AusIMM Conferences

Brisbane, Australia
19–21 October

# Mill Operators 2026

## Conference Proceedings



Proudly sponsored by

geopyörä

# Mill Operators Conference 2026

**19–21 October 2026**
**Brisbane, Australia**

The Australasian Institute of Mining and Metallurgy
Publication Series No 5/2026




Published by:
The Australasian Institute of Mining and Metallurgy
Ground Floor, 204 Lygon Street, Carlton Victoria 3053, Australia

© The Australasian Institute of Mining and Metallurgy 2026

No part of this publication may be reproduced, stored in a retrieval system or transmitted in any form by any means without permission in writing from the publisher.

All papers published in this volume were peer reviewed before publication.

The AusIMM is not responsible as a body for the facts and opinions advanced in any of its publications.

ISBN 978-1-922395-61-0

# Advisory Committee

Reg Radford
*FAusIMM*
*Advisory Committee Chair, Gold Fields*

Dr David Seaman
*FAusIMM, Paradocs Metallurgy*

Suzy Lynch
*MAusIMM, Orway Mineral Consultants*

Ben Wraith
*MAusIMM, Gekko Systems*

Luke Vollert
*Volpro*

Fran Burgess
*FAusIMM(CP), Broken Hill Mines*

Paul Petrucci
*MAusIMM, Newmont*

Dr Rob Coleman
*FAusIMM, Core Enterprises*

Jacqueline Reinhold
*AAusIMM, BHP*

# AusIMM

Julie Allen
*General Manager, Events*

Michelle Portelli
*Senior Event Manager, Events*

Sasha Pell
*Senior Manager, Conference Growth*

Sharon Lim
*Program Manager, Events*

Siobhan Rocks
*Marketing Manager, Events*

# Reviewers

We would like to thank the following people for their contribution towards enhancing the quality of the papers included in this volume:

Peter Allen
Michael Becker
Adrian Dance
Diana Drinkwater
Tristram Fyfe
Aidan Giblett
Andrew Harris
Peter Henderson
David Hunter
Sandy Hunter
Carla Kaboth
Virginia Lawson
Karen McCaffery
Andrew Newell
Stuart Nicol
Joe Pease
Andrea Hidalgo Rocha
Brigitte Seaman
Phil Sharman
Berge Simonian
Bill Staunton

# Foreword

On behalf of AusIMM, the AusIMM Metallurgical Society (MetSoc) and the Advisory Committee, we are delighted to present to you the Proceedings of the Mill Operators Conference for 2026.

Now in its 17th iteration—and its third visit to Brisbane—and spanning almost five decades, MillOps has grown from it's first regional conference into a major mineral processing conference in Australasia. This proceedings continues the proud tradition of bringing together industry professionals, researchers, technology providers, and operational leaders to share practical knowledge, innovative solutions, and lessons learned from across the minerals processing sector.

The papers published in these proceedings reflect the breadth and depth of expertise within our industry. Covering topics including comminution, flotation, geometallurgy, mineral characterisation, process control, digital transformation, automation, artificial intelligence, and emerging technologies. The papers provide valuable insights into the challenges and opportunities confronting modern processing operations. Importantly, the proceedings captures not only technical advancements but also the practical experiences, operational improvements, and collaborative efforts that drive progress across our industry.

The strong technical papers in these proceedings is the result of a rigorous review and selection process. We received well over 100 abstract submissions from contributors across Australia and around the world, demonstrating the continued strength and relevance of MillOps within the global mineral processing community. The Advisory Committee and technical reviewers dedicated significant time and expertise to evaluating submissions and selecting the high-quality papers included in this volume. We sincerely thank all authors, reviewers and committee members for their commitment to maintaining the technical excellence of the conference proceedings.

These proceedings serve as an enduring record of the knowledge shared at MillOps 2026. They provide delegates and the broader industry with access to practical case studies, innovative research, operational learnings, and technological developments that can inform current practice and inspire future improvements. We hope the papers contained within this volume will continue to be referenced long after the conference concludes, contributing to the advancement of mineral processing knowledge and professional practice.

Beyond the technical program, MillOps remains an important forum for building professional networks and fostering collaboration across the industry. In an increasingly complex and rapidly evolving operating environment, the opportunity to exchange ideas, discuss common challenges, and learn from peers has never been more valuable. The discussions, questions, and connections formed during the conference are an essential complement to the knowledge presented within these proceedings.

We also extend our sincere gratitude to our sponsors and exhibitors for their ongoing support of MillOps. Their contribution plays a vital role in the success of the conference and helps showcase the latest technologies and services.

Finally, we would like to acknowledge the outstanding efforts of the Advisory Committee, technical reviewers, authors, presenters, session chairs, sponsors and exhibitors for their ongoing support, and the AusIMM team – the success of the conference and the proceedings is the result of their dedication, expertise and commitment to knowledge sharing across our industry.

We trust that these proceedings will serve as a valuable resource for delegates and industry practitioners alike, and that the Mill Operators Conference 2026 provides an engaging and rewarding opportunity to learn, connect, and contribute to the continued advancement of our profession.

Yours faithfully,

Reg Radford *FAusIMM*

Mill Operators Conference 2026 Advisory Committee Chair

# Foreword

Metallurgy is a diverse field, filled with passionate and energetic people. Being technical people, the individuals in the field embrace ongoing education. This is important for driving humanity forward and improving the utilisation of natural resources. The Metallurgy Symposium and the accompanying proceedings aims to achieve these things, providing a forum for people to share knowledge and teach others.

The papers from the symposium will serve as an ongoing resource for metallurgists to reflect and learn. For those who attended, it will help remind them of the important ideas and provide a stimulus for further thoughts. For those who were unfortunately unable to attend, it will be a new and exciting source of information to grow their minds.

I hope that others enjoy this as much as I do!

Yours faithfully,

Dr Stuart Nicol *MAusIMM(CP)*

Metallurgical Society Chair

# Sponsors

## Major Mining Partner

BHP

## Major Conference Sponsor

MOLYCOP
A tega company

## Platinum Sponsors

FKK

MAGOTTEAUX

Metso

## Gold Sponsors

CLARIANT

elecmetal

## Silver Sponsors

GR ENGINEERING SERVICES
ENGINEERING CONSULTANTS AND CONTRACTORS

Newmont

Rockwell Automation

SYENSQO

## Technical Session Sponsors

Ausenco

SEDGMAN

## Stand Up Dinner Sponsor

ORICA Digital Solutions

## Exhibition Lounge Sponsor

HARMONY™

## Conference App Sponsor

GROWTH

GROW WITH US

## Lanyard Sponsor

WEIR

Mining technology for a sustainable future

## Lunch Sponsors

ERIEZ

InterChem®

## Coffee Cart Sponsors

ALS

DREDGE ROBOTICS

## Strategic Roadmap Sponsors

Lycopodium

Newmont™

## Notepad and Pen Sponsor

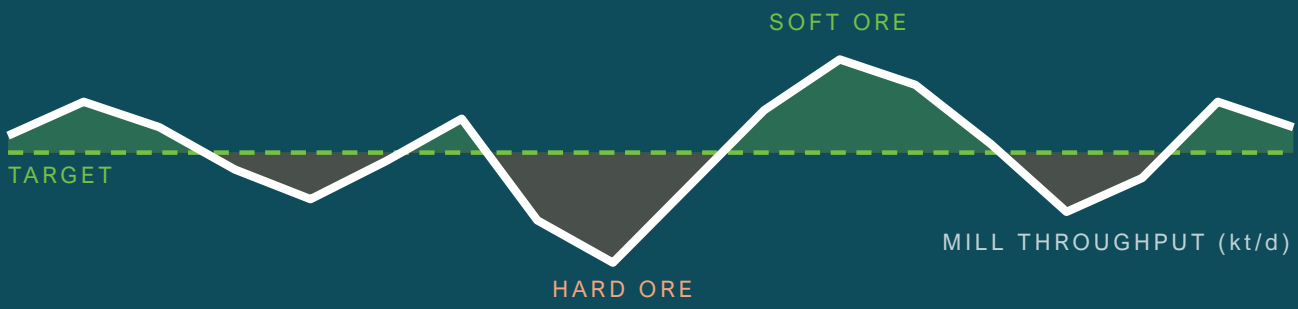
SCANTECH

*Process control specialists*

## Conference Proceeding Sponsor

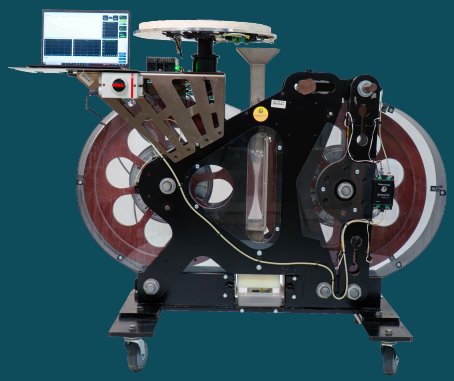
geopyörä

# Struggling to meet production targets?




## The mill is your bottleneck!

Ore hardness decides how many tonnes the mill can take, and it varies across the ore body.
Yet it is rarely known before the ore arrives.



## You can't optimise what you haven't measured.

Geopyörä measures ore hardness on drill core or D&B chips.
Geomet AI maps it across the whole ore body,
giving operations four levers to pull:

| | | |
|---|---|---|
| 1 | **Mine planning** | Schedule ore by hardness |
| 2 | **Drill & blast** | Match every blast to the rock |
| 3 | **Blending** | Feed the mill a steady diet |
| 4 | **Process control** | Set the mill for the ore ahead |

**Increase:**

- **Throughput** — More tonnes through the mill
- **Recovery** — More metal from every tonne
- **Accelerate cashflow**

## Don't just achieve targets, EXCEED them!

geopyörä

geopyora.com

# Contents

## Mill Operators


### Mill Operators: **Keynote**

Cyclones don't grind 3
*B Putland*

### Mill Operators: **Brownfields upgrades – flotation**

Everything that glitters may be gold – flash flotation in Ernest Henry's regrind circuit 23
*E Brodie, L Killer and G Binks*

Copper flotation advanced process control for Palabora Mining Company 55
*M Erwee, M Olivier, A Malan, E Mualusi, T Ramakobya, K Machaba and L Auret*

Applying modern flotation technology to improve fine particle recovery at Cadia 65
*I Heath, W Downie and M Clark*

Advanced flotation solutions for Sepon – boosting concentrate grade and carbonate rejection in gold processing 81
*H Thanasekaran, G Huang, K Thammavong and M Behre*

### Mill Operators: **Comminution**

Pebble crushing in AG/SAG circuits – operation, dynamics and solutions 99
*S Munro, R A Bearman, P Pluis and S Haskell*

Reinstating regrind for recovery – spiral technology and sulfide circuit upgrade at St Ives 115
*T S Chan, P Henderson and R Radford*

Issues with determining the SAG mill specific energy – key drivers influencing mill selection 127
*R Chandramohan, G Lane, G Ballantyne, C Haines and C Meinke*

Evaluating grinding circuit efficiency metrics at the Newmont Tanami Operation 147
*E James, A Doll and A Giblett*

Success factors in HPGR circuit ramp-up and operation 157
*I A Lovatt, M J Cook and B Dierx*

Engineering reliability in Cadia's 40 foot SAG mill 183
*A McDonough, J Brady, M Mousaviraad and R Stephens*

Mill lining for performance – a case study of the Hidden Valley SAG mill 199
*J Pyke and M Swart*

## Mill Operators: **Data, modelling and hydromet**

Accelerating process decision-making through AI-based mineralogical analysis 223
*E Aimini, E B Bezuidenhout, C F Vos, J Y Koh and N Beaton*

Investigating unleached gold in leach tails for optimum recovery 237
*K Blackwell, A R Bax, K Barbetti, B Lim and W P Staunton*

Thirteen lessons from the battle field of metal accounting 251
*R Espinosa Gomez and P D Munro*

I'm not a Luddite – is AI real? 263
*C J Greet*

Development and application of a model-based uranium tails leach optimisation tool at Olympic Dam 269
*S J Oliver and D Bouchard*

## Mill Operators: **Design and commissioning**

Woodlawn Mine restart (take two) 287
*C R Dorsch and S Oats*

Design, commissioning and operation of the Sabodala Massawa BIOX® Plant 297
*J W Olivier, M M Faye and N H M Holder*

Autoclave preservation and recommissioning at Porgera Gold Mine, Papua New Guinea 311
*L Pundi, M Kumiye, R Palme and D Akis*

Operational readiness journey of the Mungari Operations' plant expansion 323
*M K Thompson and A G L Pratt*

## Mill Operators: **Emerging technology and tailings**

Filter aid for fine and ultrafine particles – laboratory to scale technological aspects of iron ore tailings filtration 339
*L M Faustino, M G Vieira, G R Vilela Neto, W S Silva and P Fernandes*

Integration of PGNAA for ore blending control at Kanmantoo 347
*G Noble, N Muhamad, J Rutter, T Strombotne, G Norris, J Siliezar, C Rowett and M Celona*

CSIRO's recent developments in real-time monitoring of slurry mineralogy and elemental content 365
*J O'Dwyer, Y Van Haarlem, B Ganly, B James and L Mao*

Sensor-based ore sorting at Sky Metals Tallebung Project 375
*X Yang, O Davies and C Corcoran*

## Mill Operators: **Flotation**

The application of guar gum as a talc depressant, improving copper concentrate grades in the Deflector gold-copper flotation circuit, Vault Minerals, Western Australia 385
*G D Figueroa Salguero, C Wong, M Khowira, M Whitford, C Bannon, T St John and R Hanna*

Commissioning coarse flotation at BHP Carrapateena 405
*R Jones, M Davidson, F Burns and T Fyfe*

From laboratory to industry – accelerating NaHS oxidation to increase Cadia's Molybdenum Plant run time 427
*P Sharman, C Dobson, S Gunn and M Lisso*

Opening up flotation hydrodynamics – linking gas hold-up with recovery 441
*N Walter and K Lee*

## Mill Operators: **Geometallurgy**

Application of advanced mineralogy to optimise flotation at the Hillgrove Gold–Antimony Project 457
*N Bristow and J Li*

Using the Geopyörä breakage test in a Mine to Mill application at a large copper mine 471
*M Bueno, L Lara, T de Almeida and M Powell*

Development of geometallurgical testing program for Oak Dam West, South Australia 483
*Y Li, K Ehrig and V Liebezeit*

Bridging the gap between historical test work and process design 495
*A Shaikh, C Sola and S Hunter*

## Mill Operators: **Process control and automation**

Digital twin for gold production at Ikkari Mine, Finland 509
*C Araujo, T Roimaa, V Zhukov, C Izart, R Budhathoki and S Bosman*

Grinding and flotation advanced process control integration at Goldex Mine 521
*G Gagnon, A Vargas, B Aktoprak, N Chawda and D Gudgeon*

Review of an AI-driven advanced process control system for closed loop flotation optimisation at MMG Dugald River Mine – 18 months post-commissioning 533
*W Smith, A Malcolm, J Yelland, C Martin and T Soliman*

Author index 637

# Contents

## Metallurgy Symposium

### Metallurgy Symposium: Best practice in existing plant operations

A probability-based simulation of a copper mineral processing plant 551
*S L Rayward*

Mill liner wear management – common mistakes and how to avoid disaster 553
*P Toor*

### Metallurgy Symposium: Design, operation and optimisation of key unit operations

SAG milling – the benefits of bigger balls 557
*B Cornish and R Butar*

Modernising SAG mill performance – hybrid liners for enhanced efficiency and reliability 573
*J Giron, V Grover and E Mori*

Geometry – a lesson in energy efficiency and component wear 589
*I Gurnett and A Swann*

Multi-objective optimisation of mechanical flotation cell design and operating parameters for improving coarse particle flotation hydrodynamics 591
*G Lastra, B Awatey, J J Frausto, D Deglon and K Runge*

How to use the acoustic emissions from a grinding mill for diagnostics and control 593
*R A Pax*

What works versus what sounds good – the art and engineering of scale-up 595
*J D Pease and P D Munro*

Selective thorium removal from rare earth element solutions by ion exchange 601
*B da Rocha Pereira, V L Gontijo, J Vaughan, D R C Espinosa and J A S Tenorio*

Designed for one life, engineered for the next – extending the safety, capability and economic value of ageing mill relining equipment 603
*P van Rooyen*

The cleaning stage optimisations – case studies and lessons learned 605
*M Tayebi-Khorami*

Improved copper refining at Olympic Dam – experimental study and thermodynamic modelling 607
*S Valentina, G Khartcyzov, D Shishin, J Chen, J Wen, M O'Sullivan, R West, M Shevchenko and E Jak*

The devil is in the detail 609
*D Way, R Bracey and L Ryan*

## Metallurgy Symposium: **Operating updates, newly commissioned plants and plant design**

Characterisation and flotation behaviour of copper smelter slag at Mount Isa Mines 621
*J Begelhole*

Optimising CIL carbon performance to improve recovery at PT Citra Palu Minerals 635
*R Hutasoit, S Kurniawati and M Soefihara*

Author index 637

# Mill Operators

# Keynote

# Cyclones don’t grind

*B Putland*[1]

1. Managing Director, Orway Mineral Consultants (WA) Pty Ltd, East Perth WA 6004.
   Email: brian.putland@orway.com.au

## ABSTRACT

Orway Mineral Consultants (OMC) has undertaken hundreds of grinding circuit optimisation studies in mineral processing plants globally. In undertaking these, several common problems are encountered repeatedly, irrespective of other variables. One re-occurring problem is cyclone control.

The cyclone in grinding circuits plays a critical role in classifying the particles, separating the product from material requiring further grinding. They are selected and configured to achieve a target grind size under optimal conditions for the project: pressure, water split, feed and overflow density. However, the performance of the cyclone within the circuit is more influenced by ore properties, mill power draw and feed tonnes, ie specific energy input and energy requirement of the ore. This can be highly variable in some operations, resulting in a product which does not meet specifications.

The question of best practice cyclone control is frequently debated but the pros and cons are not often well-understood holistically within the context of the overall comminution circuit performance. When the product size of a circuit goes out of specification, many control systems adjust the water balance in the circuit to constrain the product size, or metallurgical teams look to optimise cyclone pressure, number of cyclones operating, water addition or components. When considered from first principles, this doesn’t make sense as the cyclones do not undertake any grinding and classification efficiency is a minor contributor. The misunderstanding appears to stem from attempts to optimise the unit process (classification) in isolation from the system (grinding). Actions taken to control the grind size in a grinding circuit are different to what is done to theoretically adjust the cut size of a cyclone.

This paper discusses common problems seen with cyclone operation and control and discusses the OMC recommended cyclone control philosophy to maintain equilibrium and stability in grinding circuits. Several case studies are presented demonstrating the benefits.

## INTRODUCTION

Over the many grinding circuit optimisations undertaken by Orway Mineral Consultants (OMC), several common problems are encountered.

One re-occurring problem is the approach to cyclone control. A common misconception in the industry seems to be that cyclones can be forced to produce a desired grind irrespective of other milling circuit variables, with many control systems adjusting the water balance and cut size of the cyclone to constrain the product size, without making any other changes. We know that cyclones do not perform any size reduction, they only undertake classification, so why should adjustment of the cyclones be undertaken to control the entire milling circuit to a target grind size?

The answer is the cyclones shouldn’t be used to try and control to grind in isolation from the greater milling circuit. The major factors that actually influence the achievable grind-size are the feed particle size distribution (PSD), throughput rate, ore characteristics, delivered grinding power, and grinding efficiency factors such as grinding media, classification efficiency and milling density. These are the variables that must be influenced and adjusted as best as possible to maintain a target grind. The cyclones should simply be set-up to classify as efficiently as possible at whatever grind size the milling circuit is capable of achieving at a target overflow density. If the economics support an adjustment in grind size, then the aforementioned milling parameters should be leveraged in a controlled way to achieve this, rather than attempting to effect the change solely via the cyclones. This often requires a change in throughput rate. Trying to implement change solely through the cyclones only leads to grinding circuit instability and production losses, which will be demonstrated in the operating examples presented in this paper.

There are two primary control schemes for operating hydrocyclones within a closed grinding circuit which are based around the fundamentals of cyclone operation. The cut-point of a cyclone is influenced by both the operating pressure (centrifugal force) and slurry density (slurry viscosity and hindered settling-effect). This gives rise to operation using one of the two primary philosophies, either constant pressure/flow and variable feed density, or constant feed density and variable pressure/flow. In each case, the aim is to stabilise both variables as much as possible while also managing the cyclone feed hopper level. Typically, one variable is controlled using cyclone feed water addition and the other variable with pump speed and/or number of cyclones online. The key to either approach is that it is integrated properly into the greater circuit control which also considers feed rate, milling density, mill speed and power draw etc. Theoretically, both philosophies can achieve the objectives, however the way comminution systems respond to circuit changes and disruptions in each case is very different, making one methodology much more effective in the majority of applications.

## CONSTANT DENSITY

Operating cyclones at constant feed density and with variable flow rate (pressure) had been the dominant trend in grinding circuit installations over the last few decades. Prior to then most cyclones operated constant pressure as the cyclone feed pumps were fixed speed. Targeting constant cyclone feed density, the water addition to the discharge hopper is varied to maintain a constant feed density to the cyclones. The pump speed is modulated to maintain the level in the mill discharge hopper. The number of cyclones online is then adjusted to keep the pressure within in a target band. There are variations to this, with the use of the pump speed and number of cyclones exchanged to control the other variable. In both cases, the outcome is the same – density is tightly controlled and the flow rate is variable.

In a grinding system, if the ore hardness or throughput increases, the achievable grind size increases if the input power and grinding efficiency is fixed. However, when operating with constant feed density, the cyclone cut point does not change in response to this which causes the circulating load to increase. This increases the flow to the cyclones, which increases cyclone feed pressure. The increase in pressure in turn decreases the cut point of the cyclone (product becomes finer), causing the circulating load to increase further. The logic then typically brings online more cyclones in an attempt to maintain the pressure within a band. This further inflates the recirculating load and in a way that makes it difficult for the process to recover without creating more grinding circuit instability.

Operators, or the greater control system, must quickly adjust operation of the milling circuit to avoid losing control, resulting in the circuit spiralling into high recirculating loads and high cyclone pressure, at which point the cyclones rope. Switching cyclones in or out only temporarily stabilises pressure fluctuations without solving the root cause: the cyclone cut point is misaligned with the grind size that can be achieved by the mill, considering power, feed size, and ore characteristics.

In this case, either the control system needs to reduce throughput (increase specific energy input to reduce the grind size) or the operators need to increase the cyclone feed density set point manually (increase the target grind size) so that the cyclone cut point and achievable grind size are in equilibrium. Due to the spiralling cause and effect response, the action of the control system, and operators, must be fast when operating under this philosophy, changing and adjusting set points before the recirculating load has been inflated. In many cases the operators do not want to reduce the throughput rate, as this loss in throughput may be economically suboptimal when compared to recovery losses at a coarser grind. As a result, any logic that is designed to reduce throughput rate to keep a tight grind size is often disabled. If throughput rate is not adjusted, the cyclone feed density must be manually or automatically adjusted to maintain the equilibrium in the circuit. The density/grind relationship is often not well understood and so this change isn't made. What often happens in this situation is the circuit is forced to operate in a disconnected way, attempting to maximise throughput while also attempting to enforce an arbitrary target grind.

If the pressure increases too much before adding a cyclone, or spikes when taking one offline, the water split is impacted and cyclones will often rope, forcing coarse material/grit out in the overflow which relieves the circulating load. If the system operates continuously close to the limit of the achievable grind, the operators may not even notice this is happening. Often only one cyclone will

rope, bleeding coarse material out of the circulating load into the overflow. The average grind is therefore coarsening naturally to achieve equilibrium, albeit in an uncontrolled way with coarse particles reporting to downstream processing. Every cyclone opened or closed causes instability and an off-specification overflow PSD during the transition. For this reason, regular cyclone switching should be avoided and reserved only for significant throughput step changes.

Constant density can be a useful approach where grind size is critical and tight control is required to avoid producing out-of-spec or unsaleable product due to poor liberation of gangue, eg in some magnetite concentrators. However, in this case, it is still important to modulate throughput to maintain the grind size rather than adjusting the number of open cyclones, since every cyclone opened or closed causes instability and an off-specification overflow PSD during the transition.

## CONSTANT PRESSURE/FLOW CONTROL

The alternative approach of constant flow with variable feed density is the preferred control method for plants handling fluctuating ore characteristics and operating parameters, due to its greater overall stability. In this configuration, the pump output speed is set to maintain a cyclone pressure set point. Water addition to the hopper is modulated to maintain the hopper level set point and the number of cyclones is selected to maintain the overflow density in a set band. Alternatively, the pump speed can be adjusted to maintain the hopper level and water addition to pressure. This provides tight control of the hopper level with the cyclone pressure/feed flow modulating slightly around the set point.

Using this philosophy, if the circulating load changes because the circuit is out of equilibrium, the cyclone feed density varies automatically, changing the cut point of the cyclone to converge to the achievable grind of the greater circuit. It essentially eliminates the frequent manual intervention required from the operator in the previous approach which prioritises throughput rate. Under such an operating system, the product size can drift coarser or finer, however the power is always fully utilised and the circuit is stable. The cyclone cut point matches the grinding capability of the mill at all times while tightly controlling the recirculating volume flow.

As the circulating solids increase, the cyclone feed density increases and associated product size increases. If the circulating solids decrease, the cyclone feed density decreases, and a finer product size is produced. The circuit is self-compensating and thereby prevents rapid changes in circulating load. In essence, the circuit will reach an equilibrium product for a given ore type, grinding power input and feed rate. The operator or control system focuses on adjusting the new ore feed rate, mill density etc to achieve the desired grind, always maximising throughput at the target grind for the ore characteristics and available power. At constant pressure, cyclone feed (CUF) density can be correlated to $P_{80}$. Pressure control does not imply wide fluctuations in feed density and generally the stability of both pressure and density improve when using this philosophy. Further, it often gives better stability of key variables such as mill power draw due to the better controlled recirculating volume flow, thus achieving a better and more stable grind than circuits that suffer the instability described in the constant density approach. When using this control philosophy, the cyclone pressure should be selected so that the cyclone underflow density is high to optimise water split (high 70s low 80s %solids depending on the ore) but below roping conditions. Cyclone underflow density should be measured at regular intervals over a shift or when a blend change has occurred. The pressure set point should be adjusted periodically to achieve the target cyclone underflow density. The ability to optimise underflow density, and therefore cyclone water split and efficiency, is another advantage of this control philosophy.

Cyclone switching, or the number of cyclones operated, should be adjusted to maintain the cyclone overflow (COF) within a target density range. Cyclones should not be taken in and out of circuit based on changes in circulating load. Adjusting the number of operating cyclones should be based on the calculated or measured cyclone overflow density, with a low value triggering a cyclone to be closed and a high value opening one. Changes in the number of operating cyclones is therefore infrequent and only required with large and sustained changes in fresh feed rate. This is best automated and requires the total water input to be measured, preferably not making changes more frequently than at 15 min intervals and ideally much less frequently. Over-automating cyclones to switch on and off too often is in most cases much more detrimental than operating a high or low

cyclone overflow density. Circuits without a tight overflow density target, ie circuits which dilute following grinding or those that feed a thickener, typically don't need to switch cyclones at all.

## IMPACT OF CONSTANT PRESSURE ON GREATER CIRCUIT OPERATION

Operating at constant pressure and maintaining stable recirculating flows affects the entire grinding system, not just classification efficiency and cyclone performance. Slurry flow rate and viscosity in closed-circuit mills influence power draw and breakage rates by changing the slurry pool size, superficial velocity and viscosity of the slurry in the mill. In extreme cases, it can also impact the charge distribution and media consumption rates due to media ejection.

Consistent and optimised flow-through a mill improves power utilisation and grinding efficiency in both semi-autogenous grinding (SAG) and overflow discharge ball mills. For closed-circuit SAG mills, stable flow enhances load control by minimising the impact of slurry pool fluctuations. The stable recycle stream (mass and pulp density) enables adjustment of grind size and throughput. Once stable and controlled, both circulating load (slurry pool size) and milling density (viscosity) can be used to change the breakage within the mill and therefore manipulate throughput and grind size.

If no downstream cyclone overflow density restriction exists, the number of cyclones operated can be used to target a grind size. Increasing the number of cyclones online will dampen coarse rock breakage due to increased slurry pooling, which in turn reduces throughput, where throughput is adjusted to meet the SAG mill load weight set point, resulting in a finer grind. Conversely, fewer cyclones online will reduce pooling and increase coarse rock breakage, increasing throughput and coarsening the grind.

Constant flow around the SAG mill combined with constant cyclone underflow also allows for more effective use of mill feed water addition to control the milling density. Changing the milling density can then also be used to adjust breakage – higher milling density for more abrasion, lower for increased coarse rock breakage. Without applying constant cyclone pressure control, the changes to mill feed water addition also impacts the cyclone pressure, which impacts the circulating load and cyclone underflow density, dampening or negating the attempted change in milling density and causing instability.

The constant pressure control also allows better control of the mill rock load and power draw allowing high mill power utilisation and throughput for a target grind size. This is seen in both SAG and ball mills.

These improvements extend further, beyond comminution and classification, often enhancing recovery in gravity circuits and flash flotation cells through more consistent preconcentration, feed flows, and slurry densities.

## INEFFECTIVE CYCLONE CONTROL PHILOSOPHIES

A control strategy commonly observed is density control within a cyclone pressure band, which constrains the product size but with no feedback to throughput control. This frequently results in an unstable and inefficient circuit. If this is combined with an unconstrained target overflow density, extremely high circulating loads can result. The result is high superficial velocities in a ball mill, ball ejection, grinding inefficiency and high cyclone and pump wear. If it is necessary to constrain the product size to within a tight range, the control logic must cascade back to incorporate adjustment of the feed rate. This often doesn't occur because the circuit feed rate is only modulated to maintain a SAG mill load weight, or the primary operating objective is to maximise throughput rate within an acceptable grind range.

Another scenario often observed is the addition of water to the cyclone feed hopper to achieve a target overflow density. This works at times if the current number of cyclones for the overflow density is operated, however, often there is a mismatch, and too many cyclones are in operation. This results in artificially inflated circulating loads of accumulated fines and/or high cyclone feed densities often to the point that the cyclone's ability to change the cut size with density is compromised. The resulting product size distribution is high in fines for the achieved $P_{80}$ (flat PSD slope), resulting in inefficient application of energy and unstable operation with the cyclones prone to roping with any circuit disruption. This is typically seen when finer grinds are targeted ($P_{80}$ 106 micron or less) and a high

overflow density is required (plus 45 per cent solids) for downstream processing. Cyclone switching exacerbates the issue with cyclones opened in an attempt to stabilise the pressure with each process disturbance, often resulting in extremely high circulating loads. As the system spirals, the operator often encounters a practical constraint, either pump capacity or number of available cyclones, and is forced to reduce throughput rate. Upgrading of the physical constraint is not uncommon, further exacerbating the problem by allowing for even higher recirculating loads.

Other variants include attempting to control both cyclone pressure and density too tightly and quasi-variable cyclone feed density and pressure while attempting to maintain an overflow density target. Neither of these scenarios provide stable flow and operation, making it difficult to achieve high cyclone classification efficiency.

## DIFFICULTIES IN IMPLEMENTATION

Operations have at times struggled with implementation due to external factors. Often there is a need to tackle a root cause rather than the symptom, which has not always been understood. These constraints are typically related to either design, understanding or motivation, including:

- Lack of understanding of general comminution theory by operations teams, particularly around the interaction of variables across different unit processes, resulting in a lack of confidence/support for modifying and tuning the control system.
- Competing strategies and advice from engineers, consultants and vendors, confusing and dividing site teams.
- Poor engineering designs leading to limited water being available for use in control in the cyclone feed hopper, flat launder or hopper angles requiring excessive flushing water, poorly integrated gravity or flash flotation circuits, or piping of intermittent flows into the cyclone feed hopper.
- Faulty, missing or damaged instrumentation and control valves for water addition.
- Ineffective mechanisms for assessing, implementing and documenting change.

## CASE STUDIES

OMC has worked across many comminution circuit configurations and scales of operation, successfully utilising pressure control of cyclones to achieve greater process objectives. In many cases this has been leveraged to increase throughput, in other mining-constrained scenarios to produce a finer grind without compromising throughput and in some to reduce operating expenditure (OPEX). These examples include Bozshakol, Cobre Panama, Sentinel, Geita, Mt Carlton, Tarkwa and Tropicana, not all of which are published, to name a few. To demonstrate the impact of applying constant pressure control, five case studies from published papers are discussed. These case studies are Damang, Greenstone, Leinster, Mako and Sentinel, all with different circuit configurations and different optimisation goals, illustrating the universal application and benefits. The projects and the benefits are summarised in Table 1.

**TABLE 1**

Benefits achieved (case studies).

| Benefit | Damang | Greenstone | Leinster | Mako | Sentinel |
|---|---|---|---|---|---|
| Increased throughput | Y | Y | Y | Y | Y |
| Finer grind | Y | | Y | | Y |
| Improved energy efficiency | Y | | Y | | |
| Improved stability and control | Y | Y | Y | Y | Y |
| Increased power utilisation | | | Y | Y | Y |
| Reduced operating costs | Y | Y | Y | Y | Y |

## Damang

The Damang comminution circuit comprises tertiary crushing followed by SAG-ball milling (SABC). The SAG mill receives 100 per cent tertiary crushed feed (-32 mm) and operates in closed circuit with a pebble crusher. The SAG discharge screen undersize reports to the ball mill circuit, closed with cyclones, with partial cyclone underflow treated via a gravity circuit and tails returning to the cyclone feed hopper. The cyclone overflow reports to a pre-leach thickener prior to the carbon-in-leach (CIL) circuit. The circuit initially achieved 4.75 million tonnes per annum (Mt/a) with product $P_{80}$ of approximately 120 µm (Lovatt *et al,* 2023).

The optimisation occurred in three phases – stabilisation control, optimisation control and long-lead modifications. Stabilisation control focused on implementing simple control loops that automatically stabilise the process in response to typical disturbances. These loops stabilised cyclone and SAG mill operation to remove unnecessary variation and allow for critical set points to be adjusted in a more controlled way. Significant improvements were achieved in both cyclone and SAG mill performance without the need for an Advanced Process Control (APC) system. The existing system on-site was switched off prior to OMC's involvement. The site team was able to implement all phases with remote support via MillROC, including recommendations, education, data analysis, implementation of logic and tuning.

Phase 1 consisted of three control areas which were intended to achieve automated stabilisation of the circuit, providing the foundation for all other optimisation activities. These loops not only removed the need for frequent operator intervention to maintain stability during normal process upsets, but they also allowed for previously uncontrolled key process variables to be controlled to operator set points. The loops were designed to complement each other, allowing the system to automatically reach grind equilibrium for the available power draw and incoming ore hardness. Previously, the operator attempted to force the desired grind size from the cyclones without consideration of the factors that determined the product including mill power input and feed properties. This historically caused the recirculating load to spiral out of control until a physical constraint was reached. The excess flow-through the ball mill resulted in loss of power draw, further exacerbating the state of imbalance.

Cyclone operation was historically unstable and labour intensive, with frequent manual switching of cyclones to cope with roping around the cluster. The grind was also variable as a result, with frequent grind excursions and prolonged instances of grit reporting off the trash screen. The original control had pump speed controlling hopper level, and water addition to the hopper in manual. This case study is an example of upstream throughput constraint, where the client was interested in exploring improved gold recovery at a finer grind size without reducing the throughput rate. Test work suggested that a $P_{80}$ of 106 µm was a significant inflection point for liberation, however the client had not been able to test this on the plant.

A constant pressure approach was selected to assist in achieving the grind target. Having full control over the operating pressure of the cyclone enabled the operators to fine-tune the pressure set point, catering for spigot wear to maximise underflow density without roping. This allowed the water split to be optimised, which minimised fines reporting to underflow, while also controlling the recirculating load within the constraints of the cyclone feed pumps. This approach is well suited to operations, with the throughput rate controlled directly to a grind size. The cyclone feed density was set to adjust automatically with throughput rate changes to converge to the grind size that is achievable with the available power. This was applicable at Damang because of the fine feed size to the SAG mill ie essentially two-stage ball milling with safety overrides for any load excursions in the primary mill. This removed the need for the operators to adjust the cyclone feed density set point, and importantly, allowed for improved control of the circulating load and density control in both mills. This allowed a higher power draw to be sustained, enabling either higher throughput rates or a finer grind.

The control loops implemented were pump speed to control to the cyclone feed pressure set point, and water addition controlling hopper level. The number of cyclones online was rarely adjusted, only when there was a significant step change in throughput. The following observations were made:

- Ball mill cyclone control was fully implemented by the site operations team with no requirement for an expert control system. The system became the default control approach from July 2022.

- Significant improvement in grind stability, eradicating grind size blowouts above $P_{80}$ 150 µm (see Figures 1 and 2).
- Reduction in incidents of roping causing grits to report to trash screen. The reduced roping was expected to improve agitator life and reduce CIL tank sanding, increasing the live volume for leaching.
- Reduction in the need for frequent operator intervention to switch cyclones in an attempt to manage roping events.
- A reduction in flow around the circuit (ball mill and cyclones) and increased mill power draw without an increase in ball charge level (see Figure 3 with the effect observed at two ball charge levels).

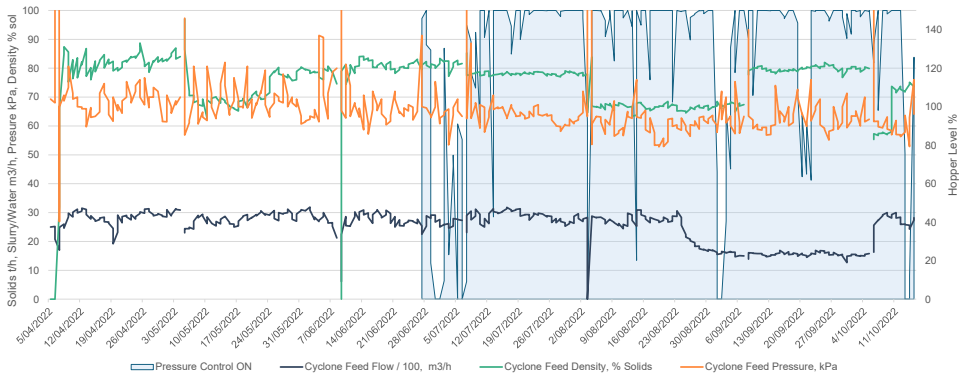



**FIG 1** – Six month trend for cyclone control running.

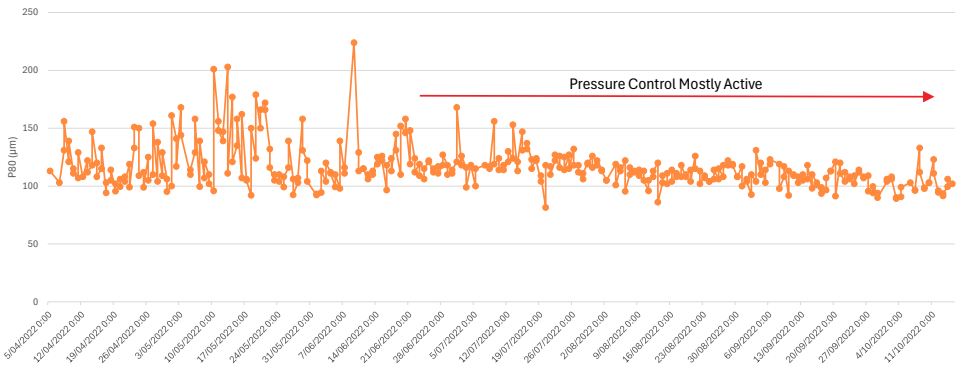



**FIG 2** – Six month trend for leach feed grind size.




**FIG 3** – Ball mill power draw versus cyclone feed flow – October.

The combined effect of the described changes was not only a sustainable increase in power draw, but also an improvement of energy efficiency. Comparing the key operating parameters from the

baseline it was evident that the primary objective of achieving a finer grind without sacrificing throughput rate was met.

The change in grind was gradual with the implementation of Phase 1, allowing for the grind to be decreased in a controlled way.

The cyclone pressure control was not perfect in this case but typically maintained the cyclone pressure within a 10 kPa range when the control was operated, which is adequate, especially considering that the variability in cyclone pressure was reduced from 15 per cent to 2.5 per cent. Fewer cyclones were operated and roping was ultimately eliminated. The grind variability was reduced by more than half, with a 5.7 per cent bonus increase in throughput achieved at the finer average grind, see Figure 4.

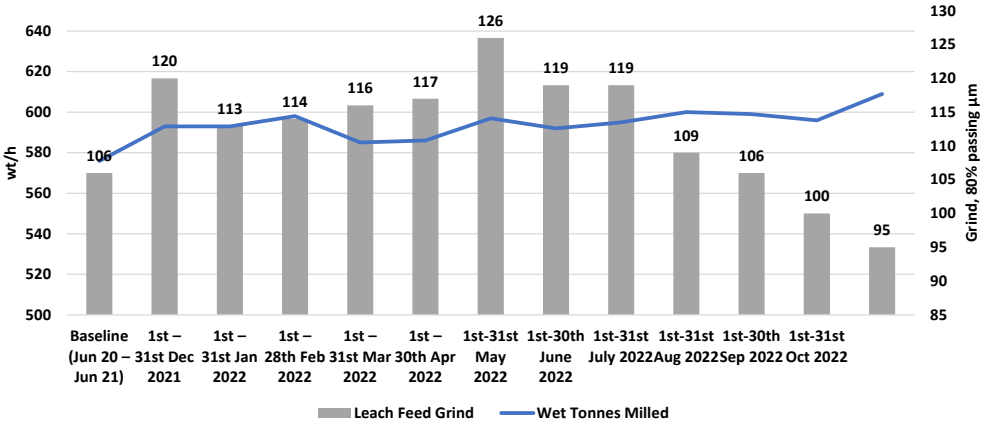



**FIG 4** – Damang throughput and grind trend.

Analysis of the circuit operating work index ($W_{io}$) showed a reduction in $W_{io}$ from around 18.2 kWh/t to 16.8 kWh/t. This indicates an improvement in circuit grinding efficiency of 7.6 per cent.

Key overall achievements were:

- Reduction in grind variability and finer average grind, exceeding the original target (see Table 2). This allowed the client to explore achievable recovery improvements in full-scale production to feed into cost-benefit analyses.
- 5.7 per cent increase in throughput.
- 7.6 per cent reduction in energy requirements, reflected in the increased throughput rate and finer grind.
- Improved circuit stability, greatly reducing incidences of cyclone roping requiring operator intervention.

**TABLE 2**

Baseline and results.

| | | Baseline | | Oct 2022 | |
|---|---|---|---|---|---|
| **Parameter** | **Units** | **Average** | **Std** | **Average** | **Std** |
| Feed rate | wet t/h | 575 | 48.8 | 608 | 41.7 |
| SAG power | kW | 5044 | 177 | 5120 | 207 |
| Ball mill power | kW | 4770 | 235 | 4760 | 129 |
| Grind $P_{80}$ | µm | 120 | 2.8 | 95 | 1.2 |
| Cyclone feed density | % | 79.6 | 3.49 | 71.2 | 2.28 |
| Cyclone pressure | kPa | 119 | 18 | 113 | 2.8 |
| $W_{io}$ | kWh/t | 18.2 | 0.817 | 16.8 | 0.711 |

Following Phase 1, throughput was later increased and the grind coarsened in an efficient and stable manner. The operator had full control over the balance between the throughput and grind size in the circuit, without experiencing cyclone instability during transitioning of set points.

## Greenstone

The Greenstone gold mine is located in the north-western part of Ontario, Canada and is owned and operated by Equinox Gold Corporation (EQX). The comminution circuit at Greenstone was designed to process competent ore at 10 Mt/a using an High Pressure Grinding Roll (HPGR)-ball milling circuit (Olmsted *et al,* 2026).

During the first sustained operating periods at Greenstone, with the cyclones manually operated, it was observed that the cyclone feed pumps were at times running at maximum output and with high variability inflow and density. Wear rates were also high on the pumps and, in the absence of a standby unit, the mill operating time was significantly reduced. This was exacerbated when running the gravity circuit due to the fluctuating addition of screen and fluidising water. Unstable operation of the upstream HPGR and wet screen circuit was also contributing to instability. The cyclone feed pump was causing instability and was a circuit bottleneck, restricting throughput ramp-up.

The team implemented the following controls to stabilise the cyclones:

- water addition to maintain mill discharge hopper level set point (SP)
- pump speed to control cyclone feed pressure SP
- number of cyclones adjusted to keep the cyclone overflow density in a target band.

The cyclone pressure control loop was fast acting because of the fast response of pressure to pump speed changes. The water addition to hopper was a slower tuned loop, allowing the hopper to operate within a band rather than a fixed level. The number of operating cyclones was adjusted ie a cyclone brought online or offline depending on feed rate and water balance to maintain the cyclone overflow density in a target range.

Using this philosophy, the product size could drift, however the mill power was being fully utilised and the circuit was stable. Typically, the relationship between cyclone feed density and grind can be used as a proxy to automatically control the fresh feed rate (throughput to grind). However, the ultrasonic density gauges were not reliable enough for this final loop to be implemented at Greenstone. The operations team is in the process of upgrading these to nuclear density gauges, after which it is planned to implement the throughput to cyclone feed density control. In the interim, the operators have been coached on when to adjust throughput rate SPs to maintain the grind at the required target using manual wet grind determinations, however they typically operate to a downstream circuit constraint.

Figure 5 presents the average cyclone feed pressure before and after implementation of the pressure control. After implementation, the number of cyclones online and pressure SP was slowly reduced while monitoring cyclone overflow and underflow density. This resulted in a lower circulating volume, with pressure maintained in a tighter band between 70–80 kPa. This removed loading on the pumps, alleviating this as the bottleneck and allowing room for additional feed. Figure 6 shows how the circuit throughput was increased, unconstrained by the previous discharge pump bottleneck through the implementation of the cyclone control philosophy.

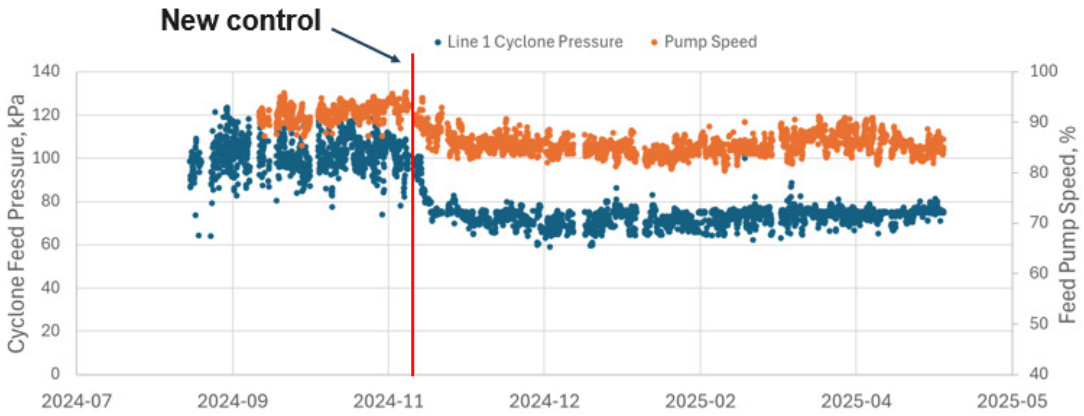



**FIG 5** – Cyclone feed pressure and pump speed.

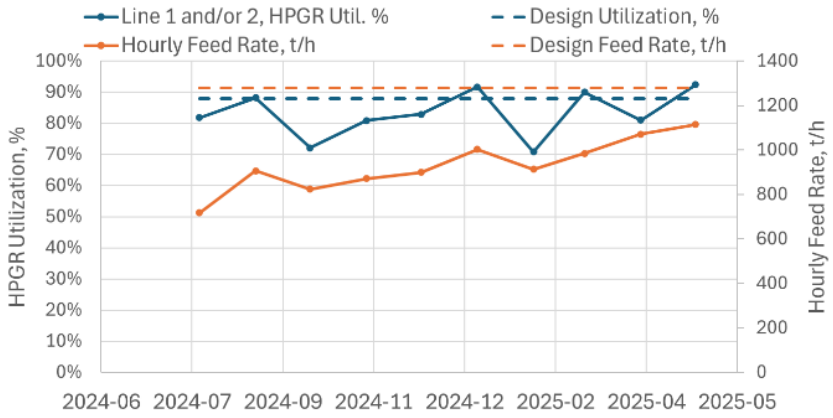



**FIG 6** – Grinding circuit utilisation and feed rate.

## Leinster

The 3 Mt/a Leinster grinding circuit consists of a closed-circuit SAG mill (7 MW) with a flash flotation cell treating 100 per cent of the cyclone underflow. An adjacent ball mill (1.6 MW), closed with its own cluster of cyclones, is fed from a portion of the flash flotation tails reporting to the ball mill discharge hopper. A cyclone overflow product $P_{80}$ size of 120 µm was targeted for the downstream flotation circuit (Harris, Hasset and Mazare, 2023).

The circuit suffered from a highly variable SAG mill load and low milling density and typically operated with high circulating loads around the SAG mill. The cyclone pressure was manually regulated with constant switching of cyclones to maintain the pressure between 80–120 kPa. The cyclone feed pump speed was adjusted to control the hopper level and no water was typically added to the discharge hoppers. The feed rate to the ball mill, coming from the flash flotation tailings bleed, was dictated by the SAG mill circulating load rather than responding to the ball mill power utilisation. The result was a highly variable grind size ($P_{80}$ 100–250 µm).

To regain stability, the control philosophy was revised by OMC. Key process control loops including SAG mill weight and milling density control were implemented, as well cyclone pressure control loops on both the SAG and ball mill cyclones. The cyclone pressure control was implemented based on adjusting cyclone feed pump speed to target a cyclone pressure set point rather than cyclone switching, and mill discharge water addition was adjusted to maintain the discharge hopper levels.

Historically, the frequency of cyclone switching was influenced by both the mill feed rate and the proportion of material being bled to the adjacent ball mill. The SAG mill feed rate was influenced by both discharge grate pegging at times and blockages on the bleed stream feeding the ball mill, further contributing to the overall circuit instability. The cause-and-effect nature of the old control philosophy that targeted symptoms rather the root causes is illustrated in comparison to performance when the pressure control was implemented, refer Figure 7.

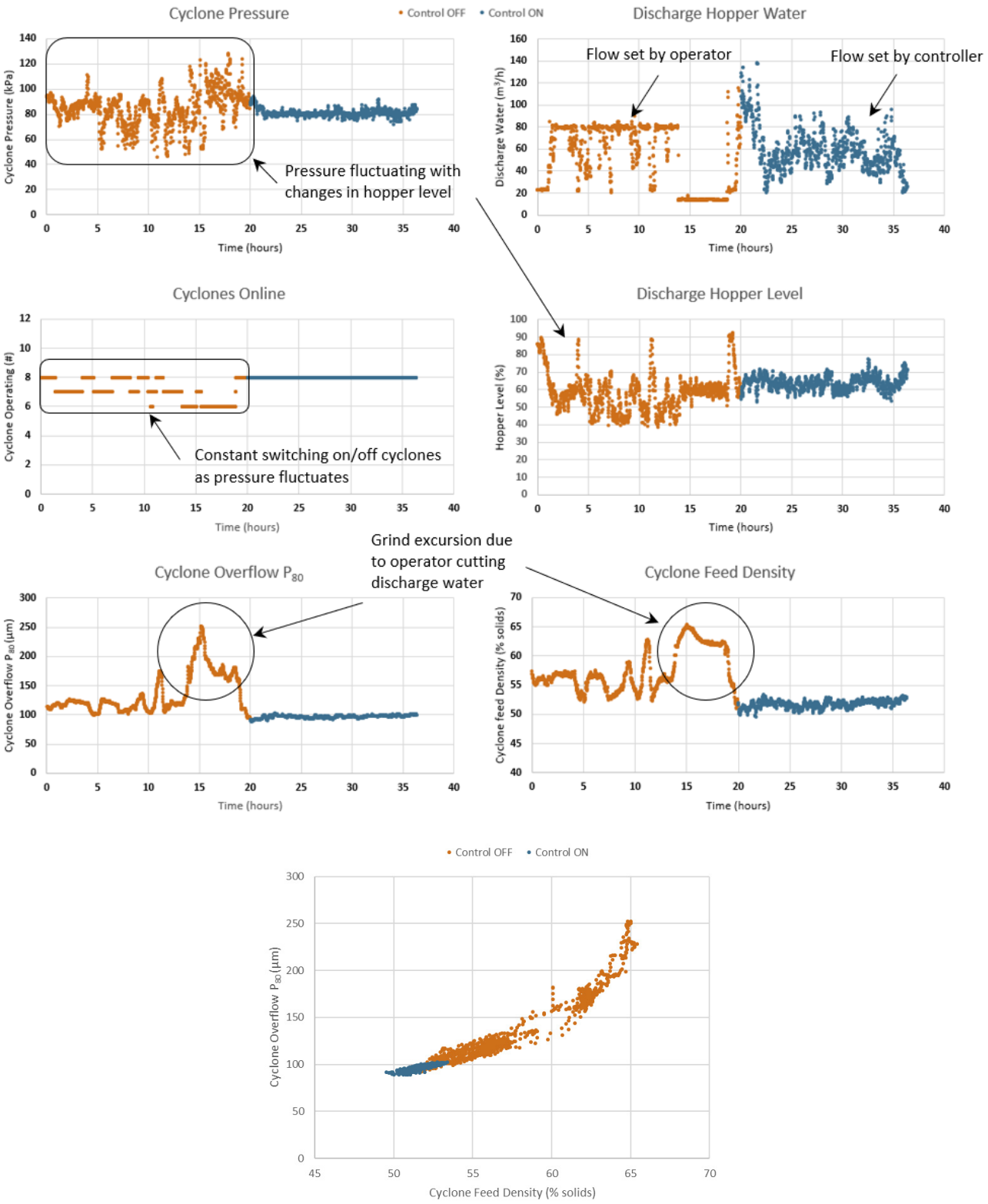



**FIG 7** – Pressure on/off comparison (Leinster).

The instability of the circuit was exacerbated by fluctuating cyclone pressure which also caused changes in the cut size and affected the amount of material returning to the mills as well as the density of the slurry in the mill. This caused variability in the mill performance which then amplified the instability back to the cyclone feed and made stabilisation even more difficult. As soon as the pressure was stabilised, the whole circuit steadied out and fluctuations due to changes in recycle flows were removed from the system. Stabilising the pressure was achieved using discharge water addition to maintain a stable flow into and out of the discharge hopper. Once implemented, the

operator only needed to manage instability due to changes in fresh feed flows rather than fluctuations in both new feed and recycles.

With the implementation of pressure control, both the cyclone feed flow and density operated in a much narrower band and the correlation between cyclone feed density and overflow product size was very strong, allowing the cyclone feed density to be used as a reliable proxy for overflow $P_{80}$ size when required. The relationship between overflow $P_{80}$, as measured by the on-stream particle size analyser (PSA) and cyclone feed density, is illustrated in Figure 7 with performance when pressure control was on and off shown for comparison.

The pressure control ON data not only enables a tighter spread of $P_{80}$ for a given feed density but also illustrates how much more stable the cyclone feed density/grind becomes with pressure control implemented. This is a natural side-effect of stabilising the recycle flows, stabilising grinding as well as classification which is often under-emphasised.

The impact of the changes made to cyclone control spread to many areas of the circuit. As the flows through the SAG mill stabilised, SAG mill power utilisation improved (+7 per cent) and the breakage rates stabilised. The final grind size $P_{80}$ reduced significantly, by almost 40 µm, and stability of the overflow product size and flows to flotation improved with a reduction in coefficient of variation (standard deviation/mean, CoV) 25 per cent to 2.5 per cent. Critically, the grinding efficiency, as indicated by the change in $W_{io}$ reduced by around 8 per cent. A summary of the benefits is presented in Table 3.

**TABLE 3**

Impact of pressure control (Leinster).

| Parameter | Pressure control | Average | Avg % change | CoV % | CoV % change |
|---|---|---|---|---|---|
| Cyclone pressure, kPa | On | 81 | -4.1 | 3.7 | -77.7 |
| | Off | 85 | | 16.4 | |
| Cyclone feed density, % Solids | On | 51.8 | -10.0 | 1.2 | -80.1 |
| | Off | 57.5 | | 6.3 | |
| SAG power, kW | On | 5776 | +7.3 | 1.7 | -55.3 |
| | Off | 5382 | | 3.7 | |
| Cyclone overflow $P_{80}$, µm | On | 97 | -28.3 | 2.5 | -90.0 |
| | Off | 135 | | 25 | |
| $W_{io}$, kWh/t | On | 19.7 | -8.0 | 5.5 | -57.5 |
| | Off | 21.4 | | 12.9 | |

A histogram and bar chart showing the 95 per cent Confidence Interval for the $W_{io}$ is shown in Figure 8 to demonstrate the improvement in stability with the confidence interval reducing from over 3 to less than 1 kWh/t.

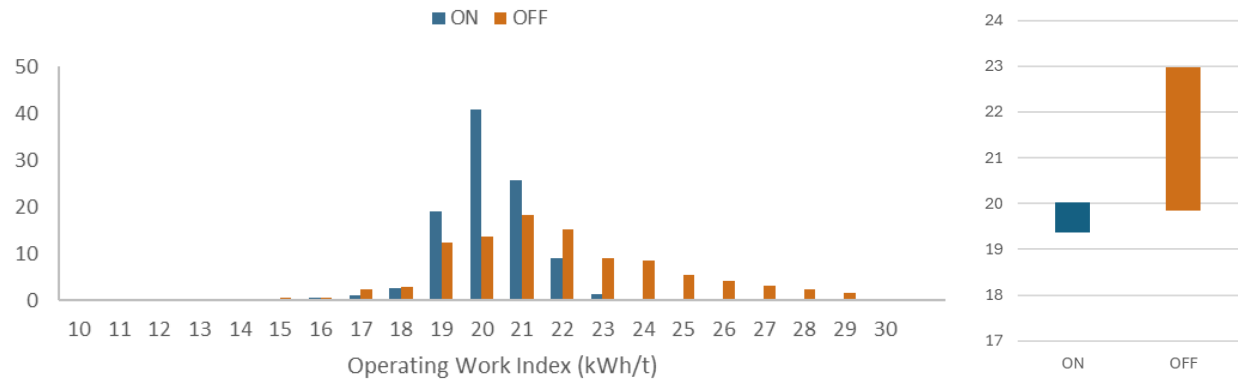



**FIG 8** – Pressure control on $W_{io}$ (Leinster).

## Mako

The Mako Gold project is located in Senegal. The 8 MW single-stage SAG mill with recycle crusher was operating at around 250 t/h, but with the cyclones consistently roping, flooding the trash screen with grits. Water to the discharge hopper was manual and cyclones were switched to control within a SP pressure band, often leading to 10+ open cyclones operating and a resulting recirculating load of over 600 per cent.

A constant pressure control logic was applied at Mako, allowing optimisation of the cyclones and leading to circuit stability. This stopped the cyclones from roping, stabilising the cyclone overflow grind size. Cyclone switching was no longer required, resulting in consistent flow around the mill and increased stability (Putland and Sciberras, 2019).

What is not understood by many operators and is illustrated in this case is the impact that flow through a single stage SAG mill has on breakage. Changes in slurry flow through the mill (volume and density) changes the slurry pool size, impacting both power draw and coarse ore breakage rates. The Mako ore was extremely competent (Axb 25) and aggressive breakage conditions aided by a low slurry pool level is required to coarsen the grind and maximise throughput.

The Mako circuit now only operates with four cyclones and with a reduced circulating load of approximately 200 per cent. Breakage has been maximised to optimise the product size ($P_{80}$ 130–140 µm), increasing throughput. The constant flow and optimised milling density allows for excellent SAG load control. This has allowed optimisation of the SAG mill power close to maximum with the circuit often averaging 96 per cent SAG mill power utilisation over a set of liners.

The use of the constant pressure control with the associated benefits, when combined with other optimisation projects overtime, has allowed the Mako circuit throughput to increase from 250 t/h to over 285 t/h, a more than 14 per cent increase.

## Sentinel

The Sentinel Copper Project (Sentinel) is located in the North-western Province of Zambia. Staged commissioning started in October 2014, with commercial production declared on November 1, 2016. The yearly production target was set at a 55 Mt/a to produce approximately 230 000 t per annum (t/a) of copper. OMC provided remote grinding support (RGS) for Sentinel from May 2017 with weekly evaluations to assist site with feedback on the comminution performance, circuit stability, bottlenecks, and potential circuit improvement strategies (Butar *et al,* 2019).

The circuit comprises secondary crushing followed by two trains of SABC circuits comprised of 28 MW SAG mills and 22 MW ball mills. There is a product scalping cyclone stage between the SAG and the ball mills with the option to bleed some of the scalping cyclone underflow back to the SAG mills as well as forward to the ball mills. The ball mills are in closed circuit with cyclones.

A number of circuit changes and trials were implemented while ramping up the circuit during the second half of 2017 and the first half of 2018 with the major changes referenced in Table 4.

**TABLE 4**

Optimisation initiatives (Sentinel).

| RGS period | Mill train | Trial description | Start date |
|---|---|---|---|
| 1–8 | Train 1 and 2 | Cyclone pressure control | May 2017 |
| 5–8 | Train 1 | T1 SAG (radial) grate slots change from 60 mm to combination of 50 and 60 mm | Jun 2017 |
| 5–8 | Train 2 | Ball Mill retaining ring installed | Jun 2017 |
| 5–8 | Train 1 | Limit SAG CUF bleed back | Jul 2017 |
| 5–8 | Train 1 and 2 | Increased BM ball charge | Jul 2017 |
| 9–12 | Train 1 and 2 | Improved gyratory crusher closed side set management | Oct 2017 |
| 9–12 | Train 1 and 2 | High intensity blasting and blasting pattern | Nov 2017 |
| 9–12 | Train 1 and 2 | Optimised mill and cyclone inspection schedule | Dec 2017 |
| 13–16 | Train 2 | Limit SAG CUF bleed back | Feb 2018 |
| 13–16 | Train 2 | 140 mm SAG mill balls | Apr 2018 |
| 13–16 | Train 2 | SAG Reline and Vortex grates | Apr 2018 |
| 13–16 | Train 1 and 2 | Cyclone 350 mm Vortex finder | Apr 2018 |
| 17–20 | Train 1 and 2 | Improved secondary crushing utilisation | Jun 2018 |
| 17–20 | Train 1 | 140 mm SAG mill balls | Jul 2018 |
| 17–20 | Train 2 | T2 SAG grate (Vortex) slots change from 60 mm to combination of 50/55 and 60 mm | Jun 2017 |
| 17–20 | Train 2 | 125 mm SAG mill balls | Aug 2018 |

Figures 9 and 10 depict how the Sentinel circuit throughput and cyclone overflow grind changed for Train 1 (T1) and Train 2 (T2). The grinding circuit product size was manually measured by operators and checked against online PSD instrumentation. The throughput stabilised towards the end of the analysis period but was slightly below design.

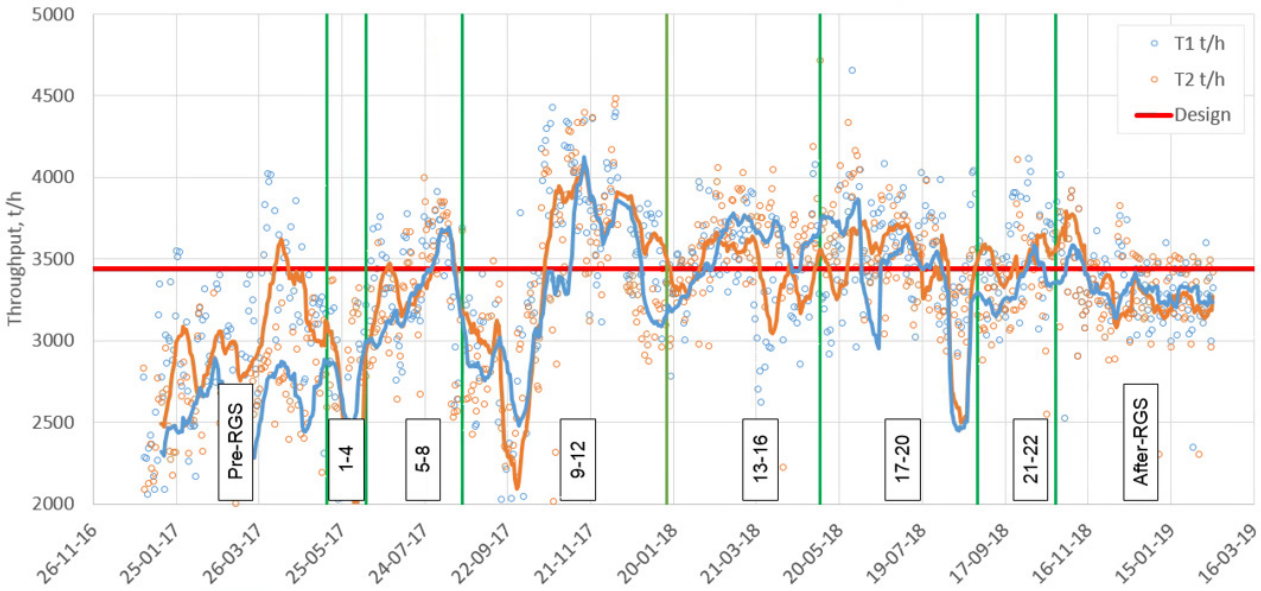



**FIG 9** – Mill throughput.

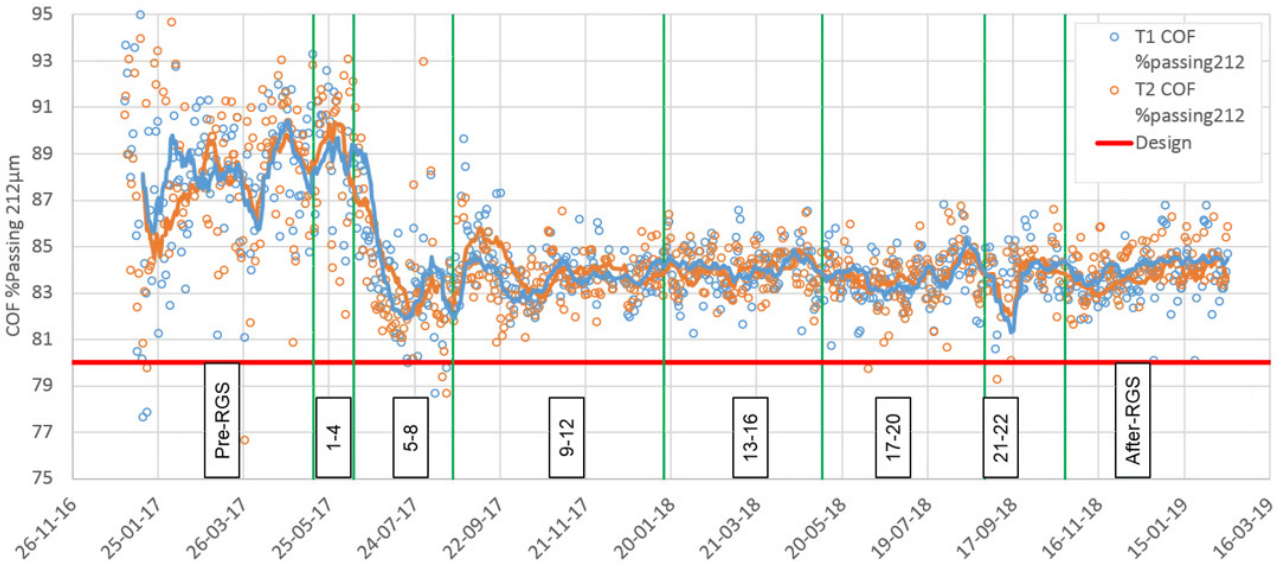



**FIG 10** – Grinding circuit product size (% passing 212 µm).

The grind had stabilised significantly after the change in control philosophy and though coarser than before change was still finer than design, which presented further opportunity to increase throughput. The power utilisation of the milling circuit was also increased from 60 per cent to 70 per cent of installed power to around 83 per cent to 84 per cent for T1 and T2, respectively over the period analysed. This was due to the reduction in flow through these large mills, which was both dampening power draw and increasing media ejection, exacerbated at higher mill speeds. The reduction in flow reduced the superficial velocity in the mill, allowing for operation at higher ball charge and speed without excessive media ejection, which enabled an increased sustainable power draw.

It was identified during design that the mills will not be able to fully utilise the installed power consistently, ie the SAG mill could only draw 26 MW of the available 28 MW consistently due to volumetric constraints. That means 7 per cent of the SAG mill power cannot be drawn. Investigations to increase power draw continued and improved after this period of analysis.

Table 5 gives a statistical extract of the feed rate, cyclone overflow percent passing 212 µm and power utilisation (as a percent of installed power) over the periods of analysis.

**TABLE 5**

Statistical analysis of optimisation initiatives (Sentinel).

| Parameter | | Pre RGS | RGS 1–8 | RGS 9–16 |
|---|---|---|---|---|
| Date | From | 01/01/17 | 14/05/17 | 21/08/17 |
| | To | 13/05/17 | 20/08/17 | 06/05/18 |
| **T1 feed rate, t/h** | | | | |
| Average | | 2992 | 3144 | 3429 |
| Std. dev. (%) | | 15.7 | 17.8 | 15.2 |
| **T2 feed rate, t/h** | | | | |
| Average | | 2582 | 3121 | 3403 |
| Std. dev. (%) | | 14.7 | 15.0 | 14.1 |
| **T1 COF % passing 212 µm** | | | | |
| Average | | 87.9 | 84.9 | 84.0 |
| Std. dev. (%) | | 3.9 | 3.7 | 1.4 |
| **T2 COF % passing 212 µm** | | | | |
| Average | | 88.2 | 85.1 | 83.9 |
| Std. dev. (%) | | 3.9 | 4.4 | 1.3 |
| **T1 Power utilisation** | | | | |
| Average (% of installed power) | | 70 | 72 | 80 |
| Std. dev. (%) | | 15.6 | 20.1 | 17.8 |
| **T2 Power utilisation** | | | | |
| Average (% of installed power) | | 63 | 73 | 80 |
| Std. dev. (%) | | 18.0 | 14.3 | 16.4 |

Overall, changing the cyclone control philosophy to constant pressure resulted in the most notable improvement to circuit stability and efficiency, as shown in Figure 9. This was significant to the overall operation of the comminution circuit, as the cyclone operation was not only responsible for achieving an efficient grind size but also enabled optimisation of flow which facilitated better utilisation of the available circuit power. The gradual change in grind under equilibrium conditions also allowed the throughput to be linked to grind size when the circuit was not SAG mill limited. Average recirculating loads decreased from around 380 per cent and 550 per cent, for the Train 1 and Train 2 ball mills respectively to 202 per cent to 243 per cent. This effectively halved the superficial velocity in the ball mills, which greatly improved the overall circuit performance, allowing higher ball mill power draw.

Achieving stable control of the cyclone cluster allowed the recirculating load of the circuit to be brought back in line with target design figures, alleviating the load on the auxiliary equipment and leading to other less obvious benefits, such as reduced discharge pump power draw, reduced wear on the pumps, pipeline, and cyclone wear components, as well as reduced superficial velocity through the ball mill. A common practice in daily operation was to vary the number of cyclones online to address short-term operating instability, particularly relating to the cyclone feed density or pressure. This artificially increases the recirculating load due to reduced separation efficiency, which in turn results in near grind size material returning to the mill and being ultimately, over-ground. Under constant pressure control the recirculating load can be controlled by matching the circuit feed rate to the target number of online cyclones. The reduced recirculating load had other less obvious benefits, such as reduced discharge pump power draw, reduced wear on the pumps, pipeline, and cyclone wear components, as well as reduced superficial velocity through the ball mill.

Figure 11 illustrates how the recirculating load variability changed over time, as the recirculating load was progressively shed. Figure 12 shows the corresponding systematic reduction in the number of online cyclones.

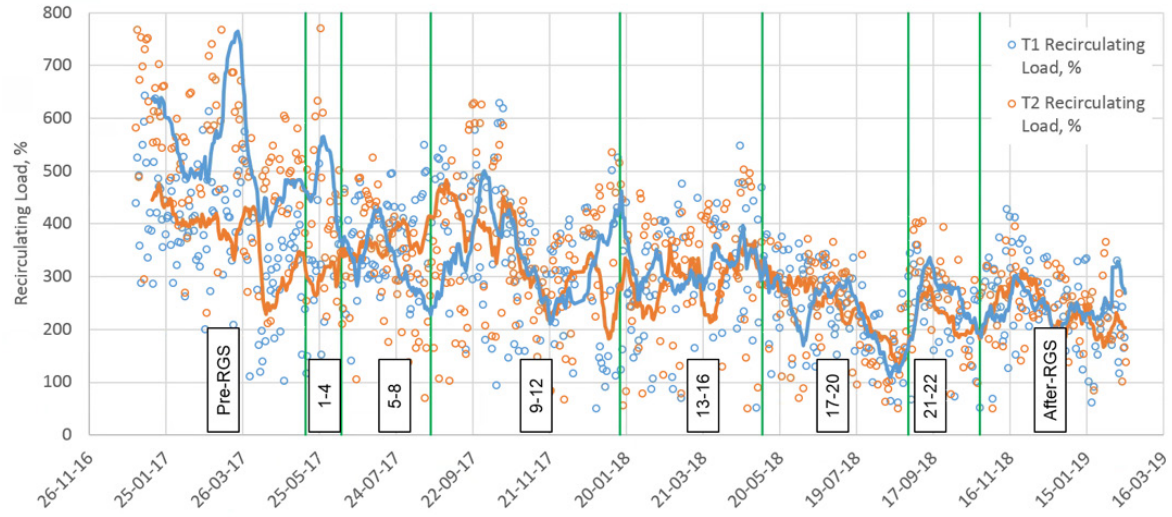



**FIG 11** – Train 1 and 2 ball mill recirculating load changes.

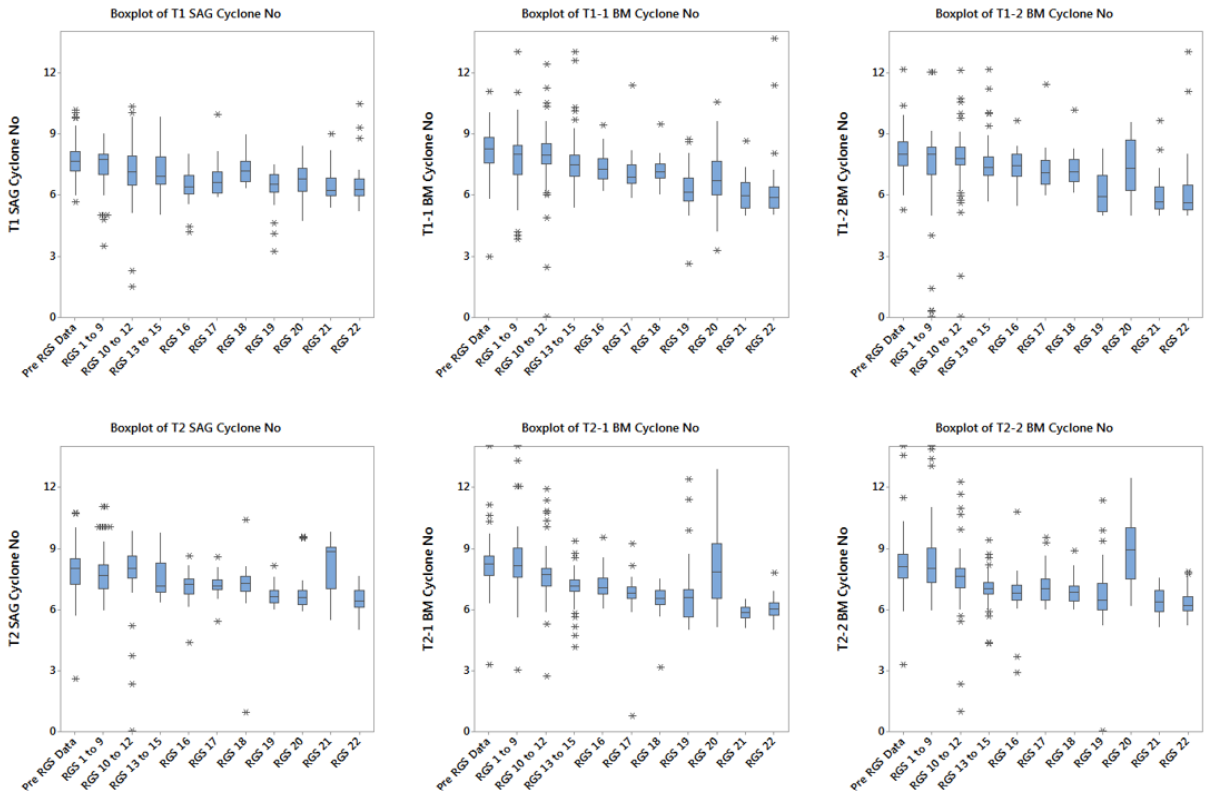



**FIG 12** – Box plot of online cyclones.

It is important to note that this evaluation does not take into account intangible benefits associated with improved circuit stability, such as reduced equipment downtime due to blockages or improved metallurgical performance due to stable operating conditions. These benefits are particularly important for flotation operations.

## CONCLUSIONS

The main concept is to use control of the water addition to the cyclone feed hopper to maintain circuit (flow) stability, as this variable is typically very responsive and is simple to implement on-site.

Once stability is achieved, the circuit can be controlled to reach the desired grind size, with cyclone feed density as a proxy, by adjusting relevant process variables such as feed PSD, ore blending, grinding power, fill level, mill speed, milling density, circulating load, classification efficiency, and throughput rate. SAG circuits can alternatively be operated to a mill load weight set point to optimise throughput, while maintaining a stable but variable grind size.

Operating at constant pressure and maintaining stable flows affects the entire grinding system and the critical variables that influence the achievable grind size, not just classification efficiency and cyclone performance. Slurry flow rate and viscosity in closed-circuit mills influence power draw and breakage rates. Consistent and optimised flow through a mill improves power utilisation and grinding efficiency in both SAG and overflow ball mills. For closed-circuit SAG mills, stable flow enhances load control by minimising the impact of slurry pool fluctuations. Stabilisation of the recirculating stream (mass and pulp density) also enables better adjustment of grind size and throughput using variables like milling density.

Improved power utilisation for longer periods of time is ultimately what is required to achieve a finer and more consistent grind, not simply adjusting cyclone feed density set point. These improvements extend beyond comminution and classification, often enhancing recovery in gravity circuits and flash flotation cells through more consistent preconcentration, feed flows, and slurry densities. OPEX savings in pumping power, cyclone and pump wear, and mill media consumption are also positive by-products.

The primary optimisation objective should be to establish stability through constant pressure operation. When obstacles arise during the implementation of the philosophy, it is essential to identify the root cause and adjust operating practices and equipment constraints, rather than merely trying to address the symptoms by modifying the proposed constant pressure control philosophy. If challenges persist with implementation, this indicates the presence of additional circuit issues that may require modifications and potential capital investment.

## ACKNOWLEDGEMENTS

I would like to acknowledge the excellent work undertaken by the authors of the papers used as case studies in the paper. Furthermore, I would like to thank the assistance from a number of OMC team members in preparing the paper and Lycopodium Limited for allowing me to publish.

## REFERENCES

Butar, R, Becker, M, Putland, B, Lovatt, I and Kock, F, 2019. Continuous improvement at Sentinel (with remote grinding support), in Proceedings of the 7th International Conference on Semi-Autogenous and High Pressure Grinding Technology (SAG 2019), Vancouver, British Columbia.

Harris, A, Hassett, P and Mazare, F, 2023. Leinster Nickel Mine—comminution circuit optimisation, in Proceedings of the 8th International Conference on Semi-Autogenous and High Pressure Grinding Technology (SAG 2023), Vancouver, British Columbia.

Lovatt, I, Lombaard, M, Kuutor, K and Arthur, S, 2023. Optimisation of the Damang comminution circuit, in Proceedings of the 8th International Conference on Semi-Autogenous and High Pressure Grinding Technology (SAG 2023), Vancouver, British Columbia.

Olmsted, A, Bélanger, F, Barstad, G, Scinto, P and Lovatt, I A, 2026. Ramp-up of the HPGR comminution circuit at Greenstone Gold Mine: a review of circuit improvements, in Proceedings of the 58th Annual Canadian Mineral Processors Operators Conference, Ottawa, Ontario.

Putland, B and Sciberras, R, 2019. Hard rock – crush it or let it break itself, in Proceedings of the 7th International Conference on Semi-Autogenous and High Pressure Grinding Technology (SAG 2019), Vancouver, British Columbia.

## Mill Operators

# Brownfields upgrades – flotation

# Everything that glitters may be gold – flash flotation in Ernest Henry's regrind circuit

*E Brodie[1], L Killer[2] and G Binks[3]*

1. Metallurgist, Evolution Mining, Cloncurry Qld 4824. Email: eve.brodie@evolutionmining.com
2. Senior Metallurgist, Evolution Mining, Cloncurry Qld 4824. Email: lindsey.killer@evolutionmining.com
3. Senior Metallurgist, Evolution Mining, Cloncurry Qld 4824. Email: gabriella.binks@evolutionmining.com

## ABSTRACT

An opportunity to improve gold recovery at Ernest Henry Operations concentrator was identified through survey analysis and supported by a favourable gold price environment. Plant survey data indicated a recirculating load of gold within the regrind circuit, enriching cyclone underflow grades from 2 g/t to 25–50 g/t Au. This may result in overgrinding, smearing and surface degradation of these particles, further contributing to gold losses in the cleaner circuit (Mitchell, Evans and Styles, 1997).

Following recovery method evaluation, flash flotation was identified as the most appropriate method for recovering gold from the regrind circuit. Flash flotation was tested on a laboratory and pilot scale with JKSimFloat modelling prior to the final investment decision.

A Metso fabricated SkimAir® flash flotation cell was installed and then commissioned in March 2025. Post-commissioning mineralogical assessment, modelling, and regression analysis of plant data have indicated improved gold and copper recovery due to the removal of gold-bearing particles from the regrind circuit, via the SkimAir cell.

Gold and copper recoveries of 78 per cent and 58 per cent from the regrind circuit, with respect to rougher scavenger concentrate, have been measured, equating to an overall plant recovery uplift of 1.06–1.99 per cent gold and 0.52 per cent copper at 90 per cent confidence. A reduction in fine gold (-20 micron) reporting to the conventional cleaner circuit and ultimately being lost to the cleaner tailings stream has also been observed.

Moreover, the dissolved oxygen demand of the downstream cleaner feed stream has reduced since the SkimAir operation, presenting more favourable conditions for sulfide flotation using xanthates.

## INTRODUCTION

Ernest Henry Operations is located approximately 35 km north-east of Cloncurry, in the north-western region of Queensland, Australia. It is one of the largest Iron Oxide Copper Gold (IOCG) deposits in the country (Cloutier *et al,* 2025). The deposit was initially mined through an open pit operation but is now exclusively accessed via underground mining methods. The mine utilises sub-level caving, a technique where ore is extracted from below, allowing the surrounding rock to collapse under gravity for easier extraction. The December 2025 Ernest Henry Ore Reserve estimate is 73 Mt at 0.75 per cent copper and 0.46 g/t gold for 550 kt of contained copper and 1100 koz of contained gold (Evolution Mining, 2026a).

The Ernest Henry copper-gold deposit is hosted in a hydrothermal breccia pipe plunging at roughly 45° to the south, bounded between two shear zones (Figure 1). The deposit is hosted entirely in felsic intermediate metavolcanic rocks, within a unit of the Mount Fort Constantine Volcanics, formed approximately 1800–1750 million years ago. Regionally these lithologies lie adjacent to a large meta-diorite body which traverses the deposit from the south-west to the north-east.

Mineralisation is associated with a matrix supported hydrothermal breccia that is enveloped by crackle veined potassium feldspar altered meta-volcanic rocks (Evolution Mining, 2023). The matrix is largely composed of magnetite, quartz, biotite, chalcopyrite, pyrite, fluorite, gold, molybdenite, uraniferous minerals and potassic feldspar. Other gangue minerals in the matrix consist of chlorite, calcite, dolomite, barite, apatite, muscovite, garnet, scapolite, sphene, rutile and tourmaline (Ryan, 1998).

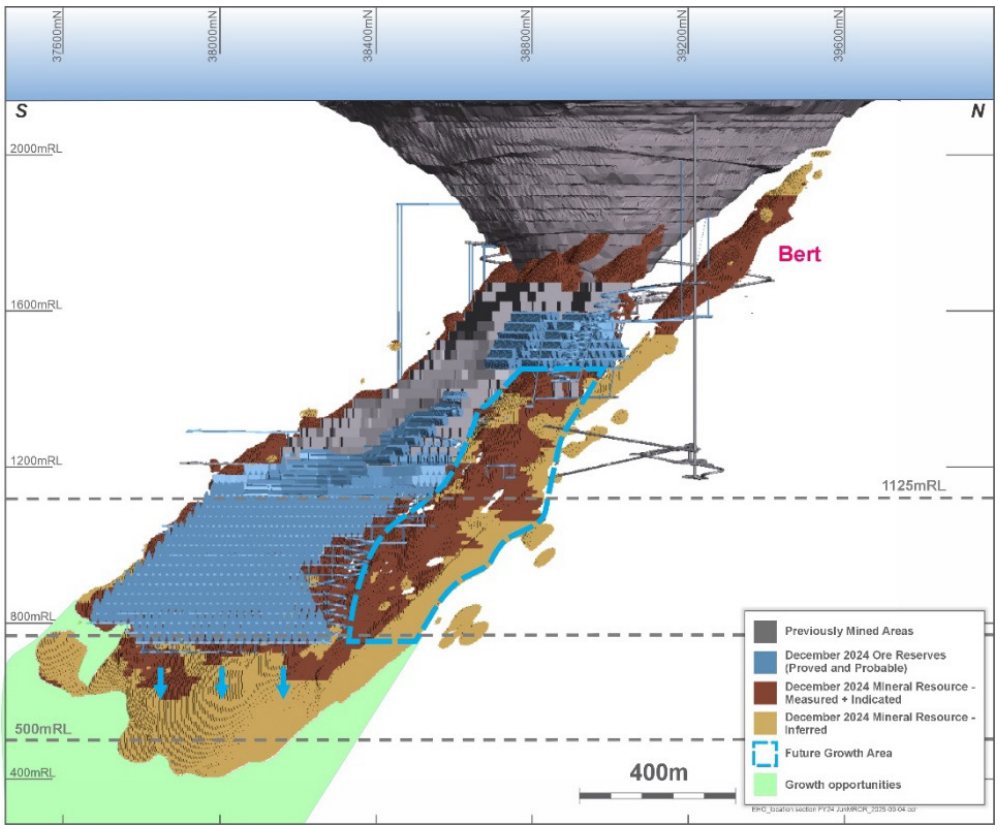



**FIG 1** – Ernest Henry orebody (Evolution Mining, 2026b). NB: The information shown is extracted from the release titled 'Annual Mineral Resources and Ore Reserves Statement' dated 1 May 2026 and available to view at <www.evolutionmining.com>. The Company confirms that it is not aware of any new information or data that materially affects the information included in the release and that all material assumptions and parameters underpinning the estimates in the release continue to apply and have not materially changed. The Company confirms that the form and context in which the Competent Persons' findings are presented have not been materially modified from the Reports.

Chalcopyrite is the sole copper-bearing mineral and, together with pyrite, represents the only significant sulfide phases. Sulfides constitute 1–20 per cent of the breccia matrix and occur as fine to medium-grained disseminations commonly associated with magnetite. Gold occurs predominantly (>98 per cent) as native gold-electrum (65–95 wt per cent Au), with minor contributions from sylvanite and sulfide-hosted gold. It is believed that gold precipitation was closely associated with, but preceded some of the chalcopyrite deposition, as indicated by the lower gold and copper ratios of late-stage chalcopyrite rich veins. Although arsenic, fluorine and uranium minerals are present, concentrations are generally below deleterious thresholds (Evolution Mining, 2023).

## Process description

Mined ore is crushed underground prior to being conveyed and hoisted onto the coarse ore stockpile (COS). The COS has a storage capacity of up to 200 kt and a minimum working volume of 20 kt. Ore is reclaimed from the COS by two apron feeders before being conveyed to the grinding circuit.

The grinding circuit comprises a 11 MW SAG mill (10.4 m Ø × 5.1 m) and a 5.5 MW ball mill (6.1 m Ø × 8.5 m) operated in a closed AB configuration with a nest of 3 × 800 mm Ø and 5 × 650 mm Ø CAVEX cyclones. The SAG mill discharge stream is screened across a vibratory screen (3 m × 9 m, 4–5 mm slots), with the screen oversize returned to the SAG mill feed by a series of conveyor belts. The screen undersize is combined with the ball mill product and is pumped to the primary cyclone pack. The cyclone underflow stream is directed by gravity to the ball mill, while the overflow stream reports by gravity to the rougher flotation circuit.

The Ernest Henry Operations (EHO) flotation circuit comprises a rougher train and three stages of dilution cleaning. The rougher train consists of nine Wemco Smart Cells (127 $m^3$) arranged in five banks. The concentrate produced by the first rougher bank is directed to the third stage of cleaning. The concentrate produced by the remaining four rougher banks reports to the regrind circuit.

The regrind circuit is composed of a Vertimill (1 MW), operated in closed circuit with a nest of 6 × GMAX15 cyclones. The overflow from the regrind cyclones reports to the first cleaner stage. The underflow from the regrind cyclones can report to a SkimAir flash flotation cell via a feed box, with the tailings flowing into the Vertimill. The concentrate produced from the SkimAir can either be directed to the final concentrate sump or third stage of cleaning.

The cleaner circuit is operated in a counter current fashion where concentrate progresses from cleaner Stage 1 to Stage 2 to Stage 3, with dilution water added to Stage 2 and Stage 3. Cleaner Stage 1 utilises eight OK50 cells, while Stages 2 and 3 utilise eight and five OK16 cells respectively.

The tailings from both cleaner Stage 1 and the rougher train are combined and directed to a 55 m diameter tailings thickener. The thickened tailings are pumped to the tailings storage facility (TSF). The final concentrate produced from cleaner Stage 3 is thickened in a 25 m diameter concentrate thickener prior to filtration using a 144 $m^2$ Larox pressure filter. The filtered concentrate is hauled by road train to Glencore's Mount Isa Copper Smelter.

The processing flow sheet of the EHO concentrator is illustrated in Figure 2.

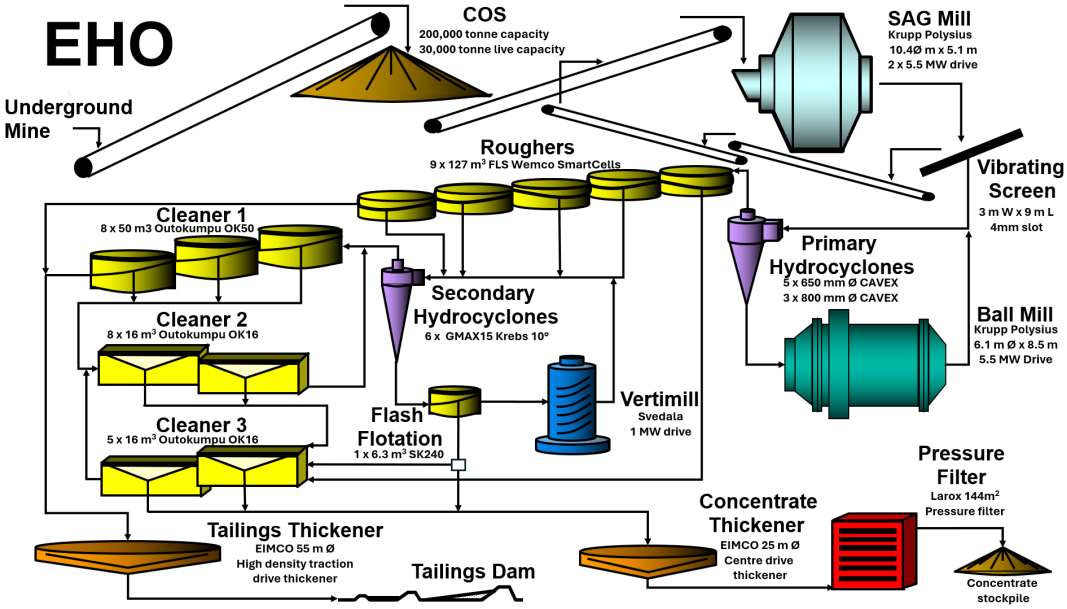



**FIG 2** – Simplified process flow sheet of EHO concentrator.

Historically copper recoveries from the rougher and cleaner circuits have ranged from 96–97 per cent and 99 per cent, respectively, yielding an overall copper recovery of 95 per cent. Gold recoveries from the rougher and cleaner circuits were approximately 89 per cent and 90 per cent, respectively, yielding an overall gold recovery of 78–80 per cent. The process produces a bulk copper-gold concentrate grading on average 26.5 per cent copper and 12 g/t gold. Pyrite is well liberated but remains the main gangue mineral in the concentrate due to the aggressive flotation conditions applied to achieve 99 per cent copper cleaner recoveries, with high dosages of xanthate in the first stage of the cleaner.

## Background

A survey of the primary and regrind circuits was conducted to further investigate the gold distribution within the inter circuit streams. The survey indicated a gold recirculating load of 400 per cent in the primary circuit and 1750 per cent in the regrind circuit (Figure 3). The level of enrichment in the regrind circuit presented as a primary target for further investigation, due to mineralogical studies indicating that up to 90 per cent of gold minerals in the downstream cleaner tailings were liberated

(Coombs, 2025). It was hypothesised that the recirculation within the regrind circuit was generating fine liberated gold. The gold losses in the cleaner tailings were ultra-fine particles (<6 micron), while the $P_{80}$ into the cleaner circuit is 20–30 microns. Pease, Curry and Young (2005), indicated that fines may not float well when mixed with coarse and composite particles, these fine particles require more flotation time and collector.

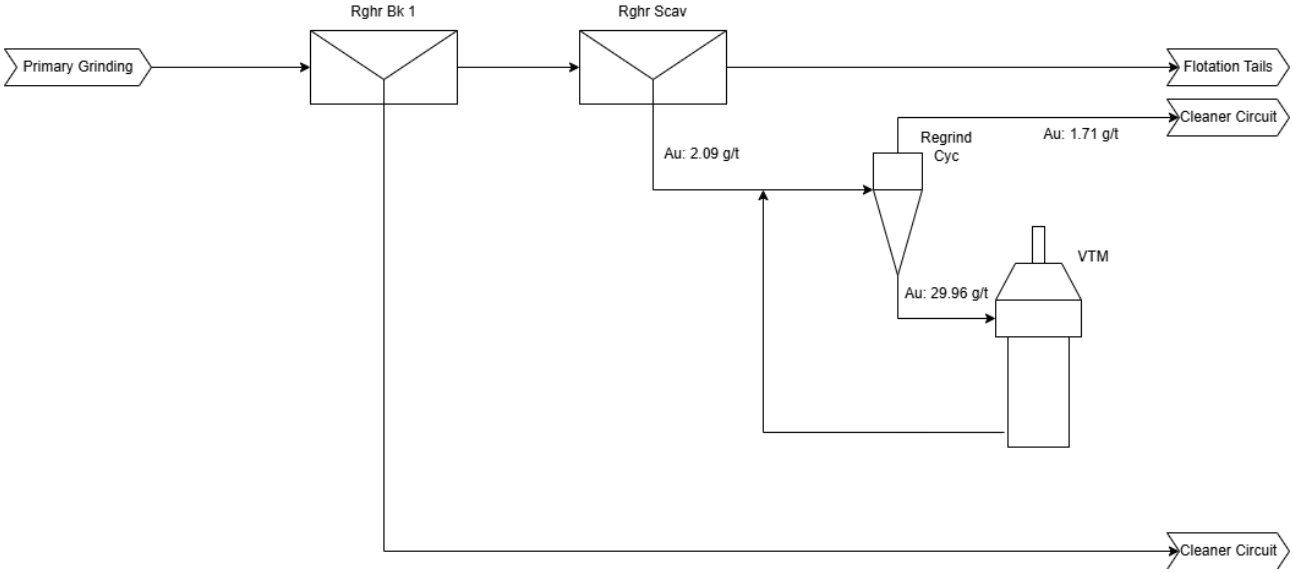



**FIG 3** – Simplified process flow diagram with gold assays from a survey in 2022.

## Recovery method options analysis

Several alternative methods for recovering fine liberated gold particles identified in the cleaner tails were evaluated alongside flash flotation. These methods are outlined here:

- Gravity concentration (Knelson) on regrind cyclone underflow.
  - External test work completed by Consep findings:
    - 27 per cent Gravity Recoverable Gold (GRG) in rougher scavenger.
    - Indicated up to 6.8 per cent gold recovery of cyclone feed by the installation of two QS48 Knelson concentrators.
  - Subsequent on-site pilot plant findings:
    - Low yield, 1.49 per cent gold unit recovery.
    - Concentrate bed erosion due to high specific gravity of pyrite which is in high concentration.
- Gold-specific collector (Aerophine 3418A) added to cleaner circuit.
  - Plant block trial findings:
    - No statistically significant increase to overall gold recovery observed.
- Open circuit configuration of IsaMill to liberate particles <20 microns while removing recirculating load in regrind circuit.
  - Pilot IsaMill findings:
    - Slurry pulp chemistry conditions less favourable for flotation due to closed system grinding.
    - Capital investment required to re-aerate flotation pulp following grinding to restore mineral floatability.
- Cleaner Tail Cyanide Leach

- 2023 scoping study findings:
  - 85 per cent of gold in the cleaner tails can be recovered by cyanide leaching based on cyanide-leach bottle roll tests completed by ALS Metallurgy Perth.
- Negative NPV, largely driven by high cyanide consumption as a result of copper and sulfur cyanocides in cleaner tail.

## Flash flotation technology overview

Flash flotation is a method of recovering well liberated, fast floating valuable mineral particles by mineral flotation before recirculating back to the grinding mill (Newcombe, Bradshaw and Wightman, 2012). By removing valuable minerals early, flash flotation reduces circulating loads and prevents over grinding. Additionally, the technology will act as a scalper and moderate feed grade fluctuations into the conventional flotation circuit, providing stability to the process.

Typically, flash flotation is carried out in a primary grinding circuit for material that has misreported to a coarse stream of a classification system, normally the cyclone underflow. The primary cause of fine, well-liberated particles reporting to cyclone underflow is the bias of high solids specific gravity particles toward the underflow, combined with the inherent inefficiency of cyclones (Niskala 2025, personal communications).

Application of the technology isn't limited to the primary grinding circuit cyclone underflow but can be utilised successfully on the ball mill discharge without classification, or in the regrinding circuit. Slurry flow should be always driven by gravity in a flash flotation circuit; hence cyclone clusters require to be elevated to a higher level than would normally be required.

The concentrate produced by flash flotation is preferably final grade, but a separate flash cleaning stage can be utilised to clean the concentrate and reach final grade if required. Ore suitability for flash flotation and for potential flash cleaning should be determined by laboratory test work.

Metso's SkimAir® flash flotation cell, has a unique cylindrical tank with a conical bottom designed to promote efficient discharge of coarse tailings mitigating the risk of sanding (Figure 4). The SkimAir geometry is well suited for regrind circuits, where solids specific gravities can reach up to 4.2 t/m$^3$ and slurry density sitting at 60 per cent w/w are common (Niskala 2025, personal communications). Typical SkimAir applications involve coarse and abrasive material, which requires a special control philosophy for the tailings discharge valve to avoid premature wear and minimise sanding.

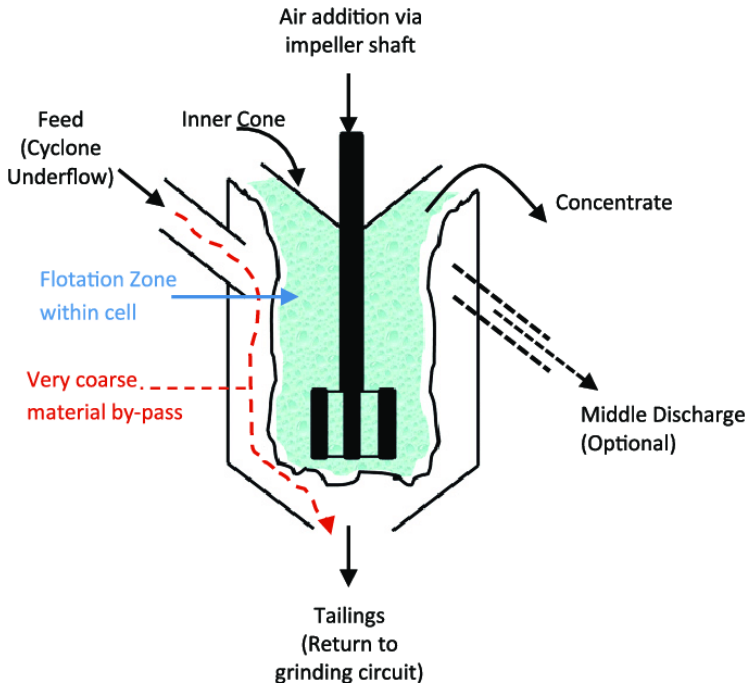



**FIG 4** – Schematic of a flash flotation cell (Newcombe, Bradshaw and Wightman, 2012).

# FLASH FLOTATION SCOPING TEST WORK

## Laboratory scale test work

Findings from quarterly mineralogy reports and plant surveys led to a laboratory test program designed to simulate installing a flash flotation cell on the regrind cyclone underflow. This test work program follows the SkimAir flash flotation laboratory procedure supplied by Metso.

### *Methodology*

The aim of this test work was to collect flotation kinetic data in order to assess the suitability of Ernest Henry process mineralogy for flash flotation.

The laboratory test work was completed on-site using a 5 L JKTech batch bottom driven flotation cell. A regrind cyclone underflow composite was collected using a half-moon sample cutter and immediately transported to the on-site laboratory. The sample was diluted to 45 per cent solids by weight using freshly collected process water. The slurry sample was then slowly transferred to the batch flotation cell with the agitator set to 1200–1250 rev/min to prevent sanding of the cell and ensure particle suspension. Appropriate reagents were added dependent on the test scheme; these included collectors Potassium Amyl Xanthate (PAX) and Aerophine 3418A (Syensqo), and Flotanol 50 (Clariant) frother. The laboratory flotation tests were carried out by following the Metso flotation procedure.

It is noted that the batch flotation tests have limited ability to predict plant recovery, as the float feed sample was taken from the current regrind circuit recirculating load, which differs significantly from the conditions expected after flash flotation cell installation. Following installation, the gold grade in the SkimAir feed is expected to decrease because a large portion of the gold will be recovered and diverted. This change will, in turn, influence flotation kinetics and overall recovery.

Numerous laboratory flotation conditions were tested, including varied air rate, cell agitator rev/min and Aerophine 3418A/PAX dosage. A summary of the test conditions which produced viable results is presented below in Table 1. The purpose of the laboratory test work was to gain a series of recovery and grade data from an operating plant stream.

**TABLE 1**

Summary of laboratory flotation test conditions.

| Test ID | Date | Air rate (L/min) | Agitator speed (rev/min) | Frother add. (ppm $H_2O$) | PAX add. (g/t Cu) | Aero add. (g/t Cu) | Start pH | Start eH (mV) |
|---|---|---|---|---|---|---|---|---|
| FF S2 | 03/09 | 8.0 | 1200 | 8.1 | 13.9 | 0 | 9.41 | 68 |
| FF T4 | 19/03 | 10.5 | 1200 | 10.4 | 0 | 6 | 9.02 | 69 |
| FF T14 | 28/04 | 10.5 | 1250 | 8.6 | 0 | 15 | - | - |
| FF T17 | 03/05 | 10.5 | 1250 | 8.1 | 0 | 21 | 9.02 | 72 |
| FF T18 | 03/05 | 10.5 | 1250 | 8.1 | 0 | 23 | - | - |
| FF T19 | 27/05 | 11.0 | 1250 | 8.4 | 0 | 21 | 9.02 | 57 |
| FF T20 | 27/05 | 10.1 | 1250 | 13.8 | 0 | 26 | 9.03 | 65 |
| FF T24 | 22/07 | 9.3 | 1200 | 8.0 | 0 | 23 | 8.6 | 77 |
| FF T25 | 22/07 | 9.5 | 1200 | 8.0 | 0 | 34 | 8.5 | 77 |

A summary of the copper grade recovery curves where results were viable are presented in Figure 5.

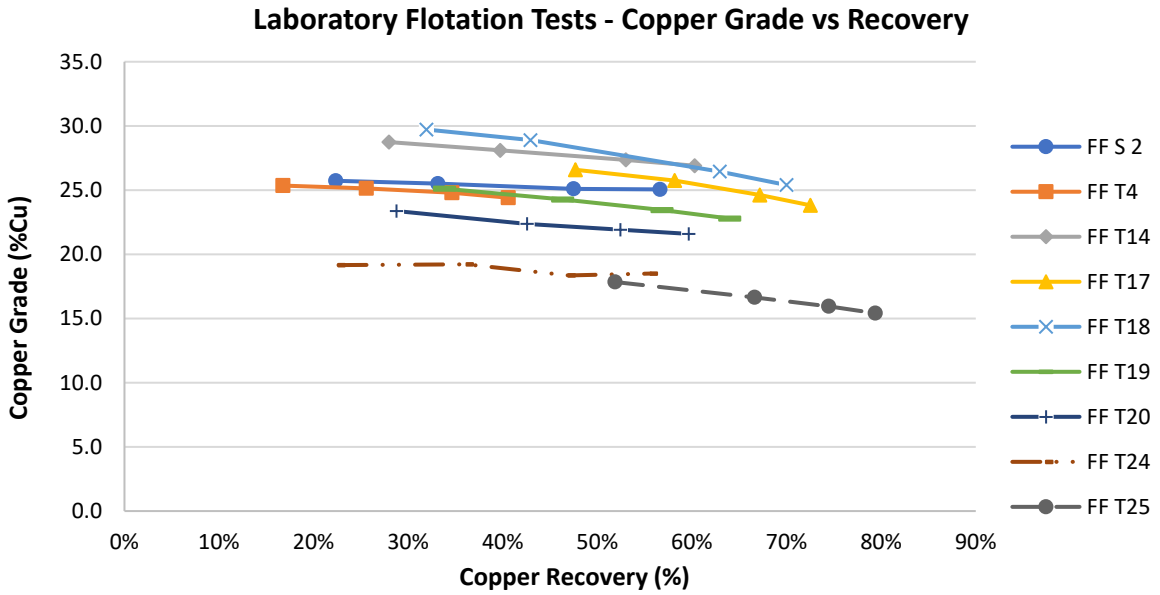



**FIG 5** – Laboratory flotation flash flotation test work – copper results.

### *Summary of results*

Laboratory batch flotation test results indicated recoveries ranged between 20–60 per cent and 45–70 per cent for gold and copper, respectively. The flotation kinetics observed in these scoping tests suggest that flash flotation technology may be applicable. This is supported by Erkan, Ekmekci and Altun (2022), who demonstrated that laboratory scale flash flotation of an ore containing both free and sulfide-associated gold achieved gold recoveries of up to 60 per cent across a particle size range of +212 to -38 micron. The engineering test work from Wiluna Mines indicated similar kinetics, with 40 per cent gold recovery after 1 min and up to 80 per cent recovery after 2 mins of flotation time (Toussaint and Richardson Consulting Engineers Pty Ltd, 1994). Although Ernest Henry batch tests indicated strong kinetics, the results were variable and further test work was required to confirm suitability.

The copper grade and recovery curves found in Figure 5, illustrate copper concentrate grades above 20 per cent were achievable. Whilst all tests were completed on different samples, changes in collector and pH resulted in a change to copper concentrate grade, gold and copper recovery. The test work consistently confirmed the ability to produce a product close or within final copper grade specification from the regrind cyclone underflow at up to 60 per cent gold recovery. Pilot and mineralogical studies followed to further understand the grade and recovery of minerals under continuous operation from an operating plant stream.

### *Laboratory float test work mineralogy*

Composite samples collected from various EHO process streams within the regrind circuit were sent to Expert Process Solutions (XPS) for unsized gold deportment mineralogy after the laboratory test work program. The mineralogy within the regrind circuit consisted primarily of pyrite (48–88 wt per cent) as there is upstream rougher scavenger circuit operation consisting of high xanthate dosage and shallow froth depth. Specifically, the regrind cyclone underflow stream consisted of 86 wt per cent pyrite, 3 wt per cent chalcopyrite and the remaining being silicate gangue. Free gold (60 per cent) and electrum (40 per cent) was 67 per cent liberated and the average liberated grain size was between 13 and 23 micron (Gordon, 2022). The liberation of the gold minerals in the regrind cyclone overflow, also known as cleaner feed, was 36 per cent in comparison. Gordon (2022) commented liberated and free precious metals recirculating in the regrind cyclone underflow are heavy and coarse. The liberation (>60 per cent) of gold minerals and chalcopyrite within this stream provided further insight for future test work.

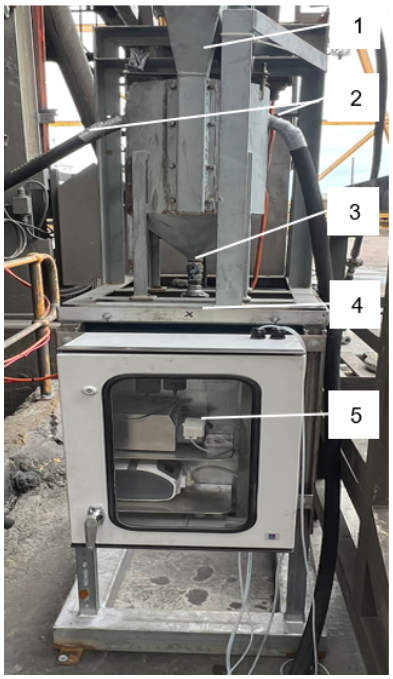
## Pilot scale test work

Following the laboratory test work results and mineralogical characterisation, a 0.25 t/h SkimAir (SK0.25) was piloted on-site to further evaluate the viability of flash flotation technology at EHO. The pilot test work was aimed to obtain:

- Cu/Au recovery and final product grades.
- Pulp chemistry conditions.
- Cell operating pulp density.
- Results to confirm reagent scheme (Aerophine 3418A versus PAX).
- Results to compare to laboratory test work.
- Inputs for flotation modelling to determine the net impact of flash flotation on overall circuit, ie rate constants for Cu/Au/NSG (non-sulfide gangue).

### *Methodology*

The pilot SkimAir cell was installed at ground level at the regrind circuit (Figure 6). Multiple spear samplers were designed to produce 0.15–0.6 $m^3$/h of slurry from a flanged regrind cyclone underflow pipe. The sample directed was to the SkimAir cell by gravity via a 1-inch hose.




| | |
|---|---|
| 1 | Feed Box |
| 2 | Concentrate sampling points |
| 3 | Manual tailing valve |
| 4 | Tailings sampling point |
| 5 | Reagent pumps (collector, frother, lime) |

**FIG 6** – Pilot plant layout.

A two-week pilot program was carried out by the on-site metallurgy team in September 2023. The tests were completed by the following method. Slurry was fed to the cell, and the tail ball valve was manually manipulated until slurry level reached steady state. Test conditions such as flow rate, pulp chemistry and reagent addition were manually measured, while air addition was monitored by a rotameter. After 10 mins of steady state at the test conditions, the concentrate and tailings stream samples were repeatedly cut into 10 L buckets. The pulp samples were analysed for percent solids and elemental analysis (base metal, titrations and fire assay Cu, Au, Ag, S, Fe, As, F, and U). Some reserve was made available for particle sizing.

### *Summary of results*

The pilot test variables were residence time, superficial air velocity, collector and pulp pH. Summarised ranges shown in Table 2.

**TABLE 2**

Range of pilot test variables.

| | Residence time (min) | Superficial air velocity (cm/s) | Aerophine g/t | pH |
|---|---|---|---|---|
| **Min–max** | 1.6–8.7 | 0.25–1.12 | 0.19–17 | 7.8–11.9 |

Initial tests illustrated a linear relationship between mass recovery and collector dosage, with copper and gold recoveries up to 90 per cent being recorded as shown in Figure 7. The initial high recoveries were associated with poor chalcopyrite selectivity as final copper concentrate grades ranged between 5–10 per cent copper.

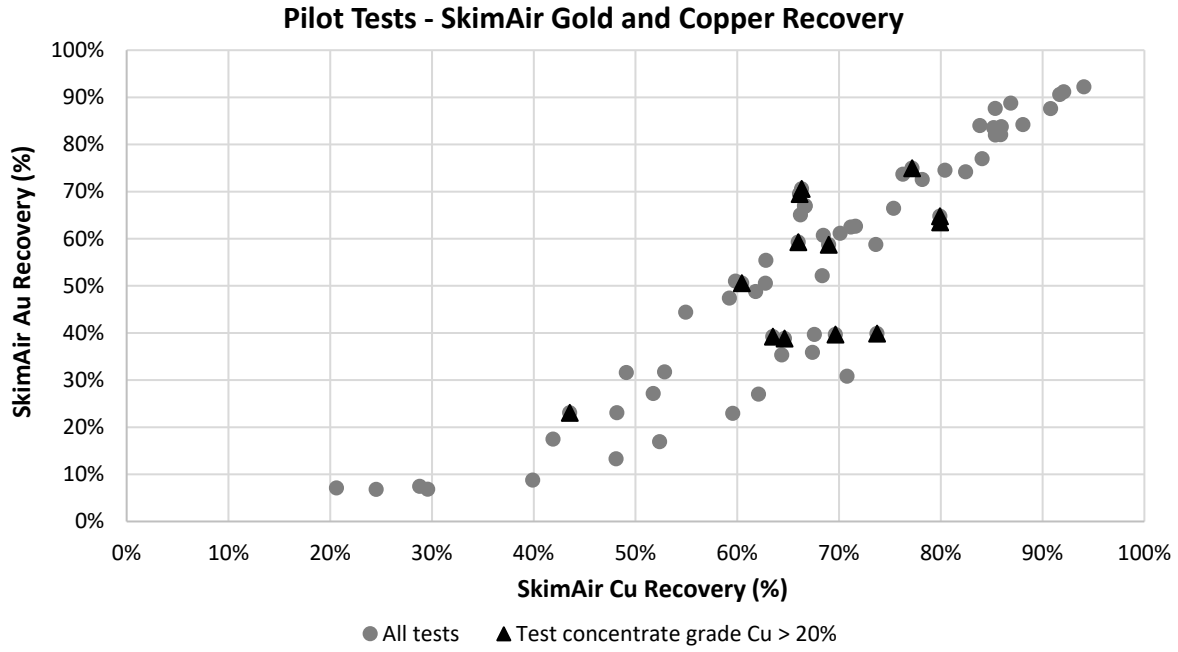



**FIG 7** – Gold and copper pilot test recovery relationship.

To produce copper concentrate grades closer to final concentrate specification, the following variables were fine-tuned:

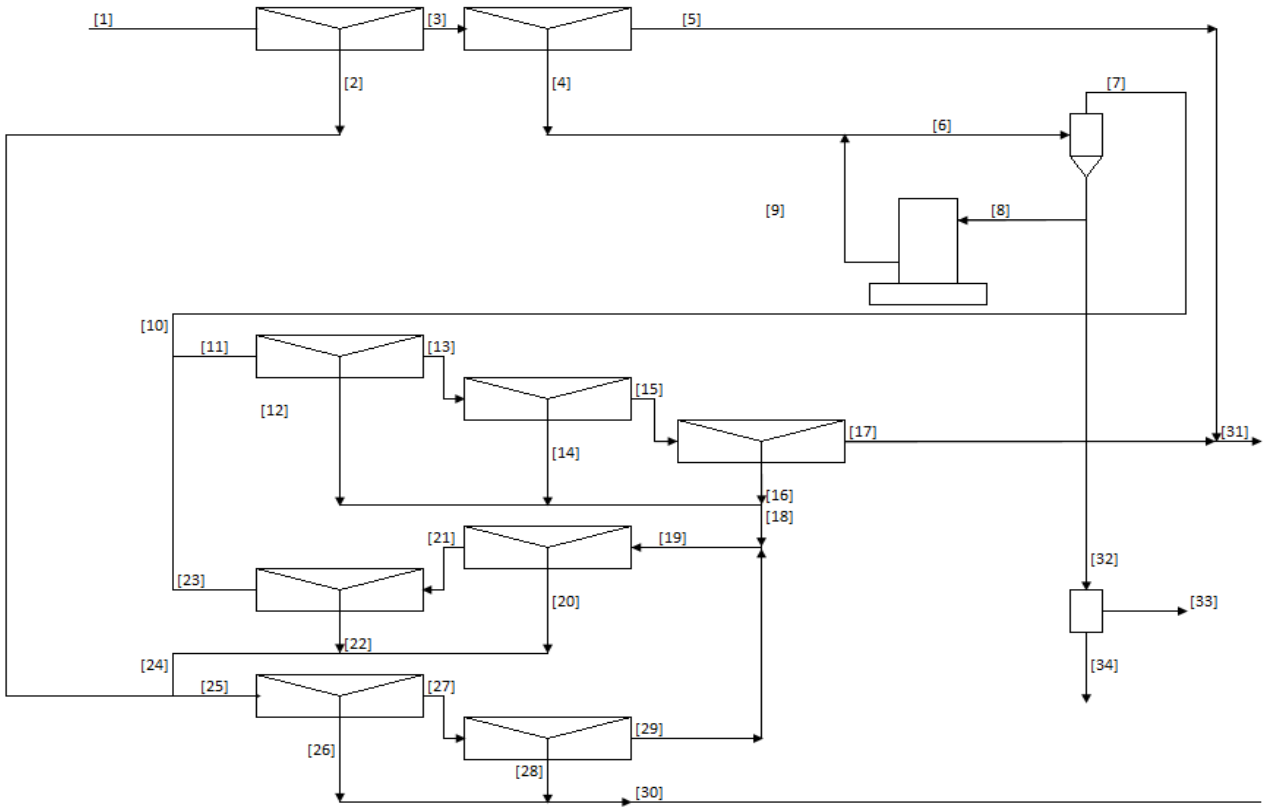
- Increased froth surface area by removing the froth crowder.
- Reduced mass pull from 8–15 per cent to 3–6 per cent.
- Increased pH for pyrite depression to 11.5–11.9.
- Decreased Aerophine 3418A dosage to 30 g/t.Cu.

Additionally, laboratory cleaner flotation tests completed on the SkimAir concentrate proved the concentrate could be upgraded without further grinding if required. The cleaner laboratory flotation test results indicated that operating at pH > 11.5, combined with > 20 g/t Cu collector dosage, resulted in gold recovery above 95 per cent. In the laboratory tests where collector was not added, copper recoveries were approximately 90 per cent whereas gold recovery was below 20 per cent.

## *Pilot flotation survey*

Whilst the pilot plant was on-site, a flotation survey was undertaken to build a JKSimFloat model to more comprehensively simulate the impacts of the installation of a flash flotation cell on the overall circuit. The recirculating load of gold did not change within the regrind circuit during piloting due to the pilot's relative size to the circuit.

The survey was completed over 2 hrs with five cuts at 30 min intervals. The sample points are shown in Figure 8. Laboratory hot float tests were also completed on relevant streams during the survey to provide the kinetic inputs required to complete modelling of the circuit.




| | | | | | |
|---|---|---|---|---|---|
| 1 Rghr Feed | 7 RG Cyc O/F | 13 C1B1 Tail | 19 C2 Feed Comb | 25 C3 Feed Comb | 31 Final Tail |
| 2 RB1 Con | 8 RG Cyc U/f | 14 C1B2 Con | 20 C2B1 Con | 26 C3B1 Con | 32 SK Feed |
| 3 RB1 Tail | 9 RG Mill Dsch | 15 C1B2 Tail | 21 C2B1 Tail | 27 C3B1 Tail | 33 SK Con |
| 4 Scav Con | 10 Clnr Feed | 16 C1B3 Con | 22 C2B2 Con | 28 C3B2 Con | 34 SK Tail |
| 5 Rghr Tail | 11 C1 Feed Comb | 17 Clnr Tail | 23 C2B2 Tail | 29 C3B2 Tail | |
| 6 RG Cyc Feed | 12 C1B1 Con | 18 C1 Con Comb | 24 C2 Con Comb | 30 Final Con | |

**FIG 8** – Flotation survey sample points.

### *JKSimFloat modelling*

Metso was engaged to generate a JKSimFloat model using the survey results to simulate the impacts of the installation of the SkimAir cell on the overall circuit. The model output summary provided by Metso is shown in Table 3.

This simulation aimed to extrapolate the pilot plant performance of flash flotation to plant scale using a 1:1 basis (Walshe *et al*, 2019). It should be noted that simulation of metallurgical performance has inherent difficulties due to complex chemical and physical phenomenon involved in froth flotation.

**TABLE 3**

Pilot test work JKSimFloat modelling output.

| Stream | Solids t/h | | | Au Grade (g/t) | | | Au Recovery (%) | | | Cu Grade (%) | | | Cu Recovery (%) | | |
|---|---|---|---|---|---|---|---|---|---|---|---|---|---|---|---|
| | Current | Flash | Flash and Froth Washing | Current | Flash | Flash and Froth Washing | Current | Flash | Flash and Froth Washing | Current | Flash | Flash and Froth Washing | Current | Flash | Flash and Froth Washing |
| Rougher Feed | 865.6 | 865.6 | 865.6 | 0.47 | 0.47 | 0.47 | 100.0 | 100.0 | 100.0 | 0.84 | 0.84 | 0.84 | 100.0 | 100.0 | 100.0 |
| Ro1–2 – Con | 20.4 | 20.4 | 20.4 | 10.51 | 10.51 | 10.51 | 52.5 | 52.5 | 52.5 | 28.96 | 28.96 | 28.96 | 81.3 | 81.3 | 81.3 |
| Ro3–9 – Tail | 775.3 | 775.3 | 775.3 | 0.07 | 0.07 | 0.07 | 12.4 | 12.4 | 12.4 | 0.04 | 0.04 | 0.04 | 4.0 | 4.0 | 4.0 |
| Regrind Cyc Feed | 230.3 | 219.0 | 224.4 | 23.72 | 2.36 | 2.36 | | | | 1.62 | 1.04 | 1.02 | | | |
| Regrind Cyc – O/F | 69.8 | 66.7 | 68.2 | 1.94 | 0.19 | 0.19 | | | | 1.52 | 0.97 | 0.96 | | | |
| Regrind Cyc – U/F | 160.5 | 152.3 | 156.2 | 33.20 | 3.31 | 3.31 | | | | 1.66 | 1.07 | 1.05 | | | |
| SkimAir Feed | 0.3 | 152.3 | 156.2 | 31.24 | 3.31 | 3.31 | | | | 1.62 | 1.04 | 1.02 | | | |
| SkimAir Con | 0.01 | 3.1 | 1.7 | 423.37 | 41.56 | 76.58 | 1.3 | 32.0 | 31.9 | 22.86 | 13.29 | 24.14 | 0.04 | 5.7 | 5.6 |
| Cleaner 1 Feed | 80.4 | 76.7 | 78.3 | 2.42 | 0.57 | 0.56 | 47.7 | 10.7 | 10.8 | 1.41 | 0.92 | 0.91 | 15.6 | 9.7 | 9.8 |
| Clnr1B3 – Tail | 65.9 | 64.8 | 66.1 | 0.38 | 0.20 | 0.20 | 6.1 | 3.2 | 3.2 | 0.11 | 0.10 | 0.10 | 1.0 | 0.9 | 0.9 |
| Cleaner 2 Feed | 18.1 | 15.3 | 15.6 | 11.34 | 3.85 | 3.80 | 50.4 | 14.4 | 14.5 | 6.33 | 4.75 | 4.71 | 15.8 | 10.0 | 10.1 |
| Cleaner 3 Feed | 28.0 | 25.8 | 25.9 | 12.90 | 9.41 | 9.38 | 88.3 | 59.3 | 59.4 | 24.98 | 25.55 | 25.47 | 96.1 | 90.5 | 90.6 |
| Clnr3 Con | 24.4 | 22.3 | 22.4 | 13.54 | 9.60 | 9.57 | 80.9 | 52.5 | 52.6 | 28.28 | 29.09 | 28.99 | 95.0 | 89.4 | 89.5 |
| Final Conc | 24.4 | 25.5 | 24.1 | 13.54 | 13.54 | 14.29 | 80.9 | 84.5 | 84.4 | 28.28 | 27.14 | 28.65 | 95.0 | 95.1 | 95.1 |
| Final Tails | 841.2 | 840.1 | 841.4 | 0.09 | 0.08 | 0.08 | 18.4 | 15.5 | 15.6 | 0.04 | 0.04 | 0.04 | 5.0 | 4.9 | 4.9 |

The results above show by employing a flash flotation unit operation in the regrind circuit, gold recovery can be increased through recovering gold to concentrate before overgrinding and surface degradation can occur. Simulations performed using the model developed indicated that a net increase in overall gold recovery of above 3 per cent can be achieved, with no measurable increase in copper recovery observed. Notably, several assumptions were made in the creation of this model:

- Change to the coarse, liberated portion of copper within the SkimAir cell was not present in the model.
- A 1:1 scale up was applied using the pilot and survey results, in line with industry standard practice (Walshe *et al*, 2019).
- No sizings were integrated into the model, ie unsized model generated.

Given the test work results, a project team was formed in 2024 consisting of site metallurgists, mechanical engineers, process control engineers, electrical engineers and operational personnel. The project was evaluated technically and financially, and an investment decision was made to purchase a SkimAir 240 (SK240) from Metso.

# DESIGN

## Design criteria

Based on the laboratory test work, pilot test work and simulations, the design criteria for the cell is presented below.

- Froth surface area: 2.5–3.5 $m^2$
- Froth carry rate: 1.37–1.92 $t/m^2h$
- pH range: 9.3–11.9
- Cell feed rate: 240 dry t/h
- Pulp SG: 1.98 $t/m^3$
- Feed solids: 67 wt per cent
- Volumetric air rate: 63–252 $Nm^3/h$.

## Process flow diagram

The operability of the SkimAir cell, along with its expected influence on the downstream flotation circuit, was heavily considered during the design phase of the process flow diagram (Figure 9).

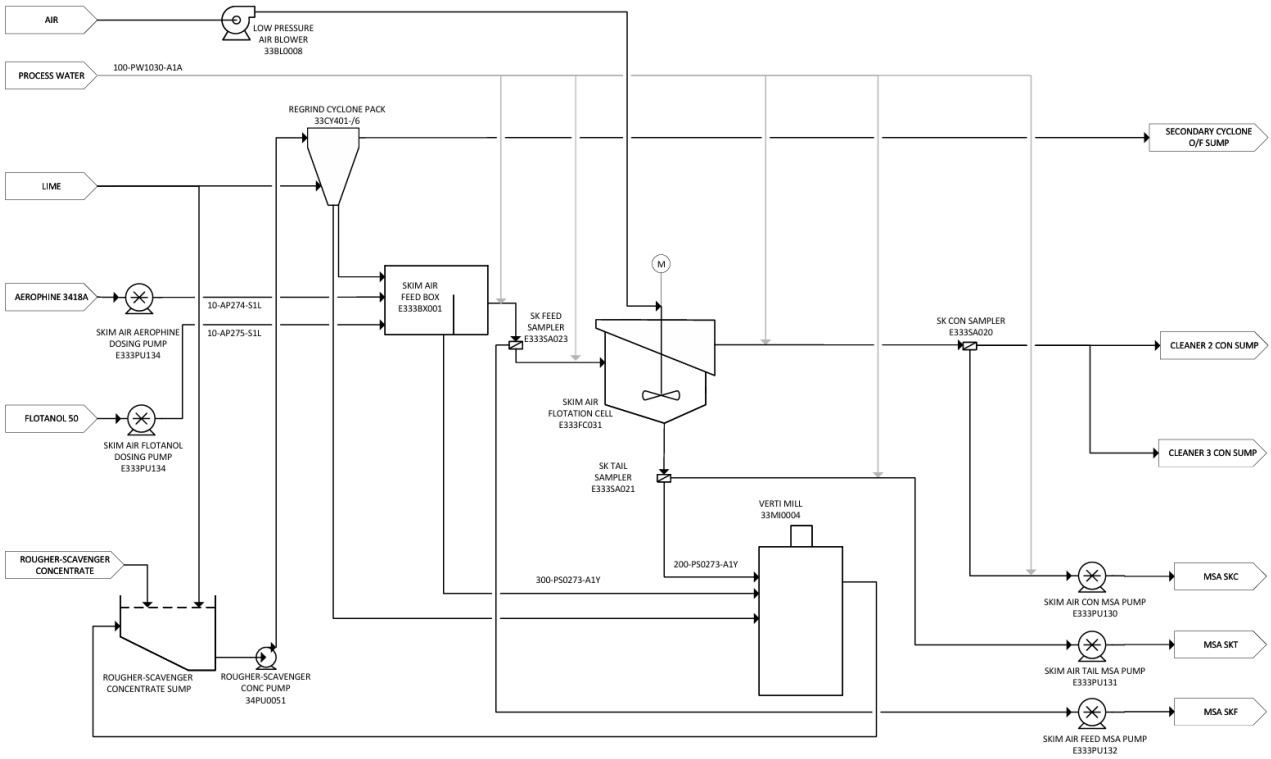



**FIG 9** – SkimAir process flow diagram.

The online process control objective was to produce a high-grade copper concentrate at the maximum copper and gold recovery. To support this, feed, tailing and concentrate lines were fitted with metallurgical samplers and pumps directing slurry to the existing online MSA. The configuration of samplers, dilution water and slurry pumps was a deliberate investment in new infrastructure as part of the project. The resulting MSA copper assays provided a calculated recovery and grade every 15 mins. Therefore, operations could respond and manipulate collector addition, air flow rate and froth depth accordingly. The three additional shift samples were included in the fire assay gold analysis workflow. The short-term copper MSA assay feedback and shift gold assays from the flash circuit provided data to the plant metallurgists for ongoing optimisation.

## Plant layout considerations

The plant layout was engineered with the collaboration between site personnel, consultants and Metso engineers. The objective was to retrofit the new infrastructure according to recommendations, in view of previously documented learnings from other installations (Paki and Erepan, 1997).

Given the pulp density of 1.98 t/m$^3$ in the Ernest Henry flash flotation feed, and in flash flotation applications more broadly, maintaining appropriate slurry velocity throughout the circuit is essential. Unique to this application, 80 per cent passing particle size of the regrind cyclone underflow (SkimAir feed) was 65–75 micron, compared to typical installations in primary grinding circuits fed with primary cyclone underflow (Newcombe, Wightman and Bradshaw, 2013; Cardenas *et al,* 2016).

To satisfy the Metso engineering specifications, the regrind cyclones were elevated 4.3 m to place the SkimAir cell between the cyclone cluster and Vertimill, shown in Figure 10. Due to final height limitations, an alternate feed box was fabricated compared to the standard Metso feed box. The installation of new structural steel and supporting infrastructure for the cyclone raise was completed within an existing planned five-day concentrator shutdown. The remaining steel work and cell installation was completed during plant operation. This led to challenges and interactions due to plant services surrounding this area, requiring planning and skilled labour contractors.

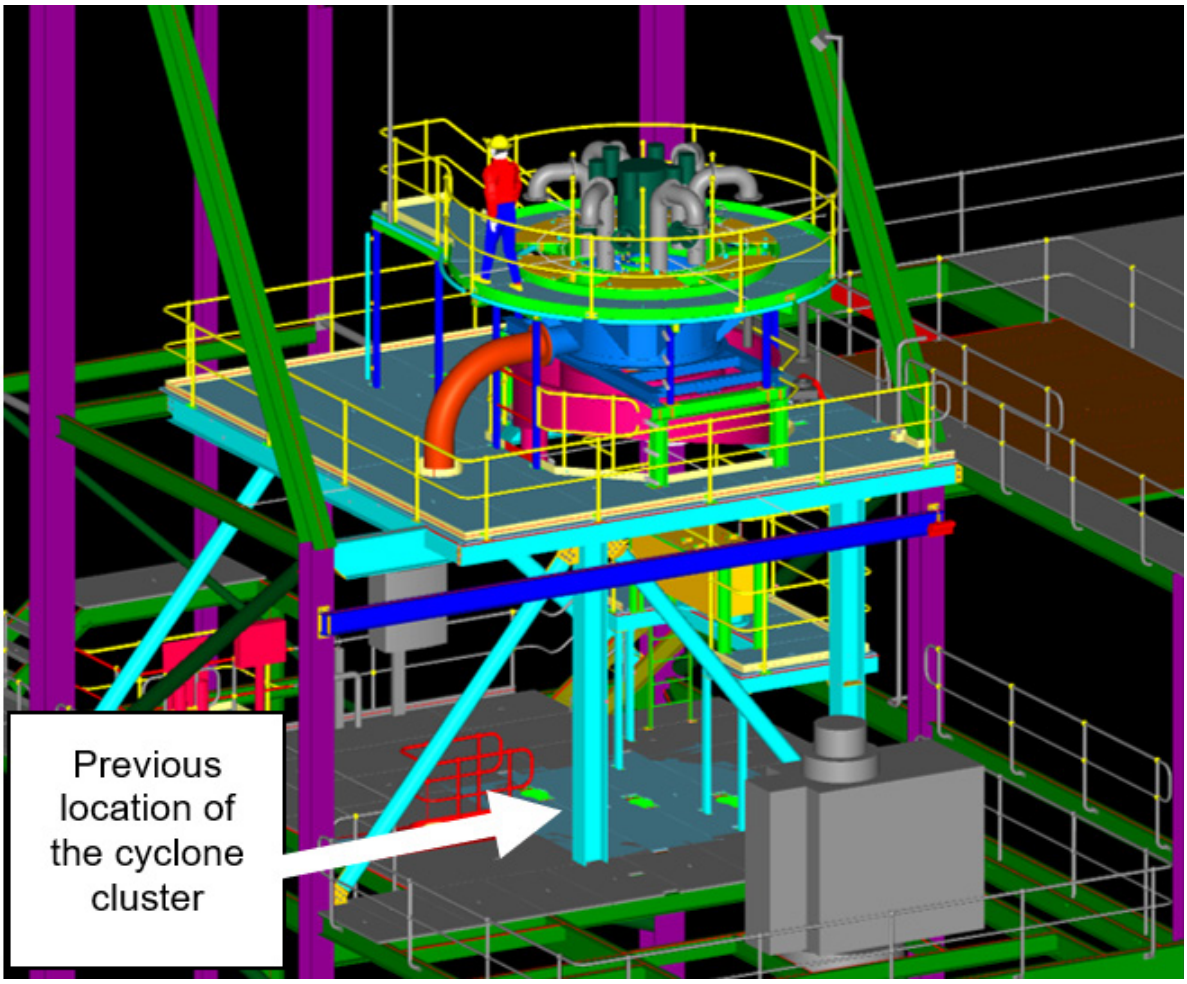



**FIG 10** – 3D Model of the regrind cyclones raised.

## Commissioning

Extensive time and effort was directed to developing a detailed commissioning plan for the project team during the dry and wet commissioning periods. This aimed to ensure that all systems and components of the new infrastructure were constructed, installed, tested and operated according to the design and operational requirements.

The commissioning process was staged as follows:

- **C0 – Pre-commissioning:** Construction team verifies that each item of plant or equipment is installed in accordance with the design and approved scope, with no power energised or equipment operated.

- **C1 – Dry commissioning:** Inspection and no-load energisation by the commissioning team to confirm design compliance, focusing mainly on electrical testing and review of electrical test packs.
- **C2 – Wet commissioning:** Testing of individual or integrated plant items under benign load (air or water) to demonstrate stable operation, beginning with utilities, and supported by OEM representatives as required.
- **C3 – Ore (Product) commissioning:** Introduction of ore and process fluids to confirm stable operation at defined parameters, with increasing involvement of operations, maintenance, and reliability teams while overall control remains with the commissioning team.

The time invested in planning the commissioning was justified through timely commissioning of the SkimAir and auxiliary equipment. Commissioning started on 27th February 2025, with the plant running full time as of 13th March 2025.

### *Lessons learnt*

A debrief with the on-site project team highlighted the following recommendations for future brownfield projects:

- Conduct a project timeline review during the planning phase with all stakeholders (electrical, mechanical, and instrumentation) to optimise the critical path for execution.
- Undertake a formal, multidisciplinary post-HAZOP sign-off to minimise late-stage design changes.
- Include ancillary equipment in the engineering work package to reduce rework during construction.
- Complete the criticality of spares assessment prior to commissioning.

## RESULTS

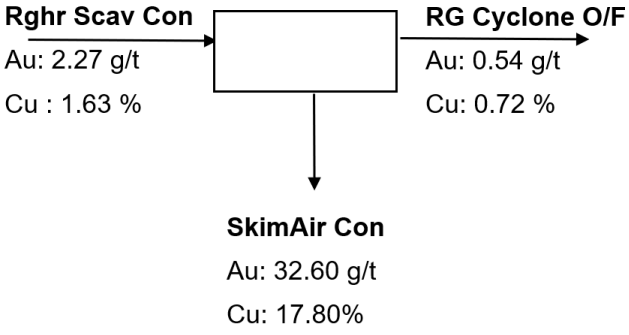
## SkimAir on/off survey

Two surveys were conducted at similar process conditions while the SkimAir was ‘on’ and ‘off’ to evaluate the impact of the newly installed equipment.

The recirculating load of gold prior to the installation of the SkimAir was 1750 per cent, which was reduced to 337 per cent based on the survey results. Whilst it was expected the recirculating load of gold had stabilised after 12 hrs, the surveys were separated by 48 hrs and were each conducted over a period of 2.5 hrs.

The flotation surveys indicated that the SkimAir was recovering:

- 77.7 per cent gold from the regrind circuit.
- 58.4 per cent copper from the regrind circuit.




The overall circuit performance for the SkimAir on/off survey is shown in Table 4. The survey results were mass balanced using JKSimFloat.

**TABLE 4**

SkimAir on/off survey results summary.

| Survey | Feed (t/h) | Au in Feed (g/t) | Cu in Feed (%) | Au Recovery (%) | Au in Concentrate (g/t) | Cu Recovery (%) | Cu in Concentrate (%) |
|---|---|---|---|---|---|---|---|
| SkimAir On | 837.9 | 0.49 | 0.88 | 83.0 | 12.8 | 95.7 | 26.5 |
| SkimAir Off | 837.6 | 0.44 | 0.91 | 79.4 | 11.2 | 94.2 | 27.4 |

The results show improved gold and copper recovery with the SkimAir online compared to when it was offline, although no statistical significance can be drawn from this data. The slight difference in copper and gold head grade between the surveys is within expected standard deviation of normal operation.

### *Survey size by recovery analysis*

Gold and copper size by recovery analysis was completed on the survey samples with respect to the flash and the overall cleaner circuit. It was hypothesised that the SkimAir would improve the overall gold cleaner recovery by collecting sufficiently liberated gold particles before they are overground in the regrind circuit's recirculating load.

Figure 11 highlights the impact of the SkimAir cell on size-by-size copper recovery in the regrind circuit. The SkimAir recovers 94 per cent of the +106 micron fraction in the regrind circuit, with respect to the rougher scavenger concentrate, with an overall sized recovery of 61 per cent prior to the cleaner stage. The removal of a proportion of these particles in the regrind circuit, through the SkimAir's additional residence time, reduces the regrind circuit circulating load and may limit particle overgrinding.

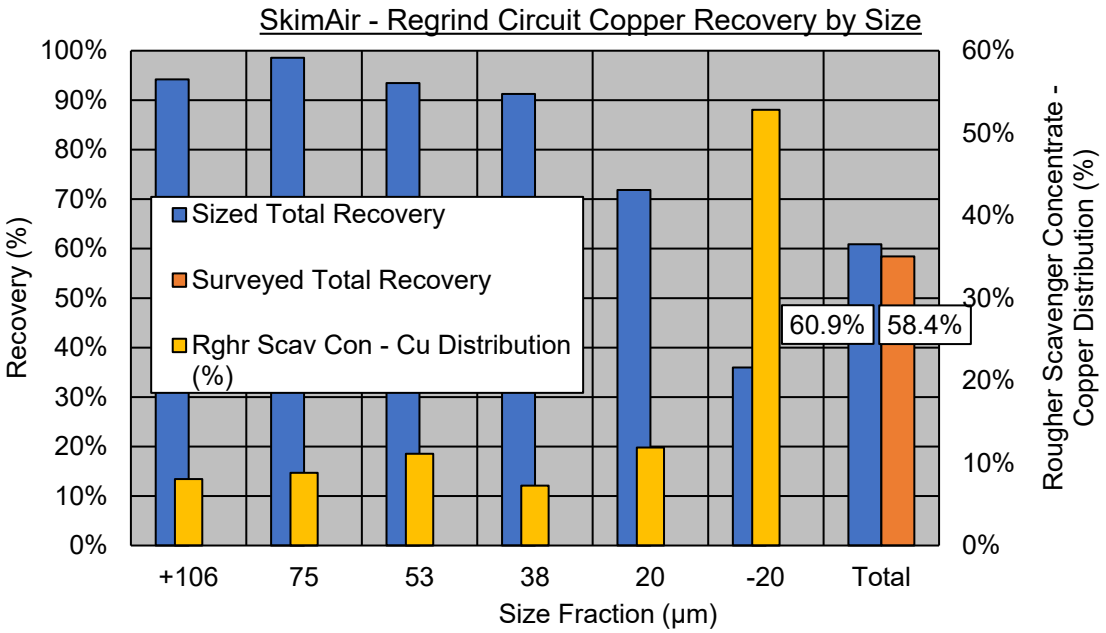



**FIG 11** – Regrind circuit copper recovery by size.

Figure 12 highlights the cleaner circuit copper recovery by size with the SkimAir on and off. Improved recovery performance is observed for the 75 to -20 micron fractions under the on condition, with slightly lower performance in the +106 micron fraction. This is hypothesised to reflect the earlier recovery of the +106 micron fraction upstream via the SkimAir. Further, the improved recovery in the finer fractions (75 to -20 micron) may be associated with enhanced downstream flotation conditions in the cleaner circuit, potentially through a combination of:

- Increased residence time.
- Changes in pulp chemistry associated with low-pressure air injection via the SkimAir.

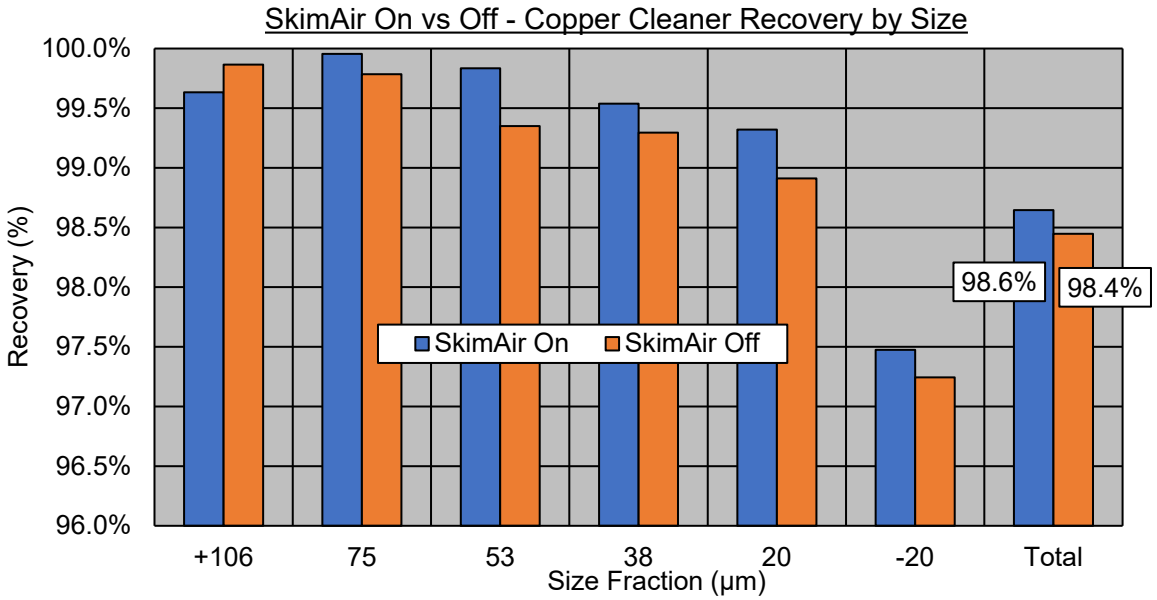



**FIG 12** – Cleaner circuit copper recovery by size with SkimAir on and off.

Similar to the copper results, the SkimAir cell recovers a high portion (95 per cent) of the gold particles (+212 to +53 micron size fractions combined) from the regrind circuit with respect to the rougher scavenger concentrate, with recovery decreasing with particle size (Figure 13). The total surveyed gold recovery from the regrind circuit with the SkimAir online was approximately 78 per cent.

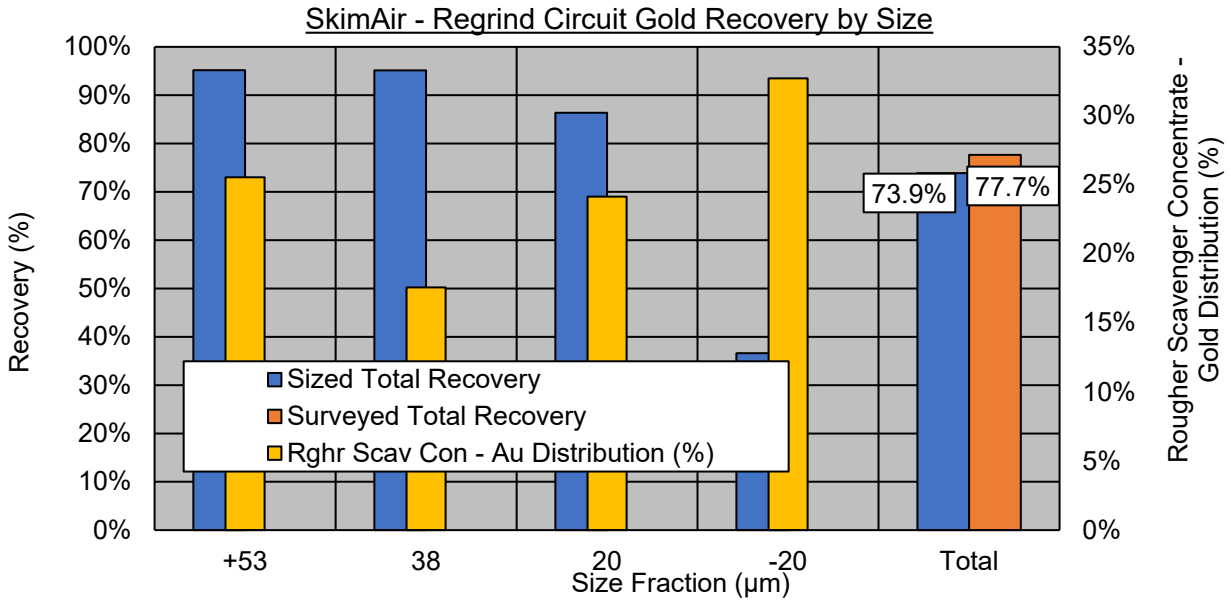



**FIG 13** – Regrind circuit gold recovery by size.

Figure 14 highlights improved cleaner circuit gold recovery across all size fractions with the SkimAir online, with the most notable improvement observed in the fines fraction (20 to -20 micron). As discussed above, this is hypothesised to be associated with earlier recovery of particles from the regrind circuit via the SkimAir cell, which may reduce overgrinding of liberated gold into the ultrafine (-20 micron) fraction and contribute to the improvements observed.

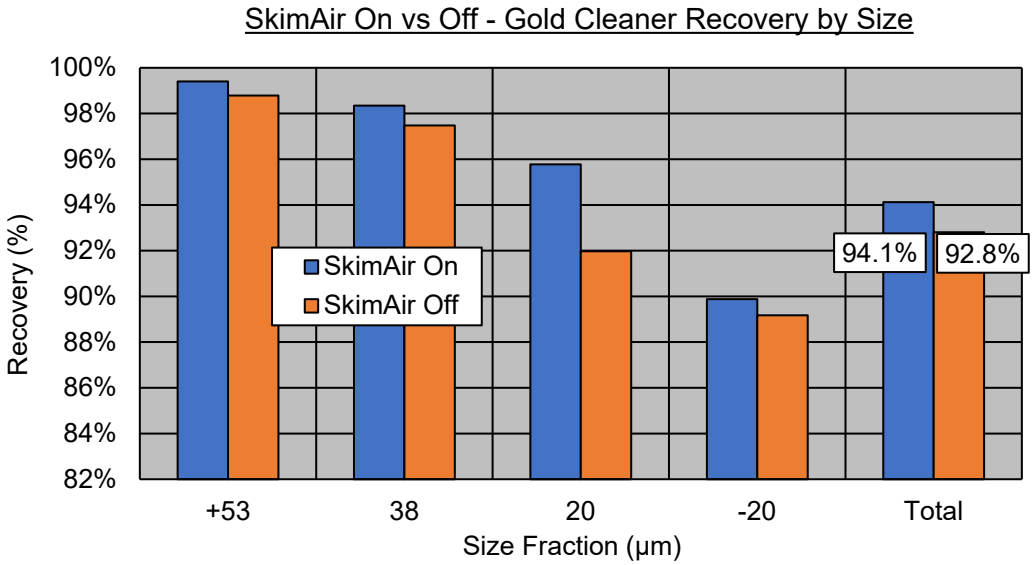



**FIG 14** – Cleaner circuit gold recovery by size with SkimAir on and off.

### *Survey pulp chemistry analysis*

A pulp chemistry survey was conducted during the SkimAir on/off survey to characterise the profile of the regrind and cleaner flotation circuit. The Eh, pH and dissolved oxygen were recorded and compared (Figure 15). Points that are not parallel to the water-oxygen line indicates that consumption of oxygen is occurring, leading to a greater reductive environment, this can be seen for the SkimAir off between points 1 and 2. It is known that the oxidation of pyrite contributes to increased acidity (Santos, Silva and Duarte, 2016). Consequently, the diagram indicates that electrochemical reactions are occurring within the VTM, leading to reductions in both pH and Eh. In comparison, under the SkimAir on condition, there are reductive interactions between the cyclone underflow and the VTM. However, despite the pH adjustment in the flotation cell (with lime added to raise it to pH 11.5), the resulting changes remain aligned with the water-stability line.

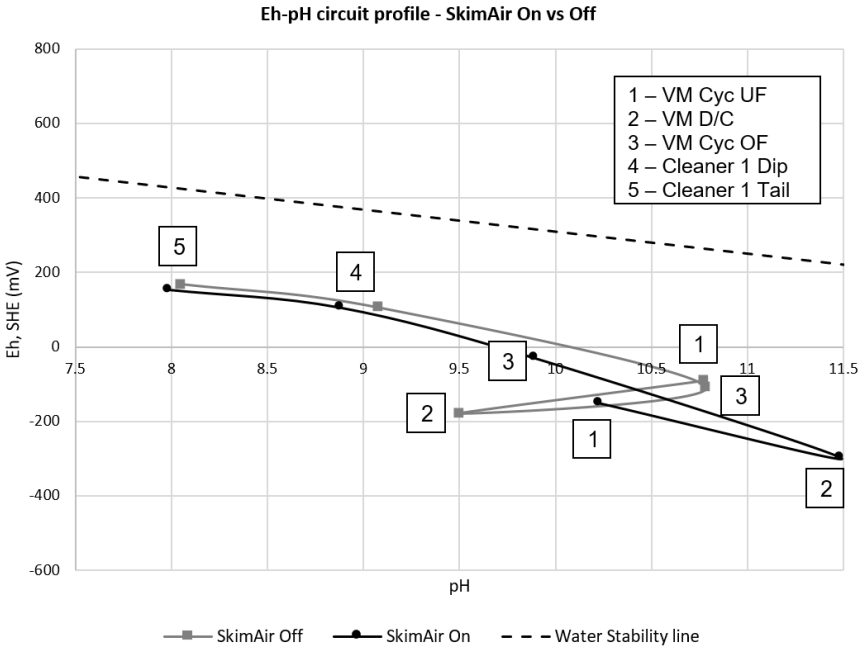



**FIG 15** – Eh-pH circuit profile comparing SkimAir on versus off.

The decay in dissolved oxygen demand was modelled using a first order rate equation of the cleaner feed conditions (Figure 16). The SkimAir on has a lower oxygen demand value of 0.16 $s^{-1}$ compared to 0.20 $s^{-1}$. This was compared with the cyclone overflow decay, which indicated a 0.04 $s^{-1}$ difference

in the dissolved oxygen demand, being more favourable towards the SkimAir on condition. Therefore, it is hypothesised the improved pulp chemistry conditions from the SkimAir is due to:

- Injection of oxygen through the flotation cell (100–170 $Nm^3/h$ of low-pressure air).
- Possible secondary effect of reduction in pyrite reporting to the cleaner circuit due to earlier recovery.

Based on the observed pulp chemistry conditions, the SkimAir presents more favourable conditions for sulfide flotation using xanthates within the downstream cleaner circuit. This arises from a reduction in ferric ions and improved stability of dixanthogen in pulp allowing for improved selective recovery of sulfide minerals.

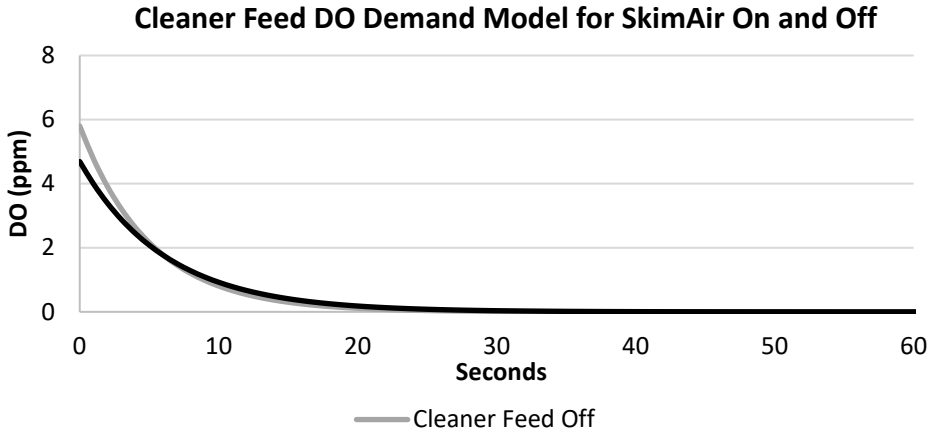



**FIG 16** – DO demand predicted model – cleaner feed.

### *Cleaner throughput change*

The diversion of 2.4 t/h of material from the cleaner feed to the SkimAir concentrate resulted in reduced froth carry rates (FCRs) in the cleaner circuit. This effect was identified during the initial feasibility study and subsequently confirmed through surveys conducted following SkimAir commissioning, as shown in Table 5.

**TABLE 5**

Cleaner circuit froth carry rates and lip loadings.

| Bank | Cell No. | SkimAir Off FCR ($t/m^2h$) | SkimAir On FCR ($t/m^2h$) | SkimAir On LL ($t/mh$) |
|---|---|---|---|---|
| Clnr 1 Bank 1 | 17 | 0.23 | 0.07 | 0.03 |
| | 16 | 0.13 | **0.09** | 0.04 |
| Clnr 1 Bank 2 | 15 | 1.40 | 1.06 | 0.46 |
| | 14 | 0.12 | **0.14** | 0.05 |
| | 13 | 1.28 | 0.71 | 0.25 |
| Clnr 1 Bank 3 | 12 | 0.16 | 0.04 | 0.04 |
| | 11 | 0.08 | 0.68 | 0.51 |
| | 10 | 0.08 | 0.03 | 0.02 |
| Cleaner 2 Bank 1 | 25, 24, 23, 22 | 0.23 | 0.22 | 0.09 |
| Cleaner 2 Bank 2 | 21, 20, 19, 18 | 0.04 | 0.05 | 0.02 |
| Cleaner 3 Bank 1 | 30, 29, 28 | 1.20 | 1.01 | 0.60 |
| Cleaner 3 Bank 2 | 27, 26 | 0.09 | 0.11 | 0.06 |

The FCRs shown in Table 5 are generally below the recommended range of 1–2 t/m$^2$h for cleaner cells, even pre SkimAir installation. This is attributed to a decrease in plant throughput since the EHO concentrator was first commissioned in 1997. The lip loading values are within recommended limits, and there are no apparent issues with lip availability across the cells.

Efforts to increase crowding, particularly in cleaner 1, have been implemented since commissioning. An additional six and five froth crowders were installed in cell 16 and cell 14, respectively, which has visually improved froth mobility. During an upcoming shutdown, a further six crowders are planned for installation in cell 17 and cell 16, reaching the current practical maximum of 12 froth crowders per cell without major modification.

## Statistical analysis

Raw process data from January to July 2025 were used to statistically compare the impact of the SkimAir before and after. The three different statistical methods used were:

1. Paired T-test.
2. Multiple linear regression.
3. Comparison of regression lines.

The aim of using three different tools is to infer a quantitative and qualitative conclusion of a change to copper and gold recovery with, in some cases, small data sets.

### *Paired t-test*

A paired t-test was conducted using the limited available data set, pairing consecutive periods in which the SkimAir was on and off during commissioning. A shift that was denoted to 'on' was if the SkimAir was online for >50 per cent of the shift, and shift composite samples were used for analysis.

The paired t-test compares the mean difference between the two conditions so that the effect of time (as a proxy of feed grade) is blocked out (Napier-Munn, 2014).

The null hypothesis is that the SkimAir does not have a significant effect on overall gold and/or copper recovery (P value > 0.10). To account for changes in head grade and mill throughput on recovery performance, a variance in SkimAir on and off shift performance against the EHO recovery models was made. A summary of the gold and copper recovery to model t-tests are shown in Table 6.

**TABLE 6**

Gold (left) and copper (right) recovery to model paired t-test results.

| Gold recovery | | |
|---|---|---|
| **t-Test: paired two sample for means** | **SkimAir On** | **SkimAir Off** |
| Mean | 1.41% | -0.39% |
| Variance | 0.001 | 0.001 |
| Observations | 9 | 9 |
| Pearson correlation | 0.293 | |
| Hypothesised mean difference | 0 | |
| df | 8 | |
| t Stat | 1.394 | |
| P(T<=t) one-tail | 0.100 | |
| t Critical one-tail | 1.860 | |
| P(T<=t) two-tail | 0.201 | |
| t Critical two-tail | 2.306 | |

| Copper recovery | | |
|---|---|---|
| **t-Test: paired two sample for means** | **SkimAir On** | **SkimAir Off** |
| Mean | -0.03% | -0.18% |
| Variance | 4.672E-05 | 6.428E-05 |
| Observations | 9 | 9 |
| Pearson correlation | -0.397 | |
| Hypothesised mean difference | 0 | |
| df | 8 | |
| t Stat | 0.357 | |
| P(T<=t) one-tail | 0.365 | |
| t Critical one-tail | 1.397 | |
| P(T<=t) two-tail | 0.730 | |
| t Critical two-tail | 1.860 | |

For overall gold recovery to model with the SkimAir online, the $P < 0.10$, therefore the SkimAir has a statistically significant effect on overall gold recovery to model.

For overall copper recovery to model with the SkimAir online, $P > 0.10$, therefore the SkimAir does not have a statistically significant effect on overall copper recovery to model.

Therefore, the estimated gold recovery when the SkimAir is on is +1.8 per cent ± 0.73 per cent at 90 per cent confidence limits. However, it should be noted that the data set is small, comprising of nine historical pairs. Calculations recommend at least 58 pairs are needed to protect against Type I and Type II errors for gold recovery. To further apply an on/off method, a 120-day trial would be required. Due to the risk of gold recovery losses, both from the expected gains above and the circuit instability caused by switching the SkimAir on and off, a formal on/off trial was not conducted. In addition, identifying the point at which the recirculating gold load in the regrind circuit stabilised after switching the cell on and off would prove difficult with changing grades and mill throughput, further complicating a potential longer trial. Therefore, additional statistical techniques such as multiple linear regression analysis were employed to infer the difference between recovery with the SkimAir on and off using a larger data set.

### *Multiple linear regression analysis*

Multiple linear regression is a method used to model the relationship between one dependent variable and two or more independent variables by fitting a linear equation. This technique helps to understand how the dependent variable changes when any of the one independent variable is varied, while others are constant. For the SkimAir performance analysis, the same variables used in the regression of the EHO operational gold and copper models, namely mill throughput, final concentrate copper grade, and primary feed copper and gold grades, were included, with an additional variable representing the SkimAir operating status (on or off).

The null hypothesis is that the SkimAir does not have a statistically significant effect on overall gold and/or copper recovery ($P > 0.10$). Data collected between January and July 2025 were used for this analysis. For both gold and copper recovery, the SkimAir on/off $P < 0.10$, therefore the running of the SkimAir has a statistically significant effect.

The regressed impact of the SkimAir running on overall gold recovery is +1.062 per cent, with a 90 per cent confidence interval ranging from 0.326 per cent to 1.798 per cent. For overall copper recovery, the impact is +0.517 per cent, with a 90 per cent confidence interval ranging from 0.231 per cent to 0.802 per cent. The summary of gold and copper regression analysis is shown in Table 7.

## TABLE 7

Summary of gold and copper recovery regression analysis.

**Gold recovery**

| **Regression statistics** | |
|---|---|
| Multiple R | 0.595 |
| R Square | 0.354 |
| Adjusted R Square | 0.345 |
| Standard Error | 0.030 |
| Observations | 303 |

**ANOVA**

| | **df** | **SS** | **MS** | **F** | **Significance F** |
|---|---|---|---|---|---|
| Regression | 4 | 0.150 | 0.037 | 40.794 | 2.97E-27 |
| Residual | 298 | 0.274 | 0.001 | | |
| Total | 302 | 0.424 | | | |

| | **Coeffic-ients** | **Standard Error** | **t Stat** | **P-value** | **Lower 95%** | **Upper 95%** | **Lower 90.0%** | **Upper 90.0%** |
|---|---|---|---|---|---|---|---|---|
| Intercept | 62.336% | 7.272% | 8.572 | 5.6E-16 | 0.480 | 0.766 | 0.503 | 0.743 |
| SAG t/h | -0.015% | 0.003% | -5.153 | 4.7E-07 | -0.021% | -0.010% | -0.020% | -0.011% |
| Cu Final Con Grade | 0.798% | 0.252% | 3.172 | 1.7E-03 | 0.303% | 1.293% | 0.383% | 1.213% |
| **SkimAir on/off** | **1.062%** | 0.446% | 2.382 | **1.8E-02** | **0.185%** | **1.940%** | **0.326%** | **1.798%** |
| Au Feed Grade | 21.905% | 3.017% | 7.260 | 3.4E-12 | 15.967% | 27.842% | 16.927% | 26.883% |

**Copper recovery**

| **Regression statistics** | |
|---|---|
| Multiple R | 0.455 |
| R Square | 0.207 |
| Adjusted R Square | 0.199 |
| Standard Error | 0.012 |
| Observations | 303 |

ANOVA

| | **df** | **SS** | **MS** | **F** | **Significance F** |
|---|---|---|---|---|---|
| Regression | 3 | 0.011 | 0.004 | 26.074 | 5.203E-15 |
| Residual | 299 | 0.042 | 0.000 | | |
| Total | 302 | 0.053 | | | |

| | **Coeffic-ients** | **Standard Error** | **t Stat** | **P-value** | **Lower 95%** | **Upper 95%** | **Lower 90.0%** | **Upper 90.0%** |
|---|---|---|---|---|---|---|---|---|
| Intercept | 95.089% | 1.310% | 72.570 | 6.8617E-192 | 92.510% | 97.667% | 92.927% | 97.251% |
| **SkimAir on/off** | **0.517%** | 0.173% | 2.981 | **0.003** | **0.176%** | **0.857%** | **0.231%** | **0.802%** |
| Cu Feed Grade | 3.799% | 0.782% | 4.860 | 1.90262E-06 | 2.261% | 5.338% | 2.509% | 5.090% |
| SAG t/h | -0.004% | 0.001% | -3.362 | 0.001 | -0.006% | -0.002% | -0.006% | -0.002% |

### *Comparison of regression lines*

The comparison of regression lines involves analysing models to determine if their slopes and intercepts differ significantly. This method helps in understanding whether different groups or conditions have distinct linear difference.

The comparison usually proceeds in four stages:

- Assessment of significance of the two linear correlation coefficients, to ensure that the two data sets show sufficient correlation to justify the method.
- Comparison of the residual variances of the two lines, to determine if they came from the same population.
- Comparison of the gradients – if they are different the lines are different, and the comparison can proceed no further.
- Comparison of the separation of the lines (the intercepts can also be compared).
    - The separation of the lines usually provides a more reliable estimate of the difference (ie the improvement) because it removes the effect of the range and distribution of the x-variable (Napier-Munn, 2014).

Shift gold recovery versus gold feed grade was compared before and after SkimAir installation through comparison of regression lines. This technique detected a statistically significant effect on gold recovery when SkimAir is on (P = 8.433 E-10). The mean improvement was estimated to be 1.99 per cent ± 0.53 per cent for overall gold recovery at 90 per cent confidence, depicted in Figure 17.

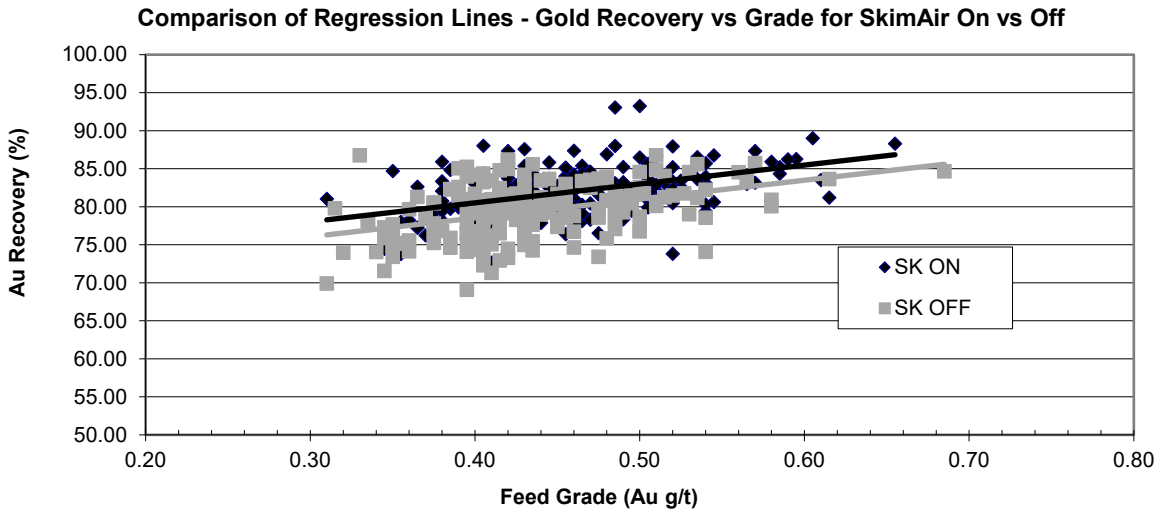



**FIG 17** – Comparison of regression lines gold recovery versus grade.

Shift copper recovery versus copper feed grade did not detect a significant effect on recovery when SkimAir is on due to the data set scatter having a statistically significant difference.

## Mineralogy

Quarterly mineralogy from across the circuit were analysed for Particle Mineral Analysis (PMA) and Trace Mineral Search (TMS) at ALS Kamloops. The shift samples from Q2 2025, post SkimAir commissioning, were filtered for extended downtime and any clear outliers, and were then mass balanced and subsampled to generate composites for mineralogical analysis. The results of this analysis are described herein.

Coombs and Ma (2025) summarised the following points in the mineralogical analysis report:

- Copper recovery for the Q2 2025 period was 95.4 per cent, increased from 94.6 per cent in Q1 2025. Copper assays of the rougher and final tailing samples provided measured slightly

lower grades compared to the Q1 samples, while the cleaner tailing assays were more significantly lower for Q2 compared to Q1.

- Concentrate copper grade was unchanged at 26.9 per cent copper, though gold content increased from 11.7 g/t for Q1 to 12.7 g/t for Q2.
- Gold recovery was increased to 83.5 per cent in Q2, according to the mineralogical metallurgical balancing completed, compared to 80.4 per cent in Q1. The rougher tailing assays for Q2 would be considered within sampling and analytical errors of gold assays for Q1, however, the cleaner tail and final tailing gold assays were lower for Q2.

Figure 18 provides a mineral composition summary of the SkimAir feed, concentrate and tailings streams.

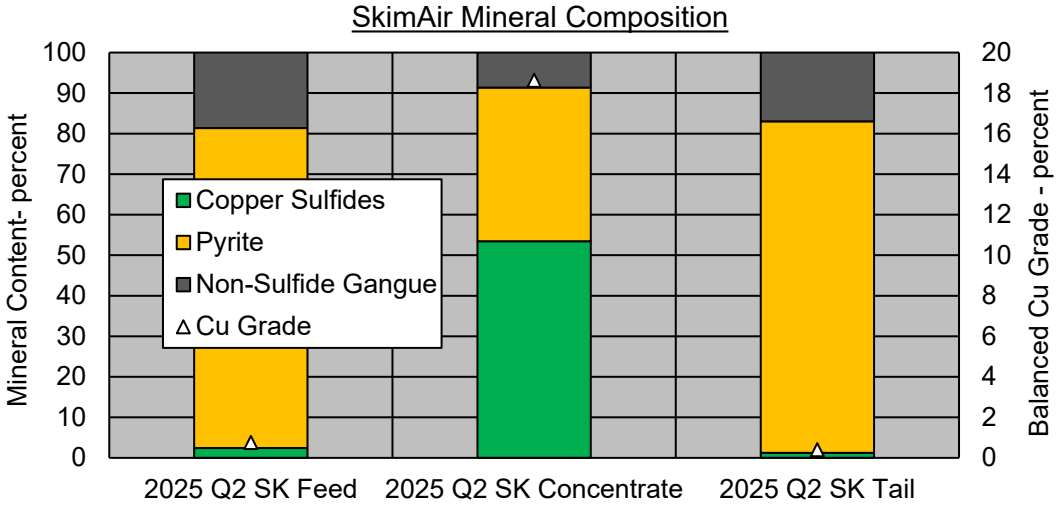



**FIG 18** – SkimAir feed, concentrate, tail mineral composition.

### *SkimAir feed*

The SkimAir feed consisted primarily of pyrite (80 per cent), which presented a high degree of liberation (96 per cent) as seen in Figure 19. Comparatively, the ratio of pyrite to copper sulfides was 32:1, with the chalcopyrite and gold presenting lower liberation of 36 per cent and 31 per cent respectively and chalcopyrite having relatively significant association with pyrite (17 per cent).

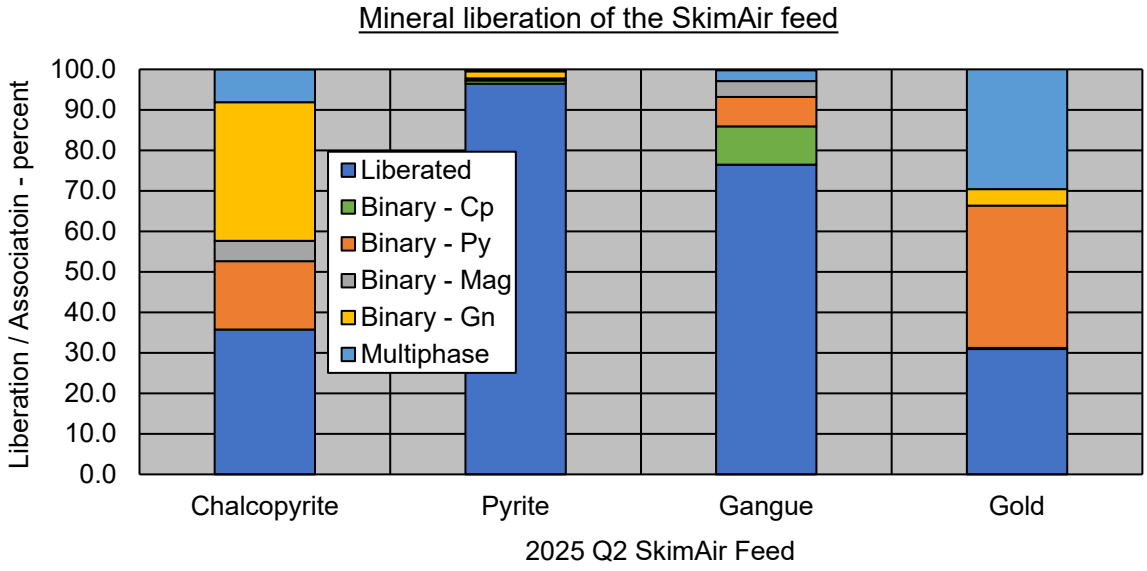



**FIG 19** – Mineral liberation of the SkimAir feed.

The gold surrounding the SkimAir was mainly present as gold-silver mineral electrum (AuAg), with minor amounts of native gold (Au) also detected. Liberated gold presented about 30 per cent of the gold in feed, with gold adhered to pyrite slightly higher at 35 per cent (Figure 19). There may be opportunity to grind finer in the regrind circuit to liberate this gold, however, this may increase the challenge of selectivity against pyrite for concentrate recovery.

### *SkimAir concentrate*

The SkimAir concentrate consisted primarily of chalcopyrite (53 per cent) and pyrite (38 per cent), both of which had high degrees of liberation at 82 per cent and 87 per cent respectively (Figure 20).

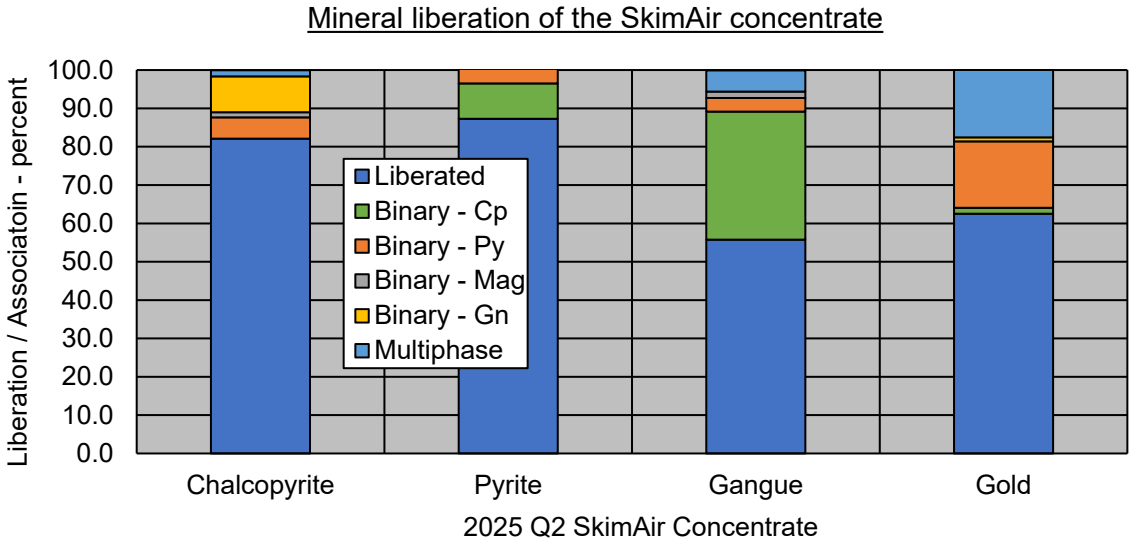



**FIG 20** – Mineral liberation of the SkimAir concentrate.

The cell is operating below the mineralogical grade-recovery limit (40 per cent copper recovery is theoretically achievable at a maximum concentrate grade of 27 per cent Cu), with current performance at 37.5 per cent recovery and 18.6 per cent Cu grade. However, this performance is expected due to the high pyrite to chalcopyrite ratio in the feed, with only 3 per cent of pyrite in feed being recovered (Coombs, 2025). This also reinforces the requirement for the high pH slurry target of 11.5 for pyrite depression to produce an in-specification copper concentrate grade.

For the gold recovered to concentrate, 63 per cent is liberated, 17 per cent is binary to pyrite, and only 2 per cent binary to chalcopyrite (Figure 20). The gold recovery achieved by the cell was 18 per cent, with one third of the gold in feed recovered by the cell.

SkimAir cell recovery by size analysis with respect to the SkimAir feed was also completed on the Q2 composite samples. Copper recovery generally improved with decreasing particle size, except for the fine -20 micron fraction, where ultrafine particles begin to lose bubble-particle attachment efficiency, resulting in copper recovery losses despite sufficient liberation. The cell recovered the coarse particles +106 micron of gold well at 40 per cent, with the -106+53 micron fraction decreasing to 9 per cent. As the size continues to decrease, the recovery performance improves (Figure 21).

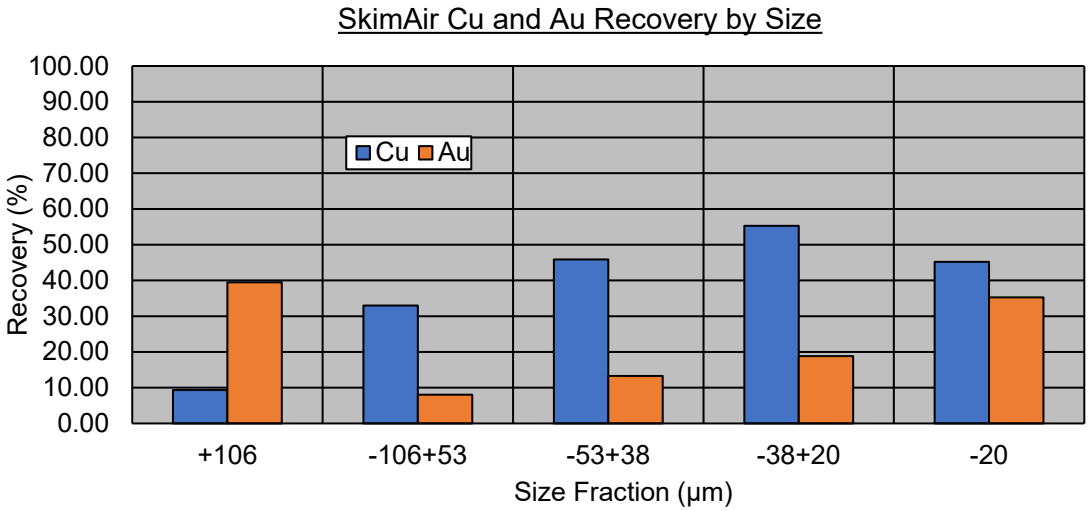



**FIG 21** – SkimAir Cu and Au recovery by size.

### *SkimAir tail*

The SkimAir tailings consisted of 81.8 per cent pyrite, again highly liberated at 97 per cent, with 1.2 per cent chalcopyrite at lower liberation (28.1 per cent). Gold in the tailing was partly liberated (30 per cent), partly in binary with pyrite (34 per cent) and partly in multiphase (36 per cent) (Figure 22). Losses associated with pyrite are likely influenced by the cell's selective operating conditions, including high pH and low collector dosage, which is again driven by the high chalcopyrite to pyrite ratios in the feed.

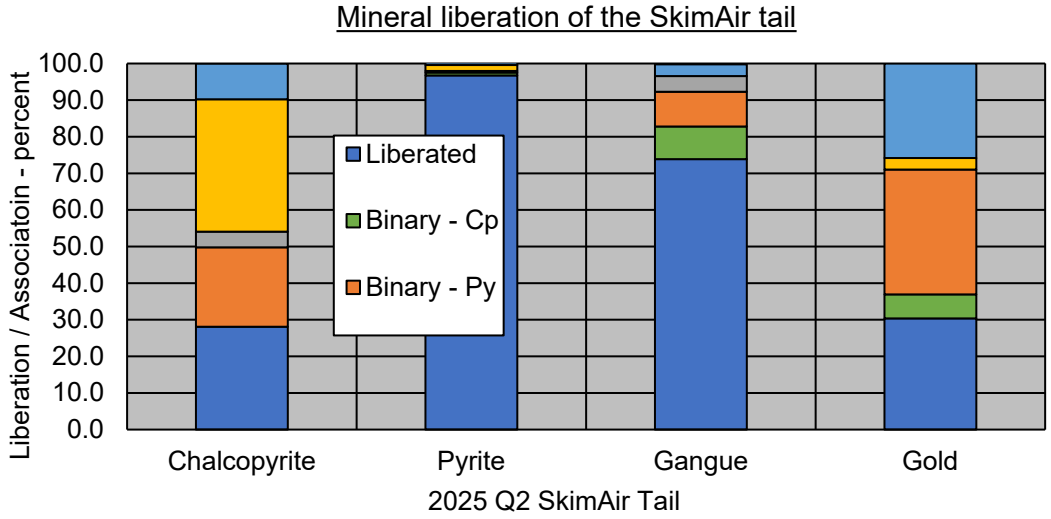



**FIG 22** – Mineral liberation of the SkimAir tails.

Table 8 summarises the distribution of gold area by class of association. It is observed that 30 per cent of the gold reporting to the SkimAir tailings is present as liberated particles, with no liberated gold observed in the -38+20 micron size fraction. This indicates that the SkimAir is effectively recovering all liberated gold at the target regrind circuit $P_{80}$ of 20–25 micron. Liberated gold present in the -53+38 micron size fraction is recirculated to the Vertimill, where further size reduction provides an opportunity for recovery in the -38+20 micron fraction upon redirection back to the SkimAir circuit.

**TABLE 8**

Distribution of gold area by class of association – KM7714 SkimAir tailing Q2 2025.

| Sample | Au distribution by size – % | Lib | Adhesions to: | | | | Inclusions within: | | | |
|---|---|---|---|---|---|---|---|---|---|---|
| | | | Cp | Py | Gn | MP | Cp | Py | Gn | MP |
| SkimAir tailing Q2 2025, +106 µm | 0.9 | - | - | - | - | 68 | - | 11 | 5 | 16 |
| SkimAir tailing Q2 2025, -106+53 µm | 32.6 | - | 20 | 9 | - | 44 | - | 16 | - | 11 |
| SkimAir tailing Q2 2025, -53+38 µm | 26.4 | 87 | - | 8 | 1 | 2 | - | 2 | - | <1 |
| SkimAir tailing Q2 2025, -38+20 µm | 25.6 | - | - | 56 | - | 11 | - | 25 | 3 | 6 |
| SkimAir tailing Q2 2025, -20 µm | 14.5 | 51 | - | 18 | 15 | 15 | - | 1 | - | 1 |
| **SkimAir tailing Q2 2025, Overall (calculated)** | **100** | **30** | **7** | **22** | **2** | **20** | **-** | **12** | **1** | **6** |

### *Cleaner tailings*

The cleaner tailings gold grade decreased from 0.44 g/t in Q1 to 0.29 g/t in Q2, corresponding to an improvement in cleaner gold recovery from 90.5 per cent to 93.1 per cent. This significantly contributed to the overall gold recovery improvement for Q2, as no significant difference in rougher gold recovery improvement was noted.

Figure 23 illustrates a reduction in liberated gold reporting to the cleaner tailings, and size-by-size assays indicate a decrease in particles finer than 10 micron from 41 per cent in Q1 to 28 per cent in Q2 (Figure 24). This trend demonstrates that SkimAir is effectively recovering a greater proportion of liberated gold prior to overgrinding in the Vertimill, thereby reducing losses to ultrafine fractions observed prior to SkimAir installation.

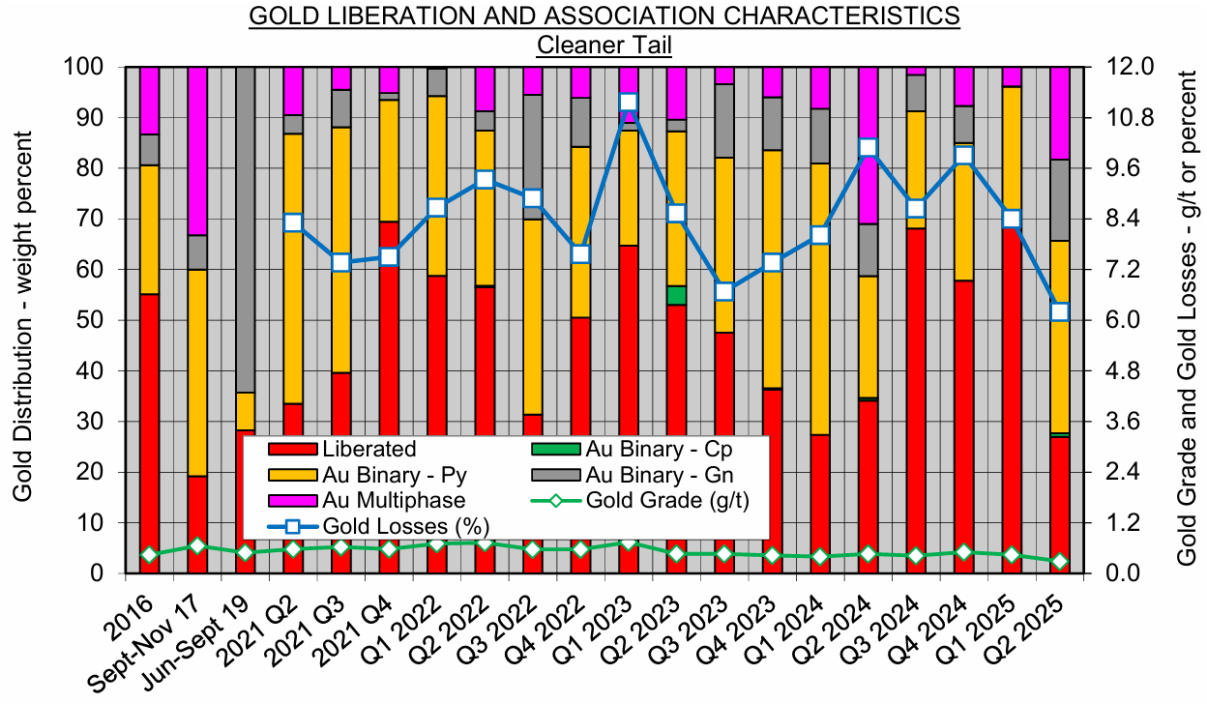



**FIG 23** – Gold liberation and association characteristics of the cleaner tail.

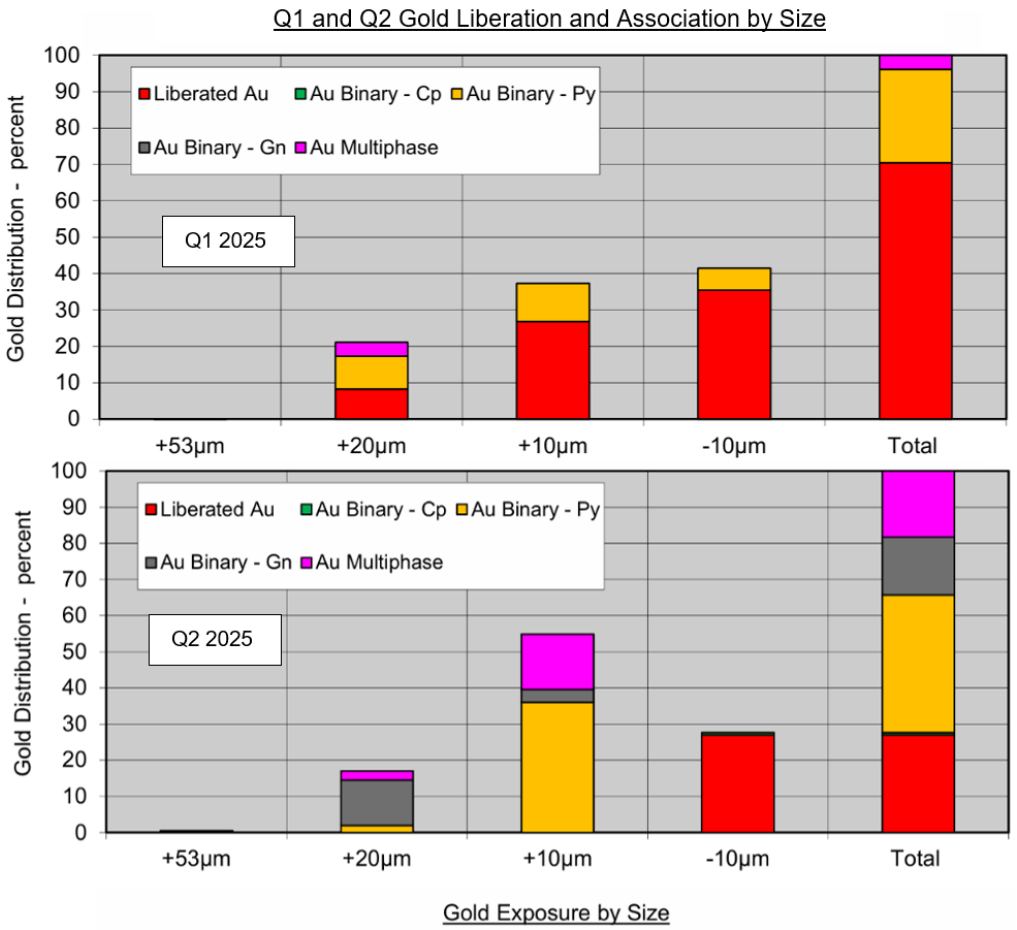



**FIG 24** – Q1 and Q2 gold liberation and association by size.

The shift cleaner tailing samples are composited weekly for routine sizing analysis. A pre and post SkimAir installation cleaner tailing composite was sent for gold analysis by size to quantify change in cleaner circuit performance. Figure 25, shows a reduction of gold losses in the ultra-fine size fraction in the cleaner tails shift sample, from 67 per cent pre SkimAir, to 46 per cent post SkimAir, along with a reduction in grade for those samples from 0.48 g/t to 0.32 g/t.

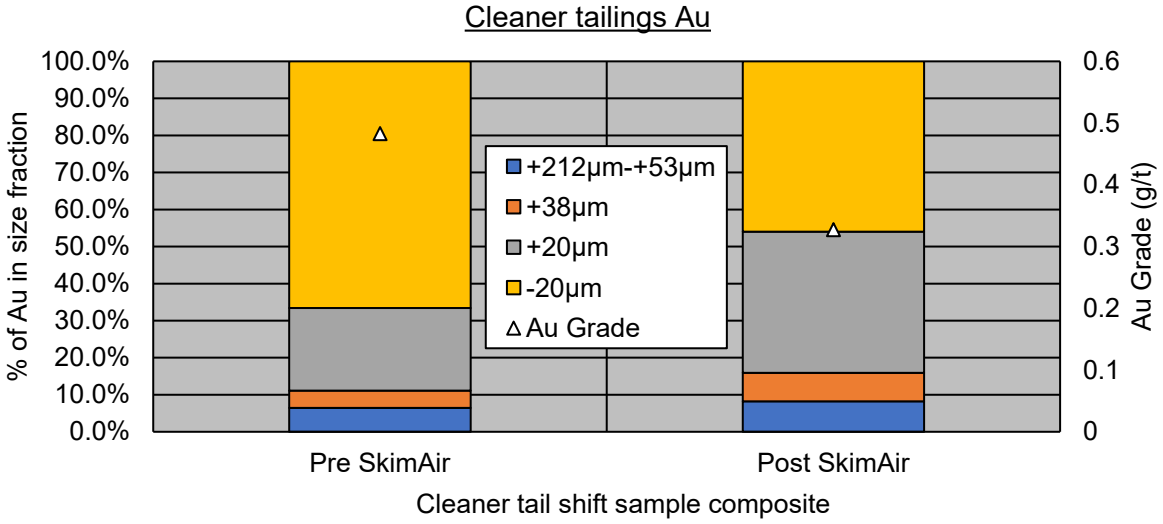



**FIG 25** – Pre and post SkimAir cleaner tailings gold by size.

### *Size by cleaner recovery*

Size by cleaner gold recovery analysis was completed comparing Q1 and Q2 mineralogy composite samples, cleaner feed, primary concentrate and cleaner tails (Figure 26). Negligible difference was observed for the -106+53 micron fraction, whereas a 3.5 per cent and 8 per cent recovery improvement for the -53+20 micron and in the ultra-fines fractions respectively was observed. This aligns with Figure 25.

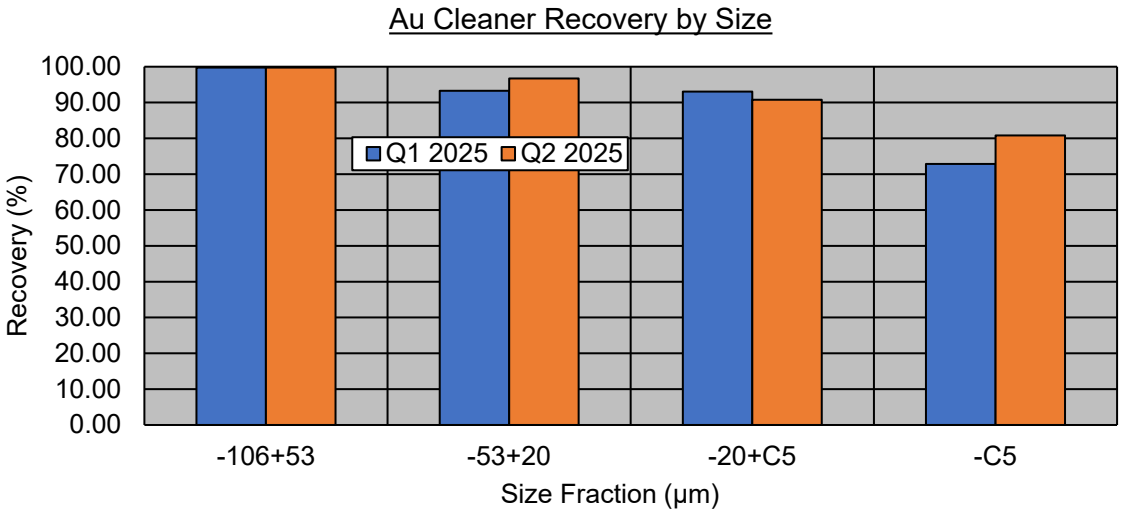



**FIG 26** – Gold cleaner recovery by size.

## FUTURE WORK

Since installing and initially commissioning the SkimAir, work has been ongoing to optimise the performance of the cell.

## Factorial trial

To assist in determining optimal operational parameters for the cell, a factorial trial was undertaken between late August and early September 2025. This trial varied air, Aerophine 3418A (g/T Cu), pH, and level between the upper and lower operating bands that the cell has typically operated between since commissioning.

The trial, conducted over eight shifts, used a full factorial design with the four variables (air, reagent, pH, and level) tested in duplicate. A summary of the low and high set points used, and the proposed set point range from the trial, is shown below in Table 9.

**TABLE 9**

Factorial optimisation trial high and low set points.

| Parameter | Low set point | High set point | Recommended set point from factorial |
|---|---|---|---|
| Air | 80 $Nm^3/h$ | 170 $Nm^3/h$ | 140–170 $Nm^3/h$ |
| Level | 380 mm | 450 mm | 390–450 mm |
| Reagent (Aerophine 3418A) | 60 g/T Cu | 160 g/T Cu | 80–120 g/T Cu |
| pH | 10.5 | 11.5 | 11.2–11.5 |

Each of the 16 cases were run in random order within two blocks, allowing 2.5 hrs to achieve steady state. Some runs were shortened due to plant conditions, with sampling guided by metallurgical judgment and online copper assay trends.

At steady state, feed (SKF), tails (SKT), and concentrate (SKC) were sampled every minute for 15 mins, producing duplicate samples (S1 and S2). Duplication by case and sample enabled the estimation of sampling error and assessment of statistical significance.

Through these tests and Yates and MATLAB analysis, the following conclusions were made:

- Copper recoveries were maximised at high air, deep froth levels*, high reagent and low pH* (where * denotes statistical significance).
- Gold recoveries were maximised at high air, high reagent* and low pH*.
- SkimAir concentrate is diluted with pyrite with increasing reagent* usage and lower pH*.
- There is significant variability in the results between Block 1 and 2, however, both sets indicate similar trends with just the magnitude varying. Some gold data from Block 2 was filtered due to nugget effect affecting assays.
- Low pH and high Aerophine trials typically drive down the SkimAir concentrate grade sharply. This negatively affected cleaner performance (low PAX, high cleaner tails results).
- There is high recirculating load around the circuit, requiring 1–2 hrs for it to reach steady state.

## Mass pull optimisation

Simulation results on the reconfigured flotation circuit indicated that increased mass pull at the SkimAir could lead to both improved gold and copper recoveries for the overall circuit. Based on these results, several operating parameters were adjusted at the SkimAir to increase mass pull to understand effects to overall circuit copper and gold recovery.

With changes to operating parameters, the SkimAir mass pull was successfully increased. This was indicated by reduced SkimAir concentrate grades and increased SkimAir concentrate percent solids readings from the MSA. However, it was also observed that the increased mass pull influenced other areas of the circuit. This includes:

- Increased SkimAir mass pull generally resulted in an upwards trend in SkimAir copper and gold recoveries, indicated by CuSUM analysis.
- Reduced cleaner feed grade and mass flow to cleaner circuit due to higher mass recovery from SkimAir cell (SkimAir concentrate is sent directly to final concentrate sump).
- Less aggressive cleaner operation, with CuSUM analysis showing decreasing Air and PAX addition and deepening of levels, which was required to maintain final concentrate grade targets, due to the extra dilution of final concentrate from SkimAir material.
- A decrease in overall circuit copper and gold recovery was observed because of the less aggressive cleaner circuit operation, again indicated by CuSUM analysis.

## Concentrate redirection trial

Simulations performed in JKSimFloat identified that increasing the SkimAir mass pull may result in an improved circuit overall gold recovery, whilst maintaining cleaner circuit performance. To enable this, the SkimAir concentrate would require to be diverted to the cleaner 2 concentrate sump to undergo an additional stage of cleaning to ensure concentrate grade is saleable. Further, Coombs and Ma (2025) suggested that given the relatively high liberation of pyrite in the SkimAir concentrate, directing the stream to the third cleaner stage may be beneficial, though may result in losses of gold (Coombs and Ma, 2025). An on/off trial was commenced to evaluate this option, however enough data points to establish a statistical significance are yet to be collected at time of writing.

# CONCLUSIONS

The installation of the SkimAir® flash flotation cell in the Ernest Henry regrind circuit has delivered a statistically significant improvement to overall circuit gold recovery through recovering liberated mineral prior to undergoing overgrinding. This is demonstrated through the gold recirculating load

reducing from 1750 per cent to 337 per cent, with the SkimAir recovering 78 per cent of gold and 58 per cent of copper from the regrind circuit.

Paired t-tests and multiple linear regressions analyses consistently confirmed a statistically significant improvement to gold recovery ranging from 1.06–1.99 per cent at 90 per cent confidence limits. These shift performance findings slightly differ to the Q2 mineralogical data, which showed a 3 per cent increase in plant gold recovery and a reduction in cleaner tailings grade from 0.44 g/t to 0.29 g/t when compared to Q1 prior to the SkimAir's installation, due to the aforementioned sample filtering and compositing process applied.

Mineralogical analysis confirmed preferential recovery of liberated gold and chalcopyrite, despite a high pyrite to chalcopyrite feed ratio. Selective operation at elevated pH limited pyrite recovery to 3 per cent, maintaining concentrate quality. Size-by-size analysis demonstrated reduced ultrafine gold losses (<10 micron) to cleaner tailings, and confirmed all liberated gold in the -38+20 micron size range was recovered by the SkimAir, further validating the recovery improvements observed.

The SkimAir circuit also improved downstream pulp chemistry by reducing dissolved oxygen demand and pyrite oxidation, creating more favourable conditions for cleaner flotation.

Overall, the SkimAir® installation has proven to be an effective strategy for enhancing gold recovery in the Ernest Henry concentrator and demonstrates the broader applicability of flash flotation within regrind circuits for IOCG operations.

## ACKNOWLEDGEMENTS

The authors would like to acknowledge Evolution Mining for their approval to publish this work. The authors would also wish to thank the Ernest Henry Metallurgy, Processing, Maintenance and Engineering teams, who all contributed to the successful installation and commissioning of the SkimAir cell. Special thanks go to the companies who made this project possible, Metso, in particular Peter Bourke, Batu Aktas and Jyry Niskala for their technical support, JK Tech, Thu Nguyen and Diana Felipe for their surveying and mass balancing expertise, and Helen Coombs and Wendy Ma from ALS Kamloops for their mineralogical analysis and reporting.

## REFERENCES

Cardenas, H, McGrory, M, Webb, G, Paredes, J, Setiagani, R, Villaspir, K A, Manguba, L E and Rodolfo, A, 2016. Didipio flash flotation and gravity recovery circuit, in *Proceedings 13th AusIMM Mill Operators Conference*, pp 123–126 (The Australasian Institute of Mining and Metallurgy: Melbourne).

Cloutier, J, Ford, A, Huston, D, Haynes, M, Schofield, A, Doublier, M, Sanchez, G, Duan, J, Goodwin, J, Beyer, E, Fraser, G, Cheng, Y, Waltenberg, K, Burnham, A and Czarnota, K, 2025. Iron oxide copper–gold potential of Australia using a hybrid data- and knowledge-driven approach and its implications for the formation of IOCG mineral systems, *Ore Geology Reviews*, 184.

Coombs, H and Ma, W, 2025. Mineralogical evaluation of Ernest Henry concentrator process streams quarter 2 2025, report KM7714 (ALS Mineralogy: Kamloops).

Coombs, H, 2025. Mineralogical evaluation of selected process streams following skim cell commissioning, report KM7610 (ALS Mineralogy: Kamloops).

Erkan, E, Ekmekci, Z and Altun, E, 2022. Comparison of flash flotation and gravity separation performance in a greenfield gold project, Physicochemical Problems of Mineral Processing, 58(3):146979.

Evolution Mining, 2023. Ernest Henry mine life extended to 2040 – ore reserves doubled (Evolution Mining: Sydney).

Evolution Mining, 2026a. Annual mineral resources and ore reserves statement as at 31 December 2025 (Evolution Mining: Sydney). Available from: <https://evolutionmining.com/wp-content/uploads/annual_mineral_resources_and_ore_reserves_statement.pdf>

Evolution Mining, 2026b. FY26 Half Year Financial Results and Interim Dividend (Evolution Mining: Sydney). Available from: <https://evolutionmining.com/wp-content/uploads/fy26_half_year_financial_results_and_interim_dividend.pdf>

Gordon, H, 2022. EHM concentrator circuit unsized Au deportment (XPS – Expert Process Solutions).

Mitchell, C J, Evans, E J and Styles, M T, 1997. A review of gold-particle size and recovery methods (British Geological Survey: Nottingham).

Napier-Munn, T, 2014. Statistical methods for mineral engineers: how to design experiments and analyse data, issue 5 (Julius Kruttschnitt Mineral Research Centre).

Newcombe, B, Bradshaw, D and Wightman, E, 2012. Development of a laboratory method to predict plant flash flotation performance, Minerals Engineering, 39:228–238.

Newcombe, B, Wightman, E and Bradshaw, D, 2013. The role of a flash flotation circuit in an industrial refractory gold concentrator, Minerals Engineering, 53:57–73.

Paki, O K and Erepan, P C, 1997. Implementation of flash flotation in the Ok Tedi grinding circuit, in Proceedings Sixth Mill Operators Conference, pp 125–131 (Madang).

Pease, J D, Curry, D C and Young, M F, 2005. Designing flotation circuits for high fines recovery, in Proceedings Centenary of Flotation Symposium, pp 905–912.

Ryan, A J, 1998. Ernest Henry copper-gold deposit, in Geology of Australian and Papua New Guinean mineral deposits (ed: DA Berkman and DH Mackenzie), pp 759–768 (The Australasian Institute of Mining and Metallurgy: Melbourne).

Santos, E C, Silva, J C and Duarte, H A, 2016. Pyrite oxidation mechanism by oxygen in aqueous medium, Journal of Physical Chemistry C, 120(5):2760–2768.

Toussaint and Richardson Consulting Engineers Pty Ltd, 1994. Skim Air flotation project: preliminary engineering, report prepared for Wiluna Mines Limited (Toussaint and Richardson Consulting Engineers Pty Ltd: Perth).

Walshe, M, Mattsson, T, Bourke, P and Grau, R, 2019. Large mechanical flotation cells – advantages and scale-up considerations, in MetPlant 2019, pp 176–191 (The Australasian Institute of Mining and Metallurgy: Melbourne).

# Copper flotation advanced process control for Palabora Mining Company

*M Erwee[1], M Olivier[2], A Malan[3], E Mualusi[4], T Ramakobya[5], K Machaba[6] and L Auret[7]*

1. APC Engineer, Stone Three, Somerset West, Western Cape 7130, South Africa. Email: monique.erwee@stonethree.com
2. Head of APC, Stone Three, Somerset West, Western Cape 7130, South Africa. Email: marnus.olivier@stonethree.com
3. APC Engineer, Stone Three, Somerset West, Western Cape 7130, South Africa. Email: annelette.coetzee@stonethree.com
4. Metallurgist, Palabora Copper (Pty) Ltd, Phalaborwa, Limpopo 1389, South Africa. Email: eric.mualusi@palabora.co.za
5. Metallurgist, Palabora Copper (Pty) Ltd, Phalaborwa, Limpopo 1389, South Africa. Email: tshire.ramakobya@palabora.co.za
6. Metallurgist, Palabora Copper (Pty) Ltd, Phalaborwa, Limpopo 1389, South Africa. Email: kabelo.machaba@palabora.co.za
7. Senior Process Data Scientist, Stone Three, Somerset West, Western Cape 7130, South Africa. Email: lidia.auret@stonethree.com

## ABSTRACT

Flotation represents the most important separation process in the copper processing circuits, where even small recovery losses at flotation carry significant economic cost. Ensuring stable and optimal operation parameters of copper flotation circuits is critical to the sustainable extraction of copper mineral. This paper discusses the design, implementation and evaluation of circuit flotation process control at the copper concentrator of Palabora Mining Company in South Africa. The scope of the work covers rougher, cleaner and recleaner froth control systems as well as their associated concentrate sumps. Advanced regulatory control is implemented in a hierarchy that layers concentrate production, sump levels, mass pull, cell pulp levels and cell air addition. Froth metrics such as froth velocity and froth bubble coverage are used as constraints in the advanced process control scheme. The performance of the advanced process control solution is evaluated in terms of stability (reduced sump level variability and incidences of overflow/emptying events) based on before/after analysis. The effect of throughput and feed grade changes was also investigated.

## INTRODUCTION

Flotation control at large-scale copper operations is challenging for well-established reasons: feed grade and mineralogy vary on timescales from hours to months, process interactions between cells within a bank are coupled through hydrostatic pressure, recirculating loads introduce long apparent delays, and the most informative metallurgical measurements (concentrate grade, tails grade, recovery) are available only once per shift or less. Industrial flotation control is typically layered as a hierarchy of base-level regulatory loops (air addition, pulp level), an advanced or supervisory layer that coordinates the air and level set points toward a higher-level objective such as mass pull or grade, and an optimisation layer (Shean and Cilliers, 2011). Model-predictive control has received the most academic attention at the supervisory layer but has seen limited sustained industrial adoption, owing to the difficulty of deriving and maintaining sufficiently accurate dynamic models under variable feed (Bergh and Yianatos, 2011; Le Roux *et al,* 2020). Advanced regulatory control (decentralised loops augmented with constraint switching, cascade and decoupling elements) is more widely deployed in practice, offering robustness to model uncertainty and simpler commissioning while retaining much of the coordinating benefit of a supervisory layer (Olivier *et al,* 2025; Skogestad, 2023).

Instability and variability in industrial flotation circuits propagate through banks: concentrate/tails from one bank reports to an intermediate sump that feeds the next, so a surge in an upstream bank propagates downstream as a sump-level excursion, and uncontrolled sumps propagate these disturbances directly to the cells they feed. Intermediate sumps are most usefully operated not at a fixed level but as buffers, absorbing inflow variation so that pump discharge remains smooth. This

principle is known as averaging level control, which trades tight level regulation for minimised throughput variability (Marlin, 1996). Conventional averaging controllers act only once the level approaches a limit; the ramp horizon integral gap controller (Gous *et al,* 2023) instead schedules its gain on both the current level and a short-horizon forecast, beginning to act before the level leaves its band and thereby reducing overshoot under fast inflow disturbances. At Palabora Mining Company (PMC), where rougher surges were observed to propagate instability through the cleaner and recleaner banks, stabilisation of the concentrate sumps was adopted as the primary control objective and the first step toward sustained metallurgical improvement.

Camera-based froth measurements have been applied to flotation monitoring and control since the late 1990s (Cipriano *et al,* 1998; Kaartinen *et al,* 2006; Brooks and Munalula, 2017) and the inference of concentrate grade from froth imagery remains an active research topic (Aldrich *et al,* 2010; Aldrich, Avelar and Liu, 2022). Robust grade inference under industrial conditions has nonetheless proven elusive, so froth-derived signals are more reliably used as indicators of froth condition (velocity, stability and coverage) than as direct grade measurements. In the present work, froth velocity and froth coverage from froth sensors are used as operating constraints within the mass-pull advanced process control (APC) layer, bounding the regime into which individual cells may be driven rather than serving directly as controlled variables.

In this work, we discuss flotation APC for PMC. Prior to the APC implementation, the flotation circuit operated without closed-loop sump level or mass-pull control. Rougher surges caused the concentrate sumps to fluctuate, which propagated instability to the downstream cleaner and recleaner banks. No feedforward control existed to counter rougher surge events, and operators managed individual cell air and pulp level set points manually. These conditions motivated an APC investment targeting circuit stabilisation as a first step toward sustained metallurgical improvement.

This paper presents the design, implementation and statistical performance evaluation of the resulting APC solution. The control structure section describes the four-layer hierarchy, encompassing sump level stabilisation and mass-pull control as its primary layers, layered above decoupled per-cell froth depth and per-cell air addition control. The data analysis section describes the comparison methodology and key results, including the trendline comparison (Napier-Munn, 1998) used to account for the effect of feed grade and throughput variation on the recovery comparison. The purpose of the current APC installation is circuit stabilisation, a requirement before subsequent metallurgical performance optimisation can be targeted in future projects. Conclusions and future work are presented in the final section.

## PROCESS DESCRIPTION

PMC operates a block-cave copper mine and on-site concentrator near Phalaborwa, Limpopo, South Africa. The flotation section (Figure 1) receives conditioned slurry from the grinding circuit via FPS01 and processes it through a three-stage flotation circuit: rougher, cleaner and recleaner banks.

The rougher bank consists of seven mechanically agitated cells (FT101–FT107), fed from the milling final product sump (SMP407) and producing a rougher concentrate that reports to the rougher concentrate sump (SMP18 and SMP22) as well as a rougher tails stream. The rougher concentrate sump feeds forward to the cleaner circuit.

The cleaner circuit comprises five cells (FT201–FT205) producing a cleaner concentrate reporting to two parallel cleaner concentrate sumps (SMP20 and SMP23), which in turn feed the recleaner bank, as well as the cleaner tails, which reports to SMP19 and is recycled back to the rougher feed.

The recleaner bank consists of four cells (FT301–FT304) that produce the final concentrate, which reports to the recleaner concentrate sump (SMP21), and the recleaner tails is recycled to the cleaner feed.

Seven physical concentrate sumps, grouped into six controlled level loops (SMP18 and SMP22 share a loop), are within the APC scope: SMP407 (milling final product), SMP18 and SMP22 (rougher concentrate), SMP20 and SMP23 (cleaner concentrate), SMP19 (cleaner tails recycle) and SMP21 (recleaner concentrate). Sixteen flotation cells are within the APC scope. Each cell is equipped with individual air addition control and dart valve-based froth depth control. Froth velocity and froth coverage measurements from top-of-froth sensors are available for all cells and are used

as constraints within the APC mass-pull layer. All measurements and final control elements are interfaced through the plant control system, and minute-level historian data from these instruments underpin the stability analysis presented later in this paper.

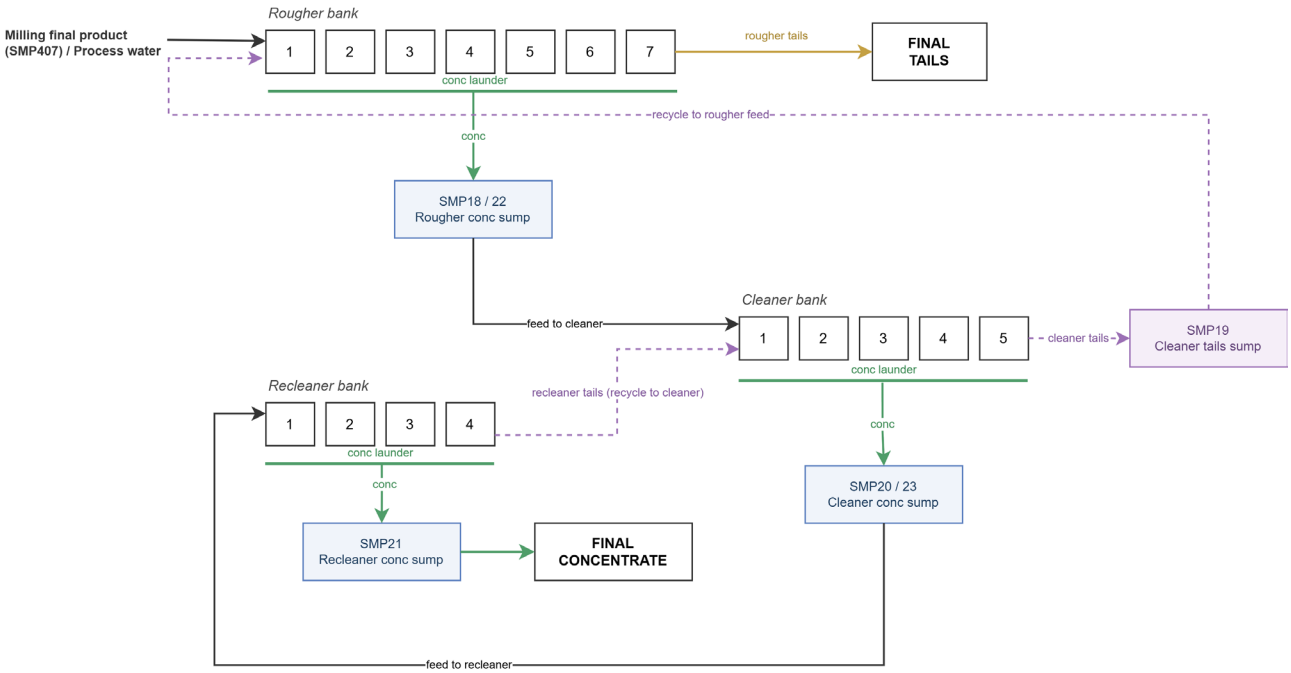



**FIG 1** – Flotation circuit overview.

Feed to the circuit over the analysis period had a mean copper grade of approximately 0.45 per cent Cu. Throughput averaged approximately 1100–1160 t/h over the periods compared.

## CONTROL STRUCTURE

The APC is implemented as a hierarchical advanced regulatory control system communicating with the plant process control system (PCS) via OPC (Open Platform Communications). The PCS provides hardware interfacing to field instruments and final control elements; the APC reads the full OPC state at each execution cycle, computes the required control actions, and writes manipulated variable set points back via OPC. The execution cycle of the APC is configured to run at a fixed sampling rate. The control hierarchy consists of four layers, described below from outermost to innermost. Figure 2 provides an overview of the control structure for a single bank.

A hierarchical advanced regulatory approach was selected over model-predictive control for three reasons: robustness to model uncertainty under variable feed mineralogy, transparency to operators and metallurgists (each layer can be inspected, enabled or disabled independently), and maintainability by site personnel without specialist model identification effort. This is consistent with reported industrial experience, where simpler decomposed control structures achieve much of the benefit of a centralised optimiser at a fraction of the maintenance burden (Le Roux *et al,* 2020; Skogestad, 2023).

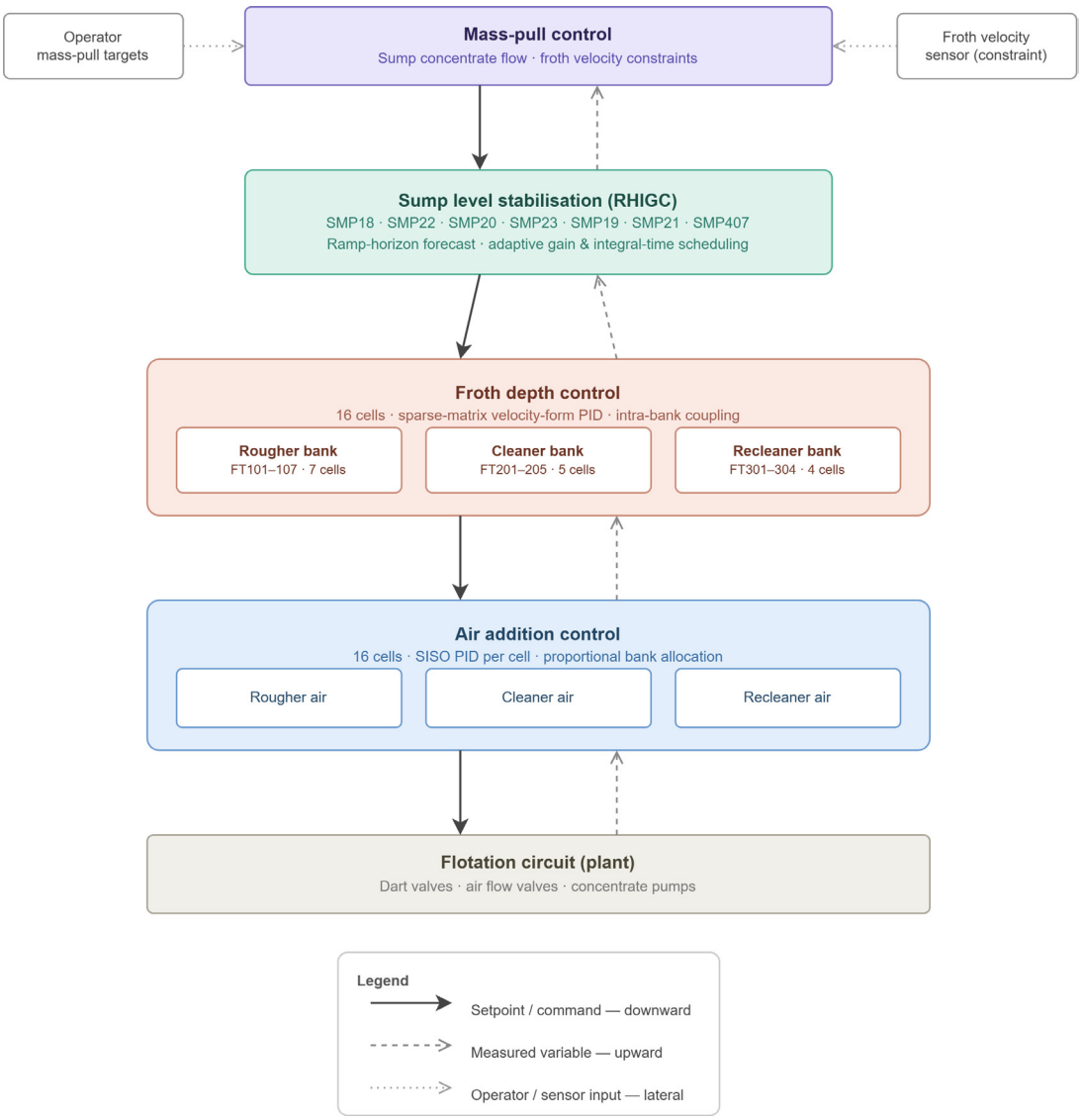



**FIG 2** – Control structure block diagram: four layers (mass pull, sump level, per-cell froth depth, per-cell air addition), with arrows showing set point flow and measured variable flow.

## Mass-pull control

The outermost layer maintains measured concentrate flow from each of the three concentrate sump groups (rougher, cleaner and recleaner) within operator-specified minimum and maximum limits. It issues incremental changes to the bank-level froth depth set point and the bank-level total air set point for the cells feeding each sump.

A distinguishing feature of the PMC APC implementation is the use of froth velocity and froth bubble size distribution measurements from the top-of-froth sensors as a constraint within this layer. Each cell has configurable minimum and maximum froth flow limits inputted by the operators. If a proposed mass-pull step would drive any cell's froth flow outside its permitted band, the air and froth depth contributions for that cell are withheld or reduced. This prevents the mass-pull layer from inadvertently pushing individual cells into hydrodynamically unfavourable regimes while still allowing the rest of the bank to respond. Bank-level set point changes are distributed to individual cells according to operator-set per-cell limits, where any portion of a set point change that cannot be absorbed by cells at their current set point limits is redistributed to cells with remaining headroom.

## Sump level stabilisation

Each of the seven concentrate sumps is subject to averaging level control, with the objective of keeping sump level within configured limits while minimising unnecessary pump speed variation. The ramp horizon integral gap control (RHIGC) algorithm (Gous *et al,* 2023) is applied, as described

in Olivier *et al* (2025): gain scheduling is driven by both the current level and a short-horizon linear forecast, ensuring the controller begins acting more aggressively before the level actually reaches a limit rather than after. A first-order lag filter removes measurement noise before the level measurement enters the controller.

## Per-cell froth depth control

Froth depth across all 16 cells is maintained at set points by manipulating the dart tails valve positions. Because flotation cells within a bank are hydraulically connected (dart valve movement in one cell alters the hydrostatic back-pressure on adjacent cells), independent single-input single-output (SISO) control of each cell is insufficient, and a multivariable decoupled control approach is required (Kämpjärvi and Jämsä-Jounela, 2003; Olivier *et al,* 2025). The implemented controller accounts for the level and valve position of both the cell itself and upstream cells when computing the dart valve output for each cell, thus lessening the inter-cell coupling. Feedforward compensation is also included to reduce the impact of measurable upstream flow disturbances, such as changes in feed flow to the rougher feed sump and sump discharge rates feeding the cleaner and recleaner banks.

Each cell is equipped with two dart valves on the tails discharge. The froth depth controller computes a combined output for the assembly, which is then allocated between the two valves via split-range logic. The dominant (more open) valve carries the larger share of the command to maintain fine-grained adjustability (via the second valve) across the full operating range, while both valves are kept above a minimum opening to prevent sanding.

## Per-cell air addition control

The purpose of air addition control is to maintain a target aeration profile across each bank. Each cell's air flow is regulated by an individual PID (proportional-integral-derivative) controller tracking a per-cell set point. These per-cell set points are derived from the bank-level total air set point (issued by the mass-pull layer) distributed across cells according to operator-configured target fractions, with any portion that cannot be absorbed by cells at their set point limits redistributed to cells with remaining headroom.

# DATA ANALYSIS

## Periods of comparison and data cleaning

The performance of the APC is assessed by comparing two operating periods using daily shift composite metallurgical accounting data:

- **Baseline (before APC):** 91 operating days prior to APC commissioning start (November 2025), of which 51 days satisfied the data cleaning criteria described below (n = 51).
- **APC ON:** 38 days from APC go-live (5 December 2025) to the start of an unplanned long shutdown due to widespread flooding that affected the plant (12 January 2026), of which 26 days satisfied the data cleaning criteria (n = 26).

Data was cleaned to retain only days representing nominal operating conditions. Days with throughput below a minimum operating threshold were excluded. During the APC ON period, APC utilisation exceeded 98 per cent of operating hours.

The primary objective of the flotation APC is to improve circuit stability, reducing the propagation of upstream variability to downstream banks. Circuit stability improvements are shown in terms of improved sump level and cell level/aeration control. Circuit stability improvements is a necessary, but not sufficient, condition for metallurgical performance improvement. Once an operational point can be maintained with low variability, optimisation control can be considered in collaboration with metallurgical oversight (this constitutes future work). Metallurgical performance improvement was not the goal of the APC implementation, and no statistically significant difference in metallurgical performance (ie also not deterioration in performance) can be concluded (larger sample sizes are required). Analyses done for this purpose included means and standard deviations comparisons,

multivariate ordinary least squares (OLS) regression, and the trendline comparison approach of Napier-Munn (1998).

## Circuit stability

### *Sump levels*

The purpose of the sump level control is to let sumps serve as buffers (sump level allowed to vary between upper (overflow risk) and lower (insufficient pump head risk) limits) to keep sump discharge flows at reduced variability. The RHIGC controller prioritises smooth pump speed over a tight level set point, allowing the level to move freely within its operating band so that inflow disturbances are absorbed by the sump rather than passed straight through to the pump. Figure 3 shows sump level time series for the before APC and APC ON periods, with exclusion zones (overflow risk, level above 90 per cent; insufficient pump head risk, level below 10 per cent) indicated. The percentage of operating time that the rougher concentrate sump level exceeded 90 per cent (a proxy for overflow risk) reduced from 16.2 per cent to 10.0 per cent. Cleaner concentrate sumps (SMP20 and SMP23) reduced from 9.6 per cent and 9.7 per cent to 6.1 per cent and 6.2 per cent respectively. SMP21 (recleaner concentrate) sump level varies between near-full and mid-level in both periods, which points to the intermittent, low-volume nature of recleaner concentrate flow. The recleaner circuit produces a relatively small and variable stream, and the sump dynamics seem to be driven by process intermittency more than by controllable disturbances. This is worth investigating further as part of future tuning work.

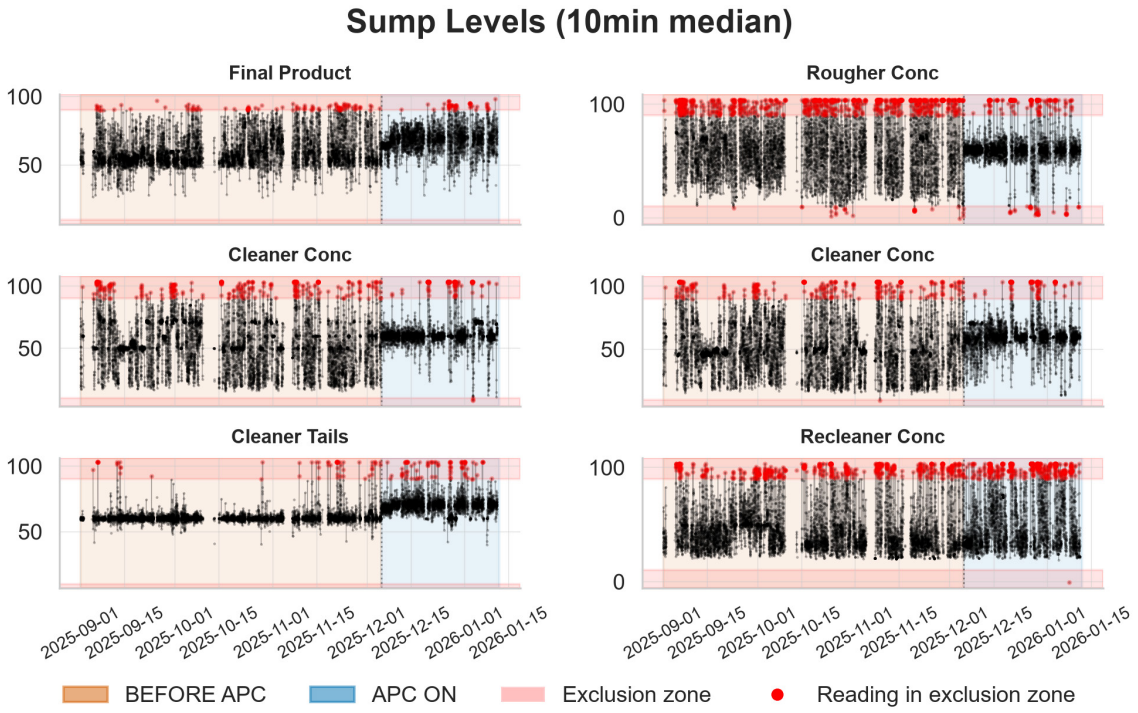



**FIG 3** – Sump level time series (median-downsampled to 10 minute sample period). Exclusion zone: >90 per cent or <10 per cent. Before APC period is shown as a light orange patch in each plot (before 5 December 2025); APC on period is shown as a light blue patch (after 5 December 2025); and exclusion zones are light red patches.

Table 1 provides variability statistics for the sump levels, quantified as the coefficient of variation (CV) and the mean absolute deviation (MAD) from the operating-band midpoint, reiterating the improvements of five of the six controlled level loops.

**TABLE 1**

Sump level stability: coefficient of variation (CV) and mean absolute deviation (MAD) from operating-band midpoint, before APC versus APC ON (seven physical sumps grouped into six controlled level loops).

| Sump | Function | CV (before → after) | MAD (before → after) | MAD reduction |
|---|---|---|---|---|
| SMP407 | Final product | 21.5% → 17.6% | 13.6 → 8.8 | 35% |
| SMP18/22 | Rougher conc | 40.4% → 31.8% | 20.4 → 11.6 | 43% |
| SMP20 | Cleaner conc A | 37.5% → 19.5% | 17.7 → 6.7 | 62% |
| SMP23 | Cleaner conc B | 41.0% → 21.9% | 19.4 → 8.2 | 58% |
| SMP19 | Cleaner tails | 17.1% → 16.2% | 11.5 → 7.6 | 34% |
| SMP21 | Recleaner conc | 47.2% → 49.5% | 22.8 → 23.8 | −5% |

### *Cell levels and aeration*

Control error for air addition and froth depth control was quantified as the percentage of operating minutes where the relative error |PV − SP| / SP × 100 exceeded 5 per cent, computed from minute-level sensor data.

Froth depth control error improved substantially across the rougher bank. Cells 4–7, which had control errors between 67.7 per cent and 73.5 per cent before APC (ie spent most of the operating time more than 5 per cent away from set point), reduced to 21.0–27.6 per cent after APC go-live. Cells 1–3 improved more modestly, from roughly 12–29 per cent to 22–23 per cent, with Cell 1 already well-controlled before APC. In the cleaner bank, Cells 3 and 5 improved materially, while Cells 1 and 2 remained high in both periods. Finally, the recleaner cells (1 and 2) improved from approximately 33 per cent to approximately 22 per cent. Some cells showed marginal deterioration or no improvement, likely attributable to instrumentation limitations or operating constraints on specific valve assemblies.

Aeration control error was generally low and close to the 5 per cent threshold before APC, as operators were actively managing individual cell air flows. After APC, most cells maintained or slightly improved aeration control; a small number of cells (notably Rougher 4 and 5) showed increased aeration error under APC. This warrants further investigation: the APC was issuing air set points consistent with its mass-pull targets, but the underlying process response on those cells may require tuning adjustment or has a physical explanation (eg blower capacity constraints or cell configuration differences). Figure 4 summarises the froth depth and aeration control comparison per cell.

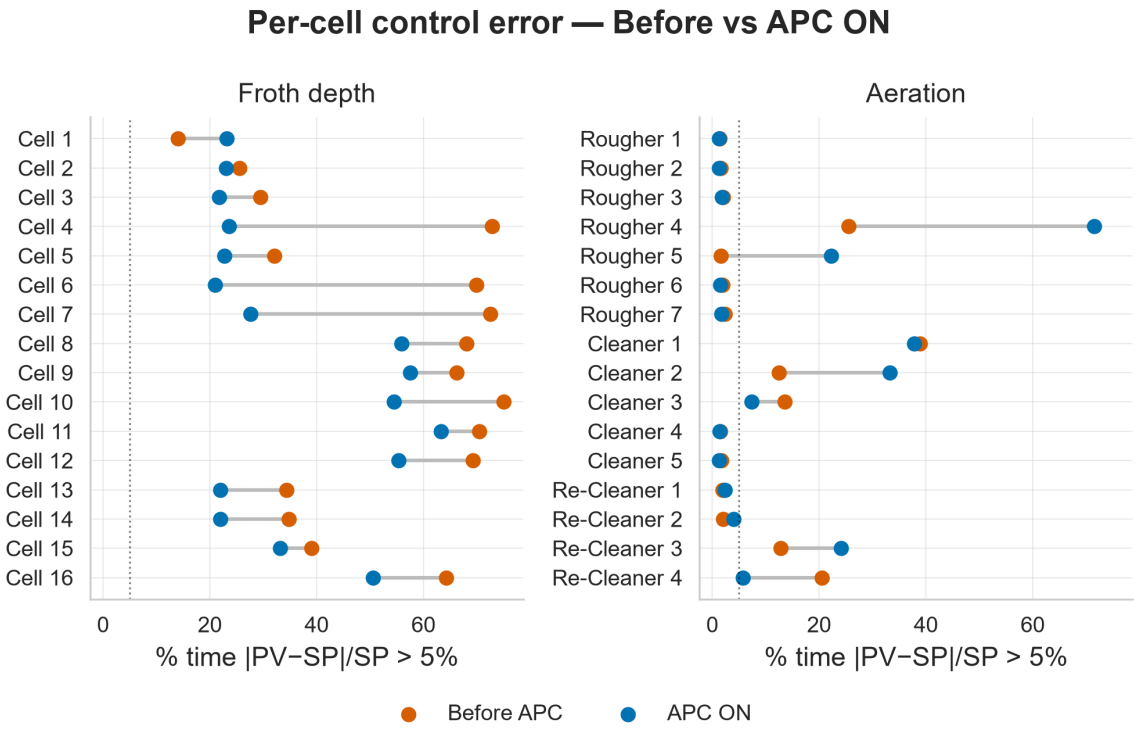



**FIG 4** – Flotation cell froth depth and aeration control comparison: % time spent in state of large control error.

## Metallurgical performance

Table 2 summarises the key production statistics for both periods. Disturbance variables that affect the KPIs are shown first (feed grade and throughput): feed grade was essentially unchanged, and throughput was slightly lower in the APC ON period. The concentrate grade decrease reflects the operator-set recovery-grade trade-off (through mass-pull target setting) and was deemed operationally acceptable. Being able to operate at a specific operating point on the recovery-grade curve with low variability is a benefit of APC.

**TABLE 2**

Metallurgical key performance indicators: before APC (n = 51) versus APC ON (n = 26), mean ± standard deviation.

| Metric | Before APC (n = 51) | APC ON (n = 26) |
|---|---|---|
| Feed grade Cu (%) | 0.45 ± 0.04 | 0.45 ± 0.04 |
| Throughput (t/h) | 1162 ± 103 | 1096 ± 99 |
| Cu recovery (%) | 78.3 ± 2.9 | 79.5 ± 2.2 |
| Tails grade Cu (%) | 0.10 ± 0.01 | 0.10 ± 0.01 |
| Conc grade Cu (%) | 26.8 ± 4.1 | 23.6 ± 3.2 |

A multivariate OLS regression model was fitted to isolate the impact of feed grade, throughput and APC status (see results in Table 3). The APC code (0 for before APC and 1 for APC ON) shows a positive coefficient, although the 95 per cent confidence interval for this coefficient spans zero, with a p-value of 0.176. The trendline comparison approach for plant trial comparison (Napier-Munn, 1998) can be seen in Figure 5.

**TABLE 3**

Multivariate ordinary least squares (OLS) regression: recovery (%) ~ feed grade Cu + throughput + APC code (n = 77, $R^2$ = 0.141, adjusted $R^2$ = 0.106).

| Variable | Coefficient | Std error | t-stat | p-value | 95% CI |
|---|---|---|---|---|---|
| Intercept | 72.8 | 5.0 | 14.6 | < 0.001 | [62.9, 82.7] |
| Feed grade Cu | 21.6 | 8.1 | 2.7 | 0.010 | [5.3, 37.8] |
| Throughput (t/h) | −0.0035 | 0.0029 | −1.22 | 0.23 | [−0.009, 0.002] |
| **APC code** | **0.88** | **0.64** | **1.37** | **0.18** | **[−0.40, 2.16]** |

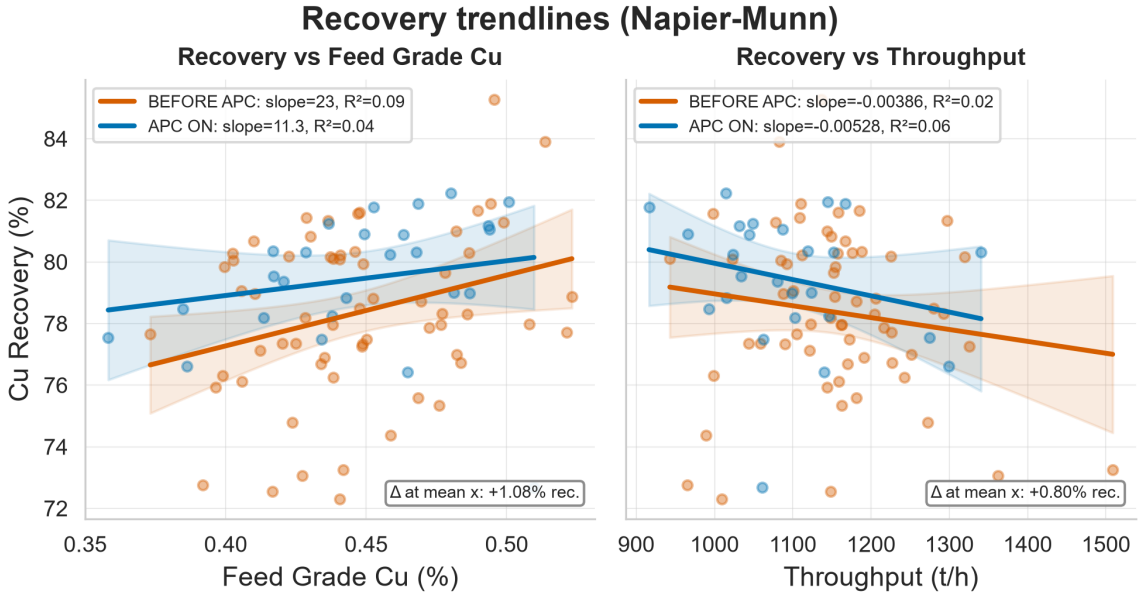



**FIG 5** – Trendline comparison (Napier-Munn, 1998) for the effect of feed grade and throughput on recovery (before APC versus APC ON).

## CONCLUSIONS

An advanced regulatory control solution was designed and implemented at PMC's copper flotation circuit, covering 16 flotation cells across rougher, cleaner and recleaner banks with seven associated concentrate sumps. The control architecture includes mass-pull control (including operator constraints from froth velocity measurements from on-cell sensors), sump level stabilisation using a ramp horizon integral gap control algorithm, decoupled per-cell pulp level control with dart valve assembly management, and per-cell aeration control. Most literature reports flotation APC for single banks, while this application is for an entire circuit.

The results show that APC delivered improvements in circuit stability at PMC. The sump level stabilisation results are consistent with the primary design intent: by smoothing concentrate sump levels and reducing overflow risk, the APC removes the main source of disturbances.

The stabilisation benefits change how the circuit is operated: operators manage bank-level mass-pull targets and per-cell constraint bands rather than individual valve and air set points, and the constraint-handling structure keeps individual cells out of hydrodynamically unfavourable regimes without operator intervention. The application also demonstrates that averaging level control, well established in tank farm and refinery service, transfers directly to flotation concentrate sumps, where buffer capacity is the main defence against surge propagation.

Future work at PMC includes extending the performance analysis over the full post-shutdown operating period, automating the grade-recovery optimisation loop once reliable online grade measurements are available, and advancing the use of froth velocity and froth bubble size distribution measurements from soft constraints to closed-loop controlled variables within the mass-pull layer.

## ACKNOWLEDGEMENTS

The authors thank the operators and metallurgists at Palabora Mining Company for their collaboration and support throughout the APC implementation and analysis, and acknowledge Palabora Copper (Pty) Ltd for approval to publish this work.

## REFERENCES

Aldrich, C, Avelar, E and Liu, X, 2022. Recent advances in flotation froth image analysis, *Minerals Engineering*, 188:107823.

Aldrich, C, Marais, C, Shean, B J and Cilliers, J J, 2010. Online monitoring and control of froth flotation systems with machine vision: a review, *International Journal of Mineral Processing*, 96:1–13.

Bergh, L G and Yianatos, J B, 2011. The long way toward multivariate predictive control of flotation processes, *Journal of Process Control*, 21:226–234.

Brooks, K and Munalula, W, 2017. Flotation velocity and grade control using cascaded model predictive controllers, *IFAC-PapersOnLine*, 50(2):25–30.

Cipriano, A, Guarini, M, Vidal, R, Soto, A, Sepúlveda, C, Mery, D and Briseño, H, 1998. A real time visual sensor for supervision of flotation cells, *Minerals Engineering*, 11:489–499.

Gous, G Z, Wiid, A J, le Roux, J D and Craig, I K, 2023. Advanced regulatory control techniques for improved averaging level control performance, *Industrial and Engineering Chemistry Research*, 62(38):15578–15587.

Kaartinen, J, Hätönen, J, Hyötyniemi, H and Miettunen, J, 2006. Machine-vision-based control of zinc flotation – a case study, *Control Engineering Practice*, 14:1455–1466.

Kämpjärvi, P and Jämsä-Jounela, S-L, 2003. Level control strategies for flotation cells, *Minerals Engineering*, 16:1061–1068.

Le Roux, J D, Oosthuizen, D J, Mantsho, S and Craig, I K, 2020. A survey on the status of industrial flotation control, *IFAC-PapersOnLine*, 53(2):11854–11859.

Marlin, T, 1996. *Process Control*: *Designing Processes and Control Systems for Dynamic Performance* (McGraw-Hill: New York).

Napier-Munn, T J, 1998. Analysing plant trials by comparing recovery-grade regression lines, *Minerals Engineering*, 11:949–958.

Olivier, M, Auret, L, Motlhagodi, M, Priyambodo, A and Moswete, S, 2025. Advanced process control design and implementation at Motheo copper flotation circuit, paper presented to MEI Flotation ‘25 Conference, Cape Town, November.

Shean, B J and Cilliers, J J, 2011. A review of froth flotation control, *International Journal of Mineral Processing*, 100:57–71.

Skogestad, S, 2023. Advanced control using decomposition and simple elements, *Annual Reviews in Control*, 56:100903.

# Applying modern flotation technology to improve fine particle recovery at Cadia

*I Heath[1], W Downie[2] and M Clark[3]*

1. Supervisor – Metallurgy, Newmont Mining Corporation, Orange NSW 2800.
   Email: isaac.heath@newmont.com
2. Specialist Process Engineer, Newmont Mining Corporation, Orange NSW 2800.
   Email: william.downie@newmont.com
3. Metallurgist, Newmont Mining Corporation, Orange NSW 2800.
   Email: meghan.clark2@newmont.com

## ABSTRACT

The Concentrator 2 circuit at Newmont's Cadia Operation completed a substantial brownfield expansion in 2022. The expansion objective was to increase throughput whilst maintaining gold and copper recovery. The brownfield footprint constraints for the flotation circuit expansion necessitated pursuing modern flotation technology over conventional solutions.

The Concentrator 2 flotation flow sheet prior to the expansion consisted of a conventional rougher-scavenger circuit upgrading to a regrind, two-stage cleaning circuit; utilising a Jameson Cell as the second stage cleaner (recleaner). The proposed expansion reduced the existing rougher-scavenger cell residence time by 28 per cent. Gold and copper recovery was forecast to reduce if no consideration was made to the residence time, due in part to a reduction in recovery of liberated fine particles (<20 microns). Brownfields constraints precluded conventional solutions to offset the residence time loss; a Z8500 Jameson Cell was instead selected at the head of the roughers due to its fast flotation kinetics, small footprint, and ability to recover fine particles. The rougher Jameson Cell and additional modification to the upstream comminution circuit, including an additional tertiary VTM-4500 Vertimill™, allowed a throughput increase whilst maintaining the flotation feed grind size target and recoveries. Additionally, due to its high degree of liberation, the cleaner-scavenger concentrate was redirected to the recleaners. This change reduced mass flow to the regrind circuit, which allowed for an improvement in mineral liberation, enhancing overall circuit recovery.

This paper gives an overview of the flotation technology and circuit changes made in Concentrator 2 at Cadia. It will discuss the results of pilot plant test work, operational challenges and recovery performance pre and post commissioning of the rougher Jameson Cell and redirection of the cleaner-scavenger concentrate.

## BACKGROUND

Concentrator 2, formerly the Ridgeway Concentrator, was commissioned in 2002 as nominally a 5 million ton per annum (Mt/a) plant to process Ridgeway Sub-Level Cave (SLC) ore. Consisting of a conventional rougher-scavenger flotation circuit with two-stages of conventional cleaning and regrind mill producing both a copper-gold concentrate and gravity dorè. The Ridgeway plant was smaller than the neighbouring Cadia Hill plant. Over the intervening years to 2017 the plant was progressively expanded to a nominal 7 Mt/a plant and transitioned from processing 100 per cent Ridgeway SLC ore to 100 per cent Cadia East ore. The concentrator was renamed 'Concentrator 2' in 2017 following the transition to 100 per cent Cadia East ore and will be referred to as Concentrator 2 from here on, no matter the feed source (Edmunds *et al,* 2021).

Ridgeway and Cadia East are both copper-gold deposits, however the mineralogical characteristics varied owing to the different geological formation conditions of each. The primary copper sulfide species within both Ridgeway and Cadia East ore was chalcopyrite and bornite, however the proportion and mineral texture vary between the deposits. Gold was present in both as native gold with lesser electrum. The primary concentrate dilutant to both Ridgeway and Cadia East ore was pyrite, however Cadia East contains a higher proportion of fluorine bearing non-sulfide minerals. To maintain fluorine in concentrate within marketable limits, froth washing was deployed on all concentrates produced while processing Cadia East ores. Wash water promotes the rejection of liberated non-sulfide fines recovered through entrainment (Akerstrom *et al,* 2018).

The Concentrator 2 flotation circuit was expanded in 2016 to support the transition to 7 Mt/a, with two additional OK100 scavenger cells, one VTM1250 regrind mill, one regrind batch centrifugal concentrator and a E3232/8 recleaner Jameson Cell. The Jameson Cell technology was selected to replace conventional tank cell recleaners due to it's superior froth washing capability. The Concentrator 2 basic process flowsheet is shown in Figure 1.

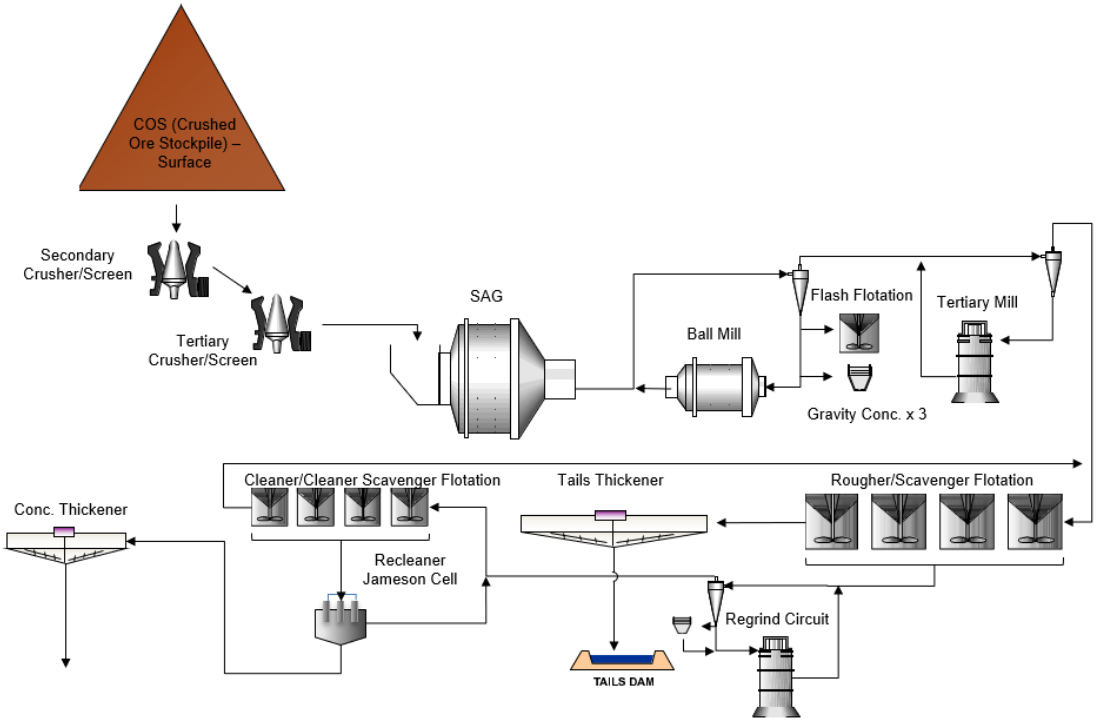



**FIG 1** – Concentrator 2 process flow sheet between 2017 to 2022.

Between 2018 and 2022 the average grind size from the comminution circuit was 80 per cent passing 140 micron ($P_{80}$ 140 µm) and the flotation feed grade was 0.35 to 0.4 per cent copper. Rougher-scavenger concentrate was 100 per cent reground to a nominal $P_{80}$ of 25 µm, achieving approximately 80 per cent Au recovery and 86 per cent copper recovery at 27 per cent copper concentrate grade. The size by liberation of copper sulfide minerals within Concentrator 2 final tails from this period is presented in Figure 2, which shows a typical distribution of composite coarse to intermediate particles and liberated fines losses. This is typical of many flotation plants, and has been well cited in the literature as the 'elephant curve' first published by Lynch *et al* (1981).

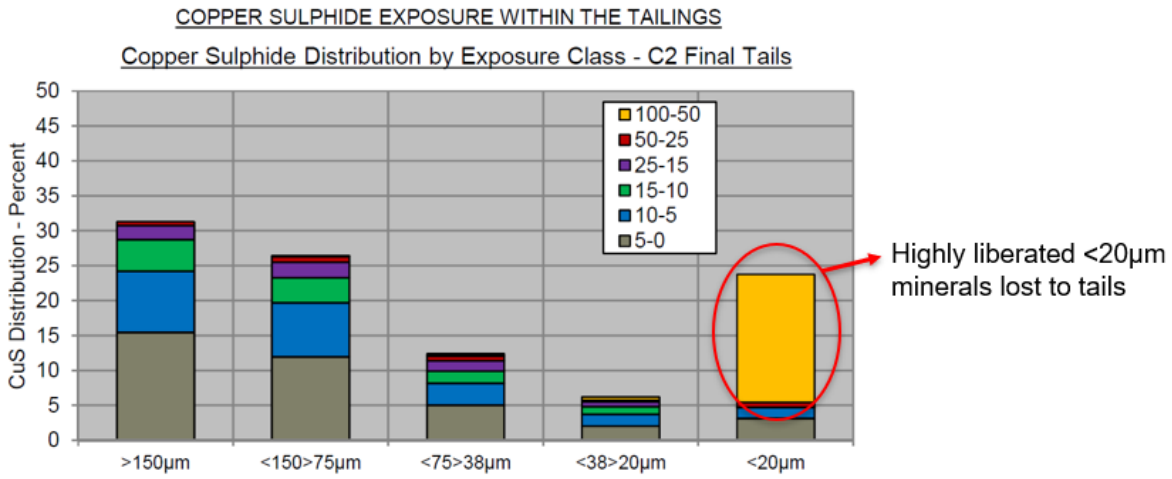



**FIG 2** – Size by liberation of Concentrator 2 copper sulfides in final tails – 2019. Note: Exposure refers to the percentage of a copper sulfide bearing particles' two-dimensional surface that is exposed copper sulfide mineral.

The Cadia Expansion Project (CXP) completed all feasibility studies to expand the underground mine in 2019 and the processing plant in 2020. The objective of the feasibility study was to extend the current mine life, increase the annual tonnes mined and milled and increase overall metal recoveries. The pathway defined from the feasibility for Concentrator 2 was more conventional when compared to Concentrator 1. Note that Concentrator 1's expansion will not be discussed in this paper. Concentrator 2 was tasked with increasing annual throughput by 30 per cent through additional comminution power whilst maintaining metal recovery and copper concentrate grade in line with pre-expansion levels. Rougher flotation residence time was seen as the largest constraint to maintaining or uplifting recovery, as the conventional circuit was operating with a residence time of 17 mins. Without any additional roughing capacity, the residence time was expected to drop as low as 11.7 mins, equivalent to a predicted 1.6 per cent recovery loss. Any countermeasure to recovery loss was required to fit within a constrained brownfield environment. Additional tank cells were not preferred due to the site layout restrictions. Jameson Cell technology was seen by Cadia as a viable alternative to conventional tank cells and better suited to the area limitations.

Maintaining concentrate quality was a key design consideration throughout the expansion project. While copper concentrate grade itself was not a significant constraint, the recovery of fluorine-bearing gangue minerals to final concentrate required careful management. Consequently, the objective was not simply to maintain copper and gold recovery, but to achieve this while preserving concentrate quality through effective fluorine rejection. Froth washing of streams reporting to final concentrate therefore remained a critical requirement in the evaluation, selection, and application of flotation technologies.

In order to better understand the opportunities to improve recovery of fine copper and gold bearing minerals, key streams were surveyed in 2019 for detailed mass balancing and mineralogical analysis. In addition to assisting with detailed design of the Jameson Cell installation, a further objective of the survey was to look for opportunities to increase mass pull in the rougher-scavenger circuit to improve circuit recovery and better utilise available capacity in the cleaning circuit. The circuit configuration at that time consisted of rougher-scavenger concentrate, regrind mill discharge and cleaner scavenger concentrate reporting to the regrind cyclone feed hopper. A key focus of the survey was to better understand the particle size and liberation of the cleaner scavenger concentrate and whether there was benefit gained by directing it to the regrind circuit.

This paper details the Jameson Cell piloting and laboratory investigations, equipment design, commissioning observations and results from the first few years of operation. The paper also details the test work, equipment selection, and commissioning outcomes associated with the cleaner scavenger concentrate redirection.

# LABORATORY AND PILOT TEST WORK

## Rougher Jameson Cell

### *Pilot testing*

A pilot campaign was conducted at Cadia on Concentrator 2 flotation feed between August and September 2018 using the L500 pilot Jameson Cell. 55 separate surveys were completed with 31 tests using froth washing and 24 without froth washing. The pilot testing results are detailed in Figures 3 and 4; demonstrating concentrates of final grade quality (26 per cent+Cu) can be produced in a single stage of flotation from the feed stream at ~120–140 µm $P_{80}$ and 0.35–0.40 per cent copper. Froth washing showed a distinct influence, maximising concentrate grade by minimising entrainment.

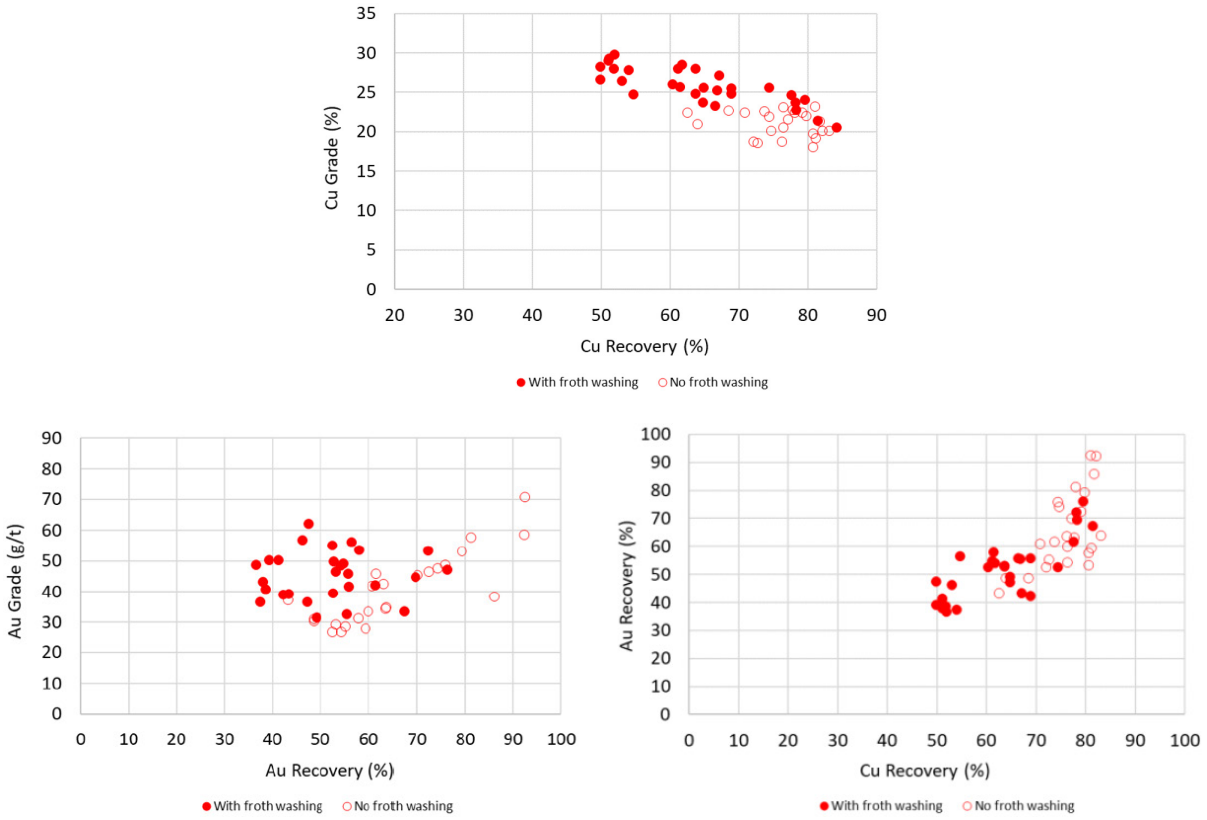



**FIG 3** – L500 pilot results – copper and gold.

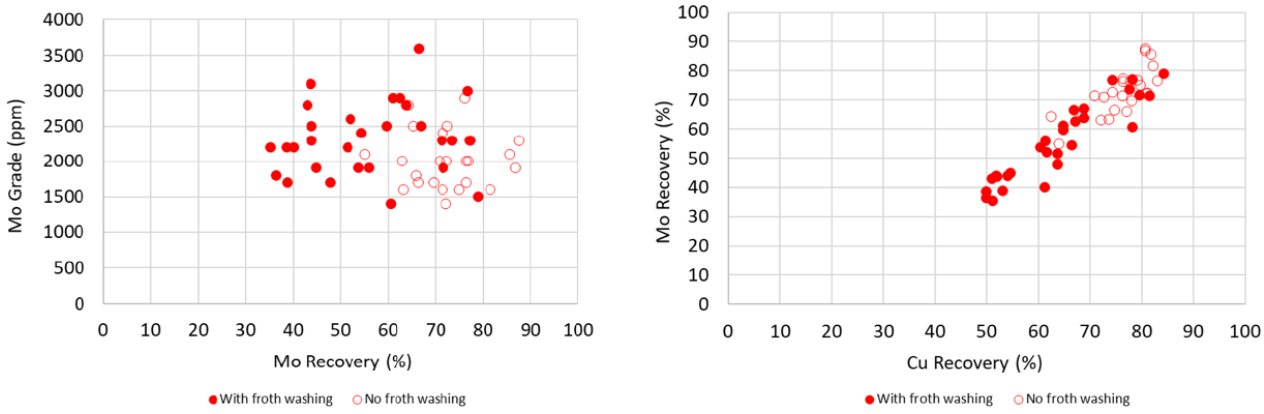



**FIG 4** – L500 pilot results – molybdenum.

The results indicate that sufficient liberated copper sulfide minerals are present in the rougher flotation feed at the nominal primary grind target of 140 µm. The findings from pilot testing were advantageous to design as they provided the justification for an option to operate the Rougher Jameson Cell in a scalper duty as an alternative to conventional roughing, theoretically improving fines recovery by removing the potential for fines to build-up as a recirculating load within the conventional cleaning circuit and possibly being lost to tails because of surface oxidation.

In addition to the Jameson Cell, a Concorde Cell was also piloted on Concentrator 2 feed material. While the Concorde Cell demonstrated promising performance, the Jameson Cell achieved a stronger overall grade-recovery response under the tested conditions. Based on the pilot data and site operating experience, the Jameson Cell was put forward as a preferred technology to provide extra roughing capacity across the rougher/scavenger bank.

Notable from the pilot test work was the molybdenum recovery and the selectivity with copper, attributed to the high mixing intensity and small bubble size characteristic of the Jameson Cell technology (Jameson, Harbort and Riches, 1991).

The Cadia East Ore is known to be a disseminated orebody with a relatively fine median copper sulfide grain size of 50–100 µm (Figure 5). Future panel caves (PC) PC1–2 and PC2–3 are observed to have finer median copper sulfide mineralogy than the current production caves PC1–1 and PC2–1|2. Therefore, the ability to operate in either scalping or roughing mode based on the feed characteristics of the ore was incorporated into the flow sheet design.

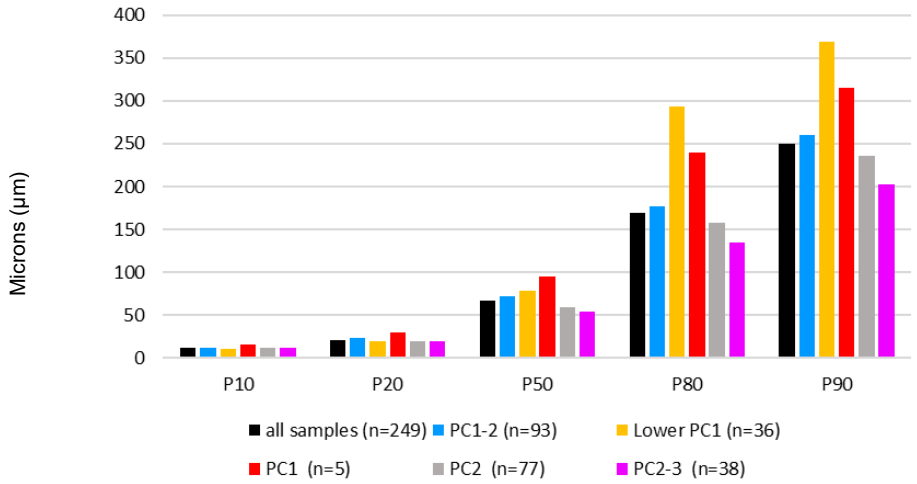



**FIG 5** – Median copper sulfide grain sizes – Cadia East deposit by panel cave.

## *Laboratory testing*

A laboratory test work program was executed in 2020 during the project feasibility phase to further understand the ore characterisation and flotation response. Concentrator 2 flotation feed samples, gathered over a number of plant conditions, were exposed to both size by assay shown in Figure 6 and size by mineralogical analysis (although optical mineralogy below 11 µm was not pursued on these samples). Key findings from the investigations were:

- The Concentrator 2 flotation feed contained 30–40 wt per cent -11 µm particles. 90 per cent of observed chalcopyrite and bornite grains were fully liberated in the -20 µm +11 µm size fraction.
- It is likely therefore that the -11 µm size fraction would exhibit similar levels of copper sulfide mineral liberation.

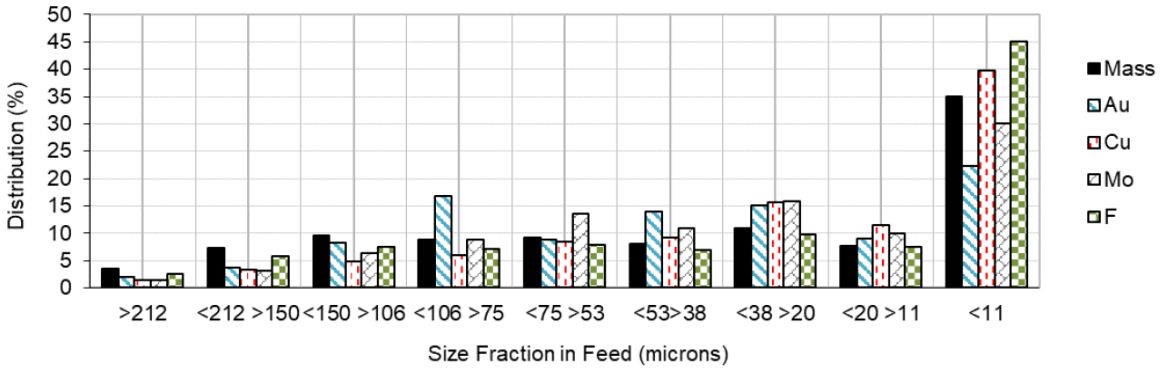



**FIG 6** – Size by assay distribution of Concentrator 2 rougher-scavenger feed.

Locked cycle dilution cleaning laboratory flotation tests were performed on the samples of Concentrator 2 rougher-scavenger feed. Dilution cleaning tests 'simulate' the impact of froth washing on the final concentrate. The results of the dilution cleaning tests are detailed in Figure 7. The grade recovery curve observed supports the pilot and optical mineralogical observations that a portion of the rougher-scavenger feed has sufficient liberated copper sulfides present to support a rougher-scalper option. Above the 70 per cent recovery point, the grade/recovery curve dips sharply,

indicating that further recovery to final concentrate requires regrind of the remaining insufficiently liberated copper sulfide particles.

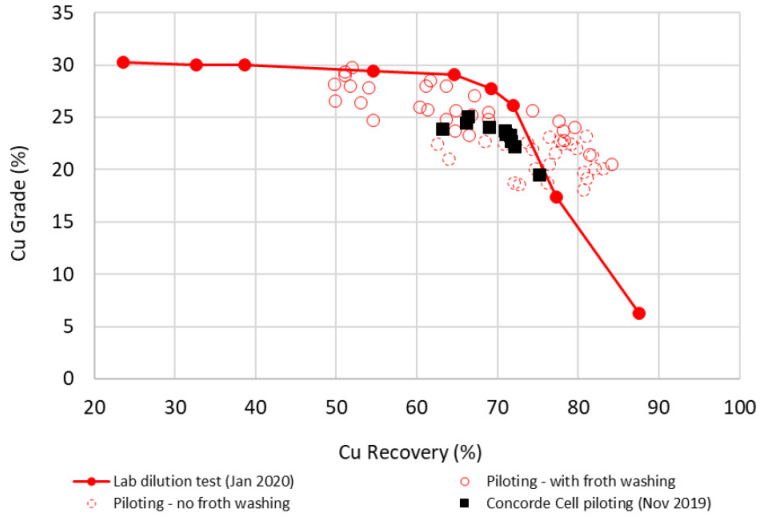



**FIG 7** – Laboratory dilution cleaning results (2020) overlaid on Jameson Pilot (2018) and Concorde Pilot (2019).

## Cleaner scavenger concentrate redirection

### *Mineralogical testing*

During the 2019 survey, detailed mineralogical analysis was conducted on the cleaner scavenger concentrate stream. The goal of this analysis was to better understand liberation characteristics of the concentrate and determine if there were any benefits to additional regrinding. The results shown below in Figure 8 highlight two important things:

1. A high proportion (80 per cent) of the copper sulfides in the concentrate were fully liberated.
2. The $P_{80}$ of the concentrate was less than 13 µm.

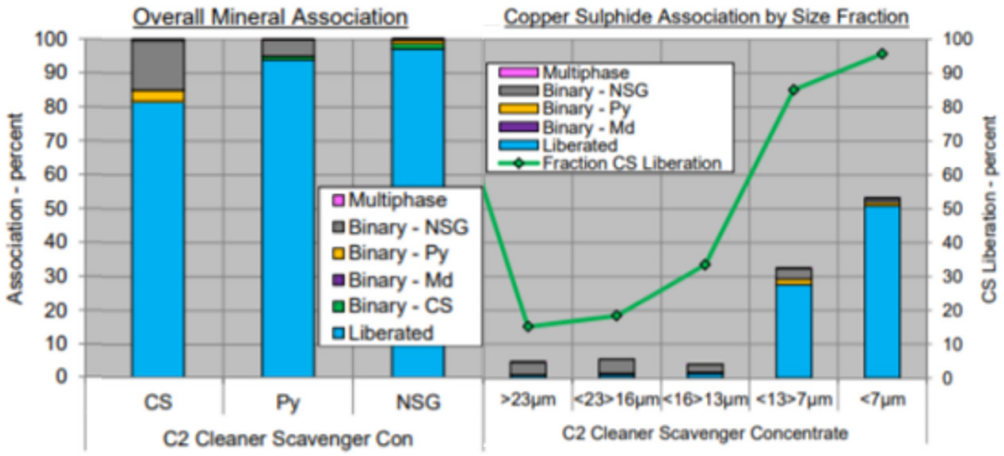



**FIG 8** – Liberation of the cleaner scavenger concentrate in Concentrator 2.

Additionally, from the circuit mass balance at the time, it was determined that 60 $m^3$/hr of cleaner scavenger concentrate was reporting to the regrind cyclone feed hopper. Through redirection of this stream, mass pull from the roughers could be increased by 60 $m^3$/hr resulting in an increase in both gold and copper recovery.

## Rougher Jameson Cell

The design for a rougher or rougher scalper Jameson Cell was based on pilot data and benchmarked against other operations pilot data through the equipment vendor. The Concentrator 2 pilot data and liberation characteristics of the feed material show it is possible to produce concentrate of final grade quality, as there are sufficient liberated particles present in the feed stream. It was concluded that, in the case of Jameson Cells, final concentrate quality is independent of head grade and dictated only by the amount of liberated, valuable mineral in the stream. The upgrade ratios defined for design were 70 and 93 for rougher and rougher scalper respectively, based on a feed grade of 0.30 per cent Copper. The design point of the rougher and rougher-scalper duty points is as defined in Figure 9 and Table 1.

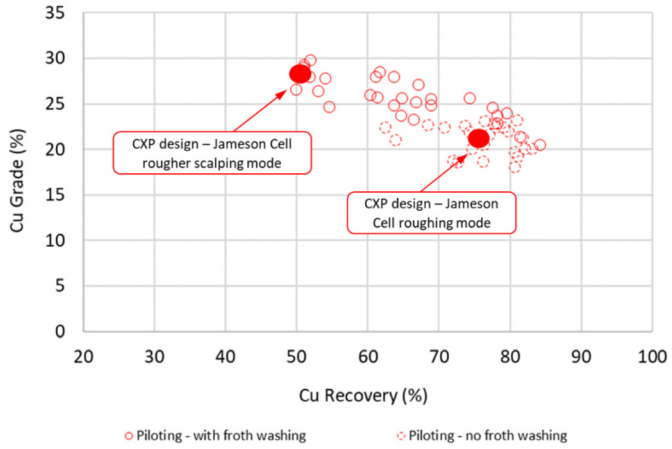



**FIG 9** – Concentrator 2 rougher Jameson Cell design points.

**TABLE 1**

Design point for the rougher Jameson Cell.

| Description | Fresh feed | Downcomer feed | Feed grade | Froth carry | Concentrate grade | Recovery | Recovery |
|---|---|---|---|---|---|---|---|
| Units | dt/h | % Solids (w/w) | % Cu | t/h/m$^2$ | % Cu | % Cu | % Mass |
| Rougher | 1255 | 35 | 0.30 | 0.50 | 21 | 75 | 1.1 |
| Rougher-Scalper | 1255 | 33 | 0.30 | 0.25 | 28 | 50 | 0.5 |

The Jameson Cell in a rougher duty was not considered novel, with multiple published cases of rougher duty Jameson Cells in metalliferous operations since 1997 (Pokrajcic *et al*, 2005). However, the Z8500 selected is the first-of-its kind integrated unit, combining the internal recycle from the 'E-Type' cells and the central distributor of the 'B-Type' cells. The Z-Type cell was selected due to the significant space constraints associated with the installation of new equipment. This presented novel hydrodynamic risks to the design in terms of internal froth/slurry separation characteristics. Computational fluid dynamics of the cell hydrodynamics were utilised to determine the acceptability of internal volume and surface area. The other notable difference is the large 500 mm downcomer, which can accommodate over 300 m$^3$/hr, compared to the conventional 280 mm Jameson downcomer ~90 m$^3$/hr flow rate. This is achieved through a larger internal orifice of 90 mm in the case of a 500 mm downcomer. No pre-screening was installed ahead of the rougher Jameson Cell, creating a potential risk of foreign material entering the cell from the upstream grinding circuit and causing blockages or equipment damage.

The physical size of the rougher Jameson Cell is dictated by the mass flow rate. Despite the relatively high mass feed rate, the low copper feed grades presenting to the rougher Jameson Cell result in low froth carry rates and lip loadings. This presented risks in terms of froth stability and control during

operation, however application of froth crowding was considered practicable, if required, during operation. The general arrangement, as shown in Figure 10, was approved and ordered for construction on the basis as this paper has discussed.

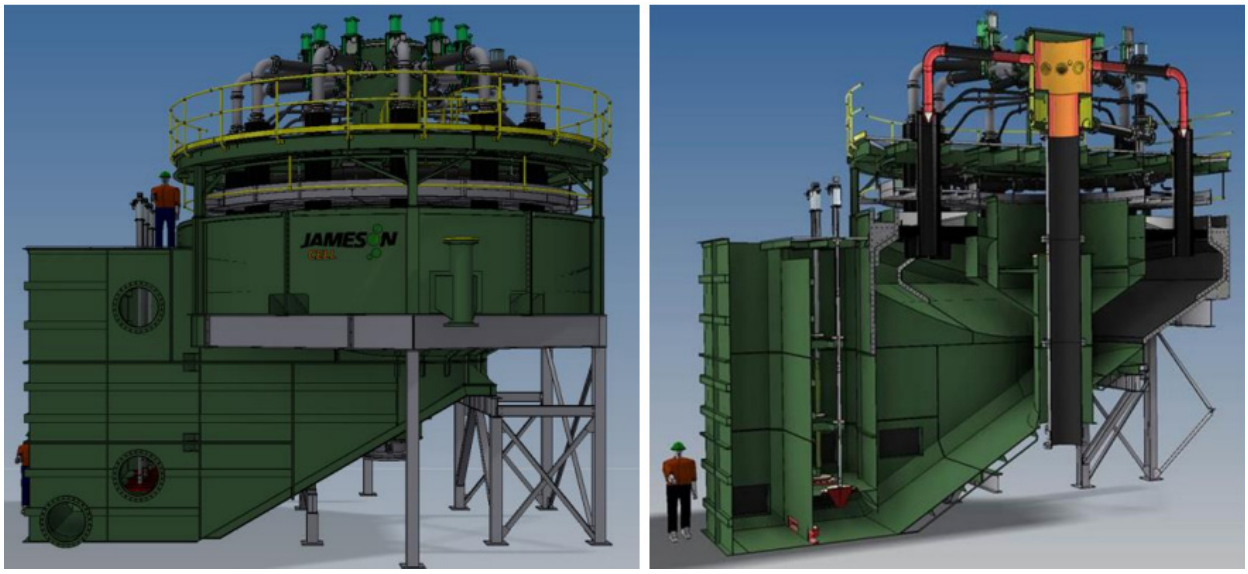



**FIG 10** – Z8500/12 Jameson Cell.

## Cleaner scavenger concentrate

At the time this project was initiated, cleaner scavenger concentrate was gravity fed into the regrind cyclone feed hopper. However, to send this material to the final stages of cleaning, a new hopper, pumps, piping and additional valves were required. This meant a significant amount of capital was required and due to the benefits of the project being marginal when compared to CXP, design and execution of the cleaner scavenger concentrate redirection was delayed.

As part of CXP, many pump and hopper upgrades were required. As a result of these brownfield upgrades, the old Concentrator 2 regrind cyclone feed hopper and some redundant final concentrate pumps were able to be repurposed for this project. This significantly reduced the capital costs and payback period for the project.

The decision was made to have the option to either send the cleaner scavenger concentrate to the recleaner bank or the final cleaner Jameson Cell. This allowed operational flexibility to control concentrate grade, with the material able to be cleaned twice (recleaners then Jameson Cell) or once (straight to the Jameson Cell). The option to return this material to the new regrind cyclone feed hopper was also maintained in the event there was unplanned downtime on the new cleaner scavenger concentrate transfer system. After multiple challenges and delays the cleaner scavenger concentrate project was fully commissioned in mid-2023.

As of November 2023, the Concentrator 2 flotation flow sheet in Figure 11 was specifically targeting fine liberated particles by the novel application of flotation technologies and key process stream changes.

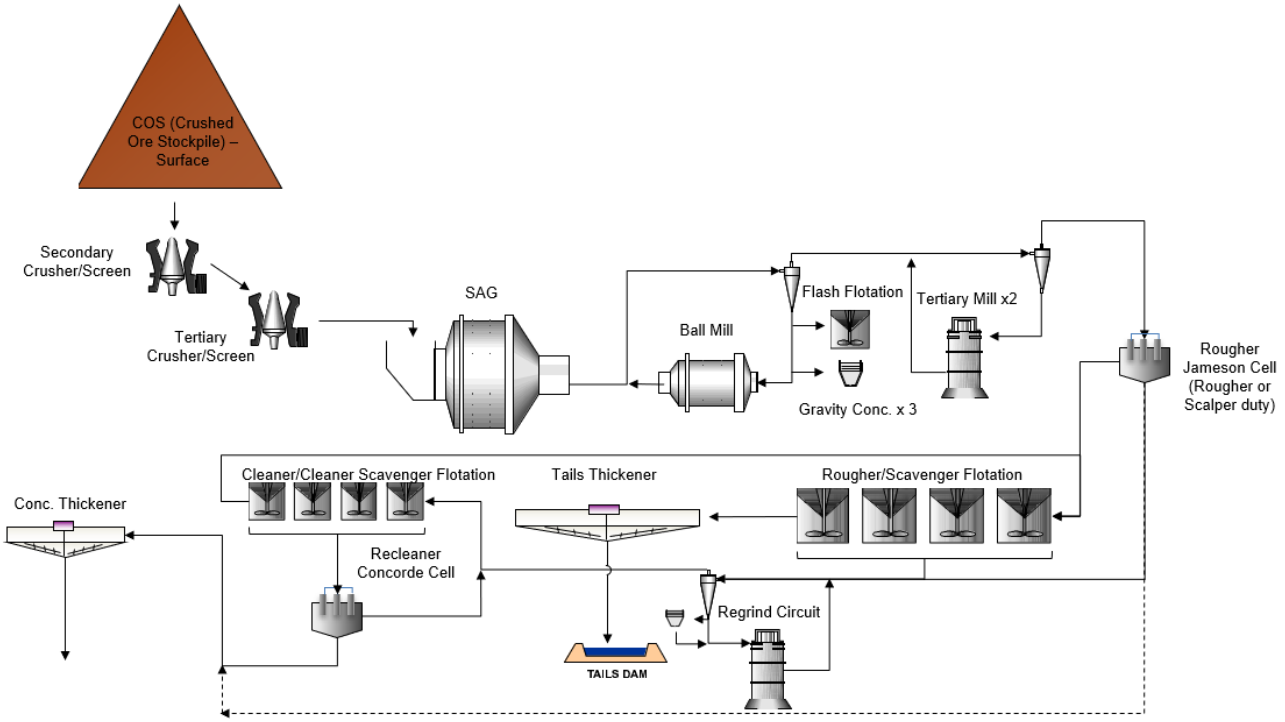



**FIG 11** – Concentrator 2 process flow sheet post Cadia Expansion Project and CSC commissioning 2023.

# OPERATIONAL RESULTS

## Rougher Jameson Cell

The Rougher Jameson Cell was commissioned at Cadia, producing first concentrate in September 2022. The cell has operated at design utilisation right from commissioning and its grade/recovery performance is presented in Figure 12. The Z8500/12 proved robust at making target concentrate grade in the rougher duty, but not in achieving the recovery observed during piloting. This was hypothesised to several operational, mechanical and metallurgical shortcomings, which this paper will expand on and how they were planned to be overcome. Whilst the Jameson Cell itself has underperformed, the overall circuit has achieved the required recovery, and therefore any shortcoming has been made up in the conventional rougher-scavenger circuit. This can be seen below in Figure 13.

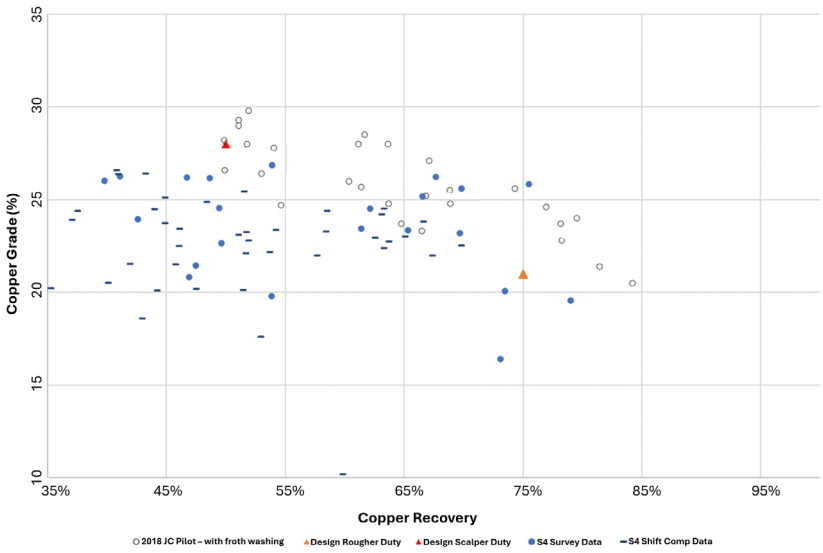



**FIG 12** – Rougher Jameson Cell commissioning copper grade-recovery data.

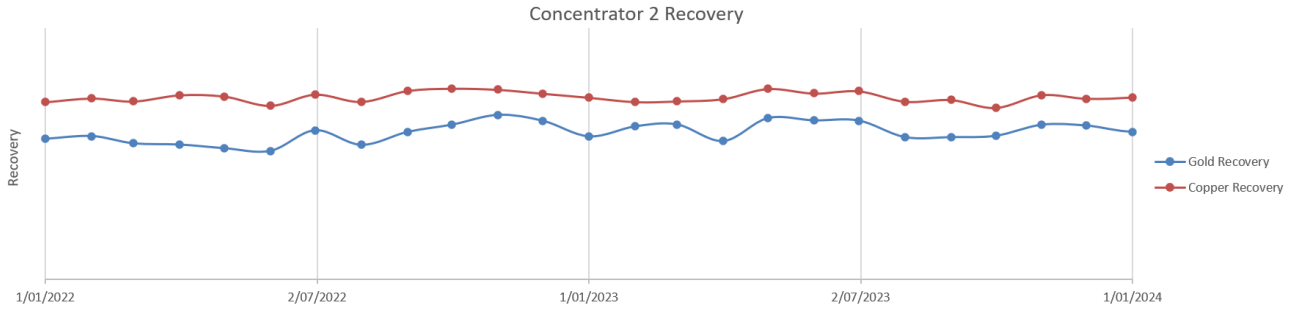



**FIG 13** – Concentrator 2 recovery pre- and post-commissioning of the rougher Jameson Cell.

### *Metallurgical benchmarking survey data*

In mid-2023, two full benchmarking surveys were completed on the Concentrator 2 flotation circuit. The surveys were designed to compare the overall plant performance, on a size by recovery basis, for the two design cases; rougher-scavenger and rougher-scalper. Size by assay mass balanced results of the Rougher Jameson in Rougher mode are shown below in Figure 14. Recovery in the coarser size fractions was poor as expected, however the poor recoveries observed in the fine size fraction (-5 µm) were not expected. The grade achieved is inline with design; therefore, the reduction in recovery is either due to less available liberated fines in the feed, a surface chemistry issue or an issue inherent to the operating conditions of the full scale Z8500/12 cell. Overall copper and gold recoveries observed in the rougher Jameson Cell are highlighted in Table 2.

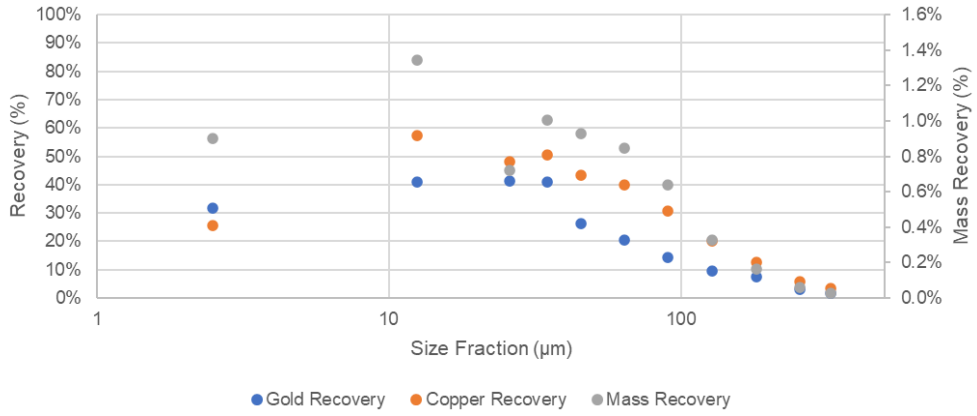



**FIG 14** – Gold and copper recoveries by size for the rougher Jameson Cell.

**TABLE 2**

Design versus actual recoveries and concentrate grades for the rougher Jameson Cell (August 2023 survey).

| | Cu recovery (%) | Cu grade (%) | Au recovery (%) | Au grade (g/t) | Concentrate percent solids (%) |
|---|---|---|---|---|---|
| Design | 77 | 21 | 66 | 22.2 | 40 |
| Actual (rougher duty) | 38 | 20 | 27 | 23.7 | 28 |
| Actual (scalper duty) | 25 | 22 | 23 | 27.3 | 20 |

Comparing the feed metal distributions in all size fractions helps to understand if the grain distribution has changed. Comparing Figure 6 and Figure 15 show that there has been an increase in the amount of flotation feed gold and copper in the coarser size fractions (>212 µm) and marginally less reporting to the slimes (-11 µm). However the proportional reduction in metal contained within the <11 µm fractions does not account for the recovery variance to design. Therefore the reduction in

recovery is not due to a change in feed distribution alone. Additional factors contributing to the below design recovery are discussed further in the Operational Learnings and Corrective Actions section.

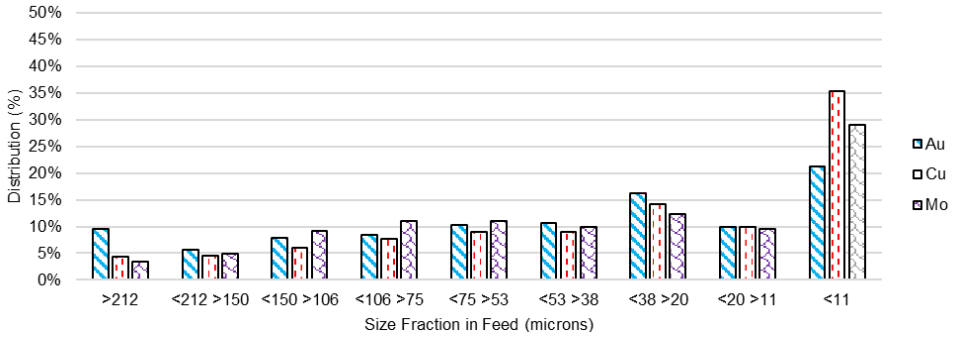



**FIG 15** – Size by assay distribution of Concentrator 2 rougher-scavenger feed (August 2023 survey).

Mineralogy was completed on the Rougher Jameson concentrate from the August 2023 survey. The copper liberation was seen to decrease with increasing size fraction. Recovery of copper sulfide particles in the +60 µm size fraction was seen to significantly decrease the grade of the concentrate. The recovery of composite particles indicated that the concentrate could be reground to improve copper sulfide liberation, supporting operation of the cell in a rougher duty as opposed to a scalper duty.

## *Operational learnings and corrective actions*

### Lip loading, froth carry rates versus design

It became apparent during commissioning that maintaining a consistent mass pull rate from the rougher Jameson Cell was a challenge. One key contributing factor was that the design lip loadings and froth carry rates were not being achieved, as detailed in Table 3. The main driver for not being able to achieve the design lip loadings and carry rates was the large surface area of the cell along with difficulties maintaining a stable froth phase. The lip loading of the cell was successfully improved with the addition of lip extenders, however the froth carry rates were still significantly lower than design. A 40 per cent increase in frother consumption was observed post installation of the rougher Jameson Cell, with approximately 75 per cent of the total flotation circuit frother dosed to the rougher Jameson Cell.

**TABLE 3**

Rougher Jameson Cell design versus actual concentrate flows, lip loadings and froth carry rates.

| | Design | Actual | Actual (with lip extenders) | Actual (with crowders and lip extenders) |
|---|---|---|---|---|
| Concentrate flow (t/h) | 11.7 | 3–8 | 5–8 | 5–8 |
| Lip loading (t/m) | 0.15 | 0.04–0.11 | 0.16–0.25 | 0.16–0.25 |
| Carry rate (t/m$^2$) | 0.44 | 0.14–0.36 | 0.23–0.36 | 0.45–0.72 |

To improve the froth carry rates and reduce frother consumption in the rougher Jameson Cell, froth crowders were scoped and installed to assist with the transportation of the froth phase to the concentrate lips. In collaboration with the vendor, a downcomer clamped froth crowder design was developed and installed in February 2024, as shown in Figure 16. The froth crowders are designed to be adjustable, with a maximum reduction in froth surface by 50 per cent. The crowders have allowed the Jameson Cell to operate at deeper froth depth and reduced frother dosage rates.



**FIG 16** – Installed froth crowders in the rougher Jameson Cell.

### Density and air to pulp ratio versus design

The rougher Jameson Cell was designed to operate at an air to pulp ratio of 0.5 and a feed density of 35 per cent solids. To achieve this air to pulp ratio, approximately 2000 $m^3$/hr of air is required. It became apparent early after commissioning that achieving these air rates was not possible due to poor froth stability driven by the high froth carry area and low mineral loading. Froth crowding made a substantial improvement to the stability of the cell, however at high throughputs, feed densities of over 40 per cent solids were observed in the Jameson Cell and violent boiling in the cell was seen when the air rates were increased too high. A contributing factor to the high densities in the cell was the choice to run the cell without wash water due to water distribution constraints, froth instability and nominal rougher duty. The boiling in the cell made consistent mass pull extremely difficult and reduced the grade of the concentrate. Blockages of the airlines to the downcomers on the rougher Jameson Cell are also seen to be a consistent problem during operating periods of low air-to-pulp ratios, due to very high vacuum pressures which induces slurry ingress to the downcomer's airline. This was made more operationally problematic by the ace valves being located at air distributor end of the downcomer supply airline.

These challenges with air-to-pulp ratio and subsequent lower cell superficial gas velocity are believed to be causing the below design recovery observed in the survey data shown. It is hypothesised that the rougher Jameson is not sufficiently recovering fines, as seen in Figure 14, due to below design air rates.

### Process control improvements

In addition to the froth crowders and lip extenders installed on the rougher Jameson Cell, a model predictive controller (MPC) was developed to maintain a consistent concentrate mass pull from the rougher Jameson Cell. The controller allows operators to enter a concentrate mass pull set point and the controller then will make gradual changes to frother, air addition and froth depth to maintain the target mass pull. The controller has been optimised to become less reliant on changing the frother dosage rate and instead focuses on driving mass pull via air and level changes.

When the decision was made to send the rougher Jameson Cell to the regrind feed hopper as the preferred operating strategy, the operational strategy around the rougher Jameson Cell changed. Instead of pulling a fixed concentrate mass to maintain a suitable grade, the strategy was to maximise concentrate production without overflowing the concentrate hopper. This led to an additional controller option being implemented labelled as maximise mode. Maximise mode works in the same way as the existing MPC controller, however instead of targeting a set mass pull, it

targets a fixed concentrate pump speed of 90–95 per cent. Figure 17 shows a histogram of the concentrate pull rates achieved with the various controller options.

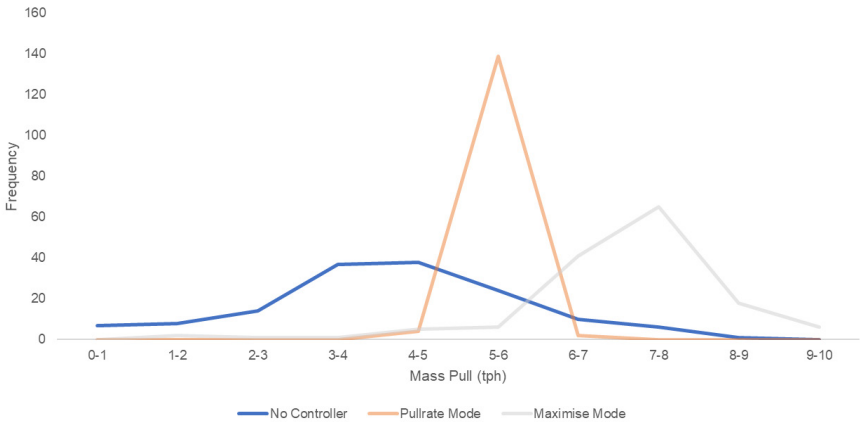



**FIG 17** – Performance of the various controllers on the rougher Jameson Cell.

## Mechanical design learnings

A critical operational issue was the repeated blocking of the slurry lens in the rougher Jameson Cell with large material due to upstream circuit issues. Approximately one year into operation, the clamping systems that held the slurry lens and pipework together started to detach during start-up. This resulted in a significant safety risk as the flexible mine hose feed pipes that formed part of the downcomers would uncontrollably move around releasing slurry into the air. The rubber shoulders on the pipework and slurry lenses, which the clamps secure against, had progressively delaminated over time. As a result, the clamps could no longer maintain a secure hold and would slip during start-up, causing the feed pipe to detach from the slurry lenses.

Designed by the site team, whip checks were installed on the rougher Jameson Cell as shown in Figure 18 to reduce the risk of downcomer and slurry lens detachment. The installation resulted in no further instances of feed pipes detaching from the slurry lenses. At the same time, Glencore Technology completed a review of the downcomer feed connection design. The original shouldered connection arrangement was subsequently replaced with a machined grooved pipe connection system incorporating Victaulic couplings. The revised design provides greater tolerance to piping deflection, improved resistance to connection damage and reduced risk of assembly-related failures.



**FIG 18** – Rougher Jameson Cell clamping arrangement.

### Operational strategy – scalper versus rougher

The Rougher Jameson Cell was installed with the option of being used as either a scalper or a rougher. The initial operational strategy was to send the concentrate to the final concentrate hopper as the cell was expected to recover fine liberated gold and copper minerals of a grade high enough to be sent directly to final concentrate.

However, Concentrator 2 struggled to meet its overall concentrate grade target. The root cause was determined to be the lower than design grade of the concentrate coming from the rougher Jameson Cell when operating as a scalper. Survey results showed that whilst the concentrate contained some fine liberated copper and gold particles, there was a significant amount of coarse particles in the concentrate, with much of this being entrained material. As discussed earlier, a multitude of operational and design issues made it difficult to run at high air rates to promote fine particle recovery, hence the decision was made to send the concentrate to the regrind feed hopper as the preferred operational strategy to maintain pre CXP concentrate grade targets.

T-test analysis of the rougher Jameson Cell operating modes showed that the tails grade achieved whilst operating as a rougher is lower than when using it as a scalper. Interestingly, the cleaner scavenger tails were significantly higher when utilised as a rougher, yet the final tails grade was lower. These numbers are shown below in Table 4. A recovery benefit of at least 0.31 per cent for Cu and 0.11 per cent for Au with 90 per cent confidence was calculated when utilising the rougher Jameson Cell as a rougher over a scalper. The benchmarking survey work completed in mid-2023 evaluated both the scalper and rougher operation of the Jameson Cell to provide insight as to why the circuit recovery was different however it was unclear from these results the driver for the difference. Given that better recoveries and final concentrate grades were achieved with the rougher Jameson Cell operating as a rougher-scavenger, this has been the preferred operating method to maximise the net smelter return at Cadia.

**TABLE 4**

Cleaner scavenger tails and final tails depending on the direction of the RJC concentrate.

| | Copper (ppm) | | Gold (g/t) | |
|---|---|---|---|---|
| Stream | Cleaner scav tails | Final tails | Cleaner scav tails | Final tails |
| Scalper | 1493 | 549 | 0.357 | 0.150 |
| Rougher | 2050 | 522 | 0.357 | 0.142 |

### Cleaner scavenger tails redirection

With the installation of froth crowders and lip extenders, the ongoing work around the rougher Jameson Cell was centred around being able to run the cell at its designed feed densities. With limited process water available to reduce the incoming density of the feed to the rougher Jameson Cell, alternative options to decrease the density in the cell were investigated.

The best solution to decrease the density in the rougher Jameson Cell was to return cleaner scavenger tails to the feed box of the cell. The cleaner scavenger tails in Concentrator 2 was originally closed to the head of the conventional roughers for reprocessing. Survey and routine plant data has consistently shown that this stream consists of fine, well liberated gold and copper particles at 12–13 per cent solids, ideal for reprocessing through the high intensity rougher Jameson Cell. By redirecting this stream to the rougher Jameson Cell feed box, a density reduction of approximately 5 per cent could be achieved, helping lower the feed density as close to design as possible without the need for additional water. A site led project was kicked off in late 2023 to complete this work.

In early 2025, the pipework connecting the cleaner scavenger tails to the rougher Jameson Cell was commissioned. It was evident early on after commissioning that the size of the recycle slots in the rougher Jameson Cell would have to be reduced to prevent the feed box overflowing. Once this issue was resolved, the cell was surveyed. The survey results showed that the new density in the rougher Jameson Cell was ~31 per cent, exceeding the initial target decrease to 35 per cent. The recovery results in Table 5 show that both gold and copper recovery increased significantly, as

expected with the lower cell densities, despite a substantial drop in feed grade since the previous survey was completed in 2023.

**TABLE 5**

Rougher Jameson Cell recoveries pre- and post-CST redirection.

| | Feed % solids (%) | Cu Recovery (%) | Cu Grade (%) | Au Recovery (%) | Au Grade (g/t) | Concentrate percent solids (%) |
|---|---|---|---|---|---|---|
| Design | 35 | 77 | 21 | 66 | 22.2 | 40 |
| Actual (rougher duty) | 40 | 38 | 20 | 27 | 23.7 | 28 |
| Post-CST redirection (rougher duty) | 31 | 56 | 19 | 43 | 18.6 | 27 |

## Cleaner scavenger concentrate redirection

The Cleaner scavenger concentrate redirection project was fully commissioned in November 2023. In the first 12 months post commissioning, the cleaner scavenger concentrate redirect had 97.3 per cent utilisation. This relieved pressure on the capacity of the regrind cyclone feed hopper, allowing the mass pull to be increased from the rougher-scavengers. Table 6 shows there was an increase in cleaner scavenger tails flow of ~55 $m^3$/hr post commissioning, reflecting the increase in rougher-scavenger concentrate flow that was gained with this change. Greater stability was also achieved in the cleaner scavengers with the implementation of a basic flow control loop that adjusts both level and air in the cells to achieve a target concentrate flow.

**TABLE 6**

Key stream flow data pre- versus post-commissioning of the cleaner scavenger concentrate redirection.

| | Cleaner scavenger tails ($m^3$/hr) | Cleaner scavenger concentrate ($m^3$/hr) |
|---|---|---|
| Pre-upgrade | 481.9 | ~55 |
| Post-upgrade | 536.4 | 89.4 |

One challenge faced when commissioning was the capacity of the darts in the first recleaner. A 20 $m^3$ tank cell, the darts didn't have the sufficient capacity to handle the additional flow of the cleaner scavenger concentrate. However, this issue was overcome by slightly modifying the cleaner scavenger concentrate pipework to feed the next three recleaner cells, a bank of 8 $m^3$ U shaped cells instead of the first recleaner cell. This change significantly helped with the froth stability, carry rates and lip loadings in the recleaner cells, improving the overall performance of the cleaning circuit.

## CONCLUSIONS

The new Z8500 cell from Glencore Technology was successfully commissioned and is now operating at Cadia. The cell has met its objective, which was to alleviate the impact of the flotation circuit residence time reduction to recovery following an uplift in throughput. Overall circuit recovery remains inline with the project design; with recovery underperformance in the Z8500 made up in the conventional circuit.

Achieving design operational parameters in the rougher Jameson Cell were not immediately possible following commissioning. Through the addition of lip extenders, froth crowders, process control improvements and density control, the rougher Jameson Cell now operates at its designed froth carry rates, lip loadings and feed density. Process water distribution was constrained; therefore, site pursued the redirection of the cleaner scavenger tails to the rougher Jameson Cell feed box as a dilution stream. These changes lifted metal recovery and concentrate grade closer to cells design.

Additionally, the fully liberated cleaner scavenger concentrate was successfully redirected to the downstream cleaning circuit, increasing the capacity in the regrind circuit and allowing an increase in mass pull from the rougher-scavengers and cleaner-scavengers.

## DISCLAIMER

This paper may contain interpretations, hypotheses, projections, and forward-looking statements that are subject to scientific variability, ongoing research, and inherent risks and uncertainties. The information presented reflects site-specific conditions and operational experience at the time of writing. The views, analyses, and conclusions expressed are those of the authors and are not intended to represent binding technical positions, standard practices, or future plans of Newmont or its affiliates. The content is provided for general technical discussion only and should not be relied upon for the design, operation, or performance of any facility or process.

## ACKNOWLEDGEMENTS

The authors would like the acknowledge to work of Campbell Haines, Glencore Technology, the team at the Julius Kruttschitt Mineral Research Centre (JKMRC), JKTech, Le Huynh and the Newmont operational, project and metallurgical teams who have contributed towards the planning, implementation, operation and optimisation of Concentrator 2. The authors would also like to thank Newmont for its support and approval to publish this paper.

## REFERENCES

Akerstrom, B, Seppelt, J, Walters, T, Bubnich, J and Seaman, D, 2018. Cleaner Circuit Optimisation at Cadia Operations, in Proceedings of the 14th Mill Operators' Conference (The Australasian Institute of Mining and Metallurgy: Melbourne).

Edmunds, R, Wilkens, M, Akerstrom, B and Haines, C, 2021. Debottlenecking of the Ridgeway Concentrator at Newcrest's Cadia Operation, in Proceedings of the 15th Mill Operators' Conference (The Australasian Institute of Mining and Metallurgy: Melbourne).

Jameson, G, Harbort, G and Riches, N, 1991. The Development and Application of Jameson Cells, in Proceedings of the Fourth Mill Operators' Conference (The Australasian Institute of Mining and Metallurgy: Melbourne).

Lynch, A J, Johnson, N W, Manlapig, E V and Thorne, C G, 1981. *Mineral and Coal Flotation Circuits: Their Simulation and Control* (Elsevier Publishing: Amsterdam).

Pokrajcic, Z, Harbort, G, Lawson, V and Reemeyer, L, 2005. Applications of the Jameson Cell at the Head of Base Metal Flotation Circuits, Centenary of Flotation Symposium (The Australasian Institute of Mining and Metallurgy: Melbourne).

# Advanced flotation solutions for Sepon – boosting concentrate grade and carbonate rejection in gold processing

*H Thanasekaran[1], G Huang[2], K Thammavong[3] and M Behre[4]*

1. Global Product Manager, Eriez, Epping Vic 3076. Email: homiet@eriez.com
2. Manager Technical Studies and Projects, Lane Xang Minerals Limited, Vientiane Capital, Laos. Email: huang.guozhi@lxml.la
3. Senior Plant Metallurgist, Lane Xang Minerals Limited, Vientiane Capital, Laos. Email: khamsing.thammavong@lxml.la
4. Technical Sales Director, Eriez, Epping Vic 3076. Email: mbehre@eriez.com

## ABSTRACT

The Sepon Gold Mine in Lao PDR undertook a flotation circuit optimisation program to improve concentrate quality by reducing carbonate (dolomite) reporting to the flotation concentrate while maintaining overall gold recovery. Although the installation of a regrind circuit improved mineral liberation, it also reduced cleaner flotation carrying capacity, resulting in lower cleaner recovery and increased carbonate entrainment. Following optimisation of the existing flotation circuit, additional flotation technologies were evaluated to address the remaining cleaner circuit limitations. Laboratory investigations followed by pilot-scale evaluations of the Eriez Cavitation Tube Column and StackCell technologies were undertaken under plant operating conditions to assess their suitability for improving flotation selectivity.

Laboratory and pilot-scale testing demonstrated that the Cavitation Tube Column rejected more than 70 per cent of the calcium contained in the rougher concentrate while maintaining stage gold recoveries of approximately 85–88 per cent. Parallel pilot trials comparing two-stage StackCell and existing two-stage Jameson Cells configurations showed that the StackCell circuit produced approximately twice the concentrate grade at comparable overall gold recovery while operating at lower mass pull and reduced concentrate calcium grade.

Based on the pilot outcomes, two Cavitation Tube Columns were installed as Phase 1 of the flotation circuit upgrade. Statistical evaluation of industrial operating data collected during six weeks of column operation (n = 75) and four weeks of offline operation (n = 47) confirmed measurable improvements in metallurgical performance. Phase 1 achieved approximately 15 per cent additional calcium rejection while maintaining overall flotation gold recovery within 1 per cent of baseline performance. Statistical analysis demonstrated a significant increase in final concentrate gold grade ($p < 0.001$) together with a significant reduction in overall calcium recovery to concentrate ($p < 0.001$), consistent with the trends observed during laboratory and pilot testing.

The Phase 1 results provided the engineering basis for approval of Phase 2 of the flotation circuit upgrade, comprising four StackCell units in the rougher flotation circuit together with an additional Cavitation Tube Column downstream of the regrind circuit. This paper presents the laboratory, pilot-scale and industrial operating results supporting the staged flotation circuit upgrade at Sepon and demonstrates the value of integrating laboratory investigations, pilot-scale validation and industrial verification when implementing flotation circuit modifications in complex gold processing operations.

## INTRODUCTION

Lane Xang Minerals Limited (LXML Sepon) operates the Sepon gold and copper operations located in the Vilabouly District of Savannakhet Province, Lao PDR. The geographical location of the Sepon mine is illustrated in Figure 1. Gold production was initiated in 2003, and more than 1.5 million ounces of gold doré have since been produced. Production was suspended in 2013 due to market conditions and other operational considerations. In June 2020, gold production was recommenced, marking the beginning of a new operational phase under Chifeng Gold.




**FIG 1** – Location of the Sepon Gold Mine and processing plant, Lao PDR.

To facilitate the restart and improve recovery from primary gold ores, significant investment was made in new processing facilities, including a flotation plant, an oxygen plant, and an elution and carbon regeneration circuit. Through these developments, the projected mine life has been extended by at least ten years.

The Sepon flotation plant was originally designed to process 1.5 Mt/a of ore. The comminution circuit is configured as a Semi-Autogenous Grinding (SAG) mill followed by a ball mill and a pebble-crushing circuit, with a target grind size of 80 per cent passing 53 microns. As shown in Figure 2, a new flotation plant was constructed and commissioned in 2020 to process carlin-type primary gold ore. The rougher flotation circuit is equipped with two Jameson Cells (E4232/10), each fitted with ten downcomers, and is followed by two 160 $m^3$ BGRIMM flotation cells. Combined concentrate from Jameson Cells J1 and J2 and rougher cells B03 and B04 reports to the cleaner Jameson Cell (J3), which produces the final flotation concentrate for transfer to the concentrate hopper.

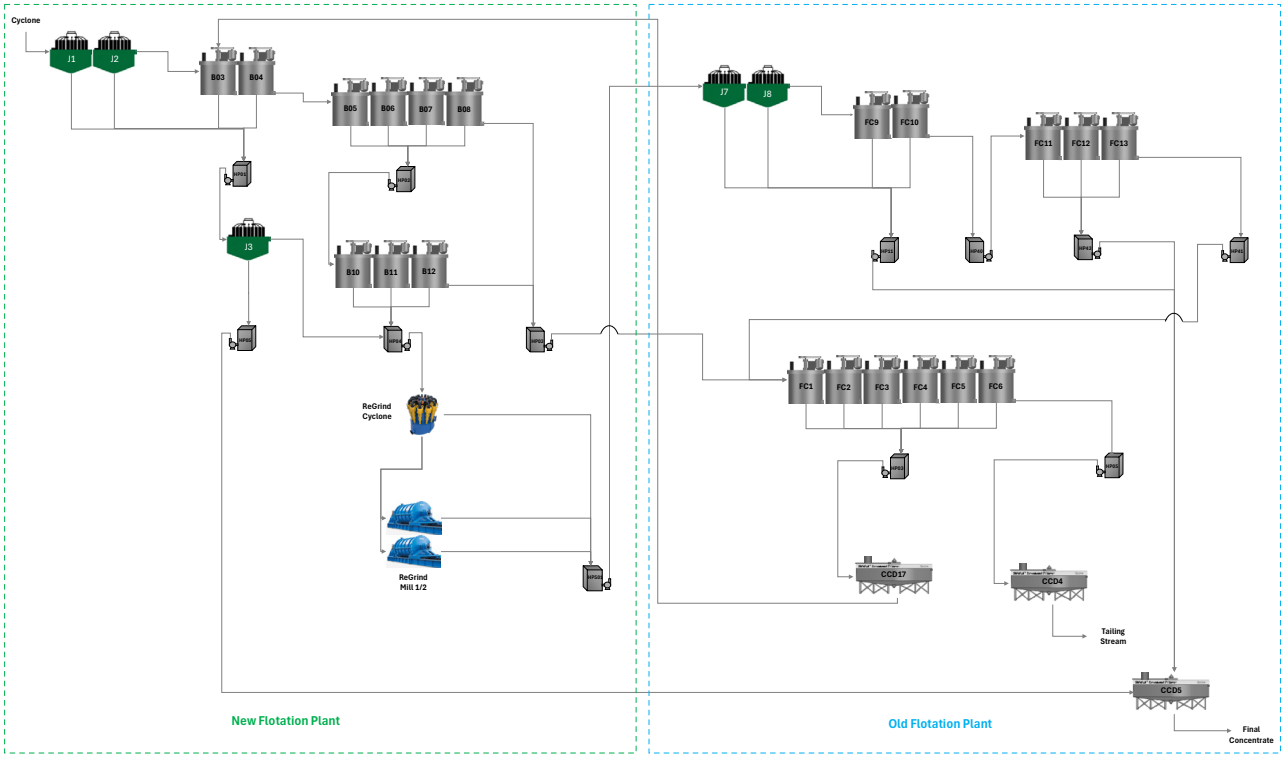



**FIG 2** – Sepon flotation process flow sheet for Carlin-type primary gold ore prior to the 2023 circuit modifications.

The old flotation plant was originally designed for processing primary copper ore; however, the regrind product from the new flotation plant continues to be treated through this circuit to provide additional cleaning capacity and improve gold recovery through increased residence time. The cleaner circuit consists of two Jameson Cells (E2514/3; J7 and J8), two Outotec OK-16 flotation cells (16 $m^3$; FC9 and FC10), and three Wemco 70 $m^3$ cells (FC11–FC13), which collectively generate the final concentrate stream. The cleaner scavenger circuit downstream of this is made up of six 70 $m^3$ Wemco cells (FC1–FC6).

## CLEANER CIRCUIT CONSTRAINTS

The increase in processing throughput from 1.8 Mt/a to 2.0 Mt/a has reduced the available residence time within the cleaner flotation circuit, resulting in diminished opportunity for selective attachment, detachment, and hydraulic classification processes to occur. Under these shortened flotation contact times, particles that would typically be rejected are instead retained in the slurry phase and more readily transported toward the froth interface.

At the same time, the higher throughput rate has imposed significant constraints on the froth phase, increasing froth loading and reducing overall selectivity. Elevated bubble crowding and suppressed drainage have increased water recovery into the concentrate, thereby enhancing the entrainment of fine hydrophilic gangue particles, most notably dolomite. These carbonate minerals do not float by true flotation mechanisms under standard operating conditions and are predominantly recovered through non-selective water entrainment. With insufficient froth residence time to permit adequate drainage, carbonate reporting to the concentrate has increased noticeably, directly contributing to higher impurity levels and elevated sulfuric acid consumption in downstream processing.

### Carbonate entrainment and downstream implications

Carbonate-rich concentrates generated under the current cleaner circuit operating conditions require substantial sulfuric acid addition during downstream processing, as the entrained dolomite reacts stoichiometrically with acid during oxidation and neutralisation stages. The elevated carbonate loading has caused acid consumption to escalate to a level that now dominates site operating expenditure, with the majority of reagent usage attributable to the decomposition of these gangue minerals rather than to the oxidation of sulfide sulfur. As a result, carbonate rejection within the flotation circuit has become a priority metallurgical objective, as improved removal of dolomite at the flotation stage has the potential to significantly reduce downstream reagent demand, lower operating costs, and improve overall process efficiency.

A recovery and gangue-rejection improvement initiative has therefore been undertaken by the processing technical team, with the following objectives:

- To retrofit the circuit with available flotation cells so that overall recovery and gangue-rejection performance can be enhanced.
- To increase the degree of mineral liberation within the cleaner circuit, thereby increasing gangue rejection, particularly the removal of carbonate minerals from the flotation concentrate.

### Implementation of the regrind mill circuit and its metallurgical outcomes

The study indicated that the installation of a regrinding circuit within the flotation circuit would enable significant carbonate rejection, with up to 40 per cent of carbonates predicted to be removed. Minor gold losses were estimated at 0–2 per cent, attributable to the presence of ultra-fine size fractions. A regrind mill circuit was installed in May 2024, with the objective of repurposing the former copper plant as a cleaner flotation circuit incorporating the two Jameson Cells. The flow sheet for the regrind flotation circuit is presented in Figure 3.

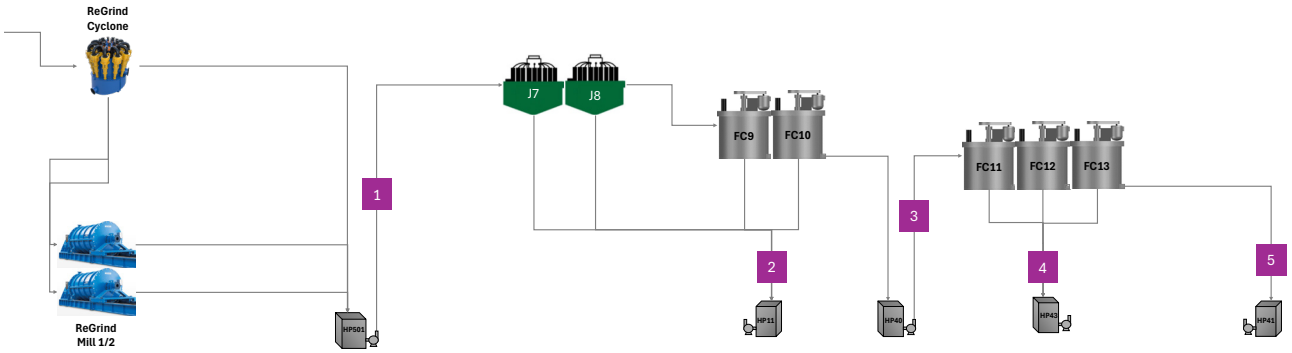



**FIG 3** – Regrind mill and cleaner flotation circuit implemented during the initial circuit upgrade.

The regrinding mill circuit was optimised to achieve a $P_{80}$ of 25–30 µm. Several plant surveys were conducted on both the regrind circuit and the modified cleaner circuit, with the resulting performance data presented in Table 1. Overall cleaner gold recovery was significantly lower than anticipated, with stage recoveries ranging from 55–70 per cent. At the global level, flotation circuit gold recovery also under-performed.

**TABLE 1**

Regrind mill circuit and cleaning circuit surveys.

| Survey 1 | 1 | 2 | 3 | Stage recovery, % | 4 | 5 | Stage recovery, % | Overall recovery, % |
|---|---|---|---|---|---|---|---|---|
| Au ppm | 2.91 | 11.75 | 2.03 | 36.6 | 6.56 | 1.15 | 52.8 | 70.1 |
| %Ca | 9.36 | 6.71 | 9.78 | 9.6 | 7.09 | 10.21 | 10.2 | 18.8 |
| %Mg | 4.60 | 3.25 | 4.69 | 4.4 | 3.41 | 4.98 | 13.3 | 17.1 |
| %Fe | 1.44 | 5.29 | 0.95 | 41.3 | 2.82 | 0.86 | 13.5 | 49.2 |
| %Org C | 0.49 | 1.37 | 0.35 | 37.4 | 0.97 | 0.22 | 47.4 | 67.0 |
| %S | 0.99 | 5.40 | 0.54 | 50.6 | 2.61 | 0.29 | 51.9 | 76.2 |
| %S_2 | 0.67 | 2.90 | 0.29 | 63.5 | 1.47 | 0.12 | 62.2 | 86.2 |

| Survey 2 | 1 | 2 | 3 | Stage recovery, % | 4 | 5 | Stage recovery, % | Overall recovery, % |
|---|---|---|---|---|---|---|---|---|
| Au ppm | 1.73 | 9.15 | 1.41 | 21.7 | 3.35 | 0.99 | 42.3 | 54.8 |
| %Ca | 11.72 | 7.51 | 12.01 | 4.2 | 9.55 | 12.59 | 15.2 | 18.7 |
| %Mg | 5.51 | 3.62 | 5.75 | 7.4 | 4.57 | 6.04 | 15.6 | 21.8 |
| %Fe | 1.07 | 4.57 | 0.78 | 32.5 | 1.71 | 0.66 | 25.4 | 49.6 |
| %Org C | 0.46 | 1.92 | 0.33 | 33.8 | 0.97 | 0.28 | 22.0 | 48.4 |
| %S | 0.79 | 4.42 | 0.41 | 52.6 | 1.65 | 0.31 | 29.9 | 66.8 |
| %S_2 | 0.47 | 2.36 | 0.23 | 58.0 | 1.14 | 0.16 | 34.6 | 72.5 |

The reduction in recovery was largely attributed to the loss of cleaning capacity following regrinding. As particle size decreased into the ultra-fine range, the available froth carry rate was substantially reduced for the same effective flotation surface area, as expected. Furthermore, selectivity within the cleaner circuit, particularly in the Jameson Cells, was below expectations. Laboratory flotation test work had indicated that enrichment ratios greater than six should have been achievable, with concentrate calcium grades of approximately 4.5 per cent. However, the plant circuit was operating

at enrichment ratios of five or lower, with calcium grades of approximately 7 per cent reporting to the concentrate stream.

## Technology evaluation strategy

The optimisation studies demonstrated that, although the regrind circuit substantially improved mineral liberation and reduced carbonate entrainment, the resulting increase in ultra-fine particles reduced the effective carrying capacity of the existing cleaner flotation circuit. Consequently, the anticipated improvements in cleaner recovery and concentrate quality were not fully realised under plant operating conditions. Further optimisation of operating parameters alone was therefore considered insufficient to overcome the remaining circuit limitations.

Following completion of the optimisation studies, a staged technology evaluation program was initiated to identify flotation technologies capable of improving cleaner circuit selectivity while maintaining overall gold recovery and integrating with the existing process flow sheet. The evaluation focused on technologies that could increase gangue rejection, particularly carbonate minerals, without requiring major modifications to the operating plant. Laboratory flotation investigations were first undertaken to establish the metallurgical potential of alternative separation approaches, followed by pilot-scale testing under representative plant operating conditions to validate metallurgical performance, operational stability and scale-up confidence prior to industrial implementation.

## Technology evaluation and pilot testing

Consistent with the technology evaluation strategy, laboratory flotation investigations were first undertaken on the Rougher 1 concentrate stream (HP01; Cells B03 and B04, collected from Hopper 1) and the cleaner scavenger concentrate stream (Cells B10, B11 and B12) to assess the potential for reducing dolomite content in the final flotation concentrate through an additional cleaning stage. The findings confirmed that up to three-quarters of the calcium contained in the rougher concentrate stream could be rejected, with only marginal reductions in stage gold recovery. The results of this test work are presented in Figure 4.

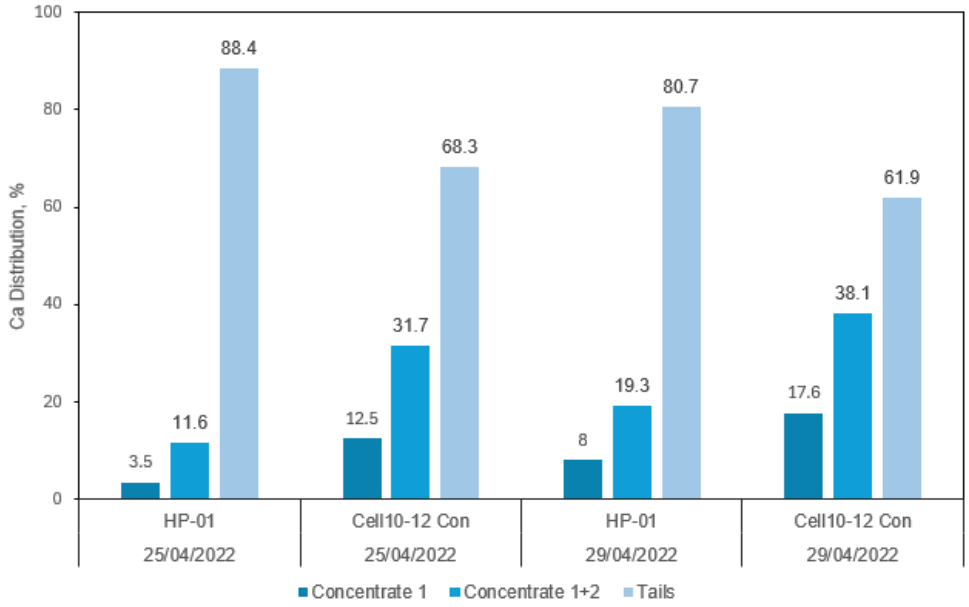



**FIG 4** – Laboratory flotation results showing calcium rejection from the rougher concentrate and cleaner-scavenger concentrate streams.

These laboratory results validated the potential to decrease the final concentrate mass by approximately 15 per cent, which would directly translate to a reduction in overall acid consumption. To further evaluate these results under site conditions, a 500 mm-diameter Cavitation Tube Column pilot unit was mobilised to site in late September 2022 for piloting on the Rougher 1 concentrate stream.

Pilot testing on the Cavitation Tube Column was conducted using the rougher concentrate stream to evaluate calcium rejection performance without compromising gold recovery. Additional on-site piloting was also undertaken on the plant's final flotation concentrate stream to further assess calcium removal capability. In parallel with the Cavitation Tube Column test work, the project team also evaluated StackCell technology for application at the front end of the rougher flotation circuit. StackCell technology was included in the evaluation because its high-intensity contacting environment and staged separation design have the potential to improve flotation kinetics and froth selectivity while operating at relatively short residence times. In addition, its compact configuration and ability to operate with deeper froth depths and wash water were considered advantageous for improving gangue rejection while integrating within the existing Sepon flotation circuit. The technology was therefore assessed for its suitability to improve early gangue rejection, reduce cleaner circuit loading, and maintain overall gold recovery under Sepon operating conditions.

The primary objective of this combined piloting program was to generate a final flotation concentrate with the lowest achievable calcium content, while simultaneously floating organic carbon as early as possible in the circuit and improving overall rougher block recovery. Recent plant survey data and laboratory test results confirmed that a final concentrate containing less than 3.5 per cent calcium could be produced from this stream; however, the existing Jameson Cells operating in this duty were unable to achieve this level of performance. To address this limitation, three StackCell pilot units were mobilised to site and operated in parallel with the Jameson Cells, with samples collected side-by-side for comparative evaluation.

A flexible feed arrangement for the pilot plant was implemented by utilising the multiplexer sample lines of the On-Stream Analyser (OSA) sampling system, or alternatively by drawing representative slip-stream samples from the pump discharge using in-line samplers. A hose pump (Flowrox LPP-T40) equipped with a variable-speed drive (VSD) was used to transfer material from a mixing tank to the pilot column and to control the feed flow rate to achieve the required residence time. A similar feed and pumping arrangement was employed for the StackCell pilot unit.



**FIG 5** – Cavitation Tube Column pilot plant installation (left) and StackCell pilot units with feed tank (right).

## CAVITATION TUBE COLUMN AND STACKCELL PILOTING RESULTS AND DISCUSSION

### Cavitation tube column pilot plant on plant Rougher 1 concentrate stream

A total of 58 pilot tests were completed using both the plant Rougher 1 concentrate stream and the plant final flotation concentrate stream. The performance of the Cavitation Tube Column treating the Rougher 1 concentrate is presented in Figures 6 and 7. Approximately three-quarters of the calcium contained in the Rougher 1 concentrate was rejected, consistent with the earlier laboratory-scale investigations. Under optimised operating conditions, stage gold recoveries of approximately 85 per cent were achieved while rejecting more than 70 per cent of the calcium reporting to the concentrate stream.

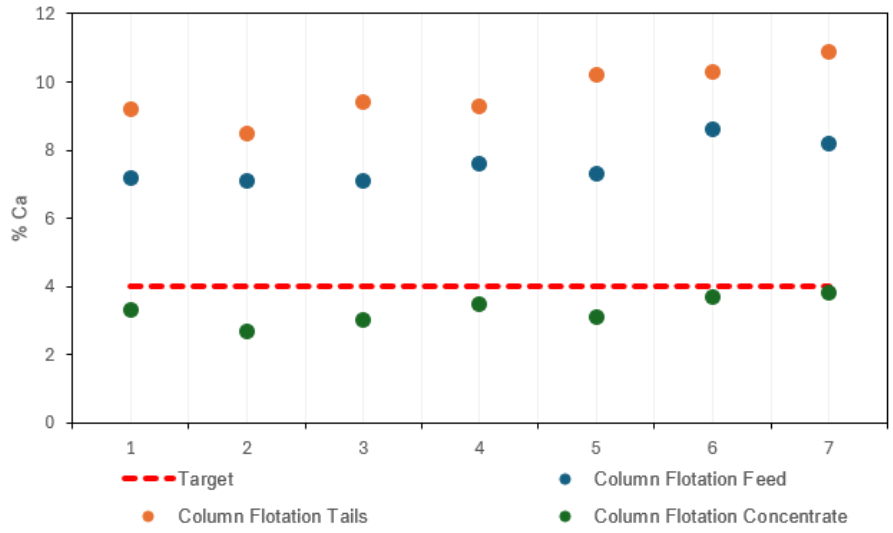



**FIG 6** – Cavitation Tube Column pilot performance treating the Rougher 1 concentrate stream (HP01), based on shift composite samples.

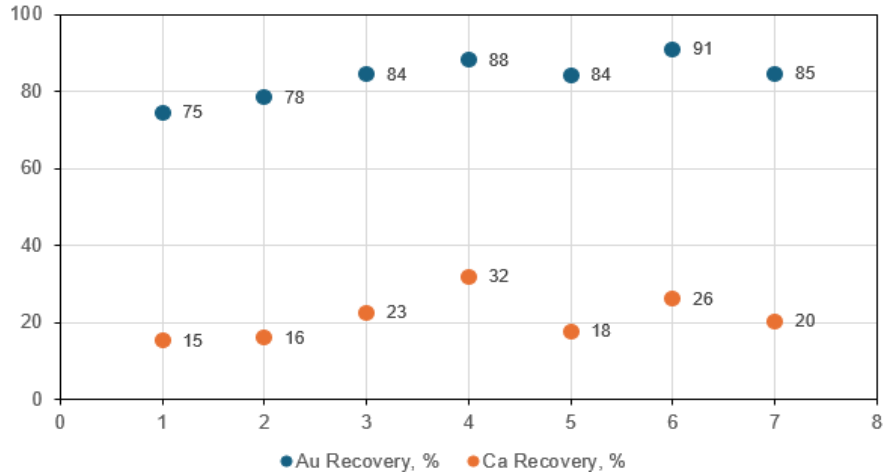



**FIG 7** – Gold and calcium recoveries achieved by the Cavitation Tube Column pilot treating the Rougher 1 concentrate stream (HP01).

The improved separation performance is considered to be primarily associated with the deep froth zone and wash-water addition employed during pilot operation. These operating conditions promote froth drainage and reduce the hydraulic entrainment of fine carbonate gangue particles while maintaining the recovery of hydrophobic gold-bearing sulfide particles through true flotation. Consequently, significant calcium rejection was achieved without a corresponding reduction in stage gold recovery, indicating that the improvement resulted from enhanced flotation selectivity rather than indiscriminate mass rejection.

The average pilot plant assays are summarised in Table 2. The concentrate calcium grade was reduced to approximately 3.5 per cent, representing a substantial improvement in concentrate quality while reducing the carbonate load reporting to downstream processing. The close agreement between the laboratory and pilot-scale results provided confidence that the observed metallurgical improvements could be reproduced under continuous plant operating conditions, supporting progression to industrial implementation.

**TABLE 2**

Balanced performance of Cavitation Tube Column pilot plant on plant Rougher 1 concentrate from HP01.

| Products | Au | Ag | S2- | S | Ca | Mg | Mass | Recovery, % | | |
|---|---|---|---|---|---|---|---|---|---|---|
| | g/t | g/t | % | % | % | % | % | Au | Ca | Mg |
| Feed | 12.2 | 10.2 | 3.0 | 3.9 | 7.4 | 3.2 | 100.0 | 100.0 | 100.0 | 100.0 |
| Concentrate | 20.1 | 14.5 | 5.1 | 6.6 | 3.4 | 1.5 | 51.3 | 84.8 | 23.9 | 24.4 |
| Tails | 3.8 | 5.7 | 0.8 | 1.1 | 11.5 | 5.0 | 48.7 | 15.2 | 76.1 | 75.6 |

## Cavitation tube column pilot plant on plant final concentrate stream

Figures 8 and 9 present the performance of the Cavitation Tube Column when treating the plant final flotation concentrate stream. Unlike the Rougher 1 concentrate evaluation, this test assessed the ability of the technology to upgrade an already cleaned concentrate by further rejecting entrained carbonate gangue while maintaining valuable mineral recovery. Approximately 50 per cent of the calcium contained in the final concentrate stream was rejected, while a stage gold recovery of approximately 88 per cent was achieved across the composite samples.

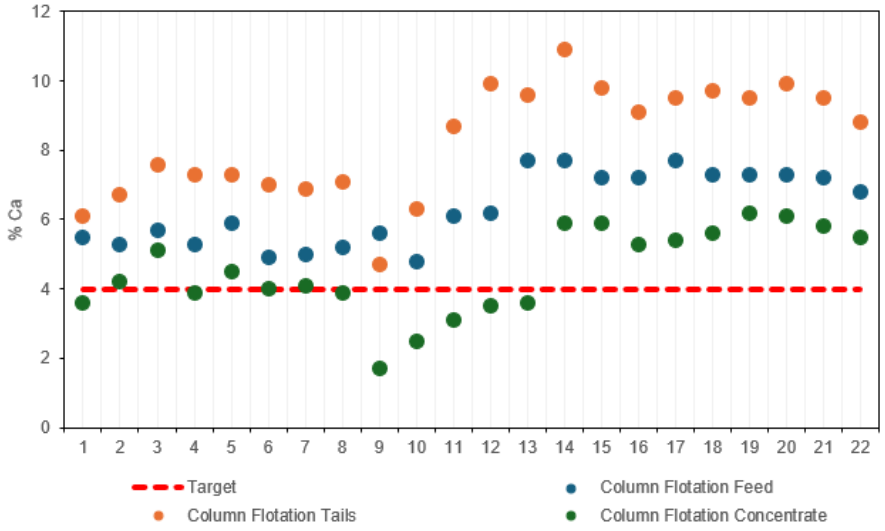



**FIG 8** – Cavitation Tube Column pilot performance treating the final flotation concentrate stream (HP05), based on shift composite samples.

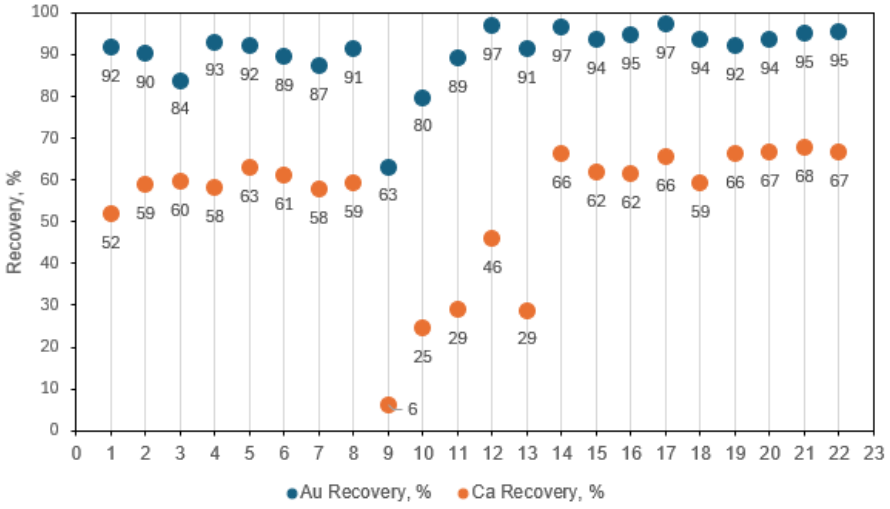



**FIG 9** – Gold and calcium recoveries achieved by the Cavitation Tube Column pilot treating the final flotation concentrate stream (HP05).

The improved upgrading performance is considered to be associated with the continued reduction of hydraulic entrainment through the combination of a deep froth zone and wash-water addition. Even after multiple cleaning stages, sufficient selectivity remained to remove a significant proportion of the remaining carbonate minerals while maintaining high gold recovery. This demonstrates that additional upgrading of the concentrate was achievable without excessive loss of valuable minerals.

The average pilot plant assays are summarised in Table 3. Concentrate calcium grades of approximately 4.5 per cent were achieved, closely matching the earlier laboratory flotation investigations. The close agreement between laboratory and pilot-scale performance demonstrated the repeatability of the metallurgical response and provided confidence that the technology could consistently deliver the concentrate quality required for downstream processing.

**TABLE 3**

Balanced performance of Cavitation Tube Column pilot plant on plant final concentrate from HP05.

| Products | Au | Ag | S2- | S | Ca | Mg | Mass | Recovery, % | | |
|---|---|---|---|---|---|---|---|---|---|---|
| | g/t | g/t | % | % | % | % | % | Au | Ca | Mg |
| Feed | 14.5 | 19.6 | 4.2 | 7.2 | 6.1 | 2.7 | 100.0 | 100.0 | 100.0 | 100.0 |
| Concentrate | 19.8 | 26.2 | 5.7 | 10.0 | 4.6 | 2.0 | 64.4 | 87.9 | 49.0 | 49.1 |
| Tails | 4.9 | 7.7 | 1.4 | 2.0 | 8.7 | 3.8 | 35.6 | 12.1 | 51.0 | 50.9 |

## StackCell pilot evaluation on the rougher flotation feed

Figure 10 compares the metallurgical performance of the two-stage StackCell pilot circuit with the existing two-stage Jameson Cells configuration operating under comparable plant conditions. The Jameson configuration comprised two cells operating in series, with samples collected as a combined concentrate from the discharge hopper. The StackCell pilot circuit also operated as two units in series, and results are presented as the cumulative grade and recovery achieved across both units.

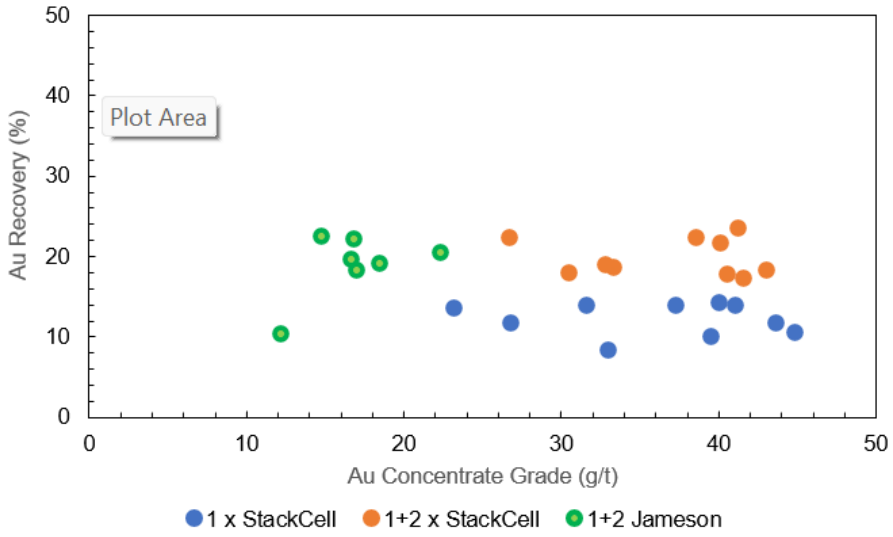



**FIG 10** – Comparison of two-stage StackCell and two-stage Jameson Cell pilot performance on the rougher flotation feed.

Under comparable overall gold recovery, the StackCell pilot circuit consistently produced approximately twice the concentrate grade while operating at substantially lower mass pull than the existing Jameson circuit. This indicates that a greater proportion of gangue material was rejected at an earlier stage of flotation while maintaining recovery of valuable minerals, thereby reducing the load reporting to the downstream cleaner circuit. The lower mass pull also reduced the quantity of material reporting to downstream cleaning stages, thereby decreasing the burden placed on the cleaner circuit.

Figure 11 illustrates the relationship between circuit mass pull and gold recovery. The pilot results demonstrate that the StackCell circuit achieved comparable gold recovery at a substantially lower circuit mass pull than the existing Jameson Cell configuration. This indicates that a greater proportion of gangue material was rejected while maintaining recovery of valuable minerals, reflecting improved flotation selectivity. From an operational perspective, the lower mass pull reduces the quantity of material reporting to downstream cleaning stages, thereby increasing effective cleaner circuit capacity without increasing flotation volume.

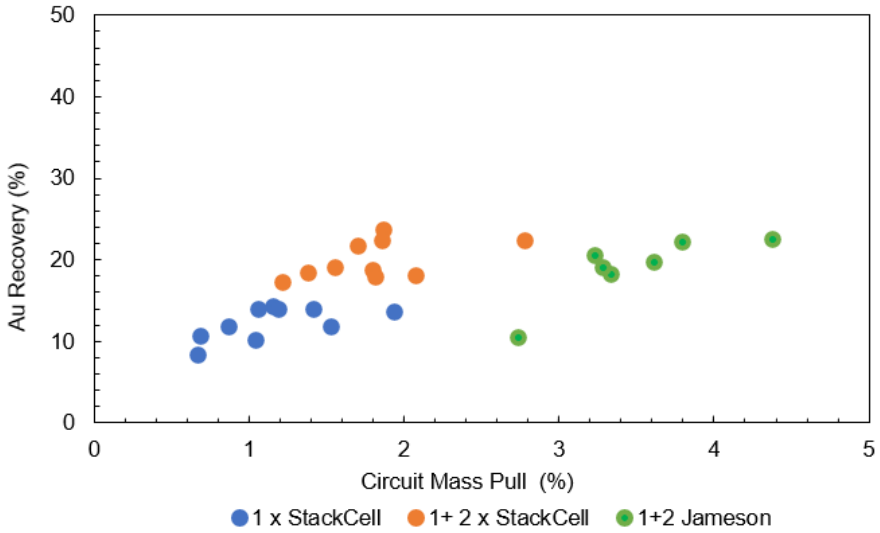



**FIG 11** – Relationship between circuit mass pull and gold recovery for the StackCell and Jameson Cell circuits.

Figure 12 demonstrates that concentrate calcium grades of ≤4 per cent were consistently achieved while recovering approximately 30–35 per cent of the gold in the rougher flotation duty. Under equivalent operating conditions, the existing flotation circuit typically produced concentrate calcium grades between 7.5 per cent and 8 per cent. The lower carbonate content generated during the pilot indicates that significant gangue rejection can be achieved at the front end of the flotation circuit, thereby reducing the carbonate load reporting to downstream cleaning stages. This early rejection strategy complements the subsequent Cavitation Tube Column cleaning stage and forms the engineering basis for the Phase 2 flotation circuit upgrade.

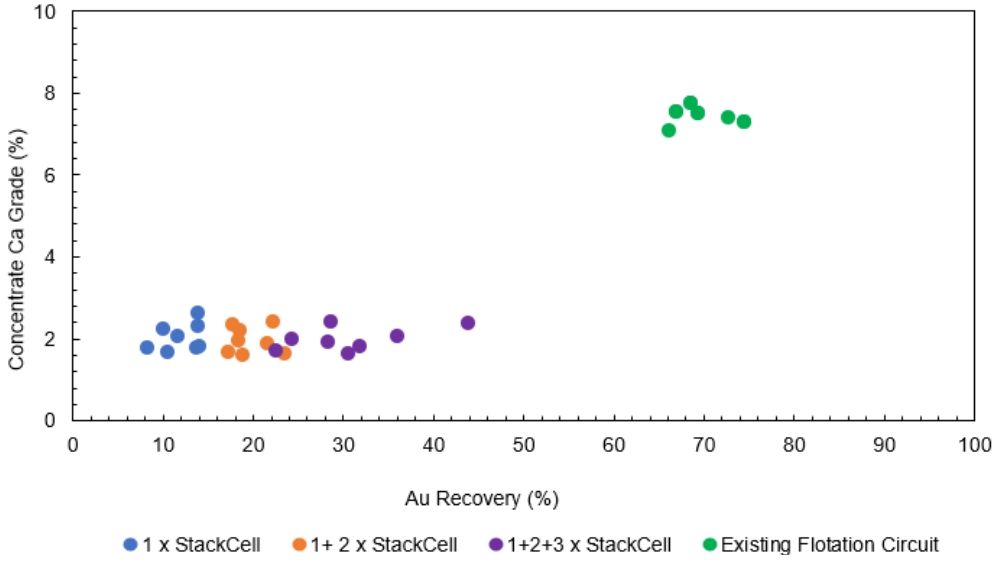



**FIG 12** – Comparison of concentrate calcium grade and gold recovery for the StackCell pilot circuit and the existing flotation circuit.

## Industrial flotation circuit development

The laboratory investigations and pilot-scale evaluations established the metallurgical basis for a staged upgrade of the Sepon flotation circuit. Rather than implementing a complete circuit replacement, the upgrade strategy progressively addressed the key process limitations identified during the evaluation program. This phased approach reduced implementation risk while allowing metallurgical performance to be verified under industrial operating conditions before proceeding with the full flotation circuit expansion.

Figure 13 illustrates the Phase 1 industrial flotation circuit developed from the outcomes of the laboratory investigations and pilot-scale evaluation. The circuit incorporated two Cavitation Tube Columns within the cleaner circuit to increase cleaning capacity and improve carbonate rejection while maintaining compatibility with the existing flotation infrastructure. This configuration directly addressed the cleaner circuit limitations identified during the evaluation program by introducing an additional upgrading stage downstream of regrinding, where selective rejection of carbonate gangue could be achieved with minimal modification to the existing plant.

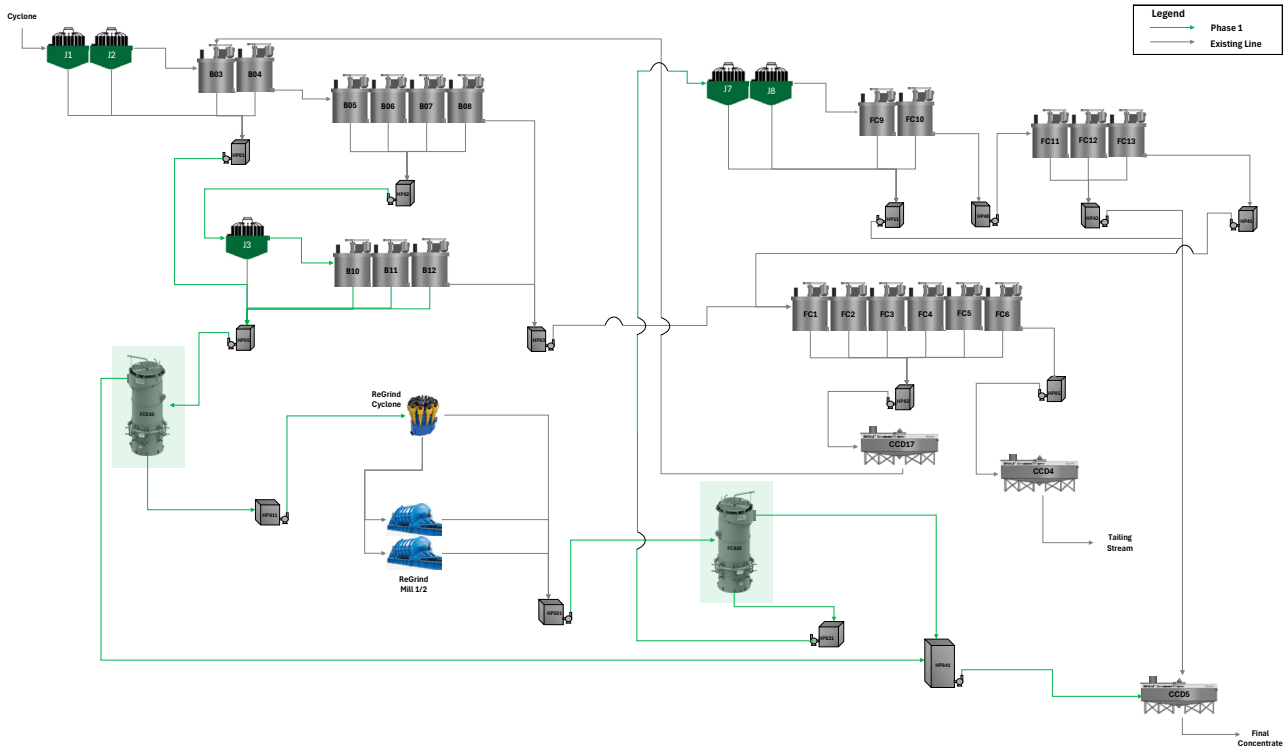



**FIG 13** – Phase 1 Sepon flotation circuit incorporating two Cavitation Tube Columns in the cleaner circuit.

Phase 1 was selected as the initial stage of implementation because the cleaner circuit represented the principal metallurgical constraint identified during the evaluation program. Installation of the two Cavitation Tube Columns provided a practical opportunity to improve carbonate rejection and verify metallurgical performance at industrial scale with relatively minor modification to the existing plant. This staged approach reduced implementation risk while generating operational experience and performance data to support the subsequent Phase 2 expansion.

Following successful implementation of Phase 1, the proposed Phase 2 flotation circuit was developed to extend the flotation upgrade strategy to the front end of the circuit, as illustrated in Figure 14. Whereas Phase 1 focused on improving cleaner circuit selectivity, Phase 2 incorporates four StackCell units ahead of the existing rougher flotation circuit together with an additional Cavitation Tube Column downstream of the regrind circuit. This integrated configuration combines early gangue rejection with enhanced cleaner circuit upgrading, thereby reducing the carbonate load reporting to downstream processing while maintaining overall flotation recovery.

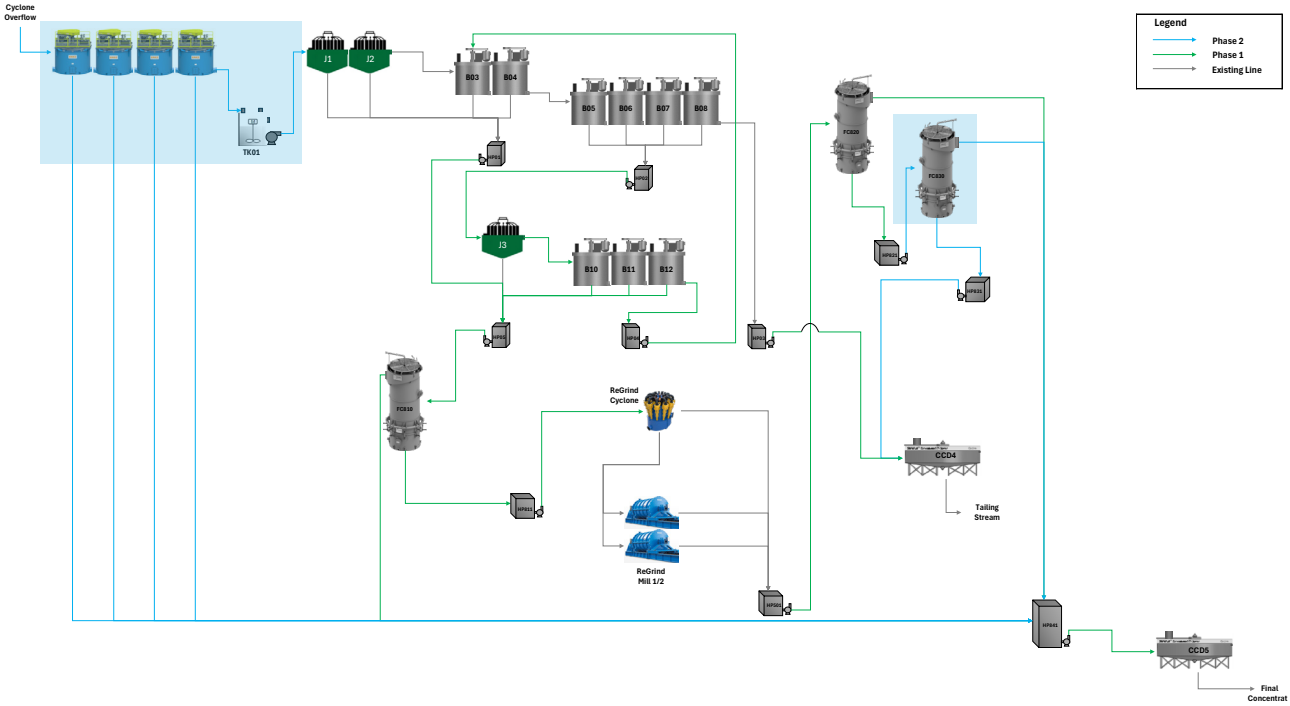



**FIG 14** – Proposed Phase 2 Sepon flotation circuit incorporating StackCell units and an additional Cavitation Tube Column.

Figure 15 presents the three-dimensional layout developed for implementation of the Phase 1 and Phase 2 flotation circuit upgrades. The compact arrangement enabled integration of the additional flotation equipment within the existing plant footprint while maintaining operational access and minimising modifications to the surrounding infrastructure. The layout also provides flexibility for future maintenance and optimisation activities without disrupting existing plant operations.

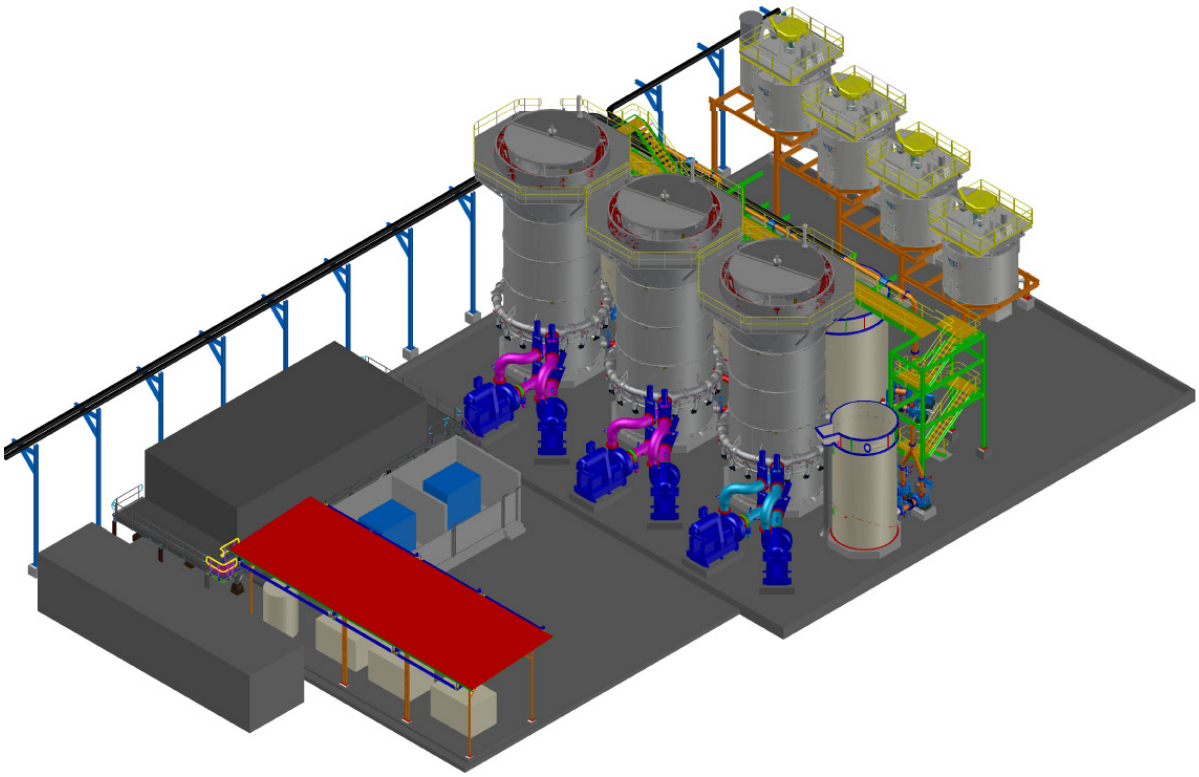


**FIG 15** – Three-dimensional layout of the Phase 1 and proposed Phase 2 flotation circuit upgrades.

## Industrial performance evaluation

Following commissioning and optimisation of the Phase 1 flotation circuit upgrade, an industrial evaluation program was undertaken to assess the metallurgical performance of the modified cleaner circuit under normal plant operating conditions. Performance was evaluated by comparing periods with the Cavitation Tube Column circuit operating (online) against periods with the circuit bypassed (offline), thereby enabling the contribution of the additional cleaning stage to be assessed under comparable operating conditions. A total of six weeks of operating data were collected during online operation (n = 75), together with four weeks of offline operating data (n = 47). The evaluation focused primarily on three key metallurgical performance indicators: final concentrate calcium grade, overall calcium recovery to concentrate, and final concentrate gold grade. These parameters directly reflect the objectives of the Phase 1 upgrade, namely improving carbonate rejection and concentrate quality under continuous industrial operation, while overall flotation gold recovery was monitored to confirm that these improvements were achieved without materially compromising plant recovery performance.

Figure 16 compares industrial flotation performance during periods when the Cavitation Tube Column circuit was operating and when it was bypassed. Although the calcium content of the flotation feed varied between the two operating periods, operation with the additional cleaning stage consistently produced a lower final concentrate calcium grade than operation without the column circuit. This behaviour demonstrates that the reduction in concentrate carbonate content was achieved through improved flotation selectivity rather than changes in feed composition alone. The industrial observations closely reproduced the metallurgical response established during both the laboratory investigations and pilot-scale evaluations, confirming that the additional cleaning stage maintained its carbonate rejection capability under continuous plant operation. These results represent an important operational outcome, as reducing carbonate reporting to the flotation concentrate directly lowers the sulfuric acid demand of downstream processing.

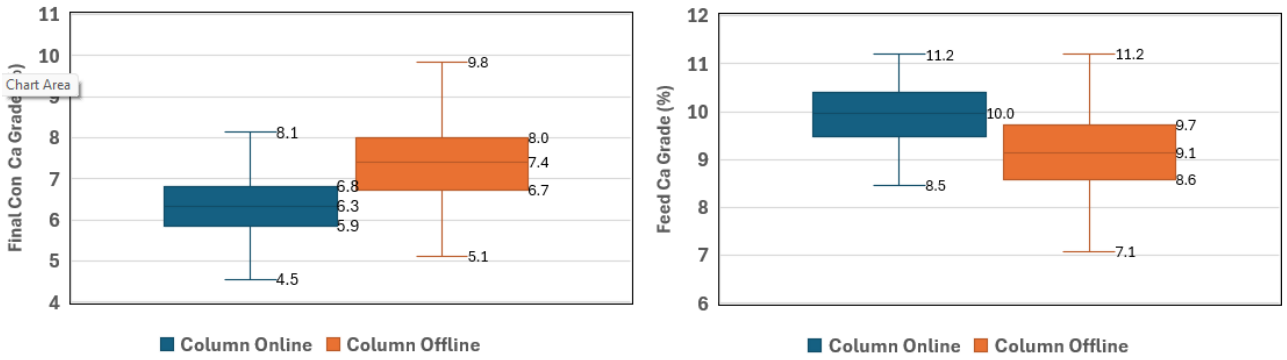



**FIG 16 –** Comparison of final concentrate calcium grade and flotation feed calcium grade during Cavitation Tube Column online and offline operation.

Figure 17 summarises the gold grade and overall flotation recovery achieved during the online and offline operating periods. While the primary objective of Phase 1 was to improve carbonate rejection and concentrate quality, overall gold recovery was closely monitored throughout the industrial evaluation to ensure that the additional cleaning stage operated within the expected metallurgical performance envelope. The online operating period consistently produced a higher final concentrate gold grade, reflecting the improved selectivity of the modified cleaner circuit. As anticipated from the laboratory investigations and pilot-scale evaluation, this improvement was accompanied by only a modest reduction in overall flotation gold recovery, representing the expected trade-off associated with increased gangue rejection during Phase 1. Importantly, the industrial operating data confirmed that the additional cleaning stage achieved its primary metallurgical objective while maintaining overall gold recovery within the design expectations established for the initial stage of the flotation circuit upgrade.

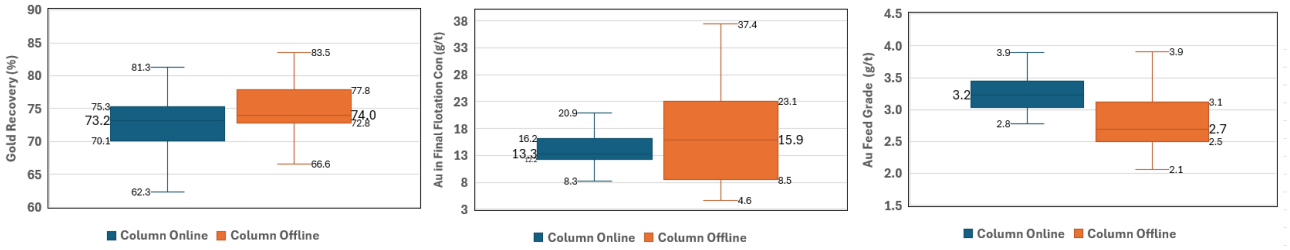



**FIG 17** – Comparison of gold recovery, final concentrate gold grade and flotation feed grade during Cavitation Tube Column online and offline operation.

## Statistical validation of industrial performance

Although the industrial operating data presented in Figures 16 and 17 showed clear differences between online and offline operation, statistical analysis was undertaken to determine whether these observations represented genuine improvements in metallurgical performance rather than normal process variability. Comparative analyses were performed using six weeks of online operating data (n = 75) and four weeks of offline operating data (n = 47). Welch's two-sample t-tests demonstrated a significant increase in final concentrate gold grade ($p < 0.001$), significant reductions in overall calcium recovery ($p = 0.00056$) and overall gold recovery ($p = 0.0045$), while the change in final concentrate calcium grade was not statistically significant ($p = 0.174$). The corresponding mean differences and 95 per cent confidence intervals are presented in Figure 18.

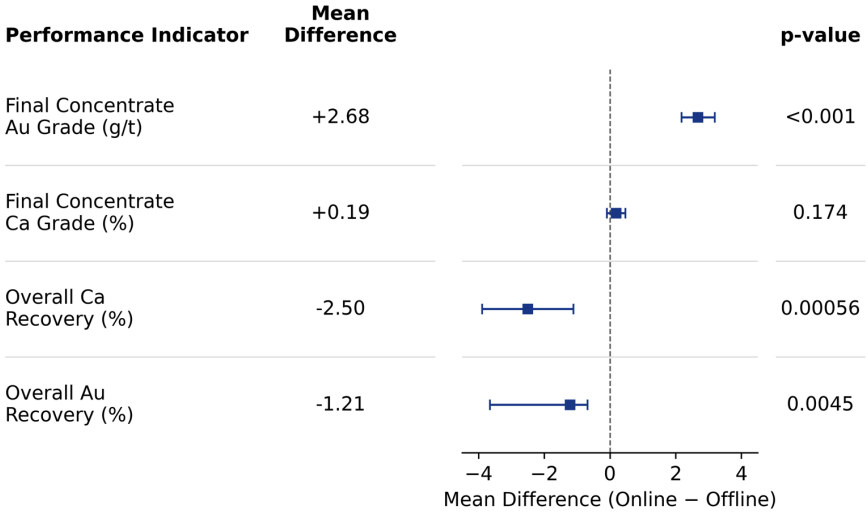



**FIG 18** – Forest plot summarising the mean differences (Online − Offline) with 95 per cent confidence intervals for the key industrial flotation performance indicators evaluated during the Phase 1 industrial trial.

Collectively, the industrial operating results and statistical analyses demonstrate that the Phase 1 flotation circuit upgrade achieved its primary metallurgical objective of improving cleaner circuit selectivity through enhanced rejection of carbonate minerals while simultaneously increasing final concentrate gold grade. The close agreement between laboratory investigations, pilot-scale evaluation and industrial operating performance provides confidence that the observed improvements reflect the underlying flotation response rather than normal process variability. Although a modest reduction in overall flotation gold recovery was observed during Phase 1 operation, this outcome was consistent with the expected metallurgical trade-off associated with increasing cleaner circuit selectivity and was considered acceptable within the staged implementation strategy. The successful validation of the Phase 1 flow sheet provided the technical basis for progressing to the second stage of the project, incorporating four StackCell units and an additional Cavitation Tube Column to further develop the industrial flotation circuit. The metallurgical performance of the complete Phase 2 configuration will be evaluated following commissioning.

## Future circuit development

The successful implementation and validation of the Phase 1 flotation circuit upgrade established the technical foundation for the second stage of the Sepon flotation circuit development. Phase 2, which is currently under construction, incorporates four StackCell units together with an additional Cavitation Tube Column to further develop the industrial flotation circuit. This expanded configuration has been designed to build upon the improved cleaner circuit selectivity and concentrate quality demonstrated during Phase 1 by integrating high-intensity flotation at the front end of the circuit with additional cleaner flotation capacity. Commissioning of the Phase 2 circuit is scheduled for Q3 2026, after which a comprehensive metallurgical evaluation will be undertaken to quantify the performance of the fully integrated flotation circuit under industrial operating conditions.

# CONCLUSIONS

This study presented the staged development and industrial implementation of an advanced flotation circuit upgrade at the Sepon Gold Mine. Beginning with laboratory investigations and progressing through pilot-scale evaluation to full-scale industrial implementation, the project demonstrated the value of a systematic engineering approach for evaluating, validating and deploying flotation technologies under operating plant conditions.

Industrial evaluation of the Phase 1 flotation circuit confirmed that the introduction of the Cavitation Tube Column significantly improved cleaner circuit selectivity by increasing final concentrate gold grade while reducing overall calcium recovery to concentrate, thereby decreasing the carbonate load reporting to downstream processing. Statistical analysis demonstrated that these improvements were significant and represented genuine metallurgical benefits rather than normal process variability. Although a modest reduction in overall flotation gold recovery was observed, this was consistent with the expected metallurgical trade-off associated with increased cleaner circuit selectivity during the initial stage of the circuit upgrade. The outcomes of Phase 1 provided the engineering basis for the Phase 2 circuit expansion, which integrates four StackCell units at the front end of the flotation circuit together with an additional Cavitation Tube Column downstream of the regrind mill. This integrated configuration has been designed to further improve overall flotation circuit performance by combining early gangue rejection with enhanced cleaner circuit upgrading.

The close agreement between laboratory investigations, pilot-scale testing and industrial operating performance demonstrated a consistent scale-up pathway from concept evaluation to commercial application. The successful validation of the Phase 1 flow sheet provided the technical confidence to proceed with the second stage of the project, incorporating four StackCell units and an additional Cavitation Tube Column to further develop the industrial flotation circuit.

This case study demonstrates that a structured, evidence-based approach to flotation circuit development can successfully bridge the gap between laboratory investigation and industrial implementation. The staged methodology adopted at Sepon reduced implementation risk while providing confidence that metallurgical improvements observed during laboratory and pilot-scale testing could be reproduced under continuous plant operation. This approach provides a practical framework for evaluating and implementing advanced flotation technologies in complex mineral processing operations.

# ACKNOWLEDGEMENTS

The authors would like to acknowledge the Sepon Metallurgy team and the many site personnel who provided essential support throughout the program, from pilot-scale testing through to post-commissioning and ongoing optimisation activities. The guidance and continued support from the Chifeng Gold corporate team are also gratefully recognised.

A special thanks is extended to the project team, whose exceptional effort enabled the complete installation of the flotation circuit in less than six weeks, ensuring the site was fully prepared for both dry commissioning and subsequent slurry commissioning. Their commitment, coordination, and execution were critical to the successful and timely delivery of the project.

Finally, the authors wish to thank the Chifeng Gold corporate team for granting permission to publish this paper.

# Mill Operators

# Comminution

# Pebble crushing in AG/SAG circuits – operation, dynamics and solutions

*S Munro[1], R A Bearman[2], P Pluis[3] and S Haskell[4]*

1. Director, Met Dynamics Pty Ltd, Woodvale WA 6026. Email: scott.munro@metdynamics.com.au
2. Director, Bear Rock Solutions Pty Ltd, Melville WA 6956. Email: ted.bearman@bear-rock.com
3. Principal, Palminco Pty Ltd, Annandale Qld 4814. Email: peter@palminco.com.au
4. Managing Director, Crushology Pty Ltd, Warnbro WA 6169. Email: stuarth@crushology.com.au

## ABSTRACT

The effectiveness of a milling circuit incorporating a pebble crusher depends on instantaneous performance, run-time, and the consistency with which the required rate and product size are delivered. This paper examines the challenges associated with each of these factors in pebble crushing circuits.

In addition to the usual application guidelines for effective crusher operation and performance, pebble crushing is subject to specific conditions which, if unaddressed, can significantly detract from both crusher performance and the effectiveness of the overall milling circuit. Consideration is given not only to the ability to achieve instantaneous process performance targets but also to the need to ensure mechanical reliability. To fully explore and understand these issues, the paper combines the authors' extensive operational experience with a mechanistic cone crusher model to illustrate and quantify their causes and remedies. Specific aspects examined include trickle feed, choke feed, mass distribution, particle size segregation, and feed size distributions encountered in pebble crusher duties.

Beyond instantaneous performance and reliability, many system effectiveness issues stem from time-based variability, including the wear condition of mill discharge grates, pebble ports, and pebble crusher liners. Steady-state snapshots can describe conditions at points during the various cycles, but they do not adequately define the impact of the transition from one operating state to another. Importantly, such transitions are a major cause of performance interruption and therefore productivity loss.

The paper investigates the main issues arising from interactions between autogenous and semi-autogenous grinding (AG/SAG) mills and pebble crushers, concentrating on the circuit dynamics. A suite of traditional steady-state and advanced dynamic process simulations is used to identify why projected performance is not always realised. The analysis considers feed presentation, operational capabilities, and the substantial variation in process performance that can result from operational strategies at the crusher and across the wider circuit. The steady-state operation assumed in most flow sheet simulations is rarely observed in pebble crushing circuits. Dynamic simulations are used to investigate and quantify the resulting effects on circuit performance, mill stability, and throughput, and to show how these effects can influence the choices made in the design and specification stages of a project.

Operational, design and capital options to realise the full throughput uplift potential of a pebble crushing–mill circuit are described and quantified. The paper also discusses how the identified issues and proposed solutions can be applied to milling circuits, together with the implications for more novel options such as high-pressure grinding rolls (HPGR) in pebble crushing duties.

## INTRODUCTION

The mining industry has expended vast amounts of effort to improve the stability of mills and milling circuits. Within many such circuits, pebble crushing is an integral component due to the improvements it can deliver to the mill and wider circuit.

The use of a pebble crusher in closed circuit with the mill and classification step, ie trommel or vibrating discharge screen, can therefore add significant value. However, there are significant challenges to be addressed to ensure the pebble crusher delivers on the design ambitions for the circuit.

If system design and optimisation methodologies are considered, the base relationship for effectiveness can be expressed in many ways, with a common form being:

Effectiveness = Mechanical Availability × Utilisation × Instantaneous Performance × Quality

Where:

- Mechanical Availability: the time during which the crusher is mechanically fit to operate.
- Utilisation: the use of available mechanical time.
- Instantaneous Performance: the performance that can be consistently achieved, often considered to be steady-state.
- Quality: the proportion of operating time during which the crusher delivers the required performance, in terms of rate and product size, to downstream processes.

Underpinning the parameters in the equation are the harsh realities of pebble crushing. Run-time comprises mechanical availability, controlled by the reliability of the crusher and the service life of components, and the utilisation of time, ie when feed is available to the crusher. These factors are based on the design of the circuit, the forces driven into the mechanical components of the crusher, and the maintenance condition. The instantaneous performance of the machine is determined by operational stability and adherence to the guidelines for the effective operation of a crusher. Quality of performance, whilst the crusher is operating, can be a hidden or forgotten element. The fact that the crusher is running and receiving feed does not, by itself, imply effectiveness.

The ‘Quality’ term referenced above is one of the challenges, particularly when taking a steady-state view, as it tends to be reduced to a single statistical metric. In reality, it is the frequency, duration, and magnitude of the disruptions to quality of crusher production that degrade mill circuit performance.

It is this transient behaviour that can lead to inadequate evaluations of pebble crusher effectiveness and therefore adversely affect overall mill circuit performance.

Given this limitation, this paper explores the use of a full dynamic circuit simulation approach, coupled with a strong practical understanding of the engineering basics, to provide an improved understanding of overall circuit performance.

The narrative used in this paper is designed to convey the logic encapsulated in the system effectiveness equation stated above, and to illustrate the following progression:

- conditions can lead to detrimental loading
- non-optimal loading reduces mechanical reliability and gives erratic process performance
- mechanical and process disruptions destabilise the milling circuit
- alternative flow sheet options may need to be considered to counteract potential disruption
- evaluation of the effects of these options is important and the use of dynamic process simulation can allow the value of the various options to be defined.

## CRUSHING BASICS AND SPECIFICS OF PEBBLE CRUSHING

Cone crushers applied to pebble crushing in autogenous and semi-autogenous grinding (AG/SAG) circuits are commonly available in three main mechanical configurations that differ in their method of closed side setting adjustment and main shaft support. The main types are bowl-adjusted designs with either a fixed or bush-mounted main shaft, and head-adjusted designs in which the shaft and head are supported by a hydraulic cylinder (Bearman, 2019a).

Although all employ compressive breakage, there is variation in kinematics and machine characteristics, including head angle, operating speed, eccentric throw, installed power, machine mass, and overall dimensions. Modern fixed-shaft bowl designs typically offer compact geometry, high speeds, and high capacity, but require tight control of operating conditions to prevent excessive loads and poor product size control. Older bush-mounted bowl-adjusted designs are robust and

operate at lower speeds and throughput, but may not deliver the same level of processing performance as the more modern variant.

Head-adjusted ('hydrocone' style) machines provide heavy structural support and controlled hydraulic positioning suited to large feed sizes and stable operation. Selection between these types of crusher arrangements for a pebble duty is therefore governed primarily by required capacity, feed characteristics, installation constraints, and preferred operating practice.

Cone crushers are widely applied in secondary and tertiary duties in hard rock mining and aggregates processing (Bearman, 2019a) as they can deliver high reduction ratios, controlled product size distributions, and required throughput, whilst offering mechanical reliability. Although often considered to be relatively 'simple' machines, a wide range of factors can influence both mechanical and process performance, as shown in Figure 1.

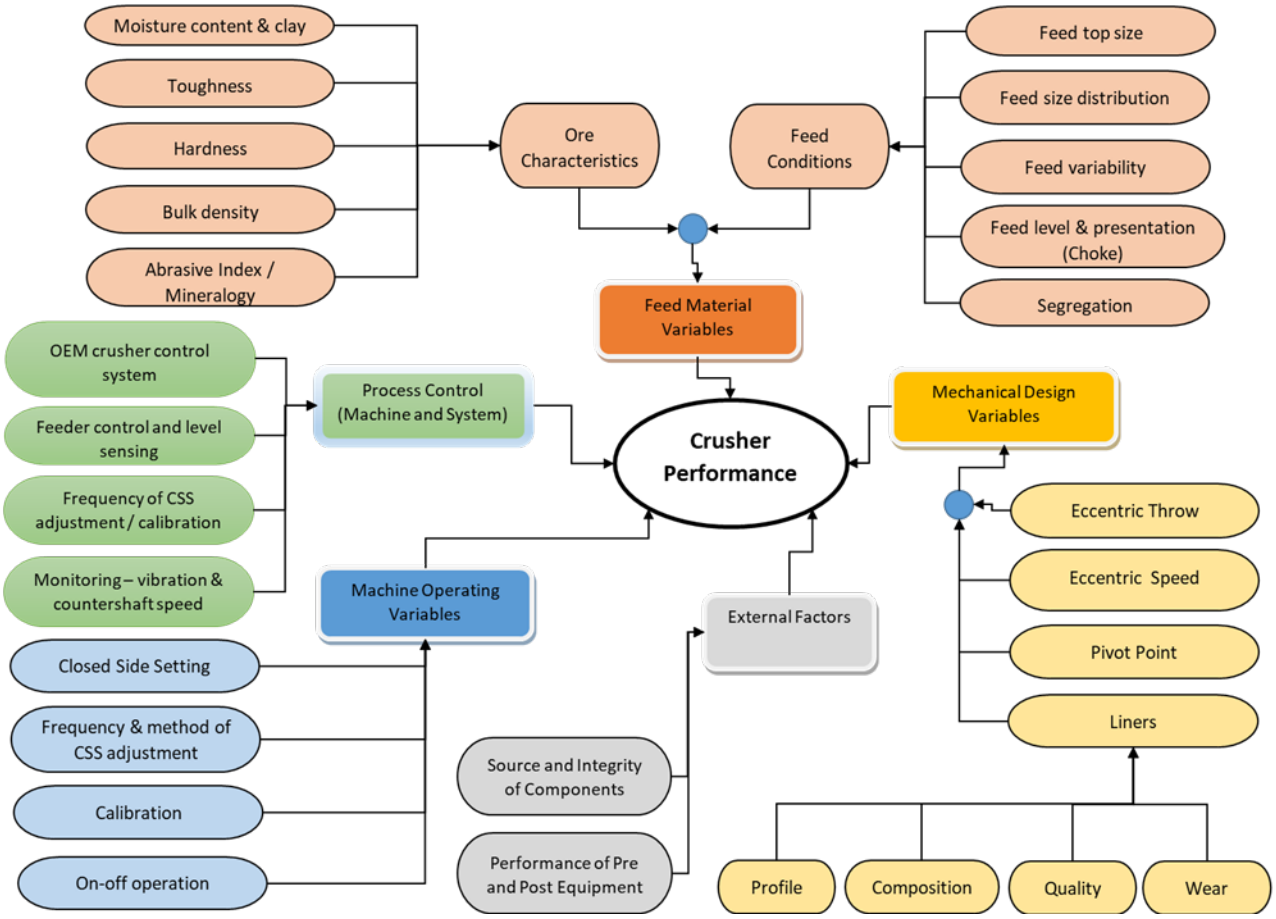



**FIG 1** – Factors contributing to the mechanical and processing aspects of cone crusher performance.

In many cases, the factors shown in Figure 1 can be rationalised down to a core consideration: cone crushers must operate with a uniform and controlled distribution of energy in the crushing cavity.

If energy application is erratic or localised:

- energy is not effectively applied to the rock for size reduction, causing degradation in instantaneous process performance.
- high and localised forces will be transmitted into the mechanical components, causing excessive stresses and leading to an increase in mechanical failures and downtime.

In terms of pebble crushing, the distribution of force is a major challenge, mainly due to:

- high competency feed, by definition, as it has survived the SAG mill at least once.
- the requirement for high reduction ratios to minimise recirculation with the mill.

- feed size distributions that can be very narrow and often bimodal.
- pebble generation rates from the mill that can change considerably over time.
- **Note:** In SAG applications, the presence of steel grinding media in the pebble stream is always a concern, which often requires the use of magnets, metal detectors, and shuttle/diversion mechanisms. For the purposes of constraining the scope of this paper, the importance of tramp metal is fully acknowledged, but it is not covered further.

As highlighted earlier, there is a need to ensure consistency of crushing performance in order to maintain mill stability.

Pebble crusher operation only needs to be compromised slightly for the challenges mentioned to be amplified. Such amplification of forces threatens the mechanical integrity and process performance of the crusher; consistency of operation is lost and disruptions to the mill are inevitable. Specific circumstances that can exacerbate the situation and cause process disruptions include:

- choke feeding, or the lack of choke feeding
- feed size segregation
- feed rate stability and surge control
- match between liner configuration and feed size distribution
- liner profile wear.

A more comprehensive summary of factors can be found in Bearman (2019b).

Two of the key operational considerations, namely feed size segregation and choke feeding, are examined in detail in the following section.

## PEBBLE CRUSHER OPERATIONAL CONDITIONS AND IMPACT ON MECHANICAL LOADING

Given the operational environment for pebble crushers, the most common problematic conditions encountered are size segregation and mass distribution. Both situations are related to feed presentation, and in each case the impact on process performance can be significant. To understand and quantify the impact of these conditions, the authors have frequently deployed the Kinematic Crusher Model (KCM) (Harding, Bearman and Munro, 2022), jointly developed by BRS and Met Dynamics in 2009. Using KCM, the implications of the operational conditions can be clearly seen and methods to alleviate issues can be implemented.

### Feed size segregation

Segregation on the basis of particle size can be a consequence of numerous aspects in the chain of feed presentation. The main areas driving segregation can be summarised as follows:

- belt loading and on-belt distribution into crusher feed bins
- trajectory of feed into bins, often due to the action or process control of a tripper or shuttle
- rilling of material within the bin(s)
- control of the bin outlet
- trajectory and flow control within the crusher feed chute.

If the segregation is not corrected before entry into the crushing chamber, different sectors of the chamber will receive variation in feed size. As the eccentric action of the crushing head is rotational, the crusher will cycle through areas of coarse and fine feed. Such variation induces extra mechanical stresses within the machine and changes the process performance of the crusher.

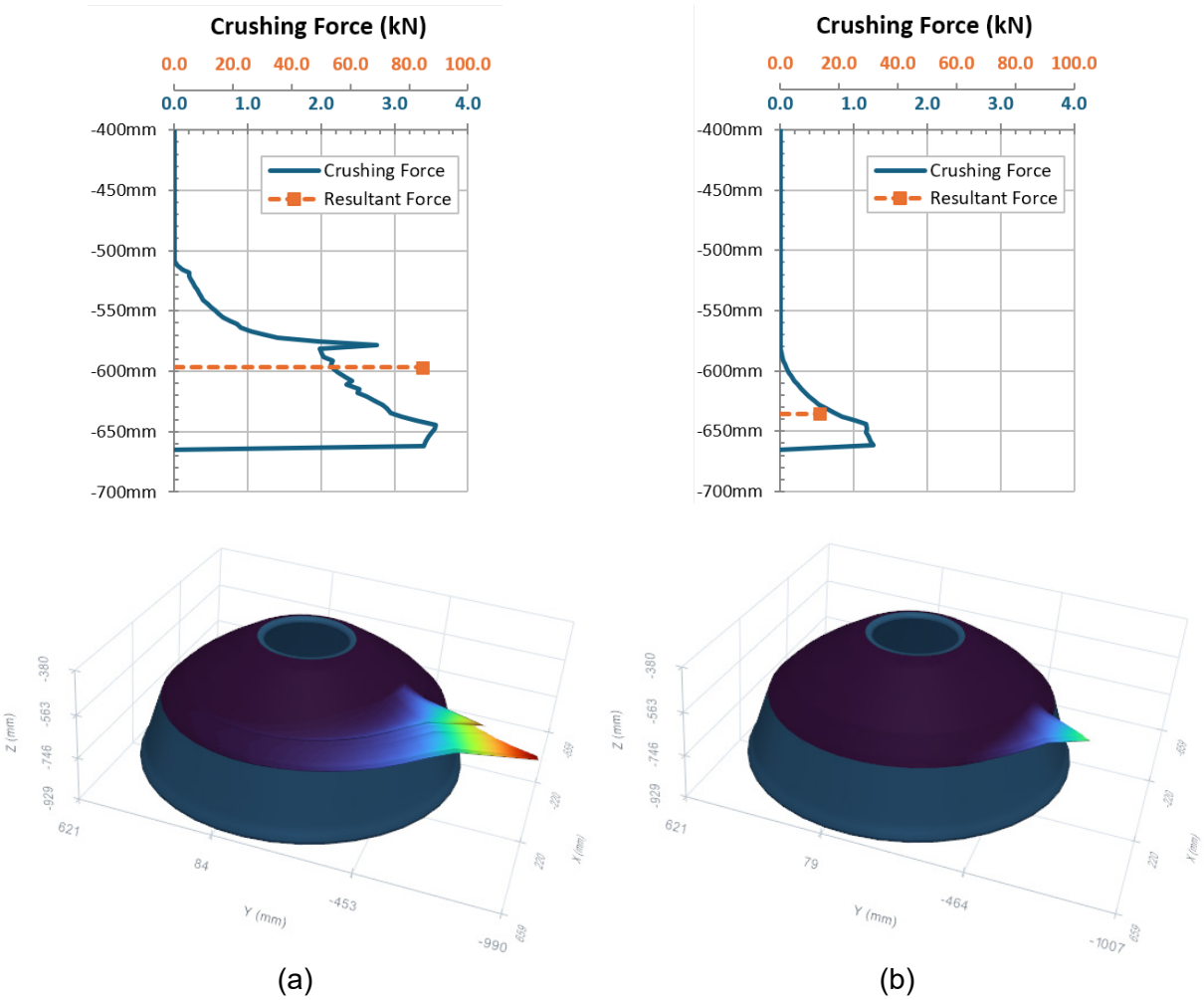
To define the effects generated in the crushing of segregated feed, KCM simulations have been run with the crusher treating the coarser and finer fractions of a typical pebble stream.

### *Changes in crusher performance due to feed particle size segregation*

Selection of the appropriate liner configuration for any crushing duty is based on the expected feed top size. As per normal practice, the maximum particle size should equate to 80 per cent of the closed side feed opening. In areas of the crushing chamber receiving the coarser part of the feed size distribution, this will therefore utilise the upper part of the chamber for the capture and nipping of the feed, with less crushing further down in the cavity. For areas receiving fine feed, the opposite is the case, with crushing being relegated to the lower sections of the chamber.

Using KCM, it is possible to examine the location and magnitude of crushing and how this will vary with the wear state of the liners.

Figure 2 presents key diagnostic plots generated by KCM for the coarse and fine feed conditions, showing the distribution of crushing force and the position of the equivalent resultant crushing force.




(a) (b)

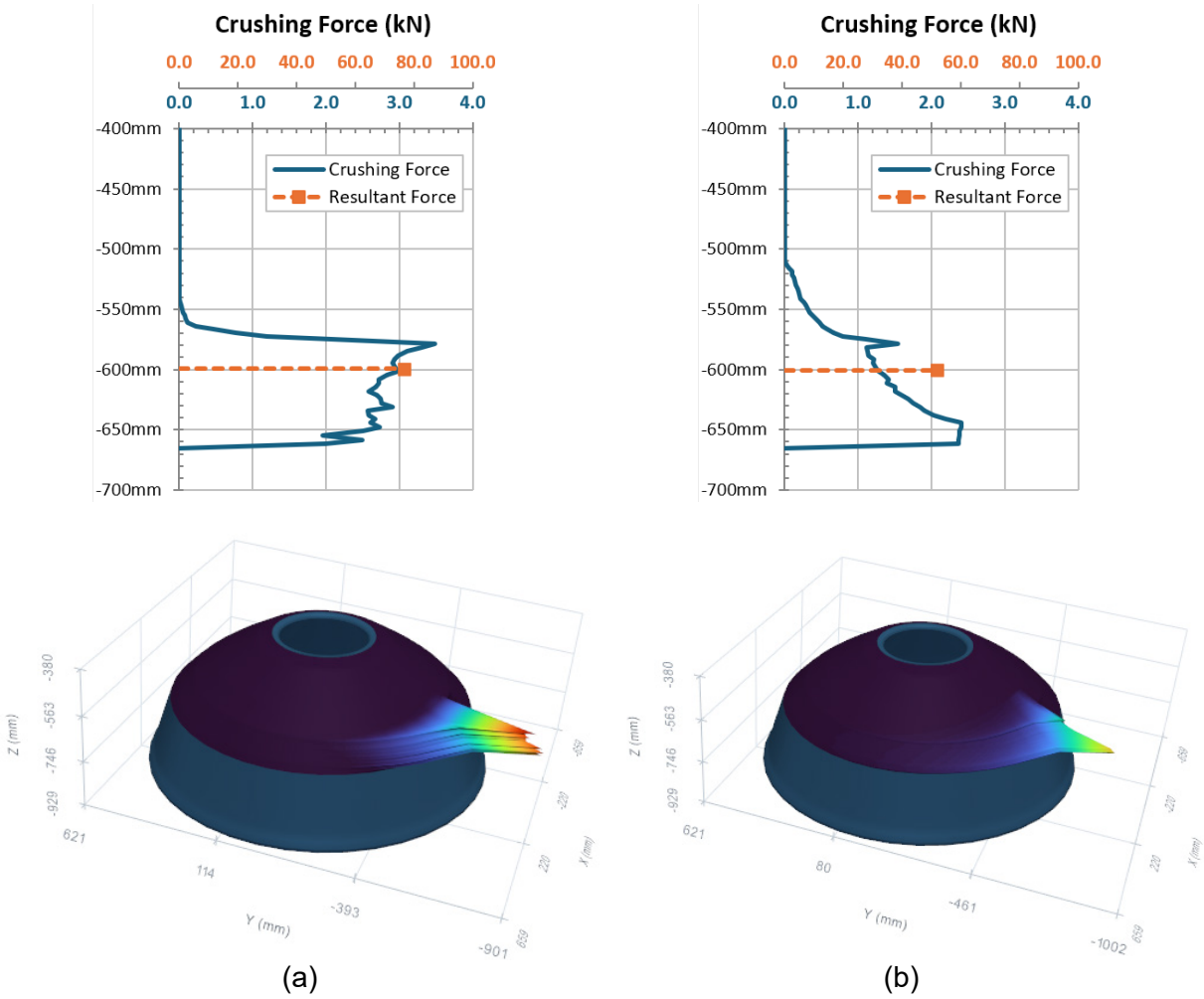
**FIG 2** – Crushing-force distributions and equivalent resultant-force positions for (a) coarse-feed and (b) fine-feed conditions. Upper plots show force distribution through the cavity; lower images show the corresponding force profile on the mantle.

## Changes in crusher performance due to cavity and circumferential filling

The other frequently observed feed presentation issue relates to the feed rate present in the various circumferential sectors around the cone head. Again, this relates to how the feed is controlled, mixed, and enters the crushing cavity.

Commonly, certain sectors will receive a full mass feed rate while others will be starved; in essence, this is analogous to certain areas being choke fed and others non-choked.

Similar to the size segregation issue, KCM can be deployed to determine the effect of this difference in mass presentation. The crushing force and position of the resultant force are shown in Figure 3 for choked and non-choked sectors.




(a) (b)

**FIG 3** – Crushing-force distributions and equivalent resultant-force positions for (a) choked sectors and (b) non-choked sectors. Upper plots show force distribution through the cavity; lower images show the corresponding force profile on the mantle.

The differences noted in the distribution of force and the position of the resultant crushing force are important as they illustrate how the spread and magnitude of force vary between conditions that can occur locally within the crushing chamber. As the crushing action moves through the cavity, the variation in force is transmitted into the internal components, causing forces to oscillate. This oscillation can be highly detrimental to the internal components, particularly bushes, as loads acting in a non-uniform fashion can deform bushes and lead to oil starvation, friction, burning, and failure.

## MECHANICAL RELIABILITY AND PROCESSING IMPACTS LEADING TO REDUCED SYSTEM EFFECTIVENESS

Crushing force information is illustrated for size segregation (Figure 2) and mass distribution (Figure 3) within the crushing cavity. As stated, the magnitude of the differences shown in the diagnostic plots is more pronounced for size segregation than for mass distribution, but in both cases the main features are:

- differences in the distribution of crushing
- distribution and magnitude of crushing force
- position and magnitude of the resultant crushing force.

The important point is not the metrics described above, but the impact on crusher performance. In terms of the distribution of crushing, some of the key considerations are:

- opportunity for progressive crushing
- generation of wear profile
- magnitude and direction of forces at key internal components.

For effective crushing, there has to be progressive size reduction through the chamber. With coarse feed, this can happen as oversize is gradually reduced as it passes through the full length of the chamber. With fine feed, however, this cannot happen. The fine feed surges through the chamber until it reaches a location just ahead of the discharge point, where one or possibly two breakage events can be applied. It should be noted that in many modern styles of bowl-adjusted cone crusher the eccentric throw can be very large, typically 60–90 mm in small to moderate-sized machines and over 100 mm in larger variants. As a result, fine material surging through a chamber can simply pass through the open side without any noticeable size reduction.

In bowl-adjusted cone crushers, the bowl is rotated to set the Closed Side Setting (CSS) and, as liners wear, to maintain the target setting. With particle size segregation, the situation can arise whereby areas of the bowl show different amounts of wear down the length of the bowl. Having this feature leads to erratic crushing, poor control of product size, and difficulty in determining the actual CSS.

Wear is a combination of mass and force at a point on the liners, so this is an obvious manifestation of uneven crushing. A more insidious situation relates to the internal mechanical components of the crusher. In all cone and gyratory crushers, various bushes are used to control motion and separate rotating components. The design of these bushes is based on the assumed position of forces generated from the crushing action. If the forces are not stable and are not acting through the position assumed in the design process, this can have serious effects on the mechanical reliability of the crusher.

## Mechanical and reliability impact

A very common symptom of uneven or unstable crushing is often referred to as ‘ring-bounce’ in bowl-adjusted cone crushers, where the adjustment ring separates from the mainframe as the clamping arrangement is unable to withstand the forces being generated within the crusher. In true ‘tramping’ events, this is a desirable feature as the movement of the adjustment ring allows uncrushable material (‘tramp’) to pass through the crusher, whilst limiting mechanical damage. However, if ring-bounce is constantly occurring due to erratic forces in the crusher, this can cause many mechanical issues that directly affect the reliability and availability of the crusher.

The main causes of frequent ring-bounce are:

- poor feed presentation and distribution (including size and mass segregation and low rates)
- excessively tight CSS
- high or low reduction ratios
- packing of fines
- poor liner wear profiles
- erratic feed rates
- presence of wet, sticky or clay-bearing feed.

Long periods of frequent ring-bounce can cause many issues, including:

- seat damage
- flexing and cracking of the crushing head, mantle, mainframe arms, and mainshaft
- high forces on eccentric bushes and bush burning, including heat damage to the body of the eccentric

- uneven or oscillating forces on the eccentric bushes (‘mid-bearing condition’)
- flexing of crusher liners, causing movement of the liner against the surface of the head (‘fretting’).

Following the primary damage listed above, cracking of key structural elements can reduce the rigidity of the crusher, allowing movement that causes further damage, such as loss of gear alignment. This is exacerbated by any areas of stress concentration due to the design, or where manufacturing processes have introduced weakness, such as casting defects or machining marks.

In bowl-adjusted cone crushers, frequent mechanical overloads can cause damage to the crushing head, adjustment ring seat bushes, mainframe arms, eccentric bushes/assembly and head ball/seat, amongst others.

In head-adjusted machines (‘hydrocone’ style), ring-bounce is not seen; instead, the forces are absorbed by the hydraulics supporting the mainshaft. In this regard, this type of machine is less prone to damage, as the hydraulics can respond to excessive force and drop the position of the crushing head to reduce the forces. However, such machines can still be damaged by excessive force, with the main areas being spider bush, mainshaft, shell tapers, eccentric bushes, and step washers and plates.

## Process performance impact

In this regard, there is both a direct impact on crusher performance and, in a broader and more important sense, an impact on the milling circuit as a whole.

At the local level of the crusher, the main effect seen is degradation of the product size generated. In Figure 4, four data sets show the crusher product size distribution generated due to size segregation and issues with mass distribution.

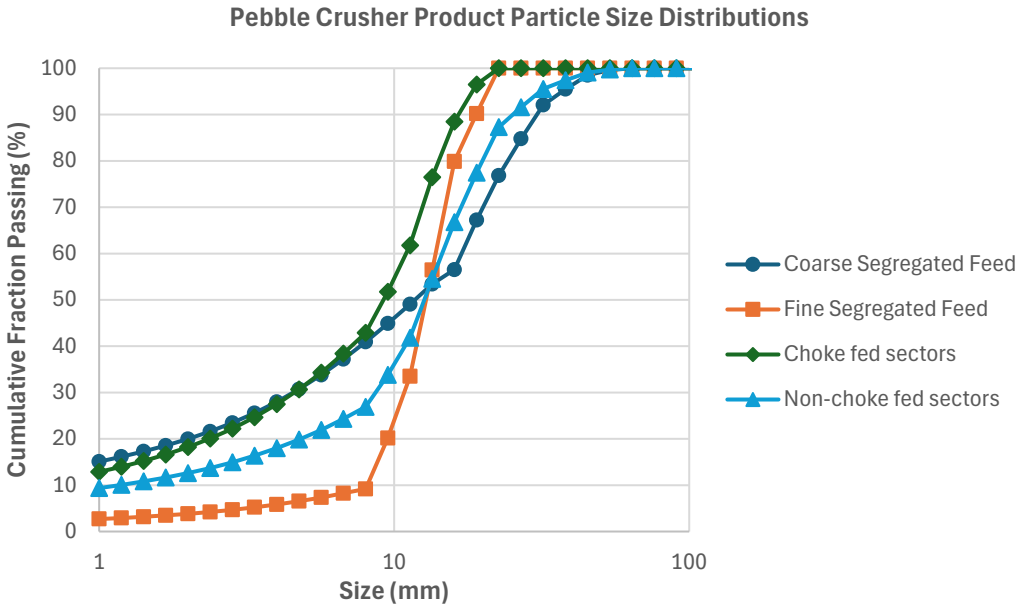



**FIG 4** – Variation in crusher product size distribution with varying operating conditions.

Figure 4 clearly demonstrates that significant changes to pebble crusher product size can be induced by poor operational conditions. Given that these conditions can be transient and difficult, or impossible, to correct in real time, they can dramatically impact the consistency of rate and product quality back to the mill. Given both the interconnected and closed-circuit nature of milling circuits with pebble crushing, this is one of the key reasons why steady-state assessments of mill-pebble circuits do not provide sufficient understanding and quantification of performance.

The following section seeks to explore options within pebble crushing and provide commentary on the value of dynamic process simulation to better define flow sheet and operational scenarios and their wider impact on the mill circuit.

## QUANTIFYING CIRCUIT EFFECTIVENESS UNDER TRANSIENT PEBBLE CRUSHING CONDITIONS

The preceding discussion has shown that segregation, cavity filling, and force redistribution influence mechanical reliability and instantaneous crushing performance. In a closed AG/SAG circuit, however, these effects extend beyond the crusher. Variability in crushed pebble size and discharge rate modifies the recycle stream to the mill, altering charge composition and load control behaviour. The result is not simply degraded crusher performance, but a change in overall circuit stability.

Such interactions are inherently dynamic. Their impact depends not only on operating conditions, but on how the system responds during transitions between conditions. To examine these time-dependent effects, a dynamic process simulation approach was adopted.

### Why steady-state evaluation is insufficient

The effectiveness framework introduced earlier defined performance as a function of run-time, instantaneous performance and quality. In pebble crushing circuits, each of these elements varies over time.

Pebble generation changes with grate wear and ore characteristics. Crusher performance varies with feed presentation. Control systems respond through transport delays and actuator limits. The circuit therefore does not operate at a single fixed condition, but moves continuously between states.

Steady-state simulation evaluates performance at isolated operating points. It cannot represent the transient redistribution of mass within the mill, the cyclic response of load control, or the interaction between crusher intermittency and mill stability. As a result, it cannot quantify the cumulative effect of repeated disturbances on throughput.

A dynamic, time-dependent circuit model was therefore used to evaluate alternative pebble crushing philosophies under realistic operating conditions.

### Dynamic circuit representation

A representative AG/SAG pebble crushing circuit was implemented as a time-stepped dynamic model within the SysCAD process simulation platform (SysCAD, version 9.3, Build 139.37069 (by KWA Kenwalt Australia Pty Ltd)). The objective was to reproduce plant-like dynamic behaviour, including material inventories, transport delays, and interacting control loops.

The circuit reflects common industrial practice. Crushed ore is reclaimed from a stockpile to a SAG mill via a belt conveyor. Mill discharge reports to a single-deck wet vibrating screen. Screen oversize pebbles are conveyed to a storage bin and then to a cone crusher. Crushed pebbles are returned to the SAG mill feed. Screen undersize proceeds to downstream grinding, which is not considered further in this analysis.

The configuration implemented in the dynamic model is shown schematically in Figure 5.

The SAG mill was represented using the Variable Rates population balance model in dynamic form (Morrell and Morrison, 1996; Valery and Morrell, 1995). Power draw and media trajectory were calculated to enable mill speed control based on both power and impact position criteria (Hilden and Powell, 2018; Powell, 1991). The vibrating screen was represented using a load-dependent classification model (Viilo, 2011; Whiten and White, 1977). These models were implemented within the Met Dynamics Models SysCAD add-on library (Met Dynamics Models, version 2.1.0 (by Met Dynamics Pty Ltd)). The pebble crusher was represented using a SysCAD add-on implementation of the Kinematic Crusher Model described earlier, allowing product size distribution to respond to operating conditions and feed presentation.

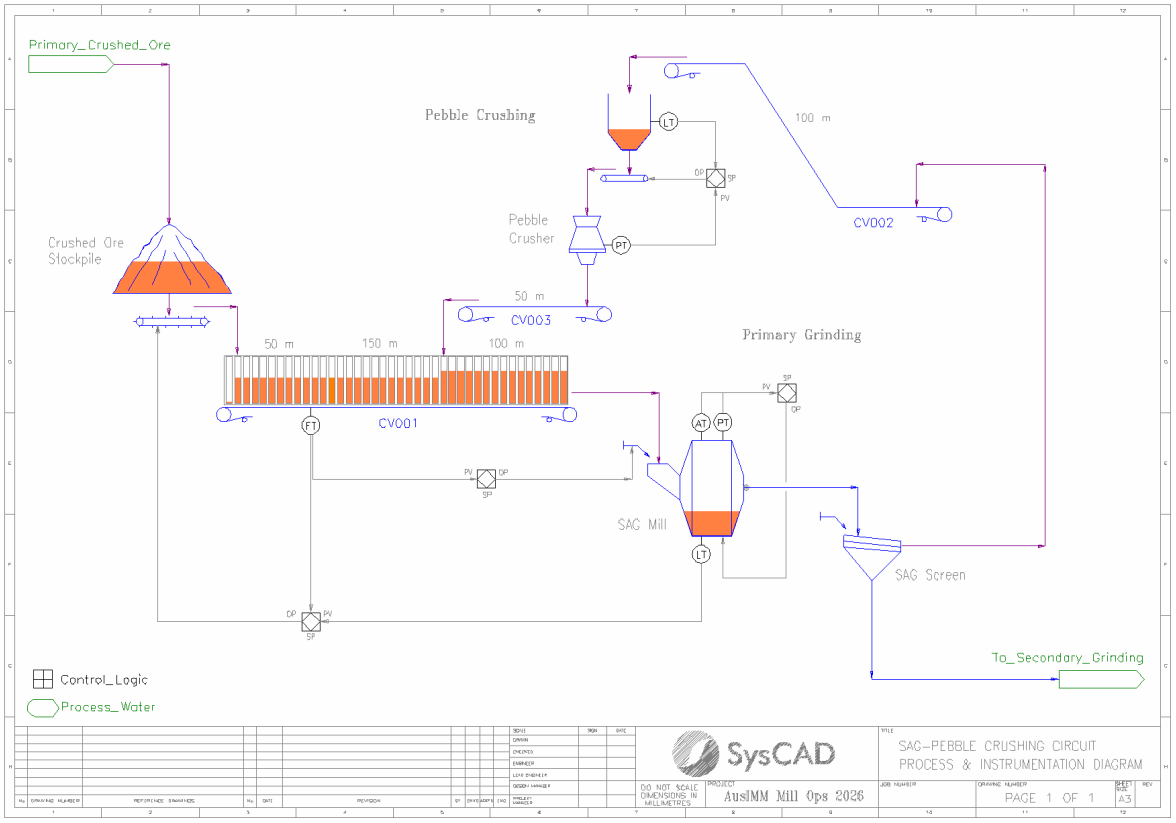



**FIG 5** – Representative SAG milling circuit with pebble crushing, as implemented in the SysCAD process simulation platform.

Survey data from an operating SAG-pebble crushing circuit were used to calibrate the model under steady-state conditions. The calibrated model reproduces measured throughput, size distributions, and power draw when simulated at the survey operating point.

Certain site-identifying details were generalised for confidentiality. The calibrated parameter set was retained unchanged for all dynamic simulations. The steady-state survey condition therefore serves as the reference from which circuit behaviour evolves as inventories and control actions vary with time.

## Behaviour of an oversized pebble crusher

A common design approach is to size a single pebble crusher for the maximum expected pebble generation rate at the end of SAG grate life. Under early grate-life conditions, the crusher is oversized relative to instantaneous pebble production. This creates a practical operating choice between continuous trickle-fed operation and intermittent choke feeding.

### *Trickle-fed operation*

In trickle-fed operation, crusher feeder speed is regulated to maintain a nominal feed bin level. The crusher operates continuously, but under partial cavity filling.

The resulting mill load and reclaim rate response over a representative operating shift is shown in Figure 6a. Mill load remains stable, and fresh ore reclaim rate exhibits virtually no variation. This case represents the baseline dynamic behaviour of the circuit and is used as the reference for subsequent throughput-change comparisons.

Under trickle-fed operation, the crusher operates away from full cavity conditions, reducing effective breakage within the chamber and shifting a greater share of size reduction duty to the SAG mill. Such trickle operation in high speed, high eccentricity cone crushers, can also lead to mechanical damage, particularly if coupled with poor fed presentation. Although dynamically stable, this mode of operation constrains achievable SAG throughput relative to higher-intensity crushing strategies

and can often reduce crusher reliability due to poor distribution of crushing forces through the machine.

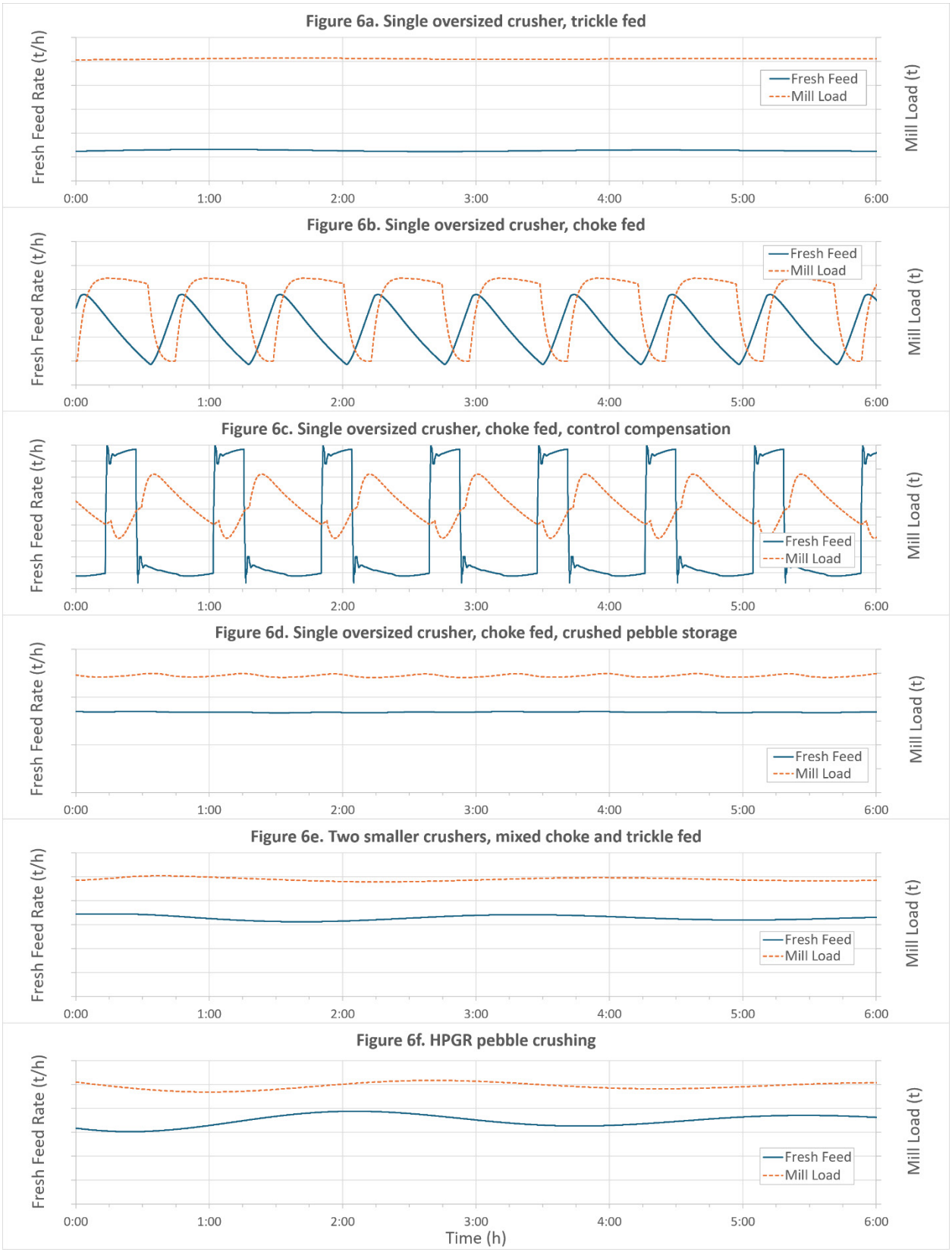



**FIG 6** – Dynamic SAG mill load and feed rate behaviour for alternative pebble crushing configurations.

### *Intermittent choke feeding*

If choke feeding is pursued to maximise crushing efficiency, a different dynamic response emerges. Because pebble generation fluctuates with grate wear and mill state, sustained choke feeding is rarely achievable. Instead, the crusher alternates between bin filling and bin depletion.

Compared with the stable baseline behaviour (Figure 6a), choke-fed operation (Figure 6b) produces pronounced variation in mill load and reclaim rate. Step changes in crushed pebble addition disturb the pebble return stream to the SAG mill, altering total feed rate and feed size distribution. The mill control system continually adjusts to re-establish the target load.

As shown in Figure 7, intermittent choke feeding increased average SAG mill throughput by 1.8 per cent relative to the trickle-fed baseline. This confirms the benefit of improved breakage under full cavity conditions, but the associated load variation limits how much of that benefit can be realised in the existing configuration.

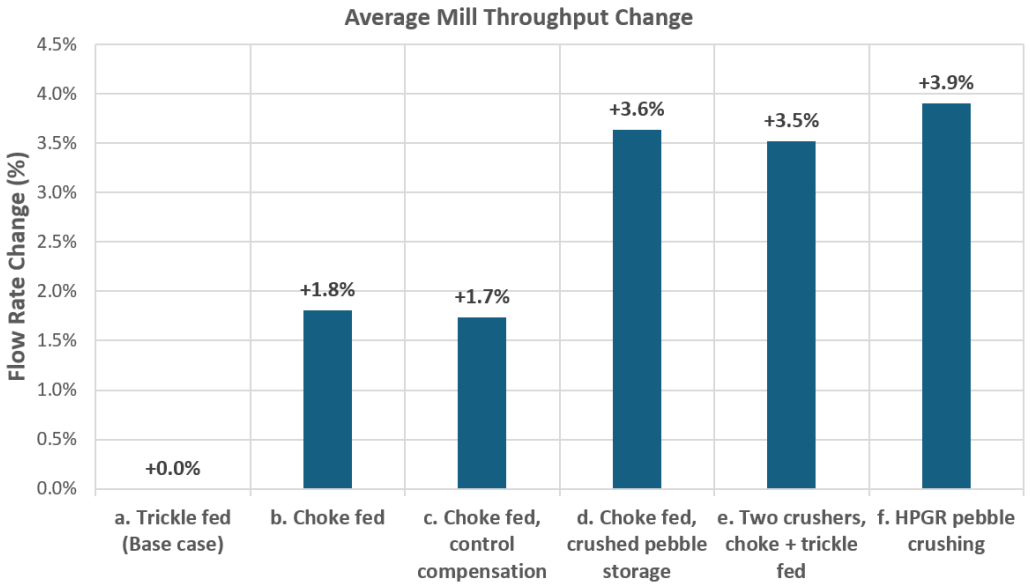



**FIG 7** – Average SAG mill throughput change by scenario.

### *Control-based compensation of intermittency*

A further case examined whether process control strategy alone could mitigate the instability associated with intermittent choke feeding.

In this configuration, fresh ore reclaim was ramped up when the pebble crusher stopped, with transport delays aligned so that total solids feed to the SAG mill remained approximately constant. When the crusher restarted, fresh feed was reduced accordingly. From a steady-state perspective, maintaining total mass flow might be expected to preserve mill stability.

The dynamic response in Figure 6c shows that this is not the case. Although total feed rate is smoothed relative to simple choke-fed operation, mill load continues to exhibit significant fluctuation during each crusher start-stop event. Substituting fresh feed for crushed pebbles alters the effective feed size distribution reporting to the mill, forcing the charge to re-establish a new internal equilibrium.

As shown in Figure 7, average throughput increased by 1.7 per cent relative to the trickle-fed baseline, but remained slightly below that achieved under intermittent choke feeding.

This result demonstrates that intermittency in pebble addition cannot be resolved through mass substitution alone. While control can moderate variability, it cannot remove the underlying structural coupling between crusher and mill.

## Decoupling strategies

The instability observed under intermittent choke feeding reflects the direct interaction between crusher discharge and SAG mill feed. Two alternative configurations were examined to reduce the impact of this interaction.

### *Crushed pebble storage*

In this configuration, crushed pebbles are accumulated in downstream storage before being metred back to the SAG mill at a controlled rate. The crusher may operate intermittently at choke conditions, but its discharge is decoupled from immediate mill demand.

The stabilising effect of this decoupling is evident when comparing the baseline response (Figure 6a) with the storage configuration (Figure 6d). The recycle stream returns to the mill at a more consistent rate, and the large load swings observed under intermittent choke feeding are effectively eliminated. As shown in Figure 7, average throughput increased by 3.6 per cent relative to the trickle-fed baseline.

From an effectiveness perspective, decoupling restores continuity while retaining higher instantaneous performance. To optimise this option, two smaller cones can be advantageous as it can extend the duration of crusher operation, compared to a single large cone that can rapidly consume available material from the feed bin.

### *Dual crusher configuration*

An alternative approach is to install two smaller pebble crushers whose combined nominal capacity equals that of the single oversized unit. One crusher operates predominantly in choke-fed mode, while the second operates in trickle-fed mode to accommodate variation in pebble generation.

This arrangement smooths crusher discharge to the mill and reduces load variation (Figure 6e) to a level similar to that achieved with downstream storage. The dual configuration delivered a throughput increase of 3.5 per cent, as shown in Figure 7.

Although the throughput improvement is slightly lower than that achieved with downstream storage, the dual configuration also introduces redundancy that could improve availability during maintenance periods.

In effectiveness terms, the combined trickle- and choke-fed operation provides a balance between crushing intensity and mill stability. Another sub-option that can be considered is the combination of dual smaller machines, with the crushed pebble storage option.

## Alternative breakage technology

The preceding cases show that instability in cone-based pebble crushing arises primarily from sensitivity to feed presentation and cavity loading. A different breakage mechanism may therefore produce different dynamic behaviour.

The cone crusher was replaced in the model with a high pressure grinding rolls (HPGR) unit configured for pebble crushing duty, consistent with published descriptions (van der Meer and Fernandez, 2015). The HPGR was represented using a power-based population balance model[2] (Torres and Casali, 2009). In order to provide some equivalence with the cone crusher options, the HPGR selected was operated to give an equivalent product $P_{80}$. As expected, the HPGR at a similar P80, will generate a finer tail to the distribution, but any advantages from this aspect would be in addition to the benefits highlighted in this paper.

Unlike the cone crusher, whose performance deteriorates under partial feed, the HPGR maintained consistent breakage across the simulated range of pebble flow rates, due to rate compensation via adjustment of roll speed. The pebble return stream to the mill remained stable without additional surge capacity, and mill load behaviour (Figure 6f) was comparable to the stable baseline case (Figure 6a). The HPGR configuration achieved a throughput increase of 3.9 per cent relative to the baseline.

Adoption of HPGR technology in pebble crushing duty imposes specific design and maintenance requirements. Roll surface condition and stud replacement must be actively managed. Roll gap selection must accommodate the full pebble size range across grate life. In SAG circuits, tramp grinding media reporting to the pebble stream require effective detection and rejection systems. This issue is less significant in AG circuits where steel media are absent.

Nevertheless, the HPGR configuration represents a dynamically stable alternative to cone-based pebble crushing while delivering improved size reduction performance.

## Implications for circuit design and effectiveness

The comparative results in Figure 7 demonstrate that pebble crushing philosophy has a measurable impact on overall circuit effectiveness.

Trickle-fed single crushers provide stable operation but limit effective crushing performance. Intermittent choke feeding increases average throughput but introduces load variation. Control-based mass substitution attempts to moderate this variation but is unable to eliminate instability. Decoupling through crushed pebble storage restores stability while retaining higher breakage efficiency. Dual crushers provide a compromise between stability and crushing intensity, whilst providing some redundancy. HPGR technology alters the dynamic response characteristics by maintaining consistent breakage across variable feed rates.

These differences are not necessarily evident in steady-state design calculations. Without dynamic analysis, the interaction between crusher intermittency, inventory response, and mill control remains hidden.

Pebble crushing effectiveness is governed not only by capacity at a single operating point, but by the consistency of performance over time. Design decisions that appear equivalent under steady-state assumptions may produce materially different outcomes when transient behaviour is considered.

Practical selection between these alternatives would also depend on capital cost and expected economic return. Structural modifications introduce additional capital and layout requirements, but may be warranted where improved stability and sustained throughput justify the investment. Control-based adjustments alone were shown to have limited ability to resolve instability arising from strong crusher-mill coupling.

Within this broader design context, dynamic simulation provides a practical means of quantifying how breakage mechanism, surge capacity, and circuit coupling influence overall mill throughput and operational stability.

# CONCLUSIONS

In designing a robust and effective pebble crushing solution, consistency of equipment operation and availability are critical if the milling circuit is to be optimised. The mechanical analysis showed that feed presentation, cavity filling, and force redistribution directly affect crushing intensity and the distribution of forces within the crushing chamber. Partial cavity loading and uneven feed conditions reduce effective breakage intensity, alter product size and are detrimental to mechanical reliability. These effects directly influence crusher performance, efficiency, and service life of key components and therefore they must be considered in any assessment of pebble crushing duty.

In a closed AG/SAG circuit, variability in crushed pebble generation and crusher operation affects the recycle stream returning to the mill and the stability of load control. The dynamic evaluation demonstrated that mill throughput depends not only on instantaneous crushing performance, but on the consistency with which that performance is delivered over time. Where variability is transmitted directly through the recycle stream, gains in breakage intensity are not fully translated into improved mill throughput. Circuit configuration therefore determines how effectively crushing performance is translated into overall mill throughput.

Dynamic process simulation provides a clearer view of the impacts of disruptions and inconsistencies arising from pebble crusher operation and availability. This enables designers to assess the trade-

off between capital and operating costs for the crusher and its associated infrastructure, and the potential loss of value in the milling circuit due to disruption.

In many cases, the authors have found that the impact of inconsistency in pebble circuits is underestimated, and therefore gaining greater insights from dynamic simulations to improve design should be regarded as a prerequisite ahead of any installation.

## ACKNOWLEDGEMENTS

The authors would like to acknowledge David Bowman (BRS) for his input and commentary.

## REFERENCES

Bearman, R A, 2019a. Gyratory and cone crushers, in *SME Mineral Processing and Extractive Metallurgy Handbook* (eds: R C Dunne and S K Kawatra), chapter 3.4, pp 391–416 (Society for Mining, Metallurgy & Exploration: Englewood).

Bearman, R A, 2019b. Crusher selection and performance optimization, in *SME Mineral Processing and Extractive Metallurgy Handbook* (eds: R C Dunne and S K Kawatra), chapter 3.6, pp 427–441 (Society for Mining, Metallurgy & Exploration: Englewood).

Harding, J, Bearman, R A and Munro, S, 2022. An investigation of gyratory crusher liner wear at the Telfer Operation using non-operational streamlined modelling, in *Proceedings International Mineral Processing Congress Asia-Pacific Conference 2022*, pp 153–168.

Hilden, M M and Powell, M S, 2018. A model of SAG mill power incorporating slurry filling and its application to real-time mill performance analysis, paper presented to Comminution ‘18, Cape Town, South Africa, 16–19 April.

Morrell, S and Morrison, R D, 1996. AG and SAG mill circuit selection and design by simulation, in *Proceedings International Conference on Autogenous and Semiautogenous Grinding Technology*, vol 2, pp 769–790.

Powell, M S, 1991. The effect of liner design on the motion of the outer grinding elements in a rotary mill, *International Journal of Mineral Processing*, 31(3–4):163–193.

Torres, M and Casali, A, 2009. A novel approach for the modelling of high-pressure grinding rolls, *Minerals Engineering*, 22(13):1137–1146.

Valery Jnr, W and Morrell, S, 1995. The development of a dynamic model for autogenous and semi-autogenous grinding, *Minerals Engineering*, 8(11):1285–1297.

van der Meer, F P and Fernandez, R, 2015. Pebble crushing by HPGR, in Proceedings International Semi-autogenous Grinding and High Pressure Grinding Roll Technology (eds: B Klein, K McLeod, R Roufail and F Wang) (University of British Columbia: Vancouver).

Viilo, K (ed), 2011. *Crushing and Screening Handbook*, fifth edition (Metso).

Whiten, W J and White, M E, 1977. Modelling and simulation of high tonnage crushing plants, in *Proceedings 12th International Mineral Processing Congress*, vol II, pp 148–158 (São Paulo).

# Reinstating regrind for recovery – spiral technology and sulfide circuit upgrade at St Ives

*T S Chan[1], P Henderson[2] and R Radford[3]*

1. MAusIMM, Project Metallurgist, Gold Fields Limited, Perth WA 6005. Email: shawn.chan@goldfields.com
2. Study Manager, HendoTEK, Perth WA 6005. Email: peter.henderson@goldfields.com
3. FAusIMM, Principal Metallurgist, Gold Fields Limited, Perth WA 6005. Email: reg.radford@goldfields.com

## ABSTRACT

Gold Fields has undertaken continuous asset optimisation programs at St Ives, focused on improving metallurgical recovery and circuit efficiency across a diverse ore profile. Historically, the site operated a dual gravity circuit, including a sulfide recovery and regrind stream centred around Inline Pressure Jig (IPJ) technology. Due to persistent operational and maintenance challenges, the IPJ circuit was decommissioned in 2020. Since then, the metallurgy team has explored alternative pathways to unlock sulfide associated gold, recognising its significant contribution to overall recovery potential.

Extensive laboratory test work demonstrated that sulfide gold can be effectively concentrated using spiral separators, followed by fine grinding to liberate locked gold. Recovery uplifts of 1.4 per cent to 9.25 per cent were observed across key ore sources, with deslimed spiral feed yielding the most consistent results. These findings led to a scoping study with Mineral Technologies and the installation of a full-scale spiral test rig in late 2023. The pilot plant, equipped with a MG12 spiral and deslime cyclone, generated operational data to validate recovery projections and inform process design.

The preferred flow sheet leverages spiral technology proven at Gold Fields' Granny Smith operation, offering a robust, low-maintenance solution tailored to St Ives' ore characteristics. Economic modelling based on conservative gold pricing indicates strong returns, with projected annual profits exceeding A$7 M in early years of operation. Gold Fields is now progressing through Front-End Engineering Design (FEED), with full-scale construction of the sulfide recovery circuit committed for post-2026 delivery.

This paper consolidates the technical rationale, historical context, and forward strategy for implementing a spiral-based sulfide recovery solution that enhances gold recovery, operational reliability, and long-term value at St Ives. It also addresses the complexities of executing a brownfields plant upgrade including legacy infrastructure constraints, integration with existing circuits, and the need to revalidate dormant assets such as the regrind mill while maintaining continuity of operations and minimising capital.

## INTRODUCTION

St Ives Gold Mine (SIGM) is located approximately 80 km south-southeast of the regional city of Kalgoorlie-Boulder in Western Australia and operates a 4.5 Mt/a processing plant treating a combination of underground and open pit ore from the Norseman–Wiluna greenstone belt. Location of the mine site and extensive deposits are shown in Figure 1.

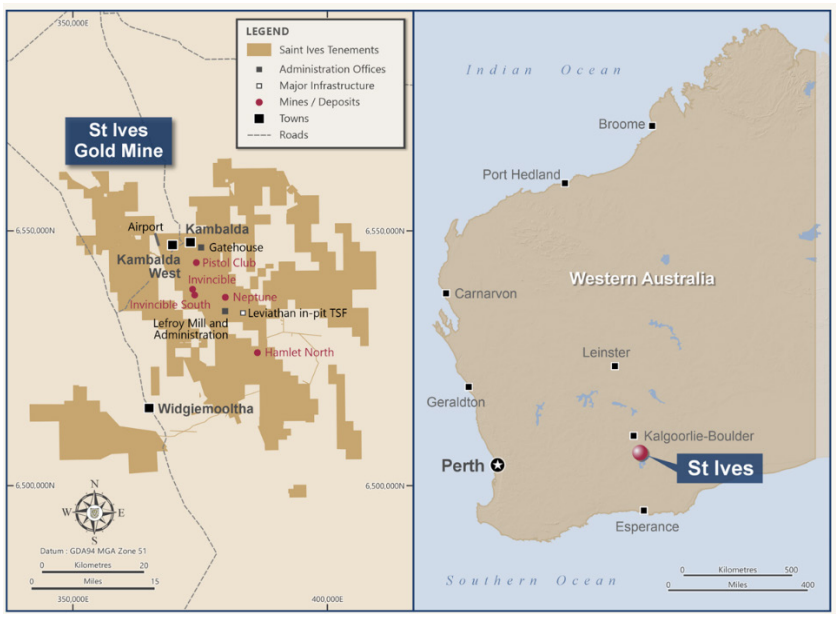



**FIG 1** – St Ives' location.

The St Ives 4.5 Mt/a plant consists of single-stage crushing, single-stage semi-autogenous (SAG) milling, gravity concentration, leaching, carousel carbon-in-pulp (CIP) adsorption, Anglo-American Research Laboratories (AARL) elution, and tailings thickening. The plant was originally designed and commissioned in 2005 with two separate gravity circuits, the flow sheet shown in Figure 2. The first circuit was a conventional gravity recoverable gold circuit employing two SB2500 Falcon centrifugal gravity concentrator units and the second circuit was a sulfide recovery circuit utilising two IPJ2400 InLine Pressure Jigs (IPJ) units and regrinding with a Vertimill® VTM-500, the concentrate streams from both gravity circuits feeding a BA3000 InLine Leach Reactor (ILR).

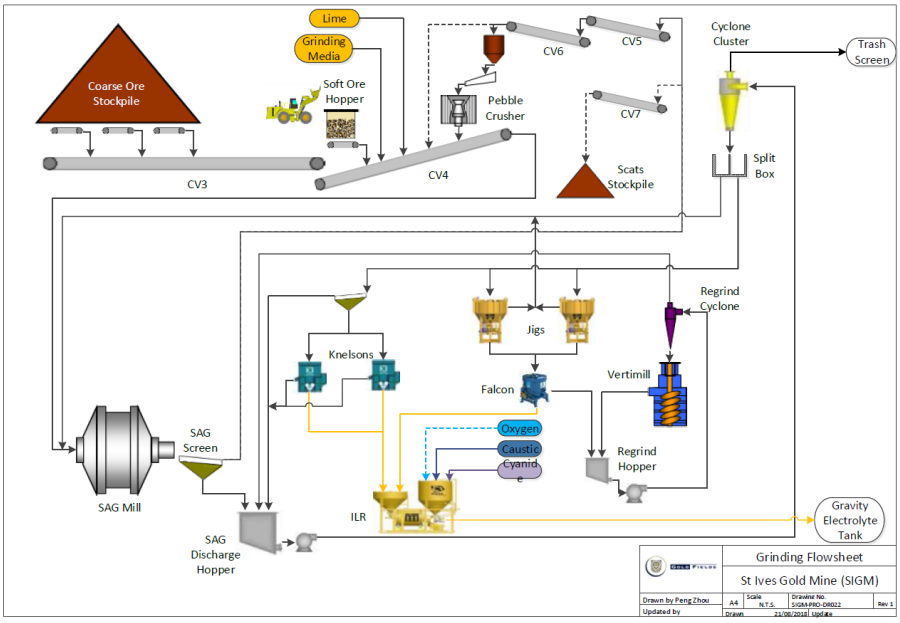



**FIG 2** – Original 2005 St Ives grinding process flow sheet.

Despite overall stable operation, periodic gold losses to tailings were observed, with evidence indicating association with sulfide minerals. Due to poor availability, high maintenance intensity, and inconsistent recovery performance, the sulfide recovery circuit had not run continuously or at full production rates for many years and frequently failed to deliver additional value to the process. In 2020 the sulfide recovery circuit was decommissioned which involved the permanent removal of the IPJ units while the concentrate regrind circuit was placed into care and maintenance. This created

an opportunity to reassess sulfide recovery options using simpler and more robust technologies, while leveraging existing infrastructure such as the regrind mill. This paper evaluates the technical and economic potential of reinstating sulfide recovery through spiral concentration and regrinding at St Ives.

## RESERVES AND RESOURCES LABORATORY TEST WORK

Following decommissioning of the sulfide recovery circuit in 2020, the resource and reserves metallurgical test work was simplified to gravity and leach extraction. Previously, when the jig sulfide recovery circuit was in operation, the resource and reserves test workflow sheet included a Wilfley wet table step on the gravity tails to mimic concentration of sulfide locked gold, followed by fine grinding of the sulfide concentrate to 38 µm prior to the leaching step.

Since the decommissioning of the sulfide recovery circuit, St Ives experienced periodic gold losses to tailings, indicating the presence of unrecovered sulfide-associated gold. St Ives reinstated and conducted test work on the gravity, sulfide concentration with fine grind and leach alongside the simplified gravity and leach extraction flow sheet for selected reserves and resource test work programmes. This was intended to build an improved understanding of the comparative recovery performance, particularly for gold locked in sulfide, and to assess the potential value of including a sulfide concentration and fine grind step. This also presented an opportunity to investigate options to reuse the decommissioned but existing Vertimill® VTM-500 to improve overall recovery at St Ives.

Comparative test work on 24-hour gold recovery was completed on Invincible, Sirius and Hamlet ore samples and presented in Figure 3. Results incorporating the Wilfley wet tabling (sulfide recovery) step indicated a strong association between gold and sulfur, and that liberation of sulfide locked gold through fine grinding of the wet table concentrate to 38 µm increased final gold recovery in all tests. The average recovery increases based on laboratory test work were:

- Invincible Orebody: 88.83 per cent to 90.6 per cent.
- Hamlet Orebody: 93.7 per cent to 95.1 per cent.
- Sirius Orebody: 84.39 per cent to 93.64 per cent.

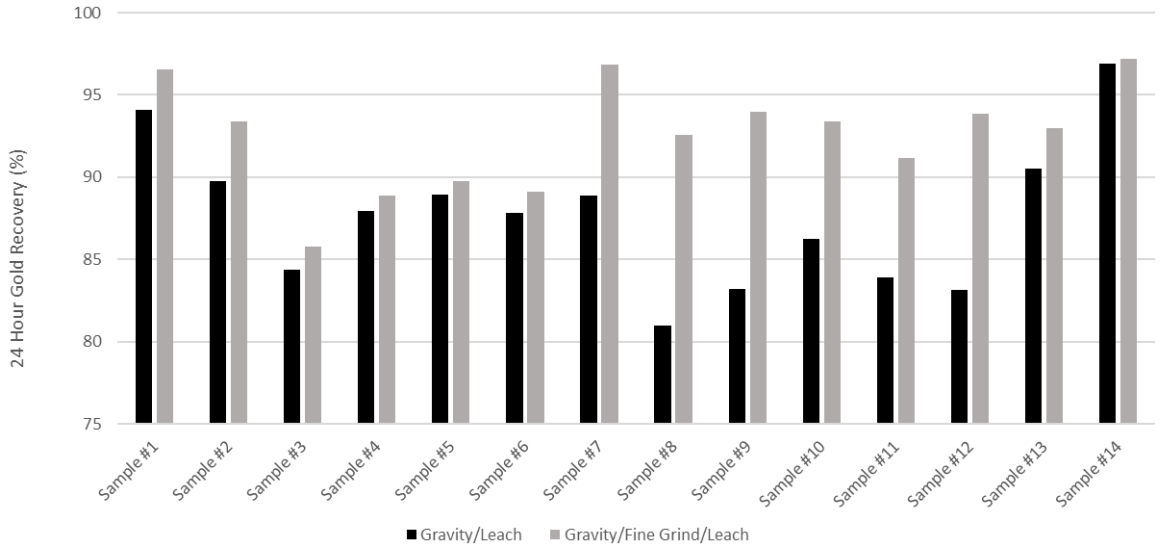



**FIG 3** – Comparative test gravity/leach versus gravity/fine grind/leach.

The largest recovery uplift was observed in ore with a higher proportion of sulfide associated gold.

Figure 3 demonstrates consistent recovery improvement across all tested ore types when incorporating sulfide concentration and fine grinding. Based on the apparent improvement between both test work, St Ives continued comparative test work on both future and existing orebodies to further validate the potential recovery gains. In parallel, options were assessed to develop a processing solution that could improve sulfide gold recovery by utilising the existing regrind mill in combination with alternative sulfide concentration technologies, rather than the previous IPJs.

## SULFIDE CONCENTRATION TECHNOLOGY SELECTION

Gold Fields already operates an established sulfide refractory circuit at the Granny Smith Mine (GSM) for over 15 years, known as the tailings retreatment circuit. This circuit deslimes the CIP tails, concentrates the cyclone underflow using spirals, and uses a Vertimill® VTM-500 to regrind the spiral concentrate. The reground concentrate is then pumped to the mill discharge hopper for CIP re-leaching. A similar type of sulfide refractory circuit employing spiral concentrators on tailings in an operating plant scale has previously been proven to be technically and economically feasible by Martins, Dunne and Delahey (1993). Considering the operational success of the Granny Smith Tailings Retreatment circuit and proven feasibility from Martins, Dunne and Delahey (1993) of utilising spiral concentrators on plant tailings, this circuit configuration was investigated as a practical solution for St Ives. The defined flow sheet for this proposed circuit is shown in Figure 4, noting that differences in ore characteristics and operational philosophy requires further validation through site-specific test work and further study phases.

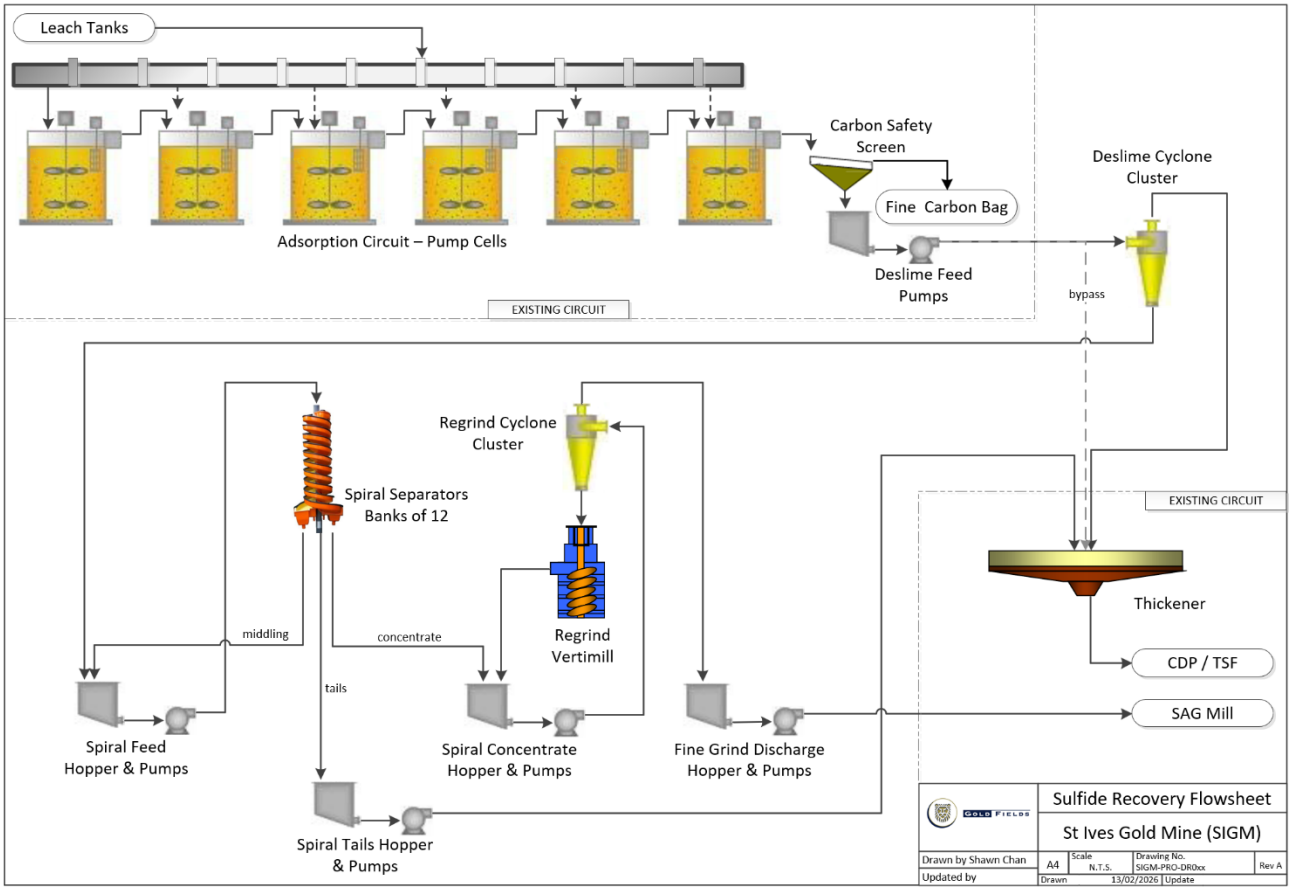



**FIG 4** – Proposed sulfide recovery at SIGM on tailings.

## Sulfide gold recovery spiral test work

A bulk composite sample of CIP tailings (average head grade 0.13 g/t Au) was sent to Mineral Technologies for preparation, including dewatering, homogenisation, and assay. Laboratory spiral test work was conducted in a closed-circuit test rig incorporating a single start FM1 spiral separator.

Release tests for benchmarking theoretical limits, were conducted on the as-received sample at a feed rate of 1.4 t/h and 29 per cent solids. These tests included dry sampling using a riffle splitter and pulverised, with the sub-samples analysed using X-ray fluorescence spectrometry (XRF) and fire assay for Au content. Three release tests were conducted with splitter positions adjusted between tests to generate different mass splits. The test work results indicate:

- Approximately 50 per cent Au was recovered at a mass pull of 10 per cent.
- Rate of recovery slows down significantly at mass pulls of sulfide concentrate greater than 10 per cent, indicating reduced separation efficiency at higher mass recoveries.

- At a spiral feed rate of 1.4 t/h and 29 per cent solids spiral feed density:
  - Concentrate mass yield of ~5 per cent assayed 1.2 ppm corresponding to a gold upgrade ratio of 9.2:1.
  - Concentrate mass yield of ~10 per cent assayed 0.8 ppm corresponding to a gold upgrade ratio of 6.1:1.
- Alignment of the Au and $SO_3$ concentration grade curves indicate that the Au has a strong association with sulfides.

CIP tailings sizing data provided from St Ives to Mineral Technologies shows that the tailings material typically contains >50 wt per cent of -38 µm slimes. A high proportion of slimes can result in highly viscous slurries which are known to reduce separation performance when using spirals. To mitigate the impact of slimes on separation performance, additional test work was conducted on deslimed feed material. Results of the test work including a deslime step are shown in Figure 5.

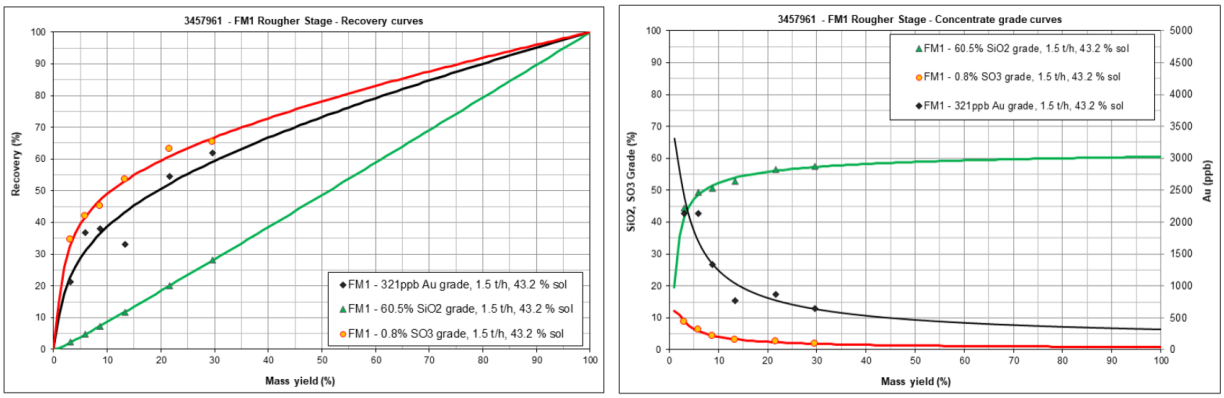



**FIG 5** – FM1 spiral recovery curves and concentrate grade curves including deslime step.

The close correlation between gold and sulfur confirms that the recovered gold is predominantly sulfide associated. The concentrate recovered from the laboratory scale spiral test work was sent to Australian Laboratory Services (ALS) Kalgoorlie for regrinding and leaching test work. This was to simulate the regrinding in the regrind mill at site after recovery by spiral treatment. The sample material was ground to a target $P_{80}$ of 38 µm, then bottle rolled for 48 hrs at 40 wt per cent solids with site water, while maintaining both pH at >9.8 and cyanide (NaCN) at 400 ppm. Samples of 1 kg mass were leached in five replicate samples, with a range of assays performed on selected solution and solid residues to understand the rate of gold recovery and mineralogy. Regrinding of the spiral concentrate significantly improved gold extraction, confirming that liberation of sulfide-associated gold is required to realise recovery gains. These results are based on laboratory-scale testing and require validation under continuous pilot or plant conditions to confirm performance at scale.

## Mineral technologies spiral pilot plant test rig and recovery test work

Following positive laboratory test work, a scoping study was undertaken to evaluate a full-scale sulfide recovery circuit using spiral separation. The study concluded that installing a sulfide gold recovery circuit on tailings is technically and economically viable however the gold recovery improvement estimate was based on laboratory test work performed on two sample set only and, therefore, introduced a high level of technical uncertainty due to the limited data set. For risk mitigation, the scoping study recommended that the site install and operate a spiral pilot plant for approximately three months and generate representative operating data to validate recovery performance and reduce scale up uncertainty.

Gold Fields worked closely with Mineral Technologies to design a modular spiral pilot plant installed in December 2023 and commissioned in January 2024. One of the key objectives was to gather sufficient data on the dominant life-of-mine (LOM) ore source, Invincible Underground, to inform potential gold recovery benefits. The long section view of the LOM orebody is shown in Figure 6. In parallel, data was collected to understand recovery benefits on a blended ore feed. The pilot plant

was operational in the first quarter of 2024 and was considered stable, well controlled and successful. The proposed sulfide recovery flow sheet on tailings is presented in Figure 4.

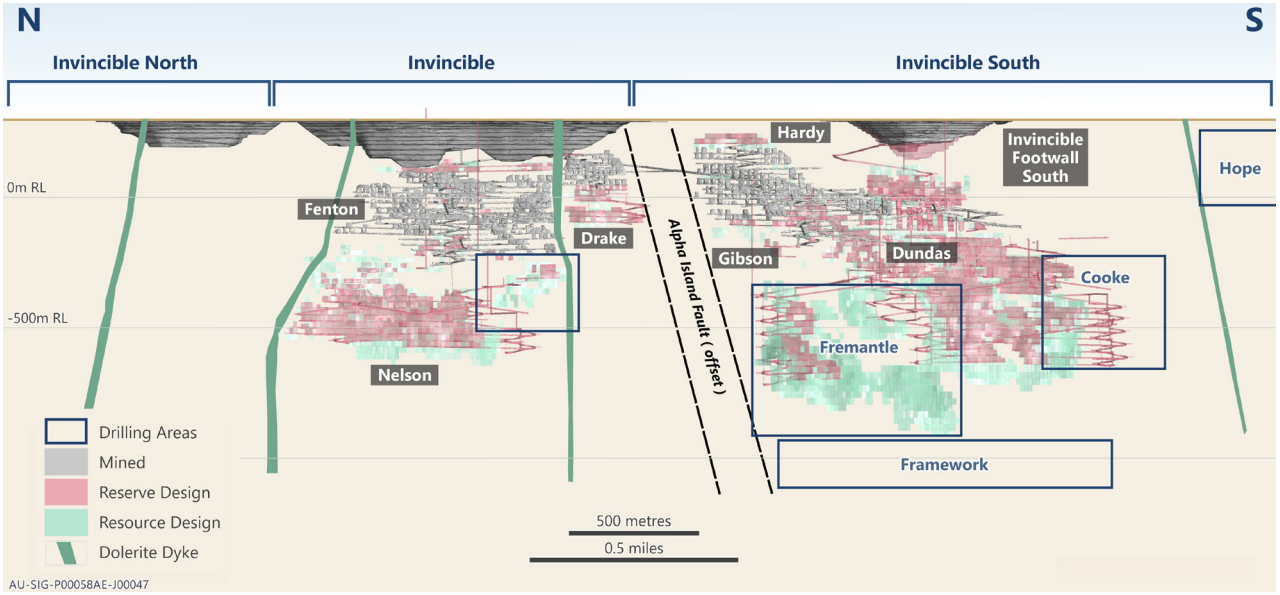



**FIG 6** – Invincible Orebody long section.

The pilot plant was configured to replicate the proposed flow sheet seen in Figure 4, with a focus on controlled sampling and flow measurement. The pilot plant comprised two primary processing stages:

- Desliming utilising a centrifugal pump that pumped adsorption tails slurry to a desliming cyclone, with the cyclone underflow reporting to the spiral separation.
- Spiral separation module utilising two variable speed-controlled pumps and one Mineral Technologies MG 12 spiral separator.

## Invincible ore parcel pilot plant metallurgical interpretation

The analysis and reporting of pilot plant data representing the unblended Invincible ore parcel considered the time required for the previous ore blend contained leach adsorption slurry to be displaced, starting 13th March 2024.

An estimated 43 125 wet tonnes were processed during the campaign at an average gold mill feed head grade and leach feed grade estimate of 3.49 g/t and 2.32 g/t, respectively. Of the 2.32 g/t leach feed grade, approximately 81.1 per cent of this gold is in the solid phase (the remaining gold deports as soluble gold), representing 1.89 g/t. The estimated plant total gold recovery during this period was approximately 93.7 per cent.

For this campaign, the sampling intervals were reduced to 6 hrs and sampled on both day and night shifts with the objective of maximising the number of data points during this period. Using a paired t-test calculation to identify minimum sample size, it was calculated that a total of 27 data points is required to achieve a 95 per cent confidence level. The undertaken sampling campaign only yielded a total of 12 data points collected, which is well below the 27 data points. However, when conducting the t-test to assess the additional recovery benefit against a null hypothesis that there is zero benefit, the p-value is extremely low at ~2.02 E-20. The calculated p-value indicates that the observed recovery improvement is statistically significant; however, the limited number of data points reduces confidence in the robustness of this result. Summarised pilot plant data and subsequent leach and gold recovery on Invincible orebody is presented in Table 1.

**TABLE 1**

Leaching and sulfide circuit KPI's.

| Statistic parameter | Spiral concentrate | | Total sulfide Au recovery (% of pump cell tails) | Additional Au oz/day benefit | Total Au recovery benefit (%) |
|---|---|---|---|---|---|
| | Leach Au recovery (%) | Leach grind size (% passing 38 µm) | | | |
| Mean | 68.9 | 70.9 | 24.9 | 17.1 | 1.5 |
| Standard error | 1.31 | 1.2 | 0.67 | 0.7 | 0.1 |
| Median | 67.8 | 69.8 | 22.9 | 17.4 | 1.4 |
| Standard deviation | 4.54 | 4.17 | 2.3 | 2.3 | 0.2 |
| Minimum | 60.2 | 65.1 | 18.8 | 13.8 | 1.2 |
| Maximum | 75.6 | 77.7 | 26.9 | 21.8 | 1.8 |

The calculated sulfide recovery in pump cell (PC) tailings of 24.9 per cent exceeds the 15.9 per cent assumption used in the scoping study. Using the balanced Invincible data set, the estimated recovery benefit is:

- Recovery of gold contained in the pump cell tails solid phase is 24.9 per cent ± 1.6 per cent.
- This equates to a total plant recovery improvement 1.5 per cent ± 0.12 per cent.

Variability in recovery was observed across the test period, reflecting changes in ore characteristics and operating conditions.

Spiral concentrate was reground to assess the effect of grind size on leach recovery. The target grind size was 65 per cent passing 38 µm, derived on 2023 GSM metallurgical accounting data for the tailings retreatment circuit. For Invincible, the nominal test work conditions for grinding were:

- 1 L of spiral concentrate at ~55 per cent solids.
- 14 kg of 12.7 mm spherical grinding media was used.
- Grind time of 12 mins.

Leach tests were conducted on reground concentrate under controlled conditions to evaluate recovery performance. The leach solution was analysed for gold on-site, and the leached solids were sent to Australian Laboratory Services (ALS) Kalgoorlie for fire assay analysis. During the Invincible ore treatment campaign, many grind versus leach recovery tests were performed daily on-site, as shown in Figure 7.

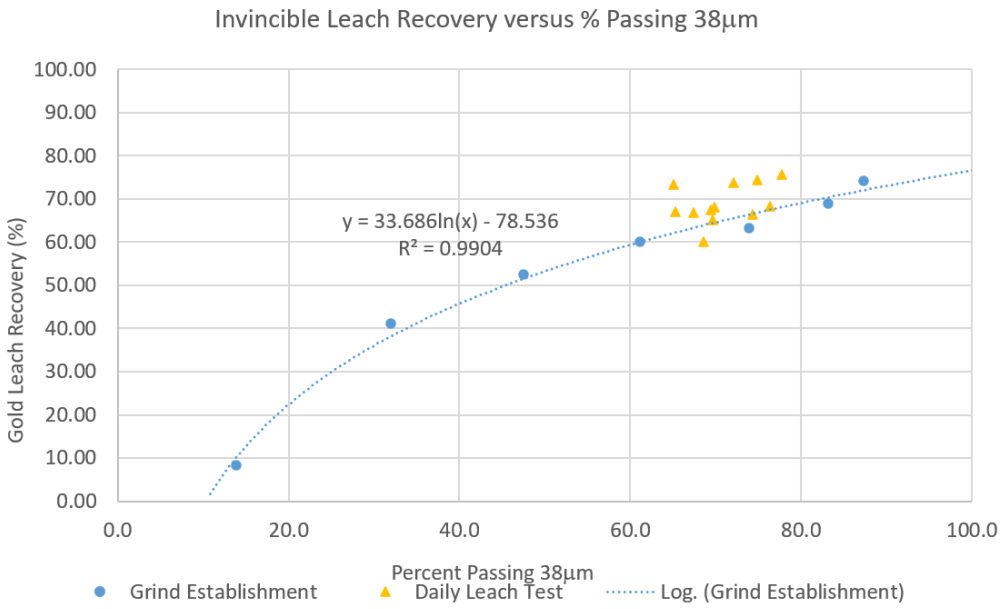



**FIG 7** – Invincible grind versus leach recovery tests.

Leach recovery was strongly dependent on grind size, confirming that fine grinding is required to liberate sulfide-associated gold. The leach test performed without grinding shows that some gold (8.3 per cent) is liberated and available for leaching without grinding. This supports the limited presence of liberated and/or coarse gravity gold that had not leached to completion in the available residence time.

The average grind size achieved was approximately 71 per cent passing 38 µm, which is slightly finer than the target of 65 per cent passing 38 µm.

## VTM-500 capacity selection

A jar mill test work was undertaken to determine the grindability of the life-of-mine ore and assess specific energy (SE) requirement to inform final selection of regrinding unit operation for the proposed sulfide recovery circuit at St Ives. In 2020, GSM had also completed a jar mill test work on their tailing retreatment circuit. Jankovic (2024) compared the St Ives jar mill test work to GSM's jar mill test work, where both operating conditions are the same (mill size, mill speed, ball filling and size, %solids), concluding that the operating work index (WiO) differences are due to the material hardness. Jankovic (2024) evaluated that the comparative 'hardness ratio' (WiO ratio) of the sulfide concentrate to be 0.68 for the target range of $P_{80}$ between 20 to 30 µm, which was of interest at the time of the evaluation.

The comparative analysis indicated that the GSM regrind Vertimill® performance can be reasonably approximated by the Bond formula calculations using an operating work index WiO of 21 kWh/t. The circuit capacity of St Ives tailings sulfide mineral concentrate was estimated based on GSM's VTM-500 circuit performance on benchmarked WiO material and jar mill test results. It was concluded that St Ives material is softer and that the operating work index of the regrind circuit should be reduced accordingly. For the St Ives Vertimill® selection, Jankovic (2024) advises selection of WiO of 14 kWh/t based on applying a correction factor of 0.68 for fine grinding to a $P_{80}$ of 20 µm. Table 2 shows the calculation results for the VTM-500 at 375 kW (referencing the existing decommissioned Vertimill at St Ives) and an VTM-500 with an installed mill power of 465 kW (based on discussed potential 20 per cent increase). Mill motor power utilisation was assumed at 95 per cent, with total mechanical and transmission losses of 7.5 per cent.

**TABLE 2**

VTM capacity bond calculations – WiO of 14 kWh/t and $F_{80}$ of 265 µm.

| | VTM-500 – 375 kW | | VTM-500 – 485 kW | |
|---|---|---|---|---|
| **Throughput (t/h)** | **$P_{80}$ (microns)** | **VTM SE @ pinion (kWh/t)** | **$P_{80}$ (microns)** | **VTM SE @ pinion (kWh/t)** |
| 30 | 51 | 11.0 | 39 | 13.7 |
| 25 | 41 | 13.2 | 31 | 16.4 |
| 20 | 31 | 16.5 | 23 | 20.5 |
| 14.5 | 20 | 22.7 | - | - |

The proposed St Ives sulfide recovery targeted a concentrate regrind feed rate to the Vertimill® at 25 dry t/h. At this target feed rate, the results indicate that the existing 375 kW installation is unlikely to consistently achieve the target grind size, while the higher power configuration provides improved grinding efficiency and reduced product size. Over-speeding the existing 375 kW Vertimill® motor to 60 Hz via a Variable Speed Drive (VSD) was assessed as a potential option to increase energy input by an estimated 20 per cent. Using the relationship shown in Figure 8, the grind size $P_{80}$ achieved when over-speeding the existing 375 kW mill motor to 60 Hz is estimated to be 32 µm. However, upon further evaluation with the electrical engineer and Vertimill® vendor, over-speeding the motor is expected to significantly reduce the life of the motor, associated bearings, and gearbox of the mill. Associated risks were further accentuated by the poor condition of the existing mill's gearbox, bearing and mill shell conditions which was noted requiring significant overhaul to operate at the new duties. Over-speeding the 375 kW motor is similar to using the next expected motor size, ie 465 kW, but with increased mechanical risk. The $P_{80}$ calculations shown in Table 2 for an installed power of 465 kW, use the same operating work index and $F_{80}$ inputs as the 375 kW motor calculations.

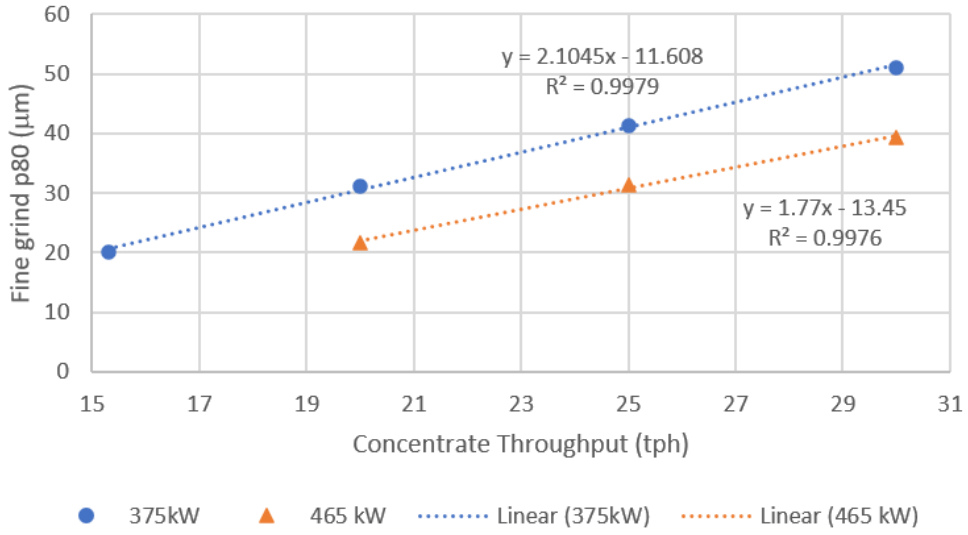



**FIG 8** – Fine grind $P_{80}$ versus throughput relationships.

It was calculated that for the design throughput of 25 t/h, the existing VTM-500 circuit with 375 kW installed power would generate a product size $P_{80}$ of ~41 µm. The recommendation from these findings were to select an VTM-500 with increased motor power input to achieve the $P_{80}$ ~32 µm product size.

## Process performance prediction

Process performance prediction utilises results from the pilot plant for Invincible Underground, along with the fine grinding power review presented by Jankovic (2024).

Figure 8 illustrates the relationship of grind size and installed grinding power at various throughputs. The relationship of interest for this study is the 375 kW relationship, which aligns with the 375 kW of installed power of the existing Vertimill®. The grind size can then be calculated at the design spiral concentrate production rate of 25 t/h using Equation 1:

$$\text{Grind size (µm)} = 2.1045 * (\text{spiral concentrate throughput}) - 11.068 \quad (1)$$

Inserting spiral concentrate throughput of 25 t/h into Equation 1, the estimated grind size for the existing VTM-500 mill with an installed power of 375 kW is 41 µm. The calculated grind size of 41 µm can then be entered into Equation 2, which is the relationship that is used for estimating the gold leach recovery of 72.6 per cent is as follows:

$$\text{Gold leach recovery} = -0.5853 * (\text{grind size}) + 96.631 \quad (2)$$

The average total gold benefit for a full-scale plant can be calculated by inserting the 72.6 per cent leach recovery estimate into pilot plant mass balance data. The average total gold benefit when applying fine grind concentrate leach recovery of 72.6 per cent is 1.54 per cent, which is the value used for further processing and financial evaluations.

## ST IVES SULFIDE RECOVERY CIRCUIT DESIGN

Results from test works discussed and pilot plant studies supported progression to feasibility study in 2024 followed by a front-end engineering design (FEED) in 2025. The feasibility study further refined the scoping study design, defining a robust and fit-for-purpose sulfide recovery circuit while employing lessons learnt from the GSM operation. Key deliverables from the feasibility study included finalisation of the process design, developing a study-level capital and operating cost estimate as well as a preliminary schedule for the execution of the project. The FEED focused on finalising design and further maturing the capital cost estimates, execution schedule and execution planning to enable effective project controls during execution and to support final investment decision. A 3D model of the proposed sulfide Recovery Circuit developed during the FEED is presented in Figure 9.

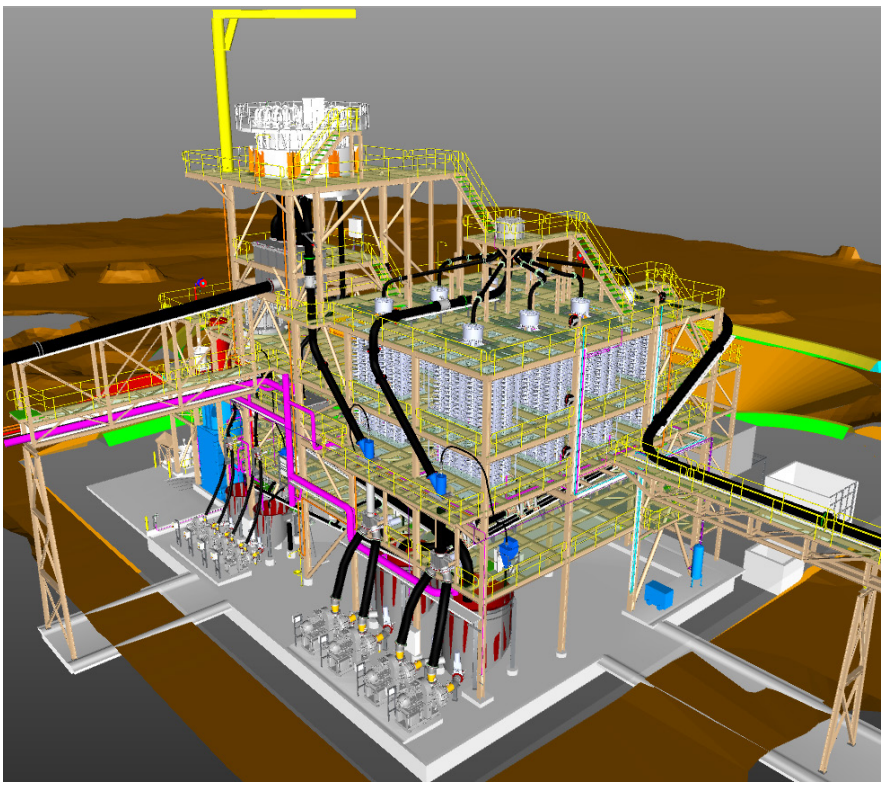


**FIG 9** – 3D model of the proposed sulfide recovery circuit.

## Process design criteria

The sulfide gold recovery circuit was designed for a capacity of 613 t/h of plant tailings with a design life of 20 years. The final design criteria was based on pilot plant performance, supported by laboratory test work and benchmarking against the Granny Smith operation. The main design criteria for the plant are summarised as follows, categorised by the three distinct unit operations of desliming, spiral concentration and regrinding:

1. Deslime cyclone classification:
    - Design capacity = 613 t/h
    - Cyclone feed $F_{80}$ = 128 µm
    - Cyclone overflow $P_{80}$ = 38 µm
    - Mass split to underflow = 54.8 per cent w/w.
2. Gravity spirals concentration:
    - Nominal feed = 325 t/h
    - $F_{80}$ = 177 µm
    - Mass pull to concentrate = 9.4 per cent w/w
    - Mass to concentrate = 25 t/h.
3. Regrind milling:
    - Nominal feed = 25 t/h
    - $F_{80}$ = 262 µm
    - $P_{80}$ = 32 µm
    - Recirculating load = 300 per cent.

The process design prioritises recovery of sulfide-associated gold while maintaining manageable mass pull and regrind throughput.

## Equipment selection

Major equipment selection was based on pilot plant performance and metallurgical test work, which included selection of eight banks of 12 Mineral Technologies twin-start spiral separators and a 485 kW VTM-500 with appropriately sized reducer and gearbox. Selection of a 485 kW VTM-500 was finalised following further discussions with study stakeholders, electrical engineer and Vertimill® vendor, noting that reusing the existing 375 kW VTM-500 at St Ives was technically not feasible to achieve design parameters, while being equally cost prohibitive to remove and refurbish the Vertimill® asset for new duties. Additionally, over speeding the 375 kW at 60 Hz by 20 per cent was mechanically flawed, with significant risks to future maintenance of the mill. Further discussions with the mill vendor indicated a motor that is next size up from the 375 kW was a 485 kW motor but required appropriate reducer and gearbox selection. Based on these discussions supported by the test work results, a higher power VTM-500 configuration was selected to achieve the target grind size and maximise recovery potential.

Other key equipment includes deslime and regrind cyclones clusters, duty-standby pump sets, primary samplers utilising in-line pressure pipe samplers and secondary samplers utilising rotary vezin sampler proven at GSM and located on all major slurry streams accompanied with a suite of density gauges and flowmeters to enable good metallurgical accounting.

# BROWNFIELD PROJECT CHALLENGES

The brownfields nature of the project introduced several design challenges. Initial feasibility study design incorporated lessons learnt from operations and maintenance of the GSM circuit coupled with recent spiral separator projects. Iterative design review process at FEED stage, with the involvement of the St Ives processing department, assisted with the final development of a robust circuit, focusing

on operability and maintainability of the new circuit, while providing consideration of the adjacent circuit maintenance interfaces as well as site specific conditions attributable to being on a salt-lake.

The other major challenge for the project is the location of the circuit, where modifications to the existing event pond is required albeit while maintaining exact same volumetric capacity post-modifications. Additionally, as St Ives is a signatory to the Cyanide Code, the project has been appropriately designed to meet the code, in consultation with the relevant internal and third party stakeholders.

## FUTURE WORKS AND CURRENT SCHEDULE

The front end engineering design was completed in Q1 2026 with the project currently progressing to the final gates of approvals for execution of the package. The sulfide recovery circuit is expected to be commissioned by 2027. The final design reflects a balance between recovery improvement, capital efficiency, and operational simplicity within the constraints of an operating brownfields plant.

## ACKNOWLEDGEMENTS

The authors wish to acknowledge the support and contribution of the St Ives and Granny Smith operations and maintenance teams, Gold Fields Limited Perth metallurgy technical support team and the numerous professionals who continuously contribute to and support operations.

## REFERENCE

Jankovic, A, 2024. Vertimill Test work Review and performance prediction, Report to St Ives Gold Mining Company Pty Ltd, report K-Rp-0005

Martins, V, Dunne, R and Delahey, G, 1993. New Celebration Tailings Treatment Plant – 18 Months Later, in *XVIII International Mineral Processing Congress*, pp 1215–1222.

# Issues with determining the SAG mill specific energy – key drivers influencing mill selection

*R Chandramohan[1], G Lane[2], G Ballantyne[3], C Haines[4] and C Meinke[5]*

1. Head of Process Optimisation, Ausenco, Vancouver BC V6E 3S7, Canada.
   Email: rajiv.chandramohan@ausenco.com
2. FAusIMM, Principal Consultant, Ausenco, South Brisbane Qld 4101, Australia.
   Email: greg.lane@ausenco.com
3. FAusIMM, Director of Technical Solutions, Ausenco, South Brisbane Qld 4101, Australia.
   Email: grant.ballantyne@ausenco.com
4. MAusIMM(CP), Technical Consultant, Ausenco, Newcastle NSW 2304, Australia.
   Email: campbell.haines@ausenco.com
5. Senior Process Engineer, Ausenco, Vancouver BC V6E 3S7, Canada.
   Email: connor.meinke@ausenco.com

## ABSTRACT

Autogenous and Semi-Autogenous Grinding (AG and SAG) mills are the most versatile comminution devices for hard rock grinding. Selecting the correct AG or SAG mill size (installed power, mill dimensions, and drive selection) for the grinding circuit duty is a crucial step in flow sheet development, as the comminution circuit typically accounts for a large share of a mineral processing plant's capital cost. Selecting the appropriate AG or SAG mill for comminution duty primarily depends on ore characteristics, feed size distribution, and product requirements (downstream processes).

Over the years, several papers have discussed how structurally altered orebodies, such as Andean ore or ore from seismically active zones, influence feed-size distribution, ore characteristics, and measured AG and SAG specific energy. These ores typically appear very competent in standard tests but show lower measured SAG mill specific energy; therefore, they do not align with the general understanding of the relationship between ore competency and SAG mill specific energy models.

This paper discusses factors affecting SAG mill-specific energy calculations that standard ore characterisation methods do not capture, and the considerations needed to improve SAG mill sizing methods.

## INTRODUCTION

Comminution equipment is the most capital-intensive and critical process equipment in hard rock mining (Lane *et al,* 2023). The Autogenous (AG) and Semi-Autogenous (SAG) mills are considered the 'modern-day workhorses' for the application. Their use and versatility make them the default major comminution device for a range of ore types and properties in various circuit configurations. Since their first application in the early 1950s, AG, then SAG, mills have treated ore with a range of feed size distributions and competence. Feeds have come from primary gyratory, secondary or tertiary cone crushers, high-pressure grinding rolls (HPGRs), pebble crushers, scalping screens or run-of-mine feed (such as those implemented in South Africa in the gold and platinum industry) (Chandramohan *et al,* 2023; Chandramohan, Lane and Morley, 2021; Powell, Morrell and Latchireddi, 2001).

The selection of a suitable AG or SAG mill is primarily determined by the ore competence (the resistance of the +10 mm material to breakage) and the feed size distribution (Morrell and Valery, 2001; Lane, 2007). These two factors influence breakage rates in the grinding mill and, in turn, affect throughput and product size distribution.

In greenfield projects, sensitivities to ore competence and hardness, the degree of rock mass fracturing, and the inability to identify these factors can lead to undersized equipment (failure to achieve nameplate throughput) or oversized equipment (higher project capital cost).

In their review of secondary crushing retrofits, Putland, Siddall and Gunstone (2004), Siddall and Putland (2007), and Chandramohan and Lane (2024), noted that some AG and SAG mills have required secondary and/or tertiary crushing retrofits to debottleneck for competent ores. Staples *et al*

(2015), Bailey *et al* (2009), and Lane (2007) reported several SAG mill-based project failures, highlighting that poor performance is primarily due to inadequate mill sizing and insufficient benchmarking during circuit design for treating competent ores.

The typical issues leading to poor performance are one or a combination of:

- insufficient or unrepresentative sampling
- poor testing protocols
- inappropriate interpretation of data and definition of design criteria
- prioritising maintenance preferences over process needs
- inaccurate mill sizing methods
- poor project management decisions.

An oversized AG or SAG mill can lead to overcapitalisation, making the project unfeasible. A review of some projects, especially for ores with high competence (circa Axb <35) and located in the Andean mountain range, indicated that the measured SAG mill specific energy is much lower than that of projects with similar ore competency values located in Canada and Australia (Foggiatto *et al,* 2022). Mills treating very competent ores in Canada and Australia are much larger or require pre-crushing, whereas Andean and some Pacific Rim ores with similar Axb values require smaller mills or no pre-crushing. The difference in capital cost for a large project, say 160 kt/d throughput, can be up to USD200M.

This paper examines potential causes of the lower measured SAG mill specific energy values compared with some calculations. The following questions focus on the key aspects of the review:

- Are we calculating the SAG mill specific energy correctly?
- Are we missing other measurements during ore characterisation?
- How do we modify our approach to capture the response of the ore in the SAG mill environment accurately?

## WHAT ARE ANDEAN OR STRUCTURALLY ALTERED ORES?

Project locations in the Andean region and operations processing structurally altered ores generally follow the subduction and collision zones between tectonic plates (Figures 1 and 2). Many copper-porphyry deposits occur along plate boundaries. Ore deposits such as Cadia and Northparkes formed on ancient volcanic arcs from the Ordovician period (circa 450 million years ago). In contrast, ore deposits such as Batu Hijau, Los Bronces, and Collahuasi formed during the Miocene and Eocene periods (circa 50–25 million years ago). Ore from these ‘younger’ ore deposits behaves differently from ore from Cadia, Northparkes and Canada. Erosion has worn away the softer components of the older deposits, leaving a consistently competent/harder feed, or a feed with lower variability in ore competence. This may explain why some ores sourced from the Western Cordillera are consistently hard and competent, as glacial movement has removed softer ore components over time. In contrast, the younger deposits may comprise a mix of soft and hard components in the mill feed, providing a distribution of competency measurements during testing.

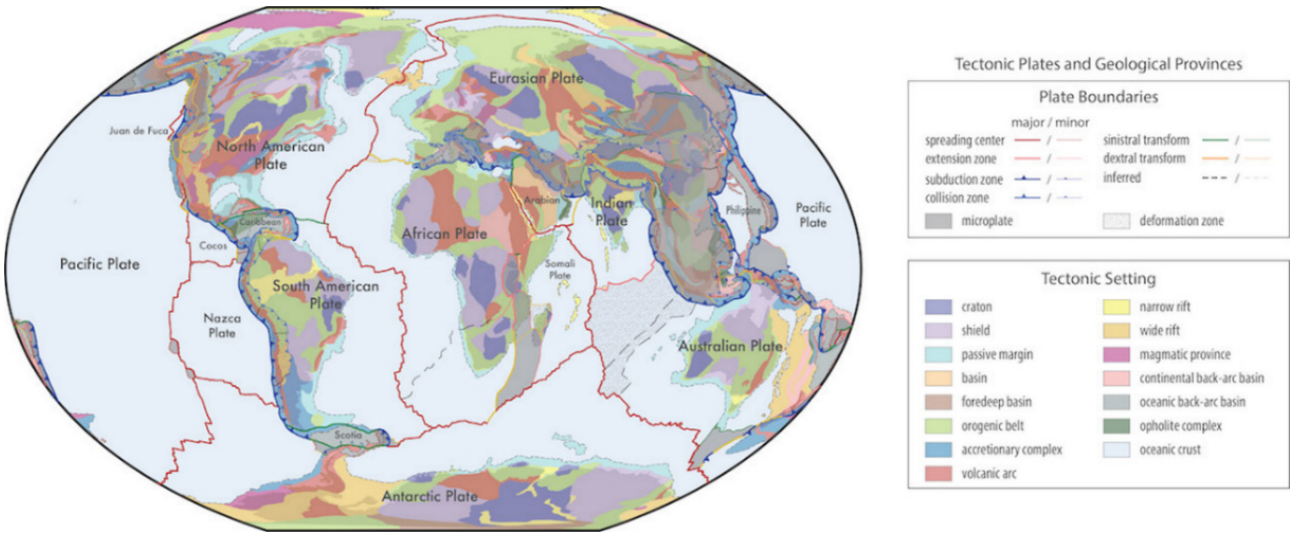



**FIG 1** – Tectonic plates and geological provinces after Hasterok *et al* (2022).

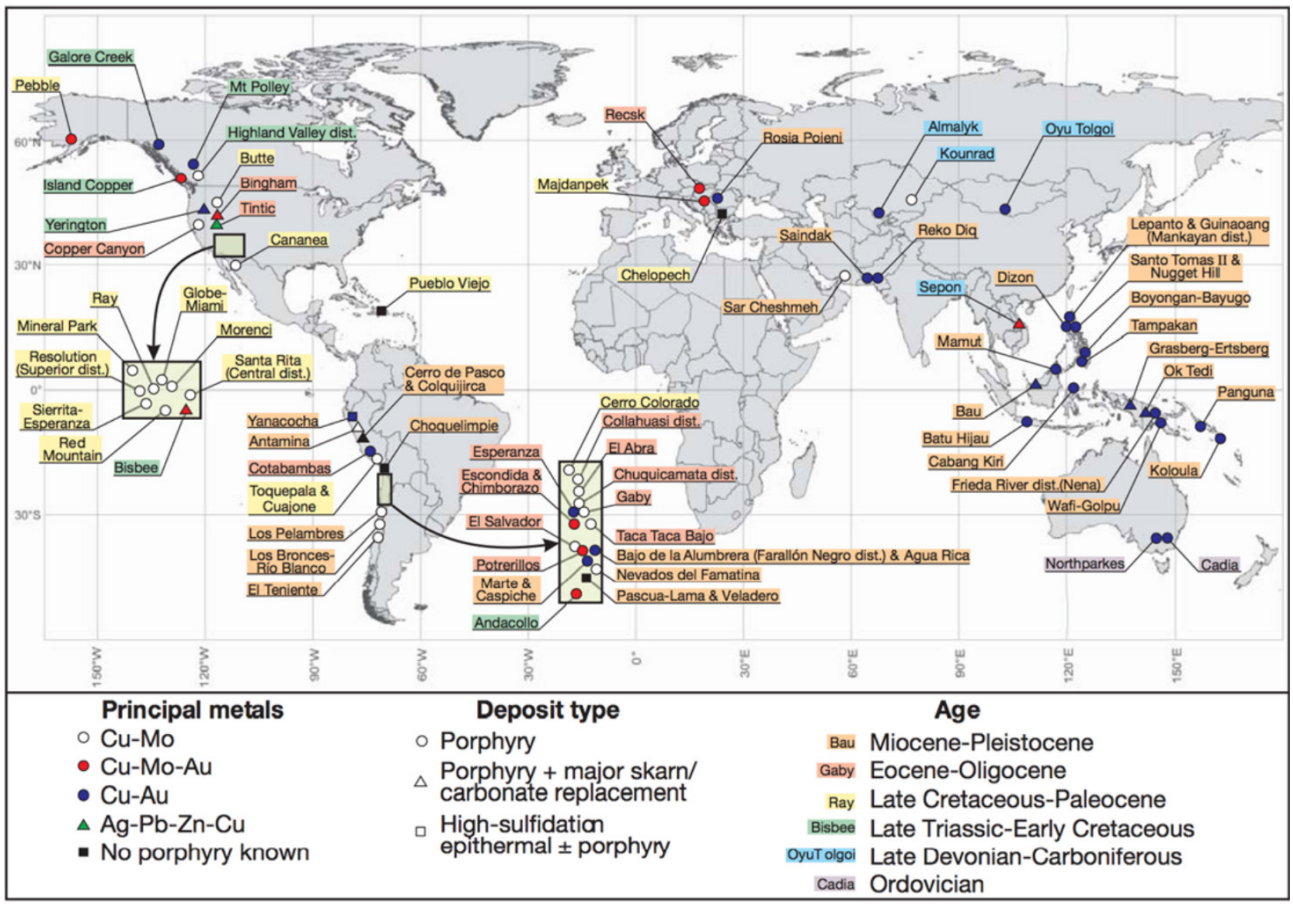



**FIG 2** – Global map of the location, age, deposit type and principal metals of major porphyry copper deposits after Sillitoe (2010). (Image sourced from Cropp, Goodall and Bradshaw, 2013).

Several papers have reported variance in measured SAG mill specific energy for the same competence (Axb) value (Veillette and Parker, 2005; Bailey *et al,* 2009; Dance *et al,* 2006; Daniel and Wang, 2014). Figure 3 presents the well-known relationship, first reported by Veillette and Parker (2005), between ore competency and SAG mill specific energy. Bailey *et al* (2009) highlight that variations of this relationship are widely used by consultants to benchmark SAG mill size and configuration across different ore types. They cautioned that there is uncertainty in SAG mill power determination for Axb values below 30 (which increases with competency) without careful review of the ore characterisation data and interpretation of the results. Based on their experience, the scatter in measured SAG mill specific energy is significant for Axb values below 25, with values ranging

from 18 to 12 kWh/t. This difference can significantly affect grinding-circuit performance if the selected mill dimensions and power do not match the ore's actual specific energy requirements.

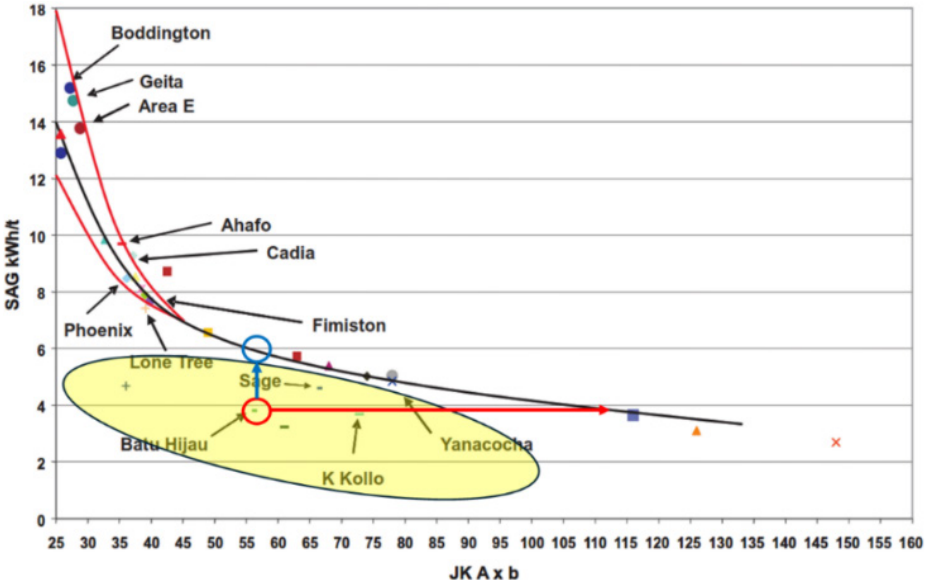



**FIG 3** – Relationship between JK Axb, and measured SAG mill specific energy values (based on Veillette and Parker, 2005; and modified after Bailey *et al,* 2009).

The yellow-highlighted region shows data from areas considered to have high seismic activity or to have undergone significant alterations – for example, Batu Hijau. Located in a high-seismicity and volcanic zone known as the Ring of Fire, Batu Hijau has a measured ore competency value of 55 on the Axb scale (moderate competence). The measured SAG mill exhibits specific energy and performance characteristics typical of a soft ore, similar to those with an Axb value of ~100 in the Australian context. Based on Veillette and Parker's general observation, the Batu Hijau's SAG mill should have had a high specific energy (Blue circle).

Foggiatto *et al* (2022) extended the data range of Veillette and Parker's Axb versus SAG mill-specific energy relationship with operations in the Andean region (Figure 4). They noted no single relationship between JK Axb and SAG mill-specific energy values; rather, it is a continuum, with the SAG mill exhibiting a wide range of specific energy for the same ore competence. Foggiatto *et al* (2022) did not identify the primary reasons for the variance. Instead, they developed a SAG mill-specific energy correction for ores from Andean and structurally altered regions, based on standard single-particle ore competency tests.

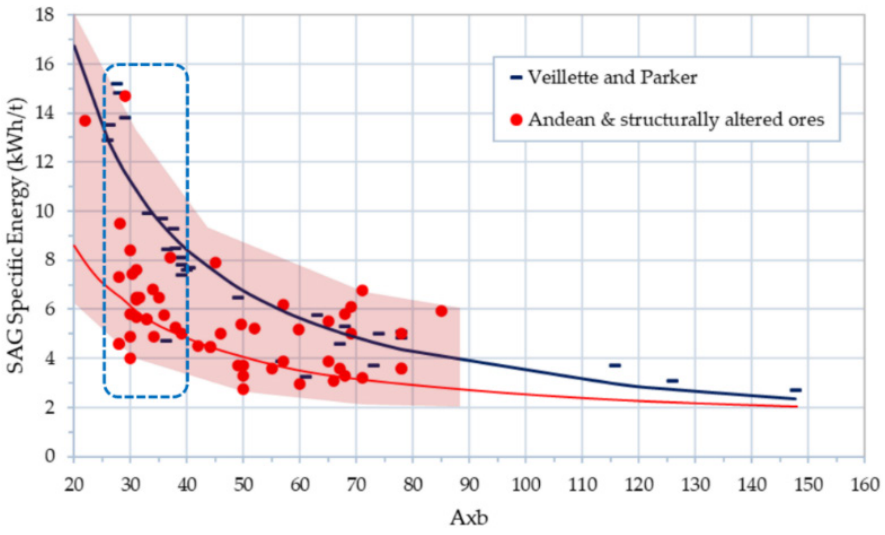



**FIG 4** – Veillette and Parker relationship mapped with Andean or structurally altered ores (after Foggiatto *et al,* 2022).

Although Foggiatto *et al's* (2022) work attempts to distinguish the general trend (Veillette and Parker's curve) between ore competency and SAG mill specific energy in the Andean and structurally altered regions, there is significant scatter in the data, with overlap between the Andean and structurally altered data and the Veillette and Parker trend, with some Andean ores apparently behaving like 'Australian ores'. For example, the area highlighted by the blue dashed box shows the specific energy range for Axb competency values between 25 and 40 – the Andean and structurally altered ores can have a range in measured SAG mill specific energy between 4 and 15 – a 300 per cent difference.

While several factors influence the measured SAG mill specific energy, there is a performance factor that is not captured during ore characterisation test work using the JKDWT or SMC test. Foggiatto *et al* (2022) stated that the variation in mill behaviour when treating ores with similar bench-scale test work results may be attributed to the macro-scale fracturing of the ore that is missed in small-scale competency tests, such as the JK Drop Weight Test (JKDWT), SMC, Geopyöra, HIT and Minpraxis (Chandramohan *et al,* 2023; Nadolski *et al,* 2024). Factors that influence macro-scale fracturing are:

- Natural occurrence due to stress during or after formation. This is often measured using the rock quality designation (RQD) during drill core logging (Deere and Deere, 1989).
- Increased blasting intensity with increasing the fines generation (a higher proportion in the mill feed below <25 mm) (Scott, Kanchibotla and Morrell, 1999).

To incorporate the effect of run-of-mine (ROM) ore fracture on SAG mill specific energy, correction factors can be applied to standard models to account for the additional fracture. Chandramohan *et al* (2015) proposed a method to correct the SAG mill F80, especially in power-based modelling, using rock quality designation (RQD) of the rock mass as a proxy, the measured ore competency DWI, and the primary crusher closed setting (CSS). The main issue with this approach is the reliance on the RQD to correct the SAG mill feed size distribution, which is based on inferred visual data from the structural integrity of drilled core. In their assessment of RQD data, Tims *et al* (2024) emphasised that the RQD methodology is inherently prone to errors in identifying domain intervals, fracture planes (open or closed), and even rubble. Several attempts have improved the measurement and the methodology, and modern core logging systems enable automated RQD assessments that reduce the need for subjective geological analysis (Elmo and Stead, 2020; Palmström, 1996; Pells *et al,* 2017). However, the authors of this paper have encountered projects with high RQD-drilled core values (>80 per cent) and corresponding higher competency ore characterisation data (Axb <35), yet have significantly lower measured SAG mill specific energy than predicted during commissioning and operation.

## ARE WE CORRECTLY MEASURING ORE COMPETENCE?

We know that ore competence affects the apparent energy efficiency of a SAG mill-based comminution circuit (Morrell, 2004; Lane, Foggiatto and Bueno, 2013). We know that circuits based on stage crushing, HPGR, and ball milling have energy requirements similar to those predicted by the Bond method using the Bond ball mill, rod mill, and impact work indices. However, as ore competence increases (generally signified by lower Axb values), a SAG mill circuit's energy efficiency reduces. This difference can be as much as 40 per cent for very competent ores. However, not all ores with measured low Axb values result in AG- or SAG-mill-based circuits with the same SAG mill-specific energy and overall energy efficiency.

Generally, in power-based modelling, the Bond crusher, rod and ball mill work index data are used to determine the required circuit-specific energy for a SAG-based circuit (Figure 5). Morrell (2004) uses Mia, Mic and Mib as a version of the Bond method, but the general formulation is similar: determining the overall circuit-specific energy based on standard ore characterisation tests. The overall specific energy for the comminution circuit is calculated from the feed and product size distributions, typically using a single-passing size (eg 80 per cent of the feed or product size). Power-based models assume that the feed and product curves are linear and parallel in the log-log size distribution plot (Figure 6).

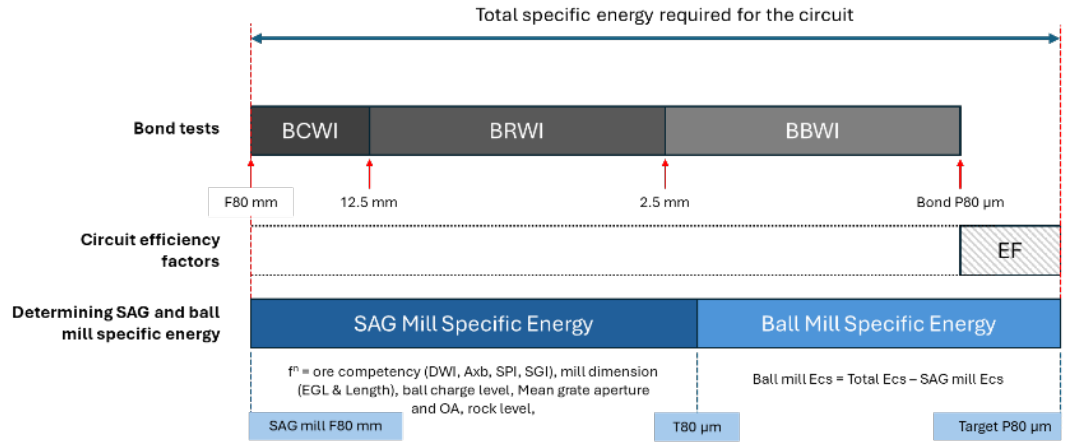



**FIG 5** – Schematic of power-based modelling approach for SAG and ball mill sizing.

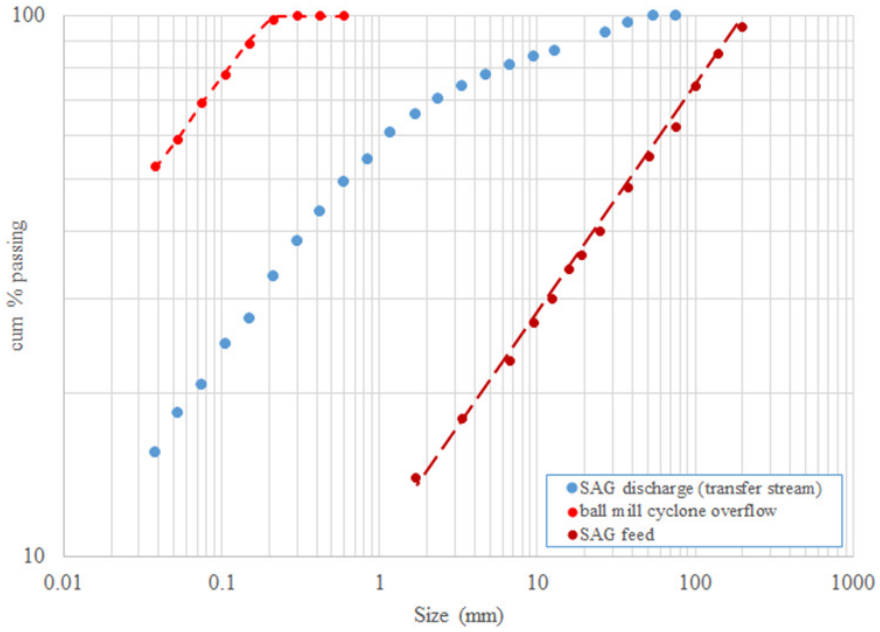



**FIG 6** – Example of size distributions of SAG mill feed, transfer and ball mill overflow streams (after Morrell, 2011).

The required SAG mill specific energy is a function of mill diameter, ball load, mill length, feed size distribution, and ore competency, where the ore competency for the same ore is derived from the single-particle and grindability tests (Lane, Foggiatto and Bueno, 2013; Barratt and Allan, 1986; Barratt, 1989; Starkey and Dobby, 1996; Siddall and Putland, 2007; Burgess, 2012; Amelunxen, Berrios and Rodriguez, 2014).

Consultants use various methods to determine the specific energy of SAG mills. While the general SAG mill-specific energy formulation is similar, some fix the transfer size (T80), whereas others vary it based on circuit and operating parameters. The transfer stream is the product size from the SAG mill discharge.

The SAG mill discharge, or the transfer stream, does not conform to the strict mathematical rule of linear, parallel curves on a log-log chart. Morrell (2011) described the transfer stream as highly complex and difficult to sample, and noted that no single equation can predict the size distribution curve from SAG mill performance. Morrell (2011) described the transfer size as an arbitrary number that can be fixed for circuit design; ie in his methodology, Morrell (2004) selected an average size of 750 µm to define the transfer size and calculate the specific energy for AG and SAG mill sizing. This number can be adjusted based on survey data, particularly for brownfield expansion (eg retrofitting secondary grinding in SSSAG circuits). For all ores, correction factors are required in the calculation to ensure that the SAG mill is sized based on the SAG mill feed size and expected transfer size

distributions. In brownfield operations, survey data can be used to model SAG mill performance; in greenfield projects, assumptions are required based on test work, particularly when T80 is used in the calculation.

Measuring the ore's competence and hardness is an essential first step in sizing AG and/or SAG mills. All comminution tests aim to characterise the ore that is being processed. However, bench-scale tests do not fully mimic the AG or SAG mill breakage environment. Therefore, comminution models or calculations are required to predict the required grinding environment. Ore characterisation aims to reduce project development risk and is a critical step in developing comminution circuit flow sheets. The following key questions are pertinent to all sizing methods in greenfield projects:

- Does the tested ore adequately represent the life-of-mine ore source?
- Which ore lithology and alteration types are dominant in the mine plan?
- Does the test method suit the ore type?

Chandramohan *et al* (2023) stated that two generally accepted approaches exist for characterising ore for AG or SAG mill sizing and selection: grindability tests and single-particle breakage tests (Figure 7). Both test outcomes are used in power-based mill-sizing models. However, only single-particle test results are used in population-balance models, where JKDWT results are used to generate the specific energy–$t_n$ relationship, a precursor to the matrix function for the breakage model. These tests are used in comminution models to estimate the specific energy required to process ore from a given feed size distribution to a target product size distribution under specified operating conditions. Therefore, the sample representation is critical for comminution equipment sizing methods.

The single-particle tests require samples with masses ranging from 75 kg (JKDWT) to 5 kg (HIT, Geopyörä) to represent the processed material. Sample selectivity and representation are critical to the sizing methodology to determine life-of-mine performance. Therefore, stringent selection criteria are required to minimise sampling bias. Small-scale tests, such as the SMC test, use ore density (specific gravity, SG) as a reference to select particles for breakage tests within one standard deviation of the mean SG value (Morrell, 2004). Geopyöra has employed a similar method to determine the SG of the ore during testing, thereby obtaining a distribution of the DWI breakage function (Bueno *et al,* 2021). Like SMC, Geopyörä and HIT aim to increase the number of tests – thereby generating a distribution of ore competency values for one rock type. Sampling bias is a major issue in single-particle tests, as only blocky rocks that survive drilling and core transport are typically selected for comminution characterisation. Chandramohan (2013) highlighted that particle-shape bias in sample selection can significantly skew competency measurements, making a sample appear either very competent or soft.

Early sizing methods (circa 1970–90s) for SAG mills relied heavily on pilot plant tests, which required at least 50–100 t of ore. These tests are costly, require sample masses that can be hard to obtain, particularly when targeting 'representative ore', and require careful planning before they are carried out. The objective of the pilot plant test is to determine the SAG mill specific energy under operating conditions that mimic actual operations.

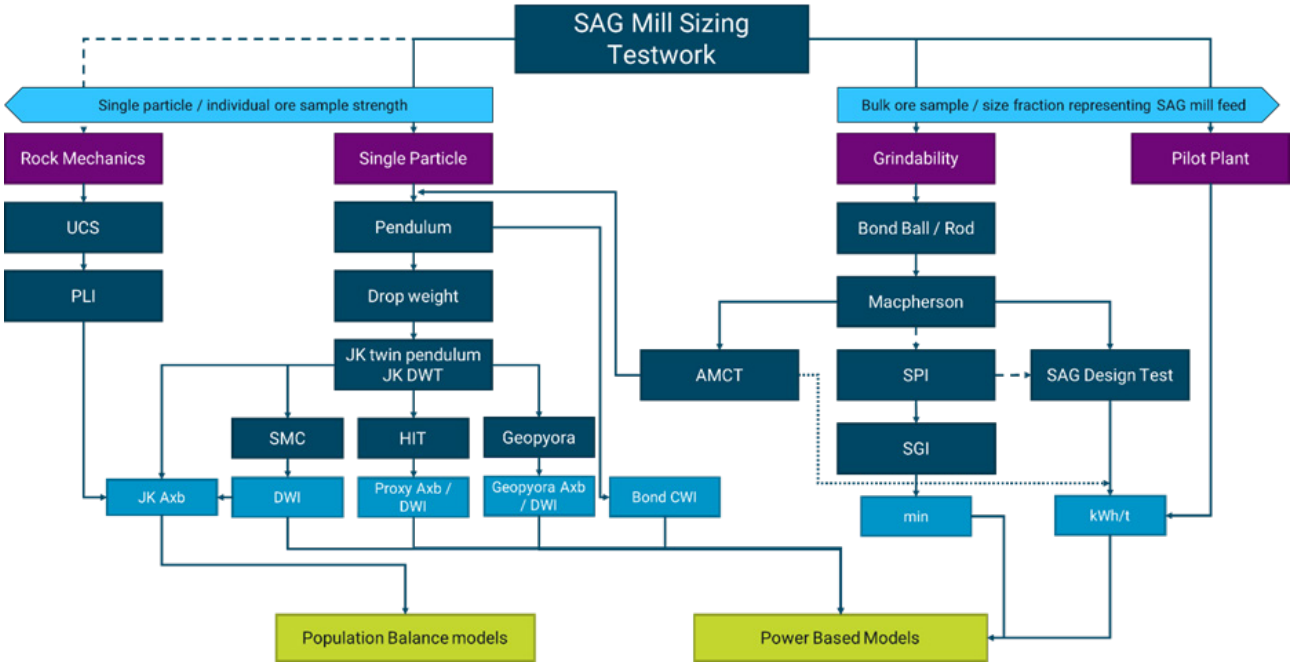



**FIG 7** – Overview of ore characterisation tests and application (Chandramohan *et al,* 2023).

Tests that use 'whole ore samples', such as the SPI, SGI, and SAG Design tests, aim to mimic 'pilot plant' test conditions using smaller samples with finer size distributions and are conducted under controlled operating conditions in open circuit. The rod mill work index is a 'whole ore sample' test that operates in closed circuit and better accounts for the variable contributions of components in heterogeneous feeds.

Chandramohan *et al* (2023) summarised that single-particle tests are better suited for ores with Axb < 75 (DWI > 4 kWh/m$^3$ and SPI/SGI > 60 min). The grindability tests, such as SGI, SPI, and SAG Design tests, are more suited to lower-competency or friable ores. The main reason for this preferred approach is that lower-competence ores are typically highly variable and mixed, comprising hard and soft components, and therefore require a test mechanism to quantify the accumulation of the harder component of the ore, which is typical behaviour in the grinding environment for highly mixed altered ores.

The high-energy impact/crush testing used by the drop-weight mechanisms of SMC, JKDWT, and HIT, or the roll-crusher-type mechanism used by Geopyörä and Minpraxis, could overestimate or underestimate specific energy, depending on particle shape, size, and orientation relative to the crushing planes. In Chandramohan's PhD work (2013), high-speed filming showed that softer ores tend to undergo significant re-breakage during crushing because lower strain rates are required for crack propagation, which would bias the measured $t_{10}$, making it appear significantly softer than it should be. The authors note that projects using single-particle tests that yield ranges above 75 (sometimes up to 250) on the Axb scale warrant caution when sizing the SAG mill, as the tested particles would have undergone re-breakage, resulting in an undersized SAG mill for the circuit duty. The Geopyörä and Minpraxis devices aim to minimise re-breakage by employing two counter-rotating rolls to crush ore samples.

Grindability tests such as the SPI, SGI, and SAG Design test better reproduce the behaviour of softer ores in the SAG mill (Bailey *et al,* 2009; Chandramohan *et al,* 2023). Because the softer components break preferentially in these tests, the measured competency (specific energy) depends on the closing screen, circulating load, fixed ball charge level, and rock level. Bailey *et al* (2009) stated that:

> *'The SPI/SGI method has been used successfully to predict performance correlations when treating soft ores, and is* ***arguably a better statistical approach*** *to sample selection and testing when compared with the JKDWT or SMC Test (or other single particle breakage tests) as the latter rely on the selection of single particles of a predetermined size and this in itself may create a bias in the test method for soft ores.'*

The main differences between the two characterisation methods are highlighted in Table 1. Fundamentally, sizing methods that use single particle tests do not rely on a closing screen to estimate the required SAG mill specific energy. Instead, competence is determined by randomly selecting, by size, hard and soft components of the ore. The average ore competence is derived from the probabilistic breakage function applied to the product-energy relationship (Narayanan and Whiten, 1988). The single-particle approach assumes that laboratory impact tests can represent the variety of breakage mechanisms occurring within a tumbling mill, including autogenous mechanisms such as self-breakage and abrasion.

**TABLE 1**

Key differentiators between single particle and grindability characterisation tests (after Chandramohan *et al,* 2023).

| Focusing question | Single particle characterisation | Grindability characterisation |
|---|---|---|
| What are the key assumptions used for AG/SAG mill sizing? | • Progeny generation is a function of matrix breakage (ie self-similarity probability breakage function).<br>• Using a single ore measurement to map the entire breakage environment history in AG/SAG mill.<br>• Hard and soft ore components in the mill feed are assumed to have an average (weighted average) ore property.<br>• No closing screen is required in the test, and the estimated specific energy for mill sizing is independent of transfer size, ball charge level. | • Accumulation of competent feed in the SAG mill defines the required specific energy for sizing.<br>• The closing screen controls the transport of the ground product and circulating load.<br>• Test outcome is based on a fixed ball and rock charge level (ergo, a fixed power input). |
| Where and how is it primarily used? | • Population balance models and power-based models.<br>• Applied as a key input variable to calculate the AG/SAG mill-specific energy (ball charge and total mill filling levels; grate/trommel classification is independent of ore competency). | • Power-based models.<br>• Calculates the mill-specific energy as a function of transfer size and predetermined operating conditions (ball charge and total mill filling levels). |
| What are the risks of using such a test for AG/SAG mill sizing? | • Population balance models are non-linear and often don't have unique solutions.<br>• Reliant on the distribution of strength tests to map the required mill-specific energy.<br>• Rock shape can bias the strength measurement. | • Reliant on the distribution of strength tests to map the required mill-specific energy.<br>• Track a single size, typically 80 per cent passing.<br>• Reliant on fixed ball charge and mill filling levels – requires operational data to modify the mill-specific energy $f_{sag}$ factors for different operating conditions ($f_{sag}$ = factors adjusting the SAG mill specific energy based on ore competency, fragmentation, mill dimensions, circuit configurations, operating parameters etc). |
| How are samples selected for the test in greenfield projects? | • Core samples are crushed or cut; only blocky or competent particles are selected for the test. | • All core samples are crushed and riffled to portion out the required mass for the grindability test. |

In grindability tests, all samples are crushed and portioned to the required mass for batch grinding. Ore competence is determined by the time required to grind the entire mill feed passing the closing screen.

Sample representation is crucial for single-particle tests, especially when individual particles are selected from the broken core for characterisation. If sampling bias is observable in single-particle tests, it should show clear deviations when benchmarking against grindability tests, especially when comparing Andean or structurally altered ores with non-altered ores.

In Figure 8, the relationships between SPI and Axb indicate no discernible sampling bias between the two characterisation methods for the same sample. The data indicate no significant difference between the model-fit power models comparing Andean ores from the high-seismic region with non-altered ores. Both single-particle and grindability tests select representative samples of the hard and soft components of the core/ore as part of their standard procedures.

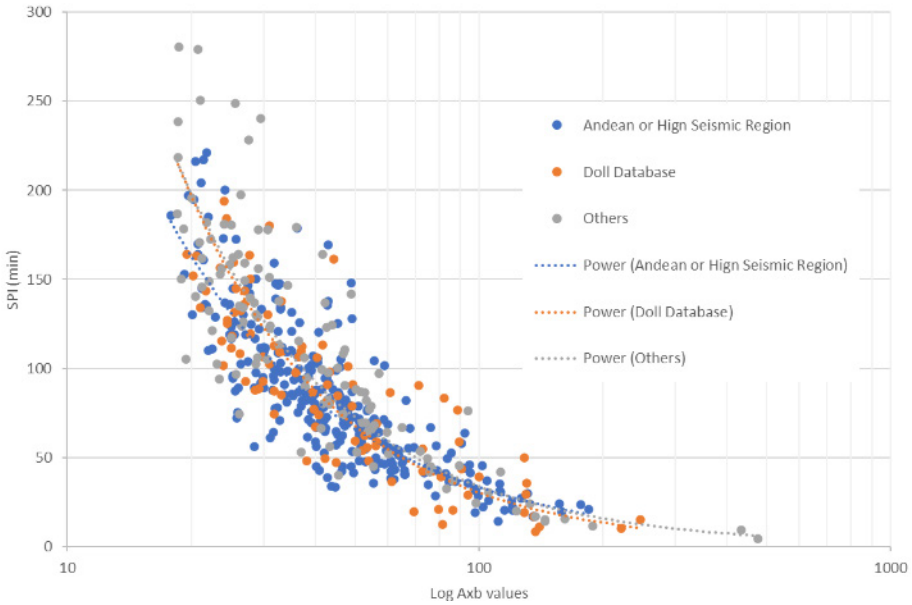



**FIG 8** – Comparison of SPI versus Axb (Doll database sourced from Doll, 2025).

If there is no evidence of sampling bias between the two characterisation methods, then other mechanisms must drive the regional variance in SAG mill specific energy, as shown earlier in Figures 4 and 7.

## How does RQD affect SAG mill specific energy?

RQD measures rock fragmentation based on visual inspection of core samples. The designation of core quality is based on the degree of fracturing within the core, with less than 10 cm (4 in) of fracturing per core section (Deere and Deere, 1989). For example, in Figure 9, the lower RQD core tray exhibits greater fragmentation than the higher RQD core tray; the two trays are visually distinct. Generally, for single-particle tests, only the competent or intact section of the core sample is selected for ore characterisation.




**FIG 9** – Examples of core RQD (sourced from Chandramohan *et al,* 2015).

Wirfiyatal and McCaffery (2011) developed a throughput model for Batu Hijau using a combination of RQD, point load index (PLI), rock mass rating (RMR) and comminution parameters such as the JKDWT. They commented that because the Batu Hijau geology primarily comprises quartz-vein mineralisation, and the general distribution of the density of the mineralisation is similar for coarse and smaller rocks, the competency of small and large rocks will be similar – ie hinting that there will be no size-effect as suggested by Morrell in the particle size versus Axb relationship (Morrell, 2004). Wirfiyatal and McCaffery (2011) concluded that the degree of core fragmentation, as inferred from RQD, primarily affects particle-size distribution rather than rock competency.

Based on the above assumption, Chandramohan *et al* (2015) used Morrell's (2004) original formulation to determine the SAG mill F80 based on the degree of fracturing in core samples (Equations 1 and 2). The assumption is that the overall bulk sample per tray (shown in Figure 9) can be lumped into the size reduction only – ie the change in the feed size distribution to the SAG mill (Foggiatto *et al,* 2022).

$$SAG\ mill\ F80 = 0.2\ \times CSS \times DWI^{0.7} \quad (1)$$

$$SAG\ mill\ F80_{if\ RQD>80\%} = 0.2\ \times CSS \times DWI^{0.7} \quad (2)$$

$$SAG\ mill\ F80_{if\ RQD<80\%} = (0.2\ \times CSS \times DWI^{0.7}) \times (0.75 \times RQD + 0.4)$$

The fundamental premise of correcting the SAG mill feed size distribution using RQD is that the ore property is:

1. Generally homogeneous and has less competency variability.
2. The smaller rocks sourced from the fragmented cores have similar strength properties to larger intact core samples.

Figure 10 presents a core tray with varying degrees of core fragmentation. The yellow zone comprises highly fractured core samples, and the red zone comprises largely intact cores. The clear colour variation between the zones highlights a transition zone or a different type of mineralisation. Depending on the competency test and required sample mass, the core sample would be crushed or cut into pieces and mixed to represent the core tray.

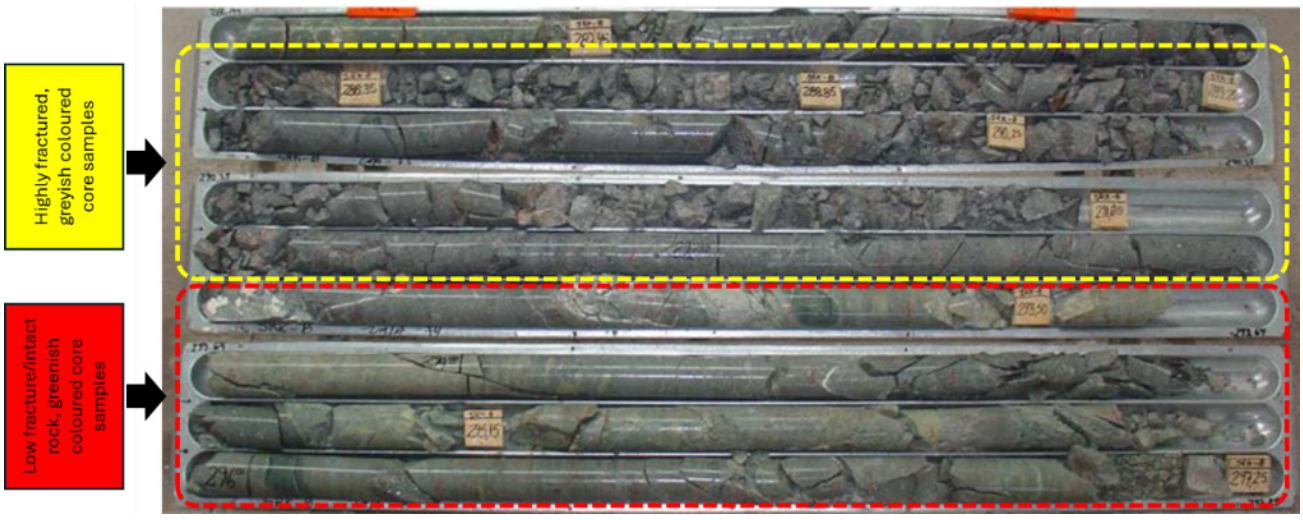



**FIG 10** – Assessing the lower RQD core sample.

Table 2 presents a hypothetical estimation of the SAG mill specific energy using the core sample presented in Figure 10. The assumption is that the entire core tray has an average Axb value of 35, and only the SAG mill F80 is modified by the degree of fragmentation as defined by Equation 2. The SAG mill specific energy is derived from the Ausgrind comminution calculation (Lane, Foggiatto and Bueno, 2013). Based on the analysis, the calculated SAG mill F80, particularly for low RQD values, can be misleading, as cores in the yellow zone may show significant fracturing, less-competent material, and more sandy or rubble-type fragmentation. The calculated SAG mill F80 value of 59 mm for the yellow zone does not match the visual observation.

**TABLE 2**

Hypothetical SAG mill specific energy estimated based on modified SAG mill F80.

| | Yellow zone | Red zone | Overall tray |
|---|---|---|---|
| Estimated RQD, % | <25 | 80 | 53 |
| Estimated Bulk Axb | | 35 | |
| Estimated DWI, kWh/m$^3$ | | 7.7 | |
| Estimated primary crusher CSS, mm | | 120 | |
| Calculated SAG mill F80, mm | 59 | 100 | 80 |
| Estimated SAG mill specific energy, kWh/t | 7.63 | 9.62 | 8.65 |

The main issue is that the degree of fragmentation, as defined by RQD, is insufficient to fully capture the rock mass's variability (see Figure 11). Tims *et al* (2024) characterised RQD as a visual oversimplification of the rock that can easily miss crucial information and misclassify the overall rock structure, particularly in intervals, breaks, and fragmentation below 10 cm, as defined by the RQD calculation (Deere and Deere, 1989).

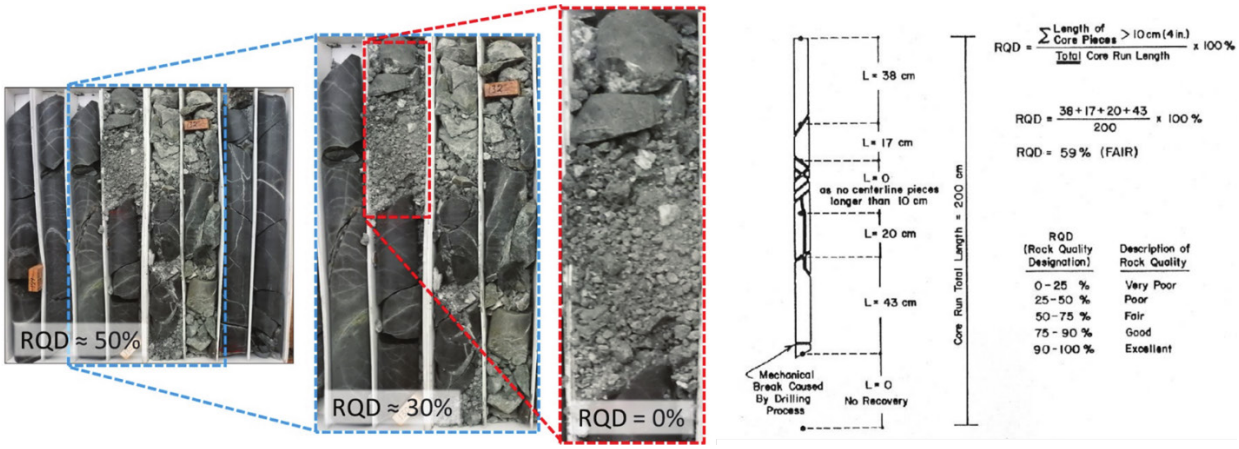



**FIG 11** – RQD does not capture the variability in the rock mass (image sourced from Tims *et al,* 2024; Deere and Deere, 1989).

For example, the three core trays classified with an RQD value of 'near zero' are visually different (Figure 12). When fed to a SAG mill, the measured F80 will differ among the three samples. Assuming the same competency value for all three samples, Sample A will likely have a higher SAG mill specific energy than Sample C. Sample C would more easily pass through the mill, resulting in a shorter mill residence time.



(a) (b) (c)

**FIG 12** – Example of RQD samples defined as near-zero percentage: (a) mechanical/drill breaks; (b) broken cores, no gouge, possible fault; (c) fault with gouge (image and analysis sourced from Tims *et al,* 2024).

In their work, Tims *et al* (2024) proposed redefining the rock mass fragmentation using a core-damage index (CDI) in addition to RQD and solid core recovery index (SCR) (Figure 13). The CDI measures the degree of fragmentation as a function of core diameter and is categorised into classes, with Class 1 denoting an intact core and Class 5 denoting highly fragmented material with broken particles representing sand or rubble.

Therefore, the same core section that is defined to have a high CDI value can have a lower RQD (section A). Similarly, a lower CDI value can indicate a medium-to-low RQD core section (Section B).

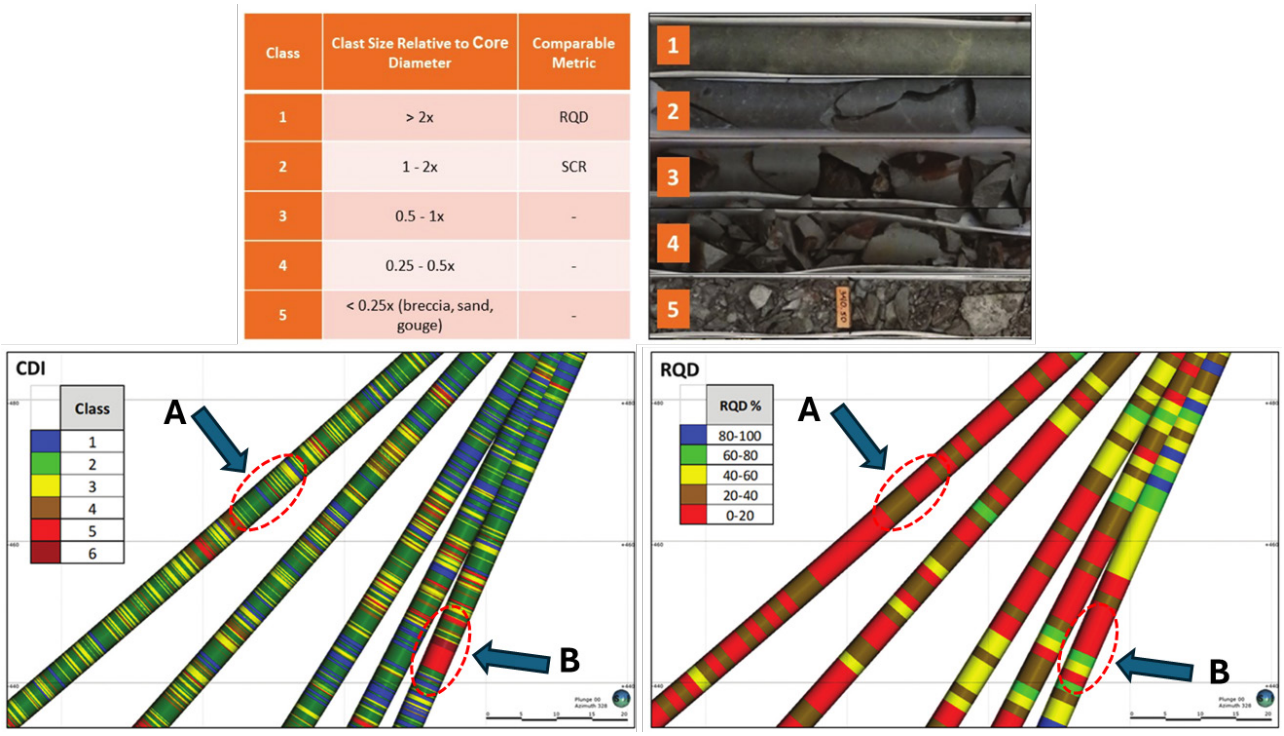



**FIG 13** – CDI and RQD classification and example (modified after Tims *et al,* 2024).

## Does rock abrasion affect the SAG mill specific energy?

The literature has established that breakage mechanisms in AG and SAG mills can be classified as impact, abrasion, compression, and attrition (Napier-Munn, 2005). This fundamental understanding led to the development of the early version of the population balance model, which was incorporated into the JKSimMet® software. The model structure was developed using Kam Leung's PhD work

(Leung, 1987). A key model component was the abrasion parameter $t_a$, measured using the JK abrasion method (Napier-Munn, 2005). The standard abrasion tumbles 3 kg of 55 + 38 mm particles for 10 mins in a 305 × 305 mm (dia × length) mill with 4 × 6 mm lifter bars. The $t_a$ is a 1/10 passing of the mean particle dimension; a lower $t_a$ value indicates a harder ore. The autogenous media competency test (AMCT), widely used by Minproc, Orway Mineral Consultants, and others, follows a similar methodology but uses larger particle sizes and a larger-diameter mill (McKen and Chiasson, 2001).

In Leung's original formulation of the AG and SAG breakage model, the $t_a$ was used to calculate the 'low energy' appearance function, and Axb was used to calculate the 'high energy' breakage function (Leung, 1987). The low-energy appearance function was applied primarily to the coarser size fraction in the mill, circa +55 mm. Early modelling of grinding survey data using $t_a$ in JKSimMet® yielded erroneous results, highlighting that abrasion alone may not adequately describe the breakage of coarse-rock; rather, lower-energy impacts or incremental damage are the main drivers (Whyte, 2005; Morrison, Shi and Whyte, 2007). Currently, the JK $t_a$ value is rarely used to calculate the appearance function in the latest breakage model in JKSimMet®; instead, the breakage model relies primarily on Axb (Hilden, 2017).

Figure 14 presents relationships between the JK $t_a$ and Axb values sourced from Alex Doll's public database (Doll, 2025). Some Andean ores (highlighted in red) have higher $t_a$ values than the mean trend (shown as equation JK $t_a$ = 0.01 × Axb). Ores with higher $t_a$ can exhibit different SAG mill performance than ores of similar competency at much lower $t_a$ values. For comparison, a Canadian operation (black data) in Quebec is shown in the same database, indicating that high-grade ores can have variable $t_a$ values. Logically, variable $t_a$ should affect SAG mill performance such that higher $t_a$ values correspond to lower mill-specific energy.

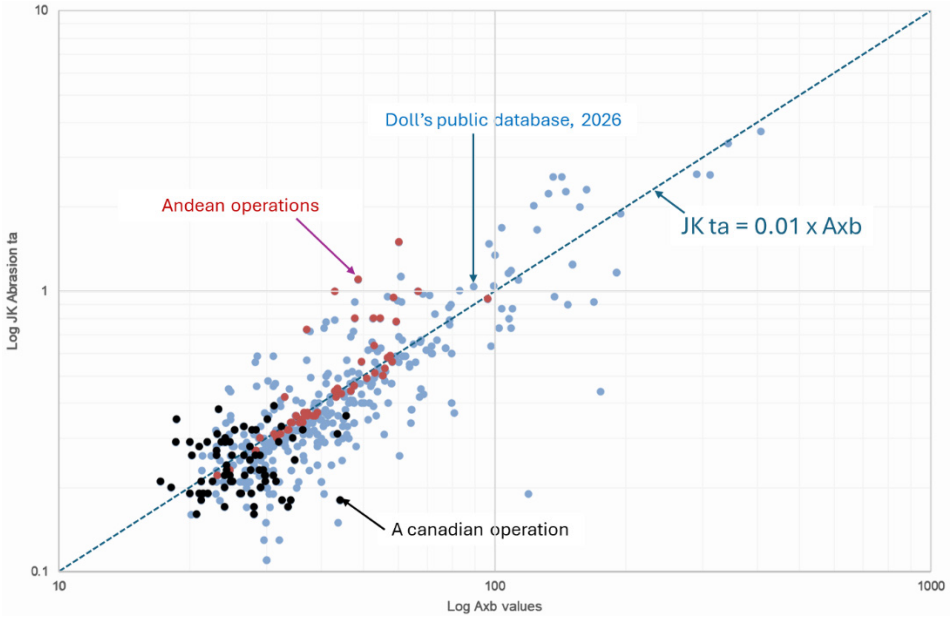



**FIG 14** – JK abrasion $t_a$ versus Axb (Data sourced from Doll, 2025).

In an early publication on the AG and SAG mill model (Morrell and Morrison, 1996), the JK $t_a$ was used to calculate the SAG mill F80. This equation is shown in Equation 3. Morrell and Morrison's (1996) formulation is different from Morrell's method (Bailey *et al,* 2009), which uses DWI and a primary crusher closed-side setting to estimate the SAG mill F80. Morrell and Morrison's (1996) model was based on primary-crusher survey data, with crushers operating at a CSS of 150 mm. The $t_a$ values were estimated from the surveyed samples of the SAG mill feed (Figure 15). Although the data show some scatter, an apparent relationship exists between $t_a$ and crusher product. Morrell and Morrison (1996) validated Equation 3 using several sets of survey data and generally noted that a higher $t_a$ value corresponded to a finer crusher product size distribution (ie a lower SAG mill F80). They noted that the variability in the measured SAG mill F80 is acceptable, given natural variations in crusher feed size distributions and operating under choke-feed conditions.

$$SAG\ mill\ F80 = CSS - \ 78.7 - 28.4 \times ln(t_a) \quad (3)$$

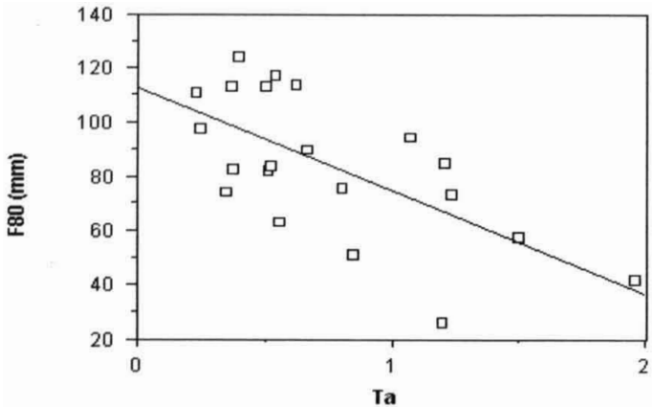



**FIG 15** – Relationship between SAG mill F80 and JK abrasion $t_a$ (Morrell and Morrison, 1996).

Figure 16 presents a SAG mill F80 comparison using Equation 1 (updated Morrell method, Bailey *et al,* 2009) and Equation 3 (after Morrell and Morrison, 1996). In Equation 1, the ore competency was Axb = 35 (DWI = 7.7 kWh/m$^3$), and the CSS was 150 mm. For a given $t_a$ value, the calculated SAG mill F80 decreases with increasing ore abrasiveness. This could mean that SAG mill feed distributions from Andean operations with higher $t_a$ values can be significantly finer (as shown in Figure 14), thereby affecting measured SAG mill specific energy values. At this stage, it is unclear whether higher $t_a$ values correspond to a lower RQD range, but without reliable RQD measurements, JK $t_a$ could likely be used to estimate SAG mill feed size distributions and calculate the required SAG mill specific energies for greenfield projects.

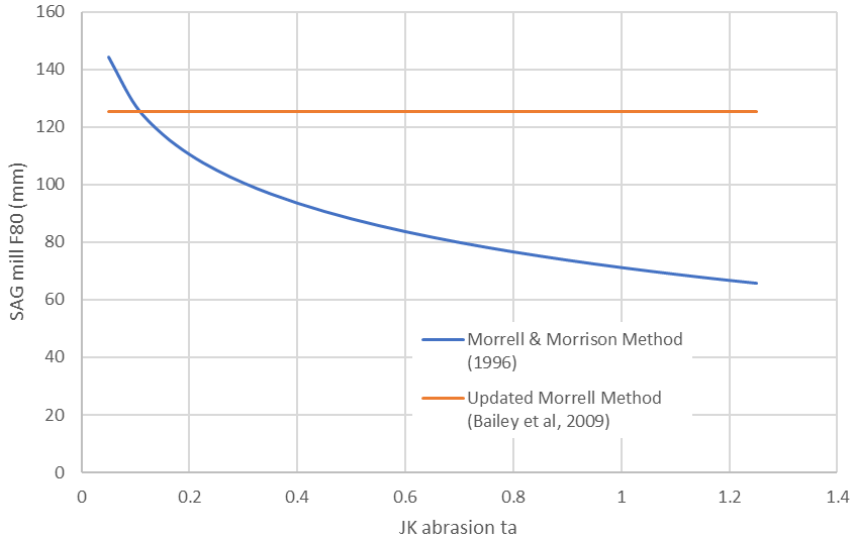



**FIG 16** – SAG mill F80 comparison using Equations 1 and 3.

## WHAT HAVE WE LEARNED FROM THE REVIEW?

SAG mill specific energy can vary significantly for the same Axb or DWI value. Andean and Pacific Rim ores can exhibit breakage that leads to significantly lower SAG mill specific energy than, for example, Australian and Canadian ores. Foggiatto *et al* (2022) and Barratt (1989) attributed this unusual behaviour to macro-scale fracturing of the ore, which small-scale tests such as single-particle and grindability tests do not capture.

There is a parameter that is not measured in our current suite of bench-scale tests. This may be due to sample particle-size bias or other ore characteristics.

Generally, ores from the Andean and high-seismic regions can be traced along subduction zones associated with plate tectonics. The most widely known copper porphyry orebodies are found in these regions, and their mineralisation generally differs from that of older ores on continental plates.

A plausible assumption is that ores from the Andean or high-seismic regions are young, in geological terms, and therefore contain both hard and soft components in the rock matrix. Most Chilean operations located in the Andean mountain range fall under this classification. Australian and Canadian Shield ores, such as those found at Cadia, Boddington, and Detour Lake, come from older, eroded rock formations that have removed softer components, leaving a consistently competent, hard-rock structure, or from geochemically different rock.

The primary aim of the assessment was to determine whether there are tell-tale signs during ore characterisation that could identify the 'effect' of macro-scale fracturing or other naturally occurring factors that impact the AG/SAG mill's specific energy measurement.

The paper aimed to answer three questions:

- Are we calculating the AG or SAG mill specific energy correctly?
    - Yes. The current methods primarily rely on ore competence and feed size distribution, which are the main 'ore-related parameter' inputs used to calculate the specific energies of AG and SAG mills. While operational factors such as ball charge levels, grate and pulp system design, and pulp densities can influence measured SAG mill specific energy values, power-based models relying on single-particle and grindability tests are benchmark calculation methods used in comminution circuit flow sheet design.
    - There is a general relationship between SPI and Axb, highlighting the interrelationship between the two results (grindability versus single-particle tests). As a check, this relationship was compared with non-Andean ores to determine whether sampling bias, particularly from single-particle tests, could account for the observed variance. The model fit is similar for both ore types, indicating that sampling bias does not significantly influence competency.
- Are we missing other measurements during ore characterisation?
    - Drilled core samples with lower RQD can contribute to lower SAG mill specific energy while maintaining high ore competence.
    - However, lower RQD cores do not always mean finer fragmentation. Tims et al's (2024) analysis of core trays with lower RQD highlighted a problem with the designation methodology.
    - Visually, cores with lower RQD (near zero) can exhibit significantly different degrees of fragmentation, ranging from sandy to blocky. When processed through the grinding mill, these ores would have variable SAG mill specific energies. Tims *et al* (2024) emphasised that automation alone would not solve the RQD issue; therefore, they introduced the core damage index (CDI) to complement RQD measurement.
    - In the absence of adequate RQD measurements, it appears that the JK abrasion parameter ($t_a$) could be a likely marker for identifying unusual ores that do not sit on the general trend presented by Veillette and Parker (2005). However, further validation is required to compare SAG mill performance between Andean and non-Andean ores.
- How do we modify our approach to capture the response of the ore in the SAG mill environment accurately?
    - In greenfield projects that depend entirely on drilled core samples to characterise the ore and estimate the likely fracturing of the rock mass for grinding mill sizing, there are two key objectives in the test to ensure enough data is collected:
        - Ensuring a representative sample is selected in small-scale comminution tests that captures the variability of the size dependency on competency.
        - Ensuring a representative description of the rock mass.
    - Generally, standard ore characterisation methods, such as single-particle and grindability tests, capture the variability of strength within the sample but overlook overall macro-scale

fracturing. RQD assesses the degree of fragmentation in the rock mass, but it can misrepresent rock quality. The proposed solutions are:

- Introduce the core damage index (CDI) as proposed by Tims *et al* (2024) as part of the core's RQD logging in the SAG mill-specific calculation.
- In the absence of an adequate RQD definition, undertake an ore abrasion test as per the JK method in parallel with ore competence measurements to correct the SAG mill feed size distribution in mill sizing calculations.

- Consider alternative methods for ore characterisation to supplement standard competence measurements. Additional data, such as geochemical analysis of core samples to identify mineral composition, could improve the prediction accuracy of SAG mill-specific energy for highly altered ores (Figure 17). The analysis method involves:
  - Hyperspectral assessment of the same section of core to determine the mineral composition as proposed by Michaux and O'Connor (2020).
  - Bulk core strength analysis using Minpraxis (Nadolski *et al,* 2024). The Minpraxis device can process full- or half-core data to determine competency (Axb, DWI, PLI, UCS) and to calculate hardness measurements using proxy bulk-strength parameters.
  - The bulk core strength samples are then validated with single particle tests using the broken core samples. Tests such as the SPI, SGI, Geopyörä, SMC, and HIT methods are suitable for small-scale comminution testing (Bueno *et al,* 2021; Morrell, 2004; Kojovic, 2016; Amelunxen, Berrios and Rodriguez, 2014; Starkey and Dobby, 1996).

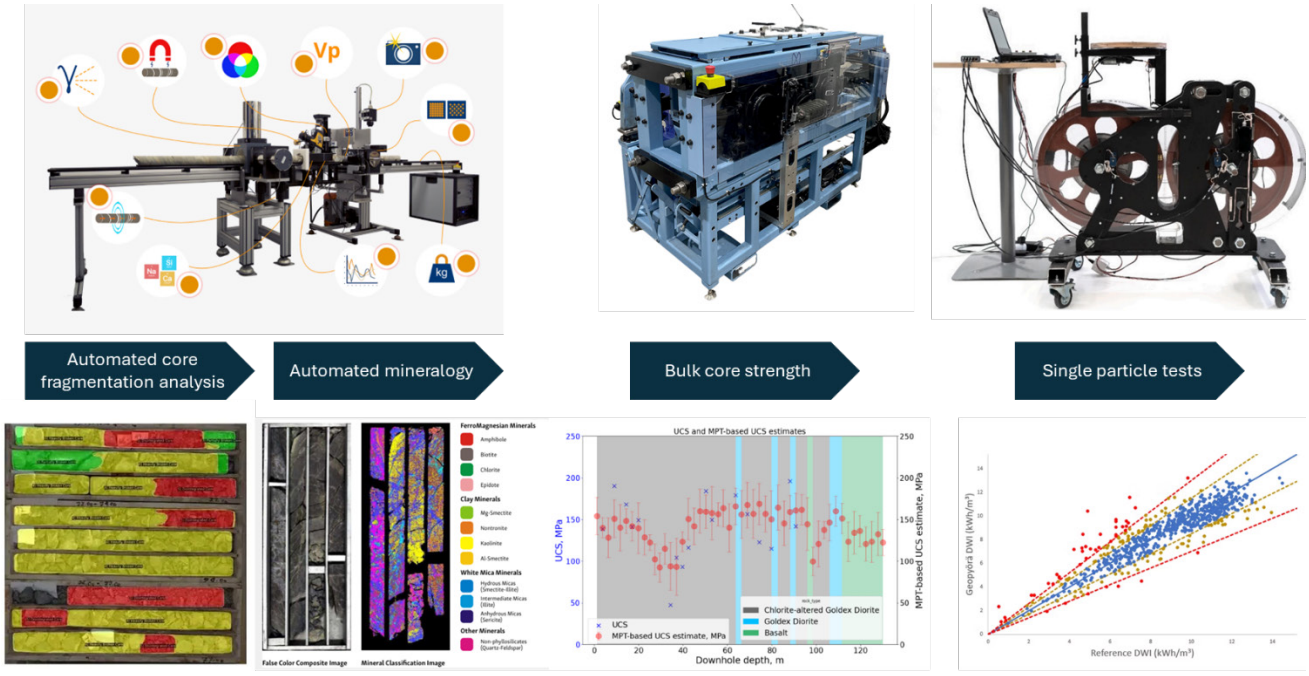



**FIG 17** – Integrated ore characterisation workflow (images sourced from Geotek multi-sensor core logger (2026), Minpraxis tester (Nadolski *et al,* 2024), Geopyörä tester (Bueno *et al,* 2021)).

As always, reviewing the test work data and interpreting the results are essential for identifying the causes of variable SAG mill-specific energy consumption. There is no single definitive method for analysing test work to size SAG mills; more importantly, understanding the data and benchmarking existing operations are just as crucial.

## ACKNOWLEDGEMENTS

The authors acknowledge Ausenco for its support and Alex Doll for reviewing the paper and providing commentary on the topic.

# REFERENCES


Amelunxen, P, Berrios, P and Rodriguez, E, 2014. The SAG mill grindability index test, *Minerals Engineering*, 55:42–51.

Bailey, C, Lane, G, Morrell, S and Staples, S, 2009. What can go wrong with comminution circuit design?, in *Proceedings Tenth Mill Operators Conference*, pp 143–149 (The Australasian Institute of Mining and Metallurgy: Melbourne).

Barratt, D and Allan, M, 1986. Testing for autogenous and semi-autogenous grinding: A designer's point of view, in *Proceedings Society for Mining, Metallurgy and Exploration,* 3:65–74.

Barratt, D, 1989. An update on testing, scale-up and sizing equipment for autogenous and semi-autogenous grinding circuits, paper presented to SAG, 1989 Conference, Vancouver.

Bueno, M, Torvela, J, Chandramohan, R, Chávez-Matus, T, Liedes, T and Powell, M, 2021. Double wheel breakage test, *Minerals Engineering*, 168:107026.

Burgess, D, 2012. A method of calculating autogenous/semi-autogenous grinding mill specific energies using a combination of Bond work indices and Julius Kruttschnitt parameters, then applying efficiency factors, in *Proceedings 11th Mill Operators Conference, MillOps 2012,* pp 37–44 (The Australasian Institute of Mining and Metallurgy: Melbourne).

Chandramohan, R and Lane, G, 2024. A review of operating data over 50 years of secondary crushing prior to AG/SAG mills, in Proceedings of the Mill Operators Conference, pp 177–194 (The Australasian Institute of Mining and Metallurgy: Perth).

Chandramohan, R, 2013. Effect of rock shapes in comminution, PhD thesis (Julius Kruttschnitt Mineral Research Centre, The University of Queensland: Brisbane).

Chandramohan, R, Foggiatto, B, Lane, G, Meinke, C, Ballantyne, G, Reeves, S and Staples, P, 2023. A review of SAG milling – history of mill selection and test work analysis, in Proceedings International Conference on Autogenous and Semi-Autogenous Grinding Technology, SAG 2023, Vancouver.

Chandramohan, R, Lane, G S and Morley, C, 2021. Operational considerations for hybrid SAG–HPGR comminution circuits, paper presented to Minerals Engineering International Comminution Conference 2021 (online).

Chandramohan, R, Lane, G, Foggiatto, B, Wang, E and Bueno, M, 2015. Reliability of ore characterisation tests, in Proceedings SAG, 2015 Conference, Vancouver.

Cropp, A, Goodall, W and Bradshaw, D, 2013. The influence of textural variation and gangue mineralogy on recovery of copper by flotation from porphyry ore – a review, in Proceedings of the Second AusIMM Geometallurgy Conference (The Australasian Institute of Mining and Metallurgy: Brisbane).

Dance, A, Valery, W, Jankovic, A, La Rosa, D and Esen, S, 2006. Higher productivity through cooperative effort: A method of revealing and correcting hidden operating inefficiencies, in Proceedings SAG, 2006 Conference, Vancouver.

Daniel, M and Wang, E, 2014. Benefits from the development of site-specific SAG mill throughput forecast models for gold, copper and iron ore concentrators, in Proceedings Procemin 2014 Conference, Santiago.

Deere, U and Deere, W, 1989. Rock quality designation (RQD) after twenty years, report prepared for US Army Corps of Engineers (Washington, DC).

Doll, A, 2025. Public grindability database, published online, Available from: <https://sagmilling.com/> [Accessed: 20 December 2025].

Elmo, D and Stead, D, 2020. The concept of representative elementary length (REL) as an effective tool to study scale effects in rock engineering problems, *Boletín Geológico y Minero*, 131(3):355–362. https://doi.org/10.21701/bolgeomin.131.3.001

Foggiatto, B, van der Wielen, K, Guerra, J, Lane, G, Chandramohan, R and Meinke, C, 2022. Prediction of SAG mill specific energy for Andean and structurally altered ores, in Proceedings Procemin 2022 Conference, Santiago.

Geotek, 2026. Multi-sensor core logging system. Available from: <https://www.geotek.co.uk/services/core-logging scanning/>

Hasterok, D, Halpin, J, Collins, A, Hand, M, Kreemer, C, Gard, M and Glorie, S, 2022. New maps of global geological provinces and tectonic plates, *Earth-Science Reviews*, 231:104038.

Hilden, M, 2017. Introducing the variable rates version 2 AG/SAG model, JKMRC seminar. Available from: <https://www.youtube.com/watch?v=2MZU_ISkL88>

Kojovic, T, 2016. HIT – a portable field device for rapid testing at site, in Proceedings 13th AusIMM Mill Operators Conference, Perth (Paper No. 107).

Lane, G, 2007. Some observations regarding SAG milling, in Proceedings Ninth Mill Operators Conference (The Australasian Institute of Mining and Metallurgy: Melbourne).

Lane, G, Dakin, P, Doddridge, T and Pyle, M, 2023. Is the capital cost of your grinding circuit too high?, paper presented to SAG 2023, Vancouver.

Lane, G, Foggiatto, B and Bueno, M, 2013. Power-based comminution calculations using Ausgrind, in Proceedings Procemin 2013 Conference, Santiago.

Leung, K, 1987. An energy-based ore-specific model for autogenous and semi-autogenous grinding, PhD thesis (Julius Kruttschnitt Mineral Research Centre, The University of Queensland: Brisbane).

McKen, A and Chiasson, G, 2001. Small-scale continuous SAG testing using the MacPherson autogenous grindability test, SGS Minerals Services Technical Paper 2001-46.

Michaux, S and O'Connor, L, 2020. How to set up and develop a geometallurgical program, GTK Report (GTK Open File Work).

Morrell, S and Morrison, R, 1996. AG and SAG mill circuit selection and design by simulation, in *Proceedings International Conference on Autogenous and Semi-Autogenous Grinding*, pp 769–790 (University of British Columbia: Vancouver).

Morrell, S and Valery, W, 2001. Influence of feed size on AG/SAG mill performance, in Proceedings SAG 2001 Conference, Vancouver.

Morrell, S, 2004. Predicting the specific energy of autogenous and semi-autogenous mills from small diameter drill core samples, *Minerals Engineering*, 17(3):447–451.

Morrell, S, 2011. The appropriateness of the transfer size in AG and SAG mill circuit design, in Proceedings SAG, 2011 Conference, Vancouver.

Morrison, R, Shi, F and Whyte, R, 2007. Modelling of incremental rock breakage by impact – for use in DEM models, *Minerals Engineering*, 20(3):303–309.

Nadolski, S, Cartes, I, Pizarro, G, Hesse, M and Moss, A, 2024. Advancing orebody knowledge with high-resolution rock strength measurement using the Minpraxis tester, in Proceedings LKAB MassMin 2024.

Napier-Munn, T J, 2005. Mineral comminution circuits: Their operation and optimisation, Julius Kruttschnitt Mineral Research Centre Monograph Series in Mining and Mineral Processing.

Narayanan, S and Whiten, W, 1988. Determination of comminution characteristics from single particle breakage tests and its application to ball mill scale-up, *Transactions of the Institution of Mining and Metallurgy, Section C: Mineral Processing and Extractive Metallurgy*, 97:C115–C124.

Palmström, A, 1996. The weighted joint density method leads to improved characterisation of jointing, in Proceedings Conference on Recent Advances in Tunnelling Technology, New Delhi.

Pells, P, Bieniawski, Z, Hencher, S and Pells, S, 2017. Rock quality designation (RQD):Time to rest in peace, *Canadian Geotechnical Journal*, 54(6):825–834. https://doi.org/10.1139/cgj-2016-0012

Powell, M S, Morrell, S and Latchireddi, S, 2001. Developments in the understanding of South African-style SAG mills, *Minerals Engineering*, 14(14):1143–1153.

Putland, B, Siddall, B and Gunstone, A, 2004. Taking control of the mill feed: Case study – partial secondary crushing Mt Rawdon, in Proceedings MetPlant 2004 (The Australasian Institute of Mining and Metallurgy: Melbourne).

Scott, A, Kanchibotla, S and Morrell, S, 1999. Blasting for mine-to-mill optimisation, technical paper, SMCC.

Siddall, B and Putland, B, 2007. Process design and implementation techniques for secondary crushing to increase milling capacity, in Proceedings SME Annual Meeting (Preprint 07-079) (SME: Salt Lake City).

Sillitoe, R H, 2010. Porphyry copper systems, *Economic Geology*, 105(1):3–41.

Staples, P, Lane, G, Braun, R, Foggiatto, B and Bueno, M, 2015. Are SAG mills losing market confidence?, in Proceedings SAG 2015 Conference, Vancouver.

Starkey, J and Dobby, G, 1996. Application of the Minnovex SAG Power Index at five Canadian SAG plants, in *Proceedings International Conference on Autogenous and Semi-Autogenous Grinding Technology* (eds: A L Mular, D J Barratt, and D A Knight), pp 345–360 (UBC: Vancouver).

Tims, S, Cate, A, LeRiche, A and Saunders, E, 2024. Automated geotechnical logging of core box images using machine learning, *CIM Journal – Rock Engineering Special Issue*.

Veillette, G and Parker, B, 2005. Boddington expansion project comminution circuit features and test work, in Proceedings Randol Gold Forum.

Whyte, R, 2005. Measuring incremental damage in rock breakage by impact, BE thesis (The University of Queensland: Brisbane).

Wirfiyatal, F and McCaffery, K, 2011. Applied geo-metallurgical characterisation for life-of-mine throughput prediction at Batu Hijau, in Proceedings of the Fifth International Conference on Autogenous and Semi-Autogenous Grinding Technology, SAG 2011. Vancouver.

# Evaluating grinding circuit efficiency metrics at the Newmont Tanami Operation

*E James[1], A Doll[2] and A Giblett[3]*

1. Plant Metallurgist, Newmont Tanami Operations, Alice Springs NT 0871, Australia. Email: ethan.james@newmont.com
2. Principal, Alex G. Doll Consulting Limited, Cork, Ireland. Email: alex.doll@sagmilling.com
3. Director, Black Swan Metallurgy Pty Ltd, Mindarie WA 6030, Australia. Email: aidan@blackswanmet.com

## ABSTRACT

Efficient comminution is core to the economic success of modern gold mining operations. At Newmont Tanami, ongoing efforts to optimise grinding circuit performance have considered evaluation and demonstration of robust efficiency methods to define performance efficiency. This evaluation uses data from a series of plant surveys performed at the Tanami operation, where both single stage ball milling and series ball milling have been used in recent history to process underground gold ore. Circuit efficiency analysis performed using this survey data evaluates the alignment between measured feed ore properties and circuit operating performance against the grinding energy requirements as predicted by conventional desktop methods. This submission therefore provides a foundation for further discussion on best practices in grinding circuit evaluation, including insights into the challenge of predicting ball mill performance in series milling configuration.

The inputs and results of the analysis will be provided in full detail specifically to allow industry professionals to follow the workings and reproduce the conclusions, thereby ensuring the paper will become a valuable reference for future studies.

## INTRODUCTION

The Newmont Tanami operation is implementing an expansion at its Dead Bullock Soak (DBS) underground mine involving a new shaft that is expected to transition the operation from its current mine constrained condition to being mill constrained. Mill feed rates post-expansion are expected to average 385 dt/h, well in excess of the 312 t/h rate targeted by the 2017 Tanami Expansion Project (TEP), as discussed by Giblett *et al* (2023). Multiple grinding surveys have been conducted over the last three years to identify potential bottlenecks within the grinding circuit during periods of current 'best case' plant performance. The surveys and supporting circuit modelling sought to identify improvement opportunities with the overarching goal of increasing plant capacity and feed rate 'sprint' capacity, while also maintaining an acceptable leach feed particle size $P_{80}$ around 75 µm.

The Granites Mill at Tanami currently sources all its ore feed from the DBS underground mine. The DBS gold deposits consist of a series of stratabound and structurally controlled Proterozoic orogenic gold deposits, which are associated with regional deformation and metamorphism. The geology of the DBS area comprises a thick succession of fine to medium grained sediments and minor intrusive rocks. These rocks belong to the Dead Bullock Formation of the Palaeoproterozoic Tanami Group. The strata are hosted in the DBS anticlinorium, a N-S oriented, east plunging fold cross-cut by several generations of faults. Two main styles of gold mineralisation have been recognised at DBS these have been designated as Callie-style and Villa style. Callie-style mineralisation characterised by coarse, nuggety, visible gold occurring in a series of sheeted thin quartz veins. Economic mineralisation most commonly occurs where these sheeted veins intersect favourable sediment units. Villa-style mineralisation is associated with disseminated pyrrhotite, pyrite and arsenopyrite, and is generally fine-grained. It is often hosted by bedding or laminations and less commonly by veins.

The Tanami grinding circuit consists of a three-stage crushing circuit with the grinding circuit fresh feed coming from a tertiary cone crusher in closed circuit with a 15 mm opening screen. The primary ball mill circuit is partially closed with a cluster of flat-bottomed cyclones, with both cyclone overflow and screened primary gravity circuit tailings combining to feed the secondary grinding circuit. These

transfer streams are combined in ‘Box 501’ as shown by the simplified grinding circuit flow sheet in Figure 1.

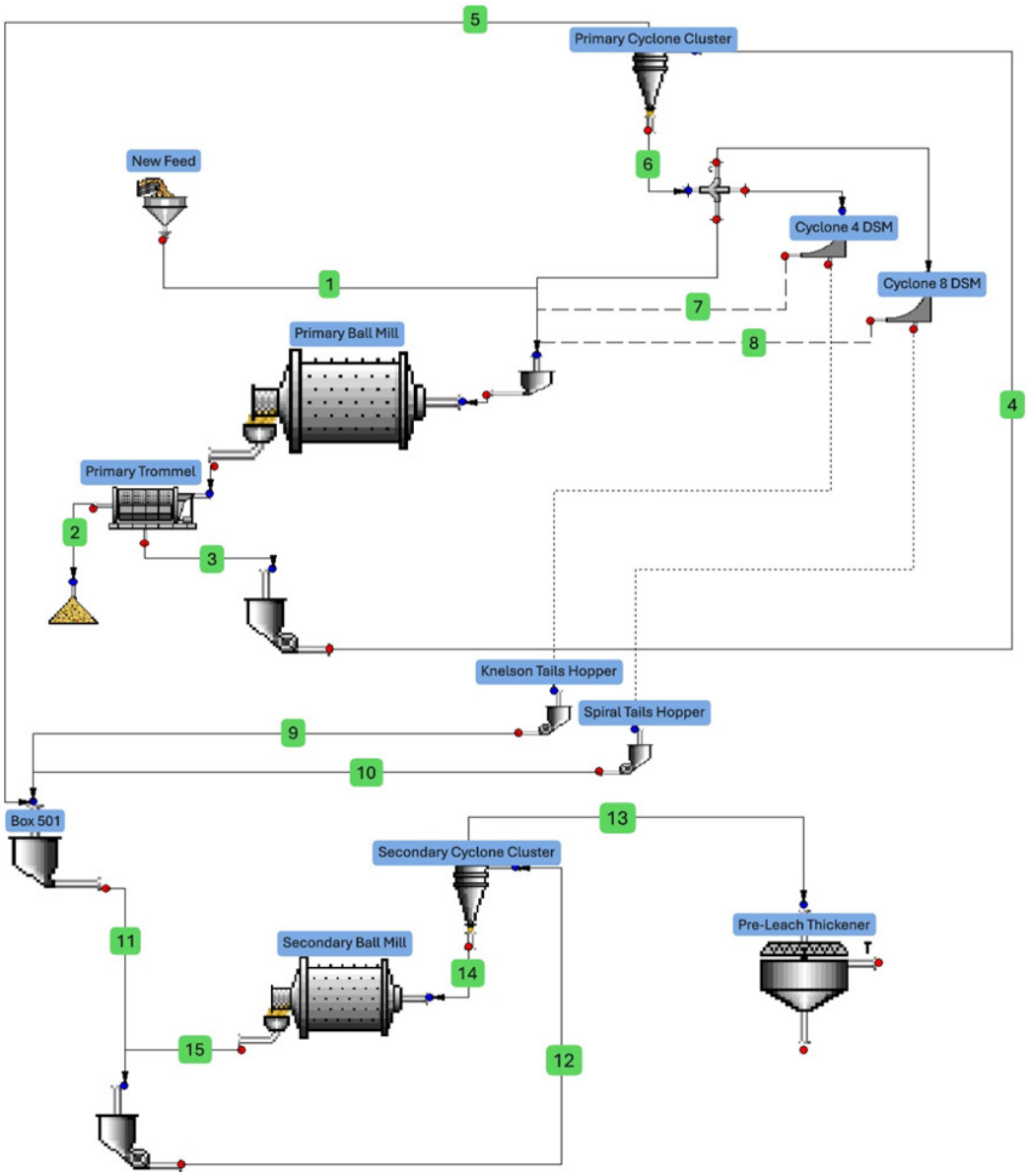



**FIG 1** – Primary and secondary grinding circuit configuration at Tanami.

A sampling campaign was conducted at the Tanami process plant on 16th August 2025 (James, 2026) for a one-hour period after the plant had operated in a stable manner for the previous hour. A primary cyclone feed sample (stream 4) was collected immediately after the one hr sampling period had ended by opening valve in the distributor to a sample collection line. After this hydrocyclone feed sample, the feed conveyor was shutdown and a belt cut was collected (stream 1) from the primary ball mill feed conveyor (CV510). The sample collection and sample mass sizes were determined using the Global Mining Guidelines Group (GMG) Guideline for sampling of grinding circuits (GMG, 2022) for the slurry and dry samples.

The objective of the survey was to observe plant operation at the current maximum demonstrated throughput rate of 406 dt/h. The primary hydrocyclone pressure was maintained at 70.5 kPa to provide for a more stable circuit during the survey as this was expected to negatively impact classification efficiency to some degree however, it allowed for higher feed rates to be maintained at steady state. The secondary hydrocyclone pressure was in its typical range around 133 kPa. The relevant survey data is summarised in Table 1, with mill power motor input values shown.

**TABLE 1**

2025 Grinding circuit survey – summary data.

| Mill feed rate (dtph) | Mill feed $F_{80}$ (mm) | Primary mill power (kW) | Primary mill $T_{80}$ (µm) | Secondary mill power (kW) | Secondary mill $P_{80}$ (µm) |
|---|---|---|---|---|---|
| 406 | 9.38 | 4744 | 324 | 2342 | 75 |

The Tanami grinding circuit survey data is interpreted in this paper to compute the grinding efficiency of both the primary and secondary ball mill by a variety of methods. The goal is to provide the industry with a reference for future grinding studies involving ball mill grinding efficiency.

## LABORATORY TEST RESULTS

Slurry samples collected at several locations in the plant during the survey were processed in the Tanami metallurgical laboratory to determine the weight percent solids and particle size distribution. These size distributions and other data collected from the plant control system were loaded into a JKSimMet model to generate plant-wide mass balances for each size class of solids.

The fresh feed CV510 sample was sent to a commercial laboratory in Perth for grindability determinations. A sub-sample of the CV510 sample was also sent to JK Tech in Brisbane for a Bond rod mill work index determination.

### Bond ball mill work index and Morrell Mib values

A series of Bond ball mill grindability tests were performed at a commercial laboratory in Perth on a sample of stream 1 collected at the time of the survey and are summarised in Table 2. The results allowed extrapolation of parameters such as work index, grams/revolution, and the Levin B value to match the $P_{80}$ sizes observed in the survey.

**TABLE 2**

Ball mill grindability test results.

| **Test closing mesh ($P_{100}$), µm** | 75 | 106 | 106* | 150 |
|---|---|---|---|---|
| **Feed $F_{80}$, µm** | 2304 | 2304 | 2264 | 2304 |
| **Product $P_{80}$, µm** | 53 | 73 | 73 | 101 |
| **grams/rev** | 0.85 | 0.94 | 0.87 | 1.06 |
| **Work index, metric** | 17.8 | 18.4 | 19.5 | 18.8 |
| **Feed %pass undersize** | 14.6 | 16.1 | 17 | 18 |
| **Levin B mWh/rev** | 20.6 | 19.7 | 19.7 | 19.1 |
| **Morrell Mib, metric** | 28.5 | 27 | 29 | 25.1 |

* Test performed earlier on the same mill feed sample.

The earlier test performed at 106 µm $P_{100}$ size appears to be an outlier, with 6 per cent variation in work index values between tests exceeding benchmarks (Angove and Dunne, 1997; Vizcarra and Wong, 2019). Regressions were performed both with and without this point, with the final calculations based on only the three values from second testing program.

As the Bond ball mill work index value is known to vary with product size, the three ball mill determinations were fitted to the equation of Josefin and Doll (2018) to determine the appropriate adjustment parameters as follows (Figure 2):

- the Bond work index Hukki Exponent (-α) is –0.525 and the coefficient $K_1$ is 167.6.
- the Morrell Mi Hukki Exponent (-α) is –0.656 and the coefficient $K_2$ is 625. The Morrell exponent on the size term $–f(P_{80}) = –0.295–P_{80}\times10^{-6}$.

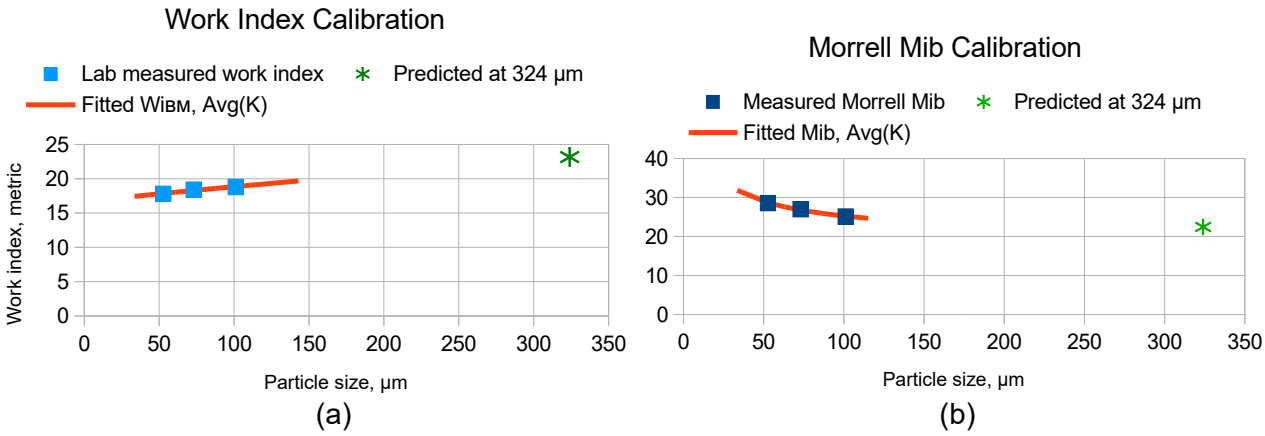



**FIG 2 –** Regression models for ball mill work index and Morrell Mib.

The Josefin regression equations for each metric are as follows:

$$Wi_{model} = \frac{K_1 x (P_{80model}{}^{-\alpha})}{10x\left(P_{80model}{}^{-0.5} - F_{80test}{}^{-0.5}\right)}, Mi_{model} = \frac{K_2 x (P_{80.model}{}^{-\alpha})}{4x\left(P_{80.model}{}^{-f(P_{80.model})} - F_{80.test}{}^{-f(F_{80})}\right)}$$

The Wi and Mib values at each grinding circuit product size according to Josefin's equations:

- primary circuit, ball mill Wi @ 324 µm = 23.2 metric units
- secondary circuit, ball mill Wi @ 75 µm = 18.3 metric units
- primary circuit, Mib @ 324 µm = 22.4 metric units
- secondary circuit, Mib @ 75 µm = 26.5 metric units (interpolated based on three tests).

A second way of adjusting the Mib value for $P_{80}$ is described in GMG (2021b):

- Mib (desired µm) = Mib(test) * ($P_{80}$ test / $P_{80}$ desired)$^{0.24}$
- Mib (324 µm) = 25.1 * (101/324)$^{0.24}$ = 19.0 metric units
- Mib (75 µm) = 27.0 metric units (one of the lab tests gave $P_{80}$ of 73 µm, suitably close to the secondary mill product $P_{80}$).

The application of Josefin's correction for the primary mill work index results in a significant correction relative to the tested work index values and has a significant impact on the assessment of the primary mill when applied in Bond calculations. The subsequent Morrell calculations have observed the primary mill Mib value correction method as per the GMG guideline.

## Rod mill work index

Two rod mill work index determinations were performed (Table 3), one at a commercial laboratory in Perth and the other at the JKTech laboratory in Queensland. It is known that the JKTech rod mill apparatus has the correct internal geometry specified by Bond and Maxson (1943) and that the commercial laboratory rod mill does not.

**TABLE 3**

Rod mill grindability test results.

| Laboratory | Test closing mesh, µm | Feed $F_{80}$, µm | Product $P_{80}$, µm | grams/ rev | Work index, metric |
|---|---|---|---|---|---|
| JKTech | 1180 | 8698 | 956 | 6.59 | 19.1 |
| Commercial Laboratory | 1180 | 9150 | 889 | 3.81 | 25.2 |

## Other grindability measurements

An SMC test was conducted on the CV510 mill feed sample reporting an A×b value of 27.7 and a Mia value of 26.1 metric units.

## GMG MORRELL AND BOND CIRCUIT EFFICIENCIES

The Morrell (GMG, 2021b) and Bond (GMG, 2021a) method for determining the grinding circuit efficiency were used to compare the industrial mill performance to the laboratory grindability test results. The Morrell method calculations were performed with and without the closed circuit crushing correction ('Ws') for comparison, as shown in Table 4.

**TABLE 4**

Morrell efficiency comparison.

| Value | Pinion | Motor | Units |
|---|---|---|---|
| Coarse Grinding (Wa) | 8.3 | 9.3 | kWh/t |
| Size Correction (Ws) | 1.0 | 1.1 | -- |
| Primary Mill Mib | 19.0 | -- | metric |
| Primary Mill Wb | 3.1 | 3.4 | kWh/t |
| Secondary Mill Mib | 27.0 | -- | metric |
| Secondary Mill Wb | 14.9 | 16.1 | kWh/t |
| **Comparison** | **Actual kWh/t** | **With Ws kWh/t (% efficiency)** | **Without Ws kWh/t (% efficiency)** |
| Primary Mill | 11.7 | 13.9 (84%) | 12.7 (92%) |
| Secondary Mill | 5.8 | 12.6 (46%) | 12.6 (46%) |
| Total Circuit | 17.5 | 26.5 (66%) | 25.4 (69%) |

The grinding circuit is consuming significantly less specific energy than predicted by the Morrell equations, 67 per cent and 70 per cent of expected kWh/t for the overall circuit. The Tanami circuit is therefore extremely efficient according to the Morrell efficiency measurement, with the secondary ball mill the dominant influence on that assessment.

The GMG Bond method was performed on the survey data using both the RWi values generated from the standard and non-standard machines, as shown in Table 5.

**TABLE 5**

GMG Bond efficiency comparison.

| Parameter | JKTech RWi | | Commercial laboratory RWi | | Actuals (Motor) |
|---|---|---|---|---|---|
| | Pinion | Motor | Pinion | Motor | |
| Rod Mill Work kWh/t | 4.1 | 4.6 | 5.4 | 6.0 | -- |
| Primary Mill Bond Work kWh/t | 5.6 | 6.2 | 5.6 | 6.2 | -- |
| Overall Bond Ball Mill Work kWh/t | 15.3 | 16.8 | 15.3 | 16.8 | -- |
| **Model Total kWh/t** | **19.4** | **21.3** | **20.7** | **22.8** | **--** |
| Primary Mill kWh/t | 9.6 | 10.8 | 10.9 | 12.3 | *11.7* |
| Secondary Mill kWh/t | 9.8 | 10.5 | 9.8 | 10.5 | *5.8* |
| **Overall kWh/t** | **19.4** | **21.3** | **20.7** | **22.8** | **17.5** |
| Overall Efficiency | | 81.9% | | 76.6% | |

The grinding circuit is consuming less specific energy than predicted by the GMG Bond equations (which use the RM Wi to characterise the size range 9356–1000 µm and the BM Wi to characterise the 1000–75 µm size range), 80 per cent to 85 per cent of expected kWh/t for the overall circuit. The Tanami circuit is very efficient according to the Bond efficiency measurement.

These findings are consistent with previous analysis of the Tanami grinding circuit (Giblett *et al*, 2023) which determined Morrell total circuit efficiency values of 70–76 per cent and Bond (commercial laboratory RWi basis) of 82–88 per cent over three surveys conducted between 2018 and 2020. Similar to the Morrell efficiency assessment, the secondary ball mill is consuming considerably less energy (55 per cent) than predicted and is therefore considered highly efficient.

The primary mill is consuming 100–113 per cent of the Bond predicted energy which might be considered good or poor depending on the chosen reference point. It should be noted that the Bond GMG guideline does not specify protocols for assessing individual components of the circuit and as such there are numerous user inputs that can materially influence these assessments. These include rod mill work index test protocols, ball mill work index testing and product size scaling protocols, and RWi/BWi transition sizes used in calculations.

## SIZE SPECIFIC ENERGY

The size specific energy (SSE) method (Ballantyne, Peukert and Powell, 2015) provides a qualitative mechanism to compare the efficiency of stages within a comminution circuit and to identify differences in the relative efficiency of each stage. As the mechanism does not qualify overall energy consumption based on ore properties, it does not provide a mechanism to judge the efficiency of the circuit in its entirety, merely to identify which components of the circuit are more efficient or less efficient than others and thereby may represent an opportunity for performance improvement. The SSE analysis for the 2025 Tanami circuit survey is shown in Figure 3.

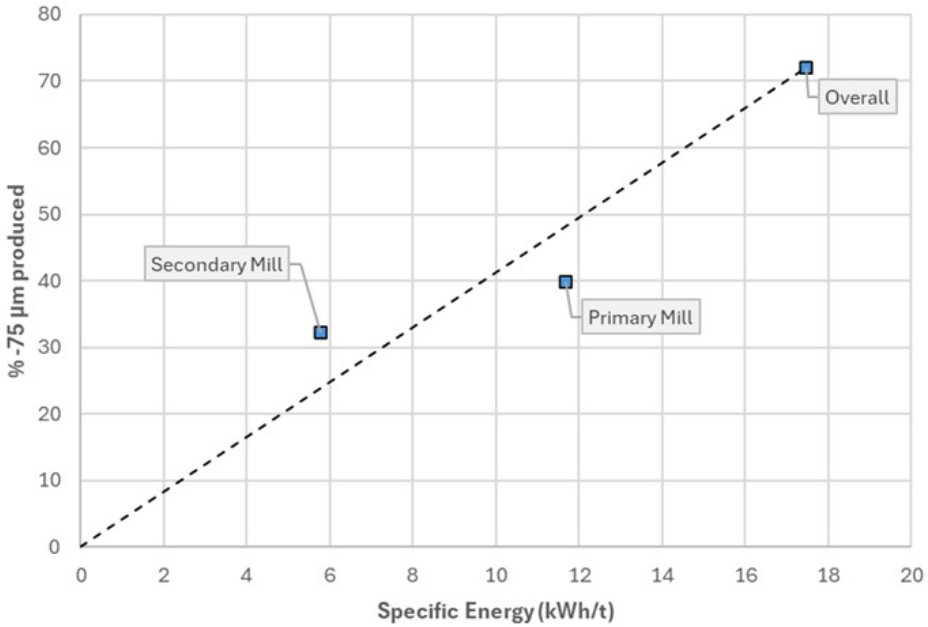



**FIG 3** – Size specific energy for the Newmont Tanami grinding circuit (2025).

The comparison shows the primary mill generating approximately 40 per cent of the final product material at a specific energy of 11.7 kWh/t, with the secondary mill producing approximately 32 per cent of the product material at a much lower specific energy of 5.8 kWh/t. In terms of specific energy per unit product, the secondary mill thereby consumes around 40 per cent less energy than the primary mill and is thereby substantially more efficient at making 75 µm particles.

## FUNCTIONAL PERFORMANCE EFFICIENCIES

The Functional Performance framework (McIvor, 2005; McIvor *et al*, 2017; Metcom Technologies, 2013) provides another tool for analysing the efficiency of ball mill circuits. It combines the standard

laboratory Bond ball mill grindability test that provides the ball mill work index with plant survey measurements permitting the performance of an industrial ball mill to be assessed in a way that accounts for ore hardness. The technique used in this analysis is a modified version of Functional Performance per Doll *et al* (2020) where the Levin B value (Levin, 1989) is used to equalise the grinding rates between the laboratory and industrial mills (Table 6).

**TABLE 6**

Functional performance efficiency.

| Parameter | Primary Mill | Secondary Mill | Comments |
|---|---|---|---|
| Product $P_{80}$ size, µm | 324 | 75 | |
| Fraction $–P_{80}$ size in mill feed | 20.8% | 20.6% | Adjusted for balance |
| Fraction $–P_{80}$ size in mill discharge | 45.6% | 34.8% | Adjusted for balance |
| Classification system efficiency (CSE) | 67% | 72% | Target is >70% |
| Mill grinding rate (fines t/h per eff kW) | 0.093 | 0.083 | |
| Lab mill grinding rate (fines t/h per eff kW) | 0.120 | 0.089 | |
| Ball mill grinding efficiency | 78% | 93% | Target is >80% |
| Overall efficiency | Acceptable | High | |

There are two efficiency measurements in Functional Performance:

1. the Classification System Efficiency (CSE) describes how much of the ball mill grinding energy is being focused on the coarse size classes, as opposed to the already product sized classes. It is computed as the average of the %retained on the target size (324 µm or 75 µm) measured in the mill feed and mill product.
   - Primary mill, feed is 79.2 per cent retained on 324 µm and product is 54.4 per cent retained on 324 µm. The CSE = (79.2+54.4)/2 = 66.8 per cent.
   - Secondary mill, feed is 79.4 per cent retained on 75 µm and product is 65.2 per cent retained on 75 µm. The CSE = (79.4+65.2)/2 = 72.3 per cent.
2. the grinding efficiency evaluates how efficiently the mill uses power to create finished sized particles and is described in terms of t/h or finished (fine) solids per effective kW consumed. Worked example per Doll (2026) contains details of the precise algorithm.

## MILL BREAKAGE FUNCTIONS

The ball mill breakage functions were computed using JK SimMet standard population balance method and using the ‘natural selection function’ of Vien (2019). The comparison of each mill feed’s 80 per cent passing size to the breakage functions are given in Figures 4 through 6.

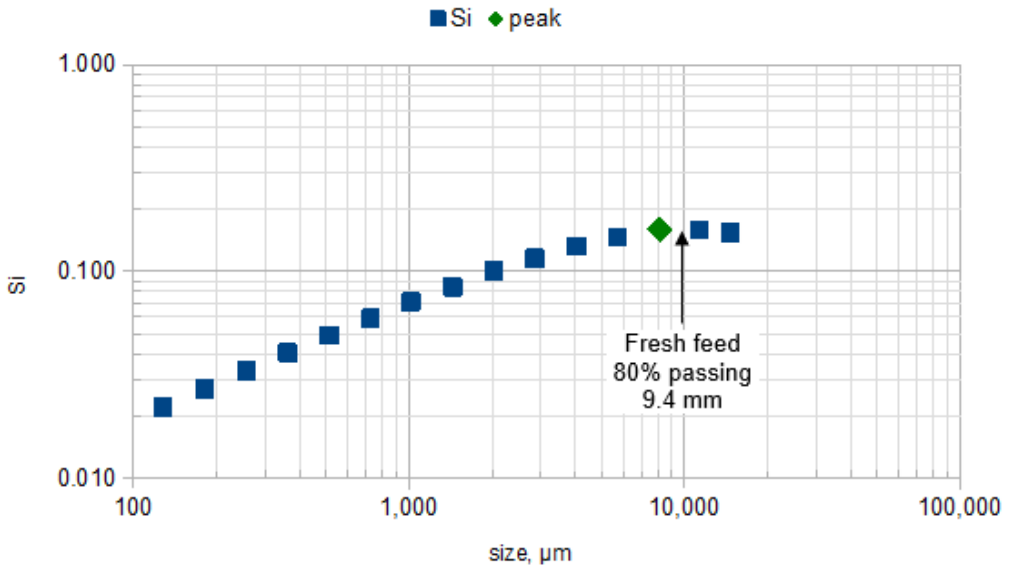



**FIG 4** – Natural selection function for the primary ball mill (peak is at 6.7 mm).

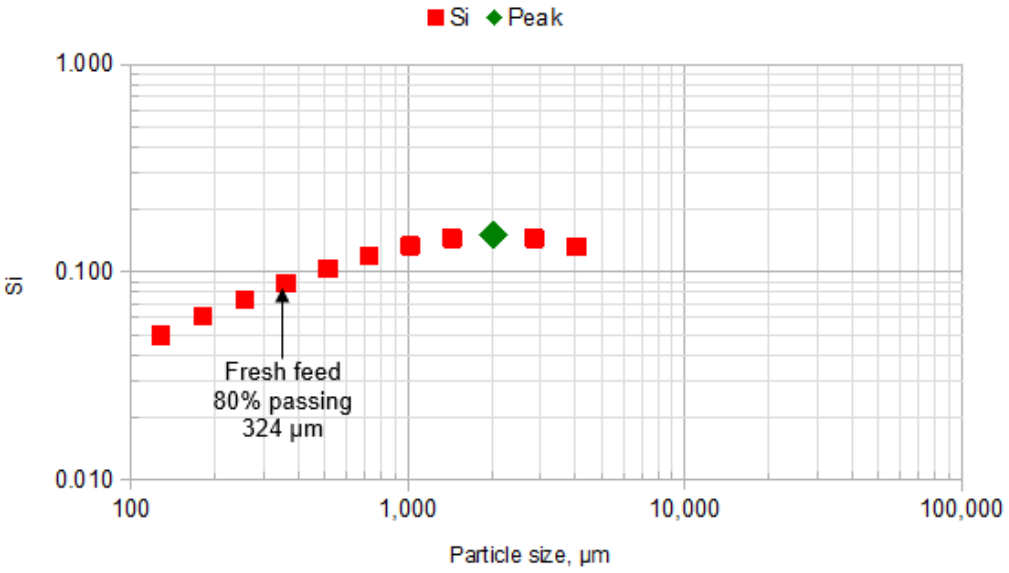



**FIG 5** – Natural selection function for the secondary ball mill (peak is at 2 mm).

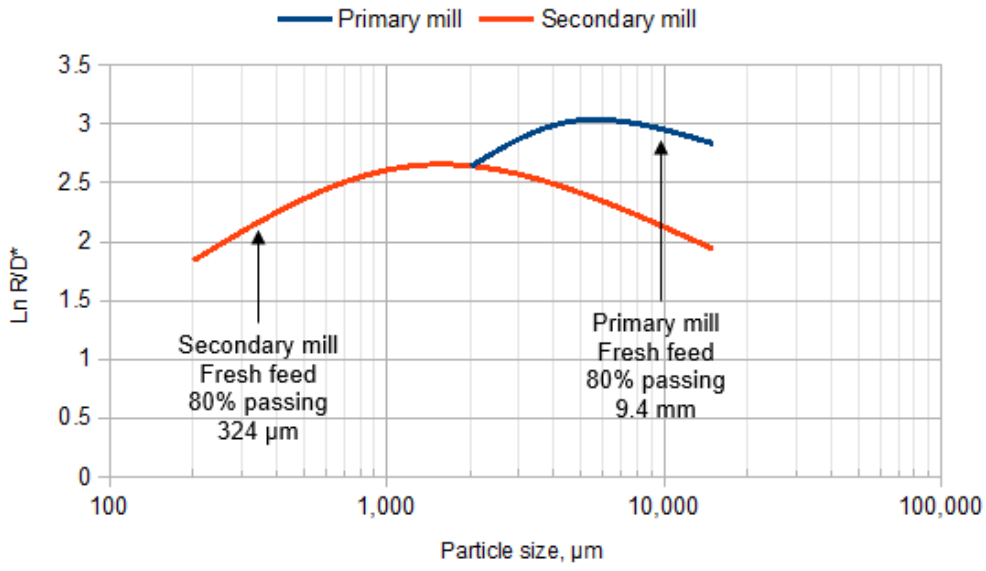



**FIG 6** – JKSimMet fitted breakage rates for the ball mills.

The primary ball mill is breakage rates are suitable for treating the fresh feed 80 per cent passing size and judged to be ‘efficient’.

The secondary ball mill is configured to treat a coarser feed (the peak of the breakage rates) than what is actually in the feed, suggesting that the media in the secondary ball mill is too coarse.

Switching to a finer ball size in the secondary mill would shift the breakage rate curve to the left, moving the peak efficiency size closer to the actual mill feed 80 per cent passing size.

These collective observations regarding the optimum breakage rates can be compared against the typical optimum ball size calculation methods of Bond (1963) and Azzaroni (1980) for the two Tanami ball mills. As shown in Table 7, the current ball sizes are aligned with Azzaroni method.

**TABLE 7**

Optimum ball size references.

| Reference | Primary Mill | Secondary Mill |
|---|---|---|
| Actual recharge size (mm) | 87 | 30 |
| Azzaroni optimum size (mm) | 83 | 35 |
| Bond optimum size (mm) | 72 | 14 |

## CONCLUSIONS

Several efficiency metrics were applied to the 2025 grinding circuit survey data for the Tanami two-stage ball milling circuit, with the results summarised in Table 8. Both stages are consequently judged to be in good health with only the breakage rate analysis suggesting that smaller media size in the secondary ball mill may be beneficial.

**TABLE 8**

Summary of efficiency measurements.

| Efficiency Metric | Primary Mill | Secondary Mill |
|---|---|---|
| Bond Efficiency | Good to poor | Extremely good |
| Morrell Mi Efficiency | Good | Extremely good |
| Size Specific Energy | Less efficient | More efficient |
| Functional Performance | Acceptable | Good |
| Natural Selection Function | Good | Opportunity (coarse media) |
| JKSimMet Breakage Rates | Acceptable | Opportunity (coarse media) |

It is notable that the conclusions of the various analysis techniques can differ substantially, with ratings for the individual mills ranging from poor or ‘improvement opportunity’ to good or extremely good. This demonstrates the need for care when assessing the outcomes of these individual methods in isolation. Conversely the value in applying various techniques to form a balanced overall assessment regarding circuit efficiency, and to derive specific insights into performance improvement opportunities, is clearly evident.

## ACKNOWLEDGEMENTS

The authors would like to acknowledge the Newmont Tanami Processing team – the Operators, Metallurgists, Metallurgical Technician and Maintenance personnel who assisted with the facilitation, planning and execution of the grinding survey. The authors would also like to acknowledge Benjamin Bonfils for his assistance and guidance to Ethan with the modelling in JK SimMet and to Newmont for permission to publish.

**Disclaimer**: This paper presents site-specific observations and modelling interpretations based on a single survey period at the Tanami operation. The results are illustrative and should not be interpreted as operational guidance, performance guarantees, or forward-looking production statements. All modelling methods contain assumptions and uncertainties, and conclusions are dependent on the specific ore characteristics and operating conditions at the time of survey. No representation or warranty is made as to the applicability of these findings to other operations or future performance at Tanami. Certain statements may constitute forward-looking statements and are subject to risks and uncertainties that may cause actual results to differ materially.

## REFERENCES


Angove, J and Dunne, R, 1997. A Review of Standard Physical Ore Property Determinations, in *Proceedings of the World Gold Conference*, pp 139–144 (The Australasian Institute of Mining and Metallurgy: Melbourne).

Azzaroni, E, 1980. Tamaño De Los Medios De Molienda Y Practica De Recarga Multiple, 3rd ARMCO Grinding Symposium, Chile.

Ballantyne, G, Peukert, W and Powell, M, 2015. Size Specific Energy (SSE) – Energy Required to Generate Minus 75 Micron Material, *International Journal of Mineral Processing*, 139:2–6.

Bond, F C and Maxson, W L, 1943. Standard Grindability Tests and Calculations, *Mining Technology*, AIME, March, pp 362–372. Available from: <http://www.onemine.org/document/abstract.cfm?docid=19041>

Bond, F C, 1963. Metal wear in crushing and grinding. 54th Annual Meeting of American Institute of Chemical Engineers.

Doll, A G, 2026. MillOps2026-Appendix [online]. Available from: <www.agdconsulting.com/examples/MillOps2026-Appendix.pdf> [Accessed: 24 July 2026].

Doll, A G, Morneau, A, Dupont, J-F and Michaud, D, 2020. A Simple Method Of Assessing Ball Mill Health Using Bond Tests And Functional Performance, Proceedings of the Annual Meeting of the Canadian Mineral Processors. Available from: <https://www.sagmilling.com/articles/37/view/2020%20CMP%20-%20Alex%20Doll.pdf?s=1>

Giblett, A, Hart, S, Davies, S and Cranley, A, 2023. Converting from Single Stage to Series Ball Milling at the Newmont Tanami Operation, Proceedings of the MetPlant Conference.

Global Mining Guidelines Group (GMG), 2021a. Determining the Bond Efficiency of Industrial Grinding Circuits. Available from: <https://gmggroup.org/determining-the-bond-efficiency-of-industrial-grinding-circuits/>

Global Mining Guidelines Group (GMG), 2021b. The Morrell Method to Determine the Efficiency of Industrial Grinding Circuits. Available from: <https://gmggroup.org/the-morrell-method-to-determine-the-efficiency-of-industrial-grinding-circuits/>

Global Mining Guidelines Group (GMG), 2022. Methods to survey and sample grinding circuits for determining energy efficiency. Available from: <https://gmggroup.org/methods-to-survey-and-sample-grinding-circuits-for-determining-energy-efficiency/>

James, E, 2026. Internal Newmont report on August 2025 grinding survey, Newmont Corporation.

Josefin, Y and Doll, A G, 2018. Correction of Bond Ball Mill Work Index Test for Closing Mesh Sizes, in *Proceedings of the 14th International Mineral Processing Conference, Procemin GEOMET 2018*, pp 200–216. Available from: <https://www.sagmilling.com/articles?topic=test work>

Levin, J, 1989. Observation on the Bond standard grindability test and a proposal for a standard grindability test for fine materials, *J S Afr Inst Min Metall*, 80(1):13–21.

McIvor, R E, 2005. Industrial validation of the functional performance equation – a breakthrough tool for improving plant grinding performance, Proceedings of the SME Annual Meeting, Preprint 05–31.

McIvor, R E, Bartholomew, K M, Arafat, O M and Finch, J A, 2017. Use of Functional Performance Models to Increase Plant Grinding Efficiency, Proceedings of the 49th Annual Canadian Mineral Processors Operators Conference.

Metcom Technologies, 2013. Workshop on Practical Tools for Maximizing Plant Grinding Efficiency, short course presented at 2013 CMP Annual Meeting, Ottawa, Canada.

Vien, A, 2019. The Natural Selection Function and Its Application to Crushing And Grinding, Proceedings of the SAG 2019 Conference, Vancouver, paper 41.

Vizcarra, T and Wong, B, 2019. Test work Variability – Implications for Grinding Circuit Design, in Proceedings of the SAG 2019 Conference, Vancouver, paper 11.

# Success factors in HPGR circuit ramp-up and operation

*I A Lovatt[1], M J Cook[2] and B Dierx[3]*

1. Principal Metallurgist and Director, Orway Mineral Consultants, Perth WA 6000. Email: ivka.lovatt@orway.com.au
2. Process Manager Specialist, Mitch Cook, Perth WA 6000. Email: mitchcook_nbn@iinet.net.au
3. Director HPGR and Process Engineering, Weir Minerals, Venlo, The Netherlands. Email: bjorn.dierx@mail.weir

## ABSTRACT

High Pressure Grinding Rolls (HPGR) technology continues to gain momentum in comminution circuits due to its established high energy efficiency, reduced operating costs and reduced emissions. However, recent implementations by 'new-to-HPGR' mining companies have revealed significant learning curves. These challenges often stem not from the HPGR units themselves, but from broader flow sheet and operational integration issues. While the success of HPGR circuit ramp-up and operation is multi-faceted, this paper focuses on operational readiness considerations for commissioning and operations teams, aimed at maximising ramp-up efficacy and ongoing operability. The paper leverages experiences from a range of recently commissioned HPGR circuits to provide suggestions and guidelines in the following aspects:

- Control philosophy considerations:
  - Integration of the HPGR into the greater comminution circuit control philosophy: how to protect the equipment and maximise mill production.
  - HPGR logic: enhancing gap control logic and integrating predictive maintenance tools.
  - Key performance variables: overview of process key performance indicators (KPIs) and essential calculated variables and trends for diagnostics.
- Process considerations:
  - HPGR feed moisture: management and troubleshooting of HPGR feed moisture and autogenous layer health.
  - Oversize feed control: understanding sources of oversized feed and correct set-up of secondary crushing plant.
  - Tramp metal: operating protocols to prevent tramp ingress and early upgrading tramp removal systems if required.
  - Operating set point adjustment: guidelines for pressure set point (SP), shims/static gap, feed density and aperture selection of the closing screen to maximise HPGR performance.
  - Flow sheet impact on operating expenses (OPEX): understanding flexibility in the circuit, experienced maintenance requirements and how these have impacted OPEX.
- Maintenance considerations:
  - Operating spares: commissioning spares and considerations for management of critical spares for robust operation.
  - Roll surface engineering: optimisation of stud patterns and surface materials to balance wear life and performance.
  - Surface repair and life cycle management: approaches to roll refurbishment and downtime minimisation.

## INTRODUCTION

This paper describes recent High Pressure Grinding Rolls (HPGR)–ball circuit projects in mineral processing, focusing on common challenges affecting ramp-up and sustained production. Insights from the engineer (Orway Mineral Consultants; OMC), operator and vendor (Weir Minerals) have

been distilled into potential focus areas for future projects with limited HPGR experience in the operations team. Emphasis is on the impact of leaner HPGR circuits and the importance of understanding inherited flow sheets early to avoid or minimise HPGR-specific pitfalls.

New-generation HPGR circuits are experiencing a resurgence of the process challenges seen during the early adoption era of HPGR technology in hard rock mineral processing. These include feed moisture, top-size control, tramp management, and circuit stability. These issues are compounded by novel challenges associated with leaner circuit designs and remote operations. The paper draws primarily on case studies from recently commissioned gold, lithium and iron ore projects supplemented by experience comparisons with more established operating sites.

## PROJECT BACKGROUND

A brief project background is provided below for major case studies considered in this paper.

### 4.0 Mt/a gold project

Construction of the process plant commenced in 2022 with first gold poured in 2024. The ore is competent, with a design Axb of 26.0 and Bond work index (BWi) of 16.9 kWh/t. An HPGR-ball circuit was selected for the attractive operating expenses (OPEX) reduction achieved via reduced power and media consumption.

The comminution flow sheet is presented in Figure 1, which feeds a CIL circuit. The run-of-mine (ROM) feed is direct tipped or front-end loader (FEL) fed through a static grizzly into the ROM bin. ROM bin product is reclaimed via an apron feeder to a vibrating grizzly (VG). The VG oversize feeds a primary jaw crusher, with the crusher discharge combining with the VG undersize to feed the secondary screen. The secondary screen top and bottom deck oversize combined and report to two parallel cone crushers. The cone crusher products combine with primary crushed ore to feed the secondary screen. Secondary screen undersize is stacked onto a stockpile. The secondary crushed stockpile is reclaimed via two apron feeders to feed an HPGR, operating in closed circuit with a single double deck banana screen (wet screening to -4 mm). The HPGR product is stored in a bin with rill window to allow for generation of additional dead stockpile. The dead stockpile is reclaimed via FEL and fed onto the wet screen feed conveyor when the HPGR is offline. During periods of reclaim, the wet screen oversize can be stockpiled and then FEL reclaimed when the HPGR is back online.

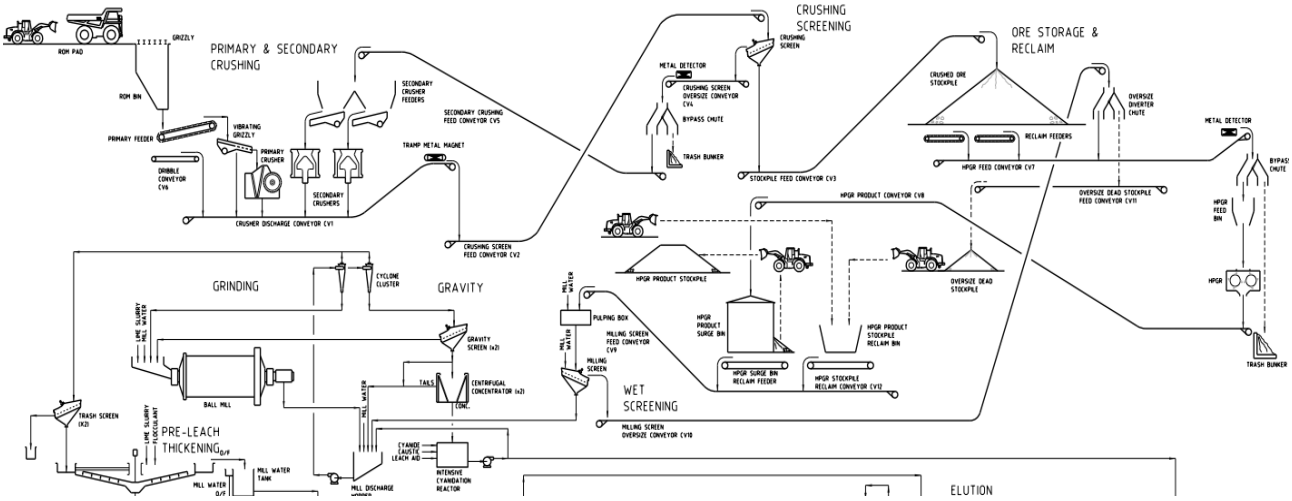



**FIG 1** – 4.0 Mt/a comminution flow sheet.

The wet screen undersize reports directly to the cyclone feed hopper, along with ball mill discharge and gravity circuit tails. The cyclone feed is pumped to a cyclone cluster (20 × Ø500 mm cyclones). The cyclone underflow feeds a single overflow discharge ball mill, with a portion split to feed the gravity circuit (2 × gravity scalping screens and 2 × KC-QS48 Knelson concentrators). The cyclone overflow report to the trash screens, with a target $P_{80}$ of 106 µm.

The major comminution equipment is as follows:

- Primary crusher – Metso C160
- Secondary screen – Vibramech 3.0 m × 7.3 m DD Banana
- Secondary crushers – 2 × Metso HP6
- HPGR – Weir RPM16 Ø1.6 m
- HPGR Screen – Vibramech 4.3 m × 8.5 m DD Banana
- Mill – NPC Ø 6.4 m × 10.70 m EGL, 7.7 MW.

The flow sheet provisions for operational flexibility include, duty/standby cone crushers, 20 hr live capacity secondary crushed stockpile, 1.5 hr HPGR product bin with rill window to additional dead stockpile, HPGR screen oversize (O/S) dead stockpile.

Much of the circuit downtime experienced in the early years is related to particle shape generated during blasting, resulting in blockages at various points in the circuit (Figure 2). Several de-bottlenecking projects are currently underway to address this to improve the run time. The ramp up curves of the three comminution areas is presented in Figure 3. The data shows that despite the below-design run time in the crushing and HPGR circuits, the flexibility available in the circuit allowed the mill ramp-up to exceed nameplate within the first six months of operation.

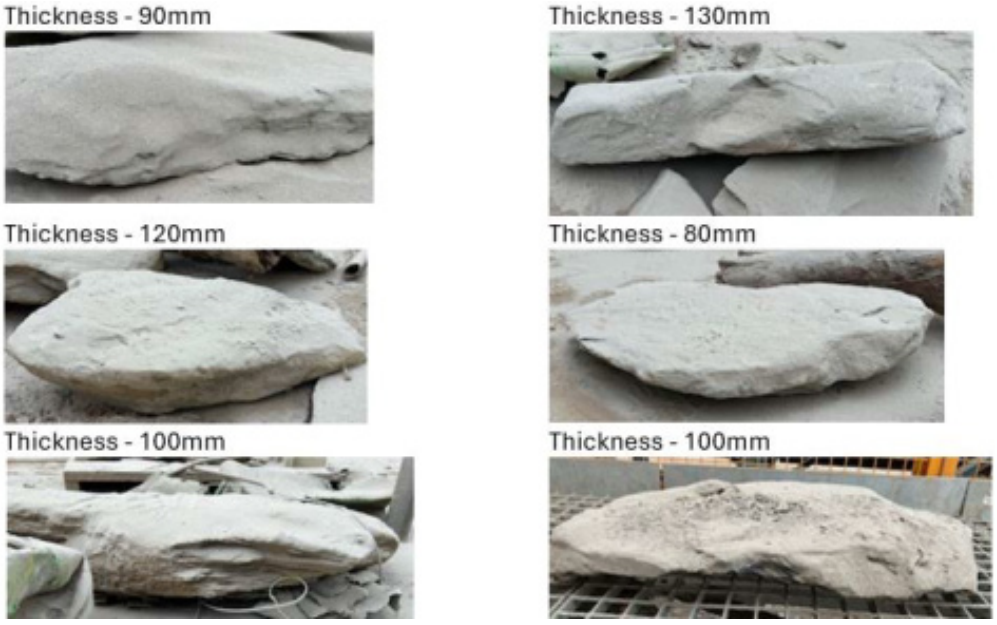



**FIG 2** – Jaw crusher product.

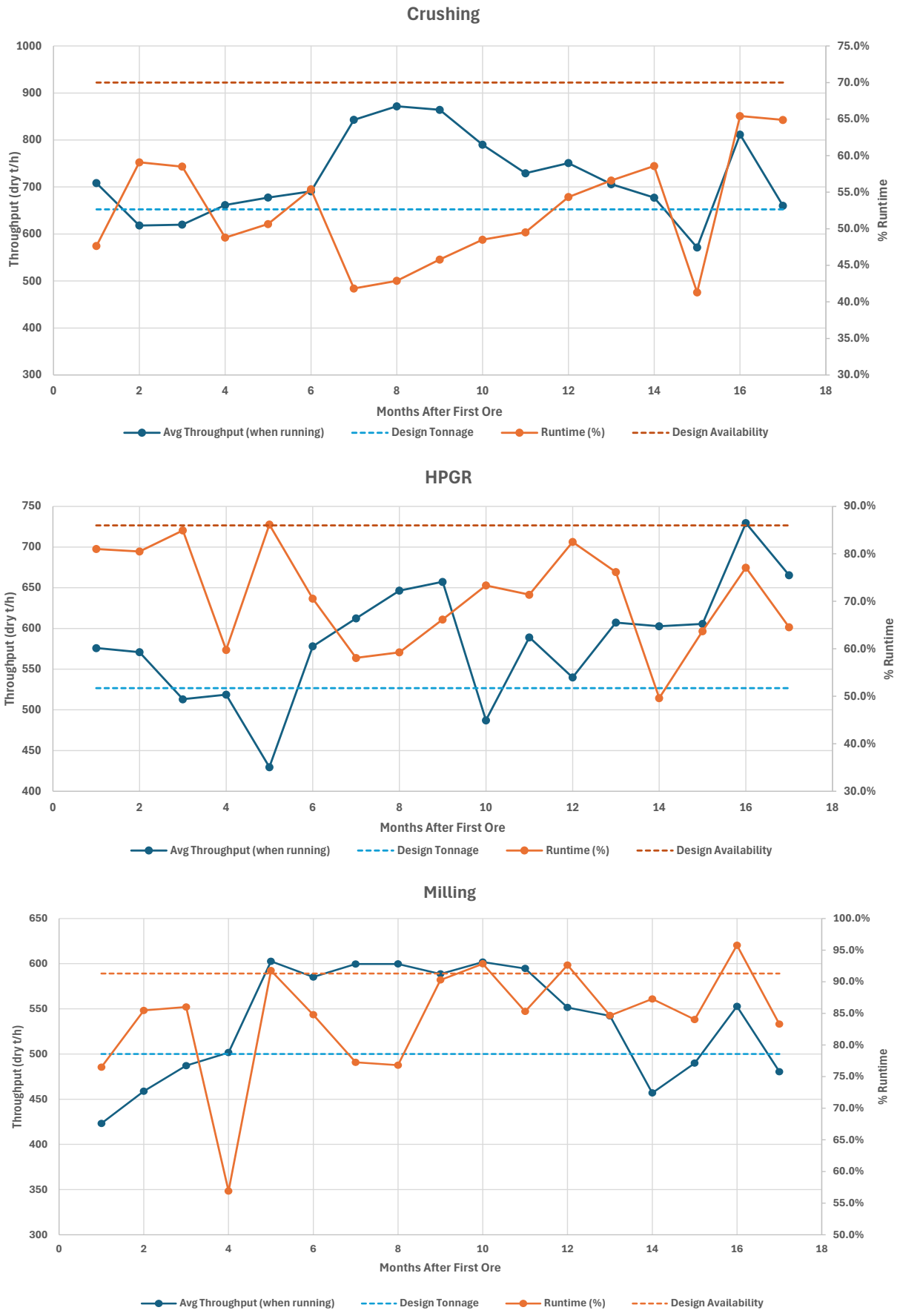



**FIG 3** – 4.0 Mt/a circuit ramp-up.

## Greenstone

The Greenstone Gold Mine is owned and operated by Equinox Gold and located in Northern Ontario. It is a ≈10 Mt/a circuit with first gold pour achieved in Q2 of 2024. Orway assisted during the ramp-up, with details published in a joint paper with the operations team (Olmsted *et al,* 2026). Below is a short summary from the paper.

The Greenstone process plant includes direct-tip primary crushing followed by closed-circuit secondary crushing, an HPGR in closed circuit with wet screening and two ball mills operating in parallel. Both mills operate in closed circuit with hydrocyclones to generate a grind size $P_{80}$ of 90–150 µm for downstream leaching. Gravity separation and intensive cyanidation circuits are dedicated to each milling train and fed via the cyclone feed pump boxes. The design Axb is 26.1 and BWi of 15.5 kWh/t. The flow sheet is presented in Figure 4. The Greenstone flow sheet is relatively lean, with only one point of surge and no standby provision in the major comminution circuit equipment. The circuit is yet to achieve nameplate at the time of writing (Figure 5). Most of the mill production losses were caused by up and downstream constraints (below-design crusher and HPGR run time as well as tails pumping constraint).

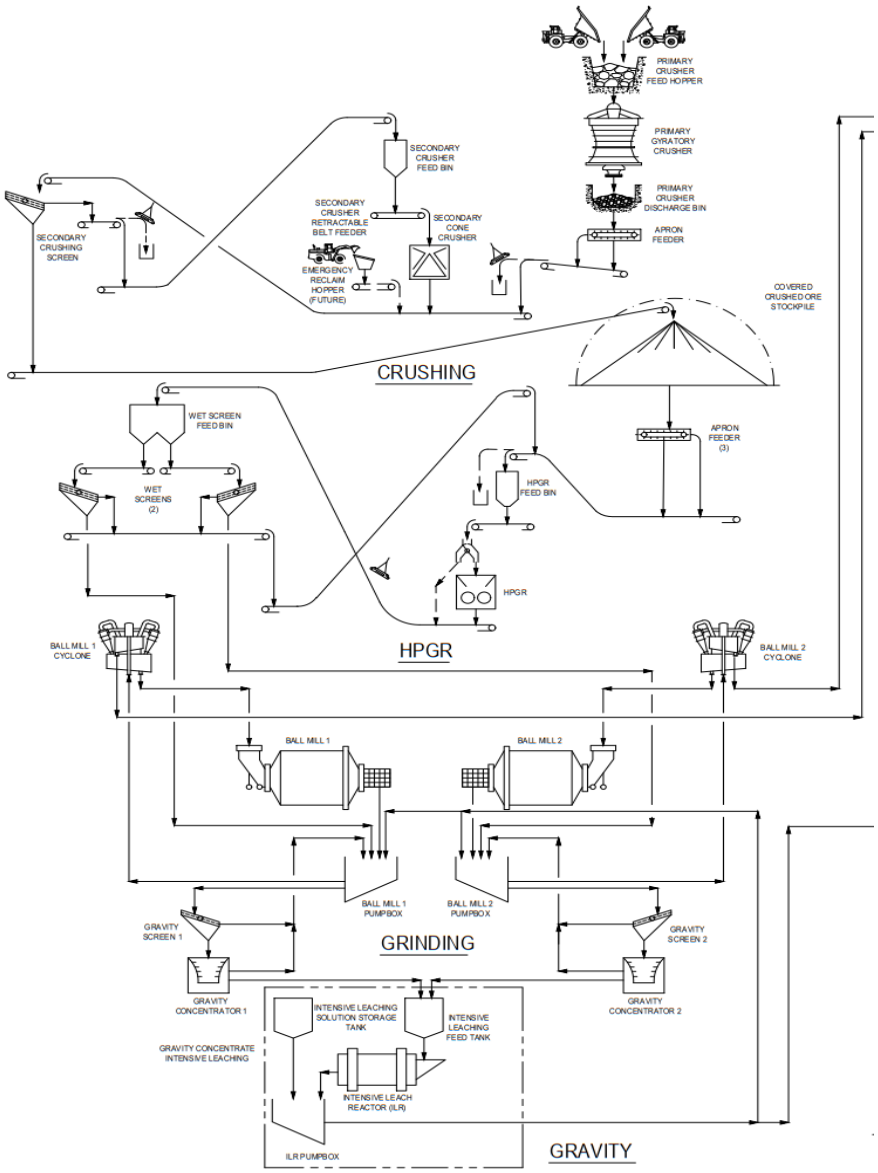



**FIG 4** – Greenstone comminution circuit flow sheet (Olmsted *et al,* 2026).

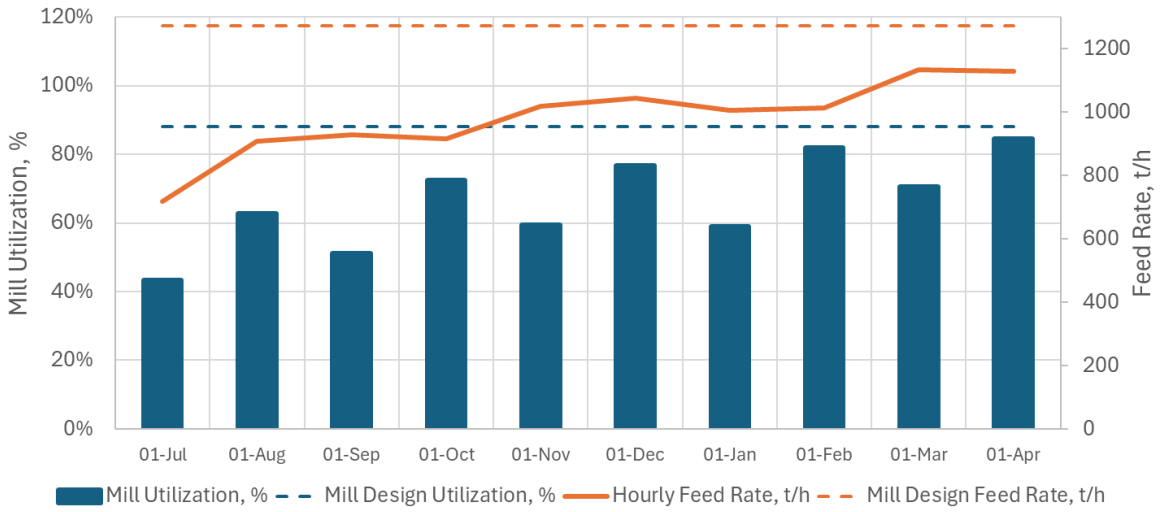



**FIG 5** – Greenstone mill ramp-up (Olmsted *et al,* 2026).

A comparison of the 4.0 Mt/a circuit and Greenstone ramp-ups is presented in Figure 6 along with additional single-unit HPGR circuit examples from the OMC database. Despite the challenges experienced at the 4.0 Mt/a circuit, the ramp-up still exceeded a Series 1 McNulty curve. This highlights the significance of circuit flexibility (both surge provisions and standby equipment) on ramp-up time.

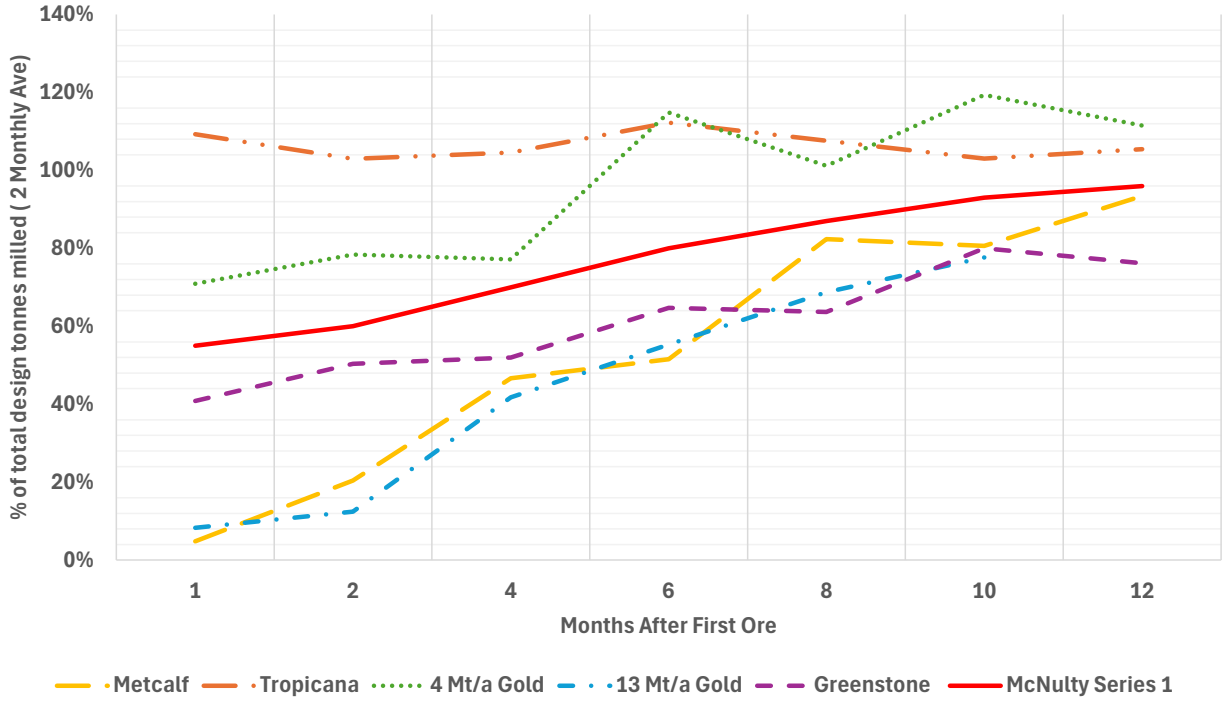



**FIG 6** – Mill ramp-up – single HPGR unit circuits.

In addition to the two case studies detailed above, examples are supplemented from the following additional case studies:

- 7 Mt/a and 13 Mt/a gold operations, Design Axb = 24.3, BWi = 16.1–18.7 kWh/t.
- 3 × lithium (spodumene) concentrators, ranging from to 2.5–10 Mt/a, Design Axb = 46.6–50.6, BWi = 14.2–15.9 kWh/t.
- 3 × magnetite concentrators, ranging from 1.5–20 Mt/a, Design Axb = 55–33.7, BWi = 13.2–18.6 kWh/t.

All are HPGR circuits operating in closed circuit with HPGR product screens. Five are with wet screening and two have dry screening in the HPGR classification duty.

## CONTROL PHILOSOPHY CONSIDERATIONS

Recently commissioned sites have generally had minimal and suboptimal automation in place within the HPGR circuits, which has contributed to premature roll failure. The following are common themes observed across recent operations:

- The HPGR is frequently in stop-start feed mode (batch operation).
- The speed of the HPGR is not integrated into the logic, resulting in surging of product, operating at higher than required speed and relying on loader intervention to manage bin levels.
- Excessive return moisture in the HPGR recirculating load where wet screening is present.
- Negative water balance in the mill (overflowing of hoppers) where the water addition is not adequately controlled.
- HPGR pressure SP selection is sub-optimal, either too high exacerbating instability or too low inflating recirculating load.
- Failure to adjust shims when required across the roll life to maintain the required static gap and healthy float on the moving roll. The trends required to monitor this are also often lacking along with the knowledge for diagnosis.
- Maintaining robust and properly tuned logic within the vendor controller, including skew management and variable speed configuration.
- All of these issues impact both process stability (production losses) and equipment wear rates.

A key issue is that the engineer's process control philosophy (PCP) does not properly integrate the two main HPGR control variables—operating pressure and speed—which are often left in manual control for inexperienced operators. While vendors provide some guidance, a more holistic, circuit-wide control approach is needed. In all recently commissioned cases reviewed, the PCP required a full overhaul to achieve stability and eliminate poor operating practices—typically after 6–12 months of commissioning, following premature roll failures and failure to reach nameplate production. The primary recommendation is to prioritise PCP development during the design phase, creating a robust control philosophy for commissioning in collaboration with the vendor, engineer, and operators. This balances process performance with equipment protection, improves reliability, and simplifies operator training by reducing manual control complexity.

Speed is typically automated to match HPGR throughput with overall circuit capacity, while pressure is adjusted to maintain healthy roll float and control recirculating load (specific energy input per pass). A recommended high-level control philosophy outline for a generic hard rock HPGR installation, is presented as an example.

### HPGR speed control

When feed to the HPGR is inconsistent, with frequent stop/start events, wear can be increased via the following means:

- The studs are more vulnerable when running at or close to the static gap (more of the feed particles are larger than the static gap). Frequent stop/start events increase the amount of time the machine operates at this vulnerable state. Particularly in combination with feed hygiene challenges during ramp-up (oversize, foreign materials etc).
- The operator adjusting the HPGR speed in large step changes or running at higher than required speed, increases wear on the roll surface (frequent acceleration of surfaces and increased operating periods of particle bed slippage). This is exacerbated when running at higher-than-required pressure SP, particularly if no further reduction in recirculating load is being achieved.

- The shut-off gate has a finite life with increased actuations significantly reducing the life of the gate (3–6 months). This is a relatively expensive consumable and has resulted in significant downtime on several operations globally. Reducing unnecessary actuations is beneficial in protecting the gate and increasing overall run time.
- Failing to maintain choke fed conditions will not only increase the risk of stud breakage but can also increase chute and shut-off gate wear caused by high impact events during surging.
- The impact of torque-controlled load balancing between the two drives needs to be considered as part of the speed control set-up. This is generally managed in the vendor PLC logic (either VFD or HPGR vendor, depending on the specific HPGR vendor's approach), and is outside of the operator's selected set points. Problems have arisen where this logic has not been set-up or tuned correctly during the commissioning. In this case the HPGR and VFD vendors should be engaged to rectify the issue.

The HPGR roll speed should be automated to maintain the required feed rate downstream to the surge stockpile and/or mill. The control philosophy recommended for conventional HPGR-ball circuits is as follows:

- Where surge capacity between the HPGR and mill is limited, the mill sets the HPGR throughput, ideally via a grind set point derived from cyclone feed density and/or online particle size analysis. If upstream or downstream constraints exist, the ball mill fresh feed rate may be manually fixed by the operator. Where surge capacity is available, stockpile or bin level instead dictates HPGR throughput, allowing operators to control surge volume and automatically maximise HPGR production when storage capacity is available.
- The HPGR screen feeder speed rate adjusts automatically to achieve the required ball mill grind or throughput SP or surge level SP, typically in a slow-acting loop as these variables have often have an acceptable band (moving average).
- When wet screening, HPGR screen pulping box water should be in ratio control to screen feed rate to maintain a constant target feed density as throughput changes. This ensures stable density to the ball mill – critical for cyclone stability – particularly given the lower solids content of the feed transfer to the ball mill in HPGR circuits (35–55 per cent w/w) compared to semi-autogenous grinding (SAG) circuits (60–75 per cent w/w). Cyclone feed hopper water is managed via a cyclone pressure control philosophy to maintain the overall mill water balance. This is especially critical where wet screening and gravity circuits coexist, as tight water balances and variability arising from gravity tails return limit available hopper water for cyclone control.
- HPGR roll speed is automatically adjusted to maintain the HPGR screen bin level using a slow-acting control loop that keeps the bin within a healthy operating band rather than a tight set point. This automation enables gradual speed changes, maintaining throughput equilibrium with the ball mill and accommodating variations in recirculating load and ore properties. Where HPGR feed hopper retention time is low (≈1 min) and long delays exist from the secondary crushed stockpile, speed safety overrides may be added at high and low hopper levels to delay trips of the feed conveyor and HPGR feed gates. However, HPGR speed should not be used for HPGR feed hopper level control, as this decouples the HPGR from downstream circuit control, disrupting equilibrium and reducing overall throughput optimisation.
- The upstream feeder to the HPGR feed hopper is used to maintain optimal hopper level at all times. This is a fast-acting loop, responding to changes in the HPGR speed and other process changes that impact the HPGR recirculating load.
- The HPGR feed (or intermediate) bin level supplying the HPGR hopper is controlled by secondary crushed stockpile feeders or by the upstream secondary crushing plant throughput set point. Where no secondary crushed stockpile exists, the secondary crushing feed rate is set to match HPGR demand, linking control back to reclaim from the primary coarse ore stockpile.

This feedback control approach has been implemented on multiple HPGR circuits and has proven effective in eliminating unnecessary stop–start events and enabling automatic ramp-up under grind control (Kock *et al,* 2015; Lovatt *et al,* 2023; Olmsted *et al,* 2026). The 4.0 Mt/a circuit example (Figure 7) demonstrates improved HPGR feed stability and elimination of feed gate actuations, while the Greenstone example (Figure 8) shows smoother HPGR speed control and improved screen feed bin level stability.




**FIG 7** – HPGR bin level logic, before and after modification, Case 1 over nine hour period.

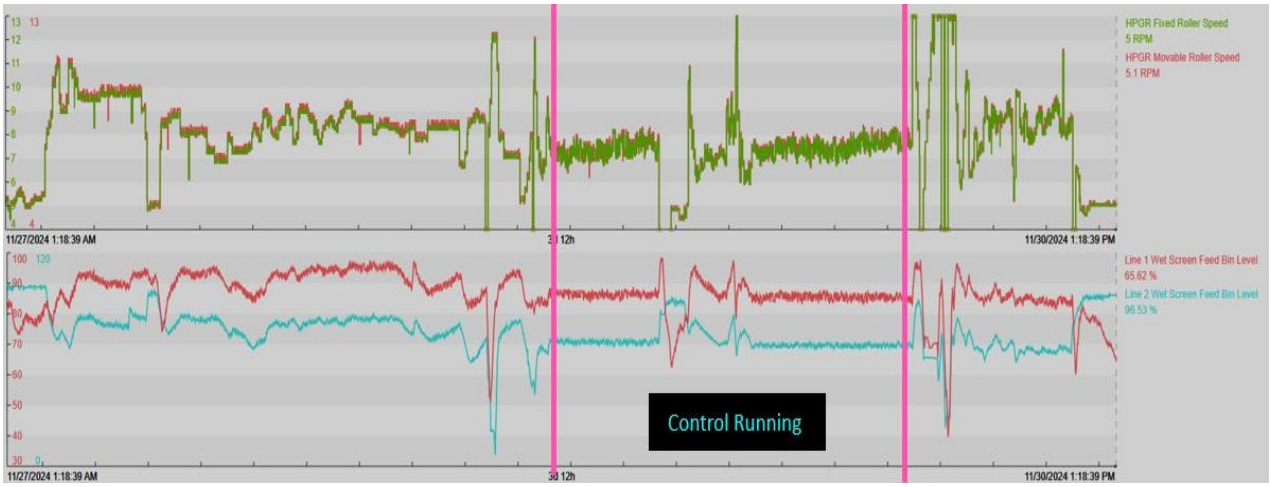



**FIG 8** – HPGR speed and bin level logic, Case 2 over three day period.

## HPGR pressure control

The other operator adjusted HPGR control variable is the pressure set point (bar), which interfaces with vendor PLC logic for skew control, often as separate control blocks. This assumes extreme skew root causes are addressed and vendor control is properly tuned. In normal operation, pressure

is adjusted only periodically to manage recirculating load as ore hardness and roll condition change – not as a routine daily or weekly control. In hard rock applications (eg gold plants), the objective is to maintain continuous roll float across the roll life while minimising recirculating load to maximise grinding efficiency. Recirculating load serves as a real-time proxy for energy transfer efficiency and can indicate whether increased pressing force delivers improved comminution. In contrast, in commodities such as lithium, where specific size fractions are targeted (eg −5 mm + 1 mm for dense media separation feed), lower pressures are often used, accepting higher recirculating loads until physical equipment limits are reached. The movable roll must float to enable efficient interparticle breakage; static operation of both rolls counteracts the HPGR comminution mechanism and should be avoided. Floating and controlled skewing are also essential for even pressure distribution, balanced bearing forces, and prevention of component overload (Rijswick *et al,* 2024).

Depending on ore characteristics, HPGR size reduction typically tapers off between 3.2–4.0 N/mm$^2$, with forces above ~4.0 N/mm$^2$ providing no further size reduction and potentially reducing gap/capacity (Figure 9). If the objective is to maximise a specific size fraction, this relationship can be exploited, as in lithium circuits. In commodities like gold and iron ore, harder ores allow higher grinding forces. Test work shows that for certain hard ores, forces above the typical range of 2.5 to 4 N/mm$^2$ can increase overall circuit capacity by reducing recirculating load (Figure 10). To maintain equipment durability at these elevated forces, HPGRs must be designed for high load, therefore operation can be limited by the machine's frame rating if this was not considered. This limit should be assessed early in commissioning by the operations team to avoid auxiliary equipment constraints that could impede ramp-up (see Greenstone example, Olmsted *et al,* 2026).

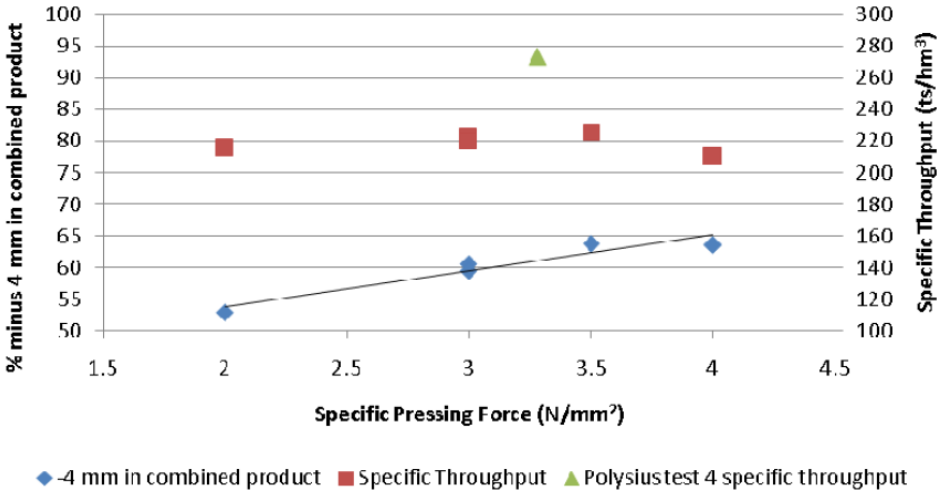



**FIG 9** – Example of pressing force relationship with size reduction.

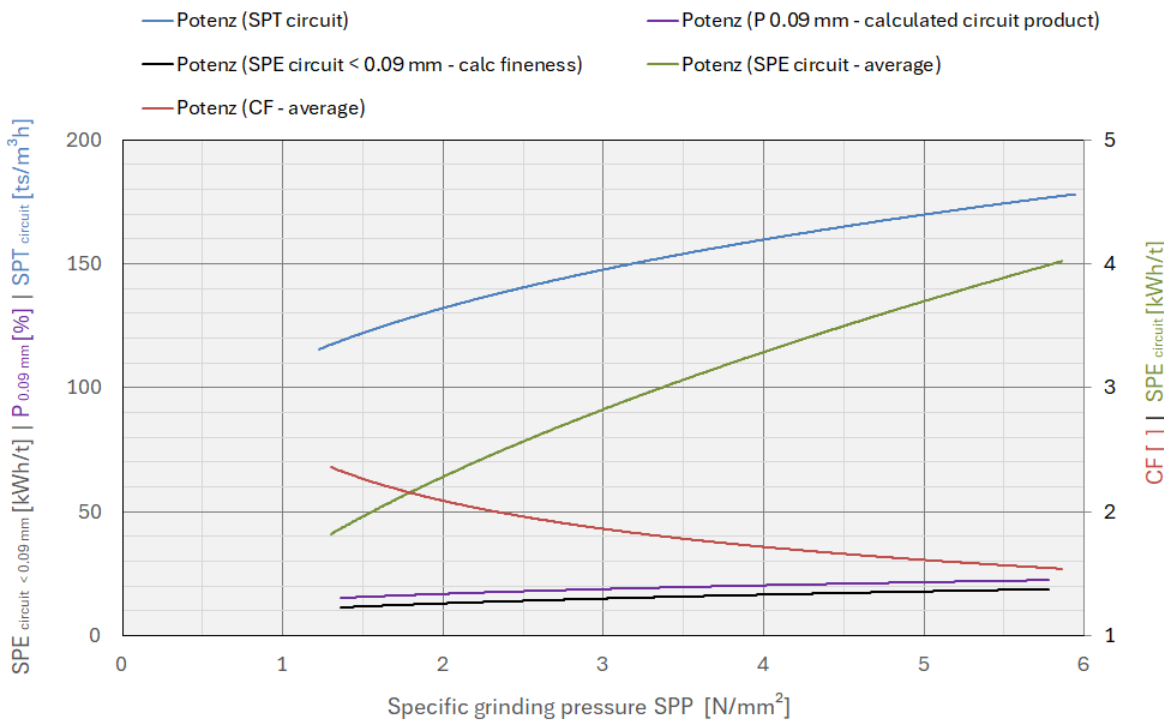



**FIG 10** – Circuit capacity versus grinding force test results for hard rock.

Optimal HPGR operating pressure is ore and process-specific and should be adjusted when major ore blend changes occur according to the impact on recirculating load (size reduction per pass). If reducing pressure has no effect on recirculating load, the lower set point should be used. Conversely, higher pressures may be warranted to increase fresh feed capacity and reduce wear on screen panels while recirculating load continues to decrease. Because pressure adjustments are infrequent, the set point can remain in manual with proper operator training, including procedures for bedding in autogenous layers on new rolls per vendor guidance. Tracking the specific pressing force via a calculated process tag, in addition to pressure in bars, is recommended for relative comparison and process monitoring.

## Static gap management

Often in newly commissioned plants the operators are not instructed on how or when to adjust the pressure SP and the metallurgists do not track the operating gap performance nor understand what to look for to ensure healthy floating is maintained across the life of the roll. The HPGR operating gap is a calculated value using two tags:

1. The static (or zero) gap is a fixed value set by the vendor, representing the roll gap with no particle bed present – typically one-third to one-half of the full operating gap. It should be maintained within ±5 mm of the vendor's initial value. As rolls wear and the roll diameters decrease, the static gap increases toward the operating gap, reducing roll float and compressed bed effectiveness, especially if wear is uneven. A pressure step test can help assess this. When roll float diminishes and pressure adjustments are ineffective, shims are removed to restore the static gap near its original value. Gap checks, often using aluminium, verify the actual gap across the roll length. Process teams typically manage this by coordinating shim adjustments with vendors or maintenance teams. Wear measurements can provide guidance but should be confirmed with physical gap checks when uncertain. Shims are usually in 5–10 mm increments, and linear transducer output should be reset during gap verification.
2. A linear displacement sensor measures the movement of the floating roll when a particle bed is present. The operating gap is calculated as the sum of the static (zero) gap and the bearing distance recorded by the sensor. Measurements are taken on both the drive and non-drive sides to assess skew, with the operating gap defined as the average of both readings. Like all

instrumentation, displacement sensors require periodic calibration, which should also be performed whenever shims are adjusted.

In the authors' experience, communication of shim and displacement sensor procedures to operations is often inadequate, requiring additional coaching during optimisation, regardless of vendor. Typically, the metallurgical team manages this, as these parameters are critical for monitoring. Proper training and trend set-up should be provided during commissioning to ensure effective oversight.

## PROCESS CONSIDERATIONS

Recent HPGR installations have experienced roll lives of 2000–6000 load hours with short-studded start-up tyres, with some units requiring three or more roll changes per annum due to atypical wear (Figure 11). Roll changes have taken 5–10 days for the new operations, and surface repair has required 2–8 hrs daily to fortnightly in these cases. Consolidated improvements in other recent but more established examples using the same HPGR technology have nearly eliminated stud breakage and extended roll life beyond 8000 hrs (Nurkazgan Cu-Au deposit in Kazakhstan, August 2023; Tuprag gold mine in Türkiye, November 2021).



**FIG 11** – Fixed roll post-removal 2025 (approximately 3200 load hrs).

Excessive HPGR surface maintenance is often linked to external process issues rather than the machine itself, though tyre composition improvements can help accommodate varying conditions. While these process challenges are well-known in the industry, operations teams new to HPGRs have frequently lacked the experience to detect and address them early. The most common process-related issues observed across recently commissioned HPGR circuits include:

- HPGR feed moisture content, both high and low moisture compromising autogenous layer health.
- Oversize feed control stemming from problematic upstream secondary crushing circuit performance results in feed top size exceeding the HPGR operating gap in all examples.
- Tramp Metal – excessive tramp metal damage is experienced on most of the sites.
- Flow sheet impact on OPEX – below-design crushing and HPGR run time has increased reliance on supplementary contract crushing and high rehandle volumes to feed the mill. Consumable rates in the crushing and HPGR circuits have also been higher than forecast during design. As a result, the OPEX of the HPGR circuit is significantly higher than budgeted.

Each of these aspects is discussed below with examples of how these issues have been addressed in recent case studies.

## MOISTURE

Moisture is essential for forming a competent autogenous layer on studded roll surfaces. Problems arise when surface (‘free’) moisture washes out the autogenous layer. The critical moisture content is ore-specific; in most gold mines with fresh rock, washout typically occurs above 4–5 per cent w/w total feed moisture. Higher moisture may be tolerated with weathered material, altered particle size distribution, or efficient wet screening, while other ore types can operate up to 12 per cent total moisture. Autogenous layer degradation can occur abruptly, even with a 0.5 per cent moisture increase. Total moisture measurements may be misleading, especially with feed segregation causing localised washout. Recommended monitoring methods for new operations do not rely solely on bulk moisture content but focus on directly tracking:

- Autogenous layer health: Conduct regular inspections of the autogenous layer for signs of thin or missing areas (example in Figure 12).
- Stud health: Measure stud protrusion in addition to stud length as part of regular maintenance practice.



**FIG 12** – Example of localised washout from visual inspection.

New studs typically start with ≈5 mm protrusion, increasing over the first few weeks and stabilising at 7–8 mm for the remainder of roll life. Continued or renewed increases indicate autogenous layer loss, washout, or mechanical gouging, shifting wear from typical tribocorrosion to aggressive cratering. Rising protrusion should prompt a review of feed moisture and static gap/roll float to ensure the autogenous layer is not being compromised.

Stud protrusion is measured with callipers from the stud top to the parent material (Figure 13) along the full roll length, usually by metallurgists during weekly or fortnightly inspections, to detect localised washout. Protrusions over 10 mm increase stud torque and risk of breakage. This is influenced by the supporting parent material ‘gum’ where valleys may tolerate slightly higher protrusion if peripheral support remains sufficient (comparative example given right in Figure 13).



**FIG 13** – Measuring high stud protrusion left, sufficient supporting gum material, Right.

Even without stud breakage, excessive protrusion reduces the usable stud length, making the remaining parent material the limiting factor for roll life (Figure 14). If clusters of studs snap, the autogenous layer is lost locally, leading to rapid cratering. Maintenance then becomes labour-intensive, with frequent replacement of large stud sections, and delayed intervention potentially voiding the remaining roll life. If protrusion is not identified early, the root cause of atypical wear can be difficult to determine at the cratering stage, as other factors (eg oversized feed, tramp metal) produce similar damage (Figure 15).

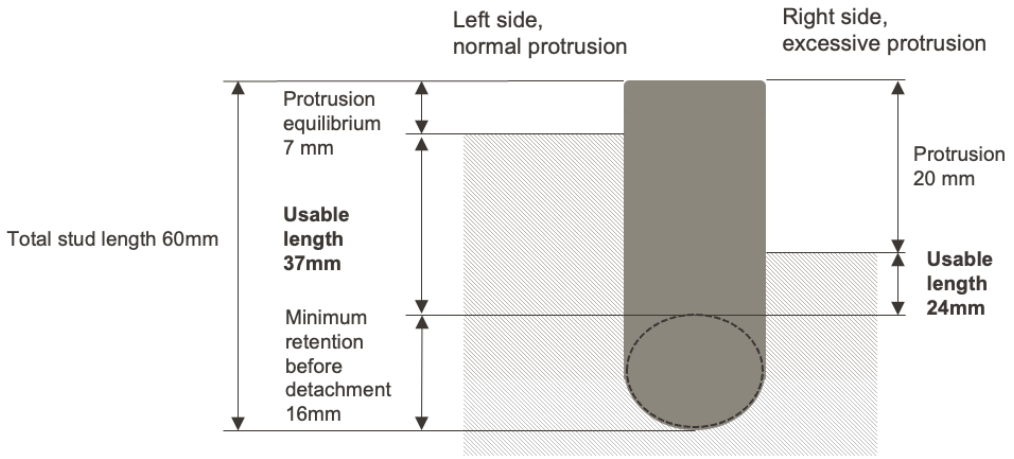



**FIG 14** – Impact on useable stud length of increased protrusion.



**FIG 15** – Later example from Figure 12 – rapid damage from segregated moisture washout.

Once high production is achieved, feed moisture and presentation should be assessed. Both excessive and insufficient moisture have caused issues in recent operations.

In two dry-screening examples (0.5–2 per cent moisture), fine misting sprays were added at the HPGR feed to maintain a stable autogenous layer. Optimisation of water addition remains ongoing, synchronising flow with roll speed to avoid over spraying.

In another site with high oxide (saprolite) content (30 per cent), washout of the autogenous layer occurred daily due to stud repairs and hosing of blocked bypass gates. Reducing oxide content to 5 per cent and eliminating these hosing practices improved autogenous layer health (Figure 16).



**FIG 16** – Localised washout observed with high-oxide blend, left; and during hosing in feed bin, right.

Wet screen performance, often neglected in early operations, is critical for moisture management and preventing premature HPGR wear. Common issues include incorrect screening material selection during design and inadequate planning for panel management. For example, two of the gold circuits experienced polyurethane top-deck panel failures within 1–2 days, compounded by insufficient spares and no established procurement process, leaving the screens compromised. It is recommended to use rubber top-deck panels for HPGR wet screening and prioritise panel procurement during operational readiness. Most operations now maintain a full set of spares on-site, additional sets on order, and remote spares in transit for each unit, including secondary screen panels.

Screen panel apertures should be adjusted to match plant constraints as they significantly impact HPGR circuit performance. Bottom-deck apertures balance circuit energy requirements and volumetric constraints – finer apertures may relieve ball mill constraints (Lovatt *et al,* 2023), while coarser apertures can increase overall production when the HPGR or auxiliary equipment is the limiting factor. Aperture settings should be reviewed regularly as ore characteristics, power costs, throughput and grind size targets change.

Routine operator checks of screen loading and oversize provide insights into HPGR health, including flake generation, feed density requirements, and tramp presence. Balancing wet screen loading can also de-bottleneck circuits and accelerate ramp-up. For example, with a 6 mm bottom deck aperture, increasing the top-deck aperture from 9.5 mm to 12 mm rebalanced deck loading accelerated ramp-up at Greenstone (Figure 17). This change reduced fines and moisture carryover, allowing higher HPGR pressing forces, decreased recirculating load, relieved conveyor constraints, and critically, improved screen life which has a significant impact on mill downtime.

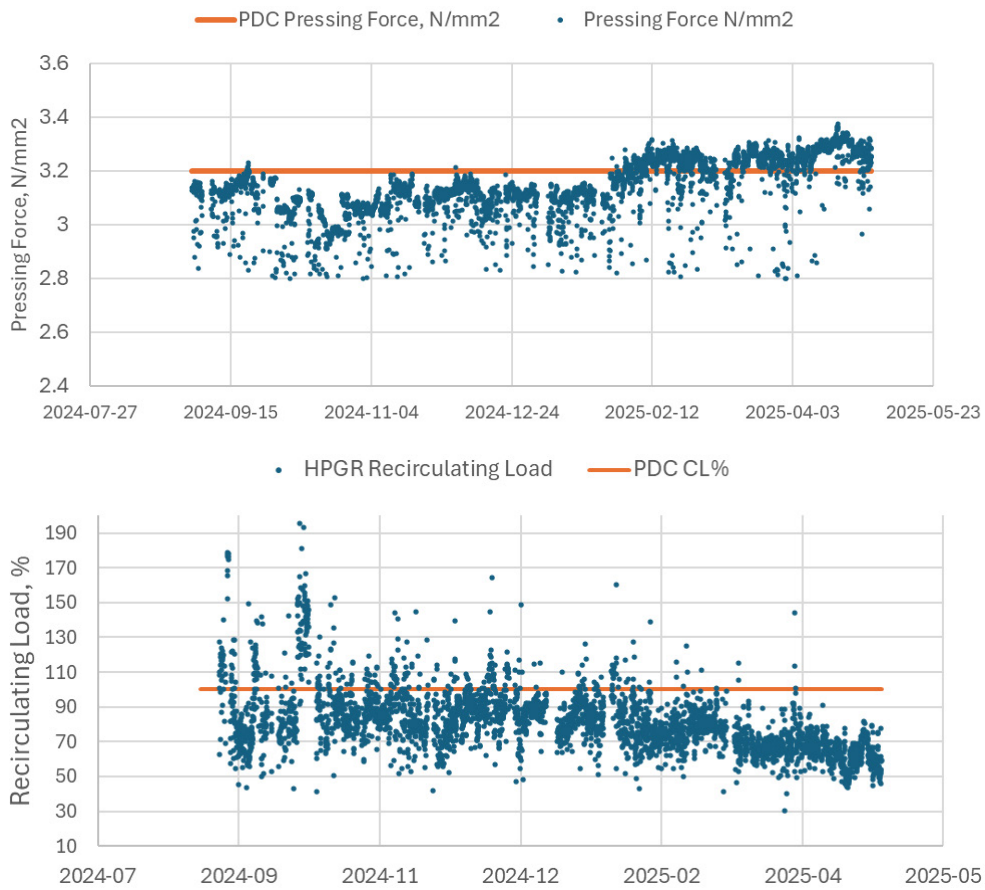



**FIG 17** – HPGR KPIs following screen aperture optimisation (Olmsted *et al,* 2026).

## Oversized feed

The particle size and hardness in the bed affect HPGR bed volume and performance. In gold processing, where HPGRs handle hard, competent ore, feed properties have a narrow influence, and the operating gap is mainly determined by roll diameter (Figure 18). The gap cannot be adjusted during operation and must rather be understood relative to the machine and any varying ore characteristics (eg compressive strength, density, swelling clay) and process conditions (eg moisture).

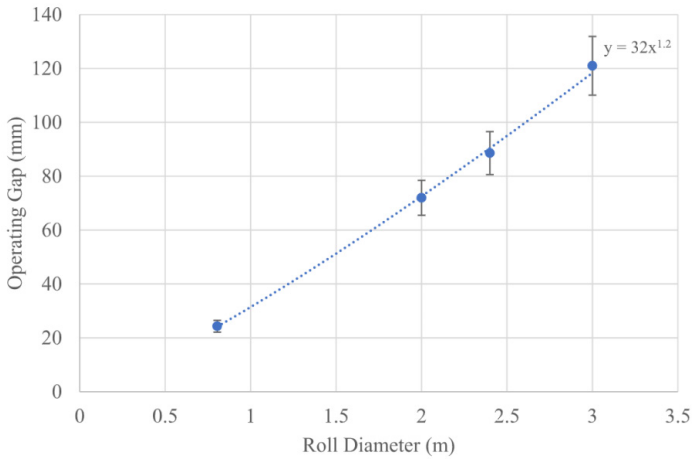



**FIG 18** – Operating gap function (Morrell, 2022).

Feed particle size must not exceed the operating gap; a single particle bridging the gap exposes studs to high impact loads, causing snapping or shattering of the tungsten-carbide studs. During design, engineers estimate the operating gap and select secondary crusher screen apertures –

typically square bottom-deck panels set ~5 mm below the HPGR gap – to allow for wear. Smaller HPGRs require finer feed to match the reduced gap.

Feed top-size problems are common, particularly when the HPGR gap relationship is not well understood. Several recent HPGR circuits started with underperforming secondary crushing plants. Lean designs, limited surge capacity and lack of standby units have led to crushing circuit run times well below design, often in the 50–60 per cent range (Table 1). All examples are hard rock, single HPGR circuits.

**TABLE 1**

% Total run time achieved in the first year of production.

| Plant area | 4.0 Mt/a circuit | Greenstone | Case 3 | Case 4 |
|---|---|---|---|---|
| Crushing | 51.4 | 57.6 | 55.0 | 56.2 |
| HPGR | 72.9 | 84.6 | 77.0 | 84.1 |
| Milling | 88.9 | 79.6* | 77.0 | 84.1 |

*Single-line operation weighted as 50 per cent run time.

Benchmark examples share common traits: primary and secondary crushers feeding a secondary crushed stockpile, with two smaller sites using jaw crushers and two larger sites using gyratories. Most circuits had little surge between the HPGR and mill (13–60 min), except the 4.0 Mt/a circuit, which has a fines surge stockpile, enabling higher early mill run time. To meet production targets despite poor crushing performance, operators have sometimes coarsened HPGR feed, resulting in oversize feed damage. Key contributing practices include:

- Premature failure of the secondary screen panels – inability to inspect without shutting down the plant leads to reduced detection of failed panels. This was particularly problematic in two cases where the Ai is 0.5–0.7 and the panels lasted seven days or less.
- Opening of the closing screen aperture size to increase the throughput rate in the limited time the crusher does run. In two cases, the aperture was opened beyond the operating gap of the HPGR, shifting the maintenance requirements from the dry screens to the HPGR rolls.
- Feeding primary crushed material (gyratory product, $F_{80}$ = 120–150 mm) directly to the HPGR during periods of secondary crusher and screen maintenance to meet production targets.
- In all four operations, contract crushing was used from the first year to supplement HPGR feed, reducing the intended OPEX savings. This practice increased the frequency of oversize rocks entering the HPGR during rehandling (Figure 19). In two cases, contract crushing supplied both secondary and HPGR stockpiles, with mill design run times still not achieved.



**FIG 19** – Oversized feed and tramp metal cleared from HPGR Screen pulping box.

The following recent examples demonstrate ways the oversized feed management has been addressed:

- Switching from slotted to square bottom-deck secondary screen panels has effectively reduced feed top size below the HPGR operating gap, especially for highly competent, slabby ore (Table 2). Although the same aperture width, the slot aspect ratio has been significant in managing feed top size to HPGR circuits given the tighter top size constraints. The 4.0 Mt/a circuit HPGR has a 45–50 mm average operating gap, where the original slotted apertures on the secondary screen bottom deck were producing feed top sizes that exceeded this. Panel open area should be reviewed to ensure sufficient screening capacity without limiting throughput, particularly if this was not considered during the design phase.
- Reducing the new screen aperture by 5 mm below the operating gap has assisted in controlling top size for longer periods where the panel wear rates have been high. Again, open area must be reviewed, along with an assessment of the top deck and secondary crusher loading to ensure adequate capacity, with set points adjusted as required.
- More stringent contract/mobile crushing and rehandle practices has prevented ingress from rehandled feed. This has included fitting protection screens to reclaim hoppers in some cases.
- Commencing capital projects as early as possible to debottleneck the secondary crushing plant, including the installation of a second parallel secondary cone crusher, has allowed for standby capacity and additional stockpile/surge capacity.
- Integration of online particle size analysis has been effective in detecting holed screen panels where inspections are difficult due to downtime.

**TABLE 2**

Impact of aperture ratio on product top size.

| Sieve size | % Passing | |
|---|---|---|
| | 40 mm × 40 mm | 40 mm × 55 mm |
| 55 | 100 | 100 |
| 50 | 100 | 96.1 |
| 45 | 100 | 92.2 |
| 37.4 | 99.3 | 91.7 |
| 22.4 | 73.3 | 62.3 |
| 16 | 57.3 | 46.7 |
| 10 | 13.9 | 35.3 |
| 4 | 28.6 | 21.5 |

## TRAMP METAL

Tramp metal, both magnetic and non-magnetic, in HPGR feed is a commonly observed critical issue across the industry. Tramp metal is most commonly introduced via the following mechanisms:

- Underground mining activities, from both current and old workings (mesh, rail, drill bits).
- Drill bits and loader teeth from open pit mining. These predominately appear in the crushing circuit with some reaching the HPGR via mobile equipment contamination. Contaminated material from the plant (ie bunker rejects and mill clean-up) is often rehandled back to the ROM, concentrating tramp metal in the circuit.
- Wear components that detach throughout the circuit (liners and wear plates).
- Mill balls via operator error or lack of adequate procedural measures to prevent mill sump clean-up material being rehandled back into the plant feed stockpiles. Inadequate operator training around tramp metal management has been observed on many new HPGR circuits globally. Balls also enter via mobile equipment which is used for multiple tasks and not adequately inspected and cleaned when leaving the mill and ball storage area.

Tramp metal is difficult to remove in HPGR circuits due to large plant scale, high loadings, and fine PSDs on conveyors compared to SAG mill scats or secondary crusher feed. Historically, large-diameter HPGRs (Ø ≥ 2.4 m) with wide operating gaps (+65 mm) and tougher, larger studs tolerated small tramp (eg mill balls ≈65 mm) with minimal stud damage damage. Examples include Boddington (Tavani, Williams and Hart, 2015), Tuprag (Weir Database), Kisladag (Weir Database), Cerro Verde (Koski, Vanderbeek and Enriquez, 2012), Metcalf, Sierra Gorda (Quadra FNX Mining Ltd, 2011; South32, 2021).

As HPGR diameters decrease, operating gaps shrink, making small tramp metal management increasingly critical. Mill balls remain the same size across circuits, so even minor tramp ingress can pose a risk. While procedural safeguards can mitigate tramp entry, experience shows that some ingress is likely, particularly during early years of operation, regardless of operator skill or plant location.

Mill balls produce distinctive stud breakage patterns reflecting their shape (Figure 20). Large tramp exceeding the operating gap can break clusters of studs, instantly removing the autogenous layer and initiating rapid cratering. This must be repaired quickly. When tramp metal enters an HPGR circuit without effective removal, it accumulates and can be seen in the screen oversize (Figure 21). Circulating metal causes repeated damage at a rate impractical for maintenance to keep up. Daily inspection of wet screen oversize provides an early indication of tramp circulation in the circuit that may be missed by poor metal detector efficacy.

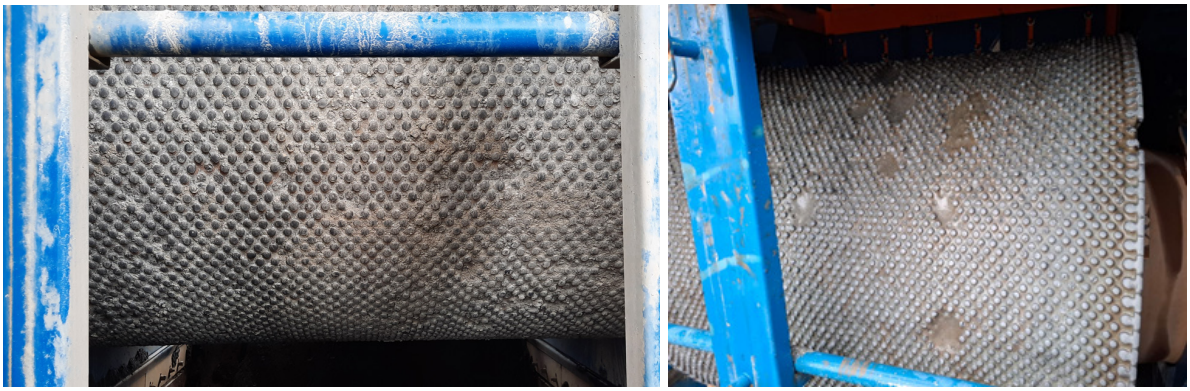


**FIG 20** – Example of tramp damage early in the roll life.

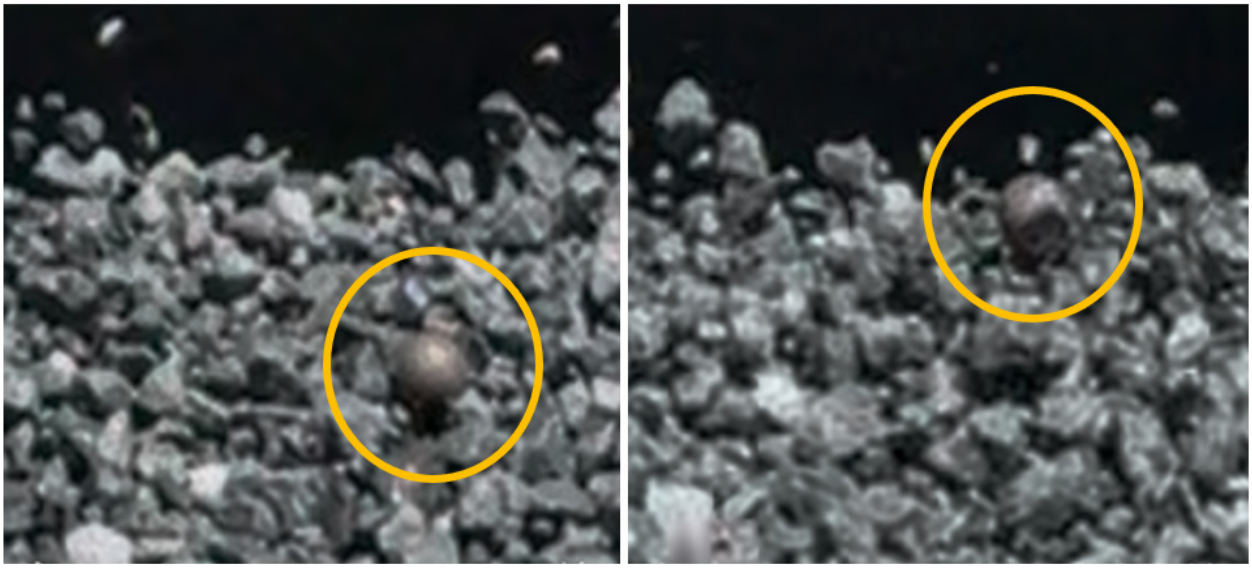


**FIG 21** – Ball in HPGR Screen O/S displaying HPGR damage.

In operations that have experienced and subsequently resolved this issue, there is usually a two-pronged approach; operating procedure/training around tramp management and upgrading tramp removal systems in the circuit.

Some specific examples from recent case studies are discussed below.

Tramp removal systems should be reviewed and prioritised during commissioning, as HPGR tyre damage from tramp is difficult to recover from and often causes early roll changes. In at least four recent cases, existing systems were inadequate, prompting upgrades. Experience with smaller HPGRs (≤ Ø2.0 m) shows that at least five metal-removal stages—such as cross-belt magnets and metal detector/diverter gates purging to grade—are typically required to control small tramp like mill balls. Single-stage magnets or detectors are generally inefficient on large conveyors. Plow systems with detectors on two recent gold plants were ineffective, causing conveyor damage and inconsistent actuation timing, and have been decommissioned.

Diverter-gate systems that purge to grade can cause piles of contaminated material, reducing magnet effectiveness and allowing ROM re-feed. Magnetite in gold and iron ore circuits can also render continuous magnets ineffective, requiring specialised detectors or non-continuous magnets. Magnetic head pulleys have proven effective in operations with significant underground contamination where magnetite is absent. Upgrades should be initiated as early as possible, as inadequate tramp control is a long-lead issue that continues to impact roll life until resolved (ideally be addressed during design).

Operating procedures should include strategies to manage contaminated feed and mobile equipment practices to avoid reintroducing tramp metal to the HPGR. At the 4.0 Mt/a, purged ore is re-treated with a mobile crushing plant fitted with magnets before returning to the main circuit. Operations teams should be trained on the effectiveness of their specific tramp removal systems and the potential impact on HPGR roll life to enable informed decisions on managing contaminated feed.

In cases where mill spillage caused ball contamination, fitting ball retainers significantly improved retention. For HPGR – ball circuits, especially with high mill superficial velocities, it is recommended to procure a ball retainer with the mill. At the 4.0 Mt/a, the retro-fitted retainer eliminated ball contamination in the wet plant area (Figure 22), a major source of tramp metal. Retainers are not foolproof, so spillage management protocols are still required. Multiple design iterations are often needed to optimise the balance between slurry flow and ball retention.



**FIG 22** – Ball mill ball retainer.

Stud design optimisation is ongoing in the new start-ups referenced in this paper. This involves making changes to the stud alloy (typically cobalt and tungsten carbide ratios), stud diameter, length

and top profile, stud density pattern and edge carbide design. A summarised overview of the design choices and consequence are summarised in Table 3. Typically, a compromise must be struck to give the best overall performance for each application. In this context, hardness refers to resistance to abrasion, which also equates to lower resistance to impact fracture.

**TABLE 3**

Roll design parameters effecting wear life**.**

| Design parameter | Consequence |
|---|---|
| Centre stud hardness | Too soft: low roll life due to limited wear resistance.<br>Too hard: can limit roll life due to excessive breakage. |
| Edge stud hardness | Must not be too brittle to avoid breakage. |
| Hardness pattern across roll width | Too hard: outer edge studs result in pronounced bathtub effect and limits achievable lifetime due to deteriorated grinding efficiency.<br>Too soft: outer centre studs cause accelerated wear and premature roll change due to edge failure. |
| Stud pattern density | Channelling of parent material needs to be prevented to avoid washouts and consequentially stud losses. |
| Stud geometry | Misalignment of feed size and stud geometry leads to increased point loading and stud chipping. Both diameter and top profile design can improve resistance to chipping across several stages of roll life. |

Tyre design decisions should be based on ore and process parameters. Initial designs are typically based on single-sample analysis which rarely reflects full-life operating conditions. For greenfield projects without operational reference, it is recommended to use start-up tyres with shorter studs to assess wear profiles and feeding conditions, reducing initial capital expenditure (CAPEX) and avoiding waste.

At steady-state, roller life can be extended with the use of longer studs, which increase CAPEX but lower OPEX per tonne. Harder studs are CAPEX-neutral and reduce OPEX but require disciplined feed size control and tramp metal management due to higher breakage risk. Minimising equipment-specific shutdowns should remain a priority to optimise overall plant availability and economics. An example of this roller surface optimisation journey from Altyntau Kokshetau, a 7 Mt/a gold mine in Kazakhstan operating a Weir Enduron RS 16 -170/180 is presented in Figure 23.

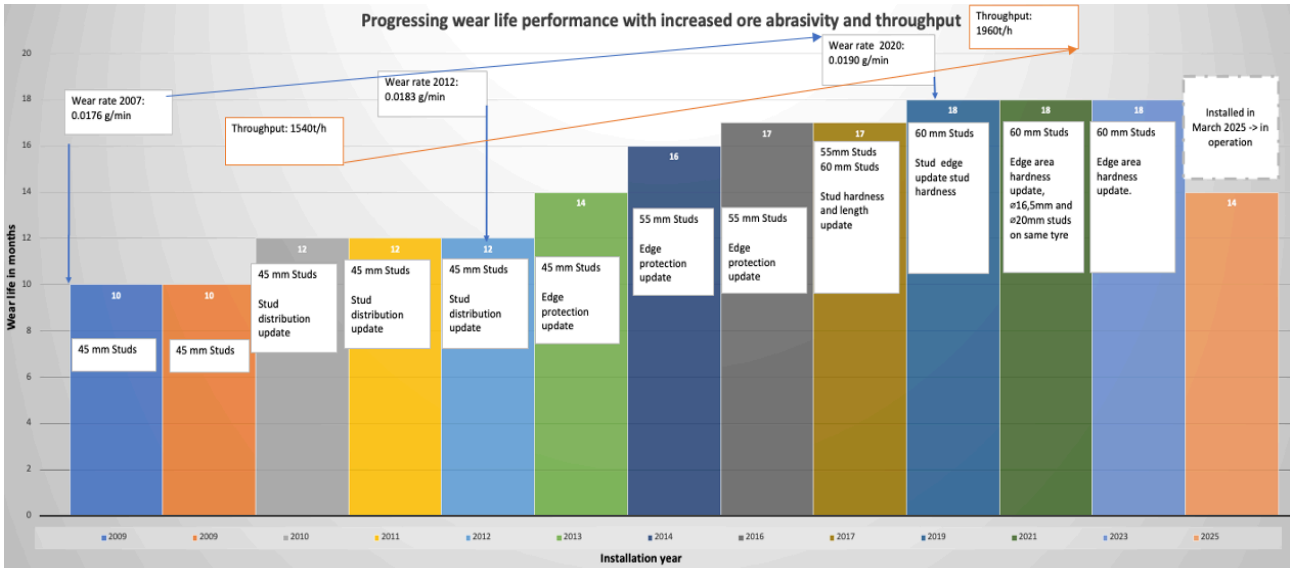



**FIG 23** – Altyntau Kokshetau roller surface optimisation.

Cheek plate design and material selection should be optimised in collaboration with HPGR vendors. While wear materials cannot fully compensate for poor feed conditions, vendors can help mitigate damage until other process issues are resolved.

In recent cases with tramp metal and oversize feed, the use of larger studs (20 mm) with higher cobalt content to increase fracture toughness to >16 MPa $m^{1/2}$, successfully reduced breakage. Similar improvements have been achieved on mature operations (Hoffman *et al*, 2023). Given long tyre lead times, spare tyres and studs should be ordered with flexibility to allow optimisation from the second tyre set onward.

In circuits with a fine HPGR screen aperture (4 mm) targeting <80 per cent passing 106 µm in the ball mill, reducing the ball top size from 65 mm to 40 mm improved grinding efficiency and lowered the ball size below the HPGR operating gap. This can serve as a stand-alone mitigation strategy where applicable.

## IMPACT ON OPEX

Mill spillage contaminated with mill balls is difficult to process, especially with wet screening and no direct mill feed option. Even with careful operation, significant slurry spillage accumulates at times, often combined with tramp-ejected material. At the 4.0 Mt/a plant, 26 000 t of such material accumulated on the ROM pad after the first year, awaiting mobile plant cleaning. This increases OPEX and introduces accounting and tracking challenges for the operation.

Supplementary contract crushing and associated rehandling costs have been an unforeseen burden in all benchmarked operations (Table 1). Low availability of primary and secondary crushers – often designed for ~70 per cent utilisation – creates a 15–20 per cent production shortfall of mill feed. In some flow sheets, such as the 4.0 Mt/a project, early operation above nameplate throughput partially offsets this loss, while in conveyor-constrained circuits like Greenstone, de-bottlenecking projects are underway (Olmsted *et al,* 2026). Replacing 15–20 per cent of mill feed with contract/mobile crushing significantly increases OPEX (and CAPEX where the mobile plant is purchased), potentially negating the operating cost savings of the HPGR and undermining the flow sheet's intended economic benefit.

At the 4.0 Mt/a project, additional dead stockpile surge increased rehandling costs, while at Greenstone, lack of surge between the HPGR and mills caused production losses. Single-unit HPGR circuits can achieve high ball mill run times (+90 per cent) early in production (Mular, Hoffert and Koski, 2015; Kock *et al*, 2015), but this depends on multiple operability factors including flow sheet flexibility. Absence of these factors in the upstream circuit in recent operations has contributed to reduced HPGR runtimes. Table 4 summarises maintenance requirements observed in the case studies from Table 1.

**TABLE 4**

Typical HPGR maintenance activities – range from benchmarked operations.

| Activity/parameter | Value |
|---|---|
| Roll life | 2300–8620 load hrs |
| Roll change time range | 5–10 days |
| Roll change time ave | 7 days |
| Cheek plate life range | 0.5–12 weeks |
| Cheek plate replacement time, average | 8 hrs |
| Stud replacement rates, average | 120–400/month |
| Inspection frequency | 1–14 days |
| Inspection time range | 1–4 hrs |

Higher-than-design oxide content has also been a cause for high contract crusher and rehandle requirement at the 4.0 Mt/a plant. High ratios of sticky, saprolite material can render the crushing circuit inoperable. If the flow sheet does not have provisions for processing problematic high-oxide blends and this is required by the mine plan, then an alternative mobile plant solution should be considered.

Due to the above factors, the costs incurred by the high volume of materials handling has been significantly underestimated in the OPEX budget, particularly for circuits that rely on HPGR product dead stockpile surge. At the 4.0 Mt/a plant, where the flow sheet requires a 3:1 ratio of handling per tonne of mill fresh feed when feeding from the dead HPGR product stockpile, material handling costs ranges between US$0.65–0.85 per tonne of total plant feed (4.0 Mt/a), depending on the number and capacity of loaders tasked with this duty. This should be considered during the design phase with consideration of purchasing dedicated mobile equipment and/or when negotiating the mining contract.

Where flow sheets are equipped with sufficient live surge capacity and duty/standby trains of major equipment (Boddington, Cerro Verde, see Vanderbeek and Gunson (2015)), or a means of producing fresh mill feed sized material as dead stockpile surge (Tropicana), then the OPEX associated with the material handling is greatly reduced. Having realistic expectations of achievable circuit run time for the specific HPGR flow sheet is therefore critical in forecasting the likely volume of supplementary feed crushing/materials handling and the subsequent impact on OPEX.

## ADDITIONAL OPERATIONAL READINESS CONSIDERATIONS

Tyre inspections are typically conducted during scheduled plant shutdowns using a straight edge and digital callipers to measure and plot wear profiles across the tyre. Visual checks assess roller surface health, with broken or missing studs repaired or replaced. Best practice is for vendors to provide a repair kit containing variable-length centre studs and different-thickness edge studs to match wear conditions and prevent excessive protrusion. This has often been overlooked in the operational readiness phase, with little or no spare studs available on-site during commissioning, and if purchased typically only new stud length.

When studs or edges can no longer be retained, welding methods can extend tyre life. Weldable tungsten carbide studs allow rebuilding of the autogenous layer, while large edge repairs can use full welding or segment welding with wear-resistant blocks for faster repair (Figure 24). Procuring sufficient replacement studs of varying lengths and weldable studs has been critical in recent start-ups due to the high replacement rates seen in Table 3. Lack of spare tyres on-site has caused production losses; spare tyres and rolls should be available on-site from commissioning where transportation times are long and/or the journey is complex. Production at the 4.0 Mt/a plant was affected due to the delayed commencement of the on-site tyre replacement facility, which only became operational 18 months after production began. An HPGR operation should never be without the ability to change tyres in the event of a premature roll failure, which can occur in as little as two weeks following major tramp damage or similar events.



**FIG 24** – Examples of tyre welding repairs: welded studs (‘Endufix’), left; edge welding, right.

The HPGR can be inspected without a mill shutdown at the 4.0 Mt/a plant, where Greenstone's flow sheet limits the inspection frequency due to the associated mill downtime. Online condition-monitoring technologies, using optical scanning and high-definition imaging (Figure 25), provide real-time feedback on roller surface health, including autogenous layer condition and stud damage. This enables operators to perform localised repairs promptly, preventing more severe washouts and reducing downtime associated with wear measurements.

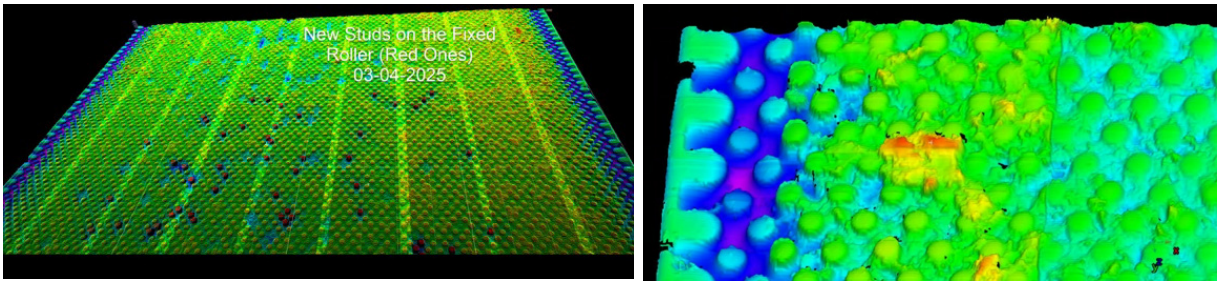



**FIG 25** – Automated tyre wear monitoring system (source: Weir HPGR).

## CONCLUSIONS

An examination of recent HPGR circuit start-ups has indicated the following critical factors impacting ramp-up and operation:

- Correct configuration of the HPGR control philosophy before commissioning, combined with targeted operator training, is critical to protecting equipment and avoiding unnecessary constraints. Early control development streamlines ramp-up training, maximises production, and prevents premature roll failure caused by improper feeding or mismanagement of key process set points.
- Feed properties including moisture, top size, and tramp metal can significantly affect HPGR circuit ramp-up. These factors should be closely monitored during start-up, with a clear understanding of the HPGR gap and timing for shim adjustments. Crushing and HPGR screen apertures should be optimised as needed, considering process requirements and material selection early in operation.
- Procurement of critical wear components should be established during operational readiness and begin at commissioning. These include tyres, cheek plates, spare studs, feed gates, and screen panels. These items are often overlooked, causing unnecessary production losses. Tyre design optimisation should start with the first set, with the production team collaborating with the vendor to address site-specific feed issues.
- The specific flow sheet inherited by the operations team has a significant bearing on the achievable run time and subsequent ramp-up time. The sooner this is defined, the sooner appropriate mitigating strategies can be implemented to meet production targets. This typically involves a combination of higher-OPEX solutions, coupled with longer-term CAPEX projects to reduce the OPEX.

## ACKNOWLEDGEMENTS

The authors wish to acknowledge the operations teams and owners of the projects referenced in this paper, who have been willing to publish their data and experiences. Your support enables our industry to progress.

## REFERENCES

Hoffman, J, Churchman, C, Ropa, J and Ramos, S, 2023. Improvement in Asset Efficiency Through Tyre Wear Life Optimisation at Cerro Verde, in Proceedings 8th International Conference on Semi-Autogenous and High Pressure Grinding Technology, SAG 2023 (Canadian Institute of Mining, Metallurgy and Petroleum: Vancouver).

Kock, F, Siddall, L, Lovatt, I, Giddy, M and DiTrento, M, 2015. Rapid Ramp-Up of the Tropicana HPGR Circuit, in Proceedings 6th International Conference on Semi-Autogenous and High Pressure Grinding Technology, SAG 2015 (Canadian Institute of Mining, Metallurgy and Petroleum: Vancouver).

Koski, S, Vanderbeek, J and Enriquez, J, 2012. Cerro Verde Concentraor: Four Years Operating HPGRs, in Proceedings 7th International Conference on Semi-Autogenous and High Pressure Grinding Technology, SAG 2011 (Canadian Institute of Mining, Metallurgy and Petroleum: Vancouver).

Lovatt, I A, Becker, M, Putland, B, Radfor, R and Robinson, J, 2023. Trade-off Realities in HPGR vs SAG Milling – A Practical Comparison of Tropicana and Gruyere Comminution Circuits, in Proceedings 8th International Conference on Semi-Autogenous and High Pressure Grinding Technology, SAG 2023 (Canadian Institute of Mining, Metallurgy and Petroleum: Vancouver).

Morrell, S, 2022. Helping to reduce mining industry carbon emissions: A step-by-step guide to sizing and election of energy efficient high pressure grinding rolls circuits, *Minerals Engineering*, 179:107431.

Mular, M, Hoffert, J R and Koski, S M, 2015. Design and Operation of the Metcalf Concentrator Comminution Circuit, in Proceedings 6th International Conference on Semi-Autogenous and High Pressure Grinding Technology, SAG 2015 (Canadian Institute of Mining, Metallurgy and Petroleum: Vancouver).

Olmsted, A, Belanger, F, Barstad, G, Scinto, P and Lovatt, I A, 2026. Ramp-up of the HPGR Comminution Circuit at Greenstone Gold Mine, A Review of Circuit Improvements, in Proceedings 58th Annual Canadian Mineral Processors Operators Conference (The Canadian Mineral Processors Society: Ottawa).

Quadra FNX Mining Ltd, 2011. Technical Report for the Sierra Gorda Project, internal report, Chile.

Rijswick, R, Onol, S, Oliveira, R and Dierx, B, 2024. To flang or not to flange?, *Minerals Engineering*, 208:108476.

South32, 2021. Investor presentation: SOUTH32 to acquire a 45% interest in the Sierra Gorda Copper Mine, internal file.

Tavani, S, Williams, C and Hart, S, 2015. Reflections on HPGR circuit operation at Newmont Boddington Gold, in Proceedings 6th International Conference on Semi-Autogenous and High Pressure Grinding Technology, SAG 2015 (Canadian Institute of Mining, Metallurgy and Petroleum: Vancouver).

Vanderbeek, J L and Gunson, A J, 2015. Cerro Verde 240,000 T/D Concentrator Expansion, in Proceedings 6th International Conference on Semi-Autogenous and High Pressure Grinding Technology, SAG 2015 (Canadian Institute of Mining, Metallurgy and Petroleum: Vancouver).

# Engineering reliability in Cadia's 40 foot SAG mill

*A McDonough[1], J Brady[2], M Mousaviraad[3] and R Stephens[4]*

1. Senior Metallurgist, Hudbay Minerals Inc, Toronto ON M5J 2V5, Canada. Email: ally.bellina@hudbayminerals.com
2. Metallurgist, Newmont Corporation, Orange NSW 2800, Australia. Email: jack.brady@newmont.com
3. Lead Mechanical Engineer, Comminution and Transportation Tech Inc, Monroe WA 98272, USA. Email: mousavi@comminutioninc.com
4. Partner, Comminution and Transportation Tech Inc, Rosland BC V0G 1Y0, Canada. Email: rob@comminutioninc.com

## ABSTRACT

Newmont Cadia's Concentrator 1 40 ft semi-autogenous grinding (SAG) mill has undergone numerous liner redesigns since commissioning in 1998. SAG mill liner design has been driven primarily by the need to handle increased ball charges, a shift resulting from the finer feed sizes produced by the upstream high-pressure grinding rolls (HPGR). The SAG mill currently operates at a 22 per cent ball charge and 2 per cent ore filling. This has resulted in recurrent feed end (FE) and discharge end (DE) bolt breakages, as well as DE grate bar fractures which directly reduce overall plant availability. Comminution and Transportation Tech Inc (CTTI) was engaged to support the site's comprehensive and ongoing root cause analysis (RCA) process using coupled Discrete Element Modelling (DEM) and Finite Element Analysis (FEA) to identify the contributing factors behind the ongoing bolting and grate bar failures.

The investigation revealed that a combination of factors caused a significant drop in bolt clamping force. This loss of pretension allowed the FE and DE liners to shift radially outwards, generating a point load on the inner end of the tapered bolt head that exceeded its fatigue limit. Systematically addressing this failure sequence has allowed the site to return from a 13 week stopgap bolt campaign life to match the 26 week liner campaign life. The grate bars primarily failed because of low Charpy impact toughness due to elevated levels of phosphorus and, in one case, residual aluminium. The failures were exacerbated by infrequent, high-energy impacts from 140 mm balls. These bars were already peened and weakened by 60 mm media becoming socketed in the pebble ports and projecting onto the grate from the top of the mill. Each of the steps in this failure sequence has been addressed, and no further grate bar failures have occurred. The successful elimination of these bolt and grate reliability issues demonstrates the value of advanced simulation techniques in solving complex engineering failures and stabilising plant availability.

## INTRODUCTION

Newmont Cadia's Concentrator 1 grinding circuit has undergone several changes since installation that have shifted the operational strategy, as described by Waters *et al* (2018). Following the Cadia East Expansion project in 2012, the flow sheet transitioned from a conventional semi-autogenous grinding (SAG), ball milling, and crushing (SABC) circuit to an upstream high-pressure grinding roll (HPGR)-fed SABC configuration. Figure 1 shows the current flow sheet with coarse ore processed through two double-deck screens in parallel and screen oversize directed to the secondary crushing circuit. Screen undersize is predominantly fed to the HPGR, with approximately 10 per cent bypassed to the SAG mill.

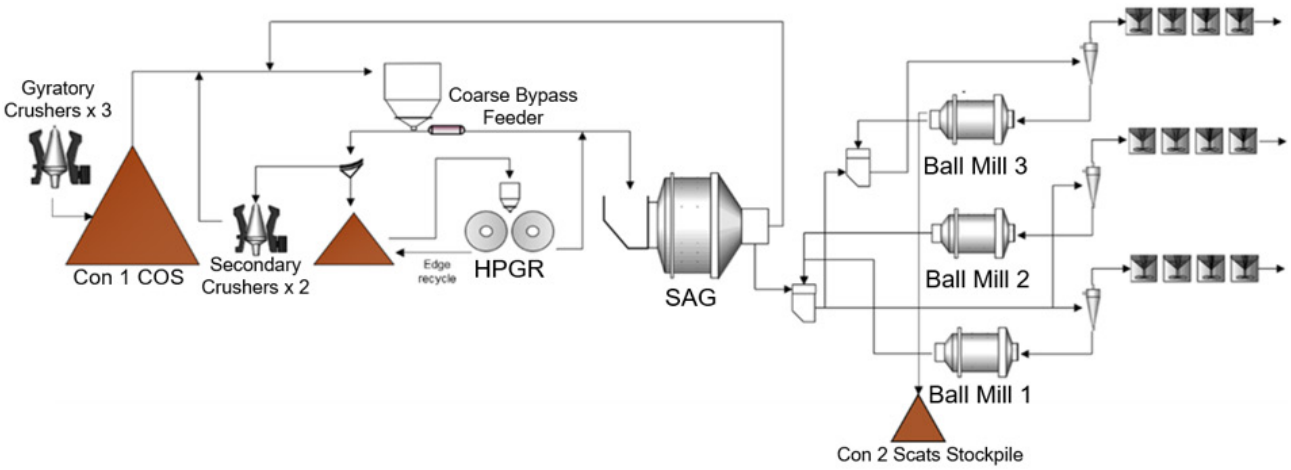



**FIG 1** – Concentrator 1 flow sheet.

Since 2017, operational conditions in the SAG mill have evolved considerably, led by a 22 MW gearless motor upgrade in 2021 (Geoghegan and Haines, 2023) that supported a progressive ball charge increase from 16 per cent to the current 22 per cent target. The $F_{80}$ to the SAG mill has dropped from 18 mm in 2016 to 14 mm in 2023, with a corresponding increase in throughput to 23 Mt/a. The current 22 per cent ball filling in the SAG mill is accompanied by an approximately 2 per cent ore filling for a total mill filling of approximately 24 per cent.

The SAG mill liners have continued to evolve since the major design changes made in 2017, as summarised by Waters *et al* (2018). Currently, the site operates on a 26 week reline campaign, with the exception of the outer pulp lifters (OPLs) and discharger cone, which are replaced at 2 year and 18 month intervals respectively. The feed end (FE) head comprises 20 rows of double-chord outer, middle, and inner liners, while the shell contains 39 rows each of FE and discharge end (DE) liners. The DE head contains 40 rows of curved grates with 30 mm and 45 mm apertures, 60 mm pebble ports, and an underlying composite pulp lifter arrangement. The current general arrangement is shown in Figure 2.

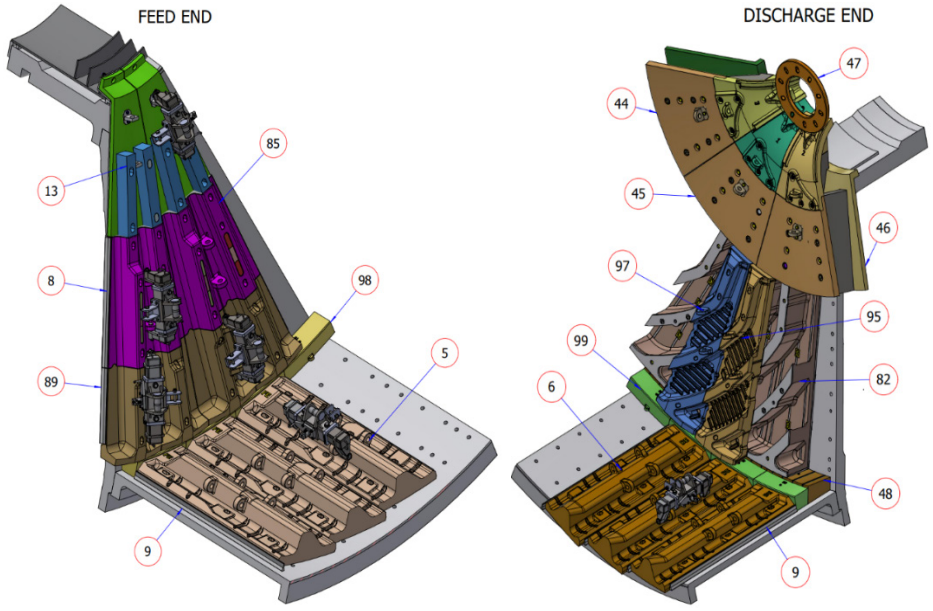



**FIG 2** – SAG mill liner system general arrangement.

## BACKGROUND

Between December 2023 and March 2024, Newmont Cadia's 40 ft SAG mill experienced a marked increase in DE and FE bolt breakages, accompanied by unexpected discharge grate bar failures. The cumulative downtime attributed to bolt-related and liner events accounted for approximately

50 per cent of the SAG mill's unplanned downtime during this period, representing a significant reliability concern for the operation.

The bolt failures exhibited reverse-bending fatigue, a failure mechanism documented in the SAG mill since 2017, but one that had markedly increased in frequency following the September 2023 reline campaign. In parallel, individual grate bars were found cracked or failed at the rib between each grate opening across approximately 25 per cent of the grates; a failure mode observed in the past but not to this extent. Though changes were made to the liner design and bolting arrangement to minimise strain, the frequency of both DE and FE bolt breakage continued to increase.

Given the severity and operational impact of these events, a root cause analysis (RCA) was initiated in collaboration with Comminution and Transportation Tech Inc (CTTI), which utilised discrete element modelling (DEM) and finite element analysis (FEA) to quantify the coupled dynamic and mechanical loading environment. This paper investigates recent as well as ongoing work done to address the bolt and grate bar failures in the SAG mill.

## BOLT FAILURES

### History – feed end bolt failures

FE head bolt breakages attributed to reverse-bending fatigue were first observed in 2017 following a transition to a single-chord liner design. This comprised 40 liners arranged in alternating high–low lifters, with each liner secured by four 300 mm M48 bolts torqued to 80 per cent proof load (5300 Nm). An RCA led to the immediate implementation of ultrasonic elongation testing (UT) to prevent tightening bolts past the yield point. A 13 week (mid-campaign) bolt replacement was also introduced, as the loose and leaking bolts were first observed at 15 weeks. Failures were concentrated on bolts 1, 2, 5, and 6, prompting the liner supplier to propose a double-chord design intended to reduce axial loading (Figure 3).

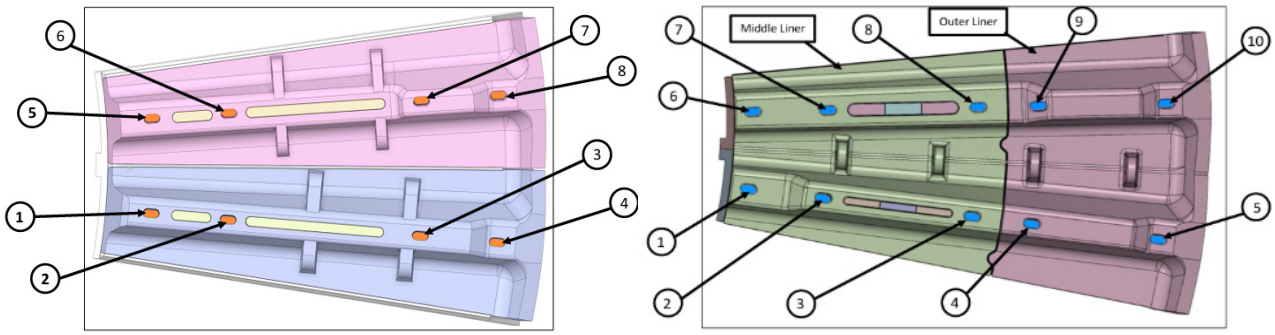



**FIG 3** – Single-chord design (left), double-chord design (right).

FEA modelling of the double-chord design predicted lower axial loads on the six middle liner bolts, but increased loading on the outer-liner bolts (positions 9 and 10). This design used a bolt ring on the mill shell that was not used for the single-chord installation (positions 9 and 4). During installation, ultrasonic testing (UT) signals for positions 9 and 4 failed because the team could not get a clear reading within the gated range set for the 300 mm bolt. This indicated that the bolt deviated (bent), causing the sensor to pick up the wall of the liner.

In September 2023, the FE was transitioned back to a 26 week bolt campaign. Failures escalated sharply after 15 weeks in service. In February 2024, 1 month prior to the scheduled reline, a middle liner with three broken bolts detached and fell into the operating SAG mill. During the liner replacement, the mill shell bolt-hole distances were measured to ensure they aligned with the double-chord liner design. It was found that there was a 14 mm discrepancy between the FE outer liner bolt-hole positions and the mill shell bolt holes. This error occurred because the dimensions for the FE outer liner were taken from a 3D scan and were not cross-referenced with mill drawings or physical measurements of the shell. As a safety measure, the FE bolt torque was reduced to 4300 Nm (65 per cent preload) for successive reline campaigns. Rectifying the outer liner bolt-hole

misalignment eliminated all geometric misalignment in the general arrangement. Inspections also confirmed all mill shell hole diameters were in good condition.

Although the misalignment was corrected in September 2024, bolt breakages persisted. Given failures also occurred on the single-chord design and at middle bolt positions, the 14 mm misalignment was ruled out as the primary root cause.

## History – OPL bolt failure

Similar fatigue failures on the OPL bolts were first observed following the February 2019 reline. As with the FE head, UT was implemented to verify bolt preload. In addition, the OPL bolt length was increased by 30 per cent to reduce the likelihood of the bolt yielding during the liner campaign; ridgeback bolts were trialled to increase contact between the bolt seat and bolt head, and the site transitioned to a composite rubber OPL design. The ridgeback bolt trial did not show any improvement. Although UT has continued to be used during installation and re-torque cycles, bolt breakage during operation persisted through to 2025.

The composite OPL design was installed in September 2021 and reduced the OPL liner weight by 62 per cent. The new design achieved its intended 2–3 year campaign life during the first installation. However, the second installation was removed after one year due to bending of the OPL back plate, which corresponded with an increase in the bolt breakage rate.

### *Metallurgical analysis – bolts*

Metallurgical analysis of both DE and FE bolts confirmed reverse-bending fatigue as the primary failure mechanism. The fatigue fractures of all analysed bolts initiated at the head-to-shank transition, with fatigue propagating through approximately 90 per cent of the bolt cross-section before final tensile overload occurred (Figure 4).



**FIG 4** – Failed bolt with final overload point in blue (right), cracked bolt (right).

No permanent bending or elongation was observed in any of the failed bolts, indicating they were not loaded beyond their yield point during installation or re-torque. The threaded regions remained in good condition, aside from minor tip damage associated with bolt removal. However, severe fretting was present on the shanks, indicating relative movement between the bolt shanks and the mill liner holes. Overall, the metallurgical findings point to a fitment-related issue either between the liner bolt hole and the bolt head, or within the general arrangement of the FE head.

### *DEM and FEA analysis*

CTTI developed detailed models of the mill liner system to conduct DEM and FEA simulations on the FE and DE liner and bolting arrangements under various operating conditions.

The operational parameters and liner conditions were divided into distinct categories:

- Ore Filling: Low ore filling (0.5 per cent) and normal ore filling (2 per cent).
- Liner State: New (simulated using a new liner scan) and worn (simulated using scans taken at the 13 week mid-point of the liner campaign).

All simulations were run at the maximum mill speed set point of 9 rev/min, while the ore and ball fillings were varied. Table 1 outlines the specific parameters used for each FE simulation. All cases were run at 2 per cent ore filling.

**TABLE 1**

FE simulation operating parameters.

| Case number | Liner status | Install date | Liner design | Ball filling (%) |
|---|---|---|---|---|
| C1– Case 1 | New | Sep 23 | 700458-2 | 22 |
| C1– Case 2 | New | | | 25 |
| C1– Case 3 | Worn | | | 22 |
| C1– Case 4 | Worn | | | 25 |
| C2 – Case 1 | New | Sep 24 | 700458-3 | 22 |
| C2 – Case 2 | New | | | 25 |

## Findings

The impact of symmetrical and asymmetrical loading on FE bolts was modelled to evaluate the effect of bolt head seating in the bolt hole. The bolt head seating refers to the way the tapered bolt head contacts the bolt seat in the liner; the engagement between these two parts is important to ensure there is no additional strain on the bolt during operation that could cause bolt breakage or liner movement.

The bolt stress contours in the simulation for asymmetric localised loading clearly align with the bolt breakages observed in the SAG mill. The high stress area predicted by FEA closely tracks the crack initiation and propagation observed in practice, with each bolt removed from the mill showing failure in the same direction (Figure 5).

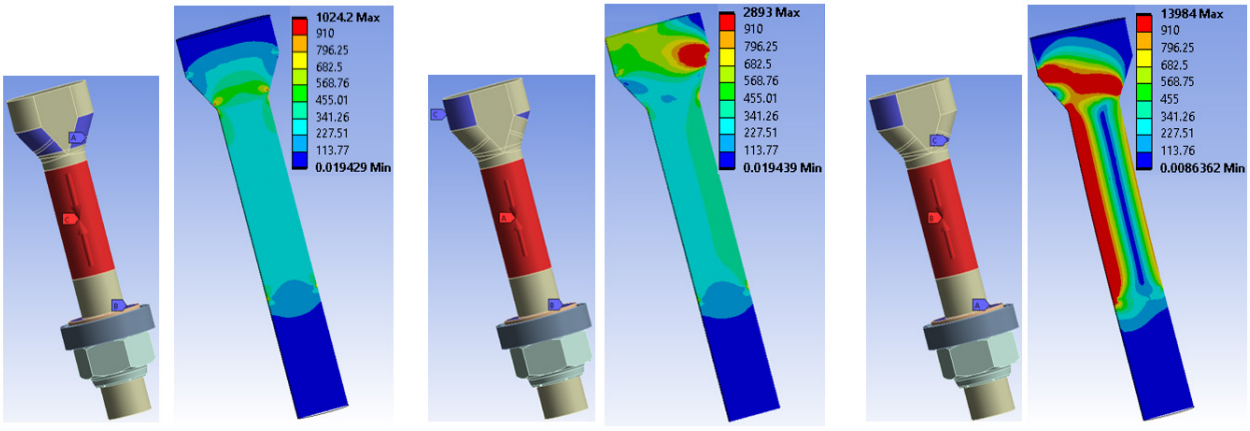



**FIG 5** – FEA modelling stress distribution contours – symmetrical maximum stress 1024 MPa (left); asymmetrical maximum stress 2664 MPa (middle); and asymmetrical localised maximum stress 13 984 MPa (right).

Onsite Dykem blue and plastigauge testing was completed to evaluate bolt head seating by torquing bolts to 8640 Nm into liner pockets on a test stand. The results were inconsistent and showed limited repeatability across multiple trials. During these tests, a significant amount of oxide mill scale (from heat treatment) was noted in the bolt holes and seats, which could cause point loading due to the uneven surface finish. However, because this scale was widespread and would likely be apparent in other non-failing liners across the mill, radial liner movement was determined to be the primary cause of the stress contours observed in Figure 5.

This radial movement is enabled by the clearance between the mill shell bolt holes and the bolt shanks, allowing the liner to shift outwardly by a few millimetres. An FEA was completed for the liner assembly with the 300 mm M48 bolts pretensioned to 65 per cent proof load. The maximum predicted stress was 178 MPa, which was well below the 13 984 MPa demonstrated in the asymmetric point loading case. Once radial liner movement was simulated, however, the stress contours mimicked the physical failures, and maximum stresses increased to 1631 MPa (Figure 6).

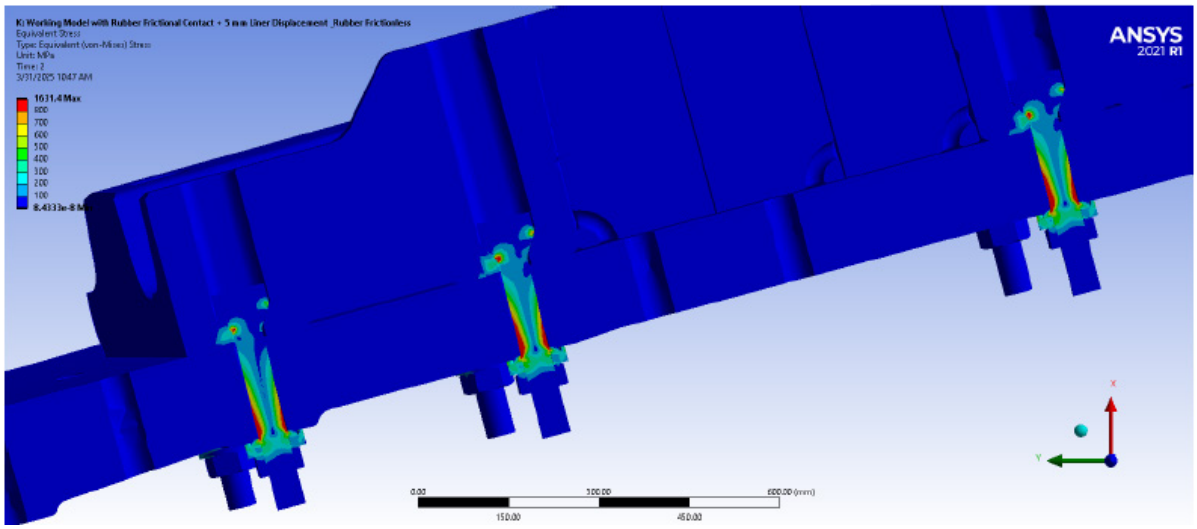



**FIG 6** – FE liner FEA and stress contours on 300 mm M48 bolts at 65 per cent proof load.

A completely flush fit between bolt seats, bolt heads, and liners is impractical because it severely delays the reline process; maintaining a reasonable design tolerance is essential to minimise mill downtime. However, the FEA results presented in Table 2 clearly explain the observed bolt failures. Increasing the relative liner displacement from 1 mm to more than 3 mm causes the bolt to tilt within the liner, resulting in asymmetric contact between the bolt head and the bolt seat. This localised contact condition more than triples the maximum stress in the bolt, substantially increasing the likelihood of yielding and fatigue damage. These results demonstrate the strong influence of relative liner movement on bolt loading and highlight the importance of limiting liner displacement during operation.

**TABLE 2**

FEA predicted max bolt stress and strain results for FE liner displacement.

| Condition | Max stress (MPa) | Max strain (%) | Min safety factor | Stress ratio | Strain ratio |
|---|---|---|---|---|---|
| Bolt pretension | 178 | 0.15 | 3.7 | 1.0 | 1.0 |
| +1 mm liner displacement | 268 | 0.16 | 2.5 | 1.5 | 1.1 |
| +3 mm liner displacement | 845 | 0.43 | 0.8 | 4.7 | 2.9 |

Evaluating these results alongside regular mill charge interactions further highlights the disproportionate impact of minor liner movement. DEM modelling generated a colour map of charge-induced instantaneous stress on the FE liners. In Figure 7 the outer liner is pressed against the rubber backing with much higher total force than the middle liner, which only partially contacts the charge and experiences highly variable stress concentrations with each revolution.

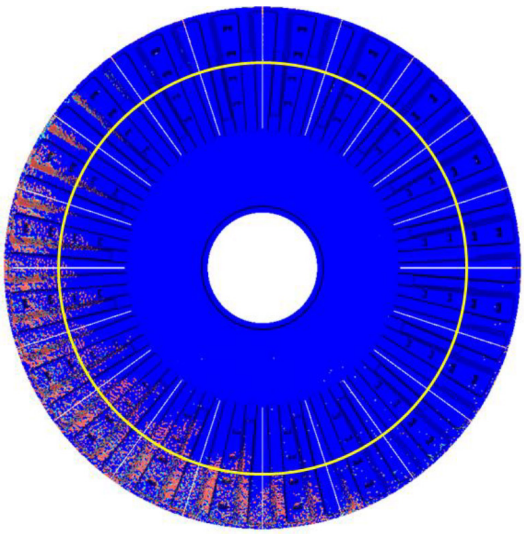


**FIG 7** – DEM 100 per cent 125 mm media and 25 per cent ball filling with new liners. Yellow circle indicates the parting line between FE middle and outer liners.

As demonstrated in Table 3, a higher ball charge results in a marginal increase in both compression forces against the shell and sliding forces in the radial and circumferential directions. Worn liners experience lower forces in due to their reduced lifter profiles. However, even at an operational peak of 340 kN, these dynamic forces remain minor compared with the severe asymmetric bolt-loading forces predicted by the FEA (Figure 5).

**TABLE 3**

DEM predicted average forces on FE liners.

| Ball filling (%) | Liner condition | Compression force (kN) | Sliding force (kN) | Total force (kN) |
|---|---|---|---|---|
| 22 | New | 199 | 226 | 301 |
| 25 | New | 229 | 253 | 341 |
| 22 | Worn | 187 | 219 | 288 |
| 25 | Worn | 214 | 244 | 325 |

Although the ball charge has increased substantially since 2017, this change is not considered a primary driver of the bolt breakages. The investigation indicates that the critical factors are minimising radial liner movement and ensuring a clean, well-prepared mating surface between the bolt head and the liner seat.

## Results and lessons learned

The bolt breakage mechanism on the SAG mill FE and DE was consistent from 2017 to 2025. With UT implemented to ensure correct pretension on every reline and bolt installation cycle, any potential loss of tension and asymmetric movement had to occur during operation. While several contributing factors were identified, the DEM and FEA completed by CTTI established that radial liner movement was the primary root cause of the asymmetric point loading.

The multi-step failure mechanism was identified as a loss of bolt tension caused by mill scale decomposition, whereby the bolt heads being twisted slightly in the bolt pocket allowed the liners to slide radially outwards to create asymmetric bolt head point loading that exceeded the fatigue fracture limits of the bolts.

The focus thereon was to minimise all radial movement by tightening tolerances between liners and using filler rings at radial parting joints, changing bolt material to a more fatigue-resistant alloy, increasing the liner bolt seating depth, and improving bolt pocket hygiene.

### *Reduction in liner tolerance*

Additional work on the FE filler rings and liners was undertaken in a staged campaign to reduce tolerances, improve liner fitment, and minimise radial parting line gaps. In September 2025, 10 mm rubber strips were added to the radial outer edges of the FE outer and middle liners as a trial to reduce gapping. Rubber was selected so that if the fit was too tight, the strip could safely peel off the liner as the reline crew installed the liner. Following successful installation, the tolerance adjustment achieved by the rubber strip was incorporated into the subsequent filler ring and liner redesigns. Due to the tight tolerances targeted, the inner 6 mm clearance between the FE outer, FE inner, and throat liners was achieved with a rubber strip, making it easily removable if fitment issues arose during installation. The designed gapping between each part of the FE head for the March 2026 reline cycle is summarised in Table 4.

**TABLE 4**

Target reduction in FE liner system tolerances.

| Tolerance (mm) | September 24 | September 25 | March 26 |
|---|---|---|---|
| FE Outer Liner to FE Filler Ring | 12 | 10 | 6 |
| FE Outer Liner to FE Middle Liner | 8 | 6 | 3 |
| FE Middle Liner to Throat Liner | 15 | 10 | 3 |

### *Bolt seat depth and clamping length*

Alongside the liner design changes, actions were taken to address the contributing causes of the bolt breakages. The bolt seat depth on the FE outer and middle liner was increased from 20 mm to 70 mm to improve bolt performance, and the bolt shank length was extended from 300 mm to 350 mm (Figure 8).

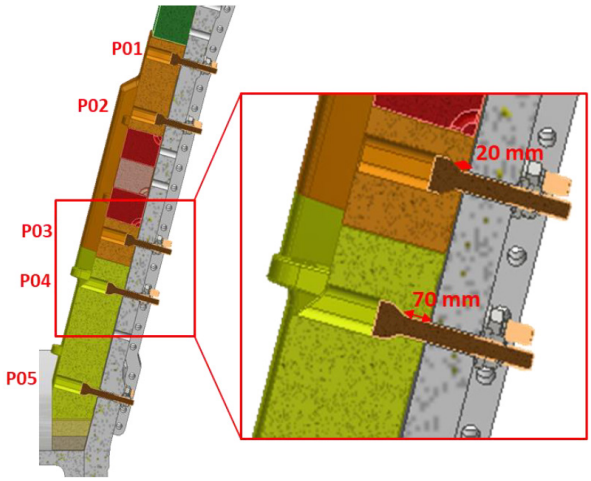



**FIG 8** – Increase in bolt seat depth for FE liners.

The increased shank length reduces the risk of bolt–liner misalignment during operation because the smooth shank engages a greater length of the liner bolt hole, providing improved lateral guidance and limiting relative liner displacement. Increased shank engagement reduces bolt tilting and the resulting localised bearing stresses beneath the bolt head. For the M48 bolts used in this application, the original 20 mm seating depth provide a shank engagement of 0.42D, whereas the revised 70 mm seating depth increases the engagement to 1.46D. Based on CTTI design practice, a shank engagement of approximately 1.5D to 2.0D is recommended for mill liner bolted joints to improve joint alignment and minimise liner movement under service loading. This recommendation is consistent with established industry best practices for highly loaded bolted joints, which emphasise maximising locating stiffness, minimising transverse bolt bending, and avoiding the transfer of lateral loads through bolt deformation whenever practical (Beardmore, 2020; Bickford, 2007; Budynas and Nisbett, 2020; VDI, 2015).

The increased shank length also improves the effective clamping length-to-diameter (L/D) ratio. This provides greater elongation under load, which distributes tensile forces more evenly to reduce the risk of premature yielding, while making the bolt less sensitive to minor angular deviations during tightening. An M48 bolt should have a minimum effective clamping length of 192 mm (48 mm × 4) or more, depending on liner thickness and mill design constraints. As demonstrated in Table 5, the FE middle liners previously failed to meet this recommended minimum threshold. In September 2025, the bolt seat depths across the FE outer and middle liners were aligned at 70 mm, successfully achieving the target L/D ratio of greater than four in the middle liners.

**TABLE 5**

Effective clamping length by bolt position.

| Bolt position | Effective clamping length (mm) | L/D ratio | Shank length in liner (mm) |
|---|---|---|---|
| P01 | 177 | 3.7 | 20 |
| P02 | 157 | 3.3 | 20 |
| P03 | 152 | 3.2 | 20 |
| P04 | 200 | 4.2 | 70 |
| P05 | 250 | 5.2 | 70 |

### *Bolt hole condition*

Since March 2025, all liner bolt holes have been sand blasted before installation to remove the oxide scale identified during Dykem testing and improve the bearing surface quality. This process removes oxide scale, burrs, and casting irregularities that can prevent uniform bolt-head seating. By providing full and uniform contact beneath the bolt head, the prepared surfaces promote the intended preload distribution while reducing localised bearing stresses, embedment, and stress concentrations that can compromise joint fatigue performance (Barrett, 1990; Bickford, 2007; VDI, 2015). This surface preparation has since become part of the standard liner installation procedure.

### *Load monitoring bolts*

Alongside the broader collaborative work with CTTI, Cadia installed load monitoring (LM) bolts on the FE and DE of the SAG mill to achieve greater granularity regarding bolt tension across the reline cycle. The steady loss of tension observed in these LM bolts during the June to December 2024 campaign subsequently provided a critical baseline for the CTTI investigation (Figure 9). The resulting strain gauge data allowed the site to predict and manage bolt issues throughout the liner campaign, playing a vital role in the strategy to return to 26 week operating cycles.

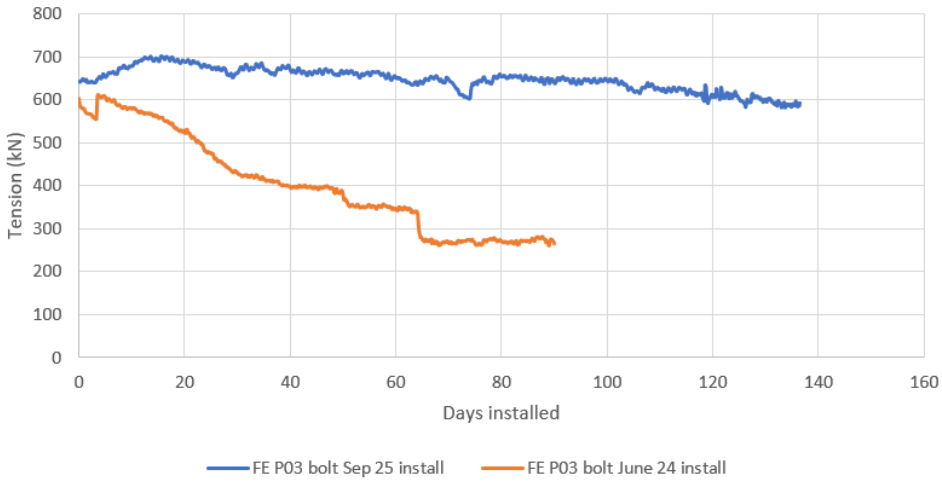



**FIG 9** – LM bolt tension readings from FE P03 comparing before and after implementation of recommendations.

Following the initial trial, the LM bolts were noted for their superior material grade compared to the standard components then in service. The 4340 alloy LM bolts feature a higher nickel content than the baseline 4140 alloy, providing enhanced ductility and fatigue resistance. Given the success of this bolt type over alternative supplier options, the remaining FE and DE positions were transitioned to the higher-grade alloy to de-risk the operational cycle.

Figure 9 illustrates the tension on FE LM bolts installed in September 2025. Several key recommendations were implemented during this stage, primarily optimising bolt hole conditions and seat depths, alongside completing Stage 1 of the tolerance reduction between the FE liners and the filler ring. Backed by these improvements, the March 2026 liner cycle successfully achieved the targeted 26 week bolting campaign.

### *Pulp lifter integrity*

Liner design changes were also implemented on the DE to minimise radial liner movement. During the March 2024 reline, two OPLs were found to be bent, and the welds attaching the internal OPL tubing—through which the grate bolts pass—to the steel spine structure had failed. These observations raised serious concerns regarding both radial movement and the structural integrity of the DE OPL components. CTTI supported the liner redesign using FEA, which resulted in increased weld support at the veins and a 20 mm increase in the back and top plate thicknesses (Figure 10).

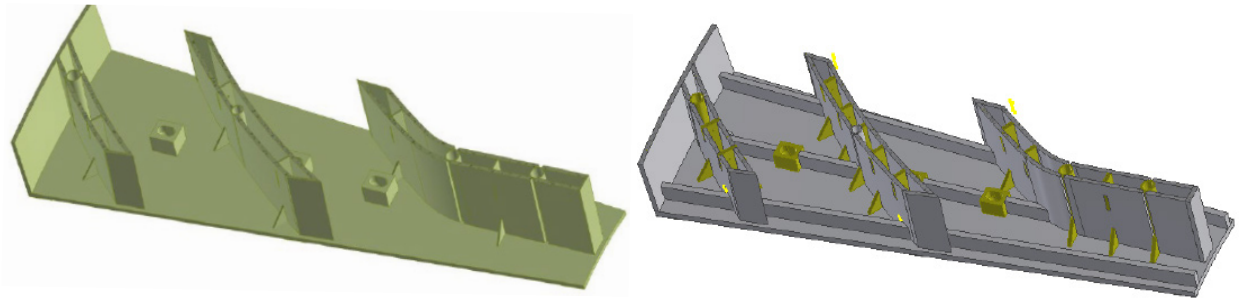


**FIG 10** – Superseded OPL design with minimal supports (left) and OPL design March 2026 with reinforced veins (right).

To improve seating against the mill shell, side pads were added to the base of the liner, and the thickness of both these and the existing corner pads was increased by 2 mm. The bolt-pad thicknesses were also modified. Each bolt pad was given a unique thickness because the flat back plate is not rolled to match the curvature of the rubber-lined inner surface of the DE cone. When these circular pads do not fully contact the shell or rubber backing, the backing plate is forced to flex during bolt tightening. This bending introduces highly localised stress concentrations at the welded joints, as illustrated in Figure 11. The revised OPL design was installed in March 2026.

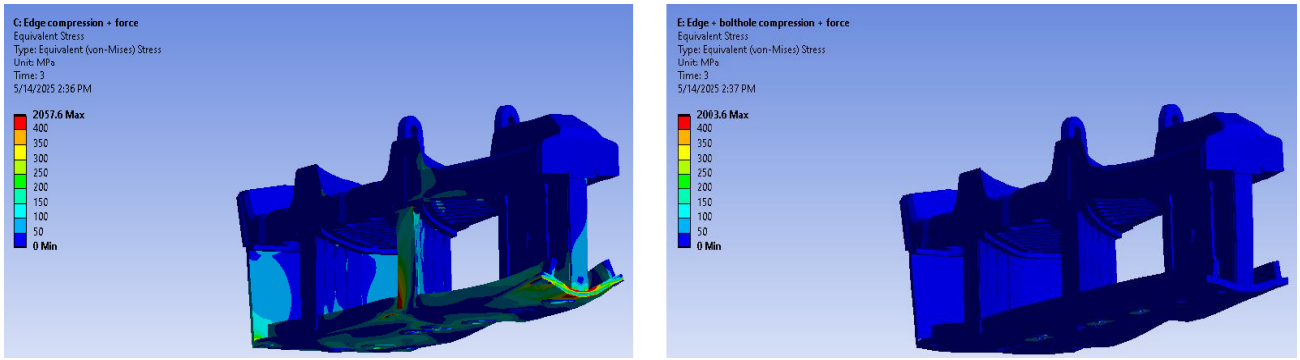



**FIG 11** – Bolt pads not in contact with mill shell (left) and bolt pads in contact with mill shell (right).

## GRATE BAR FAILURES

### History

During the September 2023 to March 2024 liner campaign, 25 per cent of the discharge grates in the SAG mill were replaced during unplanned downtime events. The first failure occurred in January 2024 and was detected by a sudden increase in oversized media reporting to the scats belt. Inspection confirmed that a grate bar on the outer radius had fractured. Following this initial event, three further downtime incidents occurred to replace grates with either failed grate bars and/or grates exhibiting visible cracking (Figure 12). All failures were located at the outer radius of the grate, specifically at the transition between the bar radius and the plate, indicating a consistent and localised failure mechanism.



**FIG 12** – Failed grate bar observed February 2024.

An important operational change prior to these failures was the introduction of a more aggressive media blend in March 2023 designed to reduce periodic, excessive scatting events. The mill charge transitioned from 100 per cent 125 mm balls to an 80:20 mix of 125 mm and 140 mm balls. Preliminary assessments of this modified blend indicated a 71 per cent increase in shear loading on the grates, but no significant increase in normal force attributable to the larger media.

#### *Metallurgical analysis*

Three grates were dispatched for metallurgical analysis. Fractography, chemical analysis, hardness testing, metallography and scanning electron microscope analysis was completed on:

- Grate from the first failure in January 2024.
- Grate with only cracking at the bars, from February 2024.
- Grate with no visible cracking from the end of the reline cycle in March 2024.

Grates 1 and 2 demonstrated a brittle failure approximately 35 mm from the wear surface. There was no evidence of ductility or casting defects on the surface, and it is likely the failure occurred instantaneously.

Chemical analysis indicated all elements were within specification except for phosphorus in Grate 1, measured at 0.047 per cent against a 0.035 per cent maximum. For inherently brittle Cr-Mo materials, elevated phosphorus is undesirable. An aluminium carbide phase (‘rock candy’ from marginally elevated residual aluminium deoxidant) was also identified in Grate 1, contributing to micro-cracking and reduced fracture toughness.

Hardness and tensile testing confirmed that all three grates met the specified material requirements, with HV20 hardness values ranging from 305 to 316. However, Charpy V-notch impact testing measured absorbed energy values of only 2–3 J, indicating exceptionally low notch toughness.

These values are substantially lower than the approximately 10–35 J typically reported for comparable high-chromium cast irons in the literature (ASTM International, 2024; Becker and Shipley, 2002; Davis, 1996; Tabrett, Sare and Ghomashchi, 1996).

While Grate 1 exhibited metallurgical defects, Grates 2 and 3 did not. Given the consistent failure location and mechanism across all failed grates, metallurgical defects were not considered the primary root cause. However, the low impact toughness of the material—despite operating in the highest-impact zone of the mill—was identified as a contributing factor.

### *DEM and FEA analysis*

The same mill conditions were modelled for the grate failures as the FE modelling, with the addition of a low ore filling of 0.5 per cent. The modelling performed by CTTI for the grates included simulating a loose FE middle liner floating in the mill charge. Although this event occurred after the first grate failed, it was important to understand whether it contributed to the uptick in grate events leading up to the mill reline in March 2024. Table 6 outlines the conditions for each DE simulation.

**TABLE 6**

DE simulation operating parameters.

| Case number | Liner status | Install date | Liner design | Ore filling (%) | Total filling (%) | Media blend (%) |
|---|---|---|---|---|---|---|
| A1 – Case 1 | Worn | Sep 23 | 700468 | 2 | 24 | 50:50 125:140 mm |
| A1 – Case 2 | Worn | | | 0.5 | 22.5 | |
| A1 – Case 3 | Worn + Dislodged FE Liner | | | 2 | 24 | |
| A2 – Case 1 | New | Sep 24 | 700512 | 2 | 24 | 80:20 125:140 mm |
| A2 – Case 2 | Worn | | | 2 | 24 | |
| A3 – Case 1 | New | | | 2 | 24 | 100:0 125 mm |
| A3 – Case 2 | Worn | | | 0.5 | 24 | |
| A3 – Case 3 | New | | | 0.5 | 22.5 | |
| A3 – Case 4 | Worn | | | 0.5 | 22.5 | |

## Findings

Three key findings relevant to the grate bar failures were identified from the DEM analysis:

- The failed FE middle liner from February 2024 did not contribute to grate bar failures.
- A 140 mm ball has a significantly higher ability of initiating a brittle failure than a 125 mm ball.
- The pebble ports transport media to the top of the charge and drop this media directly onto the grate bars.

When modelled with a dislodged FE middle liner (A1–Case 3), the liner maintained a fixed distance from the grates (Figure 13), pushed away by the charge motion without making contact.

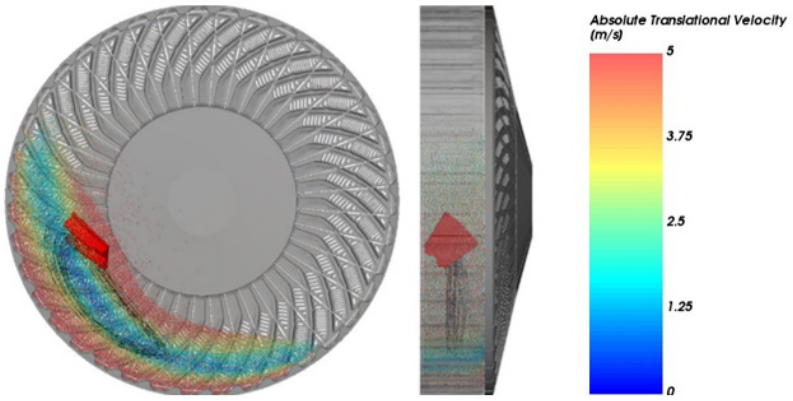



**FIG 13** – Simulation of FE failed middle liner.

Since the grate failed prior to this dislodgement, and the failure locations remained consistent, the dislodged liner was ruled out as a contributing cause.

Without the middle liner (A2 parameters), new liners showed a higher likelihood of media overshooting the toe of the charge compared to worn liners (Figure 14), supporting the operational speed cap applied during mill start-up. However, because the noise-based control in the SAG mill was inactive and unreliable at the time, the mill was exposed to impact risks post-reline regardless of the speed cap, particularly under low ore filling conditions.

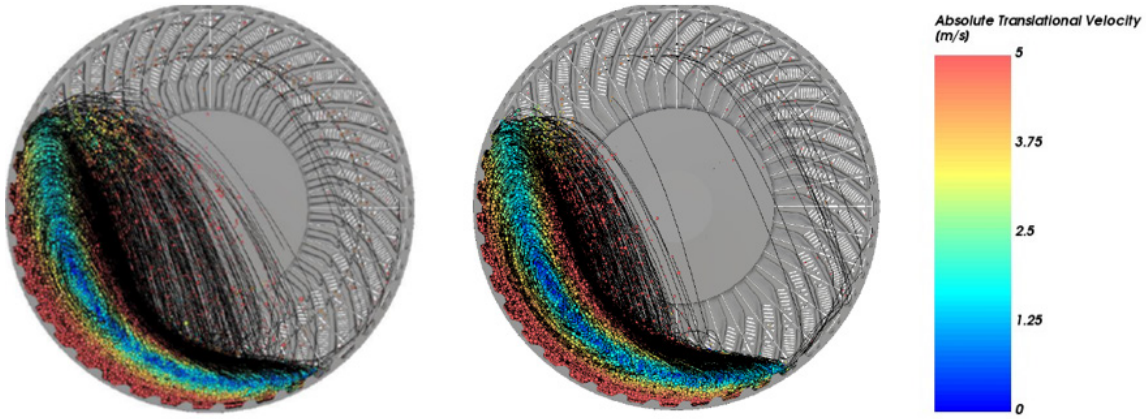



**FIG 14** – A2 Case 1: new liners, 125/140 mm blend, 2 per cent ore (left),
A2 Case 2: worn liners, 125/140 mm blend, 2 per cent ore (right).

Simulations also showed media jamming in the 60 mm pebble ports, carrying balls to the top of the charge, and dropping them 6–7 m directly onto the grate bars (Figure 15). Given the low Charpy impact toughness identified in the metallurgical analysis, this highlights the necessity of a pebble-port redesign.

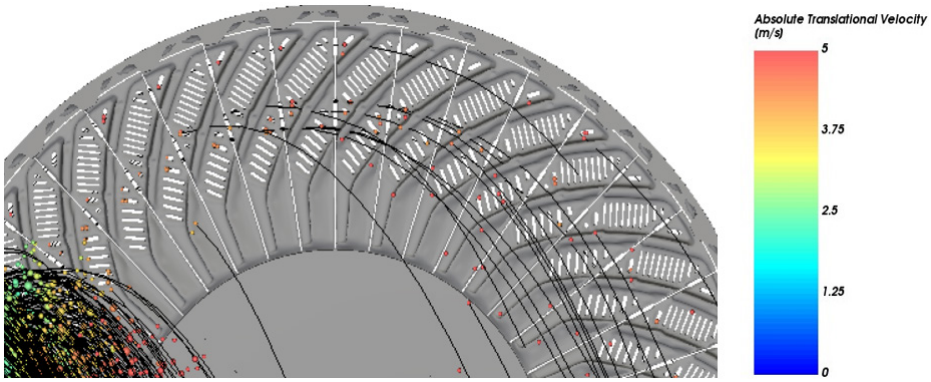



**FIG 15** – DEM modelling demonstrating media being caught in the 60 mm pebble ports.

As expected, new liners and low ore filling produced the highest maximum impact intensities. However, the two highest-impact cases occurred with 100 per cent 125 mm media charge, rather than the 125:140 mm blends. This was because the smaller media (<125 mm) is more frequently projected from the top of the charge. Figure 16 highlights the brittle fracture threshold with a red dotted line: a 140 mm ball exceeds this threshold from a drop height of just 4.5 m onto a grate bar, whereas a 125 mm ball requires a d 6.8 m drop, which corresponds to the top of the charge.

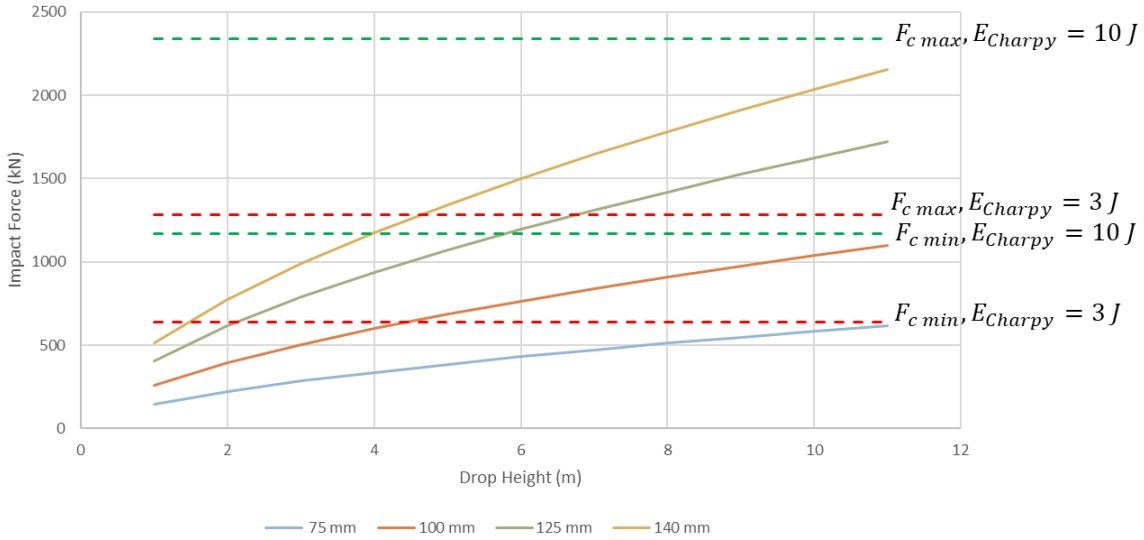



**FIG 16** – Impact force required to initiate a brittle fracture.

Therefore, removing 140 mm media is vital, due to its broader fracture-induction range (4.5 to 6.8 m). Concurrently maintaining effective noise control to prevent charge overthrow becomes critical. Redesigning the grate lifters to project balls away from the grate panels onto the charge – while also avoiding overthrow onto the shell lifters – is also another key.

## Results and lessons learned

The grate bar failures resulted from material brittleness under high operational impacts. These impacts were driven by two main factors: the introduction of 140 mm media, which carried enough energy to cause fracture when dropped from over 4.5 m, and a pebble-port design that captured and dropped balls directly onto the opposite grate bars. This risk peaked when new liners were operated with a low ore charge. Consequently, 140 mm media addition was stopped in March 2024, and the mill has since run exclusively with 125 mm media.

The DE grate has also been redesigned because of these issues including:

- A 2° increase in the pebble-port taper (to 10°) to reduce the probability of media lodging.
- Straight edges on side slots to prevent media scats from lodging between adjacent liners.
- An increased transition radius on the grate bars.
- An increased minimum bar width of 35 mm, up from the original 25 mm specification.
- Mandatory Charpy impact testing on coupons from each grate pour and heat-treatment lot to monitor toughness variations over time.

An improved noise controller, MillSlicer™, was commissioned to forcibly slow the mill during high-noise events, particularly during start-ups and ramp-downs. It provides a more sophisticated measurement of mill filling than the legacy single acoustic ear installed in 1998. The system uses five sensors to monitor impact intensity and mill charge: three shell sensors, a feed sensor, a middle sensor, and a discharge sensor. The middle and discharge sensors manage noise control, activating regularly during SAG mill start-ups and grind-outs to protect the mill. These sensors are also calibrated to provide live estimates of ore and ball filling, alerting the metallurgical team to low ore filling conditions.

Following the failures in early 2024, no subsequent grate bar failures have occurred, and end-of-life liner conditions have significantly improved.

## CONCLUSIONS

The persistent bolt reliability issues in the Newmont Cadia 40 ft SAG mill were investigated at length by the site metallurgy and reliability teams. Given the aggressive operating environment, robust liner and bolting designs are critical to maintaining mill availability. Several root-cause analyses identified the precise drivers of reverse-bending bolt breakages. Consequently, alternative hardware configurations were trialled, bolt lengths were increased, and significant structural modifications were implemented for both the OPL and FE head liners to resolve the issues.

Advanced modelling initiated in June 2024 successfully replicated the exact failure modes of the FE and DE arrangements, enabling the engineering team to isolate the root causes and mitigate outward radial liner movement. While tighter manufacturing and installation tolerances can complicate liner fitment, this study demonstrated their absolute necessity for maximising SAG mill utilisation. Maintaining precise bolt-hole dimensions, secure bolt seating, controlled liner gapping, and optimised L/D ratios is essential for ensuring uniform stress distribution and long-term operational stability.

Concurrently, the analysis of the DE grate failures emphasised the critical interplay between media selection, component geometry, and material properties. Because DE grate materials prioritise wear resistance, they are inherently more brittle and susceptible to high-energy impacts from the charge. Design features such as relief angles, transition radii, and pebble-port tapers can severely exacerbate these internal impact stresses if unoptimised. Mitigating these risks requires real-time tracking of high-risk operating conditions, which Cadia achieved by commissioning the MillSlicer™ noise-control system to proactively manage mill filling and impact intensity.

This comprehensive engineering campaign has culminated in a reliable 26 week bolt cycle on both the FE and DE assemblies for the first time since 2017. Eliminating the mid-campaign 13 week shutdowns previously required for bolt replacements—alongside minimising unplanned downtime events—has materially increased overall concentrator online time. Furthermore, the grate redesigns have prevented premature failures of the 40 ft SAG mill grates over the past 24 months. Ultimately, the deeper technical insights gained through this investigative work have optimised asset reliability and positioned the operation for sustained performance.

## DISCLAIMER

The content of this presentation reflects the presenter’s personal views and interpretations, which may include forward-looking statements that are subject to risks and uncertainties. These statements do not necessarily represent the views or endorsement of Newmont Corporation or its affiliates. Newmont has no obligation to update any statements made in this presentation. For additional information, please refer to publicly available regulatory filings.

## ACKNOWLEDGEMENTS

The authors acknowledge the contributions of the entire Newmont and CTTI teams who worked on this project:

- Metallurgy team past and present: Campbell Haines, Caitlin Geoghegan, Courtney Dobson, Steven Hart, Elias Zoghbi.
- Reliability team: Rhys Alexander, Annabelle Harding, Wendy Findlay, Henry Crossing, Sheheryar Ali.
- CTTI: Sadaf Ghorbani, Amriti Mohith, Lawrence Nordell, Malcolm Powell, Andre Langis, and Tony Facciolo (Coding Metrology Inc.).

The authors also thank Newmont and CTTI for their support and permission to publish this paper.

# REFERENCES


ASTM International, 2024. ASTM E23–24: Standard Test Methods for Notched Bar Impact Testing of Metallic Materials, ASTM International, West Conshohocken.

Barrett, R T, 1990. Fastener Design Manual, NASA Reference Publication RP-1228.

Beardmore, R, 2020. Bolted joint design, RoyMech [online]. Available from: <https://roymech.org/Useful_Tables/Screws/Bolted_Joint> [Accessed: 6 July 2026].

Becker, W T and Shipley, R J (eds), 2002. *ASM Handbook, Volume 11: Failure Analysis and Prevention* (ASM International: Materials Park). https://doi.org/10.31399/asm.hb.v11.9781627081801

Bickford, J H, 2007. *An Introduction to the Design and Behavior of Bolted Joints*, 4th edn (CRC Press: Boca Raton).

Budynas, R G and Nisbett, J K, 2020. *Shigley's Mechanical Engineering Design*, 11th ed (McGraw Hill: New York).

Davis, J R (ed), 1996. *ASM Specialty Handbook: Cast Irons* (ASM International: Materials Park, OH). https://doi.org/10.31399/asm.ash.ci.9781627085144.

Geoghegan, C and Haines, C, 2023. Maximising Concentrator 1 throughput at Cadia Valley during the SAG 20MW gearless motor drive replacement, paper presented to MetPlant 2023, Adelaide.

Tabrett, C P, Sare, I R and Ghomashchi, M R, 1996. Microstructure–property relationships in high chromium white iron alloys, *International Materials Reviews*, 41(2):59–82.

Verein Deutscher Ingenieure (VDI), 2015. VDI 2230 Blatt 1: Systematic Calculation of Highly Stressed Bolted Joints – Joints with One Cylindrical Bolt, VDI, Düsseldorf.

Waters, T, Rice, A, Seppelt, J, Bubnich, J and Akerstrom, B, 2018. The evolution of the Cadia 40-foot SAG mill to treat the Cadia East orebody: a case study of incremental change leading to operational stability, in Proceedings 14th Mill Operators' Conference 2018 (The Australasian Institute of Mining and Metallurgy: Melbourne).

# Mill lining for performance – a case study of the Hidden Valley SAG mill

*J Pyke[1] and M Swart[2]*

1. MAusIMM, Director, Solution Group – Grinding, Asia Pacific, Metso, Bendigo Vic 3550. Email: jarrod.pyke@metso.com
2. FAusIMM(CP), Executive General Manager – Processing and Operations Projects, Harmony Australasia, Milton Qld 4065. Email: morne.swart@harmonyseasia.com

## ABSTRACT

The Ø10.4 m × 5.7 m EGL (effective grinding length), 11 MW semi-autogenous grinding (SAG) mill at Harmony Gold Mining's Hidden Valley operation has undergone several liner design and operating strategy changes over its operating life. With Harmony's strong focus on operational excellence and continuous improvement, one of the key areas of collaboration with Metso was mill lining design. A drive for improved throughput, milling efficiency, and maintenance practices has resulted in a high level of optimisation and innovation.

Structural foundation concerns placed significant constraints on the mill system weight and necessitated strict control of operating speed. A heavy lining system and suboptimal mass distribution limited available operational charge mass and constrained mill performance. Various developments and innovations were undertaken by Harmony and Metso over the years to alleviate these issues and improve performance.

In 2013, development efforts focused on increasing throughput by optimising the discharge system. Grate wall improvements, using Metso Poly-Met™, aimed to eliminate pegging and increase open area to an optimal level. A pulp discharge system upgrade also improved volumetric discharge capacity. The use of rubber and composite components, rather than metallic, has allowed a reduction in system weight and helped overcome charge mass limitations as described above.

In 2015, mill efficiency was improved through optimised charge motion following the introduction of a skip-row shell lining utilising Poly-Met™. This design delivered higher milling efficiencies with an improved transfer of mill motor power to size reduction and eliminated packing events.

Although throughput was improved and liner life was stretched to greater than nine months, additional optimisation opportunities presented. Long-term operational data analysis of the updated design showed a significant improvement in mill performance following a shell reline, however a decrease in milling rates and efficiency was consistently observed after approximately six months of operation. An updated strategy was the natural next step.

With Harmony's strong focus on operational excellence and milling efficiency, the latest Megaliner™ design iteration, with a substantial reduction in pieces and improvement in fastening system, has adopted a whole-of-plant value and performance philosophy and is configured to allow quicker relines. This enables a higher reline frequency with minimal impact on annual downtime and takes advantage of the higher throughput state in the early stages of liner life.

This paper demonstrates the history and key operational data following the various optimisations and innovations that have improved SAG mill performance at Hidden Valley since 2013, with particular emphasis on the most recent innovations delivering faster, safer and more efficient relines.

## INTRODUCTION

### Geological and mineralogical characteristics

Hidden Valley is a high-altitude gold–silver mine exploiting an epithermal-style orebody hosted predominantly within altered volcaniclastic sequences and associated intrusive units. Mineralisation occurs as structurally controlled veins and disseminations, with varying degrees of hydrothermal alteration influencing both mineralogy and rock competency. The orebody exhibits moderate spatial variability in hardness, with competent primary ore zones interspersed with softer, more altered material. This variability has historically resulted in fluctuating comminution responses within the grinding circuit, particularly during transitions between ore domains.

Gold mineralisation is predominantly free-milling, with a significant proportion of the liberated gold recoverable through conventional processing routes. Silver occurs both in native form and in association with sulfide minerals, most commonly within fine-grained assemblages. The mineralogical assemblage does not contain highly refractory components; however, variable sulfide content and alteration intensity influence breakage characteristics, abrasion indices, and liner wear behaviour.

Geological and mineralogical descriptions are limited to characteristics that materially impact grinding performance, liner wear mechanisms, and downstream process stability. These attributes form the basis for the relevance of Hidden Valley as a long-term case study in grinding circuit optimisation focused on reliability, energy efficiency, and maintainability.

## Process plant flow sheet

The Hidden Valley process plant comprises a conventional hard rock processing flow sheet designed to treat run-of-mine ore and deliver a suitably prepared feed to gold and silver recovery circuits. Ore is delivered from mining operations to primary crushing facilities before being conveyed to the comminution circuit. The plant is configured as a single-line operation, with limited redundancy in critical equipment.

Following crushing, ore is processed through a single-stage semi-autogenous grinding (SAG) milling circuit operating in closed circuit with classification. The milling circuit represents the interface between the mining operation and all downstream unit operations and therefore exerts a strong influence on overall plant performance. Correctly classified mill product advances to downstream recovery operations, while oversize material is returned to the mill for further size reduction.

Figure 1 shows a simplified flow sheet of the Hidden Valley processing plant, showing primary crushing, SAG milling, classification, gravity recovery, flotation, concentrate treatment and dewatering, and tailings thickening and disposal.

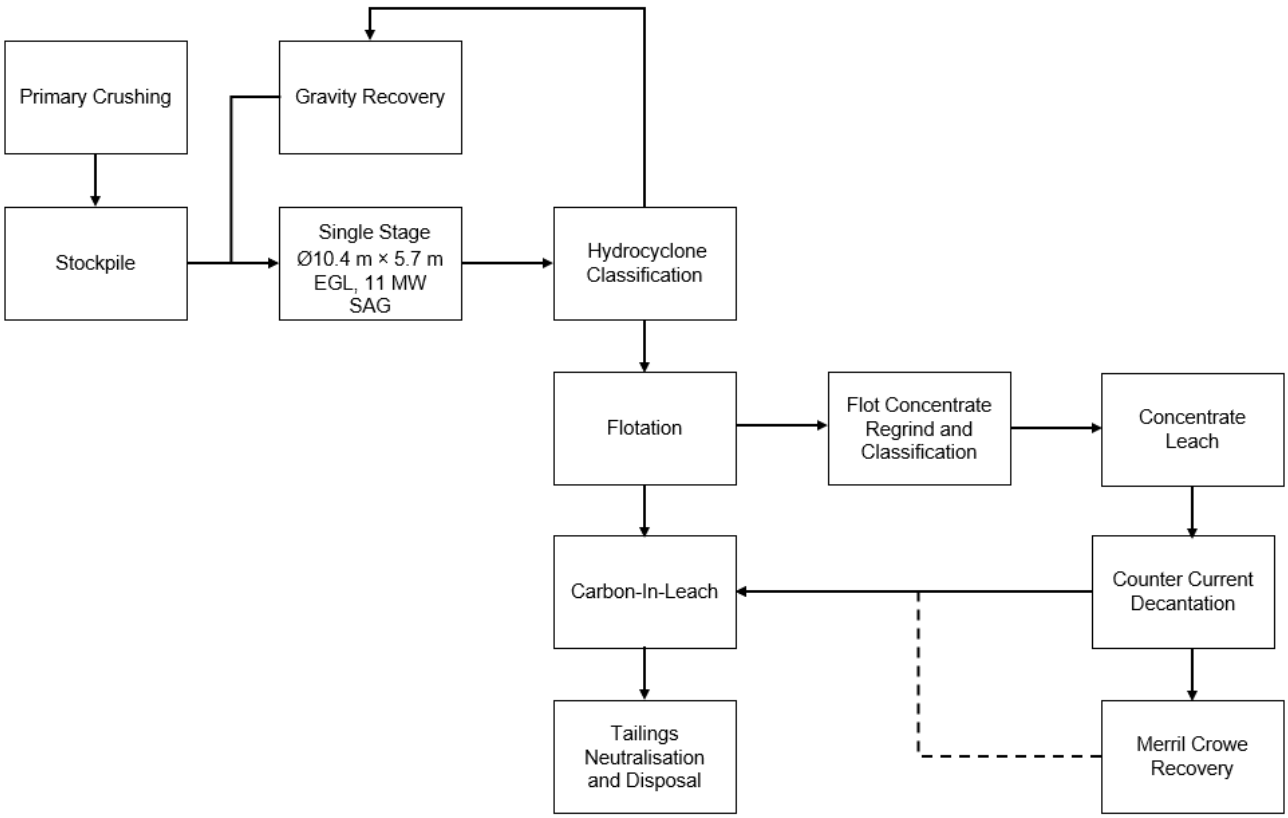



**FIG 1** – Simplified process flow sheet.

## General description of the process plant

### *Process flow*

Run-of-mine ore is delivered to the primary crusher, where it undergoes initial size reduction to enable downstream conveying and grinding. Crushed material is transferred to the SAG mill feed system, where it is combined with steel grinding media and process water before entering the mill. Within the SAG mill, size reduction is achieved through a combination of impact and attrition, governed by mill speed, charge dynamics, and liner geometry.

The mill discharge reports to hydrocyclone classification, which separates fine product from coarse material. Oversize material is recycled back to the SAG mill feed, while finer material progresses to downstream treatment.

## General performance

Over the operating life of the plant, the SAG mill has consistently functioned as the primary throughput constraint. Performance has been governed by a combination of ore competency, liner condition and geometry, charge composition, and the stability of the classification circuit. The overarching objective has been to operate as close as practicable to the mill's sustainable power and volumetric limits without inducing instability downstream. As a result, optimisation efforts have focused on maximising throughput while maintaining grinding efficiency, circuit stability, and operational reliability.

### *Operating envelope and control*

Day-to-day control targets a defined operating envelope comprising total power draw, volumetric fill (charge and slurry), feed density/solids, cyclone pressure band, and product size (using cyclone overflow $P_{80}$ as a proxy). Within this envelope, incremental set-point changes are used to stabilise charge motion, avoid pooling, and maintain consistent classification. Where ore competency increases, operating strategy typically prioritises power stabilisation and media top-up cadence ahead of feed rate escalation to preserve grind consistency.

### *Key performance indicators (typical focus areas)*

- **Throughput stability:** (eg hour-on-hour variance) Maintained to protect flotation residence times and carbon-in-leach (CIL) kinetics.
- **Specific energy (kWh/t) and power utilisation efficiency**: Monitored against grind size and ore blend to ensure energy is being converted to useful breakage rather than non-productive load.
- **Classification efficiency and cyclone performance:** Pressure, overflow density, and cut size trends to avoid circulating load excursions that can trigger grind coarsening.
- **Grind size ($P_{80}$) compliance** to downstream requirements; excursions are minimised by coordinating feed density, water addition and cyclone pressure.
- **Mechanical and maintenance key performance indicators (KPI)s:** Availability, mean time between failures on critical ancillaries, reline duration adherence.

### *Influence of liner condition*

Liner profile evolution governs charge trajectory and lift, with direct impact on breakage environment and energy utilisation. As lifters wear, reduced lift can lower effective power to breakage and drive coarsening unless compensated for through operating adjustments (media load, density, and feed rate). Predictable wear profiles support planned, fixed-duration relines and keep the mill operating within a repeatable, high-efficiency regime between shutdowns.

### *Ore variability management*

Spatial and temporal variability in hardness and abrasion index is managed through blend planning where practical, and through adaptive control in operations. Transitional domains and harder ore

pockets are handled by tightening the control envelope (overflow density and cyclone pressure), adjusting media make-up, and temporarily trading throughput for grind quality to preserve recovery stability.

### *Classification and water balance*

Stable cyclone operation is central to maintaining product size and circulating load. Control logic prioritises maintaining the pressure band and overflow density while coordinating feed dilution and sump levels to prevent roping or bypass. A consistent water balance also supports upstream power stability and downstream metallurgical performance.

### *Shutdown and reline performance*

Because the circuit is single-line, availability is highly sensitive to reline duration and repeatability. Standardised scopes, modular liner sets and pre-staged tooling have progressively reduced critical-path time and variance, improving annualised milling hours. The target condition is a calendar-based, predictable reline cadence aligned to whole-of-plant maintenance windows, rather than reactive wear-out change-outs as described later in this paper.

### *Risk controls and early-warning indicators*

Leading indicators such as rising specific energy at constant grind, increasing cyclone overflow density variability, sustained sump level excursions, or atypical bearing temperature trends are used to trigger investigation before performance degradation becomes material. Agreed trigger points guide when to adjust operating conditions, change media addition rates, or bring forward planned maintenance.

Collectively, these practices have allowed the plant to operate the SAG mill near its sustainable limits with stable grind and classification, thereby protecting downstream recovery while maximising milling hours delivered between planned shutdowns.

## Historical and future constraints

Historically, the operation faced several constraints associated with grinding circuit maintenance, including long and variable SAG mill reline durations, manual handling limitations imposed by liner mass and installation methods, and evolving safety expectations. Early liner configurations exposed a significant portion of the workforce to on-mill manual activities and were highly sensitive to execution variability, such as misalignment of reline sequencing between mill sections.

Future constraints are increasingly shaped by reduced shutdown windows, workforce availability and the requirement for predictable and repeatable maintenance execution. In response, the operational strategy has shifted towards standardisation, modular liner systems, and defined reline scopes that align with downstream processing and whole-of-plant shutdown requirements.

## Grinding circuit description and optimisation rationale

The grinding circuit is configured around a single, large-diameter SAG mill operating within a defined power draw, rotational speed, and charge volume envelope. The mill is fitted with a replaceable liner system comprising shell and head components designed to control charge trajectory, promote effective breakage, and protect the mill shell.

Grinding optimisation is essential due to the grinding circuit’s central role in controlling throughput, product size distribution, and downstream recovery performance. The SAG mill feeds gravity and flotation circuits that are sensitive to grind size variability.

## Operational challenges

Hidden Valley operates a single-line comminution circuit, which concentrates production risk on the SAG mill. The absence of parallel milling capacity elevates the importance of reliable liner life, predictable reline durations and robust shutdown readiness.

A central operational objective is to convert liner wear and mill performance into planned, calendar-based interventions through consistent wear monitoring, forecasting end-of-life windows, rolling shutdown calendars and defined trigger points.

Maintaining buffers of critical liner components, securing manufacturing and logistics windows, standardising modular liner designs and pre-staging specialised tooling are essential to sustaining a dependable reline cadence.

In a fixed-power SAG mill, excessive liner mass increases non-productive load and reduces effective grinding power. Reducing liner mass improves the proportion of installed power applied to comminution, supporting higher throughput, improved energy efficiency, reduced mechanical stress and safer, faster relines.

The operational challenges outlined above establish the framework against which liner system performance is evaluated. The following section describes the evolution of the SAG mill liner system at Hidden Valley and the design and implementation approach undertaken in collaboration with Metso.

## MILL LINING CO-DEVELOPMENT

Every grinding mill is unique; however, all mills experience continuous change, including changes in ore properties, throughput targets, maintenance requirements and asset condition. The mill lining system therefore needs to evolve with these changes, while anticipating future operational requirements.

Effective co-development of the lining design requires open sharing of information and data, and collaboration on future operational plans. The long-term partnership between Hidden Valley and Metso has led to a detailed understanding of the lining system's performance over time, wear characteristics and requirements for improvement, specifically the importance of reline efficiency and installation safety.

### SAG discharge system optimisation

In 2012, Metso was approached to review the design of the SAG mill's discharge grates due to a persistent issue of material pegging in the incumbent metallic grates, which was significantly reducing the discharge open area. As shown in Figure 2, the grates were extensively blocked with undersized grinding media, reducing open area by an estimated 50 per cent.




**FIG 2** – Comparison of rubber grates with minimal pegging and metallic grates showing heavy pegging.

A patch trial, in which 13 out of 30 metallic grates were replaced with rubber grates and Poly-Met™ lifter bars, was proposed, designed and installed in October 2012. The initial results were very encouraging, with an observed throughput increase of approximately 5–10 per cent following start-up compared with operation in the week leading up to the reline; however, this should be interpreted as indicative because operating conditions were not controlled.

The first visual inspection reinforced the positive trial results as the pegging issues had been resolved with the rubber grates. A complete set of rubber grates/Poly-Met™ lifters was procured and installed in April 2013. A further benefit to the redesign was a significant weight reduction from 68.9 t to 29.0 t and reduced part count from 165 to 138. The change from metallic loose filling segments to rubber filling segments also reduced relining risk and simplified handling.

In addition to the grate pegging issue, a broader opportunity was identified to redesign the pulp discharge system. The holistic redesign of the discharge-end head, including grate walls and pulp lifters, increased design freedom and enabled reductions in both component quantity and system weight.

In October 2013, a redesigned pulp discharge system was installed along with an upgraded discharge grate configuration. The rubber lined metallic frame pulp lifters were designed and installed, reducing the number of components from 67 to 55, as shown in Table 1.

**TABLE 1**

Pulp system design summary.

| | **Metallic Configuration** | | **Rubber Configuration** | |
|---|---|---|---|---|
| | Quantity | Mass (kg) | Quantity | Mass (kg) |
| Support Segment | 30 | 862 | 24 | 85 |
| Pulp Discharge Outer | 30 | 1,722 | 30 | 500 |
| Pulp Discharge Mid | 15 | 1,675 | 15 | 586 |
| Pulp Discharge Inner | 15 | 1,742 | | |
| Pulp Discharge Cone | 7 | 1,145 | 10 | 978 |
| Total | 67 | 136,777 | 55 | 35,610 |

A large reduction in the pulp discharge system weight, from 136.7 t to 35.6 t, was also accomplished, leading to reduced mechanical stress on the mill rotating element and bearings, providing additional capacity for charge mass if required, while also making the components lighter and easier to install.

Further benefits of rubber pulp discharge systems, beyond weight and component quantity reduction, include greater design flexibility, as they are not constrained by traditional casting limitations. In this case, an improved shape of the inner pulp dischargers opened the discharge chamber between the pulp lifters and trunnion, creating a smoother transition, as shown in Figure 3. As refined through Discrete Element Method (DEM) simulations, this design led to a reduction in modelled backflow/carry over of material to the pulp lifters, improving discharge efficiency and reducing the likelihood of discharge related constraints.

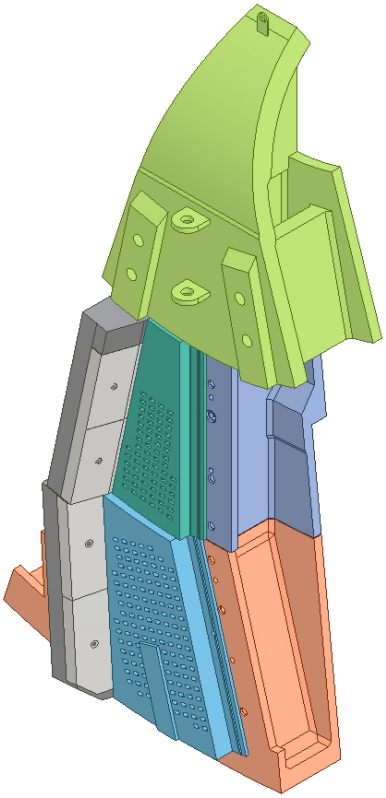


**FIG 3** – Upgraded pulp lifter design.

The complete optimised discharge-end head lining achieved a total component quantity reduction from 232 to 193 pieces and a substantial decrease in system weight from 205.7 t to 64.7 t, with the heaviest component weight reduced from 1755 kg to 978 kg.

## Shell lining optimisation – Poly-Met™ skip-row trial

Toor, Swart and Ståhlbröst (2017) describe the Poly-Met™ skip-row shell lining concept and present the Hidden Valley case in detail. The general concept of the skip-row design is to widen the spacing between shell lifter bars, whilst making the lifter bars both wider and higher, as illustrated in Figure 4. The wider spacing allows increased flexibility in lifter design, greater freedom to reduce lifter face angle where required to influence charge movement, greater penetration into the charge, a reduced potential for material to ‘pack’ between the lifters, increased service life and a potential reduction in reline frequency.

The combination of larger lifters and wider spacing increases the size of the lifting pocket between the lifters and, in turn, enhances the liner system’s ability to move larger volumes of material, particularly for large rock and grinding media.

In the case study for Hidden Valley, the shell lining was initially validated through a patch trial and subsequently converted from metallic Hi-Lo to a skip-row Poly-Met™ lining configuration. This configuration was three rings of 30 lifter bars and shell plates. The aim of the conversion was to increase milling capacity. The new design allowed an increase in lifter height from 410 mm (for the high lifter) to 500 mm. The plate width was increased to 650 mm from 230 mm, which is made possible with Poly-Met™ plates due to their greater resistance to cracking than metallic plates. A less aggressive effective charge trajectory was achieved by changing the lifter face angle from 23° to 30°.

The quantitative results presented by Toor, Swart and Ståhlbröst (2017) showed a significant increase in throughput of 13.22 per cent, accompanied by a reduction in absolute power leading to a large reduction in specific energy consumption (kWh/t) with no measurable change to product size.

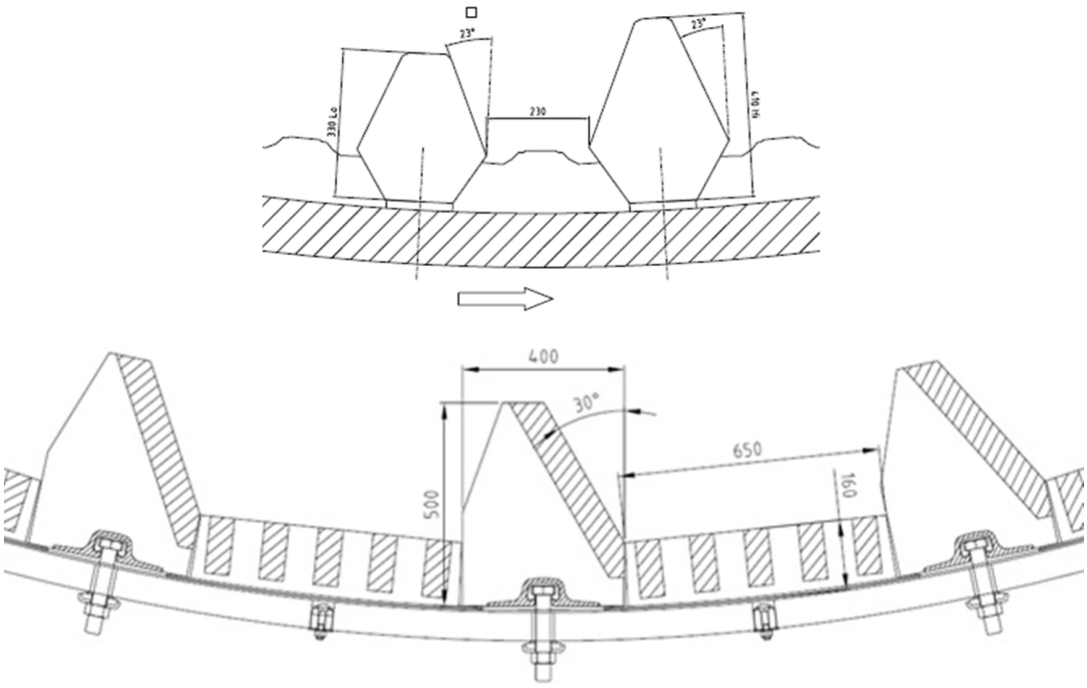



**FIG 4** – Comparison between Hi-Lo metallic and proposed skip-row designs.

In addition to the processing benefit there was a notable maintainability improvement with the updated design. As shown in Table 2, the quantity of components was reduced from 240 to 180, while the total shell lining mass was reduced from 239 t to 143 t. Further commentary on reline-time improvements through the lining optimisation process is provided later in this paper.

**TABLE 2**

Shell lining upgrade design summary.

| Metallic Configuration | | | | Polymet Configuration | | | |
|---|---|---|---|---|---|---|---|
| Section | Component | Quantity | Mass (kg) | Mass (kg) | Quantity | Component | Section |
| Shell Ring 1 | Liner | 60 | 848 | 805 | 30 | Plate | Shell Ring 1 |
| | High Lifter | 30 | 1,379 | 790 | 30 | Lifter | |
| | Low Lifter | 30 | 1,028 | | | | |
| | | | | 820 | 30 | Plate | Shell Ring 2 |
| | | | | 790 | 30 | Lifter | |
| Shell Ring 2 | Liner | 60 | 718 | 780 | 30 | Plate | Shell Ring 3 |
| | High Lifter | 30 | 1,390 | 790 | 30 | Lifter | |
| | Low Lifter | 30 | 1,041 | | | | |
| | Total | 240 | 239,100 | 143,250 | 180 | Total | |

A life cycle improvement was observed, with the new shell lining configuration requiring a complete reline every 10–12 months, depending on operating conditions. Historically, the metallic shell lining was relined on a six-month cycle of worn low lifters replaced with new high lifters.

## Shell lining optimisation – Megaliner™

Following the successful implementation of the Poly-Met™ skip-row shell lining concept, a natural step in the optimisation journey was the introduction of the Megaliner™ concept. These liners extend the benefits of Poly-Met™ technology to larger liners and use an attachment system designed to

improve installation and removal efficiency, as shown in Figure 5. This approach also improves safety and reduces installation complexity.

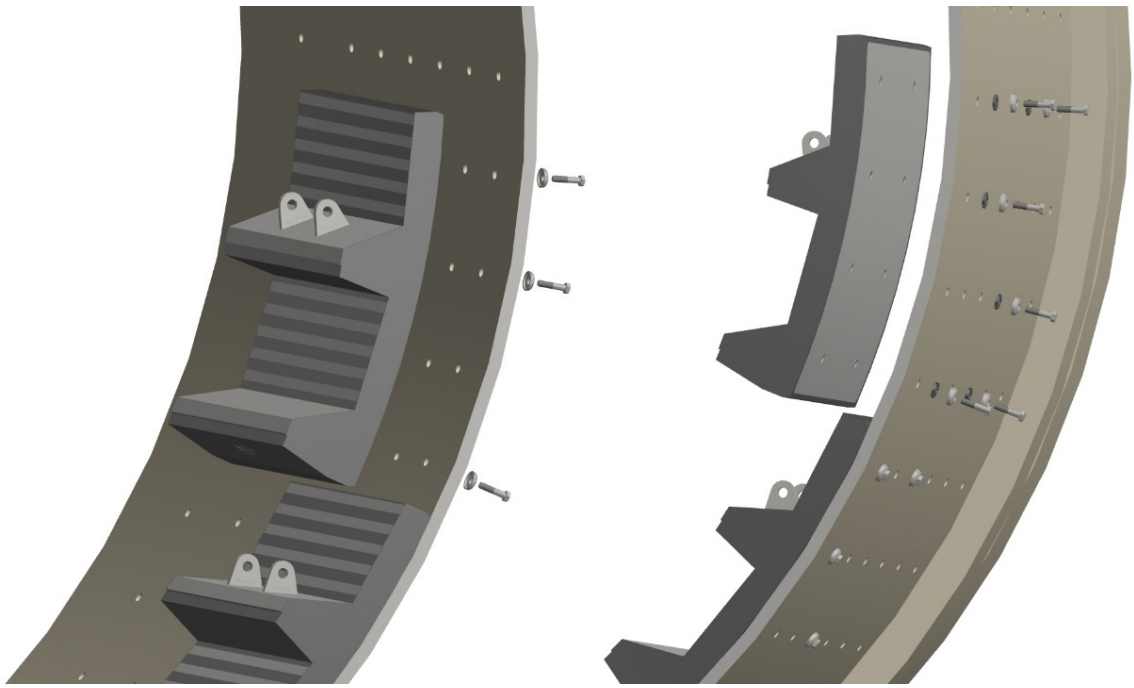


**FIG 5** – Megaliner™ attachment system.

Hidden Valley's updated shell lining design consisted of three rings of 30 Megaliner™ pieces integrating the lifter and plate of the previous design iteration. This upgraded shell lining was driven by a desire for faster and safer relines, reducing the quantity of components in the shell lining further from 180 to only 90, as shown in Table 3. This represented a further significant step change from the original metallic Hi-Lo configuration of 240 pieces. The mass of the total shell lining system marginally increased from 143 t to 147 t due to the increased mass of the liner's backing plate. The mass of the heaviest component was 1678 kg, well within the liner handler's capacity.

**TABLE 3**

Shell lining secondary upgrade design summary.

| Polymet Configuration | | | | Megaliner Configuration | | | |
|---|---|---|---|---|---|---|---|
| Section | Component | Mass (kg) | Quantity | Mass (kg) | Quantity | Component | Section |
| Shell Ring 1 | Plate | 30 | 805 | 1,678 | 30 | Megaliner | Shell Ring 1 |
| | Lifter | 30 | 790 | | | | |
| Shell Ring 2 | Plate | 30 | 820 | 1,612 | 30 | Megaliner | Shell Ring 2 |
| | Lifter | 30 | 790 | | | | |
| Shell Ring 3 | Plate | 30 | 780 | 1,619 | 30 | Megaliner | Shell Ring 3 |
| | Lifter | 30 | 790 | | | | |
| | Total | 180 | 143,250 | 147,270 | 90 | Total | |

In this case, there was no change to the profile of the lifter bar, with height and face angle remaining constant to the skip-row design and the plate thickness and width remaining unchanged. Therefore, from a process perspective and considering the relationship between mill lining and mill charge, ie the geometry and material of the lining encountering the mill charge, there was no change to the proven skip-row design from a charge-interaction perspective.

In addition to the shell lining design changes, the Poly-Met™ concept was trialled and confirmed on the feed-end head of the mill. The aim of this change was to allow consistent service life with a

reduction in component mass for faster relines. The upgraded feed-end lining delivered a weight reduction from 91.1 t to 37.9 t. Service life remained consistent with the incumbent metallic lining.

Although the Megaliner™ upgrade delivered maintainability improvements, it did not yet fully unlock substantially shorter relines, as total reline time was still constrained by feed and discharge-end head components and inching sequence.

## MILL LINING UPDATES FOR TOTAL PLANT PERFORMANCE

Hidden Valley's future constraints directed the optimisation pathway towards shorter, well-timed shutdown windows to deliver an overall increase in mill availability and throughput. Therefore, the operational strategy has shifted towards defined reline scopes that align with downstream processing and whole-of-plant shutdown requirements. Defining the optimum shutdown frequency and upgrading the liner system to support that strategy became the next step in the optimisation pathway. The challenge was clear: deliver fast, safe relines at the right time.

### Performance modelling of mill lining influence on total plant performance

Mill lining has the primary function of protecting the mill's structure, with internal wear of the shell, heads and trunnions representing a major risk factor for mill structural failure. Additionally, mill lining is vital to mill performance by transferring the power from the mill motor to the charge for comminution, acting as the first stage of classification at the discharge grates, allowing critical-size material and scats removal, and discharging material from the mill, thereby controlling residence time.

As described by Powell *et al* (2006), a poor mill lining design can have a detrimental effect on milling performance and on liner life. Conversely, an effective liner design must be tailored to the operating requirements of the specific mill; a design that performs well in one operation may not be suitable in another.

There are many cases where the scope of mill lining design may simply be to deliver the required maintenance cycle at the lowest cost, for example where the grinding circuit is currently not, or not planned to be the operational bottleneck. In these cases, the performance can be measured by the execution to plan, time between relines and cost. This was not the case at Hidden Valley.

Where the performance of the grinding circuit becomes more critical to the performance of the operation, the demands on the mill lining increase. If, as in the case of Hidden Valley, the mill reline is the critical maintenance path for plant shutdowns, the maintainability and efficiency of relining is a critical focus to the mill lining design.

Focusing on scenarios where significant mill lining design optimisation is required, the pathway for an optimum outcome can be defined as a balance of the operational performance versus risk in an environment of constraints. Adding complexity, these performance and risk factors are dynamic and change extensively over time with liner wear and processing requirements.

#### *Performance*

- Charge dynamics: The efficient transfer of power from the mill motor to the charge for material comminution. The charge dynamics are not constant over the life of the lining. Immediately after a shell reline, charge motion can be overly aggressive, increasing the potential for overthrow and ball-on-liner impacts. With wear, the lining profile can change to deliver improved charge movement. As wear progresses further, lifter profile changes and charge motion can become too passive, reducing breakage efficiency. At Hidden Valley, inefficient charge movement is mitigated against to an extent with mill operation tactics, however, change is observed, as explored deeper below.
- Mill volume: As the mill lining wears the internal volume of the EGL increases. At constant mill filling (%) the mass load will increase proportionally. Therefore, power draw for a fixed mill filling (%) increases and performance and operation are not constant over the life of the lining.
- Classification: The discharge grates are the first step in mill discharge classification with the classification and flow rates dependent on many factors, including grate aperture quantity, size,

and position, grate wall thickness, charge level and composition, mill speed, and discharge lifter height and design. The performance of the grates is not constant over time and changes with wear due to aperture expansion, reduction in grate thickness and wear of discharge lifter bars.

### *Risk*

- The mill lining's primary function is as a sacrificial wear part that protects the mill's rotating element from damage. The mill liner wear is relatively predictable in historically normal operating conditions until a critical liner profile or thickness is reached. At this point the wear behaviour becomes unpredictable, and the risk of failure is critical. All mills and their various wearing components display unique wear progression, and careful consideration is required for reline planning.
- Liner or fastening-system failure can be catastrophic. This risk is an important engineering, design and manufacturing quality consideration and is not purely time or wear-based.

### *Constraints*

There are many constraints present in operating plants, outside of the mill itself, that can limit production. These may be upstream, downstream or within the grinding circuit itself. The mill itself is a constrained unit operation with the mill size, installed motor power and drivetrain capacity being difficult and costly to upgrade. At Hidden Valley, overland conveyor and primary crusher maintenance requirements are major upstream constraints and strongly influence the practical shutdown schedule.

### *Reline time as a constraint*

For this paper, the reline time is highlighted as a primary driver of long-term operational performance. The time taken to reline a mill is a dominant driver of mill availability and is a major factor in designing mill linings. Consideration must be given to the quantity of parts to be changed, their weights and ease of installation/removal. Additional factors that contribute to reline time include the time taken to run down the plant, isolate equipment, establish a safe working environment and importantly the time taken to inch the mill to access all components.

Metso has developed a substantial database of reline execution results allowing expected reline times to be modelled. Detailed consideration is given to the piece count, liner types and procedure, ie the type and quantity of components that can be installed safely on each mill inching position. With this analysis, an understanding of the interactions between components is revealed, for example if the shell liner component count is reduced but the shell is relined together with unchanged feed and discharge-end head designs, the benefit can be limited as the total pieces per inch is not considerably reduced and the number of inches remain constant. This was evident at Hidden Valley following the first shell Megaliner™ upgrade.

In Table 4 and Figure 6, the calculated reline times for the progression in liner design iterations at Hidden Valley are shown. With the design improvements made to this point, a complete reline is expected to take 12.3 shifts of 12 hrs to complete, including re-torque requirements, however excluding plant ramp-up/ramp-down, isolations and permitting activities, compared with 16.2 shifts for the original metallic design. The regular reline of a complete mill (excluding the pulp system and feed-end inner lining) is reduced from 13.6 to 10.2 shifts.

**TABLE 4**

Reline modelling of past iterations showing 12 hour shifts of tool time, including re-torque requirements.

| | Metallic lining | Discharge Optimisation | Skip-Row Polymet | Megaliner Gen1 |
|---|---|---|---|---|
| Complete | 16.2 | 15.1 | 13.9 | 12.3 |
| Complete (exl. Pulps) | 13.9 | 13.6 | 12.4 | 10.8 |
| Complete (exl. Pulps and FE inner) | 13.6 | 13.0 | 11.8 | 10.2 |
| Shell and DE outer/mid | 10.5 | 9.0 | 7.9 | 6.4 |

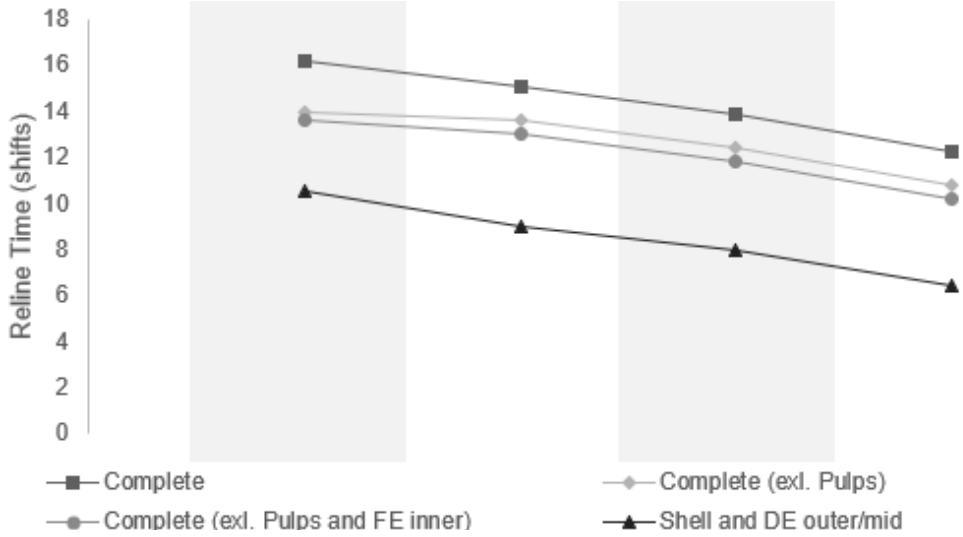



**FIG 6** – Progression of estimated reline times across liner design iterations.

### *Operational modelling and planning*

Considering these influences together allows the balance between performance and risk within a constrained operating environment to be modelled to connect mill lining design and operational strategies to whole plant performance. Scenarios can be modelled to optimise lining design and reline strategy to operational goals, ie maximising throughput, minimising operating expenditure (OPEX) and/or maximising value creation.

The modelling is complicated by competing variables, non-linear effects over time, and the fact that different liner components do not share the same service life. For example, shell, grate, pulp lifter and feed-end head components may each follow different wear and reline cycles.

To simplify the analysis, assumptions were incorporated to estimate performance over time. Historical process data, mill power modelling and 3D DEM simulations with wear progression were used to define a linear ramp-up after a trigger event, a maximum operating rate, constrained or offline periods, and a linear ramp-down period. Cost considerations were also modelled, including power, grinding media, maintenance and mill lining costs. Metso has a substantial database and understanding of mill liner costs and can incorporate this with high detail.

The modelling was intended for strategic comparison of reline-frequency scenarios rather than prediction of short-term daily throughput. Throughput data was normalised for confidentiality, and simplified linear ramp-up, steady-state and ramp-down assumptions were applied. Fixed metal prices and estimated operating costs were used for scenario comparison. DEM simulations held

operating parameters constant to isolate the influence of liner wear state on charge dynamics. Actual plant performance remains influenced by ore blend, operating strategy, downstream constraints and shutdown execution variability.

## HIDDEN VALLEY RELINE STRATEGY FOR PERFORMANCE IMPROVEMENT

Hidden Valley undertook an analysis of historic processing data and costs to optimise for reline frequency with an aim of maximising revenue. With the lining configuration at this point being the Poly-Met™ feed-end head, Megaliner™ shell and Poly-Met™ discharge-end head, the general change-out frequency was approximately 9–12 months for these components, with the pulp system remaining in service for several years and not considered. The reline frequency was focused on achieving the longest time between relines and was determined by infrequent mill lining inspections and reporting.

This created a high-risk scenario in which the lining was often pushed to the limits of its life, wear became critical, and emergency relines were required. This was particularly problematic for an isolated operation where specialist labour could not be mobilised quickly. Furthermore, it was noted that throughput ramped up following a reline, remained relatively stable for several months, then reduced almost linearly over the final life of the lining.

Historic operating data from two shell liner campaigns, defined as the period from one shell reline to the next, were investigated further. Other campaigns were excluded due to data availability and where major interruptions or restrictions obscured the liner-life performance trend. A relative daily throughput rate is shown in Figure 7 along with a 30 day moving average trend as a visual aid. All throughput data is presented relative to a designated sustainable maximum throughput rate due to raw data confidentiality.

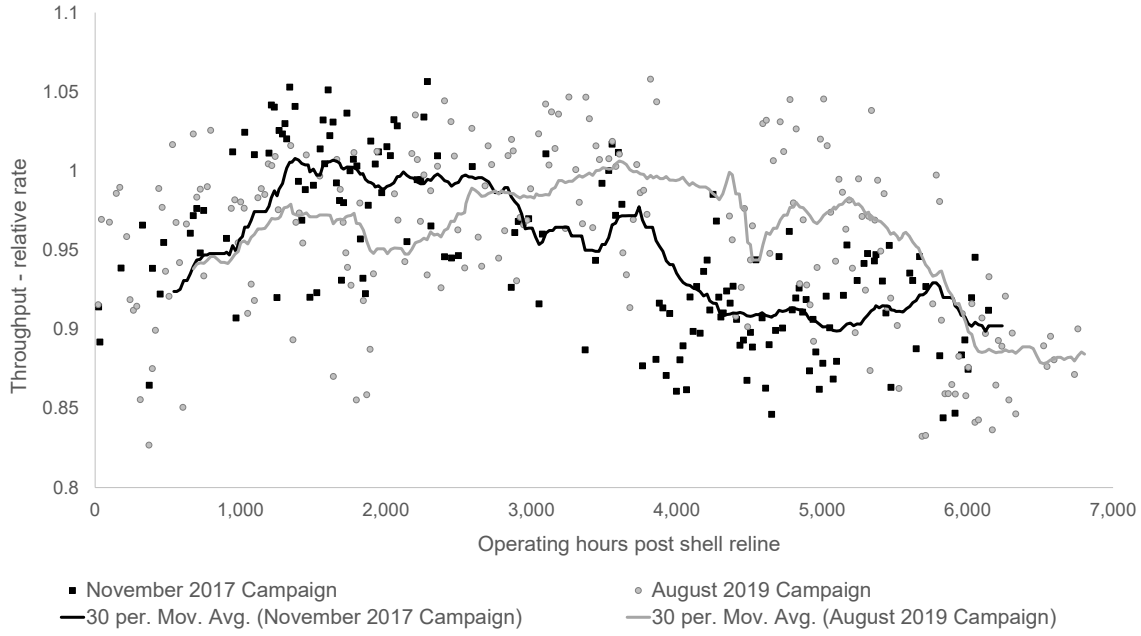



**FIG 7** – Hidden Valley SAG throughput data.

For long-term modelling, liner-life performance was simplified as follows: a ramp-up from 0.92 to 1.00 over the first 1250 operating hours, sustained throughput of 1.00 to 4000 hrs, and a ramp-down from 1.00 to 0.875 between 4000 and 6000 hrs.

To support the 4000 hr, post-reline time point as the observed inflection point of throughput performance, a relative frequency analysis of the operating data was completed and is shown in Figure 8. This compares the percentage of observations over the spectrum of throughput rates for total liner life, from reline to 4000 hrs and after the 4000 hr mark. The distribution of throughput data is shown to be higher before 4000 hrs than after 4000 hrs.

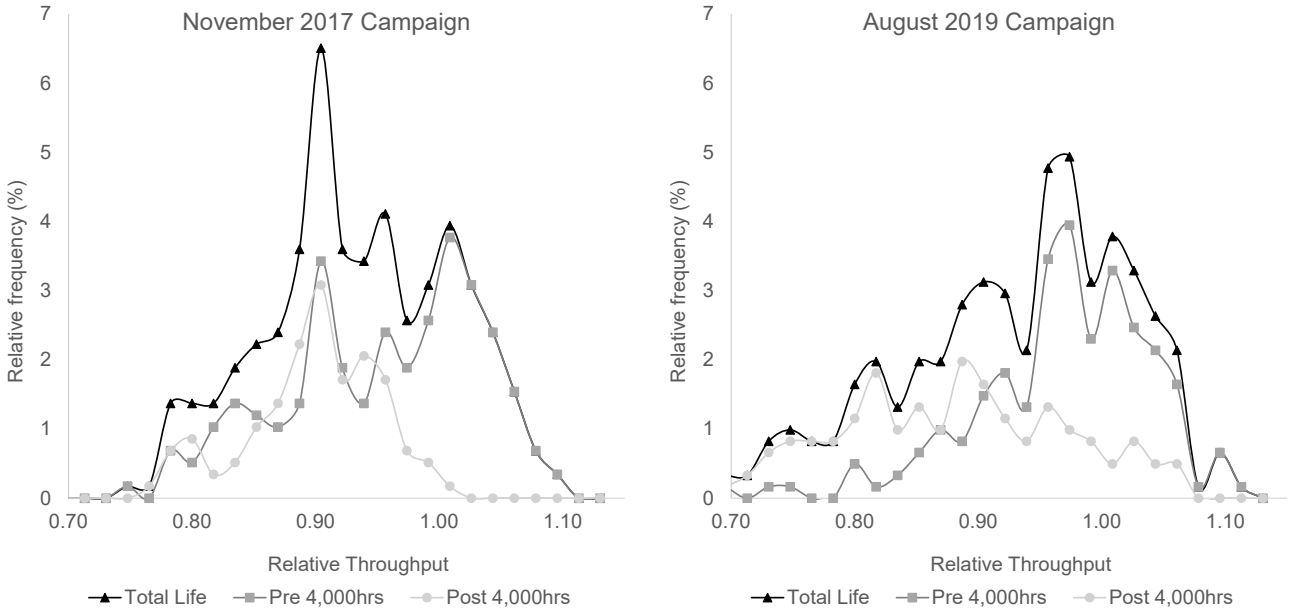



**FIG 8** – Relative frequency analysis of throughput data.

A 3D DEM study was undertaken to further understand the shell lining's wear state to charge dynamics over the life of the lining. New and worn liner profiles were extracted from the 3D wear scans, as shown in Figure 9 and 3D DEM simulations completed for each state.




**FIG 9** – New and worn liner profiles at given operational hours.

Operational parameters, including mill filling, charge filling, mill speed, media and rock particle size distributions, and density were defined to closely match normal operation and held constant across the scenarios for simplicity. In reality, operational tactics would allow manipulation of these variables and optimisation of performance for each state. The output images from the DEM study are shown in Figure 10.

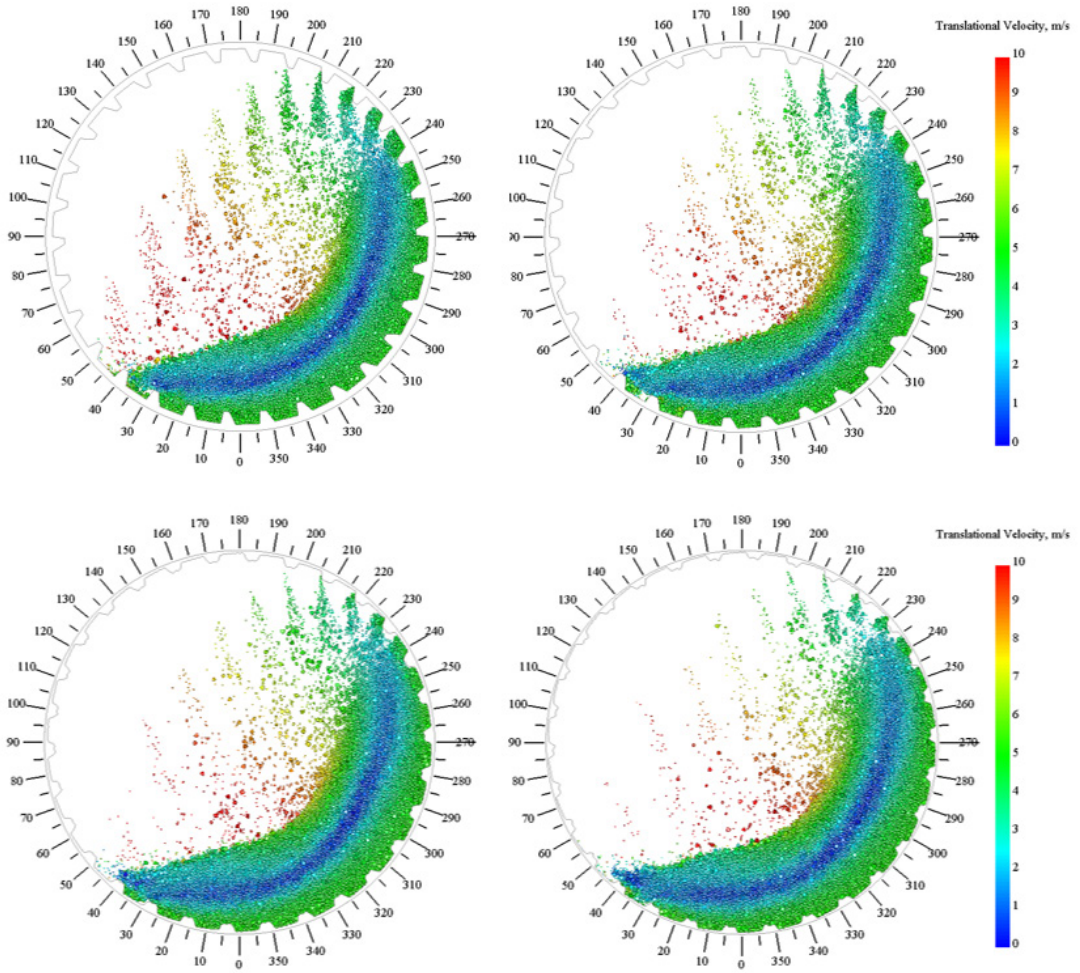



**FIG 10** – 3D DEM output images, clockwise from top left: 0, 1150, 2430 and 3400 hours.

The simulations estimated mill power draw, and impact and shear energy from all particle interactions in a 3D slice of the mill. The results are shown in Figure 11. All results are presented as relative to the highest case for simplicity and data confidentiality. When interpreting the power draw and energy results for this case, it is important to note that the mill filling percentage was held constant. Therefore, as the liner wears, internal volume increases and in turn for the same percent filling charge mass increases. Additionally, with the centre of mass of the charge moving further outward, the mill power draw increases.

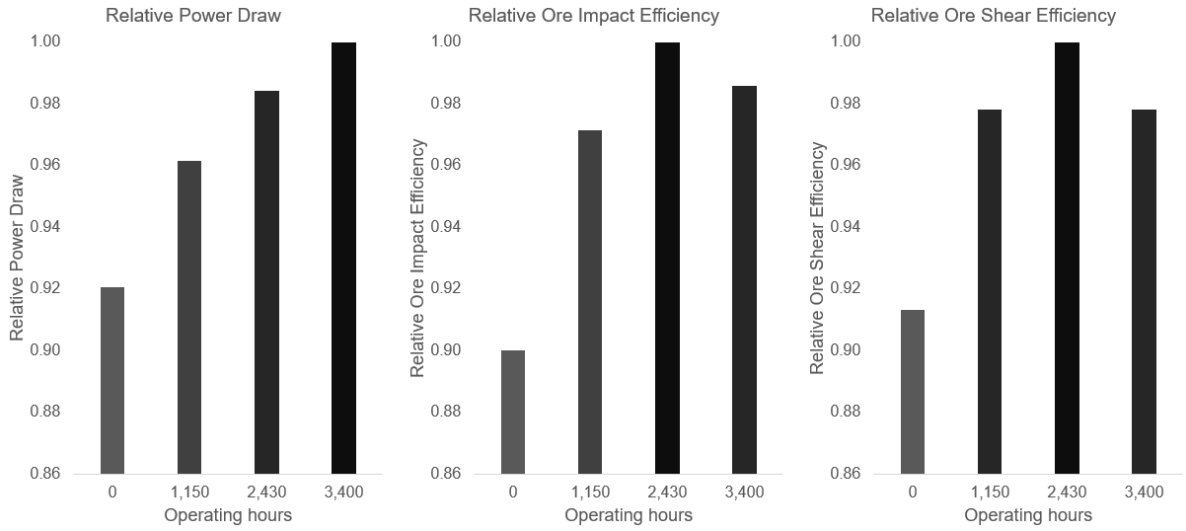



**FIG 11** – 3D DEM modelled power draw, and impact and shear efficiency.

Figure 11 shows the relative impact and shear energy efficiency, as total impact and shear energy per kWh of mill power. When normalised by power draw, higher impact and shear energy per kWh indicates more efficient use of power for comminution. In this case, as the lining begins to wear, the relative performance increases, with the best efficiency observed at 2430 operational hours. At 3400 hrs, impact and shear efficiency have begun to decrease as the shell lifters lose their capacity to move the charge effectively. Although the DEM cases did not extend to the full modelled liner life, the observed decline in relative efficiency by 3400 hrs supported the plant-data trend used in the longer-term operational model. This modelling, while not the sole evidence, supports the observed throughput trends and assumptions above.

An operational modelling and planning analysis was undertaken on this case over a five year period, with the above assumptions on performance over time taken into consideration. Assumptions included fixed metal prices and estimated operational costs. In this case, the value of throughput improvement had to be balanced against existing whole-of-plant shutdown requirements, with the constraints of the overland conveyor belt and crusher maintenance strategies factoring heavily in this analysis. A long-term reline frequency of six months was calculated as the economically optimal interval to increase throughput and metal production, with the output of a sensitivity analysis shown in Figure 12.

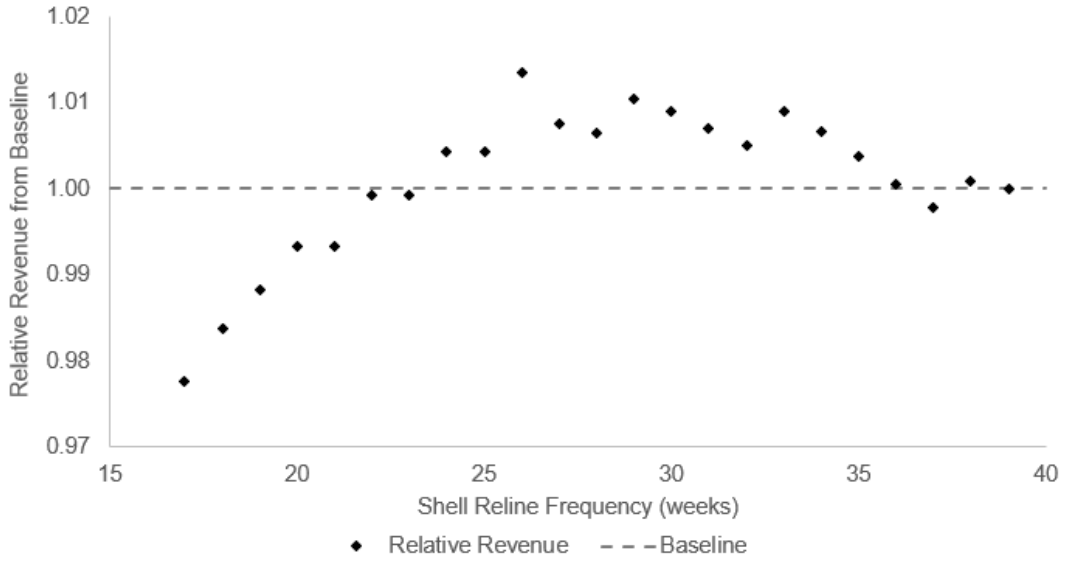



**FIG 12** – Sensitivity analysis output.

The modelling indicated a revenue increase of 1.80 per cent, as shown in Figure 13. The increased revenue was driven by a meaningful increase in average throughput rate, as the reduction of throughput rate with long-term liner life was eliminated. A minor increase in mill utilisation was expected due to the alignment of shutdowns with maintenance activities. An increase in mill lining costs was observed due to the extra relines and additional variable operating costs were factored into the calculations.

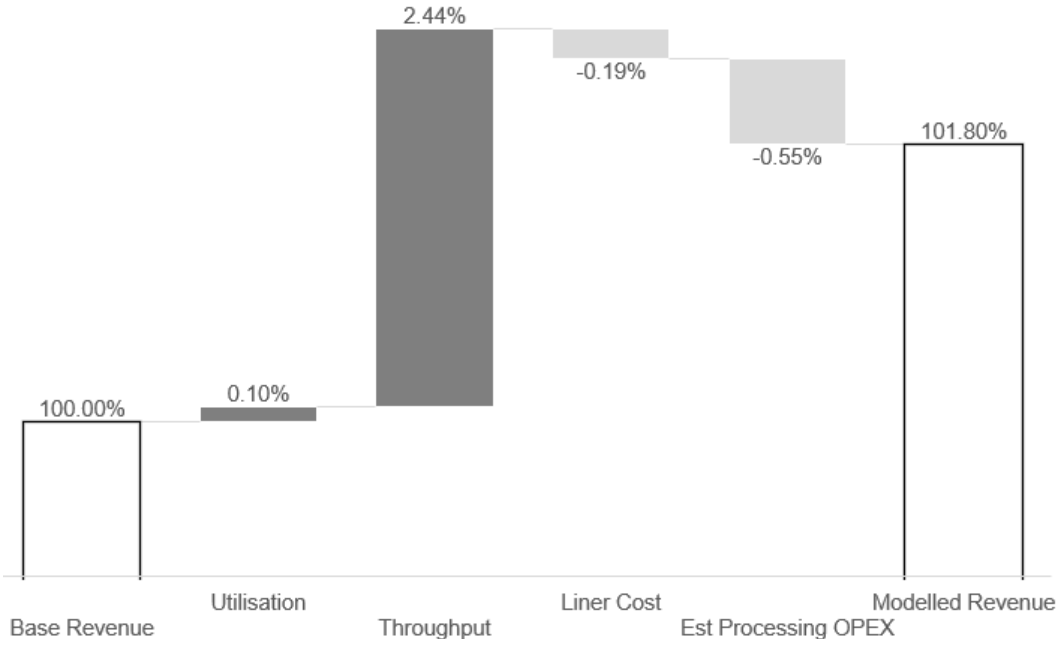



**FIG 13** – Modelling results comparing six-monthly and nine-monthly reline intervals.

## MILL LINING DESIGN UPDATES TO ENABLE THROUGHPUT PLAN WITH RAPID RELINES

To take further advantage of the optimised reline frequency, fast and efficient relines were required. Fast relines are critical in high-performance reline plans and have the potential to deliver significant throughput improvements, reduce cost and, with careful liner design, increase safety through reduced risk and exposure. The key influence of reline time is the quantity of parts to be changed, ease of change in both removal and install, and the liner handler operability. This section focuses on the design updates that resulted in a substantial reduction in component count and in turn the reduction in reline time.

### Shell lining

The updated shell liner design maintained the three rings of Megaliner™ components along the length of the shell, with each new dual-span component replacing two previous components. Each component incorporates two lifter bars and two shell plates, covering the identical space of two of the last iteration’s pieces, thus halving the total component count as shown in Table 5. A minor increase in total mass resulted from increased reinforcements. The process-facing liner profile remained unchanged, preserving the validated charge dynamics. The lining was modelled to fit through the feed trunnion opening with the liner handler in place with no apparent issues. Due to the increase in mass of each component, an upgraded liner handler was required and facilitated separately.

**TABLE 5**

Shell Megaliner™ second generation design summary.

| Shell Megaliner Gen 1 Configuration | | | | Shell Megaliner Gen 2 Configuration | | | |
|---|---|---|---|---|---|---|---|
| Section | Component | Mass (kg) | Quantity | Mass (kg) | Quantity | Component | Section |
| Shell Ring 1 | Megaliner | 30 | 1,678 | 3,323 | 15 | Megaliner | Shell Ring 1 |
| Shell Ring 2 | Megaliner | 30 | 1,612 | 3,323 | 15 | Megaliner | Shell Ring 2 |
| Shell Ring 3 | Megaliner | 30 | 1,619 | 3,323 | 15 | Megaliner | Shell Ring 3 |
| | Total | 90 | 147,270 | 149,535 | 45 | Total | |

## Feed-end head lining

A review of the feed-end head lining identified a meaningful improvement opportunity as the high quantity of components was shown to slow the reline of the shell in the last design iteration and would become more significant with the new shell design. A major redesign was required and aimed to take advantage of the Megaliner™ concept to reduce the number of components. The incumbent feed-end head lining configuration contained a total of 168 pieces, as shown in Table 6. Historically, the feed-end head lining change-out was aligned to the shell lining, however there was substantial plate and lifter life remaining, as shown in Figure 14. Wear modelling indicated that a 12 month service life may be achievable with minor modifications, but confidence was low and the risk of early change-outs high.

**TABLE 6**

Feed-end head upgrade design summary.

| Polymet Configuration | | | | Megaliner Configuration | | | |
|---|---|---|---|---|---|---|---|
| Section | Component | Mass (kg) | Quantity | Mass (kg) | Quantity | Component | Section |
| Feed Head Inner | Plate | 99 | 15 | 99 | 15 | Plate | Feed Head Inner |
| | Lifter | 64 | 15 | 64 | 15 | Lifter | |
| Feed Head Mid | Plate | 63 | 30 | | | | |
| | Lifter | 236 | 30 | | | | |
| Feed Head Outer | Plate | 450 | 30 | 1,444 | 30 | Megaliner | Feed Head Outer |
| | Lifter | 387 | 30 | | | | |
| | Filling Segment | 78 | 18 | | | | |
| | Total | 37,920 | 168 | 45,765 | 60 | Total | |

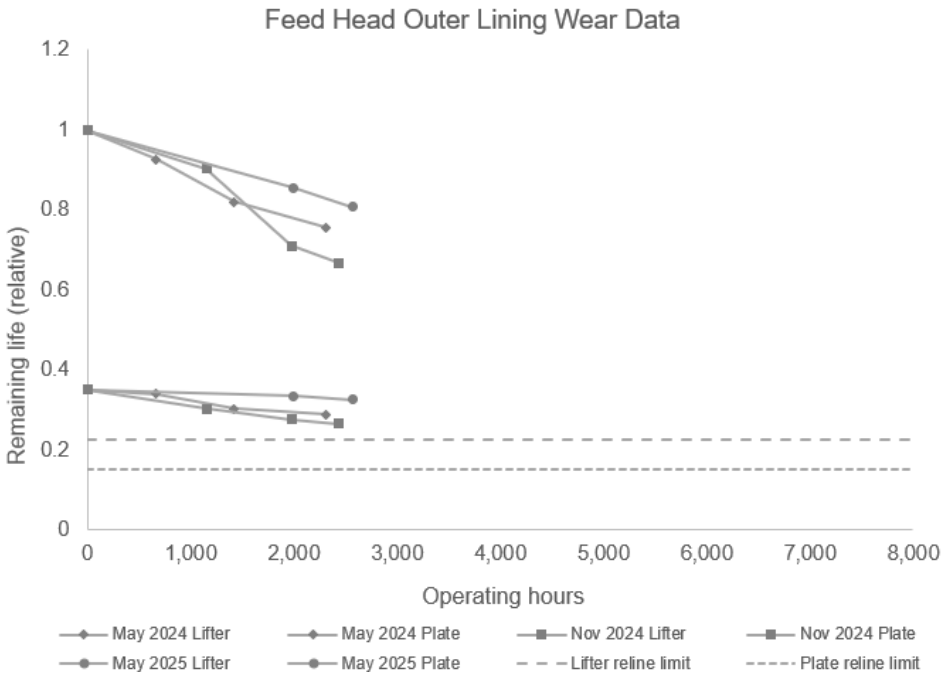



**FIG 14** – Feed-end head outer liner wear data.

The Megaliner™ for feed-end head linings has been trialled historically, however permanent installations are not common. Manufacturability of the components is complicated and requires unique tooling to be developed for each part at a high cost. The engineering requirements were complex and required detailed inspections, fitment checks and several design iterations, with the ability to fit the parts through the trunnion and manoeuvre them inside the mill as the primary design risk. 3D modelling confirmed liner-handler interaction and component manoeuvrability. A modification of the feed-end trunnion chute seal and linings was crucial to allowing a greater internal clearance diameter of the trunnion and fitment of the new feed-end head liner.

The final design, as summarised in Table 6, for the feed-end head was a single outer ring of 30 Megaliner™ pieces, each combining the two lifters of an outer and middle ring, with the two plates of an outer and middle ring, and an integrated filling segment, thus combining five components in one. To safely align with the planned 12 month service interval, the design required increased lifter height, increased plate thickness and a more robust metallic inlay. An increase in feed-end head system mass from 37 925 kg to 45 765 kg resulted. Figure 15 illustrates the Megaliner™ design.

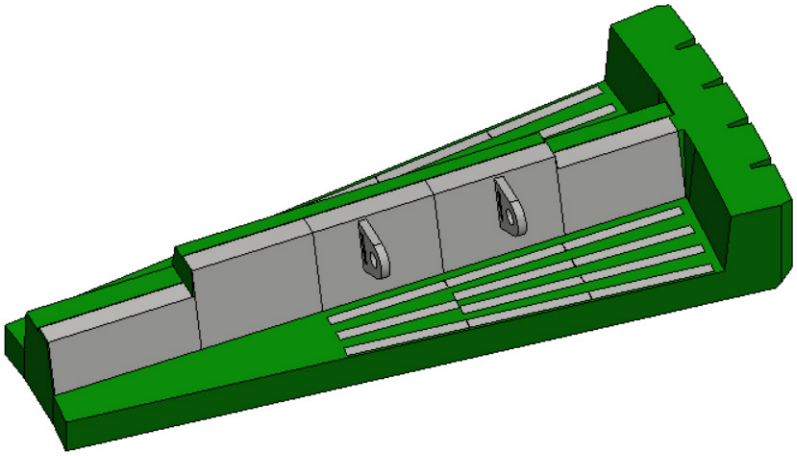


**FIG 15** – Feed-end Megaliner™ incorporating filling segment.

The inner ring design remained unchanged as it was considered very low wearing and had an infrequent reline requirement and within the foreseeable future of operation would give no tangible benefit to reline time and mill availability. An often-overlooked safety risk during relining is associated

with filling segments, which are often unsecured and require careful change-out practices. For the latest design iteration, the feed-end filling segments have been incorporated in the feed-end Megaliner™, securing them in place and removing the potential dropped object risk.

## Reduction in mill lining component count and reline time

The objective of reducing the total component count of the shell and feed-end head lining was achieved through the design changes described above. For full shell coverage using dual-span Megaliner™ components the total number of shell components has been reduced from 90 to 45, a 50 per cent reduction from the previous design and a large reduction from the original Hi-Lo metallic design of 240 pieces. The feed-end head lining has been reduced substantially from 168 individual components to 30.

As discussed above, the modelled reline time to the point of the first Megaliner™ showed a minor change in total reline times. The current liner design iteration delivers a considerable improvement in reline time as shown in Table 7 and Figure 16. With the further design improvements, a complete reline is expected to take 8.4 shifts compared to 16.2 shifts for the original metallic design. The regular reline of a complete mill (excluding the pulp system and feed-end inner lining) is reduced from 13.6 to 6.3 shifts.

**TABLE 7**

Updated reline modelling of past iterations to latest generation showing 12 hour shifts of tool time, including re-torque requirements.

| | Metallic lining | Discharge Optimisation | Skip-Row Polymet | Megaliner Gen1 | Megaliner Gen2 |
|---|---|---|---|---|---|
| Complete | 16.2 | 15.1 | 13.9 | 12.3 | 8.4 |
| Complete (exl. Pulps) | 13.9 | 13.6 | 12.4 | 10.8 | 6.9 |
| Complete (exl. Pulps and FE inner) | 13.6 | 13.0 | 11.8 | 10.2 | 6.3 |
| Shell and DE outer/mid | 10.5 | 9.0 | 7.9 | 6.4 | 5.6 |

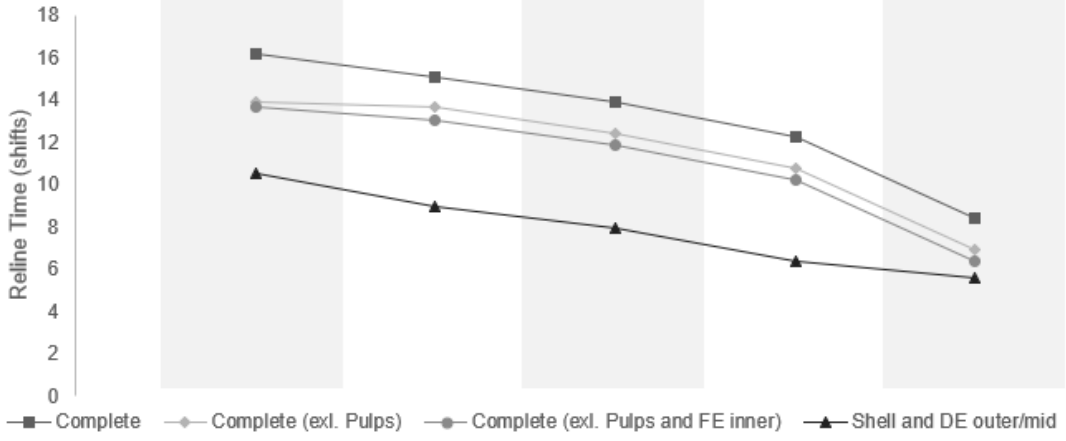



**FIG 16** – Progression of estimated reline times across design iterations, including the latest generation.

Following the design update, a revision to the long-term operational model was completed. With the faster relines, an increase in long-term mill utilisation was expected. This is modelled to deliver a further 0.55 per cent increase in revenue over the long-term. A breakdown of the results is shown in Figure 17.

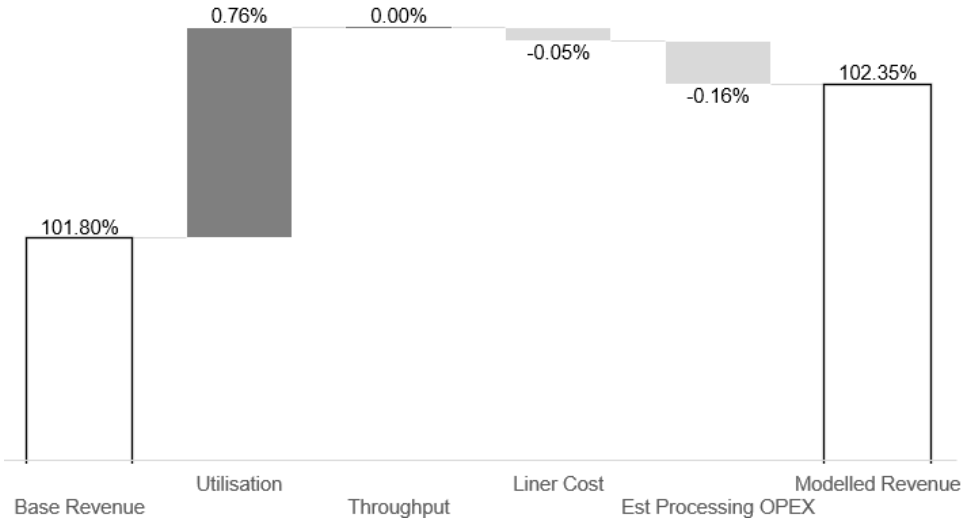



**FIG 17** – Modelling results of generation 1 to generation 2 liner design upgrade.

At the time of writing, the latest generation lining system had been installed and in operation for several months. The first shell and discharge-end reline with the new generation was recently completed in approximately 3.5 days. A deviation from the expected 2.8 days was the result of unplanned, non-liner-related delays to the reline. Condition monitoring inspections have been undertaken and the wear data for the feed-end head is shown in Figure 18. The latest projections have the lining reaching the desired 12 month service life.

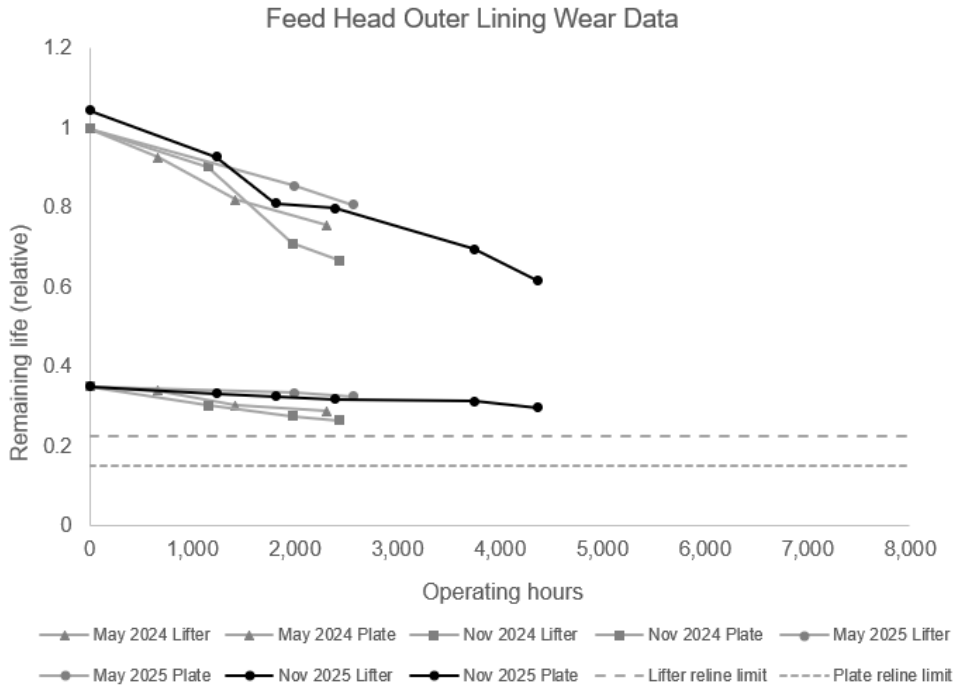



**FIG 18** – Feed-end head outer liner wear data including upgraded liner.

## CONCLUSION

Processing operations are influenced by many interacting variables, several of which are difficult to control directly. While many of these constraints are complex, mill lining offers a practical optimisation lever, and its design and maintenance strategy can deliver substantial benefits. A robust continuous improvement plan incorporating operational review, engineering and design along with future operating plans relies on a strong partnership between the operator and technology supplier.

The strategic optimisation of the mill lining system for the Hidden Valley SAG mill has delivered significant improvements in maintainability, process performance and safety. By applying a whole-

of-plant value and performance philosophy, the site was able to evaluate liner performance over both individual reline cycles and long-term operating horizons. Operational data showed that throughput declined late in shell liner life, while DEM modelling supported the link between liner wear state, charge dynamics and energy efficiency. This evidence enabled a shorter, planned reline interval to be adopted in alignment with whole-of-plant shutdown constraints.

Fast and efficient relines, enabled by creative product development and engineered design changes, are critical to this performance strategy. The iterative design optimisation has delivered considerable improvements in reline time, with the modelled 2.8 days for the commonly performed shell and discharge-end head reline representing a significant improvement over the historical nine-day relines. This increase in long-term average throughput rate and mill utilisation is modelled to deliver a potential 2.35 per cent improvement in revenue.

More broadly, this case demonstrates that mill lining is not simply a consumable maintenance item, and the longest liner life is not always optimal. When supported by product development, operational data, wear monitoring and realistic whole-of-plant modelling, mill lining can become a deliberate production-performance system.

## ACKNOWLEDGEMENTS

The authors would like to thank the Hidden Valley metallurgy and operational team for the supply of operational data and collaboration along the journey. Further thanks to the Metso team of George D’Castro, Pritesh Ranchod and Glenn Wood for on-site support, engineering and modelling.

## REFERENCES

Powell, M S, Smit, I, Radziszewski, P, Cleary, P, Rattray, B, Eriksson, K and Schaeffer, L, 2006. *The Selection and Design of Mill Liners. In Advances in Comminution* (ed: S K Kawatra), pp 331–376 (Society for Mining, Metallurgy, and Exploration, Inc.: Colorado).

Toor, P, Swart, M and Ståhlbröst, H, 2017. The Evolution of SAG Shell Lining and Introduction of the Skip Row Design, in *Proceedings of MetPlant 2017*, pp 158–184 (The Australasian Institute of Mining and Metallurgy: Melbourne).

## Mill Operators

# Data, modelling and hydromet

# Accelerating process decision-making through AI-based mineralogical analysis

*E Aimini[1], E B Bezuidenhout[2], C F Vos[3], J Y Koh[4] and N Beaton[5]*

1. CEO/Managing Director, MinDet, Brisbane Qld 4010. Email: eiman.amini@mindet.com.au
2. Senior Mineralogist, Northparkes Operation, Parkes NSW 2870. Email: byron.bezuidenhout@evolutionmining.com
3. Specialist Metallurgist, Northparkes Operation, Parkes NSW 2870. Email: francois.vos@evolutionmining.com
4. Co-Founder/Lead AI Developer, MinDet, Brisbane Qld 4010. Email: edwin.koh@mindet.com.au
5. Co-Founder/Lead Marketing, MinDet, Brisbane Qld 4010. Email: nick.beaton@mindet.com.au

## ABSTRACT

Understanding the impact of orebody mineralogy on process performance is fundamental to the exploration, design, and operation of mineral processing circuits. Beyond mineral distribution in plant feed, the liberation and association of valuable, gangue, and deleterious minerals strongly influence operational outcomes. Access to timely mineralogical data enables process engineers and Advanced Process Control (APC) systems to adjust chemistry and equipment parameters for improved performance.

Evolution Mining Northparkes Operations (NPO) has been an industry leader in incorporating mineral liberation analysis into its routine workflows, generating deep insights into how mineralogy affects key process indicators (KPIs). While conventional techniques such as scanning electron microscope (SEM)-based liberation analysis continue to provide valuable information, their high capital and operating costs, combined with slow turnaround times, limit their use for real-time decision-making.

MinDet's AI-based rapid optical mineralogy platform, Emago, seeks to address these challenges by developing a measurement system that focuses on reducing both cost and turnaround time. Emago is established to deliver critical mineralogical information within an hour of sample collection, analysing thousands of particles per minute with minimal preparation. Rather than replacing established techniques, the Emago platform complements them by targeting daily, operation-level responses to feed variability-shifting mineralogical analysis from monthly to near real-time decision-making.

This paper presents the MinDet Emago pathway and learning at NPO, outlining the challenges encountered and the improvements made to the sample preparation methodology, sensing, data acquisition and the AI algorithm. It also compares the initial results with SEM-EDS (energy dispersive spectroscopy) data, demonstrating the technology's potential to transform mineralogical analysis into a practical daily operational tool.

## INTRODUCTION

Mineral separation and concentration are typically performed after grinding, when minerals are sufficiently liberated. Among the separation technologies used for base and precious metals, froth flotation remains the most widely applied. Flotation performance is governed by complex interactions between chemical, operational, and equipment parameters (Klimpel, 1995). Numerous studies have demonstrated the influence of an ore's physical properties, pulp chemistry, and hydrodynamics on flotation recovery and kinetics (Berglund, 1991; Ralston, 1991; Kelebek, Fekete and Wells, 1995; Mathe, Harris and O'Connor, 2000; Amini, Bradshaw and Xie, 2016; Amini, Xie and Bradshaw, 2016; Amini, Bradshaw and Xie, 2017; Shahbazi, Chelgani and Matin, 2017; Amankwaa-Kyeremeh *et al,* 2023; Coleman, 2006; Forson *et al,* 2022).

While many operating variables—such as reagent dosage, air flow rate, pulp level, feed rate, and slurry density—can be measured and adjusted in real time, their optimal operating ranges are fundamentally constrained by the ore's mineralogical characteristics. Mineralogy, including the distribution of valuable and gangue minerals, the degree of liberation, mineral associations, and grain size distributions, directly controls flotation kinetics and selectivity. For example, Matsuoka *et al*

(2020) demonstrated distinct flotation responses among chalcocite, bornite, and chalcopyrite under varying pulp chemistry conditions, while Welsby, Vianna and Franzidis (2010) showed that fully liberated, mid-sized galena particles float faster than fine, coarse, or composite particles. In addition, the negative impacts of gangue minerals such as clays and pyrite on flotation performance are well documented (Farrokhpay, Ndlovu and Bradshaw, 2016; Jeldres *et al,* 2019; Jefferson *et al*, 2023; Wang *et al,* 2024). Particle-based simulation approaches further confirm that grouping particles according to mineralogical characteristics significantly improves predictions of stream composition and circuit performance (Vos, 2017).

Accurate and timely mineralogical characterisation is therefore essential to ensure that flotation circuits are maintained at an optimised state. Over the past several decades, mineralogical analysis techniques have evolved significantly. Modern automated scanning electron microscope (SEM) systems equipped with energy-dispersive spectroscopy (EDS), such as QEMSCAN, MLA, ZEISS Mineralogic, and TIMA, provide highly detailed information on modal mineralogy, grain size, and mineral associations. However, these systems are laboratory-based, expensive to operate, and typically involve long sample preparation and analysis times, limiting their usefulness for rapid process decision-making.

Online elemental analysers such as X-ray fluorescence (XRF) and laser-induced breakdown spectroscopy (LIBS) provide faster measurements and can be implemented in process streams. However, these techniques infer mineralogical information indirectly from elemental composition and therefore cannot quantify mineral associations, particle textures, or liberation characteristics. Furthermore, XRF can have limited sensitivity to light elements such as calcium and sulfur, while LIBS measurements may exhibit lower accuracy for heavier elements such as copper.

To address these limitations, several alternative optical and spectroscopic approaches have been investigated. Visible and near-infrared (VNIR) spectroscopy has been used to estimate elemental composition (Haavisto and Hyötyniemi, 2009), while reflective spectroscopy combined with chemometric analysis has been used to estimate sulfide content and particle-size fractions (Kewe *et al,* 2014). Data-fusion approaches integrating VNIR, XRF, and LIBS have also been explored for on-stream mineral identification (Khajehzadeh, Haavisto and Koresaar, 2017). In parallel, advances in optical microscopy and digital image analysis have enabled particle-level mineral identification and liberation assessment from slurry samples (Leroy *et al,* 2011; Leroy and Pirard, 2019). More recently, deep-learning-based computer vision applied to optical microscopy has demonstrated promising capabilities for estimating modal mineralogy directly from flotation pulp samples (Koh *et al,* 2024). Despite these developments, practical challenges remain in achieving rapid, representative slurry sampling, reliable grain-size quantification, and seamless integration into operational workflows. Figure 1 summarises the chronological development of mineral detection and composition analysis techniques over the past three centuries (Wright, 1942; Schulz, Sandmann and Gilbricht, 2022).

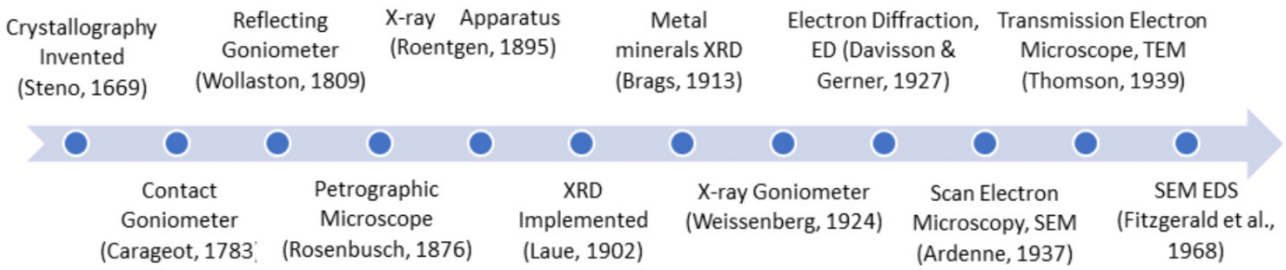



**FIG 1** – Mineral detection and composition analysis developed over the last 350 years after (Wright, 1942; Schulz, Sandmann and Gilbricht, 2022).

In response to the need for faster and more operationally accessible mineralogical measurements, this study presents the development and progress towards the validation of a rapid mineral detection system (MinDet) capable of performing modal mineralogy analysis directly on slurry samples collected from pilot-scale and full-scale operations. The MinDet platform integrates automated optical microscopy with artificial intelligence-based image analysis, capable of providing

mineralogical information with significantly reduced analysis time and sample preparation requirements.

The system is designed to overcome key limitations of existing mineralogical techniques by enabling rapid sampling, simplified preparation, and automated mineral detection. It aims to deliver actionable mineralogical information in near real time. The performance and robustness of the system are evaluated using sulfide ore samples from the Northparkes Operations (NPO) of Evolution Mining, with results compared against SEM-EDS measurements obtained using a TESCAN TIMA automated mineral analyser. This paper highlights important learnings when considering an optical system for mineralogical quantification, and demonstrates the potential of this technology to generate quantitative data towards faster process decision-making and extend the operational application of mineralogical data for flotation optimisation.

## METHODOLOGY

The MinDet bench-scale laboratory device can perform mineralogical analysis on freshly collected slurry samples obtained from flotation circuits, pilot plants, or laboratory flotation tests. The system uses a robotic digital microscope to capture high-resolution images of thousands of particles per minute. These images are subsequently analysed using a machine-vision artificial intelligence (AI) algorithm trained to identify and quantify mineral phases within individual particles.

The AI model was trained on extensive data sets generated using SEM-EDS analyses of ore particles on the sample material. The EDS spectra and morphological characteristics obtained from these reference data sets were used to train the model to recognise individual mineral grains and particle textures under reflected light microscopy. The training was initially conducted manually through collaboration between a mineralogist and AI algorithm experts. This first training data set was generated in April 2025 and is referred to as the ‘Apr-25’ data set throughout this manuscript.

Prior to deployment, each version of the algorithm undergoes a rigorous quality assurance and quality control (QA/QC) process to verify mineral recognition accuracy across multiple samples. The system’s confidence levels for mineral identification and grain delineation are continuously monitored and refined.

Microscopic images of particles were classified according to mineralogy and used to train and test the AI model. The workflow for generating labelled training data is illustrated in Figure 2. In 2026, a software package developed by MinDet was used to automate this process based on digital visual feature measurements, which was used in model development.

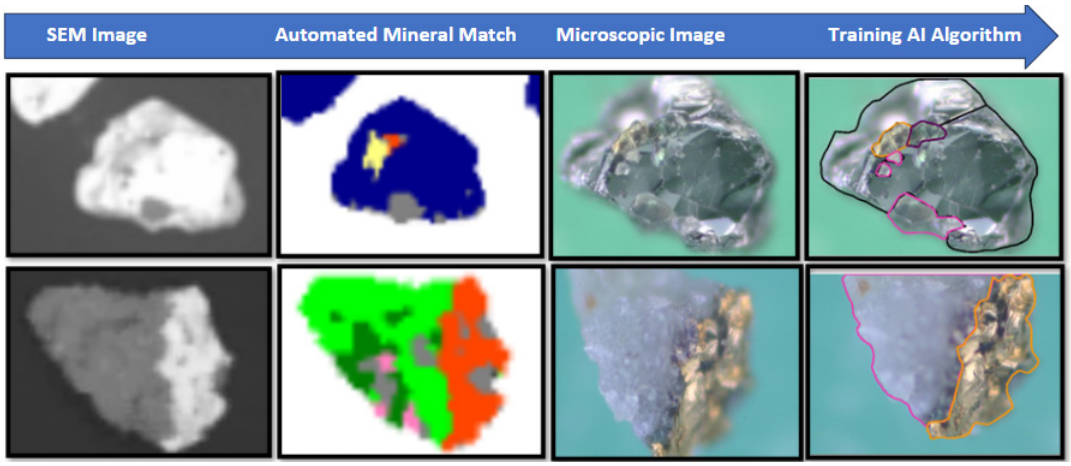



**FIG 2** – AI algorithm training procedure guided by scanning electron microscope (SEM).

Following algorithm development, slurry samples were collected from target process streams for validation. Sample preparation for MinDet analysis is rapid and straightforward. Thoroughly mix the slurry to ensure that all particles are evenly suspended throughout the mixing tank. Approximately 10 g of slurry is sub-sampled and wet-screened at approximately 20 µm to separate ultrafine

particles from the coarser fraction. Each fraction is then loaded into a transparent cuvette for scanning.

There are a couple of concerns that need to be addressed during sample preparation:

1. Removal of ultrafine particles: Surface-based analytical methods such as Emago are susceptible to the surfaces of larger particles being obscured by ultrafine material. Therefore, extra care should be taken to ensure that screening is continued until the ultrafine particles have been adequately removed from the +20 µm fraction.
2. Cuvette homogenisation: The cuvettes should be shaken thoroughly before being loaded into Emago for mineralogical analysis. This is a critical step to ensure that the sample is homogenised within the cuvette and that the surface presented for analysis is representative of the entire sample volume contained in the cuvette.

The proposed process above takes less than two hrs to prepare the sample for Emago analysis. However, adding additional size fractions may increase the sample preparation time, depending on the number of fractions added to the process. The most time-consuming step is the settling of the −20 µm fraction.

Sample grade plays an important role in determining the scanning time required by Emago. For example, a high-grade concentrate sample may require the analysis of only a few thousand particles, which can be achieved in approximately one min. In contrast, a very low-grade sample, such as final tailings, may require up to 20 mins to collect and analyse about 30 000 particles. This extended scanning time helps increase the number of sulfide-bearing particles available for analysis, particularly in the case of rare, relatively coarse particles. Separating the coarse particles and scanning them in an additional cuvette could reduce the total time required to analyse a low-grade sample.

In general, the sample preparation methodology and rapid scanning process employed by Emergo significantly reduce the time required to deliver complete mineralogical results, thereby reducing turnaround time and cost compared with conventional mineralogical techniques. Samples can also be screened into additional size fractions for separate analysis, as was performed in this study, to increase the number of sulfide-bearing particles available for analysis towards the end of the program.

The modal mineralogy generated by MinDet also enables the estimation of mineral liberation by size fraction, an important metric for optimising grinding and flotation performance. Liberation curves assist in determining the optimal grind size that maximises metal recovery while minimising energy consumption. This capability is particularly valuable for evaluating coarse particle flotation strategies (Amini, Koh and Beaton, 2025). The MinDet software includes a liberation calculation toolkit that performs these analyses in real time during sample scanning.

Up to six cuvettes can be loaded into the device simultaneously (Figure 3). The cuvettes are automatically scanned sequentially, enabling the batch analysis of multiple samples. Key parameters reported by the system include:

- particle size distribution
- bulk mineral grade
- elemental grade (calculated from mineral grades and stoichiometric composition)
- mineral liberation by size fraction
- mineral associations.

By analysing many particles, statistically robust mineralogical data can be generated rapidly. The back of the cuvettes can also be scanned to increase the number of particles analysed and improve sample representativeness. In addition, the cuvettes can be thoroughly shaken and reloaded into the device, exposing a new set of particles for scanning. The number of cuvettes loaded with the same sample can also be increased to further increase the total particle count.

The methodology was previously validated using sulfide polymetallic ore samples from four Australian operations (Amini, Koh and Beaton, 2025), where calculated elemental grades showed strong agreement with laboratory-measured grades obtained using ICP analysis.

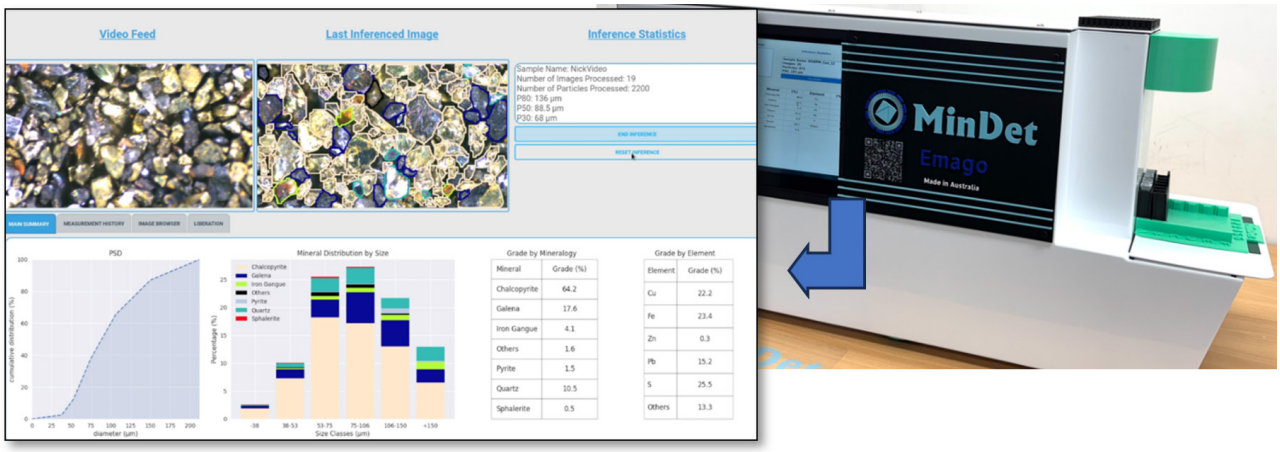



**FIG 3** – Rapid mineralogy analyser for slurry samples reports the results in real-time (Emago).

In the present study, implementation of the device focused specifically on mineral grade and liberation measurements through direct comparison with results obtained using the TESCAN TIMA system, an automated SEM-EDS mineral analyser. As part of this study, a series of analyses were conducted at NPO to determine the number of particles required to obtain statistically meaningful results when analysing both high- and low-grade samples. This included scalping particles coarser than 150 µm and loading them into a separate cuvette for analysis.

Samples were obtained from routine monthly mineralogy composites of final tailings and concentrate streams from NPO. The samples were screened into six size fractions: −20 µm, +20–38 µm, +38–53 µm, +53–75 µm, +75–106 µm, and +106–150 µm prior to preparing polished sections for SEM analysis.

Representative subsamples from April 2025 tailings and concentrate samples were analysed using the Emago system installed on-site. Representative sub splits of these samples were analysed using the TESCAN TIMA system at NPO, and the results were compared for selected mineral groups and for liberation measurements of chalcopyrite and bornite by size fraction.

These analyses were conducted as part of the Apr-25 AI model development and assessment, which provided statistically enough particles among all size fractions.

During the implementation program at NPO, composite samples were prepared by the site's mineralogy laboratory team by combining daily composites collected over six consecutive weeks from the feed, final concentrate, and final tailings streams. The samples were classified into the six size fractions described above for SEM-EDS analysis. Subsamples were taken for Emago analysis. Initially, only the −20 µm fraction was screened, generating two fractions for scanning: a fine fraction and a coarse fraction. Subsequently, the +150 µm fraction was also screened from the coarse fraction. As a result, three size fractions, −20 µm, +20–150 µm, and +150 µm, were scanned to increase the number of particles available for analysis. These analyses are referred to as 'Jul 26' data analysis in this manuscript. Several lessons were learned during this implementation process, which are discussed in the following section of this manuscript.

## RESULTS AND DISCUSSIONS

The results are presented in two sections, Apr-25 and Jul-26. The latter incorporates several methodological improvements based on lessons learned during the implementation of the device at NPO in an industrial environment.

## Minerals under optical microscopy (Apr-25)

Figure 4 presents representative examples of minerals from the major mineral classes present in the Northparkes deposit, captured using the Emago system directly from slurry samples. Thousands of such images were used to train the AI algorithm to recognise mineral groups. An example of the mineral segmentation output produced by the Emago system is shown in (Figure 5).

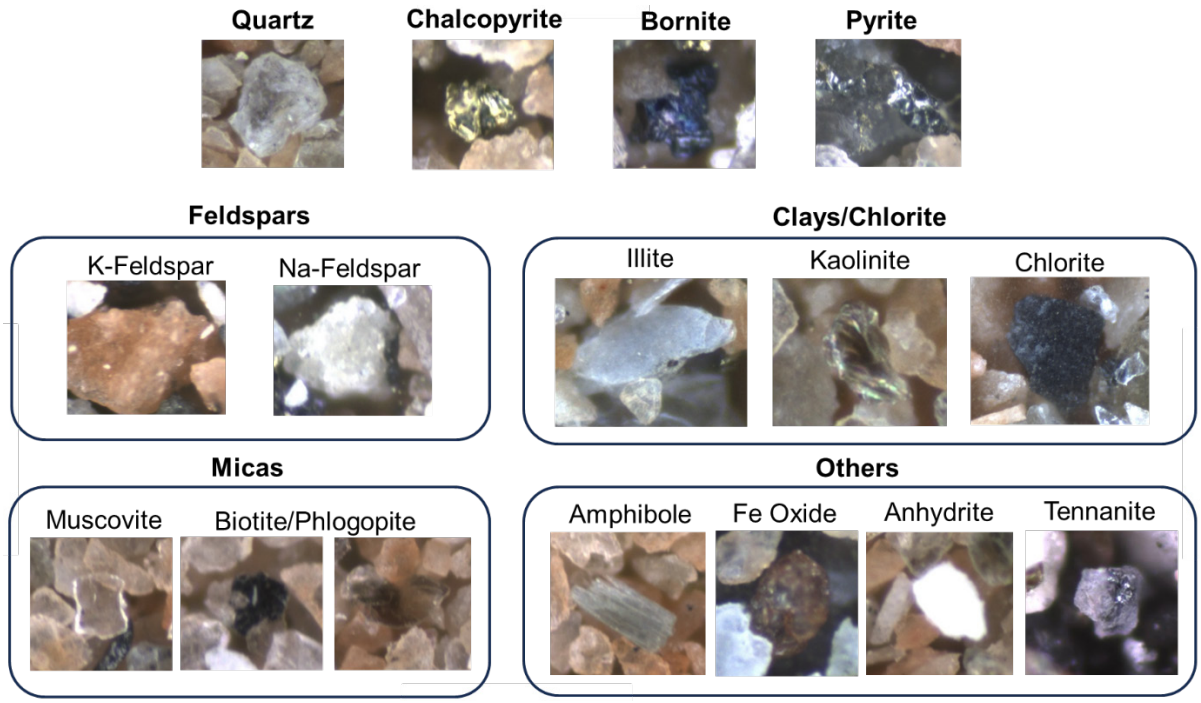



**FIG 4** – Examples of minerals in the Northparkes Operations deposit taken by the Emago machine.

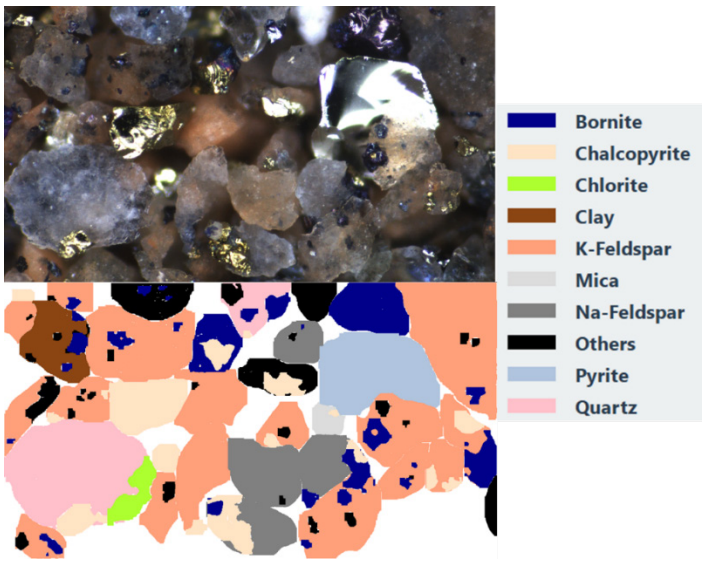



**FIG 5** – Example of the Emago mineralogy segmentation results.

## Final tails (Apr-25)

Overall, the mineral grade measurements obtained using Emago show good agreement with the SEM-EDS analysis (Figure 6). However, phyllosilicate minerals, particularly muscovite, are more difficult to measure under wet conditions because they become semi-transparent and may adhere to the cuvette walls during scanning.

In the final tailings sample, Emago slightly overestimated bornite in the +20–38 µm fraction. This discrepancy is attributed to small (<10 µm) oxidised or locked bornite grains that are difficult to

distinguish optically from dark blue gangue minerals such as magnetite or chlorite when texture information is limited.

In contrast, chalcopyrite grains within this size range remain easier to identify because few other yellow metallic minerals occur in this deposit.

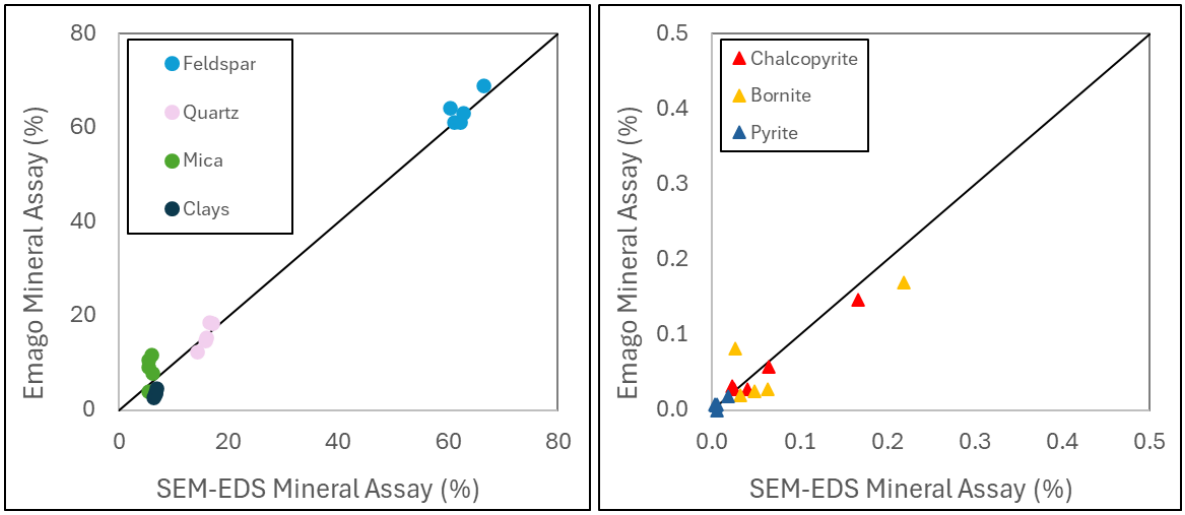



**FIG 6** – Comparison of mineral assay measurements between Emago and SEM-EDS in the final tails sample.

Liberation measurements for chalcopyrite and bornite obtained using Emago follow the same general trends observed in the SEM-EDS results (Figure 7). Most particles appear locked across the size fractions, except for the +20–38 µm fraction where a higher proportion of 80–100 per cent liberated particles is observed.

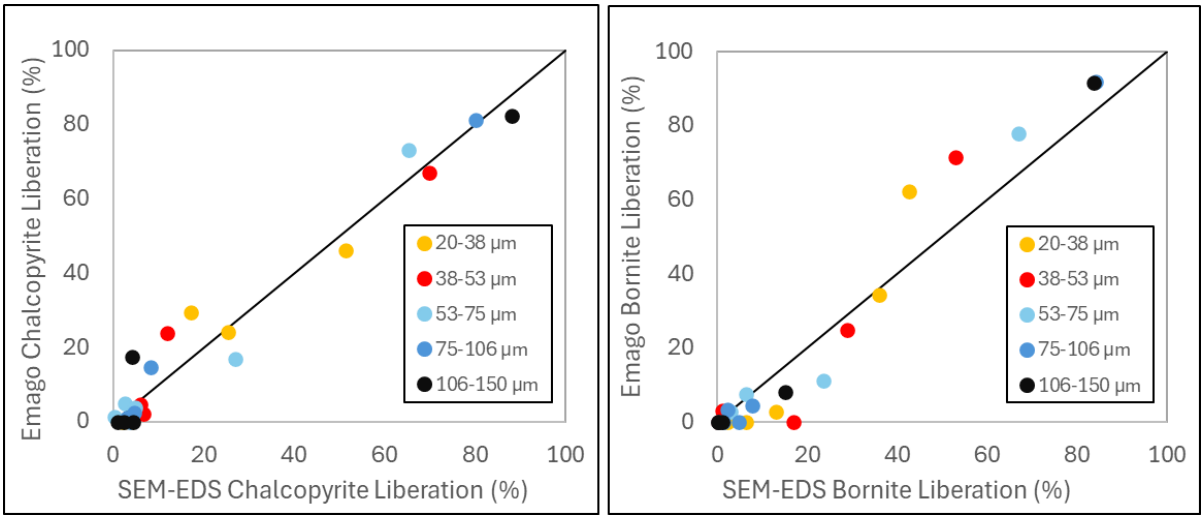



**FIG 7** – Comparison of Chalcopyrite and Bornite liberation measurements from Emago and SEM-EDS in the final tails sample.

Because the particle counts for chalcopyrite and bornite in the final tailings were relatively low (<500 particles), it remains difficult to determine whether differences between measurements arise from methodological differences—such as polished cross-section analysis in SEM-EDS versus surface projection analysis in optical imaging—or from statistical variation.

## Final concentrate (Apr-25)

In the final concentrate samples, Emago mineral grade measurements align more closely with the SEM-EDS results due to the higher abundance of mineral particles (Figure 8). However, under concentrate conditions where the image background becomes darker, transparent minerals such as

quartz and mica may occasionally be misidentified. Similar challenges occur for semi-translucent minerals such as feldspars at finer particle sizes.

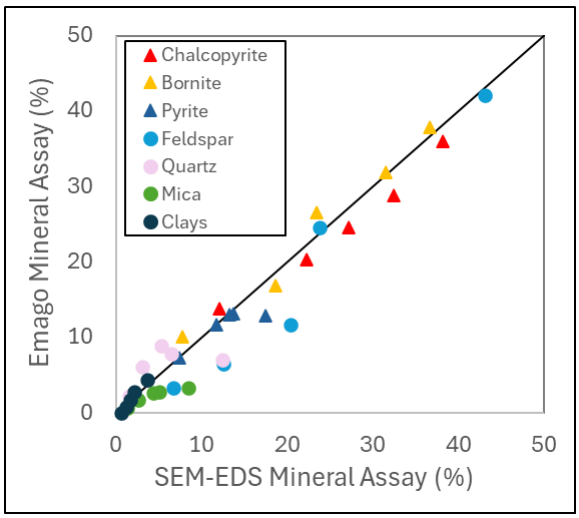



**FIG 8** – Comparison of mineral assay measurements between Emago and SEM-EDS in the final concentrate sample.

Liberation measurements obtained using Emago follow similar trends to those measured by SEM-EDS (Figure 9). Differences between the two techniques remain within an acceptable range, although it is difficult to determine whether these differences arise from methodological variation or from statistical sampling effects.

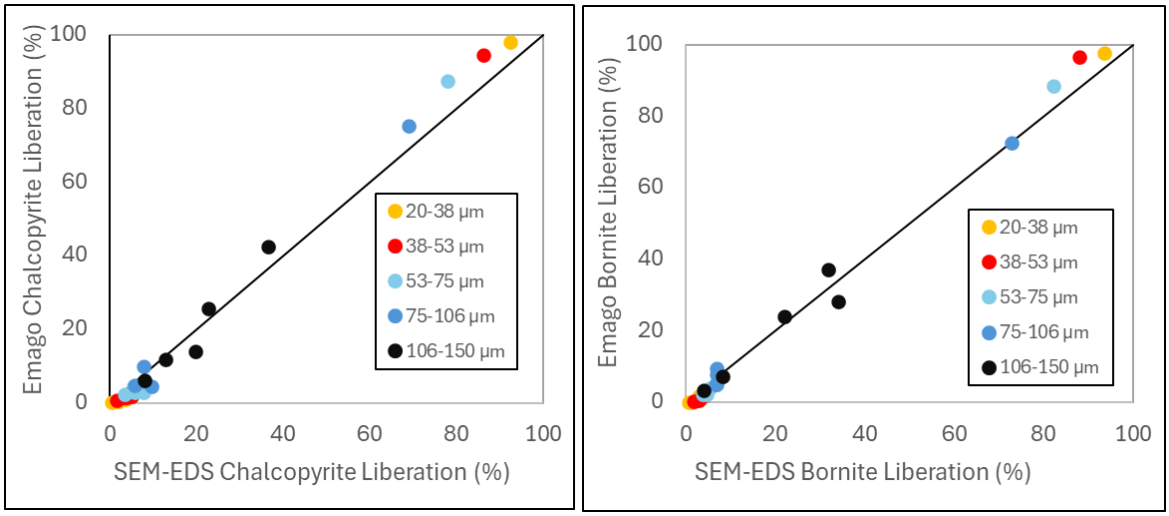



**FIG 9** – Comparison of Chalcopyrite and Bornite liberation measurements from Emago and SEM-EDS in the final concentrate sample.

## Weekly composites

Six weeks of composite samples were generated from the daily production data at the end of 2025. SEM-EDS analyses were done on the weekly sample deposits and compared with the liberation data extracted from Emago. Figure 10 compares the liberation values obtained from Emago analysis with those from SEM-EDS analysis conducted at NPO on the same sample, for chalcopyrite and bornite. The correlation obtained for these two data sets was not acceptable, especially when compared to the Apr-25 data.

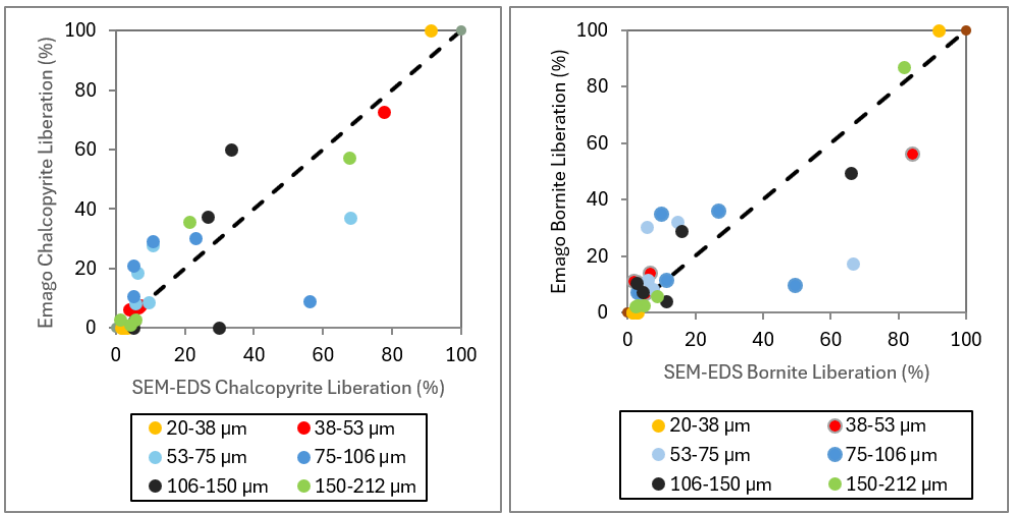



**FIG 10** – Comparison of Chalcopyrite and Bornite liberation measurements from Emago and SEM-EDS in feed for weekly composite (eg week 3).

A series of investigations was conducted to understand the source of the discrepancies, in collaboration between NPO and MinDet experts, which led to an understanding of the issues and proposed solutions to improve the optical analysis done by Emago. These are described here in further detail.

**Optically 'similar' minerals:** Some minerals are optically similar, making them difficult to distinguish at first glance; rigorous microscopic analysis is required to establish the difference. Examples are the Fe oxide group, bornite, and chlorite minerals in the NPO sample, shown in Figure 11. To address this issue, an automated feature detection algorithm was developed to distinguish these minerals from each other as part of the Rapid Mineral Identification Technology (RaMIT) software, which allows the user to find similar mineral grains within each mineral group more easily using digital tools.



**FIG 11** – From left to right – bornite, Fe oxide and chlorite mineral grains under microscope.

**Grain count:** the other source of error was the low number of observed mineral grains in low-grade samples, especially for the very coarse size fraction (eg +150 µm). For example, the number of particles identified by Emago from 210 images of both concentrate and tail for the July 2025 monthly composite is reported in Table 1, showing that the number of bornite and chalcopyrite mineral particles decreases significantly in the tail. This results in very poor statistical representativity of the readings from the low-grade samples. The locked sulfide minerals in the coarse fraction of the tail sample are of major interest at NPO, as the operational support team is eager to understand the valuable mineral loss. Particles of +150 µm size were combined with the +106 µm fraction, as the chance of reading them was low for both samples.

**TABLE 1**

Mineral grain and particle count from monthly composite July 2025.

| Size fraction | Bornite | Chalcopyrite | Total # particles |
|---|---|---|---|

| | | | | |
|---|---|---|---|---|
| **Final concentrate** | +20–38 µm | 3256 | 10 673 | 18 111 |
| | +38–53 µm | 2232 | 5978 | 11 824 |
| | +53–75 µm | 1091 | 3097 | 6677 |
| | +75–106 µm | 471 | 1621 | 4234 |
| | +106 µm | 210 | 588 | 2241 |
| **Final tail** | +20–38 µm | 5 | 5 | 46 572 |
| | +38–53 µm | 5 | 10 | 19 925 |
| | +53–75 µm | 14 | 70 | 15 788 |
| | +75–106 µm | 24 | 70 | 7379 |
| | +106 µm | 17 | 44 | 2829 |

To address the particle count issue, several approaches were proposed to increase the surface area scanned by Emago:

- Scan the whole surface area of the cuvette (six columns).
- Scan back of the cuvette as well as the front, this also helps improve the representativity of the scan if the cuvette is not shaken very well.
- Shake the cuvette again after the first scan to expose a fresh set of particles to the cuvette wall surface, and scan back and front again.
- Screen out coarse particles (+150 µm), load them into a new cuvette and scan them separately.

## Implementing the improvement (Jul-26)

As part of the sample quality assurance process, the samples for reanalysis were prepared from the SEM-EDS subsample remainders using the original feed stream particle size distribution for the weekly composites. This was done to ensure the samples in the cuvettes were similar to those used for SEM-EDS analysis. RaMIT was used to identify the optically ‘similar’ minerals by examining the digital optical features and footprint of those mineral groups, improving the bornite and chlorite mineral grain grouping process. The stream samples were separated into three particle size classes (-20 µm, +20–150 µm, and +150 µm), resulting in improved statistics for the coarse particles being scanned.

Figure 12 compares the mineral assay results obtained from Emago analysis with SEM-EDS after the improvements were applied. The correlation between the results is strong for the sulfide and gangue mineral groups.

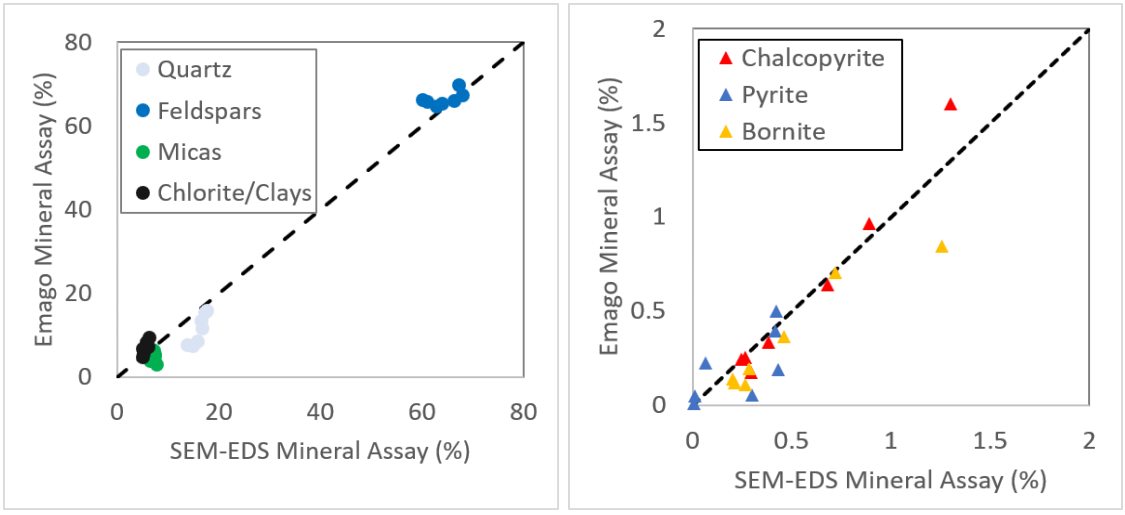



**FIG 12** – Comparison of mineral assay measurements between Emago and SEM-EDS (Week 3, Jul-26).

Initial analysis has shown significant enhancement in the liberation estimate of chalcopyrite across all size fractions, including the coarse +150 µm fraction, which is now scanned in a separate cuvette. Figure 13 summarises these results, which compared to Figure 10 (showing the results before the improvements were implemented) show a significant improvement, reducing the average absolute error for liberation from 9.5 per cent down to 5.5 per cent.

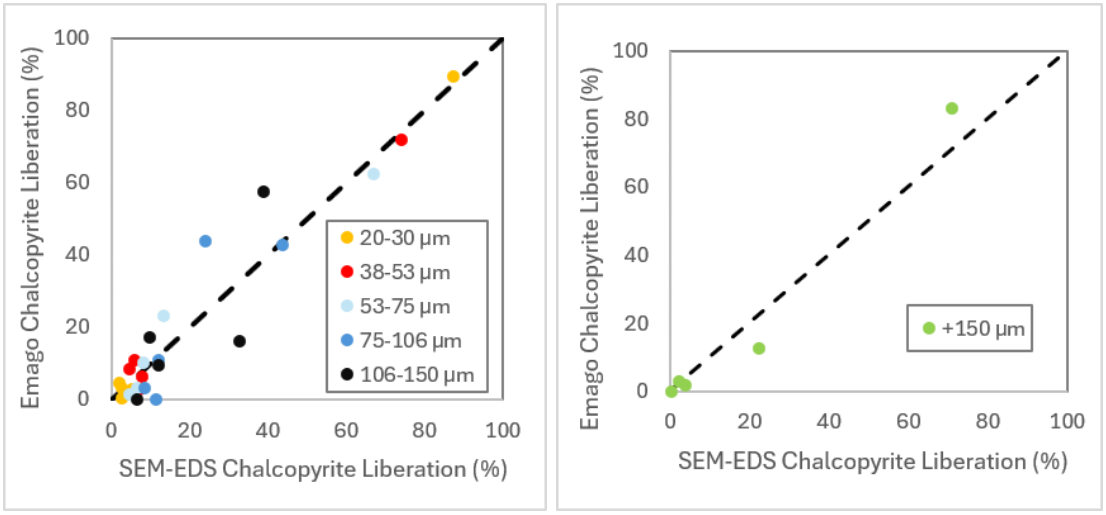



**FIG 13** – Comparison of Chalcopyrite liberation measurements from Emago and SEM-EDS in feed for weekly composite after implementation of improvements (eg week 1).

A rigorous analysis is currently being conducted by both NPO and MinDet experts on all six weeks of samples, including all mineral groups. The results and further lessons learned will be discussed in a future publication. The analysis indicates that Emago remains a strong contender for providing rapid and accurate mineral liberation data.

The authors would like to share their thoughts on the experience of implementing novel devices like Emago, which only reach success when there is investment from both the inventors and industry. This investment must come from both sides.

## Potential operational value

Despite minor differences in absolute measurements, the Emago system can reproduce mineralogical trends like SEM-EDS while delivering results within approximately one hr of sample collection. This rapid turnaround enables new opportunities for operational decision-making at the plant.

For example, operators can rapidly quantify the loss of chalcopyrite and bornite to tailings and evaluate the corresponding liberation characteristics. Such information can support operational decisions including:

- adjusting grind size to recover additional value from coarse tailings fractions (>106 μm).
- optimising reagent dosage and reagent suites to recover fine liberated particles (20–38 μm).
- monitoring the chalcopyrite-to-bornite ratio to optimise reagent selection and dosage.

Because Emago measurements are non-destructive, samples can be retained for further analysis using complementary techniques if required.

Future work will focus on integrating Emago measurements into routine plant monitoring workflows and determining the minimum particle counts required to achieve statistically robust mineralogical measurements for operational control.

## CONCLUSIONS

This study demonstrates the successful pathway towards validation of the MinDet Emago rapid mineralogy platform for analysing flotation slurry samples at Northparkes Operations. The results show that Emago mineral grade and liberation measurements follow trends consistent with those obtained using established SEM-EDS mineralogical techniques, while significantly reducing analysis time and operational costs.

Although minor discrepancies were observed in certain mineral groups and size fractions, these differences are largely attributable to optical limitations and statistical sampling effects rather than systematic errors in the methodology. Investigation of these discrepancies, conducted collaboratively between NPO and MinDet experts, identified two primary sources of error: the optical similarity of certain mineral groups (notably Fe oxides, bornite, and chlorite), and low mineral grain counts in low-grade samples, particularly within the coarse size fractions. These findings led to targeted improvements, including the development of an automated feature detection algorithm within the Rapid Mineral Identification Technology (RaMIT) software to better distinguish optically similar minerals, and revised sample scanning protocols to increase the surface area and particle counts captured by Emago. Following implementation of these improvements, the correlation between Emago and SEM-EDS results strengthened considerably across sulfide and gangue mineral groups.

Importantly, the system provides sufficiently accurate mineralogical information to support operational decision-making in mineral processing plants. The ability of Emago to deliver detailed mineralogical data within a few hours of sample collection represents a substantial advancement in the practical application of mineralogy in plant operations. This capability enables mineralogical analysis to shift from periodic laboratory reporting to a routine operational tool capable of supporting daily process optimisation.

Rapid access to mineralogical information has the potential to improve flotation performance by enabling timely adjustments to grind size, reagent strategies, and operating conditions in response to feed variability. This work also underscores that realising the full value of such platforms depends on sustained collaborative investment from both technology developers and industry partners, working together to iteratively refine and validate these tools under real operating conditions.

## ACKNOWLEDGEMENT

MinDet team would like to thank the Northparkes Operations metallurgy, mineralogy and laboratory teams, along with site management, for their support in enabling the implementation of novel technologies such as Emago at the operation. Their willingness to trial and invest in this new technology, and their ongoing support throughout the validation process, were instrumental to the success of this work.

## REFERENCES

Amankwaa-Kyeremeh, B, Ehrig, K, Greet, C and Asamoah, R, 2023. Pulp Chemistry Variables for Gaussian Process Prediction of Rougher Copper Recovery, *Minerals*, 13(6):731. https://doi.org/10.3390/min13060731

Amini, E, Bradshaw, D J and Xie, W, 2016. Influence of flotation cell hydrodynamics on the flotation kinetics and scale up, Part 1: Hydrodynamic parameter measurements and ore property determination, *Minerals Engineering*, 99:40–51. https://doi.org/10.1016/j.mineng.2016.09.024

Amini, E, Bradshaw, D J and Xie, W, 2017. Influence of flotation cell hydrodynamics on the flotation kinetics and scale up, Part 2: Introducing turbulence parameters to improve predictions, *Minerals Engineering*, 100:31–39. https://doi.org/10.1016/j.mineng.2016.10.001

Amini, E, Koh, E and Beaton, N, 2025. Rapid Mineralogy Analysis Validations for Conventional and Coarse Particle Flotation Slurries, in Flotation 25 Conference, Cape Town, Minerals Engineering.

Amini, E, Xie, W and Bradshaw, D J, 2016. Enhancement of scale up capability on Amira P9 flotation model by incorporating turbulence parameters, *International Journal of Mineral Processing*, 156:52–61. https://doi.org/10.1016/j.minpro.2016.05.001

Berglund, G, 1991. Pulp chemistry in sulphide mineral flotation, *International Journal of Mineral Processing*, 33(1–4):21–31. https://doi.org/10.1016/0301-7516(91)90040-P

Coleman, R G, 2006. Using the floatability characterisation test rig for industrial flotation plant design, PhD Thesis, School of Engineering, JKMRC, The University of Queensland. https://doi.org/10.14264/158278

Farrokhpay, S, Ndlovu, B and Bradshaw, D, 2016. Behaviour of swelling clays versus non-swelling clays in flotation, *Minerals Engineering*, 96–97:59–66. https://doi.org/10.1016/j.mineng.2016.04.011

Forson, P, Zanin, M, Skinner, W and Asamoah, R, 2022. Differential flotation of pyrite and Arsenopyrite: Effect of pulp aeration and the critical importance of collector concentration, *Minerals Engineering*, 178:107421. https://doi.org/10.1016/j.mineng.2022.107421

Haavisto, O and Hyötyniemi, H, 2009. Reflectance Spectroscopy in the Analysis of Mineral Flotation Slurries, *IFAC Proceedings Volumes*, 42(23):140–145. https://doi.org/10.3182/20091014-3-CL-4011.00026

Jefferson, M, Yenial-Arslan, U, Evans, C, Curtis-Morar, C, O'Donnell, R, Parbhakar-Fox, A and Forbes, E, 2023. Effect of pyrite textures and composition on flotation performance, *Minerals Engineering*, 108234. https://doi.org/10.1016/j.mineng.2023.108234

Jeldres, R I, Uribe, L, Cisternas, L A, Gutierrez, L, Leiva, W H and Valenzuela, J, 2019. The effect of clay minerals on the process of flotation of copper ores – A critical review, *Applied Clay Science*, 170:57–69. https://doi.org/10.1016/j.clay.2019.01.013

Kelebek, S, Fekete, S and Wells, P, 1995. Selective depression of pyrrhotite using sulphur dioxidediethylenetriamine reagent combination, in *Proceedings of the XIX International Mineral Processing Congress*, pp 181–187, San Francisco.

Kewe, T, Moffatt, N, Strobos, P, Spuy, D v, Paine, A P and Keet, K, 2014. Evaluation of the Blue Cube MQi Slurry Analyser for Application in an Advanced Control System for the Optimisation of a Gold Sulfide Flotation Circuit, in 12th Mill Operators' Conference 2014, Townsville, Queensland.

Khajehzadeh, N, Haavisto, O and Koresaar, L, 2017. On-stream mineral identification of tailing slurries of an iron ore concentrator using data fusion of LIBS, reflectance spectroscopy and XRF measurement techniques, *Minerals Engineering*, 113:83–94.

Klimpel, R R, 1995. The Influence of Frother Structure on Industrial Coal Flotation, in *Proceedings of the High Efficiency Coal Preparation: An International Symposium* (ed: S K Kawatra), pp 141–151 (Littleton: Society for Mining, Metallurgy and Exploration).

Koh, E J, Amini, E, Spier, A C, McLachlan, G J, Xie, W and Beaton, N, 2024. A mineralogy characterisation technique for copper ore in flotation pulp using deep learning machine vision with optical microscopy, *Minerals Engineering*, 205:108481. https://doi.org/10.1016/j.mineng.2023.108481

Leroy, S and Pirard, E, 2019. Mineral recognition of single particles in ore slurry samples by means of multispectral image processing, *Minerals Engineering*, 132:228–237.

Leroy, S, Dislaire, G, Bastin, D and Pirard, E, 2011. Optical analysis of particle size and chromite liberation from pulp samples of a UG2 ore regrinding circuit, *Minerals Engineering*, 24:1340–1347.

Mathe, Z T, Harris, M C and O'Connor, C T, 2000. A review of methods to model the froth phase in non-steady state flotation systems, *Minerals Engineering*, 13(2):127–140. https://doi.org/10.1016/S0892-6875(99)00159-4

Matsuoka, H, Mitsuhashi, K, Kawata, M and Tokoro, C, 2020. Derivation of Flotation Kinetic Model for Activated and Depressed Copper Sulfide Minerals, *Minerals*, 10(11):1027. https://doi.org/10.3390/min10111027

Ralston, J, 1991. Eh and its consequences in sulphide mineral flotation, *Minerals Engineering*, 4(7–11):859–878. https://doi.org/10.1016/0892-6875(91)90070-C

Schulz, B, Sandmann, D and Gilbricht, S, 2020. SEM-Based Automated Mineralogy and Its Application in Geo- and Material Sciences, *Minerals*, 10(11):1004. https://doi.org/10.3390/min10111004

Shahbazi, B, Chelgani, S C and Matin, S S, 2017. Prediction of froth flotation responses based on various conditioning parameters by Random Forest method, *Colloids and Surfaces A: Physicochemical and Engineering Aspects*, 529:936–941. https://doi.org/10.1016/j.colsurfa.2017.07.013

Vos, C F, 2017. The effect of mineral grain textures at particle surfaces on flotation response, PhD thesis, University of Queensland, JKMCR.

Wang, Z, Mu, Y, Zhang, M, Cao, Y and Li, C, 2024. Effect of clay crystal structure on froth rheology in flotation, *Powder Technology*, 435:119395. https://doi.org/10.1016/j.powtec.2024.119395

Welsby, S D, Vianna, S M and Franzidis, J-P, 2010. Assigning physical significance to floatability components, *International Journal of Mineral Processing*, 97(1–4):59–67. https://doi.org/10.1016/j.minpro.2010.08.002

Wright, F E, 1942. Methods and Instruments Used in Mineralogy, *American Mineralogist*, 27(3):145–154.

# Investigating unleached gold in leach tails for optimum recovery

*K Blackwell[1], A R Bax[2], K Barbetti[3], B Lim[4] and W P Staunton[5]*

1. Strategic Program Lead, Western Australian School of Mines, Curtin University, Bentley WA 6102. Email: kylie.blackwell@curtin.edu.au
2. Associate, Western Australian School of Mines, Curtin University, Bentley WA 6102.
3. Hydrometallurgist, Western Australian School of Mines, Curtin University, Bentley WA 6102.
4. Senior Research Officer, Western Australian School of Mines, Curtin University, Bentley WA 6102.
5. Associate, Western Australian School of Mines, Curtin University, Bentley WA 6102.

## ABSTRACT

In this paper unleached gold refers to residual solid gold in the leach tails that did not leach during processing in a CIP/CIL circuit but can be leached subsequently in the laboratory. A benchmarking survey conducted during the Amira P420G project in 2021 showed that the average gold grade of the leach tails solids from 22 sites was 0.21 g/t. At a gold price of US$4000 per ounce, the average value of the gold contained in the leach tailings solids is US$27/t. If the leach tails solids grade drops by 0.02 g/t through increased gold recovery, an additional US$2.6 M per million tonnes (Mt) of ore processed can be realised.

Understanding the causes for unleached gold is essential for leach circuit optimisation and maximising revenue. This paper presents the factors affecting gold leaching and the challenges associated with assessing the nature of the unleached gold in leach tailings. A case study is presented to illustrate the methodology to determine the nature of the unleached gold in leach tailings as well as potential options to improve gold recovery. Modelling shows a significant portion of the gold present in the leach tailings solids can be leached when subject to additional leaching time in the presence of sufficient cyanide and oxygen.

## INTRODUCTION

In almost all gold processing operations further leaching of the tails in the laboratory with cyanide and oxygen will result in additional gold recovery. This indicates that not all liberated or partially liberated gold was leached even when the ore assays for the leach tanks at the end of the leach circuit suggest leaching in the circuit is complete. This residual gold is referred to as the unleached fraction of gold in tailings. The possible causes for the unleached gold in tails are the focus of this study.

Unleached gold in tails is generally attributed to:

- inadequate leach residence time
- inadequate liberation due to full or partial encapsulation of the gold
- suboptimal reagent conditions impacting on leach kinetics
- surface coatings or passivation impacting gold leaching kinetics.

In some cases the reason for unleached gold is easily identified and attributed to inadequate or shortened leaching time in the processing circuit. Liberation studies highlight the presence of unleachable gold due to locking or encapsulation, however these studies also identify unleached liberated or partially liberated gold. Detecting and quantifying the presence of unleached liberated gold, defining optimum reagent conditions and determining if gold particles have surface coatings, all at plant scale is a significant challenge. This is often compounded by the increasingly lower gold grades where assay errors may exceed any observable differences in gold grades between successive leach tanks in the circuit.

This study utilised sensitivity modelling to examine the effect of different factors affecting the leaching rate of gold and the proportion of unleached liberated gold in a circuit with a 24 hr residence time. The modelling shows that the amount of unleached liberated gold is affected by the leach residence

time, the size and mineralogy of the free gold particles, and the cyanide and dissolved oxygen concentrations utilised within the circuit.

These findings were then applied to plant survey data collected at a Western Australian gold operation. Data collection, processing and analysis included:

- Collection of samples from all stages of the leaching circuit (solids, solutions and carbons).
- Size-by-size analysis.
- Mineralogy including gold deportment.
- Laboratory leaching test work (bottle rolls, controlled dissolved oxygen tests, size by size leaching and diagnostic leaching).

The resulting data was utilised to simulate the leaching of different sized gold particles in a multistage leach circuit.

## Gold leaching fundamentals

The dissolution of gold in alkaline cyanide solutions is an electrochemical process. Reaction 1 is the overall stoichiometric equation for the dissolution of gold.

$$4Au + O_2 + 8\,CN^- + 2H_2O \rightleftharpoons 4Au(CN)_2^- + 4\,OH^- \qquad \text{Reaction 1}$$

Gold dissolution in the presence of cyanide is a diffusion-controlled reaction. The rate that gold dissolves is determined by the rate at which:

- cyanide and oxygen are transferred from the solution to the boundary layer
- cyanide and oxygen diffuse through the boundary layer to the gold surface
- the reaction products diffuse through the boundary layer to the bulk solution.

Reaction 1 shows that stoichiometrically eight moles of cyanide ions and one mole of oxygen must reach the surface of the gold for every four moles of gold that are dissolved. When both the cyanide and oxygen concentrations at the gold surface match the stoichiometric requirements for the reaction, the rate of gold dissolution is not limited by the transport of either cyanide or oxygen.

Electrochemical theory and research have shown that the rate of gold dissolution increases linearly with the dissolved oxygen concentration ($dO_2$) when the stoichiometric cyanide concentration is present (Bax, 2022). The gold dissolution rate increases with cyanide concentration until the stoichiometric cyanide concentration is reached. The stoichiometric cyanide concentration at a given oxygen concentration is sometimes referred to as the critical cyanide concentration. Above this value the dissolution rate will plateau and any further increase in the cyanide concentration will have no impact on the gold leaching rate as shown in Figure 1.

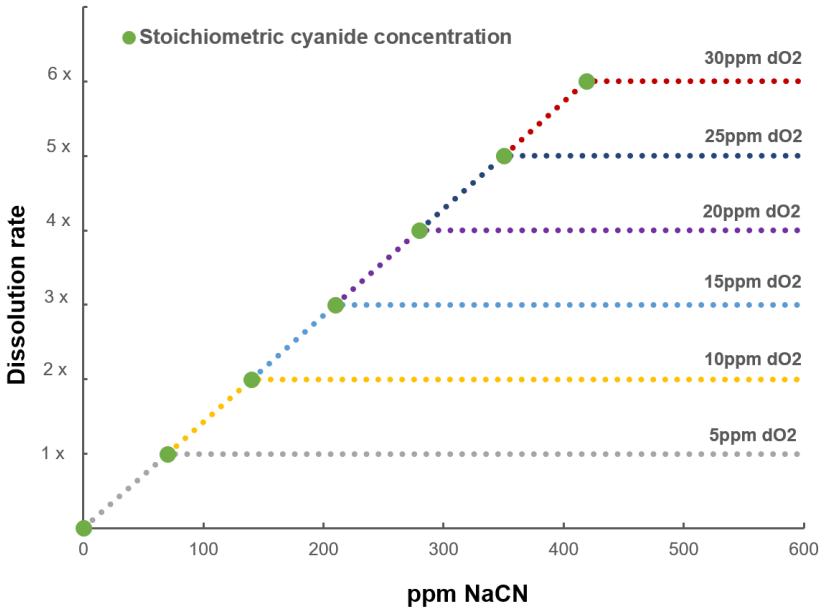



**FIG 1** – Effect of dissolved oxygen ($dO_2$) and cyanide (NaCN) concentration on gold dissolution rate.

There is a large degree of variability in the published oxygen and cyanide diffusion coefficients used to calculate the stoichiometric ratio of cyanide to oxygen concentrations (Bax, 2022). The optimum ratio varies between 11 and 24 due to differences in experimental methods and conditions. For this study the ratio of 14 ppm cyanide to 1 ppm of dissolved oxygen has been utilised (Zheng *et al,* 1995).

Other factors also affect the gold dissolution rate such as agitation intensity, temperature, gold mineralogy, viscosity. catalysts and passivating agents on the surfaces of the particles. The majority of these factors do not change significantly across gold leaching circuits and only parameters directly influenced by the addition of reagents are likely to change across the circuit. For gold leaching circuits these parameters are cyanide concentration, dissolved oxygen concentration and pH. The factors having the greatest influence on the gold leach rate are cyanide and dissolved oxygen concentrations and their concentration ratio.

## SENSITIVITY MODELLING

A model was created using a first order leach rate to simulate the leaching of different sized gold particles in a multi-stage leach circuit. The leach circuit used for the modelling comprising six tanks, with each tank having 4 hrs residence time to give a total leach residence time of 24 hrs. A slurry temperature of 45°C was used for the sensitivity modelling.

The objective of the sensitivity modelling was to examine the effect of changing reagent concentrations on the dissolution of different sized gold particles within a leaching circuit. Three different scenarios were modelled with each type of gold mineralisation: fast-leaching, average-leaching, and slow-leaching.

1. Baseline: 300 ppm NaCN and 6.5 ppm $dO_2$ in all tanks.
2. Decreasing Cyanide: 300 ppm NaCN initial concentration and 6.5 ppm $dO_2$ in all tanks.
3. Decreasing Cyanide with Stoichiometric Oxygen: 300 ppm NaCN initial concentration and optimum $dO_2$.

### Leaching rates

The leach rates used for the sensitivity test work were obtained from previous P420 gold Processing Project leaching tests that have been performed with different ores for the application of the Integrated Leaching and Liberation Model (ILLM) (Bax *et al*, 2014, 2016). The ILLM leach tests were conducted under the same conditions hence any differences between the leaching behaviour can be attributed to the composition, gangue mineralogy and shape of the gold particles.

The ILLM leach tests were conducted at room temperature (≈25°C) with 6.5 ppm $dO_2$ and 300 ppm NaCN. To provide the most accurate prediction of leaching in a full-scale leach circuit, the leach rates obtained from ILLM tests were adjusted to match temperature conditions within the circuit.

The fastest and slowest leaching gold ores were selected together with a calculated average. The measured leach rates for ILLM test work conducted on different ores is shown in Figure 2.

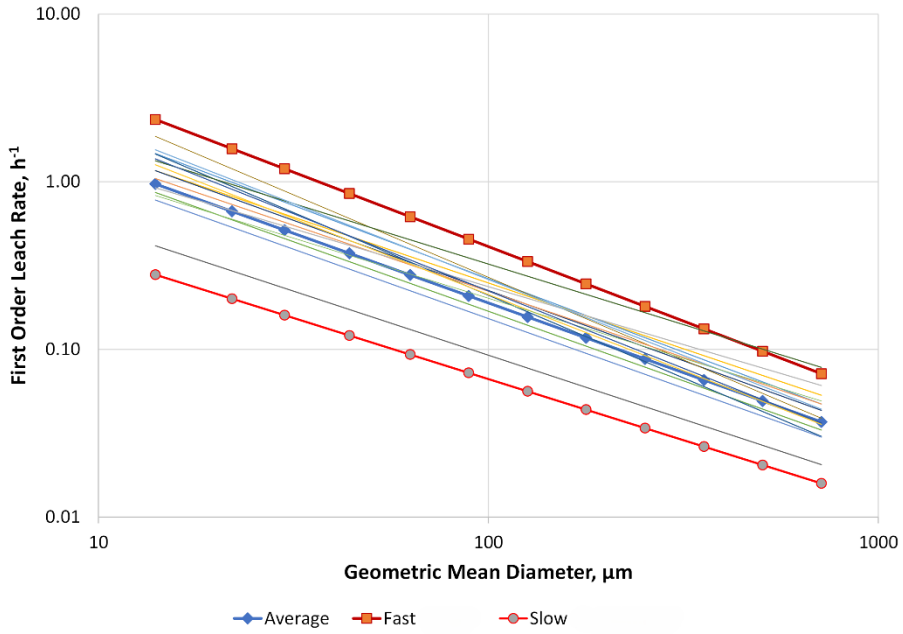



**FIG 2** – Historical ILLM leach rates for gold ores (Bax, 2022).

## Modelling outcomes

Simulations were performed for fast, average and slow leaching particles for the baseline, decreasing cyanide and decreasing cyanide with stoichiometric oxygen scenarios. The cyanide and dissolved oxygen concentrations for each set of simulations are shown in Table 1.

**TABLE 1**

Cyanide and oxygen concentrations for modelling simulations.

| | Baseline | | Decreasing cyanide | | Decreasing cyanide with optimum oxygen | |
|---|---|---|---|---|---|---|
| Tank number | [NaCN] ppm | $dO_2$ ppm | [NaCN] ppm | $dO_2$ ppm | [NaCN] ppm | $dO_2$ ppm |
| 1 | 300 | 6.5 | 300 | 6.5 | 300 | 21.5 |
| 2 | 300 | 6.5 | 234 | 6.5 | 234 | 16.7 |
| 3 | 300 | 6.5 | 195 | 6.5 | 195 | 14.0 |
| 4 | 300 | 6.5 | 168 | 6.5 | 168 | 12.0 |
| 5 | 300 | 6.5 | 147 | 6.5 | 147 | 10.5 |
| 6 | 300 | 6.5 | 129 | 6.5 | 129 | 9.3 |

The modelled final recoveries for the baseline case are shown in Figure 3a. Average and fast leaching particles with initial diameters less than 89 µm achieved more than 99 per cent dissolution within 24 hrs. For the slow-leaching gold particles, only particles less than 22 µm achieved greater

than 99 per cent dissolution within 24 hrs. This clearly shows there is a difference in leaching response for each leaching category, particularly for particles at the coarser end of the size range.

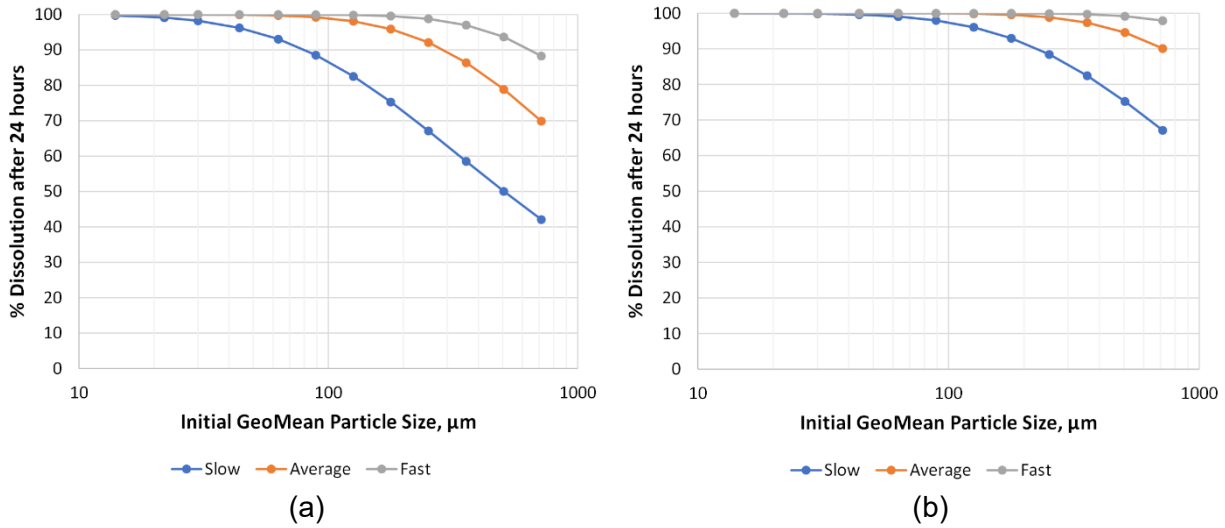



**FIG 3** – Modelled final recoveries: (a) baseline case; (b) decreasing cyanide with stoichiometric oxygen case.

The decreasing cyanide case simulations replicated the typical decline in cyanide concentration that occurs within industrial leach circuits. The cyanide concentrations were stepped down throughout the circuit whilst maintaining a fixed $dO_2$ of 6.5 ppm (Table 1). The modelled leach response for decreasing the cyanide concentration was the same as that obtained for the baseline case simulation. The explanation for this can be seen by referring to Figure 1. The calculated critical cyanide concentration for a $dO_2$ of 6.5 ppm is 91 ppm NaCN. As can be seen from Table 1, the cyanide concentration in all tanks was greater than this, indicating the leaching rate is controlled by the dissolved oxygen concentration.

For the third case the cyanide concentration was decreased and the dissolved oxygen in each tank set to match the stoichiometric requirement (Table 1). The ratio of 14 ppm cyanide to 1 ppm of dissolved oxygen was used for this calculation. The modelled final recoveries are shown in Figure 3b. The increased dissolved oxygen concentration and the corresponding increase in leaching rates increased the leach recovery significantly when compared with the leach recoveries achieved from the baseline case (Figure 3a). This effect is most pronounced for the coarsest slow leaching gold particles where the recovery improved more than 25 per cent for the 714 µm gold particles and nearly 20 per cent for the 252 µm gold particles.

The difference in overall recoveries when comparing the two cases in Figure 3, highlights the importance of operating at optimised cyanide to dissolved oxygen ratios for both fast and slow leaching ores. This result also indicates unleached gold present in tailings may be present due to unoptimised reagent conditions and insufficient leach residence time.

## SAMPLING CONSIDERATIONS

To accurately measure the extent that gold is leached within each stage of a circuit it is necessary to detect small changes in the gold content of the solids as it moves from tank to tank. It is challenging to accurately determine if gold is still leaching when the change in the gold grade between successive leach tanks is less the sampling and assay error.

The results from laboratory bottle roll leach tests on leach tailings may indicate unleached liberated gold is present in tails however it is difficult to determine if leaching is occurring within the last tanks in the circuit based on changes in the ore assays in the tanks. The issue may be that gold is still leaching at the end of the circuit, but it may not be measurable due to errors associated with sampling and assaying techniques. The question of how to quantify unleached gold in gold leaching circuits may be dependent on obtaining a statistically relevant sample.

The error associated with sampling gold particles can be calculated using the Poisson distribution. The Poisson distribution provides the ability to predict the probability that a sample of a certain mass will contain a specified number of gold particles according to the size of the gold particles and the grade of the material being sampled (Dominy, Murphy and Gray, 2011).

Figure 4 shows the relationship between the sample mass necessary to achieve 10 per cent sampling error for different sample grades and gold particles sizes. The required sample mass to achieve the desired sampling error increases exponentially with decreasing sample grade and increasing gold particle size.

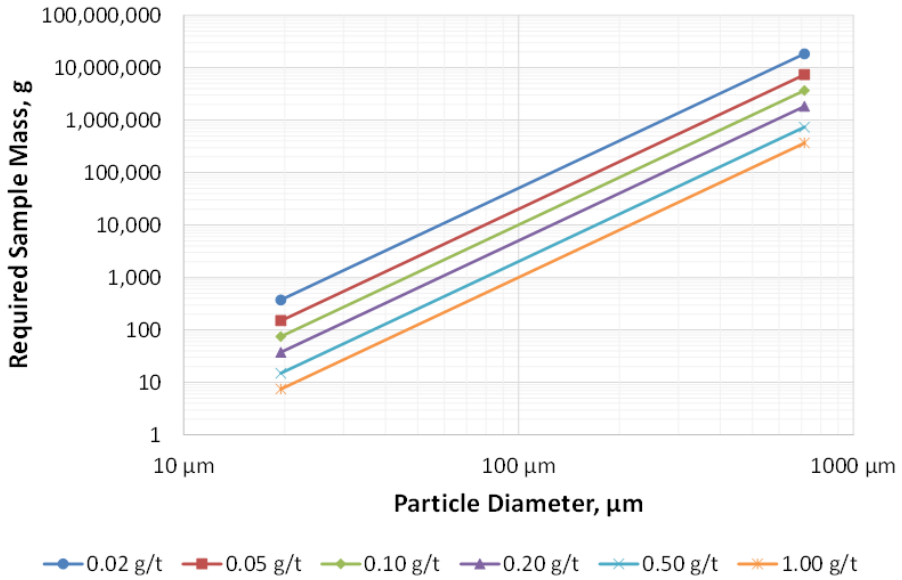



**FIG 4** – Effect of grade on sample mass required for 10 per cent sampling error (Bax, 2022).

When investigating the source of unleached gold and the often inconsistent nature of its occurrence, it is important to consider the likelihood of coarse and fine gold particles being present in the tailings streams. From Figure 4 when the gold is present as 19 µm particles only a 7 g sample at 1.00 g/t or a 374 g sample at 0.02 g/t are required. Obtaining a statistically relevant sample containing gold particles that are 19 µm in size is a relatively straightforward task.

The required sample size increases exponentially with the particle size of the gold. If gold particles are 252 µm in size, then at 1.00 g/t a 16.2 kg sample is required and at 0.02 g/t the sample size increases to 101.3 kg. If gold particles are 714 µm in size, then at 1.00 g/t a 369 kg sample is required and at 0.02 g/t the sample size increases to 18.4 t. If a lower error band or more accurate outcome is required, these sample sizes increase. Sampling and handling leach streams to determine if unleached coarse liberated gold is present becomes increasingly more complex for lower grade streams in modern processing plants.

## Size of gold particles in leaching

The shape and size of gold particles entering the leach circuit is dependent upon the milling circuit and will have an impact on unleached gold in tailings. Gold is malleable hence it behaves differently in grinding circuits. It has been observed to flatten into flakes and form into balls in the grinding circuit. Poor classification efficiency in the grinding circuit can result in coarse gold reporting to the gold leaching circuit.

To determine if coarse gold particles are likely to be contributing to the unleached gold component in tailings, it is necessary to understand what size gold particles will be at each stage within the leaching circuit.

For modelling purposes if it is assumed that gold particles are present as spherical particles, the shrinking sphere model can be utilised. It is known that not all gold particles are spherical, however it will enable calculation of the diameter of a gold particle within each stage of the leaching circuit

given the diameter of a gold particle at the commencement of leaching and the percent dissolution of the gold.

The mass of a spherical gold particle can be calculated from its volume and the specific gravity of gold. Applying a geometrical shrinking sphere model, the effect of percent dissolution on the relative particle diameter can be calculated via the following equation:

$$d_t = 2\left(\frac{d_0}{2}\right)\left[\frac{(100-Rec_t)}{100}\right]^{1/3} \quad (2)$$

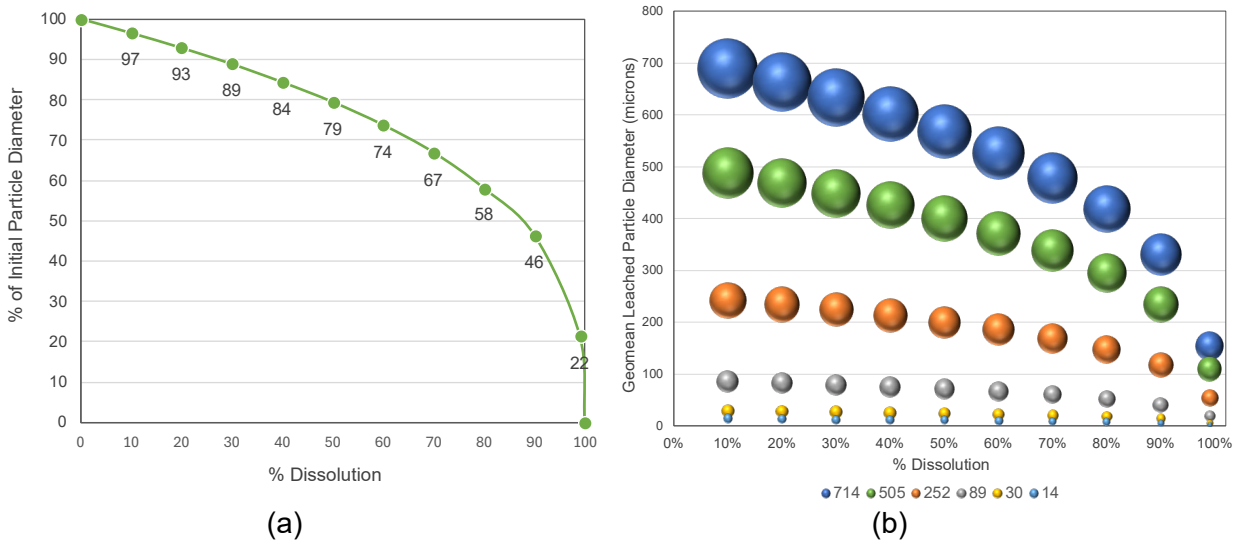
where:

$Rec_t$ is the % dissolution at time 't'

$d_t$ is the particle diameter at time 't' (µm)

$d_0$ is the particle diameter prior to leaching (µm)

The relationship between the percent dissolution and the relative particle diameter as well as the impact on leached particle diameter per size fraction is shown in Figure 5.




(a) (b)

**FIG 5** – Effect of percent dissolution on: (a) relative particle diameter; and (b) leached particle diameter.

At 90 per cent dissolution in Figure 5a the particle diameter will be 46 per cent of the initial particle diameter. For a post leach scenario in Figure 5b at 90 per cent dissolution a particle that commences leaching at 89 µm will have a diameter of 41 µm. Connecting this with Figure 4, for a tailings grade of 0.10 g/t, a minimum sample mass of 600 g would be required to be processed to determine if 41 µm gold particles are contributing to unleached liberated gold in tailings.

The final point on Figure 5b is the diameter at 99 per cent dissolution. From the model, gold particles entering the leach circuit at 30 µm have a diameter of 6 µm at 99 per cent dissolution. This indicates not only the criticality of the classification process prior to leaching but also the potential impact of coarse gold particles on ultimate leach recoveries.

## CASE STUDY – WESTERN AUSTRALIAN GOLD MINE

The aim of the study is to develop an understanding of why gold remains unleached in tails. A relatively simple gold orebody was selected as the initial case study to provide an initial baseline for comparison with more complex orebodies.

Routine bottle roll leach test work conducted by the site staff on leach tailings indicated that an additional 0.07 g/t to 0.09 g/t can be recovered after 24 hrs of bottle roll leaching. Laboratory bottle roll tests are a useful tool to monitor plant performance and aid process optimisation. For the bottle roll tests, a composite of filtered and dried daily shift samples was prepared. The bottle roll test

utilised the standard LeachWell™ Assay Tab procedure collecting solution samples at 1 hr and 24 hrs for analysis by Atomic Absorption Spectrometry (AAS).

The processing plant included two stage crushing followed by primary ball mill and secondary ball mill in closed circuit with cyclones. The gravity circuit included Knelson concentrators fed by a cyclone underflow split with gravity tail returning to secondary ball mill feed. The gravity concentrate was treated via an Acacia reactor. The cyclone overflow reported to a trash screen prior to leaching. The carbon-in-leach (CIL) circuit included nine leach tanks with a 34 hr residence time. Oxygen was used as the oxidant in Tanks 1 to 3 and air in Tanks 4 to 9. The 80 per cent passing size for the leach feed was 160 µm.

A sampling survey was conducted on-site in 2020. Samples of the leach feed and tailings were collected, as well as samples from each of the tanks. The pH, temperature, dissolved oxygen and cyanide concentrations of each sample were measured *in situ*. Slurry samples were collected, filtered and dried for subsequent size analysis and bottle roll test work. Filtered solution samples were collected for cyanide speciation and metals analysis. A separate set of samples were collected for mineralogical analysis. Ore assays from the last tanks of the leach circuit indicated that leaching had slowed or ceased (McGrath and Barbetti, 2020).

## Mineralogical results

The leach feed and leach tail were submitted to Advanced Mineral Technology Laboratory (AMTEL) for mineralogical analysis to establish the gold deportment and to probe for surface modifiers on free gold particles. A comprehensive approach was employed using multiple microbeam techniques: SEM/EDX (scanning electron microscopy/energy dispersive X-ray) to determine the composition of the gold grains, TOF-LIMS (time-of-flight laser ionisation mass spectroscopy) to analyse residual free gold grains for inorganic surface contaminants and SIMS (secondary ion mass spectrometry) to quantify solid solution and colloidal size gold in sulfide and iron oxide minerals.

The bulk mineralogy was dominated by feldspars with secondary quartz, biotite and carbonate minerals. There did not appear to be any rock mineral components which would be deleterious to leaching. Sulfide minerals form 1.4 per cent of the leach feed with pyrite dominating and minor and trace amounts of pyrrhotite and chalcopyrite respectively. Gold was present as native gold with very rare occurrences of electrum.

The following observations were noted (AMTEL, 2022):

- The leach feed contains 89 per cent potentially cyanide leachable gold. 47 per cent of the leachable gold was present as free gold grains and a further 42 per cent was unliberated but exposed gold grains in free sulfide and gangue particles (equally carried).
- Approximately 7 per cent of the leach feed gold was potentially gravity recoverable (defined as grains greater than 40 µm recoverable by Knelson concentrator).
- 22 per cent of residual gold in leach tails was exposed and potentially recoverable by optimised cyanide leaching. 15 per cent was exposed gold in silicate particles, 4 per cent was exposed associated with sulfides and 3 per cent as residual free grains.
- The majority of free gold grains remaining in the leach tails were less than 10 µm in size and may be the remnants of larger gold grains.
- Leaching of the tails to completion could lower the final leach tail by 0.041 g/t from 0.186 g/t to 0.145 g/t.
- Attaining minimum residue grade could increase total gold recovery by 3.3 per cent.
- Surface coatings did not impede free gold grain leaching.

The mineralogical analysis did not show significant surface coatings on free gold in tailings indicating that that their presence in the tailings was most likely the result of incomplete dissolution from insufficient residence time and sub-optimal leaching conditions.

## Leach circuit data

The measured circuit data collected on-site during the plant survey is summarised in Table 2.

**TABLE 2**

On-site measurements.

| Sample ID | pH | Temp °C | [NaCN] ppm | Oxidant | $dO_2$ ppm |
|---|---|---|---|---|---|
| Tank 1 | 9.43 | 43.6 | 465 | O2 | 6.8 |
| Tank 2 | 9.70 | 45.2 | 375 | O2 | 15.4 |
| Tank 3 | 9.35 | 45.0 | 480 | O2 | 20.9 |
| Tank 4 | 9.55 | 45.3 | 395 | Air | 3.9 |
| Tank 5 | 9.31 | 44.6 | 335 | Air | 1.4 |
| Tank 6 | 9.22 | 44.3 | 305 | Air | 2.9 |
| Tank 7 | 9.18 | 43.5 | 310 | Air | 1.2 |
| Tank 8 | 9.27 | 43.3 | 290 | Air | 0.6 |
| Tank 9 | 9.18 | 43.3 | 260 | Air | 0.3 |

There is a marked decrease in the dissolved oxygen concentrations after Tank 3. This can be explained by the use of air as the oxidant in Tanks 4 to 9. According to Henry's law the amount of gas that can be dissolved in a solution is directly proportional to its partial pressure. If pure oxygen (100 per cent) is replaced by air (21 per cent oxygen) the water will reach equilibrium with the 21 per cent oxygen present in air. Therefore, the maximum dissolved oxygen that can be achieved when using air will be 21 per cent of the dissolved oxygen that could be achieved by injecting pure oxygen.

The solubility of oxygen in water decreases with increasing water salinity and increasing temperature. The high salinity (approximately 125 000 ppm TDS (Total Dissolved Solids)) of the site process water and the high slurry temperatures reduce the saturation dissolved oxygen concentration that can be achieved. The maximum saturation dissolved oxygen at 125 000 ppm TDS is estimated to be 5.2 ppm for air and 24.8 ppm for oxygen at 44°C and averaged for tank depth.

## Leach circuit modelling

Size analysis was conducted on samples of the leach feed and tanks collected during the 2020 survey. Laboratory bottle roll leach tests were conducted on both the unsized material and each of the size fractions. The bottle roll test results were fitted to a first order rate equation and the leach rate (k) and leach residue grade at infinite time ($Au_e$) were calculated.

To create a leaching model, the laboratory derived leach rates were adjusted using the measured plant temperature and reagent concentrations. The leach rate was also adjusted to account for the difference in agitation intensity using corresponding plant data. The difference in agitation intensity must be considered to accurately scale-up the leaching rate obtained from the bottle roll leach test. The calculated relative leach rates at the measured dissolved oxygen concentration for each Tank is shown in Figure 6.

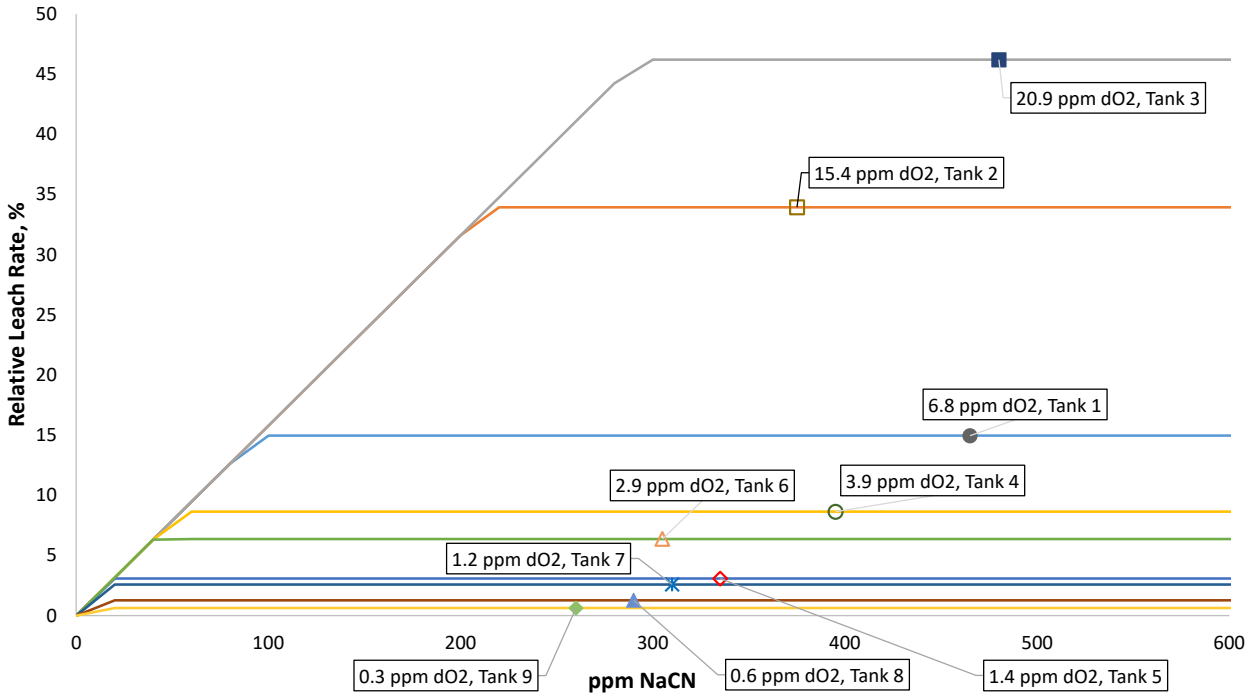



**FIG 6** – Effect of dissolved oxygen and cyanide concentration on leach rate.

The leach rate is highest in Tank 3, which had the highest dissolved oxygen concentration and lowest in Tank 9, which had the lowest dissolved oxygen concentration. The cyanide concentrations in each leach tank are much greater than the critical cyanide concentration (the inflection point on each line), consequently the leach rate is determined by the oxygen concentration and increases linearly with the oxygen concentration. In this case study it is evident that cyanide is being overdosed or conversely the tanks are deficient in oxygen.

### *Modelled leach profile at measured cyanide and dissolved oxygen*

The laboratory results, assay data and measured leach circuit conditions were used to create a baseline model to simulate leaching of gold (Bax, 2022). The modelled leach profile is compared with the measured profile from the plant survey in Figure 7a. The modelled profile utilises measured cyanide and dissolved oxygen concentrations from Table 2. There is some scatter in the data from Tank 3 onwards and this may be due to fluctuations in mill feed grade, poor classification resulting in coarse gold reporting to the leach circuit, fluctuations in gravity gold recovery and fine carbon contamination (Tank 9). The scatter in the measured assay makes it difficult to determine whether leaching has reached completion. Modelled data in Figure 7a indicates that gold leaching has slowed or ceased after Tank 3.

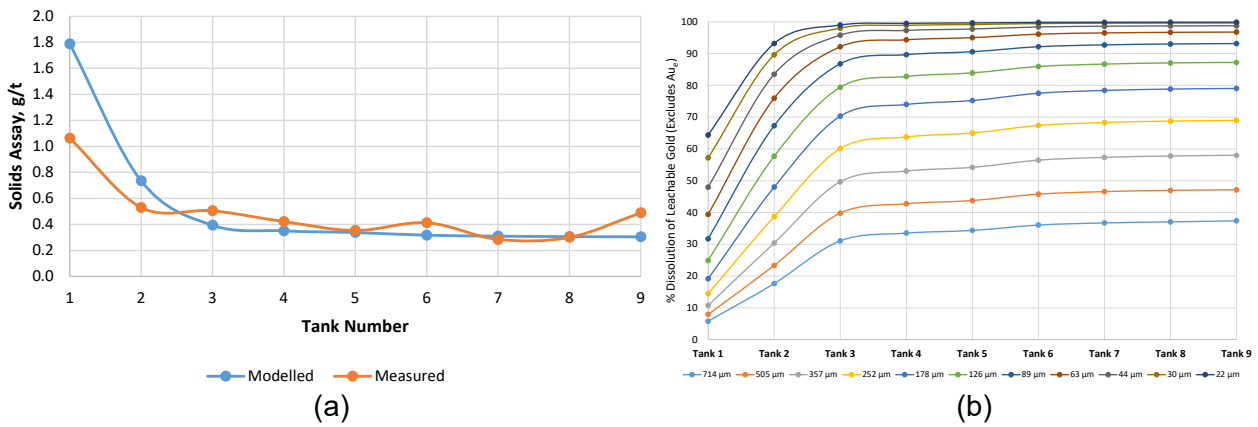



**FIG 7** – (a) Leach profile for measured cyanide and dissolved oxygen; and (b) modelled leachable gold dissolution for measured cyanide and dissolved oxygen on a sized basis.

The leach modelling can be used to get a better understanding of what is happening in the leaching circuit at the time of the survey. Figure 7b shows the dissolution of the leachable gold down the leach train for each size fraction. If we examine the modelled dissolution of leachable gold we observe a flattening of the dissolution curves after Tank 3 for all size fractions. This flattening of the curve is associated with the decrease in dissolved oxygen in Tanks 4 to 9 and the corresponding reduction in the leach rates in these tanks.

From Figure 7b gold particles less than 30 µm in the leach feed are fully leached. Less than 90 per cent recovery of the leachable gold is obtained for gold particles coarser than 106 µm in the leach feed. The modelled recovery of leachable gold from the coarsest size fraction is only 37 per cent. This highlights the importance of the classification and gravity recovery stages to ensure coarse gold does not report to the leaching circuit.

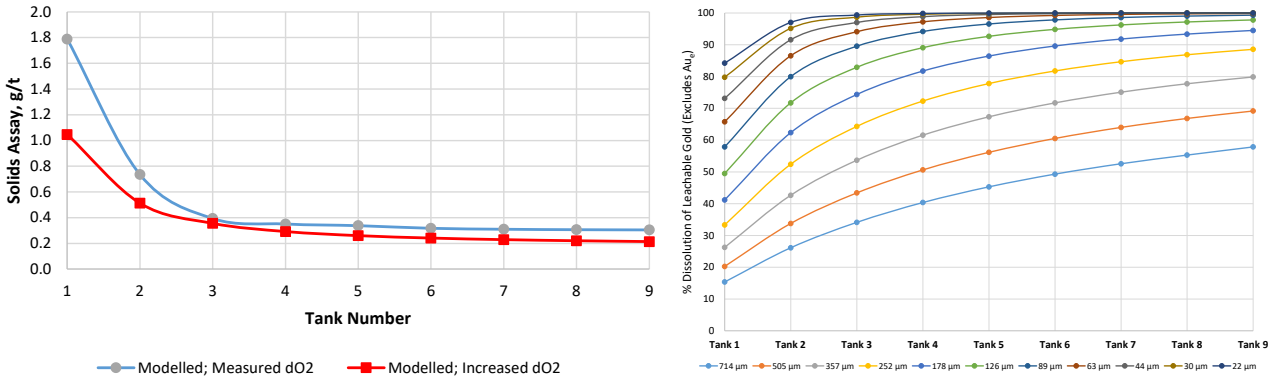
The mineralogical analysis found 71 free gold particles ranging from 2.3 to 59 µm in size with an average of 13 µm in the final leach tails. It might be expected from the modelled size data in Figure 7b that coarse gold grains were present in the leach feed, however the sampling protocol used did not collect a large enough mass to obtain a representative sample of the coarse size fractions. Analysis of a larger sample mass would be required to quantify if coarse and hence unleached liberated gold, is present in the final leach tails.

### *Modelled leach profile with increased dissolved oxygen and stoichiometric cyanide concentration*

The results of the baseline circuit modelling demonstrate the dependency of the gold leaching rate on the dissolved oxygen concentration.

To assess the potential benefit of changing dissolved oxygen concentration and distribution a simulation was performed using an assumed dissolved oxygen profile. This profile increased the dissolved oxygen in Tank 1 to 20 ppm reducing to 6 ppm in Tank 9 and adjusted the cyanide concentration to the stoichiometric (critical) cyanide concentration in each tank.

The modelled leach profile for the increased dissolved oxygen concentration is compared with the modelled leach profile for the measured dissolved oxygen conditions in Figure 8a.




(a) (b)

**FIG 8** – (a) Leach profile for increased dissolved oxygen; and (b) modelled leachable gold dissolution for increased dissolved oxygen on a sized basis.

Leaching with the increased dissolved oxygen concentrations gave a modelled tailings solids assay of 0.214 g/t. This corresponds to a reduction of 0.09 g/t when compared with the 0.305 g/t tailings solids assay obtained from the simulation with the measured dissolved oxygen concentrations. This indicates that optimising the oxidant addition may lead to a 29 per cent reduction in cyanide leachable gold present in the tailings. This result correlates with the mineralogical deportment study that estimated there was 22 per cent potentially cyanide leachable gold in the leach tails.

The modelled dissolution of the leachable gold in each size fraction is shown in Figure 8b. There is a noticeable improvement in the modelled gold dissolution for Tanks 4 to 9 when compared with the modelled gold dissolution for the measured dissolved oxygen concentrations. The recovery of

leachable gold increased from 96.7 per cent to 98.9 per cent when compared to the modelled leach profile for the measured dissolved oxygen concentrations. Notably gold particles with a geometric mean less than 63 µm are 99.9 per cent leached and the modelled recovery for the coarsest size fraction improved from 37 per cent to 58 per cent.

In addition to the increased gold recovery with the use of increased dissolved oxygen concentration, there is the opportunity for reduced cyanide addition. The oxygen capacity available on-site and the cost associated with the use of increased dissolved oxygen would have to be evaluated to assess if this scenario is viable.

## Plant survey sampling and assay errors for the case study

The size and assay analyses of the survey samples were carried out with samples weighing approximately 200 g. This results in the maximum sample weight being approximately 75 g for the minus 25 µm size fraction but only 1 g in the coarsest size fraction. As per the discussion in an earlier section, this leads to significant sampling errors in the coarse size fractions.

The combined sampling and assay errors were calculated for each size fraction in each tank in the circuit and are presented in Table 3. For this example, it was assumed that the assay error was 15 per cent. In practice it is known that the assay error will vary with the grade of the sample being analysed and the detection limits of the analysis method being used.

**TABLE 3**

Combined sampling and assay errors for sizing an assaying plant samples (%).

| Size fraction | Tank 1 | Tank 2 | Tank 3 | Tank 4 | Tank 5 | Tank 6 | Tank 7 | Tank 8 | Tank 9 |
|---|---|---|---|---|---|---|---|---|---|
| -850+600 | 2989 | 2876 | 2716 | 2683 | 2671 | 2647 | 2637 | 2632 | 2627 |
| -600+425 | 848 | 817 | 771 | 761 | 757 | 749 | 746 | 745 | 744 |
| -425+300 | 513 | 469 | 408 | 395 | 390 | 381 | 377 | 375 | 374 |
| -300+212 | 262 | 241 | 210 | 202 | 200 | 194 | 192 | 190 | 190 |
| -212+150 | 132 | 120 | 100 | 95 | 93 | 89 | 88 | 87 | 87 |
| -150+106 | 92 | 75 | 53 | 48 | 46 | 43 | 41 | 41 | 40 |
| -106+75 | 41 | 37 | 28 | 26 | 25 | 24 | 23 | 23 | 23 |
| -75+53 | 22 | 21 | 19 | 18 | 18 | 17 | 17 | 17 | 17 |
| -53+38 | 19 | 18 | 17 | 17 | 16 | 16 | 16 | 16 | 16 |
| -38+25 | 17 | 17 | 16 | 16 | 16 | 16 | 16 | 16 | 16 |
| -25 | 15 | 15 | 15 | 15 | 15 | 15 | 15 | 15 | 15 |

The main findings from the evaluation of the sampling and assay errors can be summarised as follows:

- When the sampling error is low (≤2 per cent) the combined sampling and assay error will be close to the assay error.
- The combined sampling and assay error is lowest in the finest fraction. This size fraction has the higher mass and the smallest gold particles.
- The combined sampling and assay error is highest in the coarsest size fraction. This size fraction has the lowest mass and the largest gold particles.
- The combined sampling and assay error decreases with increasing gold dissolution due to the decreasing size of the gold particles.

- A substantially larger sample mass would be required to reduce the sampling errors in coarse size fractions.

## FURTHER WORK

It is evident that cyanide concentration and dissolved oxygen concentration impact on the dissolution rate of gold in leaching circuits however there is no consistency or consensus in the literature as to the optimum cyanide to dissolved oxygen ratio. The value of the stoichiometric ratio changes with the diffusion coefficients used in the calculation and a range of 12 to 18 for the ppm stoichiometric is acceptable. There is significant scope to further examine the optimum cyanide to dissolved oxygen ratio and determine if an optimum value exists and if it is dependent on gold composition (silver/copper content), ore/gangue components or water quality.

Collection of reliable site based dissolved oxygen and cyanide concentration data sets is required to build a robust data set of leach rate data. Further work is required to achieve consistency of measured dissolved oxygen data as measurements are impacted by salinity, temperature, altitude and *in situ* measurement depth. This will allow a reliable 'average' dissolved oxygen calculation to be derived for leaching tanks.

Oxygen management strategies for oxygen and air in leaching circuits where mixed oxidants are used is an area for further investigation. This would include the potential for use of chemical oxidants in conjunction with oxygen or air to maximise efficiency for circuits where dissolution of gases is limited.

Further investigation of the effect of agitation rate, slurry density and viscosity on the leaching rate of gold.

Finalisation of the development and validation of a standardised diagnostic testing methodology for determining the nature of unleached gold in leaching circuits. This includes the ability to collect representative samples of coarse gold from leaching circuits.

## CONCLUSIONS

The factors that directly influence the dissolution rate in gold leaching circuits are cyanide concentration and dissolved oxygen concentration and their respective ratios. To achieve the optimal use of cyanide and oxygen, the ideal operating point is the point at which you are operating with stoichiometric cyanide concentration for a given dissolved oxygen concentration.

The addition of excess cyanide above the stoichiometric concentration does not improve gold dissolution as the gold dissolution rate is limited by the dissolved oxygen concentration.

Determining if coarse gold is present in leach tails requires the collection of a large sample mass to reduce the sampling errors in coarse size fractions. The collection of low mass samples may lead to misidentification of the nature of unleached gold in leach tails.

High classification and gravity circuit efficiency is critical to minimise coarse gold reporting to the leach circuit and subsequent loss to leach tail after incomplete leaching.

Measuring the dissolution of gold by means of the solids assays requires a quantifiable difference between the solids assays for the part of the circuit being studied. This can be done with a reasonably high degree of certainty when comparing the feed and tailings assays for a leach circuit. However, detecting the degree of gold dissolution on a tank by tank basis is an order of magnitude more difficult due to the relatively small differences in the solids assays and the errors associated with sampling and assaying.

Modelling provides a powerful tool to simulate the size-by-size leaching of gold and examine the effect of optimising the cyanide and dissolved oxygen concentrations utilised within leach circuits.

Modelling of the plant circuit showed increased dissolved oxygen concentrations gave a modelled tailings solids assay of 0.214 g/t. This corresponds to a reduction of 0.09 g/t when compared with the 0.305 g/t tailings solids assay obtained from the simulation with the measured dissolved oxygen concentrations.

If the 0.09 g/t reduction in leach tails solids grade is realised in the operating plant through process improvement, this would potentially increase profit by an additional US$11.5M per Mt of ore processed (based on a gold price of US$4000 per ounce).

## ACKNOWLEDGEMENTS

The authors wish to thank the industry sponsors of the Amira P420 gold Processing Technology Project (AngloGold Ashanti, Australian Gold Reagents, B2Gold, Corem, FLSmidth, Gekko Systems, Gold Fields Australia, Kemix, Newmont, Northern Star Resources, Orica Australia and SGS Canada) and the Western Australian School of Mines at Curtin University.

## REFERENCES

AMTEL, 2022. Deportment of Gold in Leach Circuit Products, Canada: Advanced Mineral Technology Laboratory.

Bax, A R, 2022. Unleached Gold in Tailings, Amira P420G Gold Processing Technology Project, Western Australian School of Mines.

Bax, A R, McGrath, J, Oraby, E A, Wardell-Johnson, G and Vaughan, J, 2014. Summary and comparison of integrated liberation and leaching test work results, Amira P420E Gold Processing Technology Project, Western Australian School of Mines.

Bax, A R, McGrath, T D H, Eksteen, J J, Staunton, W P, Oraby, E A and Wardell-Johnson, G, 2016. An Integrated Liberation-Leach Model to Evaluate Gold Liberation and its Impacts on Gravity Recovery, XXVIII International Mineral Processing Congress.

Dominy, S, Murphy, B and Gray, A, 2011. Characterisation of gravity amenable gold ores—Sample representivity and determination methods, in Proceedings of the International Geometallurgy Conference, pp 281–292 (The Australasian Institute of Mining and Metallurgy: Melbourne).

McGrath, T D H and Barbetti, K, 2020. Site Visit Summary Report, Amira P420G Gold Processing Technology Project Western Australian School of Mines.

Zheng, J, Ritchie, I, La Brooy, S and Singh, P, 1995. Study of gold leaching in oxygenated solutions containing cyanide-copper-ammonia using a rotating quartz crystal microbalance, *Hydrometallurgy,* 39:277–292.

# Thirteen lessons from the battle field of metal accounting

*R Espinosa Gomez[1] and P D Munro[2]*

1. FAusIMM, Principal Consultant, Mineralis Consultant Pty Ltd, Taringa Qld 4068. Email: respinosa@mineralis.com.au
2. MAusIMM, Principal Consultant, Mineralis Consultant Pty Ltd, Taringa Qld 4068. Email: pmunro@mineralis.com.au

## ABSTRACT

Metal accounting and reconciliation is properly considered to a part of the financial accounting process. Now production data has to be as auditable as financial data. It requires an understanding of the principles of mass balancing and metal accounting, knowledge of the equipment and capacity required to achieve the required level of accountability. It is based on a reconciled material balance which is itself derived from critical measurements. It defines production costs, revenues and inventories. It is a fundamental baseline for estimating the value of the operation.

Internal users of metal accounting information in a technical sense for a site are the departments of Process Plant, Geology and Mine. Data collected for operational control is aggregated into the metal accounting process where the inter-departmental for reconciliation.

Good quality decisions are predicated on the availability of good quality information. This is provided by metal accounting, day-to-day and for the life of the mine.

External users can be considered under the umbrella of environment, social and governance (ESG) concerns; especially governance. Therefore, the outcomes of both poor metal accounting procedures and especially malpractice, can be both a loss of reputation and consequent effects on the ‘social license to operate’.

Usually, technical papers about metal accounting subject the reader to homilies about sampling statistics or extol the virtues of a new piece of mass balancing/metal accounting software. This paper aims to liven up what many process engineers regard as a regular chore or dull subject by looking at some ‘war stories’ from the battlefield of metal accounting.

Thirteen lessons from the battle field of metal accounting are:

1. Expecting a proper reconciliation from a poor sampling system.
2. Assuming the wrong mill throughput.
3. Mass measurement and sampling systems are not run properly in a complex operation.
4. ‘Coarse gold’ mineralisation overestimated production.
5. ‘Coarse gold’ in the concentrate tank underestimated gold production.
6. What went wrong after an unnoticeable change in the process water characteristics?
7. Metal accounting system equations were ‘temporarily’ modified.
8. End of month reconciliations overcalled the company internal target during many consecutive months.
9. Inattention to the outturns.
10. Metal accounting systems did not cross process boundaries.
11. Zinc concentrate stockpile not zeroed for five years.
12. Stocks and ‘work in process’ were not converted to product.
13. Significant metal accounting issues take place in precious metals refineries.

# BACKGROUND

## Internal users

People at a mine site are familiar with the fundamental concept of metal accounting being the ‘Truth Machine’ for the interface between the departments of Process Plant, Geology and Mine. While determining production data, it drives the reconciliation process between Geology, Mine and Process Plant for defining ore resources and reserves.

## External users

Many operators would not be aware of the much wider and potentially more influential external audience for metal accounting data.

This comes under the GOVERNANCE aspect of business.

There must be compliance with statutory company regulations. These are now more prescriptive because corporate failures have highlighted gaps between what has been publicly reported by companies and stakeholder expectations.

Examples are:

- Sarbanes-Oxley Act in USA from 2002.
- UK Corporate Reform Project in 2021.

Similar prescriptive requirements for company reporting will probably just be a matter of time in Australia.

We go into further detail for what a significant outcome of these acts is.

### *Production data has to be as auditable as financial data*

Operators at mine sites should consider satisfying external audits both technically and financially as to the validity of their metal accounting practices.

‘External’ users of production data are:

- partners
- shareholders
- holders of streaming agreements receiving revenue from a percentage of production at a fixed price.

Readers should be reminded that we live in litigious times; Mineralis Consultants has done jobs involving adjudication in legal wrangles on technical issues over what quantities of metals had actually been produced.

Important ‘external’ users of production data are *Governments* where the assumed power relationship will be unequal.

Royalties and taxes – interact at three levels local, state/provincial and national.

Four recent examples of adversarial relationships between governments and mining companies:

1. Kyrgyzstan versus Kumtor (Centerra).
2. Mongolia versus Oyu Tolgoi (Rio Tinto).
3. Panama versus Cobre Panama (First Quantum).
4. Tanzania versus Bulyanhulu (Acacia Resources → Barrick).

Claims that the nation had not received a fair return from the mining company were common in the aforementioned.

A relatively small ‘error’ in metal accounting affecting royalty/taxation payments can be compounded to appear a very large sum over the life of the mine.

Cobre Panama royalty payment was US$375 million a year; 1 per cent of that over 20 years is US$75 million.

A corporate entity or operation cannot afford a loss of credibility, particularly if operating in a foreign country.

### *Malfeasance*

Examples:

- Late 1984, ‘multi-million pound’ theft of silver in Junker blocks from Britannia Refined Metals in UK.
- May 2004, alleged $34 million copper cathode theft from Codelco in Chile.
- Oct 2004, US$39 million PGM theft in South Africa.
- Dec 2009, ‘disappearance’ of $20 million in gold + silver at Royal Canadian Mint (later accounted for).
- May 2014, US$80 million copper concentrate theft from Codelco – Escondida in Chile.
- Jul 2014, US$113 million discrepancy on gold stocks at Rand Refinery, South Africa.
- Jun 2016, 38 000 t of coal ‘missing’ at Vaal Kranz Mine, South Africa.
- Mar 2021, case conclusion of theft of ‘tens of millions of dollars’ of uncut diamonds, Argyle, WA.
- Sep 2023 onward, €100 million theft of metals at Aurubis in Hamburg, Germany; apparently discovered while investigating earlier unrelated €20 million theft.

The reader wondering about the relationship between metal accounting and theft is reminded of the adage the former is the first line of defence against the latter.

Malpractice consequences are loss of reputation and social license to operate.

If an operation can’t be seen to get metal accounting right which is fundamental to vital; how could it be trusted to provide credible numbers:

- Environmental data?
- Carbon accounting?

In the following examples the reader will discern a recurrent theme of unpleasant surprises relating to notional in-process stock levels confirming the need for particular vigilance in this aspect of metal and product accounting.

## METAL ACCOUNTING LESSONS

## Expecting a proper reconciliation with poor sampling practices

### *Situation*

For two months in a row the production metal balances recorded high negative reconciliation figures.

The flotation tailing sampler in one of the processing lines had not been working for about a year and the other line used a non-compliant tailing sampler.

Since there was no combined flotation tailing sampling station, the flotation tailing values were estimated from slurry volume flows and density; periodically there were problems with the density meters.

Usually, the leach tailing sampler was not operational and even when working, was non-compliant because the cutter aperture was less than 5 mm compared with acceptable practice for a slurry stream being a minimum aperture of 10 mm.

There was no combined final tailing sampling station for the combined flotation tailing + leach tailing.

### *Learning*

Promptly repair and operate the flotation tailing sampler that had been out of action for a year. Assess if this larger sampler could be modified to also receive the second flotation tailing stream.

Promptly repair and operate the leach tailing sampler.

Assess the economics of installing a combined final tailing sampler for flotation and leach streams.

## Assuming the wrong mill throughput

### *Situation*

It took one month to resolve the mystifying situation of the actual ore feed to a rod mill grinding line being ~50 per cent higher than the 'measured' feed set point.

### *Issues*

- The mechanical maintenance crew mistakenly installed the wrong gear box to the head pulley of the rod mill feed conveyor; this increased the conveyor speed by ~50 per cent.
- The grinding line incorporating a rod mill and two ball mills experienced slurry product 'sanding' issues, including the tailings discharge launder from the plant. The operations team diligently checked every variable including rod mill feed particle size but missed the physical equipment change causing the conveyor speed increase.
- The rod mill feed weightometer was calibrated using the roller chain test method twice. Since this assumed that the conveyor speed was the 'fixed' original value, it failed to detect the problem. A full 'live load test' was planned.
- A mass balance around the grinding circuit using the particle sizing method concluded that the rod mill feed was 50 per cent higher than usual. However, the finding was ignored in favour of the more reliable 'fact' of the rod mill feed weightometer calibration showing the feed throughput was the normal value.
- Finally, when Operations discussed the problem with the maintenance people asking 'what changes if any had been made to grinding line?', the gearbox modification was discovered.

### *Learning*

- Always ask the right questions. Operations should have immediately asked if anything had been changed to the rod mill feed conveyor.
- Trite to say 'improve communication and work together among different disciplines' but what exactly was being done by the individual Maintenance and Operations sections should have been visible to each other.
- Do a proper weightometer calibration eg 'Belt speed always needs to be measured manually using a hand-held tachometer, checking the distance travelled and time, by marking the belt. All of these checks should be carried out over an integral number of at least three belt revolutions and for not less than ten minutes with the conveyor running at the beginning and end of the test'.
- Demonstrates the vital importance of 'hardware' in the metal accounting process. A sophisticated computerised metal balancing system ultimately relies on the integrity of field-based measurement equipment.

## Mass measurement and sampling systems are not run properly

### *Situation*

For two months in a row, negative adjustment above the company internal standards for the metal balance prompted an external investigation.

The metal accounting was complex and relied on many measurements; the program run as part of the daily balance required input data from over 100 streams.

### *Issues*

Poor condition/calibration of the weightometers of the two grinding mills and the two separate weightometers that were part of the combined grinding scat system.

The tonnes of ore fed to each mill were measured by a weightometer. However, one of the weightometers measured the new ore feed plus the return mill scats feed, as it was located post mill scats return. Thus, any error weighing the scats was carried to the mill feed weightometer. The scats represented about 14 per cent of the weight of the fresh mill feed.

The problem was exacerbated by the complex metal accounting system.

The input data came from weightometers, flowmeters/density meters, load cells, and sampling systems to collect measurements from the various streams; some of these data were biased. Much of the input data were either back calculated or assumed.

### *Learning*

A computerised metal accounting system cannot compensate for poor measurements. Therefore, consideration of the system requires going back to fundamentals. Primary focus must be on entry and exit streams.

## Coarse gold mineralisation overestimates production

### *Situation*

In a new gold heap leaching operation ore mineralisation occurred in a shear zone. Gold distribution was heterogeneous due to the presence of visible coarse native gold in the size range 100 µm to 600 µm. About two years after start-up the issue became noticeable, as the amount of gold produced was consistently higher than budget figures. The additional gold production could not solely be attributed to higher recoveries. Deviations of gold assays were greater than 15 per cent in precision and accuracy.

Sampling and assaying protocols were established during the exploration phase prior to start-up based on nomographs developed from early heterogeneity tests. Due to the ore characteristics the head grade had been underestimated by ore control sampling and/or assaying procedures.

*New procedures were developed for mine sample collection during blasthole drilling and new sampling protocols and nomographs to ensure an acceptable relative standard deviation to control the fundamental sampling error within ± 15 per cent.*

The scope of the sampling and assaying of coarse gold was to develop new sampling and sample preparation protocols:

- ‘Existing’ ~50 g sample versus ‘Leaching’ ~12 000 g sample.
- ‘Rotary Sampling’ protocol versus ‘Leaching’ protocol.

### *Learning*

The ‘Leaching’ protocol was better than the ‘existing’ protocol, because it used a larger sample mass (~12 000 g versus ~50 g). The ‘rotary sampling’ protocol is a good and practical alternative to the ‘leaching’ protocol, as it reduces within ±15 per cent the relative standard deviation of the fundamental error. Currently, all blasthole samples are processed using the ‘rotary sampling’ protocol, because it is simpler and safer.

## ‘Coarse gold’ in the concentrate tank underestimated gold production

### *Situation*

There was a concentrate slurry storage tank before filtration for shipping. It received concentrate from an ore with a gravity recoverable gold content ranked as ‘moderate to fine’ as per the definitions in AMIRA’s Project P420B Gold Processing Technology. While a significant portion of the coarse gold was recovered by centrifugal concentrators in the grinding circuit and treated separately, the flotation concentrates also received coarse gold coming from gravity table tailing, and any coarse gold not recovered by the centrifugal concentrators.

### *Issues*

A portion of coarse gold particles settled and accumulated at the bottom of the slurry storage tank because the mixing conditions were usually insufficiently turbulent to keep them in suspension.

The amount of gold accumulated was significant increasing over time exacerbated by operational upsets such as lower slurry % solids, power failures etc.

The significant amount of accumulated gold in these ‘traps’ contributes to abnormally high metal balance reconciliations.

### *Learning*

Slurry storage tanks need appropriate agitation systems. Operational issues require robust procedures to measure ‘gold in circuit’ and regular zeroing of inventories.

Again, another demonstration of the vital importance of having appropriate ‘hardware’ for the metal accounting process. A sophisticated computerised metal balancing system ultimately relies on the integrity of field-based equipment and measurements.

## What went wrong after an unnoticeable change in the process water characteristics?

This case comes from a flotation-leaching-CIL-Merrill Crowe-Cyanide Detox operation. Originally tailings after detoxification went directly to a storage facility with recovered water returning as process water. Then tailings went to a high compression thickener and the overflow returning as process water.

A detailed metal accounting audit occurred because there were discrepancies comparing typical differences between mine and plant head grades. There was a loss of corporate credibility in the plant metal accounting practices. The audit found that the operation applied best practices for mass measurement, moisture content, sampling, sample preparation and chemical analytical satisfactory data handling and administration.

When unaccounted gain and losses diagrams were prepared as shown in Figure 1, it was observed that for three consecutive years after the change to the tailings stream there was a permanent monthly positive bias of about 2 per cent higher recoveries.

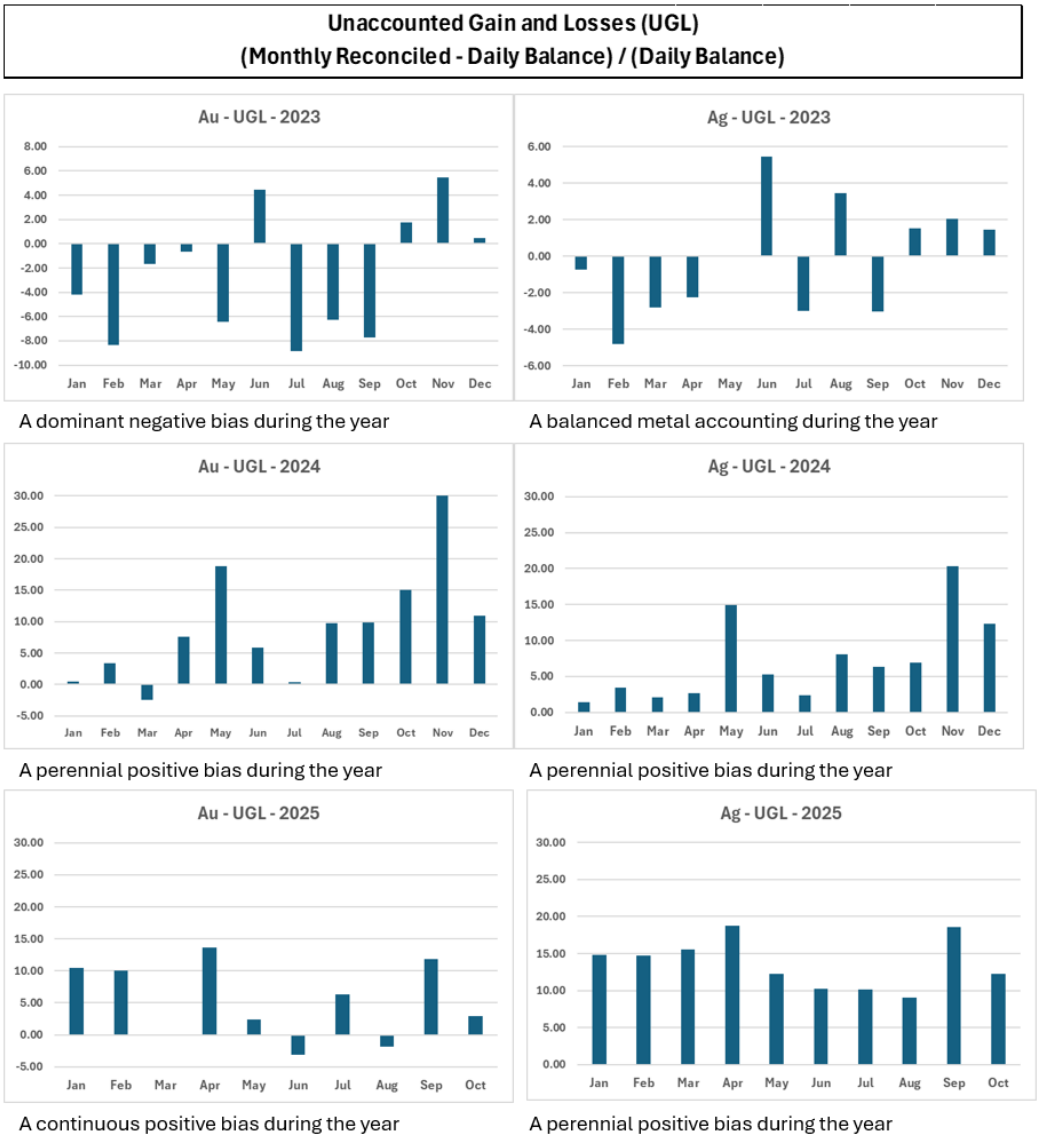



**FIG 1** – Unaccounted gain and losses (UGL) (monthly reconciled – daily balance)/(daily balance).

The daily detoxification discharge water assays had free cyanide assays generally lower that 5 ppm with total cyanide around 13 ppm. Laboratory studies had shown that more than 30 ppm of free cyanide was needed to have an effect on the gold and silver. These data were ignored. However, when reviewing procedures, it was observed that the detoxification discharge water samples once collected, had 12 hr delay without any further preparation before dispatch to the laboratory. Best practice for analysing water samples for cyanide involves immediate stabilisation by raising the pH to >12 with sodium hydroxide had not been followed.

Thus, there was sufficient free cyanide present for continuing leaching of gold and silver to be taking place in the high compression thickener.

### *Learning*

Fully investigate the potential effect of any change to the process flow sheet on the metal balance.

Continually check the adherence of all sampling and analytical methods to best practice guidelines.

The final tailing stream became the high compression thickener underflow instead of its feed.

## Metal accounting system equations were ‘temporarily’ modified

An equation in an MS-EXCEL metal accounting spreadsheet formula used to calculate the final tailings grade was temporarily modified for a one monthly reporting period due to a change in the

process to account for a temporary exit stream. This change was forgotten and remained in the metal accounting system for months, as the spreadsheet for each new month was copied from the previous one.

Reported reconciled gold head grade and recovery were significantly different from actual.

### *Learning*

When a spreadsheet-based metal accounting is used, it is essential to 'protect' all the equations and restrict the access to the system to authorised users.

Before any change is done to the system, the proposed change needs to be fully explained in a written report, which must also be approved at an appropriate level of authority, defined by the operation concerned, and retained for record purposes. When the change is done, it is important that the person responsible for the system does the change and the client understands and validates the change.

The AMIRA P754 Code of Practice for Metal Accounting Code deprecates the use of spreadsheets as a method of data entry, for the following reasons:

- does not allow controlled data entry and they are easily corrupted
- easy to inadvertently type over data, lose track of records, duplicate and improperly enter data in a spreadsheet
- justification of formulae in spreadsheets often lacks clarity, and is not always recorded with the spreadsheet
- reason for any amendments can get lost.

Mineralis Consultants takes a more lenient view on the use of spreadsheets assured that appropriate programming can 'protect' calculations with suitable procedures to authorise and document changes.

## End of month reconciliations overcalled the company internal target during many consecutive months

### *Situation*

Weightometer span error at this site had been typically ~ ±2.5 per cent.

For five years the weightometer had been calibrated every three months, during shutdowns. In the last 8 months, the span error on nine of the calibrations had been at least ~±15 per cent.

### *Issues*

The conveyor belt wear skirts had been removed as because they deemed not essential.

Consequently, large rocks spread over the conveyor belt surface hitting and damaging the load cells.

One of the weightometers had been calibrated 14 times in the last 8 months and the second weightometer 32 times in the same time period.

Weightometers were being calibrated weekly before the problem was fixed.

It took about 8 months for the problem to be fixed.

The outcome was that 18 days' worth of mill feed totalling over 1 million tonnes (Mt) of ore had to be discounted from the metallurgical balance.

### *Learning*

Follow the routine checks and the establish sound calibration procedures.

The 'siloing' issue demonstrating the need for improved communication between the different disciplines working in the process plant.

## Inattention to the outturns

The cumulative metal discrepancy between concentrator production versus smelter receipts was trended in a chart for a two-year period.

The calculation of shipped flotation concentrates to smelter for metal accounting performances paid no attention to the further reconciliation process between ‘shipped’’ and ‘received’.

Over some years it was evident that the metal values on-site were being under called by around 6 per cent for gold and copper. This additional metal production had not been taken into account in updating metallurgical recovery predictions or mill feed grade estimates; the latter being especially important in reconciling mine production and hence ore reserves.

### *Learning*

‘Siloing’ again – a sound metal accounting system uses all available data with regular reconciliation of interface streams.

This phenomenon can result from site people not having easy access to the ‘shipped’ and ‘received’ data that are used for commercial settlement.

## The metal accounting system did not cross process boundaries

### *Situation*

The mill feed weightometer calibration significantly drifted early in a month, giving plant operators a throughput value that was almost double actual throughput. The error was not discovered until a concentrate train was being loaded, and the concentrate storage silos ran empty when the train was only half full.

### *Issues*

The mainly manual system for daily metal accounting was solely based on concentrator data without feedback from downstream concentrate drying, storage and transport operations measurements until the month’s end. Thus, any gross error in the concentrator metal accounting system within the month could not be recognised.

### *Learning*

Key data measures from concentrate drying, storage silos and train load-out were recorded daily in the concentrator Metal Accounting system.

The concentrate shipment product from the site was used as the reference point and tracked daily against concentrator primary accounting measures.

## Zinc concentrate stockpile not zeroed for five years

Zinc concentrates shipments to customers from a large base metals’ operation in Australia in the mid- to late-1980s had been significantly reduced for several years because of unsatisfactory commercial terms. Thus, large stocks of zinc concentrate accumulated resulting in the zinc concentrate storage pad not being ‘zeroed’ for well over five years.

When the pad was finally ‘zeroed’ there was a discrepancy of ~20 000 t of zinc concentrate @ ~50–52 per cent Zn ‘missing’ from the book stock amount. This represented an ‘error’ of less than 1 per cent considering that well over 2 000 000 t of zinc concentrate had moved through the pad since it had been previously ‘zeroed’.

While this was not a result of any malfeasance, company accounts had to be adjusted to immediately ‘write off’ the value of 10 000 t of contained zinc metal in the two months before the end of the financial year.

### *Learning*

This was a dramatic demonstration of the cumulative effect of relatively small measurement uncertainties on stated metal production. Regular zeroing of the concentrate stocks would have avoided this unpleasant adjustment to the financial accounts.

## Stocks and 'work in process' not converted to product

Sludge was cleaned out from gold electrowinning cells but there was insufficient time to refine it to Doré bullion before the end of month closure. This required an estimation of the sludge's gold content.

The Plant Superintendent made an estimate of the amount of gold in the electrowinning cell sludge based on his experience at another operation.

His estimate used in the reconciliation was a sludge gold content of approximately ~600 oz; the actual content was later found to be less than 2 oz.

### *Learning*

Stocks and 'work in process' amounts must be accurately converted to product; this required measurement and zeroing out to avoid estimation and cumulative errors in the reconciliation. Small mass high value products such as gold are particularly prone to metal accounting errors if only estimates (more properly called 'guesstimates'?) are made.

Over the years the writers have observed a predilection amongst industry practitioners to 'estimate based on experience' rather than actually measure eg use truck and skip 'factors' rather than weighbridge of load cell data, 'drive by' data of stockpile volumes etc.

## Significant metal accounting issues take place in precious metals refineries – Example $113M less gold than in books

### *Situation*

'A serious discrepancy emerges at Rand Refinery, with Rand Refinery's customers agreeing to lend it money given an eye-popping accounting issue.' (Crowley, 2014).

Rand Refinery Ltd in South Africa, processor of about a third of the world's gold since 1920, found $113 million less physical metal than the company had booked in its accounts after adopting a new computer system.

The refinery in Germiston, a town 20 km east of Johannesburg, has 87 000 ounces of physical gold less than the amount present in its accounting records after 'implementation difficulties' with the new system, the company said in a statement today. That's worth about $113 million at today's price of $1296 an ounce.

Rand Refinery's shareholders, including AngloGold Ashanti Ltd., Sibanye Gold Ltd. and Harmony Gold Mining Co., agreed to lend the company 1.2 billion rand to help make up the difference. Howard Craig resigned as chief executive officer in May and has been replaced by Mark Lynam, who is being assisted by management consultant Accenture Plc in sorting out the issue.

Gold miners send bullion at about 80 per cent purity to the refinery, which then treats it and boosts this to close to 100 per cent. Rand, Africa's biggest processing facility for the metal, has refined almost 50 000 metric tons of gold since 1920, according to its website.

The miners, customers of the refinery, have received the prices they were expecting, leading them to conclude it was most likely an accounting problem rather than theft, James Wellsted, a spokesman for Sibanye Gold, said by phone.

AngloGold, Sibanye and Harmony made loss provisions of about $92 million between them as a result of the lost ounces. Rand Refinery has been unable to finalise its results for the year ended September 2013 because of the issue, it said.

### *Learning*

This example from a precious metals' refinery may not seem to particularly relevant to the situation in a minerals processing plant but the parable is one of the needs for vigilance about the issue of stocks in metal accounting.

Metals smelters and refineries can accumulate large stocks of materials in slags, residues, ladle 'skulls', dusts etc. An operating metric that would make the tie-up of value would be 'first past conversion of feed to saleable product'. We have seen this figure as low as <70 per cent in some cases.

A key performance indicator of achieving a high first pass conversion would decrease both stock levels and working capital hence improving the accuracy of the metal balance.

The examples mentioned above about accurately estimated 'gold in circuit' and zeroing a zinc concentrate stockpile directly relate to the stocks issue.

## CONCLUSIONS

Metal accounting and Reconciliation is the 'Truth Machine' for the interface between: Geology, Mine and Process Plant.

It determines the production data: 'driving the reconciliation process for defining ore resources and reserves'.

'Following multimillion-dollar malfeasances, new audit and corporate governance reforms now mandate that production data be held to the same auditing standards as financial data.'

The Thirteen Lessons ('War Stories') are also a remainder of the Importance of metal accounting, through lessons from day-to-day issues on: 'Sampling (3)', 'Mass Measurement (3)', 'The Metal Accounting System (3)', 'Stocks (2)', 'Outturns (1)', and 'Sample Preparation and Analytical (1)'.

## ACKNOWLEDGEMENTS

The authors wish to thank Mr Duncan Bennett, Mineralis Consultants, for providing lessons 7, 10, and 12; and Mr Aidan Giblett, Black Swan Metallurgy, for providing lesson 9.

## REFERENCE

Crowley, K, 2014. Biggest Africa refinery has $113 million less gold than in books, Bloomberg.com. Available from: <https://www.bloomberg.com/news/articles/2014-07-25/biggest-africa-refinery-has-113-million-less-gold-than-in-books>

# I’m not a Luddite – is AI real?

*C J Greet*[1]

1. Principal Consultant, Mineralis Consultants Pty Ltd, Taringa Qld 4068.
   Email: cgreet@mineralis.com.au

## ABSTRACT

A data scientist once told me that they could model a salmon farm, and that this qualified them to be able to model a sulfide flotation circuit because they knew all about AI! This was a remarkable statement and required deeper consideration.

Is it possible to model a salmon farm? And, by using their model they insisted that they could improve salmon production? Is it really AI? Can this process be applied to a sulfide flotation circuit?

The paper explores the differences between the two systems and provides an explanation as to why it is comparatively easy to develop machine learning algorithms for a Salmon farm. The same approach can be applied to a sulfide flotation circuit; however, it is not as easy to apply.

Some of the reasons attributing to the degree of difficulty in applying machine learning algorithms to a sulfide flotation circuit are described and what is required to overcome these difficulties.

## INTRODUCTION

Throughout human history there has been resistance to change and the introduction of new technology. One can only imagine the disruption fire or the wheel caused when they were first introduced to humanity.

Textile workers in England have a long history of destroying new technology which was seen as upsetting the *status quo*. As far back as 1675 ‘stockingers’ organised action against modernisation of their industry. The introduction of new cotton spinning technologies in 1768 and 1779 met with violent resistance. In the early 1800s the Luddite movement organised mass demonstrations, protests and wrecked machinery in factories that threatened their livelihoods.

Broadly, the Luddite movement were not opposed to the use of machines; they were attacking manufacturers who were trying to circumvent standard labour practices of the time, which had the potential to lower wages and significantly disadvantage the working class in Britain during a period of economic hardship.

In the modern parlance, a Luddite is generally considered to be an individual who is resistant to using new technology (for example, computers, smartphones or automated systems). In many ways AI is being viewed in the same light. That is, some believe that the unchecked corporate deployment of AI could drive down wages, eliminate entry-level career paths and concentrate wealth among a few tech monopolies.

## ARTIFICIAL INTELLIGENCE (AI)

Artificial intelligence is all a buzz with technology companies investing billions of dollars in its development, and many wishing to reap the rewards from using it. It is difficult to come up with a clear definition however Toby Walsh (National Press Club of Australia, 2026) suggests: ‘AI is getting computers to do tasks that require human intelligence’. Walsh indicates that:

- AI mimics human capabilities rather than replicating true human consciousness.
- AI does not focus on abstract thinking but is centred on functional performance or solving problems that traditionally need a human brain.
- At best AI is a collaborative tool to combine with human creativity and reasoning.

The application of AI in mineral processing is less newsworthy! However, efforts are being made.

## THE SALMON FARM

Several years ago, a group specialising in data science approached my employer at the time, indicating that they could develop algorithms that had the potential to model the flotation circuit and improve metallurgical performance. The example provided was the successful deployment of an algorithm used to control and operate a salmon farm. Management were excited and eager to apply this technology to a data set containing both pulp chemical and traditional operating data collected from a copper mine to test the capabilities of the data scientists.

In due course, several months' worth of data was provided, and the data scientists went to work. It became apparent very early in the process that the data scientists did not have a strong grasp of what minerals were, how the flotation process worked or what the data meant. Discussions to answer the data scientist's questions and explain the data did not really resolve the issues. Further, there was a reluctance to cleanse the data to remove shifts that were interrupted by shutdowns or had abnormally low (or high) head grades as this reduced the fit of their model. Their model, while indicating that the most important parameter was the air added to the fourth rougher cell, was ultimately a failure.

Upon reflection this learning experience provided some very important insights:

- Salmon require very specific water quality and environmental conditions to survive and grow. Salmon requires:
  - Water at a temperature between 8° and 14°C.
  - Dissolved oxygen concentrations of between 7–9 mg/L.
  - Fresh water for hatching and early growth, then shift to full marine salinity for adult growth.
  - A strong flow of clean water to remove waste and prevent disease.
  - A high protein diet containing fish meal, fish oil and sustainable plant proteins.

Moving outside of these boundaries resulted in the salmon becoming sick and dying. So, the normal distribution for salmon is very narrow and very easy to control. This made modelling and building a digital twin for controlling the production of salmon comparatively easy.

Data scientists are good at processing and developing relationships within data sets, however they are not expert in understanding what the data means or how the various parameters are related. Essentially, in this example the data scientist is not a flotation metallurgist and cannot be expected to understand the nuances of information provided.

Metallurgists know the mineralogy of their ore and the process. They also have a reasonable understanding of the interactions between the various parameters. The data scientist doesn't, so it is the responsibility of the metallurgist to provide an explanation of the mineralogy, the process and the data in terms that the data scientist can appreciate. For example, it is important to tell the data scientist that if the throughput is zero tonnes per hour it means the plant is shutdown and this point can be cleansed from the data set. It is not an outlier!

The normal distribution of many of the parameters in a metallurgical data set is broad. On top of this, the number of parameters provided can be large and may not necessarily cover the critical variables that impact the flotation process. Plus, the interactions are complex.

## A QUESTION OF DATA

Most well instrumented flotation plants generally have the following measurements online and available for modelling:

- throughput (t/h)
- water addition ($m^3/h$)
- per cent solids
- $P_{80}$

- reagent additions (L/min or g/t)
- air (generally as a percentage of valve opening)
- level (a percentage)
- pH
- OSA or ISA values (elemental assays (eg Cu, Pb, Zn, Fe) and percent solids) for critical process streams (eg feed, concentrate and tailing).

These parameters are perceived to be adequate for operating a plant. And there are a number of rules of thumb that apply to the data:

- The throughput and $P_{80}$ are related (ie an increase in throughput can lead to a coarsening of the grind).
- An increase in the feed grade can result in an increase in recovery.
- An increase in feed grade generally sees an increase in collector addition.
- The concentrate grade and recovery of inversely linked, that is as the concentrate grade is increased the recover tends to decrease.
- Increasing the collector addition, air and level tend to increase the recovery.

So, many of the parameters measured in the plant (as per the list above) are not independent and have an interdependence with one or more of the other parameters. These broad rules of thumb are generally common knowledge to the metallurgist but not known by the data scientist. Further, the distribution of this data is often quite broad. Figure 1 shows the distribution of the mill throughput (as tonnes per day (t/d)) and the copper feed grade for a concentrator treating a complex polymetallic ore. The mean throughput is 7095 t/d, with a spread between 5000 and 8400 t/d. Similarly, the average copper head grade of 1.81 per cent, ranging from 0.75 to 3.00 per cent. The spread is large and evident in all other parameters measured in this plant.

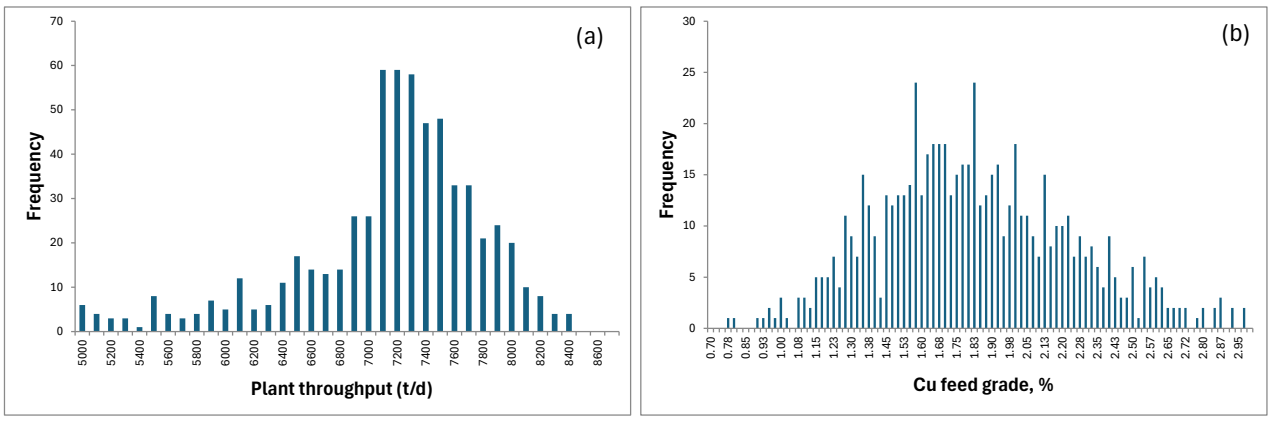



**FIG 1** – Distributions of (a) throughput, and (b) copper feed grade.

Considering the interdependence of the parameters and the broad distribution it is not unrealistic to expect that modelling this data will be difficult. Further, these parameters do not provide any information about the degree of liberation of the valuable and gangue minerals or an indication of the solution, pulp or surface chemistry of the system which are fundamental to successful flotation. It is well documented that to produce a saleable concentrate at an acceptable recovery by flotation it is necessary to prepare the valuable mineral particles such that they are well liberated from the gangue and strongly hydrophobic so that they attached to a bubble and are recovered into the concentrate process stream.

## WHAT IS MISSING

Measurement of liberation and hydrophobicity online and in real time is not currently available so there are two areas of research that could assist greatly to improve the algorithms developed for flotation plants:

1. Are there readily available proxies that could be used to infer mineralogy and hydrophobicity.
2. Create new sensors that can be used to measure critical parameters in the flotation process.

Without these advancements it is likely that the widespread adoption of model predictive control (or AI) will be limited.

In terms of proxies, utilising lime consumption data as a means for measuring an increase in either the amount of iron sulfide in the feed or the proportion of highly reactive iron sulfide for the same iron content in the feed may be a reasonable substitute for reactivity. That is, if the lime consumption increases it is probably a fair indication that the ore is more reactive probably because of an increase in iron sulfide content or type. It is therefore likely that the metallurgy is going to suffer, and it might be possible to counteract this through the introduction of oxygen in some form. While not a direct measure of liberation or hydrophobicity this type of analysis could provide indications for when the plant becomes more volatile. Further, if the volatility is measurable, it should be possible to develop strategies that lead to better metallurgical outcomes.

The measurement of pulp chemical parameters (pH, Eh, dissolved oxygen, temperature, oxygen demand and EDTA extractable metal ions) while fairly rudimentary variables they do provide insights into the chemical reactions occurring in the pulp. For instance, it is known that if the iron sulfide content increases the following changes in the pulp chemistry can be expected:

- For the same pH the lime consumption will increase.
- The Eh will shift to more reducing pulp potentials.
- The dissolved oxygen will decrease.
- There may be an increase in the pulp temperature if the iron sulfides start to oxidise.
- The oxygen demand will increase as the pulp becomes more reactive.
- The EDTA extractable metal ions are likely to increase.

These changes in pulp chemistry tend to be more favourable for iron sulfide flotation, so it is not unreasonable to expect concentrate grades and recovery of the valuable sulfide to deteriorate. Again, if these parameters were measured online and in real time it should be possible to develop strategies that lead to better metallurgical outcomes. Further, the strength of algorithms for model predictive control will improve.

Ultraviolet-visible spectroscopy (UV-vis) has been used extensively by researchers to measure collector uptake in sulfide mineral flotation. The CSIRO have extended this to measure residual collector in solution in plant pulps (Greet, Bruckard and MacKay, 2008). In effect this technology could provide insights into the hydrophobicity of the system under investigation, and if coupled with other measurements listed above could provide meaningful relationships that could be used to model flotation for improved metallurgical responses.

Tomography could offer exciting breakthroughs in measuring mineral liberation in three dimensions in a reasonable time frame. If such a sensor was commercially available, it would be possible to determine the liberation size of the valuable minerals in coarse size fractions of the rougher concentrate and use this data to drive the regrind circuit more efficiently in terms of energy consumption and metallurgical outcomes.

## FINAL COMMENTS

Firstly, I don’t consider myself to be a Luddite, I believe that technology is here to assist humans in their endeavours.

As for ‘AI’ at present it is not sentient, so it is little more than complex large language algorithms that contain the same biases as the humans who wrote the code. Yes, it is powerful and it is becoming more pervasive. I do understand that a significant proportion of the population do feel threatened as they might be made redundant by this technology. However, there is a second group who see this technology as a way of trimming the workforce to reduce costs and increase profits, not unlike the textile factory owners in the 17th and 18th centuries. But there is a third cohort who are probably more thoughtful and realise that this technology in its current form is a tool to assist in our endeavours. It is also apparent that as a metallurgical engineer I need to understand the basics so that I can check and challenge the answers given by AI.

Will AI run flotation? I suspect that someday in the future there will be sophisticated models that describe the flotation process that can be used for predictive process control that will include the complexities of mineral liberation and surface chemistry. To get there and reap the benefits significantly effort will need to be invested to develop the sensors to measure the critical parameters that make the flotation process tick.

## ACKNOWLEDGEMENTS

I acknowledge past generations who have faced change brought about by new technology and survived!

## REFERENCES

Greet, C J, Bruckard, W J and MacKay, D, 2008. Collector – Addition point and consumption, in *Proceedings of the MetPlant2008 Conference*, pp 287–301 (The Australasian Institute of Mining and Metallurgy: Melbourne).

National Press Club of Australia, 2026. IN FULL: Scientia Professor Toby Walsh Addresses the National Press Club of Australia, National Press Club of Australia. Available from: <https://www.youtube.com/watch?v=omCG6Lxjn2M>

# Development and application of a model-based uranium tails leach optimisation tool at Olympic Dam

*S J Oliver[1] and D Bouchard[2]*

1. Principal Technical Consultant, MathWorks, Sydney NSW 2067. Email: soliver@mathworks.com
2. Senior Metallurgist – Development Processing (Hydro/USX) Olympic Dam, Minerals Australia, BHP, Roxby Downs SA 5725 Email: dereck.bouchard@bhp.com

## ABSTRACT

The efficient recovery of uranium from concentrator tailings is a critical objective for hydrometallurgical operations treating complex, variable orebodies. This paper presents the development and initial deployment of a Tails Leach Optimisation Tool for a seven-tank sulfuric-acid uranium leach circuit at an Australian operation. The tool, implemented in MATLAB®, couples a phenomenological chemical-kinetic model of uranium dissolution with dynamic mass and energy balances for a cascade of continuous stirred-tank reactors (CSTRs), allowing each tank in the circuit to be modelled individually (Crundwell, 1995; Vetter, Barker and Turner, 1989).

Operational data are imported to identify key uncertainties – most notably, variable feed mineralogy and iron speciation – and to support dynamic model calibration. The calibrated model is then used to simulate plant performance, forecast operational outcomes, and optimise reagent dosing rates and tank temperature set points, subject to practical constraints on acid and oxidant addition, temperature limits and gelling risk. Preliminary application suggests that the approach can increase uranium recovery and improve reagent utilisation by enabling feed-forward, model-based decision support for operators in the presence of long residence times and delayed assay feedback (Niu *et al,* 2022).

The work builds on previous kinetic and reactor-modelling studies of uranium leaching, extending them toward a practically deployable optimisation and control tool for modern tailings leach circuits (Crundwell, 1995; Rubisov and Papangelakis, 2000; Dorfling *et al,* 2013).

## INTRODUCTION

Sulfuric acid leaching in mechanically agitated tanks remains central to conventional uranium milling, with crushed ore or flotation tailings treated in cascades of CSTRs to maximise uranium dissolution while managing acid and oxidant use (International Atomic Energy Agency (IAEA), 1990; Ring, 1979). Australian plants treating Olympic Dam–type ores process blends of uraninite, coffinite, and brannerite spanning fast to refractory leachability (Ring, 1979). Laboratory studies on synthetic analogues corroborate this behaviour: uraninite dissolves relatively quickly, coffinite more slowly, and brannerite is markedly resistant under comparable sulfate-leach conditions (Reynolds *et al,* 2018; Rashad *et al,* 2020).

In practice, this mineralogical variability combines with fluctuating feed blends, variable gangue acid consumption, and imperfect measurements to create a dynamic, hard-to-control leaching environment. Feeds originate from multiple upstream flotation and blending streams, with little scope for real-time feed control at the leach circuit (IAEA, 1990, 1993). Leach tanks operate in series, with a subset of seven in service depending on maintenance; lead tanks receive steam, sulfuric acid, and sodium chlorate additions that strongly influence dissolution kinetics. Process feedback is inherently slow, with hydraulic residence times of ~10 hrs and laboratory assay intervals of 4–6 hrs, limiting the effectiveness of purely feedback-based control strategies (Vetter, Barker and Turner, 1989; Sililo, 2016).

These interacting sources of variability limit what can be inferred from plant data alone and motivate the use of modelling to improve mechanistic understanding of leach-circuit behaviour. Approaches range from empirical regressions to phenomenological models based on mass and energy balances coupled with chemical kinetics (Crundwell, 1995; Rashad *et al,* 2020; Moussa *et al*, 2014). Dynamic CSTR-cascade models are particularly suited to process-control studies, with phenomenological

formulations offering better extrapolation and physical constraint handling than purely data-driven methods (Vetter, Barker and Turner, 1989; Rubisov and Papangelakis, 2000; Dorfling *et al,* 2013). Shrinking-core models can represent specific leach systems but are less convenient for resolving per-tank dynamics across long cascades under varying temperatures and reagent conditions (Crundwell, 1995; Bommer and Schechter, 1979). Population-balance methods provide powerful descriptions but require detailed, continuous particle-size measurements that are difficult to obtain in production environments (Crundwell, 1995).

These limitations have driven interest in optimisation-oriented modelling and control frameworks for leach circuits, including model-free adaptive control and optimisation strategies using process models or surrogates (Dong *et al,* 2023; Niu *et al,* 2022). In uranium systems, modelling efforts span laboratory-scale kinetic parameter estimation through to plant-scale dynamic models and expert systems (Sililo, 2016; Vetter, Barker and Turner, 1989). Nevertheless, real-time optimisation remains challenging because the process is slow and sparsely measured: residence times can exceed an operator's shift, assays arrive hours after sampling, and, over the same period, feed mineralogy, iron speciation, gangue acid consumption, and tank availability may change, delaying the observable impact of operating adjustments.

As a result, operators have limited ability to diagnose leach performance drivers or consistently steer the circuit toward higher uranium recovery and more efficient reagent use using intuition and delayed feedback alone. This motivates a forward-looking optimisation and decision-support tool capable of predicting 24–48 hr circuit behaviour for a given feed, plant configuration, and candidate operating strategy, while representing plant physics closely enough to support structured 'what-if' analysis and constrained optimisation under practical limits such as gelling risk and reagent caps.

In this context, a practically implementable, chemically grounded kinetic model for uranium leaching is required that can be embedded within a flow sheet-level simulator as the core of such a tool. The Tails Leach Optimisation Tool described here addresses this need by:

- Representing the key oxidation–reduction and dissolution reactions for the principal uranium species and the iron couple under sulfuric acid leaching conditions.
- Embedding these reactions within CSTR mass and energy balances for a multi-stage leach cascade.
- Calibrating uncertain kinetic and speciation parameters to recent plant operating data.
- Using the calibrated model for constrained optimisation of acid and oxidant addition and tank temperatures to maximise uranium recovery while managing reagent consumption and gelling risk.

Next, the paper outlines relevant uranium mineralogy and leaching chemistry, describes the kinetic model and plant representation, and then details parameter fitting, the response-optimisation framework, and qualitative results.

# URANIUM MINERALOGY AND LEACHING CHEMISTRY

## Uranium-bearing minerals in Olympic Dam-type ores

Uranium in iron-oxide copper–gold (IOCG)–style deposits. such as those in South Australia, commonly occurs in uraninite ($UO_2$), coffinite ($USiO_4$), and brannerite ($Uti_2O_6$), often in association with complex gangue minerals including feldspars, chlorites, and silicates (Ring, 1979; IAEA, 1993). Systematic sulfate-leach tests with synthetic uraninite, coffinite, and brannerite under conditions relevant to commercial practice show a clear hierarchy of leachability: uraninite dissolves most readily, coffinite is slower, and brannerite is significantly refractory (Reynolds *et al,* 2018; Rashad *et al,* 2020). Under typical acid sulfate-leach conditions, synthetic uraninite can be near-completely dissolved in a few hours, synthetic coffinite may require tens of hours, and synthetic brannerite may reach only partial uranium dissolution over extended residence times, with activation energies increasing from uraninite to brannerite (Reynolds *et al,* 2018).

Other kinetic studies on various uranium ores, including granitic and sandstone-hosted systems, demonstrate similarly strong dependencies on acid concentration, temperature, solid–liquid ratio,

and stirring speed, and confirm that diffusion and chemical-reaction control can both be rate-limiting depending on conditions (Moussa *et al*, 2014; Rashad *et al,* 2020; IAEA, 1990). These data provide a basis for selecting appropriate kinetic forms and parameter ranges in phenomenological models.

In plant operations processing blends of uraninite-, coffinite-, and brannerite-bearing material, the effective leach residence time required to achieve a given uranium extraction therefore depends strongly on the relative contributions of these mineral domains in the feed. Variability in ore type, particle size distribution, and mineral liberation across the feed streams translates into variability in overall leach kinetics, and, hence, in optimal operating conditions, motivating an adaptive, data-informed model calibration strategy.

## Oxidative dissolution and ferric–ferrous cycling

Under sulfuric-acid leaching conditions, the predominant uranium forms of interest are reduced uranium oxides represented here as $UO_2$ in the solid phase, and oxidised uranium represented here as $UO_3$ (with dissolved uranium commonly present as the uranyl ion, $UO_2^{2+}$) in the pregnant leach solution (IAEA, 1993). Two leaching pathways are typically considered:

- direct acid dissolution of oxidised uranium phases represented here as $UO_3$
- indirect, oxidant-mediated leaching where ferric iron acts as the oxidising agent for $UO_2$.

A convenient two-step representation for ferric-mediated oxidative dissolution is:

$$\mathrm{UO_2 + 2Fe^{3+} + H_2O \rightarrow UO_3 + 2Fe^{2+} + 2H^+} \quad (1)$$

$$\mathrm{UO_3 + 2H^+ \rightarrow UO_2^{2+} + H_2O} \quad (2)$$

Combining the two steps yields the overall uranium oxidation–reduction (redox) reaction commonly used in kinetic models:

$$\mathrm{UO_2 + 2Fe^{3+} \rightarrow UO_2^{2+} + 2Fe^{2+}} \quad (3)$$

Here, $UO_2$ in the solid phase is oxidised to the soluble uranyl species, while ferric iron is reduced to ferrous iron. Sustained $UO_2$ leaching therefore depends on continuous ferric iron regeneration via an appropriate oxidant, such as sodium chlorate, manganese dioxide, or oxygen (IAEA, 1993; Venter and Boylett, 2009). A typical ferric regeneration step in sulfate media can be represented generically as oxidation of $Fe^{2+}$ to $Fe^{3+}$, with the specific stoichiometry depending on the oxidant employed.

$$\mathrm{2Fe^{2+} + \frac{1}{3}ClO_3^- + 2H^+ \rightarrow 2Fe^{3+} + \frac{1}{3}Cl^- + H_2O} \quad (4)$$

The ferric–ferrous redox couple also underpins the measurement of oxidation–reduction potential (ORP), which is widely used as a proxy for the oxidising strength of the leach slurry. However, ORP measurements can become unreliable at low ferric concentrations or in slurries with significant interfering redox-active species, motivating the explicit inclusion of iron speciation in the kinetic model rather than relying solely on ORP control (Vetter, Barker and Turner, 1989; Sililo, 2016).

## Gangue reactions and silica gelling

Gangue mineral dissolution contributes substantially to acid consumption and can impose practical operating limits through phenomena such as silica gelling. Chlorite, feldspar, and other aluminosilicates can consume acid and release dissolved silica and aluminium, which under certain combinations of pH, temperature, and ionic strength can lead to the formation of polymerised silica gels (IAEA, 2001). These gels can impair downstream solid–liquid separation, foul equipment, and cause pumping difficulties.

Operationally, excessive acid addition in pursuit of higher uranium extraction can push the system into a regime where gangue dissolution and silica polymerisation dominate, compromising overall plant performance (IAEA, 2001). Therefore, the optimisation framework treats gelling as a soft or hard constraint, linking acid dosing and temperature to an empirical gelling index derived from plant experience and gangue dissolution models. While the current implementation focuses primarily on uranium and iron kinetics, the structure of the model allows explicit gelling reactions and solubility limits to be added in future work as thermodynamic and kinetic data are refined.

## MODELLING APPROACH

When selecting an appropriate modelling strategy for the leach circuit, both purely data-driven, non-parametric approaches and first-principles, parametric models were evaluated. Slow uranium leaching dynamics, combined with sparse plant measurements at 4–6 hr intervals, proved challenging for purely data-driven methods, which struggled to capture the long-time histories required to represent residence times of approximately 10 hrs and optimisation horizons of 24–48 hrs. Accounting for these limitations, a first-principles, chemically grounded modelling approach was selected.

The chosen framework couples a chemically motivated reaction network with dynamic mass and energy balances for each CSTR in the leach cascade. This section summarises the rationale for adopting a parametric model, the kinetic reaction network, the plant-level reactor representation, and the software environment used for implementation.

Figure 1 illustrates the simplified Simulink® uranium leaching circuit flow sheet. The plant comprises seven mechanically agitated tanks in series, fed by a mainstream and five bleed streams. Lead tanks are temperature-controlled via steam addition, and the first five tanks receive sulfuric acid and sodium chlorate dosing.

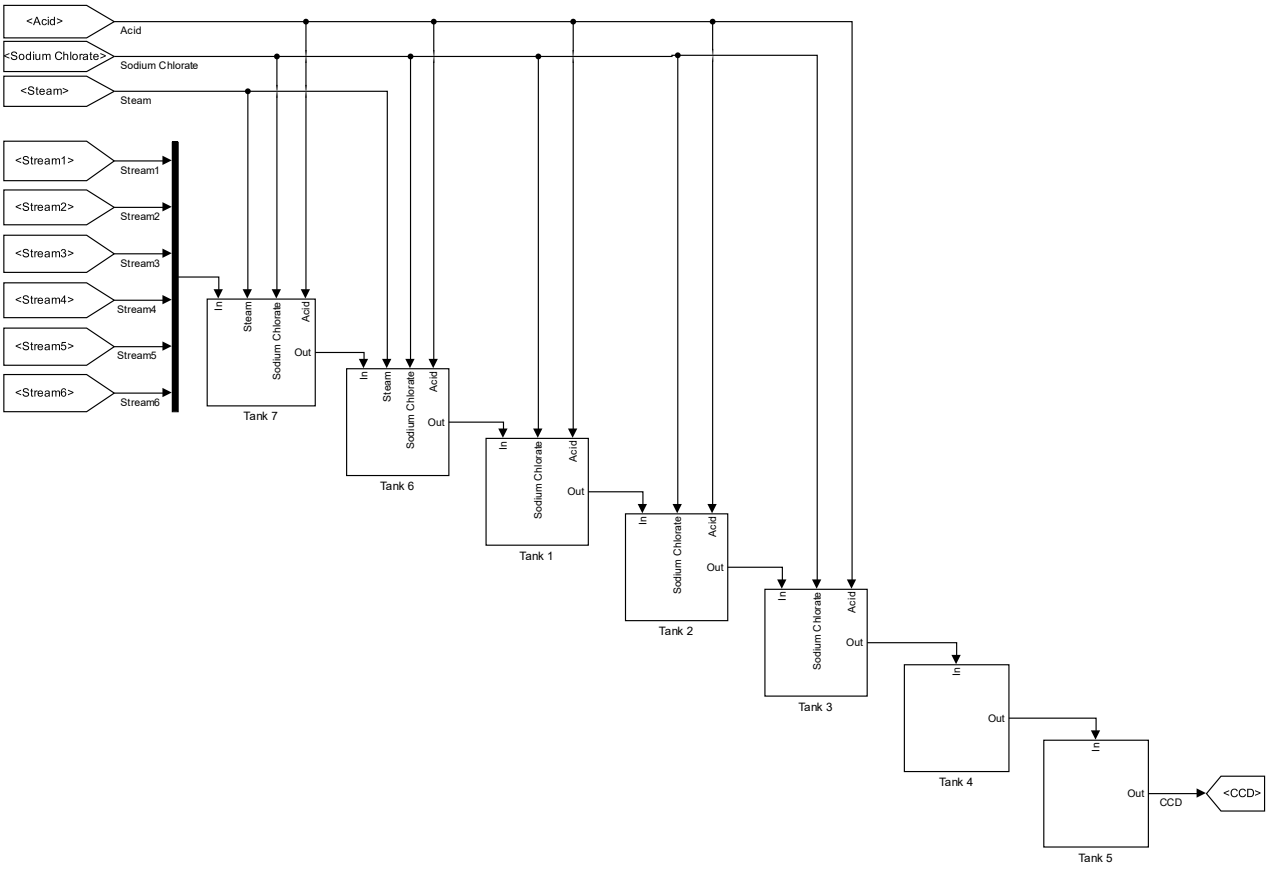



**FIG 1** – Simplified Simulink® flow sheet of the uranium leaching plant. It consists of seven tanks in series, fed by a mainstream and five bleed streams. Lead tanks are temperature controlled by steam, and the first five tanks are dosed with acid and sodium chlorate.

### Rationale for a parametric model

Purely data-driven, non-parametric modelling approaches—such as machine learning and deep learning—were initially evaluated for point-to-point uranium extraction prediction and reagent consumption based on historic operating conditions. Although Gaussian process regression (GPR) and related non-parametric models can achieve strong predictive performance within the convex hull of the training data, they exhibit well-known limitations when applied to extrapolation beyond observed operating regimes, to edge cases where key species concentrations approach zero, and

to systems exhibiting long time-history effects associated with extended residence times (Crundwell, 1995; Rubisov and Papangelakis, 2000).

With appropriate preprocessing to account for differing process delays and measurement lags, GPR-based models were found to outperform other non-parametric alternatives in terms of predictive accuracy. However, structural limitations remain. In the leach circuit examined, the effective reaction residence time is approximately 10 hrs, while concentration measurements are typically available only every 4–6 hrs, and optimisation horizons of 24–48 hr are of practical interest. Under these conditions, non-parametric models struggle to reliably capture the embedded long-memory dynamics of the system.

A parametric, mechanistic modelling framework based on chemical kinetics and reactor mass balances is therefore better suited to this application. Such models naturally embed process memory, explicitly represent reaction pathways, and enforce fundamental physical constraints, including non-negativity of species concentrations and conservation of mass (Bommer and Schechter, 1979; Dorfling *et al,* 2013).

Beyond improved physical fidelity, the parametric approach substantially reduces estimation problem dimensionality. Rather than fitting an arbitrary functional mapping from operating conditions to leach performance, a limited set of kinetic, equilibrium, and speciation parameters is estimated to reproduce observed plant behaviour. This reduction in degrees of freedom improves robustness in the presence of sparse and noisy plant data, while also enabling the systematic incorporation of prior knowledge derived from laboratory-scale kinetic studies and previous modelling efforts (Moussa *et al*, 2014; Rashad *et al,* 2020; Silillo, 2016).

## Chemical-kinetic model

The leaching chemistry is represented by a coupled network of homogeneous reactions describing:

- Oxidation and dissolution of an effective $UO_2$ solid pool (aggregating uraninite-, coffinite- and brannerite-derived $UO_2$).
- Potential direct dissolution of $UO_3$-bearing phases.
- Ferric–ferrous redox cycling, including oxidant regeneration.
- Acid consumption by gangue reactions.
- Provision for future inclusion of silica polymerisation and gelling behaviour.

Reaction rates are expressed using Arrhenius-type kinetics:

$$r_i = k_i \exp\left(-\frac{E_{a,i}}{RT}\right) f_i(\{C_j\}),$$

Where:

| | |
|---|---|
| $r_i$ | is the rate of reaction *i* |
| $k_i$ | the pre-exponential factor |
| $E_{a,i}$ | the activation energy |
| $R$ | the gas constant |
| $T$ | the temperature |
| $f_i(\{C_j\})$ | a function of relevant species concentrations |

These typically take the form of power-law dependencies on dissolved uranium, ferric and ferrous iron, hydrogen ion, and oxidant concentrations (Crundwell, 1995; Rashad *et al,* 2020).

The model aggregates different uranium minerals into effective $UO_2$ and $UO_3$ pools, with separate rate constants to capture the differing leachability of uraninite-, coffinite- and brannerite-like domains (Reynolds *et al,* 2018; Silillo, 2016). Effective parameters—including the $UO_2/UO_3$ feed ratio, $Fe^{2+}/Fe^{3+}$ speciation and apparent rate constants for uranium oxidation, gangue dissolution, and redox regeneration—are treated as tuneable during model calibration.

The reaction network shown in Figure 2 is implemented using SimBiology® (The MathWorks, Inc., 2025b), which enables graphical definition of species, reactions, and kinetic laws, and automatically generates the corresponding system of ordinary differential equations (ODEs) from mass-balance principles. Deterministic ODE solvers are used for simulation, facilitating batch-scale studies for sensitivity analysis and comparison with laboratory and pilot-plant leach tests, consistent with prior leaching-reactor modelling studies (Rubisov and Papangelakis, 2000; Dorfling *et al,* 2013).

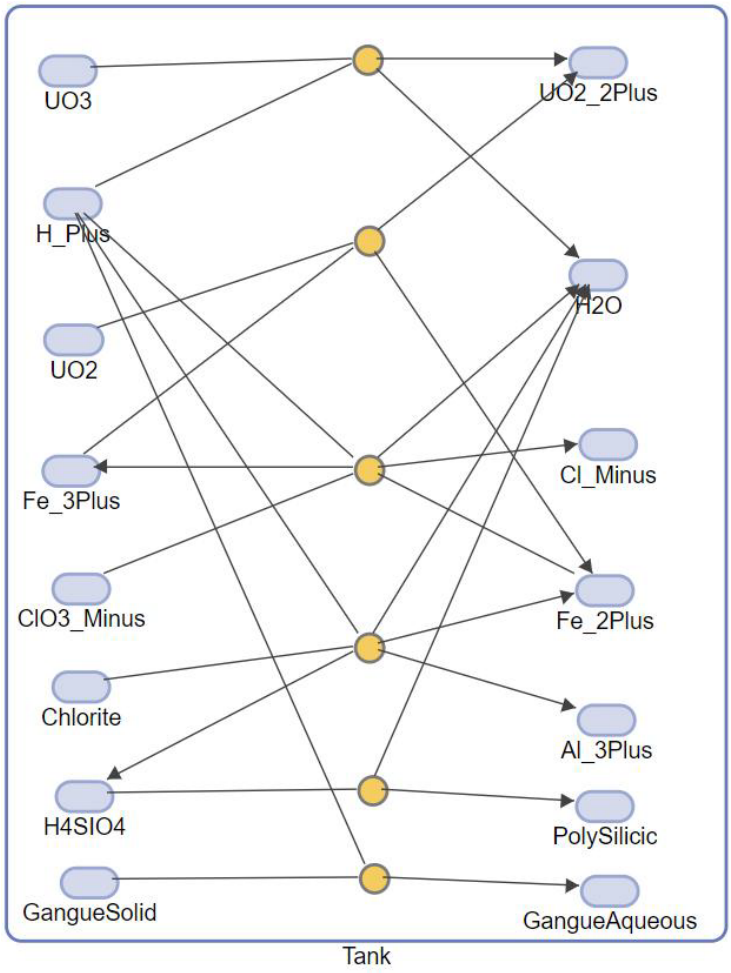



**FIG 2** – U leaching reaction kinetics model in SimBiology®. Out of the 15 species included in the model, the following are involved in the primary reactions. UO3 and UO2 represent the two solid uranium species $UO_3$ and $UO_2$. UO2_2Plus represents the dissolved uranium $UO_2^{2+}$. Fe_2Plus and Fe_3Plus is $Fe^{2+}$ and $Fe^{3+}$. ClO3_Minus is sodium chlorate. H_Plus is acid.

Figure 3 shows representative batch-simulation results from the first-principles kinetic model. As acid concentration ($H^+$) approaches zero, direct dissolution of $UO_3$ ceases, and uranium recovery proceeds only through oxidation-assisted dissolution of $UO_2$ using the remaining sodium chlorate. Excess acid is consumed by gangue reactions. For clarity, only seven of the 15 modelled species are shown.

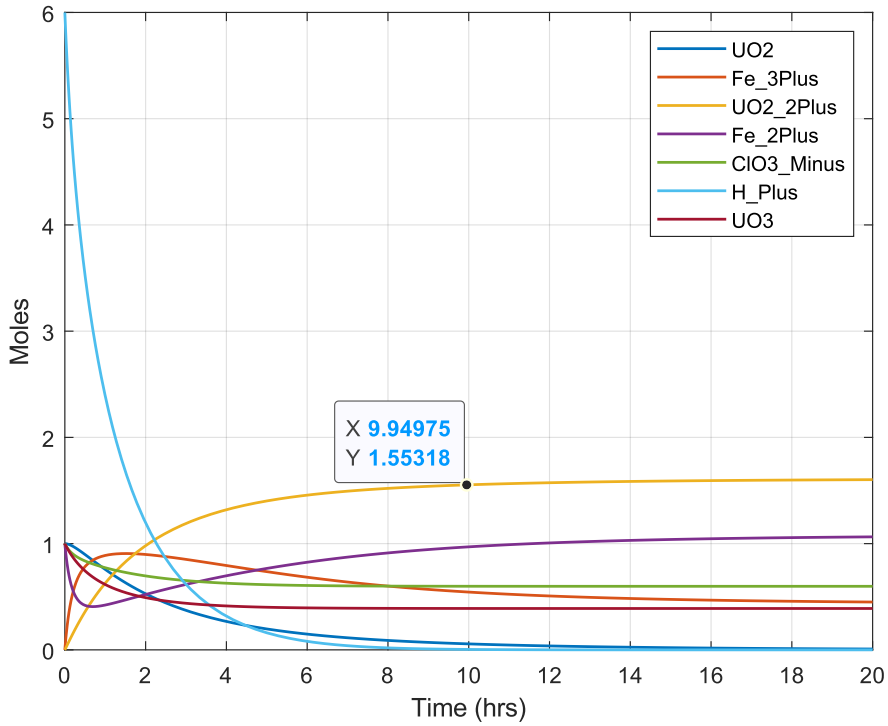



**FIG 3** – Batch simulation results from the first principal modelling approach. Notice when the acid (H_Plus) approaches zero, the direct leaching of $UO_3$ (UO3) stops. At this point, only the remaining $UO_2$ (UO2) continues to leach to uranium liquor $UO_2^{2+}$ (UO2_2Plus) using the remaining Sodium Chlorate (ClO3_Minus). The excess Acid (H_Plus) is consumed by leaching the gangue material. Only seven out of the 15 modelling species concentrations are shown here.

## Plant and reactor modelling

Once validated at the batch level, the ODE system generated in SimBiology® is exported to MATLAB® and embedded within a Simulink® flow sheet model. These ODEs provide the reaction-source terms for dynamic mass and energy balances within custom CSTR blocks.

The leach circuit is represented as a cascade of CSTRs corresponding to the mechanically agitated tanks. The nominal configuration comprises seven tanks in series, with between three and five in operation at any time, depending on maintenance. Each tank is modelled as a perfectly mixed reactor with specified slurry volume, temperature, feed, and discharge flow rates, and reagent-addition streams for acid, oxidant, and dilution water (Vetter, Barker and Turner, 1989; IAEA, 1993).

Dynamic mass and energy balance equations are adapted from standard CSTR formulations (The MathWorks, Inc., 2025a) and generalised from single-reaction examples to a vector-based implementation incorporating the full kinetic reaction network. Similar approaches have been applied in uranium leaching and related hydrometallurgical reactor models (Crundwell, 1995; Bommer and Schechter, 1979). An energy balance accounts for steam heating, reaction enthalpies, and heat losses, although in practice, tank temperatures are often tightly regulated via steam flow.

Each leach tank is represented by a separate CSTR block, and the blocks are connected in series to form the complete circuit flow sheet. Mainstream feeds, multiple bleed streams, reagent-dosing lines, bypasses, and tank-availability flags are parameterised, allowing all practical operating modes to be simulated within a single model. Plant operating data—including flow rates, tank levels, temperatures, acid and oxidant addition rates, oxidation–reduction potential measurements, and periodic uranium and iron assays—are fed into the model as inputs or calibration targets.

This phenomenological CSTR-in-series representation follows earlier dynamic uranium-leaching models developed for process-control studies, which demonstrated that such models can capture the dominant dynamic behaviour relevant to control and optimisation even when some kinetic parameters remain uncertain (Vetter, Barker and Turner, 1989; Sililo, 2016).

## PLANT OPERATIONAL OPTIMISATION

The objective of the optimisation framework is to leverage the calibrated dynamic leach-circuit model to predict plant behaviour over a 24–48 hr horizon, enabling operators—and potentially an automated supervisory control layer—to make informed decisions regarding leach-plant set points. This forward-looking capability is particularly valuable given the long residence times of the circuit and the delayed availability of key measurements.

A central challenge is that leaching dynamics vary not only with plant configuration (eg tank availability and reagent-dosing locations) but also with changes in feed mineralogy and chemistry, which are only indirectly observed. Optimisation-driven routines are therefore used both to continuously adapt model parameters to current operating conditions and to identify operating strategies that improve metallurgical and economic performance.

### Numerical optimisation approach

The same Bayesian optimisation framework employed for model parameter fitting is repurposed for response optimisation, with the objective function redefined to reflect economic or metallurgical performance and the decision variables taken as time-varying control set points. For each candidate operating strategy, the dynamic CSTR-cascade model is simulated over the forecast horizon using calibrated kinetic parameters and anticipated feed conditions. Model outputs—including uranium extraction, acid and oxidant consumption, and gelling-risk indicators—are aggregated into a scalar objective function, with penalties applied for constraint violations.

This approach treats the underlying simulator as a black box, allowing the use of complex, highly non-linear models without requiring analytical gradients. It naturally accommodates discrete or piecewise-constant control moves and can handle non-convex objective landscapes. The primary trade-off is computational cost, which is mitigated through parallel simulation, careful selection of surrogate models and dimensionality reduction in the decision space (Niu *et al,* 2022).

Figure 4 illustrates a representative Bayesian-optimisation response surface, showing evaluated operating points (blue markers), the current best solution (red star), and the next candidate selected by the acquisition function (black marker), which balances exploration and exploitation.

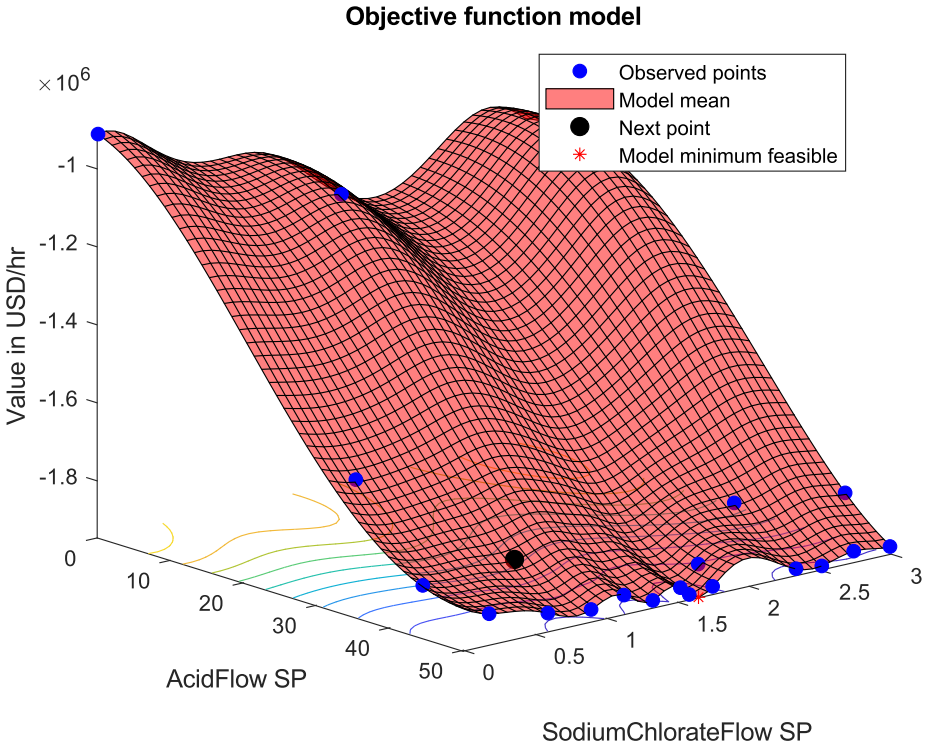



**FIG 4** – Bayesian Optimisation response surface. Include points for each function evaluation (blue dots), current maximum point (red star), and next point based on the Bayesian optimisation's acquisition function that balances exploration and exploitation trade-off (black dot).

## Model parameter fitting

Model calibration is performed on a rolling window of recent plant data, typically spanning approximately one week, to ensure that the model tracks slow changes in feed characteristics, equipment condition, and measurement biases. In this context, the fitted parameters represent uncertainty in the effective feed composition and reactivity under the current plant configuration.

The following effective parameters are adjusted during calibration:

- The ratio of $UO_2$ to $UO_3$ in the feed ($UO_2/UO_3$ ratio), representing the relative contributions of more readily leachable and refractory uranium species.
- The ratio of $Fe^{2+}$ to $Fe^{3+}$ in the feed ($Fe^{2+}/Fe^{3+}$ ratio), capturing the redox state of iron entering the circuit.
- Effective rate constants for the primary $UO_2$ oxidation reaction, dissolution of refractory $UO_2$ species, ferric regeneration and gangue acid consumption.
- Parameters associated with an empirical gelling-risk index, linking acid addition and temperature to the likelihood of silica-related operating issues.

Calibration is formulated as an optimisation problem in which the parameter vector is chosen to minimise a weighted sum of squared deviations between model predictions and measured plant variables over the calibration window. Typical calibration targets include dissolved uranium concentrations and iron speciation at selected tanks, overall uranium extraction across the cascade and, where available, oxidation–reduction potential measurements (Vetter, Barker and Turner, 1989; Sililo, 2016).

Bayesian optimisation, as implemented in the MATLAB® Statistics and Machine Learning Toolbox™, is used as the outer-loop optimiser. A surrogate model—typically based on Gaussian process regression—is constructed to approximate the mapping from parameter values to the calibration objective, and an acquisition function selects promising parameter sets for evaluation. This approach is well suited to noisy objective functions and modest-dimensional parameter spaces, particularly when each function evaluation requires a computationally expensive dynamic simulation.

Each candidate parameter set is evaluated by simulating the leach circuit over the calibration period using recorded operating data as inputs and computing the discrepancy between simulated and measured uranium and iron concentrations. Best-performing parameter sets are propagated forward as initial conditions or priors for subsequent calibration windows, providing continuity over time.

Figure 5 compares model-predicted uranium species inventories with available plant measurements for a representative calibration period. Although spot measurements of dissolved uranium were available only for a single tank, the model captures the progressive depletion of solid uranium species and the corresponding increase in dissolved uranium along the cascade.

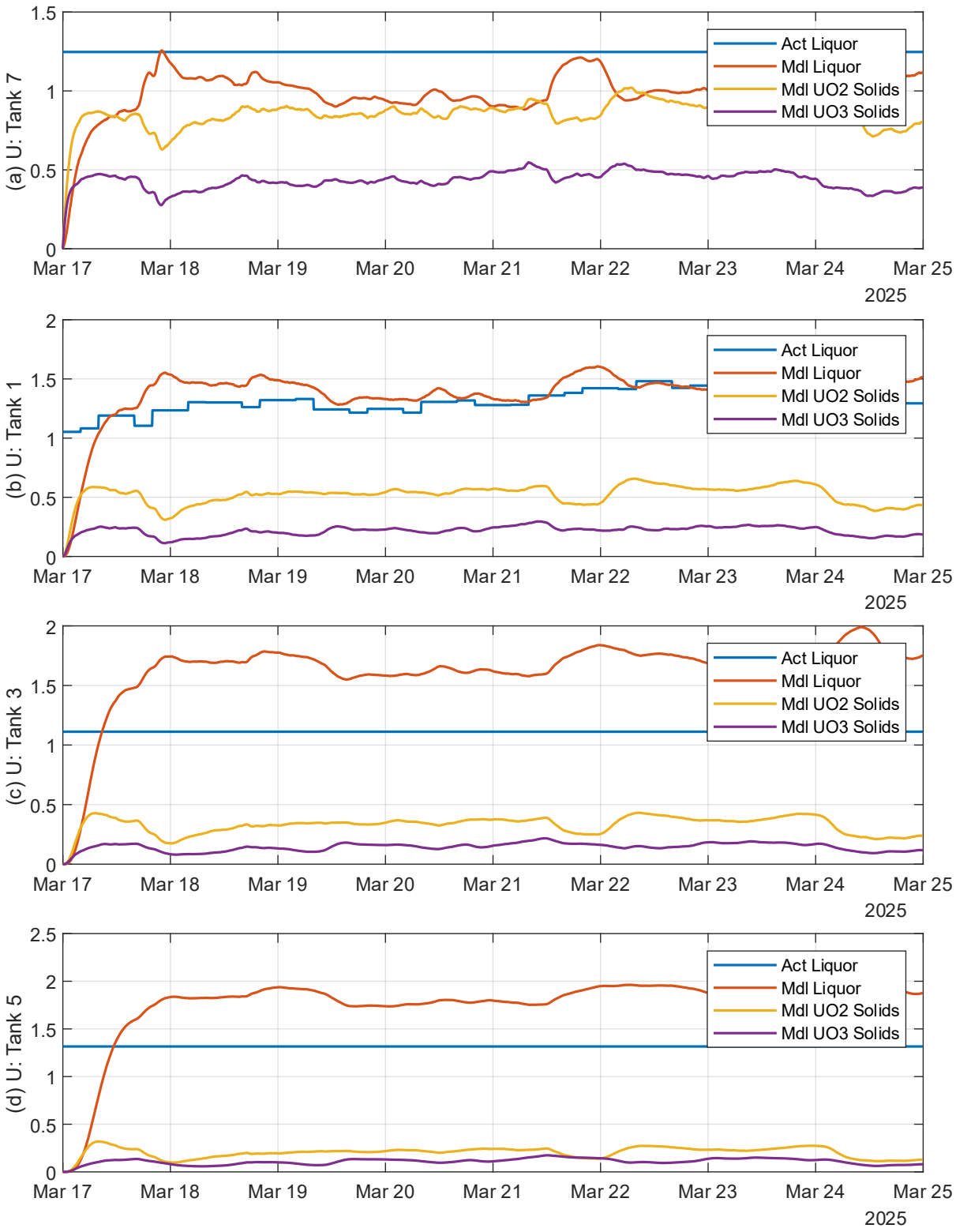



**FIG 5** – The model of uranium species concentrations in moles compared with the measurements. In this case, only spot measurements of the dissolved uranium in liquor (Act Liquor) were captured for tank 1, which in this configuration, is the second tank in series. During this test, four tanks (Tank 7, 1, 3, and 5) were active. Notice the concentration of the uranium in solids (Mdl UO2 Solids and Mdl UO3 Solids) reduces as it moves through the tanks, and that the relative concentration of the dissolved uranium in liquor (Mdl Liquor) increases.

Figure 6 shows the model's accuracy at predicting uranium leached one day ahead compared to the actual uranium leached. These results simulate the tools usage training the model based on the last seven days of plant operational data and then simulating the model one day ahead to determine a

predicted value of leached uranium. This procedure was swept forward through time. The average predictive performance was 82.5 per cent. In most cases, deviations were due to step changes in material processed, outages, or plant operational changes during the model simulation period.

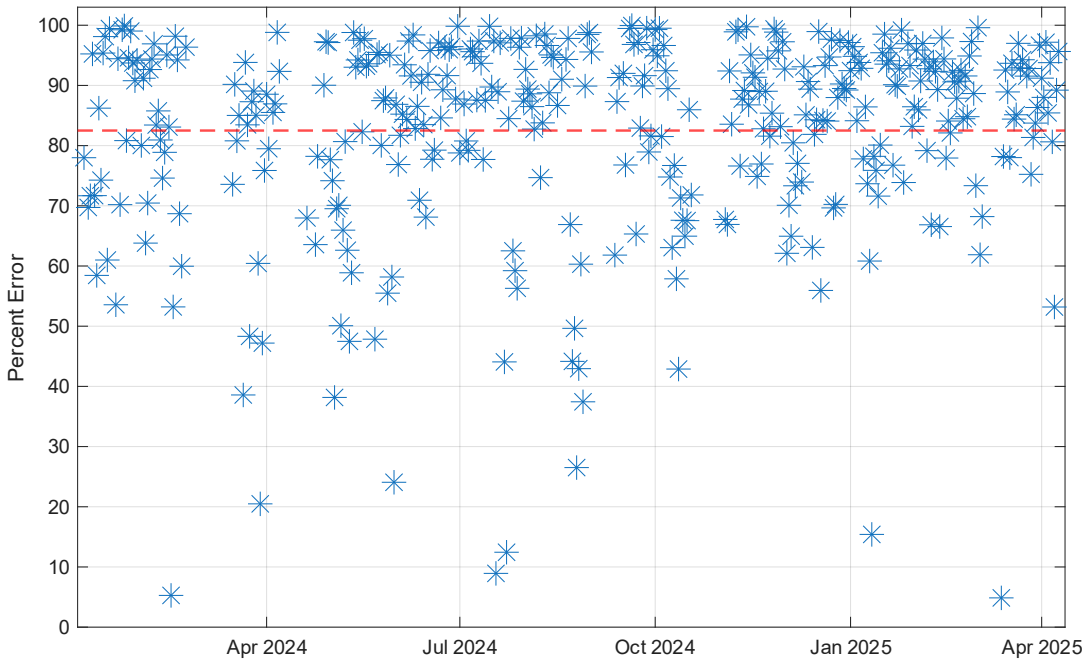



**FIG 6** – The accuracy when comparing the actual and model-predicted amount of leach uranium (blue dots) and the mean accuracy of 82.5 per cent (red dotted line). For each evaluation point, the model is fitted to the prior seven days of data and then simulated forward to predict the total leached uranium for the next day.

## Response optimisation

Once calibrated, the model is operated in predictive mode to evaluate the impact of alternative operating strategies over a 24–48 hr horizon. The primary optimisation objective is to maximise uranium recovery from the feed while constraining acid and oxidant consumption to economically and operationally acceptable levels. A secondary objective is to avoid operating regimes associated with elevated gangue dissolution and silica gelling risk.

The principal decision variables considered are:

- sulfuric-acid dosing rates to the lead tanks
- sodium-chlorate dosing rates
- tank-temperature set points.

These variables are represented as piecewise-constant or slowly varying profiles over the forecast horizon, subject to actuator limitations such as maximum ramp rates and dosing capacities. The optimisation algorithm searches over admissible control profiles to identify those that provide the best trade-off between uranium extraction and reagent usage while satisfying all process constraints (Niu *et al,* 2022).

The optimisation objective is expressed in economic terms as plant profit, defined as the value of recovered uranium minus reagent costs. While simplified, this formulation provides a transparent link between metallurgical performance and operating decisions and can readily be extended to include additional cost terms.

Figure 7 presents representative response-optimisation results, comparing baseline and optimised operation. Although set points were adjusted at the start of the optimisation window, the impact on uranium recovery became evident only after approximately 12 hrs, reflecting the long residence time of the leach circuit and underscoring the importance of predictive optimisation.

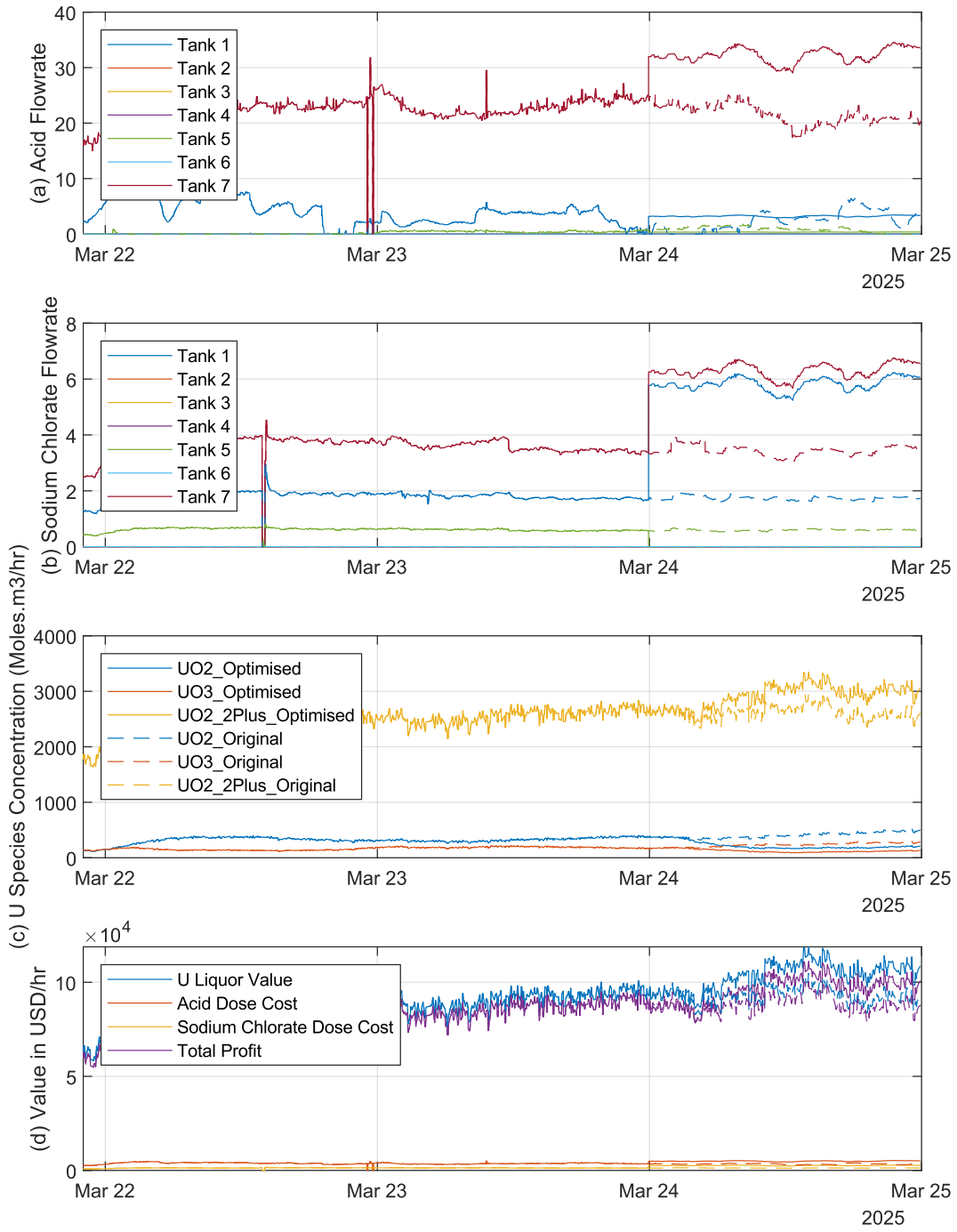



**FIG 7** – Response optimisation results highlighting the difference between the original response before tuning (dotted line) and the optimised response (solid line): (a) acid flow rates to each tank; (b) sodium chlorate flow rates to each tank; (c) uranium solids and dissolved in liquor; and (d) operations total profit (uranium value – reagent costs).

## Constraints and gelling considerations

The optimisation is subject to a range of constraints reflecting equipment limits, safety considerations, and product-quality requirements. These include:

- Upper bounds on tank temperatures to protect rubber-lined vessels and limit excessive gangue dissolution.
- Bounds on acid and oxidant dosing rates imposed by pumping and storage capacities.
- Limits on allowable changes in redox potential and pH to avoid off-spec solution conditions.

- Soft or hard constraints on a gelling-risk index, informed by empirical correlations between dissolved silica, aluminium, temperature and pH, as well as plant experience (IAEA, 1993).

In the current implementation, gelling risk is handled conservatively through constraints on combinations of acid dosing and temperature known to elevate risk. Future work will focus on embedding an explicit silica-polymerisation sub-model, drawing on broader hydrometallurgical and autoclave-leaching literature (Rubisov and Papangelakis, 2000).

## TAILS LEACH OPTIMISATION TOOL WORKFLOW

The Tails Leach Optimisation Tool is implemented as a user-interface-driven application designed to support operational decision-making for uranium leach circuits. A typical session is initiated by an operator or site metallurgist to assess current plant performance, update the model to reflect prevailing conditions, and identify operating set points for the upcoming production period.

The workflow is structured as an iterative, closed-loop process comprising the following stages:

- **Data import and context selection –** Plant operating data are imported directly via a live connection to the site data historian (AVEVA PI). Key process variables—including flow rates, temperatures, reagent-dosing rates, and available assay data—are downloaded and reviewed within the tool. The user selects a recent time window representative of current operating conditions, providing the context for subsequent model calibration and optimisation.
- **Model parameter fitting –** Initial parameter values and admissible bounds are defined for the subset of model parameters that characterise the effective feed composition and reaction kinetics. The user may adjust these parameters manually, guided by metallurgical experience, or invoke an automated optimisation routine to perform parameter fitting. The fitting process aligns the model with recent plant behaviour, ensuring that predictions reflect current feed characteristics, plant configuration, and operating state.
- **Response optimisation and set point selection –** With the model calibrated, it is used in predictive mode to evaluate plant behaviour over a 24–48 hr forecast horizon. The user can explore ‘what-if’ scenarios by manually adjusting sulfuric-acid dosing, sodium-chlorate addition, and tank-temperature set points, or can launch an automated optimisation routine to identify set point profiles that maximise plant performance subject to operational constraints. Once a preferred strategy is selected, the resulting set points can be exported for implementation in the plant control system.

By providing a virtual environment in which operating strategies can be tested before implementation, the workflow enables operators and site metallurgists to experiment safely with changes that would be impractical to evaluate directly on the physical leach circuit. Given the long residence times and delayed feedback inherent to uranium leaching operations, this capability is critical for reducing operational risk, improving confidence in set point changes, and supporting more proactive, optimisation-driven plant operation.

## RESULTS AND DISCUSSION

The optimisation procedure was evaluated using approximately one year of historic plant operating data. For each simulated operating day, a rolling window of the preceding seven days of plant data was used to calibrate the model, after which the fitted model was applied to predict and optimise leach-plant performance over the subsequent 24 hr period. Across this back-testing exercise, the model predicted plant leaching performance with approximately 90 per cent accuracy for more than 80 per cent of the evaluated days. In these cases, the optimisation routine identified operating strategies that improved predicted plant performance, most commonly through increases in one or both reagent addition rates.

Model performance was sensitive to the selection of the historical data window used for calibration. Windows that coincided with plant shutdowns, major maintenance events, or sensor failures resulted in poorly conditioned models and degraded predictive performance. During the back-testing exercise, an automated data-selection procedure was applied to filter unsuitable calibration periods; however, this procedure was not exhaustive. The quality of the selected calibration window therefore

remains a key operational risk, particularly if unsuitable data are inadvertently selected during routine tool use.

The procedure is also sensitive to changes in feed material during the prediction horizon. While the rolling-window calibration captures gradual changes in feed properties, abrupt shifts in mineralogy or chemistry occurring after calibration can reduce forecast accuracy. Selection of an appropriate calibration-window length therefore involves a trade-off: windows that are too long risk averaging over changing feed characteristics, while windows that are too short may contain insufficient information to reliably estimate model parameters.

Due to confidentiality constraints, results are presented qualitatively, with emphasis on model behaviour and the practical utility of the tool as an optimisation and decision-support system. Calibration studies indicate that the phenomenological model reproduces the dominant trends in uranium extraction and iron speciation across the leach-tank cascade under varying feed compositions and operating conditions. In particular, the model captures the sensitivity of overall extraction to acid and oxidant dosing, feed redox state and tank temperatures, consistent with published kinetic studies and established plant experience (Crundwell, 1995; Rashad *et al,* 2020; Reynolds *et al,* 2018).

Operators interact with the optimisation tool through a graphical interface that displays predicted profiles of uranium concentration, redox potential, acid consumption, and gelling-risk indicators across the tanks and over time for candidate operating strategies. By comparing these scenarios, site metallurgists gain insight into the dynamic response of the circuit and can select set points that balance uranium recovery, reagent cost, and operational risk. In this way, the tool supports a transition from reactive, feedback-only operation based on delayed assays toward more proactive, feed-forward decision-making informed by mechanistic understanding of the leaching process (Sililo, 2016).

## CONCLUSIONS

A chemically grounded kinetic model for sulfuric-acid uranium leaching has been developed and embedded within a dynamic CSTR-in-series representation of a seven-tank leach cascade treating flotation tailings. The model captures the principal oxidative dissolution pathways for $UO_2$-bearing minerals, ferric–ferrous redox cycling, and gangue acid consumption, and is calibrated to plant operating data using Bayesian optimisation. The calibrated model forms the core of a Tails Leach Optimisation Tool that searches over feasible profiles of acid and oxidant dosing and tank temperatures to improve uranium recovery while managing reagent consumption and gelling risk.

By embedding phenomenological kinetics within a flow sheet-level simulator, the approach combines the extrapolative robustness of first-principles models with the flexibility of modern optimisation algorithms. The work builds on earlier studies of uranium-leach kinetics and dynamic reactor modelling by extending these concepts into a practically deployable decision-support framework for contemporary tailings leach operations (Crundwell, 1995; Vetter, Barker and Turner, 1989; Rubisov and Papangelakis, 2000; Dorfling *et al,* 2013).

Future work will focus on:

- Refining the representation of uranium mineralogy by explicitly distinguishing uraninite-, coffinite-, and brannerite-derived contributions.
- Incorporating an explicit silica-gelling sub-model and associated constraints.
- Extending the optimisation framework to include downstream solid–liquid separation and solvent-extraction units.
- Exploring tighter integration with model-predictive control frameworks for closed-loop implementation, building on recent advances in model-based and model-free leach-circuit control (Dong *et al,* 2023; Niu *et al,* 2022).

Further validation of the reaction-rate expressions through targeted laboratory testing would also strengthen confidence in the kinetic formulation. In this context, hybrid approaches that combine

mechanistic models with data-driven techniques may offer a pathway to identifying non-linear influences not fully captured by the current rate laws.

## ACKNOWLEDGEMENTS

The authors acknowledge BHP's innovation team for supporting the initiative, and the Olympic Dam operating site's metallurgy and operations teams for providing data and process insight. Thank you to colleagues involved in the implementation of the model and the software application.

## REFERENCES

Bommer, M P and Schechter, R S, 1979. Mathematical modelling of in-situ uranium leaching, *Society of Petroleum Engineers Journal*, 19(6):393–400.

Crundwell, F K, 1995. Progress in the mathematical modelling of leaching reactors, *Hydrometallurgy*, 39(1–3):1–20.

Dong, S, Zhang, Y, Zhou, X, Niu, D and Wang, X, 2023. Model-free adaptive control of hydrometallurgy cascade gold leaching process with input constraints, *ACS Omega*, 8(7):6559–6570.

Dorfling, C, Akdogan, G, Bradshaw, S M and Eksteen, J J, 2013. Modelling of an autoclave used for high pressure sulphuric acid/oxygen leaching of first stage leach residue, Part 1: model development, *Hydrometallurgy*, 139:16–25.

International Atomic Energy Agency (IAEA), 1990. Manual on laboratory testing for uranium ore processing, IAEA-TECDOC-313 (International Atomic Energy Agency: Vienna).

International Atomic Energy Agency (IAEA), 1993. Uranium extraction technology, Technical Reports Series No. 359 (International Atomic Energy Agency: Vienna).

International Atomic Energy Agency (IAEA), 2001. Manual of acid in situ leach uranium mining technology, IAEA-TECDOC-1239 (IAEA: Vienna).

MathWorks, Inc, 2025a. CSTR Model, MATLAB and Simulink, Model Predictive Control Toolbox documentation, The MathWorks, Inc, USA. Available from: <https://www.mathworks.com/help/mpc/gs/cstr-model.html> (Accessed: 9 March 2026).

MathWorks, Inc, 2025b. SimBiology Documentation, MATLAB and Simulink documentation, The MathWorks, Inc, USA. Available from: <https://www.mathworks.com/help/simbio/index.html> (Accessed: 9 March 2026).

Moussa, M A, Daher, A M, Omar, S A, Khawassek, Y M, Haggag, E A and Gawad, E A, 2014. Kinetics of leaching process of Uranium from El-Missikat shear zone Eastern Desert, Egypt, *Journal of Basic and Environmental Sciences*, 1:65–75.

Niu, D, Liu, X, Liu, Y and Jia, M, 2022. Optimisation control of hydrometallurgical leaching process based on IDE-MPC, *Minerals Engineering*, 176:107341.

Rashad, M M, Mohamed, S A, El Sheikh, E M, Mira, H E, Abd El Wahab, G M and Zaki, S A, 2020. Kinetics of uranium leaching process using sulfuric acid for Wadi Nasib ore, South western Sinai, Egypt, *Aswan University Journal of Environmental Studies*, 1(2):171–182.

Reynolds, H S, Ram, R, Liu, X, Niu, G, Shanks, R A, Bhargava, S K and Pownceby, M I, 2018. Kinetics of uranium extraction from coffinite – a comparison with other common uranium minerals, *Transactions of Nonferrous Metals Society of China*, 28(10):2135–2142.

Ring, R J, 1979. Leaching characteristics of Australian uranium ores, *The AusIMM Proceedings*, pp 1483–1497.

Rubisov, D H and Papangelakis, V G, 2000. Sulphuric acid pressure leaching of laterites – a comprehensive model of a continuous autoclave, *Hydrometallurgy*, 58(1):89–101.

Sililo, B L, 2016. Modelling uranium leaching kinetics, MSc thesis, University of Pretoria.

Venter, R and Boylett, M, 2009. The evaluation of various oxidants used in acid leaching of uranium, in *Proceedings of the Hydrometallurgy Conference 2009,* pp 445–456 (The Southern African Institute of Mining and Metallurgy: Johannesburg).

Vetter, D A, Barker, I J and Turner, G A, 1989. A dynamic uranium-leaching model for process-control studies, *Journal of the South African Institute of Mining and Metallurgy*, 89(11):347–354.

# Mill Operators

# Design and commissioning

# Woodlawn Mine restart (take two)

*C R Dorsch[1] and S Oats[2]*

1. Processing Specialist, Develop Global Limited, Tarago NSW 2580.
   Email: carl.dorsch@develop.com.au
2. Metallurgy Superintendent, Develop Global Limited, Tarago NSW 2580.
   Email: steven.oats@develop.com.au

## ABSTRACT

Woodlawn is a polymetallic volcanogenic massive sulfide deposit located in the Lachlan Ford belt in New South Wales. The mine has had a long operating history beginning with open cut production in 1978, conversion to underground in 1987, first mine closure in 1998, first restart in 2019 and second mine closure in 2020. In 2022, Develop Global Limited (Develop) acquired the project and updated the plant design to address historical issues which eventually lead to the second re-commissioning in 2025.

The complex ore deposit is split into two distinct mineralisations: the ‘clean copper ore’ which contains predominantly chalcopyrite and the ‘polymetallic ore’ containing chalcopyrite, sphalerite and galena. Develop’s treatment strategy was to segregate the clean copper ore, allowing the opportunity for the concentrator to maximise the recovery of copper where minimal competing sulfides are present. Due to the simpler nature of this flotation, the restart project focused on starting the plant on the copper ore first in March 2025. This strategy was significantly beneficial due to identifying plant problems early on, promoting faster cash flow for the business, setting up effective training for new operators while conserving the high-value polymetallic ore that’s more challenging to process than simple copper ore. The metallurgical and operational lessons from the copper ore processing provided momentum to help achieve successful ramp up of the polymetallic ore. Overall, 2025 saw great success, with key targets achieved and improvement opportunities identified ready for 2026.

## INTRODUCTION

The Woodlawn mine is a zinc-copper-lead-gold-silver volcanogenic massive sulfide (VMS) deposit located in the Lachlan Fold belt in New South Wales, Australia – 250 km south-west of Sydney and 50 km north-east of Canberra. The mine has had a rich operating history treating ore from open pit, underground and satellite deposits. The Woodlawn deposit was discovered in the late 1960s with the open cut mining commencing production in 1978. This period had multiple owners with Rio Tinto converting to underground mining in 1987 and Denehurst Limited taking ownership from 1987 until its closure in 1998. Heron Resources Limited acquired the project in 2014 with the objective to treat combined underground and reclaimed tailings. The construction of the new concentrator was completed in 2019 with production recommenced, however the operation was placed under care and maintenance from 2020 due to being financially unsuccessful through low metal prices and the COVID pandemic. Develop acquired ownership in 2022 with plans to restart the underground operation and achieve concentrate production in the first quarter of 2025.

The processing plant is designed to produce three separate metal concentrates through sequential flotation, with additional capacity for a gangue pre-float. Previous owners left behind a relatively new concentrator with a strong skeleton and a long production history to learn from. From a processing perspective, the brownfield focus was to address historic issues through process flow design changes, rationalise and replace equipment and repurpose existing assets, to match the change in mining and processing philosophy.

## GEOLOGICAL SUMMARY

Multiple known massive sulfide lenses exist which are characterised into two major mineralisation categories: copper-rich and polymetallic (McKay and Hazeldene, 1987). Figure 1 illustrates the extent of Woodlawn underground workings and drilling. The open pit mined the near surface mineralisation which was predominantly massive pyrite with variable sphalerite, galena and chalcopyrite in a single massive zone of complex ore (Fitzgerald and Singer, 1990). The copper-rich

material includes pyrite-chalcopyrite, chlorite, quartz and calcite with minimal galena and sphalerite present. The polymetallic material is fine to medium grained massive pyrite-sphalerite-galena-chalcopyrite with similar gangue minerals inclusive of talc, muscovite and barite (Downes *et al,* 2017). The polymetallic ore also exhibits higher precious metal content (Ag, Au) and a comparatively high copper content, thus making it a substantially higher revenue driver for the Woodlawn mine.

Develop's operating strategy was to segregate and campaign each material to maximise recovery potential of the copper-rich ore. This provides optimal copper flotation conditions due to containing fewer competing sulfides which could dilute the final concentrate.

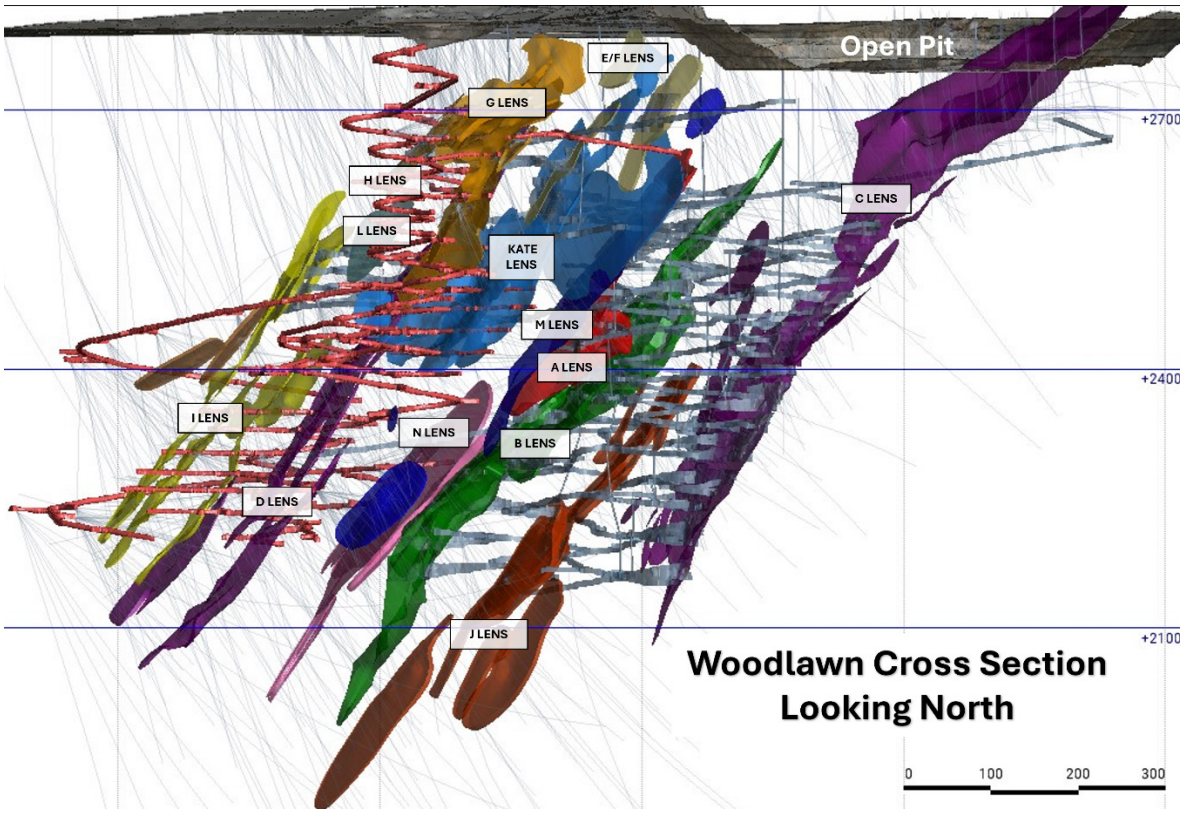



**FIG 1** – 3D model of Woodlawn deposit showing extent of underground workings and drilling.

## PROCESS PLANT DESIGN

The concentrator is designed to treat underground ore at an annualised rate of 0.85 Mt/a. The ore is crushed to a target $P_{80}$ of 8 mm through three stages of crushing. Crushed product is sent to a closed-circuit ball mill and cyclone configuration which grinds the ore down to a $P_{80}$ of 75 µm.

The flotation circuit comprises a gangue pre-float, followed by a copper, lead and zinc differential flotation sequence. Gangue pre-float concentrate is discarded to final tails to remove undesirable talc material ahead of the differential flotation circuit. The sequential copper, lead and zinc circuits each include a regrind stage on the rougher and scavenger concentrate streams prior to cleaner flotation to produce three separate concentrates. Concentrates are thickened and filtered for road transport in sealed containers. Tailings from the flotation plant are thickened for recovery of process water and underground paste fill, with slime tailings deposited into the tailings storage facility. The flow sheet is summarised in Figure 2.

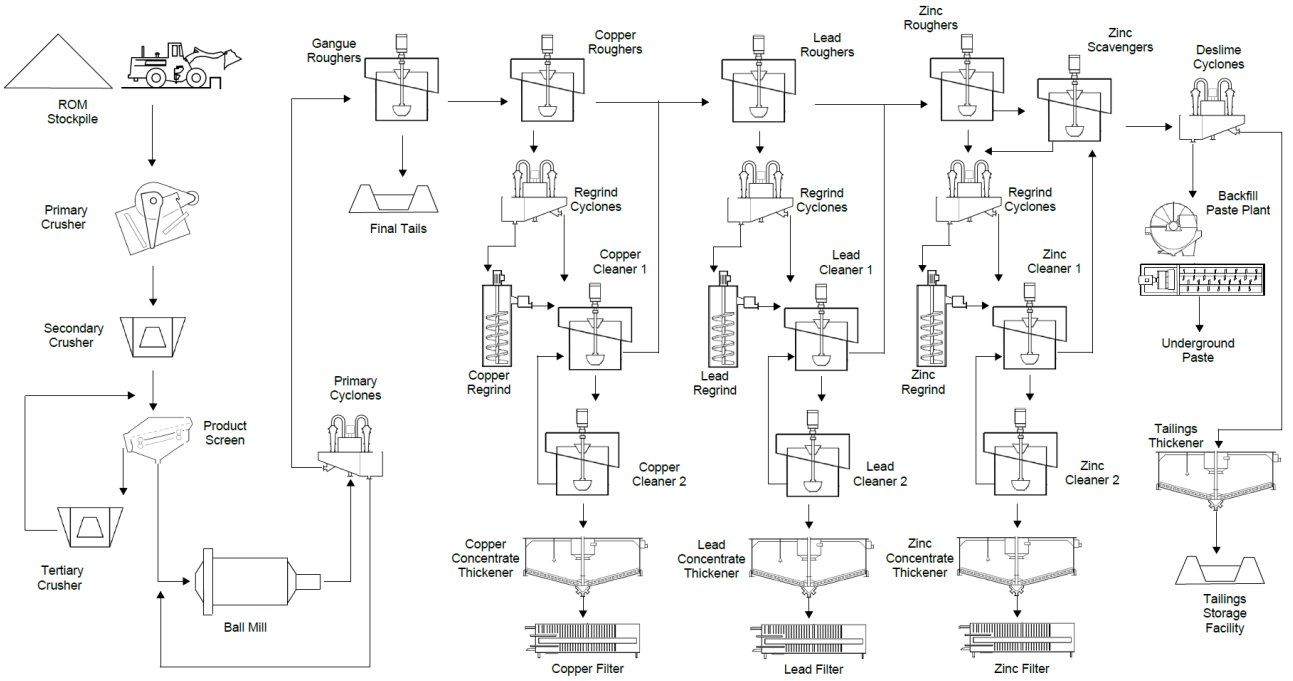



**FIG 2** – 2025 Woodlawn simplified processing flow sheet.

## MAJOR DESIGN CHANGES BY DEVELOP

The design changes were focused so that the concentrator would process only fresh underground ore, hence removing the requirement for tailings retreatment. Historical issues were reviewed for any additional improvement opportunities.

Significant structural and vibration dampening work was completed on the primary jaw crusher. A tertiary crusher was added to the revised flow sheet to provide three-stage crushing of the ore to achieve target mill feed size of less than 8 mm at 135 tonnes per hour (t/h). Crushed product feeds a fine ore bin which was modified to overflow onto a reclaimable crushed ore stockpile. A reclaim feeder and conveyor can be used to re-feed this stockpiled material to decouple the crushing and grinding circuits to improve plant operability and availability.

The flotation circuit was simplified for all three product streams. The rougher and scavenger concentrates reported to a regrind stage followed by two-stage cleaning. The option to close circuit cleaner tails to improve metal recovery was installed post-commissioning.

Existing bulk reagent mixing and dosing systems were updated and utilised where suitable. Given the complexity of the orebody and intricacies of polymetallic flotation, intermediate bulk container (IBC) dosing skids were installed for concentrated liquid reagent dosing duty.

Historical performance indicated the requirement for improved water treatment and management. To manage water chemistry, process water is treated in reaction tanks at elevated pH which then reports to a clarifying circuit re-purposed from the historic tails retreat circuit to remove precipitated metal ions and solids. Antiscalant is set-up to dose the process water and raw water systems to manage gypsum formation throughout the processing plant**.** The process water system was upgraded addressing reliability problems and the fire water circuit was decoupled as a standalone circuit.

The metallurgical and analytical laboratories were both upgraded to provide self-sufficient on-site metallurgical and assay capabilities to expedite commissioning and optimisation of the processing plant.

## PREPARATION IS KEY

Develop approached the restart project by contracting the major redesign and engineering work to an external engineering firm, whilst taking on the refurbishment and operational style works through internal resources. This allowed a larger mechanical, electrical and operational group to be

established well before commissioning of the plant. This significantly improved familiarity of the processing plant and infrastructure as well as provided cost savings compared to packaging the restart works to include refurbishment.

In parallel with flow sheet modifications, a strong focus was placed on full pump rebuilds and inspections, repairs to historically problematic areas with extensive instrumentation and control systems checks prior to start-up. Addressing these legacy reliability issues before commissioning proved essential to achieving a stable and controlled ramp up, reducing unplanned downtime and allowing the operational team to focus on process optimisation rather than mechanical integrity.

Human resources and recruitment play an under-appreciated but critical role. Onboarding more than 250 personnel in a short period demanded fast and efficient processes and competitive industry remuneration to secure scarce talent while ensuring site culture was set on strong foundations. Extensive flotation operational experience was a prerequisite for filling key roles including supervisors, seniors and superintendents. This created a platform to provide knowledge and expertise across the business for less experienced personnel.

Bringing in personnel with previous Woodlawn and similar commissioning experience was critical in identifying problematic areas and legacy issues that were not always evident from drawings or documentation. This experience assisted in identifying improvement opportunities and developing a practical understanding of existing infrastructure, particularly legacy tailings dams and complex, often inefficient, site-wide pipework that had evolved over multiple operating periods.

Procurement and vendor management brought their own complexities: onboarding more than 500 vendors, negotiating with original equipment manufacturers and managing the long lead times. Legacy vendor relationships required careful rebuilding with trust established over time. Similar challenges were encountered with reagent procurement, where storage capacity to mitigate long lead times was initially underestimated and subsequently expanded.

As with most projects of this nature, a detailed punch list was developed during the preparation phase to track outstanding mechanical, electrical, instrumentation and operational tasks required prior to start-up. While many activities were completed collaboratively, maintaining momentum proved challenging as additional personnel came online during this period. New team members were required to familiarise themselves with the plant, site structure and systems while simultaneously contributing to punch list closure.

In this environment, a positive working culture became an important enabler of progress. Open communication, shared ownership of tasks and a collective focus on the overall start-up objective helped balance learning with execution. This approach ensured that critical tasks continued to be completed efficiently despite the evolving team composition and complexity of commissioning. While all opinions were considered, effective delegation and maintaining an adaptable punch list proved critical. Progress was ultimately driven by having a team willing to make timely, informed decisions and accept accountability for outcomes, allowing change to occur quickly despite uncertainty.

While historical knowledge and expert input were invaluable, a degree of iterative learning under live operating conditions was unavoidable. There is a practical limit to what preparation alone can achieve without testing systems under operating loads, particularly for the finer technical details of a polymetallic concentrator. A fast, efficient and effective response across mechanical, electrical, control and technical teams proved pivotal in driving timely changes and continuous improvement once the plant was live.

## COPPER FLOATS FIRST

A project schedule review identified a business opportunity to prioritise the early completion of the copper flotation circuit by feeding the circuit with a mobile crusher. Sections of the orebody contain low galena and sphalerite bearing material to allow for segregation and treatment of a clean chalcopyrite feed to aid commissioning of the milling and copper flotation section of processing plant. This strategy would defer the commissioning of the crushing and Pb-Zn flotation circuits but provided multiple benefits to the operation and business.

The success of the copper-first strategy was not only driven by metallurgical simplicity, but by fast responses, rapid fault finding, prioritisation and execution across disciplines. This allowed issues to be resolved while their impacts were still small, preventing minor problems from compounding into larger operational constraints. The operational issues arising from commissioning were easier to handle simply due to managing less online equipment. Uncontrolled mechanical and electrical faults in the circuit could be rectified with faster response times. Incorrect control logic or mechanical failures for reagent dosing was identified and rectified immediately rather than hours after the fact. A large majority of the expected bottlenecking of undersized pumps and piping was identified at this stage; a relatively common occurrence in commissioning (McCarthy, 2003). The process of increasing pump capacity and pipe sizes was scoped, prioritised and executed on any downtime opportunities. A big question around the On-Stream Analyser (OSA) performance was also answered in this period. The calibration curves developed years ago could still produce an 'accurate enough' result even considering the two machines had been idle, powered down and living in the harsh high and low temperatures experienced in rural Australia for multiple years.

Reducing the three-product differential sequential flotation system to a single copper flotation stage drastically simplified the process. Operational readiness training prior to the plant start-up was valuable but seldom. Effective training only truly began once the plant was live. For many, it was their first time seeing a processing plant in operation – even those directing the works and providing the training were still finding their footing on a new site. The newcomers with less experience provided a lot of excitement and enthusiasm to contribute, but it was difficult for them to be proactive without knowing or understanding minerals processing. This was managed by grouping the newcomers with other experienced personnel across all departments to train and supervise. Furthermore, the early metallurgical findings proved to be vital for the coming months. The difficulties and shortfalls experienced early on resulted in achieving grade recovery targets faster on clean copper ore and provided critical plant understanding prior to treating the polymetallic material. The progression of the copper circuit performance is illustrated in Figures 3 and 4.

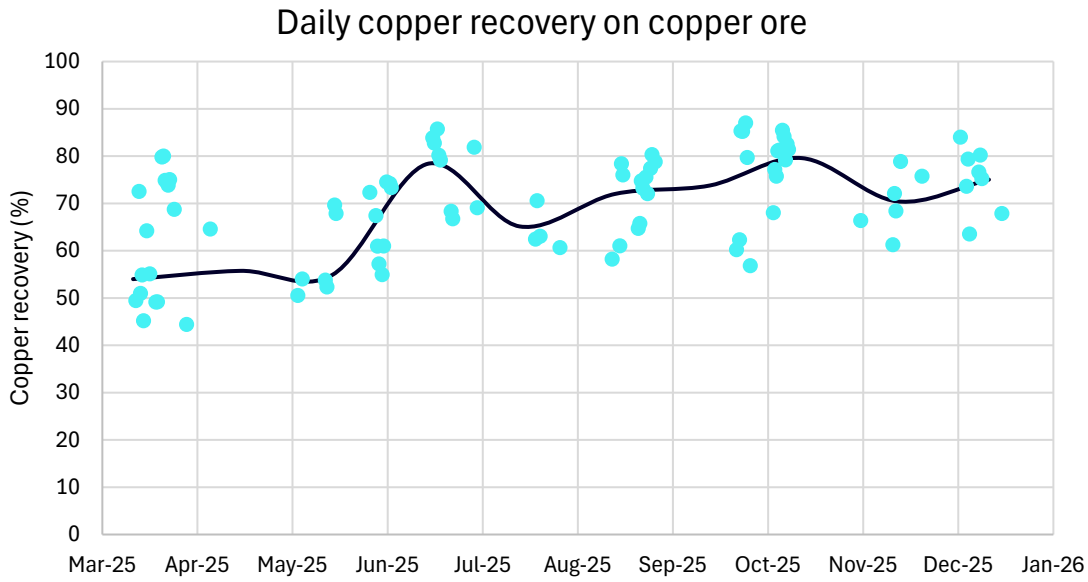



**FIG 3** – Copper ore campaign shift data since start-up (only inclusive of production days where saleable copper concentrate grade was achieved).

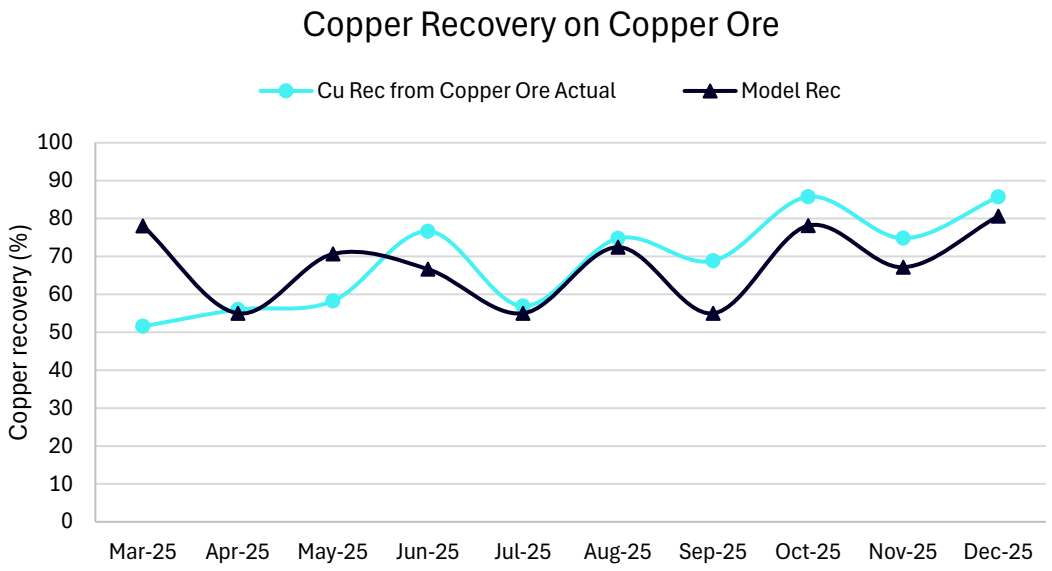



**FIG 4** – Monthly reconciled copper recovery from copper ore against model recovery.

As expected, the change in commissioning strategy did come with some challenges beyond just metallurgy – primarily the organisation and deployment of labour. Each task would have to be re-defined as critical for the copper pathway or low priority to be deferred down the track. Communication throughout a project is always critical with effective communication taking a lot of time and effort (Davidson, 1995). Managing multiple work fronts highlighted the blurred lines between contractor scope and in-house responsibilities, presenting more as a constant squiggle rather than a neat line. Adjustment of the execution strategy goes against 'rules of thumb' (Lane *et al,* 2016), but the benefits outweighed the troubles. Tight timelines and aggressive schedules left little room for scope creep and required getting the detail right upfront to avoid costly mid-stream changes. The dynamic between contractors and in-house teams added another operational wrinkle. With Develop pushing to start-up sections of the plant while the engineering contractor was still working in those same areas, managing the interface became an exercise in patience and negotiation. Yet these challenges were met with persistence and an underlying positive culture.

The first filter cycle of copper concentrate was dropped on March 11th, 2025 achieving the ambitious target for first production. The assay of this copper concentrate returned 25 per cent copper, with the re-commissioned laboratory accuracy confirmed by off-site independent testing. Producing saleable concentrate immediately would remove any requirements for long-term segregation of material or blending strategies in the concentrate shed. Produced copper concentrate was despatched in smaller 1000 t shipments using plastic lined general-purpose containers which provided two benefits: faster cash flow for the business and additional time to set-up the filters to consistently produce concentrate under transportable moisture limit (TML). The copper-first strategy provided faster cash flow, a simpler training pathway for new operators and a narrower focus on operational bottlenecks.

## MAINTAINING THE MOMENTUM

With some early stress-testing of the plant completed on the copper rich ore, it was now time to move onto the more technically challenging polymetallic material. The first polymetallic ore for the restart project was fed into the mill on April 6th, 2025. The steady mill throughput from continued high availability and utilisation of the mill (runtime achieving 93 per cent for the first 3 months of production) helped maintain stable feed conditions to troubleshoot and optimise the flotation circuit. A similar approach as before, the pumping bottlenecks were identified early on and scoped for remedial actions immediately. Although metal deportment to concentrates was initially off target while developing an understanding of the conditions required to achieve the best selectivity, saleable copper, lead and zinc concentrates were again produced from early on.

On polymetallic ore, the chalcopyrite-galena selectivity in the copper circuit and the sphalerite-pyrite selectivity in the zinc circuit proved challenging. The multitude of reagents for effective polymetallic flotation are required but can also be detrimental when there are so many possible levers to pull. With reagent adjustments showing variable results, mineral liberation was investigated. Samples were organised for full automated mineralogy analysis, however this required time to turn around results – approximately 2–3 months from despatch. Optical mineralogy assessments can provide a faster turn-around but are still close to a month from despatch. Fortunately, there was sufficient regrind capacity in each circuit to test an increased power draw to produce a finer cleaner flotation circuit feed. The change demonstrated no tangible improvement in flotation performance on any circuit with the only consequence being higher moistures from the filters struggling to effectively dewater finer product. Similar tests were conducted in parallel in the metallurgical laboratory with the same outcomes. As a result, the regrind mills were configured to produce a regrind product of approximately 25 µm. This decision was ultimately validated with automated mineralogy analysis after the fact demonstrating that:

- Chalcopyrite was 92–94 per cent liberated in copper concentrate with 81–85 per cent of galena liberated.
- Sphalerite was 93–95 per cent liberated in zinc concentrate with 81–82 per cent of iron sulfides liberated.

Historical investigations had identified the potential benefits of pre-cycloning the zinc circuit feed and having separate reagent conditioning to improve selectivity against pyrite (Heyes and Phelan, 1988). This was added to the test work list for confirmation; however, the focus at this stage was to maximise the installed design.

The nameplate design throughput of 108 t/h was achieved in the second month of production. Through a combination of crushing circuit improvements to reduce feed size and grinding circuit optimisation, the mill was pushed to 125 t/h in month three. The nature of the orebody and the design criteria split the ramp up definition into two separate categories – achieving target recovery at saleable concentrate grades from treatment of copper rich ore and treatment of polymetallic ore. Figure 5 details the category 1A McNulty curves used to compare the ramp up phase – considering the concentrator is designed with standard processes using well known and established technologies (McNulty, 1998). The main consideration here is that the Woodlawn project is classified as a brownfield expansion.

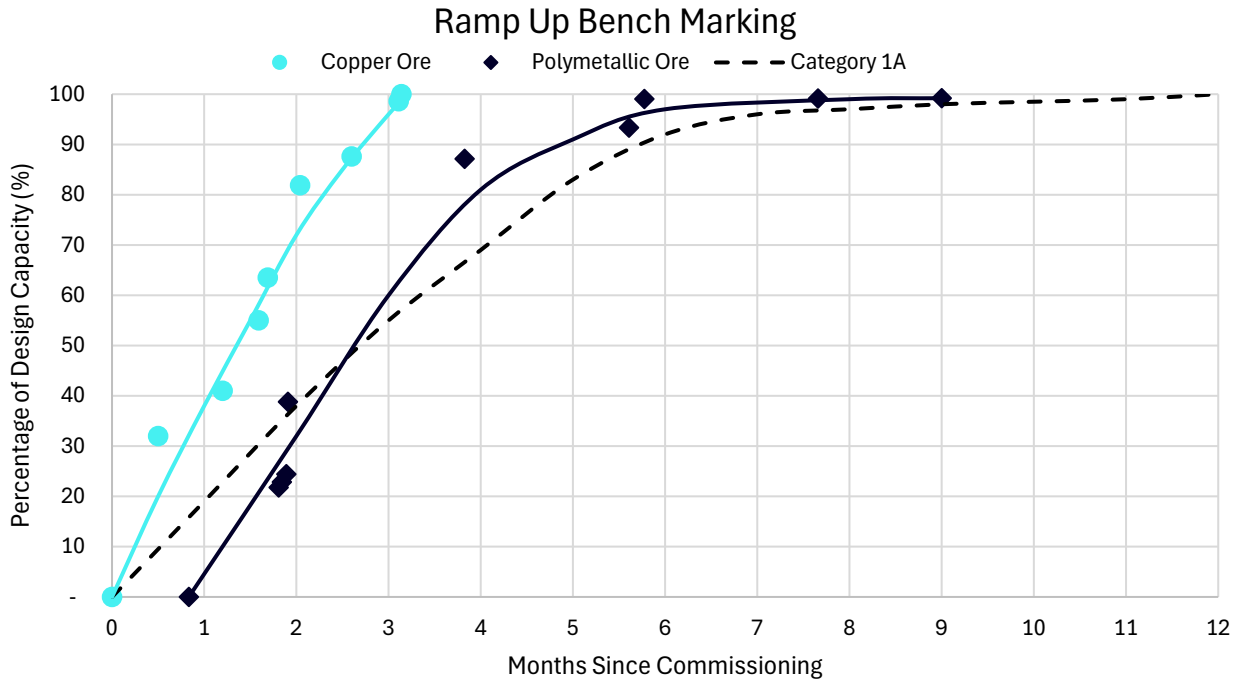



**FIG 5** – McNulty Category 1A benchmarks against Woodlawn restart (first month – March 2025).

Creating a competent mineralogy program from monthly composites was one of the items that had to be done correctly from the start. The focus was primarily on polymetallic ore due to the more complex selectivity issues and the potential value gain. Fortunately, management was in full support of the structured program with built in costs on the budget and additional costs for ad hoc analysis as required – a must in the metallurgy world but sometimes uncommon once operating (Butcher, 2019). On top of this, a large expenditure dedicated to a fully equipped metallurgy laboratory with a crusher, rod and stirred mills, ROTAP sieve shaker, laser sizer, two flotation machines and a cyclo-sizer. A strong emphasis was placed on the value of the last item due to a cyclo-sizer providing readily available size-by-assay analysis and a large cost saving for ongoing mineralogy. This of course required metallurgy technicians with the skills and experience to operate the equipment properly.

## WHAT IS NEXT?

Early 2026 finalised the ramp up period for the Woodlawn mine. Name plate throughput and copper ore treatment targets had been exceeded leaving the final stages of the polymetallic ore ramp up to be completed prior to the commencement of the next financial year. The continued opportunity for metallurgical improvements and optimisations will be throughout the life-of-mine due to the complexity of the orebody.

In 2025, the copper dominant ore achieved 88 per cent copper recovery at 21 per cent copper concentrate grade which was above the expected performance. Size by assay analysis on surveys shows the losses were predominantly in the fine fraction with 42–48 per cent of copper existing in the sub C5 size fraction as depicted in Figure 6. This analysis would lead to a review on optimal grind size and cyclone efficiency across the primary grinding and regrind stages, however the influence of these changes on polymetallic ore treatment must also be appreciated. The recirculation of copper cleaner tail back to the copper rougher can improve chalcopyrite recovery, but at the expense of concentrate quality. The best performance has been achieved and maintained in an open circuit configuration, with future work assessing options to reduce the production of the material as slimes.

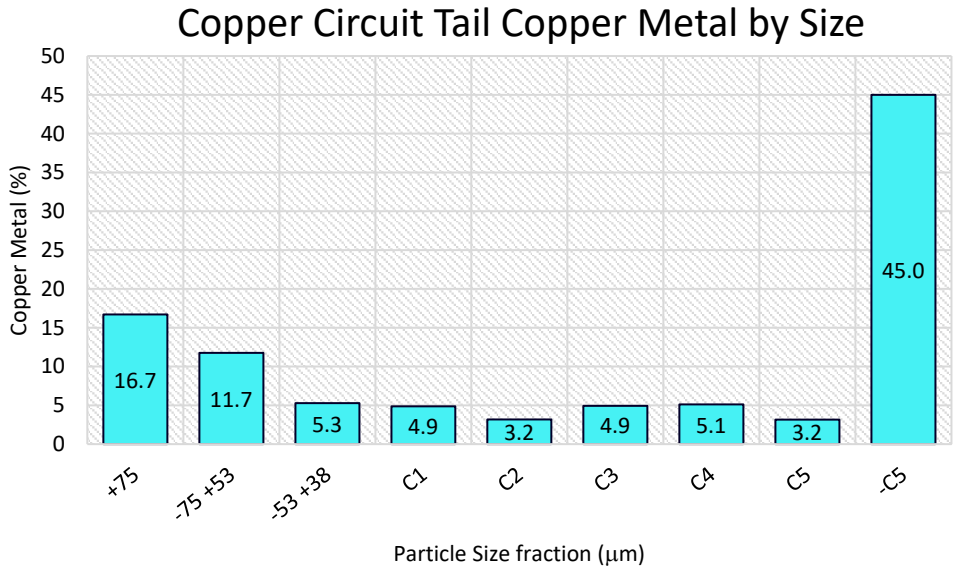



**FIG 6** – Woodlawn copper ore copper circuit final tail size by assay.

With polymetallic ore making up approximately 75 per cent of the life-of-mine, the focus for 2026 continues to be prioritising any improvements on the treatment of this ore. The precious metal content and the head grades of the ore make it the primary revenue driver for the Woodlawn mine. With mineralogy indicating relatively effective liberation characteristics, chemically optimising selectivity in the flotation circuit is the primary strategy. Chalcopyrite-galena selectivity has been tested with alternative collectors and depressants with the most successful lab-scale result from a di-thiophosphate (DTP) collector conditioned with high pH and dextrin. This test work has been

converted into current ongoing plant trial. Sphalerite-pyrite selectivity has shown mixed results in the laboratory, but some early improvements were noted with the use of naphthalene sulfonate at elevated pH. Plant trials using sodium iso-propyl xanthate (SIPX) and naphthalene sulfonate showed some indications of improvement but as with most trials, additional time is needed to provide statistical confidence.

## CONCLUSIONS

The second restart of Woodlawn demonstrated that technical decisions alone do not deliver a successful commissioning. An appreciation of historical operation played an integral role in applied design changes. Above all, the restart reinforced that success is fundamentally driven by people. Having the right individual, those willing to make difficult decisions, take accountability and drive a clear path forward proved more important than assembling a team of recognised technical specialists alone. These individuals are not always identifiable through resumes, but are often sourced through industry connections, reputation and prior working relationships.

A supportive decision-making culture was also critical during commissioning. The ability for individuals to make and drive decisions without fear of disproportionate negative consequence enabled issues to be addressed quickly. Not all decisions delivered the intended outcome; however, an environment that accepted measured failure as part of the learning process proved far more effective than delaying action in pursuit of certainty. In practice, controlled trial, review and adjustment accelerated operational understanding and improvement reinforcing that learning is rarely achieved without occasionally getting outcomes wrong.

The optimism across site created momentum through all commissioning phases. While early successes were achieved, the operation quickly recognised that the real work had only just begun.

## ACKNOWLEDGEMENTS

The authors wish to acknowledge all personnel involved in the Woodlawn restart project – including those who supplied key historical information from previous operation of the mine.

## REFERENCES

Butcher, A R, 2019. A practical guide to some aspects of mineralogy that affect flotation, in *Flotation Plant Optimisation* (ed: C J Greet), second edition, 4:137–156 (The Australasian Institute of Mining and Metallurgy: Melbourne).

Davidson, G, 1995. Woodlawn Mine – an underground operation review, in *Proceedings of the Underground Operators' Conference*, pp 259–263 (The Australasian Institute of Mining and Metallurgy: Melbourne).

Downes, P M, Jones, S A, von Perger, D A and Hine, K, 2017. Woodlawn Zn–Cu–Pb–Ag deposit, in *Australian Ore Deposits* (ed: G N Phillips), pp 781–784 (The Australasian Institute of Mining and Metallurgy: Melbourne).

Fitzgerald, D J and Singer, R P, 1990. Ore reserves at Woodlawn Mine, NSW, in *Ore Reserve Estimates,* pp 125–134 (The Australasian Institute of Mining and Metallurgy: Melbourne).

Heyes, G W and Phelan, J M, 1988. The application of separate conditioning to improve zinc metallurgy at Woodlawn Mines, in Proceedings of the Third Mill Operators' Conference (The Australasian Institute of Mining and Metallurgy: Cobar Branch).

Lane, G, Foggiatto, B, Dakin, P, Tew, A and Deonarain, N, 2016. A review of the options in concentrator layout, paper presented to Procemin 2016 – 12th International Mineral Processing Conference, Santiago, October 2016.

McCarthy, P, 2003. Managing technical risk for mine feasibility studies, in *Proceedings of the Mining Risk Management Conference 2003*, pp 21–27 (The Australasian Institute of Mining and Metallurgy: Melbourne).

McKay, W J and Hazeldene, R K, 1987. Woodlawn Zn–Pb–Cu sulfide deposit, New South Wales, Australia: an interpretation of ore formation from field observations and metal zoning, *Economic Geology,* pp 141–164.

McNulty, T, 1998. Innovative technology: its development and commercialization, in *Managing Innovation in the Minerals Industry* (ed: M Kuhn), pp 1–14 (The Australasian Institute of Mining and Metallurgy: Melbourne).

# Design, commissioning and operation of the Sabodala Massawa BIOX® Plant

*J W Olivier[1], M M Faye[2] and N H M Holder[3]*

1. Senior Process Engineer, Metso South Africa, Centurion, Gauteng 1685, South Africa.
   Email: waldemar.olivier@metso.com
2. Production Manager, Sabodala Gold Operation, Senegal.
   Email: moustapha.faye@endeavourmining.com
3. BIOX® Expert, Sabodala Gold Operation, Senegal.
   Email: nicolaas.holder@endeavourmining.com

## ABSTRACT

Sabodala Massawa is the largest gold producing mine in Senegal and one of Endeavour Mining's cornerstone assets. The Sabodala Massawa gold mine is in the south-east of Senegal, approximately 650 km from Dakar and forms part of the Birimian Greenstone Belt. The mine was recently expanded with the addition of a new 1.2 Mt/a BIOX® production facility to treat high-grade refractory resources. The BIOX® processing facility adds an incremental gold production of 1.35 Moz over the life of the mine. Construction of the USD 290M BIOX® production facility was launched in April 2022 with wet commissioning of the plant commencing in February 2024. First gold from the BIOX® circuit was completed on 28 April 2024 with the plant achieving commercial production on 1 August 2024 (Endeavour Mining, 2024).

The BIOX® circuit consists of one backup reactor and six BIOX® reactors configured as three primary reactors operating in parallel and three secondary reactors operating in series. BIOX® product is washed in a three-stage counter current decantation (CCD) circuit with the resulting BIOX® solution treated in a two-stage neutralisation circuit consisting of six tanks in series. The neutralised product reports to a single water recovery thickener with the overflow solution recycled back to the BIOX® plant as process water.

This paper covers the main BIOX® design criteria and highlights some novel design approaches adopted for this project. Successful factors behind the BIOX® inoculum build-up and commissioning activities are discussed, pointing out some key take aways for future projects. The performance of the BIOX® circuit over the first year of commercial operation is reviewed with insights provided on where the performance deviated from the design targets. The main challenges experienced during the first year of operation are discussed concluding with initiatives that are underway to further improve the performance of the BIOX® circuit.

## INTRODUCTION

Sabodala Massawa (SM) is the largest gold producing mine in Senegal and one of Endeavour Mining's cornerstone assets. The Sabodala Massawa gold mine is in the south-east of Senegal, approximately 650 km from Dakar and forms part of the Birimian Greenstone Belt. The mine was recently expanded with the addition of a new 1.2 Mt/a BIOX® production facility to treat high-grade refractory resources. The BIOX® processing facility adds an incremental gold production of 1.35 Moz over the life of the mine. Construction of the USD 290M BIOX® production facility was launched in April 2022 with wet commissioning of the plant commencing in February 2024. First gold from the BIOX® circuit was completed on 28 April 2024 with the plant achieving commercial production on 1 August 2024. In this paper the Design, Commissioning and Operation of the SM BIOX® Plant for the first year of operation, is reviewed.

## PROCESS DESCRIPTION – SULFIDE TREATMENT PLANT

The Sabodala Massawa (SM) sulfide treatment plant was designed to process high-grade refractory ore at a nominal throughput of 1.2 Mt/a (dry basis). The processing facility comprises of ROM tip and blending stockpiles, followed by primary crushing using a jaw crusher with a crushed ore storage bin and overflow stockpile. The comminution circuit is configured as a SABC circuit with a recycling pebble crushing stage, delivering a final grind size of $P_{80}$ 90 µm. A gravity concentration circuit is

included, featuring a dedicated intensive cyanidation leach reactor (ICLR) and gold electrowinning and smelting to produce doré. The flotation circuit consists of two roughers, three scavengers, and five cleaners, with flotation tailings reporting to a tailings thickener. Concentrate is further ground in a stirred mill to $P_{80}$ 45 µm before being directed to a concentrate thickener (Endeavour Mining, 2024).

The plant includes a 256 t/d BIOX® circuit for oxidation of sulfide concentrate, followed by a three-stage CCD circuit for washing and recovery of the oxidised product. A two-stage neutralisation circuit stabilises the acidic BIOX® liquor, with the product reporting to a water recovery thickener. The oxidised material is then treated in a CIL circuit for gold leaching, after which an $SO_2$/air cyanide destruction circuit reduces weak acid dissociable cyanide in the tailings. The plant also incorporates a six-tonne AARL desorption circuit, including carbon acid wash, elution, and regeneration stages, with final gold recovery achieved through electrowinning and smelting to produce doré. Tailings from the process are deposited in a dedicated lined TSF compartment for the storage of BIOX®-neutralised product and CIL tailings.

## PROCESS DESIGN – BIOX® CIRCUIT

The SM BIOX® circuit consists of one backup reactor and six BIOX® reactors configured as three primary reactors operating in parallel and three secondary reactors operating in series. The key design criteria for the SM BIOX® circuit are included in Table 1. A more detail description of the circuit follows this table.

**TABLE 1**

Sabodala Massawa BIOX® circuit design criteria.

| Parameter | Unit | Design | Acceptable range | |
|---|---|---|---|---|
| | | | Max concentrate feed | Max sulfide grade |
| **Meteorological data** | | | | |
| Maximum dry bulb temperature | °C | 45.0 | 45.0 | 45.0 |
| Maximum wet bulb temperature | °C | 25.3 | 25.3 | 25.3 |
| **BIOX® feed rate and composition** | | | | |
| $S^{2-}$ | % | 18.7 | 17.0 | 20.8 |
| Fe(T) | % | 18.9 | 17.3 | 21.1 |
| $CO_3^{2-}$ | % | 4.60 | 3.60 | 5.60 |
| As | % | 6.90 | 6.33 | 8.09 |
| Plant productivity | % | 90.1 | 90.1 | 90.1 |
| Plant capacity (nominal) | t/a | 84 091 | 96 018 | 67 739 |
| Plant capacity (design) | t/d | 256 | 292 | 206 |
| Sulfur feed rate (design) | t/d | 47.9 | 47.9 | 47.9 |
| Sulfide removal (design) | % | 94.4 | 93.8 | 95.0 |
| **BIOX® feed parameters** | | | | |
| Total BIOX® residence time | days | 6.33 | 5.52 | 7.85 |
| Operating slurry temperature | °C | 41 | 41 | 41 |
| Total bio-oxidation air requirement | $Nm^3/h$ | 40 693 | 34 640 | 30 765 |
| BIOX® cooling tower duty | kW | 14 207 | 12 127 | 11 028 |
| **Counter current decantation** | | | | |
| Wash water ratio (wash water – feed solids) | | 8.06 | 7.59 | 8.06 |
| Number of CCD stages | | 3 | 3 | 3 |
| % solids in thickener underflow | % | 35.0 | 35.0 | 35.0 |

| Parameter | Unit | Design | Acceptable range | |
|---|---|---|---|---|
| | | | Max concentrate feed | Max sulfide grade |
| Ferric concentration in feed to CIL | g/l | 0.50 | 0.50 | 0.50 |
| Required settling area | $m^2$/t/h | 12.0 | 12.0 | 12.0 |
| **Neutralisation** | | | | |
| Residence time per stage | hour | 1.20 | 1.11 | 1.54 |
| Number of stages | | 6 | 6 | 6 |
| Controlled pH in stage 3 | | 4.5 | 4.5 | 4.5 |
| Controlled pH in stage 6 | | 7.0 | 7.0 | 7.0 |
| **Water recovery thickener** | | | | |
| Settling area required for combined feed | $m^2$/t/h | 14.0 | 14.0 | 14.0 |
| % Solids in thickener under flow | % | 25.0 | 25.0 | 25.0 |
| Number of thickeners | | 1 | 1 | 1 |

The BIOX® feed preparation commences with flotation concentrate thickener underflow undergoing regrinding to achieve a particle size of approximately 75 per cent passing 45 µm and greater than 99 per cent passing 150 µm. The reground slurry is subsequently pumped via an on-stream analyser (OSA) to either high-grade or low-grade surge tanks. These surge tanks, designed to provide a combined residence time of approximately 48 hrs, ensure feed continuity during upstream interruptions and dampen variability in feed grade. Concentrate is withdrawn from both tanks in controlled proportions using variable-speed pumps to maintain a consistent sulfide sulfur grade. The slurry is diluted to approximately 20 per cent solids by the addition of process water to each pump discharge line. Flow rates and solids concentrations are accurately monitored using magnetic flow meters and slurry densitometers to ensure precise feed rate control into the BIOX® reactors.

The combined BIOX® slurry feed is sampled, equally distributed, and dosed with nutrients prior to entering three primary bio-oxidation reactors. Partially oxidised slurry overflows from the primary stage into three secondary reactors arranged in series to achieve further oxidation. Reactor operating conditions are tightly controlled to sustain optimal bacterial activity. The slurry temperature is maintained at 41°C (±0.5°C) using internal cooling coils to dissipate heat generated by exothermic reactions, while dissolved oxygen and pH are regulated within defined control ranges. The fully oxidised slurry then flows by gravity to the counter-current decantation (CCD) circuit.

Within the CCD circuit, dissolved iron, sulfur, and arsenic species are removed from the BIOX® product through a series of three thickeners operating in counter-current configuration. The circuit operates at relatively low feed slurry densities (<8 per cent solids) to promote efficient settling and washing. A Turbodil™ system is employed in each thickener to enhance dilution and flocculation performance. Thickener underflow is pumped to agitated interstage mixing tanks ahead of each thickener, where it is combined with overflow solution from the subsequent thickener. Wash water is introduced at a controlled rate into the mixing tank upstream of CCD stage 3 to maximise washing efficiency. The final underflow from CCD stage 3 is directed to pH adjustment tanks, while the overflow from CCD stage 1 is routed to the neutralisation circuit.

The acidic overflow from CCD stage 1 is treated in a six-stage neutralisation circuit. Limestone is added in stage 1 to raise the pH to approximately 4.5, followed by lime addition in stage 2 to achieve a pH of 6.5–7.0. The neutralisation tanks are both agitated and aerated, and incorporate a recycle stream to enhance reagent utilisation and to stabilise the pH profiles. Process slurry flows sequentially between tanks via launders, with the final neutralised effluent reporting to the water recovery thickener (WRT). The WRT facilitates process water recovery, producing a clarified overflow that is recycled to the process water system, while the underflow is discharged as BIOX® tailings.

BIOX® services include high-efficiency, low-pressure air blowers supplying process air to both the BIOX® reactors and neutralisation tanks. The blowers are equipped with aftercoolers to reduce air temperature to below 60°C prior to dispersion onto the BIOX® slurry via spare rings. Reactor temperature control is achieved by cooling water that is circulated through internal cooling coils, with heated water returned to evaporative cooling towers for heat rejection. Cooled water is subsequently recirculated to the reactors. The water system incorporates chemical dosing for biocide control, corrosion inhibition, and scale prevention, with automated blowdown regulated by conductivity to maintain water quality within specified limits.

## MAIN BIOX® DESIGN CONSIDERATIONS

The Sabodala Massawa BIOX® design is well aligned with the BIOX® GIII design principles, with various strategies implemented to minimise the impact of ore variability on plant performance. Variability of less than 20 per cent per day on key elements such as sulfide sulfur and arsenic is targeted to maximise microbial performance. The inclusion of an On-Stream Analyser (OSA) offers significant upside for future upgrades to advanced process control. Robustness and operability were key focus areas in the design of the CCD and neutralisation circuits, ensuring reliable operation under varying conditions. Notably, the introduction of radial foam launders represented a first for the BIOX® technology, while the adoption of Blower Optimiser 4.0 done to reduce power consumption and improve overall system performance.

### Design for variability

#### *BIOX® design covers a wide operating range*

The BIOX® feed concentrate composition and design feed rate were informed by geometallurgical modelling conducted by Mine Scope Services on behalf of Endeavour Mining. This work was based on extensive data collected across three Sabodala Massawa deposits, enabling the mineralogy and degree of refractoriness of the various orebodies to be well defined. Variability in ore and concentrate composition needed to be minimised to ensure sustained high levels of bacterial activity within the BIOX® reactors. Key parameters included, but were not limited to, the following:

- Sulfide sulfur grade, as this dictates concentrate throughput and the level of sulfide oxidation achieved across the BIOX® circuit.
- Mineralogical balance of pyrite (acid-producing), arsenopyrite, and carbonate minerals (acid-consuming) to limit reagent consumption for BIOX® reactor pH control.
- Control of both the rate of change and maximum concentrations of arsenic (%As) and antimony (%Sb), as elevated levels can negatively impact bacterial activity above certain thresholds. Although BIOX® circuits have demonstrated the capability to treat concentrates with antimony grades of up to 10 per cent (Fosterville BIOX® plant, Australia) and arsenic grades of up to 20 per cent (Coricancha BIOX® plant, Peru), more conservative operating targets were adopted for the SM BIOX® circuit.
- Iron-to-arsenic (Fe:As) molar ratio in the BIOX® feed concentrate, with a minimum molar ratio of approximately three typically required to ensure the formation of a stable ferric arsenate ($FeAsO_4$) precipitate in the neutralised product solids.

Strategies encompassing mining practices, ore stockpiling, and plant feed blending were developed to minimise any negative impacts on the BIOX® circuit resulting from rapid changes in the grades of these minerals and elements.

#### *On-stream analyser*

As part of the objective to minimise concentrate grade variability into the BIOX® circuit, an on-stream analyser (OSA) was incorporated into the plant design to provide ongoing quantification of total sulfur, iron, arsenic, antimony, calcium, magnesium and % solids of the two BIOX® feed stock tanks as well as the BIOX® feed steam.

The Courier® 8X SL analyser installed for this purpose provides real-time, automated elemental measurement for mineral processing circuits using Laser-Induced Breakdown Spectroscopy (LIBS). This technology enables simultaneous quantification of both light and heavy elements directly from process slurry that allows for the monitoring of carbonates and other acid consuming minerals that affects the limestone or acid consumption in the BIOX® reactors. This capability allows for improved BIOX® feed grade control and accelerates metallurgical decision-making related to the effective operation of the BIOX® circuit.

### *Dual stock tanks*

The SM BIOX® plant is equipped with dual feed stock tanks to provide a combined feed slurry retention time of 48 hrs. This is operated as a high-grade and a low-grade stock tank based on the sulfide sulfur content in the stock tank feed slurry.

Underflow from the concentrate thickener is pumped to the feed distribution box ahead of the high-grade and low-grade BIOX® feed stock tanks. The Plant Control System (PCS) diverts the thickened flotation concentrate in the BIOX® feed distribution box to either the high or low-grade BIOX® feed tanks by opening the appropriate feed valve leading to the tank. The selected tank is based on the sulfide sulfur grade in the feed slurry as measured by the OSA and compared to the target sulfide sulfur grade set point range for the high and low-grade BIOX® feed tanks. The BIOX® feed slurry density and flow rate, pumped from either or both high and low-grade BIOX® feed tanks is measured using nucleonic density gauges and electromagnetic flowmeters fitted with transmitters on each of the high and low-grade feed lines. Slurry is feed from these stock tanks to the BIOX® circuit in a specific ratio to achieve the target BIOX® sulfide sulfur feed grade and the dry solids feed rate to the BIOX® circuit, as set by the metallurgist.

## Design for operability and maintainability

### *BIOX® superstructure*

The SM primary BIOX® reactors are each fitted with eight cooling coil banks equally spaced around the diameter of the reactor. The location of these coils creates challenges for cooling coil maintenance when a conventional superstructure, configured as a dual beam construction with cross bracing, is used. Lycopodium Minerals developed an innovative superstructure design that provided unobstructed access to all the cooling coil banks when serviced by a mobile crane. This type of superstructure comprises of a square centre section supporting the agitator gearbox, with four support beams bridging out from to the top edge of the reactor at 45° horizontal angles to the centre structure.

### *Launder design and configuration*

Slurry from the primary BIOX® reactors overflow via riser pipes into deep U-shaped launders which delivers the partially oxidised slurry to the first secondary BIOX® reactor. The height of launders for the SM BIOX® application were increased from the conventional design with additional height added in areas such where a step change in the launder is located and prone to foaming build-up. Pneumatically operated gate valves are also used to direct slurry in both the reactors and overflow launders to allow various circuit configurations. Access to various control gate valves for maintenance purposes was provided via cat ladders and smaller platforms running below the main BIOX® walkway. This launder has proven to be very robust with no and has eliminated foam spillage completely.

### *Radial foam launders*

In order to assist with foam management inside the primary BIOX® reactors, two radial foam launders were fitter per reactor. These foam launders collect foam from the reactor once a certain operation level is exceeded and directs the foam into the BIOX® bund areas via dedicated rundown pipes. This prevents the reactors from overflowing when extreme foaming conditions are experienced. BIOX® spillage pumps are near the discharge point into the bund that allows for the easy return of BIOX® slurry to the BIOX® reactors once foaming conditions have stabilised. These launders were found to

be very effective for handing of excessive foaming conditions as were experienced during commissioning and plant ramp-up periods.

## Design for efficiency

### *BIOX® agitators*

The oxygen requirements for sulfide oxidation are high, and low-pressure air is injected into the reactors via sparge rings installed below the agitator turbines. The use of dual OKTOP agitator combining an OKTOP® 3115 top impeller with an OKTOP® 3105 bottom impeller, offers significant performance advantages in BIOX® applications. The dual-pumping configuration used in BIOX® reactors enhances aeration efficiency while simultaneously reducing foam levels by entraining foam back into the slurry, thereby improving the performance of the reactor. The result is a more energy-efficient system, achieving a signification reduction in agitator power draw due to optimised hydrodynamics and improved slurry flow stability.

### *Blower selection and control*

For the SM BIOX® project, the low-pressure air demand is met by three ZHL8–1.9M integrally geared turbo blowers, each with an installed power of 1250 kW. These blowers deliver 100 per cent oil-free, clean air in compliance with ISO 8573-1 Class 0 standards. Adjustable inlet guide vanes enable energy savings of up to 9 per cent during reduced air-flow operation, while the superior oil-free turbo air ends provide an optimal combination of high air flow and low energy consumption. Adoption of Blower Optimiser 4.0 was done. This advanced control capability and wide turndown range allow for optimisation of air consumption through a dissolved oxygen (DO) control loop, utilising the online DO measurements for each BIOX® reactor.

### *BIOX® reagent consumption*

The BIOX® cultures are kept active in the reactors by controlling the slurry conditions within specific ranges. The slurry pH is maintained between 1.4–1.6 (primaries) and 1.2–1.4 (secondaries) by means of timer-controlled additions of limestone slurry from the ring main. The addition of sulfuric acid to the reactors is controlled manually since acid addition is required infrequently. The sulfide mineralogy in combination with the carbonate content in the BIOX® feed concentrate, dictates whether the concentrate will be acid consuming or acid producing during bio-oxidation. While pyrite is acid-producing, both arsenopyrite and the decomposition of carbonate minerals consume acid. Optimisation studies were conducted during the feasibility study phase of the SM project to define the optimum mining ratio of North Zone (NZ) to Central Zone (CZ) ore to minimise reagent consumption for BIOX® pH control. HSC software simulations performed on various ore feed blends indicated that a NZ:CZ ratio close to 3 (ie 75 per cent NZ: 25 per cent CZ) will result in the BIOX® circuit to be pH neutral with neither acid nor limestone required for BIOX® pH control.

## Risk mitigation

As BIOX® is a biologically driven process, the rate and extent of sulfide oxidation is inherently dependent on the health and robustness of the microbial cultures. Operational risks therefore centre around sudden deviations in key parameters, including slurry temperature, pH, dissolved oxygen concentration, and concentrate feed composition that will negatively impact on the microbial activity. Critical design and operational considerations include ensuring the continuous availability and reliability of essential services such as agitation, aeration, and reactor cooling, as well as minimising operational errors that could introduce toxic elements such as hydrocarbons into the BIOX® system.

Despite robust process design and sound operating practices, process upsets and unplanned incidents do occur over the life of a BIOX® plant, with varying impacts on circuit performance and availability. In particular, an extended downtime event may be experienced that is characterised by a complete loss of bacterial activity. These events are most commonly associated with prolonged interruptions to critical utilities such as power, air supply, and cooling. Recovery from such events requires the re-establishment of the activity of microbial cultures within the reactors, generally involving a feed ramp-up period of approximately 18–25 days to regain design throughput. The

following section outlines the risk mitigation strategies implemented to minimise the frequency and impact of such incidents on the operational performance of the SM BIOX® plant.

### *BIOX® backup reactor*

The time to regain activity in batch mode is a function of the nature of the stress effect, activity levels of the plant prior to the incident as well as the volume of active inoculum supplied to the primary reactors daily. The volume of inoculum slurry available will also impact on the rate of ramp-up to full production. The backup inoculum is contained in a single BIOX® reactor with similar functions and services to a full-scale BIOX® primary reactor. The backup reactor is operated in batch mode to ensure that a large volume of activate BIOX® inoculum is available should supplementation of the microbial cultures in the operational BIOX® reactors, be required. Based on a trade-off study considering the cost and production impact of various backup reactor volumes, a reactor size of 300 $m^3$ was chosen to be optimal in the case of the SM BIOX® plant.

### *Backup power*

The SM BIOX® project incorporated a new dedicated power station to preferentially supply the BIOX® circuit, independent of the existing mine and plant infrastructure. This comprises of three new 6 MW HFO generator sets to provide the additional base load. Supplemental backup power was provided by two new 1.6 MW diesel generators, enabling critical BIOX® equipment such as the low-pressure blowers, BIOX® agitators, and cooling-water distribution pumps to be returned to operation within a 15 min time frame.

### *BIOX® operational support and knowledge transfer*

A major project risk identified for the SM project was for the BIOX® circuit to cause intermittent or reduced production during the plant commissioning and ramp up stages. This risk was mitigated by the employment of BIOX® experts, metallurgist and shift supervisors with substantial BIOX® plant operational experience. The allocation of Metso and Mine Scope consultations for the first 6 months of SM operation provided additional support and oversight. Sufficient training (formal and informal) was also provided for all plant operators to limit the occurrence of incidents and accident that may compromise BIOX® performance and safety.

## PLANT CONSTRUCTION

Construction of the 1.2 Mt/a SM sulfide treatment plant was completed on budget, on schedule in under two years. Over 3.5 million work hours have been completed during the project execution with zero lost-time injuries recorded. The plant achieved commercial production on 1 August 2024 (Endeavour Mining, 2024).

Displayed in Table 2 is the timelines of the main construction activities of the SM sulfide treatment plant. A high-level breakdown of the project capex cost is included in Table 3.

**TABLE 2**

Construction milestones of the SM sulfide treatment plant.

| Year | Month | Milestone |
|---|---|---|
| 2022 | March | EPCM Project Team Kick-off |
| | April | DFS published and construction launched |
| | May | Bulk earthworks commenced |
| | October | Civil works commenced |
| 2023 | June | Plant SMP works commenced |
| | September | E&I works commenced |
| | December | Powerplant energised |
| 2024 | February | Dry Commissioning commenced |
| | March | Wet Commissioning commenced |
| | April | First gold delivered |

**TABLE 3**

Capex cost breakdown for the SM sulfide treatment plant.

| Description | Cost (US$M) |
|---|---|
| Treatment plant | 106 |
| Reagents and services | 35 |
| Infrastructure | 55 |
| Other construction | 27 |
| **Sub-total** | **223** |
| Management costs | 33 |
| Owners project costs | 34 |
| **Total** | **290** |

## BIOX® INOCULUM BUILD-UP

Inoculum build-up is often a key area of concern for project teams, as it has a significant influence on the overall commissioning schedule. Successful execution requires careful planning of concentrate supply through the various stages of the inoculum build-up program, as well as ensuring adequate operator availability and appropriate training to support the process.

To address these challenges, the SM strategy focused on procuring a turn-key offering to cover the first four stages of inoculum build-up for the BIOX® circuit. In parallel, third-party concentrate was sourced to allow BIOX® inoculum build-up to progress alongside full-scale plant construction and commissioning. This approach enabled the on-site build-up of 60 $m^3$ of active and inactive BIOX® inoculum within a period of 4.33 months, ultimately fast-tracking the full-scale plant commissioning. Please see more details on the various inoculum build-up phases included under Table 4.

**TABLE 4**

Duration of the various SM BIOX® inoculum build-up phases.

| Phase | Description | Duration (days) |
|---|---|---|
| A | Inoculum Re-Activation (4 × 10 L Bench Reactors) | 7 |
| B | Tank A Inoculum build-up (100 L Reactor, Bench Inoc) | 7 |
| C | Tank B Inoculum build-up (500 L Reactor, Tank A Inoc, FV BIOX® Solution) | 12 |
| D | Tank D Inoculum build-up (10 $m^3$, Tank A–B Inoc, FV BIOX® Solution) | 82 |
| E | BIOX® Backup reactor build-up (300 $m^3$, Tank A–C Inoculum stored in IBCs) | 24 |
| | **Total (days)** | **132** |
| | **Total (months)** | **4.33** |

The Inoculum Build-up Container (IBC) comprises the tanks, agitators, pumps, and heating and cooling systems required to build-up the required inoculum volume on-site. Once installed, the container functions as a fully equipped BIOX® metallurgical laboratory, complete with all necessary process diagnostic instrumentation and laboratory equipment, excluding analytical facilities. In addition, the IBC is a valuable tool for the training of new SM plant operators. Displayed in Figure 1 is an image of the installed IBC, with photos of training provided to plant personnel included as Figure 2.

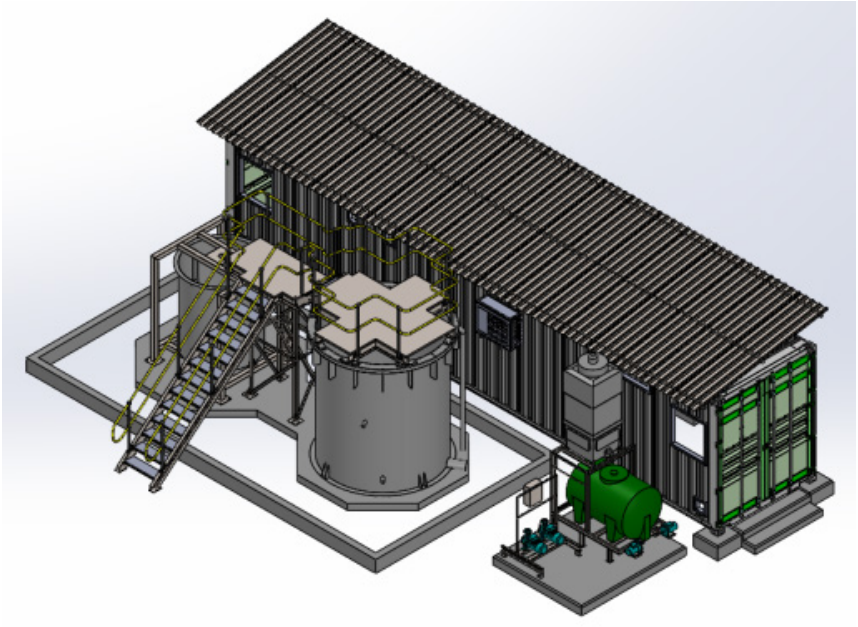


**FIG 1** – SM inoculum build-up container, reactors and services.



**FIG 2** – SM plant personnel undergoing practical training in the IBC.

The success of the Sabodala BIOX® inoculum build-up program can be attributed to several key factors, including the effective operation of the inoculum build-up container plant, the availability of various concentrate and inoculum sources, and the development of a strong, diversified BIOX® cultures during the build-up program. This success was further reinforced by the expertise of an experienced site team and the exceptional commitment and hard work of the operators.

## FULL SCALE BIOX® CIRCUIT COMMISSIONING

The SM Sulfide Treatment plant achieved commercial production on 1 August 2024, less than four months after the first gold pour. All circuits have operated in line with expectations, with nameplate capacity achieved by late Q3–2024. In October 2024, the processing rate averaged 3250 t per day that is equivalent to 101 per cent of the nameplate capacity. From the point at which all the BIOX® reactors were brought online, the ramp-up to nameplate capacity was achieved within a six-month

period. Please see more details on the various SM full scale plant inoculum build-up phases included under Table 5.

**TABLE 5**

Duration of the various SM full scale BIOX® inoculum build-up phases.

| Phase | Description | Duration (days) |
|---|---|---|
| 1 | P2 build-up (500 $m^3$ RAW Water, 160 $m^3$ Backup Inoculum, Galaxy Conc) | 24 |
| | P1 build-up (Transfer slurry from P2 to P1 due to unplanned maintenance) | 14 |
| 2 | S2 build-up (850 $m^3$ RAW Water @ pH 1.5; P2 Inoculum, SM Conc) | 8 |
| 3 | P2 build-up (500 $m^3$ RAW Water @ pH 1.5; 100 $m^3$ Backup Inoc, SM Conc) | 5 |
| 4 | S3 build-up (500 $m^3$ RAW Water @ pH 1.5; S2 Inoculum, CCD#1 Solution) | 9 |
| 5 | P3 build-up (400 $m^3$ RAW Water @ pH 1.5; CCD#1 Solution, SM Conc) | 4 |
| 6 | S1 build-up (800 $m^3$ RAW Water @ pH 1.5; CCD#1 Solution, 100 $m^3$ Inoc) | 3 |
| | **Total (days)** | **67** |
| | **Total (months)** | **2.20** |

The success of the full-scale plant start-up was built on a strong bacterial culture and sound operating principles. The availability of a third concentrate provided valuable operational flexibility. A suitably sized backup reactor has proven to be extremely valuable for both commissioning and ongoing operations. Reliable power and blower air supply during commissioning is critical and requires a high availability. Overall, a robust microbial culture has been successfully established at the SM BIOX® plant and demonstrated strong resilience under various adverse operating conditions.

## OPERATIONAL PERFORMANCE – FIRST YEAR OF OPERATION

Displayed in Table 6 is the performance during of the SM BIOX® Circuit from Q2 2024 up to Q1 2025, as compared to the design parameters.

**TABLE 6**

Performance of the Sabodala Massawa BIOX® Circuit: Q2 2024–Q1 2025.

| Parameter | Value | | |
|---|---|---|---|
| | Design | Q2–Q4 2024 actual | Q1 2025 actual |
| BIOX® feed concentrate tonnage (t/d) | 256 | 170 | 245 |
| BIOX® feed availability (%) | 90.1 | 96.0 | 99.5 |
| BIOX® feed concentrate $S^{2-}$ grade (%) | 18.7 | 11.0 | 10.7 |
| BIOX® circuit $S^{2-}$ oxidation (%) | 94.4 | 93.7 | 96.0 |
| BIOX® power consumption (kWh/t BIOX® feed) | 260 | 342 | 276 |
| Power unit cost (US$/kWh) | 0.12 | 0.11 | 0.11 |
| BIOX® CIL recovery (%) | 95 | 94 | 93 |
| BIOX® cyanide consumption (kg/t BIOX® feed) | 28.6 | 8.1 | 11.5 |

During Q3 2024, the BIOX® feed tonnage was progressively ramped up to the design rate. In Q1 2025, the BIOX® circuit operated marginally below the design capacity of 256 t/d. This was primarily due to a reduced mill throughput combined with a lower-than-design flotation mass pull during the period. This BIOX® feed tonnage profile for this period is graphically in Figure 3. The reduced throughput was accompanied by a lower sulfide sulfur feed grade, mainly because of lower-than-design sulfide grades in the ore feed. During H1 2025, BIOX® throughput was impacted by crusher and mill maintenance activities; however, peak throughput progressively improved, reaching up to

10 per cent above design nameplate capacity for periods in June 2025. An increased proportion of fresh ore relative to transitional ore from the Massawa Central Zone resulted in improved flotation performance and higher overall recoveries.

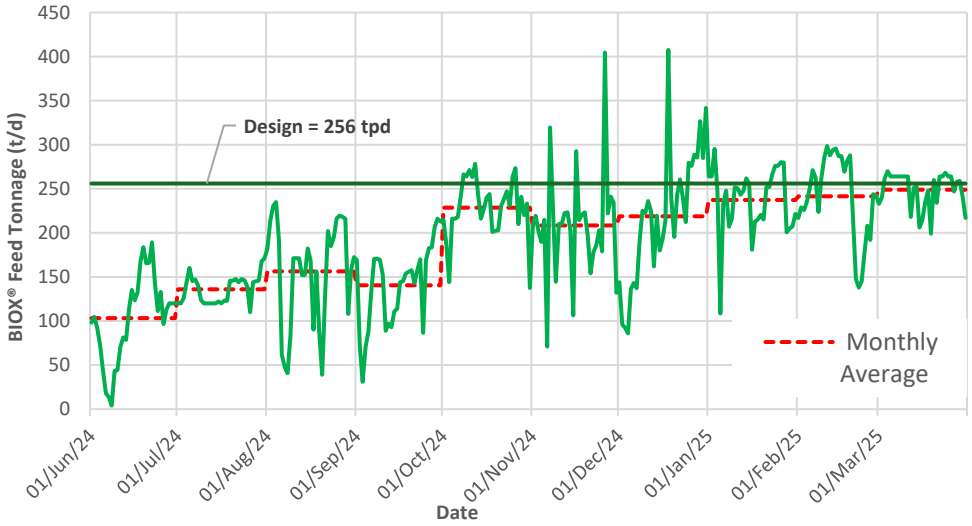



**FIG 3** – BIOX® feed tonnage to the SIM BIOX® circuit: Q2 2024–Q1 2025.

The sulfide sulfur oxidation level remained high for most of the indicated period, as shown in Figure 4. Lower oxidation levels were experienced during September 2024, caused by a reduction in bacterial activity resulting from BIOX® blower downtime, which left the BIOX® circuit without air for an extended period. The circuit, however, fully recovered from this incident, demonstrating the resilience of the SM BIOX® bacterial culture. BIOX® power consumption during Q2–Q4 2024 was higher than the design value, as agitator power draw and blower air requirements were still being optimised.

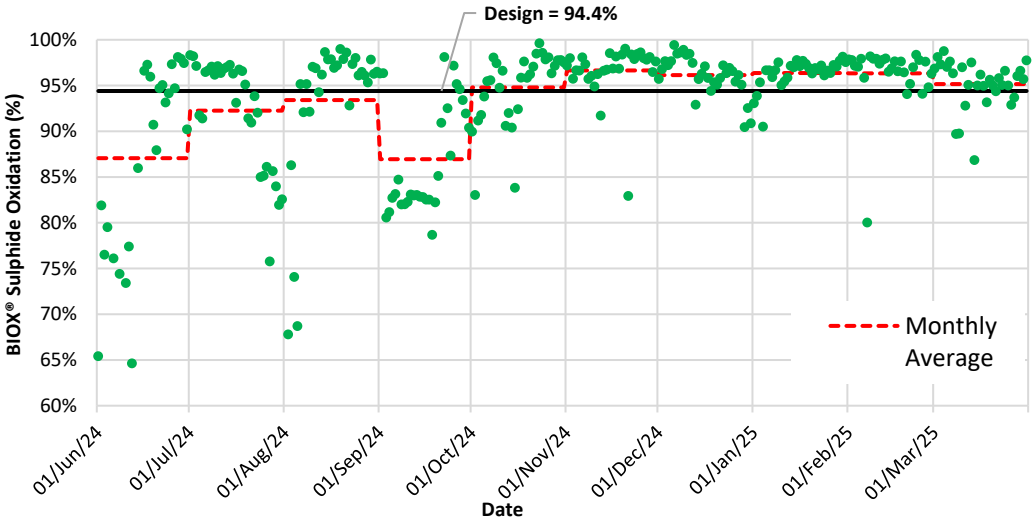



**FIG 4** – Sulfide oxidation profile for the SM BIOX® circuit: Q2 2024–Q1 2025.

As shown graphically in Figure 5, BIOX® CIL recoveries were high for most of the period, achieving levels close to the design target of 95 per cent. The dip in CIL recovery observed in October 2024 can be attributed to lower BIOX® sulfide oxidation levels experienced during September 2024. The reduced CIL recoveries in Q1 2025 are attributable to an increased feed rate, which resulted in higher oxygen demand and increased barren solution losses.

Cyanide consumption in the CIL circuit treating the BIOX® product was substantially lower than the design value. This is likely due to the lower sulfide feed grade and differences in feed concentrate mineralogy associated with the processing of transitional ore in the plant feed.

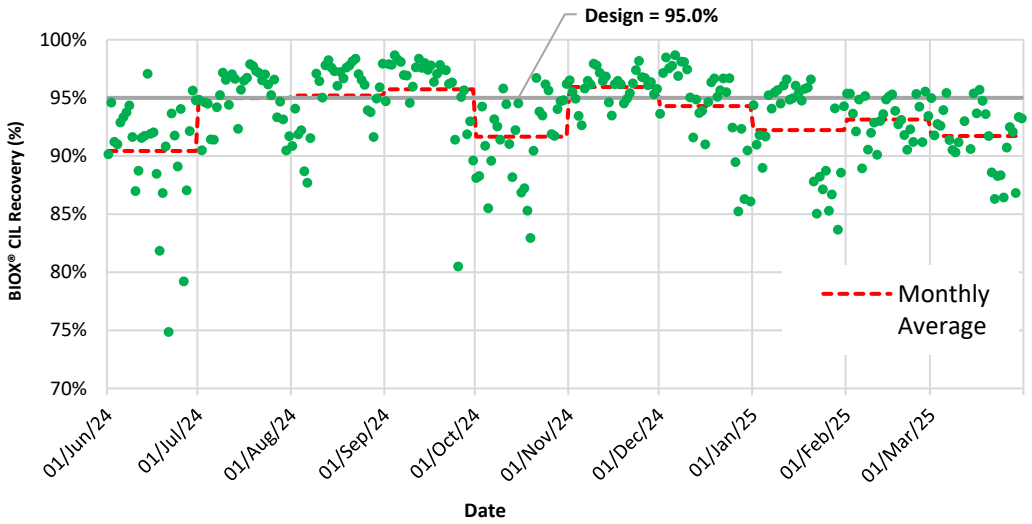



**FIG 5** – Gold recovery profile for the SM BIOX® CIL circuit: Q2 2024–Q1 2025.

The reagent consumptions achieved during the indicated period is compared against the design values listed in Table 7.

Limestone and sulfuric acid consumption during the indicated period were minimal, due to a near optimal ratio of acid-consuming and acid-producing minerals in the BIOX® feed concentrate. BIOX® defoamer consumption was also kept to a minimum through effective washing of the flotation concentrate combined with stable BIOX® operation. Higher lime and limestone consumption in the neutralisation circuit was mainly driven by milling circuit optimisation activities, which resulted in a lower slurry solids concentration. BIOX® nutrient consumption was marginally higher than the design value, with optimisation test work planned for H2 2025. Consumption of all other reagents was in line with design levels. The main contributors to reagent operating costs for the period were limestone for neutralisation (43.3 per cent), lime for neutralisation (24.2 per cent), followed by BIOX® nutrients (22.8 per cent).

**TABLE 7**

Reagent consumptions of the SM BIOX® circuit: Q2 2024–Q1 2025.

| Reagents type | Type and supply size | Consumption (kg/t BIOX® feed) | |
|---|---|---|---|
| | | Design | Actual |
| **BIOX® pH control** | | | |
| Limestone | Limestone, (tipper truck) | 66 | 0.65 |
| Sulfuric acid | Sulfuric acid, (1185 kg IBC) | 10.2 | 0.14 |
| **Neutralisation pH control** | | | |
| Limestone | Limestone, (tipper truck) | 298 | 323 |
| Lime | Lime, quick, calcium oxide (bulk tanker) | 41.7 | 46.0 |
| **Flocculant** | | | |
| CCD thickeners | Flomin DP9439, (25 kg bags) | 0.35 | 0.41 |
| Water recovery | Flomin 9629 (25 kg bags) | 0.15 | 0.19 |
| BIOX® nutrients | Pre-mix combined nutrients bag (1250 kg) | 7.20 | 9.86 |
| BIOX® de-foamer | Surfynol DF-110 L defoamer (175 kg/drum) | 2.01 | 0.02 |
| Cooling water reagents | Biocide (ST-40/Nalco 7330), Corrosion inhibitor (3DT-129), Antiscalant (Nalco 7348/3DT-120) | - | 0.22 |

## OPERATIONAL CHALLENGES AND OPTIMISATION INITIATIVES

Several operational challenges were encountered, including OSA sample flow issues caused by the existing piping configuration, as well as failures of the BIOX® feed and CCD underflow peristaltic pump hoses and gearbox seals. Additional constraints were identified in the CCD overflow pumping capacity, while the CCD rake drives experienced challenges following commissioning. Mechanical issues were also encountered with the limestone mill drive assembly, where the roller liner began peeling off. Extended downtime of the BIOX® blower occurred due to PLC-related issues. Furthermore, a failure in a section of the S1 BIOX® reactor floor plate welding was identified and required corrective action.

A number of improvement initiatives were identified to enhance overall plant performance, including optimisation of limestone and lime consumption, refinement of the Geomet blend, and improvements to dissolved oxygen levels in the CIL circuit. A plant-wide pumping capacity assessment was conducted, followed by targeted upgrades. In parallel, maintenance and operating strategies were strengthened to improve plant uptime from 92 per cent to greater than 95 per cent. These efforts were supported by accurate on-site test work to enable rapid assessment of ore characteristics, as well as the implementation of on-stream analysis upstream of BIOX® to monitor sulfide ratios and key elements such as arsenic, antimony, and iron (Endeavour Mining, 2025).

## CONCLUSIONS

The successful start-up of the SM BIOX® plant was premised on the establishment of a strong bacterial culture and sound operating principles, with the availability of a large mass of third concentrate providing valuable operational flexibility. A suitably sized backup reactor has proven to be extremely valuable during both commissioning and ongoing operations.

Reliable power and blower air supply during commissioning is critical and requires high availability. Overall, a robust microbial culture has been successfully established at the SM BIOX® plant, demonstrating strong resilience under operating conditions. The inclusion of in-tank foam launders and deep-section product launders represents a significant design improvement.

During Q1 2025, the BIOX® circuit operated marginally below the design throughput of 256 t/d. This was primarily due to low mill throughput combined with a lower-than-design flotation mass pull during the period. This was accompanied by a lower sulfide sulfur feed grade, mainly resulting from lower-than-design sulfide grades in the ore feed. Despite this, BIOX® sulfide oxidation levels and gold recovery in the CIL circuit were operating close to design levels.

A number of improvement initiatives have been identified to enhance overall plant performance, including optimisation of limestone and lime consumption, refinement of the Geomet blend, and improvements to dissolved oxygen levels in the CIL circuit.

## ACKNOWLEDGEMENTS

The authors would like to thank Endeavour Mining Sabodala Massawa Mine and Metso South Africa for allowing the publication of the paper.

## REFERENCES

Endeavour Mining, 2024. Sabodala–Massawa site visit presentation, 18 November. Available from: <https://www.endeavourmining.com/investors/presentations> [Accessed: 12 January 2026].

Endeavour Mining, 2025. Corporate presentation – 9 June 2025. Available from: <https://www.endeavourmining.com/investors/presentations> [Accessed: 12 January 2026].

# Autoclave preservation and recommissioning at Porgera Gold Mine, Papua New Guinea

*L Pundi[1], M Kumiye[2], R Palme[3] and D Akis[4]*

1. Senior Metallurgist, New Porgera Limited, Enga Province, Papua New Guinea. Email: lpundi@npltd.com
2. Senior Projects Metallurgist, New Porgera Limited, Enga Province, Papua New Guinea. Email: mark.kumiye@npltd.com
3. Superintendent Project Metallurgist, New Porgera Limited, Enga Province, Papua New Guinea. Email: r.palme@npltd.com
4. Processing Technical Service Manager, New Porgera Limited, Enga Province, Papua New Guinea. Email: akisd@npltd.com

## ABSTRACT

The Porgera Gold Mine in Papua New Guinea placed its Processing Plant under care and maintenance in April 2020, leaving four large autoclave reactors offline. A proactive preservation program was implemented: autoclaves were safely drained and filled with a low-density acidic solution of pH<4 and held at atmospheric pressure and temperature for over two years. The introduction of steam-boiler heating to maintain internal temperatures of 20–30°C was applied after inspection in 2022. This approach preserved brick hydration and sustained chemical passivation of linings, while preventing thermal shock and corrosion during the idle period. Conditions were closely monitored through routine inspections and temperature logging, and final inspections and minor repairs were completed before recommissioning and start-up.

Recommissioning commenced in December 2023, after more than three years of care and maintenance. A carefully sequenced ramp-up was executed across all units, following equipment supplier protocols for brick curing as well as internal operational procedures. A gradual, controlled increase in vessel pressure and temperature was applied to each autoclave, mitigating risks during start-up. Operator refresher training was undertaken ahead of the restart to ensure safe execution. The outcome was exceptional: all four autoclaves were successfully recommissioned with zero brick lining failures and no major relining or structural repairs required. The Pressure Oxidation circuit was restored to normal operation on schedule and within budget in July 2024, achieving design throughput shortly after restart.

This case study highlights the effectiveness of structured preservation and recommissioning strategies in autoclave operations. By maintaining controlled thermal and chemical conditions throughout care and maintenance, Porgera demonstrated that long-term idle autoclaves can be safely and efficiently restarted. The lessons learned provide a benchmark for future shutdowns of operating plants and recommissioning projects in high-sulfide gold processing environments.

## INTRODUCTION

The Porgera Gold Mine is located in the Enga Province of the Western Highlands of Papua New Guinea (PNG), approximately 130 km north-west of Mount Hagen and 600 km north-west of the capital, Port Moresby. The project is a large-scale, high-sulfide gold operation where gold recovery relies on pressure oxidation (POX) to treat refractory sulfide ore. The processing plant has historically operated at a rate of 5.7 million tonnes per annum (Mt/a), treating ore from the open pit and underground mines, plus stockpiles.

In April 2020, the Porgera processing plant was placed into care and maintenance following expiration of the operation's Special Mining Lease (SML), resulting in the shutdown of the pressure oxidation circuit and four autoclave reactors. Given the strategic importance of the POX circuit and the expectation of eventual restart, a deliberate decision was made to implement a structured preservation program rather than allowing the autoclaves to remain idle.

Prolonged shutdown of autoclave vessels presents significant risks, particularly to refractory linings and pressure-retaining components. Loss of brick hydration, uncontrolled corrosion, and exposure

to ambient temperature fluctuations can result in lining degradation and increase the likelihood of failure during recommissioning. These risks are compounded by the high temperature and pressure conditions experienced during start-up, where thermal shock can lead to catastrophic lining damage if preservation has been inadequate.

The objective of this paper is to document the preservation and recommissioning strategy applied to the Porgera autoclaves following an extended care and maintenance period. The paper describes the technical approach adopted to maintain refractory and vessel integrity, outlines the controlled recommissioning process, and presents the operational outcomes achieved. The scope is limited to autoclave preservation and restart considerations, with the intent of providing a practical reference for similar operations facing long-term shutdown scenarios.

## PLANT AND AUTOCLAVE CIRCUIT OVERVIEW

Porgera employs both Open Pit and Underground mining, from which ores from these sources to the Processing plant is predominantly refractory in nature.

The flotation circuit target concentrate grade is 14 per cent sulfur. The flotation concentrate is ground in the regrind mills to achieve a cyclone overflow of 92 per cent passing 38 µm. Pulp density of the resulting ground product is increased from 10–12 per cent to 48–50 per cent w/w in a concentrate thickener and is stored in concentrate storage tanks. These tanks provide approximately a buffer of six days between flotation and the oxidation section of the plant. From the storage tanks, the concentrate is pumped to a train of three carbonate reaction tanks, where the fresh feed is mixed with a portion of acidic recycled oxidised slurry to destroy most of the carbonates in the concentrate. Carbonate destruction reduces the release of carbon dioxide in the autoclaves and thereby improves the oxygen utilisation.

After carbonate destruction, the feed is directed to the four autoclaves. The reaction is self-sustaining once started, and quench water is added to each of the five compartments to control the reaction temperature as required. Oxidised slurry is discharged from the autoclave under pressure, along with the vent gases, into a flash vessel that is equipped with a gas scrubber system to control acidic and fine solid emissions. From there, the oxidised slurry is treated in a wash circuit comprised of two 35 m diameter stainless steel high-rate thickeners which operate counter-currently. The Concentrate thickener overflow is used as the acid wash water in the autoclave discharge thickeners. Fresh water is also added when required. The washed and thickened slurry is fed to the carbon-in-leach circuit at 45 per cent w/w.

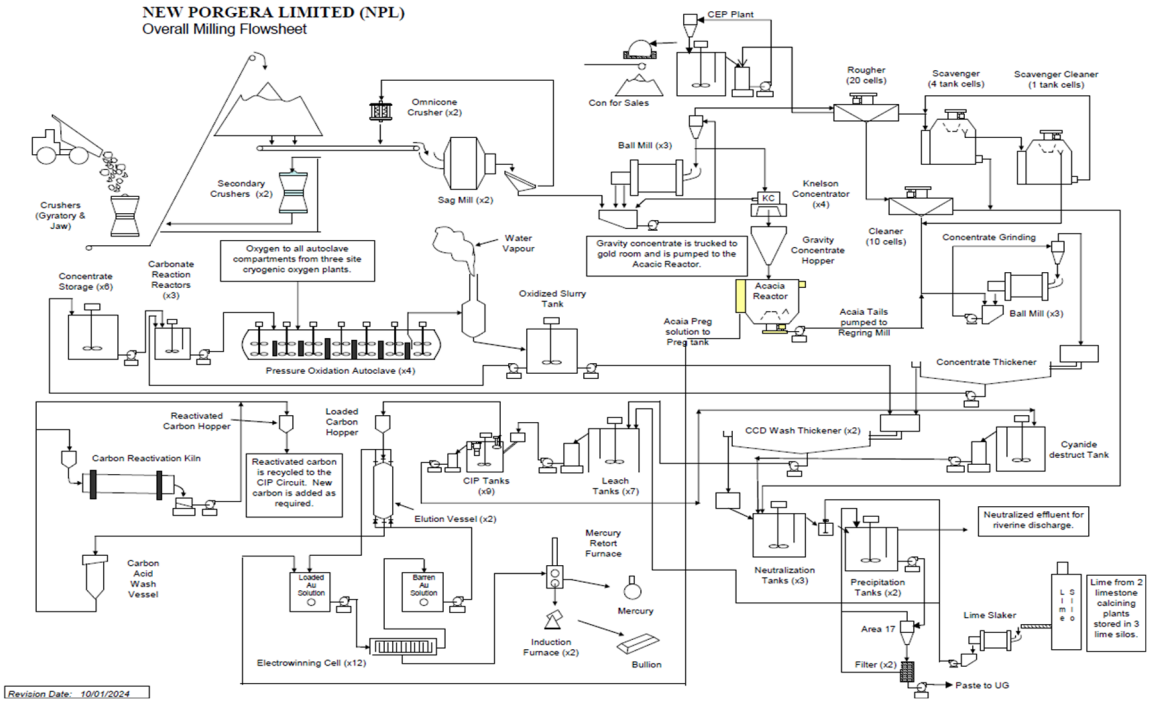



**FIG 1** – Porgera gold process flow.

## Autoclave design and operating parameters

### *Autoclaves*

- Four autoclaves are used to oxidise gold-bearing pyrite concentrate.
- Autoclaves 1, 2, 3 and 4 measure 3.57 m internal diameter by 25.1 m long.
- Each autoclave is fed using a high-precision, high-pressure diaphragm pump, referred to as Autoclave Feed Pumps (GEHO Pumps).
- All Autoclaves are fitted with seven 110 kW titanium agitators; compartments 1–4 agitators are operated on variable frequency drive. Compartment 5 (last compartment) agitators have fixed drive motors which uses its power draw as a proxy for the compartment 5 level.
- The autoclave shell is carbon steel, lined with lead and acid-resistant brick to resist the corrosion/abrasion generated by the pyrite oxidation.
- Operating pressure is 1750 kPa, and the average operating temperature across the autoclave is 198°C.
- The autoclaves are baffled into five compartments, with the first feed compartment three times the size of any of the other four, to ensure that sufficient sulfur in the feed is oxidised in the first compartment to bring the feed slurry autogenously up to the operating temperature.
- The effective working volume of each autoclave is 160 $m^3$.

### *Discharge tanks*

- Each autoclave is discharged through a choke assembly (52 mm) into a 3.5 m diameter × 10.5 m flash tank where heat is dissipated and steam generated during slurry cool down to 95°C.
- Oxidised slurry from the flash tanks is collected in a 13 m diameter × 13 m stainless steel oxidised slurry tank, complete with a 45 kW agitator.
- A portion of the slurry is recycled (28–30 per cent) to the autoclave feed to react with the carbonates and maintain acid balance in the autoclave feed for pyrite oxidation.

## Normal operating conditions

The typical operation throughput, pressure, and temperature for the autoclaves are detailed in Table 1.

**TABLE 1**

Operating data.

| | | |
|---|---|---|
| **Feed sulfur** | 8.5–9.5 | % |
| **Feed rate** | 75–90 | $m^3$/hr |
| **Autoclave operating temperature** | 196–200 | °C |
| **Autoclave operating pressure** | 1750 | kPa |
| **Oxygen overpressure** | 650 | kPa |
| **Oxygen utilisation** | 90 | % |
| **Nominal resident time** | 60 | min |
| **Sulfide oxidation** | 98 | % |
| **POX availability** | 85 | % |

## Historical operating performance and design improvements

Extensive research on improving oxygen mass transfer and dispersion in autoclaves was conducted on-site. The 'Oxygen Sparger Cap' was designed to produce a specific gas-dispersion sparger that disperses the high volume of oxygen needed during pyrite oxidation and prevents impeller flooding.

### *Design principles at Porgera*

The design is central to the POX process, where refractory gold-bearing pyrite is oxidised to allow for later cyanide leaching:

- **Anti-flooding geometry**: The Oxygen Sparger Cap profile is specifically engineered to prevent impeller flooding. In high-pressure autoclaves, standard impellers can become 'engulfed' by oxygen gas, leading to poor oxidation. The conical hub directs gas bubbles outward into the high-shear zone.
- **Oxygen dispersion**: Oxygen is sparged directly beneath these impellers. The design ensures that gas is broken into extremely fine bubbles, increasing the surface area for oxygen mass transfer into the acidic slurry.
- **Sulfide oxidation**: This efficient dispersion is what allows the oxidation of sulfides at temperatures exceeding 180°C and high pressures within the five-compartment autoclaves.

### *Implementation context*

- **Mechanical set-up**: These units are typically the lower impeller on a dual-impeller shaft. The upper impeller (often a hydrofoil) provides global mixing, while the Oxygen Sparger Cap handles the intense gas-liquid contact at the base.
- **Operational optimisation**: Highly skilled professionals at Porgera have worked on debottlenecking these circuits. Improvements involve adjusting the oxygen distribution across compartments and refining the mechanical durability of the impellers against the highly abrasive slurry.

### *Maintenance schedule*

Autoclave Maintenance Schedule for Porgera:

- 9-monthly inspections: Conduct inspections every nine months, focusing on the face-course brick and mechanical components to ensure they are in good condition and functioning properly.
- 5-yearly full face course brick change out: Every five years, a complete change of the face course bricks should be performed to maintain the integrity and efficiency of the autoclave.
- 15-yearly full rebrick: A comprehensive rebricking of the autoclave should be carried out every 15 years to address any wear and tear and to extend the lifespan of the equipment.

This schedule is crucial for maintaining the operational efficiency and safety of the autoclave. Regular maintenance can prevent unexpected failures and costly downtime.

# AUTOCLAVE PRESERVATION STRATEGY DURING CARE AND MAINTENANCE

## Brick preservation planning

After the Mine shutdown in April 2020, the autoclaves were batched out and boxed up.

In October 2022, DSB Brick Supplier (Germany) was contacted to further review the preservation of the autoclaves to ensure the reliability of refractory and other critical autoclave components is maintained until restart, as below:

- Fill the Autoclave with slurry or sulfuric acid up to the height of the first overflow compartment wall. So that the filling height throughout the complete autoclave is at that height.

- When the autoclave liquid is a slurry, run the agitators to keep the solid particles in the liquid phase, so they will not settle down. There is a risk that any settlement will get solid, rock hard, and difficult to remove for the new start-up.
- No need for the agitator to turn once the autoclave liquid is just acid.
- Maintain autoclave temperature between 15°C and 30°C. Acid concentration in the slurry or just acid below 10 g/L sulfuric acid, but at least pH<4.

Also, as part of the planning, a risk assessment was done before autoclave draining and filling.

## Autoclave draining and chemical conditioning

The process of draining and filling the autoclave with a dilute acid solution involves several critical steps to ensure safety and efficiency.

Initially, the dump tank is emptied to remove any existing contents. It is then filled to approximately 18 per cent capacity with the discharge from the autoclave.

To prepare for the autoclave filling, water is added to the dump tank until the level reaches 90 per cent. This step is crucial, as it helps reduce the solution's temperature, solids, pH, and acid content.

Before proceeding with the filling of the autoclave, samples from the dump tank are collected and sent to the assay laboratory for analysis of temperature (15–30°C), pH (<4.0), and sulfuric acid (<10 g/L).

The dilute acid solution is then transferred through a filling hose equipped with an injection fitting. This solution comes from the oxidised slurry recycle line and is discharged into the autoclave filling flange, especially targeting compartments 1A and 2.

Throughout the filling process, operators utilise an infrared temperature gun to monitor the temperature, ensuring it remains within safe operational limits. This procedure emphasises the importance of careful monitoring and controlling chemical properties to maintain safety and process efficiency during autoclave operations.

## Monitoring, inspections and maintenance activities

During the preservation period, a comprehensive assessment of each autoclave was conducted, focusing on the integrity of the brickwork. This involved a series of hammer tests performed collaboratively by the Processing, Maintenance, and DSB teams.

Key findings:

- significant loss of integrity on the vapour phase was observed
- the bricks remained in good condition, indicating that the slurry phase was performing adequately
- temperature across autoclaves was recorded at a notably low 15°C. This is well below the optimal range for effective operation. Each autoclave was only half-filled with acid, which is insufficient for maintaining proper operational parameters.

The recommendation from the DSB is to fill all autoclaves 1–4 with acid up to the 12 o'clock position and apply external heat from the outside. The best temperature is between 20°C and 30°C. This temperature adjustment is crucial for improving the efficiency and effectiveness of the autoclaving process.

## Temperature control and heating method

The temperature control and heating method for the autoclave is designed to ensure optimal conditions during the preservation period, following recommendations from DSB. The plans involve specific heating and cooling protocols aimed at maintaining the internal shell temperature within a defined range.

Heating phase: The first step involves heating the autoclave shell using steam boilers until the internal temperature reaches 30°C.

Cooling phase: Once the internal temperature reached 30°C, the heating was halted to allow the shell to cool down naturally. This natural cooling is important to prevent thermal shock and potential damage to the autoclave structure.

Reheating phase: The temperature was monitored closely, and when it dropped to 25°C, reheating commenced. This cycle ensures that the shell temperature is effectively maintained within the target range of 20°C to 30°C. The maximum shell temperature is 35°C.

Figure 2 and Table 2 illustrate a daily report that exemplifies how the operation of the autoclave boiler was monitored throughout the preservation period.

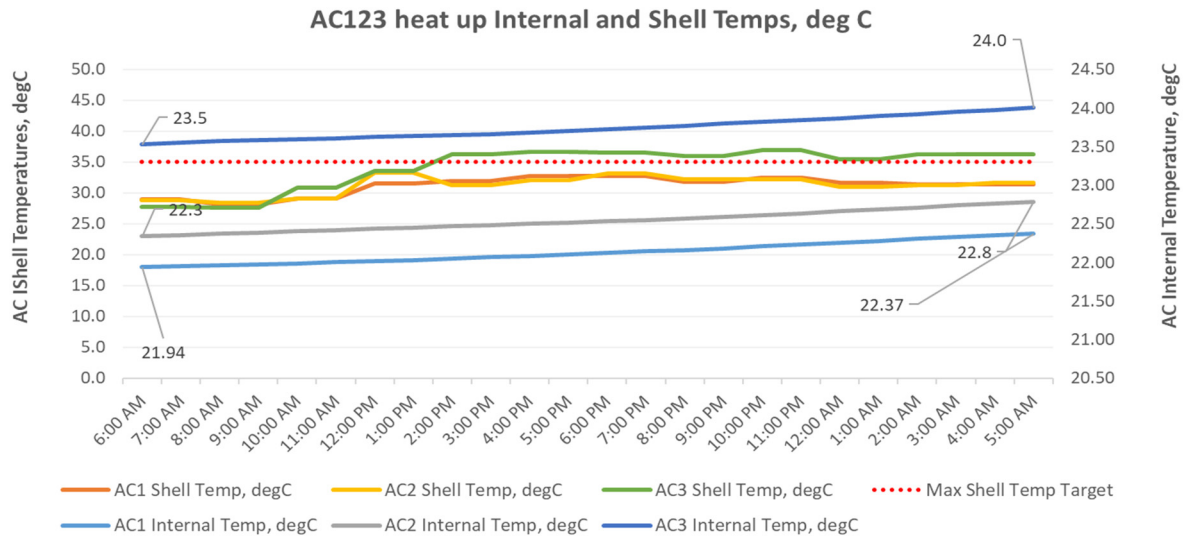



**FIG 2** – Porgera Autoclave internal and shell temperature monitoring trends.

**TABLE 2**

Porgera Autoclave internal temperature and heat-up rate monitoring.

**Autoclave Internal Temperature & Heat-up Rate for the last 24hr and Expected Temperature in the next 24hrs**

| Autoclave | Current Temp,˚C | Heating Rate,˚C/h | Temp on 13-Jan-23 |
|---|---|---|---|
| 1 | 22.5 | 0.018 | 22.91 |
| 2 | 22.7 | 0.019 | 23.12 |
| 3 | 24.0 | 0.020 | 24.48 |

| Estimated days to reach 30˚C Internal Temperature | | | | Estimated days to Cool from 30˚C - 25˚C | | |
|---|---|---|---|---|---|---|
| Autoclave | Current Temp,˚C | Heating Rate,˚C/h | Temp to reach 30˚C | Cooling Rate, ˚C/hr | Boiler Start-up Temp, ˚C | Boiler Start-up Date. |
| 1 | 22.5 | 0.018 | 29-Jan-23 | -0.02 | 25 | 10-Feb-23 |
| 2 | 22.7 | 0.019 | 28-Jan-23 | -0.02 | 25 | 10-Feb-23 |
| 3 | 24.0 | 0.020 | 29-Jan-23 | -0.02 | 25 | 10-Feb-23 |

## RECOMMISSIONING APPROACH

The re-commissioning of the Autoclave has been staged into four main groups as follows.

Terminology:

Wet Commissioning means that the Equipment has been tested, checked, and run to demonstrate that the Equipment is ready for operation, but excludes the introduction of raw or other process feed materials (no slurry).

Hot Commissioning means that the Equipment has been tested, checked, and run to demonstrate that the Equipment is ready to be placed into operation, subject to any actions or outcomes that do not comply with commissioning requirements.

Stage 1 – Pressure oxidation circuit refurbishment:

- Primary stage where all maintenance checks are done on mechanical, electrical, and instrument components. The reliability inspections, quality assurance, and checks of pipes, vessels, and valves.
- Processing Operations reviewed boundary isolation steps, standard operating procedures, and risk assessments to facilitate all required maintenance.
- Developed a commissioning checklist in preparation for recommissioning the plant.

Stage 2 – Pressure oxidation pre-commissioning:

- Fixed Plant Maintenance and Process Control team do checks to ensure all equipment is boxed, and instrument and control checks are done, and sign off permits before handing over to the Processing Operation team.

Stage 3 – Pressure oxidation Wet Commissioning:

- Performance testing of all autoclave vessels and their services connected and tested:
  - Air supply systems (Process and Instrument air).
  - Boiler (Maximum Steam production) Steam Lines to Ring Main and Autoclave/Blow down and check for leaks and activators.
  - Seal Water Systems to Autoclave agitators.
  - Quench Water System, Recycle-> Feed to Scrubber, Close discharge valve A and Open valve B, Fill Flash Tank with Choke water.
  - Flash discharge tank A pumps and control logics with water through choke (Quench pumps).
  - Dump Tank advance pump and Recycle pumps with water to Wash Thickener # 2.
  - When all discharge end tests PASS, Stop Choke water addition and run out water in the system.
  - Test discharge valve A&B for Autoclave.
  - Test Pressure according to the Pressure Temperature Curve; discharge when the compartment 5 level increases, oxygen line purging with quench regularly to avoid blockages.
  - Test Concentrate Storage Tank 1&2 forwarding Pumps and Oxidised Slurry Recycle and Carbon Reaction Tank 3 interlocks are still functional.

Stage 4 – Pressure oxidation Hot Commissioning:

The hot commissioning of the autoclave systems involved the integration of oxygen and slurry to facilitate the testing of crucial interlocks, specifically focusing on the GEHO pumps and the pressure/temperature interlocks associated with the autoclave feed and oxygen header.

Commissioning Steps:

- Preparation of Autoclave: The autoclave was pressurised and brought to the designated operating temperature. Minimum oxygen levels were established to begin the commissioning process.
- Interlock Testing: Conducted tests on interlocks with oxygen present in the autoclave vessels to verify their operational readiness. Ensure that the GEHO pumps responded correctly to various operational scenarios involving oxygen and slurry.
- Pressure Safety Valve/Pressure Control Valve Testing: All Pressure Safety Valves (PSV) and Pressure Control Valves (PCV) were tested while the feed was active. Pressure was gradually increased to assess the trip limits and ensure that the safety system functioned as intended.

The hot commissioning of the autoclave with oxygen and slurry was completed, demonstrating the reliability of the system's interlocks and safety protocols.

## Recommissioning timeline and preparation

The recommissioning of the pressure oxidation circuit was a comprehensive process that spanned over 12 months of preparation, commissioning, and start-up phases.

A thorough field risk assessment was conducted by the Processing leadership team to identify potential risks and undesirable events associated with the recommissioning process.

This assessment not only highlighted risks but also outlined appropriate controls and mitigation strategies to address these risks before commencing any inspection or recommissioning activities.

Effective timeline management was crucial in ensuring readiness for start-up. This involved a detailed scheduling process that was fundamental in coordinating various tasks and activities.

Fixed Plant Maintenance planners were responsible for managing maintenance planning and schedules, ensuring that maintenance tasks were completed in a timely manner to support the overall recommissioning efforts.

Concurrently, operations experts were tasked with managing the operational schedule, overseeing the execution of operational activities essential for the successful start-up of the circuit.

## Autoclave circuit pre-commissioning inspection and operational checks

Before the recommissioning of the pressure oxidation circuit, Ferox Global was engaged to assist in identifying circuit design risks, recommending appropriate controls, providing technical support in implementing these controls, and identifying additional condition-based risks and their corresponding controls. Below are key recommendations based on their inspections and findings:

- Monitor valve operation and service life, and to either explore a return to the Original Equipment Manufacturer (OEM) sealing rings or to seek a design modification should the polymer component become a cause for concern.
- The flash underflow pipes spools be redesigned for ease of replacement of high wear sections, wear-resistant lining materials such as ceramics be investigated, and a preventative replacement strategy be aligned with circuit maintenance opportunities.
- Upgrade all control panels to be aligned with those installed on GEHO 1 and 4, for improved field operability and troubleshooting capability.

## Brick inspection and refurbishment

In September 2023, an internal inspection of three autoclaves was conducted. The inspection revealed that autoclaves 1, 2, and 3 require minor brick repairs. The impingement block was placed to last for years. The joints were pointed, and the scale was cleared from under the impingement block.

These repairs were completed, and all autoclaves were deemed suitable for restart by the OEM.

Subsequently, autoclaves 1 and 2 were brought online in April 2024, following the heat-up guidance provided by DSB.

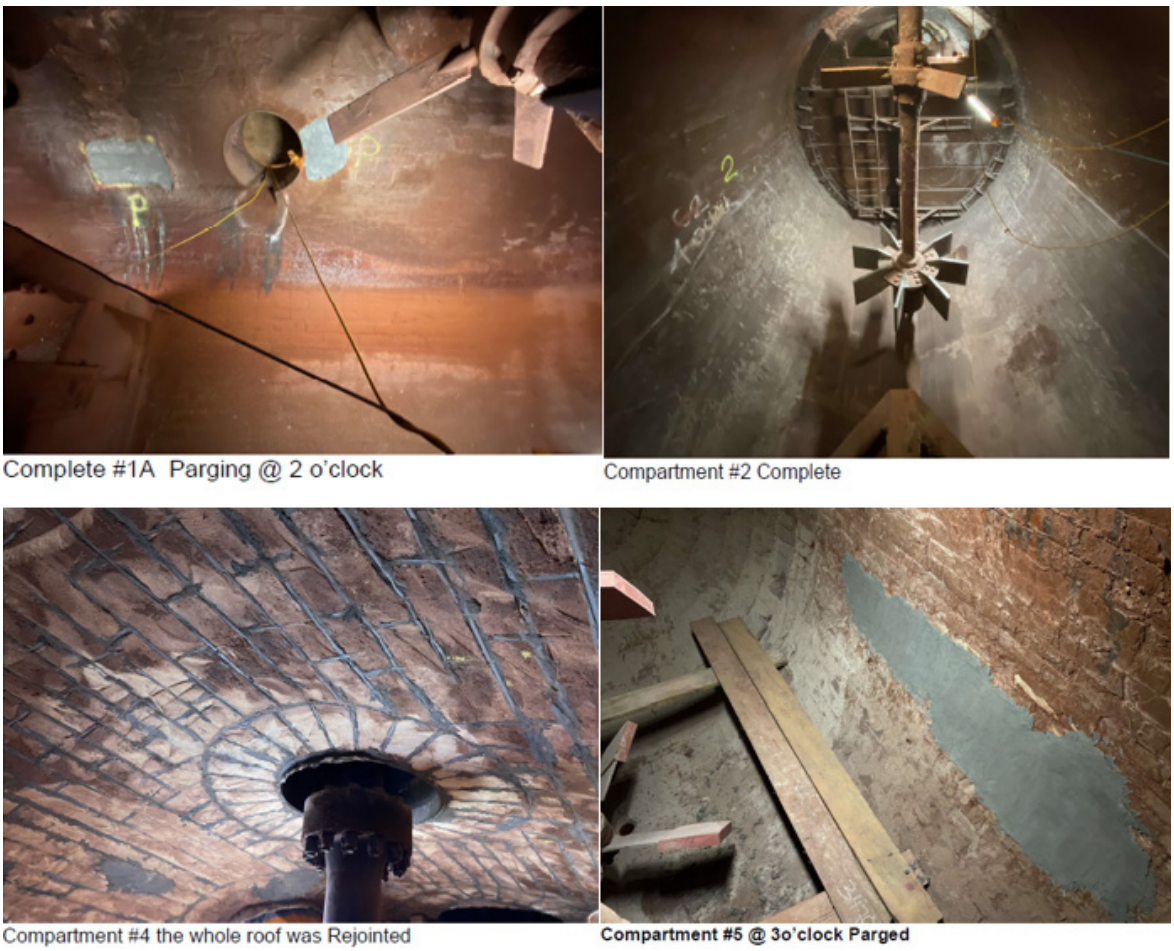



**FIG 3** – Autoclave 1 brick refurbishment.

## Autoclave curing and start-up

The physical behaviour of a brick lining inside a steel vessel during heating up, cooling down, pressurisation, and depressurisation differs significantly from that of the steel vessel itself. Therefore, DSB has issued specific instructions and recommendations for start-up, commissioning, and operations:

- Sudden drops in pressure or temperature can be detrimental to the brick lining. It is essential to avoid such occurrences, and any pressure drops exceeding 35 kPa/h must be reported to DSB immediately.
- Each heating and cooling cycle imposes stress on the brick lining. To prolong its life, these cycles should be minimised wherever possible.
- It is critical to adhere to the specified temperature and pressure gradients to extend the lifespan of the brick lining.

Proper management of these factors will help ensure the integrity and functionality of the lining throughout its operational life.

Autoclave brick curing and heat-up process, as aligned with DSB, is summarised in Table 3, along with the chart in Figure 4.

**TABLE 3**

Restart brick curing and heat-up process.

| Event | Heat-up & Cooling Rate | Duration (hrs) | Cumulative (hrs) | Temperature |
|---|---|---|---|---|
| Completion Lining | | 0 hrs | 0 hrs | 25°C |
| Air-curve | | 36 hrs | 36 hrs | 25°C |
| Filling clave with acid | | 6 hrs | 42 hrs | 25°C |
| Soaking of bricking | | 12 hrs | 54 hrs | 25°C |
| Lower Liquid Level | | 2 hrs | 56 hrs | 25°C |
| Heating | 5°C/h | 15 hrs | 71 hrs | 100°C |
| Holding | | 6 hrs | 77 hrs | 100°C |
| Heating | 10°C/h | 9 hrs | 86 hrs | 190°C |
| Holding | | 6 hrs | 92 hrs | 190°C |
| Add O2 and Process Slurry (FEED ON) | | 6 hrs | 98 hrs | 190°C |
| Cooling down to 100°C | 20°C/h | 4.5 hrs | 102.5 hrs | 100°C |
| Holding | | 2 hrs | 104.5 hrs | 100°C |
| Cooling down to 80°C | 20°C/h | 1 hrs | 105.5 hrs | 80°C |
| Air Cool | | 12 hrs | 117.5 hrs | 30°C |
| Inspection of Bricklining | | | | 30°C |

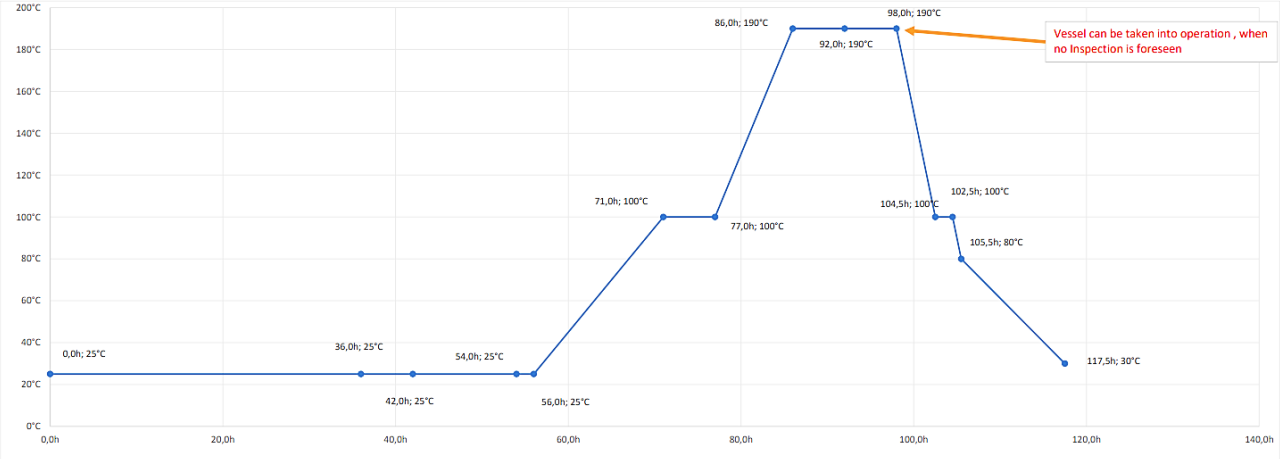



**FIG 4** – Porgera Autoclave brick curing and heat-up process chart.

## Monitoring and inspection during recommissioning

During the recommissioning phase, Ferox Global continues to monitor the performance of Autoclaves 1 and 2 after start-up. Inspection findings and recommendations are as follows.

### *Conditioning monitoring*

- Extensive condition monitoring was performed during the start-up of Autoclave 1 and also on Autoclave 2 agitators. Vibration analysis on Autoclave 2 agitators identified three gearboxes with high-speed bearing outer race defects.
- Thermographic images were also taken on Autoclave 1 agitator gearboxes, motors, and mechanical seals with guards removed. Slightly elevated temperatures were noted on Autoclave 1 agitator gearbox compartments 1A and 4. This appears to be normal, as there is no vibration signal of concern on either gearbox. Breathers were removed and replaced. The Autoclave 1 compartment 4 mechanical seal was found to be approximately 10°C hotter than the adjacent seals.

- Thermographic scans were taken on the Autoclave 2 agitators whilst the autoclave was at 100°C and filled with acidic water. No issues were identified. Thermography was also performed on the autoclave shell.

### *Autoclave 1 monitoring, Autoclave 2 commissioning, and Autoclave 3 start*

Three agitator gearboxes (C1A, C2, and C3) were replaced on Autoclave 2 due to high-speed shaft and non-drive end bearing faults that were detected via vibration analysis. Faults were confirmed during the dismantling of the gearboxes. The failure mode appears to be common across the gearboxes. It was recommended that the ARMS Engineering root cause analysis report be revisited, actions reviewed and implemented to prevent recurrence.

Thermal imaging was also performed on the autoclave shells to monitor for temperature variations beyond the expected temperatures, which may indicate degradation of the lining system. All autoclaves presented normal temperature profiles at 150°C internal temperature.

However, once at operating temperatures of approximately 200°C, autoclave 2 exhibited an elevated temperature profile across all compartment liquid zones, with temperatures of greater than 115°C indicated on compartments 1A, 1C, 2, 3, and 4. The manufacturer of the lining system recommends that the shell not be exposed to temperatures of 115°C or greater for an extended period due to the risk of lead-lining damage.

It is recommended that site technicians perform shell temperature monitoring at regular intervals and with increased frequency following process excursions such as vessel depressurisations. It is also recommended that a trigger-action response plan (TARP) be developed to guide an appropriate response to the identification of shell temperature recordings that indicate a likely change in the integrity of the lining system.

## RESULTS AND OBSERVATIONS

The recommissioning process of all autoclaves has been completed successfully. Notably, each autoclave was brought back online without the necessity for major brick relining or structural repairs. This outcome underscores the effectiveness of proper long-term preservation planning strategies.

Before preservation and recommissioning, each autoclave underwent a thorough assessment. This included inspections of the structural integrity and functionality of critical components.

The adherence to regular maintenance schedules contributed significantly to the successful recommissioning process. Routine checks and preventive measures ensured potential issues were addressed before they escalated.

All autoclaves demonstrated operational readiness upon recommissioning, with no major faults detected. This includes optimal performance in pressure and temperature settings.

## Issues encountered and mitigation measures

### *Boiler operation*

Encountered issues such as boiler trips, scaling, unstable fuel supply, and water treatment inconsistencies can disrupt steam supply, affecting temperature and temperature and pressure control inside the autoclave. A plan was in place to install a water softener and a demineralised water system, and to overhaul logic controls.

### *Recruitment and training*

Challenge to recruit experienced operators, provide training, and conduct competency assessment. Since the experienced operators had left after the Mine shutdown, it was challenging to hire and train recruits in preparation for start-up.

### *Flange, piping, and valve leakages (autoclave discharge end)*

The discharge end of the autoclave is prone to leaks due to high temperature, pressure cycling, and acidic slurry. These conditions accelerate wear and fatigue in flanges, piping systems, and valves. A proper QA/QC check needs to be done before signing off.

### *Low feed sulfur grade*

Low Sulfur content in the Ore feed will impact Autoclave operations as per the design operating parameters. Will have to review with experts to change Autoclave operations for low feed Sulfur grade <10 per cent S.

### *Autoclave operations*

Minimising high Sulfur discharge (>0.5 per cent S2-) remains an ongoing operational challenge, particularly during transitions such as switching between autoclaves or bringing a standby unit online.

## LESSONS LEARNED

The process of draining the autoclave and subsequently filling it with an acid solution was executed effectively in accordance with the recommendations provided by DSB. This method proved to be crucial for preventing corrosion and maintaining the integrity of the autoclaves during the preservation phase.

The findings and recommendations from both DSB and Ferox Global were invaluable throughout the preservation and recommissioning processes. Their thorough inspections ensured that all autoclaves were assessed and maintained in optimal condition, thereby minimising the risk of operational issues upon recommissioning. This structured approach to monitoring was essential for the successful operation of the autoclaves.

## CONCLUSION

The preservation strategy implemented during the care and maintenance period was highly effective, ensuring optimal conditions for nearly 3.5 years leading up to the recommissioning.

The recommissioning process was executed smoothly and safely without any lost time injuries and significant environmental non-compliances, adhering to both the established schedule and budgetary constraints.

This positive outcome not only ensures operational reliability but also confirms the sound condition of the equipment.

The success of this project sets a strong benchmark for future care and maintenance initiatives, demonstrating best practices in preservation and recommissioning processes.

## ACKNOWLEDGEMENTS

The authors wish to thank the Porgera site Operation and Maintenance teams for their professional and cooperative approach to preservation and recommissioning of Autoclaves during the care and maintenance period leading up to start-up.

The contributions by DSB Brick Supplier (Germany) and Ferox Global were invaluable to the success of the preservation and recommissioning of the Autoclaves.

# Operational readiness journey of the Mungari Operations' plant expansion

*M K Thompson[1] and A G L Pratt[2]*

1. MAusIMM, Principal Metallurgist, Evolution Mining, Perth WA 6000.
   Email: matthew.thompson@evolutionmining.com
2. FAusIMM(CP), Principal, Adrian Pratt and Associates Pty Ltd, Hampton Vic 3188.
   Email: adriangpratt@bigpond.com

## ABSTRACT

Evolution Mining (Evolution) is the owner and operator of Mungari Operations (Mungari), located 600 km east of Perth and 20 km west of Kalgoorlie in Western Australia. Mungari is an established mine site with all major infrastructure in place. In September 2023, Evolution approved a capital investment of $250 million for the Mungari processing plant expansion, increasing its capacity from 2 million tonnes (Mt) to 4.2 Mt/a (per annum) (Evolution Mining Limited, 2023). The brownfield expansion of the processing facility maximises the use of the existing plant, with significant additions including the front-end crushing and milling circuits, installation of a larger gravity circuit and an expanded leach circuit.

This case study focuses less on the design and construction of the plant expansion and instead details the activities undertaken by the Operational Readiness team that were critical to the project's overall success. The paper also highlights key recommendations and lessons learned. Throughout the paper, the authors aim to impart knowledge and experience to the reader, rather than provide an exhaustive plan, and to offer key insights and recommendations for mineral processing professionals seeking to implement operational readiness plans at their sites. In summary, the case study demonstrates that success in any Operational Readiness team largely depends on ensuring the right people are in the right roles and have access to the required processes, training, tools, consumables, and other resources to commission the plant and maintain long-term operations safely.

## INTRODUCTION

Evolution Mining (Evolution) is the owner and operator of the Mungari Operation (Mungari), which is located 600 km east of Perth and 20 km west of Kalgoorlie in Western Australia. Figure 1 shows the location of the Mungari Operation as well as Evolution's other Australian assets. Mungari is an established mine site with all major infrastructure in place.

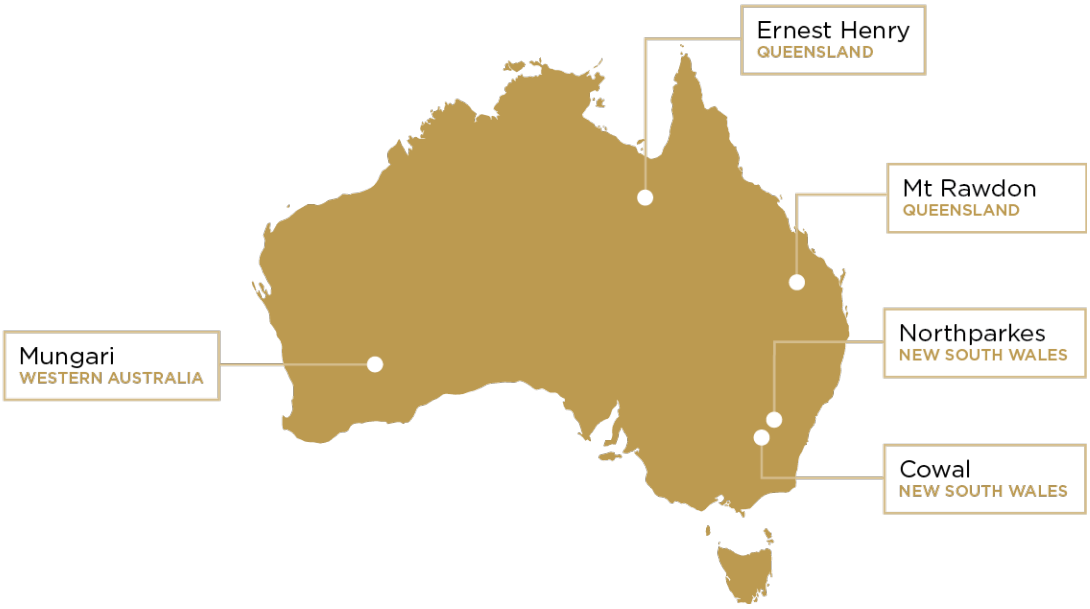



**FIG 1** – Mungari Operation location.

Evolution approved a capital investment of $250 million in 2023 to expand the Mungari processing plant from 2 Mt to 4.2 Mt per annum (Evolution Mining Limited, 2023). The plant expansion unlocked an additional resource base, reduced all-in-sustaining costs (AISC), extended mine life, and provided uplift to site gold production capacity.

The expansion to the processing facility maximised the use of Mungari's existing plant, with the main modifications being to the front-end crushing and milling circuits and installation of a larger gravity circuit and two new leach tanks. Capital expenditure commenced in FY24 with the engagement of a key contractor partner to deliver the project, with commissioning and ramp-up underway in FY26.

Development of the regional open pits was required to match the increased processing capacity delivered by the Mungari Expansion Project. This required upfront capital for infrastructure construction at each site. Pre-production capital requirements include the development of haul roads, water supply and dewatering, communication systems, offices and ablutions, workshops, fuel storage and explosive magazines, and a mining camp to service the regional operations.

The purpose of the Operational Readiness (OR) process at Mungari was to ensure that the Processing department and its functional areas were prepared to receive the handover of the expansion project and to operate the expanded plant safely at its intended production levels. Key goals were focused on ensuring that; new risks were identified and controlled, workforce capability was enhanced with relevant training support available, and spares and consumables were on-site prior to commissioning. To give effect to this purpose, Evolution used an operational readiness framework centred around people, processes, relationships, tools and equipment. This framework was the basis for developing an operational readiness plan (ORP) for the project (Evolution Mining Limited, 2024). This plan ensured that the people, processes and systems required to safely deliver effective systems of work were implemented prior to the completion of the plant expansion. The ORP enabled the smooth transition of project facilities, plants and assets to an operating plant that achieves the approved business plan objectives and specific project deliverables (Pratt, 2023).

Both the OR framework and plan were aligned to deliver the desired outcomes of:

- Ensuring everyone returned home safe every day.
- Having plans and controls in place to manage new risks.
- Maintaining community and public support.
- Achieving production ramp-up in line with the business plan and limiting downtime events.
- Ensuring the new in-pit tailings storage facility (IPTSF) was constructed and made ready prior to plant commissioning.
- Ensuring all consumables and maintenance spares were available at commissioning.
- Creation of the required training and safety documentation and ensuring all members of the operations team were trained and competent to operate the new plant.
- Establishing a sustainable business.

Any delays or failures in achieving these outcomes could have significantly impacted the project (Figure 2).

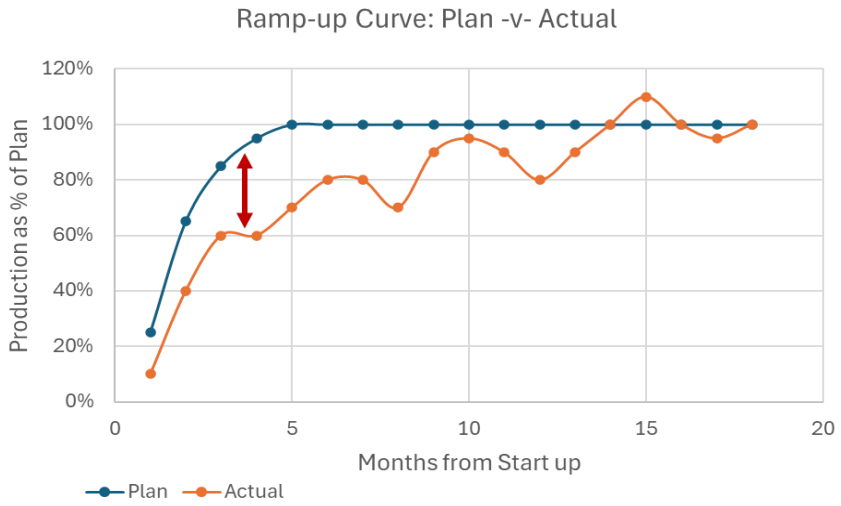



**FIG 2** – Illustrative ramp-up scenario showing the potential for value destruction (Source: Adrian Pratt and Associates).

Operational readiness touched every aspect of the Processing department during the plant expansion project; however, as a brownfield project, the scope and scale of this work varied across the department's functional areas. In essence, it involved ensuring the right people were in place, with the proper training and access to the right processes, tools/software/consumables, and equipment to safely start and sustain the operation and achieve the project's objectives. In detail, it meant that the OR team was directly focused on ensuring that; the operations team received training and had access to useful and practical reference material, the maintenance team had the requisite spares at their disposal with the means and knowledge to maintain the new plant, and the metallurgy team understood the new process and were empowered to lead the department technically through the ramp-up.

The achievement of these outcomes depended on the successful implementation of the following operational readiness activities to set the tone and context:

- Establishing the right operational readiness organisational structure.
- Selecting the right people for the right roles.
- Creating 'buy-in' and ownership for the operations team as future owners.
- Promoting a collaborative and effective operating environment.
- Establishing effective operating processes and controls.
- Establishing strong external relationships.
- Selecting the right tools and consumables for operations.

## PLANNING

A decision was made to establish an Operational Readiness team that was partially independent from both the project and site teams during the completion of the Feasibility Study. Early planning considered that relying on the site operations team to manage operational readiness in addition to their current responsibilities would result in a sub-standard outcome in both areas. The chosen approach allowed the OR team to work in parallel with the progress of plant construction, engaging and developing a level of ownership among the site team in the decisions being made. Importantly, this meant that the operations team, as future owners, were able to continue their day-to-day work while still being involved in the direction of operational readiness at an appropriate level. In this way, it was envisioned that the OR team would serve as an important interface between operations and the project team, facilitating a high level of site ownership upon completion and an efficient transition to commissioning activities.

Planning for operational readiness began approximately 15 months before the expected practical completion date. This provided ample time for planning and recruitment and aligned with the progression of detailed design commitments, which the engineering contractor primarily addressed.

To support OR scope development, a framework was developed to provide the foundation for identifying and completing required activities and for reporting progress.

The framework for operational readiness addressed the:

- Ownership and leadership of operational readiness for the Mungari Expansion Project within the Site Leadership Team (SLT).
- Establishment and use of a common workflow structure for operational readiness at Mungari.
- Communication within Mungari, and more broadly as necessary, regarding progress.
- Links between operational readiness tasks and Mungari's Operational Risk Register and Mine Operating System (MOS) to incorporate the expanded plant operations into the broader Mungari operation.

The operational readiness framework for the Mungari Expansion Project acknowledged Mungari's existing departmental structures and the functional areas they supported. Functional areas are typically led by a manager or superintendent at Mungari, and work planning under the OR scope was developed in tandem with these leaders. It was critical to engage directly with the departmental leaders to ensure that key activities were identified and included within the Operation Readiness Plan (ORP). A key part of these early interactions was setting the expectation that, whilst the OR team were ultimately responsible for delivering on these requirements, there would be a continuous and consistent build-up in involvement and ownership from the site team. This was to ensure that the site team, as future owners of the expanded plant, would be able to assume responsibility at handover and lead through plant commissioning.

The workflow structure, illustrated in Figure 3, was applied to each department and its functional areas. The purpose of this approach was to align the broader business objectives with the tasks undertaken by each of the operation's functional areas and to support the commencement of the expanded operations in line with their targeted outcomes. Importantly, a common workflow across functional areas ensures a consistent approach to operational readiness, facilitates shared learning, and promotes cohesion in reporting on operational readiness progress. This integration offers a real, practical understanding of an operation's actual state of readiness.

It was the responsibility of the General Manager and the SLT to operate the Mungari operation and its associated infrastructure at production levels aligned with the approved business plan. Therefore, their roles have the most scope to influence the completion of operational readiness work. Their ownership and commitment to the operational readiness process as a coordinated and cohesive effort are key to its success. At Mungari, the leadership of the SLT provided the OR team with:

- A level of importance and prioritisation on operational readiness tasks that was communicated to the wider business.
- Direct access to funds required to expedite spares purchase.
- Access to personnel for direct internal secondments, which supported the OR scope.

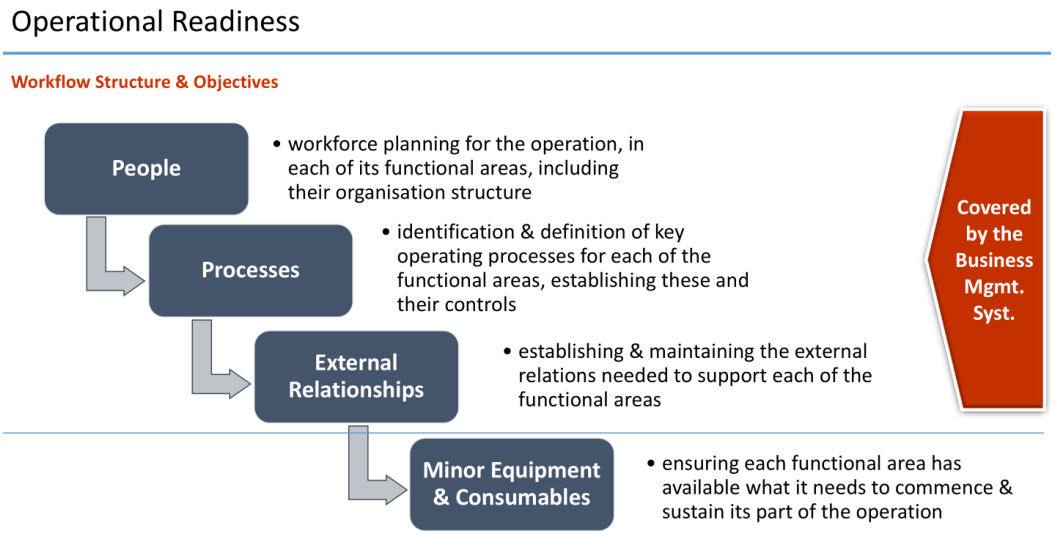



**FIG 3** – ORP workflow structure (Pratt, 2023).

There was an important link between Mungari's Operational Risk Register and the ORP, as it helped focus operations on what needed prioritisation from the outset, ensuring that the expanded operation successfully met its targeted production outcomes and integrated seamlessly into the wider Mungari operation. The Operational Risk Register is an enduring document that Mungari maintains and monitors throughout the asset's life to identify, assess and mitigate all risks to the operations. The ORP supported the Processing department and its functional area leaders in preparing and establishing expanded operating systems and processes and was informed by the Risk Register to identify and prioritise key operational readiness tasks that enable productive, sustainable operation. A key example of this was the integration of the new IPTSF.

The risks associated with tailings storage facilities are well known and comprehensively documented within the Mungari Risk Register, though the construction of the new IPTSF necessitated a review and update to risk management processes. This review formed an important aspect of the OR scope, with work undertaken to ensure that the operational changes brought forth from the introduction of a new type of tailings storage were adequately identified and documented across the site's risk management plans, critical control processes, verification plans, and safe work practices.

## BUILDING THE TEAM

As previously discussed, arguably the most critical goal of the operational readiness plan was to ensure that the site operations teams were highly engaged in the process and developed a high level of ownership in the outcome. The OR team needed to generate a high level of trust among stakeholders across the project and site operations teams. To achieve this, the Processing Lead of the plant expansion, previously the Metallurgy Superintendent at Mungari, was appointed as the Manager – Processing OR. Two additional appointments for OR Superintendent roles were made from Evolution employees who had previously held roles as the Processing and Maintenance Superintendents at Mungari. These appointments placed people in key OR positions who were not only skilled and competent in their respective areas but also maintained existing relationships and a high level of trust with members of both the site and project teams.

With the key leadership roles within the OR team solidified, the next phase of building the team required establishing clarity on scope, critical roles, and responsibilities. In practice, this meant building on the OR framework to define a clear and concise responsibility and reporting matrix, a scope of work, and a workflow structure. The first step in this process was to define the roles and responsibilities for preparing and managing the ORP's work.

Specifically, the ORP roles included:

- General Manager Mungari Operations (GM MGO): ORP endorsement and support for Operations Manager leadership to deliver against the ORP's outcomes and objectives.

- Mungari Expansion Project Manager: contribution to and support of the ORP process by ensuring the timely availability of project information, cooperation and coordination with the Mungari Expansion Project team when required.
- Operations Manager: accountability for managing the compilation of the Mungari Expansion Project's ORP and the coordination between the Operations team managers to ensure the effective delivery of plan outcomes and objectives.
- Manager – Processing OR: responsibility for facilitating, mentoring, monitoring, auditing, and reviewing OR progress against the ORP and distribution of this information to all required levels of the business.
- Operations team management: Mungari's SLT and functional area leaders for operational and support-focused work groups. Responsible for the leadership and coordination of their teams to deliver the ORP requirements as they relate to their areas of operation. This includes building their teams, preparing their operating processes and associated procedures, collaborating with other site leaders to support their completion of work, developing community and regulatory relationships as appropriate, and ensuring they have access to the equipment required to perform their functions effectively.

With key roles and stakeholders identified, progress was made toward finalising the remaining members of the OR team. A key requirement was to establish a clear scope of work and schedule to clarify the team's headcount and skill sets. The OR scope is discussed further in the next section, though broadly, the work streams fell under the following:

- OR Management and reporting.
- Processing readiness.
- Maintenance readiness.
- Commercial.
- Sustainability, environment and community.

With scope areas defined and roles clarified, the operational readiness team structure was developed. This is shown in Figure 4. The broader intent infilling these positions was to prioritise engagement and involvement with the site operations team, where appropriate and where it could have the greatest impact. This resulted largely in the secondment of personnel directly from a related role at Mungari to the OR team, either full-time or part-time. This was most apparent in the maintenance and processing areas, where leading hands and supervisors were seconded to the OR team to deliver key work packages. This practice ensured that critical work was completed in accordance with the operations team's preferred approach and to the exact quality required for seamless integration into the operation. A good example of where this was successful was the secondment of mechanical and electrical supervisors into the OR team. These appointments provided key operational personnel with leading roles in the direction of the wider maintenance strategy, an ability to build the plant assets structure tree in the most efficient way, and to direct the integration of new software to streamline future planned maintenance tasks.

To complete the remaining activities, the OR team was supported and complemented by input from external resources. These external engagements provided the team with access to skill sets that were not available within the Mungari site team. In the case of the Mungari project, relevant subject matter experts were engaged to support the development of the plant maintenance strategy, the generation of key documentation, and the updating of Mungari's Computerised Maintenance Management System (CMMS). Similarly, the substantial workload of updating and developing new operating manuals and safe work instructions was supported by external contractors. As part of the expansion project, Mungari also developed the first In-Pit tailings storage facility for use at the operation, and this activity was deemed to require additional subject matter experts and engineering support for design, permitting, and operational readiness. In all this work, the Mungari department managers and the leaders of functional areas within their teams provided substantial support to the Operational Readiness team, with several personnel seconded from their site roles to support its formation.

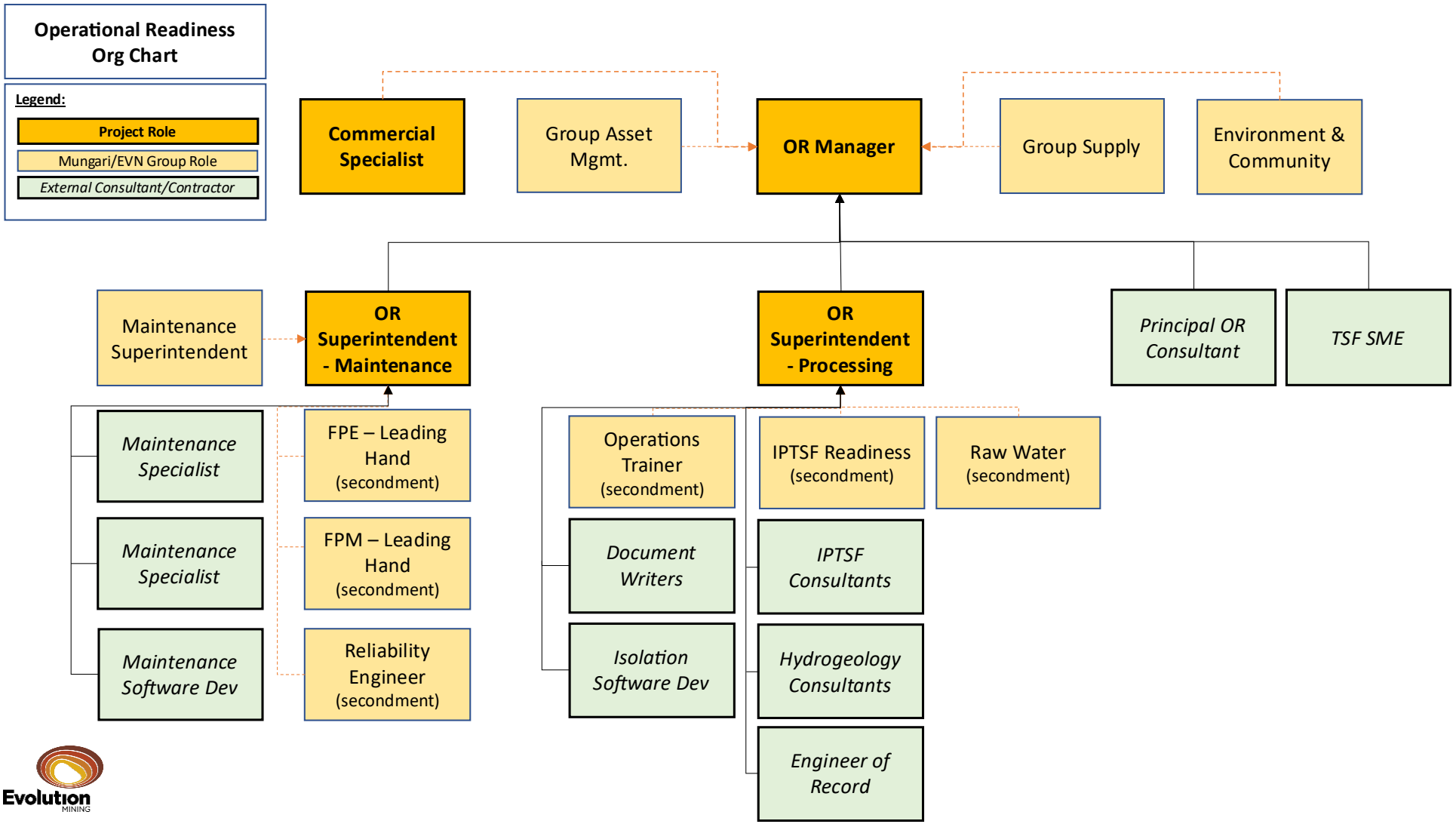



**FIG 4** – Operational readiness organisation structure within the Mungari Expansion project.

# OPERATIONAL READINESS SCOPE OF WORK

## Key formation activities

The development of the OR scope for the Mungari Expansion Project began with the completion of three critical tasks. Where practical and appropriate, these tasks were undertaken with the assistance and involvement of site personnel and external consultants to assess the operational readiness of key areas via a staged approach consisting of:

- Operational Readiness Gap Analysis.
- Operational Readiness Risk Assessment.
- Plant Asset Criticality Analysis.

The OR gap analysis took advantage of reference material generated throughout the Feasibility Study phase, which captured key OR actions arising from design reviews, risk assessments, hazard and operability studies (HAZOPs), and related activities. Review of this checklist was undertaken in collaboration with site Managers and leaders of functional areas, to identify key scope items that were required to ensure OR success. Importantly, this activity was fundamental in better defining the battery limits of the OR work and what was agreed to be clearly out of scope of the OR Team's remit.

Whilst many forms of risk assessment are typically carried out through the various study phases and project maturity, few are solely focused on how expansion activities impact the daily operating level. The goal of the OR risk assessment was to create an operational risk assessment specifically for the processing area that adequately identified any new or modified risks as a direct impact of the Mungari Expansion Project. While the majority of risks had been previously identified, the risk assessment was integral to identifying additional critical areas of high-risk work, such as confined space and working at heights, where greater OR focus was required to generate the necessary working procedures and critical control plans.

This step, while aiding in identifying key OR scope items, also allowed prioritisation of actions based on risk severity and specified clear accountability across the functions. Actions from the risk assessment were added to the OR scope of work or, where more suitably aligned, were allocated to the site operations team for completion.

The plant asset criticality analysis was arguably the single most important OR activity from the maintenance perspective. With any plant expansion, processing maintenance activities are understood to require significant time and resources, as such, a dedicated asset criticality assessment was undertaken to ensure this key area of work was well defined. A collaborative workshop over three days with key members from the Processing OR, MGO Processing, and Group Technical teams was undertaken to develop a 'whole of plant' asset criticality ranking. This intensive workshop reviewed and ranked the relative criticality of all 643 new pieces of equipment encompassing the plant expansion. Key outcomes of the criticality assessment workshop were:

- Driving the requirements for budgetary spending on insurance, critical, commissioning, and operating spares.
- The development of a robust and practical maintenance strategy.
- Providing direction to the development of routine maintenance documentation.
- Creation of the basis of the expanded plant structure tree and bill of materials.

## Scope development

Output from the three key activities described above provided a clear direction for the OR team to prioritise and progress further tasks. The body of work fell into four broad work streams, as described below. Whilst not an exhaustive review of tasks, the following summarises the main items the OR team highlighted as critical to the successful and sustained ramp-up of the expanded plant.

## Processing

The expansion of the Mungari plant brought with it two key new areas within the operations flow sheet that were unfamiliar to the existing operations team, in SAG milling and thickening. Unsurprisingly, operator training and familiarisation formed a significant portion of the OR scope. In conjunction with the Processing leadership group, the OR team took the opportunity of the plant expansion to assist with the development of a new competency-based operator training and role progression program. An entirely new training documentation package was generated for the Processing team to deliver an entire coursework package complete with training material and assessment guides. The training material aligned with nationally recognised coursework, providing aligned learning to support the development of team members in completing their Certificate IV in Process Plant Technology. The training material was aligned to a verification matrix, allowing processing staff to progress materially in their career as competency was demonstrated.

Other activities that supported the training and readiness of the processing team included:

- Opportunities for short-term secondments at other sites within the Evolution portfolio to provide direct exposure to SABC circuits.
- Dedicated commissioning and post-commissioning support from key Original Equipment Manufacturers (OEMs).
- An intensive three-day familiarisation and training program.
- Integration of operations staff in the dedicated commissioning team.
- Specific distributed control system (DCS) and PI Process Book training.

Integral to any plant expansion, whether greenfield or brownfield, is the development of the necessary procedures and documentation required to safely operate the new plant. To reliably inform this documentation update, a review of the processing operating strategy was undertaken to fully inform key tasks, required headcount, and required expertise. A complete review of the operational activities required for the successful operation of the expanded plant was conducted with the Processing leadership team. This fed into benchmarking the activity workload against the current headcount for Process Operators, Day Services, Gold Room, and Dewatering Technicians. In forming the strategy, the outputs from the Operational Risk Assessment workshop were key, as new activities had already been identified.

For the Mungari expansion, over 350 new documents were created for processing operations, including:

- Start-up and shutdown procedures.
- New/updated safe work instructions.
- Training documentation and assessments.
- Confined space procedures and rescue plans.
- Isolation procedures.
- Critical control plans and verifications.

As part of the Mungari expansion, a new IPTSF was constructed from a recently exhausted open pit in proximity to the processing plant. Whilst not considered an overly complex process, the IPTSF was the first undertaken at Mungari and, by extension, the first for Evolution Mining. The OR team was responsible for all aspects of readiness for the IPTSF, including:

- Managing all community engagement, environmental review, permitting processes and heritage aspects of the approvals process.
- Manage the drilling, construction, and commissioning of monitoring bores. Including gathering baseline monitoring bore data prior to tailings deposition.
- Plan the commissioning and operational ramp-up plans, providing all requisite documentation and training to the operations team.

- Develop dedicated operator training documentation in line with the operations strategy and training matrix.
- Engage directly with consultants, subject matter experts, and the site tailings Engineer of Record.

Upon review, the updates required in the Metallurgy space were thankfully relatively minor. Several new procedures were generated to capture new activities, for example, primary crusher belt cuts and thickener underflow samples, though the complexity of these was modest. The primary activity centred on the changes required to the metallurgical accounting procedure, including updating sampling locations and revising the accounting software. The metallurgy team was also integral to the development of the initial SAG mill reline strategy and took a lead role in identifying the planned reline frequency for the new mill and crushers as a key input for the long-term production planning.

## Maintenance

The activities within the maintenance scope were heavily supported by the existing maintenance team members, who were critical to the successful outcomes. The existing maintenance team contained several personnel who were at Mungari during the original Greenfield plant construction, and as such brought with them a clear understanding of operational readiness and a wealth of relevant experience. As reflected in the organisation chart the OR team was readily supplemented with team members seconded from the maintenance team and supported with external contractors for more of the repetitive or specialised tasks.

As mentioned previously, the Plant Asset Criticality Analysis was a key activity in the wider scope development for the Maintenance function. The resulting assessment rating informed and guided the development of the overall maintenance strategy, enabling the establishment of a robust strategy and a high-reliability plant. In effect, the implemented strategy was largely a continuation of the existing maintenance approach, though effort was placed on practices that could add further value, minimise re-work and optimally integrate technology. Key outcomes from the maintenance area strategy development were:

- Develop the required planned maintenance activities, informed by existing procedures and vendor installation, operation, and maintenance (IOM) manuals.
- Review and recommend suitable condition monitoring strategies for critical assets.
- Identify training requirements for the maintenance team for any equipment that was new to Mungari and required a specific skill set. For example, the servicing and operation of a power station.
- Review and benchmark final maintenance manhours, driven by the strategy, and review headcount to ensure adequate manning.
- Develop a critical spares purchase plan that prioritised the purchasing for future capital budgets.

With the addition of over 600 new plant items, potential duplications to be managed and many hundreds of items to be rationalised and removed from stock, the integration of maintenance items was a significant area of work. These items had to be managed physically, with space allocated within the existing maintenance warehouse structure, but also electronically, with changes made to the CMMS to accurately reflect the new plant structure tree. The Pronto system was used to create work strategies for any new equipment and infrastructure. All master data was loaded into Pronto before the handover of the Project, in compliance with site standards. Key actions regarding inventory management included:

- New fixed plant infrastructure introduced by the Mungari Expansion Project to be integrated into the current Mungari CMMS.
- Rationalisation of current spares holding stock and optimisation of storage space.
- Review and make obsolete redundant equipment and make their spares inventory obsolete in Pronto.

- Update and integrate changes to the Pronto plant structure tree.
- Develop and integrate the new plant assets, spares, and bill of materials into Pronto, including the ANSI (Amend New Stock Item) processes.
- Identify and integrate new registerable (classified) plant in the existing site management system for these assets.

A considerable suite of maintenance documentation was required in the form of new and updated maintenance plans, isolation procedures and safe work instructions. These documents were largely informed by a review of certified vendor data from equipment suppliers and contractors. In particular, the IOM documents were paramount to ensure that the required maintenance plans and frequencies were identified, spare lists and bills of materials could be generated, and equipment spares were ordered. All maintenance plans were developed in accordance with the Evolution standard, with a focusing first on developing strategies for critical equipment and then leveraging current strategies for common equipment to reduce the overall development workload. Statutory requirements were highlighted, including, but not limited to, updated testing and tagging registers, residual current devices (RCDs), conveyor/stop buttons and new registerable plant.

## Commercial

The commercial scope area focused predominantly on building upon the outputs of the maintenance scope as key equipment spares were identified, to ensure that these items were available on-site prior to commissioning. The major goals for this workstream were directed at ensuring logistics for the expansion were embedded in the existing Mungari supply chain, and the development of long-term goods and supply contracts with the largest OEMs, targeting fixed price agreements, surety of supply and long-term support.

The identification of critical spares requirements was primarily guided by the results of the Asset Criticality Assessment Workshop. This was then reviewed in conjunction with the recommended maintenance strategies alongside vendor recommendations to formulate a priority list of all critical, commissioning and operating spare parts. Commissioning spares were procured as part of the equipment purchase packages. Any commissioning spares that were not used during the commissioning process were transferred to the operation’s spares inventory.

All operational spares and consumables requirements were defined during OR execution, taking account of vendor recommendations obtained through the equipment procurement process and the maintenance strategies adopted by Mungari. As more detailed engineering was completed during the Execution phase, these operational items were detailed with part numbers and current costs. These spares were procured directly through the operation’s budget with assistance from the Operational Readiness team.

Specifications of first fills and reagents were generated for the various facilities in the scope, and a first fills list was prepared. The OR team worked directly with the Evolution Group Commercial team to ensure that existing reagent and consumables contracts are updated to satisfy the requirements of the expanded plant. Additionally, new supply contracts were developed and negotiated to procure SAG mill media and thickener flocculant, again with the assistance of the Evolution Group Commercial team.

## Sustainability, environment and community

An integral part of the Operational Readiness Plan was ensuring that Mungari obtained the necessary approvals from the relevant government departments to commence construction and operation at the higher throughput rate. Specifically, these approvals included:

- Plant expansion:
  - Department of Energy, Mines, Industry Regulation and Safety (DEMIRS) Mining Lease.
  - Department of Water and Environmental Regulation (DWER) Works Approval.
- Cutters Ridge in-pit TSF:

- DEMIRS Mining Lease.
- DWER Works Approval.

To deliver on these critical requirements, the OR team worked directly with the Mungari Sustainability and Environment teams. Significant community and stakeholder engagement was required for all approval submissions, which was led by the Mungari team. The Environment team managed approvals, submissions, and communications with the relevant departments, with the OR team providing the required design inputs and information to support this process.

## CONCLUSIONS

Overall, the outcome for the Mungari Expansion Project was a safe, productive, and efficient ramp-up of the expanded plant. The work executed by the OR team, in collaboration with the site operations teams, was critical to this successful outcome. A key marker of this success was that the processing operations personnel at the Mungari operation were ready and able to take full ownership of the plant during the commissioning and ramp-up phases upon the project's practical completion.

The plant was commissioned safely, ahead of schedule and achieved planned production rates. While the author has limited ability to provide a more detailed overview of the production metrics during the commissioning period, a high-level overview of the ramp-up curve is shown in Figure 5 below. As shown in Figure 5, the plant was able to quickly deliver production rates at approximately 80 per cent of the plan within 2 months. Over the next few months, typical troubleshooting and debottlenecking activities were carried out, allowing the plant to exceed overall planned production rates within 6 months from start-up. From the 6 month point, the plant was able to sustain total production at rates that met or exceeded planned output.

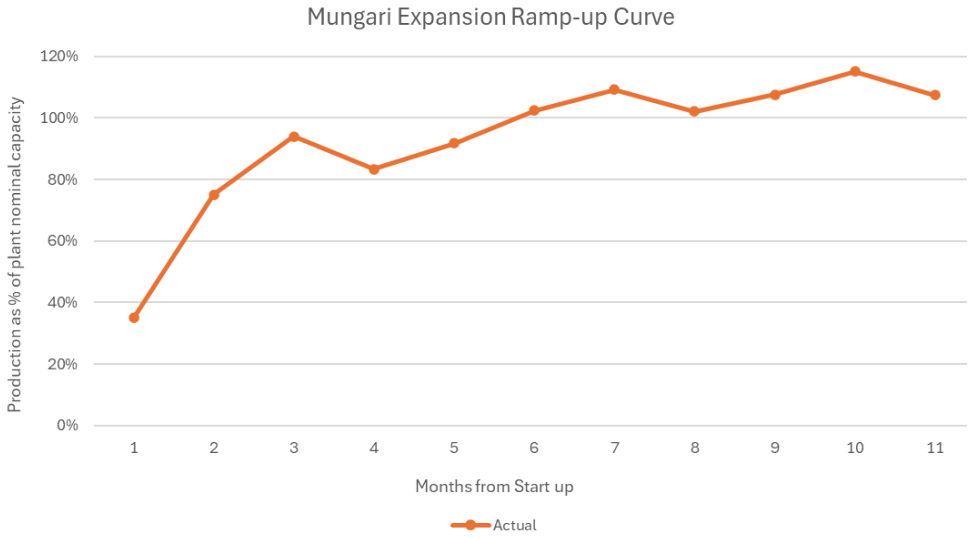



**FIG 5** – Mungari expansion actual ramp-up curve.

A subsequent review of the operational readiness team's work highlighted several key successes and lessons learned, some of which are summarised herein.

Evolutions OR experience at Mungari identifies two key areas for consideration for other similar projects in the future:

- Key Successes: the specific initiatives highlighted as making a significant contribution to the OR team's ability to address challenges at Mungari.
- Lessons Learned: the insights gained from communication and interactions required to support the operating sustainability after commissioning.

## Key successes

- Development of off-site training courses for plant operations team members, which allowed personnel to completely focus on the content away from the distractions of the existing plant operations.
- Organisation of site visits for plant operations team members at other Evolution sites. This opportunity provided team members with hands on training and familiarisation with the operation of thickeners and SAG mills that were new additions to the Mungari flow sheet.
- The OR team was able to support the maintenance team via digitisation of the site's preventative maintenance platform. This provided significant improvements to the daily maintenance function, streamlining planned maintenance activities and limiting manual paperwork.
- Implementation of a software-based isolation management system that provided the Processing department with an online tool that not only identified all isolation points for new and existing equipment but was also tailored to fully integrate with the existing isolation permitting procedures.
- Development of a competency-based training, assessment and role progression program for the plant operations team.

## Lessons learned

### *Vendor data*

A key lesson learned during the Mungari Expansion Project was that greater emphasis needed to be placed on the timely provision of data from contractors and/or vendors. In some cases, the late provision of vendor data significantly impacted the ability of the OR team to progress the maintenance scope of work and, importantly, make timely purchases of spares to ensure these arrived before commissioning. A key change to address this would be to ensure that the provision of required data is well detailed as early as possible, and key dates for data delivery are agreed to upfront.

### *Spares expediting*

During the planning phase, the number of operating, commissioning and critical spares required for the plant was largely underestimated. As the team progressed through the maintenance scope, it became clear that the vast number of items would put a strain on the site-based warehouse team. It was ultimately decided that the OR team would provide additional support in managing logistics of the critical spares, though the warehouse team were supportive of managing the logistics of tracking and cataloguing the balance of commissioning and operating spares.

At this time, an external partner was engaged to manage the logistics, tracking and expediting of the critical spares and work with the operations team. This level of support did not extend to the commissioning and operating spares, as the intent was to engage the warehouse team in the process and following the existing logistics pathway the site had maintained. Unfortunately, this led to several items from within the scope of the commissioning spares arriving on-site late, one of which resulted in more downtime than would have otherwise been incurred. Identifying this need and bringing this external partner onboard earlier to include management of the entirety of spares, would have facilitated an improved outcome in this space.

### *Plant area walkdowns*

An important activity undertaken towards the finalisation of any construction project is the completion of plant area walkdowns. The walkdowns give the project team an opportunity to ensure construction has been completed per the original project scope of work. The OR team used these area walkdowns to further engage the site teams by involving operations, maintenance, and technical personnel in these activities. In addition to capturing any potential scope gaps, this further enhanced ownership from the site team.

This engagement needs to be carefully balanced with the wider project outcomes, as KPIs between the EPC contractor, project team, and operations team can be misaligned. A key lesson for the Mungari project was to ensure that these plant area walkdowns were conducted as early as practical to ensure all punch list items could be captured and alignment gained on the subsequent categorisation of the items.

### *Equipment inspection and test plans (ITPs)*

An important tool in ensuring that key mechanical equipment is operationally ready is the ITP supplied by the OEM. These plans are imperative for the safe construction of equipment and detail important steps regarding the commissioning and readiness processes. A key function of the OR team was to ensure that these ITPs had been followed, with specific attention paid to readiness aspects. Significant benefits were achieved by bringing in the site operations team members to undertake these final tasks, further building on the site's ownership of the plant.

## ACKNOWLEDGEMENTS

This paper summarises the operational readiness work of a dedicated group of people at Evolution's Mungari Operations, particularly the entire Processing Department, which worked tirelessly to ensure the success of the plant expansion. The Authors acknowledge and celebrate their contributions to the project's success. The Authors would also like to thank Evolution Mining for their review, support and permission to publish this paper.

## REFERENCES

Evolution Mining Limited, 2023. Mungari mine life extended to 15 years at 18% lower AISC and higher production [online]. Available from: <https://evolutionmining.com/investor-centre/asx-announcements/> [Accessed: 01 September 2026].

Evolution Mining Limited, 2024. Evolution Mungari Gold Operation – Process Plant Expansion, Operational Readiness Plan, internal report, Evolution Mining Limited.

Pratt, A G L, 2023. Operational Readiness – what is it and how to get it done?, in *Proceedings of the 14th Underground Operators Conference 2023*, pp 156–175 (The Australasian Institute of Mining and Metallurgy: Melbourne).

## Mill Operators

# Emerging technology and tailings

# Filter aid for fine and ultrafine particles – laboratory to scale technological aspects of iron ore tailings filtration

*L M Faustino[1], M G Vieira[2], G R Vilela Neto[3], W S Silva[4] and P Fernandes[5]*

1. Tailings Program Manager, Clariant, Belo Horizonte MG 31710-400, Brazil. Email: livia.marques@clariant.com
2. Senior Specialist Engineer, Samarco, Belo Horizonte MG 30130-141, Brazil. Email: marcosg@samarco.com
3. Specialist Engineer in Innovation, Samarco Anchieta ES 29230-000, Brazil. Email: gil.ribeiro@samarco.com
4. Specialist Engineer, Samarco, Mariana MG 35420-970, Brazil. Email: wanderson.silva@samarco.com
5. Field Application Manager, Clariant, Belo Horizonte MG 31710-400, Brazil. Email: pierre.fernandes@clariant.com

## ABSTRACT

New global industry standards and regulatory changes regarding mining tailings management are driving installation of tailings filtration plants to decommission existing tailings dams. Several studies are underway to enable the dry stacking of dewatered ultrafine tailings, either independently or co-disposed with sandy tailings and/or waste rock. Dry Stacking technology emerges as an alternative for tailings disposal in a scenario that does not require tailings dams. Previous full-scale investigation at the Samarco concentrator has showed that adding a maximum of 5 per cent slimes caused a 35 per cent decrease in tailings filtration rate compared to 100 per cent flotation tailings. Furthermore, this mixture jeopardised geotechnical aspects such as material workability during dry staking due to the higher cake moisture and rheological properties posed by the clay minerals. After the development and optimisation of an alternative filter aid chemistry, plant trials with a new reagent showed improved filtration performance by maximising throughput to additional 75 per cent and reducing cake moisture in 1 to 2 percentage points for the feed blend of 94 per cent flotation tailing and 6 per cent slime tailing (equivalent to 30 per cent of total slime generation). Moreover, the dry stacking of the dewatered material showed enhanced workability, permeability and compressibility. The results achieved motivated the continuous implementation of the filter aid in Samarco's total tailings, which enables life expansion of existing slime disposal structures, as well as potential life of mining extension.

## INTRODUCTION

Samarco Mineração S.A. resumed its mining and iron ore beneficiation operations in December 2020, adopting a naturally confined mined-out pit as an interim facility for the disposal of ultrafine tailings produced during the iron ore desliming stage, internally designated as *slurry*. In parallel, the sandy tailings generated in the flotation circuit are subjected to mechanical dewatering using vacuum disc filtration, after which the filtered material is disposed of via dry stacking (Samarco Mineração S.A., 2023). Figure 1 presents a simplified schematic of the production flow sheet, emphasizing the generation and management routes of the two distinct tailings streams (Vilela *et al,* 2025).

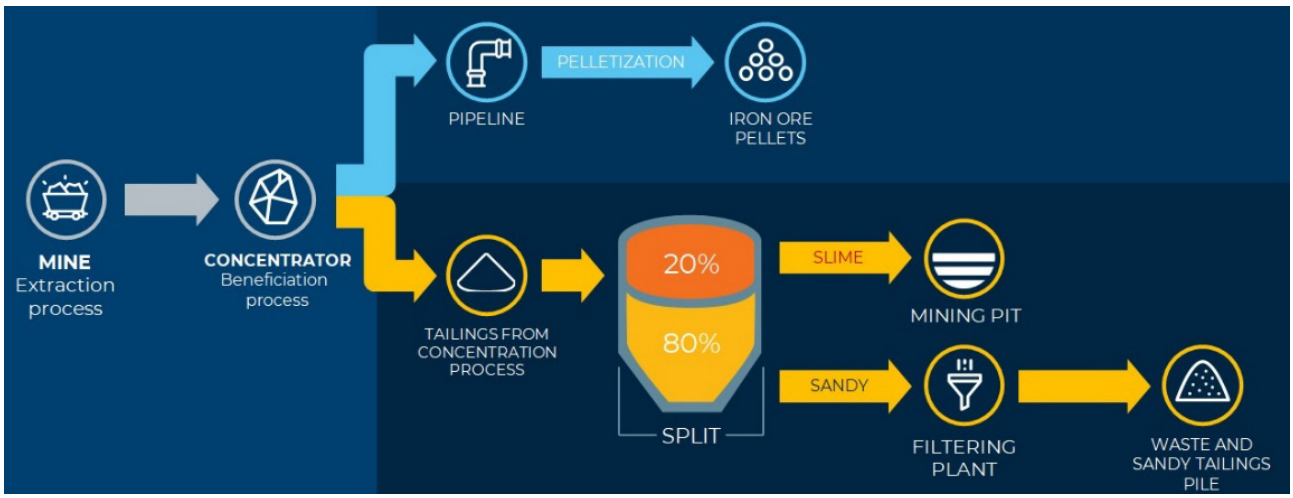



**FIG 1** – SAMARCO simplified flow sheet for tailings disposal.

Ongoing studies are focused on enabling the incorporation of ultrafine tailings (slimes) into the filtration and disposal system, either as a standalone filtered product or through co-disposal with sandy tailings and/or waste rock. The inclusion of slimes in the filtration stage is a critical requirement for the effective implementation of dry stacking, as it allows for a fully dewatered tailings management strategy and the consequent elimination of reliance on conventional tailings dams. In this context, dry stacking emerges as a risk-mitigation alternative for tailings disposal; however, its technical feasibility depends strongly on the performance of filtration equipment and on the geotechnical performance of the resulting mixtures, particularly with respect to workability, trafficability, and post-deposition stability. Accordingly, several studies have been conducted to assess industrial scale filtration and geotechnical parameters and to define operational envelopes that ensure safe and sustainable dry stacking of tailings containing ultrafine fractions.

On the forefront of tailings filtration implementation, Brazilian plants have progressively optimised key operational and design parameters, such as feed solids concentration, particle size distribution, filtration technology selection, filter media characteristics, applied pressure differentials, and cycle times in order to meet the performance indicators required for dry stacking operations (França; Rezende; Silva, 2024).

In parallel, significant research efforts have been directed toward overcoming the limitations imposed by strong capillary forces and the high specific surface area associated with ultrafine particles, which negatively affect filtration rates and residual moisture content. In this context, the application of chemical additives as filtration aids has been extensively investigated to enhance dewatering efficiency. Flocculants, surfactants, and coagulants have been evaluated for their ability to modify tailings structure and water–solid interactions during filtration. These reagents are known to influence surface and interfacial phenomena by altering particle zeta potential, pulp rheology, and liquid surface tension, thereby affecting floc size distribution, floc strength and permeability, pulp viscosity, and particle wettability, ultimately leading to improved filtration performance and reduced cake moisture (Mamghaderi *et al,* 2021; Pearse, 2003; Johnson *et al,* 2016; Vilela *et al,* 2025).

Filter aids enhance tailings filtration performance by modifying cake microstructure and interfacial phenomena, leading to reduced specific cake resistance, accelerated cake formation, increased cake permeability, and lower residual moisture content, thereby maximising achievable filtration rates. These effects are typically achieved through changes in particle aggregation, pore-size distribution, and capillary pressure within the filter cake.

Although the application of filter aids in concentrate filtration is well established and widely practiced—often relying on reagents that promote rapid floc formation and high permeability—both laboratory-scale investigations and industrial trials have demonstrated that chemical formulations effective for concentrate filtration are frequently ineffective or even detrimental when applied to tailings. This discrepancy is primarily attributed to the markedly different physicochemical characteristics of tailings, including higher ultrafine content, broader particle size distributions, elevated specific surface areas, and stronger capillary forces, which demand tailored reagent

selection and dosage strategies. Consequently, the development of filter aids for tailings filtration requires a distinct approach focused on controlling cake compressibility, pore connectivity, and water retention mechanisms rather than solely enhancing initial settling or flocculation efficiency (Pearse, 2003; Wakeman and Tarleton, 2005; Johnson *et al,* 2016; Mamghaderi *et al,* 2021).

Accordingly, filter aids specifically engineered for tailings applications play a critical role in improving the dewatering efficiency of mixed tailings streams, enabling the achievement of target moisture contents required for dry stacking. Advances in polymer-based technologies promote controlled aggregation of mineral particles into flocs with optimised size and structural integrity, thereby minimising the entrapment of water within flocculated structures. Laboratory-scale filtration tests conducted on samples comprising coarse flotation tailings blended with varying proportions of ultrafine material (5–20 wt per cent) derived from the desliming stage of iron ore processing demonstrated at least a twofold increase in filtration rates, as illustrated in Figure 2.

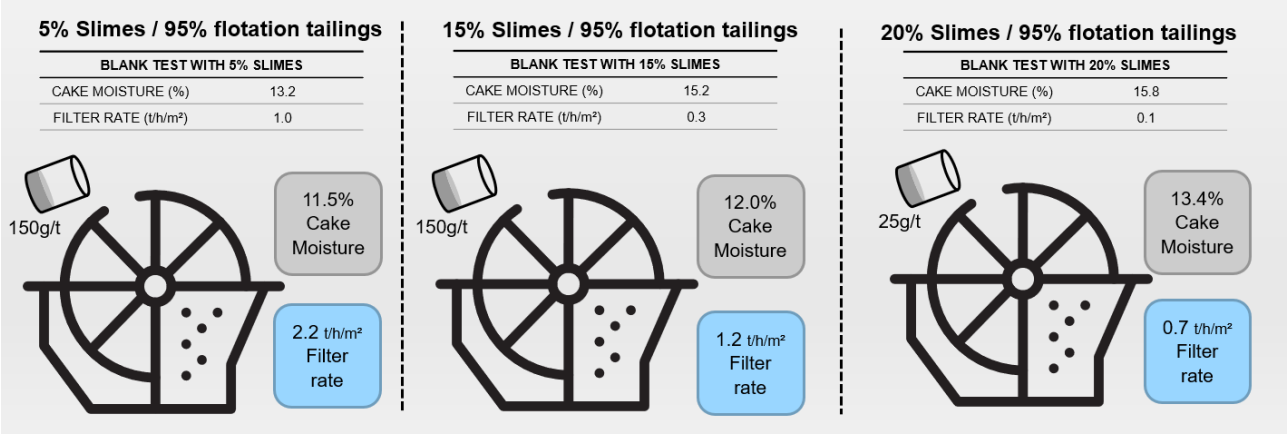



**FIG 2** – Laboratory filtration results (leaf test bottom-feed) with the filter aid FLOTICOR™ FA 17416.

Considering the enhanced filtration performance observed for the filter aid (FLOTICOR™ FA 17416) under laboratory conditions, subsequent efforts were directed toward assessing the scalability and industrial applicability of these products. Leveraging SAMARCO's extensive operational experience with vacuum disc filtration in both pellet feed and flotation tailings dewatering, the suitability of this technology for processing blended tailings streams—comprising sandy tailings and ultrafine tailings—was initially investigated through laboratory-scale leaf filtration tests (Vieira *et al,* 2023). The results obtained, particularly for the 90/10 blend (90 wt per cent sandy tailings and 10 wt per cent ultrafine tailings), demonstrated significant performance gains and provided the technical basis for advancing to full-scale industrial trials at SAMARCO's sandy tailings filtration plant.

Therefore, the primary objective of this study was to determine the maximum ultrafine tailings percentage in the mixture among the tested compositions (5 per cent to 15 per cent ultrafine tailings) using vacuum disc filter technology (in plant scale) for the dewatering of tailings mixtures intended for dry stacking. For this purpose, plant trials were conducted using the filter aid CLARIANT FLOTICOR™ FA 17416 with the goal of adding at least 5 per cent slimes (95 per cent coarse tailings) to the disc filter, keeping or reducing cake moisture and keeping filter rate higher than equal or higher than 1 t/h/m$^2$.

To test the mixtures on an industrial scale, modifications were made to the plant's industrial circuit. As observed in Figure 3, part of the underflow from the ultrafine tailings' thickener was directed, in a controlled manner, to the filtration feed tank. This control was achieved using a densimeter, flowmeter, and control valve, allowing for the addition of 5 per cent to 15 per cent of ultrafine tailings mass into the mixture fed into the filtration plant.

As illustrated in Figure 4, Clariant and Samarco implemented a dedicated filter-aid dosing system designed to deliver the reagent to the two slurry distribution lines feeding the six vacuum disc filters installed at the facility. In parallel, experimental trial pads were constructed using the filtered tailings mixtures to systematically evaluate geotechnical performance parameters, such as trafficability,

workability, and compaction index. These trials also aimed to assess the influence of filtration aid addition on downstream material handling operations, such as conveying, spreading, and mechanical compaction of the filtered tailings.

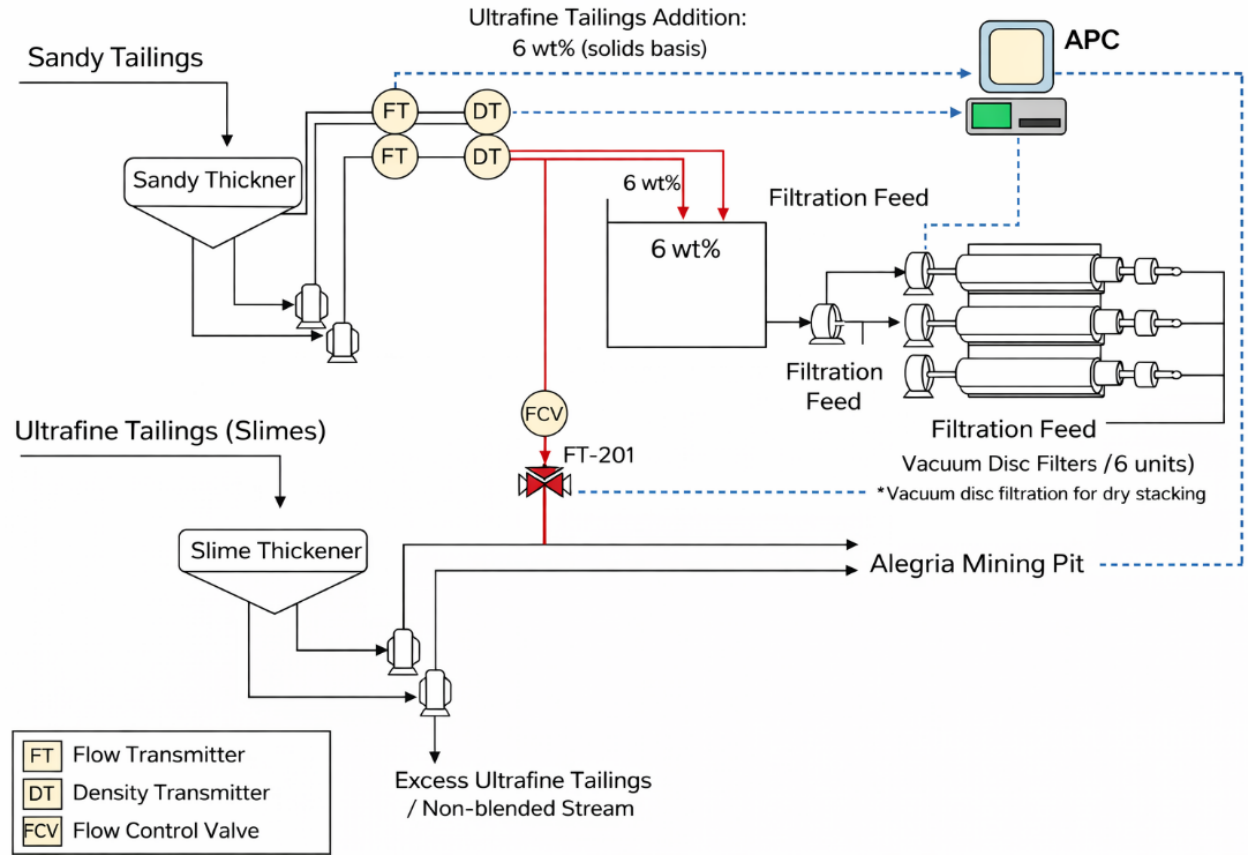



**FIG 3** – Plant modifications for industrial tests: Simplified process flow sheet showing the controlled blending of sandy tailings and ultrafine tailings (slimes) upstream of vacuum disc filtration. The ultrafine tailings addition is regulated via flow and density measurements to maintain a target solids ratio in the filtration feed, while excess slimes are diverted to the Alegria Mining Pit.



**FIG 4** – Clariant equipment set-up for plant trials.

## METHODOLOGY

### Mineral samples

During each experimental campaign, grab samples were collected at hourly intervals from the discharge of the vacuum disc filters in operation for determination of residual moisture content. Upon

completion of each test, the hourly samples were composited to obtain a representative sample of the filtered tailings blends (slimes plus coarse tailings). The composite samples were subsequently analysed to determine particle size distribution and bulk chemical composition using standard laboratory procedures, such as laser diffraction (Malvern Mastersizer) and X-Ray Fluorescence.

## Plant trials program

Each industrial-scale test campaign was conducted over 26 hrs for several days over one year. Initial trials were executed during the scheduled monthly maintenance shutdown of one of the two beneficiation plant production lines, thereby reducing the mass flow rate to the filtration plant by approximately 50 per cent. This operational strategy was adopted as a risk-mitigation measure to prevent potential filtration plant instability and unplanned beneficiation plant shutdowns, given the initially unknown filtration performance of tailings mixtures containing ultrafine material.

Subsequent test campaigns were performed with the beneficiation plant operating at nominal throughput, except for tests involving a 10 wt per cent ultrafine tailings fraction, for which the unit filtration capacity was reduced by approximately 50 per cent. Consequently, trials with 10 wt per cent ultrafine tailings were restricted to periods coinciding with the scheduled shutdown of one beneficiation line.

In all test campaigns, the filter aid FLOTICOR™ FA 17416 was continuously dosed and delivered to the slurry distribution system feeding the six vacuum disc filters. The proportion of ultrafine tailings in the feed mixture was continuously monitored and controlled at the filtration feed tank. Filtered tailings produced during the trials were conveyed to a designated area for the construction of experimental test pads, which were subsequently used for the evaluation of relevant geotechnical parameters.

## RESULTS AND DISCUSSION

Table 1 summarises the principal outcomes obtained during the industrial-scale filtration trials conducted with the addition of filtration aid. For mixtures containing 5 wt per cent ultrafine tailings, the filtration performance achieved with filtration aid addition was comparable to that previously attained under industrial operation with sandy tailings alone. For 5 per cent slimes, the results further indicate that, once the optimal filtration aid dosage (determined in several laboratory trials) was reached, additional reagent dosages did not result in measurable improvements in unit filtration rate (UFR) nor further reductions in residual moisture content. In contrast, mixtures containing 10 wt per cent ultrafine tailings caused a 50 per cent reduction in filtration productivity compared to sandy tailings alone, which is attributed to the significant proportion of particles finer than 10 µm (15 to 16 per cent wt per cent). This reduction in unit capacity implies the need for a proportional increase in the number of filters in operation to maintain the target solids throughput.

**TABLE 1**

Results of filter aid plant trials.

| Feed* Tailings mixtures | Filter aid FLOTICOR FA 17416 | Filter rate (t/h/m$^2$) | Cake moisture (%) | % passing 10 µm |
|---|---|---|---|---|
| 95/05–13/04/23 | NO | 1.5 | 12.8 | 7.5 |
| 95/05–28/11/23 | YES | 2.1 | 13.2 | 10.7 |
| 94/06–22/05/24 | YES | 1.8 | 12.1 | 10.6 |
| 93/07–05/12/23 | YES | 1.8 | 12.2 | 16.2 |
| 92/08–19/12/23 | YES | 1.1 | 12.0 | 15.8 |
| 90/10–13/12/23 | YES | 1.2 | 12.0 | 16.2 |
| 90/10–11/04/24 | YES | 0.8 | 12.8 | 15.2 |

*Feed rate ranging from 840 t/h to 980 t/h (to six disc filters) at 50 per cent solids wt per cent.

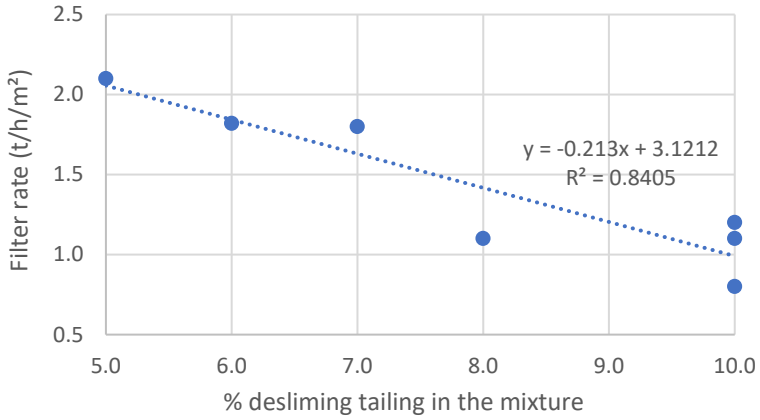



**FIG 5** – Filter rate as a function of the percentage of slimes in the mixture tailings.

Based on the experimental results obtained and considering the current configuration of six vacuum disc filters, expanding to a total of ten units upon the recommissioning of Beneficiation Plant 2 in 2025—the following operational thresholds are proposed for the future adoption of filtered tailings mixture disposal:

- **Ultrafine tailings content ≤ 6 wt per cent** (≤ 10 wt per cent passing 10 µm): no operational constraints are anticipated for the filtration process.
- **Ultrafine tailings content between 6 and 7 wt per cent** (approximately 10–16 wt per cent passing 10 µm): moderate operational constraints are expected, requiring mitigation measures such as evaluation of alternative filter cloth materials, implementation of undercloth systems, and/or development of tailored filtration aid formulations.
- **Ultrafine tailings content between 7 and 10 wt per cent** (approximately 10–16 wt per cent passing 10 µm): significant process limitations are anticipated, necessitating capital investment in additional filtration capacity to maintain target solids throughput.
- The influence of the fraction of material passing 10 µm on filtration performance warrants further investigation to define robust operational envelopes and to establish this parameter as a primary process control variable. Moreover, additional factors, including ore typology and mineralogical composition, are expected to affect filtration behaviour and must be systematically evaluated through further testing to delineate reliable operating ranges for industrial-scale tailings filtration.

In the experimental test dry-stack field, the incorporation of filtration aid resulted in a marked enhancement of material workability, leading to more uniform and reproducible geotechnical compaction responses, as evidenced by reduced compaction gradients and lower parameter variability. Trafficability assessments conducted under high-precipitation conditions further demonstrated a substantial improvement in equipment mobility across the deposited material. Overall, the use of filtration aid promoted compaction behaviour of the 95:05 tailings mixture that more closely approximates the performance observed for conventional flotation tailings disposal in the absence of ultrafine material. Nevertheless, additional systematic testing is required to fully characterise the underlying mechanisms and to quantify the long-term implications of filtration aid addition on geotechnical performance.

## CONCLUSIONS

The application of the filtration aid FLOTICOR™ FA 17416 enabled the filtration plant to process tailings mixtures containing up to 5 wt per cent ultrafine material under operating conditions comparable to those employed for sandy tailings alone. For this mixture, an average unit filtration rate of 2.0 $t \cdot h^{-1} \cdot m^{-2}$ and a mean filter cake moisture content of 12.8 per cent were achieved. When the ultrafine tailings content was increased to 10 wt per cent, the unit filtration rate decreased to 1.1 $t \cdot h^{-1} \cdot m^{-2}$ despite the use of filtration aid, indicating that the 90/10 sandy-to-ultrafine tailings blend represents the practical upper limit for vacuum disc filtration under the evaluated conditions.

A strong inverse relationship was identified between unit filtration rate and ultrafine tailings content within the tested range, with a coefficient of determination ($R^2$) of 0.84. In contrast, no clear correlation was observed between ultrafine tailings content (5–10 wt per cent) and filter cake moisture, which remained within a narrow range of 11.9–13.2 per cent.

Furthermore, the incorporation of filtration aid resulted in a pronounced improvement in the workability and trafficability of the filtered material in the experimental test pads, yielding field behaviour comparable to that observed for tailings disposed without the addition of ultrafine fractions.

## ACKNOWLEDGEMENTS

The authors acknowledge Samarco Mineração S.A. for technical and operational support, and Clariant for its collaboration in the development and scale-up of chemical solutions for tailings filtration.

## REFERENCES

Costa, N, Bicalho, L, Fernandes, P & Silva, W 2021, Filter aids to improve iron ore tailings filtration, in Proceedings of Tailings 2021, Gecamin, Santiago, Chile.

Faustino, L, Bicalho, L, Almeida, P & Silva, W 2023, Filter aids to improve coarse and ultrafine gold tailings filtration, in Proceedings of Tailings 2023, Gecamin, Santiago, Chile.

França, P, Rezende, VA & Silva, WS 2024, Disposal of filtered tailings and associated waste in Brazil – the PDER Alegria Sul (Samarco) case, in Proceedings of the AusIMM Conference on Tailings Management, The Australasian Institute of Mining and Metallurgy, Melbourne.

Gil Vilela, MV, Silvério, W, Fernandes, P & Faustino, L 2025, Technological aspects of iron ore tailings filtration and dry stacking, in Proceedings of the SME Annual Meeting 2025, Society for Mining, Metallurgy & Exploration, Denver, CO.

Mamghaderi, H, Aghababaei, S, Gharabaghi, M, Noaparast, M, Albijanic, B & Rezaei, A 2021, 'Investigation on the effects of chemical pretreatment on the iron ore tailing dewatering', Colloids and Surfaces A: Physicochemical and Engineering Aspects, vol. 625, article 126855, https://doi.org/10.1016/j.colsurfa.2021.126855

Pearse, MJ 2003, Historical use and future development of chemicals for solid–liquid separation in the minerals industry, Minerals Engineering, vol. 16, no. 2, pp. 103–108.

Samarco Mineração S.A. 2023, Management report 2022, Samarco Mineração S.A., Belo Horizonte, Brazil.

Vieira, MG, Silva, AB, Vilela Neto, GR, Cunha, MS, Nascimento, TJS & Matos, VE 2024, Testes industriais de filtragem com misturas de rejeito arenoso e lama, in Proceedings of the 23º Seminário de Mineração (ABM Week – 8ª Edição), ABM, São Paulo, Brazil.

Vieira, MG, Totou, AR, Vilela Neto, GR & Cunha, MS 2023, Avaliação do uso de um auxiliar de filtragem em testes de filtragem de laboratório de misturas de rejeito de minério de ferro, in Proceedings of the 22º Simpósio de Mineração, ABM, São Paulo, Brazil.

Wakeman, RJ & Tarleton, ES 2005, Solid/liquid separation: equipment selection and process design, Elsevier Butterworth-Heinemann, Oxford, UK.

# Integration of PGNAA for ore blending control at Kanmantoo

*G Noble[1], N Muhamad[2], J Rutter[3], T Strombotne[4], G Norris[5], J Siliezar[6], C Rowett[7] and M Celona[8]*

1. Senior Product Applications Specialist, Thermo Fisher Scientific, Adelaide Airport SA 5950. Email: garry.noble@thermofisher.com
2. Applications Specialist – Minerals, Thermo Fisher Scientific, Adelaide Airport SA 5950. Email: nur.muhamad@thermofisher.com
3. Business Development Manager – Mining and Mineral Processing, Thermo Fisher Scientific, Adelaide Airport SA 5950. Email: jon.rutter@thermofisher.com
4. Senior Product Applications Specialist – Minerals, Thermo Fisher Scientific, San Diego CA 92121, USA. Email: tom.strombotne@thermofisher.com
5. Surface Manager, Kantra Copper Limited, Kanmantoo SA 5252. Email: glenn.norris@kantra.com
6. Metallurgy Superintendent, Kantra Copper Limited, Kanmantoo SA 5252. Email: jose.siliezar@kantra.com
7. Technical Services Manager, Kantra Copper Limited, Kanmantoo SA 5252. Email: caitlin.rowett@kantra.com
8. Plant Metallurgist, Kantra Copper Limited, Kanmantoo SA 5252. Email: michael.celona@kantra.com

## ABSTRACT

Variability in ore feed grade and mineralogy can affect flotation stability, reagent demand and metallurgical performance. At Kanmantoo, crusher feed is prepared by reclaiming material from run-of-mine stockpiles according to a planned blend based on geological information. While this approach provides a target feed grade, the actual sequence of material delivered to the crusher can be affected by ore heterogeneity, stockpile segregation and reclaim practice. Until recently, there was no continuous elemental measurement between the crusher and the coarse ore stockpile to show how closely the realised feed matched the planned blend.

A Thermo Scientific cross-belt analyser using prompt gamma neutron activation analysis (PGNAA) was installed on the crushing circuit discharge conveyor feeding the coarse ore stockpile (COS). The analyser provides continuous bulk measurement of copper, sulfur and other elements before the material enters the final stockpile buffer.

A post-commissioning study was undertaken to determine whether this measurement could provide useful information for ore-blending control. Factory and site validation were used to confirm analytical performance. Minute-level measurements from the cross-belt analyser and the AnStat-430, a dedicated flotation-feed X-ray florescence (XRF) slurry analyser, were then used to establish the effective process response between crusher product and flotation feed. This timing relationship was subsequently applied when comparing the planned blend estimate, the realised cross-belt analyser measurement, the slurry analyser measurement and independent reconciled feed shift composite assays.

The commissioning results show that the planned blend average does not fully describe either the realised crusher-product grade or the variability within a blend. Grade changes measured by the cross-belt analyser remained evident downstream after stockpile and milling attenuation, while independent shift composite assays provided further confirmation that the upstream measurement was representative of the material subsequently processed.

The study demonstrates that the cross-belt analyser provides a timely and process-relevant measurement suitable for supporting ore-blending decisions at Kanmantoo. The next stage is to use the measurement in a controlled operator-assisted blending trial to determine whether active response to the measured grade and variability can deliver repeatable improvements in feed stability.

## INTRODUCTION

The Kanmantoo processing plant, located 55 km south-east of Adelaide, is a conventional crush–grind–flotation concentrator with a capacity of 3.6 Mt per annum and currently treating approximately

1.8 Mt per annum of copper–gold ore as the underground mine ramps up. Recommissioned in early 2024 to support the transition from open pit to underground mining, the plant produces a copper concentrate containing gold and silver credits.

The Kanmantoo operation processes ore from a structurally complex underground deposit within the Kanmantoo Province. Mineralisation is hosted in vein-dominated and stockwork systems comprising chalcopyrite within pyrrhotite-rich sulfide assemblages, with minor pyrite. High-grade zones are commonly associated with brecciated sulfide stockworks that are spatially irregular and difficult to predict precisely from drill data. Kanmantoo has integrated underground scanning techniques to improve the data density in its grade control system (Rowett, Rolley and O'Rielly, 2024).

As underground mining advances through these structurally controlled domains, short-scale changes in copper grade, sulfide abundance, and associated gold content occur over relatively small mining blocks. These variations manifest as time-dependent fluctuations in ROM feed delivered to the plant. Ore variability can influence flotation response, reagent demand, mass pull and metallurgical recovery (Dobby, Kosick and Amelunxen, 2002; Bulled and McInnes, 2005; Millar and Wraith, 2022).

Managing this variability before it reaches flotation is therefore an important component of stable concentrator operation. Grade control models and laboratory assays provide essential planning inputs but operate at low temporal resolution. Downstream online analysers improve visibility but are subject to process residence times that delay detection of feed changes.

Consequently, processing plants often respond to variability only after its effects have propagated through comminution and flotation circuits. This reactive cycle reinforces conservative operating strategies and limits overall process efficiency (Hodouin *et al,* 2001; Shean and Cilliers, 2011).

At Kanmantoo, underground ore is delivered to designated run-of-mine (ROM) stockpiles according to estimated grade and material classification. Crusher feed is prepared by reclaiming material from these stockpiles in proportions defined by a blending schedule. The plan establishes a target average grade, but it cannot directly measure the sequence produced after mining, truck haulage, stockpiling and loader reclaim. Variability can therefore remain within a blend even where the planned average is appropriate.

Following crushing, the ore is conveyed to the coarse ore stockpile (COS), which provides additional buffering before milling. The degree of blending provided by the COS varies with stockpile inventory levels and reclaim practices. Segregation of coarse and fine material during stacking, combined with selective reclaim, particularly during periods of low stockpile inventory, can introduce short-term grade variability. Prior to installation of the cross-belt analyser, changes in ore chemistry were only detected downstream at the flotation-feed slurry analysers or through flotation Shift Composite sampling.

Cross-belt elemental measurement provides an opportunity to move this visibility upstream. Prompt gamma neutron activation analysis (PGNAA) provides continuous bulk elemental analysis by irradiating conveyed material with neutrons and measuring the characteristic gamma radiation emitted by the constituent elements. Neutron and gamma-ray penetration capability (eg Shue, Faw and Shultis, 1996) enables volumetric analysis of the full cross-section of conveyed material. This is advantageous for primary crushed material; however analyser design and calibration methodology are critical for ensuring representative analysis under normal plant operating conditions (eg Noble and Ferguson, 2020; Rutter *et al,* 2020; Noble, Strombotne and Gordon, 2024).

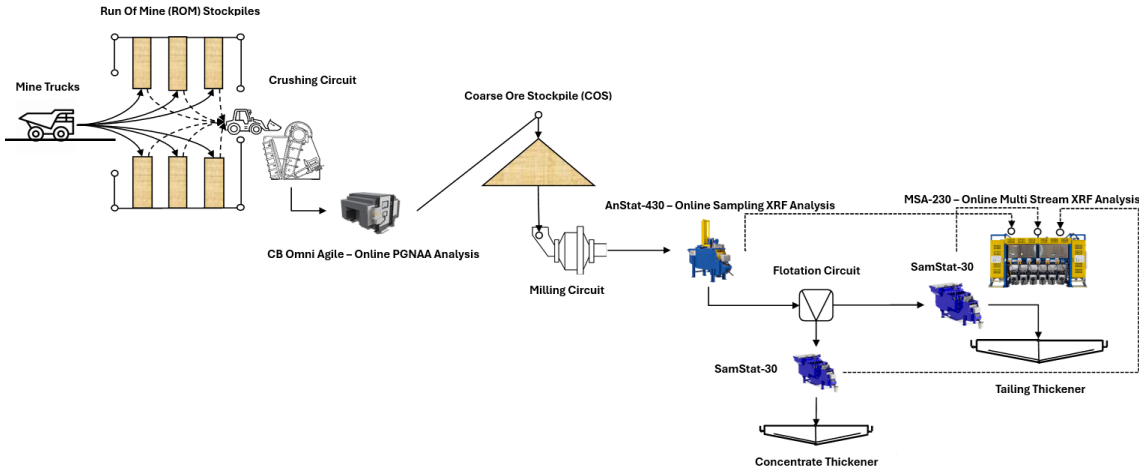
For the Kanmantoo application, the required measurement needed to operate on primary crushed ore, analyse the bulk stream upstream of the COS and provide information at a time scale relevant to ROM reclaim decisions. Laboratory and composite sampling provide important independent grade information but are not available at this temporal resolution. The existing slurry analysers provide high-frequency information but are downstream of the stockpile and milling circuit. A cross-belt PGNAA measurement was therefore selected to fill this measurement gap.

A cross-belt analyser was installed on the crushing circuit discharge conveyor feeding the COS. The analyser provides continuous measurement of copper, sulfur and other calibrated elements. Figure 1

shows the cross-belt analyser installation and its position relative to the ROM stockpiles, crushing circuit, COS and downstream slurry analysers.



(a) (b) (c)




(d)

**FIG 1** – (a) CB Omni Agile installation; (b) installed analyser; (c) analyser over the conveyed ore stream; and (d) Plant flow diagram showing locations of CB Omni Agile and AnStat-430.

The purpose of the commissioning study was to determine whether the cross-belt analyser could provide a sufficiently stable, timely and representative process measurement to support improved ore-blending control. The study did not attempt to demonstrate that active blending control had already improved plant performance. Instead, it addressed the preceding question: whether the measurement provides a suitable basis on which such a control strategy can be developed.

## METHODOLOGY

### Factory calibration and site validation

The analytical configuration of a PGNAA analyser depends on the expected elemental composition of the material, belt loading and measurement geometry. Kanmantoo supplied elemental and mineralogical information from the underground operation so that the required calibration ranges could be defined. The calibration included copper and sulfur as the principal elements relevant to ore blending, together with the major gangue elements required to represent the overall ore chemistry.

Modular reference standards were manufactured to span the expected elemental ranges and were measured at representative belt loadings during factory calibration. The reference standards were subsequently transported to Kanmantoo and measured during site commissioning in April 2026 and again in July 2026. The cross-belt analyser incorporates a belt-scale input to account for changes in material loading during operation and enable tonnage-weighted averaging.

Analytical performance was assessed by comparing the measured values with the reference-standard values. Root Mean Squared Deviation (RMSD), Normalised RMSD (NRMSD) and linearity were used to evaluate calibration and validation performance. Table 1 summarises the copper and sulfur results used to confirm that the analyser retained its factory performance after installation. The full multi-element calibration and validation results are provided in Appendix A.

**TABLE 1**

Summary of copper and sulfur factory calibration and validation performance.

| Performance | Cu RMSD | Cu NRMSD | Cu $R^2$ | S RMSD | S NRMSD | S $R^2$ |
|---|---|---|---|---|---|---|
| Factory calibration, February | 0.010% | 0.50% | 0.9998 | 0.049% | 0.78% | 0.9995 |
| Factory validation, February | 0.012% | 0.58% | 0.9997 | 0.052% | 0.83% | 0.9994 |
| Site validation, April | 0.007% | 0.33% | 0.9999 | 0.078% | 1.24% | 0.9986 |
| Site validation, July | 0.007% | 0.36% | 0.9999 | 0.065% | 1.04% | 0.9990 |

## Establishing the process response using cross-belt and slurry analysers

The cross-belt analyser is located immediately downstream of the crushing circuit and upstream of the COS. The slurry analyser measures flotation-feed after stockpiling, grinding and associated process residence time. Direct comparison of the two signals therefore requires allowance for the time taken for changes in crusher product to become visible at flotation feed.

Minute-level copper measurements from both analysers were used to determine this effective process response. Cross-correlation was evaluated over a range of time shifts and at different short-term averaging intervals. The strongest relationship occurred at approximately 41 mins using 5 min averages and approximately 46 mins using 15 min averages. A nominal 45 min response was therefore adopted for subsequent commissioning comparisons, with 40–50 mins regarded as the practical operating range.

The derived lag is an effective process response rather than exact parcel tracking. Material entering the COS is mixed and dispersed through stockpile reclaim, grinding and flotation-feed residence. Figure 2 shows the correlation response used to establish the nominal alignment.

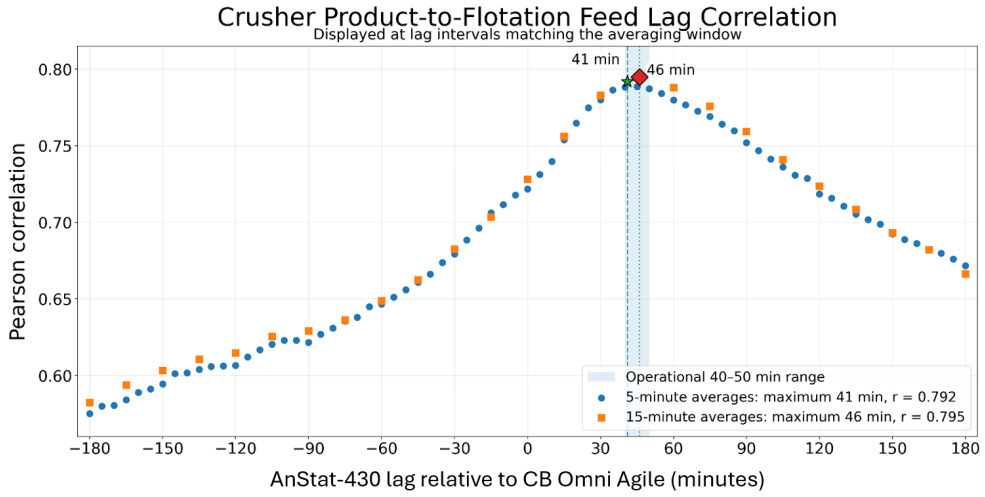



**FIG 2** – Correlation analysis supporting an effective crusher product-to-flotation feed response lag.

The slurry analyser comparison was restricted to the period before 16 June 2026. After that date, recommissioning of a flash flotation cell upstream of the slurry analyser changed the material stream presented to the analyser, so the original relationship could no longer be assumed to remain directly comparable.

## Comparison of planned and measured ore grade

Recorded blend start and finish times were used to associate the planned ROM blend estimate with the corresponding cross-belt analyser measurements. The planned blend estimate represents the intended average grade based on the nominated ROM source proportions. It is a planning value rather than a direct measurement of the material delivered to the crusher.

Cross-belt analyser measurements were averaged over each blend using throughput data so that periods carrying greater tonnage had greater influence on the calculated mean. The same minute-level data were used to describe the grade distribution within each blend. The commissioning data set contained 146 blend periods with sufficient valid cross-belt analyser coverage for comparison with the planned blend estimate. Detailed weighting and data-quality criteria are provided in Appendix A.

## Applying the process response to downstream validation

The nominal 45 min process response was then used to relate the crusher-product measurement to downstream measurements. The slurry analyser provided high-frequency flotation-feed measurements during the pre-change commissioning period and was used to determine whether short-term grade changes measured upstream remained observable downstream.

Reconciled feed provided an independent assay-based comparison. These results are based on physical 12 hr shift composite samples adjusted through the site end-of-month reconciliation process. The recorded database timestamps identify the shift composite rather than the exact start of physical sampling, so the corresponding cross-belt analyser analysis windows were moved 45 mins earlier to account for the effective process response.

The aligned comparisons therefore assessed four complementary information sources: the planned blend estimate, the continuous cross-belt analyser crusher-product measurement, the downstream flotation-feed slurry analyser measurement, and the independent reconciled feed shift composite assay. Sixty-four independent shift composites contained sufficient data to compare the planned estimate, the tonnage-weighted cross-belt analyser result and reconciled feed on the same time support. This independent comparison was treated as the principal validation of whether the upstream measurement represented the grade subsequently processed through the plant.

The main paper focuses on the process interpretation of these comparisons. Detailed weighting calculations, statistical tests, method-agreement analysis and data-quality criteria are provided in Appendix A.

# RESULTS

## Calibration remained stable following installation

Factory and site validation showed that the analyser retained a consistent response after installation. Copper validation performance was particularly stable, with NRMSD between 0.33 and 0.58 per cent and $R^2$ values of approximately 0.9997 or higher across factory and site validation. Sulfur also maintained a strong linear response across the validation measurements.

The July validation reproduced the performance observed during April commissioning, providing confidence that changes observed in the operating data were associated with changes in conveyed material rather than short-term drift in the calibration. The full multi-element results are provided in Appendix A.

## Cross-belt analyser measurement provides useful advance warning

Comparison of the minute-level cross-belt analyser and slurry analyser measurements established an effective crusher-product to flotation-feed response of approximately 40–50 mins. A nominal value of 45 mins was adopted for the remainder of the analysis.

This response time is operationally important because the cross-belt analyser detects a grade change before the same change becomes visible at flotation feed. The measurement therefore provides an interval in which the observed material can be related back to ROM reclaim and crusher-

feed activities. The lag should not be interpreted as exact tracking of an individual parcel of ore, but the relationship was sufficiently consistent to align the upstream and downstream measurements for evaluation of grade trends.

## Cross-belt analyser measurement of within-blend variability

The cross-belt analyser showed substantial grade variation within individual periods that were represented in the blending system by a single planned average. Across 146 matched blend periods, the median within-blend coefficient of variation was 9.19 per cent and the median P10–P90 range was 0.184 Cu percentage points. Forty-nine blend periods had a coefficient of variation above 10 per cent.

These results show that blend performance has two distinct components. The first is whether the average realised grade is close to the target. The second is whether the material sequence around that average is sufficiently stable. A planned blend can therefore be correct on average while still containing significant short-term variation. Conversely, a relatively stable feed can remain consistently above or below the planned target. These conditions require different operational responses and cannot be distinguished from the planned average alone.

Comparison of the planned blend estimate with the realised cross-belt analyser average also showed weak blend-to-blend tracking. The planned value should therefore continue to define the target, but it should not be treated as a measurement of the material actually delivered to the crusher. Figure 3 illustrates the planned estimate, realised weighted mean and within-blend grade range.

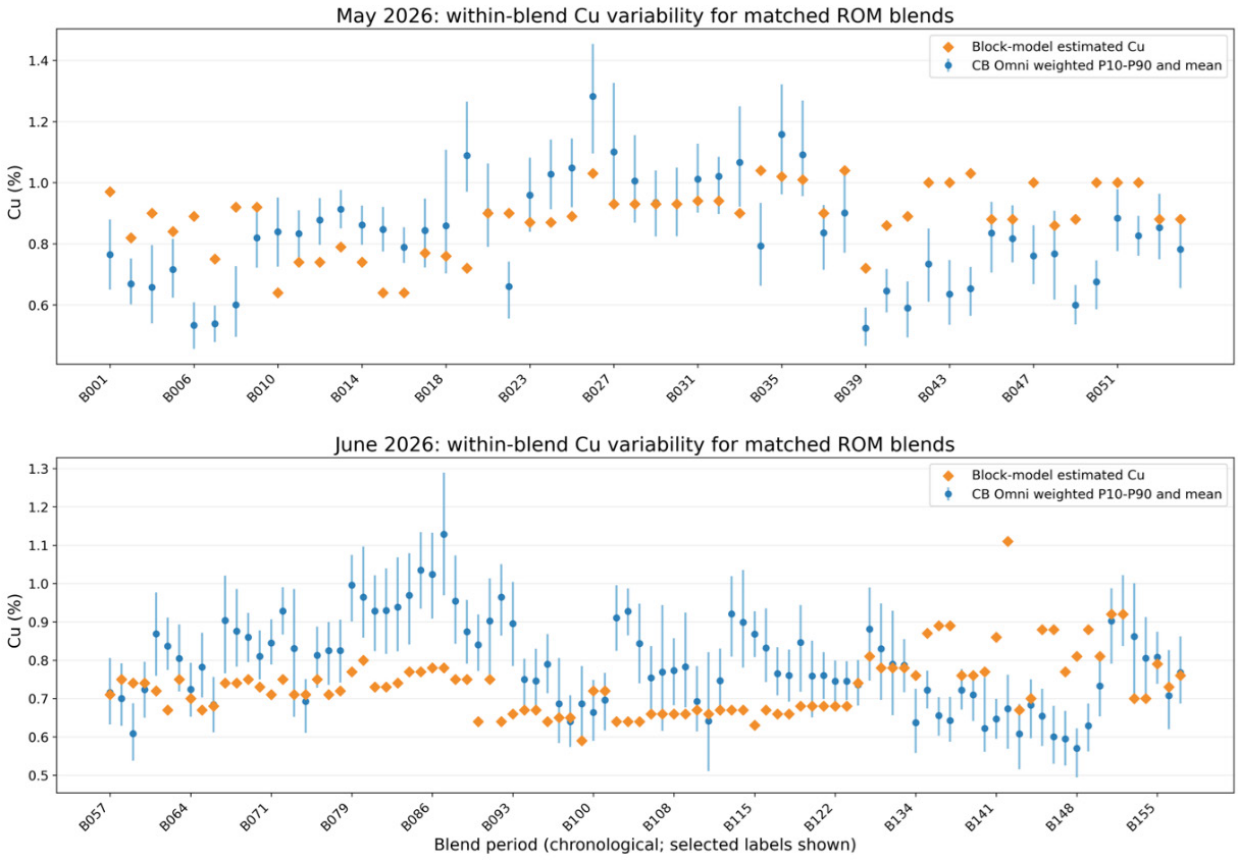



**FIG 3** – Blend-period comparison showing the planned Cu estimate, cross-belt analyser weighted mean and measured P10–P90 grade range.

## COS feed grade changes remain evident at flotation feed

After applying the effective process response, the cross-belt analyser and slurry analyser measurements showed a clear relationship during the comparable period, prior to the circuit change. For the 73 retained blend periods, the correlation between the blend-period cross-belt analyser and

slurry analyser values was 0.784. Averaging the aligned measurements over five-minute intervals produced a similar relationship.

The magnitude of short-term variability was lower at flotation feed than at crusher product. Median coefficient of variation (CV) decreased from 9.44 per cent at the cross-belt analyser to 5.75 per cent at the slurry analyser, while the median P10–P90 width decreased from 0.198 to 0.112 Cu percentage points. This behaviour is consistent with physical blending and dispersion through the COS and grinding circuit.

Importantly, the upstream variation was attenuated rather than eliminated. Grade changes measured before the COS remained sufficiently strong to be detected downstream. This provides an important link between the upstream measurement and plant operation: the cross-belt analyser is not only detecting local variation on the conveyor, but a component of that variation remains present in the material subsequently presented to flotation. The attenuation of within-period variability is shown in Figure 4.

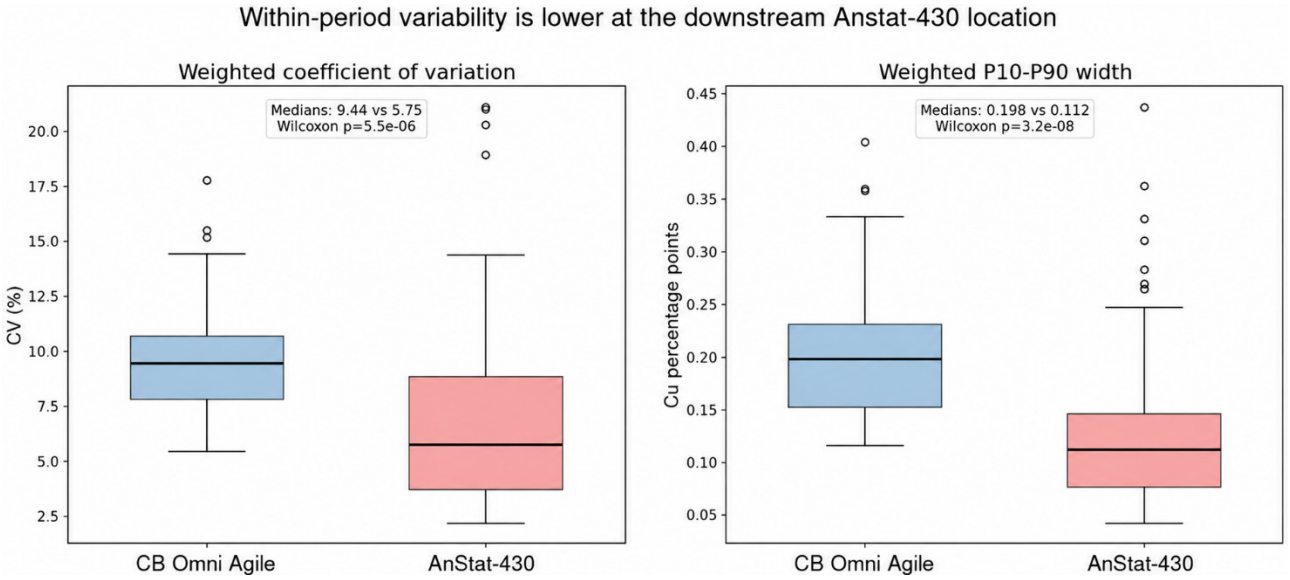



**FIG 4** – CB Omni Agile and AnStat-430 comparison showing aligned blend-period mean grade and attenuation of within-period variability.

## Independent shift composite assays support the upstream measurement

The reconciled feed shift composite comparison provided the strongest independent validation because it uses an assay-based downstream measurement rather than another online analyser. For the 64 independent shift composites, the planned blend estimate showed only a weak relationship with the downstream assay, whereas the cross-belt analyser showed a strong relationship with reconciled feed. These comparisons are shown in Figure 5.

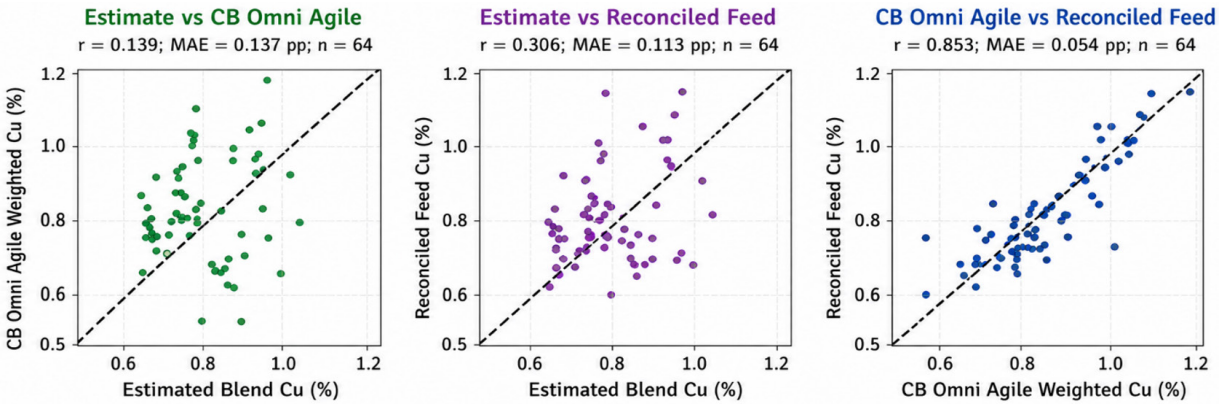



**FIG 5** – Comparison of planned blend estimate, cross-belt analyser and reconciled feed shift composite.

The correlation between cross-belt analyser and reconciled feed was 0.853, compared with 0.306 between the planned estimate and reconciled feed. The mean absolute error between cross-belt analyser and reconciled feed was 0.054 Cu percentage points, less than half the corresponding error for the planned estimate comparison.

The measurements should not be expected to agree exactly. The cross-belt analyser measures coarse conveyed ore continuously before the COS, whereas reconciled feed is a 12 hr composite measured after stockpiling and milling. Nevertheless, the substantially stronger relationship between these independent measurements shows that the realised crusher-product measurement is a better representation of downstream feed grade than the planned blend average.

Detailed method-agreement analysis in Appendix A did not identify a stable permanent correction that should be applied to the cross-belt analyser calibration. The relationship varied between commissioning periods, and further independent campaigns and direct dynamic crusher-product sampling are required before any calibration adjustment is considered.

## Suitability for blending control

The commissioning work was designed to determine whether the cross-belt analyser provides a suitable process measurement for future ore-blending control. Table 2 summarises the evidence against the practical requirements used in the study.

**TABLE 2**

Evidence supporting use of cross-belt analyser for ore-blending decision support.

| Requirement | Commissioning observation | Finding |
|---|---|---|
| Stable analytical response | Factory, April and July validation remained consistent | Verified |
| Measures realised bulk feed | Cross-belt measurement is located on crusher product before the COS | Verified |
| Provides useful lead time | Effective downstream response approximately 40–50 mins | Verified |
| Detects within-blend variability | Median CV 9.19%; median P10–P90 width 0.184 Cu pp | Verified |
| Tracks downstream plant feed | CB Omni Agile–AnStat-430 correlation 0.784 | Strongly supported |
| Supported by independent assay | CB Omni Agile–reconciled feed correlation 0.853 | Strongly supported |
| Calibration correction justified | Relationship varied between commissioning periods | Not established |
| Active blending benefit demonstrated | Commissioning data set was observational | Requires controlled trial |

Taken together, the results demonstrate that the cross-belt analyser meets the measurement requirements needed to support ore-blending decisions at Kanmantoo. The planned blend remains essential because it establishes the required target. The cross-belt analyser provides the complementary information that was previously missing: what grade was actually delivered, how variable that material was within the blend, and whether a persistent deviation is developing before the material reaches the COS.

This creates the basis for an operator-assisted blending strategy. A persistent low realised mean may indicate a need to increase the proportion of higher-grade material or review the assumed source grade. A persistent high mean may provide an opportunity to preserve high-grade inventory.

High variability around an acceptable mean instead indicates a sequencing or mixing problem and may require more frequent alternation of ROM sources.

The appropriate next step is therefore not automatic control, but a controlled operator-assisted trial in which changes to ROM reclaim are deliberately recorded and their effect on upstream and downstream variability is measured.

## CONCLUSIONS

The commissioning study demonstrates that the cross-belt analyser is suitable as an upstream process measurement to support improved ore blending at Kanmantoo.

Factory and site validation confirmed that the analyser maintained stable analytical performance following installation. Comparison with the downstream slurry analyser established an effective crusher-product to flotation-feed response of approximately 40–50 mins, providing useful advance visibility of grade changes before their downstream effect is observed.

The cross-belt analyser also demonstrated that a single planned blend average does not adequately describe the material delivered to the crushing circuit. Significant variation occurred within many planned blend periods, and the realised blend-period grade showed only a weak relationship with the planned estimate. The measurement therefore provides information about both average grade and short-term variability that is not available from the blend plan alone.

After allowing for the process response, grade changes measured by the cross-belt analyser remained evident in the downstream slurry analyser signal, although their magnitude was reduced by mixing through the COS and grinding circuit. Independent reconciled feed shift composite assays provided the strongest validation, with the cross-belt analyser representing downstream feed grade substantially better than the planned blend estimate.

The commissioning results support use of the cross-belt analyser as the primary upstream measurement for an operator-assisted ore-blending strategy. They do not demonstrate that active control has already reduced downstream variability, nor do they support applying a single permanent calibration correction.

The recommended next phase is a controlled operator-assisted blending trial using the realised rolling grade, within-blend variability and persistence of deviations to trigger documented changes in ROM reclaim. Success should be demonstrated by a repeatable reduction in crusher-product variability followed by a corresponding improvement in the applicable downstream measurement.

## REFERENCES


Bland, J M and Altman, D G, 1986. Statistical methods for assessing agreement between two methods of clinical measurement, The Lancet, 1(8476):307–310.

Bulled, D and McInnes, C, 2005. Flotation plant design and production planning through geometallurgical modelling, in Proceedings Centenary of Flotation Symposium, Brisbane, Australia, 5–9 June 2005 (The Australasian Institute of Mining and Metallurgy: Melbourne).

Dobby, G, Kosick, G and Amelunxen, R, 2002. A focus on variability within the orebody for improved design of flotation plants, in Proceedings 34th Annual Meeting of the Canadian Mineral Processors, Paper 5 (Canadian Institute of Mining, Metallurgy and Petroleum: Ottawa).

Hodouin, D, Jamsa-Jounela, S-L, Carvalho, M T and Bergh, L, 2001. State of the art and challenges in mineral processing control, Control Engineering Practice, 9(9):995–1005, doi:10.1016/S0967–0661(01)00088–0.

Linnet, K, 1993. Evaluation of regression procedures for methods comparison studies, Clinical Chemistry, 39(3):424–432, doi:10.1093/clinchem/39.3.424.

Millar, A and Wraith, B, 2022. Ore variability and process plant performance – the impacts to revenue, in Proceedings IMPC Asia-Pacific 2022, Melbourne, Australia, 22–24 August 2022, pp 34–43 (The Australasian Institute of Mining and Metallurgy: Melbourne).

Noble, G and Ferguson, S, 2020. Understanding ore heterogeneity and effective bulk ore sorting using PGNAA/PFTNA, in Proceedings Preconcentration Digital Conference 2020 (The Australasian Institute of Mining and Metallurgy: Melbourne).

Noble, G, Strombotne, T and Gordon, K, 2024. Online Elemental Analysis of Copper Concentrator Feed Utilizing PGNAA Technology, in Proceedings SME XXXI IMPC International Mineral Processing Congress, National Harbor, Washington DC, USA, 3 October 2024.

Rowett, C, Rolley, P and O'Rielly, D, 2024. Opening the geologists tool box – building a grade control system, in Proceedings International Mining Geology Conference 2024, Perth, Australia, 7–8 May 2024, pp 231–242 (The Australasian Institute of Mining and Metallurgy: Melbourne).

Rutter, J, Scott, M, Odiar, N, Federov, M and Francois-Bongarcon, D, 2020. Quantification of surface sensor representivity of primary crushed ore for bulk ore sorting, in Proceedings Preconcentration Digital Conference 2020 (The Australasian Institute of Mining and Metallurgy: Melbourne).

Shean, B J and Cilliers, J J, 2011. A review of froth flotation control, International Journal of Mineral Processing, 100(3–4):57–71, doi:10.1016/j.minpro.2011.05.002.

Shue, S L, Faw, R E and Shultis, J K, 1996. Fast neutron thermalization and capture gamma-ray generation in soils, in Proceedings HSRC-WERC Joint Conference on the Environment, Albuquerque, New Mexico, pp 596–613.

# APPENDIX A – DETAILED DATA ANALYSIS AND STATISTICAL SUPPORT

## Measurement support and data preparation

The commissioning comparisons combined measurements made at different process locations and over different time supports. The planned ROM blend estimate represents one calculated mean for each blend period. The cross-belt analyser provides minute-level measurements of coarse crusher product together with throughput. The slurry analyser provides approximately minute-level flotation-feed measurements but did not have a corresponding throughput tag in the supplied data set. Reconciled Feed is based on physical 12 hr shift composite samples adjusted through the site reconciliation process.

A minimum of 40 per cent valid measurement coverage was applied to period-based comparisons. Isolated cross-belt analyser spike readings associated with non-operating plant or equipment conditions were excluded because they were not representative of normal ore feed.

Cross-belt analyser values were tonnage-weighted so that higher-tonnage intervals made a proportionally larger contribution to each period average:

$$G_CB = \text{sum}(G_i \times Q_i \times \text{delta_t_i}) / \text{sum}(Q_i \times \text{delta_t_i}) \quad \text{(A1)}$$

where:

- G_i is cross-belt analyser Cu grade
- Q_i is analysed tonnes
- delta_t_i is the valid duration represented by each reading

Slurry analyser values were time weighted because a throughput signal was not available:

$$G_SA = \text{sum}(G_j \times \text{delta_t_j}) / \text{sum}(\text{delta_t_j}) \quad \text{(A2)}$$

Nearest-neighbour temporal support was capped at 90 seconds so that longer data gaps were not bridged.

Within-period variability was characterised using weighted standard deviation, coefficient of variation, weighted P10 and P90 values and the P10–P90 width:

$$CV_w\ (\%) = 100 \times s_w / G_CB \quad \text{(A3)}$$

$$\text{P10–P90 width} = P90_CB - P10_CB \quad \text{(A4)}$$

The reconciled feed database records shift composite results using nominal 06:00 and 18:00 labels. The physical sampling periods are 02:00–14:00 and 14:00–02:00 respectively. Applying the nominal 45 min upstream response gives corresponding cross-belt analyser analysis periods of 01:15–13:15 and 13:15–01:15.

## Statistical methods

Pearson correlation was used to assess linear tracking between paired grade series, while Spearman correlation provided a rank-based check with lower sensitivity to outliers. Paired t-tests, Wilcoxon signed-rank tests and sign tests were used to assess paired differences where appropriate.

Ordinary least squares regression was used for prediction, whereas Deming regression was used for method agreement because both the cross-belt analyser and reconciled feed contain measurement and sampling-support uncertainty (Linnet, 1993). Bland-Altman analysis was used to separate average bias from the expected difference between individual paired measurements (Bland and Altman, 1986). Heteroskedasticity- and autocorrelation-consistent tests and moving-block bootstrap methods were used where temporal dependence in repeated process data could affect inference.

Mean absolute error (MAE) was used as a readily interpretable measure of pair-level discrepancy:

$$MAE = \text{sum}(|y_i - x_i|) / n \quad \text{(A5)}$$

Statistical methods used for detailed commissioning analysis and their interpretation are provided in Table A1.

**TABLE A1**

Statistical methods used for detailed commissioning analysis and their interpretation.

| Method | Purpose in this study | Important interpretation |
|---|---|---|
| Pearson correlation | Measures linear tracking between paired grade series | High correlation shows that signals move together; it does not prove exact agreement |
| Spearman correlation | Measures monotonic tracking with reduced sensitivity to outliers | Provides a rank-based check on Pearson correlation |
| Paired t-test | Tests whether the mean paired difference differs from zero | A non-significant mean can occur when positive and negative differences cancel |
| Wilcoxon signed-rank and sign tests | Non-parametric tests of paired difference magnitude and direction | Useful when differences are not normally distributed |
| Ordinary least squares (OLS) | Predicts reconciled feed from CB Omni Agile while treating CB Omni Agile as the predictor | OLS assumes negligible error in the x-variable and can attenuate the slope when x also has uncertainty |
| Deming regression | Compares two methods while allowing uncertainty in both axes | More appropriate than OLS for method agreement between CB Omni Agile and Reconciled Feed |
| Bland-Altman analysis | Quantifies mean bias and limits of agreement | Shows the likely difference for an individual bucket, not only average tracking |
| HAC and moving-block bootstrap | Allows for temporal dependence in repeated process data | Avoids treating every time-adjacent observation as independent |

## Planned blend estimate versus realised crusher product grade

The equal-period average difference was not statistically significant, but this does not indicate close agreement for individual periods. Positive and negative residuals cancelled in the overall mean, while the low correlation, MAE and wide agreement limits show that individual planned blend values often differed materially from the realised crusher product grade. The sign test also showed that cross-belt analyser was higher more often than lower, even though the average magnitude was not significant under equal weighting.

The Bland-Altman view separates average bias from agreement for an individual blend period. The mean cross-belt analyser minus planned difference was only +0.019 percentage points, which is consistent with the non-significant equal-period paired test. However, the 95 per cent limits of agreement extended from -0.315 to +0.353 percentage points, and seven of the 146 periods fell outside those limits. The small overall mean difference therefore resulted partly from positive and negative residuals cancelling across periods; it does not mean that one planned blend value accurately represented each realised crusher product period. The wide limits show that a fixed correction factor would not resolve the blend-to-blend differences. For operational use, the planned grade should remain the target, while the cross-belt analyser should be used to measure the realised mean and short-term distribution. The planned-versus-realised comparison and agreement assessment are shown in Figure A1.

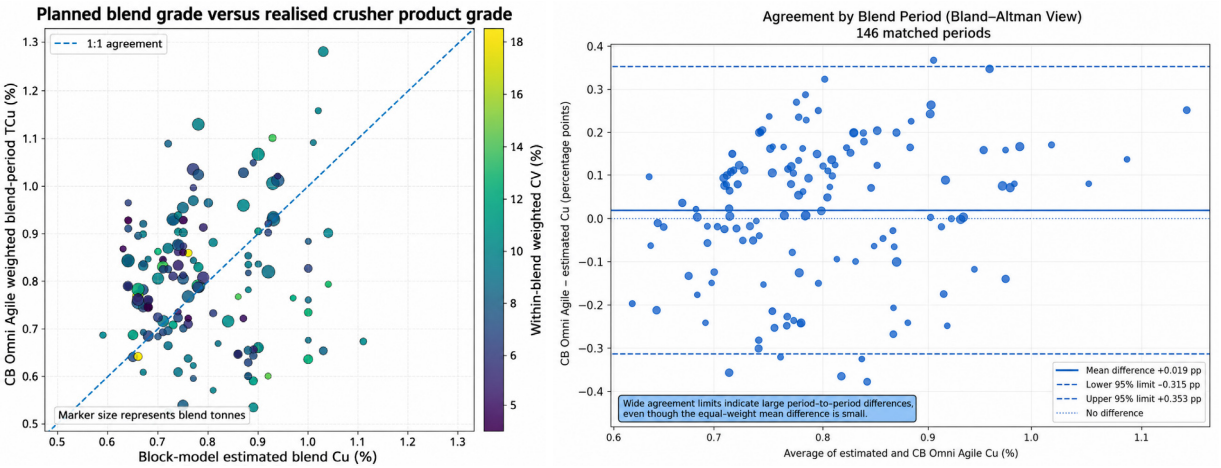



**FIG A1** – (a) planned blend Cu versus CB Omni Agile weighted Cu; (b) Bland-Altman assessment for 146 matched periods, with mean difference and 95 per cent limits of agreement.

When the periods were weighted by production tonnes, the planned estimate was 0.7810 per cent Cu and CB Omni Agile was 0.8289 per cent Cu, a difference of +0.0479 percentage points or approximately +6.1 per cent relative. Clustered analyses were significant at shift and date levels. This result is important for contained-metal reconciliation, but it is not interpreted as analyser calibration bias because the planned estimate and the process measurement describe different supports and the residual also includes blend execution, dilution, timing and source-grade uncertainty.

The May and June time-series comparison of planned blend Cu, filtered CB Omni Agile minute readings, CB Omni Agile weighted blend averages and aligned reconciled feed Cu is shown in Figure A2.

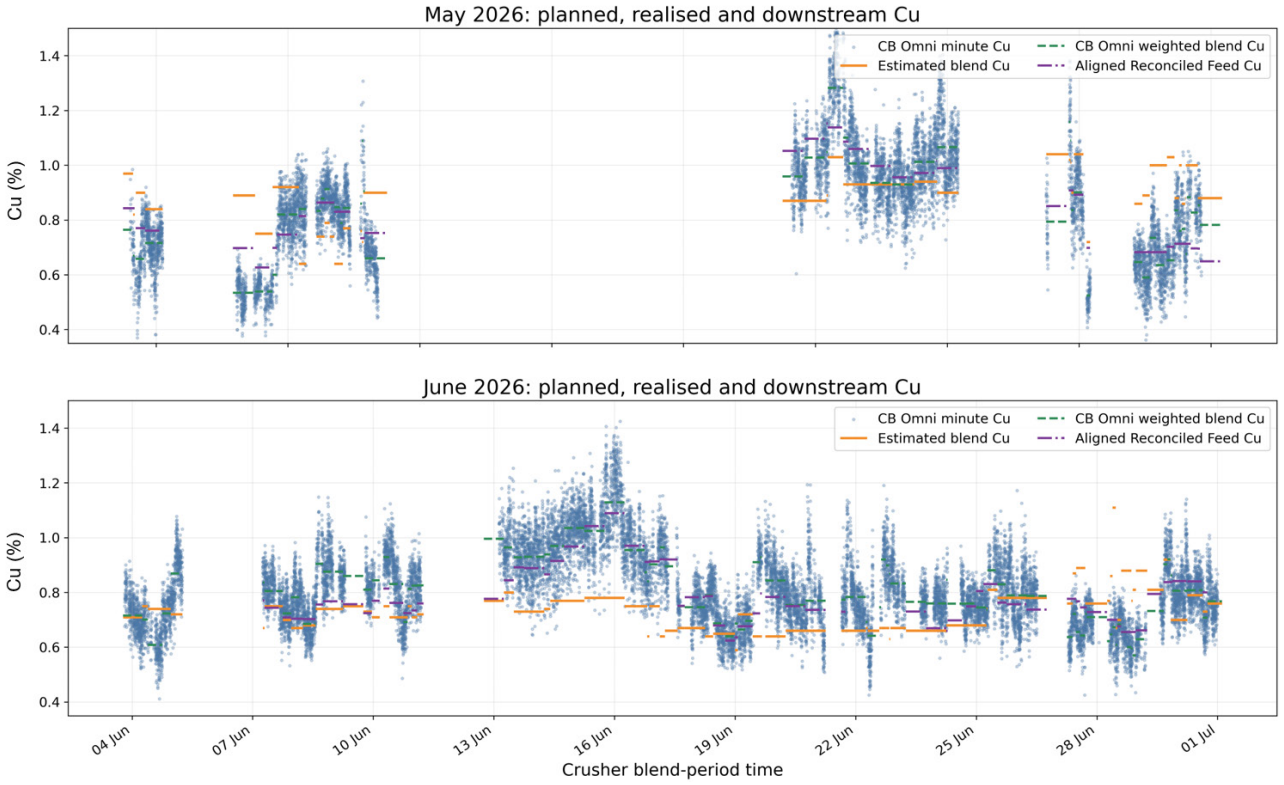



**FIG A2** – May and June time-series comparison.

## Cross-belt analyser and slurry analyser relationship

The time lag-aligned readings show that grade changes measured after the crusher were commonly visible at flotation feed after the broad process delay. The relationship strengthened when the signals were averaged over five-minute intervals, consistent with removal of short timestamp jitter and response noise. The slurry analyser mean was lower than cross-belt analyser for the selected period, but the difference should not be interpreted as a direct calibration bias because the instruments measure different material states and use different weighting supports.

Figure A3 shows the comparison between the 73 blend periods. The correlation between the blend-period cross-belt analyser and slurry analyser values was 0.784.

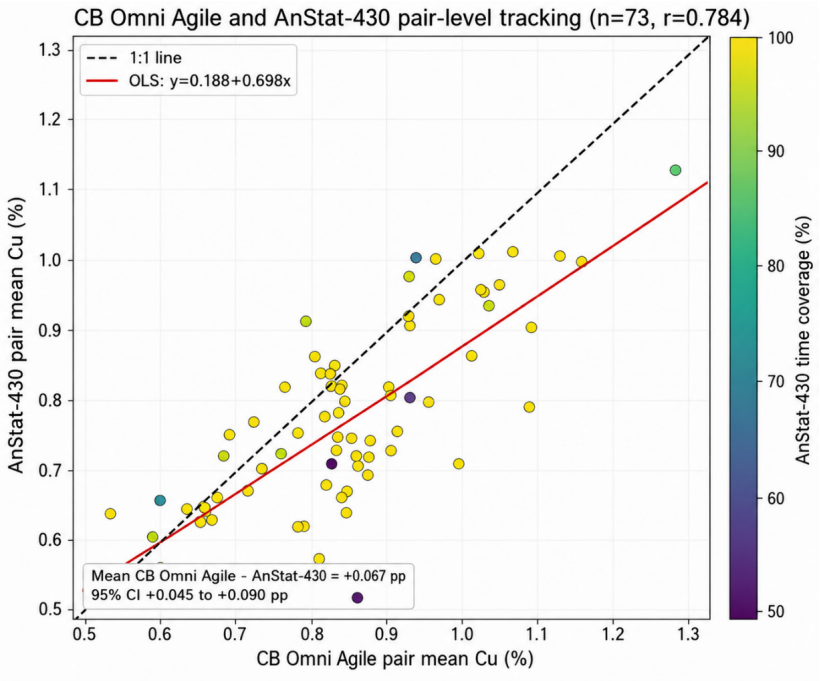
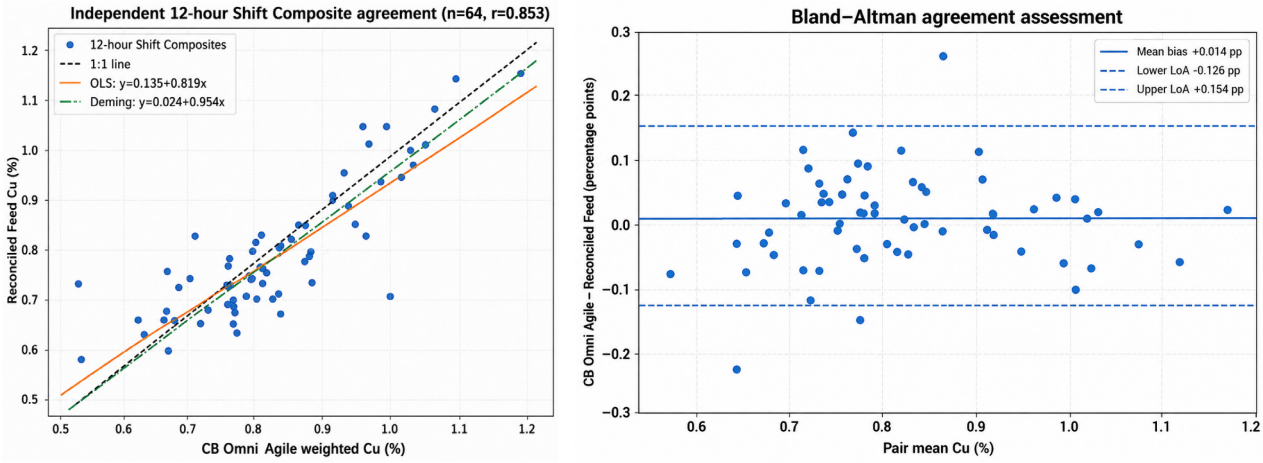



**FIG A3** – cross-belt analyser and slurry analyser blend-period comparison.

## Cross-belt analyser and reconciled feed method agreement

Figure A4 summarises the cross-belt analyser and reconciled feed comparison analysis for 64 independent shift composites.




(a) (b)

**FIG A4** – Cross-belt analyser and reconciled feed comparison.

The full-period data did not establish a consistent bias. The Deming slope confidence interval included one and the intercept interval included zero, indicating that a fixed proportional or constant correction was not supported. Deming regression is the more appropriate agreement method because both cross-belt analyser and reconciled feed contain measurement and support uncertainty. OLS remains useful for prediction but treats the cross-belt analyser as an error-free predictor.

For the independent 12 hr shift composites, the mean cross-belt analyser minus reconciled feed bias was +0.014 percentage points. The 95 per cent limits of agreement were -0.126 to +0.154 percentage points, with 61 of the 64 paired shift composites lying within those limits. The limits were substantially narrower than those for planned blend Cu versus cross-belt analyser, showing that the realised upstream measurement agreed more closely with the downstream shift composite assay than the planned estimate agreed with the realised crusher product.

The paired difference did not vary significantly with pair mean, so there was no evidence of proportional bias over the observed grade range. Nevertheless, an individual 12 hr pair can differ materially because the two values have different sampling supports and are separated by stockpiling and milling. The result supports the cross-belt analyser as a process-relevant measurement for grade tracking and blending decisions, but it does not make the cross-belt analyser and reconciled feed interchangeable measurements.

The whole-period mean difference did not remain constant through the commissioning campaign. Across the May shift composites, the mean cross-belt analyser minus reconciled feed difference was -0.0165 percentage points; across June it was +0.0315 percentage points. Figure A5 shows the difference comparison.

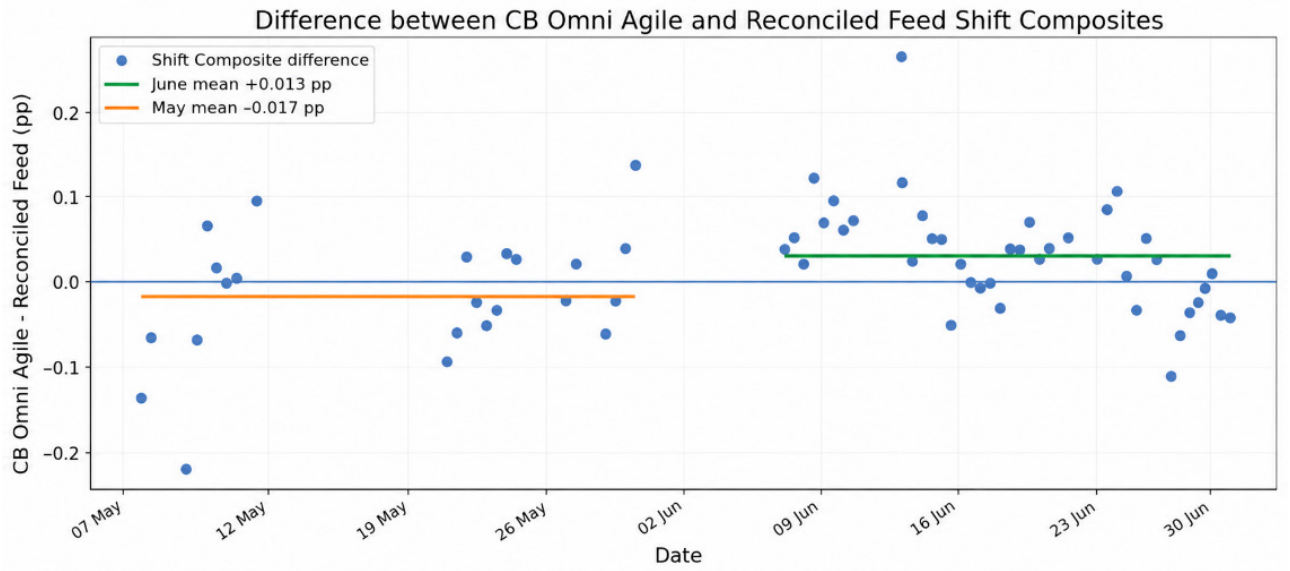



**FIG A5** – Cross-belt analyser and reconciled feed shift composite comparison.

## Detailed commissioning comparison statistics

Key comparison statistics across the commissioning data sets are consolidated in Table A2.

**TABLE A2**

Detailed comparison statistics across the post-commissioning study.

| Comparison/support | n | Pearson r | MAE (pp) | Mean difference | Additional agreement/variability evidence |
|---|---|---|---|---|---|
| Planned estimate versus CB Omni Agile (blend periods) | 146 | 0.116 | 0.141 | CB Omni Agile – estimate = +0.0194 pp | Paired t-test p = 0.172; 95% Limits of Agreement -0.315 to +0.353 pp |
| CB Omni Agile versus AnStat-430 (pre-change periods) | 73 | 0.784 | - | CB Omni Agile – AnStat-430 = +0.0673 pp | Five-minute aligned bins r = 0.785; 95% CL for period r = 0.676–0.859 |
| CB Omni Agile versus AnStat-430 variability | 73 | - | - | - | Median CV 9.44% versus 5.75%; median P10–P90 0.198 versus 0.112 pp |
| Planned estimate versus reconciled feed (132 blend-period records) | 132 | 0.181 | 0.119 | - | Descriptive support; repeated shift composite values |
| CB Omni Agile versus reconciled feed (132 blend-period records) | 132 | 0.778 | 0.071 | - | Reconciled Feed within CB Omni Agile P10–P90 for 90/132 records (68.2%) |
| Planned estimate versus CB Omni Agile (independent shift composites) | 64 | 0.139 | 0.137 | CB Omni Agile – estimate = +0.0367 pp | p = 0.272 |
| Planned estimate versus reconciled feed (independent shift composites) | 64 | 0.306 | 0.113 | reconciled feed – estimate = +0.0225 pp | p = 0.0139 |
| CB Omni Agile versus reconciled feed (independent shift composites) | 64 | 0.853 | 0.054 | CB Omni Agile – reconciled feed = +0.0142 pp | Spearman 0.8038; Limits of Agreement -0.126 to +0.154 pp |
| CB Omni Agile versus reconciled feed method agreement | 64 | 0.8528 | 0.0545 | +0.0142 pp (+1.75% relative) | OLS: y = 0.1355 + 0.8190x, R2 = 0.727; Deming: y = 0.0240 + 0.9538x; paired t-test p = 0.116; HAC p = 0.226 |

## Full multi-element calibration and validation

The full calibration included $SiO_2$, $Al_2O_3$, Fe, CaO, MgO, S, $Na_2O$, $K_2O$, $TiO_2$, Mn, Cu and Co. The reference standards were measured in the factory to validate performance prior to shipping the CB Omni Agile to site. During commissioning in April, the reference standards were measured on-site to validate analyser performance. The reference standards were measured again in July to validate performance and demonstrate the stability of the calibration.

The Root Mean Squared Deviation (RMSD) is a measure of the accuracy of the analysis relative to the reference values of the standards. RMSD can also be divided by the range of each analyte to provide a Normalised RMSD (NRMSD), which is a measure of relative performance. The squared Pearson correlation ($R^2$) is used to assess the linearity of the measured results relative to the reference values. Table A3 summarises RMSD, NRMSD and $R^2$ for factory calibration, factory validation and the April and July site validations.

**TABLE A3**

Calibration and validation performance by analyte.

| | Analyte | $SiO_2$ | $Al_2O_3$ | Fe | CaO | MgO | S | $Na_2O$ | $K_2O$ | $TiO_2$ | Mn | Cu | Co |
|---|---|---|---|---|---|---|---|---|---|---|---|---|---|
| RMSD | Factory calibration – Feb | 0.373 | 0.244 | 0.133 | 0.084 | 0.323 | 0.049 | 0.048 | 0.058 | 0.016 | 0.006 | 0.010 | 0.003 |
| | Factory validation – Feb | 0.273 | 0.292 | 0.120 | 0.094 | 0.286 | 0.052 | 0.059 | 0.063 | 0.013 | 0.004 | 0.012 | 0.003 |
| | Site validation – Apr | 0.350 | 0.267 | 0.112 | 0.078 | 0.255 | 0.078 | 0.031 | 0.051 | 0.018 | 0.007 | 0.007 | 0.002 |
| | Site validation – Jul | 0.327 | 0.346 | 0.093 | 0.092 | 0.238 | 0.065 | 0.050 | 0.058 | 0.013 | 0.007 | 0.007 | 0.003 |
| NRMSD | Factory calibration – Feb | 1.24% | 1.81% | 0.89% | 4.21% | 6.46% | 0.78% | 3.21% | 1.15% | 1.61% | 1.29% | 0.50% | 3.07% |
| | Factory validation – Feb | 0.91% | 2.16% | 0.80% | 4.68% | 5.72% | 0.83% | 3.93% | 1.26% | 1.26% | 0.71% | 0.58% | 3.32% |
| | Site validation – Apr | 1.17% | 1.97% | 0.74% | 3.91% | 5.09% | 1.24% | 2.05% | 1.02% | 1.76% | 1.35% | 0.33% | 2.48% |
| | Site validation – Jul | 1.09% | 2.56% | 0.62% | 4.62% | 4.76% | 1.04% | 3.33% | 1.15% | 1.34% | 1.43% | 0.36% | 3.29% |
| $R^2$ | Factory calibration – Feb | 0.9990 | 0.9973 | 0.9993 | 0.9853 | 0.9718 | 0.9995 | 0.9915 | 0.9990 | 0.9981 | 0.9988 | 0.9998 | 0.9926 |
| | Factory validation – Feb | 0.9993 | 0.9961 | 0.9994 | 0.9817 | 0.9717 | 0.9994 | 0.9870 | 0.9986 | 0.9987 | 0.9996 | 0.9997 | 0.9912 |
| | Site validation – Apr | 0.9988 | 0.9967 | 0.9995 | 0.9876 | 0.9775 | 0.9986 | 0.9971 | 0.9991 | 0.9976 | 0.9984 | 0.9999 | 0.9951 |
| | Site validation – Jul | 0.9990 | 0.9945 | 0.9997 | 0.9822 | 0.9810 | 0.9990 | 0.9910 | 0.9989 | 0.9986 | 0.9982 | 0.9999 | 0.9915 |

# CSIRO's recent developments in real-time monitoring of slurry mineralogy and elemental content

*J O'Dwyer[1], Y Van Haarlem[2], B Ganly[3], B James[4] and L Mao[5]*

1. Research Team Leader, CSIRO, Sydney NSW 2234. Email: joel.odwyer@csiro.au
2. Research Group Leader, CSIRO, Sydney NSW 2234. Email: yves.vanhaarlem@csiro.au
3. Research Team Leader, CSIRO, Adelaide SA 5064. Email: brianna.ganly@csiro.au
4. Research Team Leader, CSIRO, Sydney NSW 2234. Email: ben.james@csiro.au
5. Senior Metallurgist, Glencore, McArthur River Mine, NT. Email: lester.mao@glencore.com.au

## ABSTRACT

The CSIRO Mineral Resources X-ray Technologies Group develops industrial X-ray analysis instruments for real-time measurement of elements and minerals in process stream slurries. X-ray fluorescence (XRF) is widely used in mineral processing plants to measure concentrations of precious and base metals such as gold, platinum, nickel and copper for process control and plant monitoring. However, mineralogy is often the most important physical property affecting beneficiation efficiency.

CSIRO has also developed and patented specialised X-ray diffraction (XRD) technology to monitor the mineral composition of slurries directly on-stream in mineral processing plants. This approach removes the complexities associated with traditional laboratory XRD analysis of slurries and enables real-time mineralogical monitoring.

The high-accuracy XRF and world-first online XRD technologies have been combined into a slurry analyser known as the Mineral and Elemental Analyser (MEA). The MEA is an autonomous, stand-alone unit that measures a continuous slurry flow of up to 120 L/min and reports results at intervals of 5–10 mins. The MEA has been installed in several processing plants in Australia, where it monitors elements and minerals critical for evaluating plant process performance.

This paper outlines a recent field trial in which the combined XRF and XRD technologies were tested at the McArthur River Mine zinc–lead concentrator in the Northern Territory. The study had two objectives: to measure concentrations of gangue minerals, including quartz, mica and phyllosilicates, to determine the total silica ($SiO_2$) content of concentrate streams; and to demonstrate measurement of key elements in the process slurry. The trial demonstrated a measurement accuracy of 1.77 wt per cent (13.6 per cent relative) for total silica and showed good real-time measurement of sphalerite, galena, pyrite, Zn, Pb, Fe and Cu.

## INTRODUCTION

CSIRO Minerals Sensing and Sorting (SaS) is a world leader in the development of advanced online sensing technologies for mining and mineral processing. SaS has developed online X-ray analysis systems capable of monitoring the mineral and elemental compositions of process stream slurries in real-time. Recent advances in X-ray technology and data processing allow access to minerals and elements at much lower detection levels than previously possible. CSIRO's latest technology uses novel, patented X-ray diffraction (XRD) and X-ray fluorescence (XRF) analysers to directly measure key mineral phases and elements in a process stream. These two measurement technologies have been combined into a single analysis system called the Mineralogy and Elemental Analyser (MEA), which provides a complete measurement solution for process stream composition.

The mineral and elemental composition of process stream slurries are both important parameters used to optimise flotation circuits in mineral processing plants. Tracking these parameters enables increased extraction of target metals and reductions in energy and material costs during processing (Li *et al,* 2019). Typically, slurry composition is monitored by sampling at regular time intervals and analysing samples in a laboratory using conventional analytical techniques such as benchtop XRF, benchtop XRD, and mass spectrometry (Ben Amar *et al,* 2022). These methods are time-consuming and often require labour-intensive subsampling and sample preparation. Turnaround times for laboratory assays are typically in the order of 1–2 days, which leads to many critical process control

decisions being made on intuition and experience, rather than quantitative information. Real-time data from online analysers resolve these issues, enabling process control to be both automated and continuously controlled (Rybok *et al,* 2022).

Mineralogical information about slurries is considered more valuable for optimising flotation processes than elemental information alone (Wang *et al,* 2020). Despite this, XRF, which provides only elemental information, is most commonly used for online slurry monitoring because it is relatively straightforward to install in a processing plant (Ben Amar *et al,* 2023; Brooks and Koorts, 2017). Limited success has been achieved using elemental XRF data to infer mineralogical information (Wang *et al,* 2024); however, direct measurement of mineralogy is preferred in many optimisation scenarios (Wang *et al,* 2020). For example, online XRF typically cannot measure light elements such as silicon due to absorption of their low-energy characteristic X-rays by the window between the probe and slurry. As a result, XRF is generally unsuitable for online monitoring of silicate mineral concentrations. Traditional XRD methods are also rarely used in online slurry analysers due to the need for moving parts and specific sample presentation requirements. CSIRO's patented XRD technology overcomes these challenges by using energy-dispersive X-ray diffraction, which requires no moving parts; an earlier version of this technology is described by O'Dwyer and Tickner (2019).

The MEA technology was trialled at the McArthur River Mine (MRM), operated by Glencore Metals Australia, as an online analysis solution for monitoring total silica ($SiO_2$) content in flotation concentrate slurry. Silica is a contaminant in the zinc concentrate produced at MRM and must meet strict thresholds specified by zinc smelters. The primary objective of the trial was to demonstrate measurement of silicate minerals in flotation concentrate streams using the MEA's XRD capability. Secondary objectives included analysis of sulfide mineralogy and associated elements. This study presents results from field testing conducted in December 2024 using the MEA analyser on the MRM first-stage cleaner concentrate stream.

## THE MINERAL AND ELEMENTAL ANALYSER

The MEA, shown in Figure 1, consists of two independent analytical instruments: 1) an X-ray diffraction analyser that performs mineral analysis; and 2) an X-ray fluorescence (XRF) system that measures elemental concentrations. These instruments are mounted to an 80 L launder tank that accepts a continuous flow of slurry from the plant at a rate of up to 120 L/min. The MEA independently measures the slurry density via a weight measurement of the slurry in the tank. The support frame of the launder tank is mounted on six strain six gauges that are used to measure the slurry mass. Slurry density and solids loading are calculated from the weight and known volume of the tank. During operation, the analyser continuously measures the slurry in the tank and reports results to the plant in 5–10 min intervals.

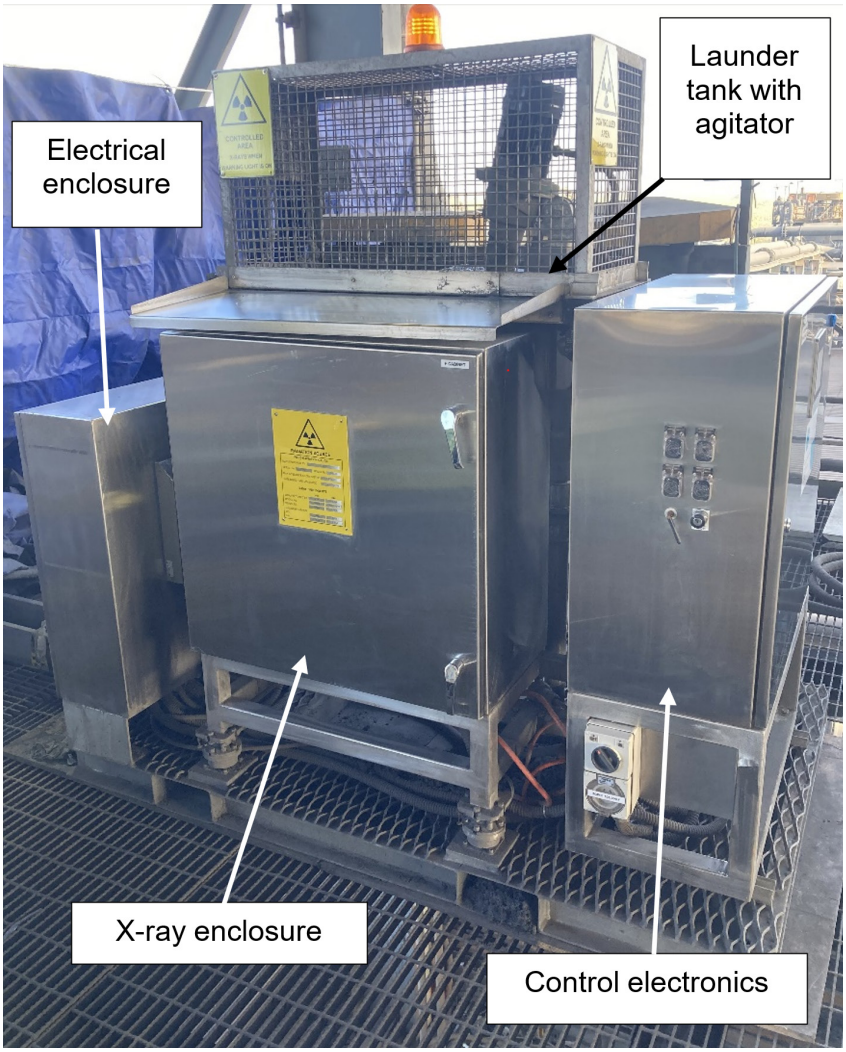



**FIG 1** – MEA Analyser, consisting of an 80 L launder tank, two X-ray enclosures and cabinets for the control electronics. The analyser's footprint is 1.85 × 1.2 m.

## Measurement technologies

The MEA's unique ability to perform on-stream mineral analysis has resulted from the development of patented energy-dispersive X-ray diffraction (EDXRD) technology that is highly optimised for on-stream measurement applications. EDXRD differs significantly to the conventional XRD systems found in analytical laboratories, which require specialised preparation of a sample before a measurement can be conducted. This precludes laboratory techniques from being used in plants for real-time process monitoring. An EDXRD analyser, in contrast, requires no sample preparation, enabling its use for bulk analysis of process stream slurries. The technique also requires no moving parts, is less mechanically sensitive and uses simpler X-ray detector systems compared to laboratory diffractometers, leading to a less expensive and more rugged instrument.

Elemental analysis is performed using CSIRO's state-of-the-art XRF technology. The system provides high accuracy, optimised analysis on elements of interest. The XRF system works simultaneously with the EDXRD analyser to provide fast, accurate stream composition data that can be used by plant control systems to make decisions about optimisation strategies. The combined measurement of both mineralogy and elements extends analysis capabilities of standalone XRD and XRF instruments.

## TECHNOLOGY TRIAL

### Installation

The MEA was installed by MRM site staff on the upper platform of the concentrate flotation shed, where the environment is relatively clean and the analyser is less vulnerable to damage. The first stage cleaner concentrate stream was pumped to the analyser from a sampling point on the second flotation cell using a small peristaltic pump at a rate of about 60–80 L/min. The discharge from the MEA was directed to an existing Outotec Courier 6× OSA. Feed to the analyser was controlled by a manual valve, which could be used to either feed or bypass the analyser, as well as throttle the feed flow rate. The inflow pipe and valve arrangements are shown in Figure 2 alongside the MEA installation at MRM.




**FIG 2** – The MEA installation at MRM (left) and Slurry feed/bypass control. The slurry flow rate to the MEA was controlled using a manual value (right).

MRM is located in the Northern Territory near the Gulf of Carpentaria, approximately 930 km south-east of Darwin. The high year-round temperatures and seasonal heavy rains experienced at this location present a particular challenge for sensitive analytical equipment. Seasonal average temperatures and humidity levels for the past 30 years (1991–2020) are given in Table 1.

**TABLE 1**

Climate statistics for McArthur River Mine. Data averages are averages over the 30 years from 1991 to 2020. Source: Bureau of Meteorology, Statistics Summary for McArthur River Mine Airport.

| | Summer | Autumn | Winter | Spring |
|---|---|---|---|---|
| Mean Min Temp (°C) | 25.0 | 20.4 | 12.9 | 21.0 |
| Mean Max Temp (°C) | 35.4 | 34.2 | 30.9 | 37.5 |
| Mean Relative Humidity (9 am) (%) | 69 | 60 | 47 | 49 |

Due to the extremes of temperature and humidity at MRM, a temporary hut was erected around the MEA, shown in Figure 3, to semi-isolate it from the external environment. A portable industrial air conditioning unit was used to cool the interior of the hut to below that of the surrounds. This solution

ensured the analyser was protected from extremes that can affect the reliability of the system's electronic and analytical devices.



**FIG 3** – Air-conditioned hut constructed to provide a cool environment for the MEA.

## Operation

The MEA was used to measure the first-stage cleaner concentrate stream, which has a solids loading of 15–25 wt per cent and an average $SiO_2$ concentration of 10–11.5 per cent. Measurements were performed by filling the tank with slurry and measuring for 2 hrs. Following each measurement, a subsample of the slurry was collected for laboratory assay, and the tank was flushed before filling with the next slurry sample.

The operation of the MEA in this way is referred to as 'batch mode' and was used to prevent gypsum precipitating from the slurry and forming scale on the inner surface of the tank. Scaling occurred when the elevated-temperature slurry (~50°C) was pumped continuously through the analyser. It was found that, when operating in batch mode, the slurry cooled to ambient temperature, significantly slowing the precipitation process. For permanent operation, the slurry will need to be cooled before entering the MEA, allowing continuous-flow operation to be utilised. A total of 17 batch samples were measured.

## RESULTS

Following the measurement of each cleaner concentrate slurry sample and the completion of the laboratory assays, the MEA XRD spectra were analysed using CSIRO's proprietary analysis software. The concentrations of the mineral phases are obtained by fitting the XRD spectra using an algorithm that is based on the crystallographic properties of the mineral phases in the samples and the physics of the XRD process used by the analyser. By fitting the spectral data, the diffraction peaks can be extracted mathematically, and their intensities determined. The intensities of the peaks are proportional to the weight fractions of the minerals present, allowing their concentrations to be measured. Calibration curves are created by linear regression analysis of the peak intensities using the laboratory assays as the 'true' concentration values.

The measurement results presented here were calculated using the 'leave-one-out' analysis method, which is a technique used to assess the accuracy of a measurement process without the calibration model having knowledge of the sample being analysed. Using leave-one-out, one sample from the measured set is removed and a calibration curve is created using the remainder of the samples. The calibration curve is then applied to the removed sample and its composition is determined. This process is repeated until all samples have been removed and their composition calculated. This is a good test of an analyser's true measurement accuracy since the samples whose composition is being calculated is 'blind' to the calibration.

The results of the MEA analysis of total $SiO_2$ plotted against the laboratory XRD assay data are shown in Figure 4. A mineralogical breakdown of the silica mineral phases is also given in Figure 5. Mineral concentrations are expressed as weight-percentages (wt per cent), which represent the mass of a mineral/constituent present in the slurry divided by the total mass of slurry solids, expressed as a percentage.

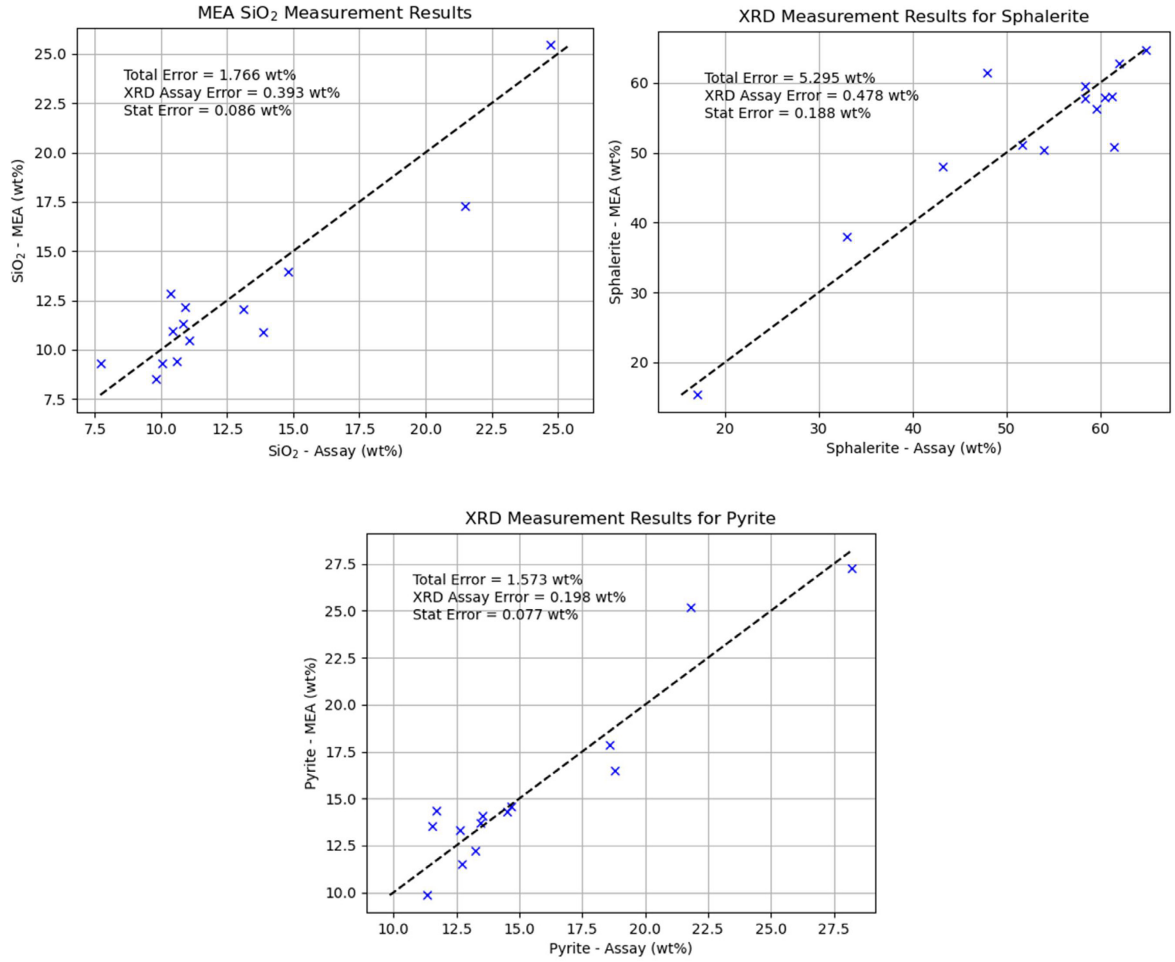



**FIG 4** – MEA XRD measurement results for total $SiO_2$ (top left), Sphalerite (top right) and Pyrite (bottom).

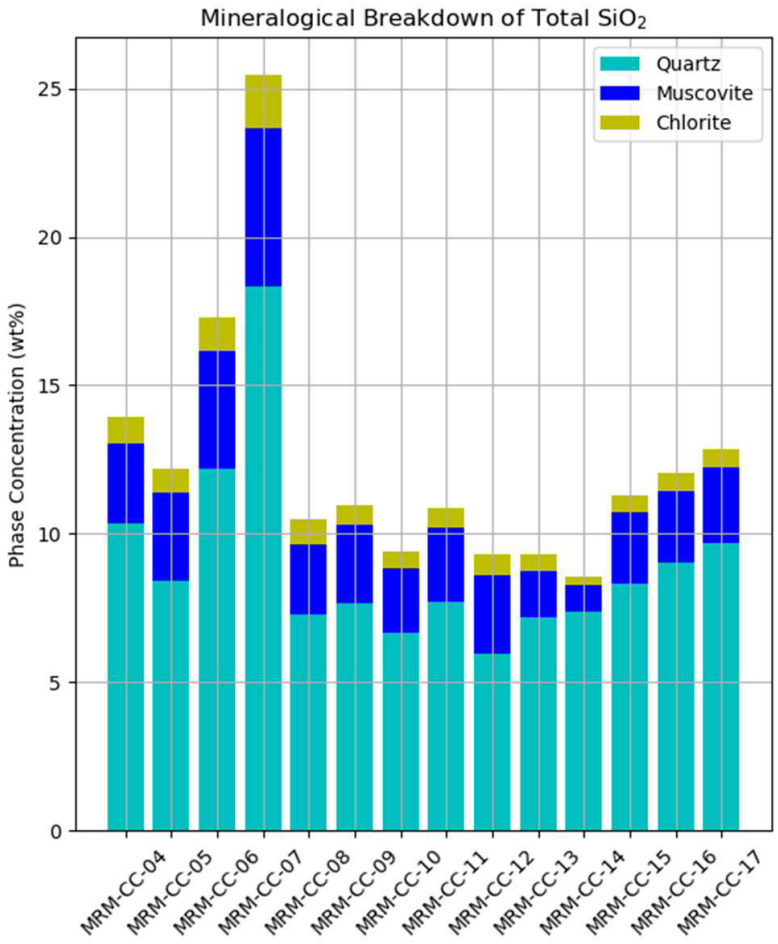



**FIG 5** – MEA XRD measurement of the silica-bearing mineral phases in cleaner concentrate slurry.

These results represent the accuracies for a measurement time of 2 hrs. For total $SiO_2$, good accuracy of 1.77 wt per cent is obtained (13.6 per cent relative) over the wide range of $SiO_2$ concentrations in the samples 7.5 to 25 wt per cent. Analysis of sphalerite and pyrite also showed good accuracies, both returning relative accuracies of 10.1 per cent. The statistical error shown on the plots is determined by the total number of diffracted X-rays counted during the measurement, which is a function of the total measurement time. Increasing the measurement time improves the statistical error, while reducing the measurement time has the opposite effect. Here, the statistical errors are only a small fraction of the total error (<<1 per cent) and therefore increasing the measurement time would provide an insignificant improvement. The dominant source of error in these measurements is sampling errors induced by the laboratory assay process, as explained in the next section.

An interesting feature of the $SiO_2$ analysis results are the two unusually high concentrations values above 20 wt per cent (MRM-CC-06 and MRM-CC-07 in Figure 5). These samples were measured during a time when a plant upset occurred. A process failure in the cleaner concentrate circuit resulted in some first cleaner tails being mixed with the concentrate stream. The tails contain much higher $SiO_2$ and Fe (pyrite) concentrations and lower Zn (sphalerite) grade, thus the $SiO_2$ concentration spiked. The rapid increase is obvious when viewing the data as a time trace (Figure 6). The increased $SiO_2$ was easily detected by MEA, as was the rapid decrease after the upset was resolved. This is a clear demonstration of the MEA's ability to monitor changes in $SiO_2$ in real-time.

Analysis of the XRF data shows similarly good agreement between the MEA measured results and the elemental assays for Zn, Fe and Cu, shown in Figure 7. Total errors of 5.30 wt per cent, 0.66 wt per cent and 0.09 wt per cent were achieved respectively. Similarly for the minerals, the statistical errors are insignificant.

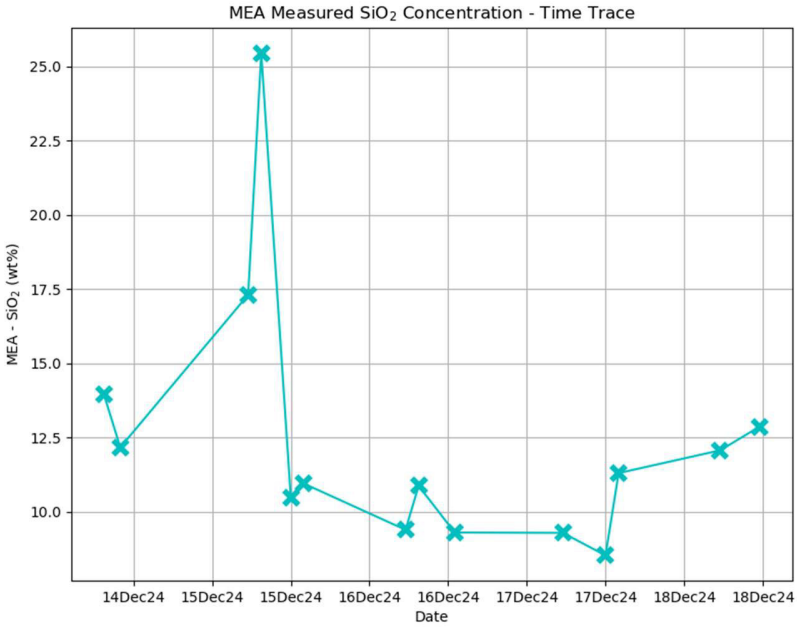



**FIG 6** – Time trace of the $SiO_2$ concentration measured by MEA. The large spike occurred as a results of a plant upset. MEA detected the upset in real-time.

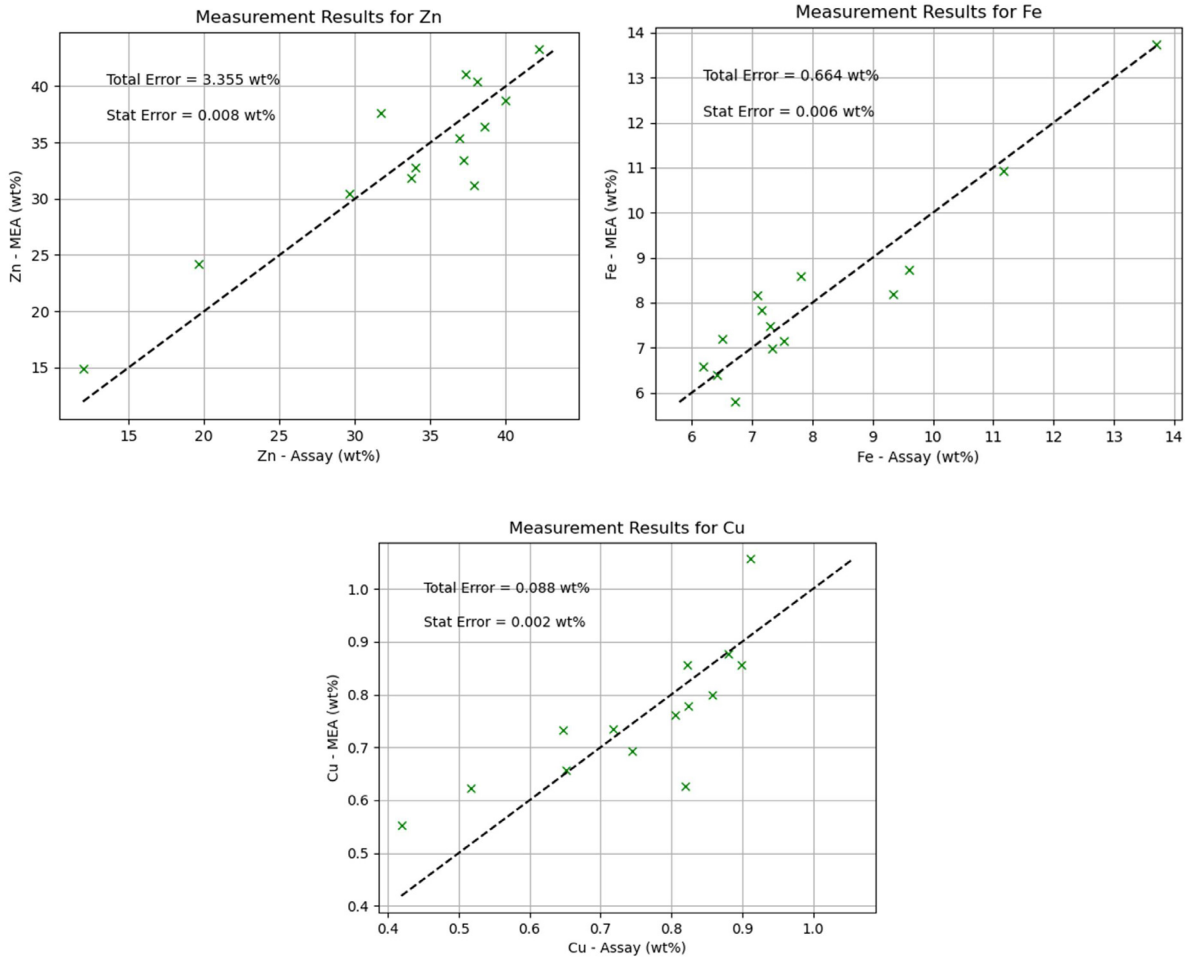



**FIG 7** – MEA XRF measurement results plotted against the elemental concentrations determined by laboratory assay.

## Sampling

A summary of the measurement accuracies obtained for the minerals and elements in the stream are given in Table 2. Overall, the accuracies from the 2 hr batch measurement showed good agreement with the laboratory assays. The largest source of error for both the XRD and XRF analyses were sampling errors associated with the collection of material from the launder tank.

**TABLE 2**

Results summary for the measurement of cleaner concentrate slurry with the MEA.

| **Mineral** | **Accuracy (wt%)** | **Range (wt%)** |
|---|---|---|
| $SiO_2$ – Total | 1.77 | 7–25 |
| • Quartz | 0.95 | 6–18 |
| • Muscovite | 2.38 | 2–13 |
| • Chlorite | 1.01 | 1–8 |
| Sphalerite | 5.30 | 17–65 |
| Pyrite | 1.57 | 11–28 |
| **Element** | | |
| Zn | 3.36 | 13–43 |
| Fe | 0.66 | 6–14 |
| Cu | 0.09 | 0–1 |

Collecting a representative subsample from a large volume, such as the launder tank of the MEA, is a challenging exercise that is prone to error, so much so that there are branches of science, engineering and mathematics dedicated to producing solutions. The magnitude and source of the sampling errors are not known, since the samples required to perform the measurements to quantify these errors were not collected. However, an assumption can be made that inhomogeneity of the slurry within the launder tank plays a significant role in the errors seen in these measurements. The ‘dip’ method used to collect samples from the tank may have resulted in some compositional bias. Future calibration of the analyser would require a more robust sample collection method, as well as quantification of the sampling.

## CONCLUSIONS

The technology trial of the MEA has demonstrated the analyser’s capability to measure the total $SiO_2$ content of first stage cleaner concentrate slurry at the MRM processing plant. Additionally, the MEA successfully measured the sphalerite, galena, pyrite, Zn, Pb, Fe and Cu concentrations of the slurry stream during the trial.

CSIRO is currently producing a new, upgraded model of the MEA to replace the existing version, which was installed and trialled at MRM. The new model – the ‘MEA-Beta’ – has several important technical advantages over the previous ‘Alpha’ version, which will enable it to operate more reliably, with less downtime and deliver significantly increased performance from the XRD system. The upgrades to the system include:

- A higher power XRD system, which is more reliable and decreases measurement times by up to 10×. Faster analysis is important when the analyser is used to measure multiple streams.
- Simplified X-ray assemblies that allow technical plant staff to perform routine maintenance on the analyser.
- Automated X-ray analyser commissioning and alignment following maintenance.
- Upgraded operating software that provides plant staff with more control over the analyser.

## ACKNOWLEDGEMENTS

CSIRO would like to thank Glencore and the McArthur River Mine for the opportunity to demonstrate the MEA technology. CSIRO acknowledges the efforts of MRM metallurgy management and technical service team Daniel Smith, Jose Siliezar, Lester Mao, Matthew Potter, Khanh Nguyen, Aden Cross and Daniel Knott and for providing support throughout the trial.

## REFERENCES

Ben Amar, I, Roudjane, M, Griguer, H, Miled, A and Messaddeq, Y, 2022. The effect of particle size and water content on XRF measurements of phosphate slurry, *Sci Rep*, 12:17823. https://doi.org/10.1038/S41598-022-21392-0

Ben Amar, I, Thomas, A, Bachmann, C, Hafnoaui, A, Griguer, H, Miled, A and Messaddeq, Y, 2023. XRF online analyzer for measurements of $P_2O_5$ content in phosphate slurry, *Sci Rep,* 13:1–11. https://doi.org/10.1038/S41598-023-45181-5;SUBJMETA

Brooks, K S and Koorts, R, 2017. Model Predictive Control of a Zinc Flotation Bank Using Online X-ray Fluorescence Analysers, *IFAC-PapersOnLine*, 50:10214–10219. https://doi.org/10.1016/J.IFACOL.2017.08.1772

Li, H, Xu, Z, Wang, W, Liu, Y and Zhang, S, 2019. A novel technique for online slurry grade detection based on EDXRF, *Miner Eng*, 131:14–22. https://doi.org/10.1016/J.MINENG.2018.11.004

O'Dwyer, J and Tickner, J, 2019. Design optimisation of an energy-dispersive X-ray diffraction analyser, *Applied Radiation and Isotopes*, 144:5–9. https://doi.org/10.1016/J.APRADISO.2018.07.010

Rybok, L, Kowoll, T, Thomas, A, Nad, A and Bachmann, C, 2022. Online elemental analysis for process control in the mineral processing industry, *TOS Forum 2022,* 131. https://doi.org/10.1255/TOSF.142

Wang, L, Zhong, X, Wang, H and Dai, W, 2024. A mechanistic and data-driven approach for real-time online determination of ilmenite grade in pulp by X-ray fluorescence, *Miner Eng*, 218:109002. https://doi.org/10.1016/J.MINENG.2024.109002

Wang, Q, Li, F, Jiang, X, Wu, S and Xu, M, 2020. On-stream mineral identification of tailing slurries of tungsten via NIR and XRF data fusion measurement techniques, *Analytical Methods*, 12:3296–3307. https://doi.org/10.1039/D0AY00322K

# Sensor-based ore sorting at Sky Metals Tallebung Project

*X Yang[1], O Davies[2] and C Corcoran[3]*

1. Senior Applications Engineer, TOMRA, Castle Hill NSW 2154. Email: xingshi.yang@tomra.com
2. Managing Director, Sky Metals Limited, Orange NSW 2800. Email: odavies@skymetals.com.au
3. Test Centre Manager, TOMRA, Castle Hill NSW 2154. Email: chris.corcoran@tomra.com

## ABSTRACT

Sensor-based ore sorting technology represents a significant advance in the pre-concentration of tin ores, offering substantial improvements in process efficiency and resource utilisation. Employing high-resolution sensor-based systems, X-ray Transmission (XRT) sorting enables the accurate differentiation between mineralised and barren material based on density and compositional contrast. This early-stage separation enhances the grade of tin in the feed material prior to milling and traditional beneficiation, thereby reducing the mass throughput to downstream processing circuits. The resulting decrease in energy and water consumption, coupled with the potential for downsized plant infrastructure contributes to both operational cost savings and reduced environmental impact.

At the Sky Metals Tallebung Tin-Tungsten-Silver Project, ore sorting has demonstrated exceptional results. The most recent bulk study using a recovery-oriented sorting approach reported a 2.80 per cent tin sorted product at 97 per cent tin recovery in a single sorting stage. Two-stage sorting produced a 9.06 per cent tin concentrate product at 86 per cent tin recovery. The deployment of sorting technology has enabled substantial reductions in the volume of material subjected to comminution and beneficiation, thereby optimising resource allocation and enhancing process selectivity. A total feed sample of 75 t have been concentrated into a minimal mass (overall mass reduction of 92 per cent).

This paper presents the results of a comprehensive test work program evaluating the application of sensor-based ore sorting technology at the Tallebung Tin Project specifically focusing on the sensor response, mineralogical characteristics, and liberation that determine and influence sorting performance as well as the demonstration of novel AI-based techniques. The study demonstrates significant economic and environmental benefits including improved tin grades, reduced mass throughput, and minimised processing requirements.

## INTRODUCTION

Sky Metals is defining a large-scale hard rock tin resource with existing bulk tonnage Mineral Resources Estimate (MRE) defined, augmented with recent higher-grade tin zones discovered on the margins of the known deposit. The Tallebung tin deposit lies at the northern end of the Wagga Tin Belt within the central Lachlan Orogen which hosts widespread S-type and minor I-type granites strongly associated with tin–tungsten mineral systems, particularly in the Wagga-Omeo Zone where Ordovician quartz-rich turbidites and black shales dominate the sedimentary succession (Mamuse and Guj, 2013). These sediments, intruded by Silurian granitic plutons, provide the regional geological framework for several tin deposit styles, including alluvial, greisen, skarn, and vein-hosted systems (Department of Regional NSW, 2021). In the Tallebung region, the Ordovician Tallebung Group crops out as weakly metamorphosed shales, siltstones, carbonaceous mudstones and minor quartz-rich sandstones, folded into an NNW-striking structural fabric. This stratigraphy, combined with the metallogenic signature of nearby fractionated granites, reflects the tectono-magmatic conditions that produced many Sn–W occurrences across the Lachlan Orogen.

The Tallebung deposit itself represents a vein-style tin-tungsten-silver system, likely genetically linked to the Silurian-aged Erimeran Granite, which outcrops ~2 km south of the mining field and is interpreted as the principal source of mineralising fluids. Mineralisation occurs in two principal forms: (1) significant unconsolidated alluvial to elluvial tin-bearing sediments, up to 36 m thick, consisting of poorly sorted sandy-silty clays with coarse bedrock fragments; and (2) a well-developed quartz-vein stockwork zone hosting cassiterite, scheelite and wolframite.

Tin ore processing addresses several challenges, particularly regarding efficient resource utilisation and minimising environmental impact (Firsching, Spencer and Leisner, nd). This study focuses on the implementation of X-ray Transmission (XRT) sorting technology at the Tallebung Tin Project, aiming to evaluate its technical and economic viability. The results of the testing show great potential for the XRT sensor-based sorting in tin preconcentration for Sky Metals' Tallebung deposit. The combination of coarse liberation and the density contrast between cassiterite grains with host-rock makes the Tallebung deposit an ideal candidate for XRT-sensor based sorting. Ore sorting increased tin grade from 0.04–0.49 per cent to a sellable concentrate 7.23–11.86 per cent. Using TOMRA's recently released deep learning tool OBTAIN™, an improved particle classification using AI de-clustering helps accurately identify individual products at high throughput rate. Tin recovery was maintained above 97 per cent with 83 per cent mass reduction.

## METHODOLOGY

The methodology included sample preparation, sensor calibration, and performance evaluation. A bulk sample of 75 t was crushed and screened to 7–40 mm prior to arrival. The samples were then separated into two stages of test work. The first stage tests performance of the XRT sensor-based ore sorting over 4 different types of feed, and the second stage tests the effectiveness of deep learning tool OBTAIN™ on sorting efficiency. The sorting of the material is shown in Figure 1. The material is presented to a pan feeder which spreads it across the full 1200 mm width of the sorter. It then drops down a chute onto the main belt and is delivered to the separation chamber where material is imaged, classified, and separated into product and waste streams using air nozzles. For each set of tests, the feed material is sorted in two runs: the first run is a recovery-oriented run which generates a non-ejected waste, and the ejected product from the first run is then re-sorted in a concentrate run which separates the material into the non-ejected middlings and the ejected concentrate product. Analytical techniques to define tin, tungsten, and silver content were employed to assess tin grade and recovery post-sorting.

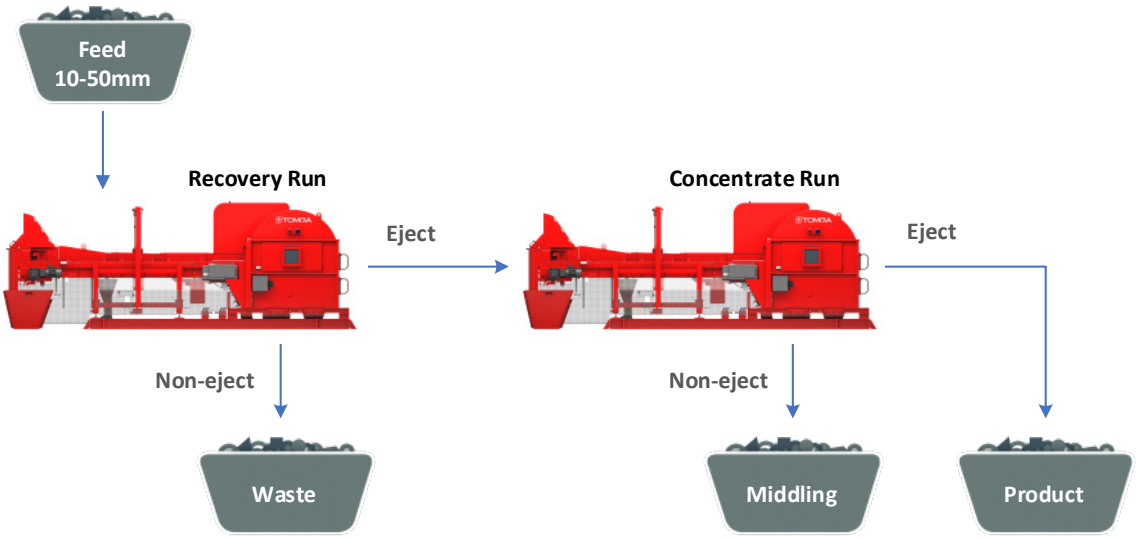



**FIG 1** – Process flow chart of the test work.

The Tallebung deposit is characterised by a relatively simple mineralogical composition, with tin primarily occurring as cassiterite. A similarly simple mineralisation emplacement encourages coarse grained, well liberated mineralisation which is integral in the most amenable sorting applications. Understanding these characteristics is essential for optimising sensor-based separation; the coarse liberation size of the cassiterite means that it does not require large amounts of energy to crush and grind prior to ore sorting as the particle size can be sorted relatively coarsely (7–40 mm).

X-ray transmission (XRT) ore sorting works bypassing X-rays through individual particles on a conveyor and measuring how much of the radiation is attenuated as it passes through each particle. The degree of attenuation depends primarily on a material's effective atomic number rather than its surface properties. In practice, XRT systems use either single- or dual-energy X-ray detectors

positioned beneath the material stream; by comparing the incoming and transmitted intensities, the system calculates a relative density or atomic-number proxy for each particle. This information is processed in real time by the sensor-based sorting control unit, which classifies particles as ore or waste and triggers mechanical ejection (typically air jets) to separate them (Figure 2). Because the measurement is taken through the rock, XRT can ignore fine coatings, weathered surfaces, and detect partial liberation, making it especially robust compared to optical methods when mineral grains are encapsulated within gangue.

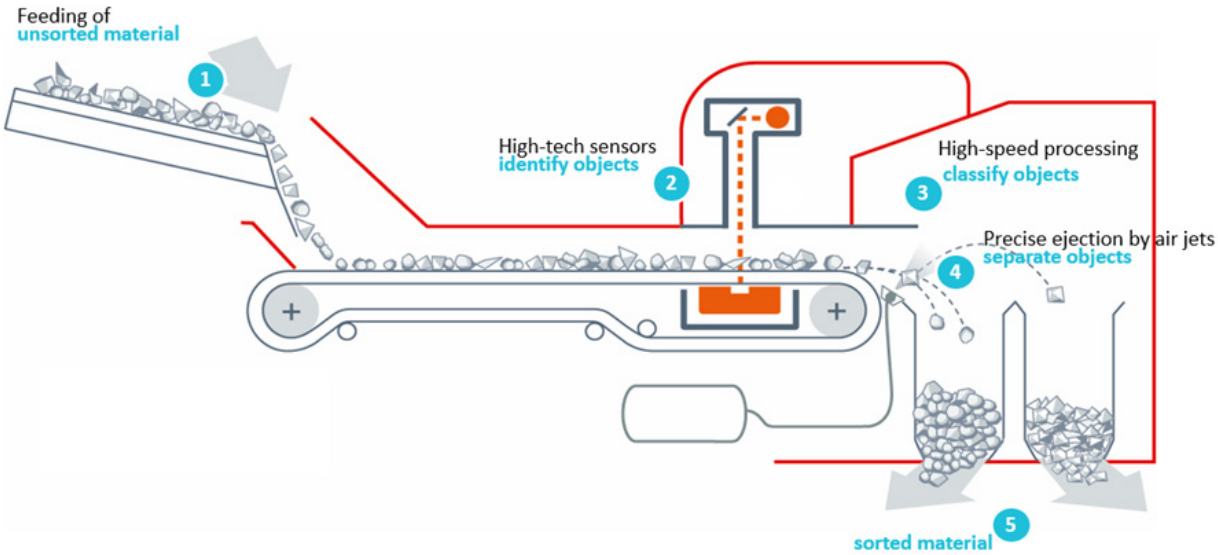



**FIG 2** – Schematic of the sensor-based sorting with XRT ore sorting.

The mineralogical property of elemental composition is primarily the atomic density as this dominates the attenuation of hard X-rays applied (Robben and Wotruba, 2019). XRT sorting is particularly effective for cassiterite ($SnO_2$) because it has a very high density and a high effective atomic number relative to common sedimentary host rocks which are primarily made up of quartz (and in the case of this deposit, lesser mica and clay minerals). When cassiterite occurs as disseminated grains or partially liberated particles within a low-density host, it causes a strong increase in X-ray attenuation that is readily detected by XRT sensors. Figure 3 shows an example of the raw XRT image and the classified image of the high density cassiterite in contrast with low density host rocks.

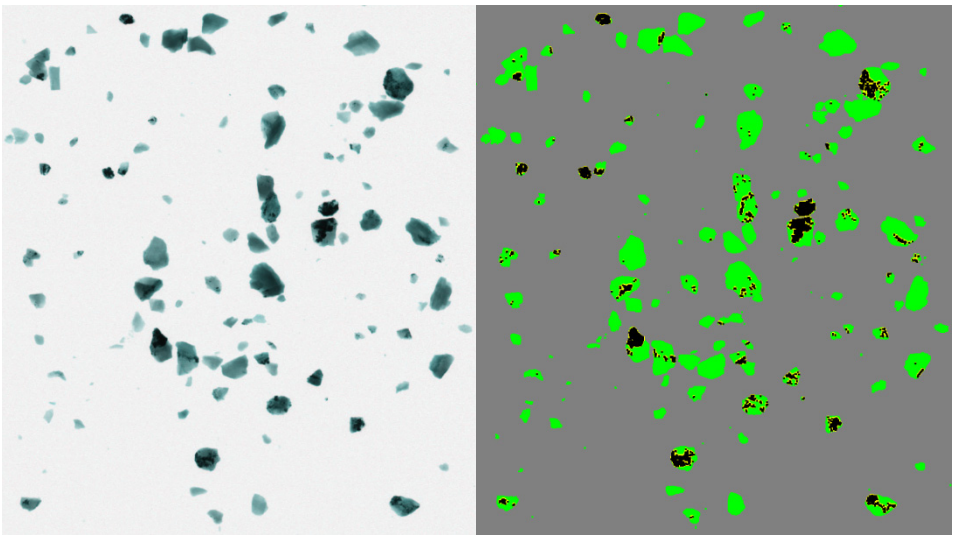


**FIG 3** – Example of raw (left) and classified (right) XRT image of the cassiterite and host rocks. Colour code of classified image: green = host rock, black = cassiterite inclusions.

## RESULTS AND DISCUSSIONS

### Stage 1 – Effect of ore minerology to sorting capabilities

The sorting program was tailored to the mineralogy of Tallebung deposit. For the stage 1 tests, the program is used for four feed samples that have similar material properties but different Sn grades. Results are shown in Figure 4. The recovery of the recovery-oriented runs of the test is largely related to the background grade of the rejected waste. For samples with relatively low feed grade (ie the T4P sample), the feed grade (Sn 0.04 per cent) is close to the waste grade (Sn 0.02 per cent) and so Sn recovery is limited to the presence and liberation of the cassiterite. For this feed, ore sorting has shown effectiveness in increasing material potential. The first run of sorting increased Sn grade from 0.04 per cent to 1.11 per cent with 98 per cent mass reduction. The concentrate run then concentrated product to 8.69 per cent Sn grade by a further 97 per cent mass reduction/deportment into the middlings fraction. For relatively higher-grade feeds (ie the T5P sample), the sorting has shown consistency in maintaining relatively low waste grade even considering higher ejection rate (and therefore increased chance of over-ejection). As such, liberation and grain size of the coarsest cassiterite grains allows for a relatively high-grade concentrate fraction which is seldom achieved in tin ore-sorting (11.86 per cent Sn @ 97 per cent mass reduction).

With increased feed grade, the recovery of tin in recovery-oriented runs increases while waste grades remain consistently low. This result demonstrates stability of sorting performance for Tallebung material. The key factor for the technical feasibility of the Tallebung material is its unique mineralogical property in XRT sensing. The sensitivity of tin product particles in XRT sensing depends on the grain size and liberation characteristics of cassiterite in the host rocks. In sedimentary environments like Tallebung, the contrast between cassiterite-bearing particles and barren gangue is very pronounced, leading to high detectability and sorting efficiency. As a result, XRT-based sorting can selectively upgrade cassiterite ores like Tallebung at coarse particle sizes, reducing downstream processing costs while maintaining high tin recovery with remarkable efficiency.

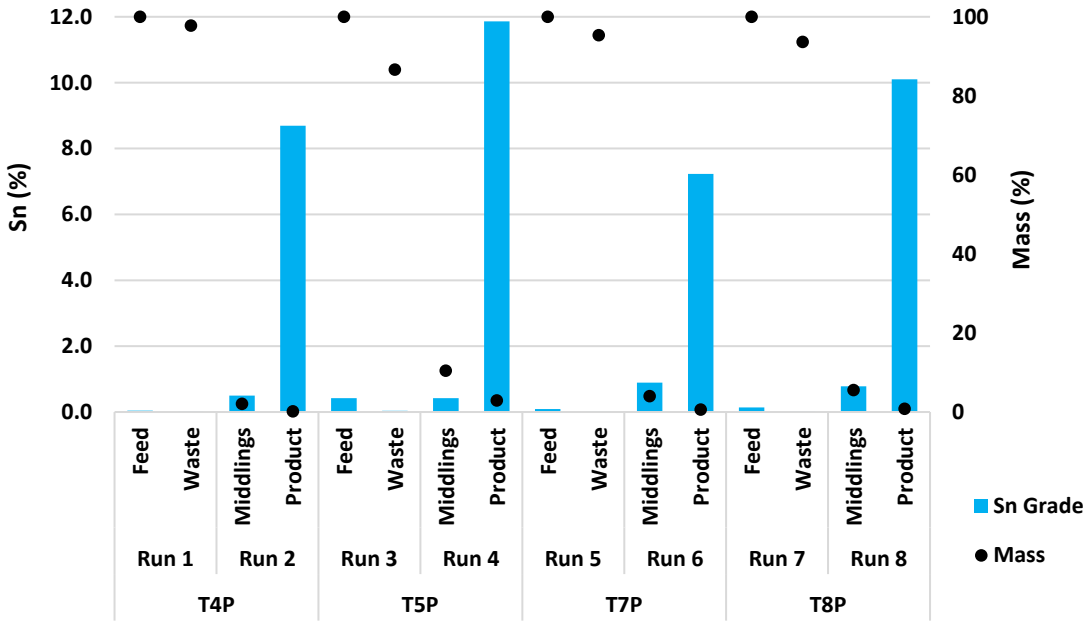
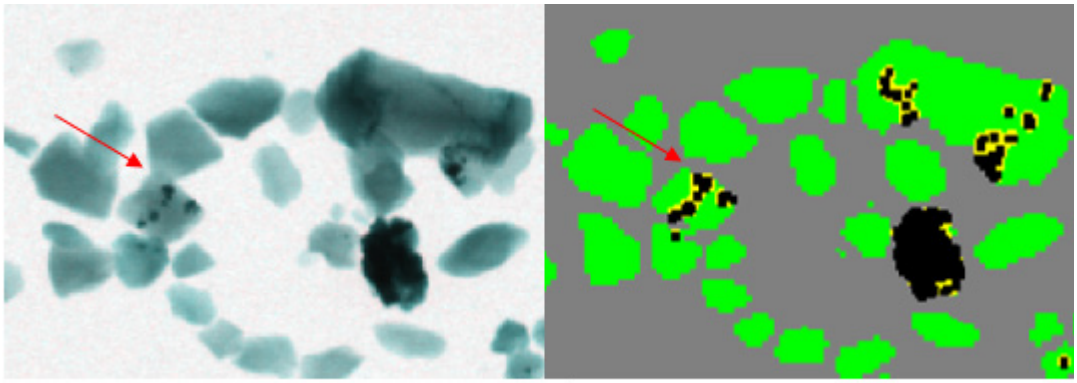



**FIG 4** – The performance of sorting in relation to deposit minerology (detailed data is available in Appendix: Table 1.)

### Stage 2 – Effect of TOMRA deep learning tool OBTAIN™

At high throughput rates, the belt occupancy of feed material increases; this measure of belt occupancy defines sorter throughput capacity. When particles cluster on the belt, a 2D detection system can have difficulties identifying, defining, and therefore ejecting product particles while ignoring waste particles. The latest TOMRA deep learning tool OBTAIN™ is designed to segment

or singulate clusters of particles by identifying and amplifying the border between individual particles through analysing the texture and shape of the cluster based on a deep-learning algorithm. Particularly effective when running high throughput rates, OBTAIN™ increases ejection resolution, decreased dilution, and improved product grades. One of the goals of the test work is to determine the effectiveness of OBTAIN™ on Tallebung material. The program uses a type of processing which identifies individual objects and ejects the area when this object meets criteria (eg % of particle containing tin). Figure 5 shows the difference of classified particles presented to the sorter at relatively high belt occupancy during Run 9 and Run 11. In Run 9 with OBTAIN™ function on, the classified images show a clear gap between previously touching particles, which allows enough room for particles to be singulated and ejected individually. In Run 11, the clustered area is defined as a whole which firstly reduces the chance to meet the ejection criteria and potentially be under-classified resulting in grade loss or secondly may over-eject all clustered waste particles if the whole area meets the criteria for ejection.



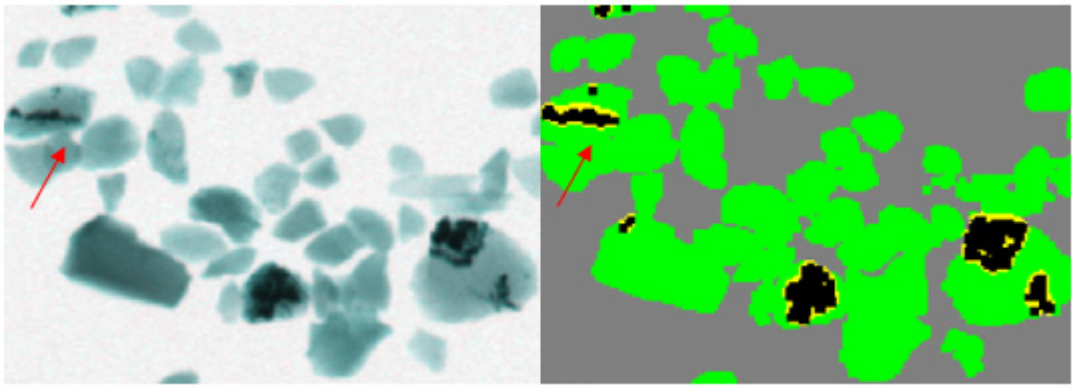




**FIG 5** – The raw and classified image of the clustered feed in Run 9 with OBTAIN™ and in Run 11 without OBTAIN™. Colour code of classified image: green = host rock, black = cassiterite inclusions.

Figure 6 shows the results from the two sets of tests using the same feed material and sorting program with and without OBTAIN™. The program for the recovery runs (Run 9 and Run 11) used in stage 2 was modified to achieve higher recovery while the program for second runs (Run 10 and Run 12) remained the same as in the first stage of test work. As a result, the tin recovery of the stage 2 recovery runs (Run 9 and Run 11) increased to 97 per cent. Although the first runs achieved similar recoveries in both tests, the test run using OBTAIN™ demonstrated a greater mass reduction and higher-grade concentrate. Due to a lower feed mass which results in a reduced occupancy, OBTAIN™ exhibits a different effect in the concentrate runs. The result of Run 10 is consistent with Run 4 which was conducted with the same conditions while Run 12 achieved similar product grade and higher mass reduction mainly as a result of two factors: (1) The higher throughput rate of the recovery runs allows OBTAIN™ to affect the sorting results to a higher degree; and (2) when OBTAIN™ is not implemented, the increase of over-ejected waste into the feed of the concentrate run means that the mass of the middlings will increase.

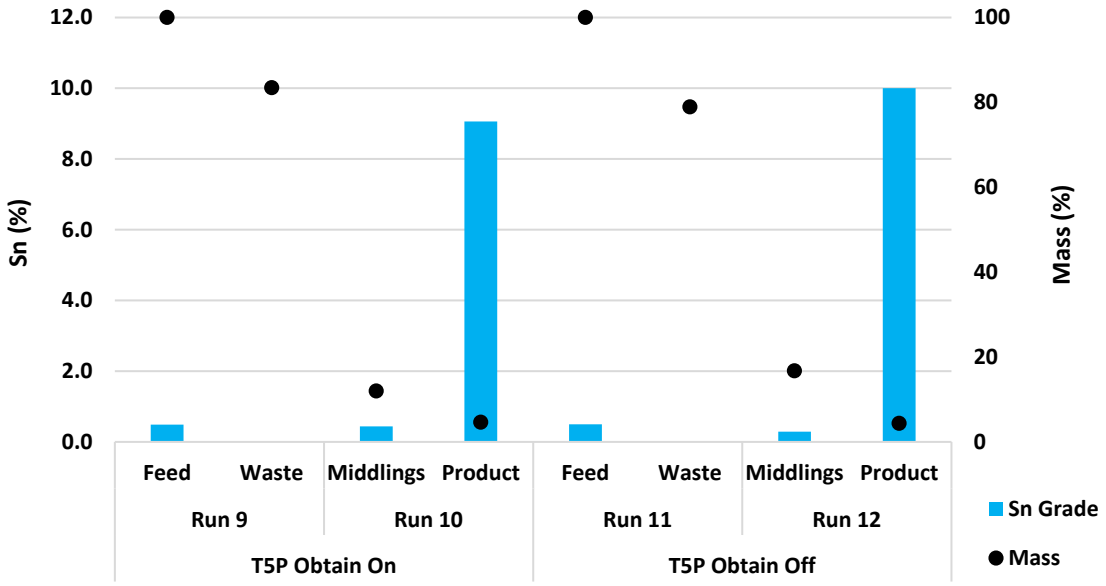



**FIG 6** – The effect of OBTAIN™ in sorting efficiency for high-grade deposit (detailed data is available in Appendix: Table 2).

Ore sorting with TOMRA sensor-based ore sorters has demonstrated strong technical and economic viability through all testing in the Tallebung Tin Project. The feed grade has been substantially improved by waste ejection which creates a very high-grade product. This helps reduce the cut-off grade of the mining process which helps unlock mine potential. The sorting process produces saleable tin product and increases middlings grade to downstream with increased processing potential for the beneficiation plant. The implementation of sorting also achieved an extremely high recovery. Minimising grade loss upfront is very important in minimising product loss throughout the beneficiation process, and the reduction in material volume at coarser size greatly reduces cost for transportation, comminution, and concentration. The waste rejection at the mining face is an economically viable option in the case of a central plant downstream with satellite mining operations and low haulage cost as a result of significantly reduced mass (Robben *et al*, 2020). The reduction in material mass leads to decreased energy and water consumption, while the reduction in plant footprint results in lower capital and operating expenditures.

Tin at Tallebung is in a mineral called cassiterite and forms large ‘nuggets’ which makes it exceptionally easy and economical to process as well as presenting many environmental benefits. The ore sorting test results demonstrate technical viability by showing that a significant proportion of low-grade or barren material can be rejected ahead of downstream processing while maintaining strong cassiterite recovery. This has the potential to reduce the mass reporting to grinding and gravity concentration, with associated benefits to downstream plant capacity, water demand, reagent consumption and operating cost. The detailed economic impact is being assessed as part of the PFS.

## REFERENCES

Department of Regional NSW, 2021. Tin and Tunsten. Available from: <https://www.resources.nsw.gov.au/sites/default/files/2022-11/tin-tungsten.pdf>

Firsching, M, Spencer, R and Leisner, J, nd. A Feasibility Study on the Detectability of Various Minerals Using Dual-Energy X-ray Imaging in XRT Sorting, Enhancing Mineral Processing Efficiency. Available from: <https://www.min-eng.com/processmineralogy24/drafts/posters/firsching.pdf>

Mamuse, A and Guj, P, 2013. The Geological Survey of New South Wales Division of Resources and Energy New South Wales Trade and Investment Maitland, NSW, 2320. Curtin University Centre for Exploration Targeting, Department of Mineral and Energy Economics, Perth: Department of Mineral and Energy Economics.

Robben, C and Wotruba, H, 2019. Sensor-Based Ore Sorting Technology in Mining – Past, Present and Future, *Minerals,* 9(9):523.

Robben, C, Condori, P, Pinto, A, Machaca, R and Takala, A, 2020. X-ray-transmission based ore sorting at the San Rafael tin mine, *Minerals Engineering*, 145:105870.

# APPENDIX

**TABLE 1**

The performance of sorting in relation to deposit minerology.

| Orebody | Test | Fraction | Sn | | | Mass | | |
|---|---|---|---|---|---|---|---|---|
| | | | % | Recovery | Cumulative recovery | kg | % | Cumulative product |
| T4P Obtain On | Run 1 | Feed | 0.04 | | | 8826.1 | 100% | |
| | | Product | 1.11* | 63% | 63% | 195.5 | 2% | 2.2% |
| | | Waste | 0.02 | | | 8630.6 | 98% | |
| | Run 2 | Feed | 1.11 | | | 195.5 | 100% | |
| | | Product | 8.69 | 58% | 37% | 14.6 | 7% | 0.2% |
| | | Waste | 0.50 | | | 180.9 | 93% | |
| T5P Obtain On | Run 3 | Feed | 0.42 | | | 8603.9 | 100% | |
| | | Product | 2.93* | 93% | 93% | 1150.5 | 13% | 13.4% |
| | | Waste | 0.04 | | | 7453.4 | 87% | |
| | Run 4 | Feed | 2.93 | | | 1150.5 | 100% | |
| | | Product | 11.86 | 89% | 82% | 252.0 | 22% | 2.9% |
| | | Waste | 0.42 | | | 898.5 | 78% | |
| T7P Obtain On | Run 5 | Feed | 0.09 | | | 7736 | 100% | |
| | | Product | 1.74* | 89% | 89% | 359.0 | 5% | 4.6% |
| | | Waste | 0.01 | | | 7377.0 | 95% | |
| | Run 6 | Feed | 1.74 | | | 359.0 | 100% | |
| | | Product | 7.23 | 56% | 50% | 48.0 | 13% | 0.6% |
| | | Waste | 0.89 | | | 311.0 | 87% | |
| T8P Obtain on | Run 7 | Feed | 0.14 | | | 12571.2 | 100% | |
| | | Product | 1.95* | 90% | 90% | 799.4 | 6% | 6.4% |
| | | Waste | 0.02 | | | 11771.8 | 94% | |
| | Run 8 | Feed | 1.95 | | | 799.4 | 100% | |
| | | Product | 10.10 | 65% | 58% | 100.0 | 13% | 0.8% |
| | | Waste | 0.78 | | | 699.4 | 87% | |

* The value of product fraction of recovery-oriented runs has been back-calculated from concentrate run assays.

**TABLE 2**

The effect of OBTAIN™ in sorting efficiency for high-grade deposit.

| Orebody | Test | Fraction | Sn | | | Mass | | |
|---|---|---|---|---|---|---|---|---|
| | | | % | Recovery | Cumulative recovery | kg | % | Cumulative product |
| T5P Obtain On | Run 1 | Feed | 0.49 | | | 251.7 | 100% | |
| | | Product | 2.84* | 97% | 97% | 41.7 | 17% | 17% |
| | | Waste | 0.02 | | | 210.0 | 83% | |
| | Run 2 | Feed | 2.84 | | | 41.7 | 100% | |
| | | Product | 9.06 | 89% | 86% | 11.6 | 28% | 5% |
| | | Waste | 0.44 | | | 30.1 | 72% | |
| T5P Obtain Off | Run 3 | Feed | 0.50 | | | 322.3 | 100% | |
| | | Product | 2.29* | 97% | 97% | 67.9 | 21% | 21% |
| | | Waste | 0.02 | | | 254.4 | 79% | |
| | Run 4 | Feed | 2.29 | | | 67.9 | 100% | |
| | | Product | 10.00 | 90% | 87% | 14.0 | 21% | 4% |
| | | Waste | 0.29 | | | 53.9 | 79% | |

* The value of product fraction of recovery-oriented runs has been back-calculated from concentrate run assays.

# Mill Operators

# Flotation

# The application of guar gum as a talc depressant, improving copper concentrate grades in the Deflector gold-copper flotation circuit, Vault Minerals, Western Australia

*G D Figueroa Salguero[1], C Wong[2], M Khowira[3], M Whitford[4], C Bannon[5], T St John[6] and R Hanna[7]*

1. Senior Plant Metallurgist, Vault Minerals, Perth WA 6000. Email: gfigueroasalguero@vaultminerals.com
2. Metallurgy Superintendent, Vault Minerals, Perth WA 6000. Email: cwong@vaultminerals.com
3. Plant Metallurgist, Vault Minerals, Perth WA 6000. Email: mkhowira@vaultminerals.com
4. Plant Metallurgist, Vault Minerals, Perth WA 6000. Email: mwhitford@vaultminerals.com
5. Plant Metallurgist, Vault Minerals, Perth WA 6000. Email: cbannon@vaultminerals.com
6. Graduate Metallurgist, Vault Minerals, Perth WA 6000. Email: tstjohn@vaultminerals.com
7. Processing Manager, Vault Minerals, Perth WA 6000. Email: rhanna@vaultminerals.com

## ABSTRACT

At the Deflector Gold-Copper Project, ore is extracted from three underground mines and hauled to the Run-of-Mine (ROM) pad before being blended and processed in the concentrator plant to produce gold doré and a copper/gold concentrate. As the central, high-grade areas within the Deflector orebodies deplete, it has been necessary for the mining front to progress outwards. The western extent of the orebody is bound by an ultramafic unit which is high in talc. This talc rich ore negatively effects the produced copper concentrate via the additional free-floating gangue material present.

To address this issue, Deflector metallurgists initially modified the flotation circuit to include a pre-flotation stage to remove the talc. However, this modification was limited to treating moderate talc blends, while periodic high-talc events lead to excessive talc contamination of the final concentrate. Several reagents were assessed via batch flotation, with guar gum emerging as the most promising candidate for talc depression. This product was selected after the evaluation of an extensive laboratory-scale reagent screening test work involving cost benefit analysis, copper increments, and safety characteristics.

Guar gum is a biodegradable product primarily used in the food industry and used as a talc-depressant in the mining industry. However, despite the potential benefits, documentation on guar gum application in concentrator plants remains limited. This is likely due to challenges in handling the product, including clumping that severely affects solution quality.

Recognising this challenge, metallurgists at Deflector, retrofitted guar addition via an unused NaHS mixing plant and dosing system to conduct diagnostic and t-test plant trials to validate laboratory scale results. The plant trial reported an improvement of at least 3 per cent copper in the concentrate without affecting recoveries. Although promising, this was lower than the expected performance based on the laboratory scale test work. This discrepancy was principally attributed to critical challenges affecting the quality of the guar solution, limitations in the selected infrastructure, housekeeping, and consistent manual handling operation.

A capex project was then approved to improve the quality of the mixing solution which included the installation of a suitable shear pump for guar mixing, upgrades of dosing pumps, enhanced stirring capacity and modified pipe work. This document outlines the plant performance improvements to date, with emphasis on the guar solution, retrofitting period, and post shear pump installation plant performance.

## INTRODUCTION

The Deflector Gold Copper Mine is located approximately 450 km north of Perth and 160 km east of Geraldton, within the Midwest region of Western Australia. Ore is sourced from the Deflector and Rothsay satellite gold and copper underground mines, typically processing feed grades of 2–5 g/t Au and less than 0.1 per cent Cu. The orebody is hosted within basaltic rocks of mafic and ultramafic composition, the latter containing higher concentrations of talc.

The ore is hauled to the Run-of-mine (ROM) and stored as finger stockpiles to manage feed grade and talc content into the processing circuit. The processing plant comprises of a three-stage crushing circuit, a single ball mill comminution circuit, a gravity circuit for gold recovery, a flotation circuit to produce a copper/gold concentrate, with flotation tails processed through a regrind mill, leaching, carbon-in-pulp (CIP) and electrowinning to produce gold doré. The processing plant operates at a throughput of around 95 t/h. For the FY26 to date (March quarter 2026), processing production comprised 593 872 t of ore milled, total gold production 58 549 ounces, and 248 t of contained copper metal in concentrate (Vault Minerals Report, 2026).

Production at the Deflector Mine commenced in 2016 (Kiddle, 2020). Historically, ore extraction has been dominated by mineralisation hosted within competent basalt units. As mining has progressed westward, the orebody has become increasingly hosted within talc-rich ultramafic lithologies. Due to the variable contact between the basalt and ultramafic host rocks, geologists use drill core logging, face mapping, and assay data to model the boundary between these lithological domains, Michael Charlesworth (July 2026, personal communication). Ore hosted within ultramafic units is segregated on the ROM and incorporated into the processing plant feed at a controlled proportion within the mill blend.

To maintain the requisite quality of the copper concentrate, ongoing improvement strategies to minimise the negative effects of talc contamination are required. Talc is a common magnesium-silicate gangue mineral containing a hydrophobic surface, allowing it to float readily (Farrokhpay, Ndlovu and Bradshaw, 2018; Ge *et al,* 2025). The flotation separation of copper minerals such as chalcopyrite ($CuFeS_2$) from talc presents a significant challenge requiring depressants (Lei *et al,* 2025).

Prior to mining of the ultramafic ore zone, the Deflector concentrator had processed ore with low levels of talc. However, this was intermittent and had negligible impact on overall concentrate copper grade. After 2024, with the increase of ultramafic (talc) proportion in the blend, concentrate grades have been declining considerably, requiring the need of prompt attention and mitigation (Figure 1).

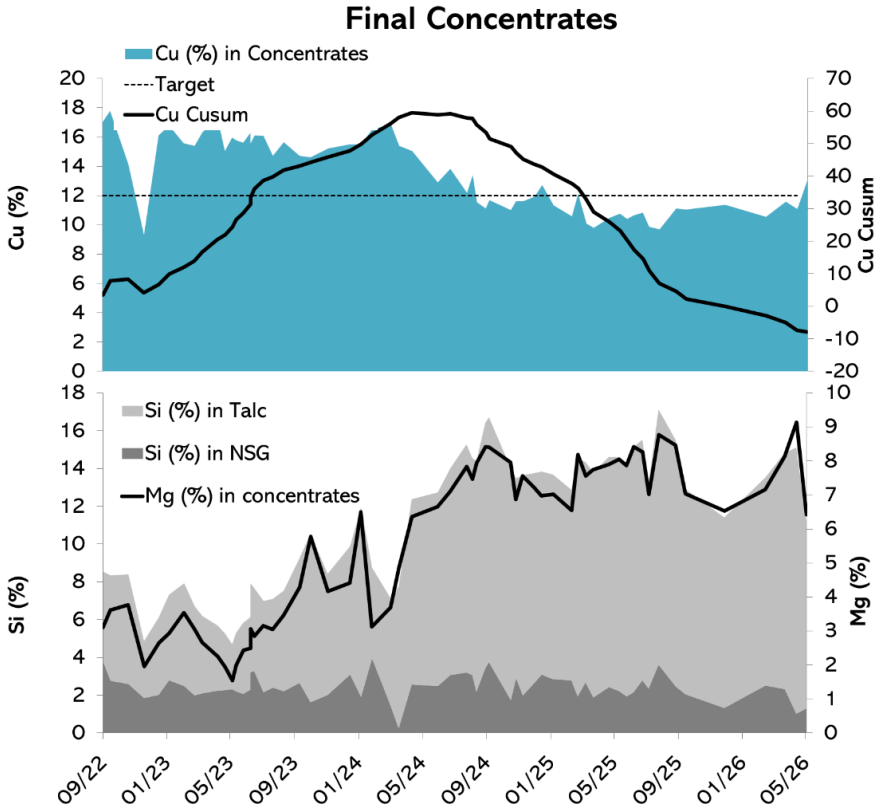



**FIG 1** – Copper concentrate decline as a function of talc content, identified using CUSUM approach (upper); and the corresponding increase in magnesium aligned with the increase in talc, as determined from silica molar calculations of final concentrates delivered since 2022 (Wong, 2026).

As shown in Figure 1 (upper plot), the cumulated sum of residuals for the copper grade (CUSUM) increased steadily, reaching a peak before declining, and stabilised towards the end of 2024. This upward trend reflects the relatively consistent copper grade produced during that period. However, following the introduction of talc in March 2024, a gradual decline in copper grade below the 12 per cent copper target is observed through to September 2025 (Figure 1 top).

The talc levels were quantified through elemental-to-mineral conversion using molar calculations based on total silica in the concentrate. This molar approach enabled the separation of silica associated with talc from silica associated with non-sulfide gangue (NSG). As shown in the lower plot, the silica from NSG remained essentially constant, whereas silica attributed to talc increased. This trend aligns with the rise of magnesium (%) in the concentrate, indicated by the dotted line beginning in March 2024 (Figure 1, bottom).

## PROCESSING STRATEGIES

Deflector is currently implementing different strategies to minimise talc contamination as talc is present in nearly all Deflector's ore sources, three main processing strategies have been implemented since 2025:

1. Ore sorting through systematic blending strategies.
2. Pre-flotation.
3. Talc depression using guar gum.

This paper focuses on recent advances in the talc depression project using guar gum within the flotation circuit.

### Ore sorting and blending strategies

Ore sorting and blending strategies are conducted in accordance with grade budget requirements. Ore sorting primarily involves categorising ore hauled from underground. Mine geologists distinguish between ultramafic and non-ultramafic material, with the former typically containing high talc concentrations. Once delivered to the ROM, the ore is allocated into designated finger stockpiles (eg Finger A, B, C etc) to facilitate controlled blending into the processing circuit.

Fingers A, B, C, D, E, and F contain the highest gold and copper grades (typically >2 to Au 8 g/t) and exhibit lower talc content. In contrast, Fingers G, LG (low-grade) and Y represent the lowest grade material (<1 g/t of Au, and 0.04 per cent Cu), and contain higher levels of talc, and are the most abundant stockpile on the ROM. There is also aged G-Off ROM (with talc) material with which started haulage and processing in 2026.

After ore sorting from underground, metallurgists define the blending strategies that operators follow when feeding the primary jaw crusher. This blend must achieve suitable gold and copper grades while maintaining acceptable talc content. Loader operators at the ROM scoop the required number of buckets from each selected finger stockpile to create the specified blend.

Table 1 presents actual blending options used by operators, where the numbers represent the number of bucket loads taken from each finger. The 'Notes' column indicates the relative proportion of Rothsay (RTH) material (typically crushing above 40 per cent in the blend) and talc proportions from ultramafic ores, in this case from Y and X fingers.

**TABLE 1**

Blending strategies prepared by metallurgists for processing in the circuit.

| Blend buckets to the crusher system | | | | | | | | | | | | |
|---|---|---|---|---|---|---|---|---|---|---|---|---|
| ROM Blend | A | B | C | D | E | F | G | LG | Y | X | GET | Notes |
| Blend 1 | 4 | | | 4 | | | | | | 0.5 | | 47% RTH, 6% Talc |
| Blend 2 | 4 | | | 4 | | | | | 0.5 | 0.5 | | 44% RTH, 11% Talc |
| Blend 3 | 4 | | | 4 | | | | | 1 | 0.5 | | 42% RTH, 16% Talc |
| Blend 4 | 4 | 2 | | 3 | | | | | 3 | 1 | | 46% RTH, 31% Talc |
| Blend 5 | 4 | 4 | | 2 | | | | | 3 | 3 | | 50% RTH, 38% Talc |

Depending on the blend selected, pre-flotation and talc depressants will be employed to improve copper floatability. At this stage, talc in the flotation circuit is visually observed (and overflowing) eg conditioning tanks, launders and sump pumps, a pre-flotation mode can be enabled to physically reject talc to final tailings.

## Pre-flotation of talc

In a standard circuit configuration, concentrate from rougher bank 1 (Ro 1) reports to the sump floor pump via the Metso Online Stream Analyser 5x (OSA) and to the final concentrate. Concentrates from roughers' 2, 3 and 4 (Ro 2, Ro 3, Ro 4, respectively) report to the mid-grade sump pump to form the mid-grade concentrate (MGC), which is also directed to the cleaner 1. The concentrate produced by the cleaners (Cl 1 and/or Cl 2) constitutes the final concentrate (FC). The rougher tails form the final tailings (FT) which are directed to the leach and CIP circuit for gold recovery. The cleaner tails are typically returned to rougher 3.

The OSA provides online stream analyses (%) of Cu, Fe, Mg, and Solids. Monitored streams include rougher 1 concentrate, flotation feed, mid-grade, final tails, and final concentrate (Figure 2). There are two OSA models for the final concentrate, one with magnesium and another one without magnesium as a guide for Operators to operate the plant when talc (Mg) is present. In addition, Potassium Amyl Xanthate (PAX), CMS41 promoter, and IF6801B frother are typical reagents dosed at controlled rates to optimise chalcopyrite recovery (copper bearing mineral in the Deflector ore). The pH in the flotation feed is also monitored which is about 7.3 to 7.5. The $P_{80}$ from the cyclone overflow (COF) in the grinding circuit to flotation is relatively coarse ranging from 150 to 180 µm.

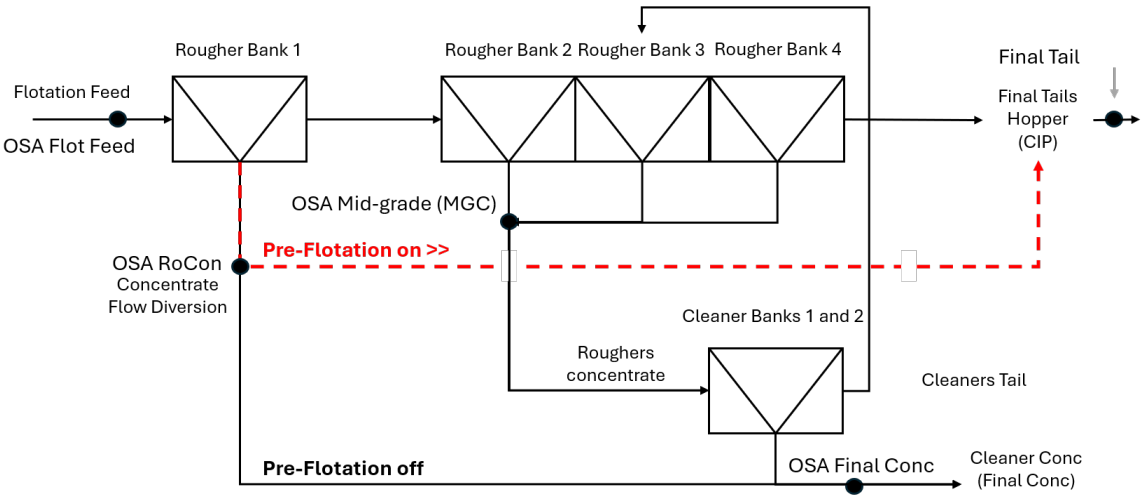



**FIG 2** – Typical flotation flow sheet including pre-flotation.

The infrastructure required for a 'pre-flotation' step was completed in late June 2024, enabling the diversion of rougher bank 1 concentrate to final flotation tailings. This approach is widely applied in operations that reject talc minerals to prevent contamination of downstream concentrates (Young

*et al,* 2006). The rougher bank 1 concentrate is directed to the rougher 4 tails hopper and ultimately to final flotation tailings to recover residual gold via cyanide leaching and CIP. Pulp levels, air, and reagents settings are adjusted specifically to float talc while avoiding copper recovery. The performance of pre-flotation is monitored through the OSA final concentrate with readings <1 per cent Cu indicating that acceptable copper losses are being sent to tailings.

Figure 2 illustrates both circuit configurations, with the dotted line indicating pre-flotation is engaged or bypassed (on/off).

Figure 3 a shows rougher 1 operating in pre-flotation mode and approaching its limits in both talc rejection and pumping capacity of floor-sump pumps (Figure 3b). Under these conditions, the final concentrate stream may fall to below <1 per cent Cu.




**FIG 3** – (a) Typical talc rejection into the launder when operating rougher 1 as pre-flotation mode; and (b) floor housekeeping associated to high talc in the circuit.

## TALC DEPRESSION PROJECT

Talc is a common magnesium phyllosilicate gangue mineral ($Mg_2Si_4O_{10}(OH)_2$) present in many copper orebodies. Its hydrophobic nature means that it floats readily (Wills and Finch, 2015; Bazar *et al,* 2021) and may cause dilution of concentrates (Young *et al,* 2006). To overcome this problem, talc is either depressed through chemical reagents or removed from the flotation circuit via pre-flotation. Talc depression is typically preferred over pre-flotation due to the inevitable copper losses associated with talc removal, as copper may be entrained in the pre-flotation concentrates (Young *et al,* 2006; Garcia and Pawlik, 2015).

As Deflector ore availability necessitated a higher proportion of ultramafic ore in the mill blend, pre-flotation alone became an insufficient control measure. To improve the recovery of copper in the circuit while maintaining concentrate copper grades, talc depression became an area of priority. The steps leading to the implantation of this are briefly described further:

- **Reagent screening:** Several talc-depressant reagents were evaluated to determine their effectiveness in improving copper concentrate grades. Most of the reagents reported significant improvements in concentrate grades without affecting recoveries.
- **Cost analysis:** From the screening tests, the most effective reagents were evaluated based on copper grade/recovery performance, costs-benefit analysis, and reagent preparation characteristics. Guar gum was found to be the most suitable option for further investigation in the plant.

- **Mixing system:** An unused NaHS mixing plant was repurposed to prepare guar gum solution for dosing in the flotation circuit to conduct statistical trials. During this trial stage, the future design of the long-term dosing system was considered.
- **Plant trial:** An on/off plant trial was successfully completed using the adapted NaHS system, demonstrating an improvement of approximately 3 per cent copper grade in the final concentrate when using guar gum and pre-flotation together. This data was used for a second review of the cost analysis.
- **Capex:** Based on the plant trial and cost analysis results, budget was submitted to management to improve the guar mixing system and improve the concentration and efficiency of guar solutions (eg guar clumping). Critical components included a shear pump, dosing pumps, a higher-capacity stirrer (for improved guar mixing), flow metre, and piping upgrades.
- **Engineering:** An engineering firm was engaged to support the installation of the overall infrastructure, alongside the Deflector Maintenance and Electrical teams to execute the required tasks.
- **Preliminary and results to date**: since the installation of the pump and subsequent optimisation of dosing strategies, copper and gold grade improvements have been observed to date. These results are presented at the end of this paper.

## Laboratory screen test work

There are currently several talc depressants available in the market for the selective depression of talc (Garcia and Pawlik, 2015; Mulvihill and Krishnan, 2021; Lei *et al,* 2025). However, literature at industrial scale using such products is scarce and therefore uncertain carrying a degree of operational risk.

A comprehensive study at laboratory scale was conducted by ALS in 2024 (ALS Australia, 2025) screening several talc depressant reagents from different suppliers including Carboxymethyl cellulose (CMC) and guar gum at different concentrations. Wet feed samples were collected from the cyclone overflow and sent to ALS Australia to conduct the trial in 4.4 L batch cells (only two tests were conducted in a 2.2 L) at 30 to 35 per cent solids concentration. The head assay of the feed contained 0.15 per cent Cu, 2.60 g/t Au and 7.6 per cent Mg. Batch flotation tests were undertaken (without replicating the pre-flotation stage) collecting four concentrates over a 22 min laboratory residence time. The reagent scheme used in the plant as used in the laboratory tests. The reagents were dosed in the rougher stage and in the second or third batch concentrate to enhance talc depression.

## Grade-recovery curves varying reagent dosage

Grade-recovery curves for gold and copper are presented below for the selected reagents varying dose rates between Celect HPD (CMC) and guar gum. As can be seen in Figure 4, in all instances, the depressants were able to improve concentrate copper and gold grades while maintaining recovery. Optimum copper grade/recoveries were observed at 350 g/t reagent addition (250 g/t in the first concentrate and 100 g/t in the second concentrate) for both CMC and guar in comparison to the baseline Figure 4a). There is a clear improvement in gold as well (Figure 4b).

When increasing the reagents (>500 g/t) there appears to be a suppression of copper resulting in lower recoveries at respective concentrate grades. On the other hand, using a lower dose rate (230 g/t) was also sub optimal when considering the grade recovery curve for copper.

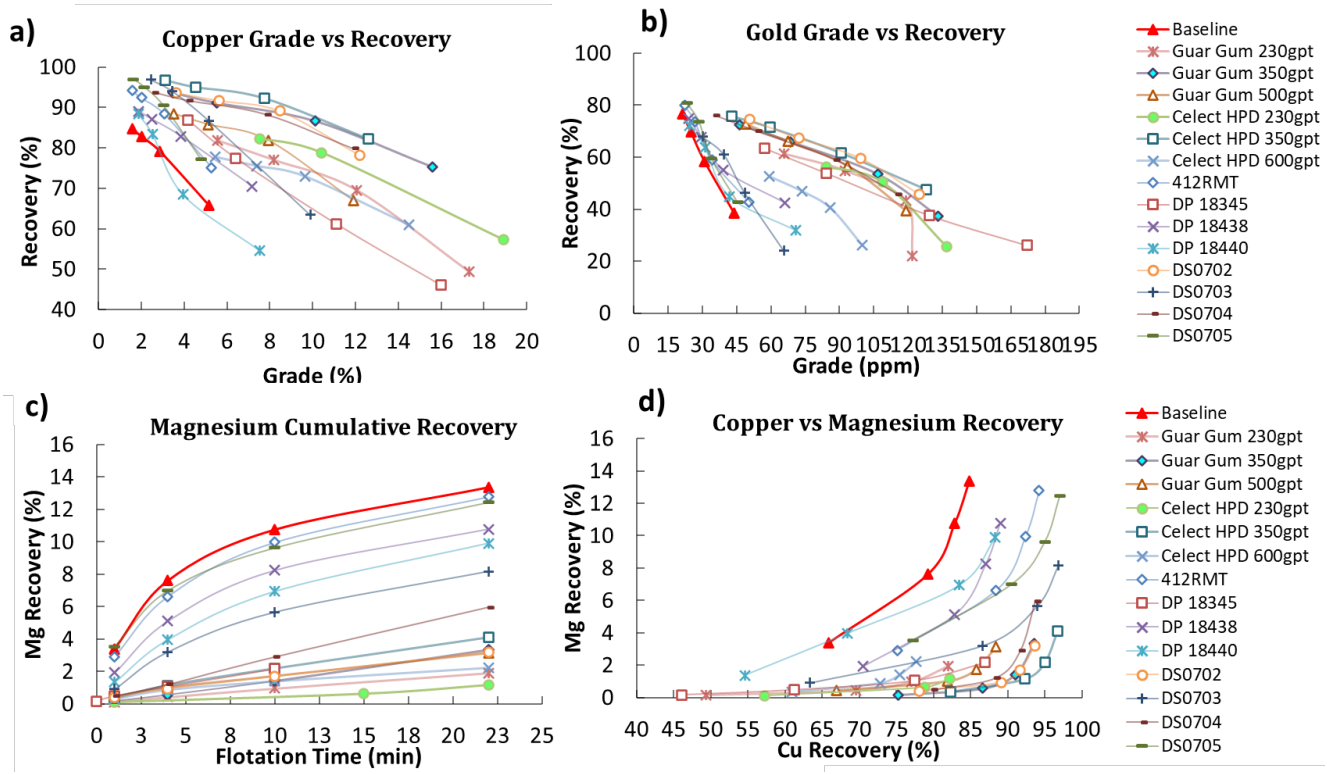



**FIG 4** – Copper, gold grade-recovery curves (a and b), magnesium cumulative recovery-time curves (c), and copper-magnesium selectivity (d).

The time-recovery of magnesium shows a notable increase for the baseline while Celect and guar gum tests show a decrease. Copper and gold grade curves illustrate an increase for most of the tests employing any depressant product. This may be attributed to a lower magnesium recovery due to talc depression. It is evident that when depressant products are present, the magnesium recovery decreases considerable in comparison to the baseline (Figure 4d).

The flotation rate of copper, gold, and magnesium was calculated using a first-order kinetic model for all tests to correlate with changes in flotation recovery. The flotation rate constant ($k$) is a parameter commonly associated with the efficiency of flotation micro-processes (Runge, 2010; Figueroa Salguero, 2019).

Table 2 presents the kinetics for each sample, along with copper and gold recoveries obtained with the different reagents. The addition of guar gum and Celect HPD resulted in an increase in flotation rate at similar concentrations, leading to recoveries of approximately 93 per cent Cu and over 72 per cent Au (Figure 5). Meanwhile, the decrease in magnesium flotation rate (0.06 and 0.08 $min^{-1}$) support the hypothesis of talc depression when such reagents are used.

**TABLE 2**

Flotation rate ($k$) of Deflector feed samples treated with different reagents including guar gum (head grade copper average 0.18 per cent Cu).

| Product ID | Reagent (g/t) | Cu k (min-1) | Au k (min-1) | Mg k (min-1) | 1st Conc - Cu % | Cu Rec inf | Au Rec inf |
|---|---|---|---|---|---|---|---|
| Baseline | 0.0 | 1.5 | 0.7 | 0.21 | 5.1 | 84.8 | 76.8 |
| Guar Gum | 231 | 0.9 | 0.3 | 0.07 | 17.3 | 93.2 | 61.3 |
| **Guar Gum** | **350** | **1.6** | **0.7** | **0.06** | **15.6** | **93.5** | **72.5** |
| Guar Gum | 500 | 1.4 | 0.8 | 0.10 | 11.9 | 93.9 | 72.8 |
| Celect HPD | 230 | 1.2 | 0.6 | 0.19 | 18.9 | 82.2 | 56.4 |
| **Celect HPD** | **350** | **1.9** | **1.0** | **0.08** | **12.6** | **93.7** | **75.9** |
| Celect HPD | 600 | 1.5 | 0.7 | 0.13 | 14.5 | 93.3 | 52.7 |
| 412RMT | 300 | 1.6 | 0.8 | 0.18 | 5.3 | 94.2 | 79.9 |
| DP 18345 | 450 | 0.8 | 0.2 | 0.07 | 16.0 | 87.0 | 62.9 |
| DP 18438 | 750 | 1.0 | 0.8 | 0.16 | 7.2 | 89.0 | 74.8 |
| DP 18440 | 750 | 1.0 | 0.2 | 0.13 | 7.5 | 88.3 | 71.9 |
| DS0702 | 350 | 1.8 | 0.9 | 0.09 | 12.2 | 93.6 | 74.6 |
| DS0703 | 650 | 1.1 | 0.3 | 0.12 | 9.9 | 93.9 | 67.8 |
| DS0704 | 450 | 1.9 | 0.9 | 0.07 | 11.9 | 93.7 | 76.1 |
| DS0705 | 750 | 1.6 | 0.8 | 0.21 | 4.8 | 94.2 | 80.8 |

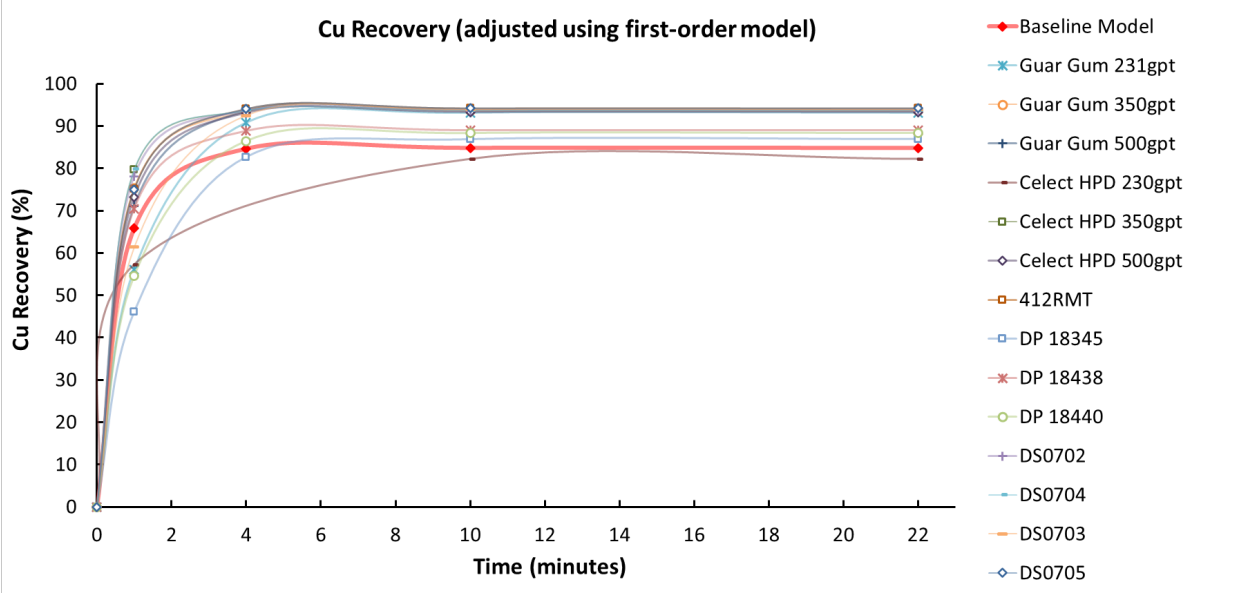



**FIG 5** – Time-recovery curve for all screened reagents, including guar gum. Note Celect HPD 230 g/t concentrates 2 and 3 were combined.

The graph presents adjusted time-recovery curves for all screened tests. Celect HPD and guar gum at 350 g/t exhibited the highest concentrate grades (>12 per cent) and adjusted recoveries of approximately 93 per cent (Figure 5).

As all products demonstrated improved performance, it was necessary to conduct a cost analysis to determine the reagent cost per tonne of saleable copper. Alongside this, a risk assessment was required to assess chemical handling and safety considerations. This evaluation supports a final decision on product selection. Guar gum and Celect HPD (a CMC-based product) were selected to be assessed in greater detail.

## GUAR EMPLOYED IN THE CONCENTRATOR PLANT

### Cost analysis

The utilisation of a talc depressant represented a significant reagent cost; therefore, an economic analysis was conducted for the assessed products and is summarised in Table 3. Using budgeted recovery (~60 per cent), milled tonnes (~765 000 t per annum), copper head grade (~0.13 per cent

and financial-related assumptions, the annual revenue was estimated for the best-performing reagents considered (guar gum and Celect).

**TABLE 3**

Guar gum yield best financial return.

| Laboratory Screening | Baseline | Guar Gum | | Celect HPD | |
|---|---|---|---|---|---|
| | 0 g/t | 350 g/t | 230 g/t | 350 g/t | 230 g/t |
| Copper Revenue | | | | | |
| Lab Rougher 1 Concentrate (%) | 5.14 | 15.6 | 17.3 | 12.6 | 18.9 |
| Lab Cum Cu Recovery (%) | 84.8 | 93.54 | 81.94 | 96.75 | 82.2 |
| 6+6 Budget Copper Feed (%) | 0.13% | 0.13% | 0.13% | 0.13% | 0.13% |
| 6+6 Budget Copper Recovered (t) | | 613 | 494 | 646 | 497 |
| Annual Saleable Cu Value (A$) | | 7,569,716 | 6,195,847 | 7,802,269 | 6,336,772 |
| Logistic Cost | | | | | |
| Cu Conc Produced (t/a) | | 3,930 | 2,857 | 5,127 | 2,629 |
| Annual Cost of Logistics (A$) | | 1,347,117 | 979,347 | 1,757,131 | 900,900 |
| Gold Revenue | | | | | |
| Lab Cum Au Recovery (%) | 76.8 | 72.5 | 61.3 | 75.9 | 56.4 |
| Annual Saleable Au Value (A$) | | 87,372,301 | 87,489,877 | 87,282,185 | 87,482,110 |
| Smelter Costs | | | | | |
| Annual Smelter Costs (A$) | | 352,032 | 253,594 | 438,116 | 247,152 |
| Total Revenue | | | | | |
| Annual Revenue (A$) | | **93,219,686** | 92,482,067 | 92,487,964 | 92,325,650 |

Based on the pricing and cost data supplied, guar gum demonstrated the best financial return when compared with Celect HPD (CMC) (Table 3).

The metallurgical performance and cost of guar (Tables 2 and 3), with consideration also given to the associated low material handling risk, meant that guar gum was selected as the most suitable talc depressant to progress to a plant trial at Deflector (Wong, Whitford and Bannon, 2025).

## Mixing system

In order to conduct plant trials, an unused NaHS mixing and storage tank system was customised to prepare guar solution and addition (Figure 6). The NaHS system consists of ~9000 L mixing tank, and an 18 900 L storage tank, and dosing and transfer pumps located at ground level. The system was retrofitted to accept guar by installing diaphragm pumps and discharge hoses to transfer the prepared guar solution to the rougher 2 conditioning tank via the flotation sump pump. The Citect interface was also updated to include guar-related tagging.

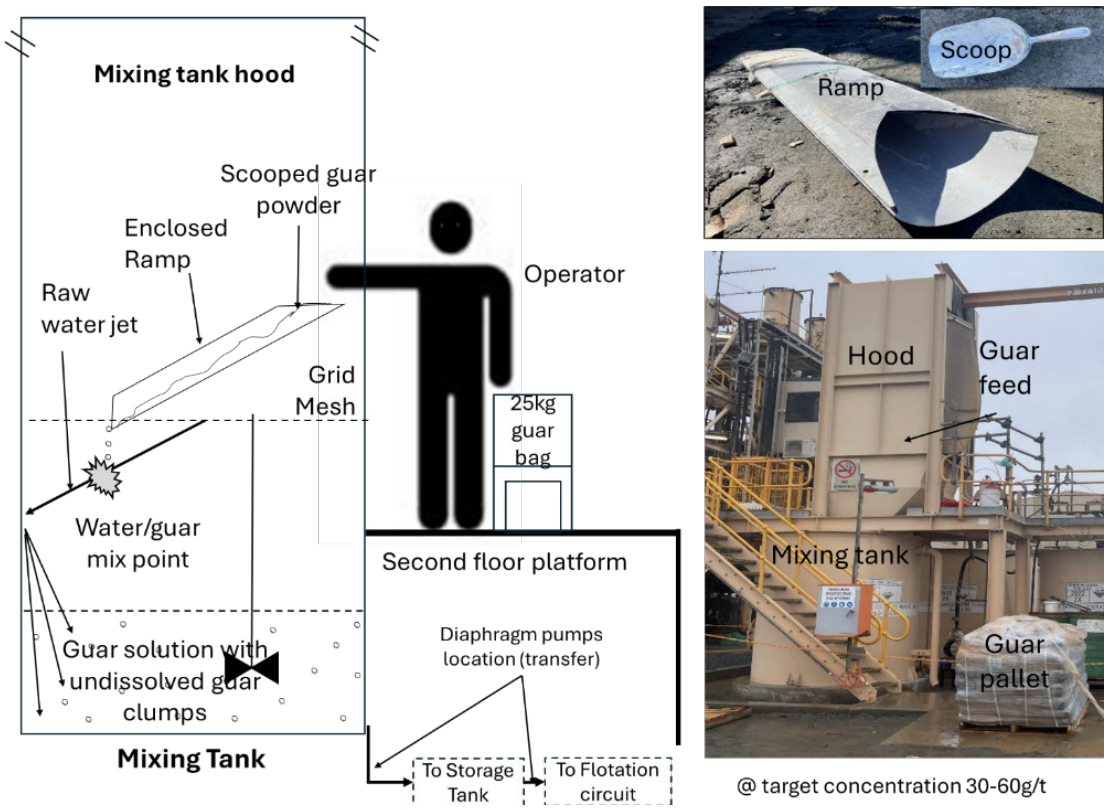



**FIG 6** – Customised NaHS mixing system adapted for guar preparation.

### *Guar mixing procedure*

The procedure for preparing guar mixes involves adding a 25 kg bag of guar powder into the mixing tank while it is filling with water to 80 per cent of its 9000 L capacity. The bag is opened manually, and the powder is poured onto an inclined enclosed ramp using a scoop. The falling guar then intersects the feed-water jet creating rapid shearing and dispersion that initiate solution formation. However, during this process not all powder is dissolved, some particles fall directly into the tank and rapidly form guar clumps ‘jelly fishes’. A mechanical stirrer remains in continuous operation to keep the guar suspended and to enhance mixing efficiency.

The water jet automatically shuts off at 80 per cent of the tank capacity, controlled by a level sensor. The guar solution is then agitated for approximately one hr before being transferred to the storage tank via diaphragm pump. A second diaphragm pump, fitted with a discharge hose, is used to deliver the guar solution to the rougher 2 conditioning tank, downstream of pre-flotation (rougher 1).

### *Guar concentrations*

The concentration of the guar solution was inferred using a Marsh funnel measurement process (Taliesin, 2025). Typically, a one litre sample of guar solution is collected and then timed (in seconds) as it flows through the Marsh funnel. This time is reference to a predefined standard curve developed from laboratory test work to estimate guar strength per cent (w/w) (Figure 7). As shown in the plot, guar concentrations greater than 0.6 per cent (w/w) are difficult to prepare due to substantial increase in viscosity (guar gum is 5000 cp).

In practice, batches prepared using one bag per mix (approximately 25 kg in 80 per cent of 9000 L), have produced concentration ranging from 0.3 to 0.5 per cent (w/w). The variability of the concentration can be attributed to several uncontrolled factors, including inaccurate tank level readings, human error during transfers, limited stirrer capacity, liquid segregation, guar clumping, and others. These issues have been progressively improved over time as the system and procedures were refined.

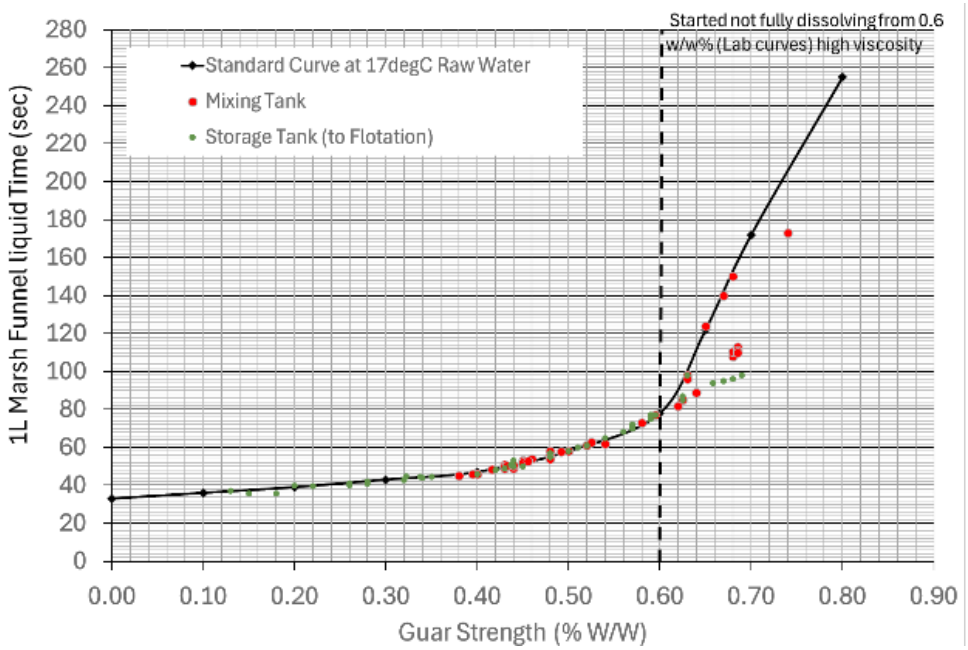



**FIG 7** – Plant guar concentrations relative to laboratory testing conditions, including records of measurements from the mixing and storage tank.

During the plant trial, and in the absence of a flow metre, the flow rate of the guar solution was measured at the discharge point by timing how long it takes to fill a 20 L bucket. Once the flow rate is known, the dry tonnes per hour (t/h) – calculated from the milled wet t/h after accounting for scats percentage and moisture content (eg 95 wet t/h at 15 per cent scats and 1 per cent moisture yields 80 dry t/h) is used to determine the guar dosage in grams per tonne milled.

The guar flow rate required is determined by the amount of talc visually observed in the circuit, which depends on the selected blend and the capacity of pre-flotation. Since the mixing system was retrofitted, guar dosages have typically ranged from 40 to 90 g/t.

The lower dosages, compared with laboratory flotation tests, are largely due to the pre-flotation stage rejecting a high proportion of talc, whereas the laboratory work did not replicate pre-flotation.

Despite the success of the plant trial, the manual mixing and dosing set-up was not without issue. Both the manual mixing/dosing process and the clearing of clumps being formed were considerable time burdens for the operations team (Figure 8).

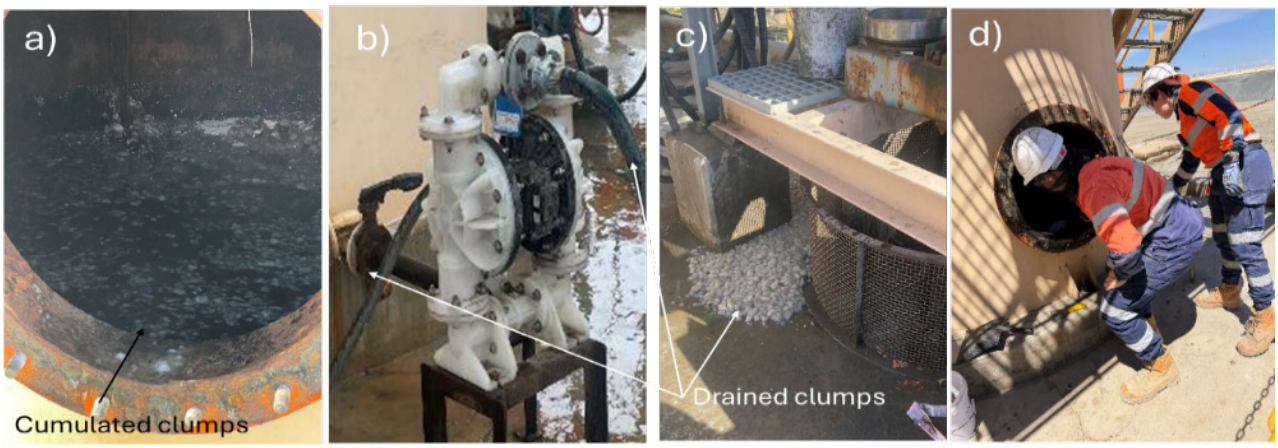



**FIG 8** – Guar-related issues in the mixing tank: (a) clumps trapped inside the tank, (b) and (c) clumps drained from spools/hoses to prevent blockages, (d) metallurgist preparing the mixing tank for cleaning.

## Statistical analysis

A statistical paired-test analysis was conducted to determine whether the addition of guar improved copper concentrate grade through talc depression in the flotation circuit.

### *On and Off plant trial as guar needed*

A paired t-test trial comprising nine paired observations at variable guar dosage (35 g/t) showed a statistically significant (3 per cent) improvement in final concentrate grade. The mean copper grade increased from 12 per cent Cu (no guar) to 15 per cent Cu (with guar). The trial was conducted from 8th May to 18th May 2025 processing an ultramafic proportion of about 23 per cent.

The p-values were low in both one- and two-tailed tests, allowing rejection of the null hypothesis at the 95 per cent confidence level and confirmed that guar addition had a statistically significant positive effect on concentrate grade. Interestingly, no significant differences were observed for magnesium content, final tails grade, or overall copper recovery (despite a slightly low p-value). These could be due to additional predictors or interactions and were not considered in this analysis.

Using the nine-pair data, a regression model incorporating feed Cu and Mg grades, guar addition (on/off), interactions terms and blend ratios. Across all models, guar addition constantly emerged as the primary significant predictor, (p-value of 0.00133), followed by feed grade (p-value = 0.02009). Magnesium showed no statistical significance (p-value = 0.4593) but was retained in the model for completeness.

The resulting model is conceptually simple, designed to illustrate the positive influence of guar gum in the final concentrate. The model is presented in Equation 1 and Figure 9 (FC = final concentrate), with Adjusted $R^2$ 0.518.

$$\boldsymbol{FC\ Cu\%} = \mathbf{17.823} - \mathbf{31.787} * \boldsymbol{Feed\ Cu} - \mathbf{0.930} * \boldsymbol{Feed\ Mg} + \mathbf{3.172} * \boldsymbol{Guar\ On/Off} \quad (1)$$

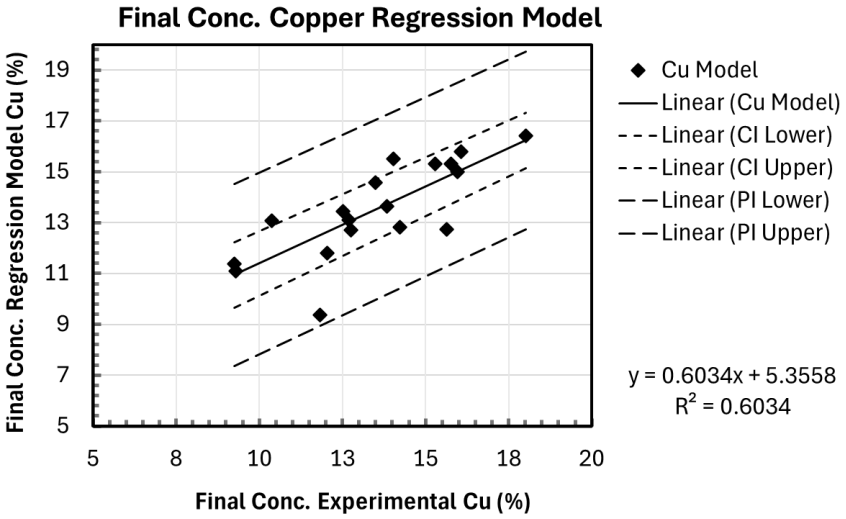



**FIG 9** – Regression model using paired t-test data (nine pairs), May 2025.

The significance of the feed-grade predictor is expected, given the influence of blend composition on flotation performance. The guar on/off predictor is similarly justified, as the presence of guar in the circuit directly contributes to talc depression and, consequently, to improvements in copper concentrate grade, as demonstrated in the preceding sections.

Nevertheless, the confidence intervals (CI) and prediction intervals (PI) exhibit a wide variability due to the limited data set, particularly in the case of prediction interval. As a result, future periods could theoretically report concentrate grades as low as 9 per cent and up to 15 per cent Cu. These outcomes could be mitigated by reducing the source of error, for example, improving guar efficiency, minimising dosing variability, increasing solution-strength consistency, managing talc levels in the blend, optimising pre-flotation performance, and others. The full data set and statistical parameters are presented in the Appendix section (Tables 5–8).

### *Cost benefit revision*

The cost benefit was then reanalysed using the copper and gold grades obtained from the pair test work reporting a variance of 3 per cent copper and gold grade of 7.1 g/t. New financial figures for 2026 budget (FY26) which includes increased milled tonnes, lower copper head grades and increased recoveries were also included as well as the same undisclosed assumptions used before (penalties, reagent costs, and others).

Using this data, a minimum annual revenue using guar gum (on) than using no guar (off) reported a revenue of A$360K per annum at 15 per cent concentrate grade.

**TABLE 4**

Plant On-Off results for a capital investment.

| Plant Trial On and Off | Guar Gum + Pre-flotation | |
|---|---|---|
| | *Off* (Baseline) | *On* (35 g/t) |
| **Copper Revenue** | | |
| Plant Trial Final Conc Cu Grade (%) | 12.01 | 15.00 |
| Plant Trial Cu Recovery (%) | 55.11 | 57.72 |
| FY26 Cu Recovered (t/a) | 512 | 512 |
| Annual Saleable Cu Value (A$) | $ 6,305,069 | $ 6,518,819 |
| **Logistic Cost** | | |
| Cu Concentrate Produced (t/a) | 4,260 | 3,411 |
| Annual Logistics Costs (A$) | $ 1,188,291 | $ 951,473 |
| **Gold Revenue** | | |
| Plant Trial Final Conc Au Grade (g/t) | 107.87 | 115.01 |
| Annual Saleable Au Value (A$) | $ 72,760,876 | $ 72,760,876 |
| **Smelter Costs** | | |
| Total Smelter Costs (A$) | $ 345,677 | $ 293,025 |
| **Total Revenue** | | |
| Annual Revenue (A$) | $ 78,005,049 | **$ 78,363,617** |

This revenue, however, is expected to increase once the statistical variance previously reported (Figure 9) is narrowed, allowing an increase of concentrate grade. Given the current limitations of the system in producing high-quality guar solution, further optimisation of pre-flotation operation and guar dosing strategies is required. A capital expenditure (CAPEX) project was submitted to address these limitations.

### *CAPEX*

A capital expenditure project (of around A$200K) was approved to acquire a fit-for-purpose guar mixing and dosing system to eliminate the persistent issue of guar clumping and associated operational challenges previously described. A high-dispersion shear-mixing pump (Powder Liquid Mixer – High shear series 620) manufactured by Mixquip Fluid Mixing Equipment ® was procured at the end of December 2025 and installed in February 2026.

Figure 10 shows the Mixquip shear pump and the live demonstration conducted by Mixquip, during which the pump successfully dissolved the guar powder/clumps.



**FIG 10** – Mixquip shear pump 620® mixing system used to dissolve guar gum clumps (modified images courtesy of Mixquip, Australia).

For the overall system upgrade, the engineering firm Verum Projects and Engineering was engaged to facilitate requirements necessary to implement this technology. Deflector mechanical maintenance and electrical departments, together with processing and metallurgy teams, have been proactively involved in the installation of the required components and associated deliverables.

The upgrade of the mixing system commenced in late-2025, beginning with electrical cabling in the field and MCC works. In mid-February 2026, a new mixing system including the Mixquip shear pump, a stirrer of higher power capacity, a reinforced lid to house the heavier stirrer, and a new level sensor in the mixing tank were installed.

Additional improvements planned include new dosing pumps from the storage tank, flow meters, piping upgrades, and sand blasting of the mixing and storage tanks, are scheduled to commenced in mid-2026.

### *Preliminary results*

*Initial response.* The quality of the guar solution improved markedly, with the Mixquip shear pumps dissolving nearly 100 per cent of the guar powder practically eliminating clump formation. The upgraded stirrer also promoted higher turbulence, improving transfer time to the storage tank. As a result of the mixing improvements, guar concentration became more consistent, while increasing in strength from 0.32 to 0.45 per cent (w/w). The circuit dose rates have remained consistent at 30 g/t to 95 g/t, however the increase in solution strength has reduced the number of mixes required.

To optimise flotation performance, guar addition points were revisited similarly than in the laboratory screening test. An additional dosing point was added to the start of the cleaner cell, where targeted depression of the talc in final concentrate was trialled (20:80 ratio of cleaners: rougher 2 guar addition).

In the example below, a thick froth layer of talc was observed forming on top of the pulp phase in the cleaner cell. Guar solution was then added to the cleaner cell which caused the talc froth to depress, allowing the copper to float and report to the launder for recovery. Figure 11 illustrates this gradual process, which occurred in less than 30 mins.

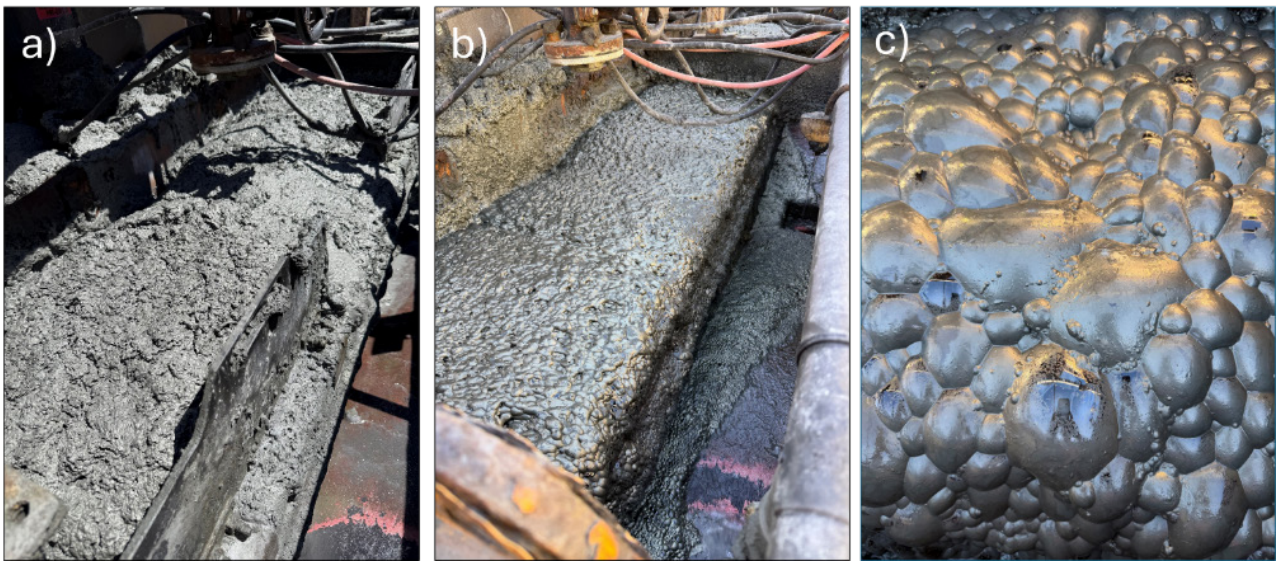



**FIG 11** – Guar effect on cleaner bank 1 cells: (a) before guar split showing a thick talc froth phase on surface obstructing copper flotation (21st February 2026); b) after removed talc froth phase, copper flotation restored; and (c) copper bubbles closeup in cell 2.

One-minute spot samples were also collected from the OSA and analysed by Intertek (Deflector's in in-house laboratory). Then 12-hours shift composites were plotted for comparisons over the same period.

The spots sample results showed an increase in copper concentrate grade from 7 per cent to 18 per cent Cu, aligning more closely with the OSA (CITECT) copper model (eg in the absence of talc). Similarly, the 12-hr shift composite samples reported improvements from 7 to 15 per cent Cu and approximately from 40 to 180 g/t for Au.

Interestingly, despite the drop in copper feed grade (dashed line) after crushing from E-Feed to ROM changing blends, both copper and gold grades remained at relatively high levels, except when affected (below 7 per cent Cu) by operational issues affecting guar supply to the circuit eg mill shutdowns, lack of raw water supply, and other related issues (Figure 12).

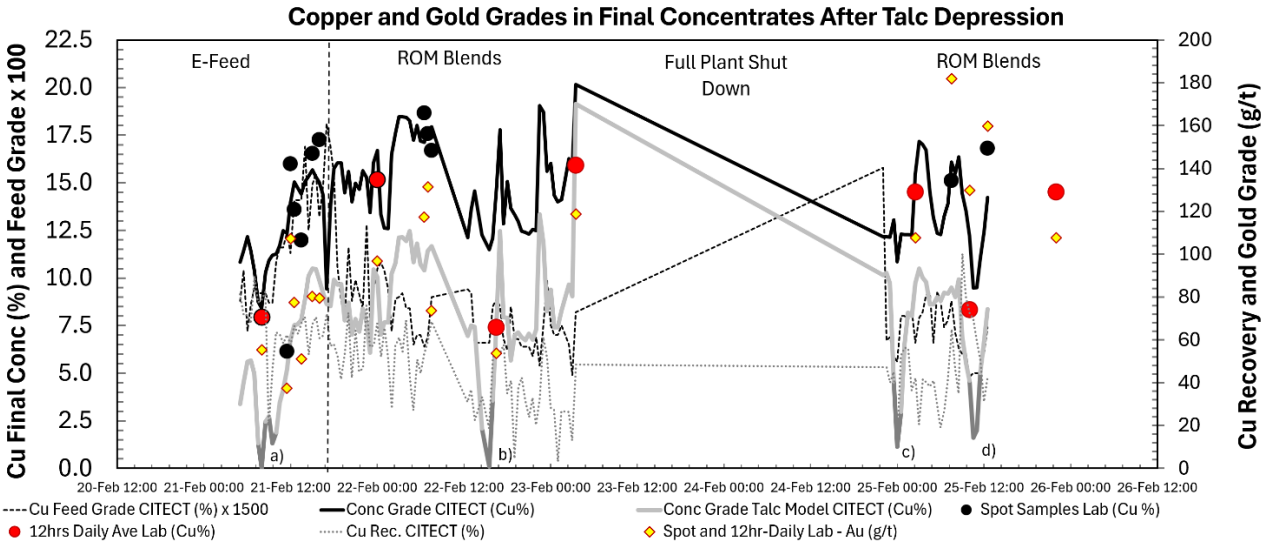



**FIG 12** – Preliminary copper flotation results after adding guar using the new shear pump and guar split into cleaners and rougher banks.

The same OSA spot samples collected during this period were analysed for nominal magnesium (representing talc-related magnesium rather than total magnesium) to assess talc depression before and after guar addition (corresponding 7 per cent and 15 per cent periods). As observed in

Figure 13, an increase in copper (15 per cent) and gold (140 g/t) grades are observed in the final concentrates with decreasing magnesium content.

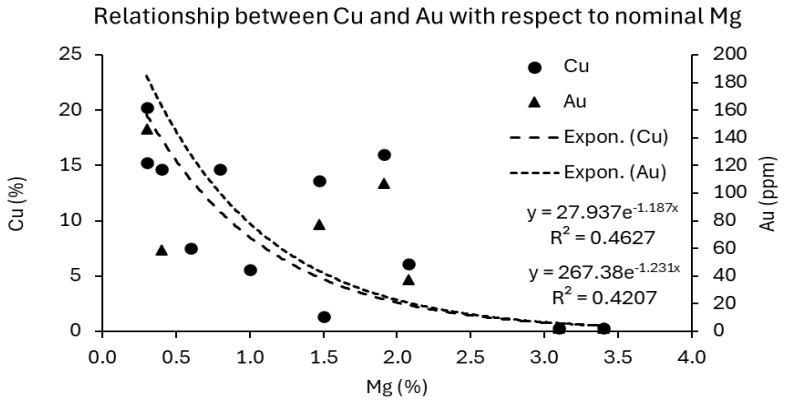



**FIG 13** – Cu and Au in function of Mg depression (talc) in spot samples collected during guar and non-guar events.

These results support the occurrence of effective talc depression, as indicated by the reduction in magnesium reporting to the concentrate, accompanied by increases in both copper and gold grades.

## FINAL CONCENTRATE GRADES TO DATE

Twenty-four-hour final concentrate samples analysed for copper and gold in the laboratory were plotted for the period from November 2025 (prior to the installation of the shear pump) to June 2026 (post-installation) (Figure 14). As observed, both the metals show an increased concentration, with copper and gold grades improving by approximately 3 to 4 per cent, consistent with the trial results reported earlier.

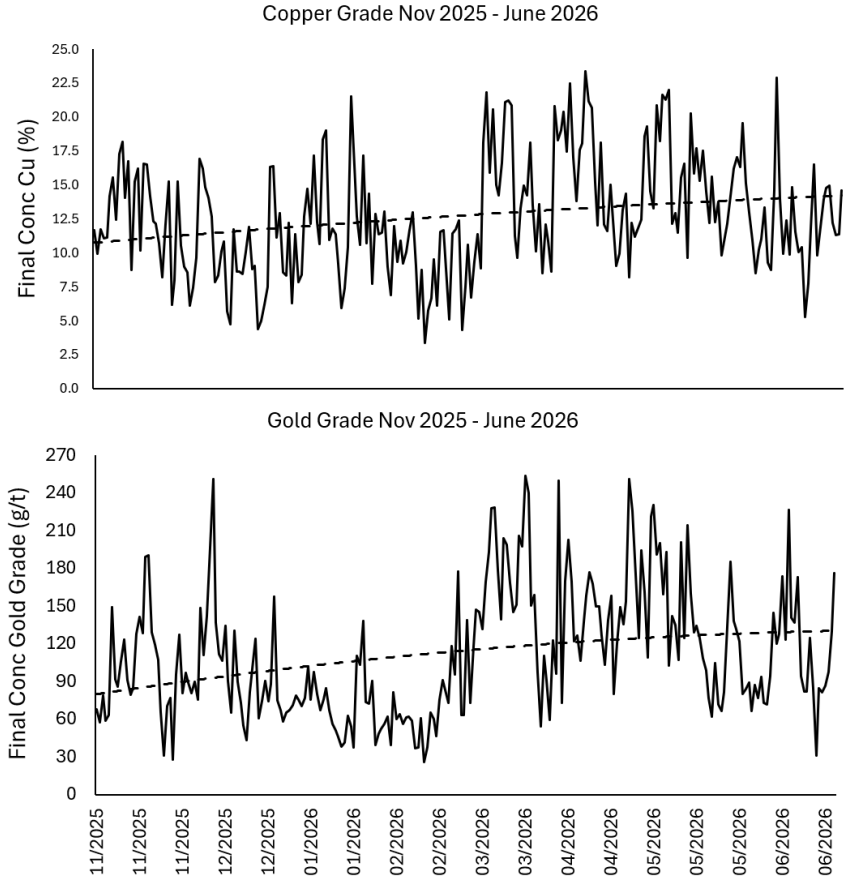



**FIG 14** – Lab assays (Cu per cent and Au ppm) Final concentrate grades – copper a) and b) gold employing guar gum as a talc depressant.

The observed variability can be attributed to changes in feed grade, Rothsay/Deflector ore proportions, troubleshooting activities, increasing operational experience, and other process factors. Nevertheless, the improvements in grades have been consistently maintained to date with operators typically dosing guar between 35–60 g/t.

It is expected that, after the implementation of pending component upgrades (eg flow metres, level sensors, and other improvements) to further reduce the statistical variability reported in the regression results (Figure 9), copper/gold concentrate grades will continue to improve.

## CONCLUSIONS

Based on the screening analysis, cost-benefit analysis, preliminary set-up and operating conditions, field observations, and statistical analyses, it was concluded that guar gum was the most suitable reagent for effectively depressing talc in the flotation circuit at Deflector.

Following the upgrade of the mixing system through a CAPEX project in 2026, higher copper and gold grades have been achieved, attributed to enhanced talc depression and improvements in pre-flotation.

Under the current system, guar addition has been delivering an approximate +3 per cent improvement in copper grade, which is aligned to the trial results. Achieving consistent and effective guar concentrations required the practical elimination of clumping, which was accomplished through system upgrades via the fit-for-purpose mixing system. Maintaining improvements to the overall system, along with strategies to manage talc at lower copper head grades, is expected to further increase concentrate grades.

Finally, copper and gold recoveries were not adversely affected by the introduction of guar in the process.

## ACKNOWLEDGEMENTS

We thank Vault Minerals and the Deflector Gold Project for permitting the publication of this study.

This work would not have been possible without the support of the plant operators responsible for producing the guar mixes.

We also extend our appreciation to the Mechanical Maintenance and Electrical teams for their essential contributions during the installation phase. Additionally, we acknowledge the ongoing engineering work performed by Verum Projects and Engineering, Australia.

Finally, special thanks go to the staff of the Intertek laboratory at Deflector for their prompt sample analysis and continued interest in the project.

## REFERENCES

ALS Australia, 2025. Talc Depression Test work, Reagent scheme and results, internal report.

Bazar, A J, Rahimi, M, Fathinia, S, Jafari, M, Chipakwe, V and Chelgani, C S, 2021. Talc flotation – An overview, *Minerals*, 11(7):662.

Farrokhpay, S, Ndlovu, B and Bradshaw, D, 2018. Behavior of talc and mica in copper ore flotation, *Applied Clay Science,* 160:270–275.

Figueroa Salguero, G D, 2019. Investigation of the effects of turbulence in flotation, PhD thesis, The University of Queensland, Brisbane.

Garcia, V C and Pawlik, M, 2015. Molecular weight effects in interactions of guar gum with talc, *International Journal Of Mineral Processing,* 138:38–43.

Ge, W, Liu, J, Cheng, Z, Gao, P, Zhu, Y, Li, H, Li, Y, Zhang, J and Yuan, S, 2025. New insights into the selective depression mechanism of galactomannan, *Flotation Separation Of Chalcopyrite And Talc, Colloids And Surfaces A*: *Physicochemical And Engineering Aspects,* 721:137263.

Kiddle, J, 2020. Deflector processing facility CIP upgrade TSF2 WWTP upgrade, *Works Approval Supporting Document,* Silverlake Resources (Deflector) Pty Ltd.

Lei, Z, Zhang, H, Tang, H, Luo, Y and Xu, P, 2025. Selective flotation separation of chalcopyrite from talc utilizing a novel carboxyl copolymer depressant, *Journal Of Environmental Chemical Engineering,* 13:117093.

Mulvihill, B and Krishnan, R, 2021. CMC mixing facility functional specifications, Renison T in Operations, Bluestone Mines Tasmania Joint Venture Pty Ltd: Gr Engineering Services.

Napier-Munn, T J, 2014. *Statistical methods for Mineral Engineers – How to Design Experiments and Analyse Data* (Julius Kruttschnitt Mineral Research Centre: Indooroopilly).

Runge, K, 2010. Laboratory flotation testing – An essential tool for ore characterisation, *Flotation Plant Optimisation*: *A Metallurgical Guide To Identifying And Solving Problems In Flotation Plants,* Spectrum Series, 16:155–173 (The Australasian Institute of Mining and Metallurgy: Melbourne).

Taliesin, S J, 2025. Guar trial update report from 20/5–28/5, Deflector Gold Project, Vault Minerals (Vault Minerals Ltd internal report).

Vault Minerals Report, 2026. March 2026 Quarterly Activities Report, Vault Minerals Limited.

Wills, B A and Finch, J, 2015. *Wills' Mineral Processing Technology*: *An Introduction To The Practical Aspects Of Ore Treatment And Mineral Recovery* (Butterworth-Heinemann).

Wong, C, 2026. Deflector concentrates shipment tracking FY26 Database (Vault Minerals Ltd internal report).

Wong, C, Whitford, M and Bannon, C, 2025. Identifying the most suitable talc depressant for ultramafic ore at deflector gold copper gold mine, Deflector Gold Mine Australia (Vault Minerals Ltd internal report).

Young, M F, Barnes, K E, Anderson, G S and Pease, J D, 2006. Jameson cell: The "comeback" in base metals applications using improved design and flow sheets, in *Proceedings of the Annual Canadian Mineral Processors Conference,* pp 331–332 (CIM Canadian Mineral Processors).

## APPENDIX

**TABLE 5**

On and off data from t-tests trial.

| Plant trial test work | | | | | Concentrate | | | Tail | | | Feed | | | Recovery | | |
|---|---|---|---|---|---|---|---|---|---|---|---|---|---|---|---|---|
| **Pair** | **Date** | **Shift** | **Pairs** | **Guar** | **Cu** | **Mg** | **Au** | **Cu** | **Mg** | **Au** | **Cu** | **Mg** | **Au** | **Cu** | **Mg** | **Au** |
| 1 | 8/05/2025 3:00 | DS | 0 | Off | 11.82 | 1.20 | 86.50 | 0.08 | 2.70 | 1.94 | 0.19 | 2.60 | 3.18 | 0.58 | 0.03 | 0.40 |
| | 8/05/2025 15:00 | NS | 1 | On | 13.50 | 1.10 | 117.16 | 0.07 | 2.40 | 1.73 | 0.14 | 2.30 | 2.20 | 0.52 | 0.04 | 0.22 |
| 2 | 9/05/2025 3:00 | DS | 0 | Off | 12.68 | 0.60 | 240.19 | 0.05 | 2.20 | 1.86 | 0.09 | 2.10 | 2.35 | 0.46 | 0.02 | 0.21 |
| | 9/05/2025 15:00 | NS | 1 | On | 18.02 | 0.70 | 150.00 | 0.04 | 2.30 | 1.73 | 0.08 | 2.10 | 2.40 | 0.58 | 0.04 | 0.28 |
| 3 | 10/05/2025 3:00 | DS | 0 | Off | 15.63 | 0.90 | 135.13 | 0.04 | 2.20 | 1.46 | 0.10 | 1.90 | 1.79 | 0.60 | 0.11 | 0.19 |
| | 10/05/2025 15:00 | NS | 1 | On | 16.07 | 1.00 | 127.19 | 0.04 | 2.10 | 1.45 | 0.10 | 2.10 | 1.94 | 0.62 | 0.00 | 0.26 |
| 4 | 11/05/2025 3:00 | DS | 0 | Off | 10.39 | 1.50 | 86.68 | 0.04 | 2.40 | 1.39 | 0.09 | 2.00 | 2.32 | 0.55 | 0.33 | 0.41 |
| | 11/05/2025 15:00 | NS | 1 | On | 15.96 | 1.00 | 73.18 | 0.05 | 2.40 | 0.98 | 0.13 | 2.10 | 1.57 | 0.60 | 0.10 | 0.38 |
| 5 | 12/05/2025 3:00 | DS | 0 | Off | 12.05 | 1.80 | 67.56 | 0.05 | 2.20 | 1.11 | 0.13 | 2.20 | 1.61 | 0.62 | 0.00 | 0.32 |
| | 12/05/2025 15:00 | NS | 1 | On | 15.78 | 1.50 | 73.42 | 0.05 | 2.20 | 1.00 | 0.11 | 2.20 | 1.64 | 0.60 | 0.00 | 0.40 |
| 6 | 15/05/2025 3:00 | DS | 0 | Off | 12.75 | 1.66 | 84.43 | 0.05 | 2.50 | 1.48 | 0.09 | 2.60 | 1.59 | 0.47 | -0.08 | 0.07 |
| | 15/05/2025 15:00 | NS | 1 | On | 14.02 | 0.65 | 190.61 | 0.04 | 2.60 | 1.50 | 0.09 | 2.70 | 2.08 | 0.54 | -0.01 | 0.28 |
| 7 | 16/05/2025 3:00 | DS | 1 | On | 15.30 | 1.70 | 154.91 | 0.04 | 2.80 | 1.89 | 0.09 | 2.90 | 2.76 | 0.60 | -0.05 | 0.32 |
| | 16/05/2025 15:00 | NS | 0 | Off | 14.23 | 1.70 | 140.40 | 0.04 | 3.10 | 1.92 | 0.08 | 2.80 | 2.88 | 0.51 | 0.13 | 0.34 |
| 8 | 17/05/2025 3:00 | DS | 0 | Off | 9.29 | 2.20 | 76.31 | 0.05 | 2.70 | 1.76 | 0.13 | 2.80 | 2.50 | 0.60 | -0.16 | 0.30 |
| | 17/05/2025 15:00 | NS | 1 | On | 12.52 | 1.80 | 70.69 | 0.07 | 2.50 | 1.50 | 0.17 | 2.40 | 2.21 | 0.58 | 0.11 | 0.33 |
| 9 | 18/05/2025 3:00 | DS | 1 | On | 13.83 | 1.60 | 77.91 | 0.08 | 1.18 | 2.50 | 0.17 | 2.16 | 2.70 | 0.56 | 1.73 | 0.08 |
| | 18/05/2025 15:00 | NS | 0 | Off | 9.26 | 2.40 | 53.63 | 0.07 | 1.26 | 2.50 | 0.15 | 1.80 | 2.30 | 0.56 | 0.63 | -0.09 |

## t-tests data

**TABLE 6**

T-test results assuming equal variance for samples with and without guar (on/off).

t-Test: Two-Sample Assuming Equal Variances

| | *Cu Conc* | | *Mg Conc* | | *Au Conc* | | *Cu Recovery* | |
|---|---|---|---|---|---|---|---|---|
| | *Off* | *On* | *Off* | *On* | *Off* | *On* | *Off* | *On* |
| Mean (%) | 12.01 | 15.00 | 1.55 | 1.23 | 108 | 115 | 55.11 | 57.72 |
| Variance | 4.582 | 2.822 | 0.337 | 0.187 | 3291 | 1938 | 0.003 | 0.001 |
| Observations | 9 | 9 | 9 | 9 | 9 | 9 | 9 | 9 |
| Pooled Variance | 3.702 | | 0.262 | | 2615 | | 0.002 | |
| Hypothesized Mean Difference | 0 | | 0 | | 0.0 | | 0 | |
| df | 16 | | 16 | | 16.0 | | 16 | |
| t Stat | -3.297 | | 1.342 | | -0.3 | | -1.189 | |
| P(T<=t) one-tail | 0.002 | | 0.099 | | 0.4 | | 0.126 | |
| t Critical one-tail | 1.746 | | 1.746 | | 1.7 | | 1.746 | |
| P(T<=t) two-tail | 0.005 | | 0.198 | | 0.8 | | 0.252 | |
| t Critical two-tail | 2.120 | | 2.120 | | 2.1 | | 2.120 | |
| Mean difference | | 2.99 | | -0.32 | | 7.14 | | 2.61 |

## Regression models

**TABLE 7**

The regression model for copper final concentrate using three key predictors.

SUMMARY OUTPUT

| *Regression Statistics* | |
|---|---|
| Multiple R | 0.776808 |
| R Square | 0.603431 |
| Adjusted R Square | 0.518452 |
| Standard Error | 1.678539 |
| Observations | 18 |

ANOVA

| | *df* | *SS* | *MS* | *F* | *Significance F* |
|---|---|---|---|---|---|
| Regression | 3 | 60.02047036 | 20.00682 | 7.100931 | 0.003914486 |
| Residual | 14 | 39.44489976 | 2.817493 | | |
| Total | 17 | 99.46537013 | | | |

| | *Coefficients* | *Standard Error* | *t Stat* | *P-value* | *Lower 95%* | *Upper 95%* | *Lower 95.0%* | *Upper 95.0%* |
|---|---|---|---|---|---|---|---|---|
| Intercept | 17.8235 | 3.324539196 | 5.361194 | 0.0001 | 10.69307337 | 24.95392819 | 10.69307337 | 24.95392819 |
| Feed Cu | -31.7867 | 12.22691657 | -2.59973 | **0.020988** | -58.01083419 | -5.5625784 | -58.01083419 | -5.5625784 |
| Feed Mg | -0.93056 | 1.223077511 | -0.76084 | 0.459378 | -3.553802506 | 1.692678221 | -3.553802506 | 1.692678221 |
| Guar (on/off) | 3.172707 | 0.79430847 | 3.994301 | **0.001331** | 1.469085005 | 4.87632947 | 1.469085005 | 4.87632947 |

## Confidence/prediction intervals data

**TABLE 8**

Calculated parameters using Linest to obtain CI and PI plotted in the regression models (Napier-Munn, 2014).

| | | | | | | | |
|---|---|---|---|---|---|---|---|
| Linest | 1.00 | -5.3E-15 | interc. | %Conf. | 95 | t.95% | 2.10 |
| SE slope | 0.20 | 2.76 | SE interc | 1-5Conf | **0.05** | SE | 1.57 |
| R2 | 0.603 | 1.57 | SE of y | n | 18 | | |
| F | 24.3 | 16 | d.f. | Xm | 13.51 | | |
| SS Reg | 60.02 | 39.44 | SS Res | SSxx | 60.02 | | |

# Commissioning coarse flotation at BHP Carrapateena

*R Jones[1], M Davidson[2], F Burns[3] and T Fyfe[4]*

1. Principal Metallurgist – Metallurgy, Carrapateena, BHP, Adelaide SA 5950. Email: rhys.jones@bhp.com
2. Lead Metallurgist – Plant, Carrapateena, BHP, Adelaide SA 5950. Email: mitchell.davidson@bhp.com.
3. Manager – Processing, Carrapateena, BHP, Adelaide SA 5950. Email: fraser.burns@bhp.com
4. Lead Metallurgist – Projects, Carrapateena, BHP, Adelaide SA 5950. Email: tristram.fyfe@bhp.com

## ABSTRACT

Carrapateena is an iron oxide copper–gold (IOCG) deposit located in the Gawler Craton, South Australia. The ore, located at depths greater than 500 m, is mined by sub-level caving methods and processed by a conventional sulfide flotation concentrator. A copper-gold-silver (Cu-Au-Ag) concentrate is produced with chalcopyrite and bornite as the main copper bearing minerals.

Carrapateena was commissioned in 2020 as a 4 mega-tonne per annum (Mt/a) concentrator, however a growth pathway to a 7 Mt/a concentrator was developed by the site processing team to keep pace with an increasingly productive mine. A key aspect of this pathway was to relax the primary grind size from the design $P_{80}$ of 75 µm to 125 µm as processing rates increased. To address associated recovery losses, a coarse flotation technology – Eriez HydroFloat® cell – was selected for use in a rougher tailings scavenger duty.

HydroFloat® laboratory studies commenced in 2019, transitioning to a pilot plant operating on-site in 2021. Through subsequent engineering phases, these studies transformed into a fully-fledged coarse flotation facility. Inclusive of three stages of desliming cyclones preparing a coarse feed to a pair of HydroFloat® cells, which recovers a coarse concentrate for treatment by a Metso Vertimill® VTM3500 for regrinding to a $P_{80}$ of 20 µm, and a two-stage cleaning circuit consisting of four Glencore Technology Jameson Cells, producing a final copper-gold-silver concentrate.

Construction of this facility commenced in 2024, with commissioning and subsequent optimisation activities occurring in 2025.

This paper outlines a process description of the operating coarse flotation circuit at Carrapateena and presents details on the commission challenges faced and optimisation path required for the circuit to achieve its design intent.

## DESIGN DEVELOPMENT

### Intent

The coarse flotation circuit was designed to enable the Carrapateena concentrator to operate at an increased plant throughput resulting in a coarser primary grind ($P_{80}$ 75 µm to ~125 µm), whilst maintaining or improving copper, gold, and silver recovery. The design intent was to:

- Recover coarse copper minerals that were being lost to rougher tailings as a result of increased throughput.
- Use of a deslime circuit for classification of rougher tailings, to produce a product that meets the feed requirements of the HydroFloat® cells.
- Produce a coarse concentrate that can effectively be reground to 20 µm and of sufficient head grade for flotation feed.
- Produce a final concentrate specification product.
- Operate reliably across a range of ore hardness, mineralogy, and throughput conditions up to 7 Mt/a.

## Delivering for future needs

The coarse flotation circuit was delivered on an accelerated schedule in anticipation of the concentrator's future throughput requirements. Carrapateena's processing rate was planned to increase from the original 4 Mt/a to 7 Mt/a, a growth pathway identified several years prior and targeted for execution in 2024. As modelling and operational data made clear, the higher throughput would inevitably drive a coarser primary grind, the site recognised the need for improved coarse particle recovery to offset the associated loss in metallurgical performance.

The project's development tracked closely with the expected production ramp-up, progressed through a series of steps with a compressed timeline:

- 2019 Lab scale test work and Concept Study.
- 2021 In field pilot plant test work.
- 2021–2022 Front End Engineering Design (FEED) Study.
- 2022–2024 Detailed engineering design.
- 2024 Construction commenced.
- 2025 First concentrate produced.

The coarse flotation circuit was fast-tracked to meet the expected increase in grind size and maintain Cu-Au-Ag recovery as the concentrator transitioned toward higher milling rates.

The circuit mimics the successful application of coarse particle flotation first introduced in a sulfide application at the Newcrest Cadia operation (Vollert *et al,* 2019) for similar objectives. Other installations in sulfide operations have included Anglo American's El Soldado operation (Arburo *et al,* 2022), this circuit was installed on a split feed basis rather than a tails scavenging application.

## HydroFloat® technology

The HydroFloat® is an aerated fluidised-bed flotation device produced by Eriez that combines the selectivity of flotation with the classification behaviour of a density separator. In operation, feed slurry is introduced at the top of the vessel and descends through an upward flow of teeter water and fine air bubbles, establishing a fluidised (teeter) bed of suspended solids.

Within this environment, fine air bubbles selectively attach to hydrophobic mineral surfaces, forming bubble–particle aggregates with a reduced effective density. These aggregates are unable to penetrate the fluidised bed and are carried upward to the overflow as concentrate, while hydrophilic gangue particles remain in the bed and discharge to underflow as tailings. A graphic of the HydroFloat® cell illustrating these operating principles is displayed in Figure 1.

Unlike conventional flotation cells, the HydroFloat® operates under low-turbulence, plug-flow conditions, which significantly increases particle residence time and reduces detachment forces. This enables recovery of coarse and partially liberated particles at sizes well beyond the effective limits of traditional flotation, typically up to several hundred microns depending on the application. HydroFloat® cells require desliming of the feed prior to flotation in order to remove barren-fine particles that would otherwise be hydraulically entrained into concentrate due to the operating principle of the cell.

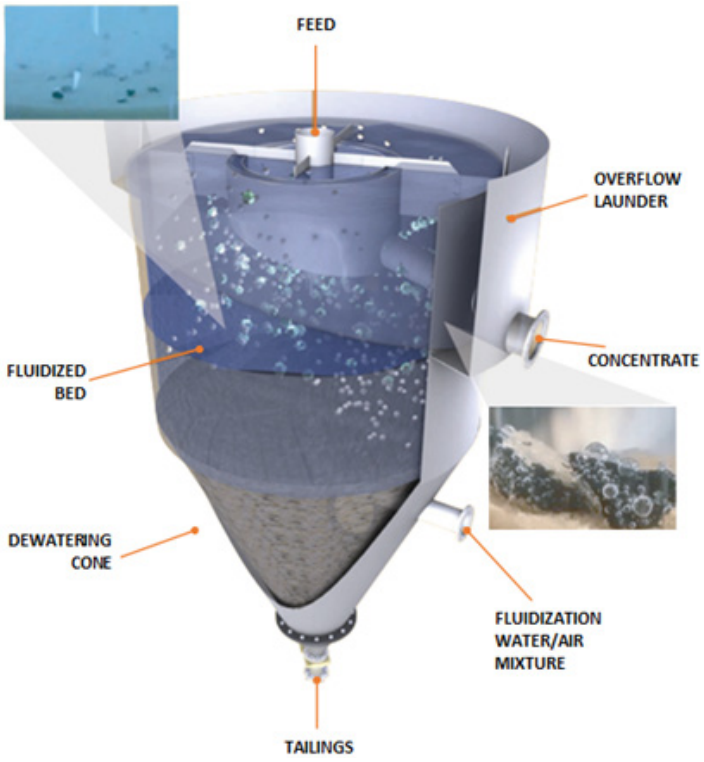



**FIG 1** – HydroFloat® cell diagram (credit: Eriez, 2026).

## Pilot plant purpose, scope, and test approach

The objective of the pilot program was to:

- Gather sufficient running data to validate previous test work results for the Eriez HydroFloat® and CrossFlow units and allow for upscaling to full size units.
- Collect sufficient flotation data to design a regrind and cleaner flotation circuit to treat the generated HydroFloat® concentrate.

The pilot plant configuration was skid mounted comprising an Eriez CrossFlow (450 mm diameter) Separator followed by a HydroFloat® Cell (400 mm diameter). The plant was fed from the concentrator rougher tailings On-Stream Analyser (OSA) sample return line. The intended hydrocyclone feed conditioner was absent, due to interstate transport restrictions during early 2021. Samples were collected as spot tests and 3–6 hr composites for mass balance and size by assay. Bulk HydroFloat® concentrate was collected from the pilot plant and a parallel laboratory scale regrind and cleaner flotation program was run in order to develop the downstream flotation flow sheet.

## Classification/desliming – CrossFlow results, cyclone options, and path forward

Early in the pilot plant run, the CrossFlow classifier desliming unit supplied for the Carrapateena pilot plant was found to be undersized for the application given the rheology of the Carrapateena rougher tailings. To improve the rheology during early stages of the pilot, the feed was diluted from 35 per cent solids to 15–20 per cent solids. Ultimately separation efficiency of the CrossFlow degraded toward hydrocyclone-like performance (fines in underflow, coarse to overflow) and was variable. Under the best measured conditions, approximately 22 per cent mass and 33 per cent copper reported to HydroFloat® feed.

During operation of the pilot plant there were occasions in which the CrossFlow was operated in such a way that there was an excess of fines reporting to the HydroFloat® feed, resulting in a loss of stability in the HydroFloat® bed. Vendor advice was for the feed preparation to HydroFloat® unit to not exceed:

- 15 per cent passing 53 µm by mass.
- 5 per cent passing 38 µm by mass.

The conclusions drawn from the pilot program were to progress with a multi-stage cyclone-based desliming circuit rather than include CrossFlow classifiers, with a target cut size as close to 53 µm as practicable (nominal ~50–53 µm) without exceeding 15 per cent -53 µm (and 5 per cent -38 µm) in HydroFloat® (HF) feed. The resultant expected performance of the deslime circuit was ~40–45 per cent mass and ~50 per cent Cu report to HF feed with ~1.15× Cu upgrade — adequate to generate a manageable HF mass pull at good coarse selectivity.

## HydroFloat® cell – operating window, reagents and performance

Throughout pilot operation, the HydroFloat® cell was able to demonstrate steady and repeatable performance provided the feed classification conditions highlighted above were met.

Achievable HydroFloat® performance (pilot) of ~20–30 per cent mass pull, ~65 per cent copper recovery from HF feed was repeatably demonstrated over a 3 month period, with a Cu upgrade ratio of ~2.0–2.5×. Test results were achieved with a teeter flux of ~18 $m^3/h/m^2$ and air fraction of ~25 per cent. By increasing the teeter flux, copper stage recoveries greater than 75 per cent could be achieved with a corresponding mass recovery increase up to 45 per cent. This higher mass pull was deemed suboptimal due to downstream circuit constraints and design implications. Overall, the combined deslime and HydroFloat® block achieved ~37 per cent copper recovery at 15 per cent mass recovery from the plant rougher tailings. A summary of the pilot plant performance data is shown in Figure 2. In Figure 3, the recovery by size achieved in the plant rougher cells together with the HydroFloat® recovery from the pilot plant is illustrated to highlight the difference in performance at coarser particle sizes.

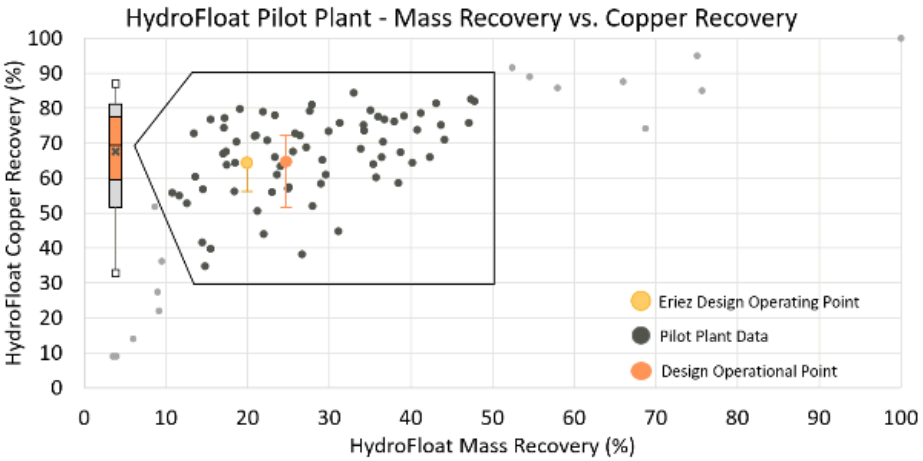



**FIG 2** – HydroFloat® pilot plant data.

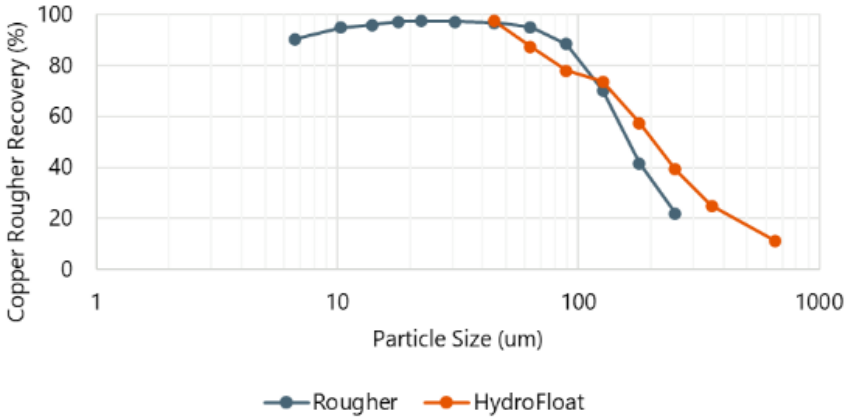



**FIG 3** – Rougher and HydroFloat® recovery versus particle size (µm).

Both the Carrapateena incumbent collector, Sodium-Ethyl Xanthate (SEX), and longer chained, Potassium Amyl Xanthate (PAX) were trialled with PAX dosed at ~200 grams per tonne (g/t) of the HydroFloat® proving to be optimal. SEX under equivalent dose rates resulted in ~5–8 per cent lower Cu recovery at similar mass pull, and equivalent recoveries when dosed at ~400 g/t SEX, no net benefit was observed from the addition of Diesel (extender) or Aerophine 3418A (promoter) as co-additions in the pilot, which has been successful elsewhere (Vollert *et al,* 2019). Based on three months of pilot operation the following recommendations were made for plant design:

- 2× 14 ft HydroFloat® cells operating with a teeter flux ~18 $m^3/h/m^2$ and air fraction ~25 per cent.
- 65 per cent stage copper recovery at 25 per cent mass recovery as operating targets.
- PAX as collector, dosed at 200 g/t with 90 seconds conditioning time.

### Regrind and cleaning – grind targets, capacity, stage recovery and final grade

A regrind and cleaning circuit test work program was run in parallel to the HydroFloat® pilot plant program utilising over 4 t of coarse concentrate produced by the pilot plant. The program consisted of kinetic roughing, cleaning and Jameson cell dilution cleaning tests as well as regrind signature plot (energy determination) development work.

The default flow sheet identified during concept level work was for a primary regrind to ~75 µm followed by roughing, then further regrind to 20 µm and cleaning. Copper recovery in roughing increased materially as grind size decreased, with ~92–95 per cent copper recovery in 40 min achieved at a $P_{80}$ between 12 and 20 µm. Coarser grinds (75–100 µm) lagged in recovery, and this evidence ruled out the dual-regrind flow sheet.

Dilution cleaner tests indicated final concentrate grades between 33 and 38 per cent Cu at 85 to 95 per cent cleaning stage recovery were achieved when regrinding to $P_{80}$ between 12 and 20 µm, with cleaning losses of approximately 2–3.5 per cent. Under laboratory conditions, a single Jameson stage upgraded the feed from around 0.3 per cent Cu to 35 per cent Cu (more than 100× upgrade) with high recovery. For scale-up from laboratory test to full scale installation, two cleaning stages plus a cleaner-scavenger were recommended and adopted.

Jameson cells were chosen for fine bubble size, intense contacting, and froth washing, suited to ultra-fine, high-upgrade cleaning. These cells were also proven and in use at Carrapateena in different duties. The design guidance emphasised long residence time and dilute conditions, with flexibility for Cleaner 1/2 inter-connections and a Cleaner-Scavenger pull-back to maximise overall stage recovery at target grades.

Given the target $P_{80}$ of less than 20 µm, a Metso High Intensity Grinding (HIG) mill was preferred due to site familiarity and energy efficiency at ultra-fine targets. Subsequent studies found that achieving a particle size reduction from ~280–300 µm to 20 µm in a single stage HIG mill was unviable due to limitations on ceramic media top size and reservations about pulling maximum power draw from the required HIG6000 without excessive rotor wear. A two-stage VertiMill (VTM)-HIG circuit was investigated but ultimately a single variable speed drive (VSD) driven VTM3500 was selected to achieve the particle size reduction in a single stage to deliver the most efficient circuit packaging. A slightly oversized mill for the duty was selected to de-risk the single stage duty and downturn ability provided by the VSD.

## COARSE FLOTATION PROCESS DESCRIPTION

The Carrapateena coarse flotation (CF) plant is configured as an integrated four-stage circuit designed to recover coarse copper particles. As illustrated in Figure 4, the circuit consists of a three-stage deslime circuit, a coarse flotation stage operating two Eriez HydroFloat® (HF) units in parallel, a regrind circuit utilising a Metso Vertimill® VTM3000 with cyclone pack in closed loop, and a staged rougher and cleaner Jameson flotation circuit.

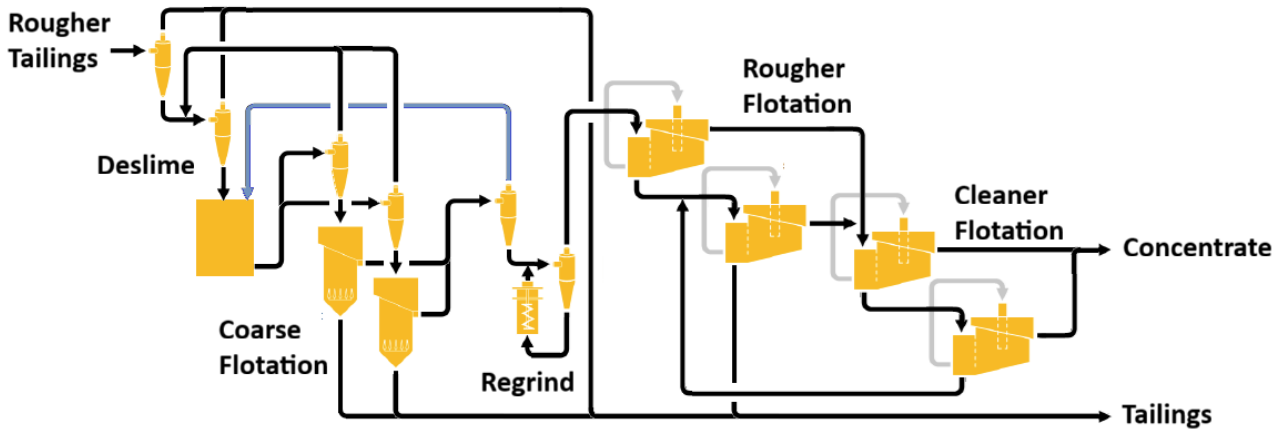



**FIG 4** – Carrapateena coarse flotation circuit – process flow diagram.

The desliming section is made up of a 26-cyclone FLSmidth 250 mm gMAX10 Stage 1 cluster with overflow reporting to tailings and underflow to Stage 2, followed by a 17-cyclone FLSmidth 381 mm gMAX15 Stage 2 cluster with overflow reporting to tailings and underflow to Stage 3. Stage 3 comprises two 8-cyclone FLSmidth 250 mm gMAX15–20 clusters fitted with CycloWash™, where overflow returns to Stage 2 deslime feed and underflow is directed to the HydroFloat® cells. Coarse flotation is undertaken in two 4.3 m diameter HydroFloat® cells, with underflow to tailings and overflow to a 16-cyclone FLSmidth 250 mm gMAX10 concentrate dewatering cluster.

The regrind circuit includes a 3750 HP VSD-driven Metso Vertimill® operating in closed loop with a 16-cyclone FLSmidth 150 mm gMAX6 cluster. Downstream flotation consists of two E6 Jameson rougher-scavenger cells in series, with tailings reporting to final tailings and concentrate feeding two E2 Jameson cleaner cells in series. The cleaner circuit provides flexibility, allowing operation as a cleaner–scavenger configuration with scavenger concentrate recycled to the cleaner feed, sequential cleaning with all concentrate reporting to final concentrate, diversion of coarse CF final concentrate to the main plant regrind circuit for additional liberation, or operation of tailings in either open circuit to final tailings or closed circuit back to the CF rougher feed.

The overall circuit process flow diagram, as designed and installed, is shown in Figure 4.

## COMMISSIONING CHALLENGES

This section summarises the key challenges, learnings, and circuit modifications encountered during commissioning, from finer-than-expected grind sizes impacting the deslime circuit, reagent performance issues, mechanical wear, and stabilisation of the HydroFloat® and Jameson flotation circuits. This also outlines how the team addressed these issues through targeted operational changes, equipment upgrades, and reagent strategy variations to improve stability, recovery, and overall circuit performance.

### Flotation feed particle size distribution

Carrapateena completed several studies with simulations based on data from 2020–2021 to understand the consequences of increased throughput on the grinding circuit product size. Based on grinding circuit surveys, modelling and simulations, the expected increase in $P_{80}$ from 4 Mt/a to 7 Mt/a was from 75 µm to 120 µm.

As production rates were increased to 7 Mt/a it was observed that the grinding circuit produced a finer product than expected. Throughput and primary grind size data from 2024–2025 are presented in Figures 5 and 6. The design 7 Mt/a objective was achieved by mid-2025, however the resulting primary grind size at this throughput rate (850–900 t/h) is finer, ranging between 85 and 100 µm compared to the expected 120 µm. This is primarily due to ore being softer within the sub-level cave (SLC) region of the Carrapateena orebody, but ore hardness is expected to increase as Carrapateena transitions to block caving in future years.

Furthermore, during commissioning and early ramp up of the CF circuit, the Carrapateena concentrator was unable to sustain long periods of throughput at the higher rates due to factors

external to the CF circuit, necessitating commissioning and optimisation of the plant around finer feed sizes. It has only been since Q2 2026, ~9 months post CF circuit start-up, that sustained 7 Mt/a operation has been achieved.

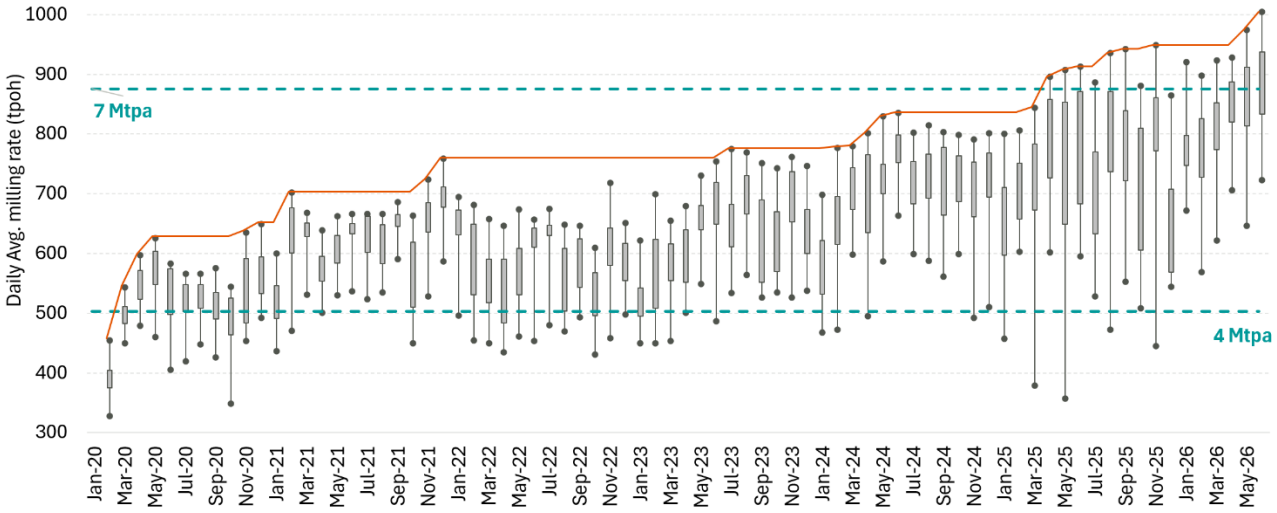



**FIG 5** – Carrapateena concentrator ramp to 7 Mt/a.

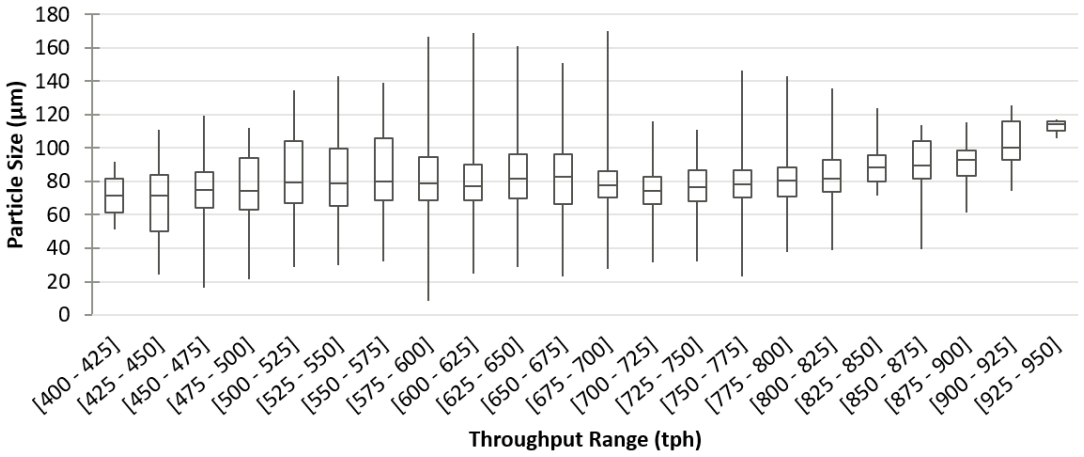



**FIG 6** – Carrapateena concentrator throughput versus flotation feed size $P_{80}$.

The finer than predicted grinding circuit product resulted in an increase in the proportion of fine material reporting to the coarse flotation deslime circuit feed. Circuit modifications were required to mitigate the greater load on the deslime circuit which is required to reject these fine particles to achieve the feed size criteria for the HydroFloat® cell.

Initial modifications to the deslime circuit included the introduction of Stage 2 and Stage 3 deslime cyclone bypasses to tailings to remove excessive recirculating loads of fines. During periods of lower throughput, operational strategies included: (a) reducing to operating one HydroFloat® cell to allow for an adequate coarse feed to establish a fluidised bed; and (b) operating at lower teeter water flows. It was found that a fluidised bed could not be maintained at lower throughputs without a critical mass flow of sufficiently coarse particles.

Surveys of the deslime circuit were collected periodically throughout commissioning. It was found that the HydroFloat® feed contained more than twice the allowance amount of fines (sub-38 µm and sub-53 µm material) when compared to the Process Design Criteria (PDC). At the time of this survey the primary grinding circuit product $P_{80}$ was approximately 90 µm compared to the targeted 120 µm. The mass splits and copper deportment through the deslime circuit are displayed in Sankey format in Figures 7 and 8, respectively, the design and actual deslime classification by size for the deslime circuit is shown in Figure 9.

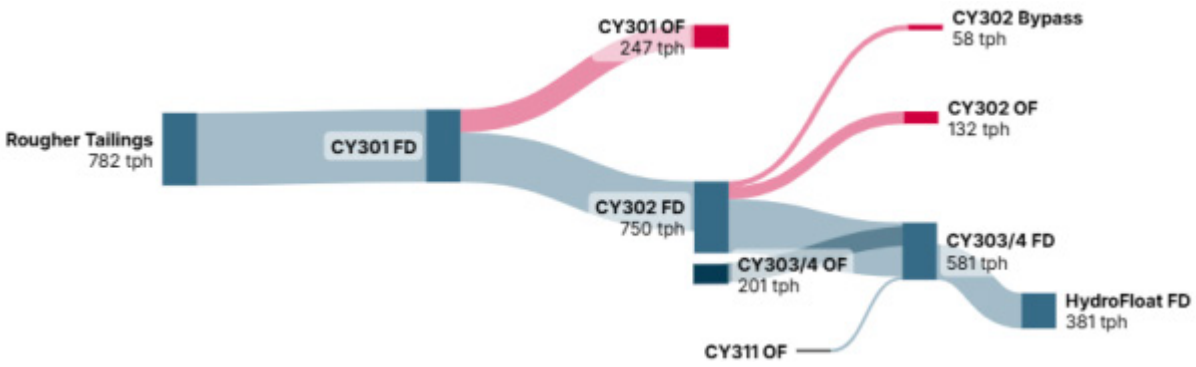



**FIG 7** – Mass flow split based on June 2025 deslime survey.

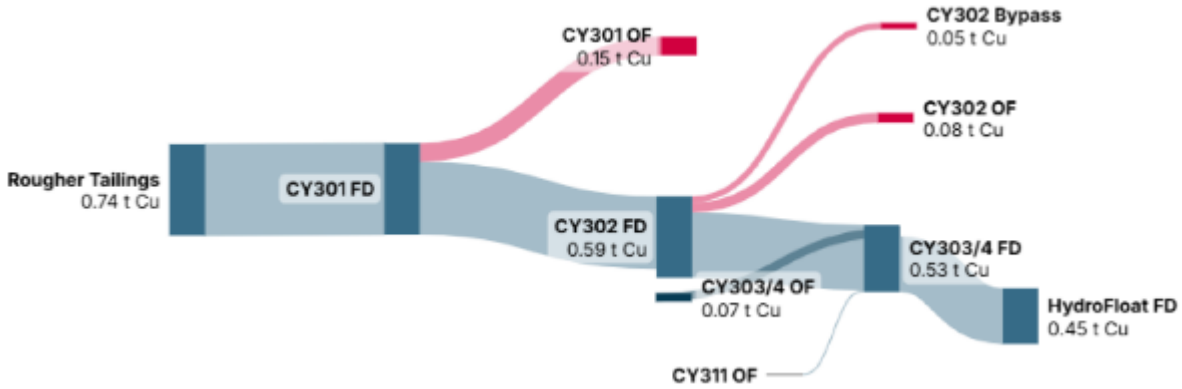



**FIG 8** – Cu metal mass split based on June 2025 deslime survey.

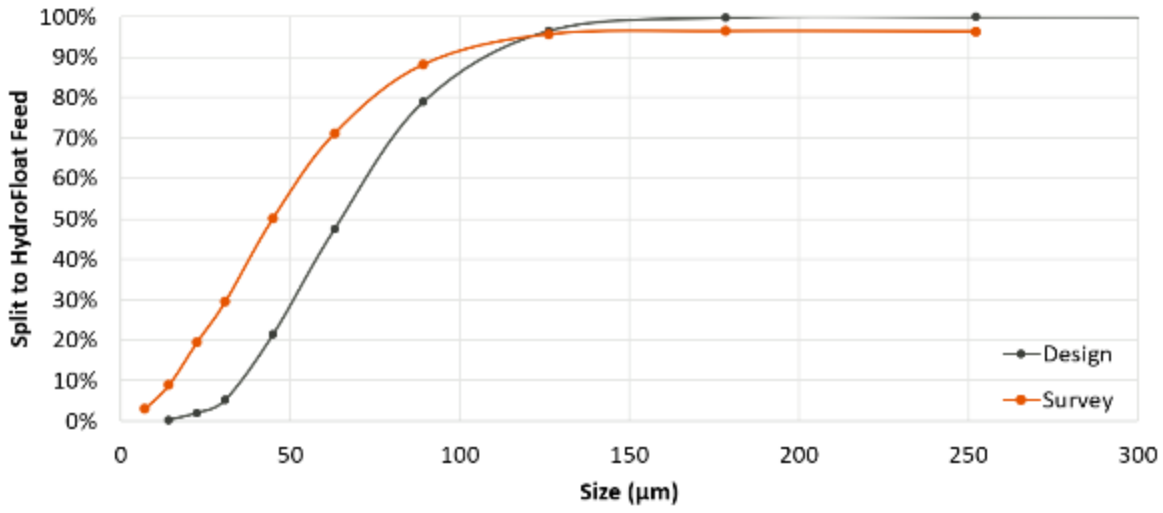



**FIG 9** – Deslime survey (June 2025) – HydroFloat® feed sizing – survey versus design.

The deslime circuit was being operated at a much finer cut size than the design, necessitated by the lower than expected primary grind size of the plant. Resultantly the feed to the two HydroFloat® cells (depicted in Figure 10) was found to be much finer than the design target case, significantly exceeding the design criteria for fines content.

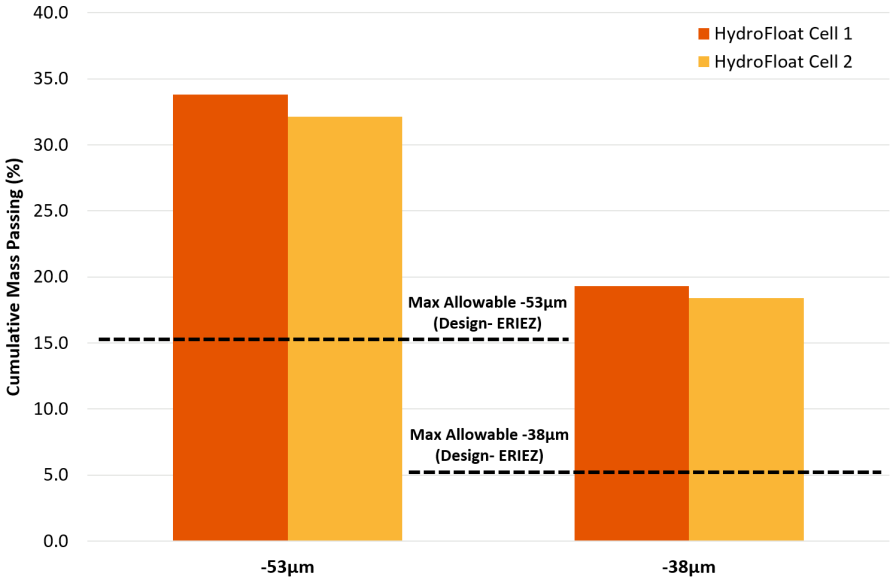



**FIG 10** – Deslime survey (June 2025) – HydroFloat® feed %mass of -53 µm and -38 µm size fractions.

## Strategies for managing the increased fines in deslime circuit

During commissioning and ramp up, because of the finer than predicted feed size distribution, a build-up of recirculating slimes load between the second and third deslime stages was identified. A strategy to manage the increase in fine particles in the circuit was developed, with the Stage 2 deslime cyclones identified as a position for a 'bleed' stream for fine material that could be rapidly implemented by blanking the underflows of two operational cyclones to reject a proportion of feed material to tailings.

Whilst this rapidly implemented change was effective at increasing circuit stability and removal of fines from the circuit, full deslime circuit survey and analysis indicated that operating the Stage 2 bypass cyclones contributed to copper losses from the mid-size fraction (25–53 µm) of approximately 7 per cent relative to deslime circuit feed.

Recommendations adopted from the survey saw the bypass shift to the third deslime stage. Two cyclones on each of the third stage deslime clusters were bypassed to tailings (via Stage 1 and Stage 2 overflow launders) instead of recirculating back to the feed of the Stage 2 cyclone cluster. This bypass provided flexibility in operation and was utilised when experiencing an increase in fines build-up in the circuit.

A further optimisation to manage fines classification is spigot and vortex finder size changes to cyclones in the Stages 2 and 3 clusters. These changes could result in improved performance and reduce the need to bypass partial streams. Due to delays in receiving parts, these changes are yet to be completed and improvements confirmed.

## Stability of recirculating loads

The deslime circuit was challenging to operate stably, exacerbated by the concentrator pushing towards a SAG mill constraint ultimately resulting in highly variable throughputs. Within the deslime circuit, the dewatering cyclone overflow reporting to the Stage 3 feed caused the most significant impacts to stability of operation, with downstream impacts on the operation of the HydroFloat® cells.

To improve stability, a strategy was implemented to control the concentrate dewatering cyclone feed pump to a minimum flow (operator set – based on plant throughput, with an added option to be a gradient scale based on throughput). The flow set point is generally higher than the feed to the hopper, meaning the hopper level is maintained by a water addition valve. This enables sufficient level control, ensures the pump does not run dry, and improves flow stability.

The same strategy was implemented on the Stage 3 feed tank, further improving overall circuit stability. The Stage 3 cyclone feed tank was designed with a larger volume to allow for surge

capacity, which was considered a successful design choice. An added deadband controller to the level has further enabled the tank to absorb surges and reduce disturbances to the Stage 3 cyclones and feed to the HydroFloat® cells.

## Robust ramp-up of coarse flotation

The HydroFloat® cell showcased a robust and rapid ramp up to design, achieving design recovery within a few weeks as demonstrated by circuit copper recoveries presented in Figure 11. A few key items ensured the success of this ramp up:

- Commissioning was led by those involved in the pilot plant operation and full circuit design, assisted by vendors for specialist support and industry experts with key knowledge and experience with HydroFloat® and coarse particle flotation commissioning at other operations.
- The availability of funds, labour and expertise to rapidly address design shortcomings during the commissioning stage was also a critical enabler of the successful ramp up.

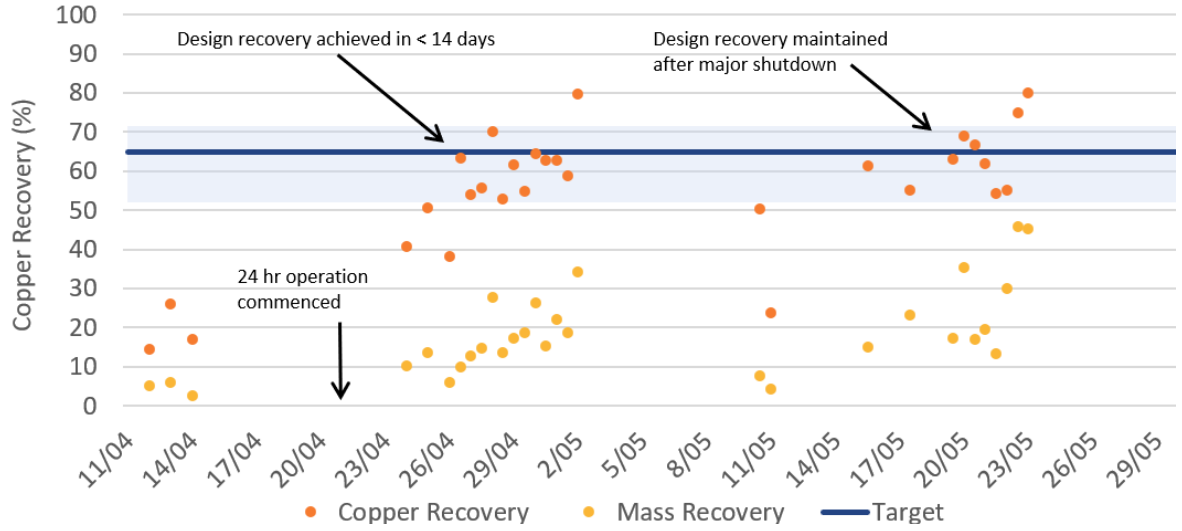



**FIG 11** – HydroFloat® commissioning and ramp up – copper recovery.

The HydroFloat® cells have operated with more stability at finer feed sizes than expected and demonstrated significantly more resilience to the presence of fines in feed as compared to the pilot and lab units. However, the load on the cleaner circuit has increased with a larger mass of fines recovered to concentrate. The pilot plant testing demonstrated that HydroFloat® stage recovery was relatively fixed for each size fraction, and this is what was experienced during commissioning. From commissioning to date, HydroFloat® stage copper recovery has been maintained at 55–70 per cent by targeting a constant mass pull from the cells. Periods of lower stage recovery are predominately driven by lower plant throughput and finer HydroFloat® feeds leading to less recoverable Cu reporting to the HF cells.

The HydroFloat® stage recovery and feed sizing on a monthly basis is shown in Figures 12 and 13.

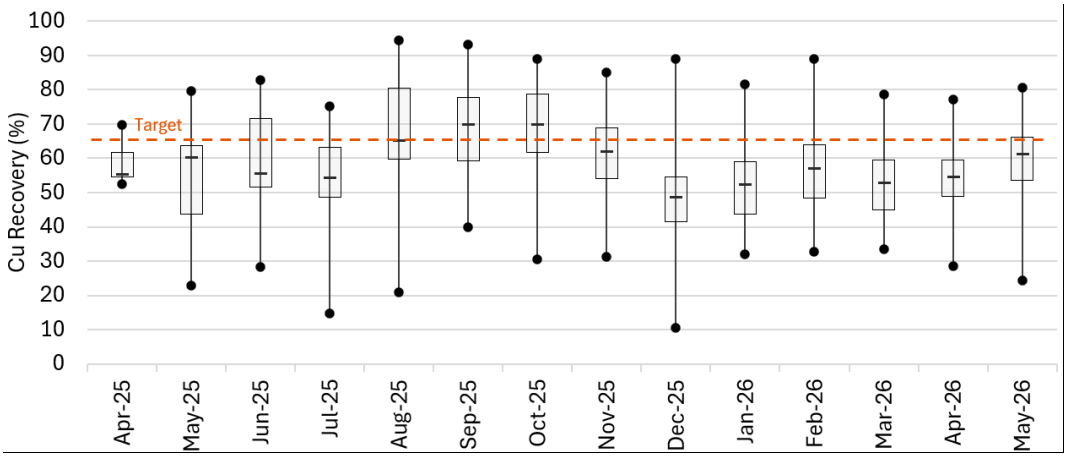



**FIG 12** – HydroFloat® copper recovery (boxplot).

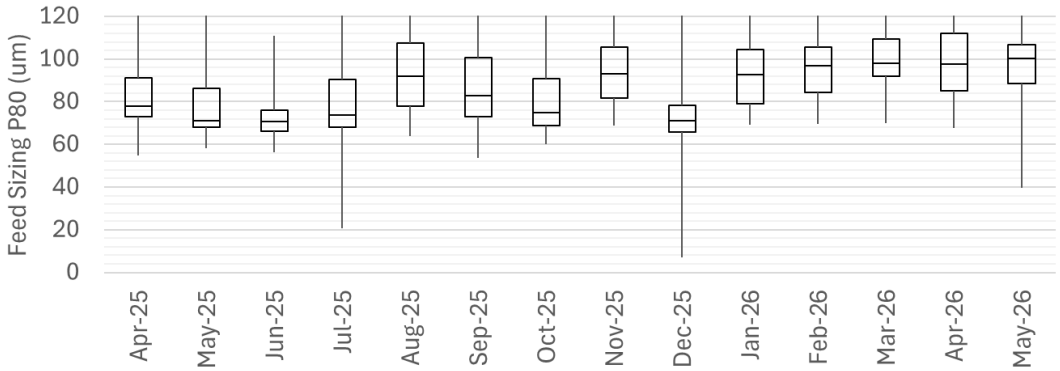



**FIG 13** – Float feed sizing (boxplot).

## COARSE FLOTATION REAGENTS

### Delayed re-commissioning of xanthate mixing

As described in Reinhold *et al* (2023), Carrapateena transitioned from SEX to Interchem INTERCOL® C4450 (a blend of dithiophosphates) as the primary collector in 2023. Pilot plant test work found that INTERCOL® C4450 would not be suitable for use in Coarse Flotation. Therefore, the coarse flotation circuit required the re-commissioning of the Xanthate mixing, storage and delivery system to the plant to allow for PAX to be used as the collector for the HydroFloat® cells.

As slurry commissioning was commenced in the coarse flotation plant, the re-commissioning of the Xanthate area was behind schedule. The site team evaluated available options including alternative reagents and the suitability of the site's current reagent suite. It was decided to trial INTERCOL® C4450 as the interim collector for coarse flotation.

### Pax performance

The use of PAX as a primary collector failed to replicate the successes experienced during the pilot plant and laboratory test work. The deleterious effect PAX had on coarse flotation performance was evident from the time it was introduced. Distinct coalescing of bubbles to the surface was observed, indicative of an unstable fluidised bed and suggesting overdose of collector. Complete froth collapse was observed within the Jameson Rougher and Cleaner flotation circuit.

Survey results in July 2025, comparing INTERCOL® C4450 and PAX confirmed the observations (see the photographs of the HydroFloat® surface in Figure 14), even at heavily reduced dosing rates. While the design PAX requirement was 200 g/t, and with dosages lowered to 1.0 g/t, the circuit continued to show unstable flotation characteristics. Surveys found INTERCOL® C4450 recovered 10–20 per cent more copper than PAX with a reduced impact to flotation downstream. Selected survey results around the HydroFloat® cells under different reagent type and addition rates are summarised in Table 1.



**FIG 14** – HydroFloat® cell: (left) using C4450; and (right) using PAX.

**TABLE 1**

HydroFloat® collector survey results – PAX versus C4450.

| Reagent | Dosage rate | Feed | Con | Tail | % Cu Rec |
|---|---|---|---|---|---|
| PAX | 1.0 g/t | 0.11 | 0.60 | 0.07 | 41.2 |
| | 1.5 g/t | 0.13 | 0.60 | 0.08 | 44.4 |
| | 4.0 g/t | 0.15 | 0.53 | 0.09 | 49.4 |
| C4450 | 4.0 g/t | 0.11 | 0.35 | 0.06 | 56.5 |
| | 8.0 g/t | 0.11 | 0.28 | 0.06 | 62.5 |

INTERCOL® C4450 was selected as the collector of choice for coarse flotation. A permanent dosing set-up for neat collector to the HydroFloat® cells was established, creating the option for neat reagent trials. During the commissioning process, several lab scale HydroFloat® tests were completed utilising PAX on fresh plant feed and the degraded performance observed in the plant was not replicable at lab scale, with lab scale results matching prior lab and pilot work.

## CLEANER CIRCUIT

The Jameson flotation circuit was initially commissioned without regrind due to the delayed commissioning of the VTM. Without a regrind circuit, the plant was able to produce a high pyrite concentrate with low-grade Cu and low impurities (Cu 1.37 per cent, Fe 45.8 per cent, S 50.4 per cent, Si 1.3 per cent). This allowed site to complete slurry commissioning of the cleaner circuit, while awaiting VTM capability, and delivered value with a proportion of Cu being recovered, with the CF concentrate diverted to the main plant regrind circuit for regrind and cleaning.

## Poor rougher froth stability – pulp chemistry investigation

Once the VTM commissioning was completed, the Rougher Jameson Cell experienced difficulties producing a stable froth. Extensive testing was conducted to identify the cause of this. Lab-scale flotation tests were performed and within lab conditions, float tests were able to produce a concentrate with grades and recoveries comparable to the design test work during piloting.

Further testing was conducted to understand the pulp chemistry conditions; pH, eH dissolved oxygen and dissolved oxygen demand. The results highlighted to the team that the flotation conditions for the rougher and cleaner circuit were far from optimal with a highly reducing environment. A high dissolved oxygen demand was also identified and hypothesised to be a cause for poor copper to pyrite selectivity, as demonstrated by Owusu *et al* (2014). Steps were taken to aerate the slurry for

improved performance by installing SlamJet® Spargers in the Jameson cell recycle pump discharge lines and also running the first Jameson cell as a pre-aeration vessel.

Test work and analysis was conducted by Uni SA and MZ Minerals on various streams across the circuit including; Ethylenediaminetetraacetic acid (EDTA) extraction, Time-of-Flight Secondary Ion Mass Spectrometry (ToF-SIMS) analysis and gas chromatography with flame ionization (GC-FID) analysis to understand the root-cause of the froth instability and collapse. The results from the EDTA extraction found minerals in the pulp oxidise rapidly, the level of oxidation in the circuit was considered normal for sulfide ores and couldn't be linked to the roughers froth instability. The ToF-SIMS analysis (image and record organic and inorganic mass spectral data) found the froth stability was not linked to modifications to the surface of minerals. GC-FID analysis found frother in solution to be within expected ranges with some accumulation in the rougher tails. Further analysis found the INTERCOL® C4450 collector was detected in higher concentration in multiple streams within the circuit. The analysis identified that the excessive collector dosage remained unadsorbed and gradually accumulated within the process water in the plant, causing disturbances to the froth phase. Ultimately this supported what the team observed when collector was turned off on the HydroFloat®.

Figure 15 shows the calculated residual collector in solution at various points in the circuit based on surveying and GC-FID analysis. Highlighted are the calculated residual collector concentration for 'good' plant conditions when a stable froth was observed on all cells versus 'bad' plant conditions in which froth collapse had occurred, with field corresponding observations shown in Figure 16. Limiting both the collector dose rate to the HydroFloat® and downstream flotation circuit was found to be the most effective solution to maintaining a stable froth allowing for the flotation circuit to function.

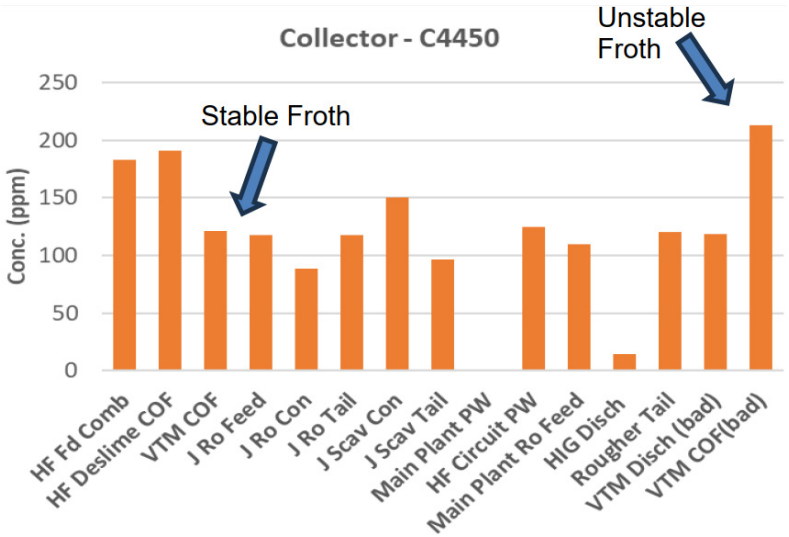



**FIG 15** – Gas chromatography results (GC-FID).



**FIG 16** – Rougher Jameson Cell froth: (left) unstable, collector overdosed condition; (right) stable, lower collector dose situation.

## Staged collector dosing

Post-GC-FID analysis with the focus of reducing total circuit collector addition, a comprehensive review of the collector addition in the circuit was undertaken. The Jameson flotation circuit proved to be very susceptible to a rapid change in performance even with low dosages of collector, and it was determined that the residual collector in the process water was creating the instability. The team performed rougher feed hot floats in the lab to compare results of collector (C4450) versus no collector.

Findings from this campaign of weekly hot floats showed that in every instance staged dosing of collector to the rougher feed in addition to dosing to the regrind feed hopper resulted in an increase in copper recovery.

Staged collector dosing was adopted to the head of the rougher and the rougher scavenger cell. To spread the dosage across the cells and reduce the undesirable impacts on the froth phase.

# STABILITY OF THE JAMESON FLOTATION CIRCUIT

As discussed previously, froth stability in the Jameson flotation circuit was difficult to achieve once the VTM was commissioned and the HydroFloat® concentrate was reground. Several changes to the operating conditions and froth geometry of the Jameson cells was necessary to improve froth stability and mobility.

## Frother

The Carrapateena orebody is known for its tenacious froth. The main flotation circuit uses little to no frother, the frother used being a weak, low glycol content frother. Early observations within the rougher and rougher scavenger Jameson cell was that the cells needed to be operated at very shallow froth depths to collect concentrate, and they were unable to produce a stable froth. This saw the team trial, and ultimately change, to a frother with a higher glycol content (glycol-ether based) with an eightfold increase in frothing strength compared with the site's standard frother.

This change in frother netted two benefits for the circuit; the ability to operate at increased froth depths (in lieu of producing a 'pulpy' concentrate) and to improve the froth transport. The on-flow impact of this change meant the HydroFloat® cells frothers would also change, and the addition rate used sparingly to reduce the risk of residual frother in process water system, impacting the main flotation circuit.

## Froth crowding

Within a few weeks of operating, it became clear there wasn't sufficient mineral loading in the circuit to sustain the open area, and that the frother change described above was in part overcoming a poorly configured froth geometry. The team promptly worked with the OEM (original equipment manufacturer) on sourcing froth crowders for the Jameson flotation circuit.

Froth crowders enabled the cells to operate at increased froth depths for improved grade control. To reduce the impacts of having no froth crowding on the cells and waiting until the OEM arrived on-site, the team resourcefully sourced blue plastic tubs (see Figure 17) to perfectly fit the width of the Jameson Cells open area, and these were used as an interim froth crowding solution. This demonstrated ingenuity in using the tools available to find a solution to the problem.



**FIG 17** – Interim froth crowder solution using plastic tubs.

Ultimately the OEM froth crowders were installed (see Figure 18) to increase the froth loading across all Jameson cells (both Rougher and Cleaners). Whilst a significant improvement, these still came with their own challenges. The design and tolerance limitations resulted in a gap between the crowder and the lip at the downcomer causing short-circuiting of pulp to concentrate, and the angle of the froth crowders are too shallow resulting in bubble coalescence surging concentrate and pulp towards the lip. Carrapateena has since worked with Glencore Technology on an improved froth crowder design.



**FIG 18** – Glencore Technology supplied froth crowders: (left) installed; and (right) 3D model.

The Jameson cell provides a key advantage in managing the concentrate grade-recovery trade-off through the application of wash water to reduce gangue entrainment. Following installation of froth crowders, modifications to wash water distribution (see Figure 19) enabled operation with a positive water bias, significantly improving gangue rejection. Plant experience demonstrated that increasing wash water to match concentrate flow reduced non-sulphide gangue (NSG) in concentrate from approximately 8–10 per cent to below 5 per cent, providing an effective control lever for maintaining concentrate quality, with further improvements expected when a feed sizing is at target of 20 µm.

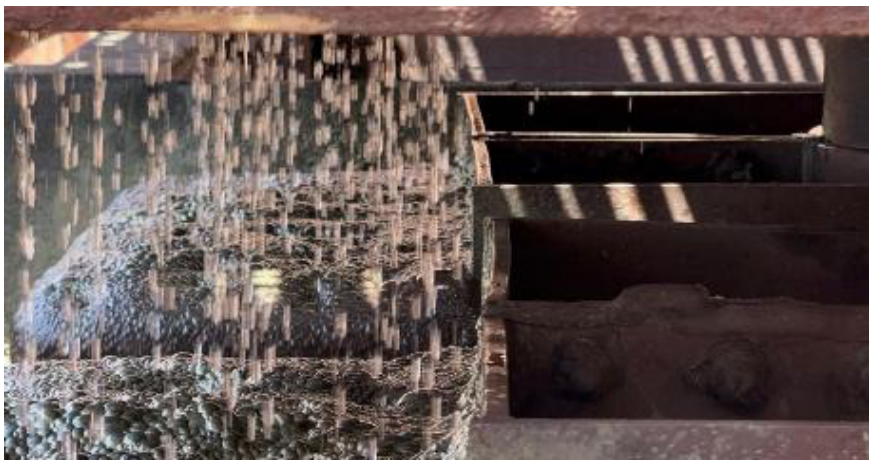


**FIG 19** – Jameson Cell – cleaner concentrate with wash water and froth crowding.

## Air and froth depth stability

Air and level control of the Jameson cells were poor as a result of the valve types (air) chosen and the dart valve and seat sizing. Air rates were fixed for a period of time due to the rapid surges in valve control. The original valve installed for air control were V-ball valves which were proved to be insufficiently fit for purpose and were changed to wafer type butterfly valves (the same style of valve used on the Jameson cells in the main flotation plant). This significantly improved the air control.

The dart valves across all cells needed to be downsized with all valves operating at less than 20 per cent opening, creating a non-linear flow and difficultly in controlling froth depth. Due to the success experienced with the main flotation plant Jameson cells, ball floats were retro-fitted by the site team and used as the primary method of froth depth control in lieu of the OEM-supplied pressure sensors.

## CF CLEANER PERFORMANCE

The Jameson flotation circuit has had incremental increases in performance since commissioning, addressing various circuit stabilising initiatives and improvements, some of which are described above. In Figure 20, the improvement in the CF cleaner circuit recovery over time is illustrated, showing both an improvement in average performance as well as a reduction in variability over time. Performance is still below target.

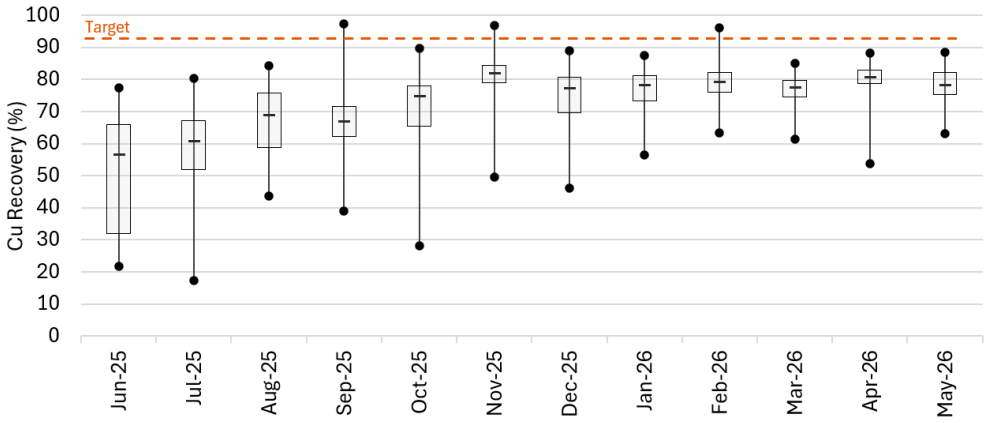



**FIG 20** – Jameson Flotation circuit stage recovery.

## Modifying the HydroFloat® operating strategy for downstream impacts

Evaluation of circuit performance identified a strong dependency between HydroFloat® performance and downstream flotation response, particularly the impact of rougher feed grade on overall circuit recovery. This prompted a review of the HydroFloat® operating strategy to better align upstream performance with downstream requirements.

Analysis highlighted that the grade-recovery relationship within the HydroFloat® is relatively weak, as demonstrated in Figure 21, with limited incremental copper recovery achieved at higher mass recovery conditions. Increasing mass recovery beyond design conditions resulted primarily in increased gangue recovery, with minimal benefit in copper recovery. This introduced two key negative impacts: increased load to the regrind circuit, reducing its ability to achieve target particle size, and dilution of the rougher flotation feed, requiring greater upgrading duty in the downstream flotation circuit.

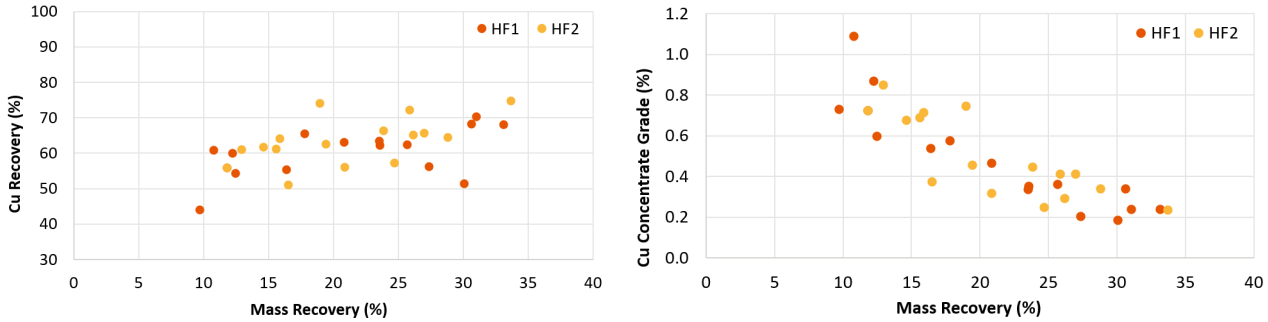



**FIG 21** – (left) HydroFloat® – mass recovery versus copper recovery; and (right) HydroFloat® – mass recovery versus Cu concentrate grade.

Based on these findings, the operating strategy has been refined to target approximately 20 per cent mass recovery (design target) and a rougher feed grade of ~0.40 per cent Cu. This represents an optimal balance between copper recovery and concentrate quality, reducing unnecessary gangue recovery while maintaining sufficient feed grade to support efficient downstream flotation and regrind performance.

## Regrind circuit product sizing

The HydroFloat® concentrate (regrind feed) is characterised by significant copper deportment within complex and binary particle associations (Figure 22), highlighting effective liberation as a key requirement for downstream flotation performance.

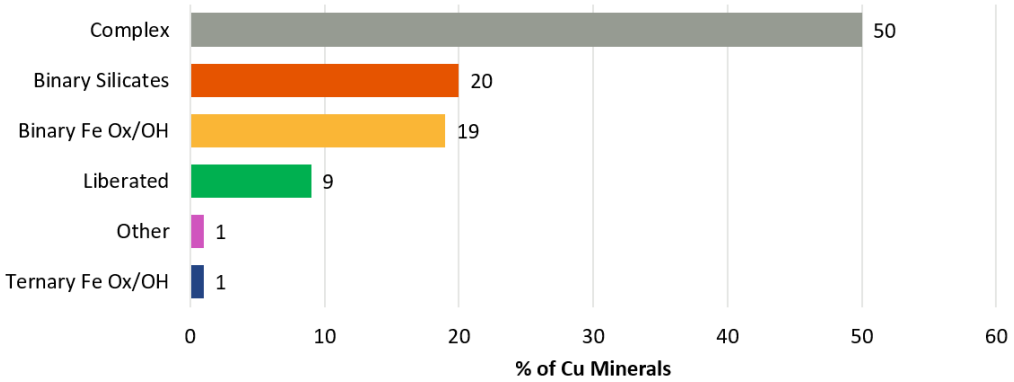



**FIG 22** – November 2025 mineralogy: HydroFloat® concentrate Cu mineral locking.

This observation is consistent with the pilot plant and downstream test work results where it was observed that a significant uplift in Cu recovery (6.8 per cent) when decreasing the grind size from 35 µm to 20 µm, leading to a regrind product size design target of 20 µm.

Due to the focus during early commissioning being on maximising flotation froth stability, regrind product size had not been an area of primary focus, with plant performance to date being unable to achieve the design target as highlighted in Figure 23, showing the regrind circuit product grind size over time.

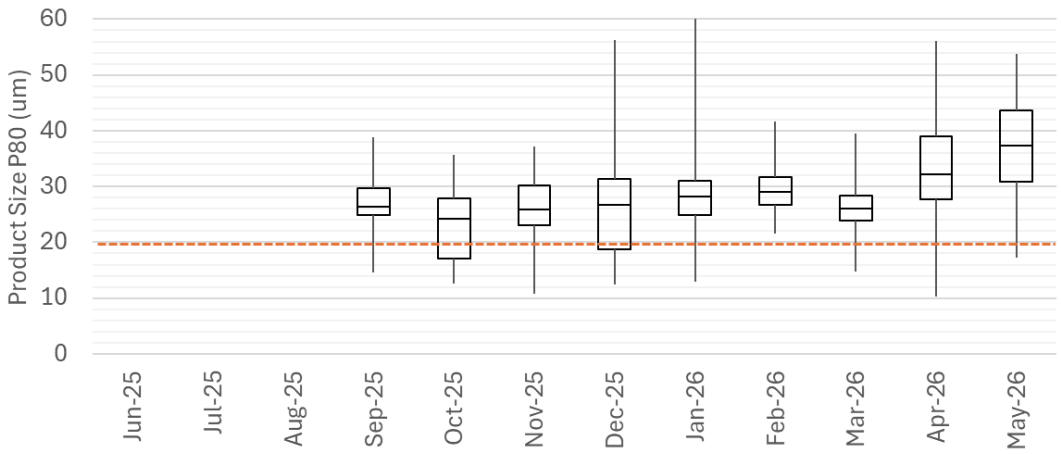



**FIG 23** – CF regrind cyclone overflow $P_{80}$.

Detailed survey work identified a strong density-driven bias within the regrind classification circuit. Cyclone performance is dominated by mineral density rather than size, with dense hematite preferentially reporting to the underflow and recirculating to the mill, while lower-density silicate particles are misclassified to the overflow at coarser sizes.

This behaviour results in a reduced utilisation of grinding energy. Hematite particles are repeatedly reground despite already meeting target size, while silicate particles requiring further liberation, bypass the mill at coarse size fractions. Mineralogy sizing highlights the magnitude of this effect, with silicates reporting to the overflow at ~39 µm compared to ~20 µm for NSG, FeOx/OH, well below the target grind size (see Figure 24).

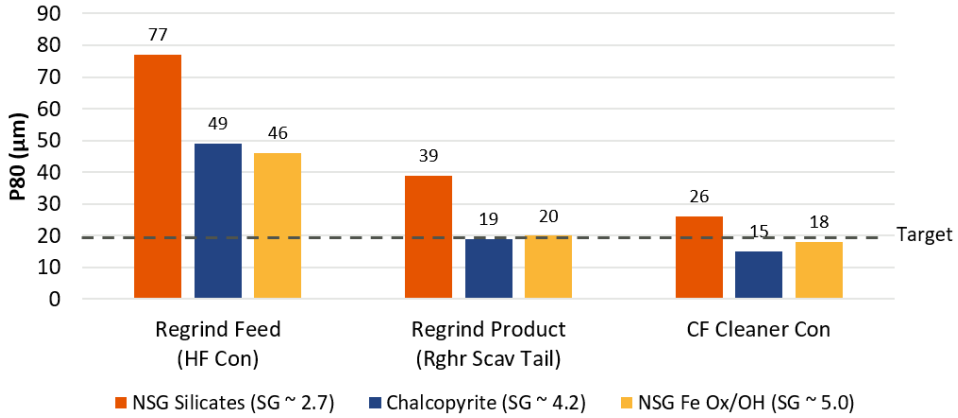



**FIG 24** – November 2025 mineralogy: mineral $P_{80}$'s across the regrind and flotation circuit.

Assay-by-size data across multiple circuit streams reinforces this mechanism. Coarse fractions have a higher silica content, while NSG FeOx/OH is concentrated in finer fractions and the circulating load. This confirms that classification is driven by density segregation rather than effective size separation, directly contributing to a coarse cyclone overflow product and limiting downstream flotation performance. Figure 25 highlights a significant quantity of +53 µm particles surviving the mill.

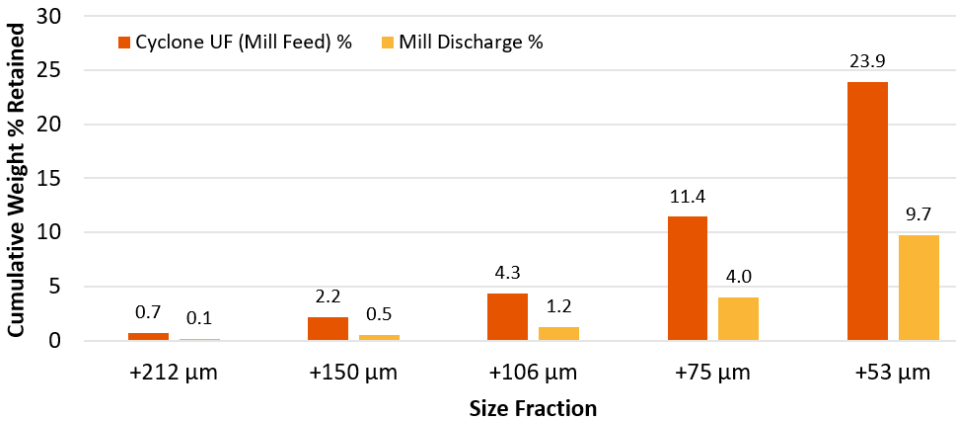



**FIG 25** – Regrind survey October 2025 – coarse fractions in mill discharge.

As a result, increasing the mill power has proven ineffective, with additional energy largely expended on already fine hematite (FeOx) rather than reducing the size of coarse silicate. The limiting factor is therefore classification behaviour, not installed grinding capacity.

A key opportunity lies in modifying the mill feed configuration. Conversion of the Vertimill® to bottom-feed operation is expected to reduce short-circuiting, improve particle residence time distribution, and increase interaction of coarse silicate particles with the grinding media. This represents a low-capital, high-impact pathway to improve grind size control and unlock further recovery in the downstream flotation circuit.

## OVERALL CIRCUIT PERFORMANCE

The design intent of the Carrapateena CF circuit was to offset the Cu recovery loss arising from relaxation of the primary grind size from 75 µm to 125 µm, in order to improve the economics of a throughput increase to 7 Mt/a. Despite key challenges identified during commissioning and ramp-up and discussed in this paper, inclusive of a finer than anticipated primary grind, the CF circuit has demonstrated robustness in operation and achieved its design intent, with overall plant Cu recoveries maintained 91.2 per cent Cu when operating at 7 Mt/a rates as compared to 90.6 per cent when operating at lower rates with a flotation feed $P_{80}$ of 75 µm. The CF circuit has been observed to provide a Cu recovery benefit of 2–2.5 per cent for throughput rates below 7 Mt/a and of 3–3.5 per cent when running at or above design throughputs. In Figures 26, 27 and 28, the performance of the Carrapateena CF circuit as a function of overall plant recovery across its ramp-up period is demonstrated.

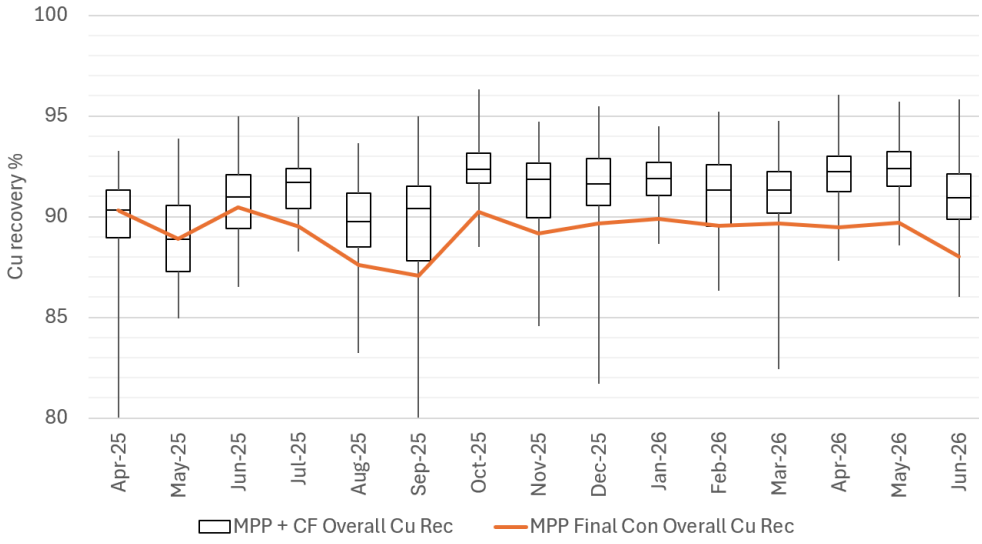



**FIG 26** – Carrapateena Cu recovery during CF commissioning and ramp-up.

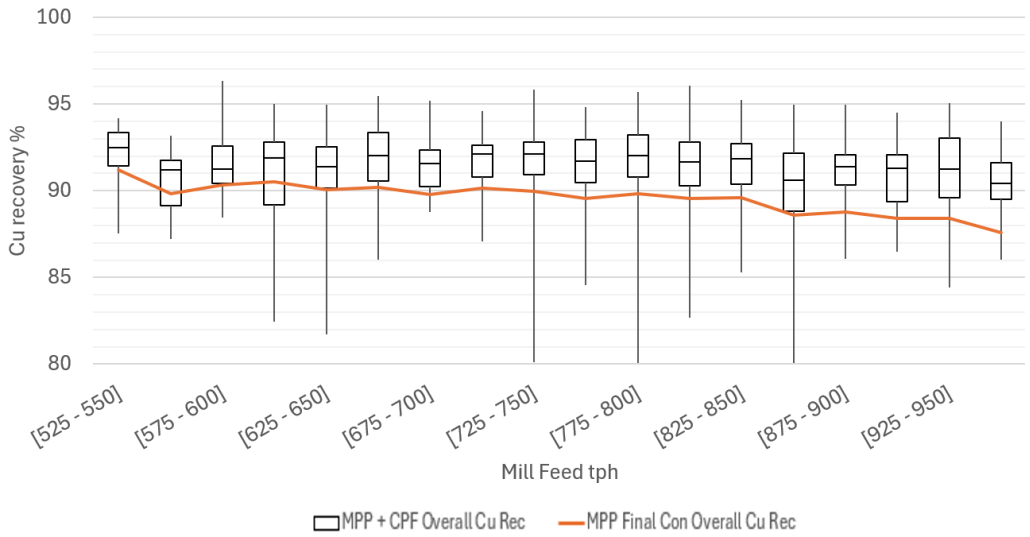



**FIG 27** – Carrapateena Cu recovery as a function of throughput.

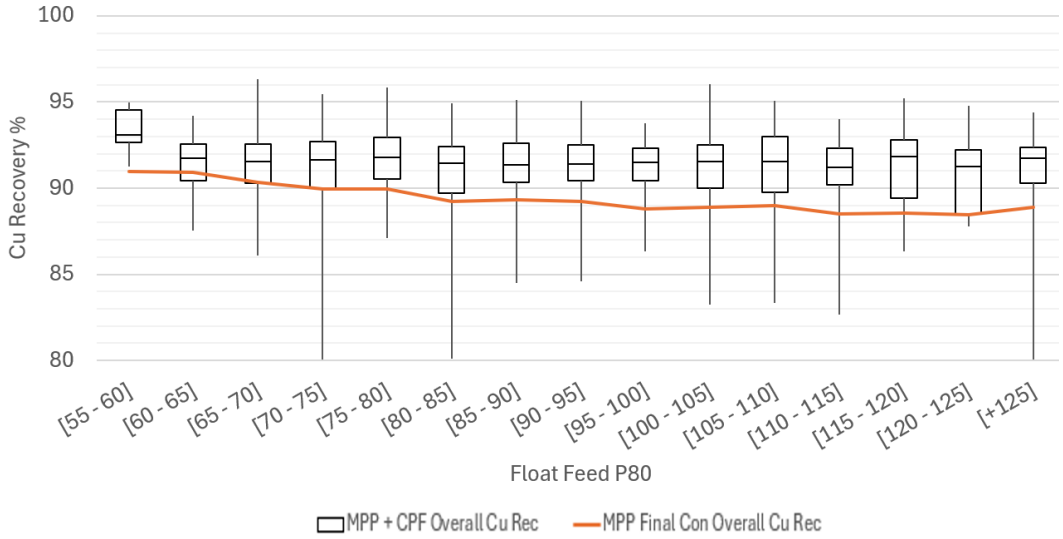



**FIG 28** – Carrapateena Cu recovery as a function of primary grind size.

The benefit derived from the CF circuit is expected to increase in the future as Carrapateena transitions into block cave mining with the harder ore increasing the primary grind size, pushing more copper to the CF circuit. A number of improvements have been identified throughout this paper with two key areas where tangible and achievable improvement is believed to be:

1. 0.15 per cent (5 per cent relative) Cu recovery uplift by maintaining HF unit stage Cu recovery at or above design of 65 per cent.
2. 0.22 per cent (6–7 per cent relative) Cu recovery uplift by enhancing Cu liberation in the CF cleaner circuit by achieving design regrind $P_{80}$ target of 20 µm.

## LESSONS LEARNED AND OPTIMISATION PATH

Commissioning and early operation of the coarse flotation circuit has highlighted that overall circuit performance is strongly governed by classification efficiency and stability across each sub-circuit, rather than individual equipment constraints. In particular, maintaining control of particle size distribution to the HydroFloat® and achieving consistent liberation in the regrind circuit have emerged as the dominant drivers of recovery.

Within the deslime circuit, the importance of cyclone configuration and operating strategy has been clearly demonstrated. Circuit performance is highly sensitive to small changes in cut size and circulating load, with sub-optimal classification directly impacting HydroFloat® feed quality. Early

operation has shown that maintaining a stable and sufficiently coarse feed is critical for fluidised bed stability and downstream performance, reinforcing the need for ongoing optimisation of cyclone configurations and operating conditions through detailed survey work.

HydroFloat® operation has proven robust, however achieving consistent concentrate production remains a key area of focus. While feed stability in terms of flow, density and pressure has improved, variability in concentrate mass pull and grade continues to propagate downstream, particularly impacting the Jameson flotation circuit. This highlights the importance of not only maintaining stable operating conditions, but also ensuring that sufficient concentrate grade is consistently delivered to the regrind and cleaning stages. Reagent selection has also demonstrated a strong influence on circuit stability and selectivity, reinforcing the need for careful reagent optimisation under site-specific conditions.

The regrind circuit has been identified as the primary constraint to achieving full circuit recovery potential. While the circuit is designed to achieve a $P_{80}$ of 20 µm, this target has not yet been consistently met, with coarse material persisting in key streams. This has a direct and material impact on downstream flotation performance, given the strong dependence of recovery on liberation at fine grind sizes. As a result, the regrind circuit represents the most significant opportunity for further recovery uplift. Ongoing work is focused on improving cyclone classification efficiency and addressing the underlying drivers of coarse particle bypass, including both cyclone configuration and mill operating conditions.

Downstream, operation of the Jameson flotation circuit has highlighted a clear trade-off between mass recovery, copper recovery, and concentrate grade. Increasing rougher concentrate flow capacity improved copper recovery; however, beyond ~80 per cent rougher recovery, an inflection point is observed where incremental copper recovery is accompanied by a disproportionate increase in mass recovery. This results in rapid dilution of concentrate grade and reduced ability to produce a ‘clean’ concentrate, reinforcing the need to operate within an optimal grade-recovery window rather than maximising copper recovery.

Reagent strategy has also proven critical, with the circuit highly sensitive to collector addition. While laboratory tests indicate improved recovery with increased collector, plant performance shows that excessive collector leads to froth instability/collapsing. This highlights the importance of managing collector addition across the full circuit, not just at the point of application.

Froth handling was another key learning, with the introduction of froth crowders significantly improving froth stability, mineral loading, and grade control. Overall, circuit performance is governed by the interaction between mass pull, reagent regime, and froth transport, requiring tight control to maintain both recovery and concentrate quality.

Finally, the abrasive nature of the coarse flotation streams has highlighted the importance of mechanical design and materials selection. Premature wear of pipework, liners and key components has impacted reliability and availability, demonstrating that durability considerations are critical when treating coarse, high-density material. Selection of more wear-resistant materials and improved maintenance strategies will be essential to ensure long-term circuit reliability.

Collectively, these learnings emphasise that successful implementation of coarse flotation requires an integrated approach to circuit optimisation, with particular focus on classification control, regrind performance, and circuit stability.

## ACKNOWLEDGEMENTS

Sincere appreciation is extended to the Carrapateena Metallurgy team, both past and present, for their ongoing commitment and collaboration throughout this work. In particular, we acknowledge the significant contributions of J Seppelt, T Philbey, and the broader leadership groups who have provided consistent support across the transition from OZ Minerals to BHP.

We also gratefully recognise the vital technical guidance, expertise, and field assistance received during the early phases of pilot plant development, test work, and commissioning. Special thanks are extended to:

- Dr M Zanin – MZ Minerals Pty Ltd

- R Dadzie – University of South Australia (UniSA)
- L Vollert – VolPro Pty Ltd
- B Seaman – Paradocs Metallurgy
- C Aisthrope and L Webb – Xenco Resources

Their collective efforts, dedication, and willingness to share knowledge have been instrumental to the progress and success of the project.


## REFERENCES


Arburo, K, Zuniga, J, McDonald, A, Valdes, F, Concha, J and Wasmund, E, 2022. Commissioning a HydroFloat® in a copper concentrator application, presented at Copper 2022, Canada.

Eriez, 2026. HydroFloat® Flotation Technology – Product Overview and Operating Principles, Eriez Flotation Division. Available from: <https://www.eriez.com/products/flotation/hydrofloat>

Owusu, C, Brito e Abreu, S, Skinner, W, Addai-Mensah, J and Zanin, M, 2014. The influence of pyrite content on the flotation of chalcopyrite/pyrite mixtures, *Minerals Engineering*, 55:87–95.

Reinhold, J, Assmann, A, Brodie, E, Van Sliedregt, J, Burns, F, Tsatouhas, G and Seppelt, J, 2023. Replacement of Sodium Ethyl Xanthate Collector at Carrapateena, presented at MetPlant 2023, Australia.

Vollert, L, Akerstrom, B and Seaman, B, 2019. Newcrest's industry-first application of Eriez HydroFloat®™ technology for copper recovery from tailings at Cadia Valley Operations, presented at Copper 2019, Canada.

# From laboratory to industry – accelerating NaHS oxidation to increase Cadia's Molybdenum Plant run time

*P Sharman[1], C Dobson[2], S Gunn[3] and M Lisso[4]*

1. Specialist – Process Engineering, Newmont Mining, Subiaco WA 6008. Email: phillip.sharman@newmont.com
2. Superintendent Metallurgy, Newmont Mining, Orange NSW 2800. Email: courtney.dobson@newmont.com
3. Manager – Ore Processing, Newmont Mining, Tanami NT 0872. Email: simon.gunn@newmont.com
4. Plant Metallurgist, Newmont Mining, Orange NSW 2800. Email: mussa.lisso@newmont.com

## ABSTRACT

In January 2022, Newmont Cadia commissioned a Molybdenum (Moly) Plant to separate molybdenite from Cadia's bulk copper-gold concentrate. The separation process uses sodium hydrosulfide (NaHS) in a flotation circuit that incorporates a High Intensity Grinding (HIG) regrind mill.

Although the plant consistently achieves its design instantaneous throughput rate, an opportunity was identified to increase run time to support delivery of annual molybdenum production targets. This opportunity was first evaluated through laboratory scale test work before being implemented on-site.

This paper outlines how laboratory-scale investigations identified methods to accelerate the oxidation of NaHS – a necessary step to eliminate the risk of hydrogen sulfide generation in the plant. Accelerating this oxidation significantly reduced the time required to ramp down the Moly Plant prior to maintenance shutdowns, thereby improving overall plant run time.

## INTRODUCTION

Newmont's Cadia Valley Operation is in the Central West of New South Wales, 25 km south of Orange. Cadia East underground ore is processed through two concentrators: Concentrator 1, which treats approximately 75 per cent of the ore, and Concentrator 2, which treats the remaining 25 per cent. Both concentrators produce a bulk copper-gold flotation concentrate as well as gold bullion. The bulk concentrate streams are combined and dewatered at Newmont's Dewatering Facility at Blayney before being transported by rail to Port Kembla for export.

In 2016, it was identified that the molybdenum (Mo) grade in Cadia East ore was increasing, with mine models predicting peaks exceeding 100 g/t Mo. Because molybdenite is naturally hydrophobic, much of it reports to the bulk flotation concentrate. This raised concerns about the molybdenum grade reaching penalty levels for existing customers, while also highlighting an opportunity to generate additional revenue by producing a separate molybdenum concentrate. A study into the feasibility of installing a dedicated Moly Plant to process the bulk copper-gold concentrate was completed and endorsed. Between 2017 and 2020, detailed study and design work progressed, leading to the commissioning of Australia's only operating Moly Plant between July 2021 and January 2022. Operational optimisation has continued since commissioning to enhance plant performance.

## MOLY PLANT FLOTATION

### Flow sheet

Cadia's Moly Plant is located adjacent to the concentrate pipeline to the Dewatering Facility in Blayney, 3 km downstream of the copper (Cu) concentrators at Cadia. Bulk concentrate is fed into two conditioning tanks as per Figure 1. Sodium hydrosulfide (NaHS), emulsified diesel, defoamer and carbon dioxide are the primary reagents dosed to the circuit. NaHS is used as a copper depressant, emulsified diesel acts as a pseudo collector for the hydrophobic molybdenite, defoamer

is used to offset the high glycol frother content from the Cadia Cu concentrators to manage tenacious froths, and carbon dioxide is used to reduce pH.

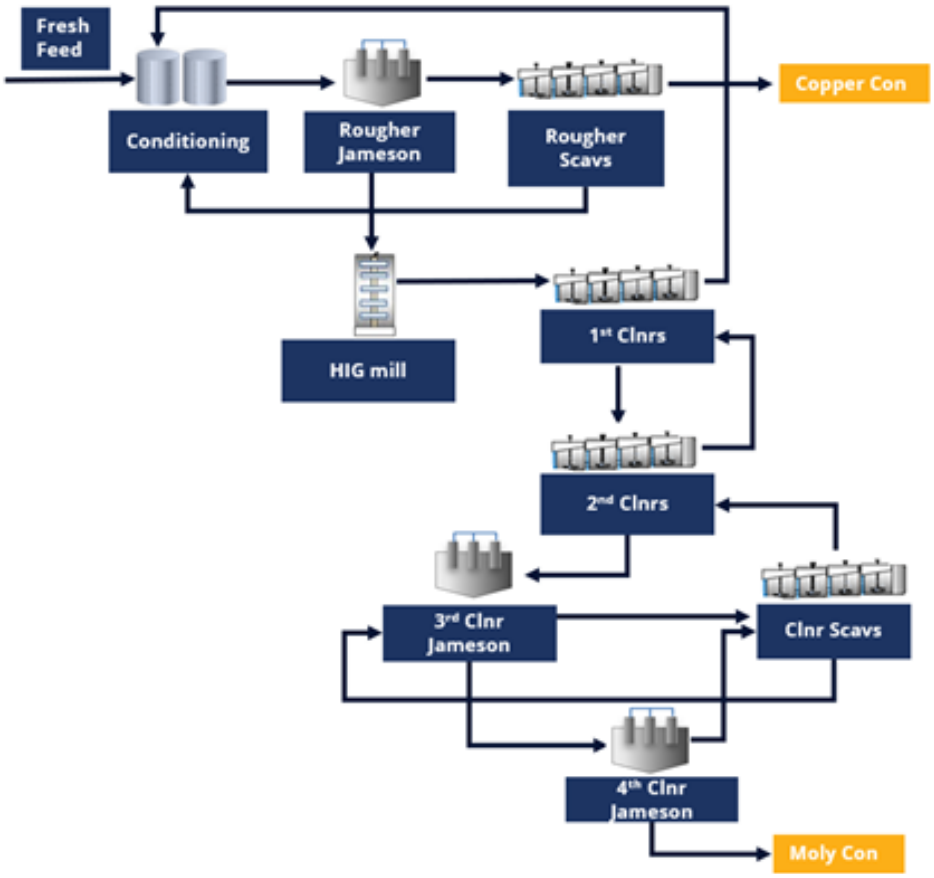



**FIG 1** – Moly Plant flow sheet.

Slurry conditioned with reagents is fed to a E2532/6 rougher Jameson Cell where it is upgraded from a fresh feed grade of approximately 0.6 per cent Mo to 10–30 per cent Mo. Concentrate progresses to a 7 m intermediate flotation thickener, to control the slurry density feeding the regrind mill and subsequent cleaning circuit. Rougher Jameson Cell tailings report to five Metso TC30 scavenging flotation cells, with concentrate recirculated to the feed conditioning tanks. Rougher scavenger tailings are copper-gold concentrate, and this is thickened and then pumped to the Dewatering Facility.

Intermediate thickener underflow material feeds a 60 kW Metso High Intensity Grinding (HIG) regrind mill prior to the first stage of cleaning. Five stages of cleaning are utilised to upgrade rougher concentrate to 50 per cent Mo. The cleaners are a combination of Metso TC5 flotation cells and Z1200/1 Jameson Cells. The tailings of all cleaning stages recirculate to the previous stage, creating five highly interdependent recirculating loads. The recirculating loads are effective at crowding out entrained Cu particles, a key penalty element in molybdenite concentrate. The final product is thickened, filtered and dried on-site with a 7 m concentrate thickener, PF60 Metso Larox filter, and Enercom Screw Dryer. Molybdenite concentrate is bagged into one tonne bulk bags and trucked to Botany Bay for shipment.

## Sodium hydrosulfide and pH

Molybdenite is separated from copper and iron sulfides using NaHS. NaHS solution dissociates into sodium ($Na^+$) and hydrosulfide ($HS^-$) ions and is dosed to decrease the Oxidation Reduction Potential (ORP) of the process slurry (Amelunxen *et al,* 2019). At an ORP of approximately -550 $mV_{Ag/AgCl}$ (Ag/AgCl reference electrode), the collector adsorption reaction on copper sulfide minerals is reversed via the following reactions. In the equations below, X represents collector.

$$2X^- + CuS \rightarrow Cu(X)_2 + S^{2-} \text{ (favoured above -550 mV)} \quad (1)$$

$$NaHS \rightarrow Na^{+} + HS^{-} \quad (2)$$

$$Cu(X)_2 + HS^{-} \rightarrow CuS + 2X^{-} + H^{+} \text{ (favoured below -550 mV)} \quad (3)$$

Excess NaHS is dosed into the process to drive the equilibrium to the right of Equation 3. The stripping of collector from sulfide minerals returns these particles to a hydrophilic state, allowing the naturally hydrophobic molybdenite to be recovered via flotation, as discussed by Amelunxen *et al* (2019).

As the ORP decreases, the pH of the slurry tends to increase, consistent with the Nernst equation, which links redox potential, pH, and temperature. Operating at elevated pH can adversely affect molybdenum flotation kinetics due to the formation of hydrophilic hydroxide species on the surface of molybdenite. This reduces the rate of molybdenite flotation and makes separation from copper increasingly difficult, consistent with the decline in the flotation rate constant above pH 11 observed by Amelunxen *et al* (2019). For this reason, the Moly Plant is operated at a target pH of approximately 10.5. Sparging carbon dioxide into the process slurry helps maintain this pH by counteracting the natural pH increase associated with NaHS addition.

A key risk when lowering the pH of slurry conditioned with NaHS is the potential formation of toxic hydrogen sulfide ($H_2S$) gas. As pH falls below 10, an increasing proportion of $HS^-$ converts to $H_2S$, as shown in Figure 2. Localised agitation can further promote $H_2S$ release by enhancing mass transfer from the aqueous phase to the gas phase. Multiple controls are in place at the Moly Plant to mitigate this risk, as outlined by Dobson *et al* (2025).

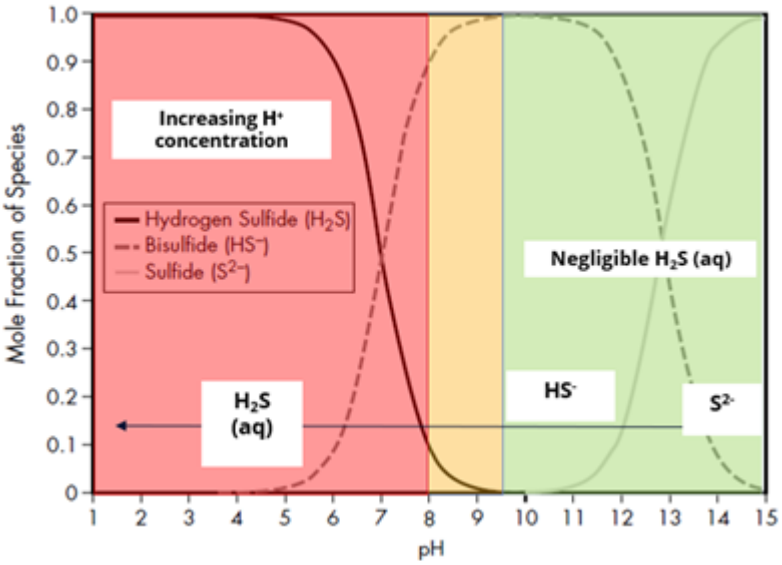



**FIG 2** – $HS^-/H_2S$ fraction versus pH.

## SHUTDOWN SAFETY

## NaHS oxidation – bleach

Moly Plant shutdowns require complete destruction of $HS^-$ in the circuit to eliminate the potential for $H_2S$ gas generation and to ensure safe confined space entry. Destruction of $HS^-$ is achieved by oxidising it to non-volatile, more oxidised sulfur species. The oxidation pathway of hydrosulfide in alkaline Moly Plant process water proceeds sequentially from $HS^-$ to elemental sulfur ($S^0$) and polysulfides ($S_n^{2-}$), then to thiosulfate ($S_2O_3^{2-}$), and ultimately to sulfite ($SO_3^{2-}$) and sulfate ($SO_4^{2-}$) as the ORP increases. During the shutdown process, slurry ORP is raised to approximately -250 $mV_{Ag/AgCl}$, equivalent to approximately -0.5 $V_{SHE}$ (standard hydrogen electrode). Although the S-$H_2O$ Pourbiax diagram in Figure 3 shows that $HS^-$ could remain thermodynamically stable at -0.5 $V_{SHE}$ under ideal equilibrium conditions, laboratory test work (Figure 4) confirms that this ORP target drives $HS^-$ to negligible concentrations well before the ORP reaches the theoretical boundary. Once $HS^-$ is converted to $S_2O_3^{2-}$, $SO_3^{2-}$, $SO_4^{2-}$, or $S^0$, $H_2S$ cannot be generated unless the system becomes reducing again.

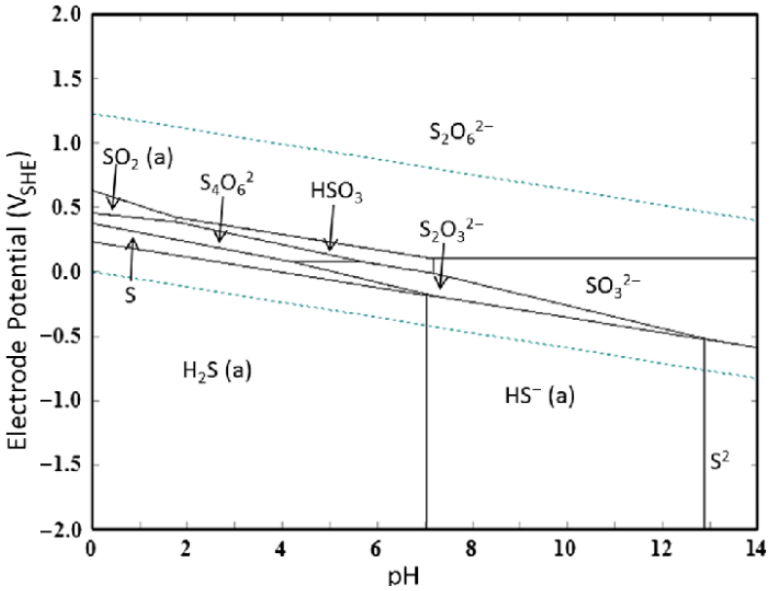



**FIG 3** – Pourbiax diagram for S-$H_2O$ system at 298K.

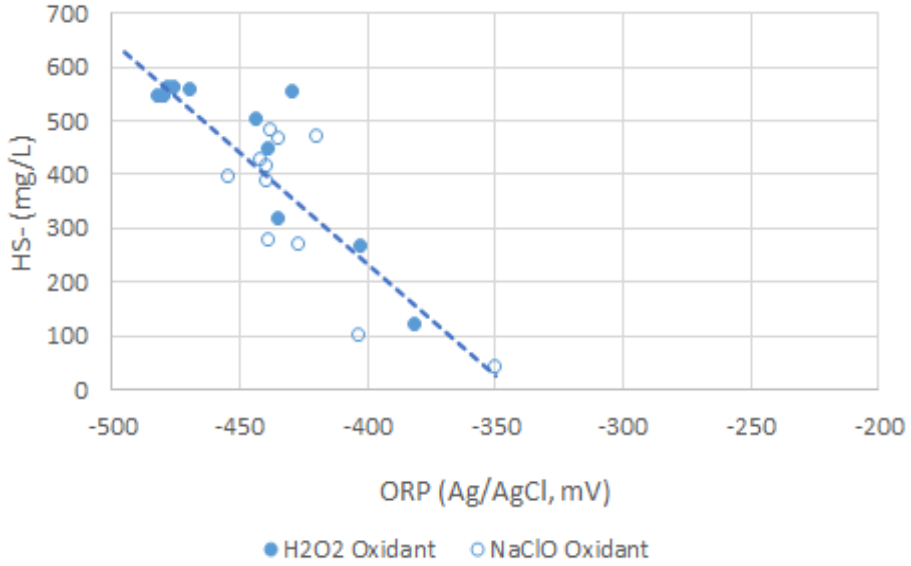



**FIG 4** – $HS^-$ versus ORP when subjected to laboratory oxidation.

The initial shutdown methodology for oxidation was to maximise air addition to the plant whilst recirculating process water. This was done via the flotation cells, thickener cones and tank injection. From this approach, the following issues were noted:

- The intense agitation from the air addition caused significant $H_2S$ off-gassing due to the increased rate of mass transfer across gas-liquid surfaces. This interrupted the Moly Plant ramp-down procedure due to off-gassing events triggering plant evacuations. This ultimately limited how much air could be added for oxidation.
- The circuit oxidation profile tended to change slowly when the ORP approached -450 mV, which was relatively far from the target of -250 mV.

To reach the -250 mV ORP target, initial plant ramp-downs required up to 100 hrs of oxidation with air. Despite these limitations, the aeration methodology was adopted as part of the shutdown procedure between January 2022 and October 2024, decreasing plant utilisation by 13 per cent each shutdown month. Laboratory test work was subsequently initiated to investigate faster methods for oxidising NaHS and reducing $H_2S$ off-gassing.

A fresh sample of Moly Plant process water was subjected to vigorous agitation for 50 hrs to impose oxidation. The oxidation of NaHS is demonstrated by the ORP/pH pathway shown in Figure 5, whereby the pH of the process water sample reduced below 10 resulting in $H_2S$ formation.

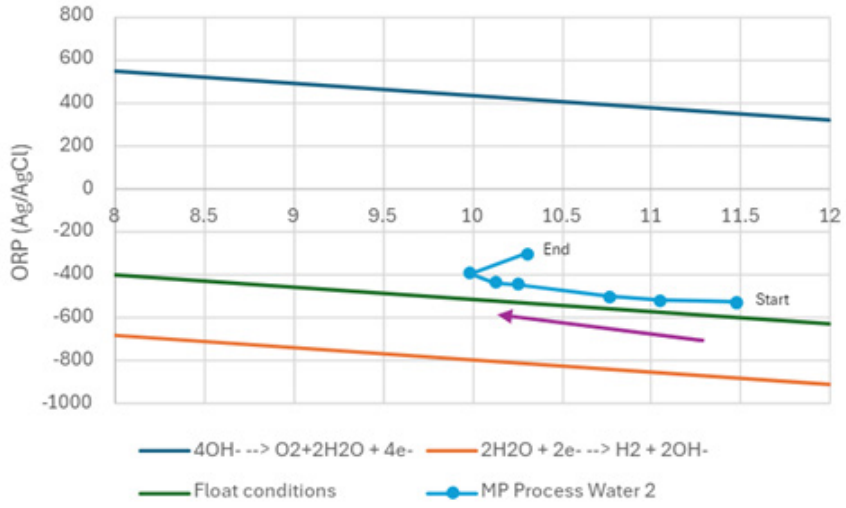



**FIG 5** – ORP/pH response of Moly Plant process water when subjected to oxidation by air.

Further test work using bleach (sodium hypochlorite, NaOCl) as a chemical oxidant was conducted to understand the process water oxidation response. Bleach was investigated as it was already approved and used on-site as an oxidant in the Moly Plant gas scrubbing system. Figure 6 shows step changes in ORP as oxidant dose increases, suggesting distinct species within the process water are oxidising.

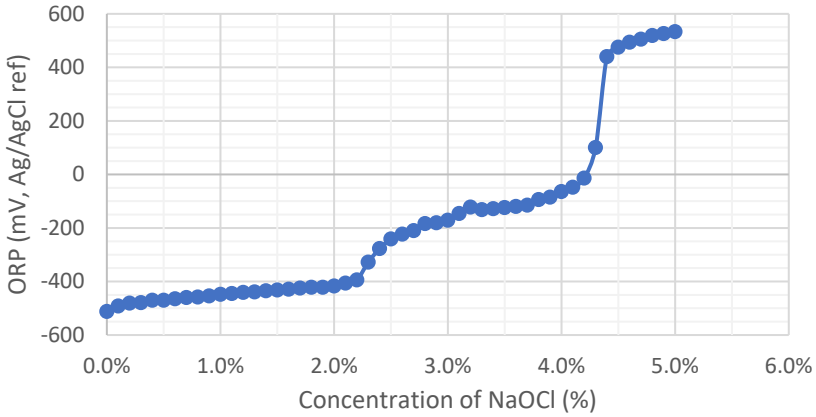



**FIG 6** – ORP response of Moly Plant process water with bleach addition.

Oxidation of $HS^-$ in process water can proceed via intermediate products such as elemental sulfur ($S^0$) and polysulfides ($S_n^{2-}$), and further to thiosulfate ($S_2O_3^{2-}$), then sulfite ($SO_3^{2-}$) or sulfate ($SO_4^{2-}$). This pathway is consistent with established sulfur oxidation mechanisms, where dissolved sulfide reacts with oxygen to form intermediate sulfur species that are progressively oxidised to thiosulfate and ultimately to sulfite and sulfate. These transformations and intermediates are well documented in the chemical sulfur cycle (Steudel, 2000). Equations 7 and 8 show the oxidation reactions that consume alkalinity, which is consistent with the observed pH decrease in Figure 5. In addition, oxidation of hydrocarbons produces hydroperoxides, which are acidic species (Equation 10). Therefore, if diesel collector hydrocarbons are being oxidised, this would further contribute to the pH reduction shown in Figure 5.

$$2HS^- + O_2 \rightarrow 2S^0 + 2OH^- \text{ (ORP couple: } HS^-/S^0) \quad (4)$$

$$S^{2-} + (n-1)S^0 \rightleftharpoons S_n^{2-} \text{ (no change in sulfur oxidation state)} \quad (5)$$

$$S^0 + SO_3^{2-} \rightleftharpoons S_2O_3^{2-} \text{(no change in sulfur oxidation state)} \quad (6)$$

$$S_2O_3^{2-} + O_2 + 2OH^- \rightarrow 2SO_3^{2-} + H_2O \text{ (ORP couple: } S_2O_3^{2-}/SO_3^{2-}) \quad (7)$$

$$S_2O_3^{2-} + 2O_2 + 2OH^- \rightarrow 2SO_4^{2-} + H_2O \text{ (ORP couple: } S_2O_3^{2-}/SO_4^{2-}) \quad (8)$$

$$2SO_3^{2-} + O_2 \rightarrow 2SO_4^{2-} \text{ (ORP couple: } SO_3^{2-}/SO_4^{2-}) \quad (9)$$

$$R\text{-}H + O_2 \rightarrow R\text{-}O\text{-}O\text{-}H \quad (10)$$

An ORP boundary is the electrode potential at which the concentration of the oxidised and reduced species in a redox couple are equal. Increasing ORP drives the system toward the more oxidised species, while decreasing ORP favours the reduced species. Boundary ORP's for the relevant sulfur couples were calculated assuming alkaline pH (pH 10–11) using the Nernst equation summarised by Chen, Chen and Peng (2020). The resulting oxidation sequence is shown in Table 1, where couples with the most negative boundary potentials oxidise first as ORP increases.

**TABLE 1**

Approximate oxidation reduction boundary potentials for sulfur redox couples at pH 10–11.

| Redox couple | ORP boundary (mV, Ag/AgCl) |
|---|---|
| $HS^-/S^0$ | -560 to -530 |
| $S_2O_3^{2-}/SO_3^{2-}$ | -200 to -100 |
| $S_2O_3^{2-}/SO_4^{2-}$ | 100 to 180 |
| $SO_3^{2-}/SO_4^{2-}$ | 150 to 220 |

To demonstrate the oxidation pathway of $HS^-$, Newmont engaged Levay and Co Environmental Services to conduct laboratory-scale test work. The program involved tracking the concentrations of $HS^-$, $S_2O_3^{2-}$, $SO_3^{2-}$ and $SO_4^{2-}$ following the addition of known quantities of oxidant, along with monitoring the ORP, as per Figure 7. The data shown in Figure 7 was from a test that was maintained at pH 9. The hollow data points represent the laboratory measurements, while the solid data points show the $HS^-$ and $S_2O_3^{2-}$ boundaries from Table 1.

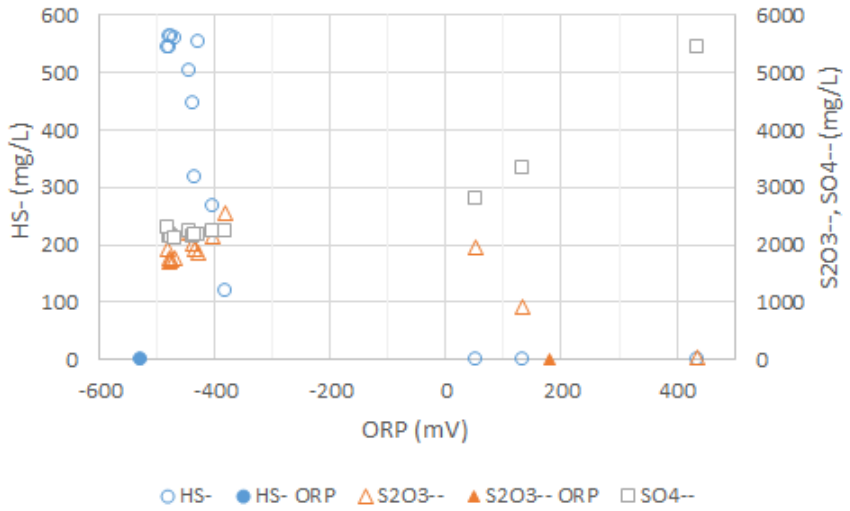



**FIG 7** – Process water aqueous sulfur species versus ORP at pH 9.

Although the theoretical ORP at which $HS^-$ should be oxidised is approximately -530 mV, as per Table 1, the test work demonstrated that $HS^-$ remained present at ORP values around -375 mV. This deviation from theoretical behaviour may be attributed to several factors: differences in solution pH, $HS^-$ oxidation kinetics being slower than the rate at which ORP responds, ORP reflecting the combined influence of all redox couples in the solution, and the presence of additional redox-active species in the process water that shift or buffer the measured potential, meaning the observed ORP does not necessarily correspond to the theoretical value for the $HS^-/S^0$ couple alone.

The data in Figure 7 shows that as ORP is increased from -500 mV to -375 mV, $HS^-$ concentration decreased and $S_2O_3^{2-}$ concentration increased, consistent with Equations 4 and 6. Within this ORP range, $SO_4^{2-}$ concentration remained relatively constant. As the ORP became positive, $S_2O_3^{2-}$ concentration decreased as it was oxidised to $SO_4^{2-}$ (Equation 8).

$SO_3^{2-}$ concentration remained below the detection limit throughout the pH 9 test work, indicating preferential formation of $S_2O_3^{2-}$ over $SO_3^{2-}$. An additional test conducted without pH control resulted in $SO_3^{2-}$ formation when the pH was above 9, demonstrating $SO_3^{2-}$ is more stable under more alkaline conditions as per Figure 3.

To achieve the -250 mV ORP target to oxidise all $HS^-$, approximately 2.5 per cent bleach concentration in process water was assumed according to Figure 6. To achieve a 2.5 per cent bleach concentration in the entire circuit inventory, it was estimated that 64 × 1000 L intermediate bulk containers (IBC's) of bleach solution would be required.

Considering the large quantity of bleach required for process water treatment, additional work was completed to identify a means to optimise the oxidation process. This included test work on a process water sample that contained Moly Plant feed slurry. The ORP pathway of a slurry sample that was vigorously agitated for 50 hrs is shown in Figure 8.

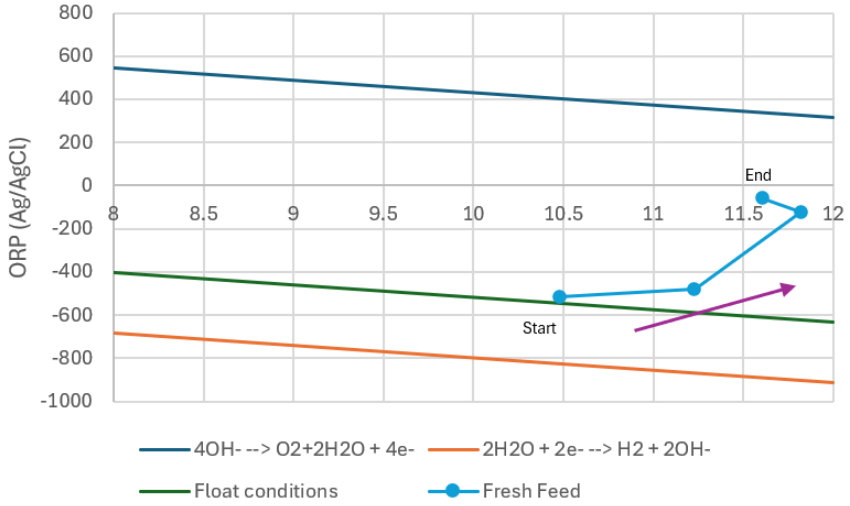



**FIG 8** – ORP/pH response of process water when subjected to oxidation with mineral slurry.

It was theorised that the minerals within the slurry consume both hydrocarbons and NaHS, as per nominal plant operation. The pH increase shown in Figure 8 is attributed to $S^{2-}$ ions (released through the reversal of collector adsorption, as per Equation 1) hydrolysing in water and producing $OH^-$ that neutralises acidic species. A plant trial using fresh Moly Plant feed to oxidise circuit water was completed on 3rd October 2024. This trial ran for 30 mins during a plant start-up. The rapid increase in rouging circuit ORP over a 30 min period led to full-scale application during the November 2024 shutdown.

In summary, it was estimated that complete oxidation of the process water would require 64 IBC's of bleach solution. However, due to site storage limitation and increased bleach demand for the gas scrubber during shutdowns, it was decided four IBC's would be used in combination with mineral slurry and air addition. During the November 2024 shutdown, fresh feed was maintained for 18.5 hrs after NaHS dosing ceased to consume some residual NaHS, after which air was added to the circuit for 16 hrs (with feed off to avoid excessive frothing). This was followed by dosing four IBC's of bleach into the circuit. As a result the total oxidation time was reduced from 100 hrs to 45 hrs.

## NaHS oxidation – hydrogen peroxide and potassium permanganate

In addition to oxidising $HS^-$ with bleach, laboratory test work involving oxidation with hydrogen peroxide ($H_2O_2$) and potassium permanganate ($KMnO_4$) was conducted to determine if the plant ramp-down time could be reduced further. NaHS feedstock solution (~20 per cent solids w/w) and a Moly Plant process water sample was supplied to Solvay during August 2024 for test work.

Two different methods were used to determine how much of each oxidant was required to oxidise the NaHS feedstock solution. Oxidation with $KMnO_4$ had a visual end point. Oxidation with $H_2O_2$ involved a potentiometric end point. The potentiometric end point was reached when the titration had a sudden change in measured electrical potential, indicating the chemical reaction between titrant and analyte was complete. The end point in Figure 9 was when 51 mL of $H_2O_2$ was dosed.

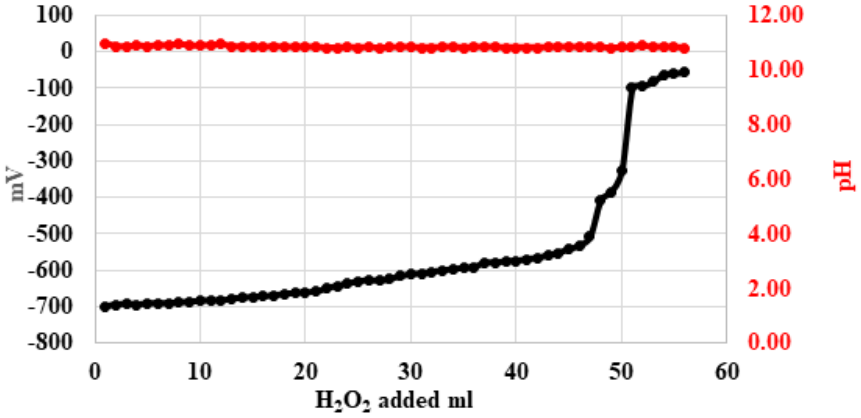



**FIG 9** – ORP/pH response of NaHS feedstock solution when subjected to oxidation with $H_2O_2$.

The composition of a Moly Plant process water sample from May 2024 is shown in Table 2. This data was used to estimate the amount of $H_2O_2$ and $KMnO_4$ required to oxidise the contained sulfur species. The oxidant consumption included consideration for the reactions shown in Table 3 and Table 4. The amount of $H_2O_2$ required to treat a tonne of Moly Plant process water was estimated to be 4.87 kg/t^ under alkaline conditions and 3.35 kg/t* under acidic conditions (Table 3). The amount of $KMnO_4$ required to treat a tonne of Moly Plant process water was estimated to be 6.21 kg under acidic conditions. Table 2 also contains a broader range of process water assays from December 2022 to July 2025, showing that the May 2024 process water sample had a relatively high $HS^-$ concentration, so the oxidant consumption is likely to be subject to variation.

**TABLE 2**

Moly Plant process water composition (mg/L), December 2022 – July 2025.

| | May 2024 | December 2022 – July 2025 | | |
|---|---|---|---|---|
| | | Average | Min | Max |
| **pH** | 11.7 | 11.4 | 10.9 | 11.9 |
| **Eh (mV)** | -363 | -345 | -405 | -314 |
| **$Na^+$** | 1800 | 2500 | 1700 | 4800 |
| **$Ca^{2+}$** | 130 | 35 | 14 | 130 |
| **$Cu^{2+}$** | 1.0 | 2.8 | 0.1 | 8.4 |
| **$K^+$** | 90 | 60 | 45 | 90 |
| **$Al^{3+}$** | 1.0 | 2.0 | 0.3 | 3.6 |
| **$Cl^-$** | 110 | 100 | 80 | 110 |
| **$HS^-$** | 495 | 270 | 85 | 495 |
| **$SO_3^{2-}$** | 117 | 130 | 35 | 270 |
| **$S_2O_3^{2-}$** | 1744 | 2200 | 1744 | 2494 |
| **$SO_4^{2-}$** | 1915 | 1190 | 894 | 1915 |

**TABLE 3**

Estimate of $H_2O_2$ needed to treat Moly Plant process water.

| Reduced sulfur species and TOC | Concentration (mg/L) | Reactions with $H_2O_2$ | Estimated $H_2O_2$ (kg/t process water) |
|---|---|---|---|
| $HS^-$ (NaHS) | 495 | $HS^- + 4H_2O_2 \rightarrow SO_4^{2-} + 4H_2O + H^+$ (alkaline)<br>$HS^- + H_2O_2 + H^+ \rightarrow S + 2H_2O$ (acidic) | 2.03<br>0.51 |
| $SO_3^{2-}$ ($Na_2SO_3$) | 117 | $SO_3^{2-} + H_2O_2 + 2H^+ \rightarrow H_2SO_4 + H_2O$ | 0.05 |
| $S_2O_3^{2-}$ ($Na_2S_2O_3$) | 2290 | $S_2O_3^{2-} + 4H_2O_2 \rightarrow H_2SO_4 + SO_4^{2-} + 3H_2O$ | 2.78 |
| Total Organic Carbon (TOC) | 153 | $C + 2H_2O_2 \rightarrow CO_2 + 2H_2O$ | 0.01 |
| | | TOTAL | 4.87^/3.35* |

alkaline conditions^, acidic conditions*

**TABLE 4**

Estimate of $KMnO_4$ needed to treat Moly Plant process water.

| Reduced sulfur species and TOC | Concentration (mg/L) | Reactions with $KMnO_4$ | Estimated $KMnO_4$ (kg/t process water) |
|---|---|---|---|
| $HS^-$ (NaHS) | 495 | $5H_2S + 2KMnO_4 + 3H_2SO_4 \rightarrow 5S + 2MnSO_4 + K_2SO_4 + 8H_2O$ | 0.95 |
| $SO_3^{2-}$ ($Na_2SO_3$) | 117 | $5Na_2SO_3 + 2KMnO_4 + 6H^+ \rightarrow 5Na_2SO_4 + 2Mn^{2+} + 3H_2O$ | 0.09 |
| $S_2O_3^{2-}$ ($Na_2S_2O_3$) | 2290 | $8MnO_4^- + 5S_2O_3^{2-} + H_2O \rightarrow 8MnO_2 + 6SO_4^{2-} + 2OH^-$ | 5.16 |
| Total Organic Carbon (TOC) | 153 | $3C + 4KMnO_4 + 4H^+ \rightarrow 3CO_2 + 4KMnO_2 + 2H_2O$ | 0.02 |
| | | TOTAL | 6.21 |

After initially estimating the oxidant demand from stoichiometric ratios, the actual $H_2O_2$ consumption was evaluated using Moly Plant process water samples. The starting pH and ORP of the process water were 10.1 and -625 mV, respectively. Following the addition of 3.0 kg/t $H_2O_2$, the pH decreased to 8.2 and the ORP increased to -336 mV. The oxidation reaction appeared to reach an end point after a total of 5.5 kg/t $H_2O_2$ had been added (Figure 10). The actual $H_2O_2$ requirement may have exceeded the stoichiometric prediction due to decomposition side reactions occurring within the process water matrix. The initial solution was transparent yellow, consistent with the presence of aqueous $HS^-$ and polysulfides ($S_n^{2-}$). Upon $H_2O_2$ addition, the sample became cloudy (Figure 11), consistent with the formation of fine sulfur particles or other intermediate oxidation products generated during the conversion of reduced sulfide species to more oxidised, non-volatile sulfur forms. The reaction time required to achieve complete oxidation under these conditions was approximately 25 mins.

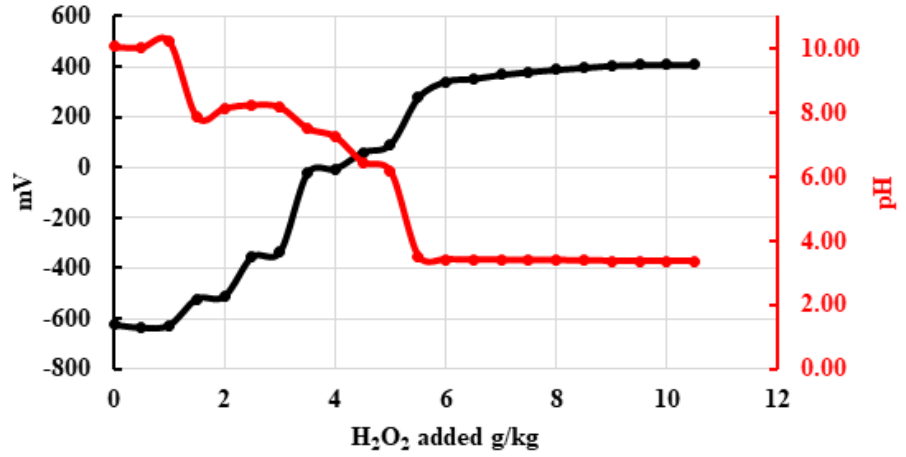



**FIG 10** – ORP/pH response of process water when subjected to oxidation with $H_2O_2$.

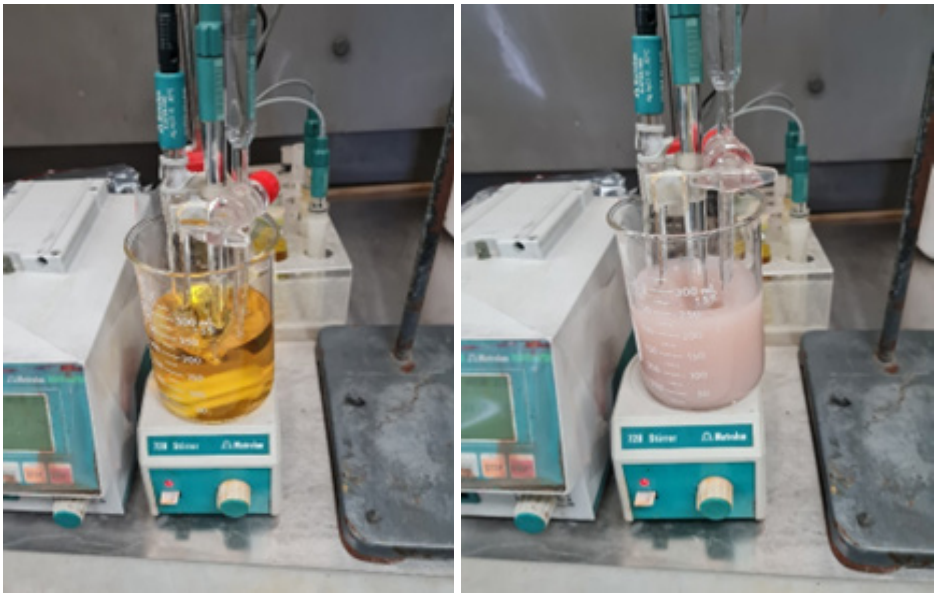


**FIG 11** – Process water appearance before and after $H_2O_2$ addition.

Oxidation test work was also conducted with pH maintained at approximately 10 using caustic soda (NaOH) to prevent formation of $H_2S$. Caustic was selected for pH control because it is fully soluble, does not introduce unwanted precipitation of solids, and allows precise pH adjustment. The initial pH and ORP of the process water sample were 9.7 and -639 mV, respectively. After the addition of 3 kg/t $H_2O_2$, the pH was held at 9.7 and the ORP increased to -374 mV (Figure 12). The clear yellow appearance of the solution remained unchanged throughout $H_2O_2$ addition (Figure 13), consistent with the formation of colourless thiosulfate ($S_2O_3^{2-}$) rather than elemental sulfur. The oxidation reaction appeared to reach an end point after a total dose of 6 kg/t $H_2O_2$, at which point the ORP was 253 mV. The reaction time required to achieve complete oxidation under these conditions was approximately 20 min. The faster reaction rate with alkaline pH is attributed to fewer intermediate oxidation steps and more favourable kinetics. At lower pH, $HS^-$ converts to $H_2S$, which can consume $H_2O_2$ through side reactions. Caustic consumption was 2.4 kg/t of process water. Only a negligible temperature change was observed during the $H_2O_2$ oxidation reaction, both with and without alkali addition.

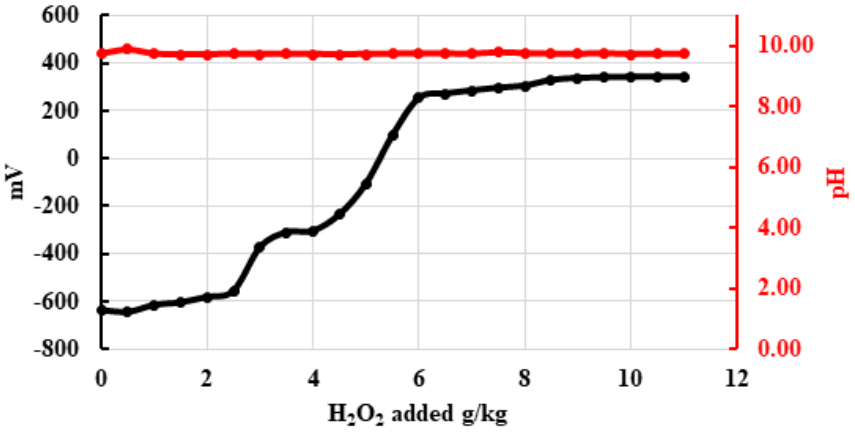



**FIG 12** – ORP response of process water when subjected to oxidation with $H_2O_2$ at constant pH.

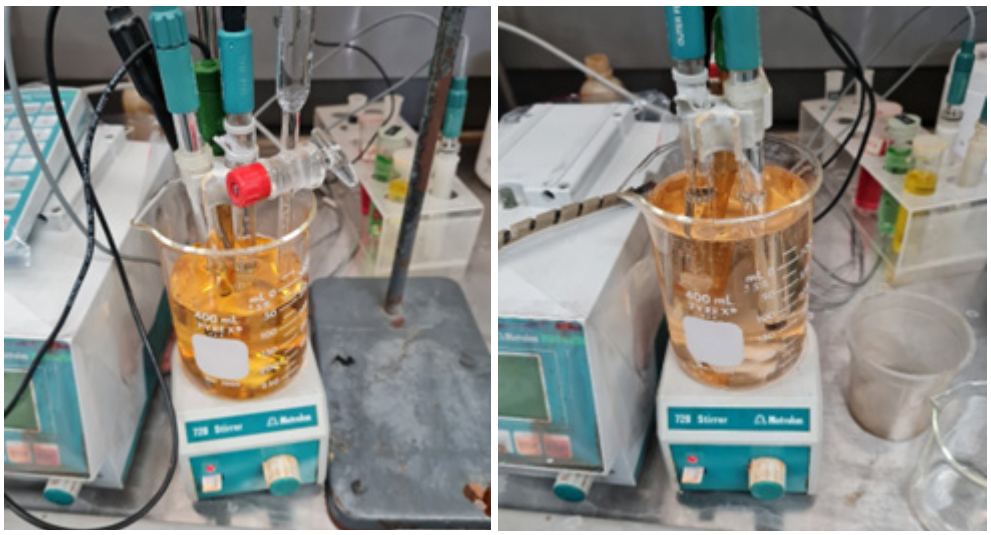


**FIG 13** – Process water appearance before and after $H_2O_2$ addition with pH maintained at 9.7.

In addition to the $H_2O_2$ trials, oxidation test work was also conducted with potassium permanganate ($KMnO_4$). A series of titrations with a standard $KMnO_4$ solution under acidic conditions confirmed that 6.15 kg/t of $KMnO_4$ was required to fully oxidise the reduced sulfur species in a Moly Plant process water sample. This result closely aligned with the predicted requirement of 6.21 kg/t. As shown in Figure 14, the solution was clear prior to $KMnO_4$ addition, transitioning to a pink, cloudy appearance at the visual end point once oxidation was complete. Acidic conditions were necessary for the $KMnO_4$ test, as $KMnO_4$ is a much weaker oxidant under alkaline conditions because it is reduced to $MnO_4(s)$ rather than $Mn^{2+}$, significantly lowering its oxidation potential. The lower pH also produced a clear initial solution because acidification converts dissolved sulfide species to colourless aqueous $H_2S$, removing the yellow polysulfide appearance evident in the alkaline starting solution for the $H_2O_2$ tests (Figure 13). The reaction time for the $KMnO_4$ test was not recorded.

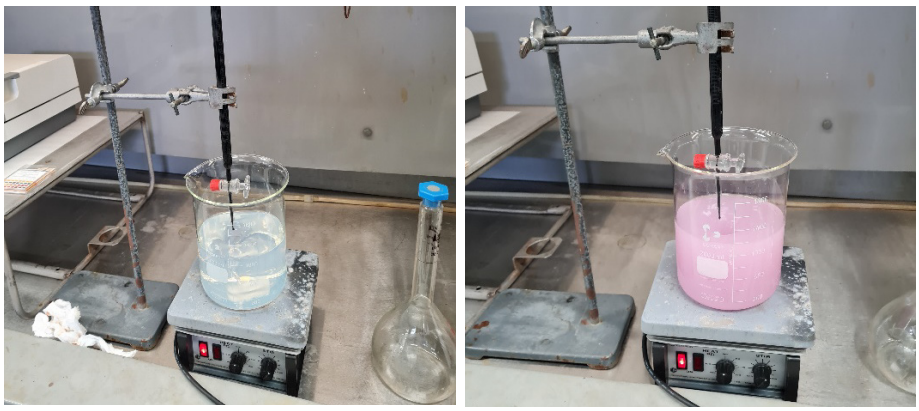


**FIG 14** – Process water appearance before and after $KMnO_4$ addition.

Laboratory-scale test work demonstrated that the reduced sulfur species present in Moly Plant process water can be fully oxidised using either $H_2O_2$ or $KMnO_4$. Oxidation with $H_2O_2$ proceeded more rapidly when the pH was maintained at 9.7 using caustic, and $H_2O_2$ showed a slightly lower overall consumption rate compared with $KMnO_4$. Both $H_2O_2$ and $KMnO_4$ are strong oxidising agents that react quickly with reduced sulfur species. $H_2O_2$ decomposes to oxygen and water, leaving no residual solids, whereas oxidation with $KMnO_4$ would result in the accumulation of manganese in the system. Effective oxidation with $KMnO_4$ also requires acidification of the process water, which increases operating cost and elevates the risk of generating $H_2S$ gas. $KMnO_4$ is additionally more expensive than $H_2O_2$. Based on these outcomes, $H_2O_2$ was selected for a full-scale trial during the plant ramp-down for the May 2025 planned maintenance shutdown. The ramp-down procedure involved maintaining fresh feed to the plant for six hrs after NaHS dosing ceased, air addition for eight hrs in conjunction with dosing two IBC's of $H_2O_2$ (60 per cent w/w concentration). Under these conditions, the oxidation process was completed in approximately 20 hrs as per Figure 15.

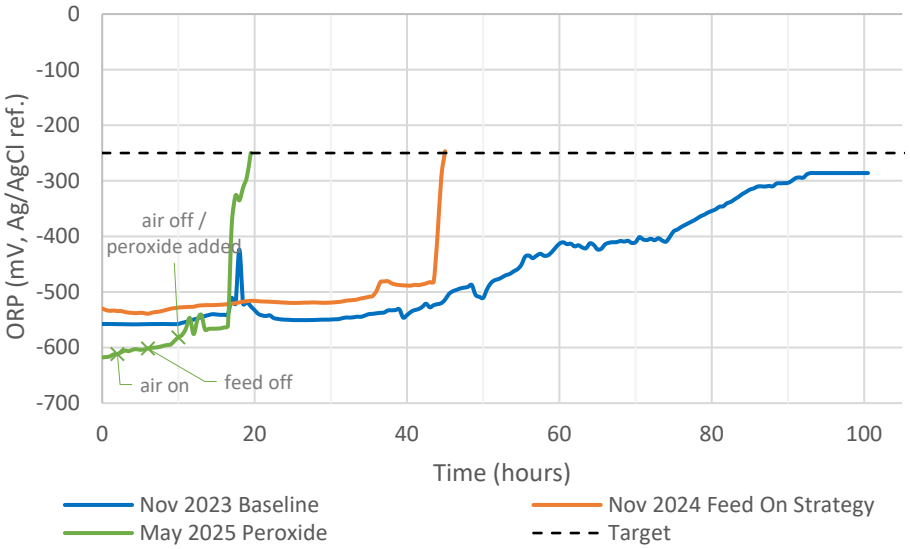



**FIG 15** – Process water ORP during November 2023, November 2024 and May 2025 shutdowns.

## CONCLUSIONS

The laboratory scale procedures were successfully translated to full-scale operation at the Moly Plant, where a combination of mineral slurry, air, and $H_2O_2$ were used to oxidise reduced sulfur species present in the process water. Full scale trials demonstrated that this approach substantially accelerated circuit ramp down prior to maintenance shutdowns.

Before optimisation test work, the November 2023 ramp down period was 100 hrs. After implementation, the November 2024 and May 2025 ramp down periods were reduced to 45 and

20 hrs respectively. This improvement increased available operating time for the Moly Plant, supporting higher annual molybdenum production and providing a platform for further optimisation.

## DISCLAIMER

This paper describes laboratory investigations and operational trials conducted at Newmont's Cadia Valley Operation under site-specific conditions, including ore characteristics, process water chemistry, plant configuration, control systems, and regulatory approvals. The information is presented for general technical discussion only and is not intended to constitute operating instructions, design criteria, or safety guidance. The handling and oxidation of sodium hydrosulfide and other reduced sulfur species involve significant safety and environmental risks. Any application of the concepts discussed requires independent engineering assessment, hazard analysis, and confirmation of compliance with applicable laws, standards, and site-specific procedures. Newmont makes no representation as to the suitability of these methods for use at other operations.

## ACKNOWLEDGEMENTS

The Moly Plant team appreciate the support of Solvay and Levay and Co Environmental Services supporting the development of test work procedures, providing reaction equations, calculations and supporting the plant trials.

## REFERENCES

Amelunxen, P, Schmitz, C, Hill, L, Goodweiler N and Andres, J, 2019. Molybdenum, *SME Mineral Processing and Extractive Metallurgy Handbook*, pp 1891–1916 (Society for Mining, Metallurgy, and Exploration).

Chen, Y, Chen, X and Peng, Y, 2020. The effect of sodium hydrosulfide on molybdenite flotation in seawater and diluted seawater, *Minerals Engineering*, 158.

Dobson, C, Sharman, P, Gunn, S and Lisso, M, 2025. Froth, flow and finesse: The journey to nameplate recovery at Cadia's Molybdenum Concentrator, presented to MetPlant Conference, Adelaide March 2026.

Steudel, R, 2000. The chemical sulfur cycle, in *Environmental Technologies to Treat Sulfur Pollution: Principles and Engineering* (eds: P Lens and L Hulshoff Pol), pp 11–53 (IWA Publishing: London).

# Opening up flotation hydrodynamics – linking gas hold-up with recovery

*N Walter[1] and K Lee[2]*

1. Senior Technical Specialist, Kemtec Mineral Processing Pty Ltd, Melbourne Vic 3207. Email: natasha.walter@kemtec.com.au
2. Group Metallurgist, Kemtec Mineral Processing Pty Ltd, Melbourne Vic 3207. Email: kenneth.lee@kemtec.com.au

## ABSTRACT

Flotation is a central unit operation in mineral processing, yet its performance is often constrained by the hidden world of cell hydrodynamics. Over the last 100 years, equipment designers have continually sought to optimise the hydrodynamics of their units. Unfortunately, conventional optimisation tools such as laboratory assays and froth imaging only offer indirect glimpses of what is really happening inside the cell, leaving operators to adjust circuits without a clear link to metallurgical outcomes.

Recent development of the FlotSense® for real time hydrodynamic measurements has enabled direct observation of individual cell behaviour. In field studies, some of which are described here, gas hold-up ($\varepsilon_g$) data has shown a strong correlation with respect to mineral recovery, as not only a descriptive parameter but also as a powerful predictor of metallurgical and operational performance. These findings highlight the importance of incorporating hydrodynamic insights when defining operational targets for individual cells.

This paper shares on-site learnings from applying $\varepsilon_g$ monitoring across nine flotation circuits representing different markets from copper, gold and poly metallic ore types. We demonstrate how reliable hydrodynamic data, can deliver measurable gains in recovery, selectivity and plant reliability. In doing so, we highlight a pathway for operations to bridge fundamental flotation hydrodynamics within everyday plant performance.

## INTRODUCTION

Flotation remains one of the most widely applied separation processes in mineral processing. Despite its maturity, day-to-day optimisation is still largely based on froth appearance, air set points and metallurgical trends, with limited insight into pulp-phase hydrodynamics.

Hydrodynamic conditions directly control collision frequency, attachment probability and bubble surface area availability. Yet operators commonly adjust air and reagents without visibility of how those changes influence usable bubble surface area within the cell. Each flotation cell operates within a hydrodynamic environment defined by air rate, impeller design/speed, bubble size distribution, frother concentration and slurry rheology. Buckingham, Walter and Lee (2025) identified that whilst superficial gas velocity ($J_g$) is frequently used as an operating reference, identical volumetric air rates do not guarantee identical dispersion. Rather, frother balance, mechanical wear, solids loading and air distribution all influence the fraction of air effectively retained within the pulp.

Gas hold-up ($\varepsilon_g$), defined as the volumetric fraction of gas within the pulp phase, integrates these variables into a single measurable parameter. Unlike airflow alone, $\varepsilon_g$ reflects both air addition and the effectiveness of its dispersion and retention. Industrial measurements show that cells operating at identical airflow frequently exhibit materially different $\varepsilon_g$ values due to mechanical and chemical variability.

The relationships between bubble surface area flux, $J_g$ and flotation performance are well established, however there has been comparatively little emphasis on how these principles can be translated into practical operating strategies. The inability to reliably measure individual cell recovery has been a practical limitation to utilise this knowledge, as the direct measurement of bubble size and surface area flux is complex. $\varepsilon_g$, however, can now be measured reliably under plant conditions due to a direct $\varepsilon_g$ measurement system, providing a practical bridge between flotation theory and operational control.

This paper presents a practical, operator-focused review of flotation hydrodynamics based on multi-site plant surveys conducted across copper, lead and zinc concentrators during 2024–2026. Direct $\varepsilon_g$ measurements were collected, enabling cell-by-cell hydrodynamic characterisation under steady-state plant conditions. These measurements were integrated with plant survey data to establish relationships between $\varepsilon_g$ and recovery. The outcomes of this work include the development of practical operational $\varepsilon_g$ thresholds, quantification of the hydrodynamic impact of staged frother addition, demonstration of the use of $\varepsilon_g$ measurements to identify mechanical wear and evaluation of the relationship between $\varepsilon_g$ and selectivity. Overall, this paper showcases how real-time hydrodynamic measurements can provide operations with actionable information to support the day-to-day process control. These measurements are an additional variable that can be used alongside conventional plant data to identify limitations, diagnose issue and guide adjustments to improve circuit stability and metallurgical performance.

## MATERIALS AND METHODS

Hydrodynamic surveys were completed at nine operations around the globe. Plant surveys are subject to head grade variability, blending changes, mechanical interruptions and sampling limitations. The methodology applied across the surveyed operations was therefore designed to be as repeatable and operationally practical as possible.

### Gas hold-up (Εg) measurement

$\varepsilon_g$ measurements were collected using FlotSense® probe technology, inserted directly into the pulp zone of operating flotation cells.

For each cell, the probe was positioned at a representative pulp depth and measurements were recorded continuously. Stable readings were averaged over the final steady-state period, with froth depth, air rate, and frother dosage recorded concurrently.

### Metallurgical sampling

Hydrodynamic measurement alone does not provide recovery data. To establish meaningful recovery–$\varepsilon_g$ relationships, plant surveys were conducted concurrently, where feasible. This occurred when flotation feed was of high enough grade to take statistically representable samples. Samples were taken of the feed, concentrate and tail of each individual cell.

Where plant conditions permitted, controlled variation of air rate and frother dosage was conducted to establish recovery–$\varepsilon_g$ relationships. This typically involved the incremental air rate adjustments with stabilisation periods between adjustments before measuring of resulting $\varepsilon_g$ and metallurgical response. While not laboratory-controlled, the consistency of observed patterns across multiple operations provides confidence in the operational relevance of the findings.

The probe is self-calibrating, enabling it to deliver reliable hydrodynamic measurements across a wide range of operating conditions, including variations in temperature, pulp characteristics, process water quality, and probe positioning.

## FLOTATION HYDRODYNAMICS

Hydrodynamics in flotation is commonly expressed in terms such as $J_g$, bubble surface area flux (Sb and $\varepsilon_g$. These parameters are well defined in the literature and provide a strong theoretical framework for understanding flotation behaviour. However, in day-to-day plant operation, hydrodynamics is experienced through recovery trends, froth behaviour, mass pull and bank stability. When developing strategies to optimise plant performance, it is important to first define the specific outcomes you want each flotation cell to achieve. For example:

- Is there enough usable bubble surface area to support recovery?
- Is that surface area distributed effectively across the bank?
- Is excessive air driving entrainment rather than selective recovery?
- Are mechanical or reagent issues limiting performance?

## Gas hold-up (Ɛg)

$Ɛ_g$ is the volumetric fraction of gas within the pulp phase, representing the proportion of the flotation cell volume occupied by bubbles at any given time. In conventional industrial mechanical cells, $Ɛ_g$ typically ranges between 5 per cent and 20 per cent, depending on operating intensity and cell condition.

In practice, $Ɛ_g$ reflects the combined influence of air addition rate, bubble size distribution, frother concentration, slurry properties and cell design. Cells operating at identical airflow set points frequently display different $Ɛ_g$ values due to variations in these parameters.

Across multiple surveyed operations, $Ɛ_g$ has consistently proven to be a more representative indicator of 'usable' air than airflow measurement alone. Airflow describes what is delivered to the cell and $Ɛ_g$ describes what is contributing to flotation. We found that plant data across copper, lead and zinc operations consistently produced three broad operating ranges for traditional flotation cells (Table 1).

**TABLE 1**

Proposed practical operating $Ɛ_g$ ranges for flotation circuits.

| $Ɛ_g$ < 5% | $Ɛ_g$ 5–15% | $Ɛ_g$ > 15% |
|---|---|---|
| Recovery limited | Good balance between recovery and selectivity | High recovery – increased mass pull |
| Insufficient bubble surface area | Stable froth structure | Higher water recovery |
| Seen often in cleaner circuits for grade control | Effective utilisation of cell volume | Entrainment of gangue |
| Higher recirculating load | Optimal rougher performance | Reduced selectivity |

These operating ranges, while not universal, were derived from multiple operations and commodities. They were consistent across hydrodynamic surveys conducted globally, operating under different ore mineralogy, liberation characteristics and reagent regimes. Although individual operating targets varied between circuits, consistent patterns were repeatedly observed within these ranges.

The proposed operating windows are practical operational guidance, providing operators with an evidence-based reference point for interpreting $Ɛ_g$ measurements and identifying cells that are recovery limited, operating at a good balance, or experiencing excessive entrainment.

## Usable air

Not all introduced air contributes equally to flotation performance. The distinction between total air supplied and usable air is central to hydrodynamic efficiency.

$J_g$ remains a convenient design parameter as it normalises air addition across different cell sizes/designs. Most mechanical flotation cells operate around nominal $J_g$ values of approximately 2 cm/s. Above roughly 2.5 cm/s, cells commonly exhibit visible 'boiling' behaviour, and below 0.6 cm/s, it may be insufficient to maintain solids suspension and promote effective bubble–particle contact.

In practice, however, plant-derived $J_g$ values are only as reliable as the airflow measurements on which they are based. Airflow meters drift out of calibration, distribution across parallel banks can be uneven and impeller wear alters effective shear at identical air rates. As a result, identical $J_g$ values do not necessarily correspond to identical gas dispersion conditions. Consequently, two cells operating at identical airflow set points may exhibit different flotation behaviour, and without direct hydrodynamic measurement, operators may incorrectly attribute this difference to reagent chemistry or ore variability. An example of this was seen in the cleaner circuit of a lead-zinc mine. The 'OK 100' flotation cells being engineered to operate at a $Ɛ_g$ of 15 per cent. However, plant survey data

showed that the actual $\varepsilon_g$ values were below the design target (see Figure 1), despite all flotation cells operating at the same volumetric air rate of 1300 $m^3$/hr, corresponding to a consistent superficial gas velocity. Under these conditions, one would expect each flotation cell in the bank to perform comparable levels of work.

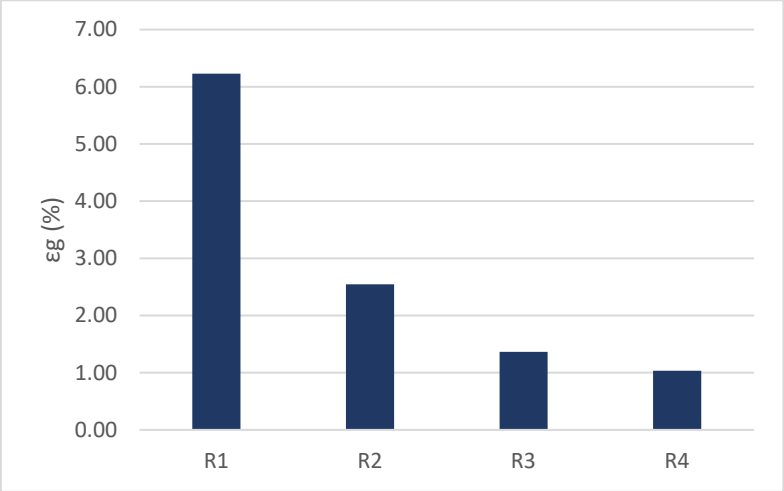



**FIG 1** – $\varepsilon_g$ profile of cleaner bank (Each flotation cell operated at 1300 $m^3$/hr).

However, this profile demonstrates that most of the flotation activity was occurring in the first cleaner cell. Downstream cells were operating below the 5 per cent recovery-limiting threshold. Operational consequences included:

- Elevated recirculating load to downstream cleaning circuit.
- Reduced effective cleaner residence time utilisation.
- Increased dependence on first cell performance.
- Potential loss of fine liberated mineral in later cells.

This imbalance was not visible through airflow data alone. Only direct $\varepsilon_g$ measurement revealed the magnitude of decline down the bank. From an operational perspective, this finding shifted focus from reagent chemistry alone to hydrodynamic distribution. Rather than increasing collector dosage to improve cleaner recovery, rebalancing air utilisation and frother distribution was identified as a more targeted intervention.

We have found that, in industrial mechanical cells, a proportion of introduced air can report to the pulp as a relatively small number of large bubbles, typically in the order of 20–25 mm in diameter. Under high air addition conditions, up to approximately 50 per cent of the total air volume may be associated with these large bubbles due to the onset of bubble coalescence. This is further illustrated by a survey completed at a copper-gold operation, where the standard deviation of repeated $\varepsilon_g$ measurements increased with air rate, indicating that dispersion became increasingly unstable as more air was introduced to the cell (Figure 2).

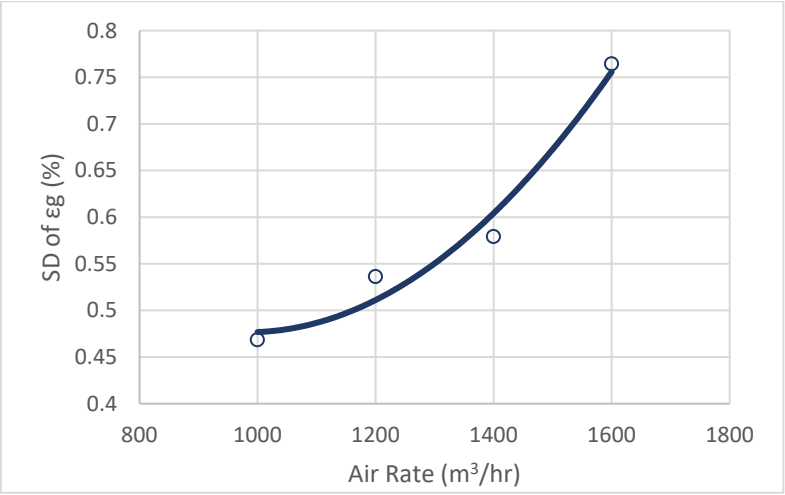



**FIG 2** – Standard deviation of measured $\varepsilon_g$ with increasing air rate.

This development of large bubbles reduces the available effective surface area for particle attachment. From an operational perspective, this means that increasing airflow to increase mass pull may, beyond the optimum point, have the opposite effect by reducing air utilisation and promoting entrainment rather than selective recovery.

As gas dispersion becomes increasingly unstable with increasing air rate, frother concentration plays a critical role in this balance, as frothers reduce bubble coalescence, stabilise smaller bubbles, and increase gas retention. In copper rougher circuits, it was found that downstream decreasing $\varepsilon_g$ was due to frother depletion rather than reduced airflow. Staged frother addition restored downstream $\varepsilon_g$ without increasing air rate, redistributing usable air along the bank and improving overall volumetric efficiency.

These observations demonstrate why airflow alone is an incomplete operating variable. What determines flotation performance is how much air is converted into stable, fine bubbles that promote particle-bubble attachment, the more meaningful variable of usable air.

Yianatos, Henríquez and Bergh (2005) further showed that while increasing $J_g$ initially increases $\varepsilon_g$ and bubble surface area flux, excessive aeration promotes bubble coalescence and increases bubble diameter. As bubble size increases, collision and attachment efficiencies decline, and the flotation rate constant can plateau or decrease despite higher air input.

The usable air concept explains how airflow adjustments can be interpreted:

- Increasing airflow without monitoring $\varepsilon_g$ may increase entrainment rather than recovery.
- Low $\varepsilon_g$ in cleaner circuits indicates insufficient usable air, even if airflow appears adequate.
- Uneven $\varepsilon_g$ distribution down-bank indicates uneven usable air distribution.
- Mechanical degradation can reduce effective shear, lowering usable air at constant airflow.

By measuring $\varepsilon_g$, operators gain visibility into how much of the introduced air is effectively contributing to flotation, allowing airflow adjustments to be targeted rather than reactive. The use of the probe enables a practical, instantaneous measurement that substantiates the claim of direct relationship between $\varepsilon_g$ and $J_g$ (Figure 3).

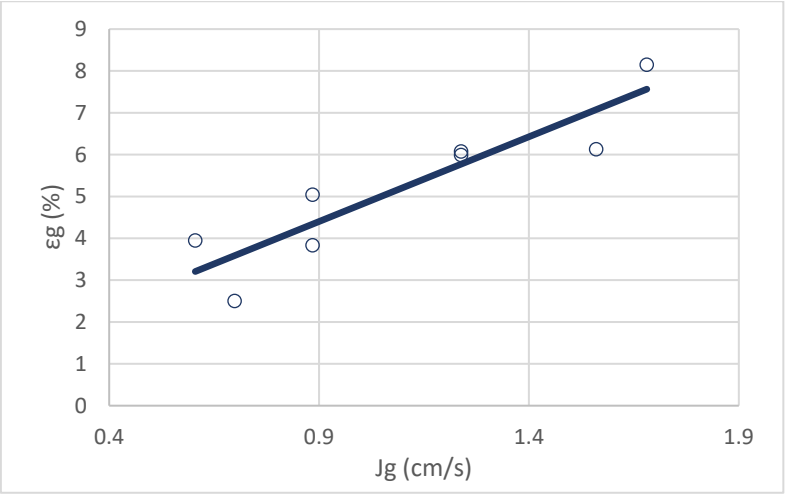



**FIG 3** – Measured relationship between $\varepsilon_g$ and $J_g$.

Rather than responding to poor flotation performance through adjusting airflow, operators can determine whether the circuit requires air adjustments, frother re-distribution or mechanical maintenance. $\varepsilon_g$ becomes an operating variable that links hydrodynamics with daily plant optimisation.

## RECOVERY DISTRIBUTION

In most flotation banks, recovery is not uniform down the bank, 70–90 per cent is usually recovered in the first few cells. This includes liberated, fast floating particles (fundamental to flotation kinetics) and targeted strategies employed to recover as much of the material in the front end as possible. Most concentrators aim to recover the majority of valuable minerals at the front end of the circuit, relying on the scavenger cells to recover the more difficult, composite particles. While this is generally accepted as the conventional approach for maximising recovery, it can inadvertently reduce mineral selectivity. If each cell were to contribute progressively to overall recovery whilst maintaining selectivity, it would allow more valuable particles to attach to bubbles further downstream, thereby reducing the loading of unwanted gangue minerals on bubble surfaces. When the scavenger cells operate with high recovery loads, more bubble surface area becomes available for less hydrophobic particles, increasing the risk of unwanted material reporting to concentrate. This leads to cleaner circuits limiting recovery and increasing recirculating load to achieve concentrate grade.

Hydrodynamic profiling with $\varepsilon_g$ probes enables visualisation of recovery distribution through $\varepsilon_g$ gradients down-bank. These profiles can indicate inefficient utilisation of installed flotation volume. Rather than allowing the full bank to contribute to recovery, hydrodynamic imbalance concentrates flotation activity into only a few of the cells. Recovery profiling is an optimisation tool for improving separation efficiency, and where appropriately applied, can contribute to improved overall recovery. However, the optimum profile is site-specific and is not a universal objective. Consequently, deliberately redistributing recovery further down the bank without appropriate evaluation may risk reducing overall circuit recovery. The balance between selectivity and recovery should be established for each operation through metallurgical evaluation.

Selectivity can be improved by distributing the recovery load more evenly across the entire circuit. By reducing mass pull in the early stages, the valuable, strongly hydrophobic minerals effectively compete for limited bubble surface area. This creates a natural crowding effect, making it more difficult for weakly hydrophobic or undesirable particles to attach, thereby improving selectivity and ultimately enhancing the ability to improve overall recovery. In a surveyed zinc cleaner circuit, elevated $\varepsilon_g$ was associated with increased water recovery and greater entrainment of $SiO_2$ to the concentrate, resulting in a consistent decline in $Zn/SiO_2$ selectivity. The work also identified an operating window where $\varepsilon_g$ was sufficient to maintain mineral recovery whilst minimising this entrainment, which indicates that improvements in concentrate grade and circuit stability can be achieved through better management of gas distribution and bubble loading.

Similarly, reducing the average unit recovery of individual cells within a flotation bank can help minimise entrainment of hydrophilic particles. Zhang, Nesset and Finch (2010) outlined that operating cells at a lower bubble flux decreases the volume of water being recovered in the froth phase and therefore reduces entrained gangue transported upward between bubbles. This provides an additional operational lever for improving concentrate quality.

This concept is consistent with the established flotation practice of froth crowding, particularly in scavenger cells. This set-up maintains froth carrying capacity and promotes selective recovery under low froth loading conditions. $\varepsilon_g$ measurements can be used in conjunction with this practice, or in operations with variability in head grades or lack of capital to retrofit froth crowders in cells.

## Implementation of recovery profiling

The implementation of $\varepsilon_g$ measurement aims to utilise the plant more effectively by recovery profiling. If flotation performance can be reliably characterised using measurable hydrodynamic parameters, advanced process control strategies can be developed based on mathematical models that aim to enhance overall separation efficiency across the circuit. Mathematical modelling by Maldonado, Araya and Finch (2012) demonstrates that achieving a flat cell-by-cell recovery profile (Figure 4) can maximise the separation of two floatable materials, thereby improving selectivity while meeting a targeted recovery. The figure below, based on a South-east Asian operation, is just one example of a potential profile that can be developed specifically for each site.

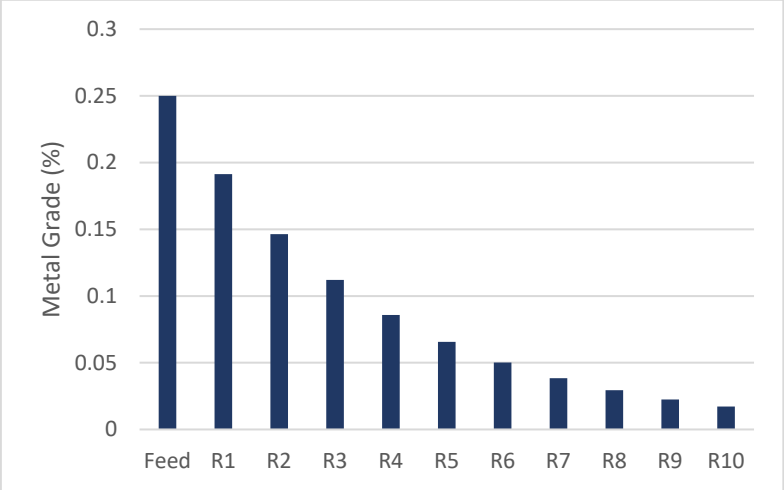



**FIG 4** – Balanced cell-by-cell recovery example.

These observations provide the basis upon which structured implementation frameworks can be developed to transition hydrodynamic characterisation into a practical operating strategy. Plant survey data consistently showed a strong relationship between $\varepsilon_g$ and individual cell recovery (Figure 5). This relationship is the basis for developing reliable strategies for predicting flotation performance using measurable hydrodynamic parameters. With this link established, hydrodynamic data can be incorporated into advanced process control frameworks to drive more consistent and efficient flotation performance across the circuit.

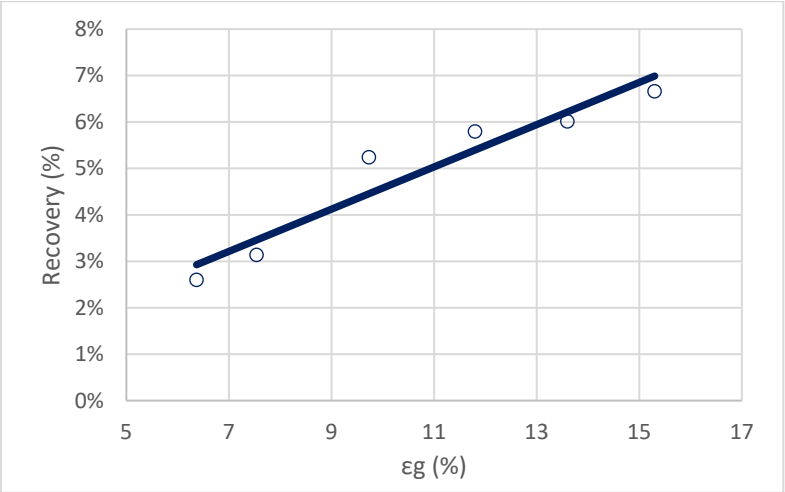



**FIG 5** – Measured $\varepsilon_g$ – recovery relationship.

By measuring individual cell $\varepsilon_g$ across a flotation bank, a hydrodynamic profile of the circuit can be established. This profile allows for metallurgical assessment of individual cell performance, but also how each cell is interacting and adding to the performance of the bank. By measuring $\varepsilon_g$ over time, and through changes in reagent addition rates, solids density, air addition and ore mineralogy, targeted profiles can be developed to improve selectivity whilst maximising recovery.

Recovery profiling can be implemented over three stages:

1. Baseline survey – measure $\varepsilon_g$ cell-by-cell under normal operating conditions to establish normal operating conditions.
2. Correlate with performance – Build relationship profile of $\varepsilon_g$ with concentrate grade, mass pull and recovery data to identify recovery and selectivity concerns within the circuit. Take individual cell surveys if plant restrictions allow.
3. Controlled adjustment – Modify frother dosage, air distribution and feed blends incrementally, monitoring shifts in $\varepsilon_g$ and how recovery responds.

The development of this profile and strategic $\varepsilon_g$ targets allows valuable minerals to be recovered progressively while maintaining selectivity, improving overall circuit efficiency and reducing unnecessary mass pull. In this way, robust and practical measurement of $\varepsilon_g$ provides a direct, measurable bridge between hydrodynamic theory and operational plant control.

## CASE STUDY

This was put into practice in a lead/zinc/silver mine in Australia. The survey aimed to assess the relationship between air rate, $\varepsilon_g$, and concentrate grade in their flotation circuit. The objective was to determine whether circuit performance limitations were chemically driven or hydrodynamically constrained.

Operating air rates below $J_g$ values of approximately 0.6 cm/s may not provide sufficient turbulence intensity to maintain full slurry suspension and effective bubble dispersion in mechanical flotation cells. Plant readings from the Pb circuit (Figure 6) indicated that the rougher and scavenger banks were operating at approximately 0.4–0.45 cm/s. At these air rates, reduced turbulence limits bubble breakup and dispersion efficiency. The consequence is a reduction in effective bubble surface area and increased probability of coarse or high-density particle de-attachment. While collector strength was adequate, the hydrodynamic environment in the rougher bank was likely limiting recovery.

In contrast, the cleaner circuit operated in a markedly different regime. The first cleaner cell was measured at approximately 2.9 cm/s, tapering to 1.3 cm/s by the third cleaner stage. This represents a significant step change in air intensity between roughing and cleaning duties.

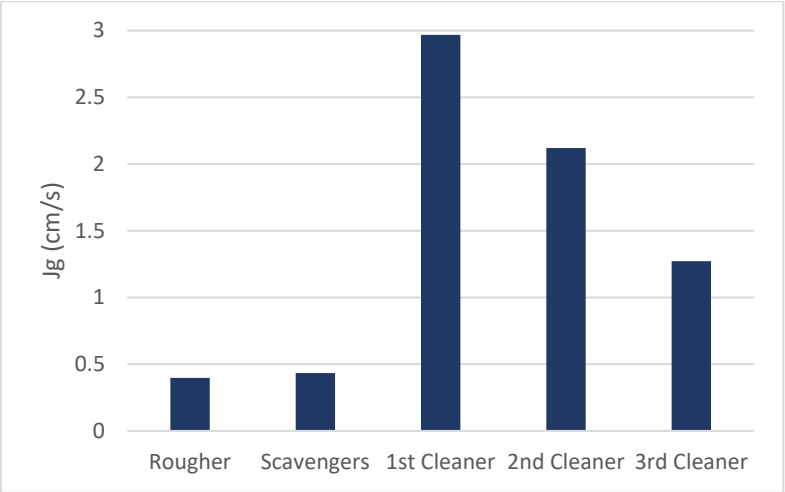



**FIG 6** – Operating $J_g$ at a lead/zinc/silver concentrator in Australia.

No dedicated frother was being applied in the Pb circuit at the time of assessment. Visual observation confirmed that the froth phase was dense, viscous and largely immobile. Froth drainage was restricted and entrained gangue had limited opportunity to return to the pulp phase. The froth structure was controlled by air rate rather than controlled froth modification.

To quantify the impact of air addition on cleaner performance, direct $\varepsilon_g$ measurements were taken in the first cell of the third cleaner bank while systematically adjusting air addition.

Based on the above average $\varepsilon_g$ results in the cleaners and issues identified with froth mobility, frother was applied to the circuit and an immediate response was seen. $\varepsilon_g$ increased to 15–20 per cent and further step testing of air addition rates was undertaken to measure the impact of $\varepsilon_g$ on concentrate grade. Measured data demonstrated a clear inverse relationship between $\varepsilon_g$ and Pb concentrate grade (Figure 7).

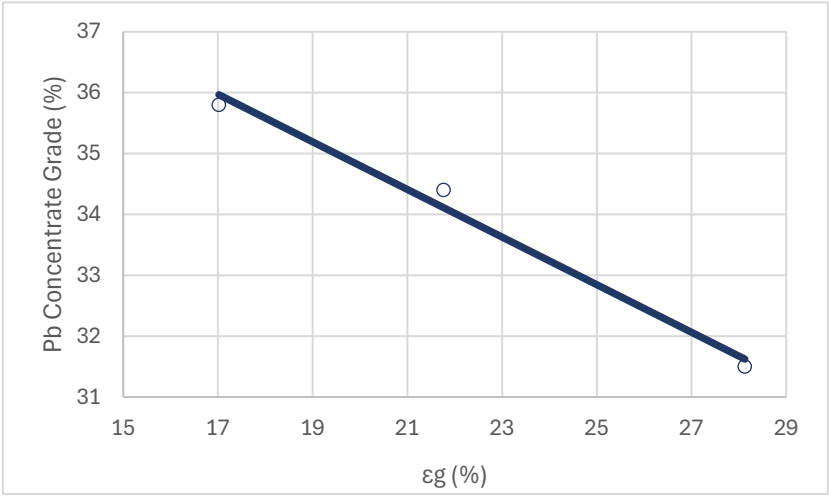



**FIG 7** – $\varepsilon_g$ – Concentrate grade relationship.

As $\varepsilon_g$ increased from approximately 17 per cent to 27 per cent, concentrate grade declined from approximately 36 per cent Pb to 31 per cent Pb. While increasing $J_g$ increases Sb and total available bubble surface area, excessive $\varepsilon_g$ in cleaner duty promotes water recovery, froth crowding, and fine gangue entrainment. The result is increased mass pull at the expense of selectivity.

Based on the measured response, an apparent operating window for the Pb cleaner circuit was identified. Concentrate grade remained highest when $\varepsilon_g$ was maintained within approximately 13–15 per cent. Above this range, grade declined progressively with increasing $\varepsilon_g$.

## STAGED FROTHER

The importance of the $\varepsilon_g$ profile was highlighted at a copper and gold processing plant in South-east Asia. Circuit analysis of the first rougher train shows that the first three cells have consistently higher $\varepsilon_g$, averaging 5.5 per cent more than the downstream cells (Figure 8). This indicates that flotation activity is strongly concentrated at the head of the bank. Frother front-loading is the principal driver: higher frother concentration in the feed zone produces smaller bubbles and higher gas retention. As the slurry progresses down the bank, frother is removed from the circuit through froth carry over, leading to depleted frother concentration, larger bubbles, and a drop in $\varepsilon_g$ values.

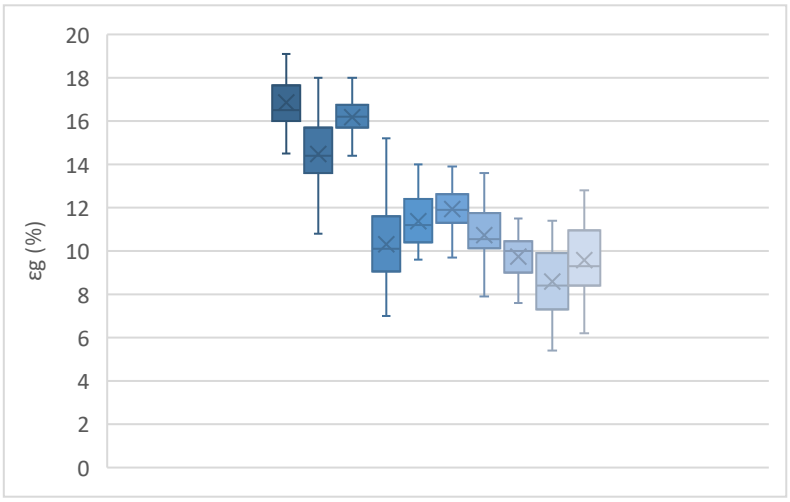



**FIG 8** – Cell $\varepsilon_g$ measurements through the first rougher bank.

Despite consistent air addition and superficial gas velocity, $\varepsilon_g$ declines markedly from cell four through to cell ten, demonstrating that air utilisation is uneven and governed by reagent availability rather than mechanical input. Additional frother is introduced at cells three and five. This is visible in the rougher bank profile (Figure 9), where localised increases in $\varepsilon_g$ and cell depth correspond to the points of reagent addition.

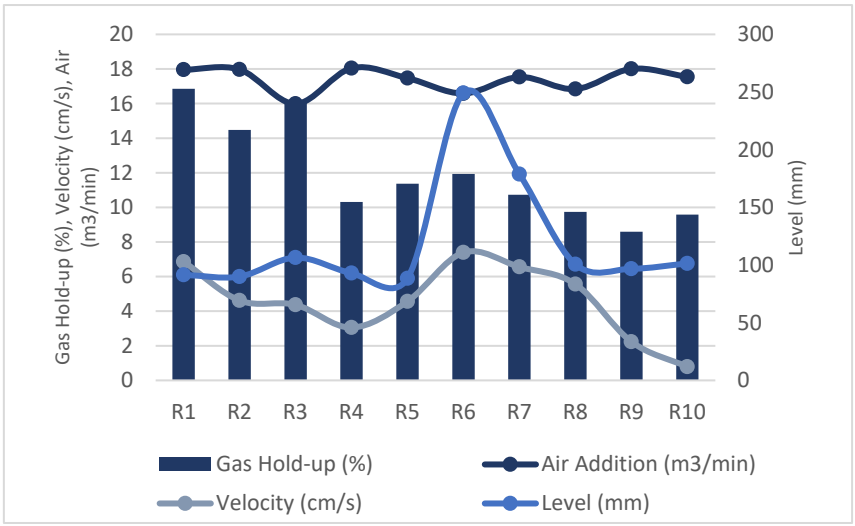



**FIG 9** – Flotation variables through rougher bank during survey.

Bubble velocity (measured by froth cameras) increases in this area despite a dip in air addition and deepening of the cells. The data confirm that staged frother addition has a measurable hydrodynamic effect, temporarily elevating $\varepsilon_g$ and impacting froth movement, as supported by Ata (2012). However, the overall profile still shows a net decline in $\varepsilon_g$, highlighting the need for more strategic methodologies to sustain downstream performance.

## MECHANICAL WEAR IDENTIFICATION

Surveys at a lead/zinc/silver mine in Australia reinforced the importance of mechanical condition in hydrodynamic behaviour. Calculated $J_g$ values across the banks ranged between 1.1 and 1.4 cm/s, consistent with design operation (Figure 10).

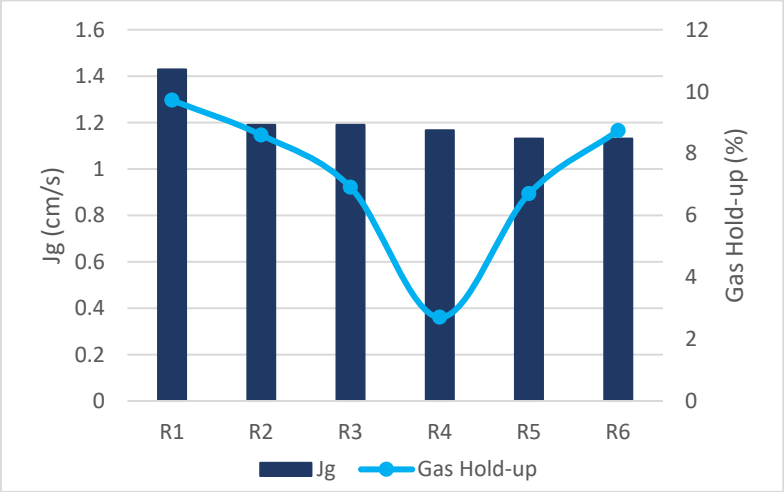



**FIG 10 –** $J_g$ profile of rougher bank.

Observed behaviour did not always align with calculated airflow. In one case, a cell exhibited visible boiling behaviour, when the calculated $J_g$ was only ~1.0 cm/s. However, as can be seen in the above figure, the measured $\varepsilon_g$ was significantly elevated relative to adjacent cells. Further discussions with site personnel revealed that some cells had received new rotors during a previous shutdown. These upgraded rotors operate at higher effective tip speeds than the older units. Such differences in cell design and equipment condition are reflected in the flotation hydrodynamic data captured. The relationship between rotor condition and $\varepsilon_g$ distribution was evident. Cells with newer or less-worn rotors consistently exhibited higher $\varepsilon_g$ relative to adjacent units operating at identical airflow set points. $\varepsilon_g$ reflects the volumetric fraction of gas retained within the pulp phase and therefore captures the combined influence of airflow, mechanical dispersion and slurry properties. Without direct $\varepsilon_g$ measurement, the observed variability would likely have been attributed to reagent regime or ore variability. Instead, hydrodynamic profiling demonstrated that mechanical condition significantly influences hydrodynamics and that identical airflow does not ensure identical bubble dispersion.

A separate hydrodynamic survey completed on a zinc circuit also demonstrated $\varepsilon_g$ measurements as a maintenance diagnostic tool. All four cells were operated at an air addition rate of 1200 $m^3$/hr. As expected, $\varepsilon_g$ generally decreased down the bank as frother concentration and solids density declined (Figure 11). Cell 3, however, had a higher $\varepsilon_g$ than preceding cells. This was without additional air or frother. Upon further investigation, it was identified that this cell had a level control valve fault (failed open), and as such froth depth could not be maintained consistently. This meant that the probe intermittently dipped into the froth layer rather than sitting within the pulp phase, leading to higher $\varepsilon_g$ values and a higher standard deviation of measurements. This anomaly identified a mechanical fault that had not been apparent from airflow measurements alone.

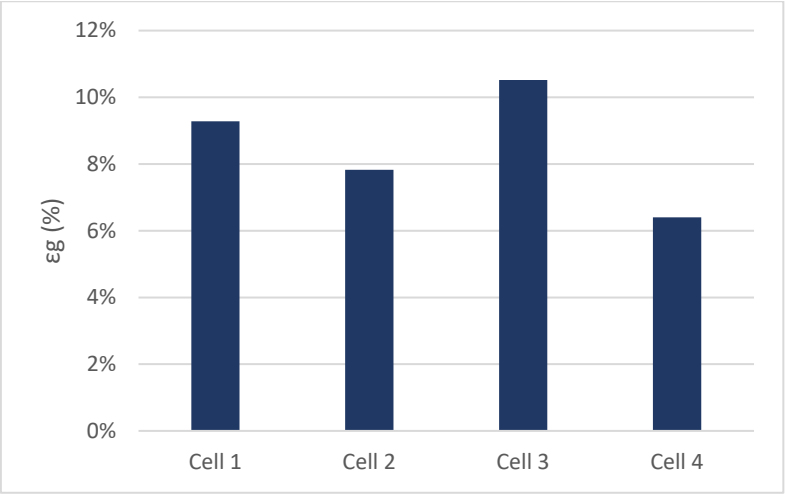



**FIG 11** – $\varepsilon_g$ of zinc cleaner cells identifying issue in cell 3.

These case studies demonstrate the usefulness of $\varepsilon_g$ measurements within the circuit, not just to improve metallurgical performance but for rapid identification of mechanical wear, instrumentation faults, or other changes in operating conditions that may otherwise remain unknown. Continuous $\varepsilon_g$ measurement has the ability to support predictive maintenance by identifying developing issues before they significantly impact performance and to assist in prioritising maintenance objectives. These measurements can also be used in reliability analysis to assess whether there is a quantifiable production or recovery impact associated with declining $\varepsilon_g$ due to wear.

## CONCLUSION

This work shows that direct flotation hydrodynamic measurements provide a practical and defensible bridge between flotation theory and practical plant control. Across multiple base-metal concentrators, consistent hydrodynamic relationships were observed that allowed practical operational guidance to be developed. Cells operating below approximately 5 per cent $\varepsilon_g$ were generally recovery-limited, those within roughly 5–15 per cent $\varepsilon_g$ achieved an effective balance between recovery and selectivity, and excessively high $\varepsilon_g$ increased entrainment and mass pull. Hydrodynamic surveys exposed patterns in circuit utilisation around the world that were easily optimised through the measurement of $\varepsilon_g$. The plant case studies demonstrated several operational applications of $\varepsilon_g$ measurement:

- Defining practical operating $\varepsilon_g$ ranges.
- Optimising frother distribution and improving the utilisation of installed flotation volume.
- Improving separation efficiency while recognising the trade-off between recovery and selectivity.
- Detecting mechanical wear and instrumentation faults.

$\varepsilon_g$ measurements extend beyond cell monitoring and provide a practical diagnostic tool for flotation optimisation and maintenance.

Now that reliable, real-time hydrodynamic measurement technology is available, $\varepsilon_g$ can now be treated as an operating variable as easily as froth velocity or air addition rate. Integrating $\varepsilon_g$ into routine plant data and advanced process control frameworks enables predictive management of individual cells, supports metallurgical target setting based on measurable hydrodynamic conditions, and provides operators with direct visibility of usable air and circuit utilisation, enabling more informed decisions on reagent strategy, air distribution and maintenance.

## ACKNOWLEDGEMENTS

We'd like to acknowledge the support of the team at Kemtec Mineral Processing and the FlotSense® team in the development and application of this technology.

## REFERENCES

Ata, S, 2012. Phenomena in the froth phase of flotation – A review, *International Journal of Mineral Processing*, pp 102–103, 1–12.

Buckingham, S, Walter, N and Lee, K, 2025. The Optimisation of Flotation Performance using Real Time Flotation Hydrodynamic Measurements, Chemeca 2025 Conference, Adelaide, Australia.

Maldonado, M, Araya, R and Finch, J, 2012. An Overview of Optimizing Strategies for Flotation Banks, *Minerals*, 2(4):258–271.

Yianatos, J A, Henríquez, F and Bergh, L, 2005. Gas dispersion measurements in industrial flotation cells, *Minerals Engineering*, 18:627–636.

Zhang, W, Nesset, J E and Finch, J A, 2010. Water Recovery and Bubble Surface Area Flux in Flotation, *Canadian Metallurgical Quarterly*, 49(4):353–362.

# Mill Operators

# Geometallurgy

# Application of advanced mineralogy to optimise flotation at the Hillgrove Gold–Antimony Project

*N Bristow[1] and J Li[2]*

1. Metallurgy Manager, Larvotto Resources, Nedlands WA 6009. Email: nick.bristow@larvottoresources.com
2. Principal Geometallurgist, AXT Pty Ltd, Belmont WA 6104. Email: jing.li@axt.com.au

## ABSTRACT

The process development phase of the redevelopment of the Hillgrove Gold–Antimony Project highlighted significant variability in flotation performance that could not be explained by conventional metallurgical test work alone. An integrated mineralogical and metallurgical investigation was undertaken to identify the fundamental controls on antimony and gold recovery and to define robust operating parameters for this complex, oxidation-prone sulfide system.

Quantitative mineralogy showed that antimony is almost entirely hosted as stibnite, occurring in texturally complex aggregates with quartz, pyrite and gold across a broad grain size range. Gold deportment analysis revealed that nearly half of the gold is associated with stibnite, either as inclusions or as invisible gold, explaining the strong coupling between Au and Sb recovery and the limited effectiveness of reagent-based separation. Thin oxidation rims on fine stibnite particles were identified as a key constraint on flotation kinetics and ultimate recovery, particularly in partially oxidised material.

Flotation testing demonstrated that liberation, oxidation state and gangue association govern metallurgical response. A primary grind size of $P_{80}$ 180 µm provided sufficient stibnite liberation while avoiding excessive fines generation, while controlled regrinding of the rougher concentrate significantly improved cleaner selectivity through liberation of ultrafine quartz. Collector comparisons showed that several reagents approached a mineralogically imposed recovery ceiling, confirming that recovery limits are controlled by oxidation rather than reagent inefficiency alone.

Collectively, these findings demonstrate that integrating quantitative mineralogy with flotation test work shifts the role of mineralogy from post-hoc explanation towards a more predictive understanding of metallurgical performance, providing a stronger basis for flotation optimisation at the Hillgrove Gold–Antimony Project.

## INTRODUCTION

Flotation optimisation in complex polymetallic sulfide systems remains a persistent challenge for the minerals processing industry. As orebodies become increasingly mineralogically heterogeneous, traditional empirical flotation test work, while still essential, often lacks the diagnostic power required to explain why certain ores respond well to a given reagent regime while others do not. This gap between metallurgical response and mineralogical cause frequently leads to sub-optimal flow sheet design, conservative operating envelopes, and elevated technical risk during project development.

The Hillgrove Gold–Antimony Project exemplifies this challenge. Despite a long production history, flotation performance has historically been variable, particularly with respect to antimony recovery and arsenic management. Previous operations relied largely on xanthate-based collectors and conventional sulfide flotation practices, achieving acceptable recoveries in some domains but struggling in others. The underlying reasons for this variability were never fully resolved, largely due to limited mineralogical resolution and an incomplete understanding of oxidation effects.

### Challenges in the mineral processing at Hillgrove Mine

The Hillgrove deposit is located near Armidale in the New England Fold Belt of New South Wales and hosts the largest known antimony resource in Australia, with significant associated gold mineralisation. Hillgrove has seen multiple waves of gold–antimony mining since the late 19th century, with modern antimony-focused operations from the 1970s and a new large-scale restart scheduled from 2026.

The gold–antimony mineralisation at Hillgrove has typical characteristics of orogenic gold deposits hosted in brittle structures at relatively shallow crustal depth (Craw and Norris, 1991; Hodgson, 1993; Goldfarb, Phillips and Nokleberg, 1998; Groves *et al,* 1998; Bierlein and Crowe, 2000). Mineralisation occurs in veins, breccias and immediately adjacent to altered wall rock. Initial mineralisation involved scheelite-bearing quartz veins, followed by arsenopyrite-pyrite-quartz-carbonate veining with associated gold and minor base metals, and these were later overprinted by paragenetically late stibnite-quartz veining with associated gold-electrum and arsenopyrite. Stibnite typically occurs as bladed or prismatic crystals, frequently intergrown with quartz and locally rimmed or veined by arsenopyrite. Pyrite occurs both as coarse euhedral grains and as fine disseminations within the gangue matrix.

These textural relationships are critical to flotation performance. Stibnite–arsenopyrite intergrowths, in particular, present challenges for selective flotation, as liberation of one mineral often implies partial liberation of the other.

Oxidation at Hillgrove is spatially variable and mineral-specific. Stibnite is particularly susceptible to surface oxidation, forming thin films of $Sb_2O_3$ and hydrated antimony oxides that significantly alter surface chemistry. Arsenopyrite and pyrite exhibit more limited oxidation under comparable conditions, leading to differential flotation behaviour.

Bulk sulfate assays provided an initial proxy for oxidation intensity, but detailed mineralogical analysis was required to understand how oxidation manifests at the particle scale and how it influences reagent adsorption and flotation kinetics.

## Limitations of conventional test work

Conventional flotation test work typically relies on bulk assays, mass balances, and grade–recovery relationships. While these metrics are indispensable, they offer limited insight into why a particular result is obtained. Without mineralogical context, it is difficult to distinguish between losses due to poor liberation, surface passivation, entrainment, or intrinsic mineral non-floatability.

At Hillgrove, early test work demonstrated clear differences in flotation response between composites, but these differences could not be satisfactorily explained using metallurgical data alone. This prompted the integration of advanced mineralogical tools.

## Advanced mineralogy tools

The TESCAN Integrated Mineral Analyzer (TIMA) is a scanning electron microscopy (SEM)-based automated mineralogy system used to quantify mineral abundance, grain size, liberation and mineral associations. These measurements provide the mineralogical context required to interpret flotation behaviour and optimise processing performance.

The intricate occurrence and distribution of gold present a difficulty for processing at Hillgrove mine, since it encompasses both free milling and refractory gold. A prior investigation (Jing, Ron and Vitor, 2024) identified gold intergrown with stibnite in the historical antimony concentrate. The relationship between gold and different sulfides must be quantified. The Automated Mineralogy Incubator (AMI), a division of AXT, has established a signature procedure for gold deportment studies. This method employs various mineral separation and measurement techniques, including gravity separators, microscopy, and TIMA, to accurately quantify the deportment of different gold types and assess their recoverability based on grain size, liberation, and association.

An ongoing geometallurgical program is also investigating the application of Laser Induced Breakdown Spectroscopy (LIBS) core scanning to extend mineralogical interpretation to deposit scale.

## Objectives of the study

Recognising the limitations of prior approaches, Larvotto Resources initiated a comprehensive metallurgical redevelopment program with the following objectives:

- Quantify the mineralogical deportment of antimony and gold across representative ore domains.

- Characterise sulfide textures, liberation, and oxidation at a resolution relevant to flotation behaviour.
- Optimise flotation reagent regimes, grind size, and regrind strategy based on mineralogical evidence.
- Develop a mineralogical framework to support future deposit-scale geometallurgical characterisation and ore domain definition.
- Establish the foundation for a predictive geometallurgical framework linking mineralogical characteristics with metallurgical performance to support future process optimisation.

# METHODOLOGY

## Composite selection and sample preparation

Multiple composite samples were prepared from channel samples to represent key metallurgical domains:

- **Resource Composite 3:** Primary sulfide ore with minimal oxidation, taken directly from the ore zone
- **Blended Composite:** Representative of average mill feed.
- **Partially oxidised Composite:** Upper-zone ore exhibiting partial oxidation and finer sulfide textures.

Composites were constructed to achieve representative Sb contributions and were prepared under controlled conditions to minimise additional oxidation.

## Flotation test work program

Batch rougher–cleaner flotation tests were conducted across a range of composites and grind sizes ($P_{80}$ 150, 180, and 212 µm). Reagent regimes included multiple collectors.

Intermediate regrind stages were incorporated in selected tests to assess the impact rougher regrind on cleaner performance.

In parallel with the flotation program, a separate LIBS-based geometallurgical program was initiated to support future predictive modelling.

## Mineralogical analysis workflow

The gold deportment study and quantitative mineralogical analysis were performed on head samples. Liberation analysis was also undertaken on the rougher concentrate, cleaner concentrate and final tailings to assess changes in mineral liberation throughout the flotation circuit.

Gold deportment was determined using the AMI precious metal deportment procedure, which incorporates gravity separation using a Superpanner. The grain size of liberated gold particles was measured manually using a stereomicroscope, and all gravity products were examined to verify separation efficiency. The cleaned gravity products were analysed for Au, S and Sb to quantify gold hosted within different mineral carriers. Automated mineralogical analysis was then used to characterise mineral abundance, grain size distribution, gold speciation and mineral associations. These analytical and mineralogical data sets were combined to quantify gold deportment within the concentrate.

Samples for automated mineralogical analysis were split to approximately 1 g, mixed with high-purity graphite powder and mounted in epoxy resin. Following curing, the mounts were polished, carbon coated and analysed using the TIMA system. Approximately 10 000–100 000 particles per sample were analysed at 1 µm resolution, providing statistically robust liberation and deportment data.

## MINERALOGICAL FINDINGS

### Antimony deportment

In Resource Composite 3, analysis confirmed that over 99 per cent of total antimony is hosted in stibnite. This finding was critical in validating a sulfide-focused flotation strategy and demonstrated that attempts to improve oxide antimony recovery would have minimal impact on overall performance. The stibnite grain size distribution is bimodal, with approximately 50 per cent of grains finer than ~60 µm and the remainder occurring at coarser sizes (Figure 1). This reflects the textural complexity of mineralisation and indicates that a single-stage fine grind would be inefficient, risking excessive breakage of fine, fragile stibnite. These characteristics support a staged grinding strategy, with coarse primary grinding followed by selective regrinding.

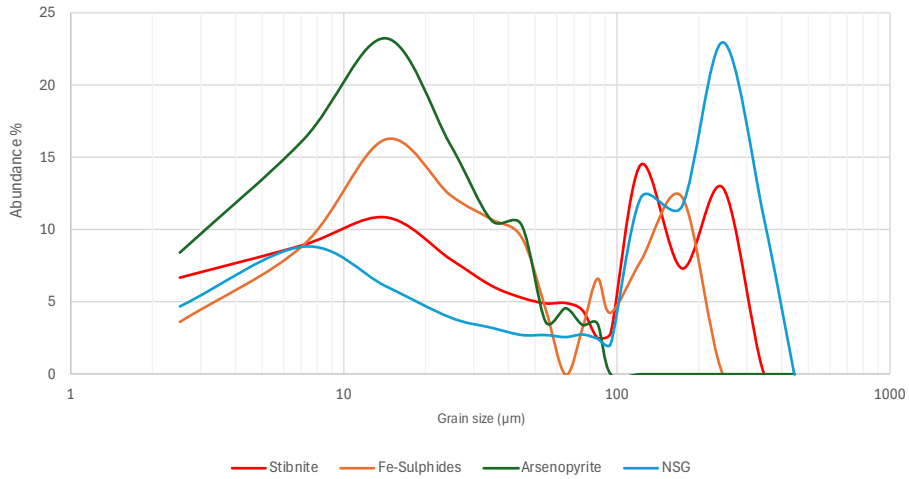



**FIG 1** – Stibnite grain size distribution for Resource Composite 3 at $P_{80}$ 300 µm.

The multiple stages of mineralisation at Hillgrove have resulted in a significant proportion of stibnite occurring in distinctive aggregated structures, characterised by brecciated stibnite fragments cemented by fine-grained stibnite (Figure 2). These aggregates commonly contain quartz, pyrite, and locally native gold (Sb: stibnite; Py: pyrite; Qz: quartz; Au: native gold), reflecting the complex paragenesis of the deposit. Such textural complexity imposes strong controls on liberation behaviour and contributes to the formation of high-grade middlings at coarse grind sizes. Liberation analysis (Figure 3) shows that at $P_{80}$ 300 µm, approximately 60 per cent of the stibnite is liberated, with a further 29 per cent present as high-grade middlings (>60 per cent stibnite by volume) and 8 per cent as intermediate middlings (30–60 per cent stibnite). Overall, approximately 90 per cent of the stibnite is amenable to flotation. These mineralogical characteristics support a staged comminution strategy, whereby coarse primary grinding in the rougher circuit is combined with targeted regrinding of the rougher concentrate to improve separation efficiency.

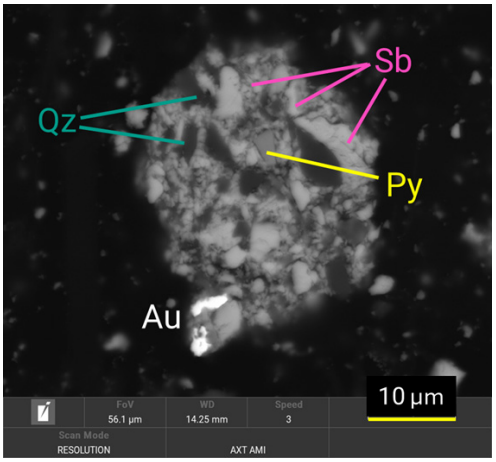



**FIG 2** – SEM image of stibnite aggregates with associated quartz, pyrite and gold.




**FIG 3** – TIMA phase images showing stibnite liberation by particle size.

## Gold deportment

Gold deportment was determined for Resource Composite 3 at a grinding size of $P_{80}$ 300 µm. The composite assayed 10.59 g/t Au and 6.69 per cent Sb. Figure 4 illustrates the principal modes of gold occurrence identified by the deportment study. Liberated gold grains (Figure 4a) are generally coarser than 40 µm and are readily amenable to gravity recovery. Exposed gold associated with stibnite (Figure 4b) typically exceeds 10 µm and is expected to report to the antimony rougher concentrate, where subsequent regrinding can further improve liberation. A significant proportion of gold occurs as ultrafine inclusions or submicroscopic gold within stibnite (Figure 4c), with additional invisible gold hosted within arsenopyrite and pyrite. These observations demonstrate the textural complexity of gold occurrence and indicate that a substantial proportion of the gold recovery is intrinsically linked to sulfide recovery.

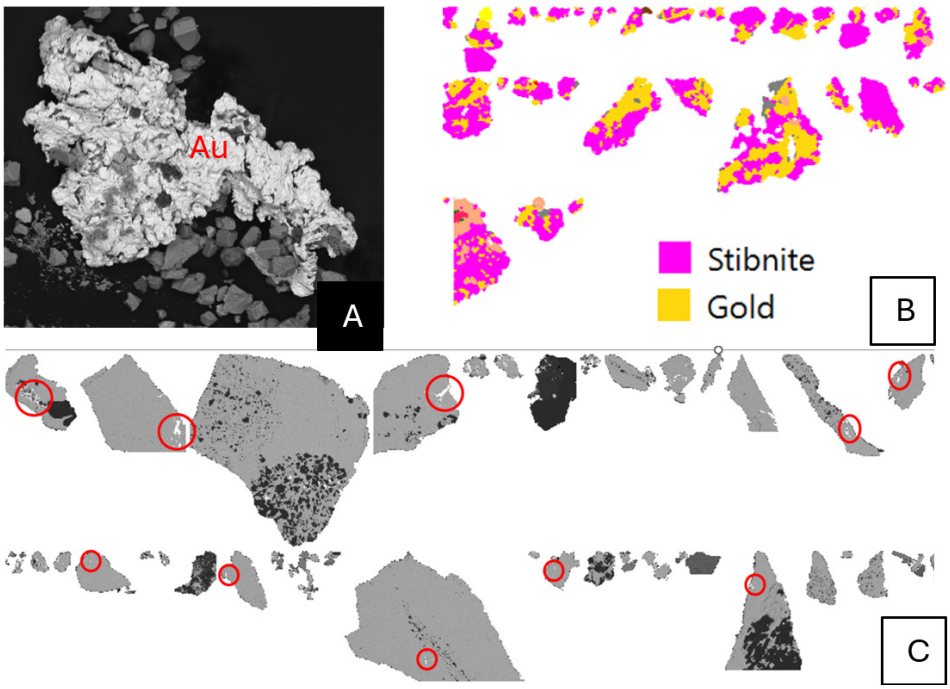



**FIG 4** – Gold occurrence in Resource Composite 3 showing: (a) liberated gold; (b) exposed gold associated with stibnite; and (c) gold locked within stibnite.

Figure 5 quantifies the deportment of gold within Resource Composite 3. Approximately 48 per cent of the gold is hosted within stibnite, either as ultrafine inclusions or invisible gold, while a further 27 per cent occurs within arsenopyrite and pyrite. Only 18 per cent of the gold is present as liberated gravity-recoverable particles, with the remaining 7 per cent occurring as exposed gold associated with stibnite. This distribution explains the strong correlation observed between antimony and gold recovery during flotation, as nearly three-quarters of the gold is hosted within sulfide minerals. Consequently, recovery of gold is fundamentally linked to stibnite recovery, limiting the effectiveness of reagent-based Au–Sb separation. Instead, improvements in gold recovery are more effectively achieved through mineralogy-driven process modifications, particularly optimisation of grind size and targeted regrinding to expose gold-bearing phases.

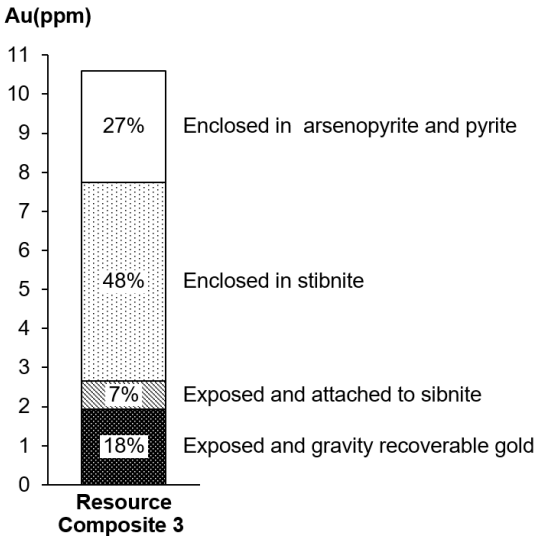



**FIG 5** – Distribution of gold occurrences in Resource Composite 3.

## Oxidation characteristics

Quantitative analysis identified the presence of antimony oxide phases in the partially oxidised composites, with oxide abundance increasing with both oxidation intensity and finer grind size (Figure 6). In the Resource Composite, antimony is almost entirely hosted as stibnite, whereas the partially oxidised material contains an elevated proportion of Sb oxide phases. While oxide antimony represents a relatively small mass fraction, thin oxidation rims are commonly developed on fine stibnite particles, particularly in the partially oxidised material. These oxidation features are typically less than 1 µm thick but exert a disproportionate influence on flotation performance by inhibiting collector adsorption and reducing flotation kinetics.

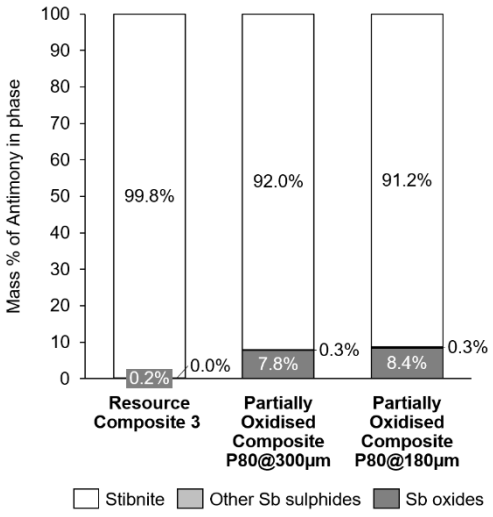



**FIG 6** – Antimony deportment by mineral host for Resource and partially oxidised composites at different grind sizes.

The presence of surface oxidation therefore imposes a mineralogically defined recovery ceiling on achievable Sb recovery under conventional sulfide flotation conditions. This mineralogically constrained recovery ceiling explains why several collectors approach similar maximum recoveries despite differing chemistries and highlights that flotation performance in partially oxidised material is controlled primarily by surface condition rather than reagent selection.

# METALLURGICAL TEST WORK RESULTS

## Grind size effects

Figure 7 shows the flotation performance of the Blended composite at different grind sizes. Sb recovery increases with decreasing grind size, with finer grinds exhibiting faster initial flotation kinetics. Differences in recovery between grind sizes are most pronounced at short flotation times and diminish as residence time increases. Beyond approximately four mins, Sb recovery approaches a plateau for all grind sizes, with minimal incremental gains thereafter. The 212 µm grind consistently displays slower kinetics and lower recovery, while the 150 and 180 µm grinds converge at longer flotation times.

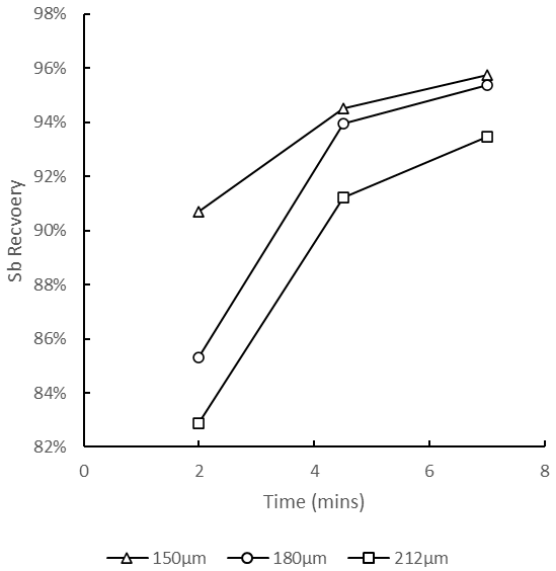



**FIG 7** – Sb recovery versus flotation time at three primary grind sizes.

The observed increase in recovery with finer grinding indicates improved liberation of stibnite. Mineralogical analysis (Figure 1) shows a trimodal stibnite grain size distribution with peaks centred at approximately 300, 150, and 20 µm. The flotation results indicate that a grind size of 180 µm is nearly as effective as 150 µm in liberating stibnite associated with the ~150 µm size fraction On this basis, and considering reduced energy consumption and the higher throughput achievable at coarser grind sizes, a design grind size of 180 µm was selected.

## Collector performance

The rougher grade–recovery curves for the partially oxidised composite shown in Figure 8 demonstrate clear and systematic differences in collector performance, confirming that collector selection has a strong influence on both Sb concentrate grade and recovery. All collectors exhibit the expected inverse relationship between grade and recovery; however, significant variation is observed in the shape, slope, and extent of the grade–recovery curves, indicating differing levels of flotation selectivity. A summary of the principal collector chemistries evaluated in this study is provided in Table 1.

Quantitative mineralogical analysis (Figure 6) shows that the partially oxidised feed contains approximately 8.4 per cent oxidised antimony, which imposes a mineralogically defined recovery ceiling on achievable Sb recovery under conventional sulfide flotation conditions. Several collectors approach this theoretical recovery limit, indicating that reduced performance at higher recoveries is

largely constrained by mineralogical factors rather than reagent inefficiency alone. Recognition of this oxidation-imposed recovery ceiling provides important context for interpreting rougher flotation performance and provides context for realistic recovery targets and the practical limits of selectivity in the rougher stage (Figure 9).

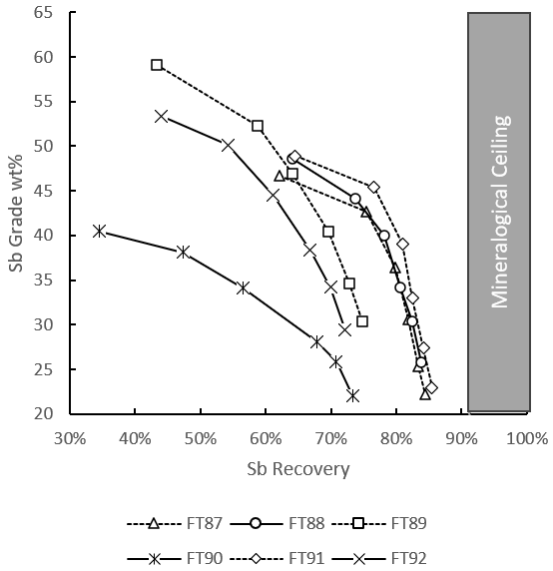



**FIG 8** – Sb grade–recovery relationships for evaluated collectors.

**TABLE 1**

Summary of collector chemistries evaluated.

| Float test | Collector chemistry |
|---|---|
| FT87 | Dithiophosphate |
| FT88 | Dithiophosphate Blend |
| FT89 | Dithiophosphate Blend |
| FT90 | Dithiocarbamate |
| FT91 | Diisobutyldithiophosphoric acid |
| FT92 | Diisopropyldithiophosphoric acid, sodium salt |

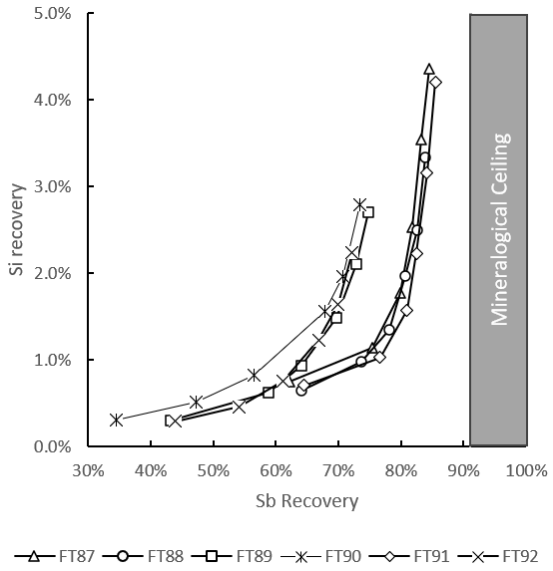



**FIG 9** – Sb – Si collector selectivity.

Collectors FT87, FT88 and FT91 define the upper performance envelope. FT87 achieves the highest Sb grades at lower to intermediate recoveries, indicating strong selectivity at modest mass pulls. FT91 exhibits grade–recovery behaviour comparable to FT87 and FT88 across much of the recovery range and shows improved grade retention at higher recoveries, maintaining similar or marginally higher Sb grades above ~75 per cent recovery. This suggests FT91 provides a broader and more robust operating window, particularly where higher recovery targets are desired.

FT88 performs similarly to FT87 at intermediate recoveries but demonstrates a steeper decline in Sb grade as recovery increases. FT89 achieves moderate grade–recovery performance but remains below the leading collectors, particularly at higher recoveries.

In contrast, FT90 consistently exhibits inferior performance, producing substantially lower Sb grades at all recoveries, indicating poor selectivity under the tested conditions. The divergence between collectors becomes more pronounced at higher recoveries, highlighting that collector choice is especially critical when targeting elevated Sb recovery while maintaining concentrate grade.

## Regrind performance

Figure 10 illustrates the effect of regrind time on Cleaner 2 grade–recovery performance for the Blended composite. Regrinding results in a substantial increase in Sb concentrate grade relative to the no-regrind condition, confirming the importance of regrind prior to cleaning. Analysis identified the presence of quartz and ultrafine quartz intimately associated with the stibnite matrix; regrinding promotes liberation of this ultrafine quartz, thereby reducing silica reporting to the cleaner concentrate and increasing Sb grade. A regrind time of 1 minute provides the most favourable grade–recovery relationship, achieving higher Sb grades at comparable recoveries than both the 0 and 2 minute tests. Increasing the regrind time to 2 minutes results in diminished concentrate grade, indicating overgrinding and a corresponding reduction in flotation selectivity.

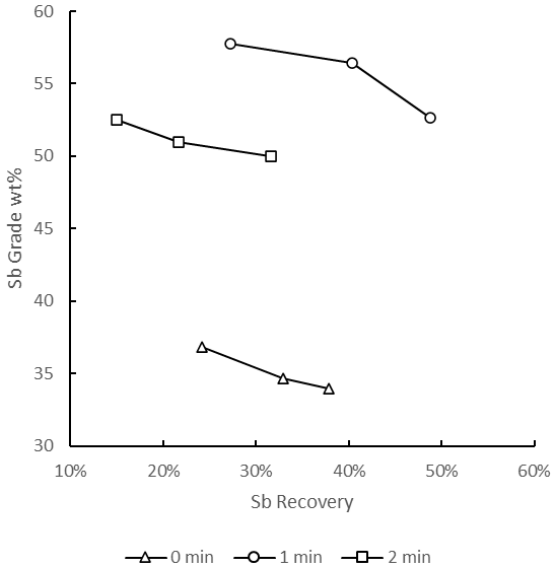



**FIG 10** – Effect of regrind time on Cleaner 2 Sb grade–recovery performance.

## Composite variability

The rougher grade–recovery responses shown in Figure 11 demonstrate distinct differences in flotation behaviour between the Blended, Partially Oxidised, and Resource Composites, tested under the same conditions. All three materials exhibit the expected inverse relationship between Sb grade and recovery; however, both the shape and extent of the curves vary markedly. The dashed vertical lines indicate the mineralogically defined recovery limits for the partially oxidised and blended/resource composites, derived from quantitative mineralogical assessment of oxidised antimony in each material. The Resource Composite delivers the most favourable rougher performance overall, maintaining relatively high Sb grades across a broad recovery range and achieving the highest Sb recoveries prior to a pronounced grade decline. This indicates that rougher recovery for the Resource Composite is largely achieved through selective flotation over much of

the recovery range, with a transition to less selective recovery mechanisms occurring only at the upper end of recovery as the mineralogically defined recovery limit is approached.

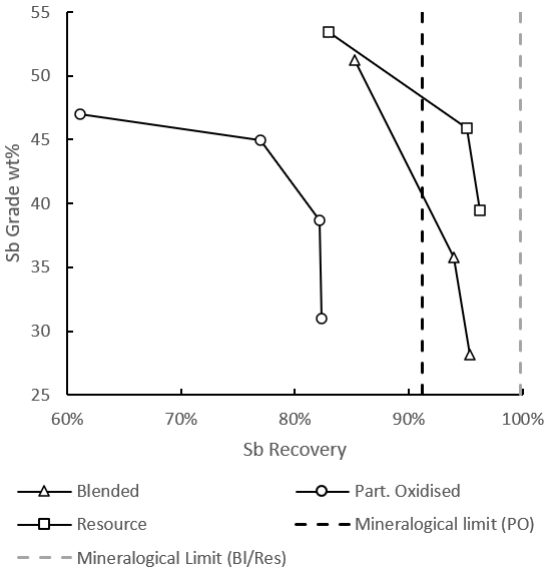



**FIG 11** – Rougher Sb grade–recovery relationships for the Blended, Partially Oxidised and Resource Composites. Dashed vertical lines indicate the mineralogically defined recovery limits derived from quantitative mineralogical assessment of oxidised antimony.

The Blended composite also exhibits a strong rougher response, achieving moderate to high Sb recoveries at comparatively elevated concentrate grades. However, when pushed toward very high recovery, the Blended composite shows an earlier onset of grade deterioration relative to the Resource material, indicating a narrower high-recovery operating window despite sharing a similar theoretical recovery limit. In contrast, the Partially Oxidised composite exhibits the earliest decline in concentrate grade with increasing recovery and a lower mineralogically defined recovery limit, reflecting the greater proportion of oxidised stibnite and reduced flotation selectivity.

Overall, the grade–recovery curves indicate that while all three composites are amenable to rougher flotation, the effectiveness and selectivity of rougher recovery vary substantially. The Resource Composite supports high recovery operation with comparatively robust grade retention up to its mineralogically defined recovery limit, whereas the Blended and Partially Oxidised composites require more conservative rougher recovery targets to avoid excessive grade dilution. The close relationship between the observed grade–recovery behaviour and the mineralogically defined recovery limits further demonstrates that oxidation intensity is a primary control on achievable Sb recovery, with reagent selection and operating conditions acting within these mineralogical constraints.

## MINERALOGICALLY INFORMED FLOW SHEET OPTIMISATION

Flotation performance at Hillgrove is fundamentally controlled by mineralogical factors rather than operating conditions alone. Antimony deportment is almost exclusively sulfide-hosted as stibnite, validating a sulfide flotation strategy and establishing that recovery is constrained by stibnite liberation and oxidation. A primary grind size of $P_{80}$ 180 µm provides sufficient liberation for effective rougher flotation while avoiding excessive generation of fines, and regrinding of the Sb rougher concentrate to $P_{80}$ 45 µm improves cleaner selectivity through liberation of ultrafine quartz. Oxidised antimony imposes a mineralogically defined recovery ceiling on achievable Sb recovery, which several collectors approach, demonstrating that recovery ceilings are primarily mineralogically constrained rather than reagent-limited. Variations in rougher grade–recovery behaviour between composites reflect differences in oxidation intensity and stibnite texture, with the Resource Composite supporting selective flotation to higher recoveries than the Blended and Partially Oxidised materials.

Based on the combined mineralogical and flotation investigations, the adopted process design comprised primary grinding to $P_{80}$ 180 µm, gravity gold recovery, antimony rougher flotation, regrinding of the antimony rougher concentrate to $P_{80}$ 45 µm prior to cleaning, followed by arsenopyrite rougher flotation incorporating regrinding of the arsenopyrite rougher concentrate to $P_{80}$ 30 µm. A mineralogically optimised process flow sheet is shown in Figure 12. The flow sheet is configured to maximise early recovery of liberated value while managing the textural complexity and oxidation sensitivity identified through mineralogical analysis shown in Table 2. A gravity separation stage is included upstream to recover liberated coarse gold, reducing downstream gold losses and circulating load. Gravity tails report to the antimony rougher circuit, where liberated and weakly locked stibnite is recovered at a relatively coarse primary grind, consistent with mineralogical evidence showing a high proportion of floatable stibnite at this size. Antimony rougher tails are subsequently treated in an arsenopyrite rougher circuit to recover gold not captured with stibnite, reflecting the strong but incomplete Au–Sb association.

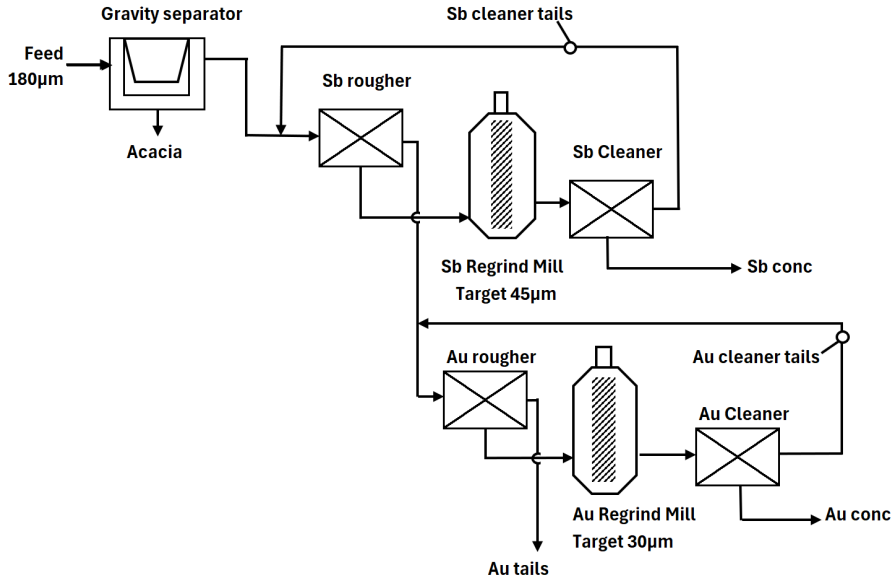



**FIG 12** – Proposed mineralogically informed process flow sheet for Hillgrove.

**TABLE 2**

Mineralogical characteristics and recommended operational focus for the principal geometallurgical domains identified at Hillgrove.

| Characteristic | Primary sulfide | Transitional | Partially oxidised |
|---|---|---|---|
| Oxidation | Low | Moderate | High |
| Liberation | Good | Moderate | Variable |
| Sb rougher recovery | High | Moderate | Oxidation limited |
| Cleaner selectivity | High | Moderate | Lower |
| Operational emphasis | Maximise recovery | Balance recovery and grade | Maintain grade |

Targeted regrinding of rougher concentrates is applied only where required to improve liberation of stibnite from quartz and sulfide gangue and to enhance cleaner Sb selectivity, while avoiding unnecessary overgrinding of the bulk feed. The individual investigations presented throughout this paper were designed to resolve specific mineralogical and metallurgical uncertainties influencing circuit performance, and collectively provided the technical basis for the adopted comminution and flotation flow sheet and operating conditions rather than representing optimisation of the complete circuit through a single integrated test program. Overall, the flow sheet adopts a staged recovery

strategy that aligns processing intensity with mineralogical characteristics, providing a robust and flexible design capable of accommodating variability across the Hillgrove orebody.

## DEPOSIT-SCALE INTERPRETATION AND PREDICTIVE GEOMETALLURGY – HILLGROVE AS A CASE STUDY

The Hillgrove Gold–Antimony Project provides a clear case study demonstrating the value of predictive geometallurgy for complex sulfide systems. Metallurgical performance at Hillgrove is not governed by head grade alone, but by mineralogical variables including stibnite texture, grain size distribution, oxidation state, and mineral association. These characteristics vary systematically across the orebody and exert first-order control on flotation kinetics, selectivity, and achievable recovery. As such, conventional geological or grade-based domains are insufficient to predict processing response.

The results demonstrate that mineralogical characteristics can be translated into practical processing domains, allowing flotation performance to be anticipated from mineralogical attributes rather than inferred solely from laboratory metallurgical test work. At Hillgrove, mineralogical data explains why recovery ceilings exist, why certain collectors perform similarly despite different chemistries, and why regrind and grind size optimisation are effective mitigation strategies rather than incremental operating adjustments.

### Mineralogical controls on metallurgical response

A limited number of mineralogical parameters were identified as dominant controls on flotation performance:

- Stibnite grain size and texture, which govern liberation, flotation kinetics, and susceptibility to over-grinding.
- Degree of stibnite surface oxidation, which suppresses collector adsorption and imposes a mineralogically defined recovery ceiling on sulfide flotation recovery.
- Gold association with stibnite, which explains the strong correlation between Au and Sb recovery and constrains separation by reagent selection alone.
- Gangue association, particularly ultrafine quartz within stibnite aggregates, which drives silica entrainment and cleaner selectivity.

These parameters consistently explained observed trends across grind size tests, collector comparisons, regrind optimisation, and composite variability, demonstrating that performance differences were intrinsic to the ore rather than artefacts of laboratory conditions.

### From mineralogy to predictive domains

By linking mineralogical attributes directly to flotation response, Hillgrove ores can be classified into geometallurgical domains based on processing behaviour rather than lithology alone:

- Primary sulfide domain, characterised by coarse, weakly oxidised stibnite with robust rougher selectivity and high recovery potential.
- Transitional domain, exhibiting moderate oxidation and variable stibnite textures, requiring tighter control of grind size and reagent strategy.
- Oxidised domain, defined by fine, surface-oxidised stibnite with reduced kinetics and lower recovery ceilings, necessitating regrind and selective reagent regimes.

These domains provide a practical framework for anticipating metallurgical response from mineralogical indicators and for designing adaptive processing strategies.

### Bridging core data and plant performance

While automated mineralogical techniques such as TIMA provide detailed particle-scale characterisation of mineral deportment, liberation and oxidation, their relatively low throughput limits application at the deposit scale. To extend these mineralogical insights across the orebody, Larvotto

Resources has commenced a geometallurgical program integrating Laser Induced Breakdown Spectroscopy (LIBS) with metallurgical test work.

The program is currently being developed to generate a predictive metallurgical database by combining high-resolution LIBS core scans with laboratory comminution and flotation test work. Representative drill core intervals are being scanned using LIBS, followed by crushing, grinding and flotation testing to quantify comminution performance, flotation response and concentrate quality. The resulting data set will be used to investigate relationships between LIBS-derived mineralogical signatures and key metallurgical outcomes, including antimony and gold recovery, concentrate grade, grinding characteristics, reagent response and costs.

The long-term objective is to establish a predictive geometallurgical framework capable of forecasting metallurgical performance directly from LIBS data. By linking mineralogical characteristics identified during resource definition drilling with downstream processing behaviour, the approach has the potential to improve ore domain definition, support mine planning and blending strategies, and enable more proactive process control during plant operation.

## Operational implications

The integration of mineralogy and flotation behaviour at Hillgrove enables proactive rather than reactive process control. Mineralogical indicators can be used to:

- Define achievable recovery targets constrained by oxidation and liberation.
- Optimise grind size and regrind intensity by ore domain.
- Guide collector selection and dosage strategies.
- Inform blending decisions to stabilise mill feed and concentrate quality.

This approach represents a shift from static flow sheet optimisation toward ore-responsive processing and demonstrates why mineralogy has a central role in the operation and long-term optimisation of complex sulfide mines.

# FUTURE WORK AND GEOMETALLURGICAL IMPLEMENTATION

Future work will focus on validating and implementing the predictive geometallurgical framework as the LIBS-metallurgical database expands to encompass a broader range of ore types, alteration styles and oxidation states across the Hillgrove deposit. The integrated data set will provide a robust foundation for the application of statistical modelling and machine learning techniques to identify relationships between LIBS-derived mineralogical signatures and key processing parameters, including comminution performance, flotation recovery, concentrate grade and reagent response. The objective is to develop predictive models capable of forecasting metallurgical performance directly from drill core, enabling more informed ore domain definition, mine planning, stockpile management and adaptive process control. As the framework matures, integration of predicted metallurgical performance with comminution characteristics and processing costs will enable incorporation into NSR models and Mine to Mill optimisation workflows, supporting mine scheduling, stope sequencing and blending strategies based on expected metallurgical performance rather than grade alone. As the database continues to mature, the predictive capability of these models will be refined and validated, supporting the transition from empirical metallurgical characterisation towards data-driven process optimisation throughout the life of the operation.

# CONCLUSIONS

This study demonstrates that flotation performance at the Hillgrove Gold–Antimony Project is fundamentally controlled by mineralogical factors rather than operating conditions alone. Quantitative mineralogy confirmed that antimony is almost exclusively hosted as stibnite, validating a sulfide-focused flotation strategy and establishing that achievable recovery is constrained by stibnite liberation, texture, and oxidation state.

Stibnite occurs across a broad grain size distribution and commonly forms texturally complex aggregates with quartz, pyrite, and gold, resulting in a significant proportion of high-grade middlings

at coarse grind sizes. A primary grind size of $P_{80}$ 180 µm was shown to provide sufficient liberation for effective rougher flotation while avoiding excessive fines generation. Targeted regrinding of rougher concentrates significantly improved cleaner selectivity by liberating ultrafine quartz and enhancing exposure of gold associated with stibnite.

Thin oxidation rims on fine stibnite particles were identified as a critical control on flotation kinetics and ultimate recovery, imposing a mineralogically defined recovery ceiling in partially oxidised material. Collector test work showed that several reagents approach this mineralogically defined limit, confirming that reduced performance at high recovery is primarily oxidation-constrained rather than reagent-limited.

Differences in rougher grade–recovery response between Resource, Blended, and Partially Oxidised composites reflect systematic variations in oxidation intensity and stibnite texture across the orebody. The study demonstrates that quantitative mineralogy provides a robust framework for understanding and predicting metallurgical variability, forming the foundation for future geometallurgical implementation at Hillgrove.

## ACKNOWLEDGEMENTS

The authors acknowledge Larvotto Resources Ltd for project access and funding, AXT PTY LTD for advanced mineralogical analysis, and IMO PTY LTD for flotation test work support.

## REFERENCES

Bierlein, F P, and Crowe, D E, 2000. Phanerozoic orogenic lode gold deposits, *Rev Econ Geol*, 13:103–139.

Craw, D and Norris, R J, 1991. Metamorphogenic Au-W veins and regional tectonics: mineralisation throughout the uplift history of the Haast Schist, New Zealand, *NZ J Geol Geophys,* 34:373–383.

Goldfarb, R J, Phillips, N and Nokleberg, J, 1998. Tectonic setting of synorogenic gold deposits of the Pacific Rim, *Ore Geol Rev*, 13:185–218.

Groves, D I, Goldfarb, R J, Gebre-Mariam, M, Hagemann, S G and Robert, F, 1998. Orogenic gold deposits: a proposed classification in the context of their crustal distribution and relationship to other gold deposit types, *Ore Geol Rev*, 13:7–27.

Hodgson, C J, 1993. Mesothermal lode-gold deposits, in *Mineral Deposit Modelling* (eds: R V Kirkham, W D Sinclair, R I Thorpe and L M Duke), *Geol Assoc Can Spec Pap*, 40:635–678.

Jing, L, Ron, H and Vitor, M N, 2024. Quantitative gold deportment study for the redevelopment Hillgrove gold-antimony ore, in *Proceedings of the Australian Journal of Earth Sciences GOLD24*, pp 189–194 (Australian Institute of Geoscientists).

# Using the Geopyörä breakage test in a Mine to Mill application at a large copper mine

*M Bueno[1], L Lara[2], T de Almeida[3] and M Powell[4]*

1. CEO, Geopyörä, Oulu 90530, Finland. Email: ceo@geopyora.com
2. Process Engineer, Geopyörä, Oulu 90530, Finland. Email: leonardo@geopyora.com
3. Data Science Manager, Geopyörä, Oulu 90530, Finland. Email: thiago@geopyora.com
4. CTO, Geopyörä, Oulu 90530, Finland. Email: cto@geopyora.com

## ABSTRACT

Mine-to-mill (M2M) programs aim to maximise comminution circuit performance by integrating blasting and milling operations. However, the effectiveness of these programs depends on a representative ore characterisation strategy to accurately quantify ore competency and its impact on the plant.

In this context, the Geopyörä device offers a fast characterisation tool that requires only a small sample mass to perform testing. The device is capable of testing both blast chips and drill core samples while delivering near real-time results through automated data processing within the Geopyörä online system (Geodata platform).

This paper presents the methodology and workflow developed to integrate the Geopyörä test into a Mine-to-Mill framework at a large copper mine. The proposed approach utilises blast-derived and core-derived samples to generate hardness parameters that were incorporated into comminution circuit throughput forecasting models. Initial validation results are presented through comparisons between predicted throughput and actual plant performance data.

In parallel, a geometallurgical modelling workflow was developed through submitting some of the samples tested on the Geopyörä to XRD analysis to obtain their geochemical data. Machine-learning techniques were applied to build the forecasting models for the Drop Weight Index (DWi) and Bond Ball Mill Work Index (BWi), allowing comminution properties to be forecasted for future ore blocks. The findings demonstrate the potential of the Geopyörä device as a practical and reliable tool for both short-term Mine-to-Mill optimisation and long-term geometallurgical modelling in large-scale operations.

## INTRODUCTION

It is well established that Mine-to-Mill (M2M) programs have significant potential to increase the throughput of comminution circuits (Grundström *et al,* 2001; Lam *et al,* 2001; La Rosa *et al,* 2015; Glauber *et al,* 2021). These improvements are primarily achieved through the optimisation of blasting to produce finer run-of-mine (ROM) fragmentation. By increasing the proportion of finer particles and reducing the top size entering the crushing and grinding stages, the load on downstream comminution equipment can be reduced, resulting in higher processing capacity and improved overall energy efficiency.

This effect is particularly pronounced in autogenous (AG) and semi-autogenous (SAG) mills, where feed size distribution directly affects their performance (Morrell and Valery, 2001). Because these mills rely partially or fully on the ore itself as grinding media, changes in fragmentation significantly influence the breakage energy distribution in the mill, which along with changes in ore competence have a direct impact on mill throughput. Studies have shown that an increased proportion of fines in the mill feed can lead to measurable increases in mill capacity (Simkus and Dance, 1998). However, blast fragmentation should be tuned to the ore competence to provide an optimal rock load in the mill, as too fine is undesirable if the ore is not sufficiently competent as the mill loses the required rock load (Powell *et al,* 2019).

### The Geopyörä breakage test

The Geopyörä is a breakage testing device designed to characterise ore competency with the use of two rotating wheels, the device measures energy loses and force at the moment of breakage for

each particle that passes through the wheels, it requires a small sample mass (around 2 kg per sample) and delivers results within a short testing time through the use of its automated data analysis system – called Geodata. Geodata generates the main industry-standard comminution parameters, including the Axb parameter (Napier-Munn *et al,* 1996), the Drop Weight Index (DWi) (Morrell, 2004), and the Bond Ball Work Index (BWi) (Bond, 1952). In addition, the device provides its own proprietary parameter, the Geopyörä Index (GPi) (Bueno, Almeida and Lara, 2024), the results become available minutes after upload.

Because the test requires only a limited sample mass and testing can be done quickly, the Geopyörä is well suited for geometallurgical applications. Drill core samples can be tested metre-by- metre, and the tested material can subsequently be submitted for geochemical or mineralogical analysis, enabling the integration of ore competency parameters with geochemical data sets.

Figure 1 illustrates the current Geopyörä device (Version 2). The upgraded version uses a newly developed software interface and an automated particle feeder system, replacing the manual feeding mechanism used in Version 1 (Bueno *et al,* 2021). The implementation of these improvements significantly improves the operational workflow by standardising sample feeding and reducing operator workload. As a result, Version 2 further improves testing efficiency and productivity while not affecting the test results.

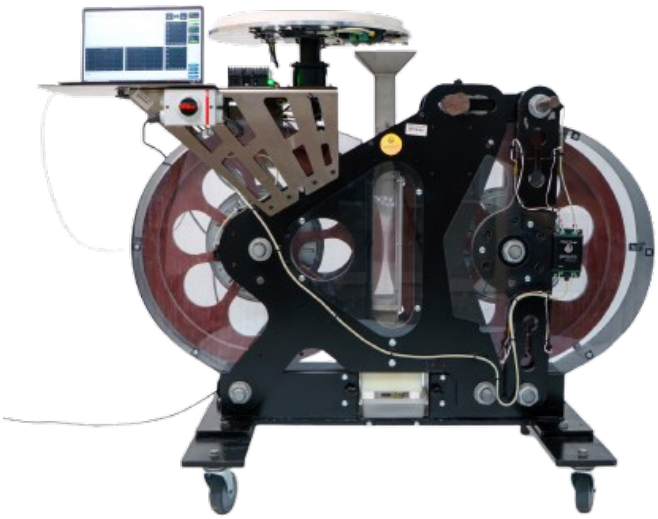


**FIG 1** – The Geopyörä V2 Breakage device.

## The Geopyörä test workflow

The procedure of the Geopyörä test is a straightforward workflow that has the potential of achieving high daily testing in a mine site laboratory, provided that proper coordination between geology, laboratory, and processing teams is established. Figure 2 presents the complete workflow of the Geopyörä test, from sample collection to the generation of final ore competency parameters.

The process starts with the collection of samples, which may be from drill core or blast chips collected directly from the pit. The gathered samples are first crushed using a laboratory jaw crusher to reduce the particles to the necessary ranges of the test. Crushed product is then subjected to a sieving stage using the sieve series presented in Table 1 to obtain required size ranges.

Two specific size fractions are selected for the test procedure. Of the two, the coarser fraction is typically used for specific gravity (SG) measurement, while the finer fraction is used in the Geopyörä for breakage testing. The use of two different sizes makes for a good workflow as it allows the SG measurement and breakage stages to happen parallel. Over the years of Geopyörä tests, the most commonly used size fractions for testing have been:

- -26.5/+22.4 for SG and -22.4/+19 for breakage.
- -22.4/+19 for SG and -19/+16 for breakage.

Only the size classes that are used need be screened from the crushed feed.

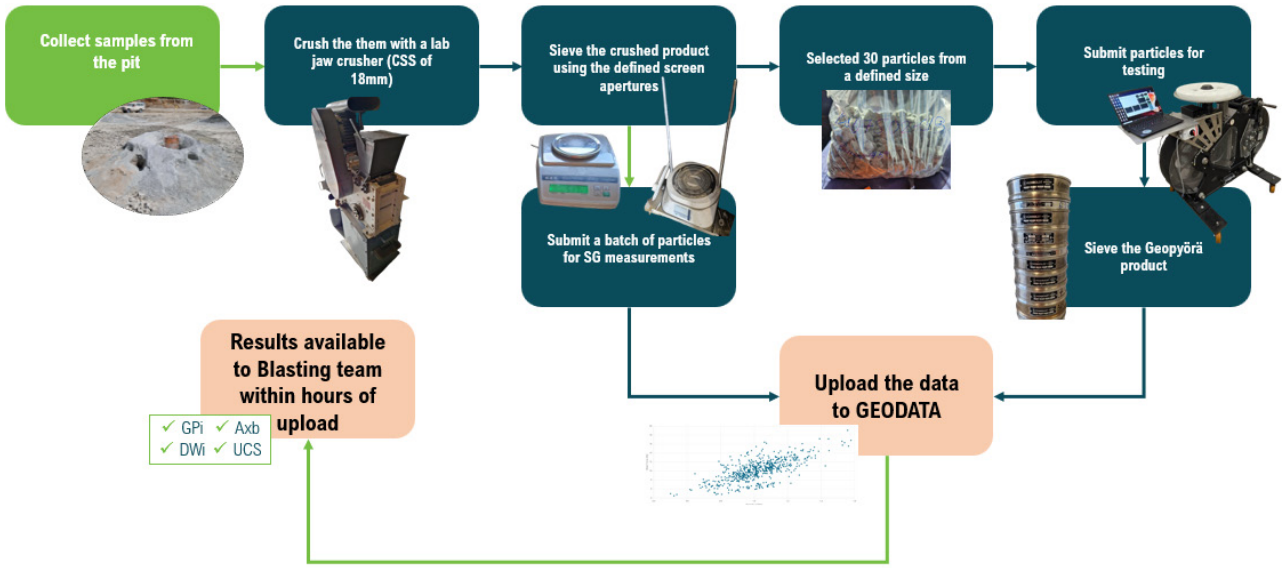



**FIG 2** – Flow chart of the Geopyörä test from sample collection to results.

**TABLE 1**

Size classes used in the Geopyörä test.

| Size class (mm) | Primary/secondary use |
|---|---|
| - 31.5 + 26.5 | SG measurement/Breakage test |
| -26.5 + 22.4 | SG measurement/Breakage test |
| - 22.4 + 19.0 | Breakage test/SG measurement |
| - 19.0 + 16.0 | Breakage test/SG measurement |
| - 16.0 + 13.2 | Breakage test/SG measurement |

Once the target particle size fractions have been selected, both the specific gravity (SG) determination and the breakage test can be conducted. Prior to testing in the Geopyörä, 30 individual particles must be selected. During this selection process, flaky or highly elongated particles are discarded, as they may pass between the wheels without experiencing breakage, particles passing between the wheels without breaking don't affect the test results as the data and the particle are removed from the data set. However, if too many pass then the test may need to be discarded due to the low number of particles that experienced breakage.

After particle selection, the breakage test is performed in the Geopyörä device. The resulting broken material is then collected at the bottom of the machine screened on a limited set of sieves to provide the key size classes needed to quantify the breakage. At the conclusion of the procedure, three main data sets are obtained: (i) the specific gravity (SG) measurement, (ii) the particle size distribution of the broken product, and (iii) a file generated by the Geopyörä machine containing force and energy measurements recorded during each breakage event. All data sets are subsequently uploaded to Geodata, the Geopyörä online processing platform, which automatically analyses the inputs and calculates the corresponding comminution parameters. Within a few minutes, the platform provides the full set of results.

Samples tested using the Geopyörä can also be submitted for further laboratory analysis, allowing continuous data generation to populate a geometallurgical model. Geochemical assays were conducted using Inductively Coupled Plasma (ICP) techniques to quantify elemental concentrations within each sample, providing detailed chemical composition data while mineralogical characterisation was performed using X-ray diffraction (XRD).

## IMPLEMENTATION OF THE GEOPYÖRÄ IN A MINE-TO-MILL PROGRAM

Understanding ore competency is fundamental for designing and optimising blasting. Accurate knowledge of breakage properties allows blast designs to be customised to the specific mechanical behaviour of the rock, which in turn maximises fragmentation efficiency and consequently increases comminution circuit throughput. Good ore characterisation is an essential step in integrating Mine-to-Mill strategies to improve downstream performance (Scott, Segui and Kanchibotla, 2000).

To make this process effective as possible, ore characterisation must be performed rapidly enough that the data is available to assist in operational decisions. In this context, the Geopyörä test offers a practical and straightforward solution. As shown in Figure 3, samples collected directly from drill chips at the mine can be tested on-site, once the test is completed, the results will be available through the Geodata platform, allowing results to be made available to the blast engineering team on the same day of testing. This enables the creation of a rapid feedback loop between ore characterisation and blasting optimisation, enhancing the effectiveness of a mine-to-program.

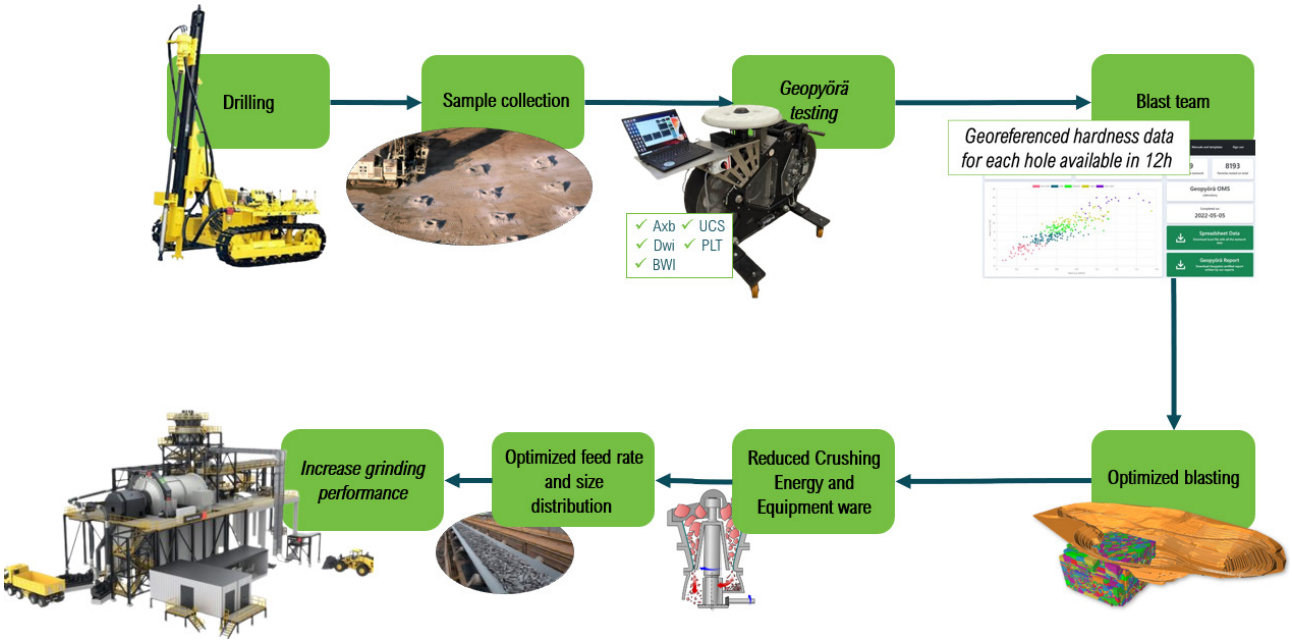



**FIG 3** – Mine-to-Mill flow chart proposed by Geopyörä.

In parallel with the Mine-to-Mill program, selected samples were also submitted for geochemical analysis to support the development of a geometallurgical model based on the results of the Geopyörä and geochemical tests. The immediate objective of the program was to generate parameters (UCS/PLA) rapidly and provide them to the blasting team, enabling adjustments to blast design and immediate operational impact.

Simultaneously, additional testing was conducted by integrating Geopyörä breakage parameters with geochemical data to develop predictive models capable of forecasting comminution properties across the orebody. This combined data set formed the basis of the geometallurgical model, enabling the prediction of comminution behaviour prior to mining and supporting the long-term optimisation of the Mine-to-Mill program. To achieve this, the products generated from the Geopyörä tests were submitted for XRD and geochemical analyses. Since the Geopyörä test does not consume the sample during breakage, the tested material remains available for subsequent mineralogical and chemical characterisation, allowing each sample to be fully utilised within the modelling workflow.

## OVERVIEW OF THE PLANT AND USE OF THE GEOPYÖRÄ

A Geopyörä testing device was used to provide ore characterisation data on-site for the development of a geometallurgical model and to supply hardness parameters to be used in the Mine to Mill program. The commissioning was completed in late 2022, and the first batches of samples were tested in early 2023.

The Geopyörä unit remained on-site during a two-year period of operation, a total of 281 samples were tested in those two years, providing a comprehensive database of breakage parameters to support blasting optimisation, throughput forecasting, and comminution modelling. Out of these 281 samples, 126 of them were also submitted for geochemical testing in order to develop the geometallurgical model.

Figure 4 shows the current comminution circuit at the copper mine where the run-of-mine ore is crushed and transported from the pit to a surface transfer station and conveyed to the concentrator via overland conveyors. At the plant, material can either report to secondary crushing or bypass directly to a coarse ore stockpile, depending on operating requirements and ore characteristics. The stockpile provides several days of live capacity to ensure continuous mill operation and facilitate maintenance planning.

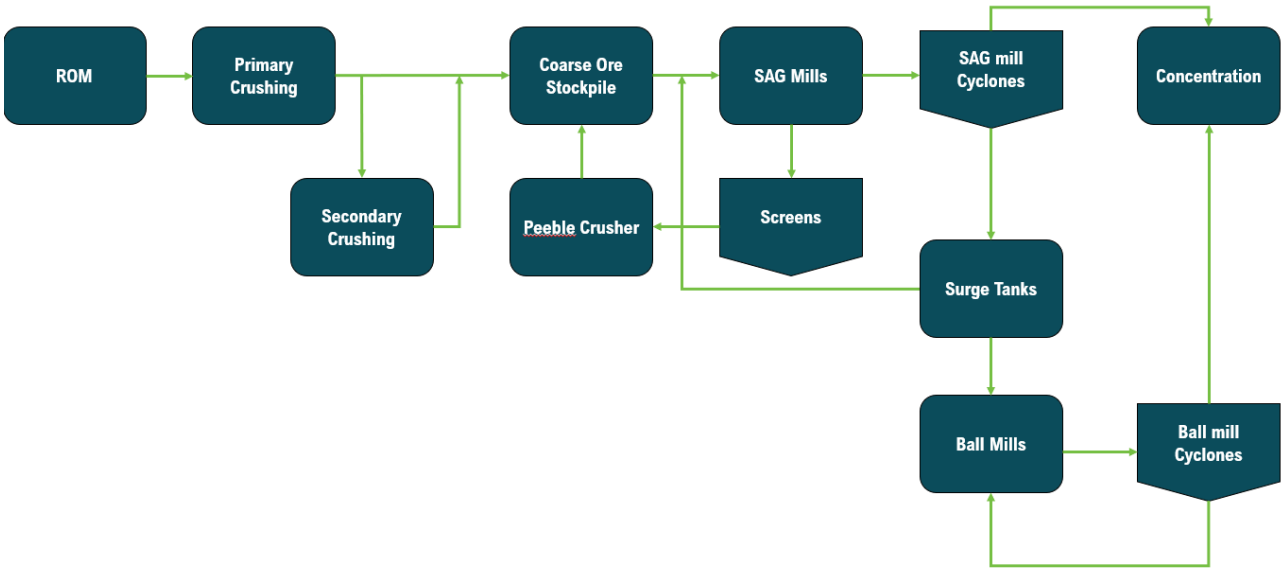



**FIG 4** – Flow sheet of the comminution circuit.

The grinding circuit consists of three high-power semi-autogenous (SAG) mills operating in combination with ball mills, all equipped with gearless drive systems. The SAG mill discharge passes through a trommel screen, where the undersize is directed to hydrocyclones for classification, while the coarse fraction is sent to washing screens and then to the pebble crusher.

The cyclone underflow is collected in surge tanks, where the material is split between recirculation to the SAG mill and feed to the ball mills. The ball mills operate in closed circuit with their own hydrocyclones. The overflow from the ball mill cyclones is directed to the concentration stage while the underflow returns to the ball mill.

The implemented testing workflow at the mine followed the framework illustrated in Figure 2, with the objective of the routine shown in Figure 3. The program included both drill core and blast chip samples. Drill core samples were tested to generate ore competency data with the products of the test been integrated with geochemical and mineralogical analyses to populate the geometallurgical model.

Blast chip samples, which represented most of the material tested, were primarily used to provide timely hardness data to support the blasting team in optimising blast design and improving fragmentation control.

## RESULTS AND DISCUSSION

Once ore competency data began to be generated from the Geopyörä, a multidisciplinary effort was initiated to develop and implement the Mine-to-Mill model, the model development had the direct involvement of Geopyörä, contractors and operation personnel. Based on the characterised breakage parameters provided (DWi, Axb, BWi and UCS), blast designs were progressively optimised with the objective of maximising the performance of the SAG mills at the plant Figure 5

shows a bench that was categorised and had its material tested on the Geopyörä; each green dot in the image represents a drill hole.

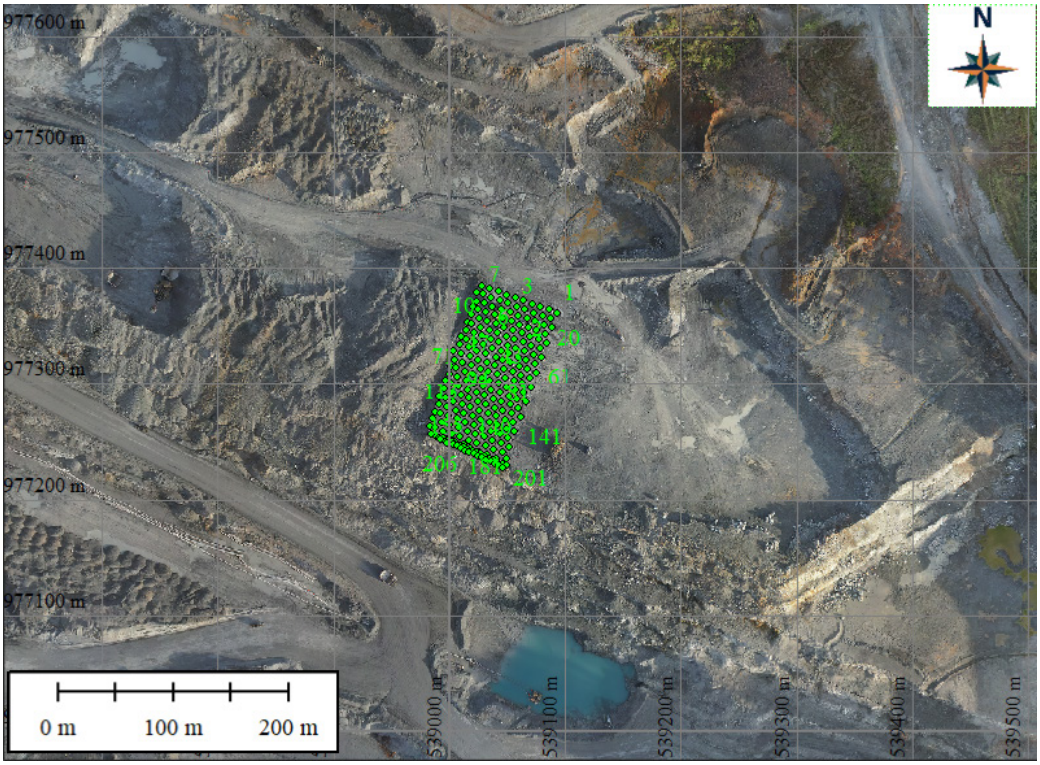



**FIG 5** – Drill Holes from the bench.

Figure 6 shows the hardness classification of the same bench presented in Figure 5. The classification was based on the Axb values of the tested samples, with the threshold values defining each category given in Table 2.

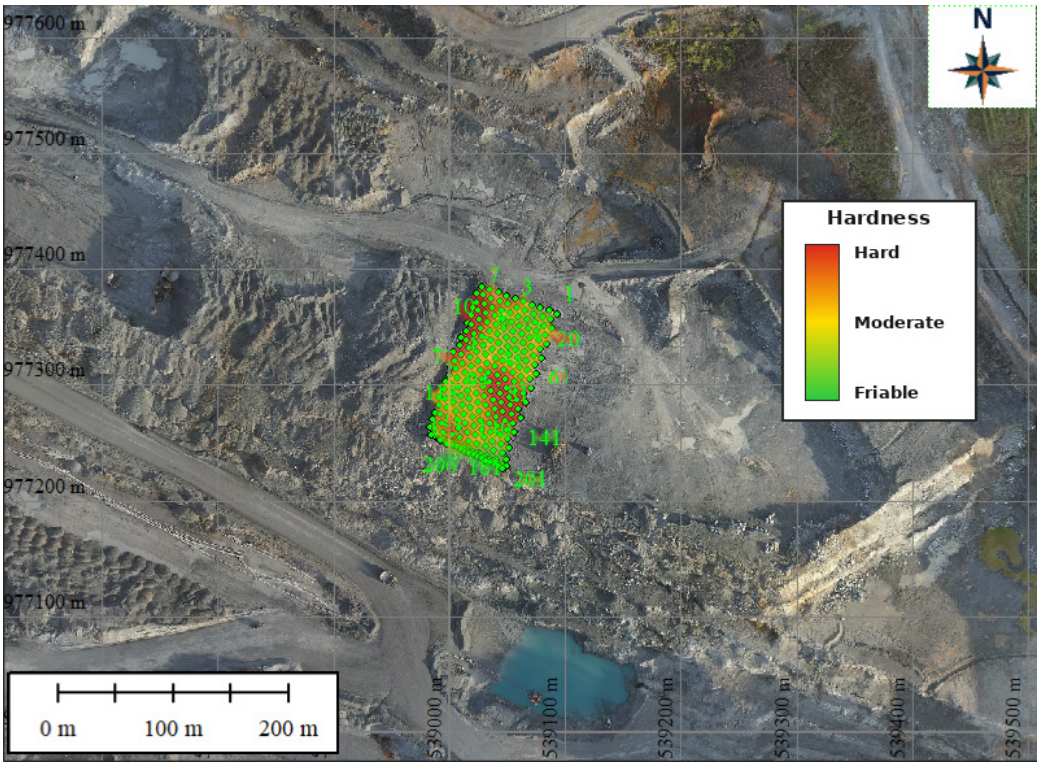



**FIG 6** – Heat map according to material hardness.

**TABLE 2**

Hardness distribution from Figure 6.

| Category | Axb Values |
|---|---|
| Friable | ≥70 |
| Moderate | >40 and <70 |
| Hard | 40≤ |

The classification was based on the Axb results of the samples tested from the bench. Those with an Axb below 40 were classified as hard, those between 40 and 70 as moderate, and those above 70 as friable.

This classification informed the blasting team's blast design, with harder regions loaded with a higher explosive charge than friable ones. Most of the bench was friable to moderate, with a noticeable cluster of competent material near hole 81 and a short band of hard material between holes 7 and 10.

Figures 7–9 present the observed operational results following the implementation of the Mine-to-Mill program in early 2022. In these graphs, the blue line represents the specific energy (kWh/t) of each SAG mill, while the orange line corresponds to the effective throughput observed. The data spans from early 2022 through the end of 2023 and illustrates the operational response of the grinding circuit following the integration of the optimised blast design in the operation.

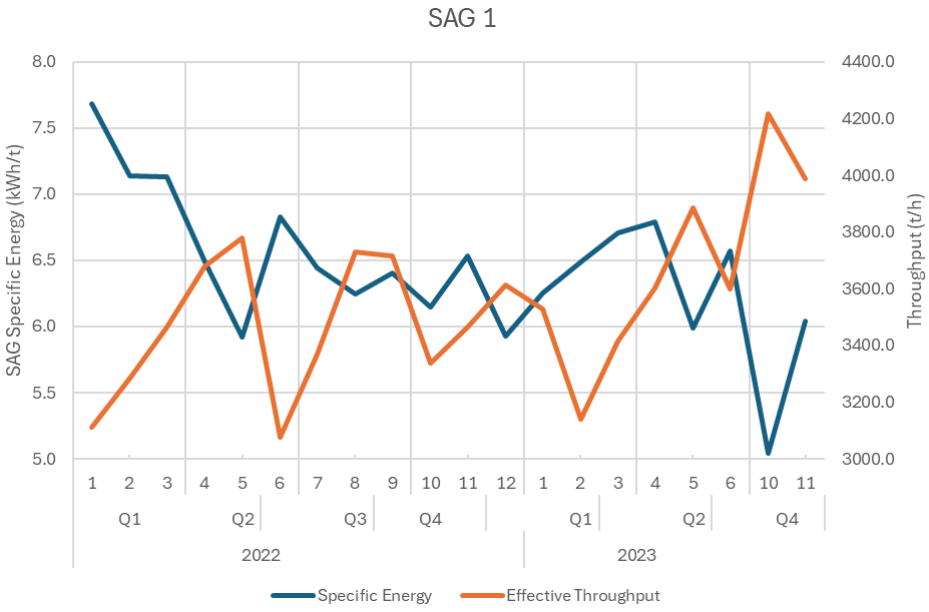



**FIG 7** – Results of the Mine to Mill program for SAG 1.

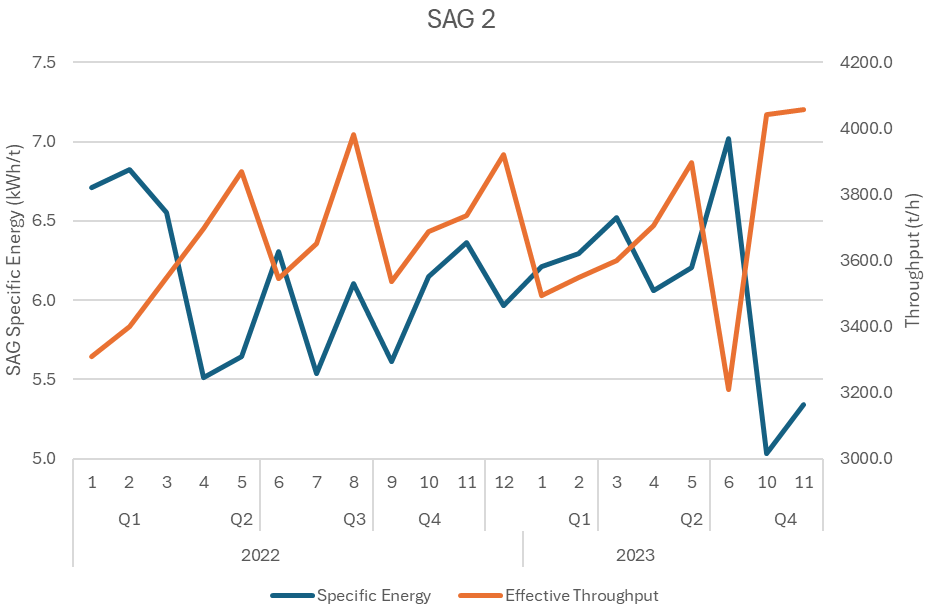



**FIG 8** – Results of the Mine to Mill program for SAG 2.

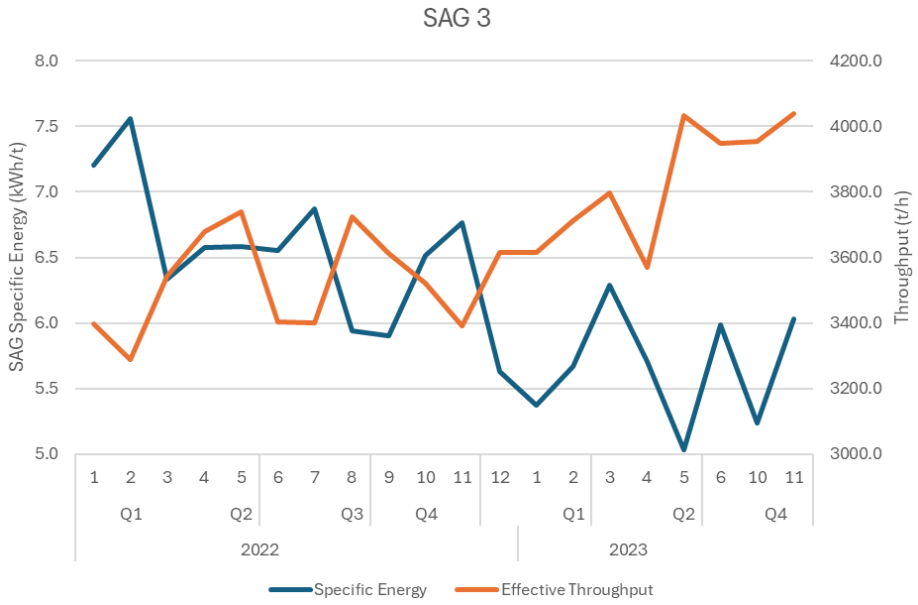



**FIG 9** – Results of the Mine to Mill program for SAG 3.

From the figures, it can be observed that all SAG mills began 2022 operating at throughputs between 3100 and 3400 tonnes per hour (t/h), with specific energy values ranging from 6.6 to 7.6 kWh/t. Following the implementation of the optimisation program, SAG Mill 1 exhibited a rapid reduction in specific energy, decreasing from 7.6 kWh/t to a sustained range between 6.0 and 6.5 kWh/t. This reduction in energy consumption was accompanied by an increase in throughput, rising from approximately 3100 t/h to around 3700 t/h within the first four months of operation.

After this initial adjustment period, the trend of both values remained consistent, with some fluctuations observed in month six of 2022 and month two of 2023. By the end of the monitoring period, the lowest recorded specific energy of 5.05 kWh/t was achieved, which coincided with the highest observed throughput for SAG Mill 1, exceeding 4200 t/h.

Similar to SAG 1, SAG 2 (Figure 8) started 2022 operating at specific energy values around 6.7 kWh/t, with a throughput of 3300 t/h. In the second half of 2022, when specific energy decreased to approximately 6.1 kWh/t (month 8), throughput increased to almost its highest recorded value of over 4000 t/h.

Throughout late 2022 and early 2023, SAG 2 exhibited moderate stability, similar to the one observed on SAG 1, with specific energy generally stabilising between 6.0 and 6.5 kWh/t and throughput varying between 3600 and 3900 t/h.

A significant improvement can be observed toward the end of 2023. Specific energy dropped sharply to approximately 5.0 kWh/t, which allowed a substantial increase in throughput, exceeding 4000 t/h. This was the highest throughput recorded for SAG 2 during the monitoring period.

Overall, SAG 2 followed the same behaviour of the described for SAG 1: the implementation of the Mine to Mill program caused reductions in specific energy, associated with improved fragmentation which in turn resulted in measurable and sustained increases in mill throughput.

Similar to SAG 1 and SAG 2, SAG 3 (Figure 9) began 2022 operating with high specific energy levels, starting above 7.0 kWh/t, with throughput around 3400 t/h. During the first half of 2022, specific energy decreased to approximately 6.5 kWh/t, which was accompanied by an increase in throughput to nearly 3700 t/h.

Throughout late 2022 and early 2023, specific energy fluctuated between 5.9 and 6.8 kWh/t, while throughput generally ranged from 3400 to 3800 t/h. The inverse relationship between specific energy and throughput remained consistent.

A more pronounced improvement was observed during 2023, when specific energy dropped to almost 5.0 kWh/t. This reduction coincided with throughput exceeding 4000 t/h, representing the highest performance levels recorded for SAG 3. Overall, the mill followed the same trend observed in the other SAG units, where reductions in specific energy associated with the Mine-to-Mill program resulted in sustained increases in throughput with a final observed throughput very close to that of SAG 1.

In addition to the operational results observed for each SAG mill, preliminary geometallurgical models were developed using the 126 samples tested with the Geopyörä that were also submitted for geochemical analysis. These models were built using machine-learning techniques, mainly Deep Neural Networks (DNN) to predict both the Drop Weight Index (DWi) and the Bond Ball Mill Work Index (BWi) parameters. Figures 10 and 11 present the parity plots for each model compared against the reference values measured directly using the Geopyörä device.

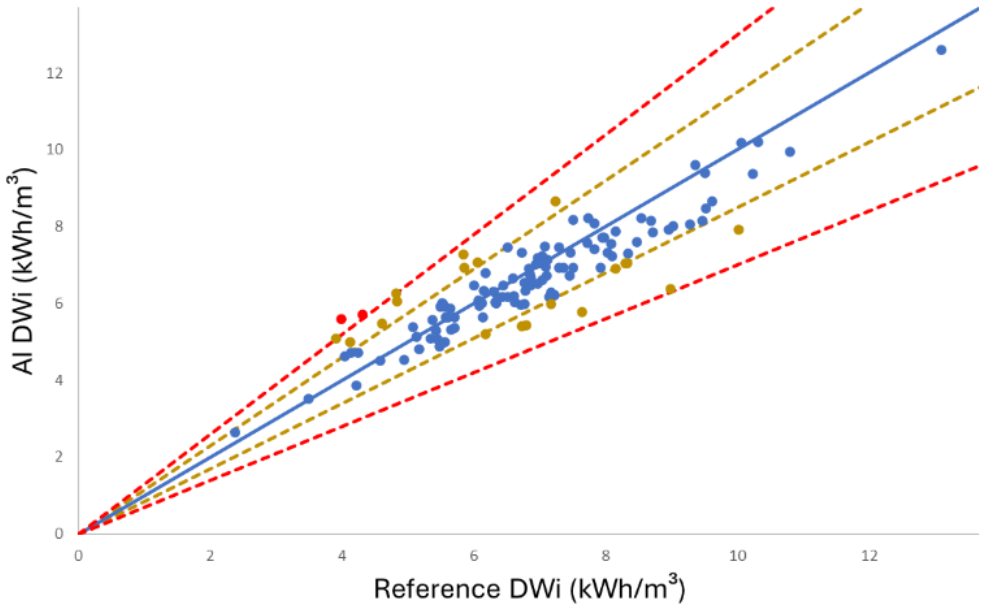



**FIG 10** – Parity Results for the Drop Weight Index geometallurgical Model.

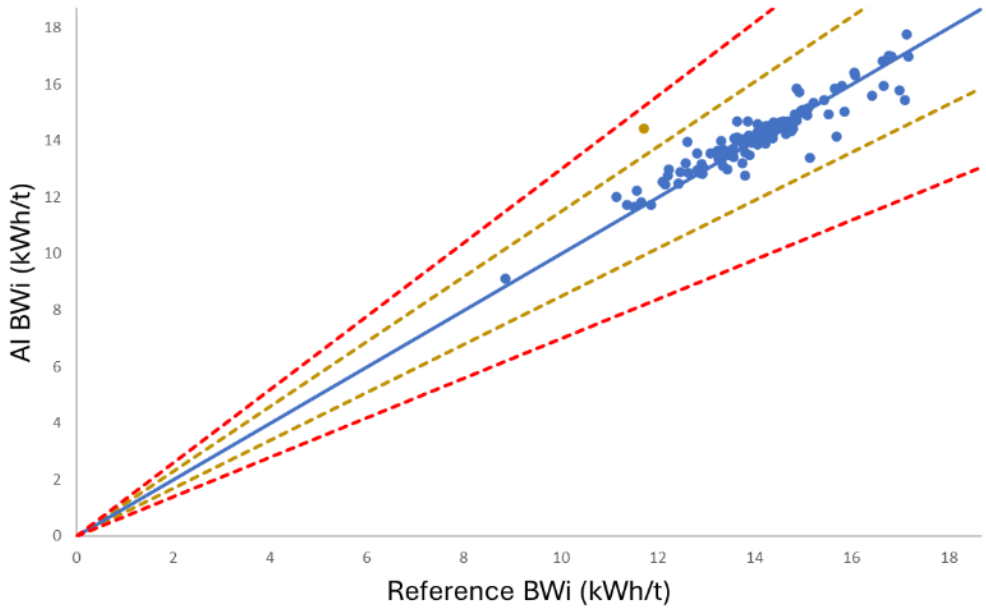



**FIG 11** – Parity Results for the Bond Ball Mill Work Index geometallurgical model.

As observed in the figures, the BWi model achieved higher predictive accuracy than the DWi model. This shows that the DNN framework was more effective at capturing the relationships between geochemical variables and the BWi parameter than those associated with DWi. This trend is consistent with previously developed models (Bueno *et al,* 2025). Despite the comparatively lower accuracy of the DWi model, its performance remained strong, with only two data points exhibiting deviations greater than 30 per cent from the reference Geopyörä measurements. These results demonstrate the capability of deep neural networks to reliably model comminution parameters based on geochemical inputs. Table 3 is an overview of the distribution of the 126 samples for both models observed in Figures 10 and 11.

**TABLE 3**

Distribution of the data on Figures 10 and 11.

| Parameter | <15% (blue) | >=15% 30%=< (yellow) | >30% (red) |
|---|---|---|---|
| DWi | 105 | 19 | 2 |
| BWi | 125 | 1 | 0 |

## CONCLUSIONS

The use of the Geopyörä breakage test within a Mine-to-Mill framework at a large copper operation showed that rapid and representative ore characterisation can have a direct impact on comminution circuit performance. The integration of the data provided by the device on operational decision-making allowed for reductions in specific energy across all three SAG mills from the plant, which in turn allowed for significant increases in throughput.

From the conducted test work, the development of geometallurgical models using Geopyörä parameters with XRD data showed strong predictive capability for both DWi and BWi parameters. The high accuracy achieved, particularly for BWi, demonstrates the potential of combining rapid breakage testing with machine-learning approaches to forecast comminution properties ahead of mining. Combining these two results highlight how the Geopyörä device can be a practical and scalable solution capable of supporting both short-term operational gains and long-term geometallurgical planning in large-scale mining operations.

## REFERENCES

Bond, F C, 1952. The Third Theory of Comminution, *Transactions of the AIME*, 193:484–494.

Bueno, M, Almeida, T and Lara, L, 2024. The Geopyörä Index: A new instrument for assessing comminution and rock strength parameters, IMPC 2024.

Bueno, M, Lara, L R, Almeida, T and Powell, M, 2025. Using neural networks to develop an AI geometallurgical model, Geopyörä, Procemin conference, Santiago, Chile.

Bueno, M, Torvela, J, Chandramohan, R, Chavez Matus, T, Liedes, T and Powell, M, 2021. The double wheel breakage test, *Minerals Engineering*, 168:106905. https://doi.org/10.1016/j.mineng.2021.106905

Glauber, E A M, Moura, F, Souza, I, Resende, F, Henrique, P J C, Ribeiro, A, Valery, W, Valle, R and Plasencia, R H, 2021. Integrated Optimization of Drill and Blast and Comminution Processes at Lundin Mining - Chapada, The 17th International Conference on Mineral Processing and Geometallurgy, Procemin-Geomet, October, online.

Grundström, C, Kanchibotla, S, Jankovich, A and Thornton, D, 2001. Blast fragmentation for maximising the SAG mill throughput at Porgera Gold Mine, in *Proceedings of the Twenty-Seventh Annual Conference on Explosives and Blasting Technique*, pp 383–399 (The International Society of Explosive Engineers).

La Rosa, D, Caron, K, Valery, W, Diaz, R and Mamani, H, 2015. Blast fragmentation impacts on downstream processing at Goldfields Cerro Corona, 11th International Symposium on Rock Fragmentation by Blasting (FragBlast 2015), Sydney, Australia, 24–26 August 2015.

Lam, M, Jankovic, A, Valery, W and Kanchibotla, S, 2001. Maximising SAG mill throughput at Porgera Gold Mine by optimising blast fragmentation, SAG 2001, Vancouver BC, 30 Sept – 3 Oct 2001 (University of British Columbia: Vancouver BC).

Morrell, S and Valery, W, 2001. Influence of feed size on AG/SAG mill performance, in Proceedings of the International Conference on Autogenous and Semi-Autogenous Grinding Technology.

Morrell, S, 2004. Predicting the specific energy of autogenous and semi-autogenous mills from small diameter drill core samples, *Minerals Engineering,* 17(3):447–451.

Napier-Munn, T, Morrell, S, Morrison, R and Kojovic, T, 1996. *Mineral Comminution Circuits: Their Operation and Optimisation*, first ed, Julius Kruttschnitt Mineral Research Centre, Indooroopilly, Australia.

Powell, M S, Bozbay, C, Kanchibotla, S, Bonfils, B, Musuniri, A, Jokovic, V, Hilden, M, Young, J and Yalcin, E, 2019. Advanced mine-to-mill used to unlock SABC capacity at the Barrick Cortez mine, in Proceedings International Autogenous and Semi-Autogenous Grinding and High Pressure Grinding Roll Technology 2019 (CIM).

Scott, A, Segui, J and Kanchibotla, S, 2000. Ore Characterisation for Mine-to-Mill Fragmentation, in Proceedings of the Fourth International Mining Geology Conference.

Simkus, R and Dance, A, 1998. Tracking hardness and size: Measuring and monitoring ROM ore properties at Highland Valley Copper, in Proceedings of Mine to Mill ’98, Brisbane, Australia.

# Development of geometallurgical testing program for Oak Dam West, South Australia

*Y Li[1], K Ehrig[2] and V Liebezeit[3]*

1. Senior Geometallurgist, BHP Copper SA, Adelaide SA 5000. Email: yan.li@bhp.com
2. Superintendent Geometallurgy, BHP Copper SA, Adelaide SA 5000. Email: kathy.ehrig@bhp.com
3. Principal Geometallurgist, BHP Copper SA, Adelaide SA 5000. Email: vanessa.liebezeit@bhp.com

## ABSTRACT

Oak Dam West is a breccia hosted iron-oxide copper-gold-uranium (IOCG) deposit located approximately 65 km south-east of the Olympic Dam deposit in South Australia. The first Mineral Resource was reported in August 2024. Resource definition, advanced exploration activities and mining studies continue. The Oak Dam West geometallurgical testing program was developed to support early-stage metallurgical evaluation and processing strategy selection for a potential copper operation within the Olympic IOCG province. This paper outlines the multi-phased development of the Oak Dam West geometallurgical testing program, from initial tests on two samples to a fully integrated framework tailored to the mineralogical and metallurgical characteristics of the deposit and proposed plant processing flow sheet. It presents the results achieved to date and includes comparisons to the other deposits in the province.

The initial sighter tests confirmed the applicability of Olympic Dam geometallurgy protocols to Oak Dam material, while highlighting the need for specific adjustments due to subtle mineralogical differences. These insights informed the first phase of testing in 2021, which focused on characterising 30 drill core samples across a wide range of mineralisation styles, including determination of the size fractions most suitable for mineralogical characterisation. Subsequent phases in 2023 and 2025 formalised a comprehensive testing matrix and flotation protocols tailored to Oak Dam mineralogy and ultimately incorporated procedural adjustments informed by emerging flow sheet concepts from the nearby Carrapateena operation. Notably, the primary grind size for flotation tests was increased to reflect the grind-size-liberation trade-off, and a pyrite depression flotation test was introduced for pyrite-rich ore to assess concentrate quality. Tests to assess by-product recovery options were included from the early phase, as was tailings characterisation.

The Oak Dam program demonstrates the adaptability of existing protocols to new deposits of the same type, while highlighting the importance of iterative refinement based on mineralogical variability and evolving processing strategies.

## INTRODUCTION

Oak Dam West, hereafter referred to as Oak Dam, is part of the Olympic Cu-Au Province and is located approximately 65 km south-east of Olympic Dam. It is classified as an Iron Oxide Copper-Gold (IOCG) deposit type. Like any other global ore deposit type, IOCGs in the Olympic Cu-Au Province (ie Olympic Dam, Oak Dam, Prominent Hill and Carrapateena) display similarities and differences (Ehrig *et al,* 2023). The deposit lies below ~750–900 m of post-mineral, flat-lying sedimentary rocks.

Mineralisation is hosted within the Oak Dam Breccia Complex which is surrounded laterally and at depth by the deformed and altered Donington Suite granitoids (~1855–1845 Ma). Highly altered and variably deformed pre-mineral mafic dykes cut the granitoids and occur as breccia clasts. The breccia complex is a mono- to polymictic hematite-granite-volcanic breccia with variable hematite-sericite-chlorite-carbonate alteration. Gawler Range Volcanic felsic dykes (~1590 Ma) cut mineralisation and are variably altered. The breccia complex is intruded by the regionally extensive, relatively unaltered ~830–820 Ma dolerites of the Gairdner Dyke Swarm. Mineralisation, based on unpublished dates, is ~1590 Ma.

The deposit can be generally characterised (Figure 1) by a central hematite-quartz-barite breccia with absent to low-grade (<0.1 per cent) copper mineralisation, irregularly surrounded by zones of high-grade, yet disseminated, chalcocite-bornite mineralisation (3 to 5 per cent Cu) and zones of variable grade bornite-chalcopyrite-pyrite mineralisation (0.5 to 2 per cent Cu). Sulfide mineralisation occurs as disseminated grains ranging in size from <0.1 to>5 mm throughout the breccia matrix (Figure 2) and sometimes in breccia clasts. Sulfide veinlets are rare.

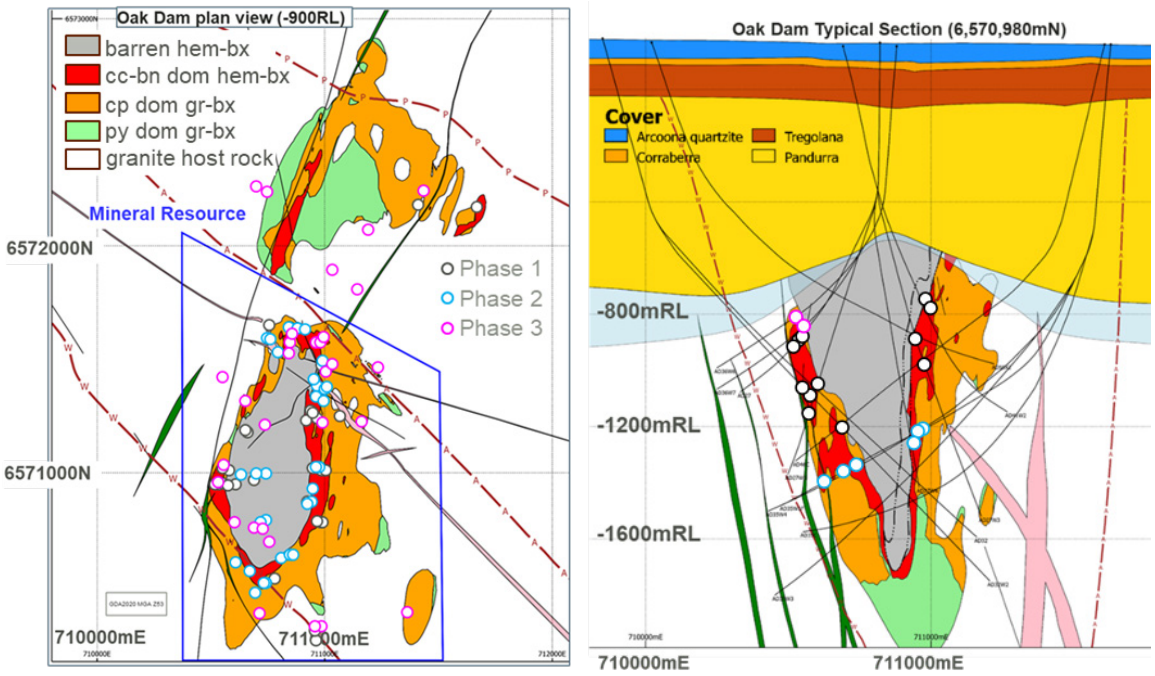



**FIG 1** – Geometallurgy sample locations across the deposit (left plan map). Sample locations are projected to one plane, hence appearing to be in the same location. The cross-section (right) portrays typical spatial variability of the major breccia and mineralisation types with depth, along with sample locations. The thin black lines are diamond drill hole traces.

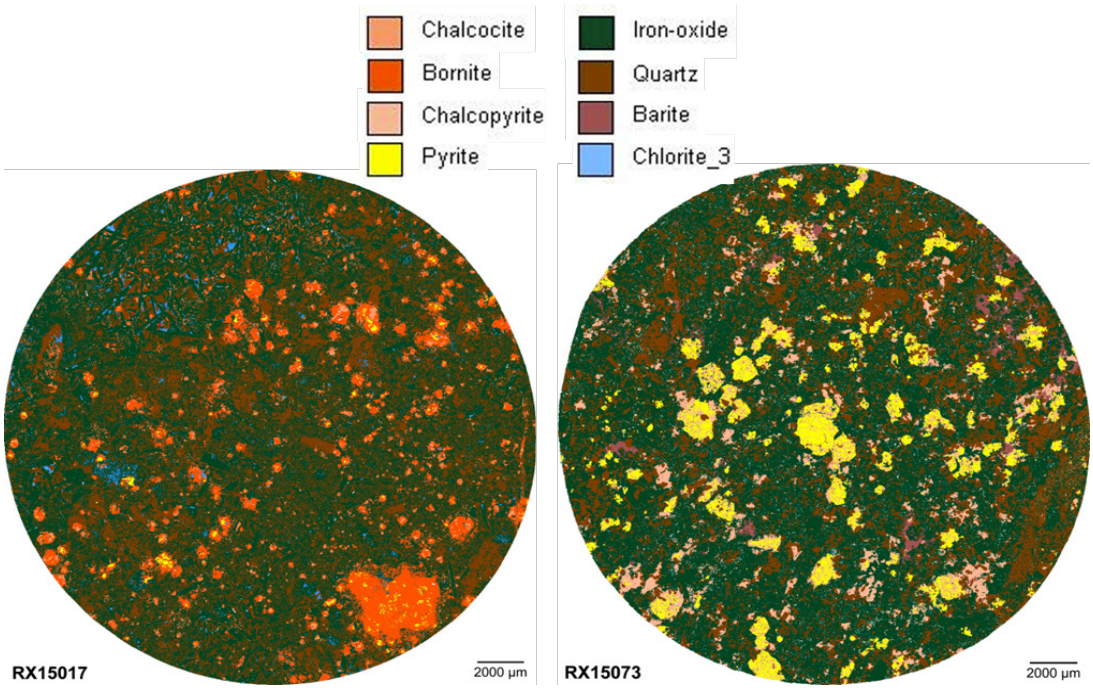



**FIG 2** – MLA false-coloured images showing typical sulfide mineral textures in polished samples of (a) bornite, chalcocite, trace pyrite, hematite, quartz, chlorite; and (b) chalcopyrite, pyrite hematite, quartz and barite.

Even though the macroscopic breccia textures of the deposit can be complex to interpret because of very high short scale variability, the geochemistry, hence mineralogy, shows systematic deposit wide trends. These trends form the fundamental geometallurgical sampling strategy. Progressive brecciation and hydrothermal alteration of the granite, replaces the original granite mineralogy (eg plagioclase, K-feldspar, quartz, biotite and amphiboles etc) with a suite of IOCG hydrothermal minerals (eg hematite, quartz, sericite, chlorite, barite, fluorite, carbonates, sulfides etc). A few of the deposit wide trends are shown in Figure 3. This data is a random subset of the drill core assay database. Hematite is the dominant Fe-bearing mineral. There is a very strong positive correlation with Fe versus bulk dry density (Figure 3a). Hematite concentration varies from <5 to ~85 wt per cent. Copper (>0.1 wt per cent) occurs in rocks with >5 wt per cent Fe and continues to increase with increasing Fe concentration, except as noted for the barren hematite breccias (lower right corner Figures 3b and d). As the intensity of the alteration increases, the primary aluminosilicates (plagioclase, K-feldspar, biotite) are first replaced by sericite and chlorite, which are ultimately replaced by hematite (Figures 3c and d). The deposit centrally located barren hematite breccias plot in the lower right corner of Figures 3b and d).

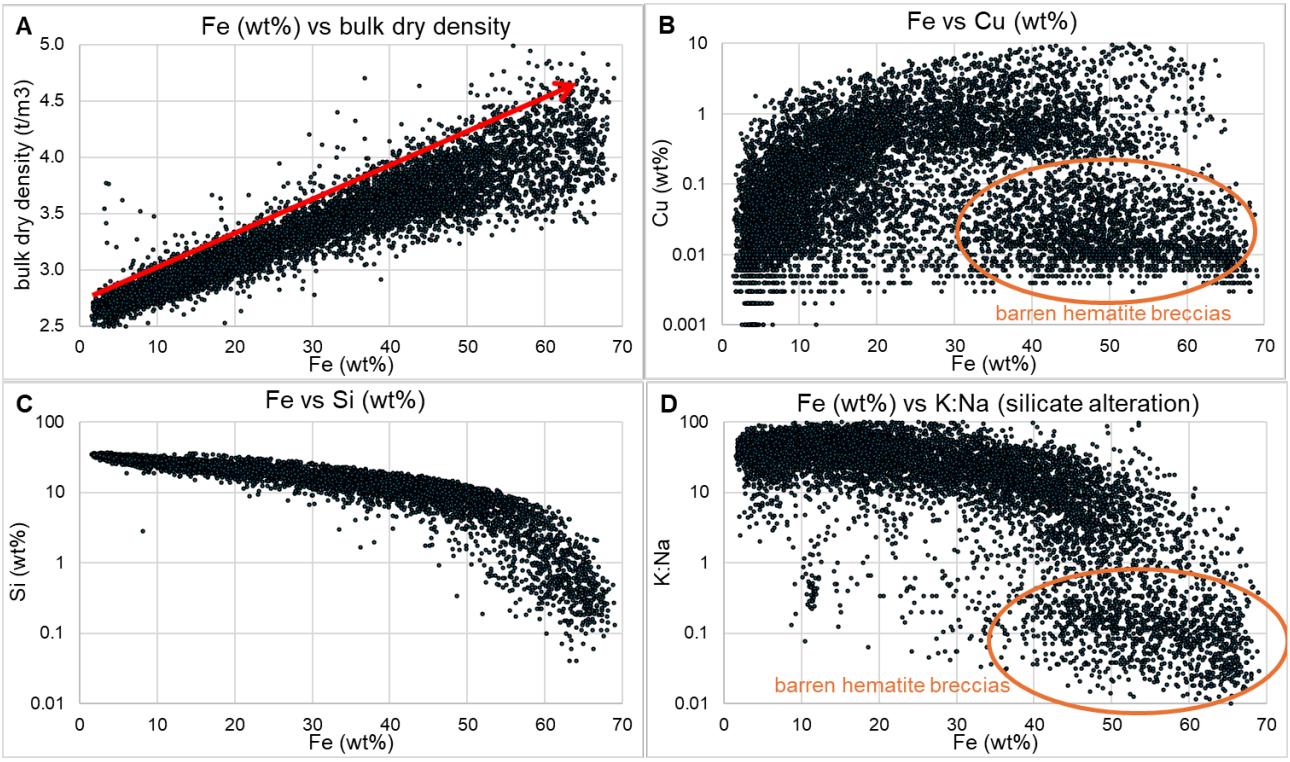



**FIG 3** – Oak Dam geochemical trends of Fe versus: (a) bulk dry density; (b) Cu wt per cent; (c) Si wt per cent; and (d) K:Na.

Ninety-three Oak Dam geometallurgy samples (20 m long samples of NQ2 diameter half core, continuous metres) were tested through three program phases over five years (2020 to 2025). Each sample consists of a single 20 m long interval from a single drill hole. The 20 m length is required to have sufficient mass to conduct the test work. Resource delineation diamond drilling was ongoing during this time. Based on the drill core available for sampling for each program phase, samples were purposefully selected to ensure 3D spatial coverage across the deposit, hence representing the potential mineralogical, hence geochemical variability. The distribution of the samples across the deposit is shown in Figure 1. Figure 4 demonstrates that the samples also represent a wide range in geochemistry both within phase and between phases, hence likely capture the mineralogical variability.

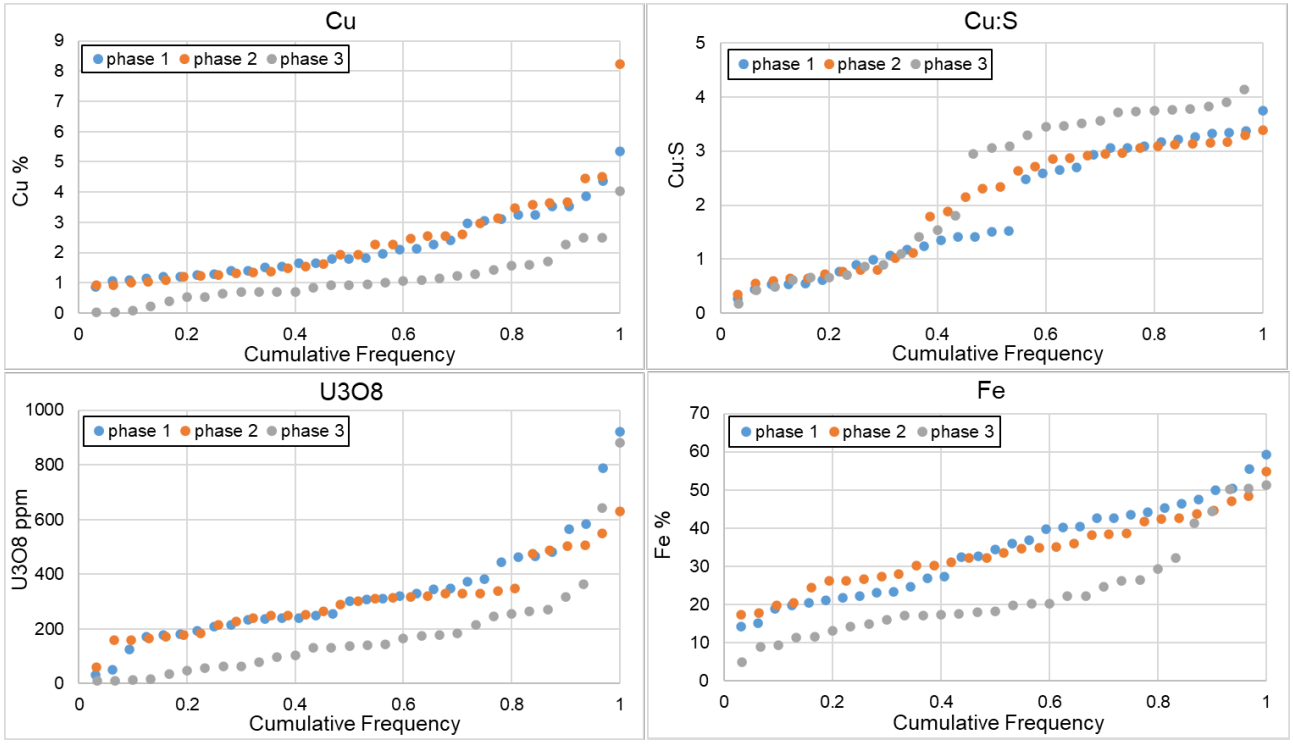



**FIG 4** – Cu, Cu:S, $U_3O_8$ and Fe distribution for samples from different phases. Note the two samples in the preliminary testing phase were combined with Phase 1 samples for the purpose of this figure. Phase 3 samples targeted overall lower Cu grade samples.

At the time of writing, the mining method and processing flow sheet were yet to be determined. Development of the geometallurgical program was intentionally iterative, with each phase building on the findings of the previous one. Learnings were incorporated into the subsequent phases. This iterative approach effectively shaped the geometallurgical program that is suitable for Oak Dam specific mineralogy, as shown in Figure 5.

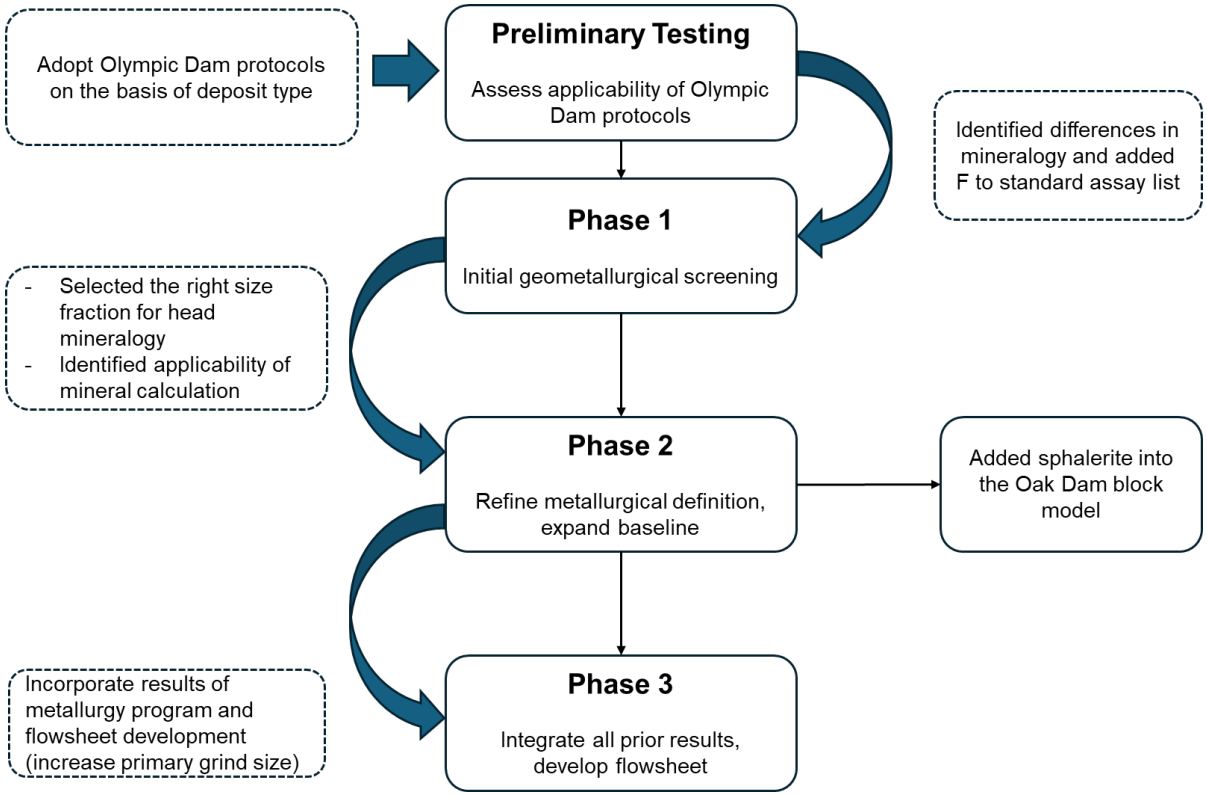



**FIG 5** – Overview of phase interactions and information pathways.

## OAK DAM MINERALOGY

While IOCG deposits in the Olympic Cu-Au Province share common mineralogy (eg minerals, abundances, grain size, grain shapes and association characteristics), process mineralogy still needs to be completed. However, in the case of Oak Dam, the length of time to establish the mineral libraries required for automated mineralogy methods such as MLA, TIMA etc was significantly reduced by simply modifying the well established Olympic Dam MLA mineralogy list. This was completed prior to commencing the Oak Dam geometallurgy program.

Modal mineralogy measurements (via MLA) were completed on the -600+425 µm size fractions for the 93 geometallurgy samples. Refer to section below (**Validation of the -600+425 µm size fraction for head mineralogy**) for the validation of using this size fraction. Table 1 lists the 18 minerals/ mineral groups which account for 99.93 wt per cent of the sample mass. The other 0.07 wt per cent consists of >43 other minerals including zircon, xenotime, albite, talc, kaolinite, and selenides, tellurides, sulfides and oxides of Cu, Co, As, Bi, Au, Ag, Mo, Sn, W.

**TABLE 1**

Modal mineralogy (wt%) of the Oak Dam geometallurgy samples.

| | Average | Stdev | Minimum | Maximum |
|---|---|---|---|---|
| **Hematite** | 44.55 | 20.77 | 5.49 | 85.08 |
| **Quartz** | 23.07 | 10.65 | 0.13 | 49.12 |
| **Sericite** | 18.87 | 11.18 | 1.18 | 49.10 |
| **Fluorite** | 2.34 | 2.64 | 0.00 | 9.90 |
| **K-feldspar** | 1.83 | 6.44 | 0.00 | 34.56 |
| **Barite** | 1.82 | 2.91 | 0.00 | 17.42 |
| **Anhydrite** | 0.16 | 0.42 | 0.00 | 2.79 |
| **Chlorite** | 1.46 | 3.21 | 0.00 | 25.80 |
| **Carbonates[1]** | 1.29 | 4.49 | 0.00 | 29.24 |
| **Chalcocite** | 1.10 | 1.45 | 0.00 | 7.83 |
| **Bornite** | 1.01 | 1.35 | 0.00 | 5.53 |
| **Chalcopyrite** | 0.81 | 0.94 | 0.00 | 4.02 |
| **Pyrite** | 0.50 | 1.24 | 0.00 | 6.98 |
| **Sphalerite** | 0.01 | 0.03 | 0.00 | 0.21 |
| **REE-minerals[2]** | 0.75 | 0.38 | 0.11 | 1.95 |
| **U-minerals[3]** | 0.03 | 0.02 | 0.00 | 0.11 |
| **Ti-minerals[4]** | 0.25 | 0.42 | 0.00 | 3.79 |
| **Tourmaline** | 0.10 | 0.16 | 0.00 | 1.14 |

Carbonates[1] = siderite, ankerite, dolomite, calcite, magnesite, rhodocrosite.

REE-minerals[2] = bastnasite, florencite, monazite, synchysite, apatite.

U-minerals[3] = uraninite, coffinite, brannerite, thorite.

Ti-minerals[4] = rutile, ilmenite, ilmenorutile.

## PRELIMINARY TESTING (FY20)

The first two samples (OKD0001 and OKD0002) from the same drill hole were collected at the start of 2020. They provided the first opportunity to assess if the established Olympic Dam geometallurgical protocols (eg sampling, sample preparation, subsampling, grinding, rougher and cleaner flotation, tailings leach) were suitable for Oak Dam material. The main objective of this phase

was to reveal any potential processing risks before committing to a large scale and more expensive test program and to confirm the similarity with Olympic Dam.

## Deposit-specific mineralogical characteristics

This phase of program provided the first detailed look at how Oak Dam's unique mineralogy would respond to Olympic Dam standard geometallurgical testing protocols.

During the rougher flotation test, larger than usual mass loss was observed for sample OKD0002. After confirming with the laboratory that all standard procedures were followed correctly, we began to investigate alternative explanations. A simple water-solubility test revealed that the sample contained some water-soluble component, with resulting liquor assay showing elevated levels of Ca and S. These findings led to the identification of anhydrite. To quickly identify the presence of anhydrite in any given sample, a 'wash test' was developed in which 50 g of solids were mixed with 100 mL of water, filtered, dried and the solids analysed. This test was then incorporated into the standard Oak Dam protocol for the next phase of the program.

Another implication of anhydrite is that some of the current assay to mineral calculations require revision. The assay to mineral calculations are used to transform the drill hole assay database into one which also contains mineralogy (Ehrig, 2006), which is the fundamental driver of processing response. In addition to mineralogical analysis via MLA on size fractioned laboratory grinding, flotation and leaching products, quantitative X-ray diffraction (QXRD) analysis is also used to measure the bulk mineralogy of the testing head samples.

### *Copper to sulfur ratio (Cu:S)*

At Olympic Dam, the copper to sulfur ratio (Cu:S) is used as an indicator of sulfide mineralogy (Ehrig *et al,* 2019) and is defined as:

$$Cu{:}S = \frac{\%Cu}{\%S - \frac{\%Ba}{4.285}}$$

The denominator of this equation represents sulfide-hosted sulfur, because at Olympic Dam essentially all sulfur occurs either in barite ($BaSO_4$) or in the sulfide minerals predominantly pyrite, chalcopyrite, bornite and chalcocite with minor contributions from sphalerite, galena and molybdenite. Subtracting barite-derived sulfur therefore provides a reasonable estimate of sulfur contained within the sulfide minerals.

At Oak Dam, however, anhydrite ($CaSO_4$) is present in addition to barite. This means that total sulfur (as determined by induction furnace infrared spectroscopy, as commonly known as LECO™) includes contributions from anhydrite, barite and the sulfide minerals. Extensive, prior experience in measuring sulfide sulfur suggests that the precision is erratic and hence insufficient for this application, especially when barite is present. Complicating matters further, calcium is present in both fluorite ($CaF_2$) and anhydrite. Therefore, there is no simple mechanism to determine 'sulfide sulfur'. The Cu:S in an ore sample cannot necessarily be used as a reliable indicator of sulfide mineralogy, as at Olympic Dam. At this stage of the program, we did not know anything about the spatial occurrence of anhydrite.

### *Fluorine assay*

At Olympic Dam, calcium concentration serves as a reliable proxy for fluorine since fluorite ($CaF_2$) is the dominant Ca containing mineral and the only F containing mineral (only very minor F in sericite) (Ehrig, 2006). As a result, fluorine content can be calculated with high accuracy from the calcium assay without the need for direct fluorine analysis.

However, at Oak Dam, calcium occurs in multiple minerals including anhydrite, ankerite/dolomite and fluorite – meaning that Ca is no longer uniquely associated with fluorine. Because calcium cannot be attributed solely to fluorite, it can no longer be used as a direct proxy for fluorine concentration. Consequently, fluorine assaying was added to the standard analytical requirement in the next phase of Oak Dam Geometallurgy program and for the routine assaying of all diamond drill core samples.

## PHASE 1 INITIAL PROGRAM DEVELOPMENT (FY21)

Initial geometallurgy screening was carried out on 30 Oak Dam samples (OKD0003 – OKD0032) during FY21 following the preliminary testing. These samples were selected to represent the various types of ore which were available from the drilling conducted in FY19 and were designed to cover a very wide range of variability in mineralogy and chemistry.

This phase of program produced the first comprehensive geometallurgical data set for the deposit, which enabled the early identification of key processing risks. The work also provided essential insight into the mineralogical variability that influences metallurgical performance, allowing metallurgical behaviour to be linked back to the deposit.

### Validation of the -600+425 µm size fraction for head mineralogy

The Olympic Dam Geometallurgy protocols include the screen sizing of a crushed charge, where the -850+600 µm size fraction is used for optical microscopy and the -600+425 µm fraction is used for mineralogical analysis via MLA. These protocols were developed because it was demonstrated that for Olympic Dam ore these size fractions were of the same chemical composition as the bulk sample – in other words, no size fractionation by assay occurred at these coarse size fractions.

To determine if this is also valid for Oak Dam, each sample charge was sized and individual size fractions analysed. Assays of the -600+425 µm fraction compares very well with the corresponding head assay. This confirms that the –600 + 425 µm fraction is representative of the bulk sample for Oak Dam material and is therefore suitable for use as the standard mineralogy fraction in the Oak Dam geometallurgy program.

### Concurrent occurrence of feldspar and chlorite

At Olympic Dam, the algorithm used to calculate mineralogy from chemical assays for resource delineation drill holes are based on some key assumptions (Ehrig, 2006). In the ore zones, the only aluminosilicate minerals present are sericite, chlorite and K-feldspar. Sericite is almost always present, while chlorite and K-feldspar may be present but not together. Possible combinations are sericite + chlorite or sericite + K-feldspar. Because of this binary nature, the K:Al can reliably distinguish which mineral pair is present, allowing the algorithm to partition elements appropriately and enables further mineral calculations.

At Oak Dam, however, this assumption doesn’t always hold. In the FY21 data set, chlorite and K-feldspar were detected together in two of the 30 samples. Violation of this fundamental assumption may introduce error into the calculated mineralogy for these minerals and reinforced the need for continued measured mineralogy. Chlorite can be deleterious in acid-leaching circuits and as the processing flow sheet had not yet been selected, it was important to understand the potential limitations of the calculated mineralogy method.

## PHASE 2 METALLURGICAL DEFINITION PROGRAM (FY23)

A further 31 drill core samples (OKD0033 – OKD0063) were tested in FY23. This phase built directly upon the learnings from the previous phase, retaining the core Olympic Dam geometallurgy framework while incorporating several Oak Dam specific adjustments identified during the earlier test work. Between the phases, there was no metallurgical program and therefore there were no changes to the protocols arising from any study. This phase of program doubled the number of geomet samples for Oak Dam but it is still a relatively small data set.

The 63 samples available at the end of FY23 were then used to make composites for metallurgical process design testing in 2024, which consumed the material. Recommendations from the composite work were implemented in the next phase of program. Details on compositing methodology for the process design and test work execution are not covered in this paper. There are important differences between sampling for process design test work, and geometallurgy sample selection which are also outside the scope of this paper.

## Drop weight index (DWi)

The JK Drop Weight Index (DWi), measured from the SMC® test, is a measure of the strength of the rock when broken under impact (kWh/m$^3$). For Olympic Dam samples, DWi typically goes up with the increasing density (or increased Fe or hematite). Figure 6 plots the Oak Dam samples with Olympic Dam DWi model. It shows that the Oak Dam samples clearly fall into two groups – samples that behave in a similar way to the bulk of Olympic Dam samples (cluster around the Olympic Dam model line), and samples which have very low DWi values across the SG range. This is consistent with other Oak Dam drill core observations which include: 1) unexpectedly low UCS measurements relative to Olympic Dam samples with similar Fe concentrations; 2) relatively rapid deterioration of diamond saw cut core in trays indicative of high porosity and the presence of weakly hematite altered yet intensively chlorite-sericite altered mafic volcanic breccia clasts; and 3) visual observation of core deterioration when handling core post processing the core for assaying.

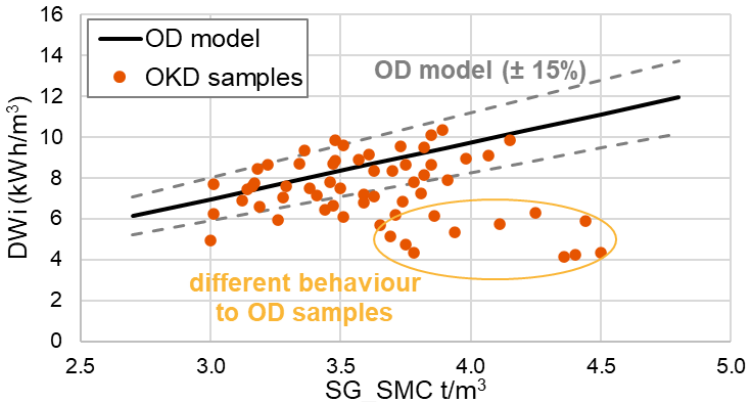



**FIG 6** – DWi results for Oak Dam, with OD model line.

## Zn and sphalerite

In the Olympic Cu-Au province, zinc occurs as sphalerite or as a trace element in carbonate minerals. When zinc occurs in carbonate minerals, its recovery to flotation concentrate is low; however, when present as the sulfide mineral sphalerite, recovery to concentrate is high (~85 per cent). Several samples produced elevated zinc grades in concentrate and MLA data shows that sphalerite tends to associate with bornite – chalcocite dominant mineralisation. Those samples typically have low mass recovery to concentrate and this amplifies the Zn grade, with levels reaching up to ~0.5 per cent in concentrate. This is significantly higher than typical Olympic Dam levels. Based on these findings sphalerite was added to the Oak Dam block model by triggering a sphalerite abundance calculation when Zn>400 ppm.

# PHASE 3 METALLURGICAL INTEGRATION PROGRAM (2025)

The 63 samples analysed in previous programs provide excellent spatial coverage and capture a wide range of chemical and mineralogical variability and identified several Oak Dam-specific requirements. In addition, metallurgical development and project study work occurred between Phase 2 and Phase 3. Phase 3 of the program aimed to incorporate these learnings at scale and validate them against a new data set. A further 30 drill core samples (OKD0064-OKD0093) were tested in this phase of program (Figure 4).

## Flotation at different primary grind size

In preliminary testing and initial program development phases (OKD0001 – OKD0032) the nominal primary grind size for flotation was set at 80 per cent passing 75 µm to be consistent with Olympic Dam. Flotation results on the first 32 samples suggested that a coarser grind could be used based on the high flotation recovery and high sulfide liberation at $P_{80}$ of 75 µm. However, no process optimisation test work was carried out prior to receipt of the Phase 2 samples (OKD0033 – OKD0063). Therefore it was decided to stay with $P_{80}$=75 µm so that any subsequent change would mean there were only two geomet data sets rather than potentially three if we chose the ‘wrong’ size for Phase 2.

In Phase 3 of the program $P_{80}$=90 µm was established for all grinding and flotation tests for all samples based on the metallurgical optimisation and project studies. To evaluate the effect of grind size on flotation performance, the earlier samples (prior to OKD0064) had a repeat flotation test at $P_{80}$=90 µm where there was sufficient material available. Figure 7 compares rougher concentrate Cu recovery at different grind size from both rougher flotation test and the rougher part of the cleaner flotation test. Overall, rougher recovery at finer grind size is slightly higher than recovery at coarser grind size but the difference between 75 µm and 90 µm is within ±1 per cent for majority of the samples, supporting the shift. Rougher concentrate Cu grade between tests of different primary grind size are also very similar. Target regrind size was kept the same to minimise impact on cleaner Cu recovery and grade.

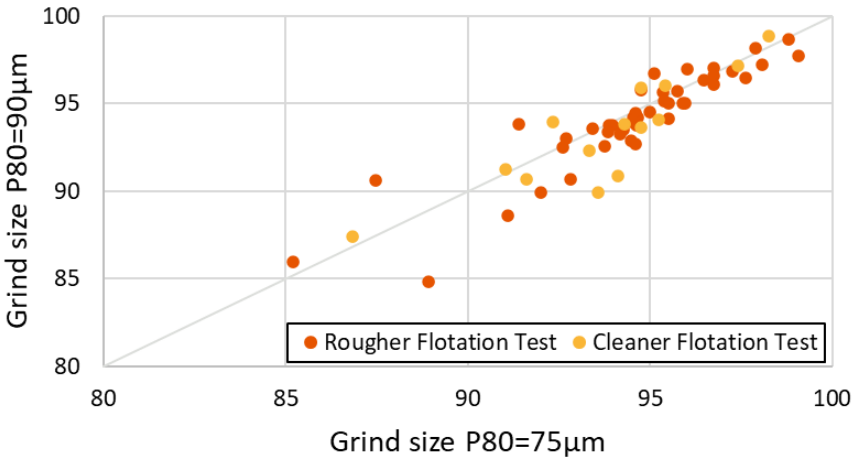



**FIG 7** – Comparison of rougher concentrate Cu recovery at $P_{80}$=75 µm and $P_{80}$=90 µm from both rougher flotation test and cleaner flotation test.

## Pyrite depression flotation test

Several samples contained high proportions of pyrite, reflected by the low Cu:S. A flotation test with a reagent regime designed to depress pyrite was conducted on those samples in this phase of program. To be consistent with the other flotation tests in this phase the primary grind size for pyrite-depression test was maintained at $P_{80}$=90 µm. XRD analysis was also performed on the resulting concentrates to quantify mineralogical responses to pyrite depression.

The Cu:S is an excellent proxy indicator for the sulfide mineralogy. Under standard flotation conditions, the Cu:S of the concentrate is usually very close to the Cu:S of the ore feed, indicating all sulfides are recovered approximately equally. This is shown for the ‘cleaner flotation test’ series in Figure 8. In contrast, pyrite depression tests on the same samples produced a clear increase in concentrate Cu:S compared with feed Cu:S demonstrating that pyrite rejection was effective.

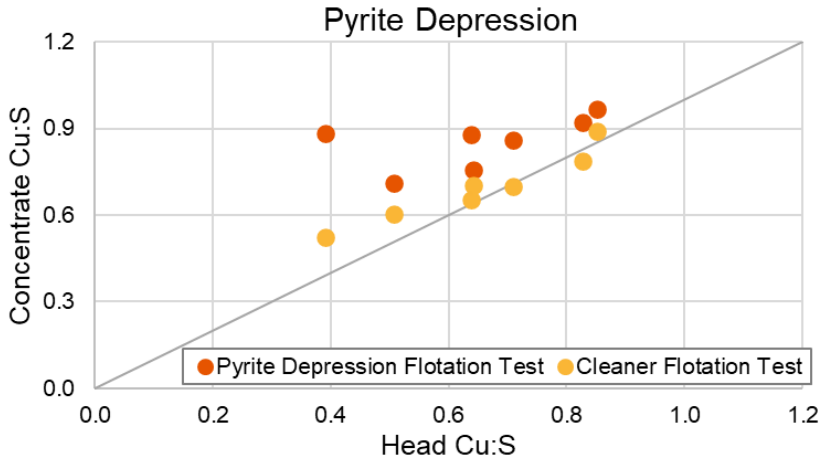



**FIG 8** – Concentrate Cu:S versus head Cu:S for normal cleaner flotation and pyrite depression flotation.

The proportion of pyrite of the total sulfide minerals in flotation concentrate also showed significant decrease after pyrite depression test (see Table 2).

**TABLE 2**

Pyrite percent of total sulfide minerals of flotation feed and flotation concentrate for pyrite depression flotation test.

| | Pyrite% of total sulfide minerals | |
|---|---|---|
| **Sample ID** | **Flotation feed** | **Pyrite depression flotation concentrate** |
| OKD0041 | 36% | 4% |
| OKD0053 | 15% | 1% |
| OKD0072 | 27% | 10% |
| OKD0075 | 18% | 7% |
| OKD0077 | 21% | 10% |

The impact of pyrite depression on concentrate quality is pronounced. Figure 9 compares Cu grade in concentrate at 80 per cent sulfides for the pyrite depression test against the corresponding normal cleaner test. The results show a clear uplift in final concentrate Cu% by 2 to 8 per cent (absolute increase Cu) confirming the effectiveness of the pyrite depression approach for reducing pyrite recovery and improving concentrate quality.

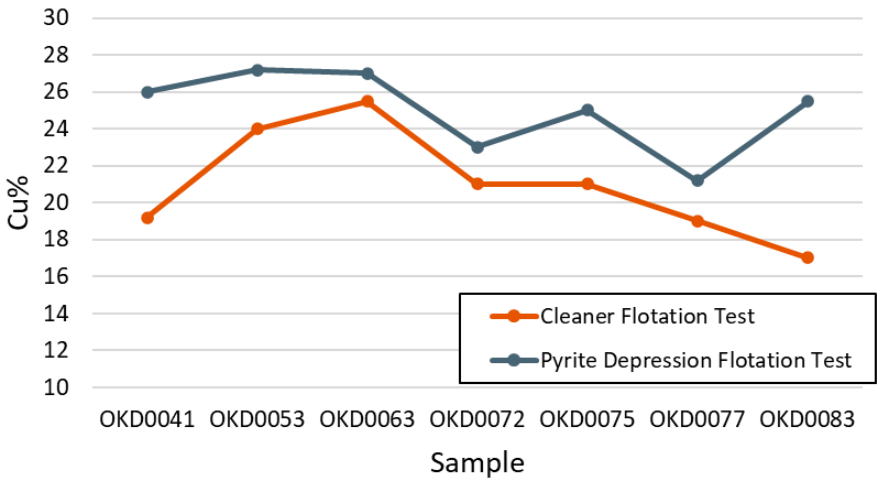



**FIG 9** – Comparison of concentrate Cu% at 80 per cent sulfide from pyrite depression flotation with normal cleaner flotation test.

## STATUS OF IDENTIFIED IMPROVEMENT OPPORTUNITIES

### Confidence in using Cu:S as a proxy for sulfide mineral abundances

Based on the mineralogy completed across the three program phases, anhydrite >0.5 wt per cent occurs only in seven of the 93 samples. While this needs to be monitored, further mineralogical and geochemical work is being conducted on the drill core samples to determine a reasonable proxy for anhydrite so that the distribution of anhydrite can be mapped across the deposit and the Cu:S proxy for sulfide mineralogy can be locally modified. The conclusion is that the Cu:S proxy for sulfide mineralogy is reliable, but not 100 per cent of the time. Spatially localised modifications to the Cu:S calculation in the resource block are required to improve the confidence in the prediction of sulfide mineral abundances.

## Calcium as a proxy for fluorine, fluorite, anhydrite and Ca-carbonates

The validation of using element proxies to estimate mineral abundances or other elements is to plot the proxy element versus the measured mineral abundance or other element. This also helps to identify the percentage on samples which fall outside of whatever precision is required. Calcium versus fluorine, fluorite, anhydrite and Ca-carbonates are plotted in Figure 10.

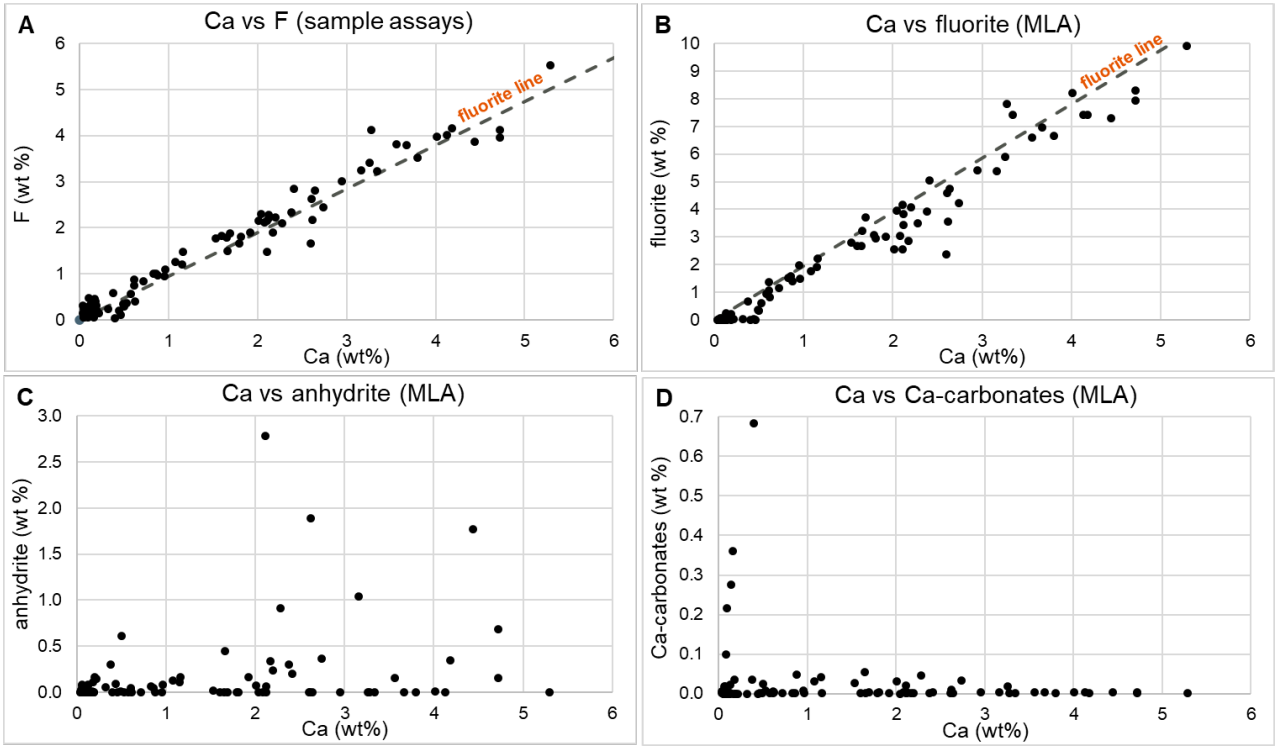



**FIG 10** – Potential use of calcium as a proxy for: (a) fluorine; (b) fluorite; (c) anhydrite; and (d) Ca-carbonates. Calcium is a good proxy for estimating fluorine and fluorite, but not anhydrite and Ca-carbonates.

### *Ca versus fluorine and fluorite*

The fluorite line labelled in Figure 10a clearly shows that there is more fluorine in some samples which is likely not associated with fluorite. It was mentioned earlier that sericite is a minor host to fluorine which is our preferred explanation. However, the data points above the fluorite line could also represent subtle differences in the precision of the calcium and fluorine assays. Data points in Figure 10b plotting below the fluorite line likely reflects the precision of the MLA measurements.

The presence of other Ca-bearing minerals, such as anhydrite and Ca-carbonates is apparent in Figures 10c-d. The conclusions from these plots are that Ca is a reasonable proxy for fluorine and fluorite, but there are 10–15 per cent of the samples which likely require modified assay to mineral calculations.

## Estimating the abundances of sericite, chlorite and K-feldspar

The current version of the assay to mineral calculations uses fixed chemical compositions for sericite, chlorite and K-feldspar. This has always been an issue because sericite and chlorite both display variable chemical compositions at Olympic Dam and Oak Dam. Recently the chemical compositions of sericite, chlorite and K-feldspar were measured via microbeam methods to establish if the variable compositions could be clustered. The next step is to use machine learning to determine if a more precise assay to mineral calculation algorithm can be developed.

## CONCLUSIONS

In general, the mineralogy of Oak Dam samples is very similar to Olympic Dam, confirming that the established Olympic Dam protocol is broadly transferable to Oak Dam material. However, the subtle

differences in mineralogy require adjustment to the assay-to-mineral calculation, notably the presence of anhydrite (an additional source of sulfur) and ankerite. It highlights the importance of testing the fundamental assumptions underpinning those protocols when applying frameworks developed for another deposit. The iterative approach with each phase building on the findings of the previous one was the right method to refine existing protocols to reflect Oak Dam specific behaviour.

Sample mass has been a key constraint towards to later phases for the program. Material was rapidly depleted due to the extensive characterisation work and the subsequent need for composite preparation for metallurgical process design test work, which limited the ability to retrospectively test alternative conditions for the full historical sample set.

Overall, the Oak Dam geometallurgical testing program has now established a robust, Oak Dam-specific framework that supports flow sheet development, concentrate quality assessment, and the future development of geometallurgical models. The results provide a strong technical foundation for progressing the project through subsequent study phases.

## ACKNOWLEDGEMENTS

The authors thank BHP Olympic Dam for permission to publish this paper. We would like to acknowledge the geometallurgy team for their contributions to this paper: Benjamath Pewkliang, Edeltraud Macmillan, Michelle Smith and Sam Slabbert.

## REFERENCES

Ehrig, K, 2006. Calculated Mineralogy of In Situ Olympic Dam Ore, BHP Internal Memorandum.

Ehrig, K, Ciobanu, C, Cook, N, Kamenetsky, V, Kamenetsky, M and McPhie, J, 2023. Similarities, yet differences: Olympic Dam, Oak Dam West, Wirrda Well, Island Dam and Acropolis IOCG deposits, Olympic Cu-Au Province, South Australia, in *Proceedings Mineral Deposits in a Changing World, 17th SGA Biennial Meeting 2023,* 1:347–350.

Ehrig, K, Liebezeit, V, Smith, M, Pewkliang, B, Li, Y and Macmillan, E, 2019. Predicting sulfide mineral abundances from drill core to smelter feed: Impact on the Olympic Dam value chain, in *Proceedings AusIMM International Mining Geology 2019*, pp 279–290 (Australasian Institute of Mining and Metallurgy: Melbourne).

# Bridging the gap between historical test work and process design

*A Shaikh[1], C Sola[2] and S Hunter[3]*

1. Process Engineer, Lycopodium, Fortitude Valley Qld 4006.
   Email: adam.shaikh@lycopodium.com
2. Lead Process Engineer, Lycopodium, Fortitude Valley Qld 4006.
   Email: christine.sola@lycopodium.com
3. FAusIMM(CP), Manager Process – Brisbane, Lycopodium, Fortitude Valley Qld 4006.
   Email: sandy.hunter@lycopodium.com

## ABSTRACT

Metallurgical test work is the cornerstone of process design, underpinning critical decisions on process flow sheet and equipment selection, reagent dosing, equipment sizing, and overall process performance. Due to the sparse and localised nature of early-stage sampling, estimating metallurgical response consistently across the entire deposit can be challenging. While sampling density does improve as projects advance, ensuring continuity and comparability of test work from early phases of study through to detailed design is critical in developing a reliable and optimised process.

This paper introduces a framework for 'bridging the gap' between historic and current test work data sets to de-risk and enhance process design. This approach leverages geometallurgical principles by integrating geological data – lithology, alteration, mineralogy, liberation and mineral association – with metallurgical test work response to create a predictive, data-rich foundation for process design. It also highlights the critical role of sample selection and test work program design in reducing technical risk in process design.

By incorporating legacy data through structured gap-filling techniques and linking it with current, variability-driven test work, this methodology reduces uncertainty in design and strengthens Mine to Mill integration. It also serves as a driver for process optimisation from concept through to operation. The result is a more robust framework from sampling to design that supports informed decision-making and maximises value across the Life-of-Mine.

## INTRODUCTION

Metallurgical test work forms the foundation of minerals process design – underpinning flow sheet development, equipment selection, reagent strategies, and performance forecasting. The reliability of this foundation, however, depends fundamentally on the representativity of the samples and the consistency of test work methodologies applied across the project life cycle. Early-stage sampling programs are typically driven by resource definition objectives and financial limitations rather than metallurgical variability requirements, resulting in sparse, spatially biased data sets that do not adequately capture the lithological, mineralogical, and geochemical heterogeneity of the orebody. Consequently, early results often lack the geometallurgical resolution needed to reliably predict processing behaviour.

As projects progress from Scoping to Pre-Feasibility and ultimately to Definitive Feasibility, test work programs expand in scope and complexity. Yet methodological discontinuities commonly arise between phases. Differences in sample selection strategy, grinding targets, analytical suites, or leaching/flotation procedures can produce data sets that are not inherently comparable. Such discontinuities increase uncertainty and often necessitate additional drilling or duplication of tests to recover confidence. This is a well-recognised issue in the broader literature, where poor sample representativity and inconsistent test work protocols have been shown to amplify apparent variability and obscure true metallurgical response (Dominy, O'Connor and Xie, 2016).

### Geometallurgy

Geometallurgy is founded on the principle that mineralogy controls metallurgy, as emphasised by Bennet and Munro (2024). Developing a metallurgical test work program that explicitly incorporates geological attributes – such as alteration assemblages, lithology, mineral associations, and mineral

liberation – is essential to ensuring that the selected samples are truly representative of the mineral deposit. By embedding these attributes into sample selection and test work design, geometallurgy provides a structured framework for understanding how geological variability drives differences in processing performance. Alignment between geologists and metallurgists achieves and maintains this representativity during exploration and sample selection (Newell, Munro and Fiedler, 2018), so that geological domaining and classification remain consistent as the project progresses. In turn, this geometallurgical approach enables early estimation of processing outcomes prior to project execution, allowing test work results to be interpreted within the context of geological domains. It also facilitates iterative evaluation between mine planning, metal extraction performance and processing cost, ensuring that design decisions remain aligned with both project objectives and the intrinsic characteristics of the orebody.

## Test work across phases of study

In addition to understanding the importance of metallurgical test work, it is necessary to ensure that test work programs are aligned with the objectives of each project study phase. Across Scoping, Pre-Feasibility (PFS) and Definitive Feasibility Study (DFS) phases, the increasing scope and complexity of metallurgical test work demands a corresponding increase in geometallurgical control. Early amenability testing provides high-level constraints on feasible extraction routes such as cyanide leaching (Marsden and House, 2006, ch3:69–98) and flotation (Jackman, 1995). However, the transition to PFS and DFS requires variability test work grounded in systematic geometallurgical domaining so that the influence of geological factors on process behaviour can be quantified (Newell, Munro and Fiedler, 2018). This includes mapping how lithology and alteration influence various factors, such as acid-consuming capacity, cyanide-consuming species, reactive sulfide populations, liberation constraints and comminution behaviour. Each of these directly affects outcomes in cyanidation or flotation processes.

## Gold extraction

Gold cyanide leaching, or cyanidation, is a method of extracting gold from ore (Dutrizac and Sunstrum, 1999). The process is conducted typically at atmospheric pressure in stirred tank reactors, where gold ore suspended in slurry is treated with a diluted cyanide solution, typically sodium cyanide, in an environment containing dissolved oxygen (DO), allowing the gold to dissolve into solution as an aurocyanide (gold-cyanide) complex (Marsden and House, 2006, ch6:233–275). This aurocyanide complex can then be recovered via adsorption, commonly onto activated carbon, from which gold is typically desorbed and recovered and then smelted into gold doré bars (Marsden and House, 2006, ch3:69–98). Besides identifying key process design parameters, gold cyanide leaching test work can be used to assess the impact of cyanide-consuming minerals within the orebody through variability test work.

Flotation is a key processing route for ores in which gold is hosted within sulfide minerals, a method commonly referred to as bulk sulfide flotation (Jackman, 1995). In this process, gold-bearing sulfides are selectively concentrated into a bulk sulfide product by aerating a pulp containing these minerals. Reagents are added to modify mineral surface chemistry and adjust the pulp redox environment (pulp potential), thereby enhancing the selectivity and overall effectiveness of the flotation response. By preconcentrating gold-bearing sulfides, the load on the downstream unit operations, such as a cyanide leaching circuit, can be significantly reduced and can potentially decrease the total cyanide consumption (Jackman, 1995), although this is highly dependent on the ore's mineralogical characteristics. Flotation is therefore suited to gold occurring within sulfide phases, though the resulting concentrate may require additional pretreatment to liberate the gold prior to subsequent extraction steps (Marsden and House, 2006, ch3:69–98).

Because both leaching and flotation responses are dependent on the metallurgical samples characteristics and test conditions, historical test work data cannot be reliably compared with new data unless it is systematically reconciled. In this context, the concept of bridging the gap becomes essential. Bridging refers to the structured reconciliation of historical and current test work data sets, enabled through geometallurgical normalisation. This process involves the alignment of all relevant test conditions – grind size, pH, free cyanide and dissolved oxygen concentration, and pulp density for cyanide leaching, and grind size, pulp density, pH, and reduction oxidation potential for flotation.

Following alignment, samples are reannotated based on their geological data, and targeted sighter tests are conducted to validate process conditions with respect to interpretations of historical results. Together, these methods allow earlier test work to be incorporated into DFS-level databases, without introducing unwarranted uncertainty, ensuring that design values are derived from the most comprehensive and geologically representative data set available.

The work presented here applies a geometallurgy-driven framework for bridging metallurgical data sets across study phases to a multi-domain gold project. By combining rigorous geometallurgical domaining, structured test work condition standardisation, and comprehensive data governance, the methodology demonstrates how legacy data can be transformed to DFS standards, improving confidence in design parameters, informing blending strategies, and strengthening the Mine to Mill integration, which is essential for robust process and economic design.

## PROJECT CASE STUDY

This case study focuses on the development of a gold minerals processing project located in Africa. The project went through three phases of design: Preliminary Economic Assessment (PEA), PFS, and DFS. This case study examines how the process design and metallurgical test work evolved across the phases of study, with a particular emphasis on gold extraction and methodologies used to bridge gaps in data. This includes the application of distinct test work and design methodologies, incorporating geometallurgical concepts to integrate multiple data sets. The test work programs undertaken in each successive study phase became progressively more detailed, providing increasingly representative assessments of ore response to metallurgical extraction methods. This progression effectively de-risked the design, improved project confidence, and provided clearer definition of the project's economic value.

### Location and geology

The exploration area covered approximately 2200 $km^2$ and comprised two key geological deposits: Main and West. The resource was situated on the andesite-rich Arabian Nubian Shield, with the western section dominated by marine sediments. The two deposits were separated by a fault system.

The Main deposit was hosted within a heterogeneous andesitic volcanic sequence where mineralisation occurred within a broad volcaniclastic-sedimentary horizon intruded by dioritic sills. These sills were characterised by intense sericitic, silicic, albite and carbonatisation alterations. Sulfides in this deposit were dominated by pyrite, with gold occurring predominantly as fine free grains, and minor silver present.

The West deposit comprised of sulfide-rich volcaniclastics adjacent to rhyolite and syenite intrusions, with pyrite as the dominant sulfide mineral. Alteration in this deposit was characterised by sericitisation, with localised carbonatisation in halos.

Across the resource, three major mineralisation styles were identified at differing depths:

1. Orogenic gold hosted in foliated schistose rock.
2. Volcanogenic massive sulfides within the Nubian volcanic sequence.
3. Rift-associated epithermal systems.

The orogenic gold deposit type also contained intrusive sheets of syenites, diorites and granitoids. Weathering was evident throughout the resource, with oxide, transition and fresh domains delineated based on oxidation levels interpreted from geological data.

### Metallurgical test work

Metallurgical test work during the PEA stage involved 12 samples with the objective of assessing the amenability of ore samples from different zones (deposits) and domains (weathering states) to gold extraction, namely via flotation and cyanide leaching. The objective of this stage was to estimate gold recovery and reagent consumptions of the resource to support financial modelling. These results enabled progression through the next financial approval gateway. Results indicated that fresh and transition domains were amenable to both flotation and cyanide leaching for effective gold recovery. Oxide domains, however, did not demonstrate amenability to flotation with results

indicating approximately half the gold recovery was achieved compared to fresh and transition domains. These findings prompted additional metallurgical test work to support identification of the optimal processing route, or flow sheet, for the project. This requirement was addressed in the PFS phase, including the optimisation of the optimal processing route.

Test work during the PFS stage expanded sample selection, utilising 56 samples across four explicitly identified pit-zones (North-East and East zones, in addition to the West and Main zones). The aim of test work in this stage was to confirm the flow sheet design for the project and the grind sensitivity of the ore across all pit-zones and domains to the selected metallurgical extraction method. A trade-off study was conducted between whole-ore cyanide leaching and flash flotation pre-concentration followed by cyanide leaching. As indicated in the PEA results, flash flotation was considered for fresh and transition domains, as oxide material was shown not to be amenable to the unit process. Thus, oxide material in the flash flotation design option was still processed wholly by cyanide leaching only.

Modelling of the test work results indicated that flash flotation pre-concentration only provided a marginal recovery increase and was not economically justified relative to whole-ore cyanide leaching. Despite pre-concentration of fresh and transition ore, which constituted around three quarters of the total resource, the increase in gold recovery observed when pre-concentrating via flash flotation was approximately 1.5 per cent compared to whole-ore leaching.

Financial modelling showed that the potential economic benefit from this recovery gain was negligible over the Life-of-Mine (LoM). This limited benefit, coupled with increased operating expenses such as power and reagent consumption, resulted in a significantly lower return on investment. Thus, the additional capital investment and design complexity associated with incorporating a flash flotation circuit could not be justified. Accordingly, for the remainder of the PFS, the objective shifted to the optimisation of the whole-ore cyanide leaching process with respect to resource variability through a variability test work program.

Variability test work is a vital component of a metallurgical test work program, instrumental in de-risking the project by quantifying the variability of the resource with respect to key design parameters. Variability test work is conducted on samples systematically selected to represent key attributes of the resource, including different ore domains, lithologies, alterations and head grades. Test work on these variability samples allows an understanding of how variations in geochemical and mineralogical characteristics affect the performance of the metallurgical extraction method, in this case cyanide leaching, enabling the development of quantitative correlations. These correlations also provide a statistical basis for estimating key operating parameters, such as reagent consumption, across the processing schedule.

For this project, a pit-zone and domain based grind sensitivity variability test work program was conducted, involving 23 sample types tested at four grind sizes to establish a grind sensitivity relationship by pit-zone and domain. Correlations between the variability samples, their optimal grind size, and cyanide leaching response enabled the development of a blending strategy.

A blending strategy is a systematic approach to combining ore from multiple sources to achieve a target plant feed composition. Maintaining consistent physical and chemical characteristics is often the primary target for plant feed, as this minimises variability in head grade, mineralogy and comminution characteristics, in turn leading to more stable plant performance. This blending strategy can then be incorporated into the mine plan, optimising plant throughput and enabling updates to the resource to assess changes in metal production per unit mined. Financial modelling completes this cycle of optimisation, where the blending strategy is used to optimise the economics of processing the resource via effective ore scheduling.

In addition to maintaining consistent feed, a blending strategy may be used to target more economically favourable ore, while uneconomic material is directed to waste rock dumps, thus not processed. These can be identified by the inclusion of low-grade samples in variability test work, assessing the impact of head grade on metallurgical response and critically evaluating this within the project cut-off grade. This also has the potential upside of expanding the resource, should low-grade samples demonstrate acceptable metallurgical performance. The blending strategy developed for this project targeted a higher feed grade for the first half of the LoM, with the aim of maximising

the return on investment earlier on in the project life. This blending strategy was further optimised and validated through the DFS test work program, supported by subsequent modelling.

Test work in the DFS stage expanded variability by introducing lithology as a third geometallurgical discriminator in addition to pit-zone and domain. As grind sensitivity was already defined by domain, optimisation work centred on cyanide leaching operating parameters including pulp-density, reagent consumption, residence time, sulfide passivation, and the effect of site water. Cyanide leaching response is governed by maintaining key operating conditions within defined control limits. These include pH, cyanide concentration, and dissolved oxygen availability. These parameters directly influence the rate of gold dissolution (Marsden and House, 2006). Optimising the rate of gold dissolution in turn affects reagent consumption, oxygen demand, leach residence time, and consequently the sizing of cyanide, lime and oxygen supply systems.

The effects of these parameters were evaluated in terms of leach kinetics and overall extraction for both valuable metals (Au, Ag) and deleterious metals (Cu, Fe, Hg), which influence reagent demand and performance of downstream processes. Following optimisation of conditions based on a mine plan representative composite, variability characterisation focused on generating a cyanide leaching response database. Responses were classified according to pit-zone, domain and lithology as per the sample selection methodology during the DFS stage, enabling geometallurgical mapping of leach behaviour. Based on the optimised cyanide leaching conditions established in the DFS phase, several cyanide leaching tests from previous phases could be reconciled into the DFS database, reducing the number of additional samples required during the DFS to populate gaps in the database to 53 samples. As displayed in Figure 1, the final database comprised 200 unique cyanide leaching tests, including seven reconciled tests from previous phases of the project.

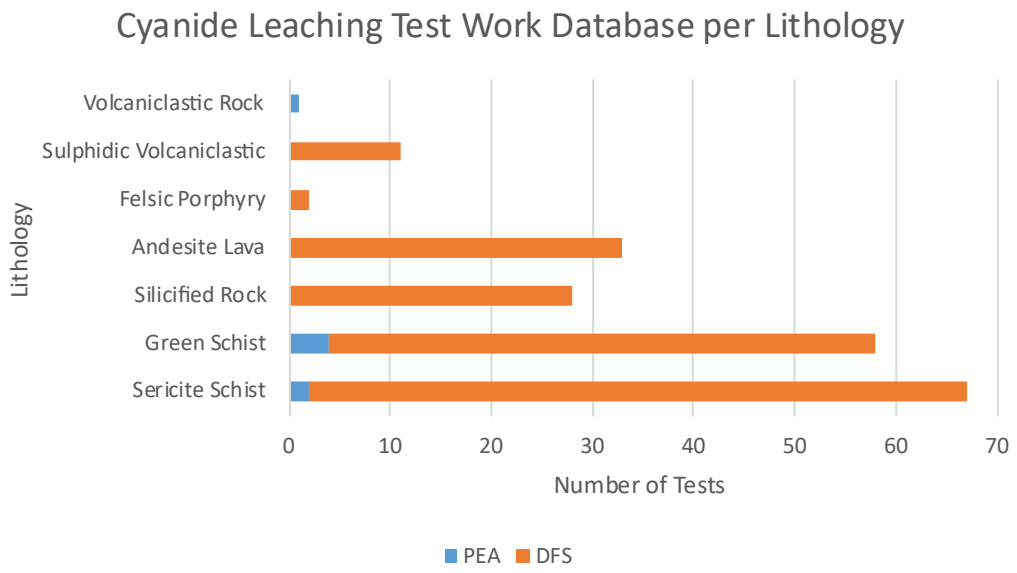



**FIG 1 –** Samples selected per phase listed by lithology type.

Figure 1 shows that the spread of samples by lithology was highly variable. For example, there were no additional samples added during the DFS phase for the Volcaniclastic Rock lithology. This was due to the sample selection methodology. For a DFS-level test work program, where samples are selected to metallurgically evaluate variability within the resource, the variability must also be with respect to the processing schedule. Another form of variability exists within each lithology due to other geological factors such as alteration and mineralogy. As a result, the variability test samples represented in Figure 1 are reflective of the processing schedule and the variability within each lithology domain.

## BRIDGING THE GAP

This was where integration of data sets, or ‘bridging the gap’, between all phases of test work became instrumental in the project’s design evolution. Consolidation of data sets from the PEA and PFS into a DFS-level design basis required a geometallurgy-driven approach to sample selection,

structured test work program execution, and step-wise investigation of process variables and process route selections, coupled with consistent documentation of key observations and decisions made throughout the three phases of study. This was achieved through a structured framework that incorporated geological domaining, spatial distribution across the orebody, mine plan representativity, and the standardisation of key process variables across all phases of test work, as illustrated in Figure 2.

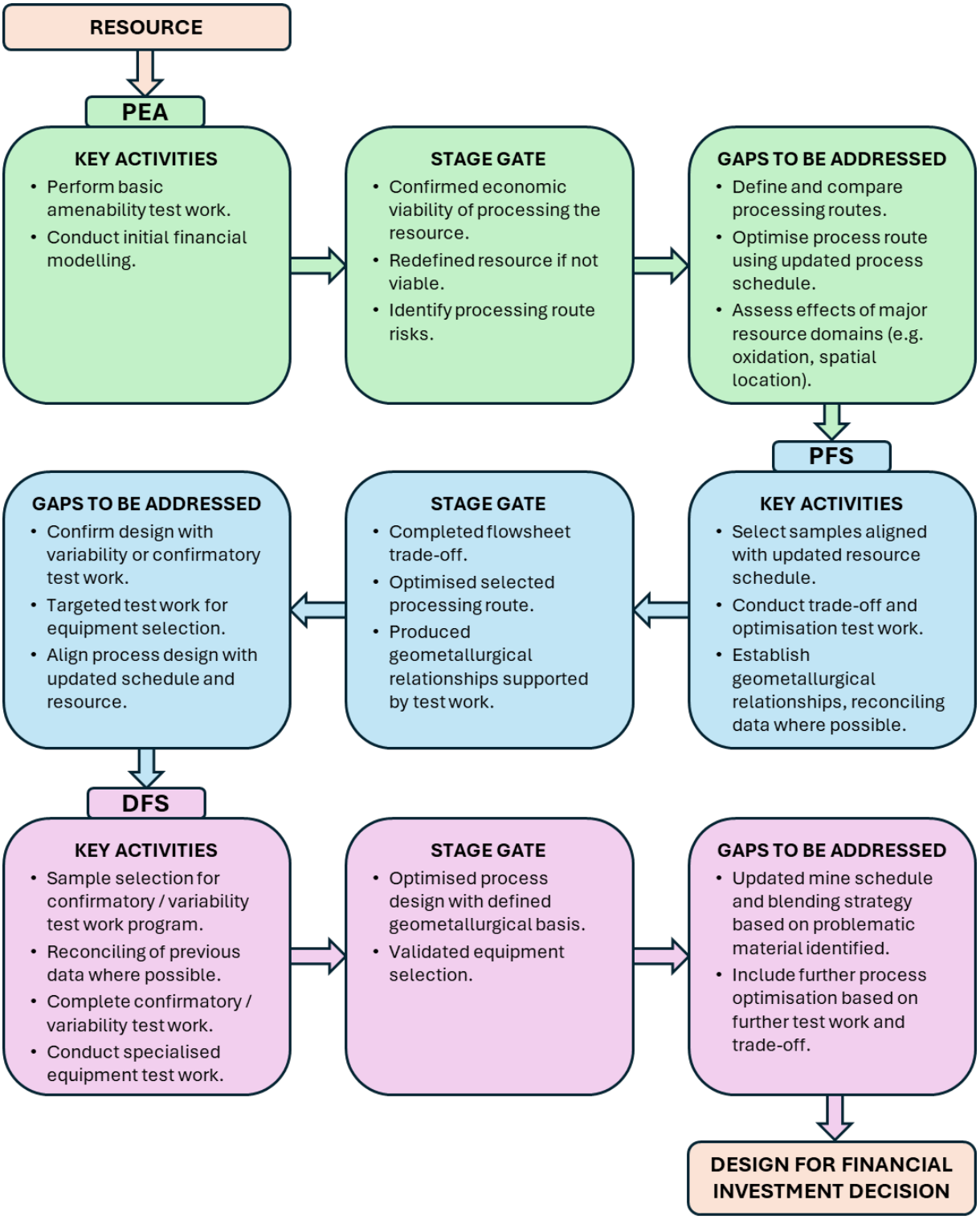



**FIG 2** – Framework for geometallurgical bridging of test work data across study phases.

The defining feature of the methodology was its iterative nature. Each study phase generated insights that revealed data gaps, limitations, or design uncertainties, which subsequently informed the objectives and scope of the next phase.

Maintaining a reliable record-keeping system was critical for reconciling historical and current test work data sets across different study phases, enabling the integration of legacy and recent data. Key geological data for each metallurgical samples; including spatial location, domain lithology, and elemental assays; together with metallurgical test work results, conditions, and objectives recorded on log sheets and archived digitally, provided a basis for consistent comparison and reconciliation. This information enables metallurgical test work results to be re-annotated against geological characteristics, facilitating the assessment and validation of relationships between test work parameters, such as grind size and process conditions, and metallurgical response in the context of geological controls including mineralogy and domain. In turn, this supported structured gap analysis to identify under-represented domains, lithologies or spatial areas within the orebody, thereby informing subsequent stages of sample selection and test work planning.

To support this process, alignment between geologists and metallurgists ensured consistent geological classification of samples (domain and lithology), thereby supporting reconciliation of test work data sets across study phases as the project and geological models matured. Key information, such as test conditions, were available from test work log sheets and digitally archived across all stages of design. Similarly, records for metallurgical samples and test work, including geological data, test conditions, and test work measurements, were maintained in a structured database encompassing both the current and previous phases of study. This framework enabled the database to mature as the project advanced, allowing historical results to be reconciled and incorporated without compromising the integrity of DFS-level design parameters.

A stage-gated metallurgical test work program implemented across amenability testing, flow sheet selection, optimisation and variability assessment provided the foundation for effective reconciliation between study phases. In turn, this systematic approach enabled results from each phase of study to be consolidated into a single, defensible DFS-level design basis. The key findings, based on evaluation of results at each stage, were used to identify gaps to be addressed in the next phase of the study. For example, grind sensitivity was evaluated during the PFS with respect to oxidation domain and spatial location; however, the influence of lithology remained unresolved. This gap was addressed in the DFS through lithology-based variability test work, enabling the relationship between lithology and cyanide leaching response to be quantified, resulting in the establishment of optimised grind sizes for each pit-zone, domain and lithology. This process also led to a systematic optimisation of the key operating parameters of cyanide leaching such as dissolved oxygen and cyanide concentration, slurry density, and residence time. The latter was optimised via the observed gold dissolution kinetic curves from the variability samples.

Further optimisations of unit processes, such as pre-aeration before cyanide leaching, were evaluated using targeted sighter tests and independently validated via further test work. Kinetic curves were generated based on observed gold extraction, and correlations established to reagent consumption to validate its effect prior to inclusion into the design. This approach enabled uncertainty in the design to be reduced by expanding data set representativity, without the requirement of additional samples, resulting in lower overall sample extraction and handling costs. It also facilitated the establishment of validated relationships between key geological characteristics, metallurgical response and process variables, in turn supporting improved confidence in process design.

# EFFECTS OF BRIDGING THE GAP

## Reagent consumption

Analysis of the consolidated database demonstrated relationships between reagent consumption and geometallurgical variability, enabling predictive mapping of cyanide and lime consumption across lithology, domain and spatial location for the Life-of-Mine. The cyanide leaching database further demonstrated correlations between unit reagent consumption, mineralogical characteristics and concentration of soluble metal species in solution. These were used to quantify mineral-specific contributions to reagent demand, such as lime consumption as a function of dolomite content, and

cyanide consumption relative to soluble metal concentrations. Lime consumption specifically, when assessed with respect to the dolomite content per domain, demonstrated the effect of dolomite as a natural alkaline buffer, in turn reducing lime consumed to maintain the leach target pH. This resulted in variance of lime consumption across domains, with oxide domains containing significantly lower concentrations of dolomite demonstrating measurably higher lime consumption rates.

The benefits of bridging the gap were further evident in the interpretation of gold leaching reagent consumption trends. Data set integration enabled the identification of correlations between cyanide and lime consumption and soluble iron concentration in solution. These relationships are presented in Figure 3.

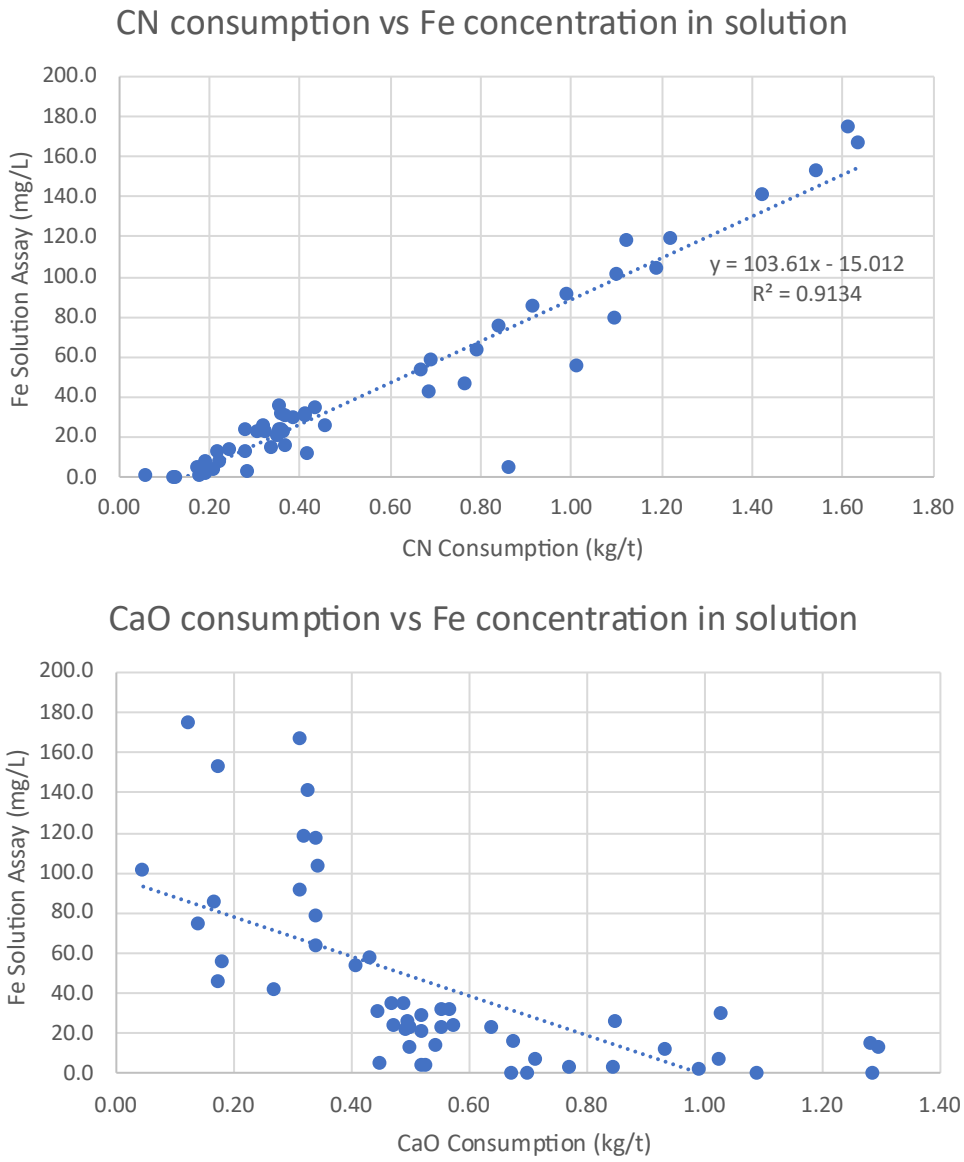



**FIG 3** – Reconciled leach solution assays and reagent consumption.

A positive correlation was observed between cyanide consumption and soluble iron concentration in solution, indicating that increased cyanide demand was partly driven by elevated soluble iron concentration in solution. In contrast, lime consumption showed an inverse relationship with soluble iron concentration in solution. By integrating these correlations with mineralogical data, it was found that elevated soluble iron concentration levels were associated with iron-bearing minerals that are reactive with cyanide under leaching conditions. This provided a strong technical basis for the inclusion of a pre-aeration step in the process flow sheet to oxidise and passivate these reactive mineral phases prior to cyanidation. Implementation of pre-aeration reduced cyanide consumption

through mineral passivation and stabilised pH during the early stages of leaching. This, in turn, lowered lime consumption and improved overall cyanidation efficiency.

By enabling the data set to be viewed holistically rather than as isolated study-phase outputs, bridging the gap improved the clarity, representativity, and defensibility of geometallurgical correlations. These enhanced correlations strengthened reagent consumption models, increased confidence in design values, and ultimately delivered a more reliable and optimised cyanide leaching process for the project.

## Process design and scheduling

In addition to process optimisation benefits, deriving correlations between geometallurgical characteristics and metallurgical outcomes established the basis to support key process design values. Through geometallurgical modelling across the processing schedule, weighted estimates of metallurgical performance could be produced to inform and optimise key blending strategies. The blending strategy for gold feed grade across the processing schedule is highlighted in Figure 4, where blending was defined by lithology. As shown in Figure 4, low recovery (<80 per cent) material was strategically blended with higher recovery material in the first half of the processing schedule. This minimised the impact that processing this material had on the overall plant recovery.

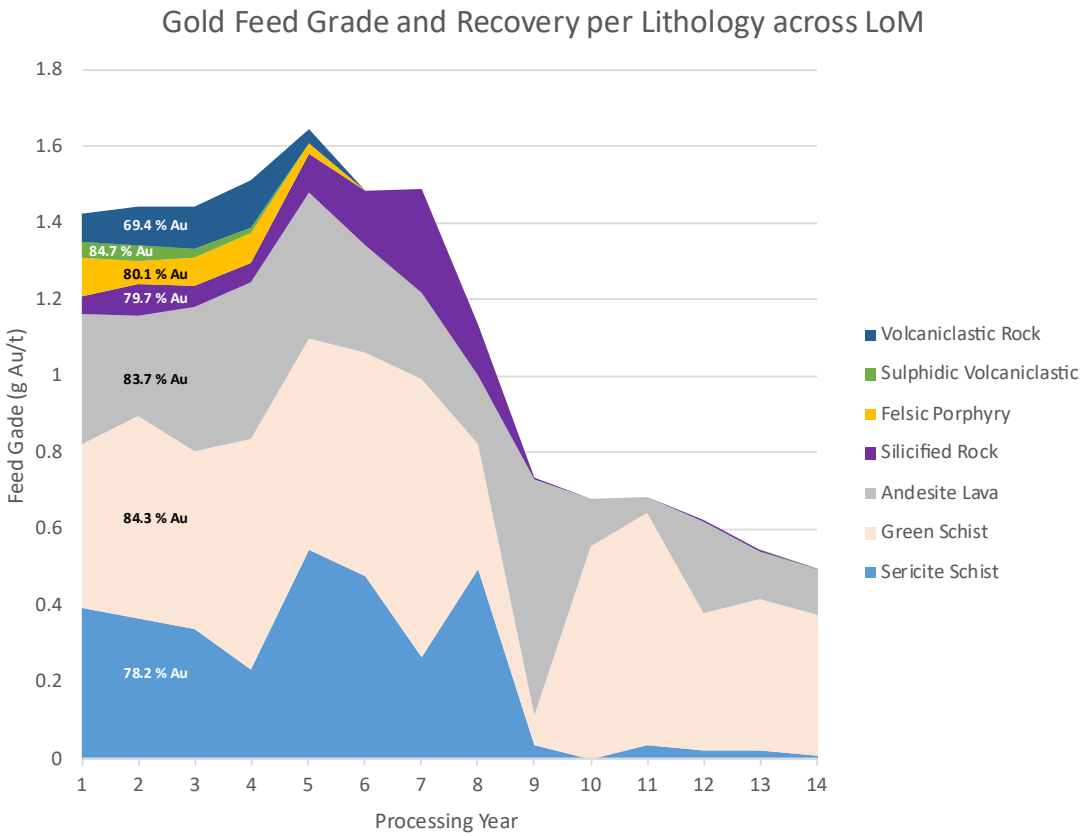



**FIG 4** – Gold feed grade over LoM with LoM weighted gold recovery per lithology.

Clearly establishing relationships such as grind sensitivity and gold dissolution kinetics of the ore by pit-zone, domain and lithology supported by variability test work led to process design values that were validated against the resource, effectively de-risking the process design. This framework enabled further blending strategies targeting over/under grinding material and minimising variance in reagent scheme and operational stability during the main phases of the process schedule to be developed.

## Economic integration

The geometallurgy-driven framework also extended into project economics by enabling both revenue and operating costs to be modelled by pit-zone, domain and lithology for each operating year within

the Life-of-Mine. Operating cost drivers such as cyanide and lime consumption were segmented by lithology, domain and pit-zone, enabling operating cost optimisation by strategic material blending. Estimating key cost and revenue drivers at a granular level of detail with respect to the resource across the project life facilitated the development of a robust financial model. Because this model was grounded in geometallurgical correlations validated through metallurgical test work, it not only de-risked the process design but also facilitated scenario-based scheduling. This supported adaptive mine-to-mill planning by balancing throughput, grinding power, and reagent demand against cash-flow targets. Ultimately, this provided a stable and defensible basis for the project to progress through the next key financial investment decision.

## Future expansion

The application of the framework also extends beyond the process design phase and provides ongoing value for evaluating future expansion opportunities. When a new resource is identified through geological exploration, its geological, mineralogical and metallurgical characteristics can be benchmarked against the existing geometallurgical database to assess its suitability for processing through the current plant. This allows potential constraints associated with the existing process plant to be identified early in the evaluation process, such as comminution circuit capacity, recovery limitations, reagent consumption or residence time requirements.

The integrated data set enables the likely processing strategies and metallurgical performance of the new ore to be assessed relative to established ore types and existing Process Design Criteria (PDC). Where the new resource exhibits different mineralogical characteristics or metallurgical responses, additional test work can be targeted to evaluate impacts on recovery, product quality and operating costs. These assessments provide a technical basis for determining whether the resource can be accommodated within the existing plant through operational strategies, such as blending, or whether modifications to the flow sheet, equipment upgrades or plant expansion are required.

Consequently, the geometallurgical database developed through the framework serves as a long-term technical reference for future expansion studies. By linking historical test work, mineralogical characteristics and process design basis, the framework supports more informed decisions regarding resource development, debottlenecking opportunities and potential plant expansions, reducing uncertainty and improving confidence in future project evaluations.

# CONCLUSIONS

This study demonstrates how a geometallurgy-driven approach can reconcile, or ‘bridge the gap’, between historical and current test work into a high-confidence basis that de-risked process design. By embedding geological attributes – such as lithology, alteration, mineral associations, and liberation – into sample selection, domaining, and data interpretation, the methodology ensures that metallurgical response is evaluated within its proper geological context. This integration enhances representativity, improves the reliability of test work outcomes, and enables meaningful prediction of key parameters such as grind sensitivity, extraction efficiency, and reagent consumption across the orebody.

Bridging the gap between earlier study phases and DFS-level requirements was achieved through the standardisation of test work conditions, rigorous data governance and building correlations between geological characteristics and metallurgical response. This approach allowed historical test work data sets to be incorporated without increasing uncertainty, substantially expanding the available data population without requiring additional drilling. The consolidated metallurgical test work database, structured by pit-zone, domain, and lithology, facilitated robust modelling of cyanide and lime consumption, gold dissolution kinetics, and blending strategies aligned with mine-to-mill scheduling.

The outcomes of this work illustrate that geometallurgy provides more than a descriptive link between geology and metallurgy. It delivers a quantitative foundation for process optimisation and economic evaluation. By establishing defensible design values, improving feed predictability, and enabling scenario-based scheduling, the geometallurgical framework reduced technical risk and strengthened the project’s financial confidence. The approach outlined here is broadly transferable and can be

applied to other commodities and processing routes, particularly where ore variability and legacy data integration present challenges.

Future work will focus on validating these correlations during plant ramp-up and applying the framework to operations data to further refine predictive capability.

## ACKNOWLEDGEMENTS

The authors thank Lycopodium for permission to display and publish this body of work, as well as the AusIMM for providing an opportunity for mining industry professionals to innovate and share ideas.

## REFERENCES

Bennet, D W and Munro, P D, 2024. Practical Geometallurgy – and let there be light, in *Proceedings Mill Operators Conference 2024*, pp 20–21 (The Australasian Institute of Mining and Metallurgy: Melbourne).

Dominy, S C, O'Connor, L and Xie, Y, 2016. Sampling and Test Work Protocol Development for Geometallurgical Characterisation of a Sheeted Vein Gold Deposit, in *Proceedings The Third AusIMM International Geometallurgy Conference 2016,* pp 97–112 (The Australasian Institute of Mining and Metallurgy: Melbourne).

Dutrizac, J E and Sunstrum, J B, 1999. The first cyanide leaching plants in Canada, *Canadian Institute of Mining, Metallurgy and Petroleum*, pp 155–159. Available from: <https://onemine.org/documents/the-first-cyanide-leaching-plants-in-canada>

Jackman, I, 1995. The Role of Flotation in the Recovery of Gold, *Canadian Institute of Mining, Metallurgy and Petroleum*, pp 426–436. Available from: <https://onemine.org/documents/the-role-of-flotation-in-the-recovery-of-gold>

Marsden, J O and House, C I, 2006. *The Chemistry of Gold Extraction*, second edition, ch3:69–98; ch6:233–275 (The Society for Mining, Metallurgy and Exploration, Inc.)

Newell, A, Munro, P D and Fiedler, K, 2018. Metallurgical test work – between a rock and a hard place, in *Proceedings of the 14th Mill Operators Conference 2018,* pp 35–52 (The Australasian Institute of Mining and Metallurgy: Melbourne).

## Mill Operators

# Process control and automation

# Digital twin for gold production at Ikkari Mine, Finland

*C Araujo[1], T Roimaa[2], V Zhukov[3], C Izart[4], R Budhathoki[5] and S Bosman[6]*

1. Senior Specialist, Simulation and AI, Metso Finland Oy, Espoo 02320, Finland.
   Email: cesar.araujo@metso.com
2. Principal Processing Engineer, Rupert Exploration Finland Oy, Sodankylä 99600, Finland.
   Email: troimaa@rupertresources.com
3. Simulation Specialist, Digital Solutions, Metso Finland Oy, Lappeenranta 53900, Finland.
   Email: vladimir.zhukov@metso.com
4. Technology Manager, Process Simulation, Metso Finland Oy, Pori 28330, Finland.
   Email: caroline.izart@metso.com
5. Senior Metallurgist, Metso Finland Oy, Pori 28330, Finland.
   Email: roshan.budhathoki@metso.com
6. Senior Manager, Digital Solutions, Metso Finland Oy, Espoo 02320, Finland.
   Email: stefan.bosman@metso.com

## ABSTRACT

Metallurgical digital twins have demonstrated success in optimising the processing performance of operational plants by integrating ore characteristics, material flows, process data and plant constraints. First-principles modelling techniques are particularly valuable for explaining process behaviour, including the planning stages of new plants or expansion of existing ones.

This study presents a comprehensive model of a gold processing site at Rupert Exploration Finland's greenfield Ikkari gold project in northern Finland. The model encompasses the minerals processing plant, including SAG mill, ball mill and gravity concentrator, the hydrometallurgical plant, including carbon-in-leach, cyanide destruction, carbon reactivation and electrowinning, and the water treatment plants, including ion exchange, reverse osmosis, gypsum precipitations and crystallisation. Leveraging advanced modelling techniques, a flexible simulation was developed with adjustable parameters to replicate the processes in accordance with various feed compositions, equipment performances and operation strategies. The simulation model incorporated the available experimental data from laboratory tests as well as the empirical knowledge of several subject matter experts.

The key findings and critical operational insights of utilising such a comprehensive model enabled the identification of optimal treatment strategies for targeted orebodies, evaluation of multiple design scenarios and alignment to operational requirements for Ikkari Project. In addition, the model evaluated hundreds of process variables throughout the process plants, providing better understanding of the overall process complexity through the detailed description of its interconnected parts.

Finally, it discusses the application of metallurgical digital twins in early-stage engineering, highlighting the insights it can provide in obtaining environmental permits, resource planning, ore blending, among other benefits.

## INTRODUCTION

The advancement of digital tools for process modelling has brought up several innovations in the fields of simulation and optimisation in the recent years. Although the concept of digital twins has existed for a long time and have been used by NASA since the 1960s (Danette Allen, 2021), it is only after the progress of computing power, software and data connectivity that its use has become more widespread. In short, a digital twin is a digital representation of an existing physical asset or process, whose purpose is to reproduce the behaviour of the physical asset or process. It is worth noting that, for the present study, our aim is to discuss it in terms of a particular process. With regards to its connectivity to the real process, the digital twin in its full implementation, should be able to ingest, in real-time, at least part of the data that is input to the physical process (eg flow rates, composition, temperature, pressure etc) and likewise calculate key performance indicators (KPIs), including a number of soft-sensors (eg conversion, recovery, efficiency, composition etc). In that

sense, the digital twin would be a playground for engineers and operators to evaluate the behaviour of their system under different scenarios through time and make informed decisions prior to taking actions on the system (Moilanen, Remes and Binder, 2023). Nevertheless, for greenfield cases where no source of online data is available, the concept of digital twin can still be applied if the user defines all the inputs to the model that are necessary for its calculations, eg input flow rates, compositions, process design rules, etc. The present paper provides a case study in which the latter concept is developed for a gold processing plant project in the northern part of Finland. The goal was to create a digital representation of the greenfield gold plant which includes minerals processing, hydrometallurgy, water treatment and the water bodies; all these interconnected and interacting with each other. Such calculations aimed at the optimisation of the process flow sheet, evaluation of environmental KPIs and production planning.

## MATERIALS AND METHODS

The process simulation used in the present study was created using the HSC Sim module of the HSC Chemistry software, version 10.8 (by Metso). HSC Sim enables the development of first-principles simulations of minerals processing, hydrometallurgy and pyrometallurgy flow sheets, integrating thermochemical and equilibria calculations to the unit operations. HSC Sim allows for the development of both static (steady-state) and dynamic (time-dependent) simulations and is the engine behind Metso's web-based digital twin platform Geminex™ (Ahmad *et al,* 2025; Moilanen, Remes and Grigoryan, 2023). After development, the HSC Sim simulation was loaded to Geminex™ and a systematic analysis and comparison of the process behaviour was done. In Geminex™, users can adjust model inputs to evaluate the effects on the model outputs. Input tables are linked to every main process area page, in such a way that operators can access them seamlessly. Such inputs cover stream quality and flow properties, as well as equipment/process parameters. It is also possible to create warnings and alarms if the variable value exceeds pre-defined alert limits, to improve user navigation of the results. In addition, users can create multiple prediction simulation scenarios cards and run them simultaneously. It gives possibility for users to easily review the simulation results at separate page to compare scenarios by checking predefined engineering or economical parameters.

## IKKARI MINE GOLD PROCESSING DIGITAL TWIN

The customer conducted comprehensive laboratory tests during the pre-feasibility studies (Rupert Resources Ltd, 2025) and possessed solid results that described the transformations involved in the processing of the ore, all the way to the water treatment. In addition to the laboratory data, the process flow diagram (PFD) for a given design of the plant has been provided, out of which the flow sheet of process simulation was based on. It is important to point out that the flow sheet design presented does not reflect the final design of the plant, which may still undergo modifications as needed. There are three main process areas in the flow sheet, encompassing the minerals processing plant, including SAG mill, ball mill and gravity concentrator, the hydrometallurgical plant, including carbon-in-leach, cyanide destruction, carbon reactivation and electrowinning, and the water treatment plants, including ion exchange, reverse osmosis, gypsum precipitations and crystallisation.

### Minerals processing and hydrometallurgy

According to the pre-feasibility report (Rupert Resources Ltd, 2025), the Ikkari deposit can be described as an orogenic hydrothermal gold system, with gold mineralisation occurring mainly in disseminated or vein related pyrite. Visible, coarse free gold can also be found. Rupert Resources has identified several different rock types in the project which can be simplified in two main groups: a felsic group and a mafic to ultramafic group. The style of mineralisation is principally controlled by the lithology. In felsic domain mineralisation can be associated to brittle fracture regime where in mafic – ultramafic domain, the mineralisation may be associated with sediment intercalation. During the pre-feasibility study, ultramafic and felsic domains ores have been characterised in terms of mineralogy, grindability and gravity recovery.

### *Feed definition and mineralogy*

The data used for the mineralogical description of the particles in the simulation comes from a study of composites for both felsic ores and mafic ores. Modal mineralogy indicates that the Felsic composite consists of quartz (41.5 per cent), plagioclase (31.3 per cent), muscovite mica (7.5 per cent), magnesite (6.9 per cent) and pyrite represents 1.4 per cent mass of the sample.

The mafic composite consists of quartz (34 per cent), magnesite (26.9 per cent), lesser quantities of muscovite (8.0 per cent), chlorite (6.2 per cent), biotite (5.6 per cent) and pyrite represent 2.9 per cent mass of the sample (Rupert Resources Ltd, 2025). The particle-based model supporting the simulation contains previously cited minerals, in different amount per ore type, in addition to gold.

Using this particle-based approach, it is possible to accurately follow the mineralogical composition of each stream in the flow sheet, providing more reliable flow density and elemental compositions. If the mineralogy is fixed in the model, gold grade, sulfur grade and magnesium grade can be adjusted, per ore type, so that variability of the ores over time can be considered. The amount of minerals is then recalculated based on these grades.

The process feed stream is constituted of a mix of felsic and ultramafic ores. The percentage of each is also an adjustable variable, that will follow the mining plan and available ore at each given year, month. The definition of the run-of-mine stream is completed by a particle size distribution, similar for both ores with a $P_{80}$ of 250 mm.

### *Crushing circuit*

The crushing circuit consists in a feed bin, a grizzly of 1000 mm associated with an open circuit jaw crusher. Product of the crushing is stored in crushed ore stockpile, before being fed to the grinding circuit, as shown in Figure 1.

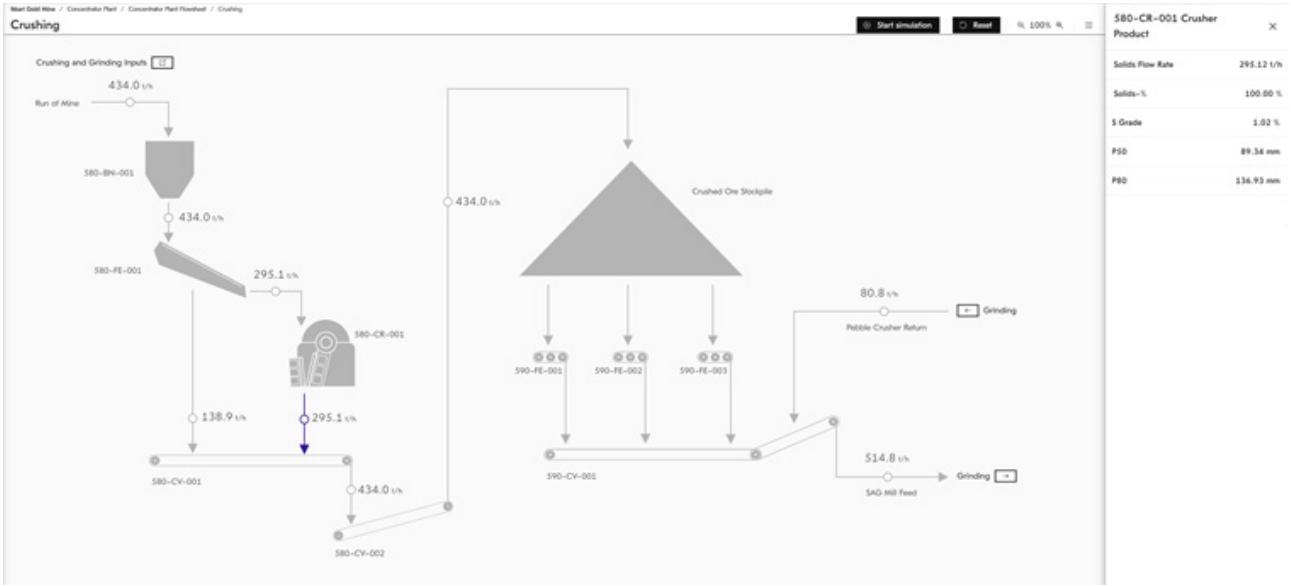



**FIG 1** – Crushing circuit flow sheet.

The grizzly screen is modelled as a simple efficiency curve distribution with oversized particles directed to the jaw crusher model. The jaw crusher model (Bengtsson and Evertsson, 2008) can simulate the product particle size distribution of the product based on the crusher's operational characteristics, including Closed Side Setting (CSS) or chamber type. The model can also predict the power consumption based on the individual ore's crushability, and the amount of each ore in the feed.

Since abrasion index is also available for both ore types, the wear rate in crusher can also be calculated based on the feed ore mix. The rest of the crushing circuit consists of mixer units, for conveyor and stockpiles, which do not transform the stream composition or size distribution.

### *Grinding circuit*

The grinding circuit consists in primary SAG mill associated to a cone crusher, followed by a closed loop ball mill – hydrocyclone, where part of the cyclone underflow is directed to gravity separation to extract coarser, already liberated gold. Figure 2 depicts the Geminex™ view of the grinding-gravity circuit.

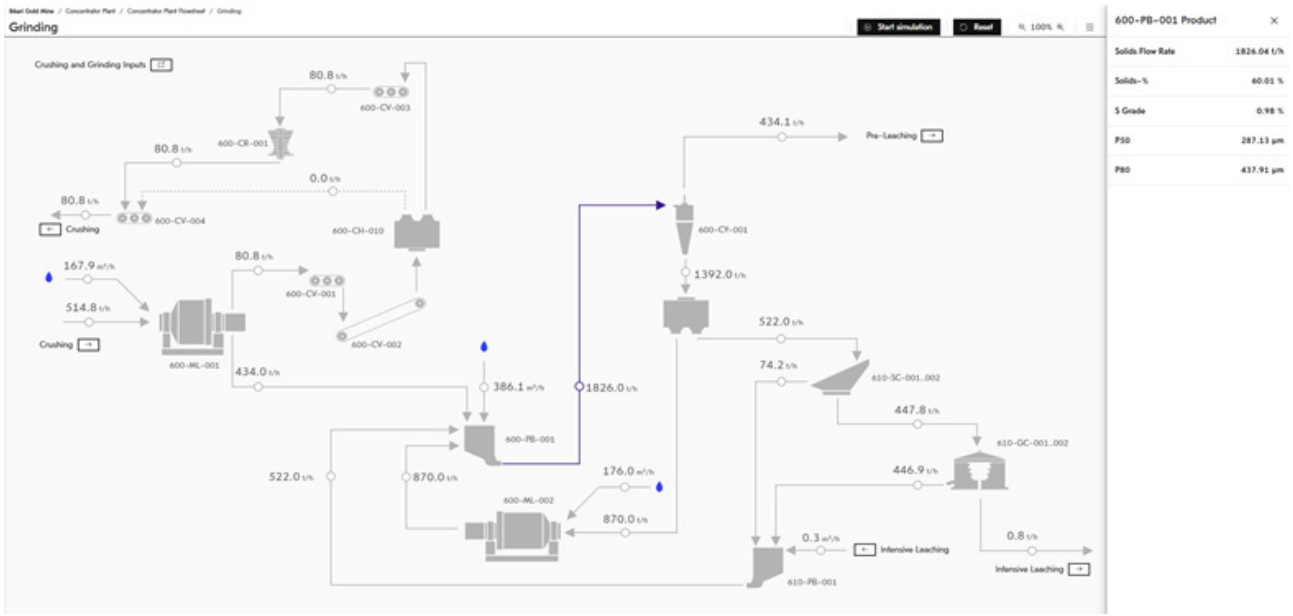



**FIG 2** – Grinding-gravity separation flow sheet.

The first model of that circuit is a SAG mill that implements a population balance model, using future mill's dimensions to calculate slurry residence time, to estimate mill power consumption and product particle size distribution. Since both ores have distinct grinding parameters (Axb, Ta, BWI) each different blend will have a different power estimation. Mill speed can be adjusted by the user and will be reflected upon size distribution and power.

The trommel oversize is directed to a pebble crusher modelled as cone crusher (Bengtsson and Evertsson, 2008) which, as well, is used to calculate the power consumption based on the ore blend.

In the next section of the grinding circuit, a sump gathers different flows to feed a cyclone cluster, also modelled as an efficiency curve, which uses feasibility studies $P_{80}$ of the overflow stream to the pre-leaching as a fitting target.

A part of that cyclone cluster underflow is directed to a ball mill, which similarly to the previously described SAG mill model, uses a population balance model and the future mill's dimension to calculate power consumption and product particle size distribution.

Finally, the rest of the cyclone underflow is directed toward gravity separation, which implement a separation per particle per size obtained in the pre-feasibility study. The gravity concentrate is directed to intensive leaching while tails are recirculated to the hydrocyclone feed sump.

As shown in Figure 3, several water addition points are present in this circuit. The water flows in this simulation are all connected and work in a close loop. In that case, the water is recirculated from the water treatment plant process which is described in further detail.

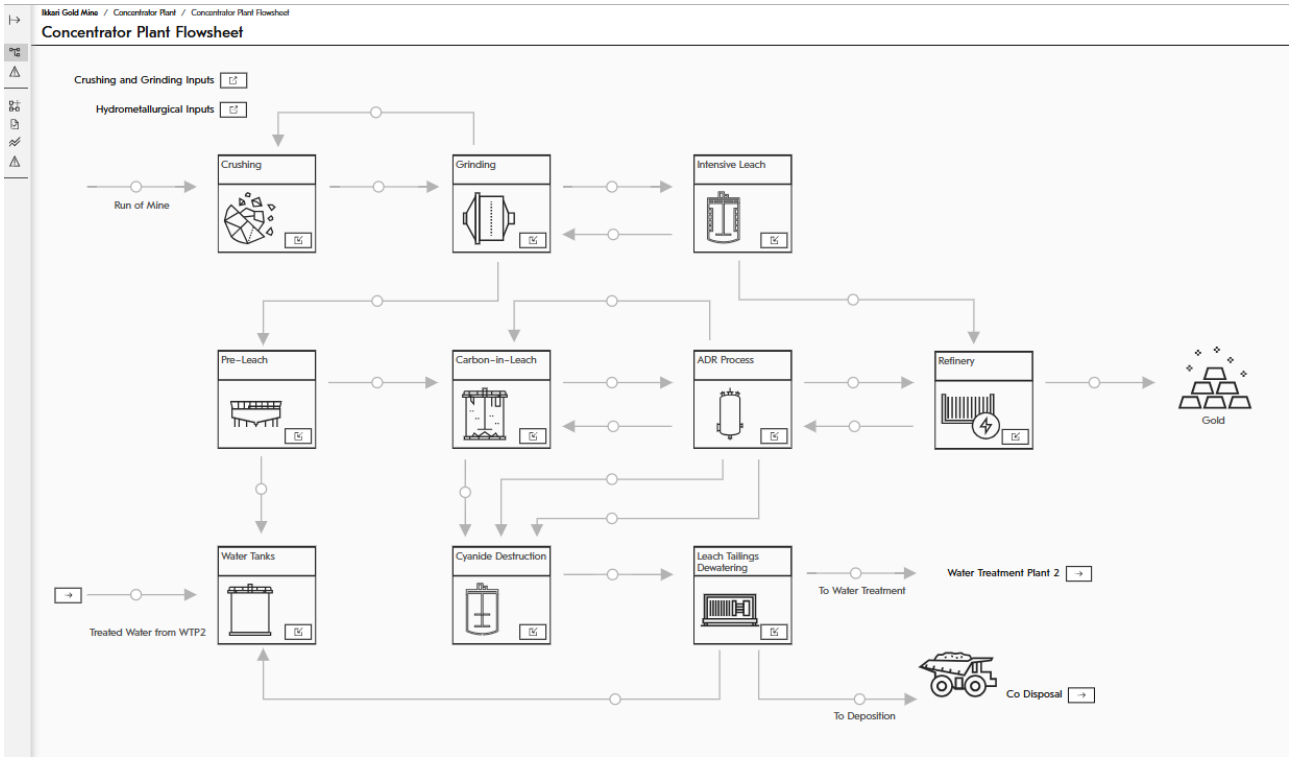



**FIG 3** – Overview of the concentrator plant flow sheet.

## Hydrometallurgy processing

The digital twin for Ikkari gold project consist of several hydrometallurgical process stages such as, intensive cyanide leaching of high-grade gravity concentrate, carbon-in-leach circuit for gold leaching with sodium cyanide solution followed by adsorption on to activated carbon, ADR (adsorption, desorption, and regeneration) process, refinery for gold recovery via electrowinning, cyanide destruction for detoxification, and leach tailing dewatering for solid liquid separation.

### *Intensive leach stage*

The high-grade gravity concentrate is leached with concentrated NaCN solution. The concentration of NaCN can be adjusted to study its impact on the process circuit. Main process input parameters are slurry pH, slurry solids concentration, NaOH stock, NaCN concentration, and gold recovery in intensive cyanide leaching. The output streams of this stage are gravity tails which are recycled back to grinding and intensive cyanidation solution which goes for gold recovery in the refinery.

### *Pre-leach and Carbon-in-Leach (CIL) process stage*

The cyclone overflow from the grinding stage is the main stream entering the pre-leach stage. The main function of pre-leach stage is to adjust the solid concentration in the slurry in a thickener. The solid concentration in the underflow and overflow streams are user input parameters. The overflow fraction of the thickener goes to process water tank while the underflow goes to CIL circuit. Figure 4 illustrates the CIL circuit view from Geminex™.

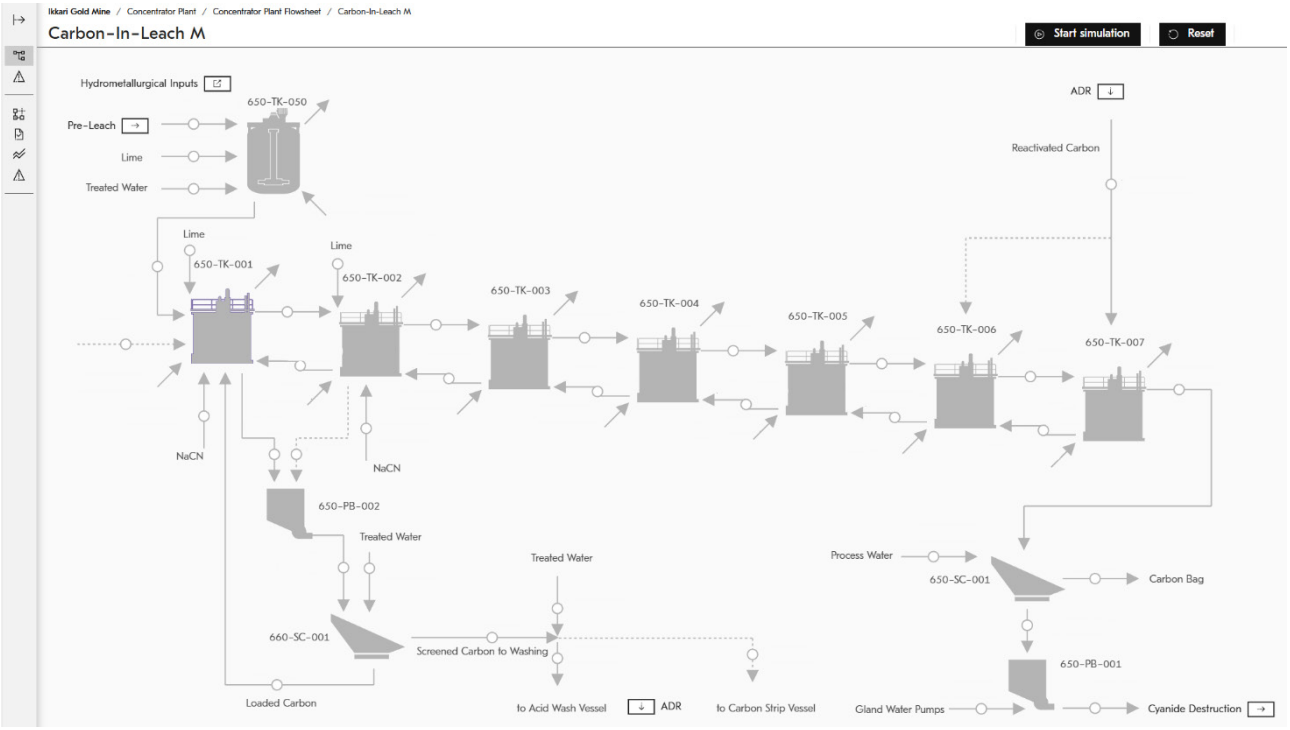



**FIG 4** – Overview of the CIL process area in Geminex™ (due to confidentiality, all value labels were removed from the picture).

In CIL circuit, the slurry first goes through a pre-aeration tank where it is preconditioned to a desired pH value using lime slurry and is also aerated with air. Both parameters are user defined in the digital twin model. The conditioned slurry goes through a series of agitated tanks (CIL1 to CIL7) in forward direction as shown in Figure 4. Whereas the activated carbon goes in a counter current flow from CIL7 to CIL1 tanks. In the present model, the carbon concentration (g/l) was taken to be the same in all tanks and was defined as a user input parameter. Thus, the impact of the carbon concentration in overall CIL process, eg in gold recovery, could be directly evaluated. In the CIL circuit, the rate of Au leaching is described in Equation 1 (Ling *et al*, 1996).

$$r_{Au,Leaching} = k_1 \cdot (CN^-)^{a_1} \cdot (O_2)^{b_1} \cdot (Au - Au^*)^{c_1} \quad (1)$$

Where:

| | |
|---|---|
| $(CN^-)$ | is the free cyanide concentration |
| $(O_2)$ | is the concentration of dissolved oxygen in the liquid phase |
| $Au$ | is the gold grade in the ore |
| $Au^*$ | is the terminal gold grade in the ore |
| $k_1$, $a_1$, $b_1$ and $c_1$ | are kinetic parameters estimated from leaching laboratory tests |

The adsorption of dissolved gold as aurocyanide complex ($Au(CN)^{2-}$) to the activated carbon is a reversible phenomenon. The gold adsorption equilibria and kinetics were calculated based on Equations 2–3, respectively.

$$Au_{Freundlich} = a_2 \cdot (Au_L)^{b_2} \quad (2)$$

$$r_{Au,Ads} = k_2 \cdot (Au_{Freundlich} - Au') \quad (3)$$

Where:

| | |
|---|---|
| $Au_L$ | is the concentration of leached gold in the liquid phase |
| $Au_{Freundlich}$ | is the equilibrium gold content in the carbon as calculated by the Freundlich isotherm in g/t |
| $Au'$ | is the gold content in the carbon in g/t |

$a_2$, $b_2$ and $k_2$ are parameters estimated from laboratory experiments

The use of kinetic expression for gold dissolution and subsequent adsorption on activated carbon in the digital twin model increases the explainability of the results and the study of the impact of leading variables such as gold grade in ore, cyanide concentration, and carbon concentration on the overall gold leaching yield, free cyanide level, and sulfate level in the flow sheet.

The gold depleted slurry then goes towards the cyanide destruction stage whereas the loaded carbon goes through the ADR (Adsorption desorption and regeneration) process where gold is desorbed from the carbon, then reactivated and recycled.

### *ADR process*

ADR process includes three principal stages such as acid washing, desorption, and carbon regeneration. The goal of the acid wash stage is to, by using dilute hydrochloric acid, remove inorganic scale, precipitated metal hydroxides, and other metal ions that foul the active sites or promote scaling downstream. The second stage involves desorption or elution of gold using hot caustic-cyanide eluant at elevated temperatures. Such aggressive process conditions drive the equilibrium to strip the aurocyanide complex ($Au(CN)^{2-}$) into the solution from the carbon. This pregnant eluate containing high gold concentration exits the column which is further treated in the refinery stage for gold recovery. On the other hand, the stripped carbon is thermally reactivated in a rotary kiln at high temperatures to restore the adsorption capacity required for a regenerative process. After quenching, the carbon is screened to remove fines and returned to the CIL circuit. The details of the ADR process are not disclosed due to confidentiality reasons.

### *Refining*

The pregnant eluate from ADR process and intensive leach solution containing gold are further treated in refinery stage to recover gold. The gold containing solution is fed through electrowinning cells where the aurocyanide ($Au(CN)^{2-}$) complex is reduced to metallic gold and free cyanide ion ($CN^-$) using electricity. The sludge from electrowinning cells goes through a filter where sludge containing gold is separated. The filtrate along with the barren solution containing cyanide ion from electrowinning cell is recycled back to the ADR process. The gold cake is further treated in an induction furnace at high temperature to obtain gold doré. The details of the refinery are not disclosed due to confidentiality reasons.

### *Cyanide destruction*

Cyanide containing solutions from CIL tailings and ADR stage are treated to remove the toxic form of cyanide into non-toxic cyanate form. Sodium metabisulfite (SMBS) and copper catalyst ($Cu^{+2}$) are used as detoxification reagents under mildly alkaline conditions. The detoxification of cyanide complexes generates sulfuric acid and lime slurry is used for the neutralisation. Weak acid dissociable (WAD) cyanide complexes are also oxidised to cyanate ($OCN^-$). However, iron-cyanide complexes required copper to coprecipitate as insoluble mixed ferrocyanides.

The concentration of SMBS and its excess factor, copper sulfate concentration and its dose, and target pH are provided as user defined variables and reagent consumptions and residual sulfate concentration are calculated in the system.

### *Leach tailing dewatering*

Leach tailing dewatering stage focuses primarily on recovering clarified water for reuse in grinding circuit and leaching stage. In addition, the tailings are also further treated for appropriate disposal. The cyanide detoxed discharge slurry reports to a tailing thickener system where flocculants aid the settling to obtain a denser underflow and a clear overflow. The clear overflow is repurposed as process water for the whole circuit and remaining overflow reports to the water treatment stage. The denser thickener underflow is filtered to separate the residue. The filtrate and wash water are recycled back to the process while the residual filter cake is reported to the co-disposal area. The main user-defined inputs are solid concentration in overflow and underflow fraction, cake moisture content, and washing efficiency in the filter.

## Water treatment

The water treatment of the plant is divided into two main process areas, namely WTP1 and WTP2. In WTP1 the contact water coming from the Raw Water Dam is mixed with recycled waters from the pressure filter and sand filter wash waters and forwarded to a flocculation-settling system. The overflow is directed to a sand filtration system and then directed to a series of two systems of ion-exchange (IX) columns. The underflow of the flocculation-settling is sent to a pressure filter where it is mixed with the underflow from the first flocculation-settling system in WTP2. The filtrate water of this filter is then mixed with the Raw Water Dam feed to WTP1 and the solid cake is collected and disposed. The wash water of the streams of the IX are sent to the crystallizer unit in WTP2. The treated water stream from the IX columns is partly recycled to the feed of WTP1, used as wash waters for the IX and sand filter system and flocculant preparation. The remaining IX treated water is routed to the Treated Water Dam, as discussed in the following section. Figure 5 provides an overview of the WTP1 process.

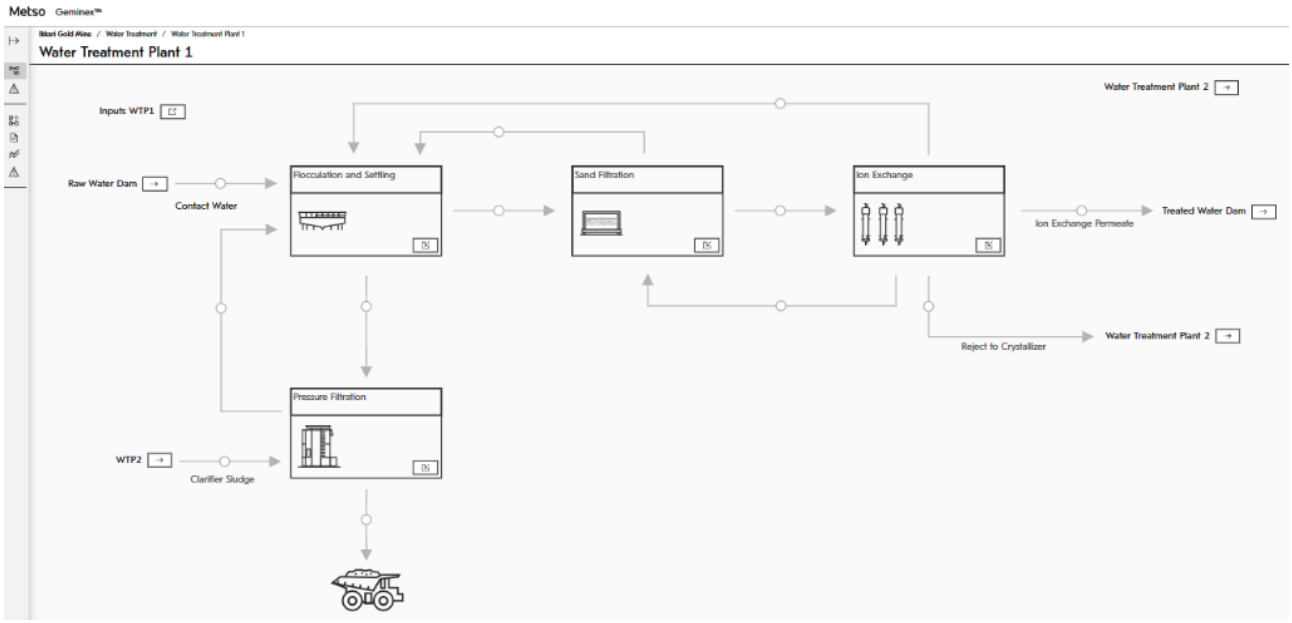



**FIG 5** – Overview of Water Treatment Plant 1 (WTP1).

The main user-defined inputs to the WTP1 are the dosing of coagulant to the flocculation-settling system, the number of sand filters in operation, the capacity of each sand filter, the sand filter filtration efficiency, the number of IX columns operating in each IX system and the IX column capacity, to name a few.

The head feed to the WTP2 process area receives as the contact water from the Water Dam and the process water from the Leach Tails Dewatering process area from the hydrometallurgy part. The feed is first treated in a flocculation-settling system, in which the underflow is routed to the pressure filter in WTP1 and the overflow is sent to a sand filter system. The effluent undergoes two stages of sequential ultrafiltration, reverse osmosis and gypsum precipitation. The treated effluent stream out of these two stages is combined with the IX wash water from WTP1 and sent to a crystalliser, where the collected salt is disposed and the evaporated water is recycled back to the first stage ultrafiltration system. The solid-containing reject streams from the first and second stage treatments are then filtered and the wash water is sent to the Raw Water Dam. Figure 6 provides an overview of the WTP2 flow sheet.

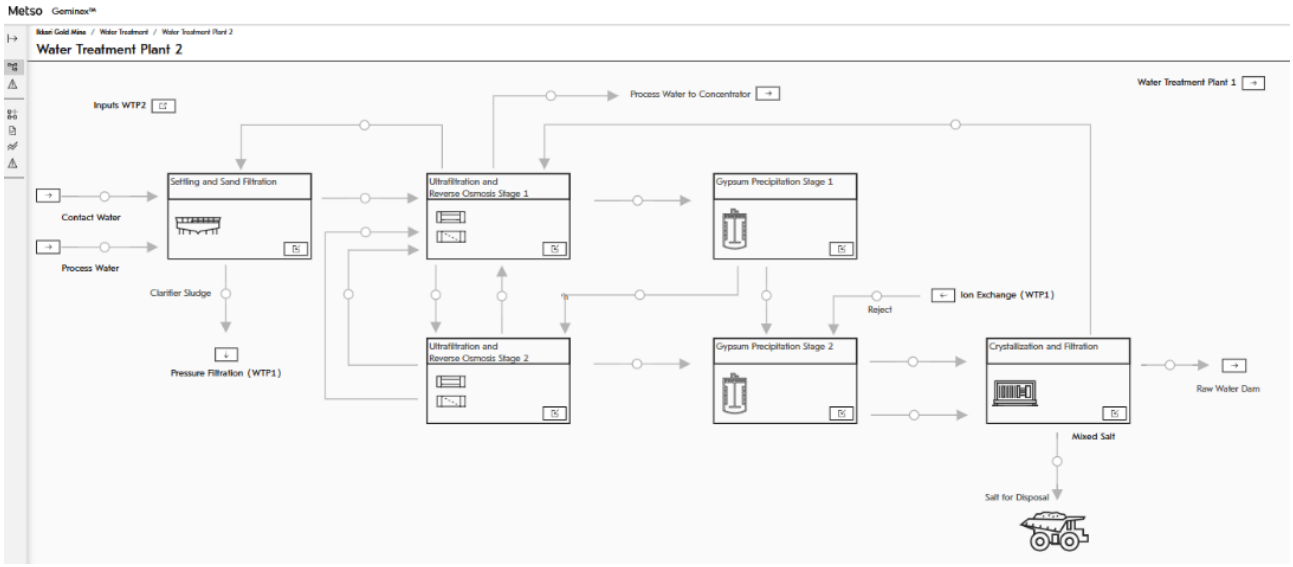



**FIG 6** – Overview of Water Treatment Plant 2 (WTP2).

The main inputs to the calculations of the WTP2 are the coagulant dosing to each of the flocculant-settlers, the number of sand filters and ultra filtration filters in operation as well as their capacities and filtration efficiency, the separation efficiencies of each dissolved species in the reverse osmosis units, the pH of the gypsum precipitation reactors and the solubilities of the precipitated salts, to name a few.

## Water storage

All water streams in this simulation model are connected, to get an accurate depiction of the water balance at all times. This includes the water gains due to precipitation in the different stockage ponds or losses due to evaporation, as well as discharges. An overview of the water storage and its connection to the process areas is depicted in Figure 7.

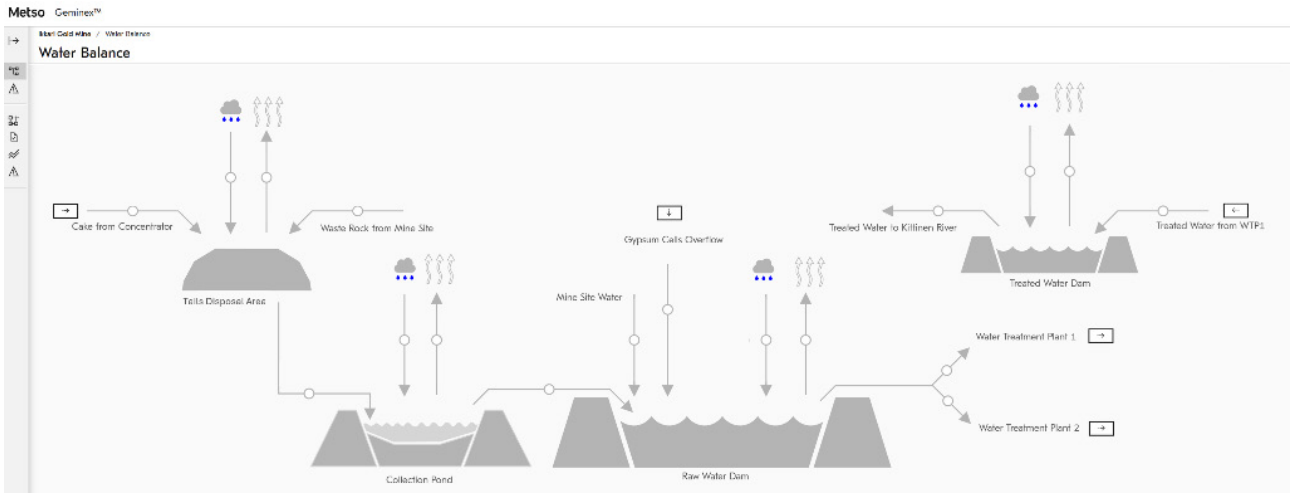



**FIG 7** – Water handling flow sheet.

The concentrator's tails filtered cake is stored in a dry stacking storing area. The rain accumulation over the tails storing area is recovered in a collection pond. Some of the collection pond water is transferred to the Raw Water Dam, together with mine site waters. From the Raw Water Dam flow, 84 per cent of it is directed to WTP1 and the remainder to the WTP2, to be reused in the concentrator plant. The water being treated from the WTP1 is stored in the Treated Water Dam before being released.

For the present study, the client provided study results showing the evolution of precipitation and evaporation over the areas of the ponds, per day over several decades, in addition to the estimation

of water flows from mine site. These data have been used to include gains and losses in the water balance. Additionally, the composition of the water in each pond is impacted by those gains and losses, the species in solution being either diluted or concentrated. It must be noted that no chemical reaction was simulated in ponds.

## RESULTS AND DISCUSSION

The model was implemented in Geminex™, Metso's digital twin platform, where the user can directly write the values for the several inputs and run a single simulation, or create simulation cards with systematic changes for scenario sensitivity analysis. The results of single simulations are displayed in the flow sheets, as in Figures 1–7. To illustrate the use of simulation cards, a couple of relevant scenarios were simulated. Firstly, the effect of ore blend composition to the crushing and grinding power consumption was analysed, and the results are depicted in Table 1.

**TABLE 1**

Ore Blend 1, 2 and 3 correspond to mixtures of Mafic and Felsic ores at the same feed rate and process conditions.

Mineral Processing KPI's

| Scenario △ | SAG Mill Recirculation, % | Ball Mill Recirculation, % | SAG Trommel Undersize, mm | P80 to CIL, µm | P80 to Gravity Concentrator, µm |
|---|---|---|---|---|---|
| Ore Blend 1 Mafic 0%, Felsic 100% | 18.67 | 211.92 | 0.40 | 96.88 | 403.42 |
| Ore Blend 2 - Mafic 100%, Felsic 0% | 18.42 | 158.70 | 0.40 | 86.06 | 397.96 |
| Ore Blend 3 - Mafic 30%, Felsic 70% | 18.60 | 194.40 | 0.40 | 93.78 | 401.63 |

The results presented in Table 1 provide insight into the operation modes of the plant and are valuable for production planning. In addition, the effect of cyanide feed to the CIL circuit was also studied. The cyanide addition was regulated by the concentration of free cyanide in the first CIL tank. The base case assumed a cyanide set point concentration in the first CIL tank of 500 ppm. Thus, three more concentration set points were evaluated, namely 250, 750 and 1000 ppm. The gold recovery profile in the CIL circuit for each of these cases are shown in Table 2.

**TABLE 2**

Gold recovery for different cyanide addition rates.

CIL Tanks Recovery, %

| Scenario | Tank 1 △ | Tank 2 | Tank 3 | Tank 4 | Tank 5 | Tank 6 | Tank 7 |
|---|---|---|---|---|---|---|---|
| CN Feed to CIL-1 250 mg/L | 43.02 | 67.34 | 71.18 | 81.47 | 91.14 | 93.03 | 94.32 |
| CN Feed to CIL 1 500 mg/l | 51.85 | 75.97 | 80.68 | 87.80 | 93.88 | 94.84 | 95.49 |
| CN Feed to CIL-1 750 mg/L | 56.83 | 80.25 | 84.65 | 90.06 | 94.70 | 95.28 | 95.71 |
| CN Feed to CIL-1 1000 mg/L | 60.42 | 82.88 | 86.83 | 91.17 | 95.06 | 95.44 | 95.79 |

Based on the results from Table 2, it is evident that a cyanide set point around 500 ppm may be sufficient for gold recovery. In addition, higher cyanide addition rates showed a detrimental effect on the effluent treatment, which was quantified by the model. Finally, for the sake of the present discussion, the influence of the total ROM feed was analysed. The base feed was assumed to be of 434 t/h and a change of +10 per cent and -10 per cent was simulated and compared. The impact of the ROM feed variation on the minerals processing KPIs are depicted in Table 3.

**TABLE 3**

Simulation results comparison.

Crushing&Grinding Power Consumption, kW — Table

| Scenario | Primary Crusher | Pebble Crusher | SAG Mill | Ball Mill |
|---|---|---|---|---|
| ROM 390.6 t/h | 33.91 | 103.11 | 3602.65 | 5309.80 |
| ROM 434.0 t/h | 33.91 | 139.39 | 4001.38 | 6057.03 |
| ROM 477.4 t/h | 33.91 | 204.30 | 4364.04 | 6796.85 |

The effects on the water treatment, water balance and hydrometallurgical process were also assessed, and the insights gathered were crucial for further optimisation of the process design. Due to confidentiality reasons, many of the insights obtained from the Geminex™ calculations cannot be described in detail. However, the digital twin was instrumental for quantifying feed quality versus weir rate in minerals processing, consumptions of reactants such as sodium cyanide, lime milk, hydrochloric acid, fresh activated carbon, among others. In addition, the CIL circuit operation was optimised together with the cyanide destruction circuit, enabling a confident decision-making and technology selection for both circuits. In the water treatment plants, the sand filtration and ultra filtration systems were all evaluated for various filter capacities and arrangements. The sensitivity of certain process units to the overall water treatment was assed and few critical bottlenecks identified. Most notably, the digital twin model was able to successfully simulate very large and wide-spanning stream recycles in the process and quantify their effects in the composition of the orebodies over a long span of operating time.

## CONCLUSION

The concentrator plant, water treatment plants and water balance of the Ikkari gold mine were modelled according to the PFDs, basic design documents, laboratory data and insights from process experts. The model built allowed for several user defined inputs, including equipment-specific performance (separation efficiency, capacity etc), reaction kinetics, solubility of compounds, flow rates, bypass ratios, etc. The use of the model and its relevant calculation inputs and outputs were used to evaluate both the overall performance of the plant, ie the ore blend ratio, the consumption of utilities, the state of the large water bodies etc, as well as process-specific key performance indicators, such as energy consumption, gold recovery per stage, particle size distribution, etc. The model was deployed to the Geminex™, Metso's digital twin platform, where the user can seamlessly navigate the different process areas, create scenarios for simulation and analyse the results and even download the results to a local computer. The present study provided valuable information for the evaluation of equipment technology, capacity and overall feasibility to the process. Several insights were obtained from such holistic approach, such that the assertiveness in decision-making process at such early-stage project has been strengthened by this tool.

## ACKNOWLEDGEMENTS

The authors would like to thank Rupert Exploration Finland, for approving discussion of the work completed in the Ikkari Mine. The authors also would like to thank Jari Moilanen and Christian Binder for their support in ideating and supporting this paper.

## REFERENCES

Ahmad, W, Takalo, V, Remes, A, Moilanen, J and Ruuska, J, 2025. Metallurgical digital twin to optimize operations throughout the life of mine, Luleå, Conference in Minerals Engineering.

Bengtsson, M and Evertsson, C M, 2008. Modelling of output and power consumption in vertical shaft impact crushers, *International Journal of Mineral Processing*, 88(1–2):18–23.

Danette Allen, B, 2021. Digital Twins and Living Models at NASA, NASA [online]. Available from: <https://ntrs.nasa.gov/citations/20210023699> [Accessed: 10 February 2026].

Ling, P, Papangelakis, V G, Argyropoulos, S A and Kondos, P D, 1996. An Improved Rate Equation for Cyanidation of a Gold Ore, *Canadian Metallurgical Quarterly*, 35(3):225–234.

Moilanen, J, Remes, A and Binder, C, 2023. Metallurgical Digital Twin for managing variability and optimizing resources, Brisbane, World Mining Congress, pp 26–29.

Moilanen, J, Remes, A and Grigoryan, A, 2023. On-line digital twin for processing plant optimization, Adelaide, MetPlant Conference.

Rupert Resources Ltd, 2025. Ikkari pre-feasibility study, NI43-101 Technical Report, [online]. Available from: <https://rupertresources.com/wp-content/uploads/2025/02/240214-_Ikkari-PFS_NI43101_Final.pdf> [Accessed: 9 September 2026].

# Grinding and flotation advanced process control integration at Goldex Mine

*G Gagnon[1], A Vargas[2], B Aktoprak[3], N Chawda[4] and D Gudgeon[5]*

1. Production Superintendent, Canadian Malartic Complex, Agnico Eagle Mines Limited, Malartic QC J0Y 1Z0, Canada. Email: gabriel2.gagnon@agnicoeagle.com
2. Project Metallurgist, Meliadine Mine, Agnico Eagle Mines Limited, Meliadine, NU X0C 0G0, Canada. Email: andres.vargas@agnicoeagle.com
3. Advanced Process Control Integrator Control, Woodgrove Technologies Inc, Toronto ON M3J 3C6, Canada. Email: batuhanaktoprak@woodgrovetech.com
4. Advanced Process Control Integrator, Woodgrove Technologies Inc, Toronto ON M3J 3C6, Canada. Email: neeleshchawda@woodgrovetech.com
5. Manager of Advanced Process Control, Woodgrove Technologies Inc, Toronto ON M3J 3C6, Canada. Email: danielgudgeon@woodgrovetech.com

## ABSTRACT

The Goldex Mine, operated by Agnico Eagle, processes ore through a conventional grinding and flotation flow sheet. While the plant layout is relatively straightforward, site conditions presented unique control challenges, particularly in managing semi autogenous grinding (SAG) mill stability and achieving consistent flotation performance under variable operating conditions. Ore hardness fluctuations and changes in feed characteristics frequently impacted circuit stability, creating challenges for operators attempting to maintain optimal throughput and recovery. To address these issues, Advanced Process Control systems were implemented on both the grinding and flotation circuits. The grinding Advanced Process Control focused on preventing SAG overloads by dynamically adjusting SAG feed rate and SAG feed density in response to changing ore characteristics and Mill Load. This reduced the frequency and severity of overload conditions, minimised operator intervention, and allowed for a more stable and consistent operation while maximising mill utilisation.

The flotation circuit presented a different challenge: the site lacked online grade measurement, limiting direct insight into grade or recovery. As a result, the flotation Advanced Process Control was developed around a strategy based on managing concentrate flow rates used as a proxy for mass pull. This approach enabled automated control of reagent dosing and cell pull rates throughout the circuit, stabilising froth behaviour and maintaining operating conditions aligned with recovery objectives. By continuously responding to process disturbances, the system helped reduce variability and improve overall circuit performance.

The results of the Advanced Process Control implementation were substantial. Flotation performance saw improvements in stability and recovery, while grinding became more robust and resilient to ore variability. In addition to metallurgical improvements, operators benefited from greater process consistency and reduced time spent responding to upset conditions. This paper highlights the control strategies deployed for both circuits, the challenges posed by limited instrumentation, and the operational improvements achieved through Advanced Process Control, demonstrating the value of advanced control technologies in maximising plant performance.

## INTRODUCTION

The Goldex Complex is located in north-western Quebec and northern Ontario. It achieved commercial production in August 2017 with Goldex underground ore and in February 2024 with Akasaba West open pit ore.

The Goldex Complex circuit is shown in Figure 1. The crushing circuit consists of one primary jaw crusher located underground and one secondary cone crusher. Crushing is followed by a conventional Semi Autogenous Grinding (SAG)/Ball Mill comminution circuit with classification by hydrocyclones. The hydrocyclone underflow returns to the Ball Mill. The Ball Mill product is treated in a gravity gold circuit that produces doré bars; the gravity tailings return to the Ball Mill and the hydrocyclone overflow reports to the flotation circuit.

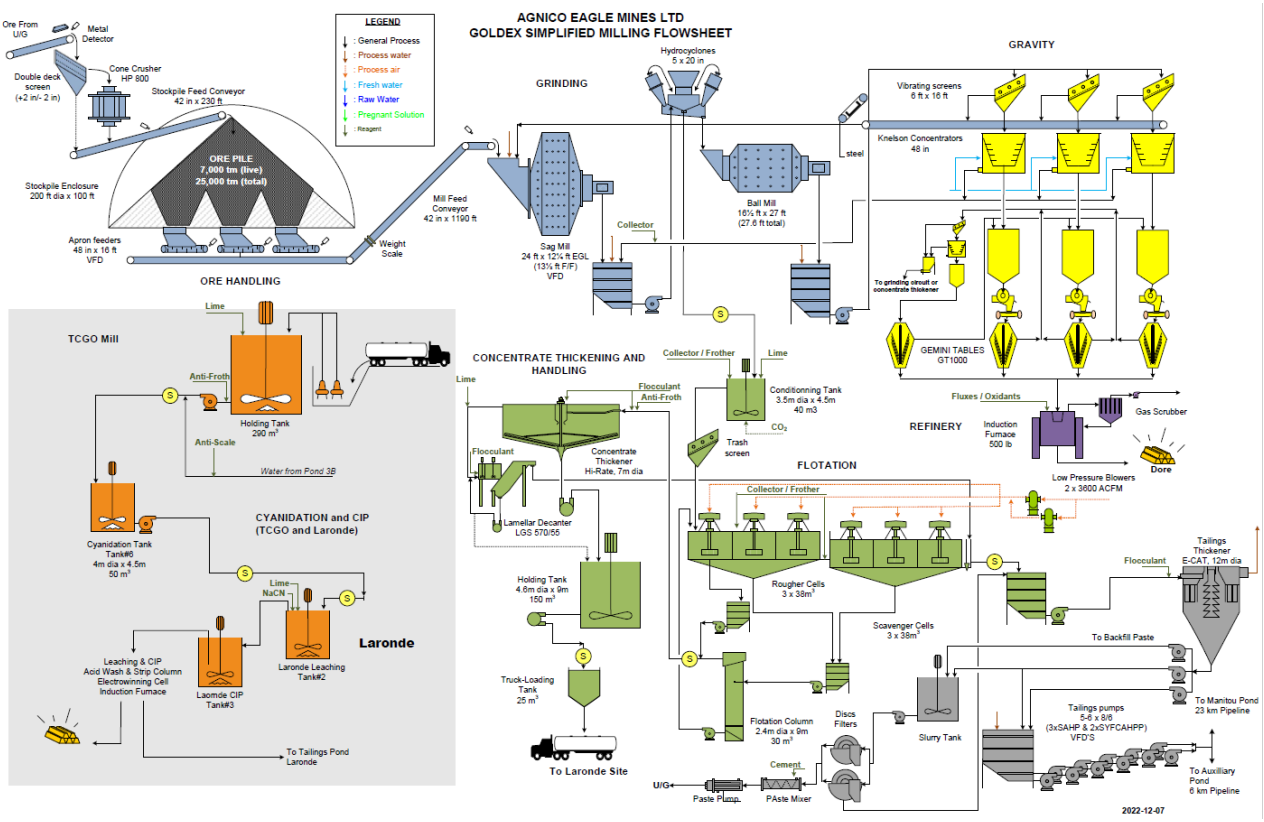



**FIG 1 –** Agnico Eagle, Goldex simplified flow diagram (advanced process control project scope highlighted in the red box).

The flotation circuit targets recovery of sulfide minerals and consists of six conventional mechanical cells and one cleaner column. The first three cells and the last three cells share level controllers. The first cell operates primarily as a rougher and produces approximately 65 per cent of the final concentrate, the first cell tailings are then processed in the remaining five conventional mechanical cells arranged as a scavenger bank to maximise recovery. The last cell discharges the final tailings to the Tailings Thickener, where the underflow is then pumped either to paste backfill or to the Manitou tailings facility. All scavengers concentrate reports to the cleaner column. The column concentrate combines with the rougher concentrate to produce the final concentrate sent to the LaRonde processing facility, while the column tailings can be returned to either the Rougher cell, or to the Scavenger circuit.

## KEY CHALLENGES FACED IN GRINDING CIRCUIT

The grinding circuit at Goldex operates under unconventional SAG mill conditions, with a feed size ($F_{80}$) typically ranging from 40–60 mm and a ball charge between 18 per cent and 20 per cent. In contrast, standard SAG mill operations generally process a coarser feed $F_{80}$ above 100–150 mm, with ball charge typically in the range of 8–12 per cent. While the SAG Mill operating conditions are aimed at increasing mill capacity, the adopted operating parameters placed the SAG mill in an intermediate regime of SAG and ball milling practices, introducing unique control complexities. This hybrid operating zone, combined with severe ore variability, posed persistent challenges to mill stability. Prior to the Woodgrove Advanced Process Control integration the SAG mill frequently encountered overload conditions, one to two times daily with cyclical behaviour that often persisted for extended periods during normal operations. Figure 2 illustrates a representative daily trend, highlighting the recurring nature and severity of these overload episodes.

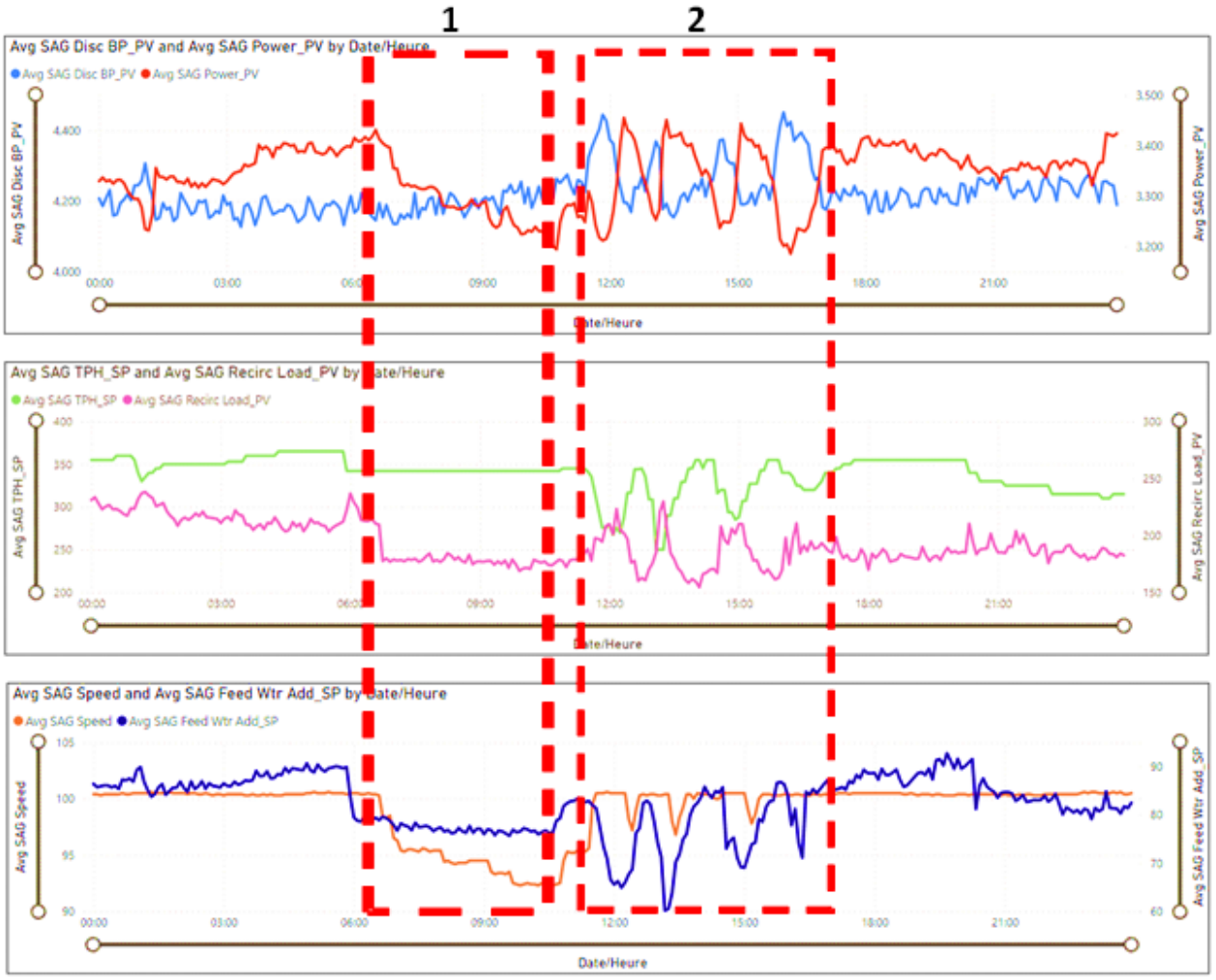



**FIG 2 –** SAG overload instances of November 1, 2022. Red – SAG power, Blue – SAG discharge bearing pressure, GREEN – SAG tons per hour_SP, PINK – SAG recirculation load, ORANGE – SAG speed, PURPLE – SAG feed density.

Prior to Woodgrove Advanced Process Control system integration, the site was equipped with a Model Predictive Control system in the grinding circuit, however this system was not found to be effective by site and remained unutilised by the Goldex team. Instead of utilising the Model Predictive Control system site relied on operator control while prioritised utilising system variables such as the SAG Mill Bearing Pressure and SAG On-Shell vibration measurement (SAG Intensity). While Model Predictive Control is a powerful optimisation method within the broader Advanced Process Control framework, its dependence on accurate process models and substantial computational resources can limit its effectiveness in highly dynamic operating environments. In the absence of explicit disturbance information, Model Predictive Control cannot predict or counteract unexpected process variations, resulting in reduced performance until corrective feedback is applied. Whereas a hybrid Advanced Process Control approach, by contrast, offers greater flexibility by incorporating a range of control strategies such as regulatory control and fuzzy logic that can adapt to limited measurements, ore variability, or complex process dynamics.

## KEY CHALLENGES FACED IN FLOTATION CIRCUIT

A key operational challenge in the Goldex flotation circuit is the absence of an online grade measurement system. This limitation compelled operators to rely solely on circuit mass flow data to balance the circuit and achieve optimal grade and recovery targets. Compounding this issue were upstream process variations, which introduced additional complexity in maintaining a stable grade-recovery equilibrium. In the absence of real-time diagnostic tools, operators frequently conducted manual inspections of flotation cells to visually assess froth characteristics and adjust mass pull accordingly. This reliance on manual intervention resulted in a labour-intensive control strategy,

characterised by continuous field monitoring, frequent sampling, and iterative testing to validate the effectiveness of corrective actions. The situation showed a critical need for either a comprehensive instrumentation layer or, at a minimum, a dual-point verification system capable of providing continuous, 24/7 performance insights to support timely and informed decision-making.

## JOURNEY TO EXCELLENCE

### Step 1 – Initiation

The control and optimisation initiative at the Goldex Complex was launched by conducting an external review of existing operational challenges, in alignment with site's current infrastructure. The goal was to identify improvement opportunities and quantify potential value gains while minimising capital expenditure. Following internal deliberations, the Goldex team sought a third-party partner with a demonstrated track record in transforming mineral processing operations through advanced control strategies, and with expertise in mineral processing and unit operation practices. Woodgrove Technologies was selected as the preferred partner to assess the circuit control challenges, evaluate potential solutions and associated benefits, and co-develop a strategic roadmap toward sustained operational excellence.

### Step 2 – Setting up the foundation

With support from Woodgrove Technologies, the Goldex team launched a targeted investigation aimed at identifying control and optimisation opportunities across the grinding and flotation circuits. A comprehensive feasibility analysis was conducted, leveraging a data-driven approach to assess current performance and infrastructure. A comprehensive data set capturing operational performance from November 2022 to February 2023, encompassing all available historised process signals was analysed. In parallel, daily metallurgical assay data for the same period was also reviewed to support performance evaluation. To ensure analytical rigour and minimise bias, the data set was systematically filtered to reduce noise and exclude transient operating conditions. Operational filters were applied to isolate steady-state periods, primarily by identifying intervals with sustained plant throughput above 250 t/hr indicative of 'normal' operation. This preprocessing step was critical to ensure that subsequent analyses and conclusions were based on representative and stable process behaviour.

For grinding, the investigation revealed that the SAG mill operates with sufficient margin in both bearing pressure and power consumption refer to Figure 3. The maximum allowable SAG power is 4000 kilowatts (kW), while the average power draw was recorded at 3278.8 kW, with MAX limit set by site at 3450 kW. Similarly, the SAG bearing pressure on the discharge end, the average was 4317 kPa, with MAX limit at 4590 kPa. Despite these margins, the SAG mill experienced classic overload conditions two to three times per day as highlighted in grinding challenges section. Also, the average throughput over the 4 months was 350 t/hr, this was 8.5 per cent less than site's targeted feed rate of 380 t/hr.

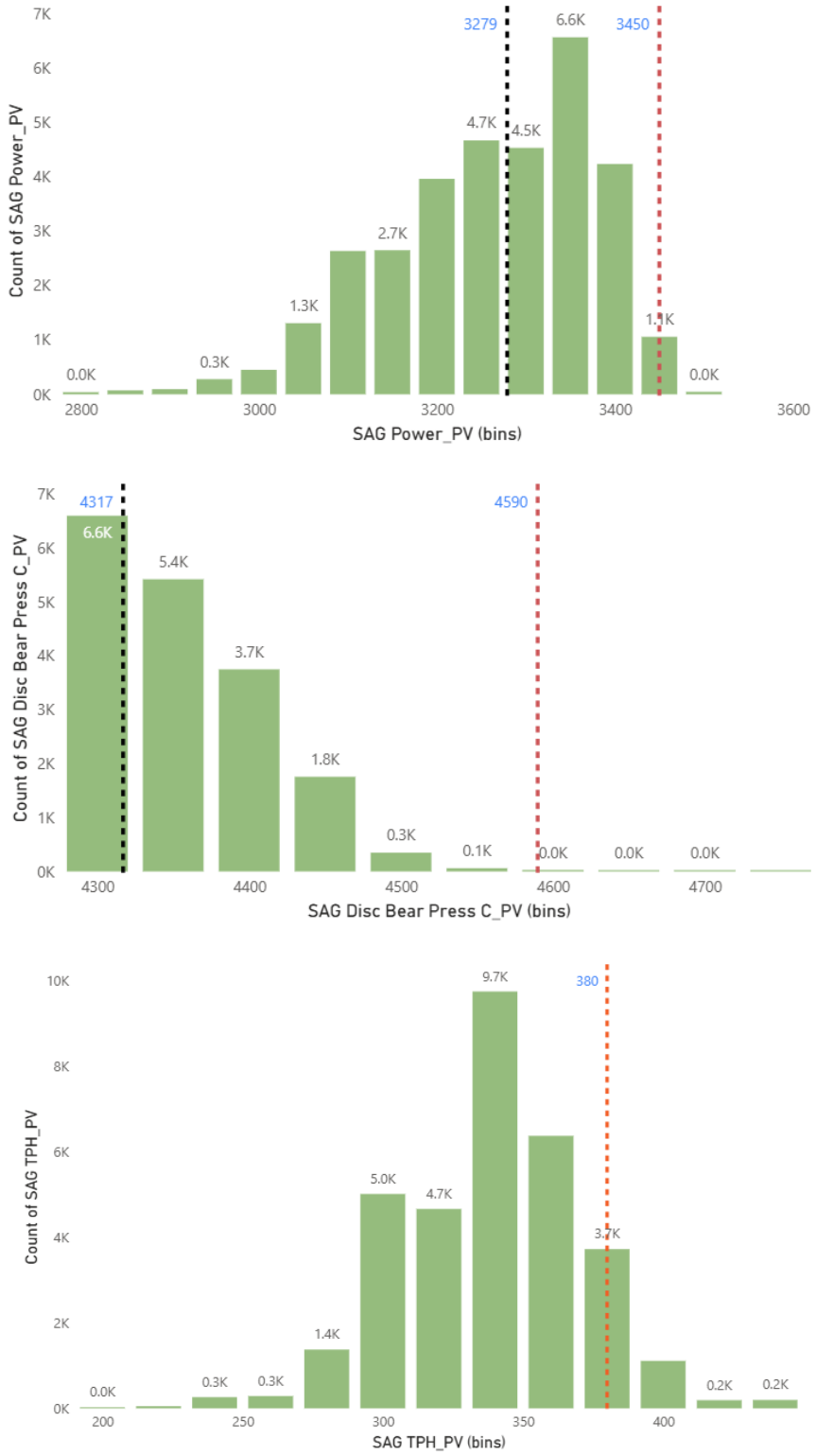



**FIG 3 –** SAG power (top), SAG bearing pressure (centre), SAG throughput (bottom) PV distribution.

During the Fit-for-Purpose review period, the Goldex operations was only treating Goldex Mine ore which only contained gold and no copper therefore the targeted investigation was focused on the performance of the flotation circuit and how it effects the gold grade and recovery. The investigation revealed that both the final tail gold and concentrate gold grades followed a strong relationship with the feed gold (comparable R2 value), which indicated that the flotation modus operandi could be revised and improved to achieve a higher grade as compared to an increase in tails with regards to the feed gold, refer to Figure 4. The flotation recovery was variable with change in feed characteristics, ranging from 71–80 per cent.

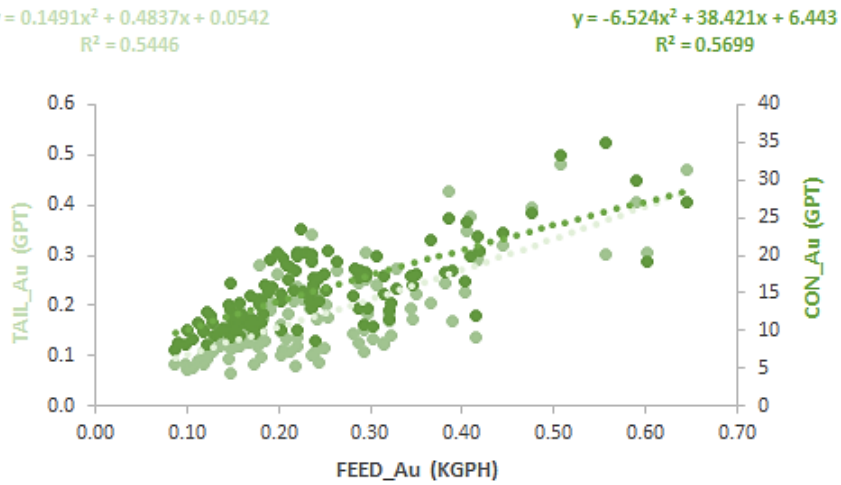



**FIG 4 –** Flotation feed gold (t/hr) versus tails and concentrate gold grade.

## Step 3 – Roadmap for success

The Woodgrove investigation revealed considerable potential for improvement by stabilising key process parameters, with projected gains in both plant throughput and metal recovery. These insights formed the foundation for a high-impact Advanced Process Control integration strategy. The proposed approach prioritised leveraging the site's existing instrumentation and stabilisation protocols, while introducing only minimal additional instrumentation to enhance operational efficiency and control robustness.

Goldex and Woodgrove jointly developed a tailored control strategy, integrating diverse technical perspectives from team members. These insights illuminated the complex nature of site operations and guided the formulation of a control philosophy that respected the unique characteristics of each circuit and adapted to the realities of the existing infrastructure. For instance, in the absence of an online grade measurement system in the flotation circuit, a combination of froth cameras and circuit mass flow data was employed to determine the optimal mass pull rate, thereby maintaining circuit balance and optimising grade-recovery performance.

The resulting strategy was reviewed collaboratively with all stakeholders at Goldex to ensure operator buy-in and alignment. This engagement formed the basis of the new control philosophy to be implemented. A multi variable control philosophy was proposed utilising SAG tonnage control, SAG speed regulation, SAG feed density control, and integrated pumpbox control for both the SAG and Ball Mill circuits using Woodgrove's Pumpbox Control® system. Woodgrove's Pumpbox Control® system is a regulatory control system designed to manages the pumpbox level, discharge density, and cyclone pressure utilising pump box water addition and pump speed controllers. Pumpbox Control® targets to deliver consistent discharge density and cyclone pressure to maintain optimum overflow cut size which is important for optimisation of the flotation circuit. These measures were designed to stabilise grinding parameters and improve throughput.

From 2024 onwards, the Agnico Eagle team began operating the Akasaba West deposit, located close to Val-d'Or (~30 km from Goldex), Agnico Eagle management decided to send the ore to the Goldex mill, as the flow sheet was compatible to recover copper, with minor modifications. The milling of Akasaba ore at Goldex also increased production flexibility to the Goldex Mine. Feeding the ore to an existing operation nearby allowed the operation of a new mine without the construction of a new mill, reducing the footprint of the mine site, and eliminating the need for a new tailings pond, reducing environmental impacts of the mining operation. However, this change required a paradigm shift and quick adaptation within the flotation operation such as changes in the existing equipment and operational philosophy. In the flotation circuit, froth cameras enabled continuous, real-time monitoring of froth characteristics, which were critical for controlling mass pull. To ensure safe and stable operation, the control strategy was built around maintaining mass flow and the circuit mass balance by regulating concentrate and tailings pumpbox levels and associated flow rates. These controls were reinforced with refined air and level regulation, designed to stabilise froth behaviour

and protect against overflows, pump strain, and circuit imbalance which is critical for optimising the grade-recovery relationship.

To facilitate effective change management and operator adoption, Goldex opted for a phased implementation approach. Phase 1 focused on Grinding Advanced Process Control integration and stabilisation, followed by Phase 2 targeting Flotation Advanced Process Control deployment. This sequencing allowed operators to gradually familiarise themselves with the new technology and ensured focused optimisation of each circuit. Implementing Grinding Advanced Process Control in the first phase also ensured a stable feed to flotation which later allowed for effective optimisation of the downstream flotation circuit. The Grinding Advanced Process Control was successfully commissioned between March 3 and May 10, 2024, followed by the Flotation Advanced Process Control between November 11 and December 11, 2024.

Goldex and Woodgrove maintained continuous, structured communication throughout the integration via regular scheduled meetings using digital platforms. This proactive engagement ensured timely escalation of concerns, alignment across teams, and rapid issue resolution. As a result, the project experienced zero delays during system tuning and commissioning, culminating in the successful deployment of a robust, safety-conscious Advanced Process Control solution. This alignment between Goldex and Woodgrove Technologies exemplified a successful synergy between operational insight and technological innovation, leveraging the combined expertise of both teams to drive mutual success and operational excellence.

## Step 4 – Integration, system tuning and training

The SAG mill optimisation strategy at Goldex was primarily based on controlling SAG intensity and power, both of which serve as proxies for mill load. By actively managing these parameters, the system was able to optimise mill loading while maximising throughput through coordinated control of SAG speed, feed density, and feed tonnage. The control logic was designed to operate within the mechanical design limits of the mill, targeting maximum throughput while maintaining grind quality monitored via mill load, reject recirculation, and cyclone feed density. Under normal and low-load conditions, the control strategy prioritised tonnage. During high or increasing load scenarios, SAG speed and feed density were employed as the first line of defence to mitigate overload risk and sustain production. Mill power was continuously monitored and regulated by adjusting SAG speed and feed density to optimise specific power consumption. Importantly, the control system was configured to detect potential overload conditions in advance, enabling timely corrective actions that reduced the frequency of mill grind-outs. The implemented Advanced Process Control logic successfully reduced variability in SAG Key Process Indicators, while delivering higher throughput at lower power consumption.

The flotation circuit optimisation at Goldex focused on controlling rougher and overall circuit mass pull through integrated use of Woodgrove Technologies' camera system, Characterization System®, and Advanced Process Control system, the Awareness Response Expert (AwaRE®). By leveraging froth velocity measurements for individual cell mass pull control, the Advanced Process Control system enabled dynamic prioritisation of cell operations boosting concentrate quality by adjusting front and back cells based on mass pull thresholds. This strategy, combined with targeted counteractions in rougher and scavenger cells, led to higher-grade recovery concentrated in early-stage cells. Enhanced circuit stability also improved feed consistency to the column cleaner stage, mitigating prior fluctuations in column level and recirculating load. Overall, the Advanced Process Control implementation significantly reduced variability in key flotation metrics, delivering improved recovery and concentrate grades beneficial to Goldex and similar operations.

To ensure the agreed-upon control strategy aligns with the measured variable targets, comprehensive data analysis was conducted. This analysis determined the optimal control range for all measured variables, ensuring effective control. The integration of this refined strategy and the results from the data analysis formed the foundation for achieving operational excellence with mechanical integrity and operational safety at Goldex.

The available instrumentation and sensor data within the circuit were integrated into closed-loop control using Woodgrove's Advance Regulatory Control®, which were embedded within the site's Programmable Logic Controller System. These controllers were configured to stabilise key unit

operations, specifically SAG mill load and flotation mass pull through dedicated control loops. At the supervisory level, Woodgrove's AwaRE® Advanced Process Control system was deployed as a global optimiser ensuring that each circuit continuously monitors its own performance while adapting to the operational state of others. AwaRE® incorporates a heuristic model built on a fuzzy-logic core and an inference engine with a multiple rule-based design to autonomously replicate the site's best operating response to each possible operational situation. The Advanced Process Control system was tuned collaboratively by Woodgrove Technologies' Advanced Process Control specialists and Goldex's experienced operators, ensuring that each layer of control logic was adapted to site-specific operating conditions. This joint effort enabled the system to maintain process stability, maximise throughput, and optimise the grade-recovery relationship across a wide range of operating scenarios. Integration was executed with a strong emphasis on safety and operational continuity. Each step was carefully coordinated with all stakeholders to prevent equipment trips, minimise process disturbances, and ensure system reliability. Valuable input from the Goldex operations team during on-site and remote support sessions led to the development of safety-focused control rules within the AwaRE® Advanced Process Control system specifically designed to protect mills and pumps from overloads, spillages, and failure risks.

Training and development of operators and administrators played a pivotal role in ensuring the long-term success and sustainability of the Advanced Process Control implementation at Goldex. The training program equipped the site operations team with a clear understanding of the AwaRE® system's functionality, enabling personnel to confidently operate, troubleshoot, and optimise the system. This empowerment fostered a culture of continuous improvement, where team members could identify enhancement opportunities and provide valuable feedback for iterative refinement. Following the full integration of the control system, the Goldex operations team demonstrated strong proficiency in utilising the AwaRE® Advanced Process Control platform, effectively translating conceptual benefits into measurable performance gains. This outcome highlights the importance of hands-on training and collaborative knowledge transfer in achieving operational excellence.

## RESULTS AND DISCUSSION – GRINDING ADVANCED PROCESS CONTROL

Improved stability was observed at the start of the tuning phase of the project. Disturbances that usually cause instability were quickly controlled by the AwaRE® Advanced Process Control system by adjusting the SAG speed, SAG feed density, and SAG feed tonnage controllers ensuring that overall productivity is optimised while the circuit load is maintained within limits. The section below outlines the performance improvements realised by the Agnico Eagle, Goldex team, in the months following the successful deployment of the Grinding AwaRE® system. The result of the advanced control system is evident in increased throughput and reduced SAG specific power along with reduction in the main SAG load indicating KPI–SAG intensity. In this document the AwaRE® performance (June 2024 and July 2024) is compared with manual operation (January 2024 and February 2024) to demonstrate the sustained benefits delivered by the grinding Advanced Process Control system on similar Akasaba ore feed. For analytical accuracy, as requested by site, after the Advanced Process Control integration was completed, only operational data exceeding 150 t/hr was considered. This threshold helps minimise noise and excludes periods affected by maintenance activities or operational disturbances, ensuring a more representative assessment of system performance.

Table 1 presents a summary of the On-Off comparison, illustrating a notable improvement in operational performance over compared period. The data reveals a 7.6 per cent increase in average throughput alongside a 9.6 per cent reduction in specific power consumption, signifying enhanced production efficiency and reduced operating costs. Furthermore, the quality KPI measured by the SAG intensity, the primary controlled variable, demonstrates higher operational intensity, indicative of improved grinding performance and a healthier SAG load state. Notably, the standard deviation of SAG intensity decreased by 30.2 per cent, reflecting greater system stability and consistency in process control.

**TABLE 1**

Impact of Advanced Process Control system on SAG productivity.

| **Production and cost key process indicators** | **Average before advanced process control** | **Average after advanced process control** | **Impact (%)** |
|---|---|---|---|
| Semi autogenous grinding tonnes [tons per hour] | 353 | 380 | 7.6 |
| Semi autogenous grinding specific energy [kilowatt-hour/ton] | 9.63 | 8.7 | -9.6 |
| **Quality key process indicators** | **Average before advanced process control** | **Average after advanced process control** | **Impact (%)** |
| Semi autogenous grinding intensity | 57 | 58.05 | 1.8 |
| Semi autogenous grinding intensity [STDV] | 4.31 | 3.01 | -30.2 |

Figure 5 illustrate the enhanced performance and stability introduced by the Advanced Process Control system in the grinding circuit. Blue bars represent the baseline performance under manual operation, while green bars depict the improved metrics achieved with Advanced Process Control implementation. The comparison clearly demonstrates that Advanced Process Control contributes to higher throughput, reduced specific power consumption, and more stable SAG intensity, highlighting its effectiveness in optimising both production efficiency and process control.

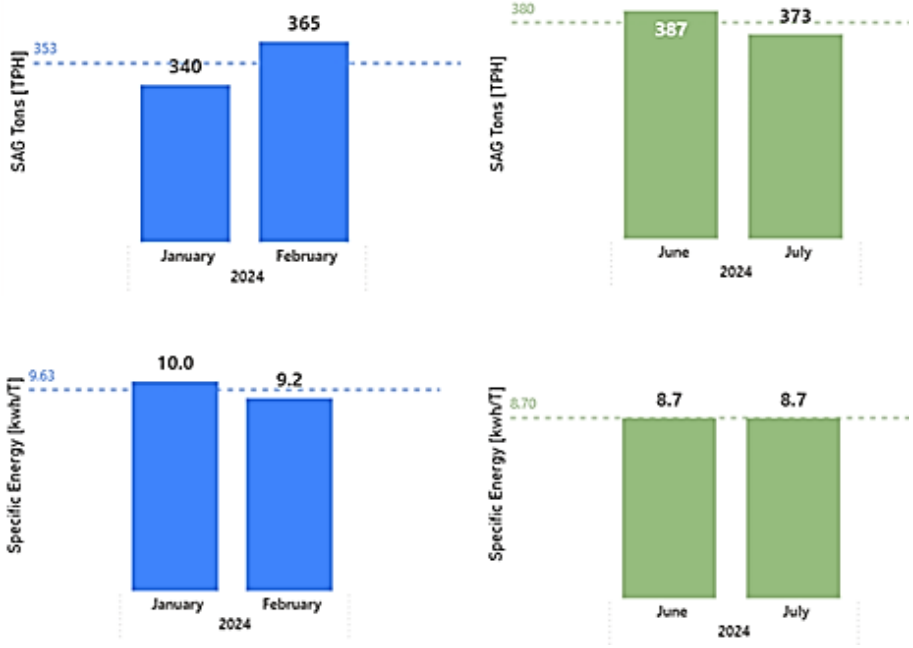



**FIG 5 –** SAG throughput (top chart) and specific power (bottom chart) performance AwaRE® OFF (blue bar graph) and ON (green bar graph).

Operational trends during the assessment phase (November 2022 to January 2023 data analysis) prior to the Woodgrove Advanced Process Control integration revealed that the SAG mill frequently experienced overloads, averaging one to two incidents per day. Figure 6 presents a trend of before and after the implementation of the Advanced Process Control system, showing a substantial reduction in overload events to fewer than ten per month. This marked decline highlights a substantial improvement in SAG mill stability and overall grinding performance.

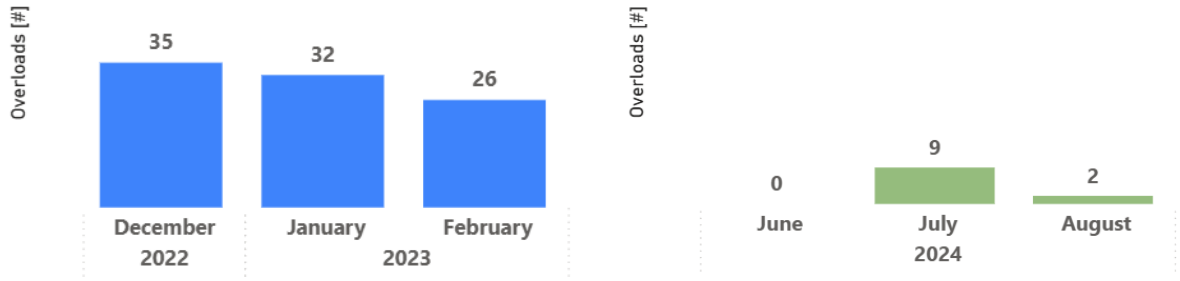



**FIG 6 –** SAG overload instances OFF (blue bar graph) and ON (green bar graph).

## RESULTS AND DISCUSSION – FLOTATION ADVANCED PROCESS CONTROL

By embedding best operational practices into the Advanced Process Control framework, the overall flotation performance showed marked improvements in terms of both productivity and product quality. The following section presents the performance gains achieved by the Agnico Eagle, Goldex team, in the months following the successful deployment of the Flotation AwaRE® system. A comparative analysis between manual operation (August to October 2024) and Advanced Process Control driven operation (January to March 2025) highlights the sustained benefits of the Advanced Process Control, particularly in terms of increased recovery and concentrate grade.

Table 2 summarises the On-Off comparison, highlighting a significant enhancement in flotation recovery following the implementation of the AwaRE® system. The data indicates a 3.8 per cent increase in average copper recovery, achieved without compromising concentrate quality. In fact, the average concentrate grade improved from 3.0 per cent to 4.1 per cent, highlighting the effectiveness of the advanced control strategy.

**TABLE 2**

Impact of Advanced Process Control system on flotation productivity

| Flotation key process indicators | Average before advanced process control | Average after advanced process control | Impact (%) |
|---|---|---|---|
| Copper feed grade [%] | 0.1 | 0.13 | 30 |
| Copper recovery [%] | 84.7 | 87.9 | 3.8 |
| Copper conc. Grade [%] | 3 | 4.1 | 36.7 |

Figure 7 illustrates the enhanced performance and operational stability resulting from the implementation of the Advanced Process Control system. In these charts, blue bars represent baseline metrics under manual operation, while green bars reflect the improvements achieved with Advanced Process Control in place. The comparison clearly demonstrates that Advanced Process Control has contributed to higher copper recovery and improved concentrate grade, despite feed grade variability.

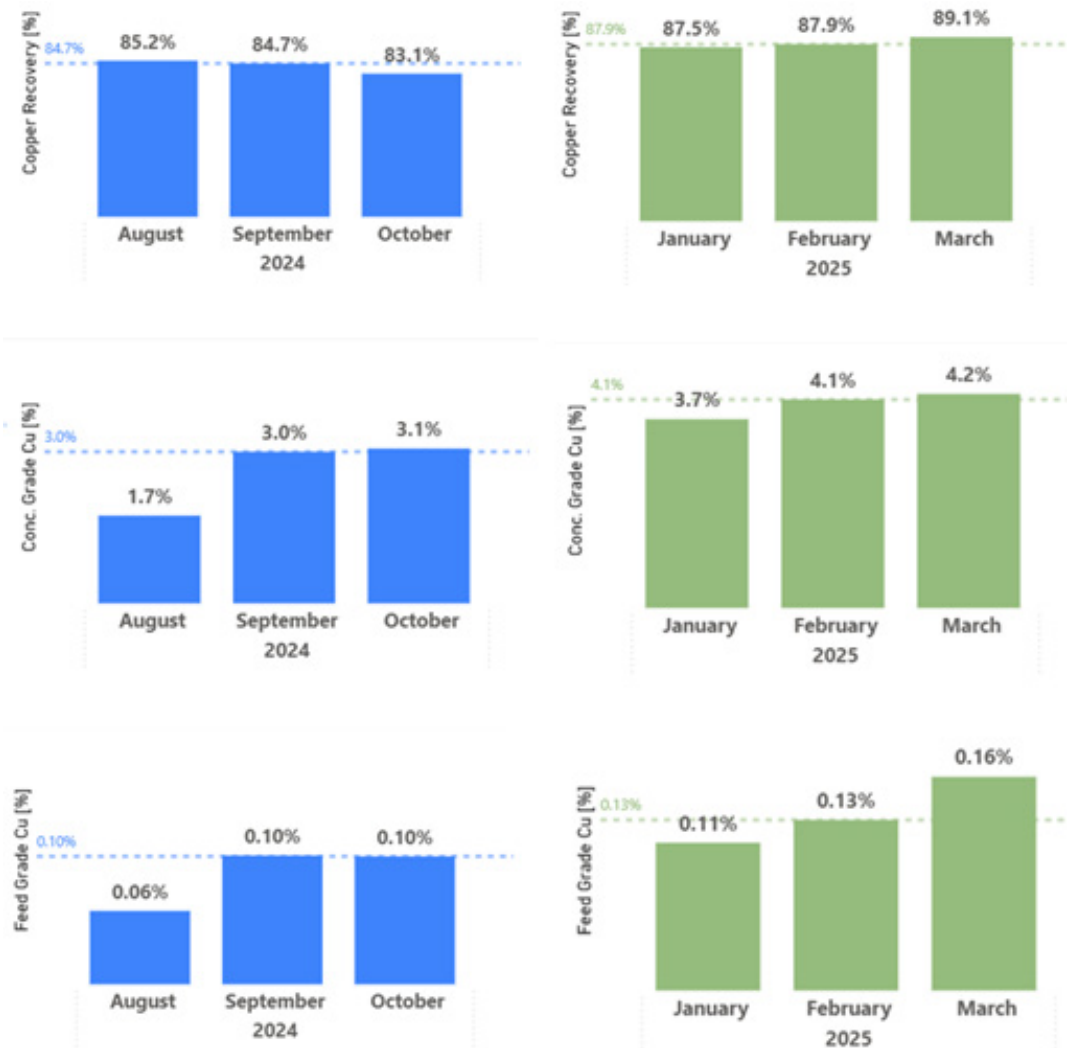



**FIG 7 –** Flotation recovery (top), flotation concentrate grade (centre), flotation feed grade (bottom) performance AwaRE® OFF (blue bar graph) and ON (green bar graph).

The overall improvement in recovery was achieved by maintaining mass pull values within a defined operational range while reducing their standard deviation. This stabilisation was accomplished through targeted adjustments by the Advanced Process Control system, including fine-tuning air flow responses and manipulating cell levels. These interventions ensured that the velocity outputs (monitored via Froth Cameras installed over each flotation cell) remained within optimal thresholds.

## CONCLUSION

The optimisation initiative at Goldex Mine began with a structured site engagement and a thorough review of operational data to identify key challenges and improvement opportunities across the Grinding and Flotation circuits. In partnership with Woodgrove Technologies, the Goldex team implemented targeted enhancements aimed at improving circuit productivity, stabilising operations, and strengthening control while maintaining a strong focus on safety and risk mitigation.

A robust control strategy was developed, integrating Advanced Process Control systems and froth cameras to enable real-time monitoring and adaptive control. These tools significantly reduced process variability, increased grinding throughput, and improved flotation recovery. Safety was embedded throughout the project life cycle from design to commissioning with protective logic layers configured to prevent equipment trips, overflows, and other operational risks.

Safety and operator training were integral to the success of the integration. Ensuring that the operations team felt confident and trusted the new system was essential for realising the full benefits of the Advanced Process Control deployment. Throughout the design and implementation phases, system safety remained a top priority.

Operator training and change management were central to the project's success. By building confidence in the system and ensuring clear communication across teams, site was well-prepared to sustain the benefits of automation. The AwaRE® Advanced Process Control system ultimately exceeded its performance targets, delivering a 7.6 per cent increase in throughput (~27 t/hr) averaging at 380 t/hr aligned to site's operating target of 380 t/hr and a 3.2 per cent gain in recovery, while reducing specific power consumption and variability across key parameters.

This outcome reflects the strength of cross-functional collaboration, disciplined project execution, and a shared commitment to operational excellence. The Goldex-Woodgrove partnership has not only addressed long-standing control challenges but also established a scalable foundation for future innovation in safe, efficient mineral processing.

# Review of an AI-driven advanced process control system for closed-loop flotation optimisation at MMG Dugald River Mine – 18 months post-commissioning

*W Smith[1], A Malcolm[2], J Yelland[3], C Martin[4] and T Soliman[5]*

1. Global Practice Lead Digital Twins, AIPC, Hatch, Brisbane Qld 4064. Email: warwick.smith@hatch.com
2. Senior Metallurgist, MMG, Dugald River Qld 4824. Email: alec.malcolm@mmg.com
3. AIPC Engineer, Hatch, Brisbane Qld 4064. Email: james.yelland@hatch.com
4. Superintendent Metallurgy, MMG, Dugald River Qld 4824. Email: catherine.martin@mmg.com
5. AIPC Engineer, Hatch, Brisbane Qld 4064. Email: tariq.soliman@hatch.com

## ABSTRACT

As of July 2026, MMG Dugald River Mine (DRM) will have operated its closed-loop digital twin for flotation optimisation for 18 months in production. This paper reviews the outcomes of one of the first operational deployments of a fully autonomous, AI-assisted process control (AIPC) systems for flotation in the Australian minerals processing sector. The authors outline both the measured metallurgical benefits and the key technical learnings associated with operating deep neural network-based technology for optimising Net Smelter Return (NSR) in a live production environment. To quantify the system's value, DRM conducted a structured, randomised on/off trial over a representative operating window, enabling a direct comparison of twin-driven and operator-driven control outcomes. The trial concluded a positive impact of +0.53 per cent Zn recovery improvement ($p$ < 0.001) by the twin, on a high baseline rougher-scavenger recovery performance exceeding 97 per cent. The trial also concluded no statistical difference in rougher-scavenger concentrate or feed grades, while the twin did achieve a significant reduction in reagent consumption through an improved multivariate control action. Time utilised in full autonomous control over the first 12 months of twin operation was approximately 75 per cent. Several post-commissioning enhancements supported these outcomes which the authors have detailed in the paper. These can be summarised as: improvements to flexible adjustment of twin set point optimisation bounds directly from supervisory control and data acquisition (SCADA), improved generalisation of the twin's internal rougher and scavenger control models; major enhancements to system infrastructure allow automated retraining of rougher and scavenger models for efficient maintenance and redeployments; and improvements in the usage of model errors in real-time to aid in short-interval self-correction of the NSR objective function calculations. Overall, the advancements achieved by the DRM team have demonstrated a new novel form of advanced process automation which contrasts significantly with traditional fuzzy logic and linear matrix model predictive control systems. Most notably, the self-learning and continuous learning aspects of the underlying AIPC systems utilised in the rougher scavenger deployment will allow greater benefits to plant metallurgists to directly model, maintain and deploy neural network-based control systems more flexibly from the plant as part of their day-to-day role. The results and findings outlined in this paper will inform both the incremental scale of the DRM rougher scavenger system to the downstream cleaner block, as well as the future application of AIPC technologies across other MMG flow sheets.

## INTRODUCTION

### Evolution of control of the DRM zinc flotation circuit

The Dugald River concentrator commenced operations in September 2017, achieving its first zinc concentrate shipment by December 2017. The flow sheet shown in Figure 1 comprises carbon pre-flotation to remove hydrophobic carbonaceous material, followed by sequential Pb–Zn flotation. Each Pb and Zn flotation circuit includes a roughing/scavenging stage with intermediate regrinding ahead of three-stage cleaning. During 2018, site priorities centred on pushing mill throughput above design to offset below plan zinc feed grades, constraining focused flotation optimisation. Annualised accounting identified zinc losses of 6.3 per cent to pre-flotation concentrate and 9.2 per cent to the

Zn circuit (scavenger tails and cleaner tails) relative to plant feed, establishing baseline targets for improvement (Smith *et al*, 2024).

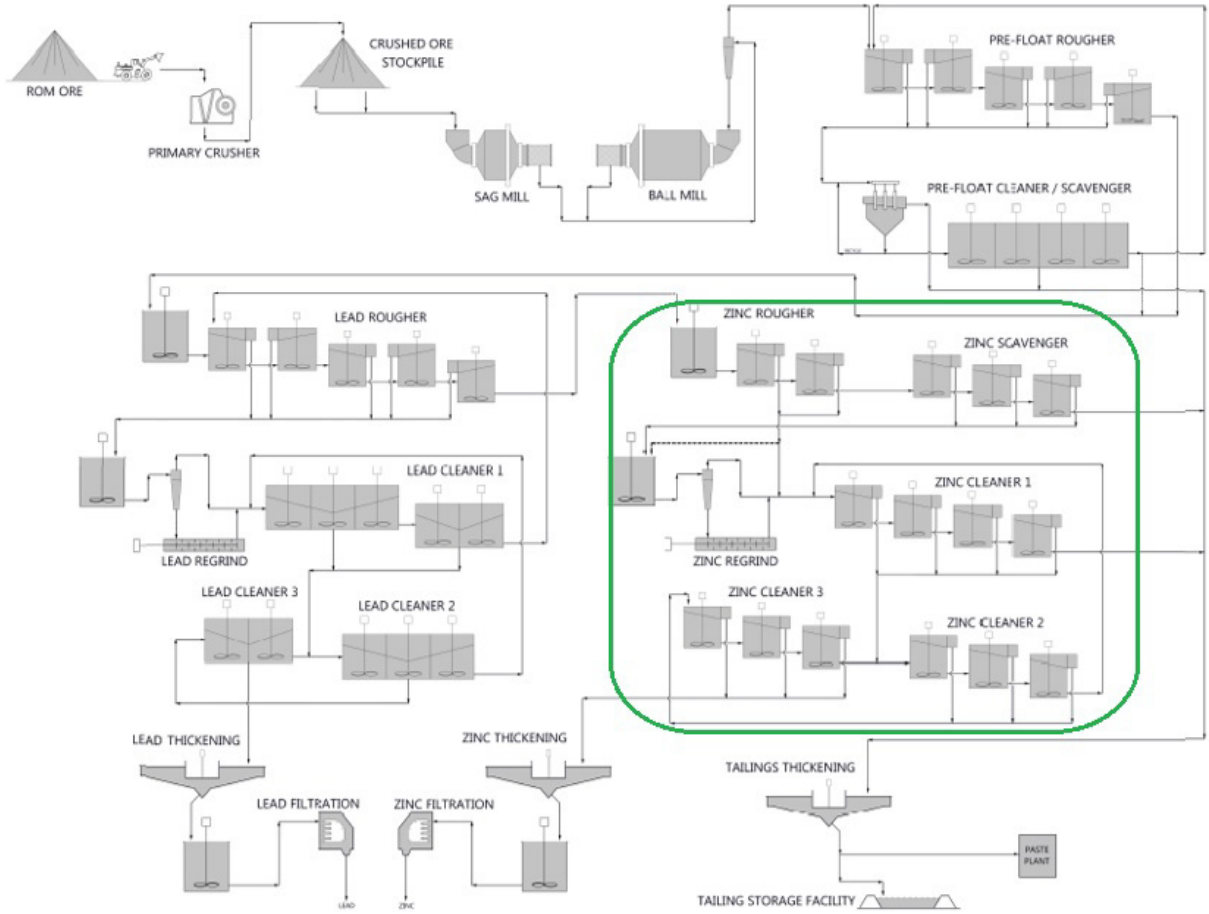



**FIG 1** – The Dugald River Concentrator flow sheet, with the zinc circuit outlined.

From 2019–2020, MMG Dugald River Mine (DRM) began an improvement program across operating practice and control which initiated continuous incremental annual uplift in Zn recovery performance. Operator guidelines were formalised for reagent addition, air distribution, and recirculating-load management and staged collector addition points were installed to enable more targeted collector usage. Significant regulatory automation was implemented, including cascade loops for all flotation variables (eg collector scaled to feed rate/grade and ratio-based set points to proportion reagents and air down-the-bank). Regrinding of Zn scavenger concentrate was also introduced to enhance liberation prior to cleaning. By 2021, Zn losses to pre-flotation were reduced from 6.3 per cent to 3.5 per cent, though Zn circuit combined losses persisted around 7.1 per cent with respect to plant feed.

Between 2022 and 2024, DRM realised additional gains via a more effective pre-flotation depressant materially decreased Zn losses to pre-flotation concentrate. For the Pb and Zn roughers, simple metallurgical target models were introduced and migrated into the control system to enable dynamic tail-grade-based collector control. Air rate, froth depth, activator, and pH remained in automatic with down-the-bank set point proportioning (notably for air), shifting operators from active manipulation to supervisory oversight of head targets.

By late 2023, a simple but solid foundation had been established for Zn rougher-scavenger control. Residual recovery variability linked to changing feed and upstream conditions remained, motivating the subsequent exploration of adaptive, model-based set point decision automation. Table 1 provides a summary of Zn circuit losses over time, leading up to the commissioning of the Zn rougher-scavenger process twin. Zn Cleaner tail loss variation from 2024 to 2025 is attributed to scavenger concentrate regrind trials and evaluation.

**TABLE 1**

Progression of Zn losses over time, with respect to Zn in plant feed, 2018–2025.

| | Recovery loss wrt plant feed (%) | | | |
|---|---|---|---|---|
| **Stream** | **2018** | **2021** | **2024** | **2025** |
| Pre-flotation concentrate | 6.3 | 3.5 | 1.8 | 2.0 |
| Zn scavenger tail | 5.9 | 4.3 | 2.9 | 2.8 |
| Zn cleaner tail | 3.3 | 2.8 | 3.0 | 3.3 |
| Total | 15.5 | 10.6 | 7.7 | 8.1 |

Prior to commissioning of the Zn rougher-scavenger twin, the univariate cascade controller list for the rougher-scavenger can be summarised as:

- Collector cascade control in specific dosage basis of g/t Zn metal units in rougher feed, where the g/t set point was allowed to ramp up and down proportionally to the error between an empirical tail grade target and the actual measured tail grade from on-stream analysis.
- Activator cascade control is specific dosage basis of g/t Zn metal units in rougher feed.
- Air rate cascade control via split/ratio control where the operator manages the head set points for the rougher and scavenger only.
- Typical lime cascade control where the lime addition is manipulated in order to hit a pH set point at the rougher conditioning tank.
- Standard automatic froth depth control.

Since the existing controllers (16 proportional-integral-differential (PID) loops in total) were generally independent from each other or otherwise represented a univariate control approach where the control room operator ultimately determined the individual set point for each cascade or automatic loop, it was hypothesized that a multivariate set point optimisation, for various feed and upstream conditions, would ultimately provide a better grade-recovery position.

## Design and commissioning phase summary at DRM

The DRM flotation twin design phase considerations, selection of the Zn rougher-scavenger as the starting point, and early feasibility level results have been well documented in previous works and will not be further summarised here (Smith *et al*, 2024).

The DRM flotation twin implementation phase has also been documented previously (Smith *et al*, 2026). The work centred on the configuration and commissioning of the closed-loop process digital twin for zinc rougher-scavenger circuit, directly integrated with the control layer to autonomously optimise the 16 flotation set points under a short-interval Net Smelter Return (NSR) objective. The implemented technology, evolved beyond fuzzy-logic and linear model predictive control (MPC) systems: a multivariate, mass-balance-plus-neural-network system that dynamically adjusts internal control relationships (eg recovery versus collector dosage) to upstream feed and grinding conditions, and is capable of routine continuous learning of control relationships without the need for manual re-tuning or re-stepping.

The implementation utilised a layered model stack as summarised in Figure 2. The model set includes linked rougher and scavenger process models predicting tail and concentrate grades, an outer recovery model and an economic model for NSR evaluation, all driven primarily by multi-stream analyser (MSA) assays validated against laboratory and shift data. Deep neural networks for capturing metallurgical relationships between process inputs and outputs were retained from the design phase, with a controlled, experiment-driven training workflow.

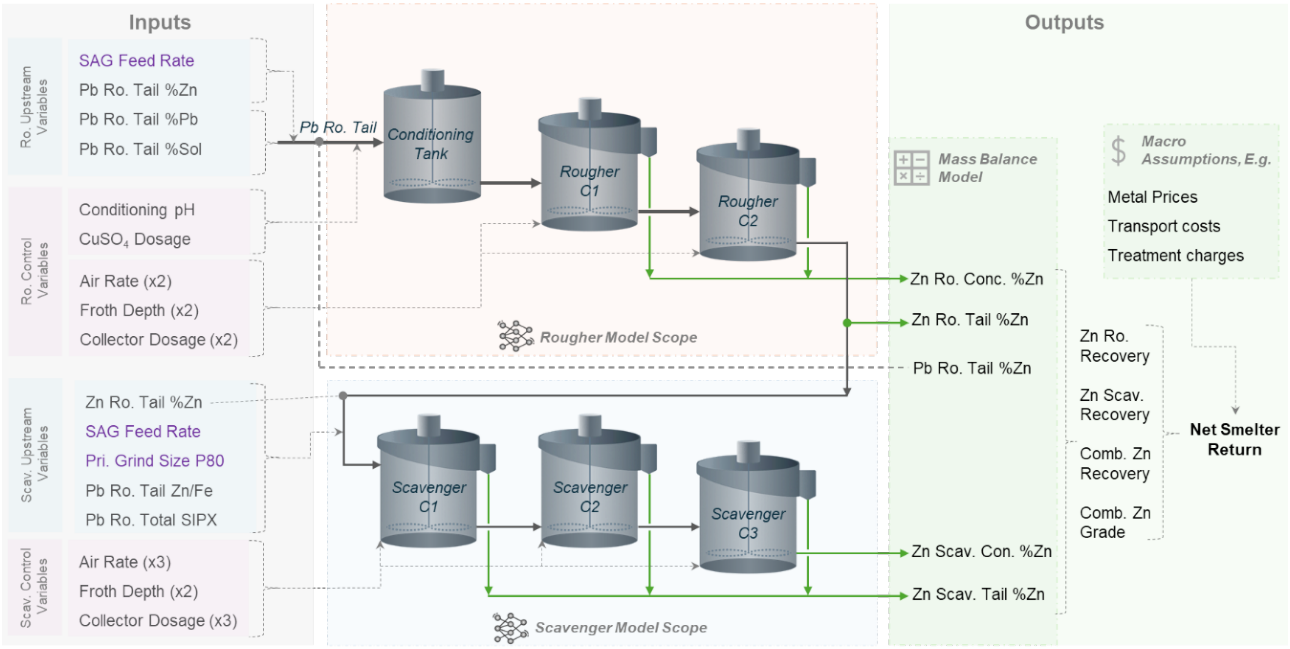



**FIG 2** – Zn rougher-scavenger conceptual model structure as at commissioning (Smith *et al*, 2026).

The set point optimisation relied on an advanced heuristic optimiser to search the non-linear neural network response surface. The production system was required to operate within a fixed 5-minute decision cycle, evaluating up to 9 million set point combinations against the NSR objective function per run. The design explicitly prioritised determinism (replicable solutions) over marginal optimality, employing multiple short repeats to confirm the final solution and a minimum-benefit threshold to prevent unnecessary set point churn and actuator wear.

Testing and commissioning progressed through layered gates (in-development, integration preparation, factory acceptance, installation, soak, site acceptance testing (SAT)), culminating in four days of continuous closed-loop commissioning activities across day and night shifts. All SAT metrics were achieved; in particular, average normalised set point movements were just 0.5–1.5 per cent of allowable ranges, evidencing frequent minor, non-disruptive adjustments. Constraint-tuning throughout commissioning showed that relaxing control variable solver limits toward data boundaries introduced a grade-recovery bias, reinforcing the need for cautious constraint management around areas of the solution space well understood by the neural networks.

Post-commissioning observations indicated that the system clearly integrated well with existing operator workflows and practices, and anecdotally reduced operator cognitive load for a crucial part of the overall flow sheet. The achievement of a closed-loop implementation from the outset however also meant that the measurement of the grade-recovery impact via a formal randomised statistical block trial (on/off trial) was relatively trivial to plan and execute.

## Post-commissioning objectives

Following the implementation and commissioning phase, the primary objectives of the post-commissioning phase were to:

- Establish the continuous learning systems, and retraining procedures and systems to enable ongoing maintenance, improvement and sustainability of the implemented process models.
- Complete further model hardening, generalisation and error management improvements to the underlying neural networks.
- Implement further operator ease-of-use aspects around constraint management, optimiser variable inclusion and other items to provide operational flexibilities to different plant and ore conditions.
- Execute the randomised block trial and quantify the final metallurgical benefit.

Like previous phases, the operational performance of the Zn rougher-scavenger implementation remained the primary focus of this phase. Other future facing objectives including the implementation of a detailed user interface (beyond the operators control system interfaces) and implementation into broader plant areas were not included in the post-commissioning efforts.

## Literature references to closed-loop AI-based control in flotation

The authors have previously summarised digital twin and AI related works in metallurgical processing (Geldenhuys *et al*, 2023; Ohenoja *et al,* 2023; Shnayder and Kalinina, 2023). Most literature to date describes offline studies regarding non-implemented systems.

Additionally, Nasiri, Iqbal and Särkkä (2025) introduce a physics-informed neural network (PINN) approach for predicting concentrate grade in froth flotation that directly addresses known shortcomings of purely data-driven neural networks. Rather than relying solely on historical plant data, the authors include flotation relationships into the learning process as soft constraints on the network outputs. These physical terms describe mass-balance and kinetic behaviour, guiding the network toward physically plausible solutions even when training data are limited or noisy, providing a form of structured regularisation. Comparative results on simulated flotation cells show that the physics-informed models achieve lower prediction error and significantly better generalisation than conventional neural networks trained on the same data sets, however this has not yet been demonstrated in production (Nasiri, Iqbal and Särkkä, 2025).

Nobahar, Xu and Dowd (2026) develop a cost-integrated, AI-based mine-to-mill optimisation framework that addresses a complementary aspect of the overall processing optimisation problem using some similar concepts. Their work focuses on modelling upstream cumulative operating cost across blasting design, screening, conveying, and semi-autogenous grinding (SAG) mill operation jointly influence across the value chain. The study emphasises predicting stage-wise operating costs and throughput as functions of design and operating variables. The methodology shares structural similarities with our approach: large-scale data (in this case from physics-based simulations rather than actual plant behaviour) are used for training a collection of sub-models (here quadratic regressions rather than neural networks), and optimisation is subsequently used to pursue a process objective over multiple sub-models. (Nobahar, Xu and Dowd, 2026).

Despite the ongoing research in digital twins that utilise AI for optimisation in mining processes, there remains little literature on the production implementation of such systems. As such, the contribution of this paper is not only the introduction of a new control technology, but rather a detailed operational evaluation of AI-driven closed-loop flotation control in sustained production.

# POST-COMMISSIONING ENHANCEMENTS

The following sections summarise a subset of post-commissioning enhancements to the rougher-scavenger flotation process twin which were ultimately important in the achievement of the final metallurgical results of the system.

## Metallurgist-managed optimisation constraints

At the time of commissioning, the control variable bounds to the twin's set point optimiser, referred to the 'engineering limits' of the system were non-exposed values existing behind the twin's configuration systems. Given the value of constraint adjustment to various operational scenarios observed both during commissioning and the weeks immediately post-commissioning, the twin's optimiser was upgraded to include an additional set of inner bounds directly configurable from the operator's supervisory control and data acquisition (SCADA) interface. Typical examples of contextual setting of optimiser constraints included shaping sodium isopropyl xanthate (SIPX) distribution and split percentages between rougher and scavenger under different upstream Pb rougher or even feed ore conditions and adjustment of air rate operating envelopes based on individual cell observations and downstream performance.

The rougher-scavenger twin was reconfigured to allow dynamic reading of the operator's constraint settings within SCADA, with additional logic checking to confirm that new constraints are not able to

be set outside the original engineering limits of the system which are governed by the machine learning domain to prevent extrapolation.

Further enhancement to the optimiser came with the recognition that at certain points in time, individual control variables may not be desired for full autonomous optimisation. For example, if a pH probe is removed from duty due to cleaning or recalibration, it may not make sense to continue to optimise leveraging pH control if that PID loop has been deactivated from cascade control. In such situations, the twin's solver can and should automatically detect the operator's selection of which control variables are available for further optimisation and customise their inclusion as manipulated variables in the solver, producing a more operationally sensible control recipe.

Finally, with respect to control variable participation in optimisation, it is also important to recognise that even though the twin may generate an optimised set point, there is no guarantee that each individual PID loop will be able to reach that value due to the potential for controller saturation at minimum or maximum output. Common examples of this include flotation air rate restrictions requiring cell reaming, or reagent flow control values reaching minimum or maximum opening positions. The Zn rougher-scavenger twin automatically detects and flag controller saturation prior to onset for operator awareness and action but does not at the time of writing autonomously adjust the relevant bound to match the current plant condition. This enhancement will occur in future releases.

## Control model improvement and generalisation over time

Prior to commissioning, the twin's rougher and scavenger models were required to be trained on process values (PV) derived from relatively discrete set point decision-making. Although natural variance in PID loop control allows for some PV variability around the set point, the discrete nature of operator selected set points can result in sparse training and testing data sets. Therefore, during the pre-commissioning model training, the models were forced to interpolate between these discrete set points with little information 'in between'.

Following commissioning however, data continued to be collected from the Zn rougher-scavenger. Since it was allowed to suggest set points in a continuous range, these gaps began to fill over time during transitions between optimal set points, helping the models to better observe previously spares set point combinations and generalise better to these conditions. The operationalisation of set points from a digital twin has been covered previously (Smith *et al*, 2026). Figure 3 demonstrates the impact of ongoing data filling for the air rate to Zn rougher cell 1. The filling process enables a clearer control curve to be established around the preferred optimal region. It is worth observing that the optimiser has approximately halved the operating envelope of the control variable, which has both advantages and disadvantages. On the positive, the optimiser is of course preventing the usage of non-optimal air rates (in this case, excessively high air rates which negatively impact both grade and recovery after a critical air rate). On the alternative view, it is important to regularly assess control bounds, and particularly time spent operating at the optimisation constraints, which may be a clear indicator for the need for additional training observations outside the constraint. Future systems will likely allow more automated collection of this data, according to calibration procedures governed by site metallurgists.

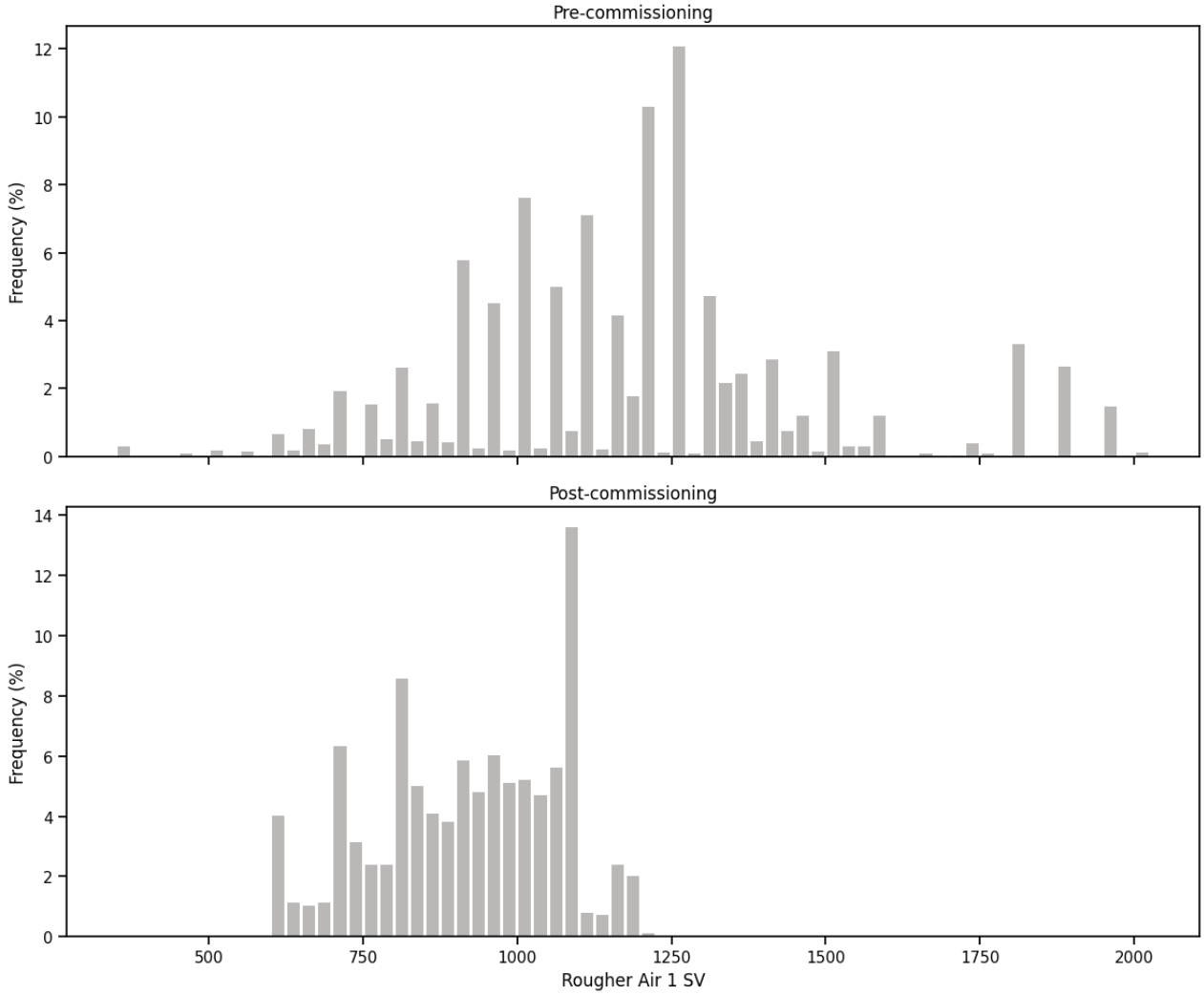



**FIG 3** – Example of distribution filling resulting from closed loop control, and continuous re-training processes. The shift in the distribution reflects the general direction of the NSR optimisation process towards lower rougher air rates.

Model generalisation was more broadly measured and assessed as the alignment of training, validation and in-production error scores (typically mean absolute error metrics and $R^2$ metrics). Throughout the first 12 months of operation of the twin, as data collection continued, it was noted that model generalisation improved with typically smaller, tighter neural network structures rather than those previously used in the feasibility and implementation phases. General reduction in network size combined with more appropriate usage of network regularisation techniques improved the continuity of the internal control relationships and typically resulted in better pre-deployment error metrics. Management of overfitting during model development and maintenance will remain a crucial issue in all applications of machine learning to metallurgical processing, simply due to the relatively small data set sizes being leveraged in many industrial contexts.

As an example of a reasonably well-developed control relationship, Figure 4 shows the predictions for Scavenger Tail and Combined Grade against Zn scavenger cell 1 SIPX dosage rate, using the model in production at February 2026. While the control variable surface is not perfectly smooth, ongoing generalisation of the model has captured relatively precise grade-recovery relationships. This example, despite only representing a single dimension of the set point optimisation, provides a simple illustration of the competing trade-offs that the NSR objective function is able to address.

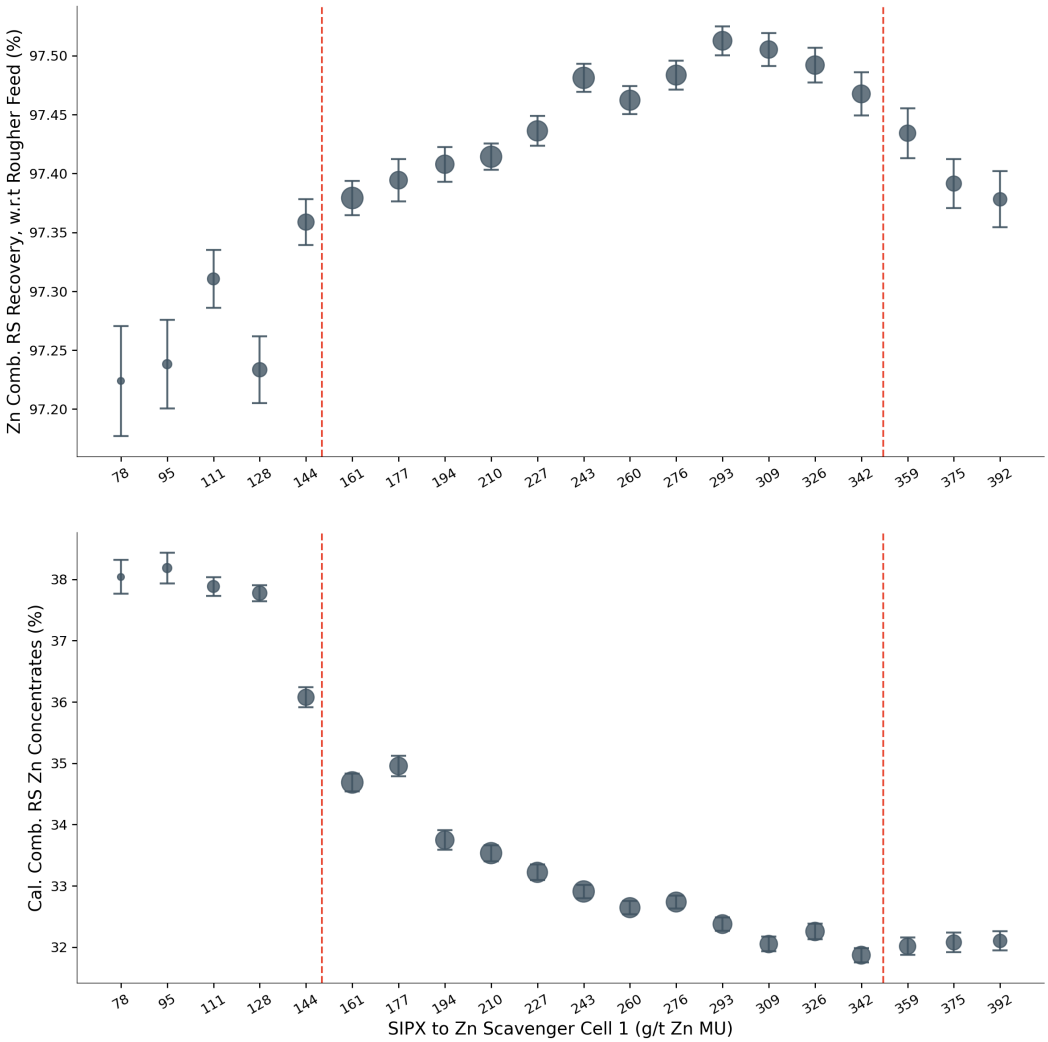



**FIG 4** – The modelled control relationships against combined rougher scavenger recovery (upper) and combined concentrate grade (lower) for one control variable: collector to scavenger cell 1. The red lines indicate typical set point optimisation bounds employed during the first 12 months, between 150–350 g/t Zn metal units. Bars denote the 95 per cent confidence interval around the prediction at each point in the control relationship.

## Control model maintenance improvements

A critical component of maintaining the twin is ensuring an efficient and thorough system is in place to enable regular, proactive model redeployments as new data becomes available. This is necessary to ensure drift over time in control relationships is captured. The long-term goal of such a system is to enable more hands-on model management from site metallurgy teams. At the time of commissioning, expanding the model training data set required a manual extraction from site to be merged with the existing data set. New models were then manually retrained as required, typically on a 8 to 10-week basis or as desired.

In June 2025, Hatch's continuous learning environment was enabled via near-real-time data streaming. This occurred through a separate IT architecture leveraging regular historian synchronisation to cloud systems, not connected or associated with the twin's production systems. This allowed the automated model retraining to begin. Whilst continual experimentation can be conducted on the model training workflow, the current iteration of the production-ready training workflow is utilised for this automated system. This contrasts greatly with traditional fuzzy logic and linear model matrix APCs (advanced process control solutions) which require manual rule adjustments, or manual re-stepping of static control relationships, which can be expensive, slow, and vendor dependent.

Each retrain creates a new version of the model in an ever-expanding catalogue, trained on data up to at most a day old. Whilst models can be produced automatically on a daily basis, replacement of the live twin's production model at this stage should not be done automatically on such a high frequency, since control relationships are unlikely to change day-to-day. Moreover, while automated retraining according to a standardised workflow is relatively trivial, the metallurgists' quality assurance procedures (QA/QC) are not. The defined model QA/QC procedures should continue to be conducted by individuals familiar with the flow sheet process and historical twin behaviours, to ensure continued sound metallurgical control responses to feed disturbances.

The QA/QC process is further complicated by the large quantum of potential control responses to many potential disturbance variable combinations (%Zn, %Fe, %Pb, %Sol, solids rate, $P_{80}$ etc). As such, the system must standardise around a key set of disturbances. This allows a repeatable comparison of optimisation results from candidate to candidate, and against the current production model. Figure 5 demonstrates an example of a standardised disturbance in which the feed zinc grade is artificially ramped from a statistically low to a statistically high value, and the response of the SIPX dosage across the five cells is examined.

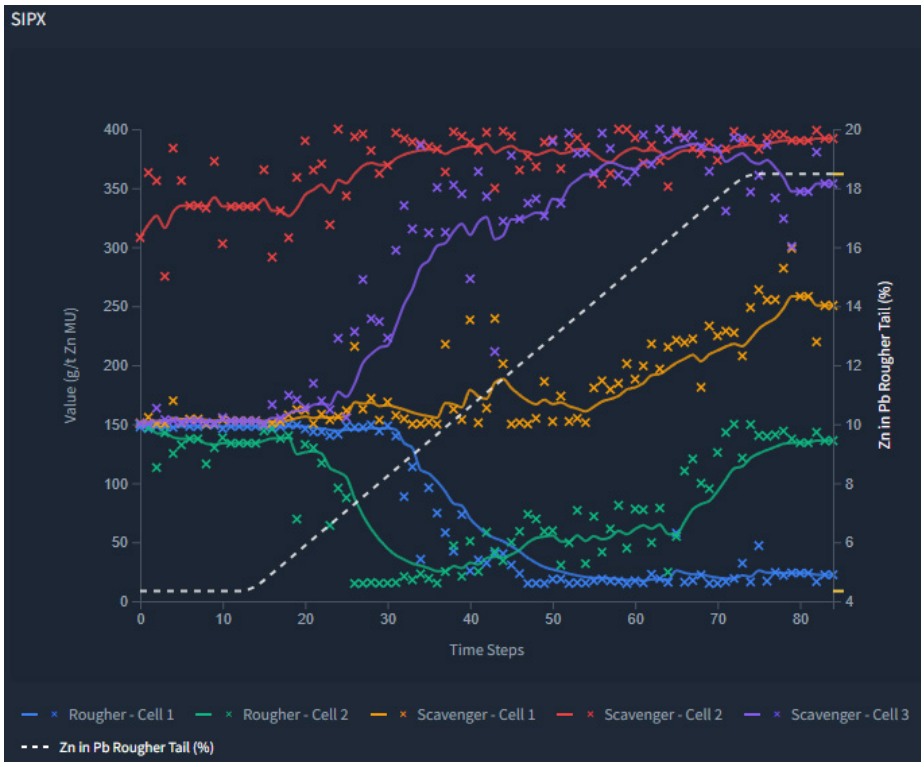



**FIG 5** – An example QA/QC response chart showing the optimised control responses of the SIPX dosages from a simulated increase in feed zinc grade. The white dotted line represents the simulated disturbance, while the coloured lines and markers represent the SIPX dosage on each of the five cells. The 'x' markers represent the raw optimisation results (not able to be executed) while the lines represent the partially smoothed set points.

The twin's SIPX responses to head grade shown in Figure 5 illustrate a repeat behaviour often observed by the twin in production. At low Zn rougher feed grades (6–8 per cent), the twin typically opts for very low rougher cell dosages. As feed grades increase (8–10 per cent), the final scavenger cell 3 ('purple') is effectively activated by the twin, rapidly shifting the dosage rate off the lower scavenger constraint of 150 g/t in this case. This shift in SIPX usage onto the Scavenger cells is initially offset by decreased usage on the rougher cells, until high feed grades are reached (>14 per cent). At higher feed grades, both rougher cell 2 and scavenger cell 1 (ie the mid-bank cells) simultaneously increase the collector dosage rate to handle the higher associated metal loading hitting the rougher.

There are several noteworthy aspects of this. Firstly, none of these behaviours were explicitly programmed by the twin but learnt by the linked neural networks and then extracted by the twin's set

point solver. Secondly, these patterns are potentially Dugald River rougher-scavenger specific, and the approach may learn different optimised control responses custom to different flow sheets and ores. Finally, the very practice of having to perform QA/QC on these models helps build solid fundamental control knowledge for plant metallurgists around the specific control patterns within one's plant, that are not immediately discernible. In the view of the authors, this type of activity will become more commonplace for plant metallurgy practitioners as this process twin technology becomes more widely adopted.

## Model error management in real-time

Any model of a real system will be imperfect and therefore have error. To assess the reliability and effectiveness of the twin's underlying models, errors must be transparently presented on every loop of the system, and operators and metallurgists should have capability to track and review these errors in real time.

In many ways, neural networks are opaque models that take inputs and provide predictions without providing direct insight to users as to how the predictions were made. Due to a lack of complete mechanistic interpretability of these systems, it can be difficult to anticipate what conditions may lead to poor performance. While extrapolation is not possible or acceptable for the DRM rougher-scavenger twin, for models of continuous variables in a high dimensional space such as this, interpolation is necessary and accuracy in different regions will vary. Unmodelled metallurgical and geological variables that impact flotation performance can further exacerbate errors. In the context of an optimisation process, poor model accuracy leads to suboptimal recommendations.

Given these risks, it is vital that systems such as these can be constantly assessed for their accuracy. Informing operators of the performance (Figure 6) allows them the control to make informed decisions about when to manually disengage the system which is crucial for building trust. Furthermore, error tracking allows the system to make quantitative self-assessments by *automatically* disengaging if errors exceed defined thresholds and warning operators. Since the model predicts performance in real-time, it can perform these self-assessments every loop before it provides a control recommendation. The DRM rougher-scavenger twin will automatically disengage and trigger a graceful fall-back to the pre-existing cascade control loop if errors breach custom statistical benchmarks established for each model during validation (pre-deployment).

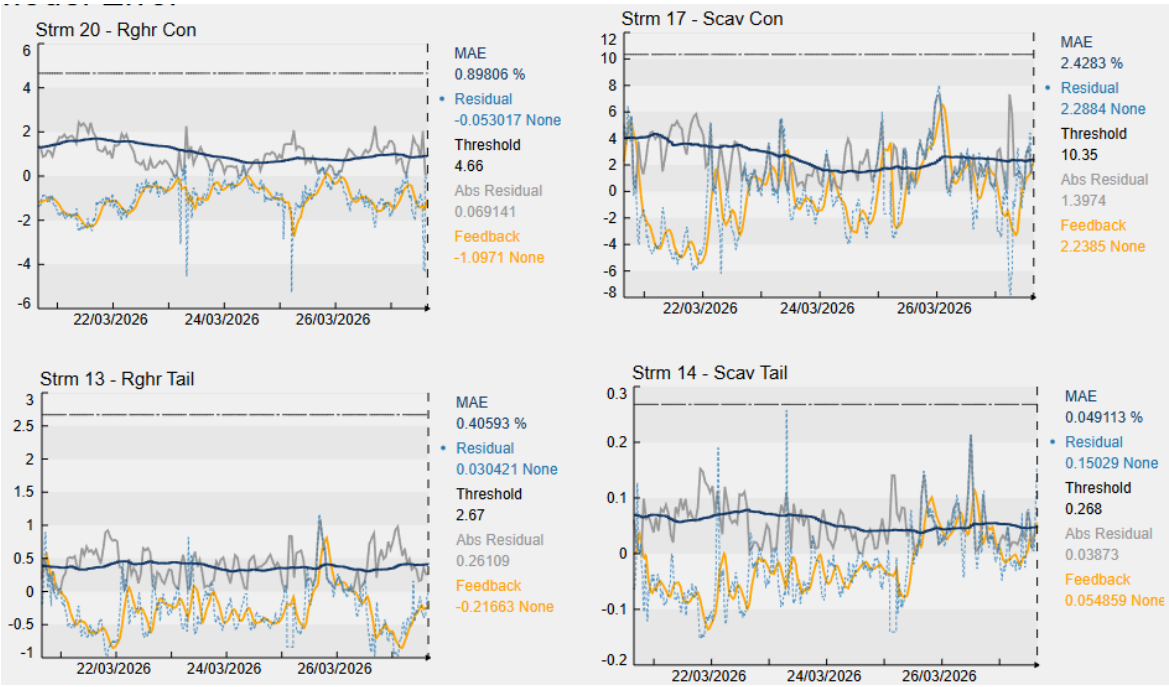



**FIG 6** – Screenshot of the plant metallurgists PI Vision interface subset, highlighting seven days of error tracking for the four neural network outputs. Raw residuals per loop are shown in blue, while the mean absolute error (MAE) which triggers automated model health disablement by the twin is shown in the dark bold line.

Additionally, since plant conditions and control usually change smoothly and slowly, prediction errors often exhibit temporal correlation and can persist over extended periods. By recording and aggregating these previous errors, the current bias in the system can be estimated and a correction can be applied to predictions made during optimisation. Notably, any estimated bias can be reapplied in real-time to every calculation of the NSR objective function. This effectively causes the optimiser to periodically self-correct, and steer residuals back towards zero. Future developments in this space will allow for the longer-term penalisation of specific incorrect or poorly performing set point combinations that were caused by poor input data or local overfitting during the neural network training process.

Bias correction should not be applied when displaying model errors and performing automated self-assessments as this would lead to an incorrect representation of the underlying process model performance and degrade trust in the model. The purpose of bias estimation is just to inform the optimiser that the model's current predictions may be trending in a consistent direction relative to actual plant measurements, and therefore the chosen set points should account for this (in the above example this may lead to a gentler set of set points). This of course assumes that actual plant measurements and estimates form ground truth, rather than the model, which is not always completely correct.

Finally, with regards to model error trending in the context of set point optimisation it is worth observing that the errors in concentrate and tail grades manifest as an overall grade-recovery position bias, relative to the NSR optimisers precise preferred position. In general, throughout the first 18 months of twin operation, the twin's models resulted in a bias towards slightly over achieving recovery, and slightly underachieving concentrate grade. Preliminary improvement of this minor issue involved introduction of sharp penalty curves for low combined rougher-scavenger concentrate grades in the NSR optimisation, configurable from the operator's SCADA.

# EVALUATION BY RANDOMISED BLOCK TRIAL

## Trial design and execution

The digital twin's performance was evaluated from July to December 2025 using a randomised on/off block trial with each block spanning at least eight shifts (four days), with the actual block duration being relatively randomised (Malcolm, 2025).

The randomised block design was chosen to account for differences in operators and staff, temperature and rougher feed ore characteristics. The criteria for a shift to be included in the analysis included:

- at least 11.5 hrs of plant runtime (95.8 per cent)
- twin enabled/disabled >90 per cent
- confounding reagent trials not ongoing
- no indication of major contaminants in plant feed (based on irregular preflotation feed pH)
- MSA available for the whole shift
- no control variables significantly saturated (unable to reach set point values)
- no significant interventions required by the operator due to unplanned circumstances.

In total the trial included 89 off shifts and 86 on shifts, for a total of 175 evaluated shifts. Results were assess based on official shift reconciled data (recorded and mass balanced independently of the digital twin software) using a two-sample t-test (Malcolm, 2025).

Given the relatively simple nature of the on/off trial, no major issues were incurred during the execution of the trial. The twin's software remained fully operational during the twin 'off' block but was simply disengaged from autonomous closed-loop control, allowing simple management of the trial according to the pre-determined trial schedule.

## Results and discussion

### *Randomised block trial results*

In each of the below statistical comparisons, the twin ‘on’ condition is represented by the red distribution, while the twin ‘off’ trial condition is represented by the blue distribution. A kernel density is provided on the y-axis, and a trend line of the kernel density estimate for ease of visually comparing distributions. Figure 7 provides the Zn rougher feed grade comparison between the ON and OFF conditions. As expected through the block randomisation process, there is no statistical difference in feed grades (both conditions 10.6 per cent Zn), and the mean rougher feed grade is typical.

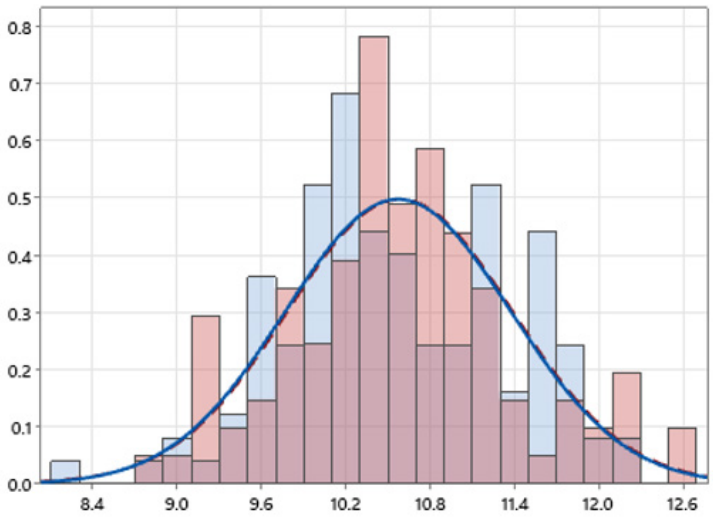



**FIG 7** – Feed grade comparisons between the twin on (red) and twin off (blue) conditions.

A statistically significant difference in combined rougher-scavenger recovery was determined by the trial of +0.53 per cent ($p$ = 0.00) higher recovery during the twin ON condition (distributions shown in Figure 8). No statistical difference in combined rougher-scavenger concentrate grade was detected, implying that the twins NSR optimisation process valued targeting higher recoveries without achieving higher concentrate grades. Note the baseline rougher scavenger recovery of greater than 97 per cent represented a relatively tough recovery improvement challenge for the twin project to meet.

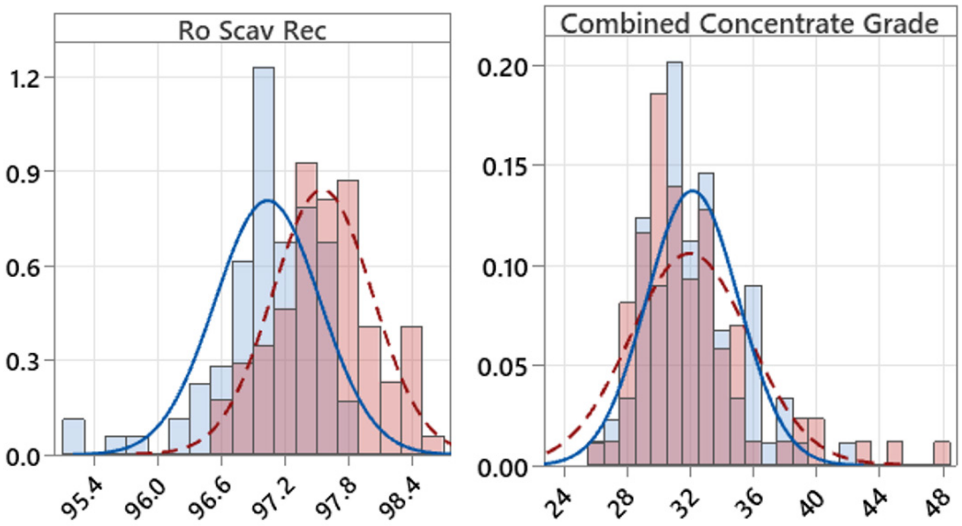



**FIG 8** – (left) the rougher-scavenger recovery comparison and (right) the combined rougher-scavenger concentrate grade comparisons between the twin on (red) and twin off (blue) conditions.

Similar results were observed for full plant Zn recovery, with reconciled results highlighting +0.38 per cent ($p$ = 0.02) during the twin ON condition. Downstream cleaner recovery indicated a 0.14 per cent reduction during the twin ON condition, however this was deemed not statistically significant from the trial results ($p$ = 0.45).

Additional interesting results were observed with both reductions in consumption of both collector (SIPX) and activator ($CuSO_4$) during the twin on condition, as highlighted in Figure 9. Collector consumption achieved a reduction from 1074 g/t Zn metal unit to 913 g/t Zn metal unit ($p$ = 0.00). It is expected that the reduction in consumption is firstly due to the usage of a full multivariate control variable optimisation in the case of the twin ON condition, and secondly due to the tendency of the pre-existing SIPX cascade controller in the twin OFF condition to chase tail grades with additional collector whenever measured tail grade exceeded the metallurgical target limit.

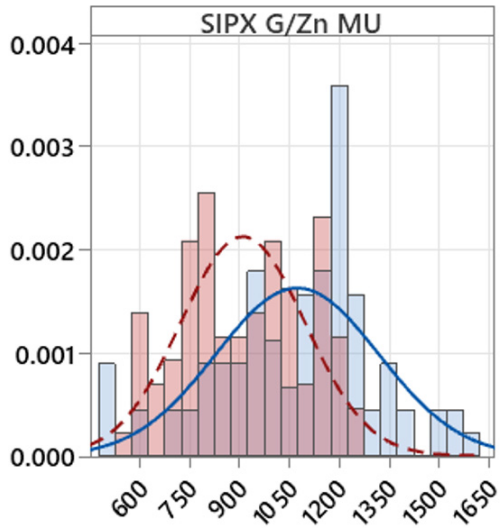



**FIG 9** – Material reduction in collector consumption during the twin ‘on’ condition (red) in comparison to the twin ‘off’ condition (blue).

Overall, the trial was considered complete by the end of December 2025, despite having reached a statistically significant result in favour of the twin ON condition by the completion of the first third of the trial schedule.

### *Time in closed loop*

Time in closed loop was previously reported spanning January 2025 to September 2025 (Smith *et al*, 2026). Closed loop time is calculated as a percentage of available time, excluding interlocked time during plant shutdown, plant start-ups, or off periods in the block trial. Figure 10 provides the closed loop utilisation metric up to March 2026.

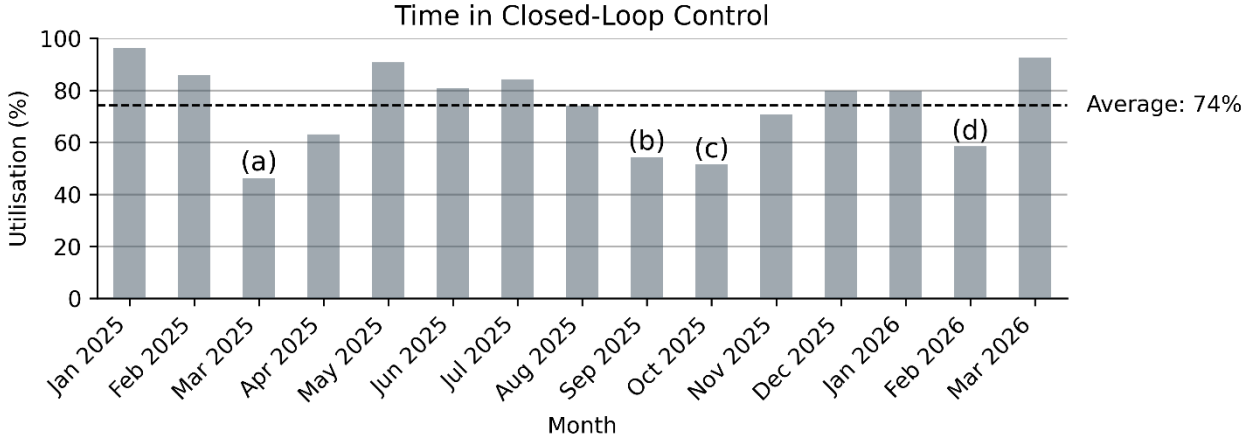



**FIG 10** – Utilised time in closed loop control since commissioning (as of 27 March 2026).

At the time of writing, the average utilisation since commissioning is 74 per cent in closed loop control. Excluding February 2026, the utilisation has been trending higher since the conclusion of the block trial in December 2025, simply due to reduced disruption associated with managing block trial conditions. The four months with low (below 60 per cent) utilisation labelled (a)–(d) in Figure 10 were associated with the following events:

- a combination of model error and negative scavenger concentrate grade impacts, resulting in the first model re-deployment.
- particle size analyser downtime, resulting in a grinding circuit-based proxy for primary grind $P_{80}$ being incorporated into the twin's model set to overcome future analyser outage.
- low SIPX addition in the lead rougher circuit required manual override of the SIPX dosage in the rougher/scavenger circuit, and temporary twin disengagement.
- a redeployment resulted in extended time out of closed loop control while awaiting readiness to engage and evaluate the updated models.

The time in closed loop control was considered positive and consistent for the first year of operations, and will continue to target maximum utilisation going forward, while allowing for some model unhealthy time to ensure reasonably effective model health evaluation thresholds.

## ZN CLEANER EXPANSION – DESIGN CONSIDERATIONS

Following the completion of the randomised block trial and formal evaluation of the rougher scavenger twin's impact on the Zn circuit performance, scoping began for the expansion of the system into the Zn cleaner circuit. Such a system would be likely characterised by three additional neural networks covering the three stage cleaner circuit and focus on further set point optimisation and advanced automation of the Zn flotation circuit as a whole. Importantly, rather than acting as individual systems, both the rougher-scavenger and cleaner blocks would be brought under a single expanded process objective function, providing a more complete estimate of NSR impacts than what has been completed to date under the rougher scavenger NSR impact alone.

The key design challenges of this future implementation shall include:

- Updated approaches to circuit mass balance modelling and dynamic reconciliation estimates to deal with unmeasured properties within the Zn cleaner circuit ahead of control model training and development.
- The requirement to manage and maintain a set of five neural network control models, necessitating ongoing innovation in model management and model QA/QC systems, more suitable for plant metallurgist usage over time.
- New challenges and opportunities to better balance rougher-scavenger and cleaner performance. For example, allowing the cleaner block to feedback systematic underperformance of cleaner feed grades and final concentrate grades to effectively drive rougher-scavenger grade constraints higher. Conversely, allowing the cleaner block to feedback systematic overperformance in final concentrate grade against NSR requirements, thereby enabling more tactical targeting of the scavenger tail grade.
- Computational time limitations to solver a wider flow sheet area problem, in combination with new, longer residence time process dynamics across that wider area.

Importantly, as emphasised in the earlier implementation and commissioning works, the system will need to undergo the same structured methodology to model validation, as well as the layered testing and operator acceptance methodologies previously published to ensure position adoption rates from commissioning onwards.

## CONCLUSIONS

In this work, the authors demonstrated the metallurgical and operational impact of a closed-loop rougher scavenger flotation twin aimed at automating and optimisation flotation set points under a Zn Net Smelter Return objective function. The system was evaluated under a randomised block trial,

which concluded a positive impact of +0.53 per cent Zn recovery improvement at high statistical confidence, on a high baseline rougher-scavenger recovery performance exceeding 97 per cent. The trial also concluded no statistical difference in combined rougher scavenger concentrate grade, while material improvement in reagent consumption rates by the twin was observed through improved utilisation of a full multivariate control action. The twin achieved a high and consistent time in closed loop control throughout the first 12 months of operation, reflecting the positive change and operator readiness work completed in the previous implementation and commissioning phases.

Several crucial post-commissioning twin enhancements supported the overall outcomes achieved by the DRM operational and metallurgical teams. These were summarised as: improvements to flexible adjustment of twin set point optimisation bounds directly from SCADA, improved generalisation of the twin's internal rougher and scavenger control models; major enhancements to system infrastructure allow automated retraining of rougher and scavenger models for efficient maintenance and redeployments; and improvements in the usage of model errors in real-time to aid in short-interval self-correction of the NSR objective function calculations.

Based on the positive outcomes from commissioning and evaluation, it was concluded by the authors that the system is now ready for the next incremental scale out of the system to include the Zn cleaner block, which would effectively place the full Zn circuit under a single closed-loop process optimisation.

## ACKNOWLEDGEMENTS

The authors would like to acknowledge and thank MMG and the Dugald River Mine team for the close collaboration and ongoing feedback throughout the design, the implementation and the commissioning of the process twin at site. The authors would also like to thank both MMG and Hatch for the opportunity to report on the findings from this project.

## REFERENCES

Geldenhuys, S, Auret, L, Deglon, D and McFadzean, B, 2023. Digital twinning of flotation processes: A business case and potential challenges, in Proceedings of the Flotation Conference 2023, Cape Town: MEI.

Malcolm, A, 2025. Dugald River Technical Note 93: Digital Twin Trial Results, internal document.

Nasiri, M, Iqbal, S and Särkkä, S, 2025. Physics-informed machine learning for grade prediction in froth flotation, *Minerals Engineering*, 227:109297. https://doi.org/10.1016/j.mineng.2025.109297

Nobahar, P, Xu, C and Dowd, P, 2026. Cost-Integrated AI Meta-Models for Mine-to-Mill Optimisation: Linking Fragmentation, Throughput and Operating Costs Across the Value Chain, *Minerals*, 16(1):73. https://doi.org/10.3390/min16010073

Ohenoja, M, Koistinen, A, Hultgren, M, Remes, A, Kortelainen, J, Kaartinen, J and Ruusunen, M, 2023. Continuous adaptation of a digital twin model for a pilot flotation plant, *Minerals Engineering*, 198(March).

Shnayder, D A and Kalinina, E A, 2023. Development of the Digital Twin for Flotation of Non-Ferrous Metal Ore Beneficiation, in *Proceedings of the 2023 International Russian Smart Industry Conference (SmartIndustryCon)*, pp 50–54.

Smith, W, Malcolm, A, Goode, I, Bai, G and Martin, C, 2024. Practical considerations in the design of flotation process twins for set point decision automation at MMG Dugald River Mine, in *Proceedings of the Mill Operators Conference 2024*, pp 159–174 (The Australasian Institute of Mining and Metallurgy: Melbourne).

Smith, W, Malcolm, A, Martin, C and Yelland, J, 2026. Commissioning a process twin for set point decision automation at Dugald River Mine, in Proceedings of the MetPlant 2026 Conference, Adelaide.

Metallurgy Symposium

# Best practice in existing plant operations

# A probability-based simulation of a copper mineral processing plant

*S L Rayward*[1]

1. Principal and R&D Director, Midas Tech, Sunshine Coast Qld 4551.
   Email: stephenr@midastech.com.au

## ABSTRACT

In this abstract, I will present the application of a probability-based simulation to a copper plant in Kazakhstan (the client). This will be of interest to mineral processors whose focus is the optimisation of the performance of mineral processing plants using a logical and elegant approach.

There are various approaches to simulate the performance of a mineral processing plant using plant survey data. A common approach is to construct unit models which are then combined by using a flow sheet visualisation framework. Conventional unit-based modelling is generally based on semi-phenomenological models. An alternative unit modelling approach is to use probabilistic models. These models are based on a relatively new mathematical approach called information theory (popularised in the 1960s). In this context, information theory means the mathematical interpretation of available information. There are advantages of the two alternative approaches (conventional and information theory), and ideally, they would be used synergistically.

In this simulation, only the information theory approach was used. The advantages of the probabilistic approach (compared to the conventional approach) are:

- More accurate results and more easily applied mass balance than the well-known flawed conventional mass balance methods.
- A natural extension of mass balance to unit model construction.
- The easily applied application of these unit models in a simulation system that focuses on a holistic approach rendering the simulation more user-friendly.
- Straightforward integration of comminution, classification and flotation rather than using separate non-compatible systems.
- This was particularly important for the client as the flow sheet involved numerous regrinds.
- The information theory approach provides an appropriate framework for extension to feedback-loop-based machine learning (also called reinforcement machine learning).

All software (for the flow sheet-based simulator) was created using Excel/VBA, which then allowed straightforward transfer of software to the client. The purpose of the simulation was mainly focused on developing a prototype. The client decided to use the prototype as a basis of developing a new independent simulation system – specifically customised for Russian speaking countries.

# Mill liner wear management – common mistakes and how to avoid disaster

*P Toor*[1]

1. Comminution Consultant, Toornado Metallurgy, Brisbane Qld 4000.
   Email: paul@toornadometallurgy.com.au

## ABSTRACT

The shutdown frequency and duration for mill concentrators is generally dictated by the primary mill reline, and this is especially true for grinding circuits with SAG mills. As a result, mill liners are routinely inspected to understand the current wear performance and forecast the service life with respect to the scheduled shutdown dates. These inspections are now typically performed using 3D laser scanners, which generate comprehensive models from millions of data points collected from the exposed liners and mill charge *in situ*. 3D scanning is a major improvement over traditional methods like manual ultrasonic measurements. However, it has not consistently reduced premature liner failures or emergency relines. A key reason for this is a poor understanding of liner wear fundamentals from mill operators and plant metallurgists. This paper revisits the fundamental principles of liner wear, its application to wear monitoring and forecasting. It highlights common pitfalls and misinterpretations in current practices, providing guidance to help operators avoid costly liner-related failures and improve the reliability of shutdown planning.

Metallurgy Symposium

# Design, operation and optimisation of key unit operations

# SAG milling – the benefits of bigger balls

*B Cornish[1] and R Butar[2]*

1. Director of Application Engineering, ME Elecmetal, Point Lonsdale Vic 3225.
   Email: bcornish@meglobal.com
2. Senior Application Engineer, ME Elecmetal, Bali 80361, Indonesia.
   Email: ramlan@meglobal.com

## ABSTRACT

Semi-autogenous grinding (SAG) milling circuits are almost always associated with high throughput mining operations with aggressive production targets. The main role of the SAG mill is to achieve and maintain the desired feed rate while the role of the ball milling circuit is to achieve and maintain the target product size. While there are a few industrial levers available to make it easier to maintain the desired feed rate, the simplest change is to increase the SAG mill ball top size.

In the SAG milling environment, rock breakage rates can be increased by using larger grinding media. The improvement can be usually measured using the throughput rate, pebble production rate, and specific energy consumption. Larger diameter (and therefore heavier) balls will result in a greater kinetic energy per impact, meaning that they can break larger and harder rocks more effectively, thus reducing the accumulation of the critical size materials. Large balls may also cause a finer particle size distribution per impact that smaller balls on the same size rocks, leading to accelerated fine particle production. While it is true that there are fewer balls per unit volume and thus less frequent impacting events than that smaller diameter balls, it is also true that there are still an enormous number of balls tumbling within the mill.

The key benefits include unlocking a wider operational range thus improve consistency and reducing ball consumption. Larger grinding media on the SAG mill could also lead to slower mill speed and/or lower ball load to maintain the fresh feed rate. There are some case studies briefly explain in the presentation that show the benefits of larger media on milling performance and media consumption. This paper provides valuable insight into optimising SAG milling performance with bigger balls; there is an extensive list of benefits with very few risks, especially on the liners.

## INTRODUCTION

Semi-autogenous grinding (SAG) circuits have several different forms, but all involve complex interactions between rock, water, and steel balls. The mill feed – particularly the top size, particle size distribution (PSD), and breakage characteristics – are the primary variables when establishing operating conditions. Doll and Tischler (2015) state that the primary role of the SAG mill is to achieve and maintain the target plant feed rate at a transfer size suitable for the ball mills to in turn achieve and maintain the target product size. Most of the challenges with maintaining the feed rate and product size originate with the mill feed, and the purpose of this paper is to demonstrate that there are benefits in moving to the next largest ball size.

## SAG MILLING BASICS

In a SAG mill, the grinding action is achieved primarily through the ore itself tumbling and impacting other pieces of ore. Lane (2007) states that steel balls are added to help break down the larger pieces of ore and these balls provide additional grinding energy, especially for harder, more breakage-resistant rock. A typical SAG circuit is shown in Figure 1.

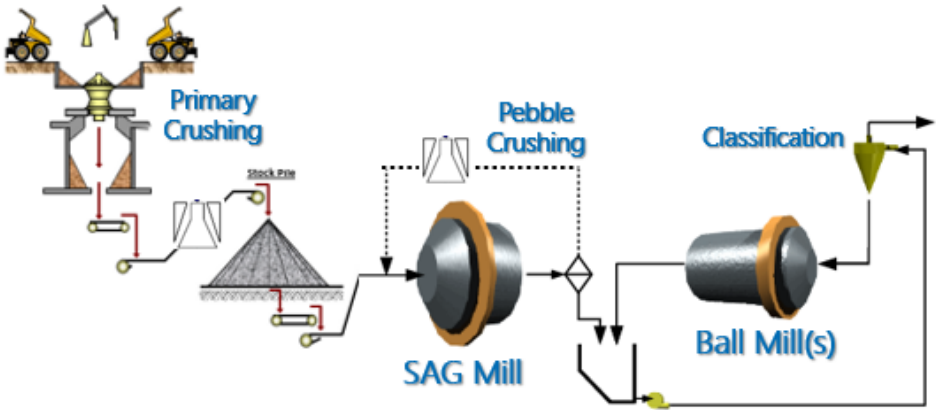



**FIG 1** – Typical SAG milling circuit.

With each mill rotation, the grinding media and the ore particles transition between having potential energy and kinetic energy. The continuous transition of these two forms of energy in this milling environment results in three main rock breakage mechanisms: abrasion, attrition, and impact. It is generally accepted that 10–20 per cent of the grinding work is impact breakage and is roughly confined to the toe region, which is small compared to the entire rotating kidney region. Figure 2 shows a typical SAG mill cross-section with the characteristic kidney, toe and shoulder regions.

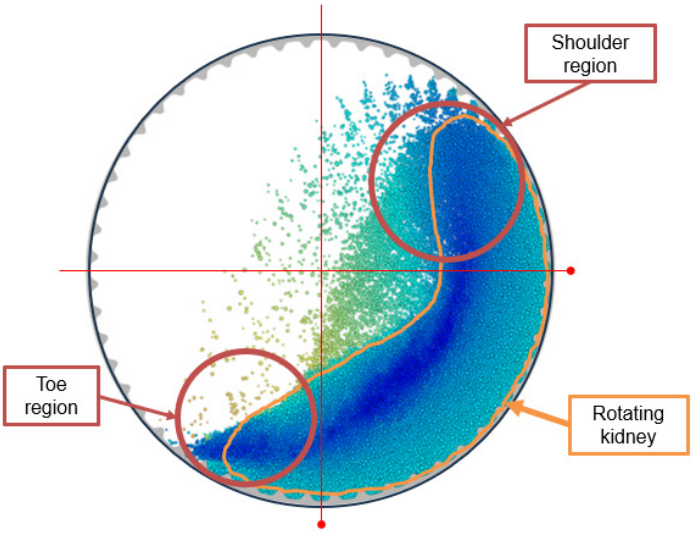



**FIG 2** – Typical SAG mill cross-section from Discrete Element Method (DEM) simulation.

The standard design utilisation of the installed SAG mill power capacity is 85–90 per cent and this allows for 10–15 per cent buffer capacity in the event of a significant disturbance causing rock to accumulate and the mill to approach an overload condition. The additional power capacity enables the mill to continue operating (usually at a much lower—or zero—feed rate) to decrease the mill rock load as quickly as possible.

SAG mill operational performance can be measured and monitored using specific energy consumption (SEC) and the fresh feed rate. These two variables capture the most basic daily grinding circuit measures of throughput (tonnes), operating time (hours), and energy consumption (kWh), further noting that the product of any operational performance data point is the power draw (kWh/t*t/h = kW).

Thus, the location of any data point (the actual power draw) can be compared to the installed power capacity. Over several months of data analysis, it can be determined when power draw should be maximised and when it is unnecessary to do so. A Plant Metallurgist needs to understand operational performance (kWh/t, t/h) before attempting to understand media performance (g/kWh, g/t, kg/h).

In the past decade it has become more common to prioritise monitoring and maintaining a target ball load and as such, instrumentation and models have been developed to continuously measure ball

loads. Such advances in measuring and modelling have enabled an increase in ball loads to well over 18 per cent. This operational strategy is referred to as barely autogenous grinding (BAG), and power utilisation can be up to 95 per cent leaving little room for unplanned grind-outs. It must be noted that BAG milling is usually associated with a fine feed size (as low as 20 mm) and perhaps an SABC2 circuit configuration (where pebbles are crushed at least twice, classified, and directed to the ball mill circuit feed).

It is also common to operate SAG mills with a high ball:rock ratio; for example, a ball load of 20 per cent and rock load of 5 per cent is a ball:rock ratio of 4. This milling environment provides high rock breakage rates but also results in occasional – and in some cases sustained – ball-on-liner impact events that at the very least increase media and liner consumption rates, and at worst result in mass ball breakage and/or broken shell liners and discharge grates. Such conditions demand high quality grinding media that can resist breakage as the excessive impacting energy accumulates within each ball; as such it is common to observe broken balls in the SAG mill rejects bunker or as a worst case, within the mill load.

## BENEFITS OF LARGER MEDIA SIZE

Ball size and ball loads have generally increased in recent years; in past decades, a 100 mm ball size was desirable with an 8 per cent steel load. Today, 140 mm and even 160 mm balls are common in 40 ft diameter SAG mills with 28 MW motors at steel loads of 22 per cent. In such a case, a ball load of 800 t is maintained by daily addition of 27 t of 140 mm balls each weighing 11.2 kg (2500 balls/day). Despite the large size, this is an enormous number of top-sized balls tumbling at any given time.

Larger diameter (and therefore heavier) balls will result in greater kinetic energy per impact, meaning that they can break larger and harder rocks more effectively. In theory, larger balls create a finer PSD per impact than smaller balls on the same size rock, perhaps leading to accelerated fine particle production. While it is true that there are fewer balls per unit volume and thus less frequent impacting events than with smaller diameter balls, it is also true that there are still an enormous number of balls tumbling within the mill.

In SAG mills, there is evidence that rock breakage rates can be increased by using larger grinding media, and the improvement can be measured as a combination of throughput rate, SEC, and pebble production rate. The physical benefits of using larger balls are summarised as follows:

- The increase kinetic energy per impact provides an increased rock breakage rate that expands operational flexibility to accommodate varying SAG mill feed size and ore competencies.
- The larger (and heavier) balls are more likely to be released earlier from the lifter resulting in an equal or lower trajectory from shoulder to toe.
- Larger balls provide a more stable rock breakage (grinding) environment, with a decrease in transient and potentially dangerous ball trajectories that may result in direct ball-on-liner impact events.
- The exposed surface area of a ball charge with larger diameter balls is less than that of a charge with smaller diameter balls, thereby leading to lower media consumption with larger diameter balls.

At a higher level, larger balls make the SAG mill easier to operate and maintain the ball load. This improved operational performance and stability provides several opportunities:

- Increase of the fresh feed rate (assuming no other plant constraints).
- Decrease of mill speed and/or ball load can be realised at the same feed rate (assuming minimal impact on transfer size) – this may result in extended liner life and operating time.
- Decrease of pebble production enables optimisation of the pebble crushing circuit.
- Further optimisation of rock load control leading to a more uniform PSD delivery to the ball mill circuit and thus improving the ball mill circuit functional performance.

Leveraging any of these opportunities effectively leads to increased metal production at a lower overall operating expenditure (OPEX). Any plant management team considering using larger SAG balls must be sure to adhere to the industry standard change management protocols and be aware of the following threats:

- Operators need to be educated that larger balls may change the mill internal dynamics, but there is no fundamental change to the risks of operating at maximum speed (78 per cent critical speed [Cs]) with low rock loads.
- Liner design, specifically grate slot size and open area, becomes more important as the benefits of the larger ball will possibly result in a slower slurry transport (pumping action) at a slower mill speed.
- Liner design, specifically the lifter attack angle, requires more consideration given that an aggressive angle may not be necessary with larger ball sizes to achieve effective impact rock breakage in the toe region.
- SAG mill feed rate control and maintaining a safe rock load to protect the liners, grates, and media is of critical importance (as always) in minimising ball-on-liner impacting – prioritising the mill feed rate over a safe rock load is never a good operating strategy.

Returning to the basic SAG mill rock breakage mechanisms (abrasion, attrition, and impaction), it is generally accepted that 10–20 per cent of the grinding work is impact breakage. Further, the impact breakage is roughly confined to the toe region, which is small compared to the entire rotating kidney region. It is postulated that larger balls extend impact breakage into the outer layers of the rotating kidney where top-sized balls (having rolled off the lifter earlier) are chattering together in a semi-confined space with much greater energy, resulting in effective impact breakage displacing a portion of the lower energy abrasion and attrition breakage.

## BALL DROP TEST WORK

ME Elecmetal initiated a basic test work program to validate the theory that the impact energy of any ball-on-rock collision depends on the mass and velocity of the ball at the time of the collision. In other words, the ball size and drop height are correlated with rock breakage and PSD. The work was conducted by the Application Engineering Team in 2017 and consisted of dropping four different ball sizes from three different heights onto similar rock samples.

The rock samples used were crushed pebbles from the Asarco Ray SAG mill; all samples were screened and verified to be 50 mm (±10 mm), and it was assumed that the minerology and breakage characteristics would be uniform between the samples. An apparatus was assembled consisting of an impact plate/stand and a metal tube to guide the ball drop and contain the broken rock particles. Ball sizes of 105 mm, 125 mm, 140 mm, and 160 mm were dropped from three different heights of 0.75 m, 1.5 m, and 2.3 m directly onto one rock sample. Each ball size and drop height combination was repeated ten times with a fresh rock sample. For each drop test, the contained broken rock was carefully collected and screened with an appropriate set of standard Tyler sieves.

Data from each of the ten tests was collated and appropriately averaged into one PSD. The $P_{80}$ of each was extrapolated and this data is summarised in Table 1.

**TABLE 1**

Average $P_{80}$ sizes (mm) for each ball size and drop height.

| Ball size (mm) | Drop height (m) | | |
|---|---|---|---|
| | 0.75 | 1.5 | 2.3 |
| 105 | 31.1 | 24.8 | 23.8 |
| 125 | 29.6 | 25.9 | 23.3 |
| 140 | 30.1 | 22.9 | 19.8 |
| 160 | 22.8 | 20.9 | 19.2 |

The $P_{80}$ data indicates a clear advantage in rock breakage for the larger balls at the lowest drop height and maintains the advantage as drop height increases.

These test work results could be considered as rather simple and intuitive, and while this is true, the level of intuition can be extended to the actual milling environment. Given the continuous transition of potential and kinetic energy and the resulting rock breakage mechanisms (abrasion, attrition, and impact), each mill rotation maintains an enormous series of impact events across a wide range of drop heights. So intuitively, a larger ball will create increased rock breakage (a decreased $P_{80}$ size) with any given drop height within the mill even with the inevitable random interactions with other balls and rock; this must include the relatively small drop heights in the semi-confined space around the rotating kidney as well as the relatively large drop heights occurring in the toe region.

It is well known that SAG mills use grinding media to create impact breakage which produces the feed for the attrition/abrasion breakage; as well, basic comminution theory states that particle size reduction to a target $P_{80}$ requires less energy as the feed size decreases. Given that larger balls reduce the $P_{80}$ size through impacting at any given drop height within the mill, the concurrent finer grinding within the rotating kidney should be more efficient.

## SIMULATIONS USING LARGER BALLS

While all SAG mills are different, the rock breakage rate curve generally has a familiar shape that features the critical size component of almost all ores as shown in Figure 3. Each of the three zones represents the basic types of rock breakage (from left to right): abrasion of finer particles, critical size impacting and attrition, and impacting of coarse particles.

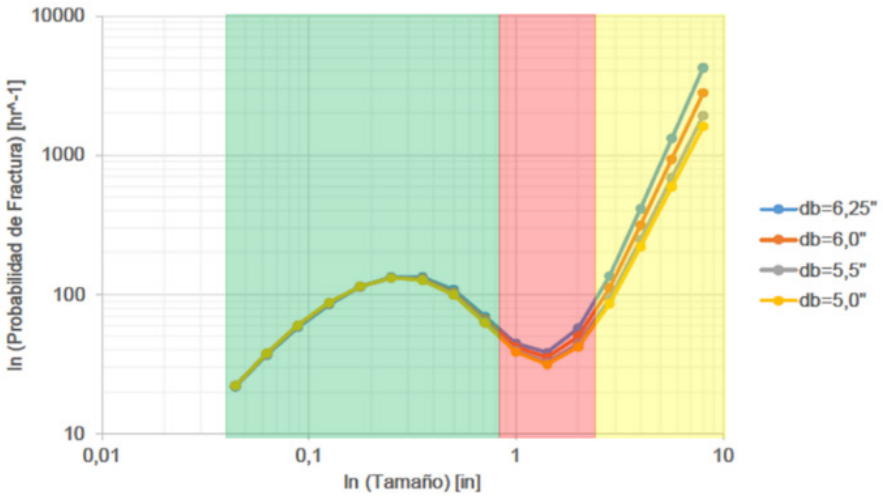



**FIG 3** – Typical SAG mill rock breakage rate curves used in simulations.

This JKSimMet chart also demonstrates the general upward shifts in the breakage rate curves of the largest particles with increasing ball size. The shifts are directly related to the increasing ball weight and the continuous cycle of transferring potential energy to kinetic (impact) energy.

For reference, Table 2 shows the actual and relative ball weights for the five ball sizes used in the EDEM® simulations by Tavares *et al* (2021). For example, a 140 mm ball is 33 per cent heavier than a 127 mm ball, while a 165 mm ball is 120 per cent heavier.

**TABLE 2**

Actual and relative ball weights used in simulations.

| **Ball size (mm)** | 127 | 140 | 152 | 160 | 165 |
|---|---|---|---|---|---|
| **Ball weight (kg)** | 8.4 | 11.2 | 14.5 | 16.4 | 18.4 |
| **Relative difference** | 0% | 33% | 73% | 95% | 120% |

Numerous simulations have been conducted across a wide range of SAG mill sizes under a wide range of operating conditions. There are some recurring themes with increasing ball size as follows:

- The overall ball and rock tumbling action (cascading and cataracting) changes very little.
- Ball trajectory is maintained or is decreased.
- The shoulder height (point at which a ball is released from the lifter) is maintained or is decreased.

These observations indicate that there is a combination of events occurring with each mill rotation: bigger balls are generally released from the lifter earlier and not lifted as high as smaller balls. It also seems that the impact region (generally the toe) is ***expanded inwards*** and there is a ***redistribution of the overall collision energy*** involving all forms of rock breakage. The most important observation is that there is very little opportunity for a top size ball to be released at the highest shoulder height and cataract directly onto a shell liner or discharge grate; physics does not support such a dangerous event.

The simulations described here were carried out using a 28 ft × 14 ft SAG mill with all operating variables within the standard range (Jb = 18 per cent, Jc = 28 per cent, grate slot = 75 mm, 1000 t/h, 4 MW). EDEM was used to model and analyse the behaviour of the mill charge, including the collision energy effects of the mill load with five different ball top sizes (Tavares *et al*, 2021).

## Overall ball size distribution

First it is important to consider the overall ball size distributions with increasing ball size as shown in Figure 4.

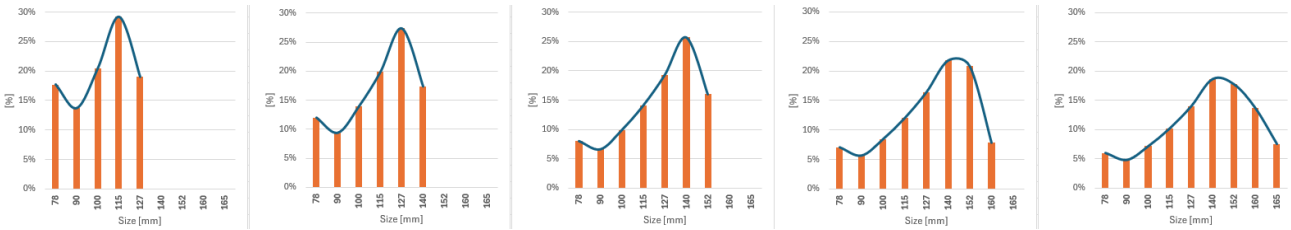



**FIG 4** – Ball size distribution used in simulations.

As the ball top size increases (from left to right), there is increasing diversity within the charge, assuming that the grate slot size is maintained (in this case 75 mm). Ultimately, this diversity enables the mill to develop a wider operating range and greater stability. The charts reveal that there are decreasing portions of smaller balls, but in a SAG mill of any size, there are still an enormous number of balls of every size fraction. Thus, the argument that larger balls lead to a larger transfer size is likely not true; unfortunately given the fact that representative sampling of any SAG mill discharge is extremely challenging, it is difficult to prove one way or the other.

## Overall collision energy

The overall collision energy increases marginally from 527 kJ to 540 kJ with increasing ball size in these simulations as shown in Table 3.

**TABLE 3**

Overall collision energy calculations.

| **Ball size (mm)** | 127 | 140 | 152 | 160 | 165 |
|---|---|---|---|---|---|
| **Overall collision (kJ)** | 527 | 530 | 536 | 539 | 540 |
| **Relative difference** | 0.0% | 0.6% | 1.7% | 2.3% | 2.5% |

This summary table confirms that the power draw and energy consumed by the operating mill remain reasonably constant as ball size is increased; this makes sense because fundamentally there is no

change to the total ball load weight or mill speed. Regarding the marginal increase in overall collision energy, this supports the assumption that bigger balls are released from the lifter at the same point (or earlier) than smaller balls. If top size balls were consistently released at a higher shoulder angle, this would indeed result in a significantly higher power draw.

Although there is minimal increase in the overall collision energy, there is a significant ***redistribution*** of the different types of collisions when using a larger top size ball. EDEM simulations define five types of collisions as follows (listed with decreasing energy):

1. Rock-on-rock (representing autogenous abrasion/attrition breakage).
2. Ball-on-rock (representing some impact breakage).
3. Ball-on-ball (representing some impact breakage).
4. Rock-on-liner (representing autogenous impact breakage).
5. Ball-on-liner (representing undesirable liner wear and breakage).

As expected in SAG milling, autogenous rock-on-rock breakage generally represents >50 per cent of the total collision energy while rock-on-liner breakage is much smaller at <5 per cent. It is important to note that although the energy involved in these collision types represents more than half of the total energy, they remain unaffected by the ball top size.

The three types of collisions involving balls are the important ones to consider in detail; understanding the redistribution of the collision energy resulting from a larger ball top size is the key to appreciating the healthy increases in desirable rock breakage and the decrease in undesirable liner collisions.

## Ball-on-rock collision energy

In SAG milling using balls of any size, ball-on-rock collision energy generally represents rock breakage in the toe region and defines the balls and rock that are lifted higher and over the rotating kidney; generally, these balls and rock have a higher trajectory as they cascade and cataract towards the toe region. In the toe region, there is a much wider range of interactions between balls and rocks of all sizes, primarily due to the characteristic maximal chaos. When a ball or rock enters this region, it undergoes a massive change in direction in a very brief period, and this near-instantaneous event defines its position (and velocity) relative to the centre of mass (CoM) for the upward journey.

In the toe region, higher velocity results in higher collision energy events, and this is true impact breakage; clearly ball size makes a significant difference in this region. The ball-on-rock collision energy increases from 150 kJ to 163 kJ with increasing ball size in these simulations as shown in Table 4.

**TABLE 4**

Ball-on-rock collision energy calculations.

| **Ball size (mm)** | 127 | 140 | 152 | 160 | 165 |
|---|---|---|---|---|---|
| **Ball-on-rock collision energy (kJ)** | 150 | 152 | 156 | 160 | 163 |
| **Relative difference** | 0% | 1% | 4% | 7% | 9% |

The increases in ball-on-rock collision energy with increasing ball size supports the assumption that balls and rock are interacting with maximum velocity and are generating the maximum rock breakage rate. This aligns perfectly with the ball drop test work described earlier and the increased generation of finer particles that feed into the rotating kidney.

## Ball-on-ball collision energy

Ball-on-ball collision energy generally represents rock breakage within the rotating kidney of the total mill load with a relatively narrow range of interactions between balls and rocks of all sizes. The kidney

can be considered as a confined space with interacting layers of balls and rock rotating around the CoM. The tumbling mass of the mill load is so chaotic and interactive that there is no opportunity for layers to be arranged by size or weight (such as within cyclone classifiers); instead, the main sorting mechanism is velocity. With each rotation, the velocity of any given rock particle or ball within the kidney is a function of when it is released from the lifter, and this determines which layer it reports to around the CoM. The earlier the release, the closer to the CoM and the lower the velocity. Further, lower velocity and proximity to the CoM results in higher compression forces, and this is true abrasion breakage; it seems likely that ball size doesn't play any role in this region close to the CoM. However, further from the CoM in the outer layers of the rotating kidney with higher velocity, a portion of the abrasion breakage is replaced by low-level impacting events, and this is where ball size begins to make a difference.

The ball-on-ball collision energy increases from 95 kJ to 110 kJ with increasing ball size in these simulations, representing the most significant change in healthy rock breakage as shown in Table 5.

**TABLE 5**

Ball-on-ball collision energy calculations.

| **Ball size (mm)** | 127 | 140 | 152 | 160 | 165 |
|---|---|---|---|---|---|
| **Ball-on-ball collision energy (kJ)** | 95 | 101 | 106 | 108 | 110 |
| **Relative difference** | 0% | 6% | 12% | 14% | 16% |

The large increases in ball-on-ball collision energy with increasing ball size supports the assumption that balls and rock are interacting with higher energy despite little movement unless (within the chaos of the next rotation) there is a shift to the outer layers where ball size has some influence.

## Ball-on-liner collision energy

Ball-on-liner collision energy is specific to the situation of a ball directly impacting a shell liner or discharge grate. In such a case, a ball of any size is released very late from the lifters and has a maximum trajectory and cataracting from shoulder to toe.

The ball-on-liner collision energy decreases from 22 kJ to 8 kJ with increasing ball size in these simulations as shown in Table 6.

**TABLE 6**

Ball-on-liner collision energy calculations.

| **Ball size (mm)** | 127 | 140 | 152 | 160 | 165 |
|---|---|---|---|---|---|
| **Ball-on-liner collision energy (kJ)** | 22 | 20 | 19 | 9 | 8 |
| **Relative difference** | 0% | -9% | -14% | -59% | -64% |

The significant decrease in ball-on-liner collision energy with increasing ball size supports the assumption that bigger balls are generally released from the lifter earlier. It also makes sense that if the total collision energy is held reasonably constant and the other forms of collision energy increase, there must be a decrease somewhere. Finally, it is critical to note that although such collisions represent the smallest portion of the overall collision energy (2–3 per cent), with any ball size there will inevitably be process disturbances creating mill grind-out events, and if sustained for extended periods with excessive mill speed, can be catastrophic – especially considering the largest ball size. However, the simulation data shows that a larger ball top size decreases the risk of such sustained events.

## Simulation collision summary

A chart representing the three collision types involving increasing ball size is shown in Figure 5.

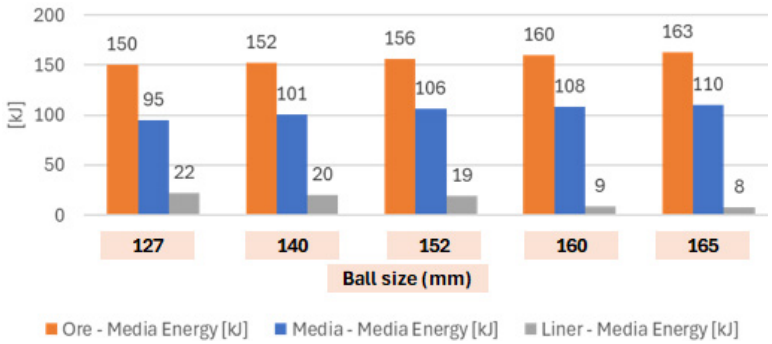



**FIG 5** – Magnitude of each ball related collision energy type from the simulations.

The redistribution of the different types of collisions with increasing ball top size is clear in this chart. There are healthy increases in the desirable abrasion and impact breakage and a decrease in the undesirable collisions that can cause liner wear and breakage if sustained over extended periods.

## Ball consumption

One of the most significant costs in SAG milling is media consumption. The physical characteristics of the ball load with any given ball top size can be calculated; this includes the following variables:

- Total ball charge surface area ($m^2$).
- Ball consumption rates (g/t, g/kWh, t/d).
- The life cycle of each ball (months).

In the case of the 28 ft × 14 ft SAG mill for this simulation, the standard operating variables (Jb = 18 per cent, Jc = 28 per cent, grate slot = 75 mm, 1000 t/h, 4 MW) were used to populate Table 7 as shown.

**TABLE 7**

Ball charge characteristics for a 28 ft × 14 ft SAG mill with increasing ball size.

| Ball size (mm) | Surface area ($m^2$) | Wear rate (g/t) | Wear rate (g/kWh) | Wear rate (t/d) | Time for top size to reject size (months) |
|---|---|---|---|---|---|
| 127 | 1501 | 292 | 73 | 7.0 | 1.8 |
| 140 | 1392 | 254 | 64 | 6.1 | 2.3 |
| 152 | 1295 | 227 | 57 | 5.4 | 2.7 |
| 160 | 1251 | 216 | 54 | 5.2 | 2.9 |
| 165 | 1209 | 206 | 51 | 4.9 | 3.2 |

The linear (or superficial) theory of ball wear considers that the consumption rate should be proportional to the total surface area of the ball load. As the ball top size increases, the actual number of balls decreases, and the total surface area decreases (even though the ball top size has a larger surface area). Ball consumption and scrap rates decrease significantly, and the life cycle of each ball is extended.

# INDUSTRIAL RESULTS OF LARGER TOP SIZE GRINDING MEDIA

Each of the following case studies represents a SAG mill operation that has changed to a larger ball size. ME Elecmetal has many customers operating a wide variety of grinding mills under various

configurations, and therefore the Grinding Media Applications Team has the privilege of access to an extensive database. All sites will remain anonymous. For simplicity, mill dimensions are in feet and media sizes will be consistent in millimetres.

## Case study 1

This operation has two parallel trains, each with a 40 ft × 26 ft SAG mill with a 28 MW reversible drive. The plant was commissioned with 125 mm media, and during this period the SAG1 and SAG2 monthly data points indicate feed rates generally below 3000 t/h (as can be seen in Figure 6 in the data points to the left).

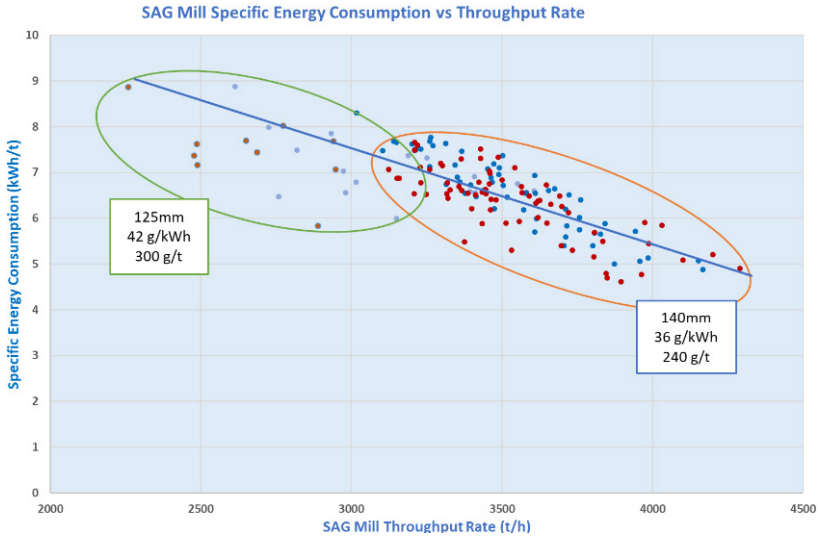



**FIG 6** – Two 40 ft SAG mills transition from 125 mm to 140 mm media.

The introduction of 140 mm media has been one of the key factors of the improvement in milling performance as larger balls enable a wider range of operation, especially the ability to accommodate changes in feed characteristics including ore hardness and feed size due to secondary crushing availability. The benefits of the change in SAG media top size can clearly be seen by the data points on the right side of the chart. The media and specific energy consumption have also decreased significantly (~15 per cent) after transitioning to the 140 mm top size.

## Case study 2

This operation includes a 40 ft × 26 ft SAG mill with a 28 MW reversible drive. The data points towards the left represent the monthly average performance of the SAG mill with 125 mm media, and variations in mill performance are clear in Figure 7 as the SAG mill struggled to maintain the target feed rate with changes in ore conditions.

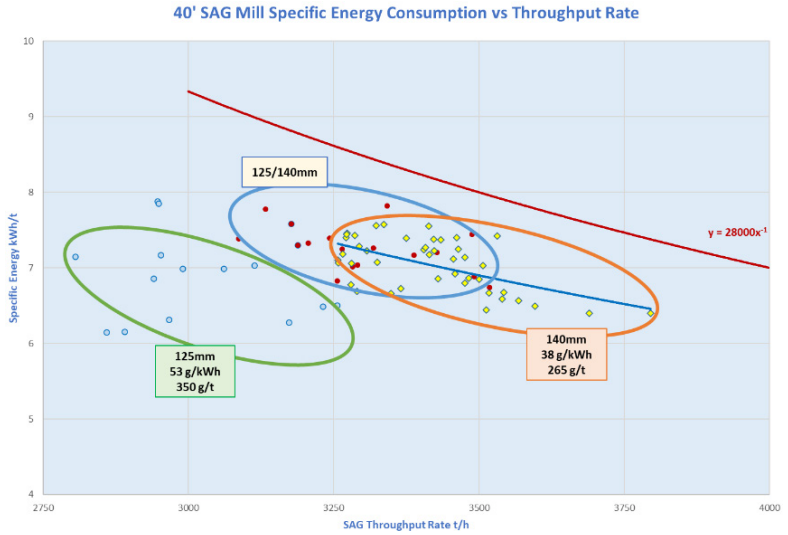



**FIG 7** – A 40 ft SAG mill transitions from 125 mm to 140 mm media.

The data points and trendline to the right represent the performance with a full transition to 140 mm media, which has resulted in improved and steadier mill performance. Data points in the middle section represent a transition period which was a risk mitigation step by the Plant Team. Media consumption figures are also included in Figure 5 and represent a 30 per cent decrease.

## Case study 3

This operation is a 28 ft × 13 ft SAG mill and is considered an extreme user of the largest available 160 mm ME Elecmetal SuperSAG balls in a relatively small mill. The SAG mill was commissioned using 125 mm media, continuing for about two years before making a transition to 160 mm, which had a significant positive impact on the throughput rate as shown in Figure 8.

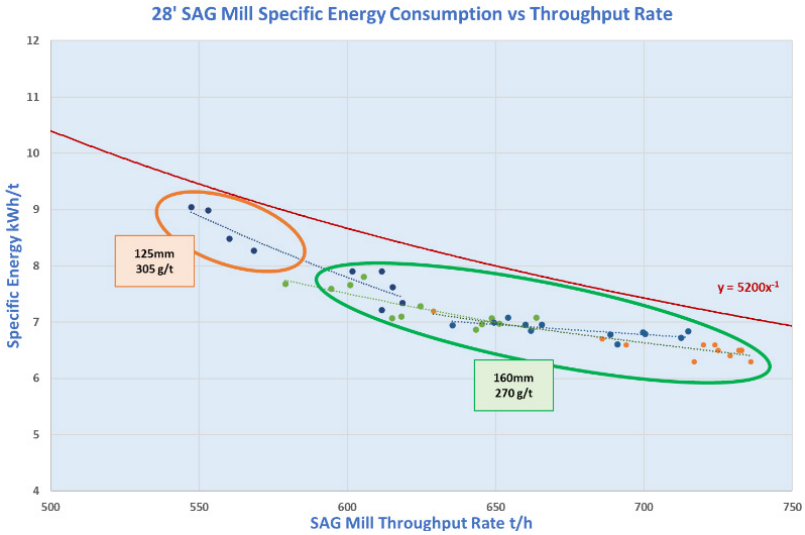



**FIG 8** – A 28 ft SAG mill transition between 125 mm and 160 mm media.

Note that there is minimal data for the 125 mm media period, but the four months to the left side of Figure 6 are considered representative of the entire two years in the 550 t/h to 570 t/h range. Furthermore, there was a definite progression of circuit improvements through optimising grate slot size, which fully utilise the increased rock breakage provided by the larger balls. The more recent data towards the right represents the next three years and clearly demonstrates a mature and consistently optimised operation.

## REINVENTING SAG MILL OPERATING STRATEGY

During the past several decades of SAG milling, mills have increased in size, throughput rates have increased, and ball loads have increased to the point where SAG mills resemble ball mills and BAG milling is a common reference. In addition, SAG mill operators are obsessed with precisely monitoring the ball load and generally attempting to increase ball loads as measurement reliability increases. In general, there are many risks involved with operating at the highest manageable ball:rock ratio with any given ball size.

This approach is understandable given smaller ball top sizes; the lower ball-on-rock and ball-on-ball collision energy means that the frequency of collisions becomes the key variable, and this is driven by the number of balls and the mill speed. However, this operating strategy also carries an increased risk of ball-on-liner collisions, and there have been an enormous number of cracked and broken shell liners and discharge grates resulting from sustained periods of mills operating at high speed in a grind-out condition.

The primary role of the SAG mill is to maintain the target plant feed rate at a transfer size suitable for the ball mills to in turn achieve and maintain the target product size. Larger top size balls make this easier to achieve and in addition drive a revised operational strategy where maintaining a precise ball load is not the priority; rather, the ball load and mill speed can be decreased while maintaining the same rock breakage rates. More specifically, process control strategies can be established to move towards the lowest possible ball load required to maintain the target feed rate and pebble production. Mill speed can also be decreased as a secondary consideration, while being maintained in the standard 75–78 per cent Cs range as often as possible, as it is known that all tumbling mills, regardless of size, generally operate most efficiently at speeds in this range. As with any transition in control strategy, it is critical to consider the entire grinding circuit and closely monitor the capacity of each unit operation.

Using this basic strategy, mill speed should be the priority for maintaining the target power draw rather than the ball load. In other words, larger balls should enable a SAG mill to operate at a safe speed at the target feed rate, with a lower ball load. Process control strategy can be modified significantly to continuously search for the lowest ball load that provides the rock breakage required to maintain the feed rate while controlling pebble production. Larger SAG balls can also drive mill speeds below 75 per cent Cs that results in a larger rotating kidney, however while this reduces the chaos (more abrasion, less impact), it increases pebble production and the opportunity for deformed media. Exceptions to this strategy would be during the first few weeks of the liner campaign when a reduced speed is sensible; another would be for SAG mills processing ores with very little resistance to breakage, in which case the mill is more of a pump than a grinding mill.

### Comminution energy curves

Comminution energy curves have been developed by Ballantyne (2019) to illustrate the benefit of benchmarking the energy intensity of comminution circuits. However, the difference in the energy is only made obvious when the ancillary and embodied energy directly related to grinding media is included, and this is significant for any operating plant attempting to reduce the carbon footprint. A case study involving a plant that has moved from AG to SAG to BAG milling is shown in Figure 9.

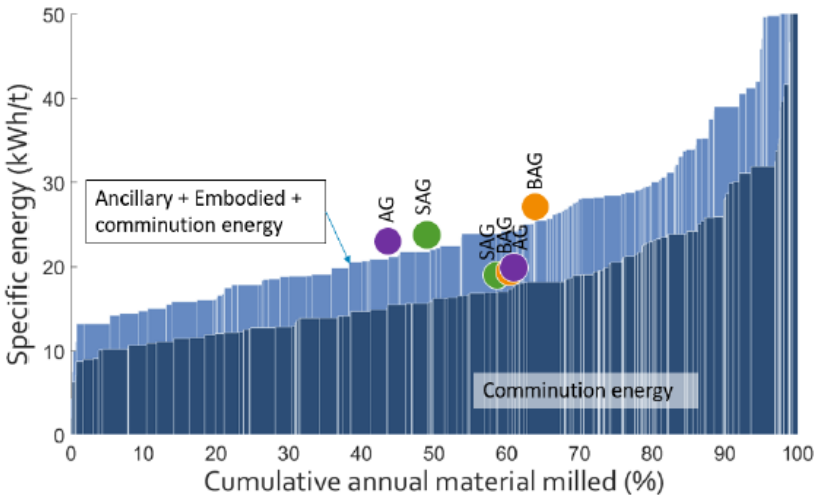



**FIG 9** – Progression from AG to SAG to BAG milling on the comminution energy curves with ancillary and embodied energy included (Ballantyne, 2019).

The data points above the comminution energy curves (in dark blue) indicate that transitioning from AG to BAG did not significantly alter the specific energy of the circuit when looking solely at the comminution equipment. However, accounting for the ancillary and embodied energy associated with grinding media gives the extended energy curves (in light blue) and the transition from AG to SAG to BAG results in significant increases in comminution specific energy. The key message here is that BAG milling comes at a significant cost (OPEX and carbon footprint) and a trend back towards SAG milling – enabled by a larger media top size – is very sensible.

## Continuous improvement projects

From a Continuous Improvement (CI) view, any project pipeline can be prioritised using an ***Impact versus Effort matrix*** (Six Sigma Development Solutions, Inc, 2024). Projects such as upgrading primary and pebble crushing circuits, installing secondary crushing, or changing grinding circuit configuration may have enormous value (impact), but come at an enormous cost (effort). Other projects such as optimising liner design through seemingly endless plant trials or installing the latest process monitoring instrumentation potentially have high value but at a high cost in terms of time consumed.

Comparing such projects to a trial of larger SAG balls, we have the likely outcome of very high value (especially if the fresh feed rate is increased) with zero additional cost and minimal effort outside of the standard plant team activities. Other CI initiatives such as increasing SAG ball loads or increasing mill speed (beyond 78 per cent Cs) have been common; while such projects also require minimal effort and have small cost increases, they have risk and may eventually result in lost operating time due to unplanned equipment failures.

SAG mill operators and designers can also discard the belief that the ball top size is determined by the feed size. This applies only to ball milling circuits where the process of managing the transfer size to product size may require a specific ball size (or blend of ball sizes). Larger SAG balls can certainly manage a larger feed size at higher rates, but larger balls will also have benefits with smaller feed sizes, and the opportunity for decreasing ball load and mill speed are more pronounced in such conditions.

Finally, as ore sources progressively become harder (lower Axb), the benefits of larger SAG balls become more measurable (fresh feed t/h, SEC kWh/t, pebble t/h). But again, even with softer ores larger balls will have benefits, especially in terms of the opportunity for decreasing ball loads and media consumption; in such cases higher mill speeds are required to maintain higher pumping rates.

# GRINDING MEDIA QUALITY

It is essential that media quality is maintained as balls become larger. It is well-known in steel metallurgy that manufacturing of reliable larger balls is much more challenging than smaller balls.

Balls that break apart under severe operating conditions will be extremely counter-productive to maintaining target feed rates and pebble production. There are several components to achieving the highest possible ball quality, but the more important ones are:

- Premium raw steel bar chemistry for optimal microstructure.
- Multiple methods for extracting undesirable gas inclusions from the raw steel bar.
- Forging and shaping steps to maximise sphericity and eliminate flat poles.
- Precise and consistent heat treatment.

As with cracked liners and grates, there have been an enormous number of occasions of mass ball breakage under severe SAG milling conditions. While ball breakage after being rejected can be considered acceptable (unless SAG balls are recovered to become ball mill media), breakage within the mill is likely to be catastrophic when excessive grate slot pegging affects the slurry transport through the mill and the fresh feed rate.

## CONCLUSIONS

Larger SAG media enables a wider operating range so the mill that can accommodate a larger range of ore characteristics while maintaining the target feed rate and operational performance. While the benefits may be easily measurable in a SAG mill constrained circuit, it is also true that the benefits can be achieved in a circuit that is ball mill limited; the same amount of grinding work can be accomplished with a lower SAG ball load. Larger SAG ball top size supports the ideal SABC circuit conditions whereby the plant is SAG mill constrained half the time and ball mill constrained for the other half.

Ball drop test work clearly demonstrates that a larger ball will create increased rock breakage (a decreased $P_{80}$ size) with any given drop height within the mill and this can be translated directly to actual SAG mill operation. Given that larger balls reduce the $P_{80}$ size through impacting at any given drop height within the mill, the concurrent finer grinding within the rotating kidney should be more efficient.

Simulations indicate that as the ball top size increases, there is increasing diversity within the charge that ultimately enables the mill to develop a wider operating range and greater stability. This diversity results in healthy increases in the desirable abrasion and impact breakage and a decrease in the undesirable collisions that can cause liner wear and breakage if sustained over extended periods.

Industrial case studies reveal that SAG milling operations have benefited from using a larger top size ball. Such benefits include an increase in feed rate or a decrease in pebble production, but there will always be an increased range of operation and improved accommodation of variable ore conditions. At a minimum, larger balls of premium quality will result in lower media consumption with all else held constant.

Any new equipment, circuit configuration, or consumable trial must be accompanied by a thorough change management process. Plant Operations personnel must be aware that the internal characteristics of the mill will change; it is simply a matter of how much. The same operational risks involving unexpected grind-outs and maintaining a safe mill rock load remain in place.

Mass manufacturing of reliable larger balls is much more challenging than smaller balls. It is essential that media quality is maintained as balls that break apart under severe operating conditions will be extremely counter-productive to maintaining target feed rates and pebble production.

Final note: In mineral processing we can rarely prove anything beyond any doubt. Grinding circuits are messy and chaotic, full of transient and random events, and our understanding is continuously evolving. The best we can hope for is to reduce uncertainty. An industrial trial involving a grinding mill can only increase or decrease confidence in the probability that our expectations are truly supported or not. But we can be sure of some things, such as the basic fact that ball consumption is correlated with ball surface area; thus, at the very least using a larger ball size will decrease media consumption.

# REFERENCES

Ballantyne, G, 2019. Quantifying the Additional Energy Consumed by Ancillary Equipment and Embodied in Grinding Media in Comminution Circuits, in Proceedings of the 7th International Conference on SAG and HPGR Technology 2019 (SAG Conference Award Foundation).

Doll, A and Tischler, K, 2015. The Engineering and Process Effects of Choosing a Motor Design Speed, in Proceedings of the 6th International Conference on SAG and HPGR Technology 2015 (SAG Conference Award Foundation).

Lane, G, 2007. Some Observations about SAG milling, in Proceedings of the Ninth Mill Operators' Conference (The Australasian Institute of Mining and Metallurgy: Melbourne).

Six Sigma Development Solutions, Inc, 2024. Impact Effort Matrix: Prioritize Projects with Our Simple Guide. Available from: <https://sixsigmadsi.com/what-is-an-impact-effort-matrix-how-does-it-work/>

Tavares, M, Rodriguez, V, Sousani, M, Padros, C and Ooi, J, 2021. An effective sphere-based model for breakage simulation in DEM, Federal University of Rio de Janeiro, Brazil.

# Modernising SAG mill performance – hybrid liners for enhanced efficiency and reliability

*J Giron[1], V Grover[2] and E Mori[3]*

1. Global Comminution Manager, Tega Industries, Panama City, Panama. Email: jennifer.giron@tegaindustries.com
2. Global Business Head, Tega Industries, Sudbury, Canada. Email: vinay.grover@tegaindustries.com
3. Senior Manager Mill, Tega Industries, Santiago, Chile. Email: ernesto.mori@tegaindustries.cl

## ABSTRACT

The performance of semi-autogenous grinding (SAG) mills is strongly influenced by liner design, which must enable rapid start-up while delivering sustained durability under high-demand operating conditions. Conventional steel liners, while proven in durability, impose limitations due to their heavier weight, resulting in elevated mechanical stress on mill components and constrained ramp-up strategies. These factors often lead to delayed achievement of target throughput and reduced operational flexibility. This paper evaluates the impact of converting from all-steel to hybrid liners on 36-ft-diameter SAG mills at two mine sites, one in Chile and one in Australia, focusing on start-up behaviour, mechanical response, and long-term production outcomes. Hybrid liners offer a reduced weight profile and a simplified installation process, which collectively lower structural stress on the mill and support higher mill speeds earlier in the commissioning phase. This enables a faster, more controlled ramp-up to full capacity without compromising safety or reliability. Operational monitoring confirmed that hybrid liners facilitated improved charge motion, reduced shell impact, and enhanced grinding efficiency. Mechanical monitoring indicated lower vibration levels and reduced stress on critical components such as bearings and drive systems. Additionally, hybrid liners demonstrated increased wear life and reduced downtime due to faster change-outs, contributing to improved mill availability and decreased maintenance demands. The findings highlight the potential of hybrid liners as a next-generation solution for large SAG mills. By supporting both early ramp-up performance and sustained high-throughput operation, hybrid liners offer a durable, adaptable alternative to traditional steel configurations in modern demanding grinding environments.

## INTRODUCTION

Semi-autogenous grinding (SAG) mills are integral components of mineral processing operations and serve as one of the primary stages of size reduction in numerous concentrator circuits. Their performance is a critical factor that directly influences overall plant throughput, energy efficiency, and metal recovery rate. Therefore, the optimisation of SAG mill operations is of major importance in mineral processing plants and has significant implications for productivity and profitability.

A particularly challenging aspect of SAG mill operation is the ramp-up phase following liner replacement. This phase involves a complex balance between protecting equipment and meeting production targets. The standard industry practice involves operating the mill at a reduced speed, typically around 66 per cent critical, after a liner change-out, before gradually increasing to the target operating speed (78–80 per cent critical). This conservative approach has been historically adopted to protect new liners from excessive impact loading and premature failure during the initial break-in period.

However, this cautious ramp-up process often results in substantial production losses, averaging approximately 5 per cent during the initial days or weeks of operation. This represents a significant opportunity cost for mining operations, highlighting the need for more optimised ramp-up strategies that can minimise downtime while ensuring equipment reliability.

The ramp-up phase is a critical period in which operators must carefully manage the trade-off between safeguarding liner integrity and maintaining production targets. Operating below the design speed reduces the impact energy and grinding efficiency, leading to decreased breakage rates and lower throughputs. This suboptimal performance can have cascading effects throughout the processing circuit, potentially affecting downstream processes and overall plant efficiency.

Conversely, accelerating the ramp-up too quickly can impose high-impact stresses on liner components and bolts before sufficient wear patterns are developed. This aggressive approach increases the risk of fatigue cracking, liner displacement, and localised damage. Such premature wear or failure of the liners can lead to unscheduled downtime, costly repairs, and potential safety hazards, emphasising the importance of a well-balanced ramp-up strategy to prevent these issues.

This paper examines the influence of SAG mill speed ramp-up following liner replacement on production performance and liner integrity. It describes the operational reasoning behind conservative start-up practices, exploring the historical context and risk-averse approaches that dominate the industry. This study also compares the behaviour of steel and Tega's hybrid liner systems under different ramp-up conditions, providing valuable insights into the performance characteristics of various liner materials and designs.

The analysis presented in this paper is based on a rich data set of operational data collected from 2022 to 2025 for a 36 ft diameter SAG mill in a Chilean copper operation. This extensive time frame allowed observation of multiple liner change-out cycles, providing a robust foundation for drawing meaningful conclusions. Key performance indicators, such as throughput, power draw, liner wear rates, and grinding efficiency for different ramp-up scenarios were examined. Furthermore, key considerations and opportunities for improving ramp-up methodologies are highlighted. This explores innovative approaches to monitoring and control during the ramp-up phase, including the use of advanced sensors and real-time data analytics to optimise processes.

Lastly, this paper also explores the economic implications of different ramp-up strategies by considering factors such as production losses, energy consumption, and maintenance.

## KEY MATERIAL PROPERTIES GOVERNING LINER PERFORMANCE

The performance and duration of SAG mill liners are strongly governed by the properties of their materials of manufacture. Among these, wear resistance is one of the most critical attributes, directly influencing liner service life and frequency of replacement. Materials with superior wear resistance can substantially extend the operating period between maintenance shutdowns, thereby improving mill availability and reducing maintenance costs.

Equally important are toughness and impact resistance, which determine the ability to withstand repeated high-energy impacts without cracking or deforming. These characteristics are typically quantified using Charpy impact tests or fracture toughness measurements. High toughness is especially vital in regions of the mill where large ore fragments or grinding media impose substantial impact forces (very commonly seen towards the discharge end of the shell, as grinding media movement is augmented by grate lifter design). In such areas, materials with an optimal combination of strength and ductility help maintain liner integrity and ensure operational safety.

Another important aspect of liner performance is material fatigue and creep resistance. Continuous exposure to cyclic stresses during mill operation can lead to fatigue damage, whereas elevated temperatures can induce creep deformation in susceptible materials. Fatigue resistance is particularly relevant in zones of high mechanical loading, whereas creep resistance is crucial for mills operating under thermally demanding conditions. Maintaining structural stability under these combined effects ensures the reliability and durability of the liner system over an extended period.

Hardness, another key material property, defines the resistance of a liner to indentation and deformation. Although increased hardness typically correlates with improved wear resistance, it must be balanced with adequate toughness to prevent brittle fracture under impact conditions. The elastic modulus of the liner material also contributes to mechanical performance, influencing its ability to deform elastically under load and recover when the stress is removed. Materials with appropriate elastic characteristics can absorb and distribute impact forces more effectively, thereby reducing localised wear and extending liner life.

Finally, corrosion resistance is a decisive factor in operations where ore or process water contain corrosive agents (or by reagents addition to the mill). Some chemicals can accelerate material degradation and lead to premature liner failure if not properly mitigated. Selecting materials or coatings with high corrosion resistance helps ensure consistent performance.

These properties must be carefully balanced to optimise the performance and longevity of the liners. The ideal combination of properties often varies depending on the specific operational conditions and ore characteristics. For example, a mill processing highly abrasive ore might prioritise wear resistance and hardness, whereas a mill processing large, competent ore particles might place greater emphasis on impact resistance and toughness.

## MATERIALS FAILURE MECHANISM

An understanding of the metallurgical characteristics of liners materials is essential for interpreting their mechanical behaviour and failure mechanisms. A brief discussion comparing steel and composite liners follows.

Conventional cast steel liners typically exhibit a pearlitic microstructure and contain medium carbon levels (0.5–0.6 per cent C), with alloying additions of chromium (2.0–2.5 per cent Cr) and nickel (0.3–0.4 per cent Ni). These liners generally possess a surface hardness of 300–330 Brinell hardness number (BHN), which gradually decreases toward the core owing to cooling-rate variations during solidification. Under repeated impact loadings, the pearlitic structure undergoes plastic deformation and strain hardening, resulting in an increase in the surface hardness to approximately 450–460 BHN during service. However, this work-hardening effect is often accompanied by the formation of microcracks, which can propagate under cyclic stresses as shown in Figure 1, ultimately compromising the structural integrity and service life of the liner.



**FIG 1 –** Peening pattern developed from repeated impact, left, versus developed cracks after weeks, right.

In contrast, the abrasion-resistant (AR) steel used in hybrid liners is engineered with a martensitic microstructure and is produced from a low-carbon, low-alloy steel system containing chromium, nickel, and molybdenum, with minor additions of titanium and vanadium. Through thermomechanical processing, fine austenitic grains are generated prior to quenching, which leads to improved toughness and resistance to crack initiation. The resulting tempered martensitic microstructure exhibits a uniform hardness in the range of 450–600 BHN throughout the liner, maintaining consistent mechanical properties over the entire service life. Table 1 summarises the comparison of the main physical and chemical properties of steel and composite liners.

Unlike conventional cast steel, AR steel used in hybrids does not undergo significant work-hardening during operation, as it is manufactured to achieve its maximum hardness from the outset. This stable and homogeneous hardness, combined with enhanced toughness and high tolerance to plastic deformation, provides greater resistance to impact fatigue and abrasive wear.

**TABLE 1**

Physicochemical properties comparison between steel and hybrid liners.

| Properties | Steel medium cast carbon alloy Cr/Mo | Laminated low carbon alloy steel Cr/Mo/Ni/others |
|---|---|---|
| Chemical composition | 0.55 to 0.8% Carbon | 0.3 maximum Carbon |
| Surface hardness | 370 BHN maximum | 400–540 BHN |
| Volume hardness | 265 to 340 BHN | 400–540 BHN |
| Manufacturing defects | Shrinkage cavity, slag, oxides, cracks | Minor oxide defects |
| Non-metallic inclusions | High MnS(FeO) | Low globular oxides and Mn sulfur |
| Microstructure | Perlite, some bainite | Mainly martensite |
| Impact toughness with room temperature notch | $10^{-3}$ joule | Over 80 Joules |
| Impact toughness without notch at room temperature | $150^{-5}$ joule | Over 250 Joules |
| Impact toughness without notch at -40°C -40°C | <5 Joule | >30 Joules |

## FACTORS INFLUENCING SPEED OF RAMP-UP

Several factors may influence the speed at which the mill can be ramped up:

- Feed ore characteristics: the physical properties of the materials being processed, including hardness, size distribution, and moisture content. Variations in ore characteristics may require adjustments in processing speed and feed water addition to maintain operating efficiency:
    - Hardness and abrasiveness: ore hardness affects the amount of energy required to break particles. Harder ores generally require more energy, which can affect the efficiency of the SAG mill. If the ore is too hard, it can slow down the ramp-up process as more time and energy are required to achieve target product size.
    - Particle size distribution: a SAG mill requires the full range of feed size distribution for balanced performance; too many coarse materials in feed will require increased residence time in the mill which translates to reduced mill speed to allow for further grinding. Too fine material on the other side allows for easier ore passage through the mill, with solids flushing out the mill faster and risking increased impact on liners by the grinding media.
- Viscosity and pulp density variations in the ore can alter rheology, influencing slurry flow in the mill and affecting the ability of the mill to ramp up efficiently. High viscosity can hinder movement and increase energy consumption. A good example is ‘clayey’ ore, which tends to absorb high amounts of water and stick to the liners, having a similar effect to a centrifuge, affecting the grinding process and wasting power.
- Mill design and mechanical condition: the overall design of the mill, including liners, lifters, grates and the interaction among these components, affects the ability of the mill to handle high speeds. Regular maintenance ensures that mechanical wear does not hinder the safe acceleration of the mill.
- Liner wear patterns: different liner materials wear differently based on the speed of operation. For instance, liners operating predominantly in cascade mode at lower speed experience more abrasive wear, whereas at higher speed the impact becomes more pronounced. Higher speeds tend to increase impact forces in the mill, which may lead to greater wear and tear on the liners, necessitating the use of materials that can withstand such impacts. The liners must be chosen for their ability to endure both abrasive and impact wear, particularly at higher

operating speeds, where the dynamic forces are amplified (Beloglazov and Plaschinsky, 2024).

- Charge motion: the liner lifter height and face angle influence the motion of the charge in the mill. The cascade and cataract motion patterns are critical for efficient grinding. As speed increases, the charge is more likely to be lifted higher and fall back into the mill aggressively (cataracting). This can cause uneven liner wear. In such cases, hybrid materials with high impact resistance are preferable to accommodate the aggressive nature of the charge at high speeds (Cleary, 2019).
- Mill load and dynamics: liner component weight also affects ramp-up speed. Properly balanced load conditions with lighter liners can enhance stability and allow for smoother acceleration without excessive wear or stress on the mill structure and bearing system, particularly for aged equipment constrained by the maximum load, reduction in ore fragmentation, or available mill motor power.
- Variable frequency drives (VFDs): the use of advanced control systems, such as VFDs, can optimise the speed of mill rotation, further enhancing energy efficiency by ensuring that the mill operates at its optimal speed.
- Mill motor capabilities: the capacity and responsiveness of the mill motor also play vital roles. A powerful motor coupled with a reliable power supply ensures the mill can achieve the desired ramp-up speed efficiently without overloading the system.
- Control systems and automation: advanced control systems optimise mill speed settings based on real-time data, ensuring the mill operates under conditions that minimise power consumption while maximising throughput (Lopez *et al*, 2023).
- Discharge system design: crucial for controlling the flow of materials out of the mill. A well-designed discharge system can facilitate the smooth removal of material and prevent bottlenecks that could otherwise slow down the mill speed ramp-up. This is because efficient discharge reduces the load within the mill, allowing for a quicker acceleration to the desired operating speed. Moreover, the grates serve to control the size distribution of the materials (rocks and grinding media scats) that pass through, thereby influencing the overall efficiency and energy utilisation. By optimising grate design, it is possible to enhance the cataracting and cascading components of the flow, leading to more efficient energy utilisation that supports faster ramp-up speeds (Cleary, 2019; Lopez *et al*, 2023).

## CASE STUDY 1 – 36 FT DIAMETER SAG MILL, CHILE

The following case study concerns a 36 ft diameter SAG mill in a Chilean copper mine, processing an average of 2500 t/h and charged with 152 mm steel balls to levels between 18–20 per cent. The mill was previously equipped with steel liners and suffered repetitive unplanned downtime due to cracked plates and bolt-breakage. The operating practice after liner replacement involved cautious speed ramp-up (8.6 rev/min, 66 per cent critical speed) to avoid liner cracking and mitigate bolt failures, features that had been historically frequent under high impact at early speed increases. Typically, the mill took between 21 and 42 days to reach the nominal operating speed (70 per cent critical speed) following a reline, with an estimated loss of throughput between 3–5 per cent, and frequent downtimes with a cumulative yearly loss time of 50 hrs. This prolonged ramp-up period reflected the conservative operational limits imposed to safeguard the steel liner and bolted fixings. Early in each campaign, the speed changes were incremental, and the operators held back until confidence in liner stability was established. As a result of the slow ramp, the production throughput during the early days post-reline was well below target and the mill operated under sub-optimal conditions for several weeks, increasing the operating costs per tonne and contributing to lower overall campaign productivity.

### Conversion to Tega's hybrid (Dynaprime) liners and revised ramp-up practice

After the conversion to Tega's hybrid liners, the operators reported that mill behaviour during ramp-up changed markedly. The hybrid liner design provided impact damping, better resistance to

crack propagation, and reduced fatigue. This enabled a more aggressive ramp-up strategy. With hybrid liners in place, the mill typically reached full or near-nominal speed in about one week post-reline. Moreover, in a recent campaign started in September 2024, the mill attained its maximum speed (9.8 rev/min) on the second day after the restart. This sharply contrasts with the three to six weeks required for steel liners.

### *Considerations for faster ramp-up*

In preparing to adopt a more aggressive ramp-up protocol with Tega hybrid liners, the following listed considerations (pre-checks) were evaluated. These safeguards and preparatory steps were intended to manage risk, validate assumptions, and ensure that the mill and production, operators, and supporting systems were ready for a faster, safer approach.

- Feed ore competency: the projected feed ore characteristics (Axb and SAG Power Index, SPI) for the four weeks after reline were revised (Figure 2), and mitigation measures established in case of a sudden feed quality change.
- Feed ore size distribution: a well-blended feed aids to absorb impact energy, reducing the severity of ball-liner or ball-shell collisions. Thus, the operations team ensured that the feed gradation, crusher, and blast fragmentation outputs would not exacerbate the impact risk during the faster ramp.
- Ball filling measurements after liner replacement: immediately after relining, the team performed precise measurements of ball filling level inside the mill. This provides a baseline reference for any required adjustments during ramp progression and ensures that the charge behaves as per the modelling and simulations.
- Mill noise monitoring: microphone sensors mounted in proximity to known ball-strike zones provided continuous feedback and alerts on critical impacts. The monitoring system was programmed to flag abrupt rises in impact noise beyond the acceptable set point of 105 dB (considered a grind-out noise condition). Furthermore, regular monitoring rounds by site personnel every four hours provide backup checks.
- Mill load checks: another important consideration was the reduced mass of the Tega hybrid liner system relative to previous steel liners. Because the hybrid liners typically weigh less for an equivalent wear life, the internal mill mass was reduced. The site recognised an opportunity to slightly increase the ball and ore load to better utilise the installed motor power, converting more of it into effective grinding throughput in the early days of the campaign.
- Finite Element (FEA) and stress analyses assessing potential liner deformation under charge pressure indicated no operating risk, with no displacements observed in the fastening zones (bolts) as depicted in Figure 3. Additionally, stress analysis of the steel inserts was conducted to evaluate their performance under highly variable loading conditions, including the impact of oversized ore, grinding media wear, and fluctuations in mill throughput.

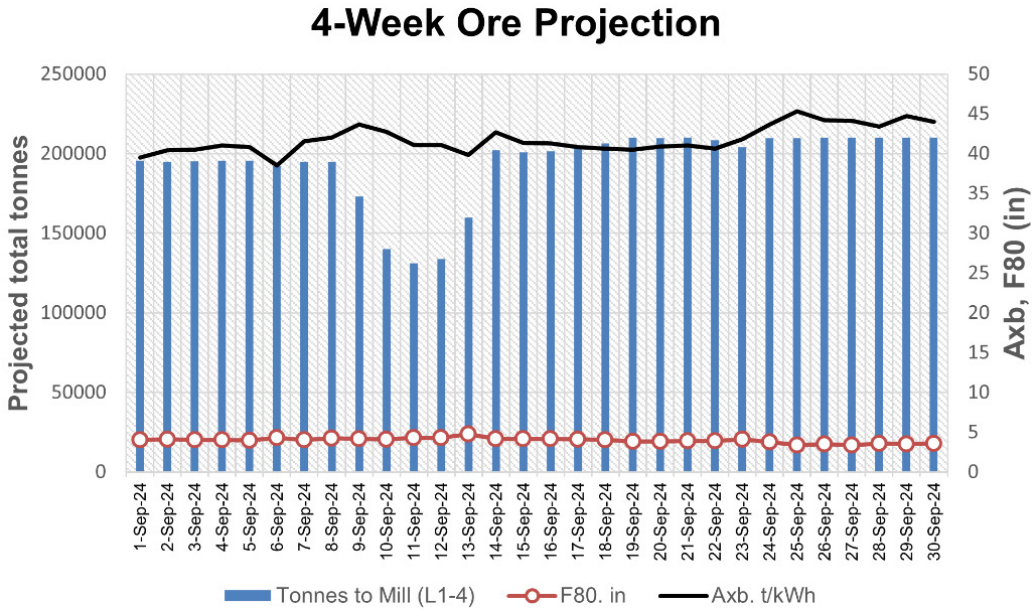



**FIG 2** – Sample of projected feed ore to SAG mill post-reline for a specific campaign.

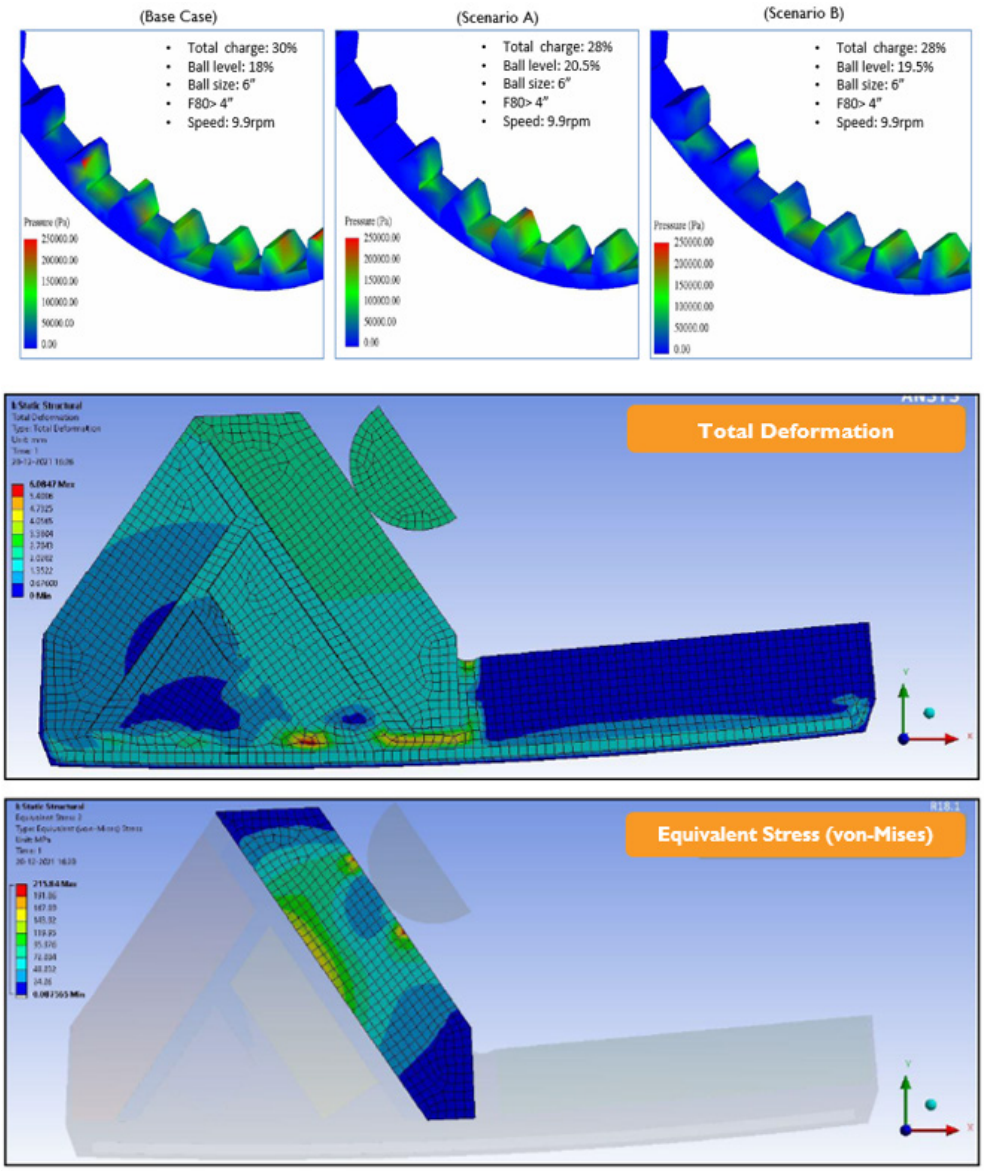



**FIG 3** – FEA analysis of liner deformation and stress.

These preparatory steps were key enablers to safely reducing the ramp-up duration while preserving liner integrity.

## Results and operational observations

Following the application of a faster speed ramp-up philosophy, several key operational improvements were observed in terms of mill performance, liner reliability, and energy efficiency.

### *Ramp-up duration*

A significant reduction in the ramp-up period was observed. Historically, the mill required between 21 and 42 days to reach nominal operating speed after a full reline with steel liners. After implementing the hybrid liners, the site registered a reduction in ramp-up time to approximately seven days, with one campaign reaching full speed as early as the second day after reline, as depicted in Figure 4. This accelerated ramp-up was achieved without compromising liner integrity.

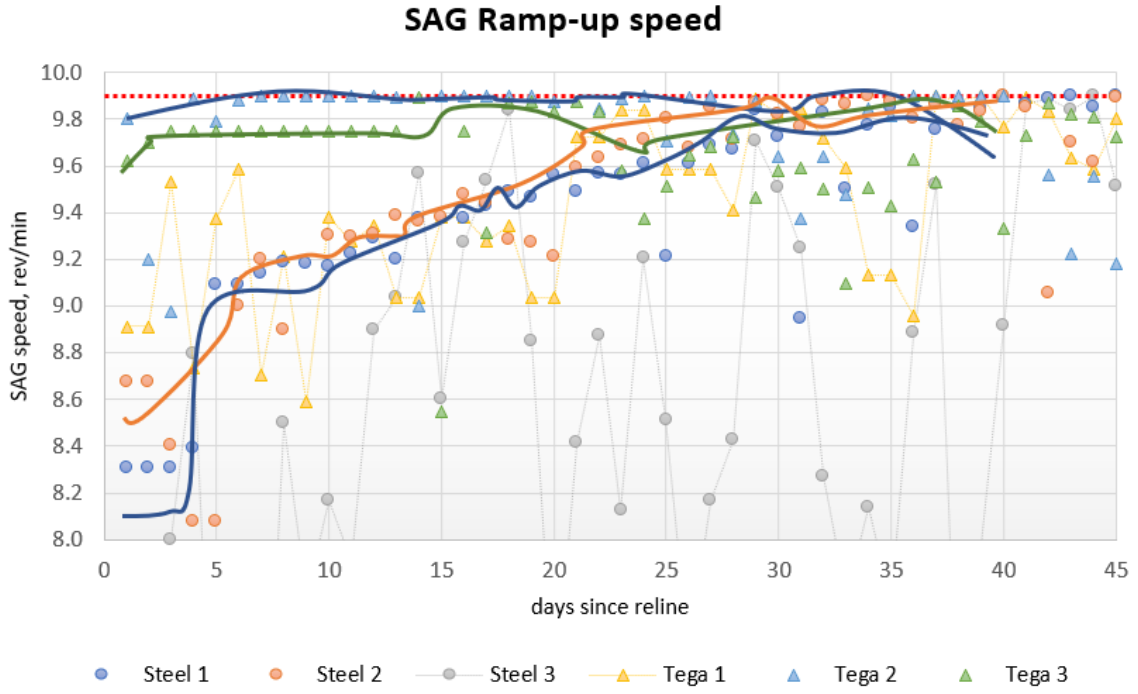



**FIG 4** – Comparison of ramp-up speeds by liner type.

### *Key performance indicators*

The operational data collected during different campaigns demonstrated improvements in several critical performance metrics of the system. As shown in the comparative Table 2, the mill feed rate increased by 6.8 per cent over the life of the campaign, rising from 2381 t/h with steel liners to 2542 t/h with Tega hybrid liners. This uplift was observed from the start-up and sustained throughout the liner life.

**TABLE 2**

KPI comparison steel versus Tega hybrids.

| Parameter | Steel | Tega hybrid | %Var. |
|---|---|---|---|
| Mill Rate, t/h | 2381 | 2542 | 6.8% |
| Speed, rev/min | 8.6 | 9.5–9.8 | 12.2% |
| Power draw, MW | 12 379 | 11 777 | -4.9% |
| SEC, kWh/t | 5.5 | 4.7 | -14.4% |
| %Solids | 71.6 | 74.1 | 3.5% |
| $F_{80}$, in | 3.8 | 4.0 | 5.1% |
| $P_{80}$, µm | 212 | 209 | -1.6% |
| Bearings pressure, kPa | 6199 | 5988 | -3.4% |
| Pebbles tph | 697 | 670 | -3.9% |
| Wi, kWh/t | 12.0 | 12.13 | 1.2% |

Another key metric was the specific energy consumption (SEC), which improved notably. The SEC dropped from 5.5 kWh/t to 4.7 kWh/t, a 14.4 per cent reduction. This indicated more efficient energy use per tonne of ore processed, suggesting improved grinding dynamics and power utilisation. In addition, the $F_{80}$ (feed size) increased from 76 to 101 mm (5.1 per cent), which implies that the mill handled coarser feed more effectively post-transition, further supporting the conclusion that Tega's hybrid liners enabled a more robust and resilient grinding performance. Figure 5 depicts a comparison of SEC by throughput ranges for steel liners versus hybrids.

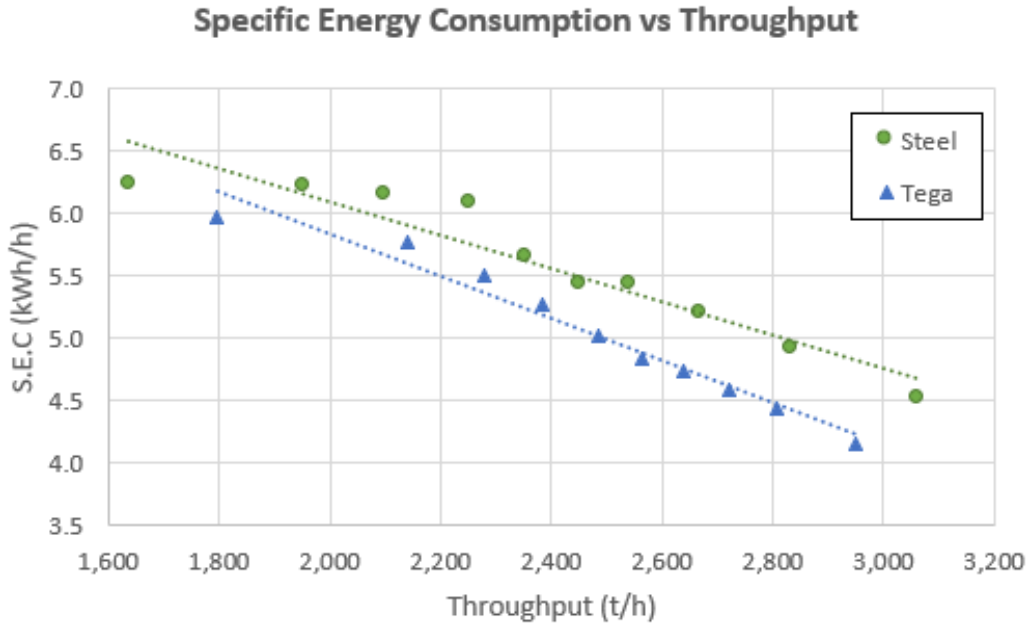



**FIG 5 –** SEC versus throughput, Tega hybrid versus steel.

Other operating parameters, such as the solid percentage and pad pressure, remained within the expected variations, and no significant adverse trends were noted. The mill speed increased from 8.6 rev/min to a range of 9.5–9.8 rev/min, aligning with the faster ramp-up strategy.

### *Acoustic monitoring*

The recorded mill noise levels were within the average range of 95–101 dB and did not indicate critical impact events. The hybrid liner system demonstrated stable acoustic behaviour, with no excessive spikes associated with ball-liner impacts.

### *Liner wear performance and reliability*

Following the implementation of a faster ramp-up speed in the SAG mill, the hybrid liners demonstrated improved wear performance and reliability. The liner life increased from 3356 to 4196 hrs, extending the interval between the relines. Furthermore, no displacement or debonding of the steel inserts was observed during the operating cycles. Likewise, no instances of liner cracking or bolt breakage were observed despite the more aggressive start-up conditions, and the unplanned loss time reduced from 50 hours per annum (h/a) to 4 h/a.

Post-installation inspections and continuous monitoring confirmed that the liners were mechanically sound for the duration of their operating life. The liner campaigns lasted 187 days on average, matching the performance expectations based on the wear modelling. Importantly, the accelerated start-up did not shorten liner life, indicating that the increased early speed and load did not adversely affect wear performance. Figure 6 illustrates hybrid liner condition during an inspection at end of service life.



**FIG 6 –** Mill inspection of hybrid liners at end of life.

For comparison, previous all-steel liner sets achieved an average service life of 130–140 days. With the introduction of hybrid liners, reline intervals have been extended to an average of 179.5 days, despite the projected life ranging from 188–206 days. This demonstrates that even under accelerated mill speeds, the hybrid liners maintain excellent wear resistance and mechanical stability, with reline timing continuing to be determined primarily by maintenance planning considerations rather than liner wear limitations. Table 3 summarises a detailed comparison of the production impacted between steel and Tega hybrids.

**TABLE 3**

Comparison of annual production – base case (steel) versus Tega hybrids.

| | Base case | Tega hybrids | Difference (Tega-base) |
|---|---|---|---|
| Liner life, hours | 3356 | 4196 | 840 |
| Liner life, months | 5.1 | 6.3 | 1.2 |
| Number of relines per annum | 2.6 | 2.1 | -0.5 |
| Longer shell liner life, % | 0 | 25% | 25 |
| Mill utilisation, % | 92 | 93 | 1.0 |
| Reline time (shell + heads), hours | 85 | 75 | -10 |
| Total reline time per annum, h/a | 222 | 157 | -65 |
| Mill rate, t/h | 2381 | 2542 | 161 |
| Mill rate, t/d | 52 572 | 56 737 | 4165 |
| Production loss due to corrective maintenance, h/a | 18.9 | 4 | -15 |
| Milled tonnage per annum, gross | 19 188 955 | 20 709 166 | 1 520 211 |
| Total loss time per annum | 241 | 161 | -80 |
| Loss time production, t | 573 251 | 408 173 | 165 078 |
| **Milled tonnage per annum** | **18 615 704** | **20 300 992** | **1 685 288** |

Plant data from 2022 to 2025 showed that Tega's Dynaprime liner:

- Reduced downtime frequency in each liner campaign, increased milled tonnage, and improved energy efficiency.
- Gave lower cumulative risk of liner damage and bolt failure during ramp-up owing to lower transmitted stress and better energy absorption and distribution by the hybrid liner.
- Allowed higher throughput earlier in the campaign, since speed could be increased sooner without waiting for safety margins or break-in periods to be proven over several days.

However, the transition also entailed certain prerequisites and required changes in execution:

- Monitoring and instrumentation: to safely accelerate the speed earlier, the operation had to rely on accurate and timely feedback on noise, impact loads, shell bolt strain, and liner behaviour.
- Engineering validation: finite element analysis, fatigue assessments, and impact simulations were performed to verify that the mill shell, liners, bolts, and supporting structure could tolerate the altered loading profile. The steel inserts and rubber bonding in Tega's hybrid liner were designed to avoid adiabatic shear failures or defects.
- Change management: operators and maintenance staff needed to shift from a deeply ingrained conservative mindset that 'slower ramp = safer operation' to one trusting the damping capacity and durability of the hybrid liner. This shift required data, trial runs, incremental steps, and adjustments to operational policies.
- Quality of liner manufacture: the effectiveness of the hybrid liner depends on consistent materials bonding, embedment, and arrangement of steel inserts, accurate geometry, and rubber properties.

## Liner endurance under increasing ore competency and aggressive mill conditions

Throughout the evaluation period, the SAG mill equipped with Tega's hybrid liners demonstrated consistent performance under changing and increasingly demanding ore. A key challenge faced by the operation was the progressive deterioration in ore grindability, which required both the liner system and milling strategy to adapt without compromising throughput.

From early 2023 to mid-2025, the ore processed by the SAG mill experienced a noticeable increase in competency, as indicated by a decrease in Axb values and an increase in SPI. Initially, the Axb values remained above 45, supporting throughput rates consistently above 2500 t/h. However, beginning in the third quarter of 2024, a distinct shift in ore characteristics was observed, with Axb values dropping to between 34 and 32, whereas the SPI increased from 59 to 80 mins. This change corresponded with a measurable decline in SAG mill throughput, with rates decreasing to between 2030 and 2190 t/h, as shown in Figure 7. The correlation between lower Axb and reduced mill rate was clear and consistent, highlighting the sensitivity of mill productivity to ore competency and the challenges to be addressed in terms of liner design.

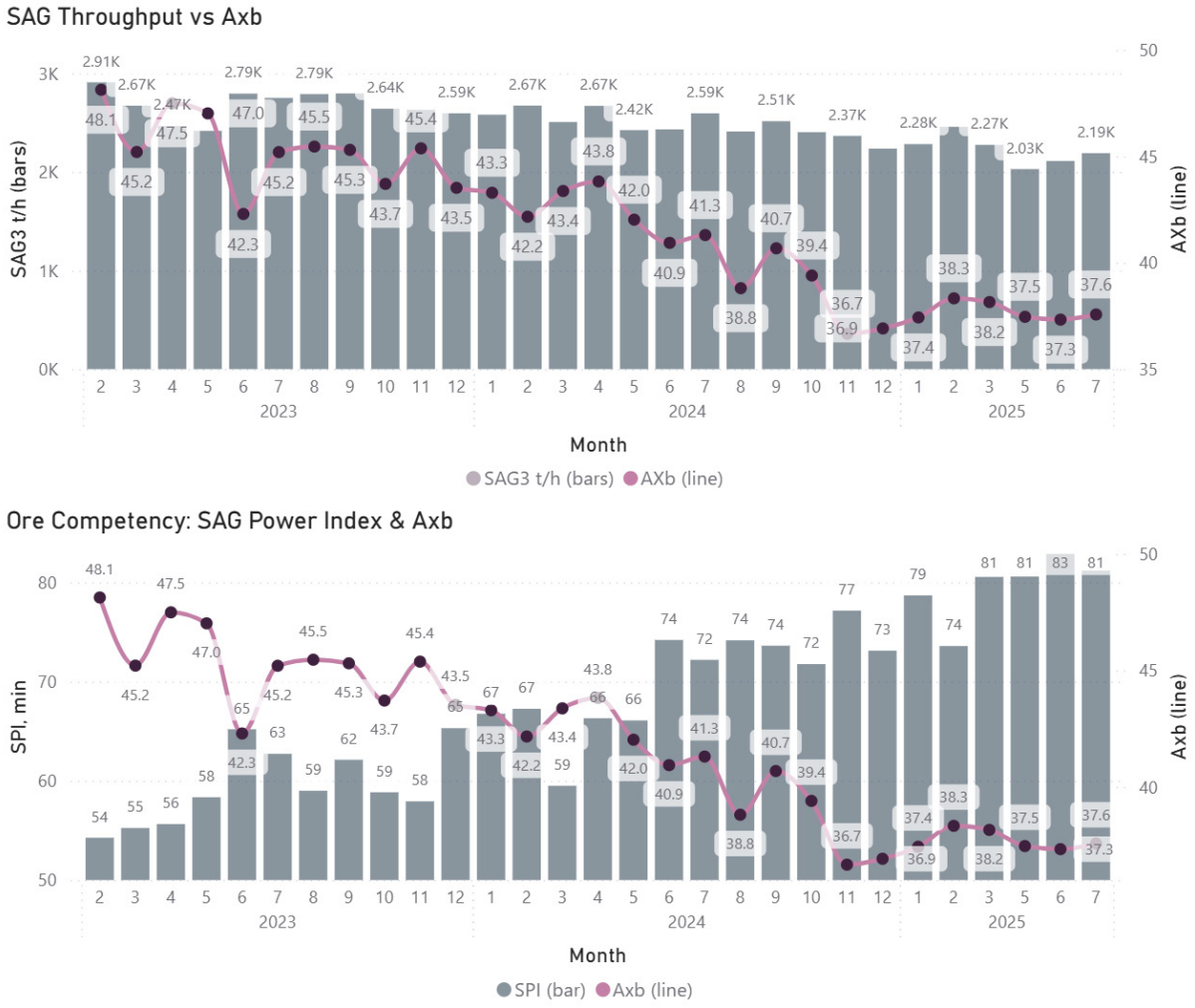



**FIG 7** – SAG throughput versus ore competency Axb and SPI.

## Operational response and strategic liner design adjustments

In response to the decrease in throughput driven by harder and coarser ore (frequently exceeding $F_{80}$ of 102 mm), site leadership initiated a set of planning and simulation exercises aimed at recovering performance. One key focus was to assess the capacity of the current liner configuration to withstand more aggressive milling conditions without sacrificing the liner. Discrete element method (DEM) simulations were performed to evaluate the liner endurance under a combination of the following intensified operating conditions (Figure 8):

- harder ore: characterised by Axb values consistently <35
- coarser feed: with incoming $F_{80}$>102 mm
- increased grinding media size: potential shift from 152 mm to 160 mm balls
- maximum allowable mill speed (9.8 rev/min).

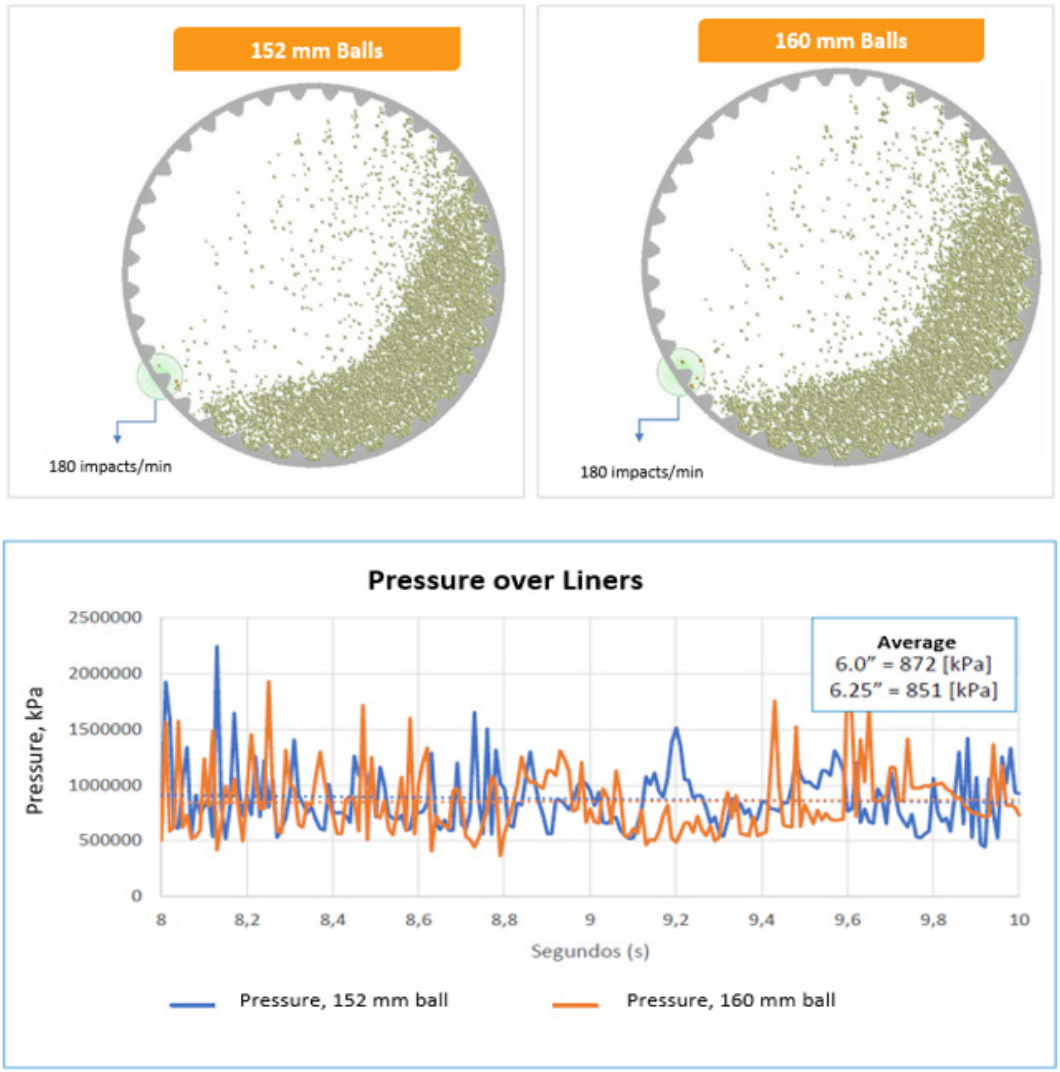



**FIG 8** – DEM simulations results for increase in ball size.

These simulations were critical for understanding how the liner system would perform in scenarios in which the impact forces and grinding pressure increase simultaneously. The results indicated that the current hybrid liner configuration retains sufficient structural capacity to withstand the added impact loadings, particularly when combined with active monitoring and optimised media charging.

With the planned implementation of larger grinding media in 2026 and a continued focus on improving throughput under tougher ore conditions, the plant aims to leverage the simulation outcomes and past campaign experiences to refine its liner and mill control strategy. These efforts will involve not only material upgrades and re-engineered liner geometry, but also tighter integration of real-time monitoring systems (impact, mill load and filling levels, feed ore size distribution, real-time liner wear monitoring.) to ensure safe operation under high energy conditions.

The endurance of the liner system in recent campaigns under changing ore characteristics provides a degree of confidence in the ability to push performance boundaries further. However, as ore competency continues to increase, ongoing validation and data-driven adaptations will be essential to sustain mill productivity and liner durability.

## CASE STUDY 2 – 36 FT × 20 FT SAG MILL AT AN AUSTRALIAN GOLD OPERATION

A second case study was undertaken at a 36 ft × 20 ft SAG mill at a gold operation in Australia. Three consecutive liner campaigns were considered: two campaigns using conventional steel liners followed by a third campaign using a hybrid liner configuration. The first steel campaign extended from April to September 2025, the second from September 2025 to March 2026, and the hybrid campaign commenced in March 2026 and remained ongoing at the time of the analysis. The analysis used hourly operating data collected between April 2025 and June 2026. Because the hybrid campaign was still ongoing, the comparison of cumulative production was normalised to the equivalent operating duration of the shortest campaign.

At 2072 equivalent running hours (Figure 9), the hybrid campaign had processed approximately 3.42 Mt of fresh feed, compared with approximately 2.81 Mt for each of the preceding steel campaigns. Over the same period, flotation feed was approximately 2.08 Mt for the hybrid campaign compared with 2.04 and 1.97 Mt for the preceding campaigns. The hybrid campaign also recorded a maximum daily flotation feed rate of 1155 t/h, compared with 1082 and 1080 t/h for the two steel campaigns. These figures should be interpreted with caution since the operating conditions were not identical. In particular, the hybrid campaign contained a measurable proportion of oxide ore, whereas the preceding campaigns contained virtually no oxide material. The hybrid campaign also operated at a lower average work index. These differences provide an important limitation to any direct comparison of throughput or energy performance.

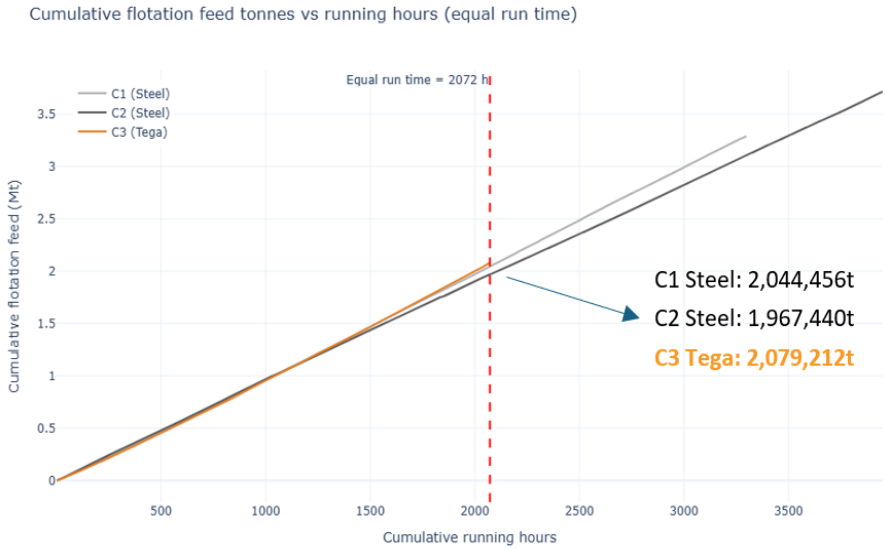



**FIG 9** – Cumulative tonnage comparison among campaigns.

The most notable observation from the second case study was the behaviour during the early stages of the hybrid campaign. A ramp-up criterion based on the first occurrence of a mill rate of at least 1000 t/h was used to compare the campaigns. The first steel campaign reached this threshold after approximately 139 running hours, while the second reached it after approximately 61 running hours. The hybrid campaign reached the same threshold after only approximately 20 running hours. The 20-hour value represents the first achievement of the selected production threshold and should not be interpreted as the point at which sustained full-capacity operation had been established. The analysis identified a later period, beginning approximately 13 days after restart, during which the mill was able to operate more consistently within the target production range. Nevertheless, the early achievement of the 1000 t/h threshold provides a useful indication that the mill was capable of entering the higher operating-rate region substantially earlier in the hybrid campaign than in the preceding steel campaigns.

This response occurred despite several constraints during the early campaign. A ball mill lubrication-system failure affected the start-up period, while interruptions and maintenance in the crushing circuit affected feed availability and stockpile conditions. Additional shutdowns occurred during the first

weeks of operation. Furthermore, the MillSlicer™ system was unavailable during much of the first four weeks, limiting the ability to directly evaluate charge trajectory and impact behaviour during the earliest part of the campaign. The operating records nevertheless show that the mill progressively returned to higher production rates as circuit conditions improved. During the early period, the mill operated at speeds of approximately 9.6–9.8 rev/min, with recorded flotation feed subsequently reaching approximately 1005 t/h and 1000 t/h on consecutive days. A later operating period recorded approximately 1018 t/h. These observations indicate that the higher production-rate region was achieved early in the campaign, although the ability to sustain production remained dependent on the availability of the surrounding circuit.

The early hybrid campaign also showed a reduction in operating work index as the campaign progressed. During the first three weeks, mean operating work index was approximately 28.2 kWh/t, decreasing to approximately 27.0 kWh/t during weeks three to six. Mean flotation feed increased from approximately 903 to 979 t/h over the same periods. The change in ore characteristics therefore needs to be considered when interpreting the production response.

The second case study provides a useful independent observation of accelerated ramp-up behaviour at another 36 ft SAG mill. However, because the hybrid campaign was still ongoing and the ore and circuit conditions differed from the preceding campaigns, the results are more appropriately interpreted as evidence of operational feasibility rather than as a controlled measurement of liner-related performance.

## DISCUSSION

The two case studies show a similar operational trend; following the introduction of hybrid liner systems, the SAG mills were able to enter their higher operating-speed or production regions substantially earlier than during the preceding steel-liner campaigns. The magnitude and form of the response differed between the operations, reflecting differences in mill configuration, ore characteristics and operating practices, but the common observation was a reduction in the period during which the mills were restricted to lower operating conditions following reline.

The Chilean case provides the more complete data set for evaluating the longer-term implications of this operating strategy because multiple hybrid campaigns were available and liner service life could be assessed. The mill reached near-nominal speed within approximately one week rather than the 21–42 days historically required with the steel configuration, while the observed hybrid liner campaigns did not experience any cracking or bolt failures that had previously contributed to the conservative ramp-up approach. The increase in liner service life observed in the evaluated campaigns provides additional evidence that the accelerated ramp-up did not result in an identifiable deterioration in liner durability.

The Australian case provides a second field observation of the early production response. The hybrid campaign reached the 1000 t/h threshold after approximately 20 running hours, compared with 61 and 139 hrs for the preceding steel campaigns. Importantly, this occurred despite several circuit interruptions during the start-up period. The result suggests that the mill was mechanically and operationally capable of entering the higher production region early in the campaign, although the subsequent ability to sustain this production depended on the availability of the upstream and downstream circuits.

The two cases should not be interpreted as controlled comparisons in which liner configuration was the only variable. Ore characteristics, feed size, work index, mill filling, operating speed, circuit availability and instrumentation differed between campaigns. The Australian case in particular contained a higher proportion of oxide ore and experienced several external constraints. Consequently, the observed throughput and energy differences cannot be assigned solely to the hybrid liner system. The more appropriate engineering interpretation is that the hybrid configuration can provide an operating envelope within which a shorter ramp-up may be feasible, provided that the mill is mechanically sound and appropriate monitoring is available. The liner configuration is therefore one component of an integrated ramp-up strategy rather than an independent determinant of production.

This distinction is important when considering implementation at other operations. A faster ramp-up should not consist simply of increasing mill speed immediately after a reline. The operating strategy should first establish the mechanical condition of the mill and the initial grinding-charge condition, while feed characteristics and expected circuit constraints should be reviewed. As speed is increased, mill power, weight, acoustic response and, where available, charge trajectory should be monitored so that the operating envelope can be adjusted in response to actual mill behaviour.

## CONCLUSIONS

Over the past two decades, substantial effort has been directed toward improving the performance of cast steel liners in large-diameter SAG mills. However, despite material and design refinements, these advances have not translated into corresponding improvements in mill availability or reliability. As modern operations continue to commission larger mills, employ higher ball loads, and process increasingly competent ores, the resulting rise in impact energy has intensified liner damage and extended reline durations, ultimately reducing effective run time compared with earlier generations of SAG mills.

The growing size and power of SAG mills have therefore accelerated the industry's transition toward hybrid liner systems. Leveraging advanced computational modelling, materials science, and decades of experience in metal–rubber bonding, Tega's hybrid (Dynaprime) liners deliver a balance between impact resistance, wear life, and energy efficiency. Field data demonstrate clear improvements, including faster ramp-up periods, increased mill throughput, reduced specific energy consumption, and a notable decrease in liner-related downtime.

As the mining industry progresses toward even larger and more demanding SAG mill applications, hybrid liners are emerging as the preferred solution, offering durability, enhanced mill performance, and improved operational sustainability. These results confirm that hybrid liners are not merely an alternative to steel, but the next evolutionary step in SAG mill lining technology for modern, high-capacity operations.

## ACKNOWLEDGEMENTS

The authors wish to express their gratitude to the numerous parties that have contributed to advancements in liner design, particularly the leadership teams at the mine that have conducted trials with the new technology.

## REFERENCES

Beloglazov, I and Plaschinsky, V, 2024. Development MPC for the Grinding Process in SAG Mills Using DEM Investigations on Liner Wear, *Materials*, 17(4):795–795.

Cleary, P W, 2019. Effect of rock shape representation in DEM on flow and energy utilisation in a pilot SAG mill, *Computational Particle Mechanics*, 6(3):461–477

Lopez, P, Reyes, I, Risso, N, Momayez, M and Zhang, J, 2023. Machine Learning Algorithms for Semi-Autogenous Grinding Mill Operational Regions' Identification, *Minerals*, 13(11):1360–1360.

# Geometry – a lesson in energy efficiency and component wear

*I Gurnett[1] and A Swann[2]*

1. Glencore Technology, Brisbane Qld 4000. Email: ion.gurnett@glencore.com.au
2. Glencore Technology, Brisbane Qld 4000. Email: andrew.swann@glencore.com.au

## ABSTRACT

The IsaMill™ has been the industry leader in stirred milling for the past 30 years, delivering energy-efficient grinding to mineral and mining operations. Over the last decade alternative stirred milling technologies have become more commercially available with a noticeable increase in industry vendors. The counter to a potentially reduced market share, is that it has forced incumbent technologies to further develop their continuous improvement cultures, to innovate and to set themselves apart. This paper describes one of these innovation journeys.

There is a common belief that a disc in an IsaMill™ 'is just a standard disc'; this can be understood as saying a 'SAG mill liner is just a liner'. Within stirred mills, internal geometry and material choice greatly influence energy efficiency and wear during operation. This paper aims to guide you through some successful methodologies to progress through the innovation cycle and provide quick ways to evaluate new geometric ideas. Using this approach, it will highlight case studies where Glencore Technology successfully developed a recently patented disc, a new spacer that reduced energy consumption by 20 per cent, and anti-media compression discs.

# Multi-objective optimisation of mechanical flotation cell design and operating parameters for improving coarse particle flotation hydrodynamics

*G Lastra[1], B Awatey[2], J J Frausto[3,4], D Deglon[5] and K Runge[6]*

1. PhD Candidate, Julius Kruttschnitt Mineral Research Centre, The University of Queensland, Indooroopilly Qld 4068. Email: g.lastra@uq.edu.au
2. Research Fellow, Julius Kruttschnitt Mineral Research Centre, The University of Queensland, Indooroopilly Qld 4068. Email: b.awatey@uq.edu.au
3. Former Research Fellow, Julius Kruttschnitt Mineral Research Centre, The University of Queensland, Indooroopilly Qld 4068.
4. Present affiliation: Minerals Sales Manager, Metso, Mexico. Email: juan.g.frausto@metso.com
5. Professor, Department of Chemical Engineering, University of Cape Town, Rondebosch 7700, Cape Town, South Africa. Email: david.deglon@uct.ac.za
6. Associate Professor, Julius Kruttschnitt Mineral Research Centre, The University of Queensland, Indooroopilly Qld 4068. Email: k.runge@uq.edu.au

## ABSTRACT

Mechanical flotation cells remain the dominant flotation technology in the mineral processing industry, but they are typically optimised for intermediate particle sizes (10–100 μm) and perform poorly when treating coarse particles. Poor coarse particle recovery is attributed to inadequate solids suspension, increased turbulence-induced bubble-particle detachment, and reduced froth recovery. Improving coarse particle flotation therefore requires effective suspension at reduced power input, together with a stable pulp-froth interface and appropriate control of bubble size and gas dispersion. However, no systematic investigation has evaluated the combined effects of cell design and operating variables on these hydrodynamic responses. Pilot-scale testing was conducted in a 1 $m^3$ mechanical flotation cell. A Design of Experiments approach was used to evaluate the effects of rotor diameter, impeller off-bottom clearance, baffling configuration, superficial gas velocity (Jg), and solids concentration. Suspension was assessed using the critical impeller speed for complete off-bottom suspension (Njs), while specific power draw, bubble size, gas dispersion, and pulp-froth interface oscillations were measured at this condition. A large rotor operated with baffles at low clearance, reduced solids concentration, and low airflow rate improved suspension and decreased power draw. However, this configuration also deteriorated gas dispersion and increased interface oscillations. Regression modelling and multi-response optimisation were therefore used to balance these competing responses, identifying an optimal configuration comprising a large rotor-stator system operated at low clearance and intermediate air rate. Relative to the standard configuration, this arrangement enhanced suspension, reduced power draw and interface oscillations, whilst maintaining adequate gas dispersion. These readily retrofittable design and operating modifications have strong potential to improve coarse particle recovery. Future work will test this hypothesis through direct flotation experiments.

# How to use the acoustic emissions from a grinding mill for diagnostics and control

*R A Pax*[1]

1. MAusIMM, Principal, RAP Innovation and Development Pty Ltd, Indooroopilly Qld 4068. Email: rpax@rapind.com.au

## ABSTRACT

Grinding mills create significant acoustic emissions which can be understood in terms of the mechanisms of their internal operation (Pax, 2001, 2012, 2016, 2017, 2026; Pax and Bevan, 2023). These mechanisms are influenced by both the feed ore characteristics and the operational practice of the grinding circuit, including feed preparation, and its circuit. Various studies of grinding circuits using permanent installations of an acoustic array as well as acoustic surveys have been executed on over 70 mills over the last 25+ years (eg Pax *et al*, 2014). This work has resulted in a tool that allows the understanding for the rapid diagnosis of grinding operations as well as providing useful outputs for the control of mills (Pax, 2011; Pax and Cornish, 2015a, 2015b; Pax and Thornton, 2019). Examples include the easy real-time detection of packing of media and ore between lifters, evaluation of changes in feed ore characteristics (including ore hardness), exceptional impacting of media against liners at several circumferential locations, an assessment of the water/slurry holdup inside the mill, the determination of optimal load (including overloading and underloading), and the evaluation appropriate or otherwise of mill operation and its circuit. This paper will discuss, in overview, the acoustic emissions derived measurement methodology (implemented in SmartNoise© software (ver 20), RAP Innovation and Development Pty, Ltd) and how they are applied to the determination to the rapid and timely production information resulting in the financial savings for production costs and reduced downtime for the grinding circuit. A more complete presentation is given by Pax (2026).

## REFERENCES

Pax, R A, 2001. Non-contact acoustic measurement of in-mill variables of SAG mills, in *Proceedings International Autogeneous and Semi-Autogeneous Grinding Technology*, (eds: D J Barratt, M J Allan and A L Mular) II:386–393 (Canadian Institute of Mining and Metallurgy: Westmount).

Pax, R A, 2011. Non-contact acoustic measurement of dynamics in mill processes for SAG/AG mills, in *Proceedings of the Metplant Conference*, pp 163–175 (The Australasian Institute of Mining and Metallurgy: Melbourne).

Pax, R A, 2012. Determining mill operational efficiencies using non-contact acoustic emissions from microphone arrays, in *Proceedings of the 11th Mill Operators Conference*, pp 119–126 (The Australasian Institute of Mining and Metallurgy: Melbourne).

Pax, R A, 2016. Using non-contact acoustics measurement to view inside a tumbling mill, in *Proceedings of the XVIII International Mineral Processing Congress (IMPC)*, paper 604 (Canadian Institute of Mining and Metallurgy: Westmount).

Pax, R A, 2017. The measurement of comminution processes in tumbling mills, *AusIMM Bulletin Magazine*, June, pp 68–71.

Pax, R A, 2026. How to use the acoustic emissions from a grinding mill for diagnostics and control, AusIMM webinar 21/5/2026. Unique ID: P-03559-Y6M9Q3-202607150121398019.

Pax, R A and Bevan, A, 2023. RAPID diagnostics and Observations of the internal operation of a SAG mill in the Context of its Grinding Circuit, in *Proceedings of the 8th International Conference on Semi-Autogeneous Grinding and High-Pressure Grinding Roll Technology* (eds: L F Hartwig, B Simonian, M Samuels and M J Allan), paper S14P5_167.

Pax, R A and Cornish, B, 2015a. Determination of particle trajectories, toe and shoulder dynamics using a non-contact acoustic array on an industrial SAG mill, in *Proceedings of the SAG Conference* (eds: B Klein, K McLeod, R Roufail and F Wang), paper 80 (Canadian Institute of Mining and Metallurgy: Westmount).

Pax, R A and Cornish, B, 2015b. A novel measurement for the internal operation of a SAG mill using acoustic sensors: A case study. in *Proceedings of the MetPlant Conference*, pp 120–128 (The Australasian Institute of Mining and Metallurgy: Melbourne).

Pax, R A and Thornton, A, 2019. Real time measurement and fast control strategies for the optimal operation of grinding circuits, in *Proceedings of the Metplant Conference*, pp 132–148 (The Australasian Institute of Mining and Metallurgy: Melbourne).

Pax, R A, Wynn, R, Mann, S and Cornish, B, 2014. Implementation of Acoustic Arrays for Semi-autogenous Grinding Mill Operation, in *Proceedings of the 12th Mill Operators Conference*, pp 273–282 (The Australasian Institute of Mining and Metallurgy: Melbourne).

# What works versus what sounds good – the art and engineering of scale-up

*J D Pease[1] and P D Munro[2]*

1. Principal Consultant, Mineralis Consultants, Brisbane Qld 4068.
   Email: jpease@mineralis.com.au
2. Principal Consultant, Mineralis Consultants, Brisbane Qld 4068.
   Email: pmunro@mineralis.com.au

## ABSTRACT

The metallurgical industry has a poor record of starting-up new technology and new processes. Though we frequently hear complaints that the minerals industry is conservative, that record suggests otherwise. Many financiers think the minerals industry is serially over-optimistic and takes reckless risks with their funds. When considering whether to lend funds, the last words they want to hear are 'innovative new technology'.

Most industry professionals are familiar with McNulty curves (Figure 1) to summarise plant start-ups. McNulty (1998) said the bad start-ups, Type 4, are often innovative technology, do not have enough pilot testing, and may have cut corners cut in engineering. A Type 4 plant takes four years to reach 60 per cent of design. We will discuss some recent major Australian plants that eventually wrestled to a Type 4 performance. And some more recent examples that fell woefully short of even a Type 4 start-up.

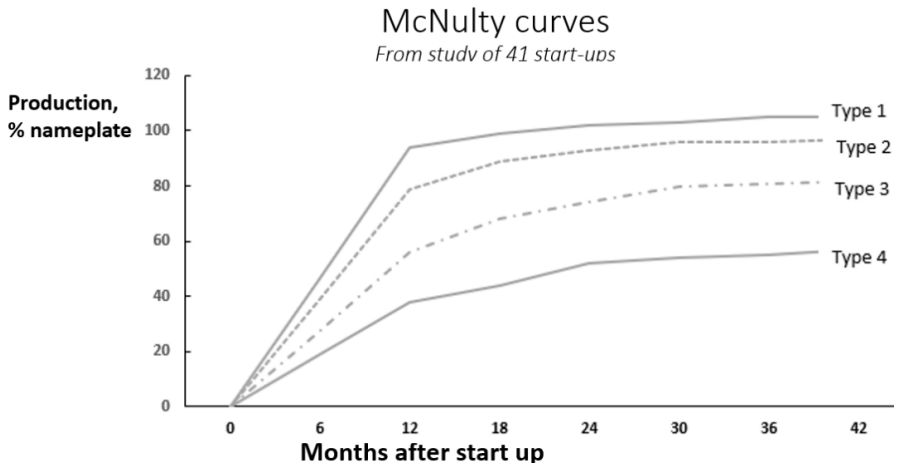



**FIG 1** – McNulty curves.

For minerals processing it appears that McNulty was an optimist. This presentation will discuss why.

## THE PERILS OF PARTICLES

In complex processing plants, the problems are not usually the novel chemistry. Chemistry is reliable and repeatable: if it works on the benchtop, it will work in a plant. Success at full scale is determined by *materials* – materials of construction, materials handling of solids, controlling precipitation (wanted or unwanted) of solids, and solids-liquids separation steps. These materials matters determine whether or not the overall production system is robust. We will discuss how such apparently prosaic matters caused dreadful start-ups of several recent Australian plants that used proven processes.

Nice (2004) reviewed the start-ups for three Western Australian nickel laterite processing plants. In Figure 2 we superimpose the results over the McNulty curves, and add a fourth plant commissioned after Nice's analysis (that commissioning was interrupted when shut the plant and wrote off their investment during the Global Financial Crisis). In all cases the chemistry was confirmed by substantial pilot plant testing. The problems were materials handling, materials of construction, and keeping all of the process elements and equipment items working consistently and in harmony. Those are engineering issues, they are not about chemistry or innovative technology – but they are

fundamental to its success. The most sobering message in Figure 2 is that the fourth plant – with the benefit of lessons from the preceding plants and a huge investment in pilot testing – was no better.

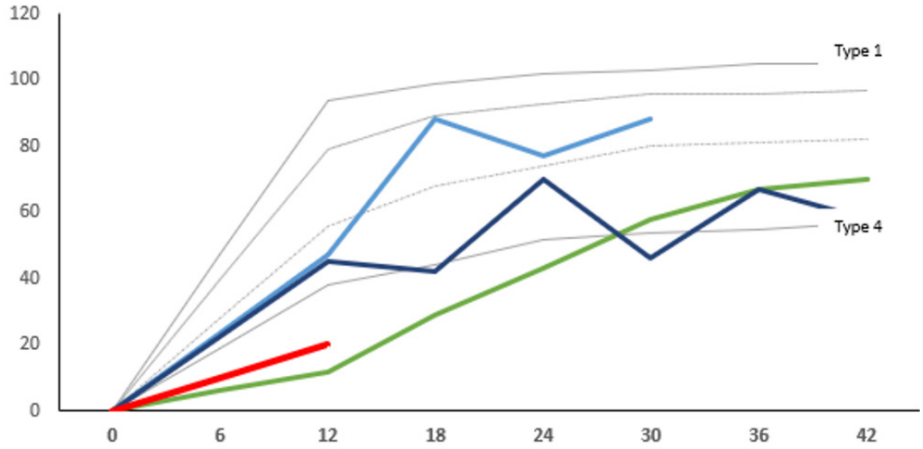



**FIG 2** – Start-up performance of four Western Australian nickel laterite plants.

McNulty related poor start-up performance to the level of innovation and whether it was matched with sufficient demonstration and engineering. That is clearly important, and it is appropriate that the industry has embraced McNulty curves. And yet, this conclusion misses a fundamental challenge in the minerals and evident in the four nickel laterite plants – we deal with particles. For gases, PV = nRT is pretty much all you need to know. For liquids, add rheology. But particles are much harder to characterise. Their behaviour changes with size and conditions, with moisture content and the presence of other particles. They build-up, or settle, or precipitate where we don't want them; they abrade equipment and vessels. This was vividly explained by Wellwood (2019). It is extraordinarily more difficult to engineer for solids than for liquids and gases. And just because well-prepared particles behaved well in the pilot plant, that doesn't mean that mountains of 'raw' particles will behave the same in your plant. That is like the difference between a first date and marriage.

Before McNulty's study, an earlier author, Edward Merrow (1988), also researched plant start-ups. His findings may be even more profound than McNulty's, but they were not as well presented and therefore have been less noticed. A workshop by Hartford (2016) later presented Merrow's results in a more familiar form, reproduced in Figure 3.

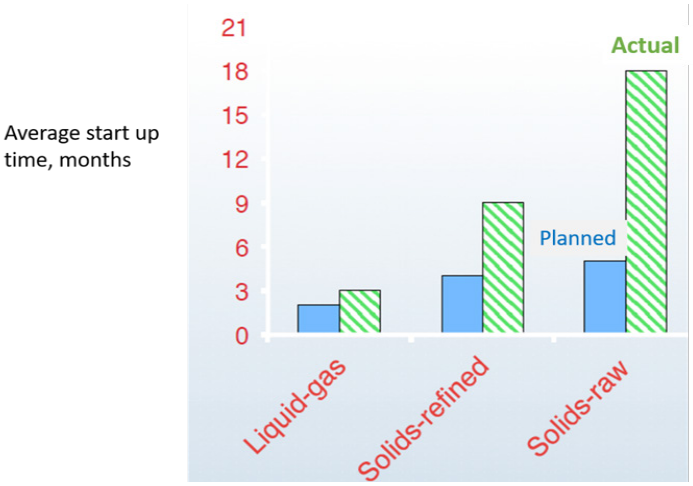



**FIG 3** – Graphical presentation of Merrow's findings.

## EVENTS VERSUS PROCESSES

The widespread myth that comminution 'consumes 3 per cent of global electricity' was disproven by the thorough analysis by Morrell (2023). He showed that the correct number is around 0.5 per cent

(less than 1/20th of current data centre consumption). Even so, comminution consumes significant energy and is an obvious target to improve efficiency.

Many proposed new comminution technologies are based on Schoenert's finding that the most efficient way to break a particle is by compression between two hard surfaces (Schoenert, 1972). That is a scientific truth. The mineral processing challenge is how to combine the *science* of breaking individual particles with the *engineering* challenge of breaking billions of particles a day, consistently, reliably, and with acceptable equipment life. Many concepts have successfully demonstrated Schoenert's principle in small scale equipment, but have failed at pilot or semi-industrial scale. Not due to the science, but due to the engineering of scaling-up equipment size; the change from single particle to billions of particles. Just as lightning is an impressive and powerful event, but we haven't yet engineered as a practical source of energy for our homes.

Binnermans and Jones (2025) describe our tendency to identify shortfalls in established technology, but may not use the same rigour to assess how a promising new technology will interact with all elements of a complex production system. They call this the 'Lindy Effect'. The general public call it 'the devil you know'.

Pease (2016) discussed the IsaSmelt copper smelting technology crossing the innovation 'Valley of Death'. The chemistry was proven and the engineering was demonstrated at two scales in commercial pilot plants. Yet the technology nearly failed at full scale due to initial short refractory life (Figure 4). Regardless of substantial effort, we didn't know enough about engineering and operating at the final scale. The owner (MIM Holdings Pty Ltd) had to persevere because it had committed copper production to the new technology. But it is not unreasonable to expect that subsequent adopters would want to see demonstration of three-year refractory life before committing. We did not expect that would take 11 years. Though, even if we had got it perfectly right first time, it would still takes at least three years to demonstrate three-year life.

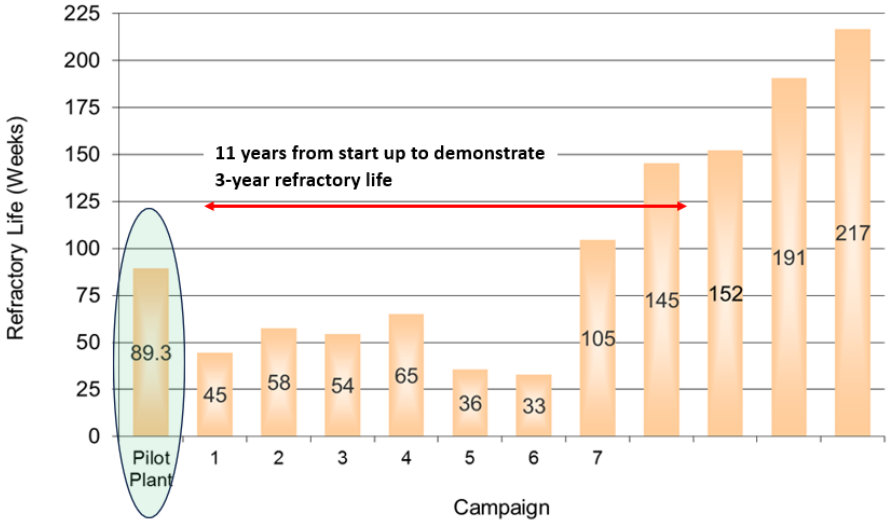



**FIG 4** – Refractory life for the first full scale copper IsaSmelt.

## CROCODILES AND DINOSAURS

When we say that the industry uses conservative, decades-old technology, we imply that this technology is a 'dinosaur' – its time has passed and it is due to be replaced. In such cases, it should be relatively easy to demonstrate that a new technology is better and more robust.

But sometimes there could also be an alternative explanation – that the technology may be a 'crocodile', perfectly evolved for its environment. In that case – underestimate it at your peril!

We will discuss an example using Figure 5, reproduced from Napier Munn (AusIMM 2016 Delprat Lecture, personal communications T Napier Munn, 2026). He presented how little crusher design had changed in 90 years (now 100 years) and asked 'Does this make this design a dinosaur or a crocodile?'. We will consider this, along with some alternative comminution technologies. If we can

better distinguish between dinosaurs and crocodiles, and identify the future crocodiles, then we can better target our innovation efforts and funding.

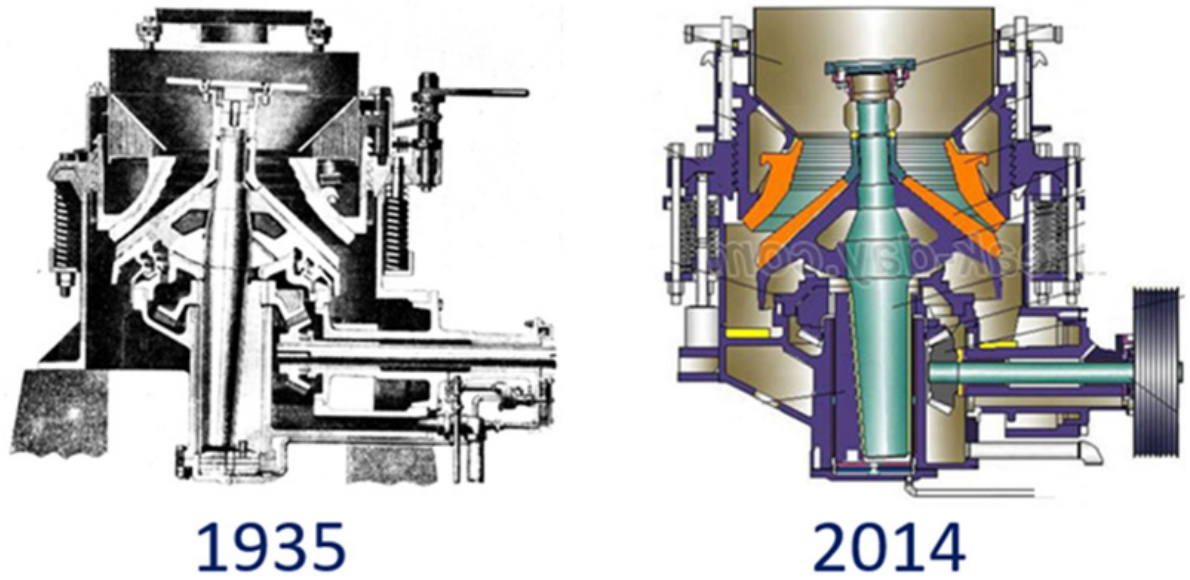



**FIG 5** – The evolution of crusher design, from T Napier Munn (personal communications, 2026).

## THE RUBIK'S CUBE OF IMPURITIES

Unlike manufacturing, the vast majority of feed to metallurgical processing plants is unwanted and uncontrolled waste. The success of a process plant does not depend on it producing copper or gold or lithium. Success depends on whether the process can methodically, sequentially and economically remove the other 99 per cent of feed derived from the rest of the elements in the periodic table. Not just to remove them (and the process additives), but to reliably and economically place them into manageable and environmentally stable exit streams, in closed-circuit and in long-term steady state – even though the feed to the plant varies.

Making the copper or lithium is the *easy* bit; anyone can do that. Our job is to solve the Rubik's cube for the rest of the periodic table while having little control over the composition of that 99 per cent of feed. We discuss this challenge using the example of hydrometallurgical processing of high-arsenic copper-gold concentrates. In spite of many attempts over half a century, this remains an important target and an unsolved puzzle.

## CONCLUSIONS

Our discussion of failed innovation is not to discourage. It is so we learn how to best focus our limited time and research funds. We would like to say that the industry is getting better at this; sadly recent performance suggests we are getting worse. Our good intentions to adopt promising new technology are dashed on the rocks (and wet fines) of materials handling and engineering. No wonder financiers – and company Directors – are cautious of the term 'new technology'.

How do we identify the engineering limits to scale up? How can we tell if an existing technology a dinosaur or a crocodile? When we find an innovation to deliver efficient events, how do we assess how to scale it up to perform reliably as a component in a complex process? How will it deal with the billions of recalcitrant particles, and manage the uncontrolled variation of 99 per cent of feed from the rest of the periodic table? How can we be certain that we can all the exit streams for the other 99 per cent within environmental limits over the long-term?

If we understand those questions and seek their answers, then we will focus our researchers and engineers on the factors most important to innovation succeeding at full scale. We will develop things that *work*, not keep failing with things that just *sound* good.

## REFERENCES

Binnermans, K and Jones, P, 2025. Lindy Effect in Hydrometallurgy, *Journal of Sustainable Metallurgy*, 11:2157–2174.

Hartford, C, 2016. Overview of Efforts in Feedstock and Materials Handling – Key Technical and Economic Challenges, DOE Biorefinery Optimisation Workshop, October 2016.

McNulty, T, 1998. Developing Innovative Technology, *Mining Engineering*, 50(10), September.

Merrow, E, 1988. Estimating Start-Up Ties for Solids Processing Plants, *Chemical Engineering*, 95(15), October.

Morrell, S, 2023. How to Reduce the Hard Rock Mining Industry's Comminution Carbon Footprint by Up to 40%, in Proceedings of the World Mining Congress 2023, Brisbane, Australia.

Nice, R, 2004. The Western Australian Nickel Laterite Projects – What Have we Learned?, in *Proceedings of the 36th Annual Hydrometallurgy Meeting*, pp 155–179, Canadian Institute of Mining, Metallurgy and Petroleum.

Pease, J, 2016. Crossing the Innovation Valley of Death, presentation to JKMRC weekly lecture, August 2016.

Schoenert, K, 1972. Role of Fracture Physics in Understanding Comminution Phenomenon, *Society of Mining Engineers, AIME, Transactions*, 252:21–26.

Wellwood, G, 2019. Bulk Solids Handing – A Chemical Engineers Perspective, in *Proceedings of the 13th International Conference on Bulk Materials Storage, Handling and Transportation (ICBMH 2019)*, pp 130–151 (Engineers Australia).

# Selective thorium removal from rare earth element solutions by ion exchange

*B da Rocha Pereira[1], V L Gontijo[2], J Vaughan[3], D R C Espinosa[4] and J A S Tenorio[5]*

1. PhD Candidate, LAREX – Laboratory of Recycling, Waste Treatment and Extraction, Department of Chemical Engineering, Polytechnic School, University of São Paulo (USP), São Paulo SP 05508-080, Brazil. Email: barbaraalvesrocha@usp.br
2. Researcher, School of Chemical Engineering, The University of Queensland, St Lucia Qld 4072, Australia. Email: v.loureirogontijo@uq.edu.au
3. Professor, School of Chemical Engineering, The University of Queensland, St Lucia Qld 4072, Australia. Email: james.vaughan@uq.edu.au
4. Professor, LAREX – Laboratory of Recycling, Waste Treatment and Extraction, Department of Chemical Engineering, Polytechnic School, University of São Paulo (USP), São Paulo SP 05508-080, Brazil. Email: espinosa@usp.br
5. Professor, LAREX – Laboratory of Recycling, Waste Treatment and Extraction, Department of Chemical Engineering, Polytechnic School, University of São Paulo (USP), São Paulo SP 05508-080, Brazil. Email: jtenorio@usp.br

## ABSTRACT

The recovery of rare earth elements (REEs) from primary and secondary resources can be hindered by impurities, including radioactive thorium (Th). Th removal prior to REE recovery is often necessary to ensure that product specifications are achieved. In this study, three ion-exchange resins were evaluated for selective Th removal from a synthetic multielement solution containing Ce, La, Nd, Sm, Gd, Dy, and Y, aiming to retain REEs in the aqueous phase. The resins were Lewatit® MonoPlus TP260, a chelating cation-exchange resin containing aminomethylphosphonic acid groups; Lewatit® MonoPlus MP64, a weak-base anion-exchange resin with a macroporous styrene-divinylbenzene matrix; and Lewatit® MonoPlus MP800, a Type I strong-base anion-exchange resin with quaternary ammonium groups. The starting solution comprises of 206 mg/L Ce, 104 mg/L La, 53 mg/L Nd, 8.5 mg/L Sm, 11 mg/L Gd, 5.8 mg/L Dy, 5.5 mg/L Y, and 50 mg/L Th. The resins were evaluated at pH 1–5 using 1.0 g resin per 50 mL solution and a 2 hr contact time. TP260 adsorbed 98–99 per cent Th and 83–97 per cent REEs, indicating that its aminomethyl-phosphonic acid groups did not provide sufficient discrimination between Th and REEs under the evaluated conditions. MP64 adsorbed 18–35 per cent REEs, while Th adsorption increased from approximately 30 per cent at pH 1 to 70 per cent at pH 5. For MP800, Th adsorption increased from approximately 20 per cent at pH 1 to 99 per cent at pH 5. At pH 5, individual REE adsorption ranged from 11 to 29 per cent, corresponding to 71–89 per cent remaining in solution. This behaviour may be related to anionic Th species interacting with MP800 quaternary ammonium groups through ion exchange. The kinetic adsorption of Th onto MP800 at pH 5 was evaluated. Approximately 98 per cent Th was removed from solution after 0.5 hr and remaining at 98–99 per cent range up to 8 hrs. These results demonstrate the potential of MP800 for selective Th removal. Future studies will evaluate primary- and secondary-resource-derived solutions to investigate matrix composition and other elements on Th removal and REE retention.

# Designed for one life, engineered for the next – extending the safety, capability and economic value of ageing mill relining equipment

*P van Rooyen*[1]

1. Global Asset Support Engineering Manager, Russell Mineral Equipment, Toowoomba Qld 4350. Email: pierre.vanrooyen@rmeglobal.com

## ABSTRACT

Mill relining machines are long-life capital assets that can remain in operation beyond the intended service intervals or support life of their original mechanical, hydraulic, electrical and control-system components. As operating hours, load cycles and environmental exposure accumulate, the probability of component wear, structural fatigue, hydraulic degradation, control-system obsolescence and failure of unsupported safety-critical components increases. Continued operation requires more than routine maintenance. It requires an engineering assessment of asset condition, residual risk and capability for the next defined period of service.

A risk-based, total cost of ownership approach integrates equipment utilisation and service history, site inspection, non-destructive testing of primary structures and major fabrications, hydraulic-system assessment, original equipment manufacturer replacement guidance, current safety requirements and the site's future operating mine-life. These inputs establish a revised condition baseline, identify degradation mechanisms and rank interventions according to safety, reliability, supportability, and operational consequence.

Life-extension activities restore critical mechanical systems, including the grapple and turntable, and replace high-wear or fatigue-sensitive components such as bearings and grapple tooling. Structural inspections determine whether major fabrications require continued monitoring, repair, or replacement. Hydraulic assessment covers coolers, circuits, controls and valves, while field and fleet data support the planned treatment of known failure modes before they result in secondary damage or unplanned loss of function. Site audit findings also provide the technical basis for deciding whether major assemblies should be retained, refurbished, or replaced.

Safety improvements focus on ageing and obsolete safety-critical systems. These can include replacement of electrical and control components, modernisation of isolation systems and access arrangements, and upgrades to emergency-stop, radio-control and operator-protection systems. Fleet operating experience is applied to remove legacy designs and incorporate verified engineering and operational improvements.

Modernisation can introduce updated control architecture, operator interfaces, and drive technologies to improve ergonomics, maintainability, and component supportability. Targeted capability upgrades may include increased liner-handling capacity, improved in-mill lighting and specialised tooling that reduces manual handling, personnel exposure on the mill charge and hot-work requirements.

The total cost of ownership assessment compares continued maintenance, major service, refurbishment, modernisation and replacement over a defined operating horizon. The evaluation considers intervention cost, deferred capital expenditure, component availability, obsolescence exposure, failure consequence, and the potential effect on planned and unplanned mill availability.

Life extension does not mean operating an asset indefinitely. It means using condition evidence, engineering analysis and defined controls to manage its changing risk profile and establish a technically supportable next life.

# The cleaning stage optimisations – case studies and lessons learned

*M Tayebi-Khorami*[1]

1. FAusIMM(CP), Principal Metallurgist, Core Resources, Brisbane Qld 4069.
   Email: m.tayebikhorami@gmail.com

## ABSTRACT

Optimising the flotation cleaning stage is a critical component in achieving high-grade concentrates without compromising recovery. The cleaning circuit acts as the final refining step in the flotation process, where selective rejection of gangue and upgrading of valuable minerals occur. However, the cleaning stage is often overlooked compared with rougher performance, despite its pivotal role in overall plant efficiency and final products quality.

Effective optimisation requires a detailed understanding of mineralogy, flotation chemistry, and circuit configuration. Key strategies include adjusting grind size to liberate locked minerals, optimising reagent regimes, extending flotation times, and modifying circuit layout. Regrinding rougher concentrates to finer sizes can improve liberation and selectivity, while targeted reagent additions such as collectors, depressants, and frothers, can enhance separation. Recirculating scavenger material to the cleaning circuit, adding dilution water, increasing residence time and wash water control are also effective approaches. Each of these strategies aims to balance concentrate grade improvement with minimal recovery loss.

In practice, however, cleaning stage optimisation is not a one-size-fits-all solution but a process of continual learning and adaptation. Achieving optimal performance is challenging as each ore type has distinct mineralogical characteristics, surface oxidation states, and mineral associations, meaning that circuit changes effective for one deposit may underperform in another. Additionally, electrochemical factors such as galvanic interactions between sulfide minerals, the presence of ultrafine particles, and slime coating on valuable mineral surfaces can significantly affect selectivity and concentrate quality. Managing these effects through controlled regrind conditions, targeted dispersants, and optimised pH and redox potential is crucial for successful cleaner performance.

This paper presents a series of case studies highlighting cleaning stage optimisation in complex base-metal and polymetallic systems. Examples include regrind and cleaner-scavenger circuit implementation in copper ores, selective depressant strategies to improve lead and zinc separation, and reagent modifications that enhanced gold and silver recovery in sulfide circuits. The findings highlight the importance of integrating mineralogical characterisation with laboratory flotation test work to guide circuit design and optimisations.

# Improved copper refining at Olympic Dam – experimental study and thermodynamic modelling

*S Valentina[1], G Khartcyzov[2], D Shishin[3], J Chen[4], J Wen[5], M O'Sullivan[6], R West[7], M Shevchenko[8] and E Jak[9]*

1. PhD student, PYROSEARCH, The University of Queensland, St Lucia Qld 4072. Email: s.valentina@uq.edu.au
2. Research Fellow, PYROSEARCH, The University of Queensland, St Lucia Qld 4072. Email: g.khartcyzov@uq.edu.au
3. Senior Research Fellow, PYROSEARCH, The University of Queensland, St Lucia Qld 4072. Email: d.shishin@uq.edu.au
4. Senior Research Fellow, PYROSEARCH, The University of Queensland, St Lucia Qld 4072. Email: j.chen5@uq.edu.au
5. Postdoctoral Research Fellow, PYROSEARCH, The University of Queensland, St Lucia Qld 4072. Email: x.wen@uq.edu.au
6. Senior Metallurgist, BHP, Olympic Dam SA 5725. Email: mark.osullivan@bhp.com
7. Process and Development Manager, BHP, Olympic Dam SA 5725. Email: robert.west@bhp.com
8. Senior Research Fellow, PYROSEARCH, The University of Queensland, St Lucia Qld 4072. Email: m.shevchenko@uq.edu.au
9. Professor, Laboratory Director, PYROSEARCH, The University of Queensland, St Lucia Qld 4072. Email: e.jak@uq.edu.au

## ABSTRACT

As the global energy transition accelerates, copper has solidified its status as a strategic mineral, presenting Australia with a unique opportunity to expand its domestic production capacity. However, the mineralogical complexity of the concentrate presents a significant challenge to efficient extraction and refining. Impurities (eg Ag, As, Au, Bi, Co, Fe, Ni, Pb, Sb, Se, Te and Zn) present in the concentrate persist through smelting and remain in the anode copper. Consequently, the removal of these elements, particularly lead (Pb), is critical because it directly determines the quality of anode copper and its suitability for downstream electrorefining. In parallel, the world's growing interest in processing secondary resources, particularly electronic waste, within existing smelting infrastructure has introduced additional complexity to impurity management due to broader and more variable feed compositions.

The present study evaluates potential strategies for reducing the Pb content of the anode copper, a framework has been developed to evaluate and optimise furnace operations to run the plant-scale trials more efficiently. This framework combines advanced thermodynamic-based process modelling (digital twin) with targeted experimental validation of the thermodynamic model. Developed using FactSage 8.3, the digital twin models the multi-stage oxidation and reduction cycles of a rotary anode furnace while incorporating industrial calibration parameters-such as oxygen efficiency and metal entrainment—to reflect the real operations deviations from equilibrium conditions. The model is supported by kinetic and equilibrium investigations conducted at the Pyrometallurgy Innovation Laboratory (PYROSEARCH), providing insights into slag-blister copper interactions and lead partitioning.

The present study revealed that a modified strategy involving targeted silica ($SiO_2$) fluxing and enhanced slag skimming can effectuate further reduction of the Pb concentration in the anode copper, compared to the current industrial practices wherein the slag is not efficiently managed. This research provides a pathway for metallurgical facilities to understand the removal of complex impurities, securing Australia's ability to process its unique mineral wealth and reinforcing its capability in the global critical minerals supply chain.

# The devil is in the detail

*D Way[1], R Bracey[2] and L Ryan[3]*

1. Manager Process Solutions, Sedgman, South Bank Qld 4101. Email: david.way@sedgman.com
2. Principal Process Consultant, Sedgman, South Bank Qld 4101.
   Email: ryan.bracey@sedgman.com
3. Senior Director, Business Development, Worley, Perth WA 6000.
   Email: lyndon.ryan@worley.com

## ABSTRACT

Progressing process plant projects from studies to construction and operations requires process design work, preliminary engineering and metallurgical studies to prove up an economic flow sheet and plant layout. This work has a reliance on basic sampling, ore characterisation, and metallurgical testing to a standard that supports sound decision-making. Often overlooked and underappreciated is the role of collaboration and multidiscipline approach employing best practices and attention to detail play to maximise the economic extraction of metal.

This paper will present examples of sampling practises often observed for copper development projects and compare these against sampling practises considered the best, with supporting evidence. Some of the benefits and pitfalls of domaining practises and tests used for comminution and flotation characterisation will be discussed for a selection of copper case studies.

Copper projects developed by Sedgman using these best practises have demonstrated a substantial uplift in net present value (NPV) by domaining of ores by different comminution and flotation characteristics. The details of one such project will be presented that yielded a 27 per cent increase in the size of the resource and 29 per cent increase in project scale. The domaining also resulted in significant changes to the comminution and flotation circuit design, maximising the economic extraction of metal. A second case study details the importance of comminution and flotation sampling in combination with geospatial considerations. These considerations enabled a new operating schedule to be proposed which resulted in a 34 per cent uplift in copper production over the first four years of the project, significantly increasing the overall project value.

The case studies presented demonstrate the importance of best practise with respect to sampling, ore characterisation, domaining and metallurgical testing to support the design basis, and technical and economic viability of copper development projects.

## INTRODUCTION

Often in mining project development the terms ‘fast track’, ‘no time for detail’, ‘project acceleration’ or even ‘skip a stage’ are used aiming to accelerate project development. The goal of this acceleration is to advance project development as to get into operation as fast as possible, initiating cash flow for the project. An example of this was the ‘Standard Concentrator’ approach to copper project development employed by a Tier one miner between 2007–2013. Antapaccay and Las Bambas were the only two ‘Standard Concentrator’ projects commissioned. These projects are metallurgically unique compared to the portfolio of copper projects held at the time which also included El Morro, El Pachon, Tampakan and Frieda River. ‘Fast tracking’ or similar concepts didn’t help with development of these later projects. Progressing from studies to construction and operations requires significant trade-off studies and process design work to prove up an economic flow sheet and plant layout which are often driven by site or ore specific requirements.

The basis of this work is a reliance on sampling, ore characterisation and metallurgical testing to a suitable standard. Often overlooked and underappreciated is attention to detail and the benefits in best practices to maximise economic extraction of metal. The basic aim should be to optimise key technical levers to maximise the economic extraction of metal. The key levers include defining the:

- flow sheet design
- production strategy

- production rate
- production efficiency
- resource scale.

## SAMPLING

Ore sampling often does not attract the attention it deserves. It is a key initial step for project development and identifying the pathway for maximum economic extraction of metal. Sampling practises should consider many things such as geological and mineralogical variation, mine schedule, sample representation, test methodology and extraction methodology. We will consider some of these focus areas in this paper and show how following what we consider best practise can lead to maximise the economic extraction of metal.

The JK Drop Weight test is a single particle test and was developed at the Julius Kruttschnitt Research Centre in the early 1990s to characterise ore according to its resistance to impact breakage. The test was an improvement over sourcing of bulk samples for pilot mill tests. These bulk samples were generally accessible ore samples, rather than representative samples. The test involves breakage testing of five particle size ranges from 13.2 mm to 63 mm at three target specific energies. The test typically requires >70 kg of rock to complete the required test work procedure. This amount of material is considered difficult to obtain by diamond drilling due to the competing demands for material for resource confirmation and other characterisation and test work programs. An adit is often suggested but they don't typically provide representative sample. Reverse circulation (RC) chips are of no value because the survivors of the RC drilling process are hard materials (Way, McKee and Pease, 2021). For diamond drilling using PQ or 85 mm size we need >5 m of continuous core at high recovery and competency to provide enough material for testing. From experience, >10 m is normally required to provide enough sample of the required particle size and mass. This amount of core and cost of the test meant that few tests were completed which did not support practitioners to define hardness variability.

This led to the development of the SMC test by Dr Steve Morrell which is another single particle test (Morrell, 2004, 2008). The SMC test requires ≥20 kg of diamond drill core and this sample mass and lower test cost supports larger quantities of samples for testing to define hardness variability. The test considers one particle size range (preferred size fraction is –31.5 +26.5 mm) tested at five target specific energies. In all, 100 discrete particles in the target size range are tested to provide the hardness characteristics. It is most important that practitioners understand the origin of these 100 particles before assigning spatial hardness parameters to a block model.

Sedgman regularly receives data from bulk samples or master composites, which were collected with the aim to establish an average performance of the ore and/or save on project development costs. This paper will attempt to demonstrate via two case studies how these practices can limit maximum economic extraction of metal. Consider the examples below for comminution characterisation testing which presents two examples of bulk or master composite samples and multiple continuous intervals of drill core that are tested independently.

Figure 1 is an example of multiple sub-samples gathered from a spatially broad area to form a bulk or master composite sample. The composite sample is likely to originate from across multiple years of production and provide an average SMC test result. However, if any of the discrete sub-samples are ≥20 kg then it is possible that the SMC test sample could originate from one sub-sample. The most likely case is that the results will represent a weighted average of a few unidentified areas once samples are mixed. Unfortunately, this means that the result is omitted or is of secondary value in the database. It is important to note, the typical procedure for sample selection for single particle comminution tests can result in unintentional sampling bias toward selection of most competent rocks (ie avoid soft-crumbly rock). Other tests such as SAG (semi-autogenous grinding) Power Index (SPI), SAG Design, Bond Ball Mill Work index (BBWi) and flotation tests using this sampling methodology will likely present weighted average results for the sampled areas and may not have any resemblance to ore characteristics expected in the process plant.

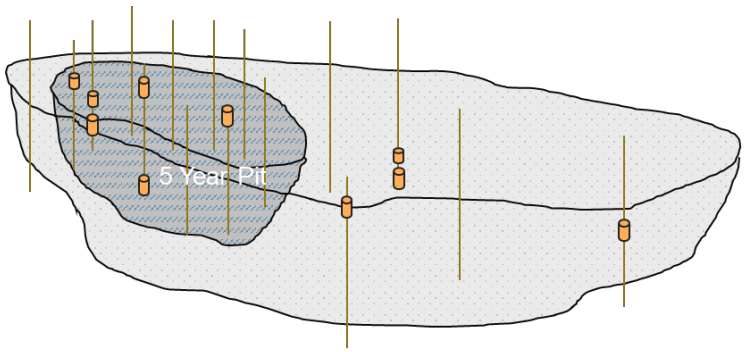



**FIG 1** – Example of multiple sub-samples gathered from a spatially broad area to form a bulk or master composite sample.

Figure 2 is an example of a continuous bulk sample gathered by combining a long continuous intersection of drill core (ie ½ HQ or 63.5 mm core from 70 m of continuous drill core). This sample is likely to present ore characteristics across multiple years of production (ie ≥5 mining bench heights). For single particle comminution tests, the particles could originate from either end or any location along the drill core. Spatial representation of the test result is lost. Other tests such as SPI, SAG Design, BBWi and flotation tests will likely present weighted average result for the sampled area and again may not have any resemblance to ore characteristics expected in the process plant.

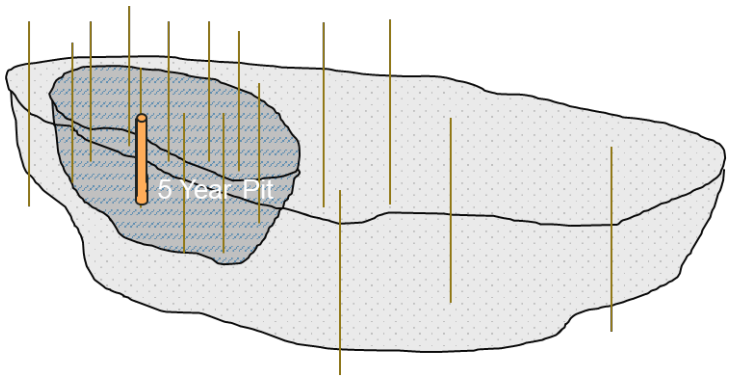



**FIG 2** – Example of a continuous bulk sample gathered by combining a long continuous intersection of drill core.

Figure 3 is an example of multiple samples of 40–70 kg. Each sample is formed by combining discrete continuous intervals of drill core from spatially representative areas. The continuous intervals are no greater than the proposed height of the mining bench. Individual characterisation and testing of samples enables test results to be spatially representative in a block model. After individual testing these samples is complete, they can be combined to form bulk, production or master composites for flotation test work. An approach the authors use specifically for SMC testing is to assign a maximum of 25–30 kg of continuous intersection for each test. This approach forces the laboratory to use a limited set of particles and if sufficient material cannot be identified as suitable for testing, then the intersection is likely very soft and/or highly fragmented. This is a good result because an understanding about the ore variability is gained and there should not be a cost for not being able to run the test. Test results for SPI, SAG Design, BBWi and flotation tests using this sampling methodology are more representative of how the ores are mined and processed according to a production schedule.

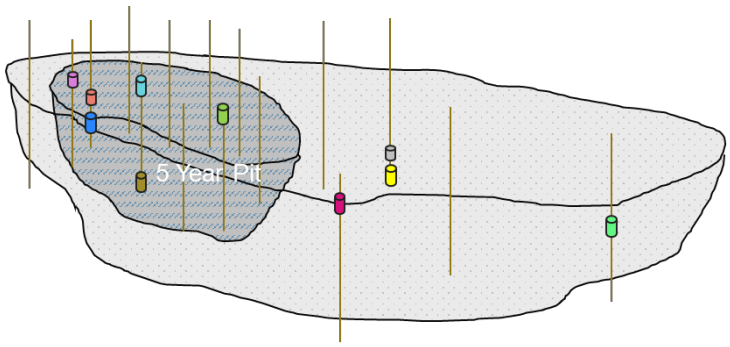



**FIG 3** – Example of multiple samples of discrete continuous intervals of drill core from spatially representative areas.

## METHODOLOGY

Two case studies of copper development projects that Sedgman was involved in are presented as examples of the importance of sampling and a methodical assessment of results. Some of the benefits and pitfalls of ore domaining practises and tests used for comminution and flotation characterisation testing will be discussed using two copper development projects that were undertaken by Sedgman.

### Case Study A

This case study considers a small to medium copper-gold project containing separate oxide, transition, and sulfide materials. The original processing schedule was developed to treat a blend of the materials in the early payback years of the project. The resource includes a couple of open pit and underground mines.

The ore domaining for comminution identified into the following three categories:

1. Oxide.
2. Transition.
3. Sulfide.

Figure 4 presents comminution results for sulfide ores and shows that they can be interpreted in two ways, and it demonstrates the importance of collecting significant variability samples. Broad assumptions, such as ‘ores get harder with depth’ do not always hold. The data identifies some early throughput rate opportunities if ores can be defined and mined selectively.

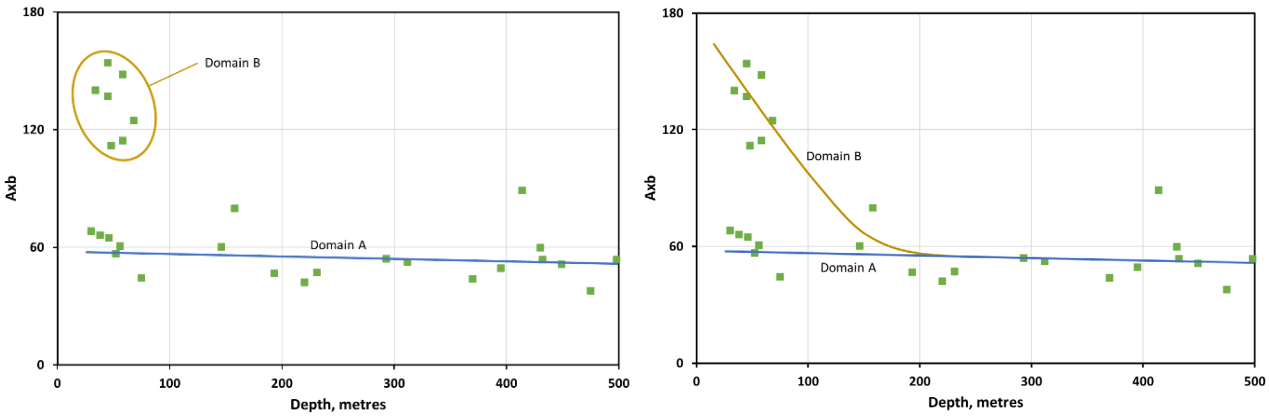



**FIG 4** – Case Study A comminution data interpretation (left) Domain B as a separate softer zone in RL >100 m. (right) Domain B trends towards domain A and >200 m RL they are inseparable.

For flotation the domaining methodology was altered from the original concept which considered all materials of equivalent flotation performance. Figure 5 presents the historical data with the Copper recovery versus copper head grade data and curve of best fit. The copper recovery was determined with a normalised copper concentrate grade of 27 per cent Cu. Sedgman reassigned the results

according to the domains identified for comminution characterisation. The separation of samples into domains was based on copper solubility in citric acid which was available but previously never used. Sedgman also omitted flotation results for blended ore domains. Figure 6 presents flotation results for the separate domains according to the three key categories identified and the new low-grade sulfide samples. It was found that most of the lower grade and poorer recovery results were associated with oxide and transition ore samples. Definition of samples into separate domains also showed that there was insufficient testing of sulfide domain samples near the cut-off grades for open pit and underground sulfides, and the copper recovery relationship with respect to copper head grade was unchanged across the copper head grade range tested. Additional low-grade samples were targeted from core samples available and flotation tested to determine the sulfide copper recovery relationship to lower copper head grades. These results showed a slow decrease in copper recovery occurring at <0.8 per cent Cu. This work shows how definition of ores into separate flotation domains resulted in ≥24 per cent increase in copper recovery at cut-off grades. Sulfide ores cut-off grade is 1.0 per cent Cu equivalent for underground and 0.5 per cent Cu equivalent for open cut ores.

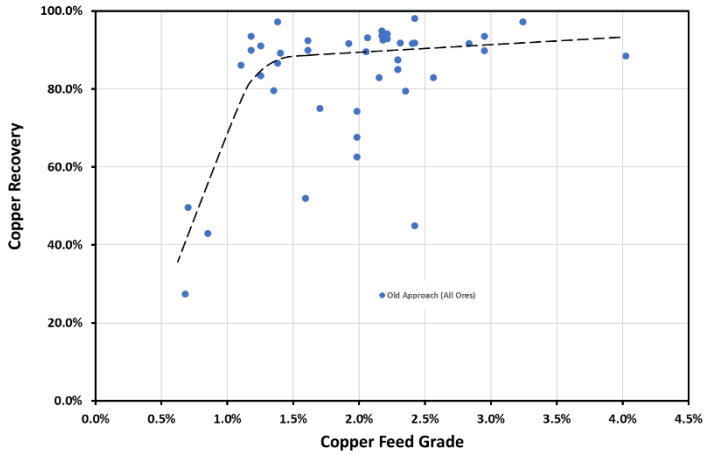



**FIG 5** – Case Study A flotation data interpretation employing the historical domaining approach with curve of best fit.

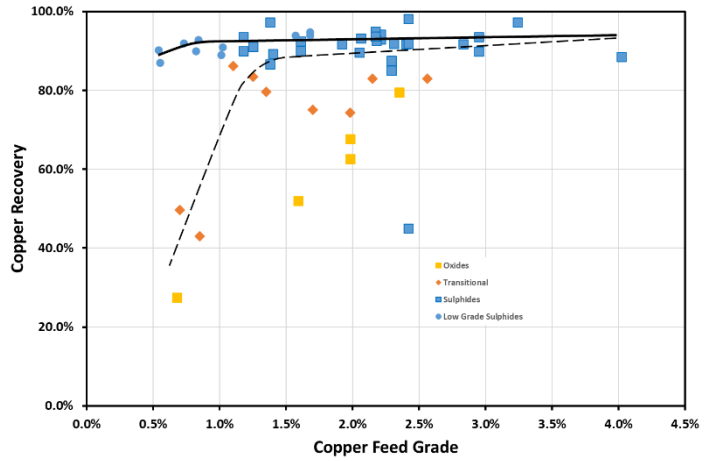



**FIG 6** – Case Study A flotation data interpretation employing the new domaining approach using the three categories (oxide, transition and sulfide) and addition of low-grade sulfide samples with curves of best fit for sulfide domains versus the historical prediction for flotation performance.

The new interpretation of results and filling in gaps in the results caused the production schedule to change. Prior to this work the sulfide ore (ore domain with highest recovery at the target concentrate grade) represented 96 per cent of the processing schedule, whereas after this work it was 99 per cent of the schedule. The sulfide domain increased because lower grade ores could be justified for the production schedule due to the improved copper recoveries. Transition and oxide domains with poorer recovery of copper decreased and only the highest head grades of these materials can be economically justified for production.

Overall, the resource scale increased by 27 per cent and the throughput rate was able to be scaled up by 29 per cent, significantly maximising the economic extraction of metal. Table 1 presents the breakdown changes with respect to content of domains, copper recovery improvement and overall effect on project strategy and economics. This project is a good example to highlight the importance of domaining and detailed procedures, and the effect that these can have on assessment on project viability.

**TABLE 1**

Summary of key changes realised from implementing proper ore domaining practises for Case Study A.

| Parameter | Change/grade, % |
|---|---|
| Original resource | |
| Oxide | 3 |
| Transition | 3 |
| Sulfide | 94 |
| Open pit cut-off grade, cu | 0.5 |
| Copper recovery improvement | +63 |
| Underground cut-off grade, cu | 1.0 |
| Copper recovery improvement | +24 |
| New resource | |
| Oxide | 0.5 |
| Transition | 0.5 |
| Sulfide | 99 |
| Increase size of resource | +27 |
| Increase scale of project | +29 |

## Case Study B

This case study considers a medium to large copper-gold project containing separate sulfide and native copper deposits. The original processing schedule was developed to treat sulfide and native copper ores at a controlled blend ratio. The resource includes numerous open pit mines but early production (>6 years) is expected to be one or two deposits only.

All native copper ores are soft. All relevant sulfide comminution data is presented for this project. The Drop Weight index (DWi) data is presented against depth and again there is no correlation between hardness and sample depth, showing that the anecdotal saying that ore hardness increases with depth doesn’t always hold true. Although the two comminution testing methods test different properties, the DWi was compared against BBWi and a broad linear relationship is observed which can potentially lead to BBWi being used as a proxy for DWi in future ore characterisation test work (see Figure 7).

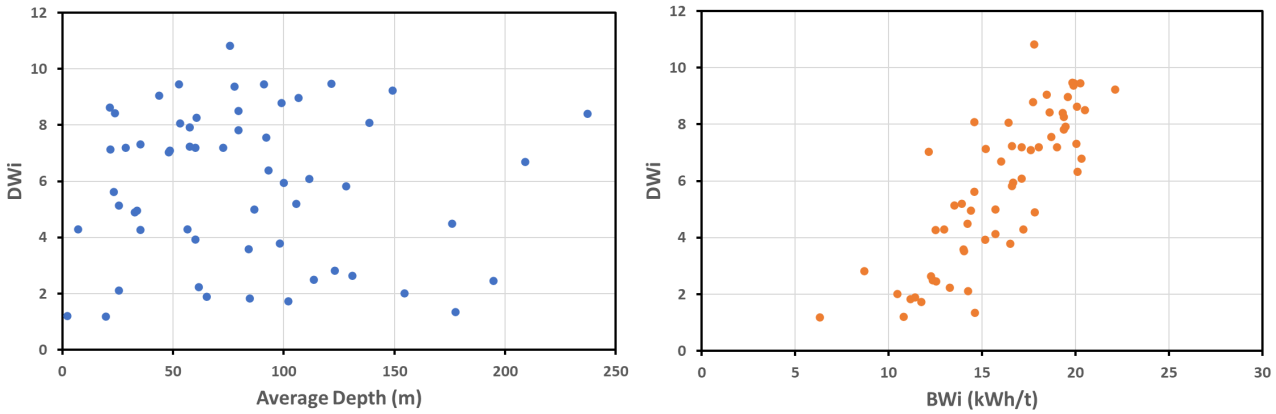



**FIG 7** – Case Study B comminution data assessment (left) DWi versus average depth showing DWi is highly variable at all depths. (right) DWi versus BBWi showing a broad linear relationship between the two separate comminution parameters.

The frequency of DWi data is presented in Figure 8 for DWi ranges covering soft, soft-medium, medium-hard and hard. Interestingly, plotting the frequency distribution this way shows almost equal number of samples characterised for each of the hardness categories. It is not surprising the comminution circuit was designed with a 75th percentile hardness DWi of approximately 8.0.

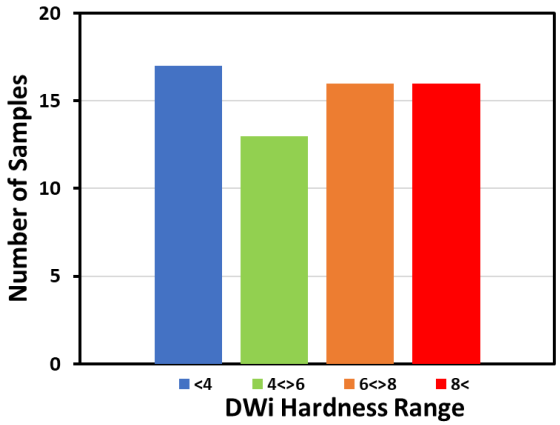



**FIG 8** – Frequency distribution of Drop Weight Index (DWi) results for comminution samples.

Due to the high variability in samples characterised, Sedgman requested that each of the samples be spatially mapped in the project block model with colour coding to represent each of the four hardness categories, shown in Figure 9. This assessment revealed that all the hardest sample to be located at one end of the deposit and the softest samples at the opposite end. The medium hardness samples were in the middle. Considering that the ore grades are very similar across the entire deposit and the overburden depth is consistent too, this information opened the way for significant project optimisation during the initial financial payback years.

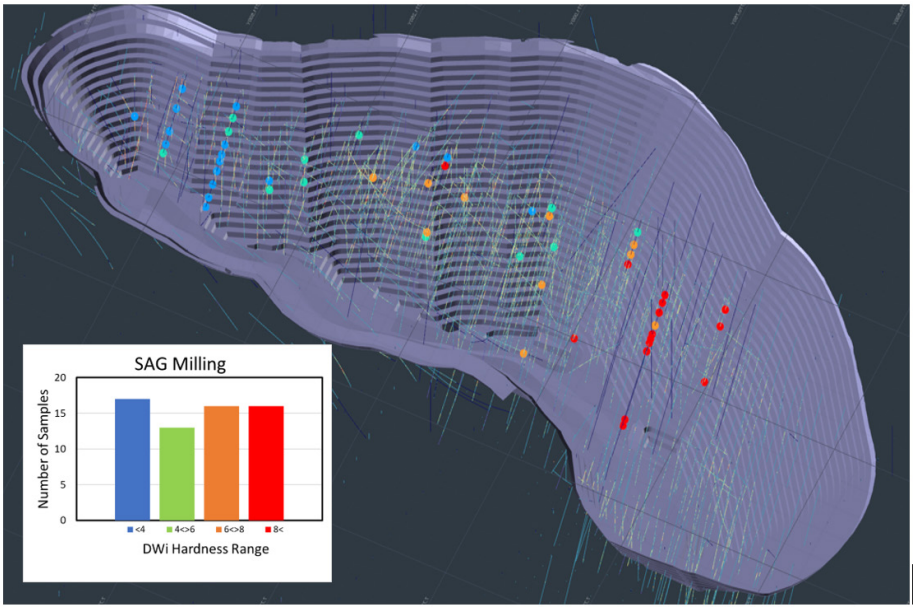



**FIG 9** – Spatial representation of the ore hardness variability across the proposed pit shell with the frequency distribution for hardness shown in the bottom left.

For this project it is particularly important to comment on the mineralogy and key characteristics of the different materials for treatment. The native copper ore is dominated by metallic copper (>85 per cent of the copper content) and is coarse grained with a $P_{80}$ ≥ 100 µm for the mineral. It needs to be pointed out that native copper mineral is malleable and ductile which means that during comminution the mineral concentrates into the coarsest size fractions, which is contrary to sulfides. The sulfide minerals are typically between 18–40 µm $P_{80}$ and easily liberate at coarse target grind sizes due to being soft and brittle. The head grade of the native copper ore is 15 per cent higher than sulfide ore and was considered higher value on that basis.

A high-level summary of the concentrate grade against primary grind size for various ore domains and blends is presented in Figure 10. Native copper samples consistently upgraded to ≥25 per cent copper grade in concentrate with a primary grind of 75 µm $P_{80}$. At primary grinds ≥100 µm $P_{80}$ this copper grade in concentrate was not achievable. Sulfide samples were optimised for flotation and locked cycle tested at coarser primary grind sizes of 180 µm and 250 µm $P_{80}$. The results are consistent with ≥28 per cent copper grade in concentrate at recoveries ≥95 per cent.

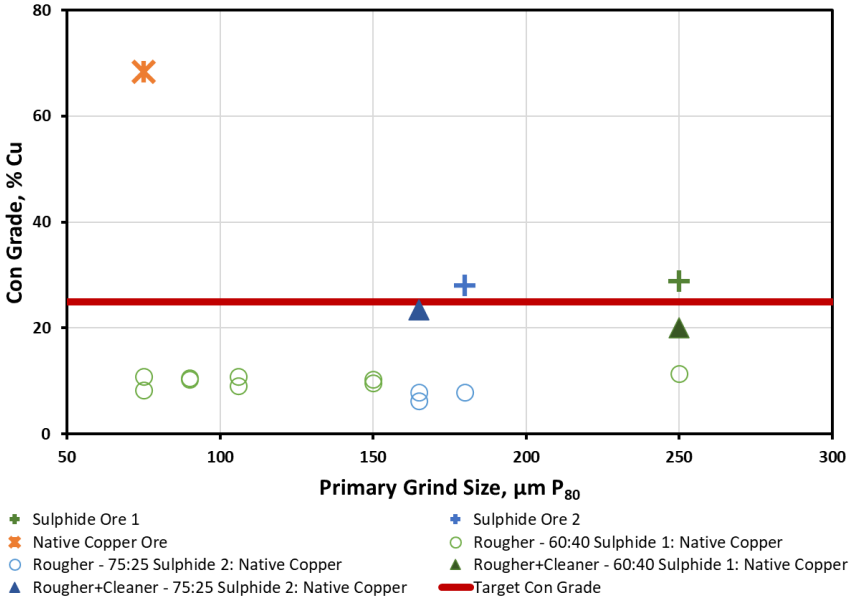



**FIG 10** – Concentrate grade against primary grind size for ore types and blends, with the target concentrate grade shown via the red line.

The production strategy to blend the sulfide and native copper ores was derived so that sulfide ore dominated the feed to the concentrator flow sheet. The sulfide: native copper ores were tested in blends of 75:25 and 60:40 to cover the most likely production scenarios. They considered that such blends would provide a softening of the feed blend and that the blended head grade of the native copper ore would naturally produce a weighted average flotation performance of the individual domains. Figure 11 shows the anticipated blended recovery targets by the blue and green lines. None of the laboratory flotation test work could support this expectation and in fact, all blended test work fell short in terms of concentrate grade target and ≥13 per cent recovery at primary grinds of 165 µm and 250 µm $P_{80}$ shown in Figure 10. The reasons for this underperformance is related to the lack of liberation of native copper in the blend at these target grind sizes and the difficulty in achieving optimum flotation performance for the individual domains once blended.

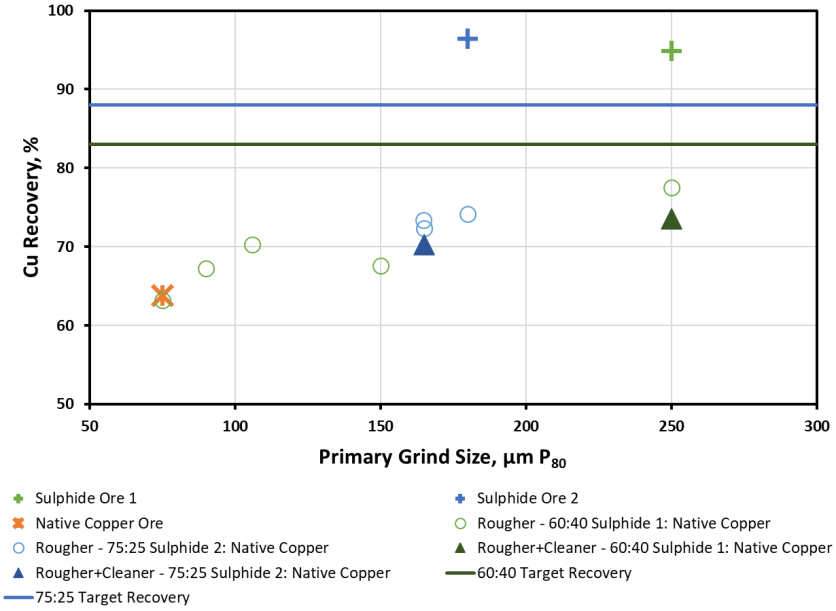



**FIG 11** – Copper recovery against primary grind size for various ore types and blends, with green line showing 60:40 sulfide: native copper target recovery and blue line showing 75:25 sulfide: native copper target recovery.

Sedgman's assessment resulted in a production strategy change and a change in key equipment selection. The overall benefits realised a 34 per cent increase in metal production compared to the base case by end of year four, as shown in Figure 12. Focus changed to be on batch processing of the different domains to maximise their respective recoveries. Treating the softer sulfide ores first (higher value ores) provided higher throughput rates at coarse primary grinds and higher copper output (throughput rate and recovery driven). The soft native copper ores were delayed for the end of mine life and could utilise a cut down version of the comminution circuit and still achieve a primary grind of 75 µm $P_{80}$ and maintain the target throughput rate, due to their soft comminution properties compared to the sulfide ores. Overall, these strategies delivered significant value to the project and resulted in the change of production strategy to enable this early value generation.

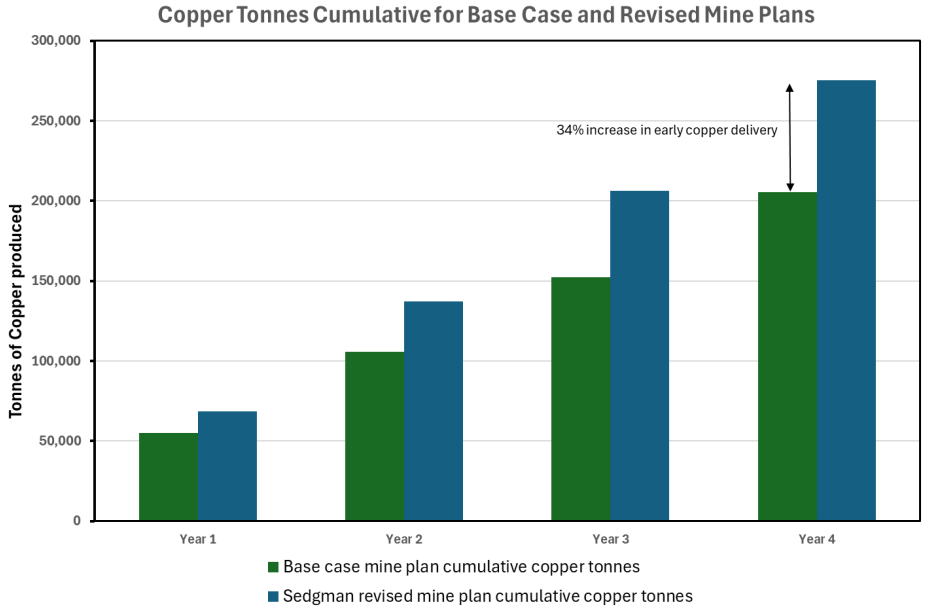



**FIG 12** – Copper production cumulative over production years 0–4 for the base case and revised mine plans.

## CONCLUSION

The case studies presented demonstrate the importance of best practise with respect to sampling, ore characterisation, domaining and metallurgical testing to support the design basis, and technical and economic viability, of copper development projects.

Case Study A presented an overall resource increase of 27 per cent thereby making the project economically viable. This increase was enabled by better definition of flotation domains, separate testing and analysis of individual domains and targeted testing of low-grade samples aimed at improving metal recoveries at cut-off grades. A lack of domaining led to poor and confusing test work results until the performance of individual components were understood. The best performing domain (sulfides) increased in overall content from 96 per cent to 99 per cent of the resource. The remaining 1 per cent of the resource was originally considered important for the initial production years but now is divided between high-grade transition and oxide domains that were delayed until late in the mine life.

Case Study B provided an overall benefit of 34 per cent increase in metal production (and value) compared to the base case by end of production year four. Although slightly higher head grade than sulfide ore, the recoverable copper content of native copper ores is significantly lower which resulted in the strategy and plant design to change. Focus changed to be on batch processing of the different domains. Detailed assessment of comminution samples and spatial 3D mapping in the block model supported softer sulfide being the early priority to maximise project value. Sulfide ores were found to have substantial soft ore available in the early production schedule, they are liberated for flotation at much coarser primary grinds and despite a lower head grade, the copper and gold production rates are higher due to much higher metal recoveries compared to native copper ores.

## REFERENCES

Morrell, S, 2004. Predicting the Specific Energy of Autogenous and Semi-autogenous Mills from Small Diameter Drill Core Samples, *Minerals Engineering*, 17(3):447–451.

Morrell, S, 2008. A method for predicting the specific energy requirement of comminution circuits and assessing their energy utilisation efficiency, *Minerals Engineering*, 21(3):224–233.

Way, D, McKee, D and Pease, J, 2021. Comminution and Mineral Separation – Geological Input to Metallurgy, *Society of Economic Geologists (SEG) Discovery*, 126:28–41.

## Metallurgy Symposium

# Operating updates, newly commissioned plants and plant design

# Characterisation and flotation behaviour of copper smelter slag at Mount Isa Mines

*J Begelhole*[1]

1. Senior Project Metallurgist, Glencore, Mount Isa Qld 4825.
   Email: jason.begelhole@glencore.com.au

## ABSTRACT

Copper smelter slag produced at Mount Isa Mines represents a complex flotation feed due to its unique mineralogical characteristics and the conditions under which it forms. Rapid cooling of molten slag during smelting and converting results in extremely fine copper sulfide grain sizes, with mineralogical analysis indicating that more than half of the copper sulfide mass is below 10 µm and approximately 27 per cent is below 5 µm. Liberation at conventional grind sizes is correspondingly limited, with only ~50 per cent of copper sulfides reporting as liberated in the RHF slag head sample. These mineralogical constraints fundamentally shape the flotation response of slag and underpin the metallurgical behaviour observed across laboratory and plant studies.

This paper presents a comprehensive characterisation of slag flotation performance across two feed blends, RHF:Magnetics (RHF:Mags) and RHF:Converter (RHF:Conv), drawing on laboratory test work and plant survey data collected between 2024 and 2026. Grind-size investigations demonstrated that both blends exhibit similar flotation behaviour despite differences in chemical composition. Reducing the grind size from the plant standard of 90 µm to ~40–50 µm produced only marginal improvements in copper recovery, whereas increasing the grind size to ~125–140 µm significantly reduced recovery and concentrate grade. These results confirm that significant improvements in liberation would require grinding to $P_{80}$ values approaching 10 µm, which is not practically achievable within existing circuit constraints.

Flotation kinetics were exceptionally fast for both blends. Laboratory tests showed that more than 80 per cent of the total copper recovery occurred within the first few minutes of flotation at standard grind sizes, with finer grinds accelerating early recovery but not materially increasing final recovery. Plant cell-by-cell surveys validated these findings, with Bank 1 alone accounting for approximately 75 per cent of the total circuit recovery, and subsequent banks contributing only minor incremental gains. This alignment between laboratory and plant behaviour highlights the strong influence of liberation on flotation rate and the limited presence of floatable copper beyond the initial rougher bank.

A reagent-screening program evaluated the influence of collector chemistry on slag flotation performance across both laboratory-prepared and hot-floated plant feeds. Despite differences in head grade, operator technique, and reagent scheme, all tests converged to a narrow final recovery range of 89–92 per cent. While certain collectors influenced early kinetics and concentrate grade, none produced a substantial increase in ultimate recovery. These results demonstrate that collector selection is not a controlling variable in slag flotation and that reagent optimisation cannot compensate for liberation limitations inherent to the slag mineralogy.

Overall, the combined mineralogical, laboratory, and plant findings confirm that copper recovery from smelter slag is governed primarily by liberation rather than reagent chemistry or circuit configuration. Improvements in metallurgical performance will therefore require strategies that enhance liberation or promote copper sulfide grain growth, such as slower slag cooling, rather than further modification of collector schemes.

## INTRODUCTION

Copper smelter slag is generated as a by-product of pyrometallurgical copper processing, produced at two principal stages: the Rotary Holding Furnace (RHF), where matte and slag separate following IsaSmelt furnace treatment of copper concentrate, and the Peirce-Smith Converters, where copper matte is further refined toward blister copper. Molten slag from each stage reports to a common slag stockpile, where it is subsequently crushed, screened, ground and processed through flotation to

recover residual copper values before disposal to a slag dam. Two feed blends are considered in this paper: RHF:Mags, comprising RHF slag combined with a magnetic slag fraction historically used to line the cooling dam wall (typically at a ratio of approximately 15 per cent by weight), and RHF:Converter (RHF:Conv), comprising RHF slag combined with approximately 15 per cent Converter slag (Begelhole, 2024a, 2024c).

Not all copper reporting to the smelter is recovered as metal or matte. During smelting and converting, fine droplets of copper-bearing matte can become physically entrained in the slag phase before sufficient settling time has elapsed (Cheng *et al,* 2017), particularly where rising sulfur dioxide gas bubbles generated during oxidation carry matte droplets across the matte-slag interface (Minto and Davenport, 1972). This entrained matte, rather than being converted through to metallic copper, reports with the slag and is subsequently lost to the slag stockpile unless recovered by downstream processing (Ruddle, 1953). Flotation of the crushed and ground slag is intended to recover this residual copper before the material reports to final tailings.

This paper presents a technical characterisation of copper smelter slag, covering its mineralogy, comminution behaviour, flotation performance across grind sizes, plant-scale validation, and reagent response. The work draws on laboratory test work and plant survey data collected between 2024 and 2026. The slag processing flow sheet is shown in Figure 1.

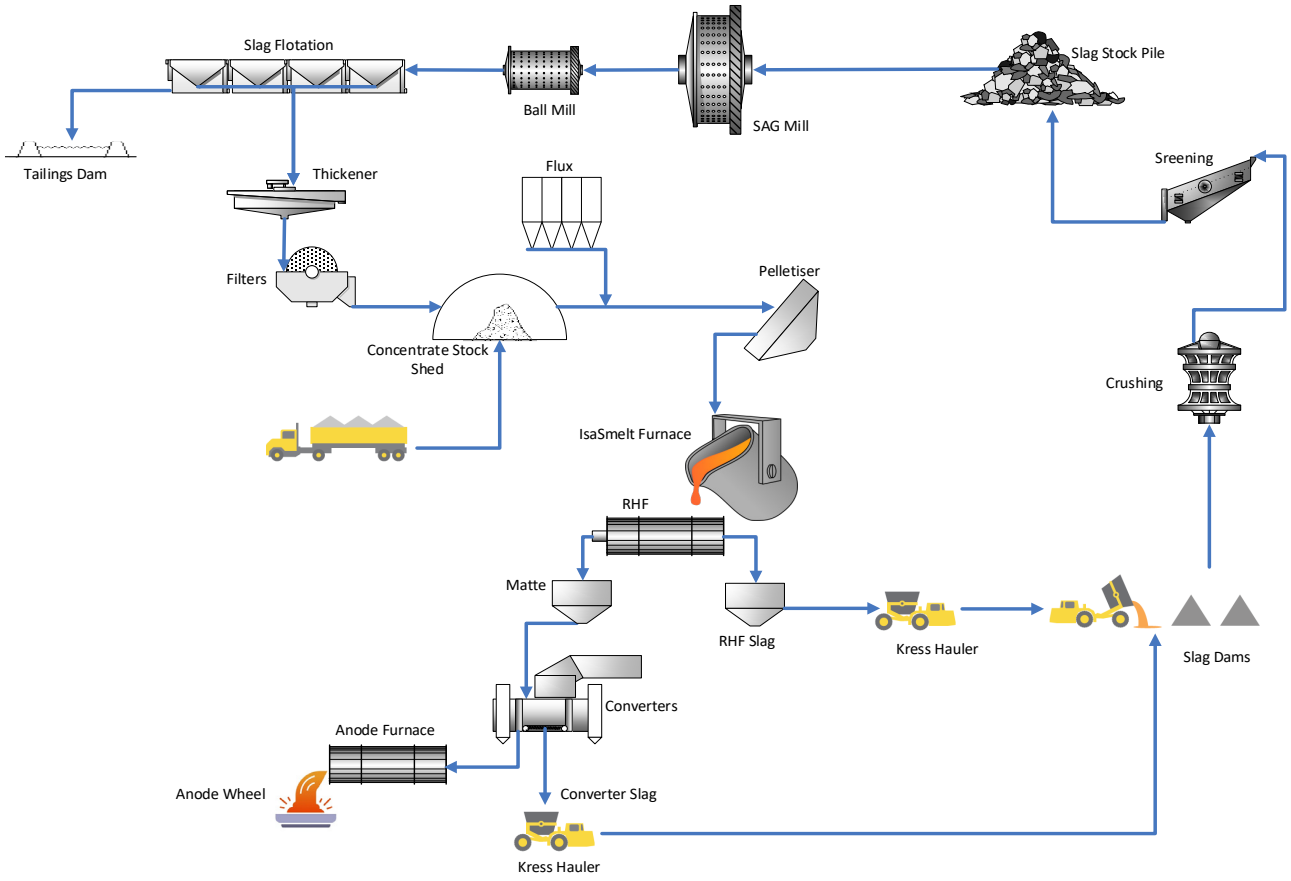



**FIG 1** – Slag process flow diagram.

It must be noted that the RHF:Mags blend is no longer processed (Begelhole, 2024b); however, it remains relevant to the test work comparisons and this paper, as several of the surveys and comparisons were conducted when this blend was processed in the concentrator. There was a magnetic separation stage after screening (Begelhole, 2024b). The non-magnetics were fed back into the smelter, and the magnetic component (Mags) was used to line the slag dam walls of new dams, and it was processed in a separate flotation process. This reduced the copper head grades without significantly affecting the other elements.

## MINERALOGY

Mineralogical characterisation of RHF slag was conducted in 2017 by XPS Consulting and Test work Services using a head sample collected from the process plant, with a $P_{80}$ of 102 µm (XPS Consulting and Test work Services, 2018). This work characterised the grain size of the copper sulfide minerals present, finding them to be extremely fine: approximately 53 per cent of the total copper sulfide mass is below 10 µm, and approximately 27 per cent is below 5 µm (Figure 2).

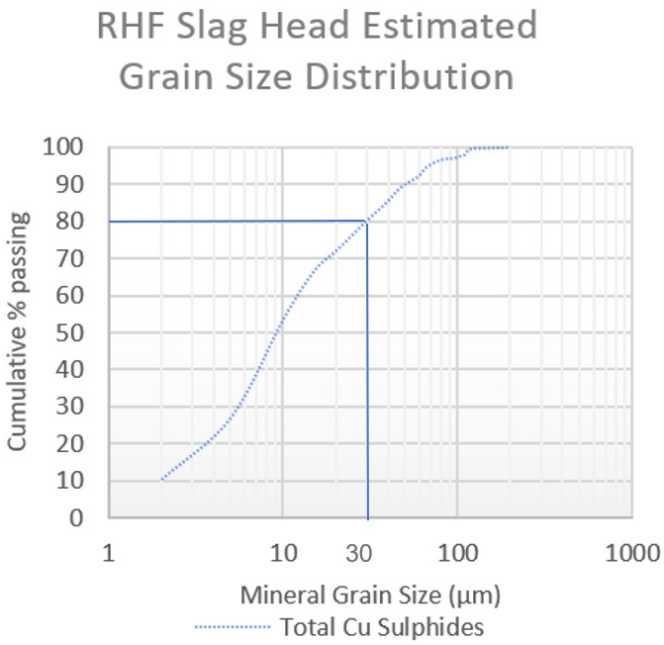



**FIG 2** – Cu grain size distribution.

The same work found that copper sulfides in the RHF slag head sample were only moderately liberated, at approximately 50 per cent (Figure 3). The locked and middling fractions were found to be associated with a combination of slag phases, iron sulfides and non-sulfide gangue (NSG).

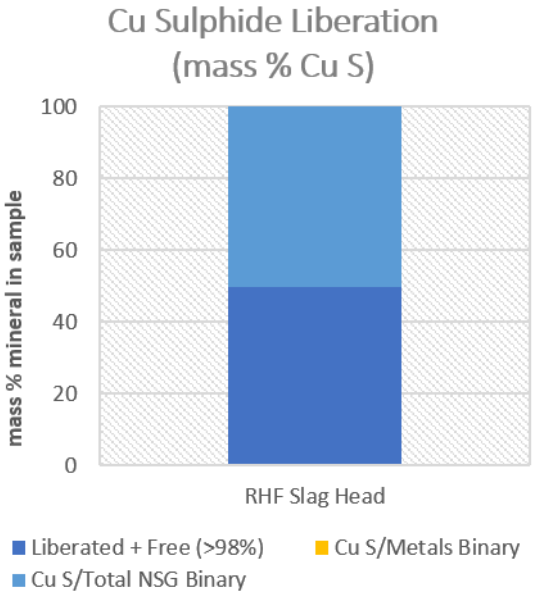



**FIG 3** – Cu sulfide liberation.

This fine grain size is attributed to the rapid cooling that molten slag undergoes during production. Slag is poured from the furnace into cooling pits or dams while still molten and cools far more rapidly than a natural orebody. Rapid cooling arrests the growth of mineral crystals: many nuclei form almost simultaneously as the liquid cools, but none are given sufficient time to grow before the system fully

solidifies. This contrasts with a natural orebody, which cools over geological timescales, allowing relatively few nuclei to form and each to grow to a substantially larger final grain size.

The mineralogy of the copper sulfide species present, principally bornite and chalcopyrite in roughly equal proportion, with chalcocite as a minor phase, is not itself unusual; it is the grain size distribution, a consequence of the cooling rate, that fundamentally distinguishes this material from a conventional ore feed. Because the ultrafine copper sulfide grain size is directly controlled by the cooling rate, slower pot cooling could, in principle, promote larger copper sulfide grain growth and improve liberation at practical grind sizes.

This fine-grain size and the correspondingly limited liberation achieved at conventional grind sizes are the central mineralogical constraints that underpin the flotation and plant performance findings discussed in the following sections.

## FLOTATION TEST WORK

Table 1 shows the head assays for the two tested blends, RHF:Mags Blend and RHF:Conv slag. During extensive testing of both blends, it was found that, despite their different chemical compositions, the physical separation was relatively similar, as observed in lab flotation tests and in the results obtained (Begelhole, 2024a, 2024c).

**TABLE 1**

Head grades for lab flotation sample charges.

| Sample | Pb (%) | Zn (%) | Cu (%) | Fe (%) | CaO (%) | S (%) | $SiO_2$ (%) | $Al_2O_3$ (%) | MgO (%) | As (%) | Ba (%) |
|---|---|---|---|---|---|---|---|---|---|---|---|
| RHF:Mags | 0.20 | 0.69 | 2.43 | 37.50 | 3.47 | 1.21 | 34.10 | 3.51 | 2.36 | 0.11 | <0.1 |
| RHF:Conv | 0.30 | 0.38 | 3.40 | 39.70 | 2.72 | 1.19 | 32.30 | 2.86 | 2.09 | 0.09 | 0.10 |

### Sample preparation

Approximately 150 kg of sample was taken from the Semi-Autogenous Grinding (SAG) mill feed stockpile. This material was crushed and screened to -2 mm using a lab jaw crusher and then placed into a large rotary splitter to produce eight portions. These portions were split and recombined three times to ensure complete mixing of the large sample. The fourth split was divided into eight portions; each portion was weighed and sub-sampled using a small rotary splitter, producing approximately 78 × 2 kg charges, and a head sample was sent for assay as a representative of the other 78 samples.

### Grind establishment

The target grind size for both the RHF:Conv and RHF:Mags blends was a $P_{80}$ of 90 µm, consistent with normal plant operating conditions for slag processing. For the RHF:Conv blend, the initial grind time of 900 sec, chosen based on the RHF:Mags starting point, proved insufficient, resulting in a coarse $P_{80}$ feed size of 242 µm. Subsequent increases in grind time progressively reduced the $P_{80}$: 123 µm at 1800 sec, 100 µm at 2100 sec, and finally 91 µm at 2400 sec, indicating that approximately 2400 sec of grinding would be required to achieve the target of 90 µm. In comparison, the RHF:Mags blend responded more predictably, with grind times of 900 sec, 1500 sec, and 1850 sec producing $P_{80}$s of 151 µm, 112 µm, and 84 µm, respectively; fitting these results gave an estimated 1800 sec to reach the same 90 µm target. The grind establishment curves for both blends are shown in Figure 4.

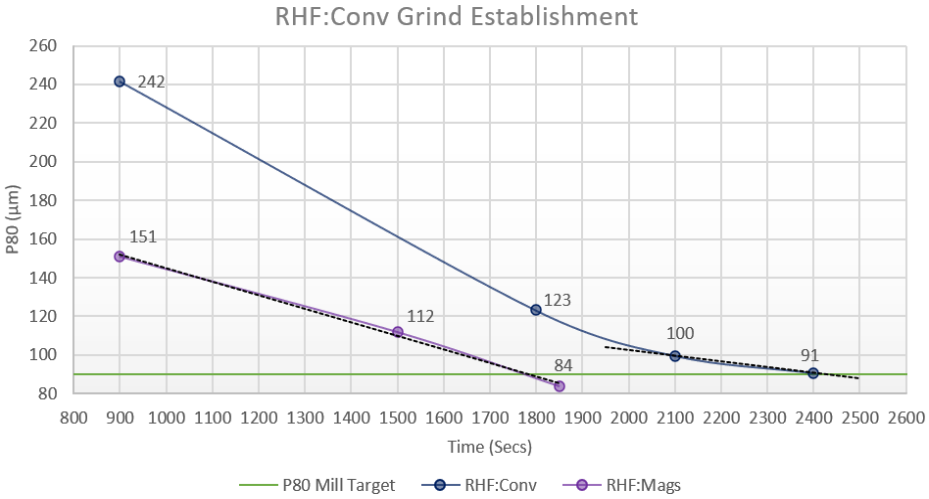



**FIG 4** – Grind establishment curves for RHF:Conv and RHF:Mags blends.

## Impact of grind size

Different grind sizes were evaluated to assess their effects on concentrate grade and copper recovery for the RHF:Conv and RHF:Mags blends. The objective of grind size optimisation is to identify the finest $P_{80}$ at which the additional grinding energy remains cost-effective, balancing the revenue from increased copper recovery against the cost of grinding. Conversely, if the same recovery can be achieved at a coarser grind, the reduction in grinding energy is also worth pursuing, as it lowers operating cost without penalising recovery or grade.

The RHF:Conv tests were conducted at grind times of 1800 sec ($P_{80}$ ~125 µm), 2400 sec ($P_{80}$ ~90 µm, the standard plant grind) and 4800 sec, which doubled the energy input but only reduced the $P_{80}$ to ~40 µm. Figure 5 shows the cumulative mass recovery for the three grind sizes. The finer grind produced a moderate increase in mass recovery, whereas coarsening the grind from 90 µm to 125 µm substantially reduced the mass recovery.

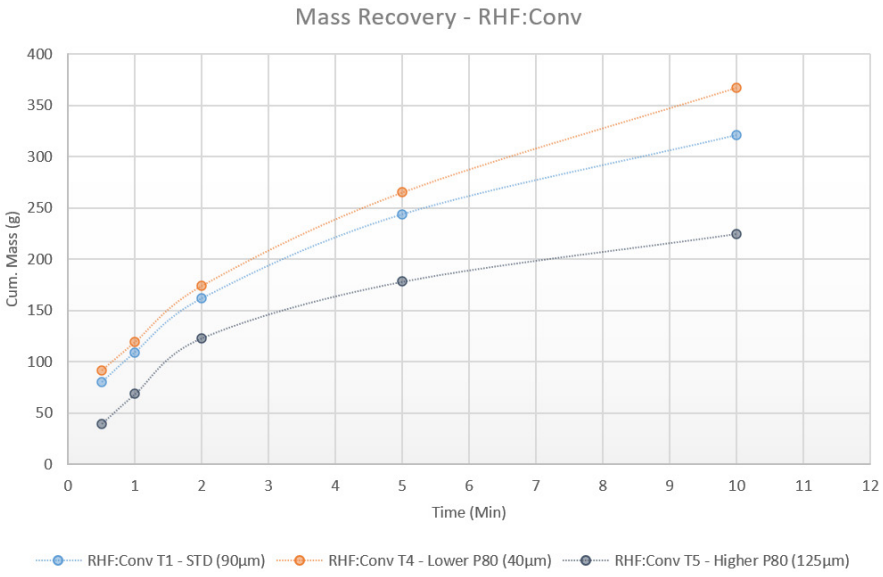



**FIG 5** – RHF:Conv blend mass recovery versus time.

Figure 6 shows the grade-recovery curves for the three grind sizes across two blends. Both blends show similar trends despite the 1 per cent increase in head grade for the RHF:Conv samples. Reducing the grind size from 90 µm to 40–50 µm produced only a small improvement in recovery and a slight reduction in concentrate grade. However, shifting the grind size to 125–140 µm noticeably lowers the concentrate grade and recovery.

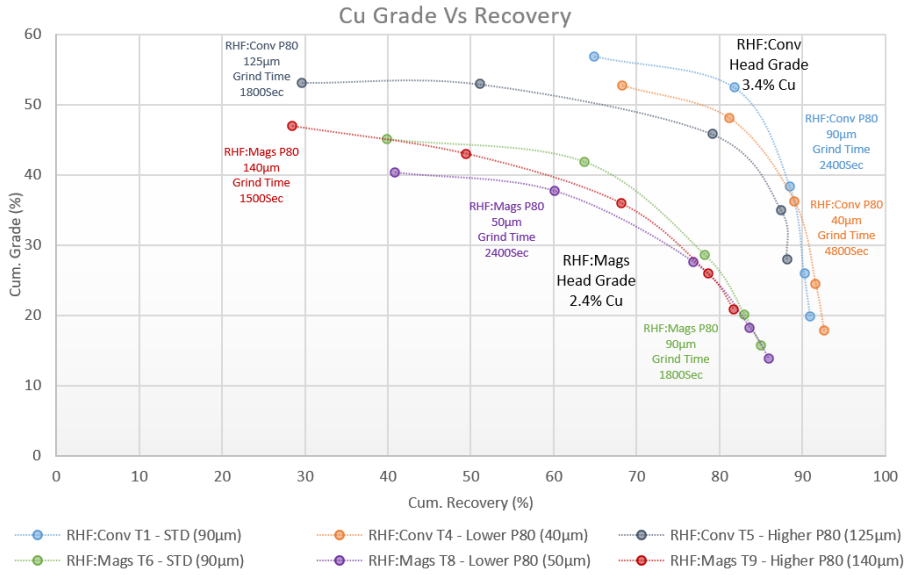



**FIG 6** – Grade-recovery curves for the different blends and grind sizes.

The decrease in performance at a coarser $P_{80}$ is due to the fine copper sulfide grains remaining locked within larger slag particles, which limits the exposure of sulfide surfaces available for bubble attachment (Begelhole, 2024a, 2024c). Conversely, the very small improvement observed when decreasing the $P_{80}$ is explained by the extremely fine grain size of the copper minerals: significant increases in liberation would require grinding to a $P_{80}$ close to 10 µm, far finer than is practical in the existing circuit. Doubling the grinding energy to achieve a 56 per cent reduction in $P_{80}$ (90 µm to 40 µm) produced a 1.6 per cent increase in copper recovery and a 2.0 per cent decrease in concentrate grade. When the economics are evaluated, the additional revenue from the recovery gain is sufficient to justify the doubled grinding cost. However, the returns diminish rapidly: recovery gains flatten as the liberation limit is approached, while grinding energy rises steeply as $P_{80}$ is reduced (Bond, 1952; Wills and Finch, 2016), so each further step finer delivers less recovery for more energy.

Observations during the three RHF:Conv flotation tests in Figure 6, with a head grade of 3.4 per cent Cu, showed little difference between 90 µm and 40 µm in this blend (Begelhole, 2024c). However, at a $P_{80}$ of 125 µm, the physical appearance of the froth was vastly different, regardless of having the same reagent scheme. The froth was lightly loaded with weak bubbles, and the very low recovery demonstrates this.

## Copper kinetics

The copper recovery kinetics for both the RHF:Mags and RHF:Conv materials show a consistent and predictable relationship between grind size ($P_{80}$) and flotation performance. In both data sets, the finer $P_{80}$s (~40–50 µm) and the standard plant grind (~90 µm) show faster initial recovery followed by an early plateau, whereas the coarser grinds (~125–140 µm) delay recovery despite ultimately reaching similar cumulative values. The similarity in kinetic behaviour across both blends indicates that particle liberation is the dominant control on flotation rate, regardless of feed type (Begelhole, 2024a, 2024c).

Figure 7 presents the copper recovery kinetics for the RHF:Mags blend across three grind sizes. Both the 50 µm and 90 µm grinds show rapid early recovery, reaching approximately 78 per cent cumulative recovery within two mins of flotation, with a final value of approximately 86 per cent. Their steep initial slopes indicate strong liberation at these sizes, enabling copper-bearing particles to float quickly. The 140 µm grind displays slower kinetics, with a lower initial recovery and a more gradual rise toward its final cumulative value; although it eventually approaches a similar overall recovery, it requires longer flotation time to do so (Begelhole, 2024a).

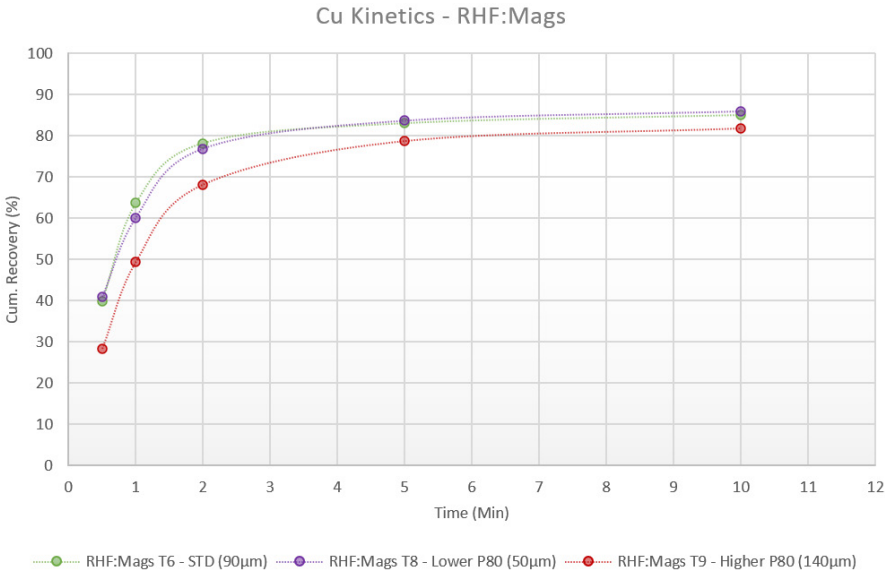



**FIG 7** – RHF:Mags blend kinetic curves.

Figure 8 shows the same comparison for the RHF:Conv blend, and the trends closely mirror those observed in Figure 7. The standard grind (90 µm) and the finer grind (40 µm) both achieve approximately 89 per cent cumulative recovery within two mins and plateau shortly after, while the coarser grind (125 µm) again shows reduced initial recovery and a more gradual approach to its final value. In both blends, liberation constraints at coarser $P_{80}$s limit early recovery and extend the time required to reach peak cumulative recovery (Begelhole, 2024c).

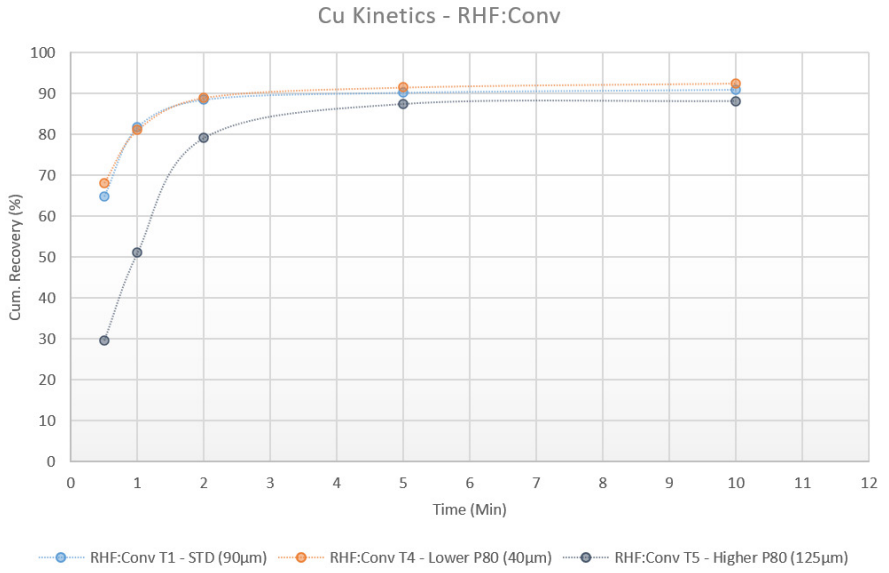



**FIG 8** – RHF:Conv blend kinetic curves.

## Grade and recovery

The grade-recovery curves for both RHF:Mags and RHF:Conv show the same fundamental behaviour: grind size controls the maximum recovery achievable. The finer grinds (40–50 µm) extend the curve to the highest ultimate recovery but sit slightly below the standard grind size in concentrate grade across the recovery range, reflecting the additional gangue recovered with partially liberated composite particles. The coarser grinds (125–140 µm) cut the curve at a lower maximum recovery because a greater proportion of the copper sulfides remain locked in gangue. The alignment of these trends across both blends confirms that grind size is the dominant control on the grade-recovery performance (Begelhole, 2024a, 2024c).

Figure 9 illustrates the grade-recovery response of the RHF:Mags blend at three grind sizes (50 µm, 90 µm and 140 µm). The standard plant grind (90 µm) reaches approximately 85 per cent recovery, and the finer grind (50 µm) extends this only marginally to approximately 86 per cent recovery. The coarser grind (140 µm) produces approximately 82 per cent recovery but at a higher final grade of 20.9 per cent Cu. This behaviour is consistent with reduced liberation at coarse $P_{80}$s, where locked copper sulfide grains report to tailings, and with reduced selectivity at fine $P_{80}$s, where gangue attached to partially liberated grains reports to the concentrate.

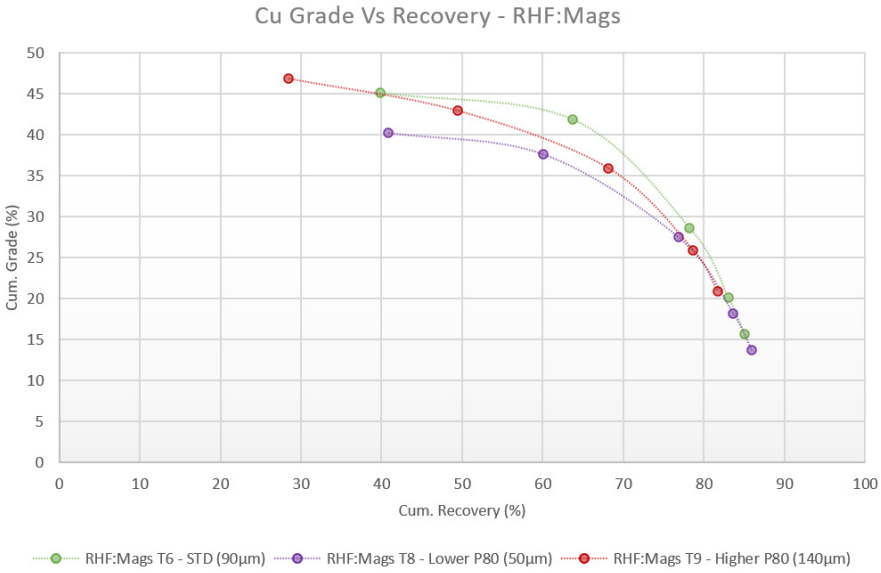



**FIG 9** – RHF:Mags grade-recovery.

Figure 10 presents the same comparison for the RHF:Conv blend, and the trends closely mirror those observed in Figure 9. The 90 µm and 40 µm grinds achieve approximately 91 per cent and 93 per cent recovery, respectively, with the 40 µm curve again sitting slightly below the 90 µm curve in concentrate grade. The 125 µm grind produces approximately 88 per cent recovery, with a final grade of 28.0 per cent Cu compared with 19.8 per cent Cu for the standard grind. In both blends, reducing the grind size below the plant standard buys a small gain in ultimate recovery at the cost of grade, while coarsening it forfeits recovery.

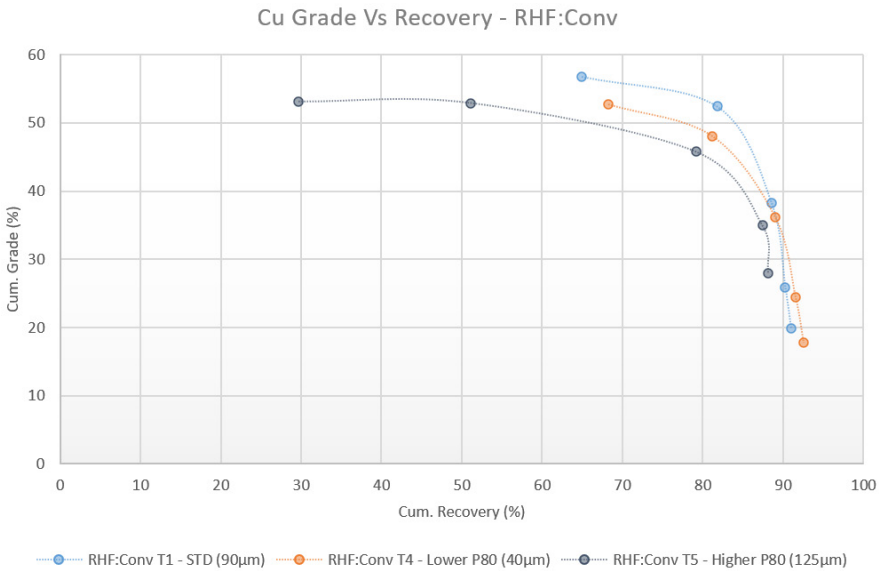



**FIG 10** – RHF:Conv grade-recovery.

## Selectivity

To quantify the selectivity of each grind size, the gangue mineral recoveries corresponding to the maximum Cu recovery achieved in each test were tabulated. This approach provides a consistent and metallurgically significant basis for comparison, as it reflects the impurity levels present when each test is pushed to its practical recovery limit. Reporting $SiO_2$, Fe, MgO and $Al_2O_3$ recoveries at these end points highlights how grind size influences gangue flotation. Finer $P_{80}$s (40–50 µm) achieve slightly higher Cu recovery but lower concentrate grades. Two mechanisms are likely to contribute: copper sulfide grains, while more exposed, remain only partially liberated, allowing gangue minerals attached to these grains to float with them; and the greater proportion of fine gangue produced at a $P_{80}$ of 40–50 µm increases the potential for entrainment into the concentrate. Entrainment was not measured directly in this program, but the similar increases in Fe, $SiO_2$, $Al_2O_3$ and MgO recoveries at the finer grinds (Table 2) are consistent with a non-selective mechanism contributing alongside composite flotation. In contrast, coarser $P_{80}$s (125–140 µm) show lower gangue recovery and higher concentrate grades, but at the cost of reduced Cu recovery due to insufficient liberation of the copper sulfide grains. The values for all tests are summarised in Table 2.

**TABLE 2**

Gangue mineral recoveries at maximum Cu recovery for each grind size.

| Test | Blend | $P_{80}$ (µm) | Cu Grade (%) | Cu Rec (%) | Fe Rec (%) | $SiO_2$ Rec (%) | $Al_2O_3$ Rec (%) | MgO Rec (%) |
|---|---|---|---|---|---|---|---|---|
| T6 | RHF:Mags | 90 | 15.70 | 84.99 | 11.00 | 10.80 | 11.64 | 9.66 |
| T8 | RHF:Mags | 50 | 13.78 | 85.91 | 12.67 | 12.77 | 13.75 | 11.44 |
| T9 | RHF:Mags | 140 | 20.86 | 81.72 | 7.10 | 6.92 | 7.63 | 6.25 |
| T1 | RHF:Conv | 90 | 19.85 | 90.96 | 12.15 | 12.73 | 13.44 | 10.42 |
| T4 | RHF:Conv | 40 | 17.83 | 92.56 | 14.34 | 15.41 | 16.20 | 13.20 |
| T5 | RHF:Conv | 125 | 27.99 | 88.18 | 7.79 | 7.99 | 8.12 | 6.74 |

Table 2 shows that finer grind sizes consistently produce higher gangue recoveries across both RHF:Mags and RHF:Conv, reflecting reduced selectivity caused by partial liberation of both copper sulfides and gangue minerals. The standard plant grind (90 µm) provides intermediate gangue recovery, balancing copper exposure and gangue rejection. Coarser grind sizes (125–140 µm) deliver the lowest gangue recoveries and therefore the best selectivity, although this comes with lower Cu recovery because many copper sulfide grains remain locked. These trends align with the grade-recovery curves presented in Figures 9 and 10, confirming that grind size is the dominant control on impurity rejection.

# PLANT PERFORMANCE

To complement the grind-size and selectivity analysis, a detailed cell-by-cell survey of the rougher-scavenger circuit was completed to quantify how copper recovery and grade progress through each flotation bank. Individual cell samples were collected using best-practice sampling methods, enabling calculation of dry mass flow, copper grade, and copper recovery for each cell, which were subsequently combined to produce downstream cumulative values. This section presents the cell-by-cell recovery profile and demonstrates how the flotation behaviour observed in laboratory kinetics is reflected in full-scale plant operation. The resulting cell-by-cell grade-recovery profile is presented in Figure 11.

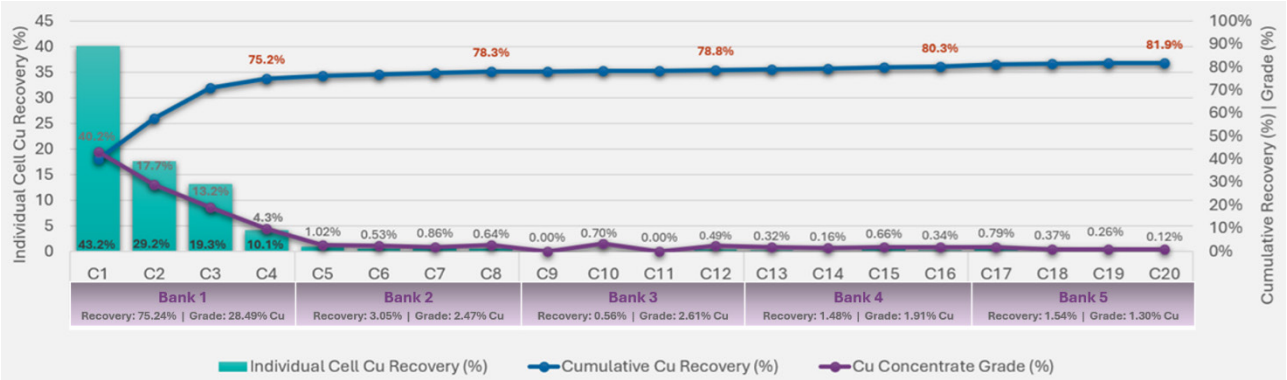



**FIG 11** – Cell-by-cell recovery profile.

The individual cell recoveries show that most of the copper is recovered in Bank 1, with Cell 1 alone accounting for approximately 40 per cent of total circuit recovery. Recoveries then decrease sharply across Cells 2 to 4, falling from 18 per cent to 13 per cent, then to around 4 per cent. From Bank 2 onward, every cell contributes less than 1 per cent recovery, indicating that only minimal amounts of floatable copper remain in the circuit after the first bank. The copper grade profile mirrors the laboratory profile, starting at approximately 43 per cent Cu in Cell 1 and declining sharply through Cells 2 to 4 before falling to below 5 per cent Cu by the end of Bank 1, consistent with the rapid early flotation observed in the lab tests.

The cumulative recovery curve rises steeply through Bank 1, reaching ~75 per cent Cu recovery, and then flattens considerably, increasing only marginally to ~82 per cent by the end of Bank 5. This behaviour mirrors the laboratory flotation kinetics, where tests T1 and T4 achieved 65–68 per cent Cu recovery within the first 30 sec and approached their final recovery within two mins. Given that Bank 1 provides a residence time similar to the early laboratory flotation interval, the cell-by-cell survey confirms the extremely fast flotation kinetics of copper in slag and validates the laboratory findings (Begelhole, 2024b).

## REAGENT SCREENING

A reagent-screening program was completed to evaluate whether collector selection has any measurable influence on ultimate copper recovery in slag, given that mineral liberation had already been established as the dominant metallurgical constraint. Two feed types were tested: laboratory-ground slag samples (T-series and R-series) and hot-floated plant feed samples (KT-series). These samples differed significantly in head grade. Table 3 summarises the head grades for both feed types.

**TABLE 3**

Head grades for KT, T and R samples.

| Sample | Cu (%) | Fe (%) | S (%) | $SiO_2$ (%) | MgO (%) |
|---|---|---|---|---|---|
| KT-Series | 5.66 | 32.7 | 2.76 | 32.8 | 2.44 |
| T and R-Series | 3.40 | 39.7 | 1.19 | 32.3 | 2.09 |

The KT feed contained substantially higher copper and sulfur, reflecting a greater proportion of copper sulfides. In contrast, the T and R feed had lower sulfur and higher iron.

Table 4 summarises the reagent schemes tested across both feed types and the corresponding final grade-recovery outcomes. The reagent schemes comprised a frother, methyl isobutyl carbinol (MIBC) or KemFroth011, with one or more collectors: sodium isobutyl xanthate (SIBX), sodium isopropyl xanthate (SIPX), sodium ethyl xanthate (SEX) and mercaptobenzothiazole (MBT). These results provide the basis for evaluating whether collector chemistry influences ultimate copper recovery in slag flotation.

**TABLE 4**

Reagent screening schemes and final grade-recovery results.

| Test | Reagent scheme | Cu grade (%) | Cu recovery (%) |
|---|---|---|---|
| T1 (baseline) | MIBC, MBT, SIBX | 19.8 | 91.0 |
| R6 | MIBC, MBT, SEX | 29.9 | 88.8 |
| R7 | MIBC, SEX | 27.0 | 89.6 |
| R8 | MIBC, MBT, SIPX | 24.9 | 89.9 |
| R9 | MIBC, SIPX | 22.3 | 91.5 |
| KT1 | MIBC, MBT, SIBX | 24.4 | 91.8 |
| KT3 | KemFroth011, MBT, SIBX | 24.8 | 91.6 |
| KT5 | MIBC, MBT, SIPX | 26.2 | 91.2 |

Figure 12 shows the grade-recovery curves for the eight reagent schemes, and across all of them, final copper recovery falls within a narrow range of 88.8–91.8 per cent, despite differences in reagent chemistry, operator, feed preparation, and head grade (Begelhole, 2026).

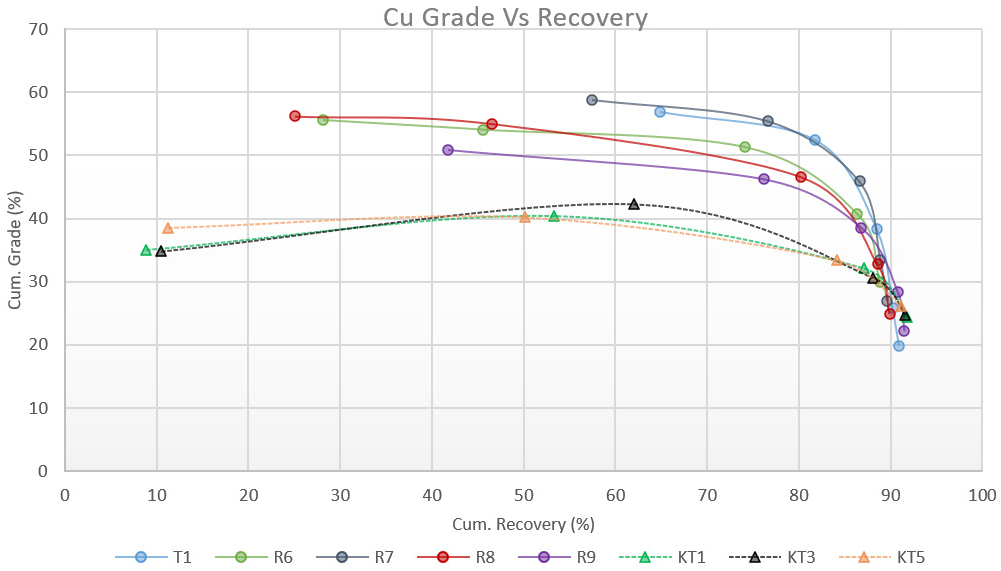



**FIG 12** – Grade recovery curves for reagent screening tests.

The reagent-screening results demonstrate that ultimate copper recovery in slag flotation is effectively reagent-independent. Xanthate-type collectors such as SIBX, SIPX and sodium ethyl xanthate (SEX) operate by chemically binding to exposed sulfide surfaces; however, particles with fully locked copper sulfides present no attachment sites and therefore cannot float regardless of collector type or dosage. As a result, ultimate recovery is controlled by the proportion of liberated sulfide surfaces, not by the specific collector used.

The grade-recovery curves in Figure 12 show two distinct clusters: one from the KT test series and one from the T and R test series. This separation is expected because the KT tests used a higher-grade feed (5.66 per cent Cu) and were conducted by Kemtec personnel, while the T and R tests used a lower-grade feed (3.4 per cent Cu) and were conducted internally. Slag flotation kinetics are extremely fast, and small differences in operator technique during the first minute can shift the early recovery points. These factors explain the variation in the curves starting positions.

However, the critical observation is that all curves converge to the same region by 10 mins, regardless of reagent scheme, operator, or head grade. Every test ends with copper recovery

between 89–92 per cent and concentrate grades between 20–30 per cent Cu. Collector selection influences concentrate grade and early kinetics. Sodium ethyl xanthate (SEX) tends to produce higher grades, SIPX slightly higher recoveries, but none of the reagent schemes tested produced a meaningful increase in ultimate copper recovery (Begelhole, 2026).

This convergence, achieved despite substantial differences in operator, feed preparation and head grade, is strong evidence that copper recovery in this material is governed primarily by mineral liberation rather than by reagent chemistry (Begelhole, 2026). Optimisation efforts should therefore focus on improving liberation rather than further modification of collector schemes.

## CONCLUSIONS

Copper smelter slag presents a unique metallurgical challenge due to its extremely fine copper sulfide grain size and limited liberation at conventional grind sizes, as established in prior mineralogical work (XPS Consulting and Test work Services, 2018). Across all laboratory and plant investigations, the dominant constraint on copper recovery was consistently shown to be liberation rather than reagent chemistry, circuit configuration, or operating conditions.

Laboratory flotation test work demonstrated that both RHF:Mags and RHF:Conv blends exhibit exceptionally fast flotation kinetics, with more than 80 per cent of total copper recovery achieved within the first few minutes of flotation (Begelhole, 2024a, 2024c). This behaviour was mirrored in full-scale plant surveys, where Bank 1 of the rougher circuit alone accounted for approximately 75 per cent of total circuit recovery (Begelhole, 2024b). Beyond this point, only marginal additional recovery was possible, confirming that most floatable copper is recovered almost immediately once exposed.

Grind size investigations validated the strong relationship between liberation and metallurgical performance (Begelhole, 2024a, 2024c). Reducing the $P_{80}$ from 90 µm to 40 µm increased copper recovery sufficiently to justify the additional grinding energy; however, the returns diminish rapidly beyond this point, as recovery gains flatten while grinding energy rises steeply. This reflects the ultrafine nature of the copper sulfides, with more than half of the grains below 10 µm, and the persistence of locked particles even under aggressive grinding conditions.

Reagent-screening work confirmed that collector selection does not meaningfully influence ultimate copper recovery. Although different collectors affected early kinetics and concentrate grade, all tests converged to the same final recovery range of 89–92 per cent when floated to extinction (Begelhole, 2026). This reinforces the point that reagent optimisation cannot overcome liberation limitations inherent in the slag mineralogy.

Collectively, these findings demonstrate that copper recovery from smelter slag is fundamentally controlled by mineral liberation. Improvements in recovery will therefore require strategies that enhance liberation or promote the growth of copper sulfide grains, such as slower slag cooling, rather than further modifications to reagent schemes.

## ACKNOWLEDGEMENTS

The author acknowledges K Lee of Kemtec for conducting the independent frother screening test work, which contributed to the reagent screening findings presented in this paper.

## REFERENCES

Begelhole, J, 2024a. Copper slag – rougher lab test work, Project Metallurgy internal technical note (unpublished), Mount Isa Mines, Mount Isa.

Begelhole, J, 2024b. Copper slag – survey, Project Metallurgy internal technical note (unpublished), Mount Isa Mines, Mount Isa.

Begelhole, J, 2024c. Copper RHF:Converter slag lab flotation, Project Metallurgy internal technical note (unpublished), Mount Isa Mines, Mount Isa.

Begelhole, J, 2026. Cu slag collectors, Project Metallurgy internal technical note (unpublished), Mount Isa Mines, Mount Isa.

Bond, F C, 1952. The third theory of comminution, *Transactions AIME*, 193:484–494.

Cheng, X, Cui, Z, Contreras, L, Chen, M, Nguyen, A and Zhao, B, 2017. Introduction of matte droplets in copper smelting slag, in *Proceedings of the 8th International Symposium on High-Temperature Metallurgical Processing*, pp 385–394 (The Minerals, Metals & Materials Society: Pittsburgh).

Minto, R and Davenport, W G, 1972. Entrapment and flotation of matte in molten slags, *Canadian Mining and Metallurgical Bulletin*, 65:70–75.

Ruddle, R W, 1953. *The Physical Chemistry of Copper Smelting*, pp 64–107 (Institution of Mining and Metallurgy: London).

Wills, B A and Finch, J A, 2016. *Wills' Mineral Processing Technology*, eighth edition, pp 111–112 (Butterworth-Heinemann: Oxford).

XPS Consulting and Test work Services, 2018. Mount Isa slag circuit composites, unpublished internal report for Glencore Mount Isa Mines.

# Optimising CIL carbon performance to improve recovery at PT Citra Palu Minerals

*R Hutasoit[1], S Kurniawati[2] and M Soefihara[3]*

1. Metallurgy Manager, PT Citra Palu Minerals, Palu, Central Sulawesi 94119, Indonesia. Email: ramces.hutasoit@citrapalu.com
2. Shift Metallurgist, PT Citra Palu Minerals, Palu, Central Sulawesi 94119, Indonesia. Email: syafira.kurniawati@citrapalu.com
3. Technical Manager, IXOM Operations Pty Ltd, Perth WA 6000, Australia. Email: muhammad.soefihara@ixom.com

## ABSTRACT

In carbon-in-leach (CIL) circuits, activated carbon is the primary lever controlling soluble gold losses, making its selection and performance critical to overall plant recovery. PT Citra Palu Minerals (CPM) sought to optimise its CIL circuit to increase overall gold and silver recovery while reducing solution losses and reagent consumption. A structured carbon screening program benchmarked six activated carbon products, using standardised kinetic and equilibrium adsorption tests for Au and Ag, attrition/abrasion resistance, and proximate analyses (ash, moisture, iodine number). Statistical analysis employed one-way ANOVA to detect overall group differences and two-sample t-tests to compare pairs of carbons.

IXOM supplied Jacobi G210S activated carbon to PT CPM. Among the candidates, G210S carbon demonstrated the highest gold and silver relative carbon activity and enhanced adsorption efficiency for CIL circuit. It also exhibited the highest attrition strength, implying reduced fines generation, lower carbon make-up rates, and improved carbon inventory stability. Furthermore, it had the lowest ash content, a critical factor linked to fewer inorganic impurities that can occupy active sites and diminish effective surface area. Collectively, these properties distinguished G210S statistically from the alternative carbons and identified it as the preferred candidate for CIL application at PT CPM.

Mass balance modelling of the CIL circuit, incorporating the measured isotherms and attrition data, predicts an improvement in soluble gold loss and reagent consumption to deliver annual benefit of more than A$300 000. Implementation will include carbon changeover, elution stage review with carbon audit, and monitoring of carbon loading and fines.

# Author index


Aimini, E 223
Akis, D 311
Aktoprak, B 521
Araujo, C 509
Auret, L 55
Awatey, B 591
Ballantyne, G 127
Bannon, C 385
Barbetti, K 237
Bax, A R 237
Bearman, R A 99
Beaton, N 223
Begelhole, J 621
Behre, M 81
Bezuidenhout, E B 223
Binks, G 23
Blackwell, K 237
Bosman, S 509
Bouchard, D 269
Bracey, R 609
Brady, J 183
Bristow, N 457
Brodie, E 23
Budhathoki, R 509
Bueno, M 471
Burns, F 405
Butar, R 557
Celona, M 347
Chan, T S 115
Chandramohan, R 127
Chawda, N 521
Chen, J 607
Clark, M 65
Cook, M J 157
Corcoran, C 375
Cornish, B 557
da Rocha Pereira, B 601
Davidson, M 405
Davies, O 375
de Almeida, T 471
Deglon, D 591
Dierx, B 157
Dobson, C 427
Doll, A 147
Dorsch, C R 287
Downie, W 65
Ehrig, K 483
Erwee, M 55
Espinosa Gomez, R 251
Espinosa, D R C 601
Faustino, L M 339
Faye, M M 297
Fernandes, P 339
Figueroa Salguero, G D 385
Frausto, J J 591
Fyfe, T 405
Gagnon, G 521
Ganly, B 365
Giblett, A 147
Giron, J 573
Gontijo, V L 601
Greet, C J 263
Grover, V 573
Gudgeon, D 521
Gunn, S 427
Gurnett, I 589
Haines, C 127
Hanna, R 385
Haskell, S 99
Heath, I 65
Henderson, P 115
Holder, N H M 297

Huang, G 81
Hunter, S 495
Hutasoit, R 635
Izart, C 509
Jak, E 607
James, B 365
James, E 147
Jones, R 405
Khartcyzov, G 607
Khowira, M 385
Killer, L 23
Koh, J Y 223
Kumiye, M 311
Kurniawati, S 635
Lane, G 127
Lara, L 471
Lastra, G 591
Lee, K 441
Li, J 457
Li, Y 483
Liebezeit, V 483
Lim, B 237
Lisso, M 427
Lovatt, I A 157
Machaba, K 55
Malan, A 55
Malcolm, A 533
Mao, L 365
Martin, C 533
McDonough, A 183
Meinke, C 127
Mori, E 573
Mousaviraad, M 183
Mualusi, E 55
Muhamad, N 347
Munro, P D 251, 595
Munro, S 99
Noble, G 347
Norris, G 347
O'Dwyer, J 365
O'Sullivan, M 607
Oats, S 287
Oliver, S J 269
Olivier, J W 297
Olivier, M 55
Palme, R 311
Pax, R A 593
Pease, J D 595
Pluis, P 99
Powell, M 471
Pratt, A G L 323
Pundi, L 311
Putland, B 3
Pyke, J 199
Radford, R 115
Ramakobya, T 55
Rayward, S L 551
Roimaa, T 509
Rowett, C 347
Runge, K 591
Rutter, J 347
Ryan, L 609
Shaikh, A 495
Sharman, P 427
Shevchenko, M 607
Shishin, D 607
Siliezar, J 347
Silva, W S 339
Smith, W 533
Soefihara, M 635
Sola, C 495
Soliman, T 533
St John, T 385
Staunton, W P 237
Stephens, R 183
Strombotne, T 347
Swann, A 589
Swart, M 199

Tayebi-Khorami, M 605
Tenorio, J A S 601
Thammavong, K 81
Thanasekaran, H 81
Thompson, M K 323
Toor, P 553
Valentina, S 607
Van Haarlem, Y 365
van Rooyen, P 603
Vargas, A 521
Vaughan, J 601
Vieira, M G 339
Vilela Neto, G R 339
Vos, C F 223
Walter, N 441
Way, D 609
Wen, J 607
West, R 607
Whitford, M 385
Wong, C 385
Yang, X 375
Yelland, J 533
Zhukov, V 509